THE SCIENCE AND TECHNOLOGY OF FLEXIBLE PACKAGING

Multilayer Films from Resin and Process to End Use

Barry A. Morris



Amsterdam • Boston • Heidelberg • London • New York • Oxford
Paris • San Diego • San Francisco • Singapore • Sydney • Tokyo
William Andrew is an imprint of Elsevier



Huhtamaki EX1036
U.S. Patent No. 11,260,624

EPL LIMITED EX1005
U.S. Patent No. 10,889,093

William Andrew is an imprint of Elsevier
The Boulevard, Langford Lane, Kidlington, Oxford, OX5 1GB, United Kingdom
50 Hampshire Street, 5th Floor, Cambridge, MA 02139, United States

Copyright © 2017 Elsevier Inc. All rights reserved.

No part of this publication may be reproduced or transmitted in any form or by any means, electronic or mechanical, including photocopying, recording, or any information storage and retrieval system, without permission in writing from the publisher. Details on how to seek permission, further information about the Publisher's permissions policies and our arrangements with organizations such as the Copyright Clearance Center and the Copyright Licensing Agency, can be found at our website: www.elsevier.com/permissions.

This book and the individual contributions contained in it are protected under copyright by the Publisher (other than as may be noted herein). All effort has been made by the author and publisher to obtain permissions to reproduce tables and figures from previous publications in this book.

Notices
Knowledge and best practice in this field are constantly changing. As new research and experience broaden our understanding, changes in research methods, professional practices, or medical treatment may become necessary.

Practitioners and researchers must always rely on their own experience and knowledge in evaluating and using any information, methods, compounds, or experiments described herein. In using such information or methods they should be mindful of their own safety and the safety of others, including parties for whom they have a professional responsibility.

To the fullest extent of the law, neither the Publisher nor the authors, contributors, or editors, assume any liability for any injury and/or damage to persons or property as a matter of products liability, negligence or otherwise, or from any use or operation of any methods, products, instructions, or ideas contained in the material herein.

Library of Congress Cataloging-in-Publication Data
A catalog record for this book is available from the Library of Congress

British Library Cataloguing-in-Publication Data
A catalogue record for this book is available from the British Library

ISBN: 978-0-323-24273-8

For information on all William Andrew publications
visit our website at https://www.elsevier.com/



Publisher: Matthew Deans
Acquisition Editor: David Jackson
Editorial Project Manager: Edward Payne
Production Project Manager: Susan Li
Designer: Mark Rogers

Typeset by TNQ Books and Journals

Preface

There are many handbooks available that describe plastics and equipment to make multilayer film. While these books provide a good list of what is possible, they often fail to provide the reader the fundamental understanding of why one material is favored over another for a particular application, or how the film or coating process affects the properties. Also, these books do not cover how the product being packaged and the end use affect the film properties.

Similarly, there are handbooks on packaging technology that provide details on the mechanical aspects of packaging equipment and outline film structures currently in use (at least at the time the book was published). These books fail to explain the principles behind packaging equipment from a unit operation's perspective (sealing, thermoforming, and so on). Nor do they give the reader a fundamental understanding of how to design a packaging structure.

There are also a few textbooks that provide an academic analysis of polymer processes. These are typically written at a level beyond the reach or desire of most packaging engineers.

My goal is to create a book that brings the science to the practitioner in a concise and impactful way, bridging the gap between standard handbooks and academic treatises. Using scientific principles, I explore (and debunk) some of the myths that have persisted in our industry. While discussing key challenges in the packaging industry, I provide a critical review of the scientific literature as well as practical explanations and tips on how to deal with the challenge. Too often packaging engineers fail to seek out the scientific literature. One benefit of this book is easy access to this literature, summarized in a meaningful way. Finally, the book provides insight into why things are done the way they are, which makes the work evergreen: the same principles can be applied to new packaging applications with new materials that are sure to come along in the future.

This book is organized into seven parts and two appendices:

1. Introduction
2. Basic processes
3. Material basics
4. Film properties
5. Effect of converting processes on properties
6. End-use considerations
7. Structure Design and Modeling

Appendix A: Writing Guide for Packaging Films and Other Multilayer Structures

Appendix B: Examples of Flexible Packaging Film Structures

The introduction provides a brief history of packaging and its benefits to society. It describes the basic functions of packaging, the packaging value chain, and what is important for each player in the value chain. It also introduces the need for multilayer films to provide the needs along the value chain in the most cost-effective manner.

Part 2 briefly describes the processes involved in the manufacture and use of multilayer films for packaging. Basic differences between technologies and why one may be favored over another for a given application are highlighted. Key unit operations and processing variables are introduced that affect properties, which are described in more detail in subsequent chapters.

Part 3 introduces resins and substrates commonly used in flexible packaging, highlighting important properties, applications, and regulatory issues. Chapters on melt rheology and polymer blending round out the basics.

Part 4 begins the heart of the book, providing detailed descriptions and analysis of the key properties of packaging films from an engineering and

scientific perspective. Drawing from personal knowledge/experiments and the scientific and patent literature, the current state of knowledge around these properties is distilled. Each chapter begins with why the property under discussion is important, how to measure it and typical values. This is followed by a discussion of the science behind how materials influence these properties. Subjects include heat sealing, barrier, physical strength, abuse resistance, adhesion, optical properties, frictional properties, shrinkage, and thermoforming.

Properties of packaging films cannot be thought of in isolation of the process used to make them. Part 5 explores the effect processing has on film properties in tandem with material properties. Three chapters comprise Part 5, the first of which explores the effect of the process on film quality. Flow instabilities and other topics that affect material selection are covered. The second chapter provides examples of how the process directly affects film properties through changes in quench rate and orientation. The final chapter looks at the effect of processing on interlayer adhesion.

How the flexible film is ultimately used—the environment it is subjected to, types of products being packaged—can influence film properties and design. Part 6 discusses the effect of the end-use environment (temperature, humidity, pressure, and irradiation), packaging—product interactions, and aging on package performance. The cost of the package is a predominant factor in any package design. Here both financial costs (film raw material and converting costs, packing line productivity, and waste due to package failure) and environmental costs are considered.

The final section brings together the ideas introduced in earlier parts into a concluding section on structure design. Principles of design, analytical methods to determine what structures are currently in use and modeling approaches are covered.

There are also two important appendices. The first is a system for writing multilayer structures, authored by my longtime colleague at DuPont, Scott Marks. His system provides a coherent method for communicating package design throughout the industry which is used in this book. The second provides some typical packaging structures that have been in use for various applications over the years. The intention is only to provide some examples and not an exhaustive, or even current, list of structures.

Taking on a project like this is a huge endeavor. I have many people to thank, too many to name individually. I want to acknowledge my friends and colleagues at DuPont who have taught me so much over the years about flexible packaging and where most of my knowledge has come from. My longtime association with the Society of Plastics Engineers and TAPPI has also enriched my understanding of polymer processing and film properties.

Finally I would like to thank my family, Kathy, Elizabeth, and Sara, for their encouragement and for putting up with my long hours of writing and editing.

Barry A. Morris
August 10, 2016

1 Introduction

The primary function of a package is to protect the product, and it is through this function society derives the most benefit by preventing food waste, enabling economies of scale in the production and distribution of goods, and aiding in the access of health care to all parts of the world. Packaging has evolved to meet the changing needs of the value chain; for example, packaging in modern times increasingly serves as a communication platform, providing content information, instruction, and a marketing message. Flexible packaging is ideally suited to meet the challenges of the marketplace and is the fastest growing form of packaging. Multilayer film technology drives this growth by allowing specialized layers with sealing, barrier, or abuse resistance properties to be combined to meet the packaging requirements in the most cost-effective manner. Adding to this is the variety of manufacturing processes that can be used to assemble these structures. Future trends will drive further specialization, which underscores the need for fundamental understanding of flexible packaging technology.

1.1 History of Packaging

Early hunter-gatherer societies likely used animal skins and other textiles to transport and store food. The development of agriculture at least 10,000 years ago coincided with the advancement of other forms of packaging. Farming fostered the growth of larger societies and the need to store food. Early granaries probably used baskets woven from various plants. The earliest evidence for basket weaving dates back about 10,000−12,000 years ago, but earlier artifacts may not have survived [1] (Fig. 1.1).

Basket weaving is the direct predecessor of pottery since baskets were used as the mold for ceramic vessels before the invention of the pottery wheel. The earliest known functional pottery vessels for storing water and food date back to about 10,000 BC [2]. The Egyptians, Greeks, and later Romans used pottery vessels called amorpha to transport a variety of food and other products. These two-handled clay pots are about half the size of today's 55-gallon (208 L) drum. They have been found on many ship wrecks from these times, indicating that they played

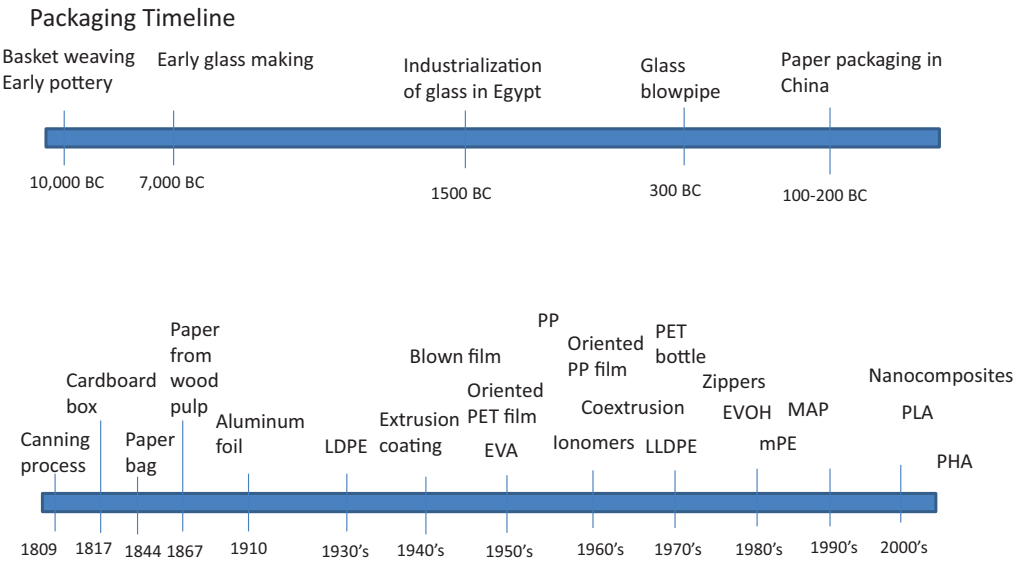


Figure 1.1 Milestones in packaging history.

The Science and Technology of Flexible Packaging. http://dx.doi.org/10.1016/B978-0-323-24273-8.00001-0
Copyright © 2017 Elsevier Inc. All rights reserved.

an important part in early civilization commerce [3] (Fig. 1.2).

An offshoot of pottery is glass, which dates back to around 7000 BC and was industrialized in Egypt in 1500 BC. The blowpipe was invented by the Phoenicians in the 3rd century BC. The modern era of glass packaging dates back to 1889 when the automated bottle making machine was developed [4].

Rigid packaging got its jumpstart from Napoleon, who in the late 1700s offered an award for improved packaging to feed his army. In 1809, Nicholas Appert of France invented a way to preserve food through sterilization and the canning process was born. One year later Peter Durand of England received a patent on various forms of packaging and is generally credited with the invention of the tin can [5,6]. Tin was later replaced by steel and aluminum.

Tin foil was marketed for food packaging in the late 1800s but left an off-taste. Aluminum foil was first produced in France and Switzerland in the early 1900s and in the United States by 1913. Neher patented a continuous rolling process in 1910; packaging was an early application. By 1921 the first foil-laminated paperboard carton was introduced. The first heat sealing foil was developed in 1938. During World War II, aluminum foil found use as a packaging medium, which helped establish it as a mainstream flexible packaging substrate [7].



Figure 1.2 Amorpha in Turkey. Photo by Tim Rogers.
Reproduced with permission under terms of the GNU Free Documentation License.

Next to animal skins, paper may be the oldest form of flexible packaging [8]. The Chinese used an early form of paper to wrap foods in 100−200 BC. The technology evolved and was transported to the Middle East, Europe, and England over the next 1500 years. Early paper was made from bark, flax fibers, or old linen rags. Wood pulp was first used to make paper in 1867. Two other developments in the 1800's contributed to paper's growing use as a packaging medium: the paper making machine and flexographic printing [9]. These developments spurred the commercialization of various packaging forms, such as the paper bag (1844), the cardboard box (1817), corrugated paper (1850), and the paper carton (1870) [8].

Paper-based packaging continued to grow well into the mid-1900s, when plastic substrates became widely available. The introduction of cellophane marks the beginning of the modern era of flexible packaging. Invented in 1908 by Jacque E. Brandenberger, a Swiss textile engineer, it initially only found limited use for wrapping candy and chocolate. This clear flexible film had one major drawback: it had very poor moisture vapor barrier, many times worse than wax-coated paper available by this time. The DuPont company acquired the US patent rights to manufacture cellophane and hired a young scientist in the mid-1920s named William H. Charch to improve the technology. By 1927 Charch had come up with a solution: a thin, transparent coating that made the film water tight [10]. This coincided with major changes in the lifestyles of American consumers. Before then, most food was purchased in open markets or small stores. The modern supermarket was beginning to come onto the scene, emphasizing self-service over customization. The availability of a crystal clear film transformed the market, allowing the store to prepackage goods in a way that the consumer could see what was being packaged. DuPont heavily advertised their miracle film to consumers for its clarity, protection, and convenience: it allowed the shopper to save time by not having to wait for a clerk to serve them [10,11]. Two of these advertisements are reproduced in Figs. 1.3 and 1.4.

By the 1960's much of the cellophane had been replaced by polyvinyl chloride, biaxial-oriented polyester (developed in the mid-1950s at DuPont, ICI, and Hoechst) [14] or oriented polypropylene



Figure 1.3 1948 Cellophane advertisement.
Courtesy of E. I. du Pont de Nemours and Company and Hagley Museum and Library [12].

(ICI, 1961) [15]. Metallized film, formed by physical or vacuum vapor deposition of a thin layer of aluminum, was first commercialized in the 1930s for Christmas tinsel. It was adapted for packaging films and paper in the 1970s [16].

Polyethylene (PE) is the largest volume plastic used in flexible packaging today, valued for its water barrier, toughness, sealability, and transparency. Hans von Pechmann first made PE, although he did it accidently when heating diazomethane in a test tube in 1898. The white waxy substance was analyzed by colleagues to contain long molecules which they dubbed polymethylene. In the 1930s, ICI developed the high-pressure free radical polymerization process for making low density polyethylene (LDPE). Commercialized in 1939, LDPE was used during World War II for radar and cable insulation. DuPont collaborated with ICI and US production began in 1943. Union Carbide and Dow Chemical were also producing LDPE by the 1950s [17].



Figure 1.4 1949 Cellophane advertisement.
Courtesy of E. I. du Pont de Nemours and Company and Hagley Museum and Library [13].

Linear low density polyethylene (LLDPE) and high density polyethylene (HDPE) were developed in the 1950s. The technology involves using a catalyst and coordination chemistry. There are three basic chemistries: chromium typically used in slurry and gas phase processes, Ziegler–Natta in gas and solution processes, and metallocene in all processes. The chromium catalyst process was developed at Phillips Petroleum in the 1950s and introduced as Marlex HDPE. Karl Ziegler (Germany) and Giulio Natta (Italy) conducted their research in the 1950s and LLDPE was commercialized in the 1970s. Metallocene PE was discovered by Walter Kaminsky and Hansjorg Sinn in Germany in 1976 and developed by Dow and ExxonMobil in the 1980s [17].

Throughout the time period between 1950 and 1990 other materials used in packaging were introduced, including ethylene vinyl acetate (EVA), ethylene acid copolymers, ionomers, polypropylene (PP), polyamide 6 (PA6), ethylene vinyl alcohol

(EVOH), polyvinylidene chloride (PVDC), polystyrene, and tie resins.

As the plastics materials advanced, so did the processes to convert them into flexible packaging. Extrusion coating is a case in point. Following World War II, in 1946 and 1947, H P. Smith developed an early process for coating LDPE onto paper. The process of today involving coating a free film onto paper was developed during the same time period by DuPont, working with Hartig Engine and Machine Co. DuPont worked closely with St. Regis Co., which was the first to make extrusion-coated products on a commercial scale. International Paper, Sealright and Egan were also early innovators. By 1957, the first LDPE-coated milk carton was commercialized. From there, the technology advanced to many other packaging forms [18].

The blown film process also developed with the advent of LDPE. The demand for waterproof packaging films with good low-temperature toughness progressed in the 1940s and 1950s, and LDPE was just the plastic to fit this need. The technology to make blown film advanced through this time period, mostly by film producers that made their own dies and ancillary equipment. Visking Company is reported to be the first company to develop PE extrusion. Most of the technology remained closely guarded company secrets until the late 1950s when resin suppliers began buying up film producers and opening up the technology to grow the market for their resins [19].

Extrusion processes were first used in the mid-1800s to make sheet of gutta-percha, rubber, and shellac. Modern looking screw extruders appeared in the mid-1930s in Germany and the United States [20]. As materials were developed, so were the sheet and other flat die processes like cast film and extrusion coating.

Combining materials into multilayer flexible packaging has been practiced since the beginning of the modern packaging era. Coatings onto paper, such as wax or clay, were used early on to provide moisture resistance. By the 1940s adhesives were being used to bond sealant layers onto substrates like cellophane and aluminum foil. Coextrusion, where the layers are combined during the film fabrication process, was commercialized for flat die extrusion in the 1960s, followed shortly thereafter for blown film [21,22].

Packaging machinery also evolved with the availability of new materials from early bag making machines to form-fill-seal machinery. The vertical-form-fill-seal machine was patented by Walter Zwoyer in 1936 [23].

Packaging forms have advanced throughout the years with ever more sophistication. Paper bags were introduced in the 1840s with glued paper sacks with gussets in the 1870s. Laminated paper cartons with aluminum foil were introduced in 1921. Wax-coated milk cartons appeared in the early 1900s [24] and the LDPE-coated version in 1957. Modified atmosphere barrier packaging for improving the shelf life of meat products came into use in the 1970s. Zippers were used in the 1950s but not extensively into flexible packaging until the 1980s. The stand-up pouch gained popularity in the 1990s.

A constant throughout the dynamic growth of multilayer flexible packaging over the past 50 years has been the continued advancement of technology, whether it is resin, substrate, process, or package form. Today there is a plethora of packaging materials and forms that are continuing to evolve as packaging needs change. While one or two layers may have been common a few years ago, now five, seven, and nine layers are the norm with some package structures utilizing hundreds of layers. Often there are multiple ways to solve a package need either by changing layers or the process. For example, a barrier film can be made by laminating a barrier substrate like aluminum foil to a heat seal film or by coextruding a barrier resin like ethylene vinyl alcohol copolymer (EVOH) with a sealant. Often the choice depends on the secondary needs of the application as well as what equipment the converter has.

1.2 Benefits of Packaging

The function of packaging is to aid in the distribution of goods for the benefit of society [25]. From an engineering perspective, the package protects the product. For a food product, this typically means it prevents spoilage or extends the shelf life of the product before the consumer uses it. Barrier and abuse resistance are two primary considerations. Barrier may involve the creation of hermetic seals, blocking light, or providing low permeation to gases such as moisture and oxygen. It also may include preventing food component migration into the package or package component migration into the food. The package may aid in the prevention of

harmful microbe growth by allowing for post packaging sterilization through techniques such as retort, radiation, or high-pressure pasteurization.

Packaging abuse comes in many forms. The package may be subjected to slow puncture, as from a sharp product within the package such as a bone or noodle. High-speed impact events may occur during filling, handling, and distribution. Cold or hot storage may be a factor. The package may be subjected to internal pressure created by elevation changes during transport. The ability to withstand such abuse must be designed into the package.

From a marketing perspective the package is an advertisement. Often it is the only mechanism the brand owner has to inform and entice the consumer. Sparkling graphics can aid in grabbing the attention of the consumer and informing the customer why he or she should purchase the product. To this end, the package often must provide a surface for printing. The entire or parts of the package may need to be transparent so the consumer can see what he or she is purchasing.

From an operations perspective, an ideal package has an efficient form factor, allowing for ease of transportation. The shape of the package impacts how many packs can fit on a pallet and on a truck. It also influences what can be put on a shelf—does it stand up on its own or does it need a peg? Can it be stacked one high on the shelf or more than one high? Such forms influence where the product may be displayed in the store.

From a legal perspective, the package performs a service by providing a medium for displaying content. Label laws in many countries require ever more space on the package to the extent that many pharmaceuticals have labels that open out to display all the requisite information. Labeling laws may require a list of ingredients, net weight, dosage, and various disclaimers. The brand owner may also want to include contact information, recipe suggestions, and so on.

The benefits of packaging to society are numerous. Packaging helps reduce world hunger, spurs economic development, enables life-saving measures in health care, and contributes to sustainability. The UN estimates that the world population will reach 9 billion people by 2043 [26], 2 billion more than in 2012. Increasing food production as well as reducing waste will be essential for feeding the world. The United Nations Food and Agriculture Organization estimates that about 1/3 or 1.3 billion tons of food are wasted each year [27]. An Institute of Mechanical Engineers study [28] concludes from 30% to 50% of food is wasted. The cause of food waste differs by country. Poor distribution and infrastructure results in substantial food loss in developing countries. Packaging can play a key role in preserving food throughout the food chain, as has been demonstrated in the developed world. Transferring best practices to the developing world will go a long way to help reduce the potential for future food shortages.

In developed countries, more food makes it to the consumer, where more is wasted. Part of this is due to excessive buying by the consumer. Packaging can also play a role here. While single-use packaging appears wasteful, portion control packaging can actually be more sustainable than bulk packaging if it cuts down on the amount of unused food. Advances in barrier and reclosable technologies may also extend shelf life at the consumer level, helping to cut food waste.

Packaging in recent years has often been demonized as part of the sustainability problem. But if the whole food chain is considered, packaging turns out to be only a small contributor to environmental stress. Büsser et al. [25] evaluates the impact of packaging on several food products. They find that the impact from packaging is minor compared with the product. For example, for coffee, cultivation and brewing make up 82−99% of the nonrenewable energy consumption and greenhouse gas emissions. Packaging only contributes about 1−5% depending on product package type. The study also considers ozone layer depletion, acidification, and eutrophication. These impacts are also not significantly impacted by the package. Similar conclusions are made for the two other food products considered: frozen spinach and butter. For frozen spinach, keeping the product cold throughout distribution, and in particular at the consumer, is found to be responsible for most of the environmental stress. Butter production overwhelms other factors, including packaging, for environmental impact. Indeed, one can conclude that the package prevents the environmental stress from being even greater due to prevention of spoilage and damage throughout distribution and use.

Although packaging can reduce the environmental impact of the food distribution process, there are still opportunities to reduce environmental stress through material choice, optimizing package-converting processes and reduction of packaging. Indeed, the recent trend toward reducing packaging

by switching from rigid packaging, such as steel cans or glass jars, to flexible packaging is driven in part by this dynamic (the other driver is economic cost). There have been a number of studies trying to compare one package type versus another. Some are of dubious standing, sponsored by special interest groups from one side or another. But intuitively, reducing the amount of material usage should reduce environmental impact. A study by the Flexible Packaging Association [29] shows substantial reduction in nonrenewable energy consumption and greenhouse gas emissions when switching from rigid or even paper packaging to plastic flexible packaging. For example, switching from glass or metal beverage containers to a plastic stand-up pouch reduces energy consumption by 50% and greenhouse gas emissions by 75%. No doubt this study is motivated by enhancing the status of its members, but nevertheless, reducing the amount of material used in a package makes inherent sense both from a financial and environmental cost perspective.

Packaging also provides numerous benefits to the health and well-being of society [30]. Medical devices packaged in easy-open, tamperproof, and sterilizable packaging ensure that instruments are safe for use in the operating room. Packaging enables pharmaceuticals to reach remote areas of the world where cold storage or sanitary conditions does not exist. Emergency relief operations depend heavily on prepackaged goods for fast delivery to areas in need.

It is no coincidence that the use of packaging has expanded in the era of mass production and merchandising [31]. Huge supply chains have developed involving unfinished parts or goods being transported from place to place. This would not be possible without packaging. Packaging has helped spur economic development by enabling self-service purchasing by consumers. It has cut the cost of distributing, promoting, and ensuring the quality of products, and servicing consumers. Packaging has replaced the sales clerk in many markets by providing information on the label. By taking cost out of the supply chain, the cost of goods sold has decreased, making products more affordable to the mass market.

Packaging does have some negative impact on society and the environment, especially when not used responsibly. These include greenhouse gas emissions during production, possible release of toxins into the environment, the scarring of landscapes from mining pits (aluminum) or clear cutting (paper), and the accumulation of plastics in our oceans [32]. Clearly, more can be done to reduce these negative consequences, such as more recycling and better collection of used packaging. But the benefits of packaging, especially flexible packaging, are numerous and generally outweigh the negatives.

1.3 Consumption Patterns

Flexible packaging has grown faster than other packaging forms over the last several decades. The primary driver has been cost. Flexible packaging generally uses less material on a weight basis than other packaging forms, resulting in less material usage as well as savings in transportation. Rigid packaging historically held the advantage in terms of reclosability (caps and lids) and high temperature sterilization, but flexible packaging has closed the gap as new technologies have been introduced.

The size of the flexible packaging market depends on how it is defined. The Flexible Packaging Association as well as PCI Films Consulting define it as follows, which is adopted here:

> *Flexible packaging, as PCI Films Consulting defines it, embraces the manufacture, supply and conversion of plastic and cellulose films, aluminum foils and papers that are used separately or in combination, for primary retail food packaging; non-food packaging applications such as pet food, DIY [do it yourself], hygiene-product overwrap, household detergents, tobacco; and certain other specialist non-food packaging sectors, such as medical and pharmaceutical packaging. PCI's definition relates specifically to value-added, converter-supplied flexible packaging (printed, laminated, coextruded or made into bags and pouches). The value of flexible packaging is measured at the packer level. This definition specifically excludes shrink and stretch films used for secondary packaging and pallet wrap, carrier bags, supermarket self-service and counter bags, silage bags, refuse sacks, industrial IBCs and other industrial packaging, etc.*
>
> **Spading [33]**

Estimates for the size of the market can be found in various market research reports [34−39] and government agencies such as the US Census [39]. These range from $17 to $26 billion for the United States, about 20% of the overall packaging market and the second largest form (after corrugated cardboard). Care must be taken when examining these reports. Differences in market definitions and the methodologies used to obtain the data can give substantially different results. Even for the same source, there may be discrepancies within the data. Estimates for the global market share of flexible packaging range from 25% to 37% for the Americas, 23% to 34% for Europe, and 27% to 33% for Asia [40−42]. The overall growth rate in 2011 was around 4−5%. The projections call for slower growth (but still greater than GDP growth) in the developed regions and much faster growth in the developing world over the next 5 years.

Food packaging is the primary end use for flexible packaging but estimates vary widely from 56% to 83% [41,44]. Other major uses include retail nonfood, industrial, institutional nonfood, and medical and pharmaceutical packaging.

A number of trends in consumption are driving change in the flexible packaging industry:

- Major retailers and brand owners continue to drive sustainability, with reduce, reuse, and recycle being the mantra. Flexible packaging has a reputation for being harder to recycle than rigid packaging forms. The industry needs to continue to cut packaging waste and lightweight to compete against rigid packaging, which has been light weighting and is easier to recycle [33].
- Legislations may force adoption of nonfossil fuel-based materials [33], but so far biosourced materials remain too expensive for mainstream use. Higher raw material costs and lack of high barrier properties have kept biodegradables and compostables a niche [33].
- Europe is considering mandates toward a "circular" economy for flexible packaging [49]. This means reusing, repairing, refurbishing, and recycling existing materials and products in a more focused way. This is driving new monomaterial approaches to packaging.
- Waste-to-energy and pyrolysis are expected to advance in the coming years to help "recycle" multilayer packaging waste [46].
- Flexible packaging remains relatively immune to global downturns [33]. Food uses outpace nonfood uses [43].
- Material costs represent on average 56% of sales. Pretax profit for converters is 4.4% [41].
- Stronger growth is expected in developing regions than in developed nations. Global personal disposable incomes are rising, and with it will come increases in purchases of packaged goods of all kinds [33]. The most dynamic markets have been China and India with growth rates of 12% and 22% per year in 2012, respectively [33,45].
- Interregion trade currently only accounts for 3.8% of world production and consumption, with Western Europe accounting for almost 60% of exports [45]. An increase in exports of flexible packaging or prepackaged goods to the United States from Mexico or Asia is anticipated [33].
- High barrier packaging is expected to grow: BOPET, PA, EVOH [40], high moisture barrier, and metallized films [33]. New clear high barrier films are coming to market that will compete against metallized films [46].
- Bags remain the largest form of flexible packaging. There will continue to be conversion from rigid packaging to stand-up pouches with gains for flat and retortable pouches [43,46].
- Flexible packaging will expand into new market segments, such as viscous condiments (beyond ketchup) and health and beauty products such as shampoos, soups, and so on. Look for more shaped flexible packaging to accent brand identities. More easy-open and reclose options will become available [46].
- The number of layers in coextrusion will continue to grow [46]. Not only do 9 layers provide greater flexibility in material combinations than standard 3 or 5 layers lines, but allow the converter more precise control over thickness of conventional 5 layer films. This is accomplished by combining layers for a single thick

layer. Better layer gauge control allows for downgauging and sustainability gains.

1.4 Packaging Value Chain

The packaging value chain consists of a number of players, as outlined in Fig. 1.5. These include the following:

- Material suppliers (resins, adhesives, substrates)
- Film/sheet converters
- Film laminators and printers
- Equipment manufacturers (converting and packaging)
- Packers (including contract packers)
- Consumer Package Goods Companies
- Wholesalers, distributors
- Retailers (rise of store brands)
- Consumer

The material suppliers furnish the raw materials for making the package. These include polymers used by the converter to make films, such as polyethylene; adhesives; and substrates, including paper, aluminum foil, and polymer films. Each of the materials has its own value chain. For example, the resin producer uses monomers such as ethylene to make the polymer. Ethylene, in turn, is produced from oil (naptha-based processes), natural gas (ethane-based processes), or biobased ethanol. It is beyond the scope of this book to dwell on these value chains. Nevertheless, one trend in the marketplace is to consider renewable-sourced monomers to make conventional oil-based polymers. Braskem has built a plant to make polyethylene from ethylene derived from sugarcane. Coca-Cola has introduced bottles made from polyester that are partially derived from biosourced monomers. As of this writing it is difficult to see whether these material substitutions will take off in the marketplace. So far, biobased monomers have been more expensive than their fossil fuel-based counterparts. The changing dynamic in ethane supply and cost, particularly in the United States with new sources of natural gas coming from new extraction technology, so far has tipped the scale toward fossil fuel-based polymers. Similar arguments can be made for new polymers derived from biosources, such as

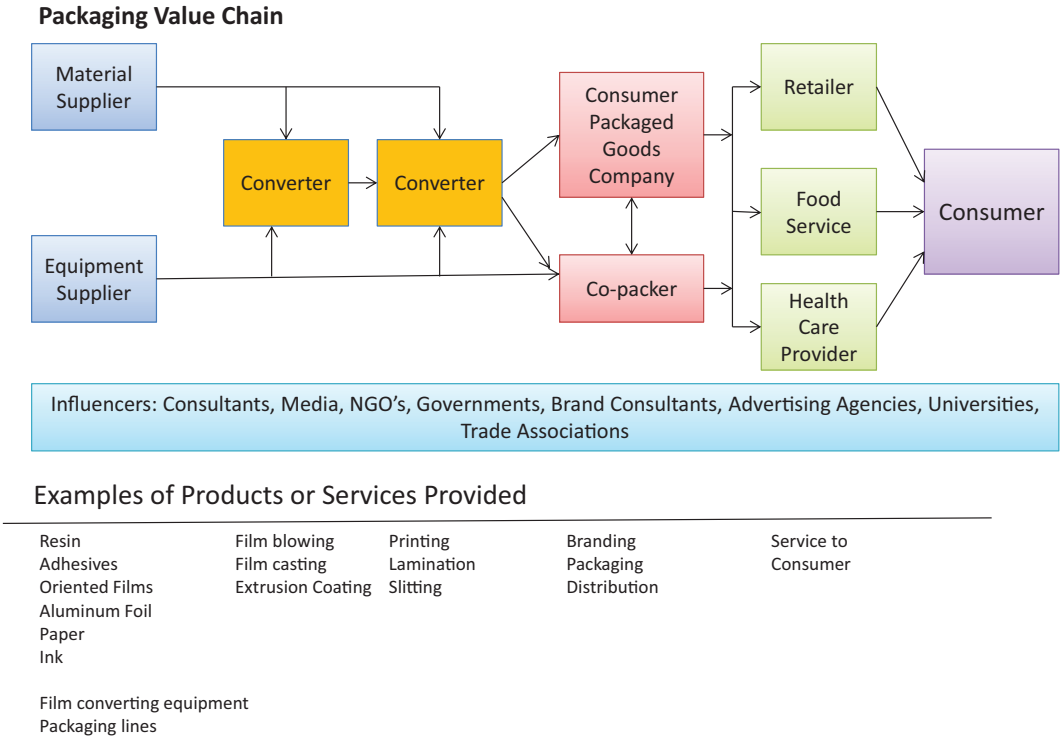


Figure 1.5 Flexible packaging value chain.

polylactic acid, starch-based polymers, and polyhydroxyalkanates. New polymers suffer from having to compete against polymers that have been fine-tuned for many years to achieve desired processibility and properties. As with any disruptive technology, it may take time before these polymers gain enough traction to be widely used in flexible packaging.

The film or sheet converters process the resins into single layer or multilayer films. Common processes for flexible packaging include blown and cast film and extrusion coating or lamination. Any of these processes may be employing coextrusion technology where more than one layer is combined to make a multilayer structure during the manufacture of the film. Orientation processes such as tenter frame or double bubble may also be used.

Film lamination and printing are often performed by the converter who makes the film, but may be done in a separate operation at another plant or company. Lamination involves combining films or substrates typically using either an adhesive lamination or extrusion lamination process. In adhesive lamination, solvent-based, water-based, or liquid solventless adhesives are used to bind the substrates together. Heat is applied after lamination to dry or cure the adhesive. In extrusion lamination, molten polymer is used as the adhesive. Cooling solidifies the polymer and locks the layers in place. Thermal lamination is a third process less practiced in the packaging industry. One example is thermal lamination of a barrier film to a single-layer tray to improve the barrier performance of the tray. The film is brought in through a secondary unwind just after the sheet is made and is still hot. The residual heat bonds the film to the sheet as pressure is applied.

Equipment suppliers provide film fabrication, lamination, coating, printing, winding and unwinding, and packaging equipment to the industry. The packaging equipment suppliers are probably the most diverse given the myriad of packaging forms on the market today. Examples include stick packs, pillow pouches, stand up pouches, juice boxes, composite cans, bag-in-box, trays with lids… There are many ways to package a product and many ways to produce a given package form.

Packers put the product into the package, often on high-speed packaging lines, seal it up and send it off for distribution. At one time the packer was synonymous with the brand owner. The brand owner did its own packing, often at multiple locations that made sense for local distribution. Increasingly, independent or contract packers have set up shop. Initially they handled overflow from the brand owners. They have since evolved to provide services for private label or even brand owners who have decided not to invest in their own lines or equipment.

Consumer Packaging Goods (CPG) Companies or brand owners control the development, production, distribution, and marketing and branding of the product. The CPG's may be local, regional, national, or international in scope. They may choose to contract some of these functions out to copackers or marketing service companies. Increasingly, retailers have created their own "private" labels that compete with traditional brand owners.

A supply chain may have distributors or wholesalers between the CPG and the retailer. The distributors take care of supplying the product to the retailer. The retailer is the company with direct access to the consumer. This is where the consumer comes to purchase the product. Increasingly, the retailer may have a component of their business online to attract customers from the Internet. Some retailers may be completely Internet-based. Retailers ultimate control which products and package forms they will accept. Large retailers, such as Walmart, are increasingly becoming more influential on packaging choices, including creating their own private label brands.

The consumer is the ultimate customer for consumer goods and many food products. Consumer preferences and purchasing decisions in the end determine which products will be manufactured and packaged.

In addition to the consumer goods industry, the food service and health-care industries are important users of flexible packaging. Packaging structures and forms for food service are often similar to that in retail, although the size or form of the package may differ. Also, labeling and graphics may be less critical for food service than retail. Medical devices, such as surgical instruments, are packaged in sterilizable flexible packaging. Blister packaging is often used for pharmaceuticals. Other industries such as electronics and automotive use flexible packaging during internal manufacturing operations as parts are moved from place to place.

Throughout the value chain there are influencers that impact packaging decisions. These influencers include consultants, package design companies, brand and advertising consultants, copackers, trade

associations, trade magazines and other media outlets, universities, and nongovernment agencies and government (especially regulators).

1.5 Needs Along the Value Chain

The needs or what is critical to quality (CTQ's) are expressed differently by various players along the value chain. The consumer drives the decisions at the brand owner or end user, which is chiefly concerned with the marketing, distribution, and safety of the product. The end-user needs are expressed in terms of the package form and features that can provide the consumer needs. Converters are generally responsible for designing and making the film for the package; their needs center on the materials and process that can satisfy the end-user needs.

1.5.1 Consumer Needs

What do consumers expect from the package? First and foremost they are looking for protection. For a food product, they want freshness and an assurance of safety. They want the product to be free of contamination, be the correct weight and not crushed inside the package. They do not want the product to leak from the package, whether it is a liquid or powder.

Information is a second need. What is the product? This may be in the form of a description or picture, or if the package is transparent, a window to the product itself. In this age of self-service, the package may also need to provide guidance as to why to buy this product over others (new flavor, new size, and so on). A list of ingredients, net weight, "use by" dates, and instructions for use may be other information expected on the package. A recycle symbol designating which recycle stream it can become part of is another feature that many consumers look for.

Increasingly, the consumer is looking for the package to provide convenience, such as easy-open features, reclosability, or shaped for on-the-go consumption.

1.5.2 End-User Needs

The end user is a term used to describe the players in the value chain that use the film to package the product. This may be the CPG or brand owner or the packer. The end user is concerned with translating the consumer needs to package function. An example for a food company is given in Table 1.1. Here the following needs are translated to packaging requirements:

- Preserving freshness of the product may require achieving certain barrier requirements, such as limiting the amount of oxygen that may permeate into the package over the intended shelf life of the product. If the barrier requirement can be quantified, the materials and their thickness can be specified to meet the target. Light barrier may also be a requirement, which can be achieved through incorporating opaque layers such as aluminum foil or metallized films, adding filler such as titanium dioxide (TiO_2) to a plastic layer or by printing. Moisture, CO_2, and ethylene barrier or transmission may also be important for ensuring freshness. Fresh produce, for example, benefits from being packaged in films with high gas transmission to allow the produce to "breath." Microperforation, a process which imparts small holes into a film, is often used to achieve such permeation.
- Freshness may also involve preventing off-flavors from migrating from the package to the product, or flavors or active ingredients in the product from migrating out.
- Preventing the product from being contaminated requires good heat seals. Sometimes the product itself, if it is powdery or greasy, may contaminate the seal area, making sealing even more demanding. The choice of the sealant can be critical in these situations.
- The seal must also be able to withstand the extreme environments it may be subjected to during shipping and handling. High altitudes may put pressure on the seal as the package expands due to the thinning of the air surrounding it. Extreme cold, as in blast freezers, or hot temperatures during filling, sterilization, or shipping may affect seal durability.
- Off-odors permeating through the package or from the package itself can also contaminate the product.
- Maintaining the correct weight involves preventing the package from leaking, which relates back to seal and barrier performance as well as puncture resistance.

Table 1.1 Example of Packaging Needs of a Food Company Based on Consumer Needs

Consumer Needs	Translates to
Freshness	Barrier and flavor retention properties
No contamination	Heat seal properties, off-odors
Correct weight	Heat seal properties
Product not crushed	Stiffness, durability
Information	Print quality

- The stiffness, puncture resistance, and impact toughness of the package all contribute to preventing the product from being crushed during transportation and distribution.
- Fulfilling the consumer needs for information may require good printing quality, which starts with having a good surface for printing. Also, it may be important for the consumer to see the product, so providing transparency or a window in the package may be needed.

The end user has a number of other needs, such as

- Processability of the packaging film on the filling equipment. This requires the film having the right stiffness and frictional properties to be easily handled. Seal performance will contribute to packaging line speed. The ability to be easily cut and to withstand the temperature during the filling process is also important.
- Compliance with food packaging regulations, such as the U.S. FDA or the European food laws.
- Ability to withstand postfilling operations, such as sterilization, pasteurization, or freezing.

1.5.3 Converter Needs

The flexible packaging converter purchases base films and resins to produce the film rollstock for the end user. Cost is a key driver throughout the value chain. The focus at this stage of the chain is providing function at the lowest cost. This usually involves combining more than one material into a multilayer film. Often there are several ways to build a packaging structure for a given application. The converter must weigh the options, considering the functional requirements, process assets they may have in place (or wish to invest in) and cost.

One decision is whether lamination or coextrusion should be used to make the multiple layer structure. Lamination involves combining two films with an adhesive or polymer melt (extrusion lamination). In coextrusion, layers are combined while in the melt during the film-converting process. Coextrusion has several attributes including

- bringing the desired properties of different materials into one structure
- reducing emissions from solvent lamination processes (although more than ever water-based or solventless adhesives are used today in adhesive lamination)
- processing multiple materials in one pass to economize on process steps, cost, and time.

Coextrusion is inherently a more flexible process than monolayer extrusion but is more complex: more extruders, more complicated flow geometries, greater potential for flow issues, higher cost of capital investment, and higher scrap costs if the waste generated during the process cannot be recycled. These factors all must be weighed by the converter when determining what process to use.

The converter must translate the needs of the end user into a cost-effective functional packaging film, using a combination of resin and process technology. An example is given in Table 1.2. Here the end-use needs are translated into material and structure design requirements:

- Barrier requirements are met by the selection of materials. Often there is a choice. For example, for high oxygen barrier, the converter may choose between a number of materials, such as aluminum foil, metallized films, AlOx- or SiOx-coated film, PVDC, EVOH, and PA. The cost, the ability to meet the other requirements of the package, and the compatibility with the converter's process will dictate which to use. For example, if transparency is required, then aluminum foil or metallized films would not be considered.
- The barrier is also influenced by the structure design. The permeation is typically inversely proportional to the thickness, so increasing

Table 1.2 Translating End-User Needs by the Converter

End-User Needs	Translates to
Barrier requirements	Selection of materials and layer thickness
Stiffness	Selection of materials and layer thickness
Heat seal performance	Characteristics of heat seal material including seal around contamination and grease resistance
Durability	Toughness of materials and interlayer adhesion
Packing line speeds	Characteristics of heat seal material including seal initiation, hot tack
Slip properties	COF, additive packages
Postfilling steps	Material temperature ranges

thickness improves the barrier, but increases cost. Splitting barrier layers may be beneficial. Protecting barrier layers such as aluminum foil from stress cracking during use may also be an effective strategy.

- The bending stiffness of the film is affected by the stiffness (modulus) of each of the layers, their thickness and their position within the structure. Stiffer layers near the outside of the film have a greater effect on increasing stiffness than near the center. As structures are downsized to meet cost or sustainability targets, these design features become increasingly important to maintain the strength and durability of the package, as well as the consumer acceptance (perception of quality).
- The chemistry of the sealant polymer affects sealability, particularly when dealing with powdery or greasy contamination in the seal area.
- Durability of the package film when exposed to puncture, impact, scratch, and other threats are influenced by the durability of the layers within the package. The adhesion between the layers may also play a role. Controlled delamination during an impact may help dissipate energy and prevent failure of the package.
- Packaging line speed is a function of how fast the package will seal. This is determined by how fast the heat arrives at the interface (film thickness and seal bar temperature) and the characteristics of the sealant. Sealants with low-heat seal initiation temperature and high hot tack strength allow for faster line speeds.
- The slip properties of the film are determined by the coefficient of friction of the film, which in turn, is often controlled by the use of additives to the polymer.
- The ability of the film to withstand postfilling steps such as sterilization, retort, or blast freezing will depend on the temperature in use ranges of the materials. Retort, for example, typically involves exposing the filled package to 121°C for 30 min or more under pressure. Materials that melt below this temperature may not be suitable.

Each of these requirements is explored in-depth in this book.

1.6 Assembling a Package: Benefits of Multiple Layers

The simplest packaging structure consists of a single material or layer. There are a number of packaging forms and applications where this works well, such as glass jars, metal cans (although cans are usually coated with an epoxy, so even seemingly single layer packages may be more than one layer), polyethylene terephthalate (PET) soda bottles, and polyethylene (PE)-produced bags. But each of these has its limitations that prevent it from being used more broadly. The glass jar is heavy and breakable; metal cans are not transparent and so cannot show the product; PET bottles lack sufficient oxygen barrier for many products and work best for liquids; and PE bags lack oxygen barrier and may be limited in the quality of printing that may be applied.

Adding an additional layer gains some functionality, often in a way that reduces overall cost (even after including the additional processing cost of making a more complex structure) over what would be needed to make a single layer perform the same function. Or more often, the multilayer structure allows the package to perform a combination of functions not possible with a single layer.

Obviously a two-layer structure consists of an inner (product side) and an outer layer. In a typical two-layer flexible packaging structure the inner layer provides sealability and the outer layer abuse resistance, printability, or barrier. Some examples are shown in Table 1.3. Common sealant layers include EVA, LDPE, LLDPE, polyethylene plastomers and ionomers. These provide low temperature sealability for fast packaging line speeds. They also may contribute to barrier performance. For example, ionomers have exceptional oil and grease resistance. By themselves, however, they often lack the stiffness, structural integrity, and abuse resistance needed for the application. This is the role of the outside layer, which also may bring additional functionality. HDPE provides moisture barrier and is often used in packaging dry foods such as cereal and crackers. PA may be used where exceptional thermoformability may be needed, such as brick packages for cheese. Oriented PET film provides an excellent surface for printing. Paper is a low-cost substrate often used in pouches and bags. With two layers, greater functionality can be achieved than either layer alone.

Three layers provide even greater flexibility in package design. The primary function of the inner layer is still sealability. The outer layer again provides abuse resistance, heat resistance (during sealing), stiffness, structural integrity, a surface for printing, and in some cases moisture barrier. The same substrates as discussed in the two-layer examples are typically used as the outer layer in three-layer structures. The center layer may provide a variety of functions. PVDC or metallization layers may be used to provide oxygen barrier. Many films are printed and laminated to a sealant layer with the print side facing inward, protected from outside abuse by the film layer. This is known as reverse printing. Adhesives may be used in the center layer to allow for lamination of two dissimilar materials. Recycle can be incorporated into the center layer for some applications. Pigments such as titanium dioxide (TiO_2) may be added to a core layer to provide light barrier. Examples of such structures are shown in Table 1.4. One example is a medical forming web. Here an ionomer, traditionally used as a sealant in flexible packaging, finds use as the core providing outstanding thermoformability and puncture resistance. Less expensive EVA or PE layers are used as the skin to bond to the Tyvek spun bond polyethylene top layer of the package. An alternative structure for this application is (PA6-tie-PE) where the PA6 provides the thermoformability and puncture resistance.

Examples of extending the concept of multiple layers to five are shown in Table 1.5. Again the inner most layer is typically a sealant layer such as PE, EVA, or ionomer. Layer 2 is often an adhesive layer followed by a barrier layer, another adhesive layer, and the abuse resistance layer. The examples shown here are all made by coextrusion. The barrier polymers, such as PA6 and EVOH, do not bond to most sealant polymers. The industry has developed tie resins to bond these materials together during coextrusion, as explained in Chapter 10. The first example is an extension of the two-layer (HDPE sealant) snack package film discussed earlier. Five layers allow the incorporation of a PA6 or EVOH layer to provide oxygen and aroma barrier. HDPE provides the moisture barrier.

The next two structures in Table 1.5 represent barrier forming webs often used in meat packaging. The ionomer sealant provides excellent sealability, especially in the presence of grease. PA is combined with EVOH to help with thermoformability as well as abuse resistance.

The final structure in Table 1.5 highlights one of the advantages five or more layers bring to operational flexibility. Here a two-layer snack package structure is made with five layers. The HDPE thickness is determined by the amount of moisture barrier needed for the application and often is greater than

Table 1.3 Examples of Functionality of Two-Layer Flexible Packaging Structures

Inner layer Function	Outer Layer Function	Example Structure	Example Application
Low-temperature sealing, easy open	Stiffness Moisture barrier	(HDPE−EVA) (HDPE-ionomer)	Cereal or cracker liner (bag in box)
Sealing	Stiffness Low cost	Paper/LDPE	Dry soup, spice pouches

Table 1.4 Examples of Three Layer Flexible Packaging Structures

Inner Layer Function	Center Layer Function	Outer Layer Function	Example Structure	Example Application
Sealing	Print	Temperature and abuse resistance printability	OPET/print/EVA	Cheese packaging
Sealing	O_2 barrier and adhesion	Temperature and abuse resistance	OPET/PVDC adhesive/EVA	Meat packaging
Sealing	Adhesion	Temperature and abuse resistance	PA/adh/mPE OPET/adh/EVA	Cheese packaging
Sealing	Recycle	Temperature and abuse resistance	(HDPE-recycle-LLDPE)	Bags
Sealing	Light barrier	Temperature and abuse resistance, moisture barrier	(HDPE−HDPE + TiO_2 −EVA)	Snack package
Sealing	Forming puncture resistance	Sealing	(EVA−Surlyn−EVA)	Medical device packaging forming web
Sealing	Adhesion	Thermoforming and puncture resistance	(PA6−tie−PE)	Medical device packaging forming web

Table 1.5 Examples of Five Layer Flexible Packaging Structures

Layer 1	Layer 2	Layer 3	Layer 4	Layer 5	Example Structures	Example Application
Sealing	Adhesion	Barrier	Adhesion	Abuse resistance, moisture barrier	(HDPE-tie-PA6-tie-EVA) (HDPE-tie-EVOH-tie-ionomer)	Barrier snack package
Sealing	Adhesion	Barrier	Adhesion	Abuse resistance, thermoforming	(PA6-tie-EVOH-tie-ionomer)	Bacon package
Sealing	Adhesion	Thermoforming	Barrier	Abuse resistance, thermoforming	(PA6-EVOH-PA6-tie-ionomer)	Meat forming web
Sealing	Adhesion	Moisture barrier	Moisture barrier	Moisture barrier	(HDPE-HDPE-HDPE-HDPE-EVA)	Snack package

what a two layer film process is designed to run. By putting the HDPE in multiple layers, the converter can easily make the desired structure. Indeed, operational flexibility is one of the primary motivations for the converter to purchase seven and even nine layer film lines. The operational flexibility gained with additional layers may also improve the control of the layer distribution within the film. Without such flexibility, the converter may resort to bumping up the thickness of an expensive barrier layer to ensure the film meets specifications. Better process control may allow the layer to be downgauged.

Table 1.6 Examples of Structures With Greater Than Five Layers

Sample Structure	Application
PE/Paperboard/PE/Al/(ACR-LDPE)	Aseptic pouch
(PP-regrind-tie-EVOH-tie-PP)	Retort bowl
OPET/print/adh/met-OPP/adh/(LLDPE-LLDPE-LLDPE)	Stand-up pouch
(LDPE-ACR)/ACR/Al/ACR/(ACR-LDPE)	Toothpaste tube
(PA6-tie-PA6-EVOH-PA6-tie-LLDPE) (PA6-tie-PA6-EVOH-PA6-tie-ionomer)	Meat forming web

ACR, *acid copolymer resin.*

The capability of additional layers also allows additional structures to be made. Some examples of such structures are shown in Table 1.6.

1.7 Packaging Trends in the Context of the Value Chain

A number of key drivers and trends in flexible packaging based on discussions by DuPont with players throughout the value chain are compiled in Table 1.7. In this analysis consumer trends and needs drive the brand owners and retailers toward behaviors that influence package innovation:

- The first is the trend toward greater health, safety, and wellness. Consumers want a healthier diet, particularly as consumers in the developing world rise out of poverty into the growing middle class. This brings with it the challenge of food safety and the role packaging plays. The implication for the brand owner is the need to improve product quality. This translates to packages and package technology that ensure safety and freshness, such as the use of quality sealants to prevent leakers, high barrier resins or coatings, and in-package sterilization.
- The consumer continues to value simplicity and convenience. Brand owners strive to improve the consumer experience with easy-open and reclosable features, packages shaped to be held in the hand and microwaveable packaging.

Table 1.7 Packaging Drivers and Trends

Consumer Trends and Needs	Brand Owner/ Retailer Implications	Packaging Implications
Health, safety, wellness	Produce quality products	Safer, fresher packages
Simplicity, convenience	Improve experience	Easy-open solutions
Offering overload	Differentiate for share	Shelf impact and experiential
Sustainability	People, planet, profits	Reduce, recycle, renewable, protect
Affordability/ value	Minimize cost—productivity; maximize profits	Lightweight structures

Courtesy of E. I. du Pont de Nemours and Company.

- The consumer is inundated with choices, especially in the developed world. The brand owner and retailer must continually innovate to gain share. This leads to new package designs that have shelf impact and give the consumer a hands-on experience. Such experiences increasingly include interactions with smart phones that may require changes in graphics and other technology.
- Sustainability continues to drive consumer choices. Retailers have also gotten involved, leading to changes in package design, content, and recyclability. An example of things to come is the transition to square 1-gallon plastic milk jugs from round ones in the U.S. market at large discount stores like Walmart and Costco [47]. The design eliminates the need for a shipping crate since the jugs are stackable. This saves labor by 50% and cuts water use (for cleaning the crates) by 60–70%. More gallons fit on a truck and crates do not need to be shipped back. They also save space in the store. Other products have followed suit, such as the switch from round to square yogurt cups.
- Finally, the consumer is always looking for value. This drives the brand owners to greater productivity to minimize cost. One consequence of this is the lightweighting of packaging

structures. A recent Flexible Packaging Association white paper illustrates the progress that has been made on this front with several examples, including the following [48]:

- Over a 6-year period the weight of a national brand hot dog package was reduced by 30%.
- A candy bar flexible package was reduced by 60% in a 6-year period.
- Cereal bag liners and stretch films have been reduced by using a tough ionomer film.
- Coextrusion technology has allowed cheese packages to be 30% lighter without sacrificing barrier performance.

Many of the strategies outlined in the FPA report, such as advances in material toughness, coextrusion, barrier resins, and equipment technology, can be taken advantage of through the concepts that will be introduced and explained in the remainder of this book.

References

[1] Scarre C. Smithsonian timelines of the ancient world. 1st American ed. London: Dorling Kindersley; 1993.

[2] De Guire E. History of ceramics, Americal Ceramic Society;2014. viewed June 15, 2016, from: http://ceramics.org/learn-about-ceramics/history-of-ceramics

[3] National Geographic News. Ancient Greek wreck found in Black Sea;2010. viewed May 18, 2013, from: http://news.nationalgeographic.com/news/2003/01/0110_030113_blacksea_2.html.

[4] Miller GL, Sullivan C. Machine- made glass containers and the end of production for mouth-blown bottles. Historical Archeology 1984; 18:83–96. viewed June 15, 2016, from: http://www.sha.org/bottle/pdffiles/MillerSullivan1984.pdf

[5] Risch SJ. Food packaging history and innovations. J Agric Food Chem 2009:8089–92.

[6] Berger KR. A brief history of packaging. University of Florida IFAS Extension, ABE321;2002. viewed May 18, 2013, from: http://edis.ifas.ufl.edu/pdffiles/AE/AE20600.pdf.

[7] Aluminumfoils.com. History of aluminum foil; 2005. viewed May 18, 2013, from: http://www.aluminumfoils.com/aluminum-foil/aluminum-foil-history.html.

[8] Hook P, Heimlich JE. A History of Packaging. Ohio State University Extension Fact Sheet, Community Development, 700 Ackerman Road, Suite 235, Columbus, OH 43202–51578, CDFS-133, viewed May 18, 2013, from: http://ohioline.osu.edu/cd-fact/0133.html.

[9] Twede D. The origins of paper based packaging. In: The future of Marketing's past, proceedings of the 12th conference on historical analysis and research in marketing, CHARM 2005, Long Beach, California, April 28–March 1, 2005; 2005. p. 288–300.

[10] Kinnane A. DuPont: from the banks of the brandywine to miracles of science. E. I. Du Pont de Nemours and Co; 2002.

[11] Bernat C. Supermarket packaging: the shift from glass to aluminum to plastic. The Atlantic; 2012. January 25, viewed May 18, 2013, from: http://www.theatlantic.com/health/archive/2012/01/supermarket-packaging-the-shift-from-glass-to-aluminum-to-plastic/251875/?single_page=true.

[12] E. I. du Pont de Nemours and Company, Advertising Department. Modern shoppers prefer food in cellophane: shows what it protects! Protects what it shows!. Dpads-1803–00308.tif. Hagley Museum and Library; 1948.

[13] E. I. du Pont de Nemours and Company, Advertising Department. New self-service meats make shopping quicker, easier: DuPont Cellophane. Dpads-1803–00320.tif. Hagley Museum and Library; 1949.

[14] Wikipedia. BoPET, viewed June 16, 2016, from: http://en.wikipedia.org/wiki/BoPET#History.

[15] Wikipedia. Innovia Films, Ltd, viewed June 16, 2016, from: http://en.wikipedia.org/wiki/Innovia_Films_Ltd.

[16] Hanlon JF, Kelsey RJ, Forcinio HE. Handbook of package engineering. 3rd ed. CRC Press; 1998. p. 117.

[17] Demirors M. The history of polyethylene. In: Strom E, Rasmussen S, editors. 100+ years of plastics. Leo Baekeland and beyond. Washington, DC: ACS Symposium Series; American Chemical Society; 2011. p. 115–38.

[18] Bezigian T, editor. Extrusion coating manual. 4th ed. Atlanta, GA: TAPPI Press; 1999. p. 1–2.

[19] Andrews WC, Williams KJ. In: Giles GA, Bain DR, editors. Technology of plastics packaging for the consumer market. Oxford: Sheffield Academic Press; 2001. p. 160.
[20] BCC Research. History of plastic sheet;2013. viewed May 18, 2013, from: http://www.bccresearch.com/blog/report-archives/history-plastic-sheet.html.
[21] Djordjevic D. Coextrusion. Rapra Rev Rep 1992;6(2) [Rapra Publishing].
[22] Frey TD, Albright JA. Coextrusions for flexible packaging. In: Baker M, editor. Wiley encyclopedia of packaging technology. New York: John Wiley and Sons; 1986. p. 199.
[23] General Packaging Equipment. History of the VFFS machine and general;2013. viewed May 18, 2013, from: http://www.generalpackaging.com/history.html.
[24] Doug and Linda's Dairy Antique Site. Wax milk containers;2013. viewed May 18, 2013, from: http://dairyantiques.com/Wax_Milk_Containers.html.
[25] Büsser S, Steiner R, Jungbluth N. LCA of packed food products: the function of flexible packaging. Düsseldorf, DE and Uster, CH: ESU-Services Ltd. Commissioned by Flexible Packaging Europe; 2008.
[26] United Nations, Department of Economic and Social Affairs, Population Division, Population Estimates and Projections Section, UN world population prospects, the 2010 revision;2010. viewed May 18, 2013, from: http://esa.un.org/unpd/wpp/index.htm.
[27] Gustavavsson J, Cederberg C, Sonesson U, van Otterdijk R, Meybreck A. Global food loses and food waste: extent, causes and prevention. Rome: Food and Agriculture Organization of the United Nations; 2011. Study conducted for the International Congress, SAVE FOOD! at Interpack2011, Düsseldorf, Germany.
[28] Institution of Mechanical Engineers. Global food. Waste not, want not;2013. viewed May 18, 2013, from: http://www.imeche.org/knowledge/themes/environment/global-food.
[29] Flexible Packaging Association. Flexible packaging, less resources, less footprint, more value. 3rd ed. 2009.
[30] SPI. The Plastics Industry Trade Association, Plastics in Packaging, viewed May 18, 2013, from: http://www.plasticsindustry.org/AboutPlastics/content.cfm?ItemNumber=636&navItemNumber=1118.
[31] Anthony S. A public service announcement for packaging?. Packaging World; 2013. February 19, viewed May 18, 2013, from: http://www.packworld.com/print/54474.
[32] Ragsdale TE. Food packaging study, A report on environmental impact. Ashland Food Cooperative; 2005. viewed May 18, 2013, from: http://www.ashlandfood.coop/sites/default/files/packaging-study.pdf.
[33] Spalding MA. A global flexible-packaging market SWOT statement to 2016. In: The converting Curmudgeon, viewed on May 18, 2013; April 21, 2013. from: http://convertingcurmudgeon.com/2013/04/21/a-global-flexible-packaging-market-swot-statement-to-2016/.
[34] Smithers Pira. Market reports;2013. viewed 18 May 19, 2013, from: https://www.smitherspira.com/MarketReports/Home.aspx.
[35] Freedonia. Industry market research;2013. viewed 18 May 19, 2013, from: http://www.freedoniagroup.com/?ReferrerId=AP-Adwords&gclid=CLPf_IiLo7cCFYyZ4AodLS4AYA.
[36] Visiongain. Packaging;2013. viewed May 19, 2013, from: http://www.freedoniagroup.com/?ReferrerId=AP-Adwords&gclid=CLPf_IiLo7cCFYyZ4AodLS4AYA.
[37] BCC Research. Plastics;2013. viewed May 20, 2013, from: http://www.bccresearch.com/index/category/code/plastics.
[38] PCI Films Consulting Limited. Flexible packaging market reports;2013. viewed May 19, 2013, from: http://www.pcifilms.com/main.asp?selection=Market Studies&subsel=Flexible Packaging Market Reports.
[39] U.S. Census Bureau. North American Industry classification system, viewed May 18, 2013, from: http://www.census.gov/eos/www/naics/index.html.
[40] Flexible Packaging Association. Report to members. 2012. viewed May 18, 2013, from: http://www.flexpack.org/PDFs/Misc_Reports/FPA_RTM2011.pdf.
[41] Homan J. European and global markets for flexible packaging. In: FPA Annual Conference, Arizona; 2012. viewed 18 May 19, 2013, from: https://www.flexpack.org/MEMONL/mo_presentations/2012_am/Jan_Homan.pdf.
[42] Smithers P. Versatility and innovation to drive global flexible packaging market, viewed on May 18, 2013, from: https://www.smitherspira.com/versatility-and-innovation-to-drive-global-flexible-packaging-market.aspx.

[43] Freedonia. Description of converted flexible packaging to 2015;2013. viewed May 18, 2013, from: http://www.freedoniagroup.com/Converted-Flexible-Packaging.html.

[44] Flexible Packaging Association. Flexible packaging facts & figures;2013. viewed on May 18, 2013, from: http://www.flexpack.org/INDUST/industry_facts_figures.asp.

[45] Converting Quarterly. Global flexible packaging market to reach $90 billion in 2016;2013. viewed on May 18, 2013, from: http://www.convertingquarterly.com/industry-news/articles/id/4600/global-flexible-packaging-market-to-reach-90-billion-in-2016.aspx.

[46] Romanik R. Eleven trends shaping flexible packaging. In: Packaging world, 2013; 2013. viewed May 21, 2013, from: http://www.packworld.com/print/54859.

[47] Rosenbloom S. Solution or mess? A milk jug for a green earth. New York Times; 2008. June 30, viewed June 10, 2013, from: http://www.nytimes.com/2008/06/30/business/30milk.html?pagewanted=all.

[48] Flexible Packaging Association. Flexible packaging lightweighting strategies and innovation. 2011. viewed June 10, 2013, from: http://www.flexpack.org/sustainable_packaging/FPA_Lightweighting_White_Paper.pdf.

[49] European Commission. Moving towards a circular economy. 2015. viewed November 29, 2015 at: http://ec.europa.eu/environment/circular-economy/index_en.htm.

2 Converting Processes

The purpose of the converting process is to transform raw materials in the form of polymer pellets or film substrates (including paper and foil) into a final packaging structure. This often involves more than one process or step that may include film formation, orientation, metallization, lamination, coating, printing, winding, and slitting. The basic processes with their starting materials and the finished products they produce are outlined in Table 2.1. Often there is more than one way to make a functional structure, the choice of which depends on a number of factors such as run length and existing assets of the converter. This chapter briefly describes the major converting processes, their key components, and processing parameters that affect the properties of the final product.

2.1 Extrusion

Extrusion is a common component of all polymer film converting processes. The extruder melts the polymer pellets and pumps it through a die, which forms the film or coating. Almost all film and coating lines use single screw extruders as shown schematically in Fig. 2.1. Polymer pellets are fed into the rear of the extruder through a feed hopper. The rate of rotation of the screw underneath the hopper determines the rate of feed and output of the extruder. This is known as flood feeding. In more sophisticated twin screw extruders and polymer compounding equipment, feeders on top of the hopper "starve feed" the extruder so that screw speed and feed rate are independently controlled. Twin screw extruders and starve feeding are rarely used in film extrusion; single screw extruders provide sufficient mixing at much lower cost for packaging converting operations.

The output of a single screw extruder increases with the diameter of the screw; as the diameter increases so does the volume of material that can be conveyed. The volume increases with the cube of the diameter from simple geometric considerations. The output scale-up is generally less than cubic, however, since other factors such as heat transfer also influence output. Typical rates can be found in Table 2.2.

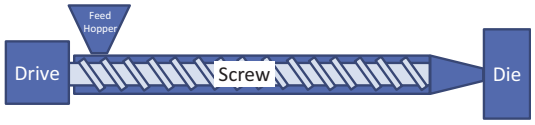


Figure 2.1 Schematic diagram of a single screw extruder.

Table 2.1 Major Converting Processes

Unit Operation	Processes	Raw Materials	Finished Product
Film formation	Blown film Cast film	Polymer pellets	Single or multilayer film
Coating or lamination	Extrusion coating Extrusion lamination Adhesive lamination	Film, paper, or foil substrate(s) Polymer or adhesive	Multilayer film
Film orientation	Tenter frame Double bubble Machine direction orienter	Polymer or sheet	Oriented film
Printing	Gravure Flexographic	Film Ink	Printed film
Slitting	Slitter	Film	Film

The Science and Technology of Flexible Packaging. http://dx.doi.org/10.1016/B978-0-323-24273-8.00002-2
Copyright © 2017 Elsevier Inc. All rights reserved.

Table 2.2 Typical Output and Specific Output for a 30:1 L/D Single Screw Extruder Running at 100 rpm

Screw Diameter		Output		Specific Output	
Inches	mm	lb/hr	kg/hr	lb/hr/rpm	kg/hr/rpm
0.75	19	8	3.6	0.08	0.036
1.0	25	13	5.9	0.13	0.059
1.25	32	30	13.6	0.30	0.14
1.5	38	50	22.7	0.50	0.23
2.0	51	120	54.5	1.20	0.55
2.5	63.5	250	114	2.50	1.14
3.5	89	600	273	6.00	2.73
4.5	114	1200	545	12.0	5.45
6.0	152	2500	1140	25.0	11.4
8.0	203	5200	2360	52.0	23.6

Frankland, J. Get smarter on extrusion sizes. Plastics Technology; July 2012. p. 22.

The key performance requirements for the extruder are to fully melt the polymer, to produce a uniform melt temperature at the die exit (which minimizes gauge variability), and to generate sufficient pressure to sustain flow through the downstream process (typically transfer tubes, screen packs, feedblock, and die). The important factors affecting performance are the screw design, operation temperatures, and screw speed. The function of the screw can be divided into three operations: solids conveying, compression and melting, and metering or pumping. Each operation occurs in about one-third of the extruder length as shown in Fig. 2.2.

Conveying is achieved by the frictional differences between the polymer pellets against the barrel and screw root as the screw rotates. The friction of the pellets against the barrel needs to be greater than at the screw root, otherwise the pellets will simply rotate with the screw. An analogy is the rotation of a screw and nut—if the nut is not held in place it will rotate with the screw as it is tightened. Screw cooling and barrel heating are sometimes used to create the differential friction for conveying. Adding grooves to the barrel can increase the solids conveying for some polymers by 20–40% [2], but care must be taken when using this approach. Some polymers may be too hard; the resultant pressure buildup may cause damage or even break the screw. This is especially true for retrofitted smooth bore systems that have not been designed for the high pressure and torque required with grooves [3]. Some polymers may be too soft—if the polymer melts in the grooves, the effect of the grooves may be negated, and the grooves can become a source of holdup and polymer degradation. Light grooves can be a good compromise for some polymers [4]. Discussion with the extruder manufacturer and the polymer supplier prior to running a new polymer on a grooved barrel extruder is advised to avoid potential problems.

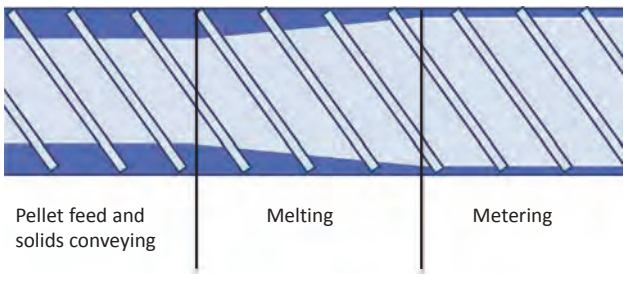


Figure 2.2 Operational design of a screw.

As the solid pellets are conveyed forward, they are compressed. In what is typically referred to as a "standard" screw design, this is achieved by slowly reducing the height of the screw channel. The ratio of the final screw channel height (metering section) to the initial (solids conveying section) screw channel height is known as the compression ratio. This ratio typically ranges from about 2:1 to 3:1 and compression takes place over approximately the second third of the screw length. As the compression takes place, friction and heat transferred from the barrel to the solid bed begin to melt the polymer.

The polymer melt forms a pool behind the solid bed that increases in width as the polymer travels down the barrel length (Fig. 2.3). Ideally, the polymer is entirely melted at the end of the compression or melting zone.

Frictional forces tend to dominate the melting process in single screw extruders. To speed up this process and increase output, many modern screw designs introduce a second flight that segregates the melt pool from the solid bed. These designs are known as barrier screws with the barrier being the second flight between the solid bed and melt pool. Forcing the separation of the melt from the solid bed increases the frictional heat on the solid bed, accelerating its melting. There are many different variations on this general scheme, including changing the width or depth of the melt pool along the screw length. One of the challenges is the transition to and from the barrier section of the screw. The pros and cons of each approach are discussed in the general literature [5–7].

The final section of the screw builds pressure in the melt to pump it through the die. The metering section output is a function of screw speed, screw geometry, pressure drop, and polymer viscosity. As the screw rotates, drag is introduced between the stationary barrel and rotating surface of the screw, propelling the melt forward. There is also a pressure-driven component to the flow, and depending on the pressure profile within the extruder, this may be positive or negative. A simple model for the drag and pressure-driven flow is given by Eqs. (2.1) and (2.2) [8]. Fig. 2.4 shows the definition of variables in these equations. Here several assumptions have been made including Newtonian flow (viscosity in independent of shear rate), fully developed flow, and no leakage across the flight tips. Despite these limiting assumptions, the sum of Eqs. (2.1) and (2.2) usually comes close to predicting the output of the metering section. These can be used as a starting point for troubleshooting [9].

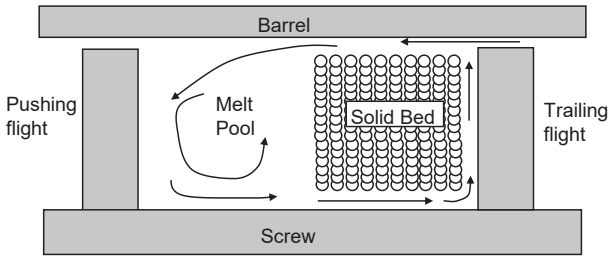


Figure 2.3 Schematic of melting in a single screw extruder.
Reproduced from Morris [55].

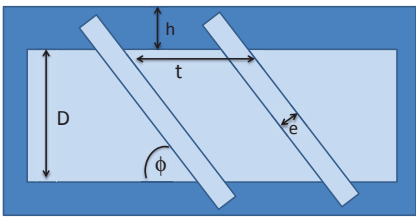


Figure 2.4 Metering section of a single screw extruder.

$$Q_{\text{drag}} = \frac{1}{2}F_{\text{d}}\pi^2 D^2 h\left(1-\frac{ne}{t}\right)\sin\varphi\cos\varphi \qquad (2.1)$$

$$Q_{\text{pressure}} = \frac{F_{\text{p}}\pi D h^3\left(1-\frac{ne}{t}\right)\sin^2\varphi\Delta P}{12\mu L} \qquad (2.2)$$

where Q_{drag} = drag flow, Q_{pressure} = pressure-driven flow, F_{d} = channel correction factor = $0.140(h/w)^2 - 0.645(h/w) + 1$, F_{p} = channel correction factor = $0.162(h/w)^2 - 0.742h/w + 1$, D = screw diameter, N = screw speed (rpm), h = screw meter section channel depth, n = number of flights on the screw, e = thickness of flight, t = flight lead (pitch), ϕ = flight helix angle, μ = viscosity of melt calculated at shear rate = $\pi ND/h$, L = length of metering section being investigated.

A good screw design will keep the pressure-driven component of flow to about 10% or less of the total flow. If the pressure-driven component becomes too high, small fluctuations in pressure can result in large changes in output, which is undesirable. In situations where precise control of output is required, a separate melt pump may be used at the end of the extruder to decouple pumping from the other functions of the extruder.

Achieving temperature uniformity at the extruder exit is critical for good gauge control coming out of the die. To reduce temperature variability in the extruder, often times a mixing element is incorporated into the screw design, typically as part of the metering section. There are a number of different types of mixing sections, three of which are shown in Fig. 2.5. Inserting pins is one of the easiest ways to redistribute flow, but stagnant areas behind the pins set up the potential for gel formation. More sophisticated designs, such as the Saxton mixer [10],

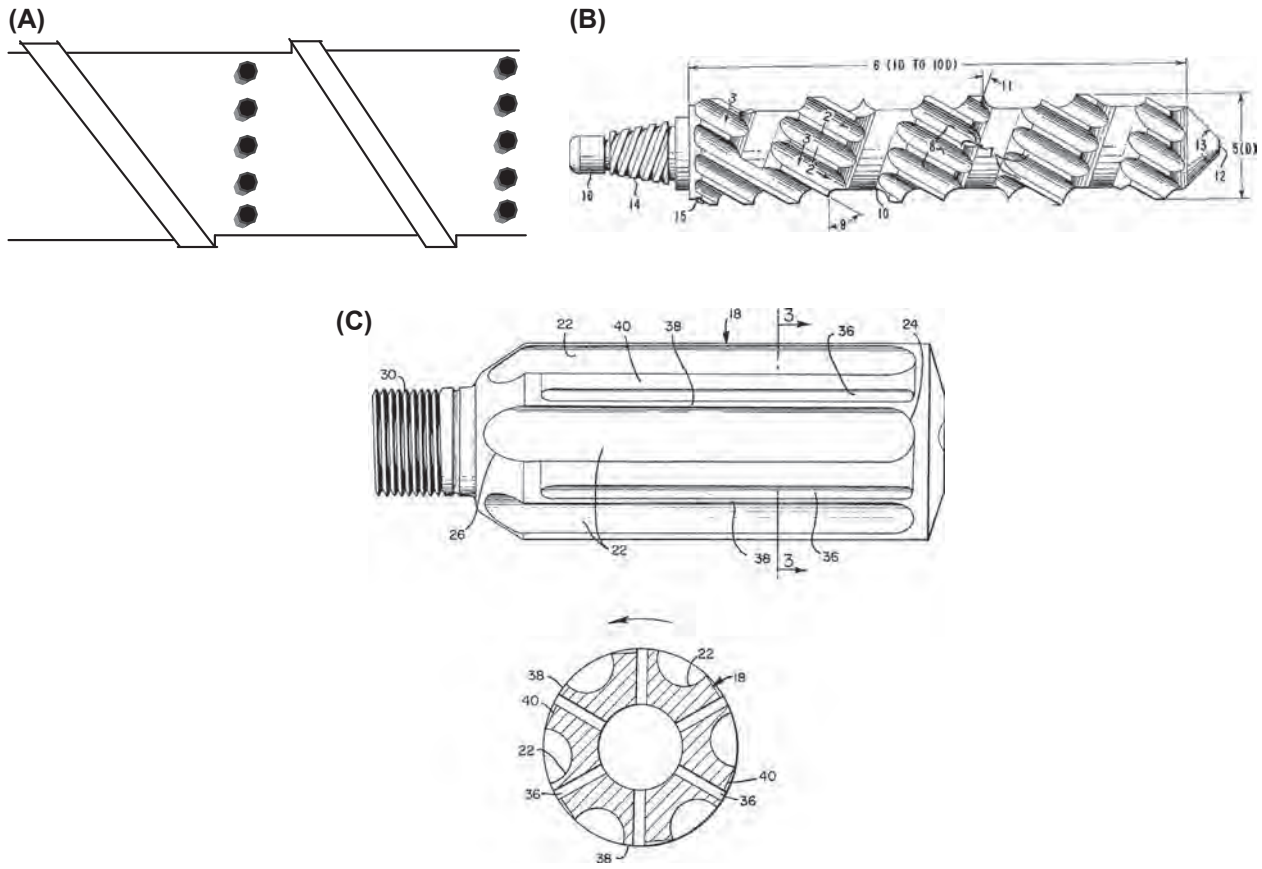


Figure 2.5 Common mixing elements used in single screw extrusion: (A) pin mixers, (B) Saxton mixer [10], (C) Maddock mixer [11].

eliminate the dead zones while dividing up the flow. In the Maddock mixer, the polymer flows down a fluted section and over a small clearance between the screw and barrel; this introduces high shear stresses to break up agglomerates. Alternatively, a static mixer may be incorporated in the transfer pipe between the extruder and die.

As the polymer flows it generates heat from viscous energy dissipation, which often dominates external heat transfer. The barrels of the extruder are typically jacketed with heaters and coolers (either water or air cooling). As the size of the extruder is increased, however, the effectiveness of the barrel heating/cooling is diminished by the reduction of surface area to polymer volume. The energy dissipation or frictional heat is a function of the shear rate times the shear stress, or the viscosity times the shear rate squared. The typical shear rate in the extruder ranges from about 10 to 100 s^{-1}. The shear rate increases with decreasing channel depth and increasing screw speed; processes requiring higher temperatures such as extrusion coating may operate with higher screw speed or shallower channels than processes trying to minimize temperatures. The viscosity of the polymer is often tailored for the process. Blown film polymers, for example, typically have a higher viscosity at a given temperature and shear rate than those used in extrusion coating to achieve sufficient melt strength and bubble stability. In extrusion coating, low viscosity and high temperatures help the polymer wet the substrate, a first step to achieve adhesion. Blown film processes are often run with barrel cooling while extrusion coating processes employ further tools such as pressure valves to try to build up temperature.

For Further Reading

1. Tadmor Z, Klein I. Engineering principles of plasticating extrusion. New York: Van Nostrand Reinhold Co.; 1970.
2. Rauwendaal C. Polymer Extrusion, 4th ed. Munich: Carl Hanser Verlag; 2001.

3. Vlachopoulos J, Wagner JR, editors. The SPE guide on extrusion technology and troubleshooting. Brookfield (CT): The Society of Plastics Engineers; 2001.
4. Campbell GA, Spalding MA. Troubleshooting & analysis of single-screw extrusion, New York: Hanser Gardner Publications; 2010.
5. Chung C. Extrusion of Polymers: Theory and Practice, 2nd ed. Cincinnati (OH): Hanser Gardner Publications; 2000.
6. Tadmor Z, Gogos C. Principles of polymer processing, 2nd ed. Hoboken (NJ): John Wiley & Sons; 2006.

2.2 Film Converting

2.2.1 Blown Film

The blown film process converts polymer resin into a plastic film. Polymer pellets are fed into an extruder, melted, and pumped out a tubular die (Fig. 2.6). In a traditional air quenched process, the tube travels up a tower where it is pinched off at the top with a nip roll. Air is forced into the middle of the tube, expanding the tube in the hoop direction as it is accelerated in the machine direction by the nip roll. The expansion occurs while the tube is being cooled by air blown across the outside of the bubble. The result is a film with orientation in both the machine and transverse directions.

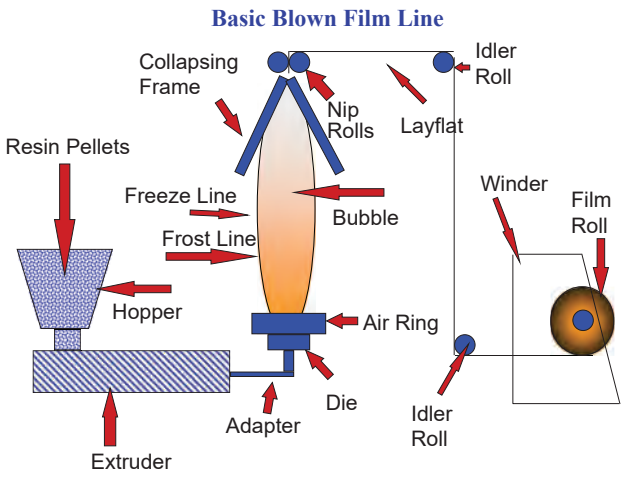


Figure 2.6 Blown film process.
Reproduced with permission from E. I. du Pont de Nemours and Company.

In a water quench system, the tube is stretched in the melt around a mandrel or guide into a water bath. The rapidly quenched film typically has less orientation and crystallinity than an air quenched film, providing better thermoforming, higher transparency, and lower stiffness.

2.2.1.1 Key Components

2.2.1.1.1 Extruder

The extruder melts and pumps the polymer through the blown film die. See Section 2.1 for details.

2.2.1.1.2 Tubular Die

The die distributes the melt into a tube with uniform flow in the axial direction at the die exit. This minimizes gauge variation in the final film. The key performance requirement is streamline flow without die lines. Doing this without excessive residence time and pressure is also important. The key factors affecting performance are uniform temperature entering the die, die design as it affects the flow geometry, die gap, and materials of construction. Spiral mandrel designs (Fig. 2.7) are typically used to distribute the flow evenly and to avoid die lines. Stacked or pancake die designs have found use in coextrusion to help thermally isolate polymers of

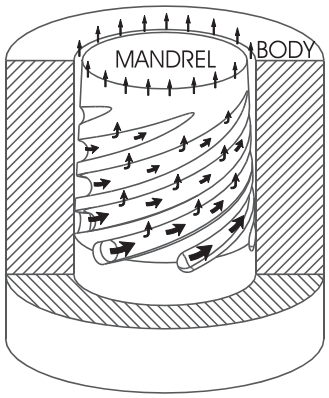


Figure 2.7 Schematic of cylindrical spiral mandrel die design.
Reproduced from Perdikoulias J. Multilayer blown (tubular) film dies. In: Wagner J, editor. Multilayer flexible packaging, technology and applications for the food, personal care and over-the-counter pharmaceutical industries. Oxford: Elsevier; 2010. pp. 97–102 with permission from Elsevier, Figure 7-3.

different viscosities or thermal stability and minimize residence time in coextrusion dies.

At the die exit, air is blown inside the bubble to inflate it (the air is entrapped by the nip at the top of the tower). The air pressure inside the bubble determines the amount of expansion, the final bubble diameter, and its layflat (one half the final circumference of the bubble).

2.2.1.1.3 Air Ring and Inner Bubble Cooling

The air ring blows air on the outside of the bubble, cooling it. Key parameters include the air flow rate, distribution, and temperature. The design of the flow manifold is also critical, as a good design can help stabilize the bubble. Poor bubble stability can result in nonuniform film thickness, line breaks, and limited output [12,13]. Most air rings today have a dual lip to better control the air flow and create a venture tube that helps seat the bubble and hold it in place. A schematic of the dual lip air ring is shown in Fig. 2.8.

Cooling by blowing air on the outside of the bubble becomes less effective as the line size gets bigger. On larger lines, chilled air is circulated inside the bubble and continuously replenished to help cool it more rapidly. This feature is known as inner bubble cooling and helps increase output. The quench rate influences a number of properties, including crystallinity, tear strength, transparency, and haze.

2.2.1.1.4 Collapsing Frame and Haul-Off

The collapsing frame, nip, and haul-off roll flatten the tube after it has been quenched. The speed of the haul-off roll determines the amount of draw in the machine direction.

The collapsing frame helps with the transition of the film from tube to layflat. The formation of wrinkles can be a problem during this transition and the design of the collapsing frame plays a role in preventing wrinkles [14].

The collapsing frame, nip, and haul-off roll are typically rotated to help randomize bands of nonuniform gauge on the wound roll. Early versions of this technology rotated the die rather than the haul-off.

2.2.1.1.5 Gauge Control

A sensor is typically used to measure the gauge across the layflat during haul-off. On lines with automatic die adjustment capability, a signal is sent back to a controller that adjusts the thickness uniformity around the circumference of the die. One approach to automatic adjustments is to selectively heat or remove heat from bolts along the circumference to flex a membrane in the die lip [15]. The thermal expansion of the hot bolt flexes the membrane, further restricting the flow near the bolt and lowering the thickness. Another approach is to

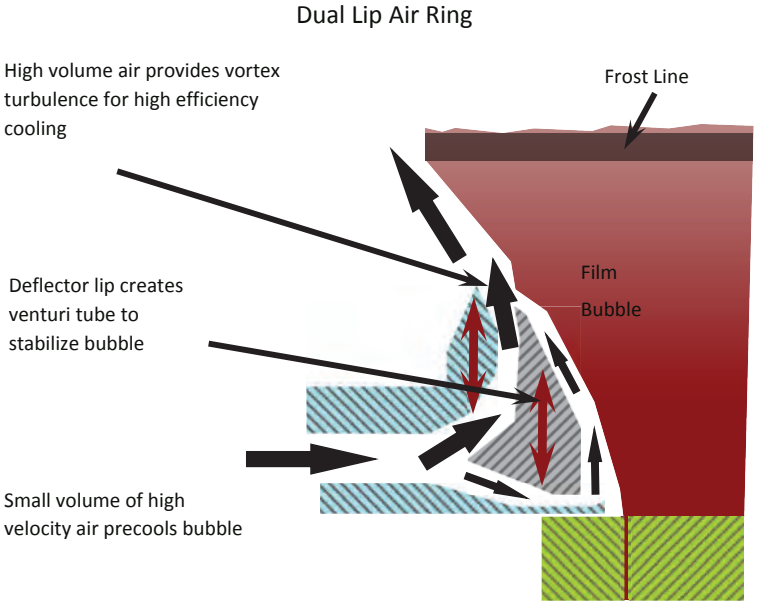


Figure 2.8 Schematic of a dual lip air ring.
Reproduced with permission from E. I. du Pont de Nemours and Company.

locally adjust the quench air speed along the air ring [16].

There are many types of online gauge monitoring technologies. Historically, gamma backscatter or capacitance techniques have been used to measure total thickness of the bubble online [17] and transmission techniques such as beta, gamma, or X-ray on flat film. Beta gauges emit beta particles (high speed electrons) from a radioactive source. The beta particles pass through the film and are detected by a sensor on the other side. The amount of particles that transmit through the film is proportional to the mass of the film. Gamma gauges are similar except that the radioactive source emits gamma rays or high energy photons. Gamma ray transmission is highly dependent on the atomic number of the material it passes through, so in some cases discrimination can be made between layers in a multilayer film. X-rays and gamma rays are essentially the same, differing by their origin: gamma rays arise from a nuclear source whereas X-rays come from high speed electrons.

Newer advances in technology, such as near-infrared spectroscopy (IR) or full spectrum IR and optical probes [18], are starting to make possible the online measurement of interior layers, such as barrier layers. Coupled with feedback control, these developments may significantly reduce layer to layer variation in coextrusion.

2.2.1.1.6 Windup

The windup is also a critical piece of equipment. There are a number of different types of winders in the market to accommodate a wide variety of possible substrates from elastic/extensible films to heavy paperboard. The types fit into three general categories (Fig. 2.9). In a center winder, torque is directly applied through the windup roll. This is the simplest method and the best for many materials, such as elastic materials and flexible packaging laminates with high caliber variation. Generally, the tension is tapered to allow for higher tension at the start of the roll to prevent dishing and telescoping, two problems that occur when the edges of the film on each wrap do not line up properly. In some systems the tapering is simply accomplished by maintaining a constant tension and relying on the natural reduction in tension as the diameter increases (with each successive wrap). Some versions of center winders have a nondriven nip roll to remove entrapped air during winding to increase roll hardness.

Surface center winders have a driven center windup roll and a driven nip. These are the most versatile winders since they utilize all the mechanisms of winding: tension, nip, and torque. Each is independently controlled. The nip roll isolates the winding tension from the process tension, allowing the surface winder to apply more torque at the beginning of the roll to ensure a tight start.

Pure surface winders, known as two drum winders, have been around for a long time. The speed of winding is controlled by two externally driven nip rolls. A third nip roll provides additional nip pressure during start-up. These winders continue to find use in the industry due to their ease of use.

For Further Reading on Winding

1. Gronewold J. Winding. In: Bezigian, editor. Extrusion Coating Manual, 4th ed. Atlanta: TAPPI Press; 1999. pp. 133−152.
2. Frye KG. Winding. Atlanta: TAPPI Press; 1991.

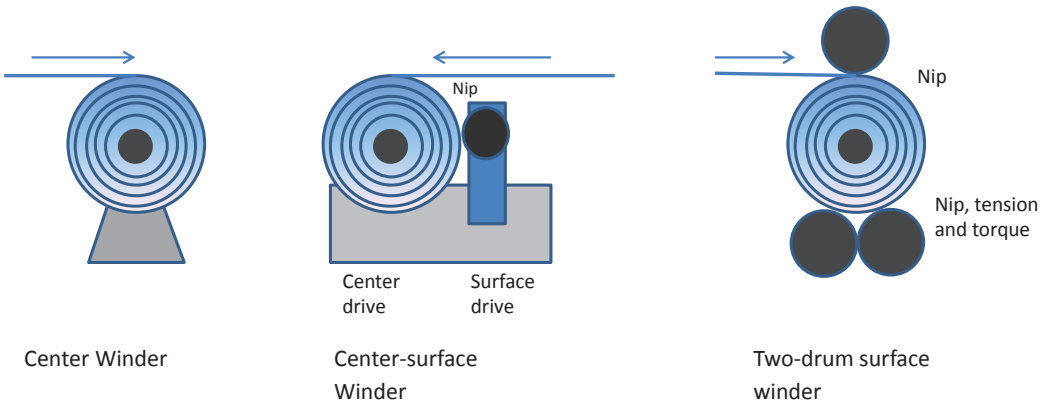


Figure 2.9 Types of winders.

3. Roisum DR. The mechanics of winding. Atlanta: TAPPI Press; 1994.
4. Roisum DR. The mechanics of rollers. Atlanta: TAPPI Press; 1996.
5. Roisum DR. The mechanics of web handling. Atlanta: TAPPI Press; 1998.
6. Smith RD. Roll and web defect terminology. 2nd ed. Atlanta: TAPPI press; 2007.

2.2.1.2 Coextrusion Blown Film

In the coextrusion process, multiple layers are combined during the film fabrication process. There are two general approaches for joining layers. One is to feed different polymer melts from multiple extruders into a combining operation prior to forming the final film shape. The hardware that performs the combining operation is known as a feedblock. Feedblocks are commonly used in flat die extrusion such as coextrusion cast film, sheet, and extrusion coating. The second approach is to form the final film shape first and then combine the melt streams. This is the approach used in coextrusion blown film.

In a conventional coextrusion blown film die, each layer has its own spiral mandrel distribution system, as described in Fig. 2.7, nestled within a larger die. This is shown schematically in Fig. 2.10. A disadvantage of this system is that the outer layers have an increasing larger flow diameter and residence time. In the late 1980's, Brampton Engineering introduced stacked die technology where a series of flat "pancakes" that distribute flow horizontally rather than vertically are stacked vertically. A flat spiral distribution is used as illustrated in Fig. 2.11. A cross section of the stacking geometry is shown in Fig. 2.12. Advantages of the stacked die configuration are reduced residence time and the ability to thermally isolate layers, which can be important for extruding thermally sensitive resins with high melt point polymers. A number of variations on these two basic geometries have been introduced into the market over the years [19].

2.2.1.3 Key Factors Affecting Properties

The properties of blown film are influenced by the stress–strain history, which is a result of the complex interplay of cooling and stretching in the machine and hoop directions. The amount of stretching in the machine direction is characterized by the take-up

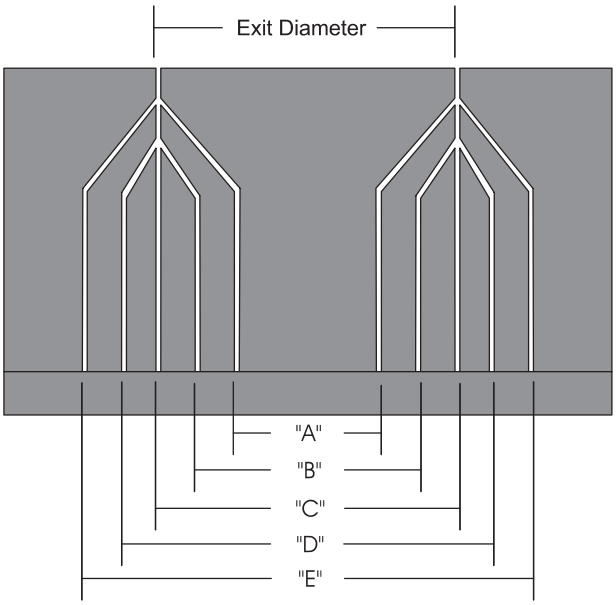


Figure 2.10 Cross-sectional schematic of a conventional cylindrical spiral mandrel coextrusion die with five nestled layers.
Reproduced from Perdikoulias J. Multilayer blown (tubular) film dies. In: Wagner J, editor. Multilayer flexible packaging, technology and applications for the food, personal care and over-the-counter pharmaceutical industries. Oxford: Elsevier; 2010. pp. 97–102, Figure 7-2.

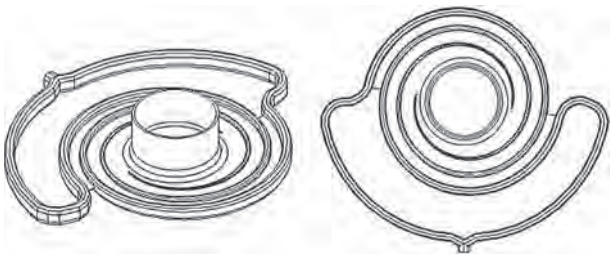


Figure 2.11 A flat spiral distribution system with two spirals.
Reproduced from Perdikoulias J. Multilayer blown (tubular) film dies. In: Wagner J, editor. Multilayer flexible packaging, technology and applications for the food, personal care and over-the-counter pharmaceutical industries. Oxford: Elsevier; 2010. pp. 97–102, Figure 7-6.

ratio (TUR), sometimes called the draw-down ratio (DDR), which is the ratio of the take-up speed to the velocity of the melt as it exits the die:

$$\text{TUR} = \text{DDR} = v_f/v_0 \tag{2.3}$$

where TUR = take-up ratio, DDR = draw-down ratio, v_f = final film velocity or take-up speed,

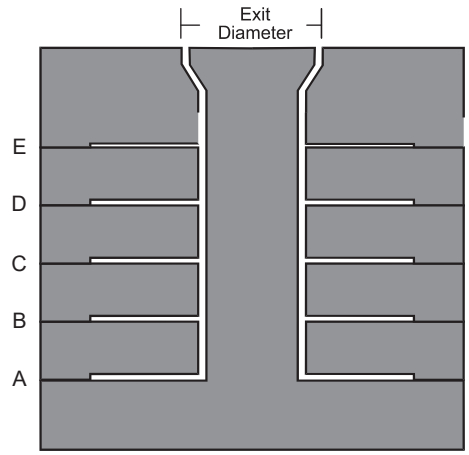


Figure 2.12 Cross-sectional schematic of a stacked type of coextrusion die.
Reproduced from Perdikoulias J. Multilayer blown (tubular) film dies. In: Wagner J, editor. Multilayer flexible packaging, technology and applications for the food, personal care and over-the-counter pharmaceutical industries. Oxford: Elsevier; 2010. pp. 97–102, Figure 7-4.

v_0 = initial velocity or velocity of melt as it exits the die.

Here the subscript "0" is used for the initial state and "f" for the final state. Stretching in the cross or hoop direction is characterized by the blow-up ratio (BUR), which is defined as the final film diameter divided by the die diameter:

$$\text{BUR} = D_f/D_0 \tag{2.4}$$

where BUR = blow-up ratio, D_f = final tube diameter, D_0 = die diameter.

Since the velocity of the polymer melt at the die exit is not typically measured, Eq. (2.3) is not in a readily useable form. A mass balance can be used to derive an alternative form of Eq. (2.3). The mass flow rate at the die exit is equal to the product of the velocity, area of the die opening, and the density of the polymer melt:

$$\dot{M} = v_0 \pi D_0 X_0 \rho_0 \tag{2.5}$$

where $\dot{M}$ = mass flow rate, v_0 = velocity of polymer at die exit, D_0 = die diameter, X_0 = die gap, ρ_0 = density of polymer melt (at die exit).

A mass balance at the takeoff roll yields the following:

$$\dot{M} = v_f \pi D_f X_f \rho_f \tag{2.6}$$

where X_f = final film thickness, ρ_f = density of polymer at the take-up roll (solid).

Here the die gap is assumed to be much less than the die diameter ($X_0 << D_0$) so that the area simplifies to the circumference times the die gap. Similarly, it is assumed that $X_f << D_f$.

Equating Eqs. (2.5) and (2.6), the following relationship for TUR (DDR) is obtained:

$$\text{TUR} = \frac{1}{\text{BUR}} \frac{X_0}{X_f} \frac{\rho_0}{\rho_f}. \tag{2.7}$$

For many polyolefins, the ratio ρ_0/ρ_f ranges from about 0.7 to 0.9. Many references ignore the density difference, but the error can be significant depending on the polymer.

The amount of stretching only tells part of the story. For an elastic solid, the stress is proportional to the elongation through the modulus:

$$\sigma_{\text{elastic solid}} = G\varepsilon \tag{2.8}$$

where $\sigma_{\text{elastic solid}}$ = stress, G = elastic modulus, ε = strain or elongation.

The modulus is a function of temperature; as the bubble cools, the modulus increases. In monolayer blown film, much of the stretching occurs near the freezing point of the polymer where the modulus and stress are highest.

Polymers are known to be viscoelastic (see Chapter 5 for further discussion on the rheology of polymers), meaning they behave like elastic solids as well as viscous fluids. For a viscous fluid, the stress is proportional to the rate of strain (also known as the rate of elongation or rate of stretching) through the viscosity:

$$\sigma_{\text{viscous fluid}} = \mu\dot{\varepsilon} \tag{2.9}$$

where $\sigma_{\text{viscous fluid}}$ = stress, μ = viscosity, $\dot{\varepsilon}$ = rate of strain or elongation.

The rate of stretching depends on the change in velocity of the polymer as it travels up the bubble and the change in bubble diameter. This in turn is a function of the cooling rate; as the polymer cools it gains melt strength that is needed to sustain the stretching of the bubble. A characteristic process time can be defined as the time it takes the polymer melt to travel from the die exit to the frost line. The frost line is an indicator of when the polymer is starting to freeze. In some films, the film becomes

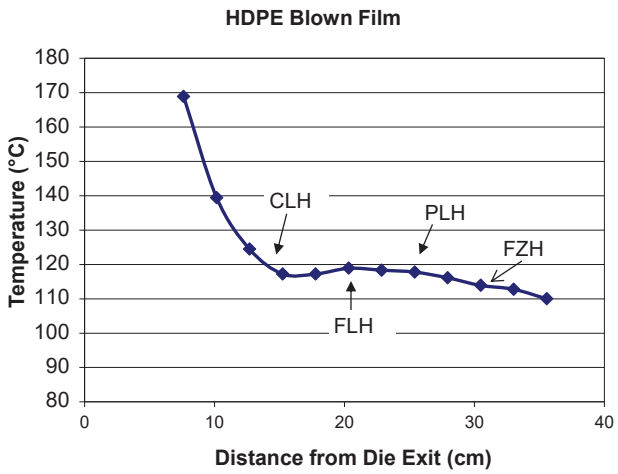


Figure 2.13 Definition of transitions in blown film. *Reproduced from Morris BA. Effect of process and material parameters on interlayer peel strength in coextrusion coating, film casting and film blowing, J Plastic Film Sheeting 2010;26:pp. 343–76 with permission from Sage.*

hazy at this point as it begins to crystallize. In other films, the frost line can be determined by where the bubble stops changing shape. The cooling kinetics can be monitored by an IR thermometer. Butler [20] has defined several transitions as shown in Fig. 2.13: the crystalline-line height where crystallization first begins, the frost line height (FLH) where the change in the bubble shape ends, the plateau line height where the temperature plateau ends, and the freeze-line height where primary crystallization ends.

The velocity (v) of an element of polymer within the extruded tube or web is equal to its change in position (z) with time (t):

$$v = \frac{dz}{dt}. \tag{2.10}$$

The instantaneous rate of strain is equal to the change in velocity with respect to distance; the strain is found by integrating the instantaneous rate of strain over time:

$$\dot{\varepsilon}(t) = \frac{dv}{dz} = \frac{1}{v}\frac{dv}{dt}. \tag{2.11}$$

$$\varepsilon(t) = \int_0^t \dot{\varepsilon}dt = \int_0^t \frac{1}{v}\frac{dv}{dt}dt = \ln\left(\frac{v}{v_0}\right). \tag{2.12}$$

Elongation occurs up to the FLH where the bubble diameter and velocity cease to change. The process time, t_f, is defined as the time it takes the polymer to travel from the die exit to the frost line. It represents the time over which the bubble is stretched. At t_f the velocity reaches its final value or v_f. Using Eq. (2.12), the total amount of strain imparted in the bubble is found by integrating the rate of strain from zero to t_f:

$$\varepsilon_{tot} = \ln\left(\frac{v_f}{v_0}\right) = \ln(\text{DDR}). \tag{2.13}$$

A typical velocity profile in blown film is shown in Fig. 2.14. The change in velocity from the die exit to the frost line is nearly linear. Assuming a linear velocity profile and integrating Eq. (2.10) yields the following equation for the process time:

$$t_f = \frac{h_f}{v_f - v_0}\ln\left(\frac{v_f}{v_0}\right) \tag{2.14}$$

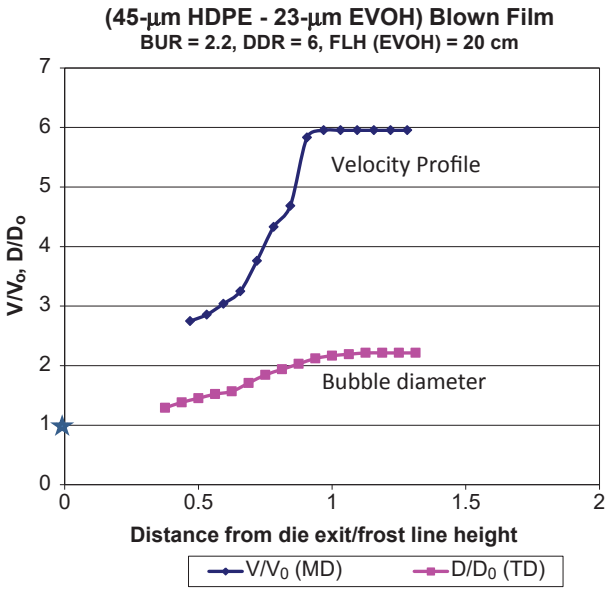


Figure 2.14 Machine direction velocity (V) and bubble diameter (D) profiles in blown film. Taken from video camera marker experiments on a two-layer film. X-axis is the vertical distance from the die exit divided by the frost line height. Data collection from $X = 0$ to 0.5 is blocked by the air ring. Value at $X = 0$ is 1 by definition.
Reproduced from Morris BA. Effect of process and material parameters on interlayer peel strength in coextrusion coating, film casting and film blowing, J Plastic Film Sheeting 2010;26:pp. 343–76 with permission from Sage.

where h_f = frost line height.

Using a mass balance, Eq. (2.14) can be recast into more easily measured parameters:

$$t_f = \left[\frac{h_f}{v_f\left(1 - \frac{[BUR]X_f\rho_f}{X_0\rho_0}\right)}\right] ln\left(\frac{X_0\rho_0}{BURX_f\rho_f}\right). \quad (2.15)$$

Butler [22], Campbell [23], and others have proposed models for the effect of fabrication parameters on property development of monolayer blown film. These are explored in more detail in Chapters 14 and 15 along with their extension to coextrusion.

2.2.1.4 Scale-Up

Kanai [24] uses a thin membrane approximation of Pearson and Petrie [25–27] to derive scale-up factors for blown film. Such factors are important for predicting process conditions that will duplicate film properties made on different size film lines. Shirodkar [28] proposes using process time (Eq. (2.14)) as a scale-up factor and shows that dart impact and tear resistance correlates well with process time. Careful examination of Kanai's scaling parameters shows that when BUR, TUR, and h_f/D_f are held constant, so too is process time.

Butler [29] has also proposed scale-up factors based on membrane models and a heat transfer analysis. The output in Kanai's analysis increases with the die gap times the square of the die diameter [30], which means that the die gap needs to be increased to maintain constant stress on the polymer flow in the die. As a consequence, the final film thickness must be changed to maintain constant properties. This is not practical in most situations. Butler proposes scaling the output linearly with die diameter. He explicitly uses the process time in his analysis, proposing a film fabrication number (known as the Deborah number in the Rheology literature) that relates the timescale of the process (Eq. (2.14)) to the relaxation time of the polymer. A comparison of the two approaches can be found in Table 2.3.

Further Reading on Blown Film

- Butler TI, editor. Film extrusion manual. Atlanta: TAPPI Press; 2005.
- Kanai T. Campbell GA. Film processing. Hanser Publications; 2011.
- Giles Jr HF, Mount III EM, Wagner Jr JR, editors. Extrusion: the definitive process guide and handbook. William Andrews; 2007. pp. 453–63.
- Perdikoulias J. Multilayer blown (tubular) film dies. In: Wagner J, editor. Multilayer flexible packaging, technology and applications for the food, personal care and over-the-counter

Table 2.3 Blown Film Scale-Up Analysis

Parameter	Kanai	Butler
BUR	Constant	Constant
DDR or TUR	Constant	Constant
T_{melt}	Constant	Constant
h_f/D_f	Constant	h_f adjusted to keep t_f constant
λ/t_f		Constant
v_0	D_0	Constant
v_f	D_0	Constant
X_0	D_0	Constant
X_f	X_0	Constant
h_f	D_0	Adjusted to keep t_f constant
Q	$X_0D_0^2$	D_0

Here h_f = *frost line height,* λ = *relaxation time of polymer,* Q = *volumetric throughput.*

pharmaceutical industries. Oxford: Elsevier; 2010. pp.97–102.

- Butler TI. Blown film extrusion. In: Vlachopoulos J, Wagner JR, editors. The SPE guide on extrusion technology and troubleshooting. Brookfield (CT): The Society of Plastics Engineers; 2001.

2.2.2 Cast Film

The cast film process involves extruding the polymer through a flat die, drawing it down to the final thickness by pinning the melt extrudate onto a rotating cold roll and rapidly solidifying it (Fig. 2.15). In the cast film process, the polymer is stretched in the molten state in the machine direction and very rapidly quenched. Blown film is stretched near its freezing point in both the machine and transverse directions while being more slowly quenched. As a result, cast film properties may differ from films of a similar composition made on the blown film process.

2.2.2.1 Key Components

2.2.2.1.1 Extruder

The extruder melts and pumps the polymer through the flat die. Details on the extrusion process can be found in Section 2.1.

2.2.2.1.2 Die

The die distributes the melt into a flat sheet. Uniform flow at the die exit across the width of the die is the critical performance requirement for the die design. Key factors influencing performance are the flow channel geometry including the manifold design, residence time, and pressure distribution. T-slot dies use a wide channel perpendicular to the die entrance to distribute the flow across the width of the die. Pressure across a preland region regulates the flow (see Fig. 2.16A.). These are more commonly used in extrusion coating. The so-called "coat hanger" dies (Fig. 2.16B) use a manifold to create equal pressure drop across the width of the die. This helps create uniform flow out the die. Most modern cast film dies use some type of coat hanger geometry.

The width of the melt extrudate can be narrowed by attaching deckles which restrict the flow at the die edges. Early versions of this technology were externally applied to the die. Modern dies have internal deckles with rods and pins that can be slid to adjust the flow at the edges [31].

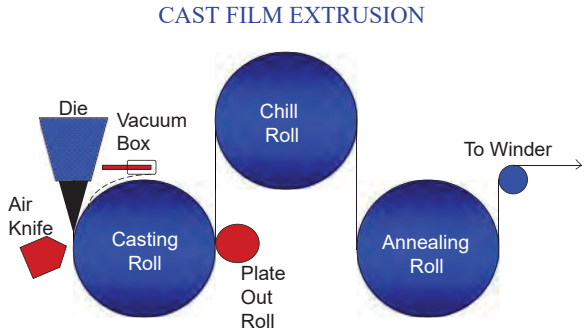


Figure 2.15 Cast film process.
Reproduced with permission from E. I. du Pont de Nemours and Company.

2.2.2.1.3 Chill Roll and Pinning Technology

After the melt curtain exits the flat die, it is drawn down to its final thickness and quenched by pinning it to a fast moving cold roll. The chill roll is usually chrome plated and internally cooled with chilled water. Two types of pinning technology are common, the vacuum box and the air knife. As their names suggest, the vacuum box draws the melt curtain onto the roll with a vacuum whereas the air knife blows air across the curtain to force it onto the roll.

Key operating parameters for drawing and quenching are the chill roll temperature and line speed (velocity of the film as it is wound up). If the

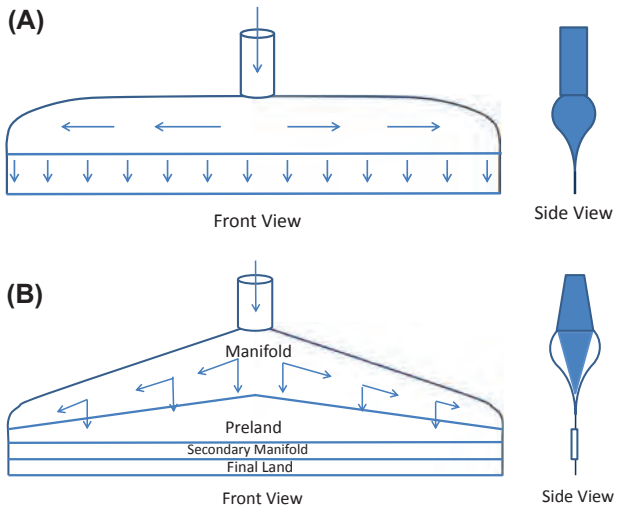


Figure 2.16 Diagram of flat die technologies: (A) T-slot die, (B) coat hanger die.

chill roll temperature is too hot, the polymer may stick to the roll. A matted surface is sometimes used to help prevent sticking. The line speed at a given extruder output determines the final thickness of the film.

2.2.2.1.4 Windup and Other Components

Similar windup technology as described in Section 2.2.2.1 applies here. Automatic gauge control can also be employed in cast film. Feedback from film gauge measurements across the web can be used to adjust the local die gap. One approach is to apply differential heat to bolts across the width of the die land [32].

2.2.2.2 Coextrusion

Two approaches are used to combine layers in flat die coextrusion; both are applied to cast film, cast sheet, or extrusion coating. In the first, each extruder feeds the polymer melt into a combining device known as a feedblock. A number of feedblock technologies are on the market. Their basic function is to combine the polymer melt streams in a way that results in a uniform layer distribution prior to feeding into the die. To help achieve uniform layer distribution, several strategies can be employed, including vanes and laminar plates. Most feedblocks allow flexibility in layer ratio and the number of layers through the use of specific plugs, pins, and other devices.

The second approach is to spread the polymer melt to its final width prior to combining the flow. Typically this is done in a multi-manifold die where the melt streams are combined just prior to the die exit. A variation on this is to employ more than one die and combine the melt streams just after the die exit.

Feedblock technology is generally less expensive and more versatile than multi-manifold die technology. Multi-manifold dies are typically designed for a specific structure. Adding more layers, for example, becomes difficult. Multi-manifold dies are less sensitive to flow instabilities and allow more diverse materials to be combined. Flow instability is covered in more detail in Chapter 13. Also multi-manifold dies allow polymers with different melt temperatures to be combined with minimal heat transfer between them. This may be important when extruding a thermally sensitive polymer with a polymer with a high melting point. Multi-manifold dies may be combined with feedblocks to further increase versatility.

2.2.2.3 Key Factors Affecting Properties

The properties of cast film are influenced by the amount of orientation and quench rate. The DDR characterizes the orientation in the machine direction:

$$\text{DDR} = \frac{v_f}{v_0} \tag{2.16}$$

where v_f = line speed (final speed of the film coming off the chill roll) and v_0 = velocity of polymer at the die exit.

A simple mass balance equating the mass flow rate at the die exit with the film at the chill roll yields:

$$w_0 X_0 v_0 \rho_0 = w_f X_f v_f \rho_f \tag{2.17}$$

where w_0 = the width of the die opening (deckled), w_f = width of the melt curtain upon contact with the chill roll, X_0 = die gap, X_f = final film thickness, ρ_0 = melt density, ρ_f = solid density.

Substituting Eq. (2.17) into Eq. (2.16):

$$\text{DDR} = \frac{w_0 X_0 \rho_0}{w_f X_f \rho_f}. \tag{2.18}$$

If neck-in of the melt curtain is small, then $w_0 \cong w_f$ and Eq. (2.18) simplifies to

$$\text{DDR} = \frac{X_0 \rho_0}{X_f \rho_f}. \tag{2.19}$$

For a given polymer, the density ratio is constant, so that the DDR is proportional to the die gap and inversely proportional to the final film thickness. For a constant die gap, the thinner the film, the more draw down, and the greater the orientation.

The quench rate in cast film is very rapid since the melt curtain is pinned directly against the chill roll. Rapid quench rates generally result in lower levels of crystallinity (for crystalline polymers). Some of the consequences of lower crystallinity are described in Section 2.2.2.4.

Another important parameter is the time in the air gap (TIAG). As is shown in later chapters, TIAG is important for adhesion and orientation since it relates

to the rate of elongation. For cast film and extrusion coating, the polymer velocity in the air gap fits well to a Newtonian fluid [33] (see Fig. 2.17):

$$\frac{v}{v_0} = \mathrm{DDR}^{\left(\frac{z}{L}\right)} \tag{2.20}$$

where $z =$ vertical distance from the die exit, $L =$ length of air gap (distance between the die exit and the chill roll).

It then follows from Eq. (2.10) to Eq. (2.12) that

$$\varepsilon = \ln\left(\frac{v}{v_0}\right) = \frac{z}{L}\ln(\mathrm{DDR}). \tag{2.21}$$

$$\dot{\varepsilon} = \frac{v_\mathrm{f}}{L}\mathrm{DDR}^{\left(\frac{z}{L}-1\right)}\ln(\mathrm{DDR}). \tag{2.22}$$

$$t_\mathrm{f} = \frac{L}{v_\mathrm{f}}\left[\frac{\mathrm{DDR}-1}{\ln(\mathrm{DDR})}\right] \tag{2.23}$$

where $\varepsilon =$ strain, $\dot{\varepsilon} =$ rate of strain, $t_\mathrm{f} =$ process time.

Many practitioners simplify Eq. (2.23) by ignoring the term in brackets. This value is typically known as the TIAG [35]:

$$\mathrm{TIAG} = \frac{L}{v_\mathrm{f}}. \tag{2.24}$$

In English units, this can be written:

$$\mathrm{TIAG(ms)} = \frac{L[\mathrm{inches}]}{v_\mathrm{f}\left[\frac{\mathrm{ft}}{\mathrm{min}}\right]} \times 5000. \tag{2.25}$$

In metric units:

$$\mathrm{TIAG(ms)} = \frac{L[\mathrm{mm}]}{v_\mathrm{f}\left[\frac{\mathrm{m}}{\mathrm{min}}\right]} \times 60. \tag{2.26}$$

Eq. (2.24) assumes that the polymer instantaneously accelerates to the final line speed as it exits the die. While not physically correct, TIAG does prove useful for explaining adhesion and other data, especially in extrusion coating. Eq. (2.23) should be used if changes are being made in DDR.

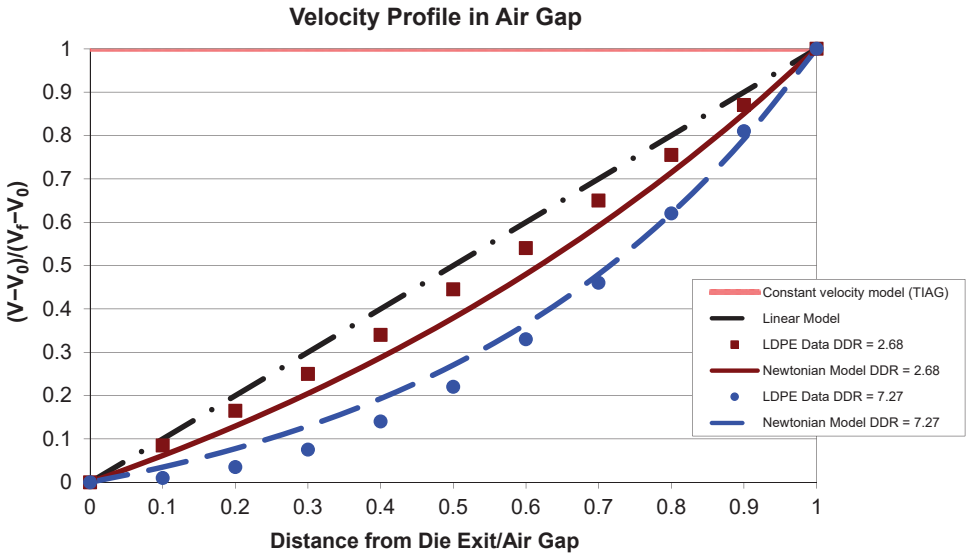


Figure 2.17 Velocity profile of polymer melt in air gap of cast film/extrusion coating. Constant model assumes $v = v_\mathrm{f}$ ($t_\mathrm{f} =$ TIAG). Linear model assumes $v = v_0 + (vL - v_0)z/L$. Newtonian model is shown in Eq. (2.20).
Reproduced from Morris BA. Understanding why adhesion in extrusion coating decreases with diminishing coating thickness. J Plastic Film Sheeting 2008;24:pp 53–88 with permission from Sage. Data for LDPE melt taken from Canning K, Bian B, Co A. Film casting of a low density polyethylene melt. Proceedings of ANTEC 1999, Annual Technical Conference – Society of Plastic Engineers. vol. 57. 1999. pp. 386–90.

Process times for cast film are typically fairly short since the die exit is positioned close to the chill roll (L is small).

2.2.2.4 Comparison of Blown and Cast Film Processes

In the blown film process, the melt is simultaneously cooled and stretched in both the machine and transverse directions over a relatively long process time (on the order of 1 s or more). Most of the stretching takes place near the freezing point. In the cast film process, the polymer is stretched primarily in the machine direction before the polymer is quenched but over a much shorter process time (on the order of 0.1 s or less). The result is that blown film typically has more crystallinity and is more balanced in orientation in the machine and transverse directions. Greater crystallinity produces a more dense film, higher haze, less transparency, and higher barrier properties. Cast film is typically softer and more transparent. It also may thermoform more easily.

In addition to these property differences, there are a number of operational differences as summarized in Table 2.4. [36–38].

- Blown film typically has greater flexibility in width (by changing BUR or using die lip inserts), which produces less trim waste and is easier to transition. As a result, blown film is favored for short runs.
- Gauge control is typically better for cast film. Variation of +/−2% or less is common for cast film versus +/−5−10% for blown film.
- Cast film lines typically run at a higher output than blown film. Blown: 5−24+ lb/circumferential inch (0.9−4.3+ kg/cm) of die; cast: 15−30+ lb/in (2.7−5.4+) of die width.
- Blown film lines typically require less capital investment than cast film lines.
- Blown film lines typically use resin with higher viscosity (lower melt index) and higher melt strength than cast film lines. Processing temperatures are also typically lower on blown film lines to help achieve good melt strength, which improves bubble stability.

Further Reading for Cast Film

- Butler TI, editor. Film extrusion manual. Atlanta: TAPPI Press; 2005.

Table 2.4 Comparison of Blown and Cast Film

Attribute	Blown Film	Cast Film
Film Properties		
Crystallinity	Higher	Lower
Haze	Higher	Lower
Gloss	Lower	Higher
Barrier	Higher	Lower
Stiffness	Higher	Lower
Thermoformability	Lower	Better
Orientation	MD and TD	MD
Operation		
Flexibility in width	More	Less
Gauge variability	More	Less
Trim waste	Less	More
Output per film width	Lower	Higher
Flexibility for short runs	More	Less
Initial capital investment	Lower	Higher

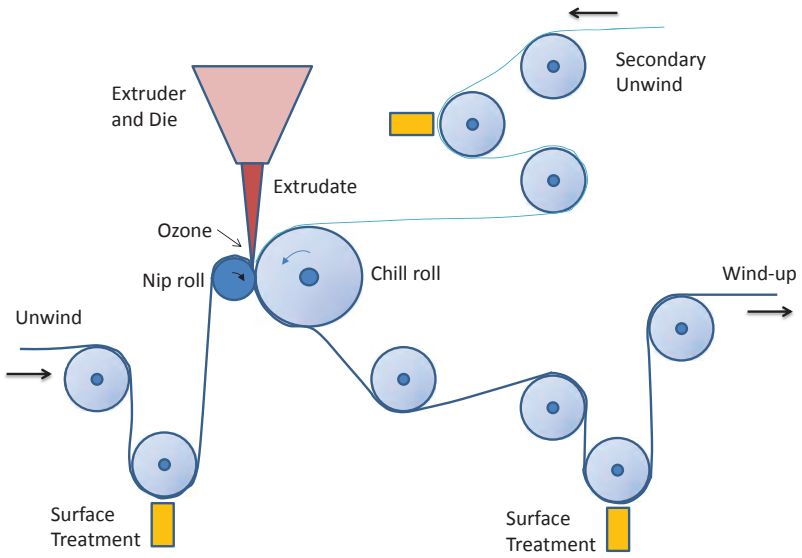


Figure 2.18 Extrusion Coating and Lamination Process.

- Ivey J. Cast film and sheet extrusion. In: Vlachopoulos J, Wagner JR, editors, The SPE guide on extrusion technology and troubleshooting. Brookfield (CT); The Society of Plastics Engineers; 2001. pp. 12-1—12-12.

2.3 Coating and Lamination

2.3.1 Extrusion Coating and Lamination

In the extrusion coating process (Fig. 2.18), molten polymer is laid down onto a solid substrate and is simultaneous cooled against a cold roll. The substrate, such as paper, foil, film, or fabric, is unwound in a continuous process and sometimes primed or treated to aid in the adhesion of the coating to the substrate. Once coated and cooled, the coating and substrate is rewound.

The extrusion lamination process uses the same equipment as in extrusion coating. Instead of coating a single substrate, two substrates are unwound and fed into the nip region. The molten polymer is laid in between to bond the substrates together.

The key components of the extrusion coating/lamination process are similar to those used in cast film.

2.3.1.1 Key Components

2.3.1.1.1 Extruder

The extruder melts and pumps the polymer through the flat die. Details on the extrusion process can be found in Section 2.1. Extrusion coating generally involves extruding the polymer at high temperatures (eg, 320°C for LDPE). To achieve such temperatures, high screw speed and narrow channel depths are often employed. A restrictor valve at the end of the extruder may also be used to help generate temperature and pressure.

2.3.1.1.2 Die

A flat die similar to that used in cast film is utilized (see Section 2.2.2.1 for details). As the polymer is drawn down from the die exit to the chill roll, it has a tendency to narrow in width. This is known as neck-in. As the melt curtain necks-in, the edges become thicker (known as edge bead). Modern "edge bead reduction" dies have adjustable flags or rods that fine-tune the flow path near the edge of the die exit. This thins out the flow to help compensate for beading.

2.3.1.1.3 Substrate Unwind and Preparation

The substrate is unwound from a roll with proper tension control. Depending on the structure and

application, the surface of the substrate may need to be modified prior to coating. A number of technologies may be used for in-line surface preparation, including:

- Flame treatment [39]. This is often used to burn off oils and other impurities on the surface of aluminum foil or to preheat paper or paperboard.
- Corona, ozone, or plasma treatment [39–42]. Ionization of various gases may be employed to change the surface chemistry of the substrate and remove impurities to promote adhesion to the coating polymer. Treatment may also be used to modify the polymer melt curtain. For example, ozone is used to promote oxidation of LDPE to improve its adhesion to polar substrates such as aluminum foil.
- Chemical priming [43]. Chemicals may be applied to the substrate to promote adhesion to the coating polymer. One commonly used primer is polyethylene imide. Others include polyurethanes and aqueous dispersions of ethylene acrylic acid copolymers. Priming is usually accompanied by in-line drying depending on the chemistry employed.
- Combinations of these technologies. For example, corona treatment may be used prior to the application of the chemical primer to ensure the primer wets the surface. Generally, the surface tension of the substrate must be 10 mN/m higher than the primer to ensure good wetting and coating [44]. Corona or plasma treatment is often used to raise the surface tension of the substrate.

2.3.1.1.4 Chill and Nip Roll

The molten polymer impinges onto the substrate as it simultaneously comes into contact with the chill roll (or the second substrate that is in contact with the chill roll in extrusion lamination). A rubber nip roll applies pressure to help ensure contact between the polymer and substrate. Bonding to the substrate is completed by solidifying the polymer through the transfer of heat to the chill roll.

The chill roll is cooled by chilled water or other cooling medium. The roll is typically chrome plated to help prevent the polymer from sticking to it. It may also be matted to aid in the release of the polymer. The polymer may contain a release agent to help prevent chill roll sticking as well.

Time and pressure in the nip are important for adhesion, particularly to porous substrates such as paper. The hardness of the nip roll impacts the length of the nip region and the pressure that is imparted. Time in the nip decreases with increasing line speed and roll hardness.

2.3.1.1.5 Windup

Like blown and cast film, windup is a key processing step for extrusion coating and lamination (see Section 2.2.1.1 for a discussion of winder technology).

2.3.1.2 Coextrusion

The coextrusion process for extrusion coating and lamination is the same as for coextrusion cast film (Section 2.2.2.2). Both feedblock and multi-manifold die technology are commercially employed in coextrusion coating/lamination. One of the advantages of coextrusion is the ability to tailor the adhesive used to bond to the substrate(s).

2.3.1.3 Key Parameters Affecting Properties

Unlike cast or blown film, the physical properties of multilayer films made by extrusion coating or lamination are primarily determined by the substrates rather than the extrudate or process. The coating or laminating polymer generally provides adhesion and/or sealing.

Adhesion is influenced by extrusion temperature, process time (or TIAG), DDR, chill roll temperature, and time in the nip. In general, higher processing temperature increases adhesion to the substrate through better wetting and, when present, chemical interaction. Increasing process time (Eq. (2.23)) or TIAG (Eq. (2.24)) increases the time for oxidation of LDPE. Oxidation creates small amounts of acids, aldehydes, and ketones that help improve adhesion to polar substrates such as aluminum foil. Increasing process time also reduces the rate of strain (Eq. (2.22)), which reduces stress and can increase peel strength performance [45]. These effects are explored more deeply in Chapter 15.

Increasing TIAG has its limits. TIAG can be increased by either increasing the air gap (L) or reducing line speed. Reducing line speed decreases productivity. Increasing air gap leads to more neck-in. Neck-in can limit coating width and cause a thickening of the coating near the edges (edge bead). The choice of polymer can influence neck-in: greater melt strength reduces neck-in. Also die design can help reduce edge bead: internal deckled dies have flags that can be adjusted to thin out the edges at the die exit to help compensate for edge bead.

Extrusion temperature also has its limitations. Excessive temperature can lead to thermal stability issues (such as cross-linking that leads to gel), generation of off-odor species and poor melt strength (greater neck-in). High temperature can also negatively affect heat seal and hot tack performance through cross-linking [53,54] or partial degradation of the coating [46].

High line speed and draw down can lead to web instabilities known as edge weave and draw resonance. The line speed or draw down where this occurs is influenced by the polymer flow characteristics (rheology).

Once the hot polymer contacts the substrate it has only a few milliseconds to wet the surface before it solidifies. Wetting is aided by the pressure from the nip. The balance between time in the nip and quench rate can influence adhesion. For paper substrates, the nip pressure helps drive the molten polymer into the pores to achieve physical bonding around the fibers. If the polymer freezes too soon, poor penetration into the paper may result in poor adhesion [47].

Further Reading for Extrusion Coating and Lamination

- Bezigian T, editor. Extrusion coating manual, 4th ed. Atlanta: TAPPI Press; 1999.
- Cooper J. Extrusion Coating. In: Vlachopoulos J, Wagner JR, editors. The SPE guide on extrusion technology and troubleshooting. Brookfield (CT): The Society of Plastics Engineers; 2001. pp. 13-1−13-16.
- Gregory BH. Extrusion coating: A process manual. Victoria (BC): Trafford Publishing; 2005.

2.3.2 Adhesive Lamination

Adhesive lamination (Fig. 2.19) is a method for bonding substrates together in a continuous roll to roll process. The technique involves applying a liquid adhesive to one or both substrates followed by subsequent curing by heat, UV light, moisture, or e-beam radiation. The adhesive may be solvent based, water based, or "solventless." Solventless adhesives are low viscosity liquids such as polyurethanes or isocyanates that are applied to one or both substrates and subsequently cured.

In dry lamination, the adhesive is applied to one substrate and dried prior to the second substrate being introduced. The dried adhesive is activated by a heated nip roll. In wet lamination, the adhesive is applied to one or both substrates just prior to the combining of the two substrates via a nip. This is followed by drying. At least one of the substrates must be porous to allow the water or solvent to evaporate.

Other lamination processes include hot melt coating and cold seal coatings.

2.3.2.1 Key Components

2.3.2.1.1 Unwind and Surface Preparation

The substrates are unwound and typically treated with flame, corona, ozone, or plasma to clean and prepare the surface for application of the adhesive. The substrate generally needs a surface energy that is 10 mN/m greater than the adhesive to achieve good wetting. The treatment removes surface oils and contaminates as well as increases the surface energy.

2.3.2.1.2 Adhesive Application

The adhesive is typically applied via a gravure cylinder. This involves a secondary cylinder that picks up the adhesive from a bath and transfers it to the applicator roll.

2.3.2.1.3 Curing or Drying

Drying is usually accomplished with heaters (such as IR heaters) or hot air flow. Curing depends on the chemistry of the adhesive. For example, UV adhesives are cured by UV lamps.

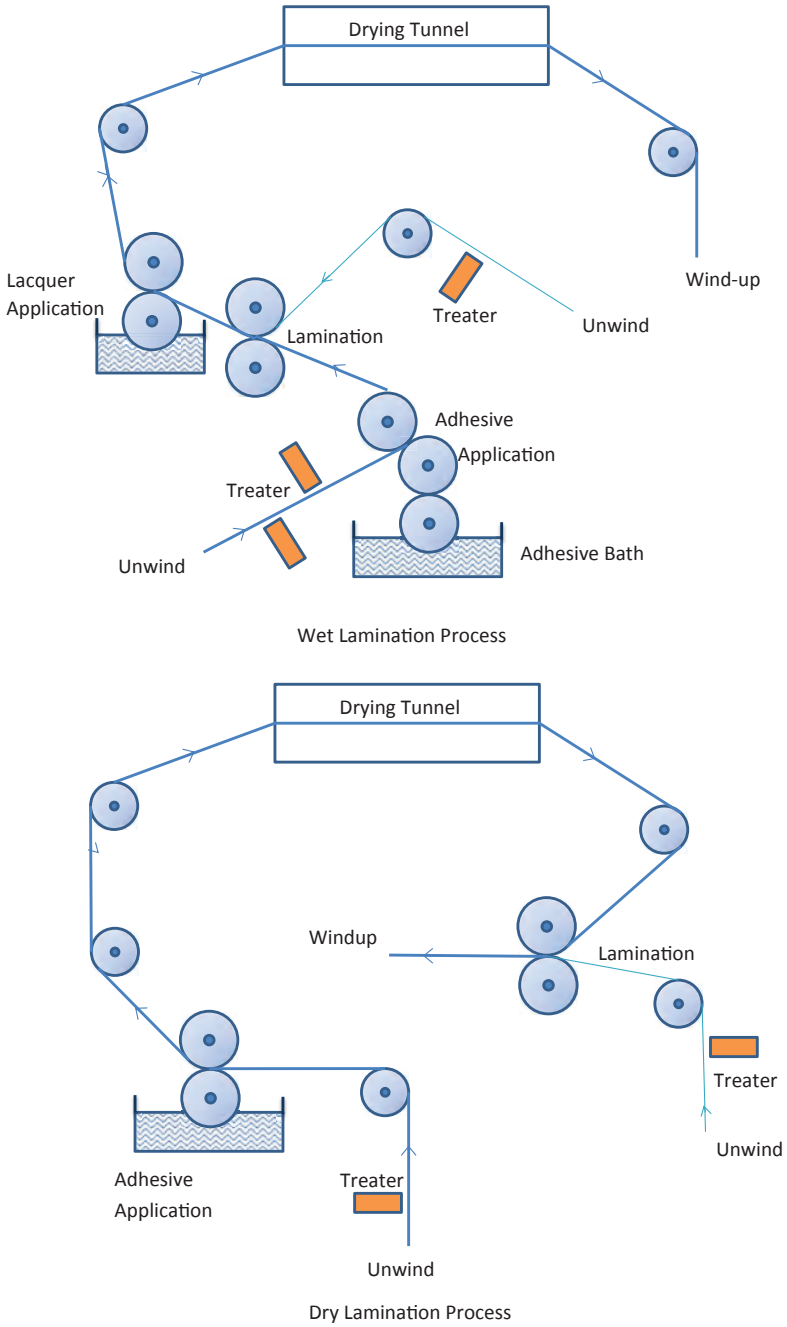


Figure 2.19 Adhesive lamination processes.

2.3.2.1.4 Windup

Proper tension control is important during lamination to prevent curl, wrinkling, dishing, telescoping, and other potential problems (see Section 2.2.1.1 for more details on winding).

2.3.2.2 Key Factors Affecting Properties

Substrate surface chemistry, adhesive chemistry, coat weight, curing conditions, and tension control are critical parameters affecting performance. The adhesive must wet the surface of the substrate as a

prerequisite to bonding. Contaminates on the substrate surface or a poor match in surface energies with the adhesive can contribute to poor wettability. Adhesion fundamentals are explored in Chapter 10.

The coat weight is a function of the adhesive viscosity, line speed, and solids content. Coat weight can affect peel strength and other properties such as barrier performance.

Drying involves evaporation of the solvent or water, or with some adhesive chemistries, curing. Drying must be accomplished within the residence time of the drying tunnel; this is a function of the line speed and drying temperature. The thermal stability of the substrate plays a role. Oriented films, for example, sag, distort, or shrink when they get too hot so care must be taken to not exceed the temperature limit. Incomplete curing can allow unreacted monomers or oligomers to migrate out of the adhesive and affect sealing or other film properties.

Tension control is important during lamination to prevent stresses from building up, which can lead to delamination. Proper tension also helps avoid problems, such as telescoping, that contribute to defective rolls.

2.3.2.3 Comparison of Extrusion and Adhesive Lamination

The selection of extrusion or adhesive lamination to make a packaging film structure often comes down to what equipment the converter has in place. Table 2.5 summarizes some of the differences. Extrusion coating generally uses less expensive materials but takes longer to line out. Thus adhesive lamination is often favored for short runs. Adhesive lamination is also favored in situations where its curing chemistry brings advantage, such as temperature resistance for retort applications [44,48,49].

Table 2.5 Comparison of Advantages of Extrusion and Adhesive Lamination

Extrusion Lamination	Adhesive Lamination
No solvents	Short job changes
Lamination of rough or porous substrates possible (eg, paper)	Lower energy use
Good flexibility of laminate	Very cost-effective at $<5000\ m^2$
Good puncture resistance	Lower capital investment
Good environmental stress crack resistance	
Cost-effective at long ($>5000\ m^2$) runs	
Low cost in resin handling and disposal	

2.4 Orientation

Biaxial-orientated polypropylene (BOPP), polyester (BOPET), and polyamide are often used as substrates in multilayer laminations or stand-alone films. Oriented polylactic acid and polystyrene films have also found use in packaging. Orientation of coextruded films of (EVA−PVDC−EVA) are used as shrink bags for primal meat packaging. Machine direction-oriented (MDO) films are used in strapping and tapes and more recently in hygienic films and synthetic paper [50]. MDO is starting to find use in coextruded films although challenges remain [50,51]. Transverse-oriented films are used as shrink sleeves.

The effect of orientation on properties is explored in more detail in Chapter 11. In general, orienting a film increases tensile strength and barrier properties while decreasing haze and elongation at break. The films are flatter and thinner than conventional films.

There are three main types of commercial processes for producing oriented film: tenter frame for transverse, machine, or biaxial orientation; double bubble for biaxial orientation; and MDO. These are depicted schematically in Figs. 2.20−2.22.

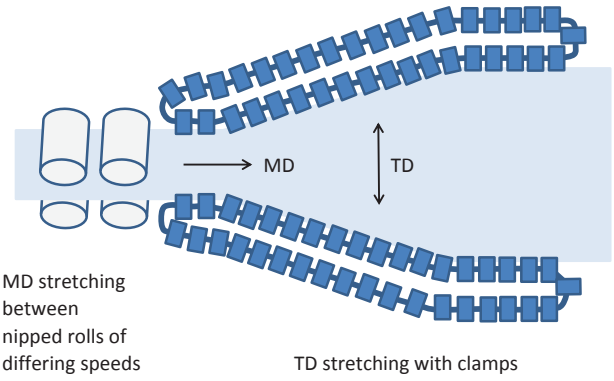


Figure 2.20 The tenter frame process.

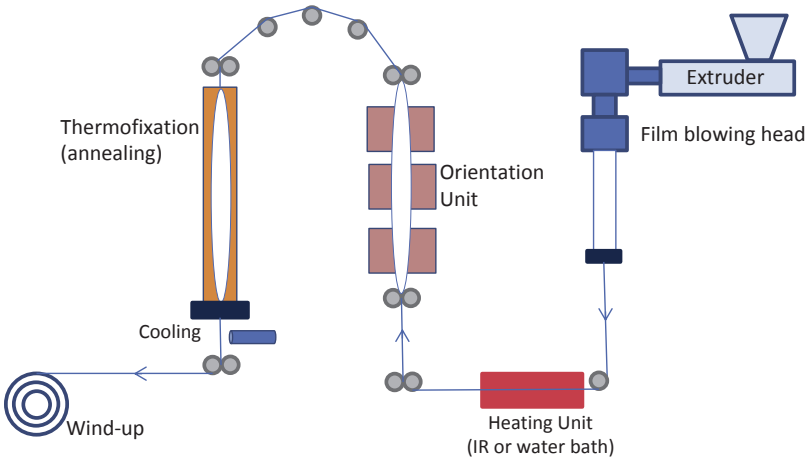


Figure 2.21 The double bubble process.

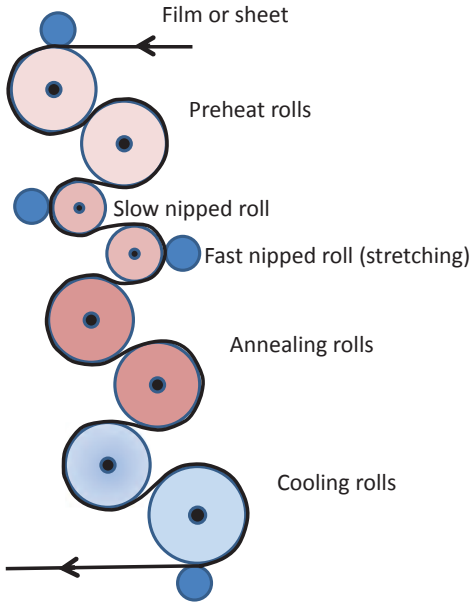


Figure 2.22 The machine orientation process.

2.4.1 Tenter Frame

In a sequential tenter frame process, polymer sheet is stretched in the machine and transverse directions in series. Typically the sheet is stretched in the machine direction first, often using heated rolls operating at different speeds (see Section 2.4.3). The film then goes into the transverse stretching oven where heaters raise the temperature of the sheet to the stretching temperature. Clamps are attached to the side of the film that are on a track that accelerates the sheet in the transverse direction. Following orientation the film undergoes a thermofixation or annealing step to improve dimensional stability. The annealing temperature is typically above the orientation temperature; the film remains clamped during annealing to prevent shrinkage and lock the orientation in place. Polymers have a memory and subsequent heating of the film below the thermofixation temperature will preserve the orientation (in a shrink film, the film is heated above its thermofixation temperature to initiate the shrinkage).

The stretching may be sequential or simultaneous. Simultaneous stretching results in more balanced orientation in the machine and transverse directions. Key variables affecting performance include the stretching temperature, annealing temperature, the draw ratio in each direction, the rate of stretching, and for biaxial orientation, the sequence of the stretching (sequential or simultaneous).

2.4.2 Double Bubble

In the double bubble process, the polymer is extruded as a tube into a water bath. The water rapidly quenches the polymer, reducing its crystallinity compared to conventional air quench blown film. The lower level of crystallinity helps in the subsequent orientation process.

Following quenching the tube is reheated to the orientation temperature using a hot water bath or IR heater. This two-step process of quenching and reheating the tube helps control the crystallinity as well as produces a more uniform temperature for orientation. The tube is expanded by blowing air inside the tube similar to a conventional blown film

process. A difference is that in the double bubble process the tube is oriented at lower temperatures, producing higher stresses during orientation. Stretch ratios are also typically much higher than in conventional blown film. As a result, double bubble films have more orientation than conventional blown films. Melt strength is also not a factor as it is in the blown film process.

The oriented film may undergo a thermofixation step in a third bubble, where the tube is reheated to the annealing temperature. This helps control shrinkage in a shrink film or improve dimensional stability in a nonshrink film.

Important factors influencing performance include the orientation and thermofixation temperatures, the BUR (transverse orientation stretch ratio), and the TUR (machine direction stretch ratio).

The double bubble process produces a film with more uniform properties in the machine and transverse directions than a sequential tenter frame process. Tenter frame processes have much higher output than double bubble processes and are the predominate method used to make BOPP and BOPET film. Double bubble processes are often used to make shrink film/bags. More recently they have found use for manufacturing barrier films [52].

2.4.3 Machine Direction Orientation

The MDO process is typically used as the first step of a sequential tenter frame biaxial orientation process but can be used as a stand-alone process as well. MDO machines consist of a set of heated rolls, often 12 or more in series. The first few rolls preheat the film to the stretching temperature. This feeds into a set of two nipped rolls operating at different speeds. The differential speed determines the amount of stretching or orientation. This is followed by annealing rolls to lock in the orientation. Finally, the film is cooled to room temperature on a set of cooling rolls [50].

The orientation temperature, draw ratio (ratio of the speeds of the nipped rolls), and annealing temperature are all important parameters influencing the final properties. Getting these rights for a given polymer is often the challenge in making good film from this process. Splitting and brittleness are two potential outcomes if not done correctly [51].

Further Reading on Film Orientation Processes

- DeMeuse MT. Biaxial stretching of film, Principles and applications. Oxford: Woodhead Publishing; 2011.
- Breil J. Biaxially oriented films for packaging applications. In: Ebnesajjad S, editor. Plastic films in food packaging, Materials, technology and applications. Amsterdam: Elsevier; 2013. pp. 53–70.
- Hatfield E. Machine direction oriented film technology. In: Wagner J, editor. Multilayer flexible packaging, technology and applications for the food, personal care and over-the-counter pharmaceutical industries. Oxford; Elsevier; 2010. pp. 113–8.

2.5 Printing

There are two general types of high speed roll-to-roll printing used in packaging: gravure and flexographic. Historically Europe favored gravure and the US flexographic, but both have gained popularity across regions.

2.5.1 Gravure Printing

In gravure printing (Fig. 2.23), an engraved metal roll is used to directly transfer the ink to the film substrate. The depressions in the engraved surface hold the ink and the ridges or unengraved portions of the roll are the nonprinted areas. The roll is immersed in a bath of ink where the etched regions pickup the ink. A blade removes the excess ink prior to contact

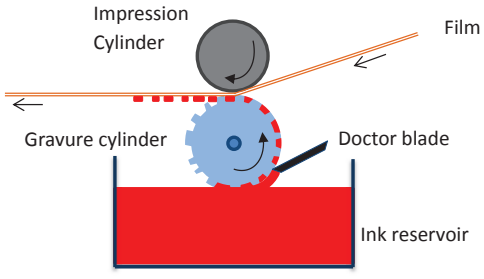


Figure 2.23 The gravure printing process.
Based on Lentz J. Printing. In: Bakker M, editor. The Wiley encyclopedia of packaging technology. New York: John Wiley & Sons; 1986. pp.554–61.

with the film. An impression cylinder on the back side of the film forces contact of the film with the depressed, ink-filled regions of the gravure roll, transferring the ink to the film. The film is passed through a dryer to drive off the solvent or water. The gravure press may contain many printing stations in-line, each for a different color of ink, or for applying cold seal or barrier emulsions.

The gravure rolls are chemically, mechanically, or laser etched to form the pattern of small cells of depressions that hold the ink. The rolls are hard and long-lasting. One of the advantages of this process is that the rolls are durable, allowing for accurate reproduction of the design over many prints at high speeds. The initial costs are high but for long runs the gravure process is cost-effective.

2.5.2 Flexographic Printing

In flexographic printing, the pattern is made into plates, typically from a photopolymer. The plates are attached to a roll. Ink is transferred from a bath to an anilox roll, which contains millions of tiny divots to take up the ink. The anilox roll then contacts the printing roll, transferring the ink to the surface of the plates. The printing roll then contacts the surface of the film. While gravure printing relies on impressing the film into the cavities of the roll where the ink resides, the ink on the flexographic plates is on the ridges of the pattern (Fig. 2.24).

The plates are relatively inexpensive, which favors flexographic printing for short runs. The quality and productivity of flexographic printing has advanced so that choosing between flexographic and gravure printing is often difficult.

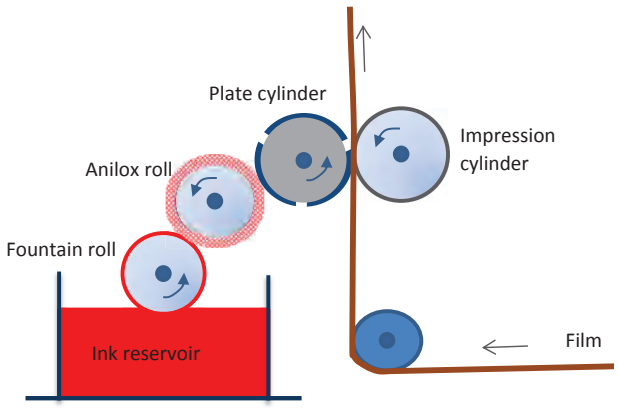


Figure 2.24 Flexographic Printing Process.
Based on Lentz J. Printing. In: Bakker M, editor. The Wiley encyclopedia of packaging technology. New York: John Wiley & Sons; 1986. pp.554–61.

Further Reading on Film Printing Processes

- Lentz J. Printing. In: Bakker M, editor. The Wiley encyclopedia of packaging technology. New York: John Wiley & Sons; 1986. pp.554–61.
- Kirwin M, Strawbridge JW. Plastics in Food Packaging. In: Coles R, McDowell D, Kirwin MJ. Food Packaging Technology. Oxford: Blackwell Publishing Ltd; 2003. pp. 211–2.

References

[1] Frankland J. Get smarter on extrusion sizes. Plastics Technology; July 2012. p. 22.
[2] Schut J. Understanding grooved feed. Plastics Technology; April 2000. viewed 29 May 2013, from: http://www.ptonline.com/articles/understanding-grooved-feed.
[3] Rauwendaal C. Polymer extrusion. Munich: Hanser Publishers; 1986. p. 246–56.
[4] Hellmuth W. Light grooved feed throat extrusion – versatile, efficient, and retrofitable. In: Proceedings of the International Polyolefins Conference 2010, Houston, TX, February 21–24. Society of Plastics Engineers; 2010.
[5] Chung CI. Scientifically designed barrier screw. In: SPE ANTEC Conference; 2013.
[6] Campbell GA, Spalding MA. Troubleshooting & analysis of single-screw extrusion. New York: Hanser Gardner Publications; 2010. p. 627–33.
[7] Rauwendaal C. Polymer extrusion. 4th ed. Munich: Carl Hanser Verlag; 2001. p. 477–90.
[8] Kramer WA, Steward EL. Single-screw extruders. In: Vlachopoulos J, Wagner JR, editors. The SPE guide on extrusion technology and troubleshooting. Brookfield (CT): The Society of Plastics Engineers; 2001. p. 1–9.
[9] Campbell GA, Spalding MA. Troubleshooting & analysis of single-screw extrusion. New York: Hanser Gardner Publications; 2010. p. 597–624.
[10] Saxton R. Extruder mixing screw. U.S. patent, US3006029. 1961.
[11] Maddock B. Mixing of thermoplastic materials. U.S. patent 3730492A. 1973.

[12] Waller P. What to do when the bubble won't behave. PlasticsTechnology; 2002. viewed 19 June 2013, from: http://www.ptonline.com/articles/what-to-do-when-the-bubble-won't-behave.
[13] Butler T. Blown film bubble instability induced by fabrication conditions. In: SPE ANTEC Tech. Paper; 2000. p. 156–64.
[14] Waller P. Blown film processes and trouble-shooting, the ultimate quality control tool. In: 2009 Flexible Packaging Summit, TAPPI PLACE; 2009. viewed on 15 June, 2013, from: http://www.tappi.org/content/events/09PLACESY/Course_Papers/waller.pdf.
[15] Gross HG. Control of the thickness distribution of blown film by changing the flow channel gap of the die over the circumference. In: SPE ANTEC Conference; 2008.
[16] Tamber H. Blown film cooling systems. In: Butler TI, editor. Film extrusion manual: process, materials, properties. 2nd ed. Atlanta (GA): TAPPI Press; 2005. p. 189.
[17] Wright D. Latest developments in on-line measurement and control of multilayer blown films: full spectrum infrared (FSIR) and air ring. In: TAPPI PLACE Conference, Portsmouth (VA); 2008.
[18] Blalock T, Heveron-Smith S. Multi-layer film measurement using dual-light interferometry. In: TAPPI PLACE Conference, Indianapolis (IN); 2004.
[19] Perdikoulias J. Multilayer blown (tubular) film dies. In: Wagner J, editor. Multilayer flexible packaging, technology and applications for the food, personal care and over-the-counter pharmaceutical industries. Oxford: Elsevier; 2010. p. 97–102.
[20] Butler TI, Patel R, Lai SY, Spuria J. Blown film frost line-freeze line interactions. In: TAPPI Polymers, Laminations & Coatings Conference; 1993. p. 13–25.
[21] Morris BA. Effect of process and material parameters on interlayer peel strength in coextrusion coating, film casting and film blowing. J Plastic Film Sheeting 2010;26:343–76.
[22] Ratel RM, Butler TI, Walton JL, Knight GW. Investigation of processing-structure-properties relationships in polyethylene blown films. Polym Eng Sci 1994;34(19):1506–14.
[23] Babel AK, Campbell GA. Correlating the plastic strain with the properties of the low density polyethylene blown film. J Plastic Film Sheeting 1993;9:246–58.
[24] Kanai T, Kimura M, Asano Y. Studies on scale-up of tubular film extrusion. In: SPE ANTEC Conference; 1986. p. 912–6.
[25] Pearson JRA, Petrie CJS. The flow of a tubular film. Part 1. Formal mathematical representation. J Fluid Mech 1970;40:1.
[26] Pearson JRA, Petrie CJS. The flow of a tubular film. Part 2. Interpretation of the model and discussion of solutions. J Fluid Mech 1970;42:609–25.
[27] Pearson JRA, Petrie CJS. A fluid-mechanical analysis of the film-blowing process. Plast Polym 1970;38:85.
[28] Shirodkar P, Firdaus V, Fruitwals H. Scale-up of LLDPE blown film. Plastics Engineering; December 1994. p. 27.
[29] Butler TI, Lai SY, Patel R. Scale-up factors effecting crystallization in polyolefin blown film. In: TAPPI Polymers, Laminations & Coatings Conference; 1994. p. 289–304.
[30] Sukhadia AM. The use of bubble kinematics in the scale up and processing-property analysis of the blown film process. In: SPE ANTEC Conference; 1994. p. 202–10.
[31] Bezigian T. A survey of current bead reduction die technology. In: Bezigian T, editor. Extrusion coating manual. 4th ed. Atlanta: TAPPI Press; 1999. p. 55–63.
[32] Kirtley. Coat weight/thickness measurement and control. In: Bezigian T, editor. Extrusion coating manual. 4th ed. Atlanta: TAPPI Press; 1999. p. 117–8.
[33] Morris BA. Understanding why adhesion in extrusion coating decreases with diminishing coating thickness. J Plastic Film Sheeting 2008;24:53–88.
[34] Canning K, Bian B, Co A. Film casting of a low density polyethylene melt. In: Proceedings of ANTEC 1999, Annual Technical Conference – Society of Plastic Engineers, vol. 57; 1999. p. 386–90.
[35] Antonov V, Soutar A. Foil adhesion with co-polymers: time in the air gap. In: TAPPI 1991 Polymers, Laminations & Coatings Conference

Proceedings. Atlanta: TAPPI PRESS; 1991. p. 553.
[36] Prinsen B. Why choose blown, cast or lamination processes to achieve barrier properties. In: TAPPI PLACE, 2009 Flexible Packaging Summit; 2009. viewed 08 June, 2013 from: http://www.tappi.org/content/events/09PLACESY/Course_Papers/prinsen.pdf.
[37] Giles Jr HF, Mount III EM, Wagner Jr JR. Extrusion: the definitive process guide and handbook. William Andrews; 2007. p. 460–2.
[38] Knittel R. Blown film versus the cast film process. SPE Extrusion Division; 1995. Viewed on 2 June, 2013 from: http://www.extrusionwiki.com/wiki/(X(1)S(0bpdnb45tivsdq450plakjus))/CC-V22-3-B.ashx.
[39] Laiho E, Ylanen T. Flame, corona, ozone – do we need all pretreatments in extrusion coating? In: Bezigian T, editor. Extrusion coating manual. 4th ed. Atlanta: TAPPI Press; 1999. p. 89–97.
[40] Markgraf DA. Corona treatment enhanced adhesion for extrusion coating. In: Bezigian T, editor. Extrusion coating manual. 4th ed. Atlanta: TAPPI Press; 1999. p. 65–74.
[41] Sherman PB. Ozonation of polymer melt for improved adhesion. In: Bezigian T, editor. Extrusion coating manual. 4th ed. Atlanta: TAPPI Press; 1999. p. 75–87.
[42] DiGiacomo JD. Flame plasma surface treatment. In: Bezigian T, editor. Extrusion coating manual. 4th ed. Atlanta: TAPPI Press; 1999. p. 121–30.
[43] Bentley Jr DJ, Singer FM. Chemical primers to enhance adhesion and other properties. In: Bezigian T, editor. Extrusion coating manual. 4th ed. Atlanta: TAPPI Press; 1999. p. 99–108.
[44] Wolf R. A technology decision – adhesive lamination or extrusion coating/lamination? In: Tappi place Conference, April, Albuquerque (NM); 2010. viewed on 11 June, 2013, from: http://www.tappi.org/content/events/10PLACE/papers/wolf1.pdf.
[45] Morris BA, Suzuki N. The case against oxidation as a primary factor for bonding acid copolymers to foil. In: TAPPI Polymers, Laminations & Coatings Conference; 2000.
[46] Schubert G, Plassmann O, Husch S. Hot tack of extrusion coatings on aluminum foil and paper – does the process always lead to the same result?. In: TAPPI PLACE Conference; 2010.
[47] Trouilhet Y, Morris. Prediction of temperature profiles across coating and substrate in the nip. In: TAPPI Polymers, Laminations and Coatings Conference; 1999.
[48] Petrie EM. Laminating adhesives for flexible packaging. Omnexus 4 Adhesives & Sealants, viewed 11 June 2013, from: http://www.packagingconnections.com/downloads/download195_0.pdf.
[49] Schetschok H, Kupsch E. Adhesive lamination vs. extrusion lamination, trends and technology update. In: TAPPI European PLACE Conference, May, Bregenz, Austria; 2011. viewed on 11 June 2013, from: http://www.tappi.org/Downloads/Conference-Papers/2011/2011-13th-TAPPI-European-PLACE-Conference/11EURO30.aspx.
[50] Breese R. Benefits of machine direction orientation (MDO) film in flexible packaging applications. Converting Quarterly; 2011. p. 32–6.
[51] Shut JH. MDO films: lots of promise, big challenges. Plastics Technology; February 2005. viewed 18 June 2013, on: http://www.ptonline.com/articles/mdo-films-lots-of-promise-big-challenges.
[52] Alexy F. Replacing aluminum in high barrier packaging with Triple Bubble® blown film extrusion. In: Multilayer Packaging Films 2012 Conference; 2012.
[53] Waghorn PE. The control of oxidation and odour in extrusion coating. Chicago: Polythene Extrusion Coaters Group; 1963.
[54] Crolius VG, Ebeling WE, Parsons RC. The effect of processing variables on the adhesion strength of polyethylene-coated aluminum foil. TAPPI 1962;45(5):351–6.
[55] Morris BA. Polymer blending for packaging applications. In: Ebnesajjad S, editor. Plastic films in food packaging, Materials, technology and applications. Amsterdam: Elsevier; 2013. p. 311–43.
[56] Lentz J. Printing. In: Bakker M, editor. The Wiley encyclopedia of packaging technology. New York: John Wiley & Sons; 1986. p. 554–61.

3 Packaging Equipment

Packaging equipment transforms the flexible film into a package form, fills it with product, seals it to prevent leaks, and prepares it for shipping. This chapter briefly describes packaging equipment commonly used in flexible packaging as outlined in Table 3.1. There are many forms of packaging equipment available on the market today. The purpose of this chapter is not to describe these in great detail but to point out some of the common features and operations. This chapter closes with a discussion of the unit operations of packaging equipment: registration, thermoforming, filling, gas flush/modified atmosphere packaging (MAP), and sealing.

3.1 Brief Description of Packaging Equipment

3.1.1 Pouch Machines

Pouches come in a wide variety of forms, such as pillow packs, stick packs, gusseted packs, and stand-up pouches. Pouch styles are differentiated by their sealing. Some general types are depicted in Fig. 3.1. Pillow packs have straight top and bottom seals or end seals with a long seal up the side. The side seal may be a lap seal, where the outside surface of the film seals to the inside surface of the same film, or a fin seal where the inside seals to the inside. In a gusseted end seal, the film is folded along the sides to provide a more rectangular profile. Three- or four-sided seal pouches and stand-up pouches are other special forms.

Pouch machines come in a wide variety of designs but generally fit into two categories: vertical form fill seal (VFFS) or horizontal form fill seal (HFFS) machines.

3.1.1.1 Vertical Form Fill Seal

As pictured in Fig. 3.2, in a common form of a VFFS line a flexible packaging film is shaped over a mandrel into a tube. The bottom and side is sealed, product is dropped into the tube from above, and the top is sealed (at the same time as the bottom seal of the next package) and cut. The sealed pouch drops onto a conveyor belt for secondary packaging and shipping.

Packaging speeds of up to 100 bags per minute are common. Bag sizes range from 5 to 25 in. (13–64 cm) for food packaging, and even longer for nonfood packaging. Typical products packaged on these lines include chips and other snacks, cereal, cookies (that are dump filled), and bagged candy. Often these packages form the inner package of a "bag and box" package structure, where the filled bag is stuffed into a paperboard secondary package. The outer package provides some degree of protection but more importantly provides a good form factor for sitting on a shelf as well as a print surface. VFFS is also often used for nonfood packaging, such as for polymer resins and fertilizer.

An important consideration for VFFS is a strong bottom seal that can withstand the weight of the product during filling. The seal is still molten at this point in the process. The ability of the seal to withstand an opening force before it solidifies is known as hot tack, an important sealing property that is covered in detail in Chapter 7.

The side seal may be a fin or lap seal, or in the case of a three- or four-sided seal, a conventional seal. The three- or four-sided seal pouch or sachet is often used for condiments, shampoo and soap sachets, oil, and sauces. Sachet machines can often be run faster than pillow pack machines since the product does not drop as far.

Stick packs are long and thin and are often used for powdered drink mixes and pharmaceuticals.

3.1.1.2 Horizontal Form Fill Seal

In a horizontal flow wrap machine, the film is formed around a mandrel in the horizontal dimension, filled with the product, sealed, and cut. This is depicted in Fig. 3.3. These high speed lines run up to

The Science and Technology of Flexible Packaging. http://dx.doi.org/10.1016/B978-0-323-24273-8.00003-4
Copyright © 2017 Elsevier Inc. All rights reserved.

Table 3.1 Examples of Packaging Equipment and Their Uses

Equipment	Package Form	Examples of Products Packaged
Vertical form fill seal	Pouches Pillow packs	Chips Cereal and other bag-in-box Cookies Nonfood: resin, fertilizer
Horizontal form fill seal (flow wrappers)	Flow wrappers	Candy bars Cookies Snack crackers/ cookies Medical products Disposable razors
Horizontal thermoform fill seal	Tray with lid, shingle packs	Processed meat Cheese Fish Medical items
Tray sealer	Tray with lid	Microwavable meals Ovenable meals Other dual oven food items
Vertical pouch	Pouches Sachets	Condiments Shampoo/soap sachets Water Oil Sauces
Vertical pouch	Stick packs	Powder drink mixes Pharmaceuticals
Horizontal pouch	Pouches	Dry soups Mixed ingredient food products Jello Cake mixes
Stand-up pouch	Pouches	Frozen vegetables Snacks Candy Liquids
Blister packaging	Carded blister packs	Pharmaceuticals

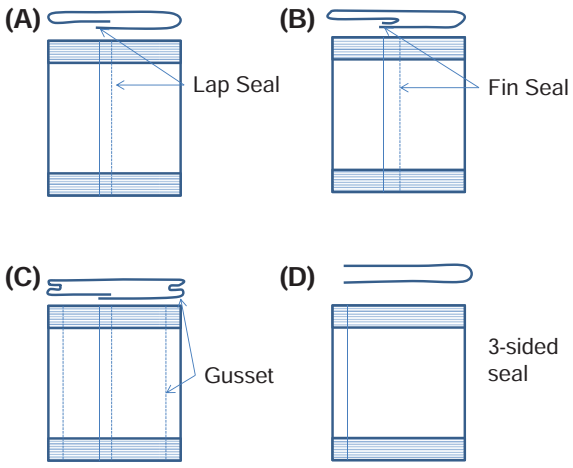


Figure 3.1 Types of seals found on pouches (A) lap seal, (B) fin seal, (C) gusseted seal, (D) three-sided seal.
Adapted with permission from Moyer G. Form/fill/seal, vertical. In: Bakker M, editor. Wiley encyclopedia of packaging technology. New York: John Wiley & Sons; 1986. p. 367–9.

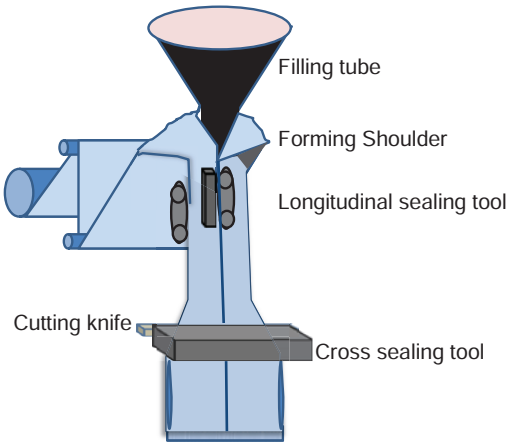


Figure 3.2 Vertical form fill seal line.
Adapted with permission from Moyer G. Form/fill/seal, vertical. In: Bakker M, editor. Wiley encyclopedia of packaging technology. New York: John Wiley & Sons; 1986. p. 367–9.

3200 in. (81 m) per minute, 400 packages/min for an 8-in. (0.2 m) package with packages from 5 to 16 in. (0.13–0.4 m) long and $^1/_2$ to 7 in. (0.013–0.18 m) wide. There may be multiple lanes to increase the number of packages per minute. The filling may be automated or manual.

Some of the products typically packaged on flow wrapper lines include candy bars, cookies, crackers, medical products, and disposable razors.

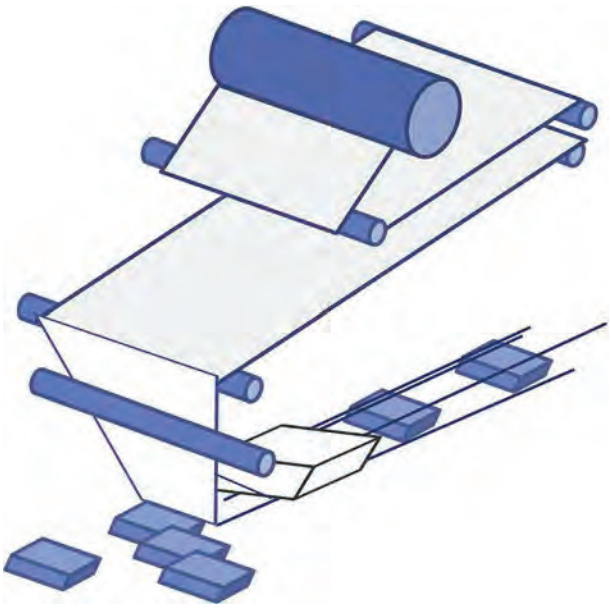


Figure 3.3 Horizontal flow wrap line.
Adapted from Hughes AA. Food packaging machinery. In: Ebnesajjad, editor. Plastic films in food packaging. Elvesier; 2013. p. 210.

Three- or four-sided seal horizontal pouch machines are used to package a variety of dry soups, spices, cake mixes, and mixed ingredient food products. Lines can run at high speed (200 packs/minute or higher) with multiple fillers and one or two webs. A variety of sized pouches can be made from small (2-in. × 2-in. or 5-cm × 5-cm) to large (8-in. × 10-in. or 20-cm × 25-cm).

The use of stand-up pouches has seen substantial growth over the last 20 years. Much of the early growth of this package came from the replacement of metal cans, where stand-up pouches offer the following advantages:

- unlimited sizes/shapes
- reduced raw material costs
- reduced storage costs
- reduced freight costs
- source reduction
- unequaled graphics.

Stand-up pouches still suffer from lower filling speeds versus cans. In recent years, stand-up pouches have replaced other forms of flexible packaging, mainly for their superior graphics and ability to stand-up and be seen (billboard effect) on the grocery shelf.

3.1.2 Horizontal Thermoform Fill Seal

In a horizontal thermoform fill seal packaging line (Fig. 3.4), a bottom forming web is registered into a heating and forming station where a cavity is thermoformed into the web, typically with a vacuum

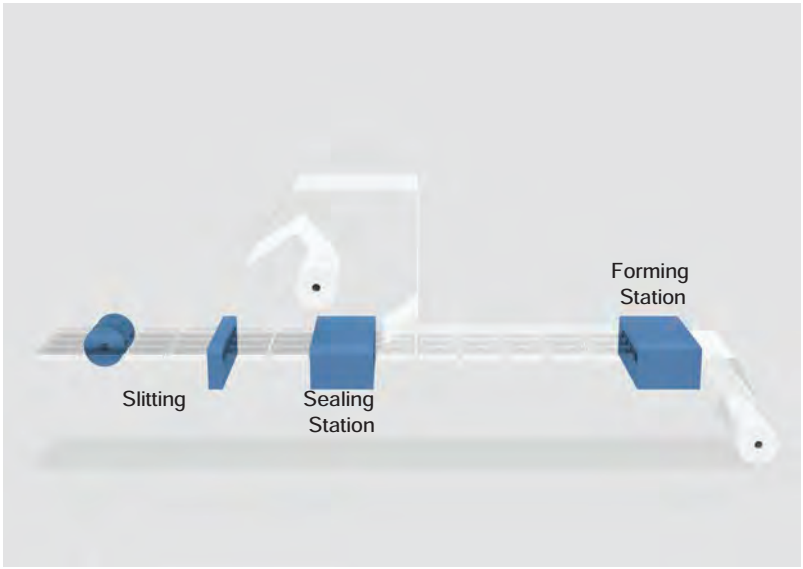


Figure 3.4 Horizontal thermoform fill seal machine.
Reproduced with permission of MULTIVAC.

and plug assist. The film then registers to a filling station where the product is laid into the cavity, either manually or automatically. A second "top" web is then laid down on top of the filled forming web, air evacuated, and if necessary gases added. [In a technology known as MAP, the gas environment inside the package is adjusted to extend the shelf life of the product (see Section 3.2.4)]. The top and bottom web are then heat sealed together. Often multiple lanes are thermoformed and filled in parallel. In a final step the individual packages are cut from the web.

The bottom forming web is often different in composition and thickness than the top web. In particular the bottom web is often thicker to accommodate the reduction in wall thickness during thermoforming. The bottom web may be flexible or semirigid with thicknesses up to about 35 mils (0.89 mm).

Typical products packaged on these lines include block cheese, processed meat, fish, and medical devices. For medical device packaging, the top web is often a porous paper or nonwoven, such as DuPont's Tyvek, to facilitate sterilization by ethylene oxide.

3.1.3 Tray Sealer

In a tray sealer (Fig. 3.5), trays are filled with product, covered with a lidding film, air evacuated and gas flushed (if necessary), and sealed. Machines are typically designed to handle a wide variety of tray materials such as paperboard, metal, and plastic [polyethylene terephthalate (PET), polypropylene, and polystyrene are the most common].

Tray sealing machines are used for a variety of microwavable and dual ovenable meals. Also various bowls and cups can be filled and sealed on the same type of equipment, making them suitable for dairy and other products.

3.1.4 Aseptic Packaging

In aseptic packaging, the food and packaging materials are sterilized and maintained in a sterile environment throughout the packaging process. The rollstock is typically a multilayer barrier film or laminate. As it enters the machine it is sterilized by gamma radiation or hydrogen peroxide. The film is formed, filled, and sealed.

Some products packaged with aseptic packaging include juices and dairy products. Individual children's juice drinks are often packaged in this way, such as the Tetra Brik (Tetra Pak) introduced in the 1980s.

3.1.5 Retail Packaging

There are three main types of flexible packaging used for display of merchandise in the retail environment: clamshell, blister, and carded skin packaging. Stand-up pouches have also grown in use in the retail sector but are addressed in Section 3.1.1.2.

3.1.5.1 Clamshell Packaging

Clamshell packaging consists of a clear thermoformed sheet, usually hinged, with a top and bottom portion. The product is placed in the cavities formed by the sheet and the sheet is welded in place.

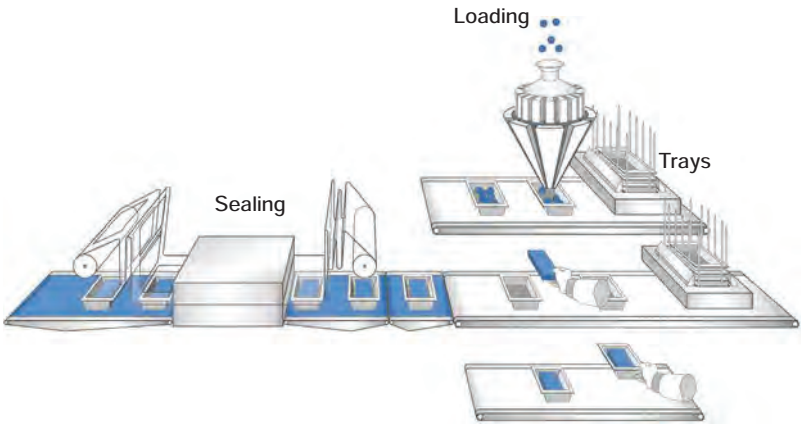


Figure 3.5 Tray sealing line.
Reproduced with permission of MULTIVAC.

Clamshell packaging has become a major form of packaging for retail goods, such as hardware goods, automotive parts and supplies, consumer goods, and household items. Polyvinyl chloride (PVC) and PET are two common materials used for retail packaging due to their combination of clarity, toughness, and low cost.

Graphics are typically provided by inserting a printed paper card within the clamshell.

3.1.5.2 Blister Packaging

Blister packaging is a form of retail packaging where the product sits in a plastic blister on top of paperboard. There are four main components to blister packaging: a preformed plastic blister, the paperboard card, a heat seal coating, and printing inks [1].

The preformed plastic blister is made of a clear plastic such as PVC or PET. The type of plastic depends on many factors including the size of the product, whether the product has sharp or pointed edges, impact resistance needs, aging requirements, and cost.

The paperboard provides stiffness and a surface for heat seal and graphics. The size and thickness depend on the product and the stresses that the package will see during its use.

A heat seal coating is applied to the board to seal the blister in place. The coating must be compatible with the board (or ink) and blister.

The printing ink provides graphics and must bond well to the substrates.

There are several types of blister packages (Fig. 3.6). In the conventional design, the blister fits over the product and its flange is heat sealed to the board. In a foldover card, the board is folded so that the blister flange sits below the top portion of the board and above the bottom portion. The bottom and top portions of the board are sealed board to board. A hole in the top portion is punched out so that the blister flange can sit below the top portion. In the hinged blister/foldover card variation, the blister folds over the product and is set in place by a sealed hinged blister. A sandwich or double card is where the blister is sandwiched between two boards (no hinge).

In a typical assembly operation, the blister is filled with the product, the paperboard is set on top, and heat sealed in place.

Blister packaging is also used in pharmaceutical packaging where aluminum foil and barrier films, such as Aclar polychlorotrifluoroethylene, are often used instead of paperboard and PVC to achieve good moisture barrier.

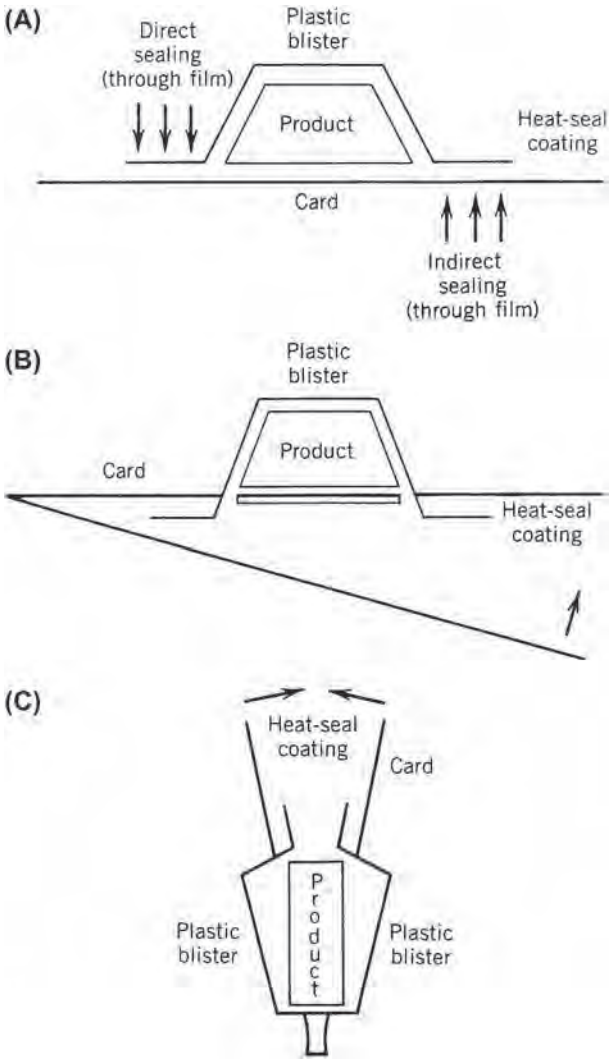


Figure 3.6 Forms of retail blister packaging: (A) conventional surface seal, (B) foldover variation, (C) hinged blister/foldover card variation.
Reproduced with permission from Gresher JM. Carded packaging. In: Bakker M, editor. Wiley encyclopedia of packaging technology. New York: John Wiley & Sons; 1986. p. 124–32.

3.1.5.3 Skin Packaging

In skin packaging, the product serves as the mold over which a heated plastic film (skin) is draped. Vacuum is drawn through a porous board to pull the film against the product and board, conforming it to the shape of the product and creating a heat seal (Fig. 3.7).

Skin packaging has four main components: the plastic film, the porous paperboard, a heat seal coating, and ink. The plastic film is typically low density polyethylene (LDPE), PVC, or ionomer. PVC is clear and inexpensive. LDPE is inexpensive but lacks the clarity of PVC or ionomer. Ionomers provide better abrasion and puncture resistance, superior drawability for high profile items, excellent resistance to board curl, better gloss, cold crack resistance, faster cycle time, and are more cost-effective/higher yield per unit weight.

The paperboard must be porous enough for the vacuum to draw the film down around the product. Solid-bleached sulfate board is often used. Clay coatings generally are not used since this reduces the porosity. In some cases the board may be perforated to achieve the desired porosity.

The board is coated with a heat seal coating, typically applied as a latex- or water-based dispersion. Ethylene acrylic acid copolymer dispersions are often used for good compatibility with LDPE and ionomer, as well as good sealability.

Inks are used for printing the board. The ink needs to be compatible with both the board and the heat seal coating.

In the skin packaging machine, product is placed on the printed heat seal coated paperboard. The plastic film is held in a frame above the product, heated, and draped over the product, while vacuum is pulled through the porous paperboard from below. The residual heat in the film activates the heat seal coating, forming a bond between the film and board.

3.1.5.4 Comparison of Retail Packaging Types

Consumer products companies are generally looking for packages that meet the following requirements:

- transparent so that the consumer can see the product
- tamper evident or difficultly to pilfer (to reduce in-store loses to theft)
- easy to display (typically on a peg)
- ability to have graphics to inform the consumer about the benefits of the product.

Choosing between the package forms is not always a clear choice. Table 3.2 gives some advantages and disadvantages for each type.

Further Reading

1. Yam Kit L. Wiley encyclopedia of packaging technology. 3rd ed. John Wiley & Sons; 2009.
2. Paine FA, Paine HY. A handbook of food packaging. Springer; 1992. p. 97–158.

3.2 Unit Operations

While there is a wide variety in design, packaging equipment shares common operations. This section explores some of the key factors that affect performance.

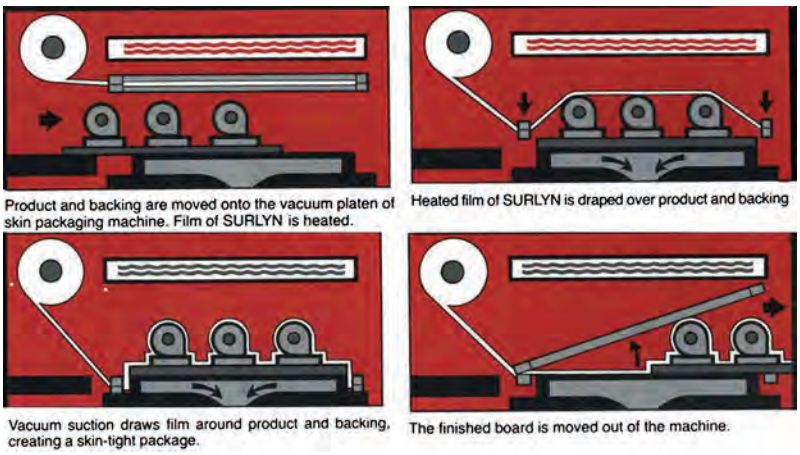


Figure 3.7 Skin packaging process.
Reproduced with permission from E. I. du Pont de Nemours and Company.

Table 3.2 Comparison of Retail Packaging Types

Attribute	Clamshell	Blister	Skin
Cost	Highest material costs	May have advantage over skin packaging if product is much smaller than the card	May have advantage over blister packaging if product is about the same size as the card
High speed/ automation	Good	Good	Typically packed on smaller, manual machines; more labor intensive
Transparency, ability to see the product	Good	Good	Good. Allows the consumer to interact with the product
Graphics/printing	Achieved with paper inserts; generally low "billboard space"	Best graphics: paperboard may be clay coated to achieve excellent graphic quality; large "billboard space"	Largest "billboard space," clay coating not used due to its effect on porosity
Retail space	Typically bulky, taking up more retail space	Easy for pegged display	Easy for pegged display
Ease of opening	Difficult to open (good for stopping in-store theft, bad for consumers)	Easier to open than clamshell	Can be designed for easy-open or difficult to open
Other	Perception of higher quality; easily allows packaging multiple items in single package		Difficult to package round items; holds products in place during distribution

Courtesy of DuPont.

3.2.1 Registration

Registration involves the controlled movement of the film through the machine while various operations are performed. Critical to quality is the movement of the film without wrinkling or distortion. Factors influencing performance include the frictional properties of the film, film stiffness, and machine design. The frictional properties of the film are generally characterized by the coefficient of friction (COF) as measured by ASTM D1894. The COF is defined as "the ratio of the force required to move one surface over another over the total force applied normal to the surfaces" [2]. Several types of COF can be measured. Static COF involves the friction between a weighted sled and the film surface as the sled is initially dragged across the surface. It is a start-up value. The kinetic COF is the measured frictional force after the force has reached a steady state. Both may be important in film registration. COF can also be measured against different surfaces. Film-to-film COF involves measuring the frictional drag on the film against itself. Film-to-metal COF involves measuring the drag of the film against a metal surface. Again, both may be important for registration.

The COF of barefoot plastic films can often be quite high, near 1. Often values of around 0.2–0.3 are desired. To achieve this, additives may be used to impart a more slippery surface on the film. These slip additives are typically fatty acid amides that bloom to the surface over time, so care must be taken to allow sufficient time for the slip agent to reach the surface before measuring COF. A more detailed discussion on the diffusion of slip agents in films is provided in Chapter 12.

Blocking of the film on the roll can be another issue. Blocking is the resistance of the film to unwind. It is particularly an issue with soft or tacky plastics, or if the film is too tightly wound. "Anti-blocking" additives are often added to the plastic to reduce blocking. These are typically inorganic materials such as diatomaceous earth, silica, or talc.

These make the surface bumpier, reducing the contact between the layers of film in the roll.

Film stiffness is important because if a film is too flimsy it may be too difficult to handle, resulting in wrinkles and other problems. If the film is too stiff, it may not bend around sections of the machinery. The bending stiffness is what is important for registration, rather than a tensile stiffness (as measured by a tensile or Young's modulus). For single layer films, the bending stiffness increases with the thickness cubed. For multilayer films, the bending stiffness is a complex relationship between the thickness, placement, and tensile modulus of each of the layers. Modeling of this relationship is described in Chapter 9.

Film strength and equipment design also play a role. Proper tension control and keeping the drag force below the yield strength of the film is important to prevent the film from stretching.

3.2.2 Thermoforming

Thermoforming involves heating the film to the forming temperature and shaping it into the form of a cavity. This typically involves drawing a vacuum to pull the film into the cavity or using a plug to push the film into the cavity or both. During the forming process, the film is drawn down in thickness in proportion to the additional area created.

Uniform thickness and layer distribution after forming as well as minimizing spring back are critical to quality. Factors that influence performance include the thermoforming temperature, plug assist design, film design/construction, draw ratio, the heating process, and time.

Most plastic materials have a range of temperatures over which they can be readily thermoformed. Since thermoforming involves biaxially stretching of the polymer, many of the same considerations for material selection and temperature as for oriented films apply to thermoforming. Forming is typically done below the melting point of the highest melting layer of the structure. Otherwise, the film may sag too much during the process, resulting in operational issues. Forming in the solid state also helps impart more orientation on the formed package, providing better strength. But too much orientation or residual stress may result in spring back, where the final shape of the package is not within the desired dimensional tolerances due to relaxation of stresses during forming.

Forming at temperatures that are too high may distort one or more of the layers. Also, some of the layers may be molten at the forming temperature. This may particularly be true for the sealant layer, which is often designed with a low melting point to achieve low temperature sealability and high line speeds. Since the sealant is an outer layer of the film, care must be taken that the molten sealant does not stick to the plug assist or mold.

When designing a multilayer film structure for thermoforming, the individual thermoforming temperature ranges of each of the layers must overlap so that a common forming temperature can be found [3]. Sometimes materials may have to be substituted to achieve a workable system.

The stretch or draw ratio and draw rate may affect formability. Some materials do not draw well. For example, standard grades of ethylene vinyl alcohol (EVOH) have limited drawing performance. At high draw ratios, they become distorted and discontinuous. Using grades tailored for thermoforming helps reduce this problem. Early on this meant using grades with higher ethylene content, but in more recent years the EVOH suppliers have come out with special grades with lower ethylene content (and higher barrier performance) [4,5]. Blends have also proven effective. DuPont showed that adding a minor amount of amorphous polyamide [6] or ionomer [7] can significantly improve deep draw thermoformability without significant impact on barrier properties. Adjustments to the thermoforming process may also be effective [8].

The thermoforming process and key resin properties, such as strain hardening, are described in further detail in Chapter 11.

3.2.3 Filling

The filling operation involves dispensing an accurate number or volume of product into the package. There are two general methods to account for the product being packaged: by count and by weight or volume. When dosing a specific count or number of items into the package, three steps typically take place: representation, detection, and product handling [9].

The objects must first be detected, typically by an electric signal, so that they can be accounted for in a control system. Detection is done by optical or nonoptical methods. A typical optical method uses a photosensor to detect the object. Nonoptical methods

use other means to "touch" the article. One method is to channel the objects into an escapement device that is designed so that the product exactly fits into a receiving device. This involves a physical touch of the article. Electrical or magnetic fields are also used for detection.

During product handling, the objects are typically channeled into single file during conveying. This facilitates counting. The articles are then accumulated and dispensed into the package.

Dry or liquid products are filled by weight or volume. The goal is to fill the container or package with a specific weight or volume as denoted on the package. Label laws often require that the package contains the amount indicated. Variability in filling or measuring inevitably occurs, generally requiring that the package to be overfilled to ensure that the law is met. The capability of the filling system to meet a target filling weight can be described by statistics. Typically the variability follows a normal probability distribution and the standard deviation can be used to characterize the variability or error. Guidelines, such as +/−3 standard deviations (99.73%), can be established to ensure compliance with laws. The specification of a filling system will be dictated by its cost and ability to minimize filling error.

The filling of dry products is done by volume or weight. Volumetric systems are less expensive and sufficient for constant density products. They are also easier to maintain than weight systems. Weight systems are generally more accurate and allow for record keeping. Their cost has come down in recent years.

There are many types of dry goods feeders, including augur, gravity fed, vibratory, belt, screw, vibration bin discharge, cascade filling, and vacuum filling. Each has its advantages and disadvantages [10]. There are a number of weighing systems on the market, the details of which are beyond the scope of this book.

In the packaging process, there are many approaches to accurately deliver the target volume or weight to the package. Some systems fill volumetrically to a point, weigh the partially filled package, and fill with a weight system to reach the goal. Others use loss in weight throughout. Multiple feeders and feeder types may be used on a single packaging line. Selection of the feeder must take into account production rate, product cost, packaging type and cost, machine efficiency, maintenance cost, equipment cost, operating cost, and layout [10].

3.2.4 Gas Flush/Modified Atmosphere Packaging

Oxygen in the headspace or entrained with the product during filling can contribute to food spoilage. Often the headspace will be flushed with an inert gas such as nitrogen or an atmosphere different from air (20.9% oxygen, 79% nitrogen, and 0.03% carbon dioxide) during filling or prior to sealing. This is known as MAP and has been in practice since the 1970s as a way to extend the shelf life of the product.

Oxygen accelerates oxidation and microbial growth; replacing the oxygen retards oxidation, reduces enzymatic reactions, and decreases loss of product water through respiration. Gas flushing involves introducing a continuous gas stream to flush air out of the package. This technique only gets the O_2 down to 2−5% and is not sufficient for oxygen-sensitive foods but allows high packing rates. In compensated vacuum gas flushing, the headspace is evacuated by pulling a vacuum and then flushed with a modified atmosphere gas. This gives lower residual oxygen than gas flushing and is sufficient for oxygen-sensitive foods [11]. Vacuum packaging is a special type of MAP where the oxygen is removed from the package without replacing it with a modified atmosphere.

A simple gas flush of N_2 may be used or other gases or mixture of gases may be introduced. Table 3.3 gives a list of commonly used gases and the reasons for their use. It should be noted that completely excluding the oxygen can lead to anaerobic microbial growth, which can be deleterious as well. An example of a harmful anaerobic bacterium is *Clostridium botulinum*.

MAP may be used in combination with active packaging, such as oxygen and carbon dioxide scavengers and ethanol and carbon dioxide emitters. The specific gas mixture used depends on the product. Typically, it involves some combination of nitrogen, oxygen, and carbon dioxide. For example, a high oxygen environment is used to preserve the color of fresh red meat, CO_2 and N_2 help prevent mold in bakery items and N_2 is used to prevent rancidity in dried goods. Other examples are given in Table 3.4.

In fresh produce packaging respiration of the product changes the atmosphere within the package with time. For the full effect of MAP, the film must be permeable. Extremely permeable packages for highly

Table 3.3 Gases Used in Modified Atmosphere Packaging

Gas	Some Common Uses in Modified Atmosphere Packaging
Oxygen	Maintain red color in fresh red meat
Nitrogen	Inert gas to replace O_2 or other gas
Carbon dioxide	Acidification of water provides direct suppression of microbial growth (>10−15% CO_2); suppresses respiration of some fresh produce and can suppress ripening
Carbon monoxide	Suppresses microbial growth at low concentrations. Also helps red meat retain its red color longer. Toxic at higher concentrations so a challenge to handle
Sulfur dioxide	Helps control mold growth and microbial growth in some foods (eg, wines, fruit juices, and so on). Some people are hypersensitive to it so under scrutiny
Ethanol	Antifungal activity; retain flavor of tomatoes
Argon	Some reports of antimicrobial effect

Adapted from information in Brandenburg J. Modified atmosphere packaging. In: Yam KL, editor. Wiley encyclopedia of packaging technology. 3rd ed. John Wiley & Sons; 2009. p. 787−94.

Table 3.4 Some Modified Atmospheres Used in Food Packaging

Food Type	Modified Atmosphere	Comment
Raw red meat	20−30% CO_2, 70−80% O_2	Red color stability, microbial inhibition
Raw poultry	25−50% CO_2, 50−75% N_2 100% CO_2 (bulk package)	CO_2 inhibits microbial growth
Cooked, cured, processed meat	25−50% CO_2, 50−75% N_2	Inhibits oxidation but food poisoning from anaerobic bacteria a concern with oxygen-free atmosphere
Fish	CO_2/N_2	Inhibits aerobic bacteria and food poisoning from anaerobic bacteria a concern. Some add O_2. Store at 3°C for less than 10 days
Fresh produce	Low O_2/high CO_2	Inhibits respiration. Composition of gas specific to different types of produce
Dairy	N_2 or N_2/CO_2	Inhibits oxidative rancidity in powdered milk, cheeses, and fat spreads

Adapted from Mullan M, McDowell D. Modified atmosphere packaging. In: Coles R, McDowell D, Kirwan MJ, editors. Food packaging technology. Oxford (England): Blackwell Publishing and CRC Press. p. 303−39.

respiring foods, such as mushrooms, bean sprouts, leaks, herbs, peas, broccoli, typically use microperforated films.

In MAP, the package contents are not sterile, as in retort or other sterilization techniques. MAP only slows the degradation mechanisms. It is usually used in combination with refrigeration. In some cases, introducing a modified atmosphere that inhibits one type of spoilage mechanism may introduce another or potentially introduce conditions that may cause concerns for food safety. For example, minimizing oxygen in the atmosphere may delay oxidation, rancidity, and growth of aerobic microbes but favor the growth of harmful anaerobic microbes such as botulism. Refrigeration, limiting shelf life, and the use of preservatives may be required to maintain food safety.

3.2.5 Heat Sealing

Heat sealing involves the fusing of films together under heat and pressure. Often, a separate sealant layer is designed into a multilayer film to achieve heat sealability to prevent distortion of other layers of the film, achieve high packaging line speeds, or to seal in the presence of product contamination. Some of the commonly used sealant resins are described in Chapter 4. A discussion of the science

of heat sealing, modeling, and easy-open technology is given in Chapter 7. Here, the types of heat sealing and the basic factors that influence the quality of heat sealing are discussed.

3.2.5.1 Types of Heat Sealing

3.2.5.1.1 Bar Sealing

Bar sealing is the most commonly used method of sealing. Heated jaws are clamped down on the outside surface of the two films being joined. Heat transfers from the jaws through the film, melting the interface. The jaws are removed and the seal area allowed to cool. One or both jaws may be heated. The surface of the jaws may be coated with Teflon or another nonstick surface to prevent sticking to the outside of the film. The jaws may have a serrated design with ridges to obtain a higher seal strength. This technique is used on many laminated and coextruded structures.

3.2.5.1.2 Impulse Sealing

In impulse sealing the bar is covered with silicone rubber and a nichrome ribbon over one or both surfaces. The ribbon is covered with a Teflon-impregnated cloth. Electric current is sent through the ribbon to heat the surface. Cooling occurs with circulating water in the closed position.

Impulse sealing is slower than hot bar sealing. It is used on tacky materials and unsupported films.

3.2.5.1.3 Hot Wire or Hot Knife Sealing

Hot wire or hot knife sealing is typically used on unsupported films. The film is cut through with the hot wire forming a bead. The method is often used on shrink films but does not result in a reliable hermetic seal.

3.2.5.1.4 Hot Air/Gas Sealing

In hot air or gas sealing, the heated gas is passed over both surfaces to be sealed. When the surfaces are sufficiently heated, the gas stream is removed and the surfaces joined between chilled jaws. This technique is typically used to seal heavy or thick packaging materials, such as coated paperboard milk cartons and toothpaste tubes.

3.2.5.1.5 Pneumatic Sealing

Pneumatic sealing is used for carded skin packaging. An object is placed on a perforated paperboard. A heated film is draped over the object and board. Air is withdrawn with a vacuum through the board, collapsing the film against the object and board. The residual heat in the film creates the seal.

3.2.5.1.6 Ultrasonic Sealing

In ultrasonic sealing, a sonic horn is used to impart sound waves to hammer or rub the films together at high frequency. The friction at the interface generates heat to create the weld. This technique is good for oriented films where direct heat may distort the film. It also works well for thick films where it takes too long to transfer the heat through the film in hot bar sealing. Other advantages over hot bar sealing include the ability to seal through contamination, less heat transferred to the product, lower operating expense (since energy is only consumed during the short sealing cycle, not continuously to heat the bars), and the potential for smaller material footprint since the seal area is typically smaller than with a conventional hot bar seal. Disadvantages include the potential for squeezing out the sealant and substantially higher capital expense [13–18].

3.2.5.1.7 Induction Sealing

Induction sealing uses alternating current applied to a metal to generate the heat for sealing. Typically this is used in lidding films containing a layer of aluminum for sealing to the mouth of filled containers. Heat is generated by the electrical resistance of the foil.

Further Reading

1. Morris BA, Darby D. Sealing, Heat. In: Yam Kit L, editor. Wiley encyclopedia of packaging technology. 3rd ed. John Wiley & Sons; 2009. p. 1089–96.

3.2.5.2 Types of Seals

There are two possible configurations used when sealing a film to itself: fin and lap seals. The most common is a conventional fin seal where the inside surface is sealed to the corresponding inside surface. In multilayer films, this means the sealant layer is sealing to itself; there are no issues with poor compatibility or adhesion.

In the lap seal, the inside surface is sealed to the outside surface of the film. With a single layer film, again there is no issue with compatibility. But with

multilayer films, the choice of the sealant must be made to ensure that it seals well to the outside layer of the film.

In horizontal thermoform fill seal processes, care should be taken to ensure that the sealant layers of the top and bottom webs are compatible. For best results, using the same sealant in each film is recommended. In lidding applications, the lidding film sealant is often comprised of a different chemistry than the container to which it is sealed. Here the sealant must be chosen to wet and adhere to the container surface.

3.2.5.3 Seal Crimper and Die Design

In hot bar sealing, the leading and trailing end seals are typically sealed using a heated mechanical crimper assembly. The crimper assembly consists of a pair of dies or crimpers that have a pattern of grooves. The grooves on the top and bottom crimpers are aligned so that the peaks on the top crimper line up with the valleys of the bottom grooves. The geometry of these groove patterns, including the angle of the groove, whether the peaks are truncated (to prevent tearing of the film), depth and size of the grooves, and orientation of the grooves are important. Orientation of the grooves or serrations is usually described in relation to the longitudinal dimension of the die or bar. Horizontal serrations are parallel to the longitudinal dimension. In a typical VFFS or HFFS end seal, horizontal serrations are perpendicular to the machine direction of the film and perpendicular to the direction of pull as the packaging is opened. Vertical serrations are oriented perpendicular to the longitudinal dimension of the seal bar. Diagonal serrations of almost any angle can be found and the design of these patterns is often more art than science.

Lako Tool [19] discusses problems associated with crimp design. The crimp pattern can affect the packaging line speed. Horizontal designs (serrations parallel to the knife cut) allow for higher line speeds than vertical designs (serrations perpendicular to the knife cut). They show data generated by the Mobil Chemical Company on several polypropylene films. Horizontal serrations allow 43–67% increase in-line speed over vertical serrations at a constant seal temperature. The horizontal serration pattern also gives a wider packaging speed window (the low end of the line speed window is determined by overheating and distortion of the seal area and the high end by poor seal strength).

Theller [20] discusses serration design. Serration angle, land length, and other aspects of die geometry can be important. “In particular, improved hot tack and decreased channel leakers have been achieved with these designs.” Theller found for a (HDPE—EVA + PB) film structure (where HDPE, EVA and PB are high density polyethylene, ethylene vinyl acetate and polybutene-1, respectively), vertical serrations produced higher heat seal strength than horizontal serrations or flat bars with no serrations (horizontal serrations and flat bars gave the same seal strength). They attributed this not to changes in molecular diffusion at the sealant interface but to orientation effects with respect to the direction of stressing. Vertical serrations act as corrugations that are perpendicular to the peel front as the sample is peeled apart. The serrations act as reinforcements, requiring extra force to flatten or stretch out the corrugation as the front moves through. Horizontal serrations are parallel to the peel front and lack this reinforcing effect.

This phenomenon of high seal strength was not apparent when they sealed a more flexible, thinner LDPE film. Indeed, the vertical serrations gave slightly lower seal strengths than the horizontal serrations or flat die. They propose a model to explain the results. The serrations create a corrugation in the seal area. The sealing force is greatest in the slanted sides of the serration and lowest at the peaks and valleys since the tool is generally rounded off to prevent breakage of the film. This results in periodic sealed and lightly sealed regions. When the serrations are vertical (perpendicular to the peel front), the measured force is the sum of the fully sealed and lightly sealed regions, resulting in a lower seal value. Since the maximum measured seal strength is recorded, the horizontal serrations result in the fully sealed value and are equal to that of the flat bar.

Vertical serration designs can result in leakers. Bower [21] describes a horizontal design that is claimed to provide more shear flow and reduce leakers. The key feature of the design is interlocking crimp patterns with at least one male “land” truncated to a lower height than the corresponding groove. Other patents describe variations on crimper designs [22–28].

3.2.5.4 Factors Influencing Performance

The primary function of the seal is to prevent leaking of the contents of the package to the

environment and ingress of the environment (such as oxygen and moisture) into the package. Factors influencing the seal performance include the following:

- sealing properties of the film
- line speed
- temperature
- uniformity of temperature across the seal bar
- uniformity of pressure across the seal bar
- package design (eg, gussets)
- weight of the product (especially for VFFS)
- contamination in the seal area.

The sealing properties of multilayer film are explored in more detail in Chapter 7. The temperature range over which a quality seal can be obtained is an important consideration. If the temperature is too low, the seal strength may be variable. If it is too high, the film may distort or tear. The optimum seal temperature range is a function of the sealing time (known as the dwell time), film thickness, and the thermal and physical properties of the film. Time and temperature are inversely related. As is described in Chapter 7, sufficient time and temperature are needed for polymer melting, diffusing and strength building at the sealant interface. Increasing the temperature generally speeds up this process until the ultimate strength is reached. In a typical heat seal curve (Fig. 3.8), the seal strength as a function of seal bar temperature is plotted. Seal strength is zero at low temperatures until at some point the seal strength begins to increase. This point is known as the heat seal initiation temperature (HSIT). At higher temperature the seal strength levels off to the ultimate seal strength. The point where it starts to level off is known as the plateau initiation temperature. The HSIT and plateau initiation temperature are related to the melting behavior of the polymer [29].

Thickness influences the time it takes the heat to reach the interface in hot bar sealing. The transfer of heat from the outside surface to the interface is roughly proportional to the square of the thickness. As a result, at a given dwell time, the HSIT may be higher for thicker films [30].

The upper end of the sealing temperature range is influenced by the physical properties of the film. Shrinkage and distortion of the film may occur at elevated temperatures. Often at the ultimate seal strength, the seal strength exceeds the tear resistance

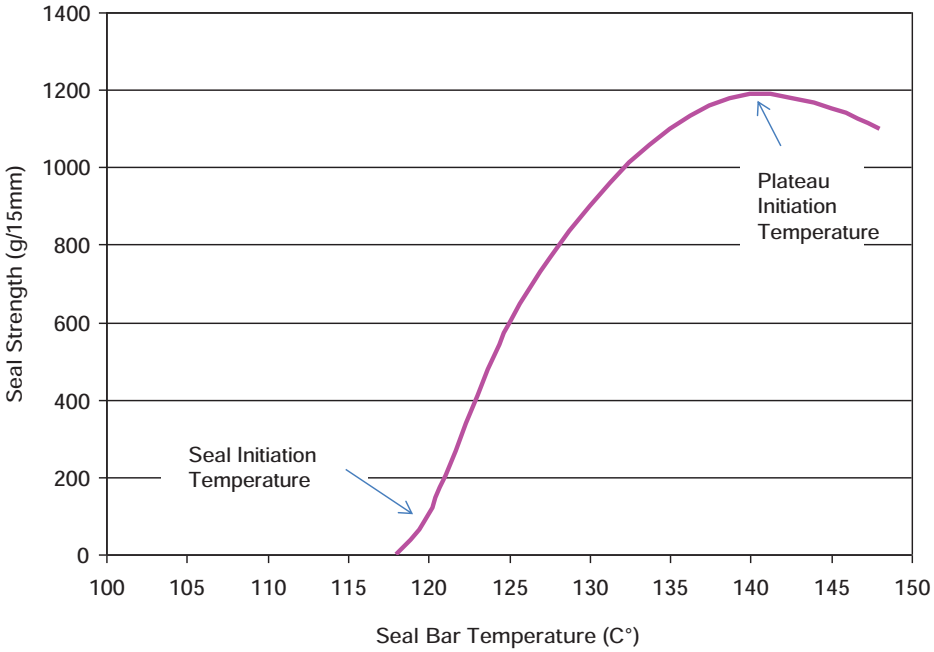


Figure 3.8 Heat seal curve. Center portion of the curve represents the heat seal window or temperature range for optimum sealing.
Reproduced with permission from E. I. du Pont de Nemours and Company.

of the film. The tear resistance may be weakened as the result of some of the film having been squeezed out during the heat seal process at high temperatures and pressures.

Increasing packaging line speed reduces the dwell time for sealing. The exact relationship between line speed and dwell time depends on the fraction of the machine cycle time devoted to sealing. With registration, cutting, and other operations, the sealing may be 50% or less of the cycle time. For example, if the machine is running at 60 packs per minute and half the cycle time is devoted to sealing, the dwell time is 60 packs/min $\times$ min/60 s $\times$ 0.5 = 0.5 s.

The seal bar temperature may vary throughout the day as the packaging machine is slowed down or sped up. The temperature may also not be uniform across the width of the bar. This is shown in a study by DuPont where measurements were made on several commercial scale packaging lines at their technical service laboratory. Four different pieces of equipment are studied using thermocouples and a data logger to simultaneously record the temperatures at three places across the seal bar. The temperature set points are chosen to represent the normal operating range of the machine. The temperatures are recorded long enough to capture drift from the on/off of the heating cycle. The trials are done in a static state with no film. Results from the study are given in Fig. 3.9. Variation from the set point is as high as 54°C.

Some of the possible causes for such variation include maintenance and cleanliness of the machine, calibration of the machine's sensors, controlling thermocouple position (is it properly situated in the thermocouple well?), and machine design

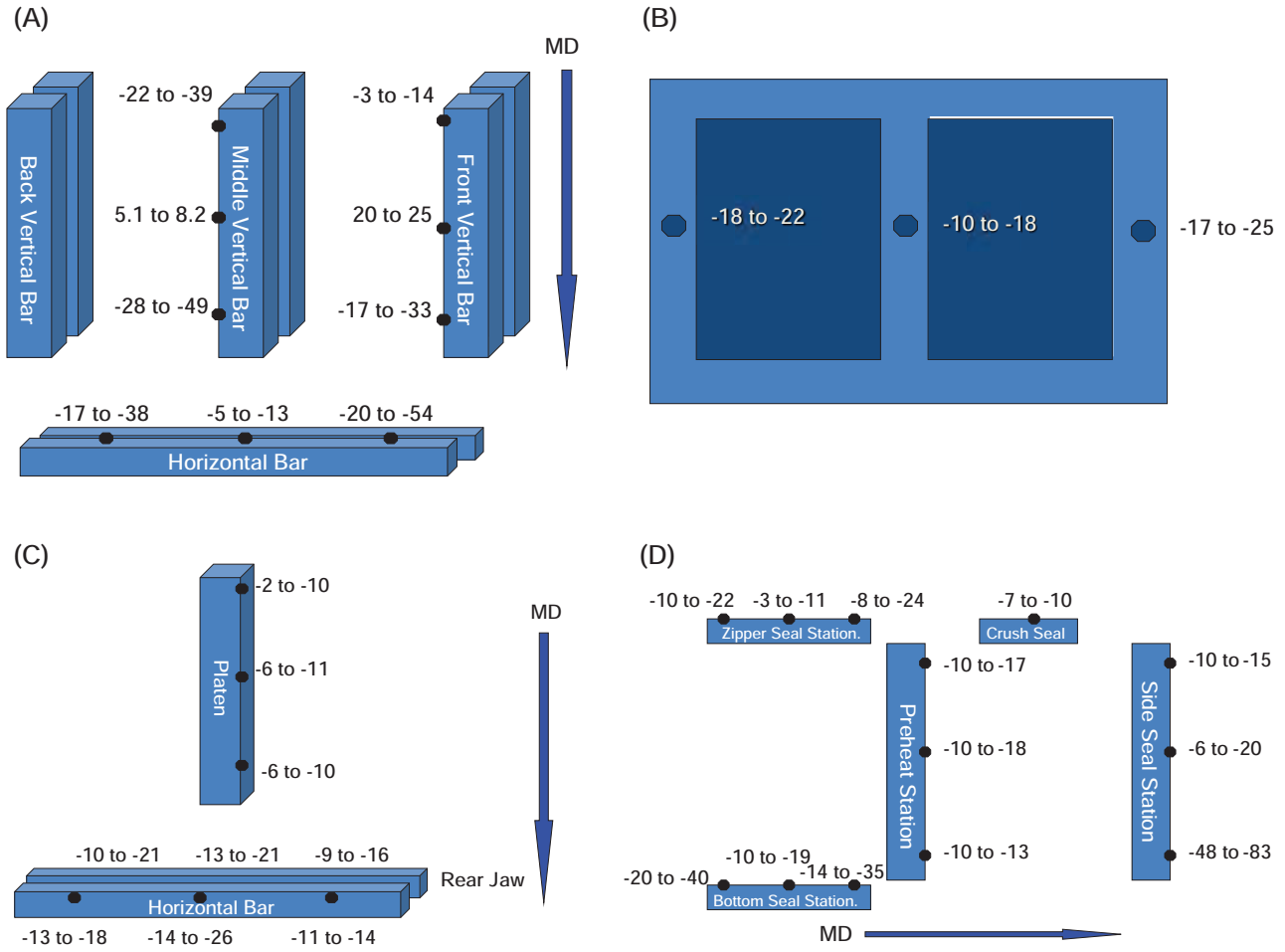


Figure 3.9 Measurements of temperature variation (deviation from set point) across heat seal bars on commercial scale packaging lines: (A) vertical liquid pouch line, (B) horizontal thermoform fill seal line, (C) vertical form fill seal line, (D) stand-up pouch line.

Reproduced with permission from E. I. du Pont de Nemours and Company.

considerations. Advances have likely been made in temperature control since this study was made, but it underscores the amount of variation that is possible.

Pressure is an another factor in seal performance. Sufficient pressure is needed for the surface of the two films to be in intimate contact for molecular diffusion to occur. Too much pressure, however, can result in squeezing out of the sealant from the seal area, causing poor seal strength and tearing. This is covered in more detail in Chapter 7. Variation in pressure across the seal bar can also result in seal issues. Misalignment of the seal jaws, bowing of long seal bars, and crimp patterns are possible causes of pressure variation.

Gussets or folds in the seal area are a particular challenge for hot bar sealing. The folded areas are thicker than the rest of the seal area, resulting in longer times needed to obtain a good seal. Gussets may also affect the pressure distribution along the seal bar with the gusseted areas experiencing high pressure and the other areas lower pressures.

Gussets also tend to spring back after sealing while the seal area is still warm and the sealant has not had time to solidify. The resistance of the sealant to opening forces such as spring back in HFFS or the weight of the package in VFFS is known as hot tack (Fig. 3.10). Hot tack is an important consideration in selecting a sealant and is dealt with in considerable detail in Chapter 7. In general, polymers with greater melt strength have higher hot tack performance.

Contamination of the seal area with powdery or greasy product during filling may affect seal performance. Equipment design can help reduce the potential for contamination, but in industrial environments contamination is always a possibility. The film may build up a static charge during handling that attracts powder contamination. Static charge mitigation is a key component for preventing contaminated seals. Optimum sealant selection may also help reduce sealing issues due to contamination. There is no generally accepted laboratory method for comparing sealing performance in the presence of contamination. This topic is discussed in greater detail in Chapter 7.

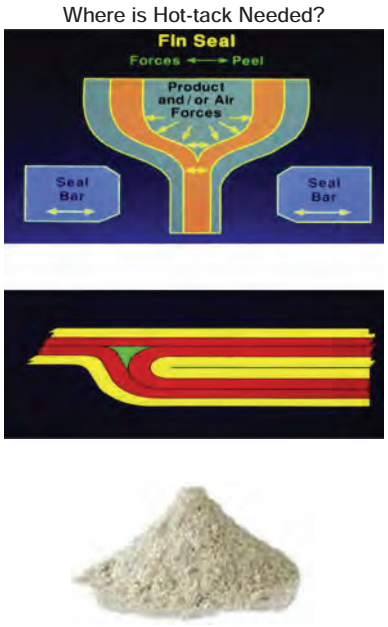


Figure 3.10 Importance of hot tack.
Reproduced with permission from E. I. du Pont de Nemours and Company.

References

[1] Gresher JM. Carded packaging. In: Bakker M, editor. Wiley encyclopedia of packaging technology. New York: John Wiley & Sons; 1986. p. 124–32.

[2] ASTM International. D1894–11: standard test method for static and kinetic coefficients of friction of plastic film and sheeting. 2011.

[3] Eval Americas. Thermoforming of Eval® resin containing structures. Technical bulletin no. 150. http://www.eval.eu/media/36418/ea%20-%20technical%20bulletin%20no%20150.pdf.

[4] Eval-Americas. EVAL™ products. http://www.eval-americas.com/us/about-eval/eval-products.aspx.

[5] Nippon Goshei. Grade lineup. http://www.soarnol.com/eng/grade/index.html.

[6] Chou RT, Deak GI, DuPont. Blends of ethylene vinyl alcohol copolymer and amorphous polyamide, and multilayer containers made. U.S. Patent 4,990,562. 1991.

[7] Fetell AI. Nylon-containing ionomer improves the performance of ethylene vinyl alcohol (EVOH) copolymers in multilayer structures. In: TAPPI polymers, laminations & coatings conference; 1997. p. 503–5.
[8] W.A. Oberle, (DuPont), 1998, Process for thermoforming EVOH barrier sheets and products relating hereto, European Patent EP0699125 B1.
[9] Madison D. Filling machinery, by count. In: Bakker M, editor. Wiley encyclopedia of packaging technology. New York: John Wiley & Sons; 1986. p. 294–5.
[10] Bardsley RF. Filling machinery, dry-product. In: Bakker M, editor. Wiley encyclopedia of packaging technology. New York: John Wiley & Sons; 1986. p. 295–300.
[11] Mullan M, McDowell D. Modified atmosphere packaging. In: Coles R, McDowell D, Kirwan MJ, editors. Food packaging technology. Oxford (England): Blackwell Publishing and CRC Press. p. 303–39.
[12] Brandenburg J. Modified atmosphere packaging. In: Yam KL, editor. Wiley encyclopedia of packaging technology. 3rd ed. John Wiley & Sons; 2009. p. 787–94.
[13] Considine D. Ultransonic packaging sealing – technology and applications review. Bartlett (IL): Herrmann Ultrasonics; March 22, 2007.
[14] Bach S, Bunk N, Majschak J-P. Effect of laminate structure and morphology on fracture mechanics and seam strength of sealed seams. In: TAPPI European PLACE Conference, Dresdon, Germany; 2013.
[15] Dun J, Bensasson S, Thürling K. Polyolefins for ultrasonic sealing. In: TAPPI European PLACE Conference, Dresdon, Germany; 2013.
[16] Thurling K, Bach S, Maschak J-P, Nase M. Influence of material parameters on the ultrasonic sealing behavior of polymer films for packaging. In: 14th International scientific conference "polymer materials", Halle, PT67; 2010.
[17] Suresh KS, Rani MR, Prakasan K, Rudramoorthy R. Modeling of temperature distribution in ultrasonic welding of thermoplastics for various joint designs. J Mater Process Technol 2007;186:138–46.
[18] Tateishi N, North TH, Woodhams RT. Ultrasonic welding using tie-layer materials. Part I: analysis of process operation. Polym Eng Sci 1992;32(9): 600–11.
[19] Lako Tool. Solutions. http://www.lakotool.com/solutions.htm.
[20] Theller HW. Heat sealability of flexible web materials in hot-bar sealing applications. J Plast Film Sheeting 1989;5(1):66–93.
[21] Bower, W.B.., (Crown Zellerbach Corporation) 1986, Heatseal die, U.S. Patent 4,582,555.
[22] Montano, L.M. and Smith, L.E.., (Lako Tool and Manufacturing) 2013, Split crimper for heat sealing packaging material, US Patent 8,387,344B2.
[23] Knauf, R.L. and Menzner, D.F.., (Marathon Cheese Corporation) 1977, Seal for plastics capable of thermoplastic sealing and means for effecting such sealing, U.S. Patent 4,001,075.
[24] Smith, L.E.., 1987, Crimper bar set for forming hermetically sealed packages, U. S. Patent 4,807,426.
[25] Smith, L.E.., (Lako Tool & Manufacturing, Inc..) 2001, Crimper assembly for sealing overlapping portions of a sheet of packaging material, U. S. Patent 6,230,781B1.
[26] Stevens, D.J.., (Cryovac Australia Pty Ltd..) 2005, Sealing assembly, U. S. Patent 6,877,542 B2.
[27] Montano, L.M. and Smith, L.E.., (Lako Tool and Manufacturing) 2011, Split crimper for heat seal packaging material, U.S. patent 7,941,991 B2.
[28] Montano, L.M. and Smith, L.E.., (Lako Tool and Manufacturing) 2004, Crimper assembly for sealing overlapping portions of a sheet of packaging material, U. S. Patent 6,736,182 B2.
[29] Stehling FC, Meka P. Heat sealing of semicrystalline polymer films. II. Effect of melting distribution on heat-sealing behavior of polyolefins. J Appl Polym Sci 1994;51:105–9.
[30] Morris BA. Predicting the heat seal performance of ionomer films. J Plast Film Sheeting 2002;18(July):157–67.
[31] Moyer G. Form/fill/seal, vertical. In: Bakker M, editor. Wiley encyclopedia of packaging technology. New York: John Wiley & Sons; 1986. p. 367–9.
[32] Hughes AA. Food packaging machinery. In: Ebnesajjad, editor. Plastic films in food packaging. Elvesier; 2013. p. 210.

4 Commonly Used Resins and Substrates in Flexible Packaging

Material selection is the key to packaging performance. This chapter introduces some of the important characteristics of commonly used materials in flexible package.

4.1 Resin and Substrate Function

As introduced in Chapter 1, the basic purpose of a flexible package is to provide protection (including structural integrity, barrier, sealing, and adhesion) and promotion (which may include aesthetics, printability, and so on). In multilayer films, a specific combination of materials is selected to meet the functional requirements in the most economical manner. Often materials used in flexible packaging provide more than one function. For example, high density polyethylene (HDPE) in a cereal liner bag-in-box structure provides stiffness, puncture resistance, and moisture barrier. As more layers are incorporated into flexible packaging, the contribution of the each of the layers has become more specialized.

4.1.1 Structural Integrity

Structural integrity involves ensuring the package has enough strength to hold up during the packaging process and the end use, has sufficient stiffness to be easily handled on the packing line and in some cases for the end use (such as for stand-up pouches), and survive abuse. Some of the specific properties that are used to gauge whether the material provides structural integrity are tensile strength, yield strength, elongation at break, modulus, tear strength, impact strength, and puncture resistance.

Stiff materials are generally used for structural integrity, such as paper, oriented polypropylene (OPP), or oriented polyester (OPET).

Temperature is a factor in selecting materials for structural integrity. High temperature may melt or distort the polymer or substrate, resulting in poor performance. Low temperatures can also be a problem, especially when it comes to toughness. Many materials become brittle at low temperatures.

4.1.2 Barrier

Moisture, oxygen, carbon dioxide, and light barrier are the four most common barrier needs in flexible packaging. Oil and grease barrier is another need for some applications. The amount of barrier required depends on the product being packaged and the shelf life requirements. Gas barrier is generally characterized by the permeability of the gas through the film. Permeability is inversely related to barrier; the higher the permeability, the lower the barrier performance. The gas barrier of many resins and substrates is influenced by environmental factors such as temperature and relative humidity (RH). It is important, therefore, to select materials that have the required barrier performance under the conditions of the end use.

Highly crystalline polyolefins such as HDPE and polypropylene (PP) are often the most cost-effective moisture barrier materials. Polyvinylidene chloride (PVDC), cyclic olefin copolymers (COCs), and chlorotrifluoroethylene (CTFE) are used for more specialized applications. Aluminum foil and metallized film are also used for moisture barrier.

Polar polymers such as ethylene vinyl alcohol (EVOH), polyvinyl alcohol (PVOH), and PVDC provide an outstanding oxygen barrier performance. Aluminum foil and metallized film also provide an exceptional oxygen barrier. Polyamide 6 (PA6) and polyethylene terephthalate (PET) provide moderate barrier to oxygen.

Light barrier is typically provided by adding opacifiers such as titanium dioxide (TiO_2) into one or more layers, through metallization, or by incorporating aluminum foil.

Oil and grease resistance is generally improved with higher crystallinity and/or polarity of the polymer. HDPE provides better oil resistance than LDPE due to its higher crystallinity. Polar polymers such as

The Science and Technology of Flexible Packaging. http://dx.doi.org/10.1016/B978-0-323-24273-8.00004-6
Copyright © 2017 Elsevier Inc. All rights reserved.

PA, PET, and PVDC also provide excellent oil resistance.

4.1.3 Sealing

The sealant layer is the innermost layer of the flexible packaging structure. Its chief function is to provide a hermetic seal to keep the contents of the package in and contamination out. For high-speed packing operations, low seal initiation temperature is desired to achieve short sealing times. Heat is applied to the outside surface of the film and transfers inward, melting the sealant. The seal initiation temperature is the minimum temperature at which seal strength is obtained (see Chapter 7 for details.) The melting point of the polymer is a primary determinate of the seal initiation temperature; above the melting point the polymer chains have mobility to interdiffuse and build strength during the sealing process. Therefore, polymers with low melting points generally make good sealants. As a class, the ethylene copolymers such as ethylene vinyl acetate (EVA) copolymer, low density polyethylene (LDPE), linear low density polyethylene (LLDPE), and ionomers have low melting points and provide low seal initiation temperature.

Other factors involved in selecting the sealant resin are hot tack (the ability of the seal to withstand opening forces prior to solidification) and seal through contamination such as greasy food or powders. The sealant may also contribute to other functions of the package such as optical clarity, puncture resistance, and stiffness.

4.1.4 Adhesion

Many of the resins and substrates used in multilayer flexible packaging do not bond well to each other. Adhesives are used to tie the layers together so that the package behaves as a single entity. There are generally two types of adhesives used in flexible packaging: liquid adhesives used in adhesive lamination and polymer adhesives used in coextrusion or extrusion coating. The liquid adhesives are water, solvent, or "solventless" adhesives that are designed to bond films together during lamination. They require heat after application to remove the solvent or water, or to provide curing.

The polymer adhesives are applied in the molten state and require cooling after application. Ethylene copolymers such as EVA, EMA (ethylene methyl acrylate) copolymer, EAA (ethylene acrylic acid) copolymer, and special maleated grades of PE are often used as tie resins. The polar comonomer helps bond to polar substrates whereas the nonpolar ethylene component of the copolymer helps tie to nonpolar substrates such as PE. The coating process may also impart polarity and functionality. For example, LDPE is often run at elevated temperatures ($\sim$320°C) in extrusion coating to promote the formation of acids, aldehydes, and ketones that help bond to aluminum foil.

4.1.5 Aesthetics

Optical clarity and transparency are important for some packaging applications. For these the substrates need to be selected to have good transparency in addition to performing their primary function. For example, a clear barrier polymer such as EVOH or PVDC would be favored over an opaque barrier such as a metallized film for a transparent package.

Printability is an another factor in selecting substrates. For good printing, paper may be treated or calendared. OPET is often favored in applications requiring a stable print surface.

4.1.6 Typical Properties

Table 4.1 provides some typical properties and test methods that characterize the functionality of various resins and substrates used in flexible packaging. These are just a starting point, as many applications have more targeted performance tests that have been developed to determine if a packaging structure will meet the needs of the end use. Most of these properties are material properties. A key consideration is translating material properties into a set of specifications for packaging performance. For example, what tensile strength or impact resistance test values are needed for the package to survive the packing and transportation process? Often, material specifications are just a starting point. In the ultimate assessment the structure is prototyped and tested on an actual packaging line to simulate the abuse it may be exposed to during transportation, distribution, and retail. This is done either in the lab or through actual shipping tests.

Table 4.2 lists some of the common resins used in flexible packaging and the functions they most often provide. Table 4.3 provides a range of typical

Table 4.1 Typical Properties for Flexible Packaging Films

Property	ASTM Method	Why It Is Important
Density	D792	Enters into cost (per area), needed for layer control
Melt flow rate	D1238	Indicates flowability in a polymer process; inversely related to viscosity and molecular weight; typically used for polyolefins
Viscosity (melt or solution)	Various	Processing
Secant or tensile modulus	D882	Helps determine how stiff the package will be; also related to strength, integrity, impact resistance, and puncture resistance
Tensile strength	D882	Important for gauging the strength of the package
Elongation at break	D882	Related to toughness
Tear strength	D1922 (Elmendorf) D1004 (Graves)	Notched or unnotched tear resistance
Melt temperature (semicrystalline polymers)	D3418	Related to seal initiation temperature; determines extrusion temperature
Glass transition temperature (T_g)	E1356 (DSC) E1640 (DMA)	Need to be above T_g to melt process; material becomes brittle below T_g
Freezing temperature	D3418	Affects how fast the film quenches in converting processes
Vicat softening temperature	D1525	An indication of temperature resistance
Impact strength	D3420 (Spencer) D1709 (Dart Drop)	High speed impact toughness
Puncture resistance	F1306, D2582	Slow speed puncture resistance
Clarity, haze, gloss	D1746 (clarity) D1003 (haze) D2547 (gloss)	Optical properties
Oxygen permeation value	F1927, D3985, F2622	Inversely related to oxygen barrier
MVTR	F1249, E96	Inversely related to moisture barrier

properties for several frequently used resins in flexible packaging. These data were taken from a number of sources. A common problem with comparing material properties from multiple sources is that differences in test methods and the method of fabricating the samples may have a significant impact on the measured values. For example, films made on cast and blown film processes will likely have differences in machine and transverse direction physical properties. Even with samples prepared on the same type of fabrication process, differences in processing conditions may impact the properties. One should be careful about comparing property data from different sources.

Table 4.2 Function of Commonly Used Resins in Flexible Packaging

Resin	Sealant	Tie-Layer Adhesive	Barrier	Structural Layer
LDPE	X	X		X
LLDPE	X			X
HDPE			X	X
PP	X		X	X
PS				X
PET	x			X
PVC				X
EVA	X	X		X
Ionomer	X	X		
EMA	X	X		
ACR (EAA or EMAA)	X	X		
Tie resin		X		
PA			X	X
EVOH			X	
PVDC			X	
PLA				X

Abbreviations can be found in Appendix A.

4.2 Commonly Used Resins in Flexible Packaging

This section provides a brief introduction to frequently used resins in flexible packaging, highlighting their chemistry, key properties and typical applications.

4.2.1 Polymer Chemistry as It Relates to Packaging Performance

The term polymer comes from the Greek "poly" and "mer," meaning many mers or repeat units. Polymers are long chain molecules made up of numerous reoccurring units or groups of atoms. A number of aspects of polymer chemistry and technology are introduced in this section that lay a groundwork for understanding the chemistry of the polymers used in packaging.

4.2.1.1 Molecular Weight

The molecular weight (MW) of a polymer is directly related to the number of repeat units on the polymer chain. The longer the chain, the higher is the MW. The polymers used in flexible packaging generally have a high MW. Polymers with low MW tend to be brittle since individual chains may be easily pulled away from the others. Polymers gain strength once they are long enough to become entangled. The entanglement MW is a characteristic of the polymer that varies with chemistry. For the most part, polymers with an MW of greater than 1000 repeat units are used in packaging [17].

4.2.1.2 Molecular Weight Distribution

An inherent consequence of the polymerization process is that not all the polymer chains are the same length. There are a number of ways to characterize molecular weight distribution (MWD), the two most common being the number average molecular weight (M_n) and the weight average molecular weight (M_w). Mathematically, these are given by:

$$M_n = \sum_{i=1}^{\infty} n_i M_i = \frac{\sum_{i=1}^{\infty} N_i M_i}{\sum_{i=1}^{\infty} N_i} \qquad (4.1)$$

Table 4.3 Typical Property Values of Commonly Used Resins in Flexible Packaging

Property	Method	Units	LDPE	LLDPE	*m*-LLDPE	mPE Plastomer	EVA (18% VA)	Ionomer	HDPE	Cast PP	OPP	BOPET	PA 6	EVOH (32 m% ethy)
Density	ASTM D792/ D1505	g/cc	0.92–0.93	0.91–0.93	0.91–0.93	0.9–0.91	0.94	0.95	0.96	0.9	0.9	1.39	1.15	1.18
Tensile strength at break (MD/ TD)	ASTM D882	MPa	26/22	50/35	53/41	60/50	31	24–37/ 23–41	80/37	45/38	140/240	200/235	90–120	71
Elongation at break (MD/ TD)	ASTM D882	%	130/540	570/850	500/700	560/750	530	300– 500/300 –450	420/4	650/700	180/60	116/91	300–900	230
Secant modulus	ASTM D882	MPa	240/290	190/220	192/201	73/77	48	150–480	1100/ 1600	480/450	1720/ 3100	4900/ 5100	600– 1000	2400–3000
Elmendorf tear (MD/TD)	ASTM 1923	g/μm	10/2.7	3/16	11/17	4/7	7	0.1–1.5	1.2	0.8/3.5		1.2/1.2	2/5	0.5/0.6
Dart impact strength	ASTM D1709A	g/μm	3.1	4	22	21		6–14	<1.5	6				
Melting point	DSC	°C	110–113	121	119	92	89	92–100	135	145–161	161	254	220	183
Vicat	ASTM D1525	°C	96	94	102	84	69	65–79	125–129					
MVTR, 38 C, 90% RH		g-mil/ m2-day	15–20	12–18	12–18	18–23	110	18–24	6–12	12.4	6	20	70	75.6
OPV, 23 C, 45% RH		cc-mil/ m2-day	8000	8500	8500	8,000– 12,000	15,000	5200 –8200	3000	2790	2300	70	280	0.5
References			[3,7]	[8,16]	[5,16]	[6,16]	[10]	[11]	[9,16]	[12]	[13,14]	[1–3]	[4]	[15]

$$M_w = \sum_{i=1}^{\infty} w_i M_i = \frac{\sum_{i=1}^{\infty} N_i M_i^2}{\sum_{i=1}^{\infty} N_i M_i} \tag{4.2}$$

where M_n, number average molecular weight; M_w, weight average molecular weight; N_i, number of molecules of chain length i; M_i, molecular weight of molecules with chain length i; n_i, number fraction of molecules of chain length i, $\frac{N_i}{\sum_{i=1}^{\infty} N_i}$; w_i, weight fraction of molecules of chain length i, $\frac{N_i M_i}{\sum_{i=1}^{\infty} N_i M_i}$.

M_n is highly influenced by the short chain molecules, whereas M_w is more heavily influenced by the longer chains. In general, $M_n < M_w$ unless all the chains are the same length. The use of M_n over M_w or other representations depends on the property; some properties correlate well with M_n, others with M_w or other variations of average MW. Modern techniques to measure MW and MWD typically employ gel permeation chromatography, which involves dissolving the polymer and detecting the size via a number of sensors, which taken together can provide information on M_n and M_w.

The ratio of M_w to M_n is known as the polydispersity index (PDI):

$$\text{PDI} = \frac{M_w}{M_n}. \tag{4.3}$$

Polymers such as PA or PET made by condensation polymerization have a theoretical PDI of 2. Polyolefins, made via a free radical or coordination catalyst polymerization process, generally have a higher PDI.

MWD influences the flow or rheological properties of the polymer. In general broad MWD polymers tend to be easier to melt process. Their viscosities tend to decrease with increasing shear rate, which has advantages in a number of polymer processes. This is discussed in more detail in Chapter 5.

4.2.1.3 Crystallinity

In some polymers, the chains organize into ordered structures known as crystals. Steric hindrances and other considerations prevent all the chains from participating in the crystals; hence this class of polymers is known as semicrystalline polymers. The noncrystalline regions are known as amorphous regions. Common semicrystalline polymers include polyethylene, PP, PA6, EVOH, and PET.

Some polymers such as polystyrene (PS) are amorphous; they lack any crystalline regions.

Semicrystalline polymers have melting and freezing points, although these generally occur over a broader temperature range than low MW molecules. The breadth of the melting point range impacts heat seal and other properties. For example, the melting point of LLDPE is often reported at 121°C, which represents the peak of the melting endotherm in a differential scanning calorimeter measurement. However, the crystals do not completely melt until around 130°C. It is this temperature that corresponds to the ultimate seal strength [18].

The long chain nature of polymers also impacts the rate of which the polymer freezes from the melt. Some polymers form crystals relatively slowly so that the fabrication process can have a substantial impact on final properties. An example is PET. Its slow rate of crystallization is taken advantage of when making film and sheet. In the APET (amorphous polyester) process, the film/sheet is rapidly quenched so that the PET remains in the amorphous state (polymer melts are amorphous since all the crystals have been melted). The resulting sheet is transparent and pliable but has poor temperature resistance. Applications include thermoformed containers for refrigerated foods. The amorphous sheet can be stretched into biaxial oriented film (BOPET). During the stretching process, the polymer chains align and organize into crystals, producing a transparent, tough semicrystalline film. In the CPET (crystalline PET) process, a nucleating agent is added to the PET so that when it is quenched into a sheet it crystallizes. The crystals form large structures called spherulites that diffract light. The resulting sheet is opaque but has good temperature stability and heat resistance. Trays made from CPET are used for packaging dual ovenable foods, which can be heated up by the consumer in a microwave or convection oven. A consequence of the large crystals is poor low temperature toughness; ethylene copolymers are often added for freezer applications to improve impact resistance [19–22].

The above example shows that the presence and morphology of the crystals affect properties. Some of the typical properties influenced by crystallinity include the following:

- Stiffness. The mobility of the polymer chains is impeded by the presence of the crystals, increasing the stiffness or modulus.

- Melting point. Higher levels of crystallinity often result in higher melting point and greater heats of fusion.
- Barrier. The crystals may impede the transport of liquids or gases through the polymer, reducing permeability.
- Optical properties. The crystals often are large enough to diffract light, causing a reduction in transparency and an increase in haze.

Polyethylene is a semicrystalline polymer. The amount of crystallinity is controlled by the level of short chain branching and is characterized by the density. Density is inversely proportional to volume. Polymer with a higher level of crystallinity has a lower volume per unit mass or higher density since the chains are packed closer together in the crystalline phase than in the amorphous phase. HDPE has a crystallinity of around 50−60% and LDPE around 20−30%. Compared with LDPE, HDPE has higher moisture barrier (lower moisture vapor transmission rate or MVTR), a higher melting point (135 vs. 110°C), higher modulus [760 MPa (110 kpsi) vs. 140−210 MPa (20−30 kpsi)], and higher haze.

The size, shape, and organization of the crystals, known as the crystalline morphology, influence properties. The differences in crystalline morphology in OPET and CPET are discussed above. Another example is PP. Standard PP forms large spherulites when made into sheet or film. Nucleating agents are often added to PP to improve its clarity. The nucleating agent forms many sites upon which the crystals can initiate. This not only increases the speed of crystallization but because so many additional sites have been created, the resulting size of the growing crystals is smaller. The smaller crystals diffract less light. The result is clarified PP.

Quench rates and orientation during film fabrication can affect the amount of crystals and their morphology. In general, faster quench from the melt to solid results in a lower level of crystallinity. Cast film often has lower haze than blown film due to the faster quench rate in cast film. Orientation also influences the morphology of the crystals. The crystals in PE, for example, have been observed to change from a twisted ribbon to a row nucleation morphology with low and high orientation processes [23].

4.2.1.4 Polymerization Process

The polymerization process affects the molecular characteristics such as MW and MWD. The three main processes for manufacturing polymers used in flexible packaging are briefly described below.

4.2.1.4.1 Free Radical

Free radical or addition polymerization involves a chain reaction with unsaturated monomers, such as vinyl molecules, forming long polymer chains. Vinyl molecules have a double bond of the type CH_2═CHX and CH_2═CXY where X and Y represent a number of possible chemical moieties, such as a hydrogen atom (ethylene), a methyl group (propylene), or a benzene ring (styrene). Not all vinyl molecules polymerize into high MW polymers. Homopolymers of ethylene (resulting in LDPE), various copolymers of ethylene and vinyl monomers such as vinyl acetate, and polystyrene are the most important examples of free radical polymers used in flexible packaging.

Vinyl free radical polymerization involves several steps:

- Free radical generation. Typically thermal or photochemical degradation of peroxide is used to generate intermediates known as free radicals, which result in very reactive unpaired electrons.
- Initiation. The free radicals combine with the vinyl molecule to add to the double bond, creating a new radical. The regeneration of the free radical is the hallmark of a chain reaction.
- Propagation. The chain radical adds successive monomers to grow the polymer chain.
- Termination. Propagation could go on indefinitely until all the monomer is consumed but for the fact that some free radicals combine to form a paired electron covalent bond and a loss of free radical activity. Typically the reaction is run so that only a small amount of free radicals are created to reduce the probability of termination.
- Chain transfer. The free radical can be transferred to other species. This may be used to control molecular weight (by creating additional polymer molecules for each radical chain initiated). It also leads to the formation of branches, which has a substantial impact on MWD and properties.

Because of the nature of the chain addition process, the MWD of free radical polymerized polymers can be broad.

4.2.1.4.2 Coordination

Coordination or stereospecific polymerization involves directing the monomers in their approach to the growing polymer chain. Most often coordination polymerization is conducted using a catalyst in the form of a slurry or supported gas phase (fluidized bed) reactor. The technology came into existence with the work of Ziegler and Natta in the 1950s, resulting in the highly successful commercialization of linear polyethylene (both HDPE and LLDPE) and PP.

Ziegler–Natta catalysts are formed by complexes of alkyls of metals from groups I–III with halides and other derivatives from the transition metals of groups IV–VIII in the periodic table [25]. Solid and supported catalysts based on titanium represent an important class, which are typically used with a cocatalyst such as organoaluminum. More recently, metallocene catalysts, representing a combination of mono and bis-metallocene complexes of titanium, zirconium, or hafnium have been developed. Complexes of transition metals with multidentate oxygen- and nitrogen-based ligands represent another class of these catalysts [26].

Chromium-based catalysts are another type of commercially important coordination catalysts used to make HDPE [27].

The mechanisms of these catalysts are beyond the scope of this introductory chapter. In brief, these catalysts control the approach and regularity of the growing polymer chain through the formation of complexes. Advances have led to a number of technologies, including heterogeneous catalysts with multimodal comonomer or MW distributions, stereospecificity (especially for PP), and narrow comonomer and MW distributions. The consequences of these catalysts on the properties of polyethylene and PP are reviewed later in this chapter.

4.2.1.4.3 Condensation

Condensation polymerization generally involves stepwise reactions that result in the loss of a small molecule such as water at each reaction step. Many polymers are produced via condensation polymerization but the two most important for packaging applications are polyester and polyamide (nylon).

For example, PET can be synthesized by reacting terephthalic acid and ethylene glycol, liberating water, as shown in the following equation:

$$n\,C_6H_4(CO_2H)_2 + n\,HOCH_2CH_2OH \rightarrow [(CO)C_6H_4(CO_2CH_2CH_2O)]_n + 2n\,H_2O \tag{4.4}$$

PET can also be polymerized by reacting dimethyl terephthalate and ethylene glycol, liberating methanol.

Following the work of Flory, a statistical analysis shows that the distribution of polymers made via condensation polymerization follows the following relationship [28,29]:

$$\frac{M_w}{M_n} = 1 + p. \tag{4.5}$$

where p, extent of reaction.

For high molecular weight polymers, the extent of reaction is large and approaches a value of 1. The PDI approaches 2.0, which has been observed experimentally. PET and nylon generally have narrow MWD, which poses some processing issues that are discussed in Chapter 5.

4.2.1.5 Molecular Forces

The nature of the chemical bonds that hold polymers together influences their properties. This section reviews the main types of molecular forces acting on polymers used in packaging.

4.2.1.5.1 Primary Bonds

The covalent bond is the primary type of molecular force linking atoms within the polymer chain. Covalent bonds form when one or more pairs of valence electrons are shared between atoms. Bonds between carbon atoms are covalent bonds.

Ionic bonds involve an electrostatic attraction between oppositely charged ions, typically a metal salt and an electron donor. Sodium chloride is an example for small molecules. Ionic bonding does not usually come into play for polymers used in packaging, except for a special type of polymer called an ionomer. Ethylene-based ionomers are used in

flexible packaging. These are ethylene methacrylic or acrylic acid copolymers that are partially neutralized with metal cations such as zinc or sodium. The ionic interactions form a cross-link-like structure that is melt reversible. Such polymers have an attractive balance of properties, especially for heat seal applications.

4.2.1.5.2 Secondary Bonds

Bonds not associated with filling the outer electron shells are generally known as secondary forces. These are considerably weaker than the primary bonds, but because they may occur in large numbers, especially between polymer chains, they can have a considerable impact on the properties of polymers.

Dipole forces exist when atoms within the molecule carry equal and opposite charges, forming a dipole moment. These molecules are said to be polar. At short distances, these forces provide an attractive force. The strength of these forces depends on the alignment of the dipoles which can be disrupted by thermal motion. Hence these forces are strongly dependent upon temperature.

A polar molecule can induce a temporary dipole moment in a nearby nonpolar molecule. This interaction between polar and induced dipoles is called an induction force. The strength of this force is dependent on the polarizability of the molecule and is independent of temperature.

Dispersion forces exist between nonpolar molecules. They arise from temporary perturbations in the electron clouds surrounding neighboring molecules, creating time varying dipole moments. They are independent of temperature and are the main secondary force acting on polymers unless strong dipoles are present.

Hydrogen bonding is ionic in character. It typically involves an interaction between hydrogen present in an acid group with a basic oxygen atom (such as in carbonyls, ethers, or hydroxyls) or nitrogen in amines or amides. They influence the properties of polar molecules like nylon and many proteins. Properties may be susceptible to moisture.

4.2.1.5.3 Effect of Bonding on Polymer Properties

The strength of a polymer's intermolecular forces impacts its physical properties. (*Inter*molecular forces refer to interactions between polymer chains, as opposed to *intra*molecular forces which involve bonding within the polymer chain.) Polymers with weak intermolecular forces are more flexible and elastomeric in nature. Strong interactions increase stiffness and strength. Polar interactions contribute to the high stiffness and strength of polyesters and polyamides. Polyethylene, which only has dispersive intermolecular forces, is more flexible. Within the polyethylene family, higher density increases stiffness. Higher density is the result of greater crystallinity, which involves closely ordered structures and interaction between chains.

The types of bonds and their strength also influence surface energies and bonding at interfaces between polymers or surfaces (inks and so on). Polar polymers are more likely to have higher surface energies for bonding to inks. As is described in Chapter 10, matching polarities is one strategy to improve bonding between polymers at an interface.

4.2.1.6 Branching and Isomerism

Beyond molecular weight, MWD, and the number and type of chemical bonds, there are other structural features of polymers that influence their properties. One of these is branching. Branching comes in two types: short chain and long chain branching (LCB). Short chain branching typically involves less than about 10 carbon atoms. In polyethylene, the presence of short chain branching arises from backbiting during free radical polymerization (LDPE) or the deliberate incorporation of short chain comonomers such as butene, hexene, and octene (LLDPE). The presence of these short chains disrupts the ability of the primary chains to form ordered structures or crystals. Increasing the amount of short chain branching reduces the density of polyethylene.

LCB involves the formation of side branches of the main chain that rival in length to the main chain. In polyethylene, free radical polymerization is conducive to the creation of long branches. LDPE is often referred to as branched PE whereas LLDPE produced via Ziegler–Natta or metallocene catalysts are referred to as linear polyethylene (even if short chains are present). Some single site catalysts allow for an occasional long chain to form [30–32].

LCB can have a substantial influence on the flow properties of polymers. Branched polymers are typically more shear thinning (viscosity decreases with increasing shear rate) and have greater melt strength than their linear counterparts. These

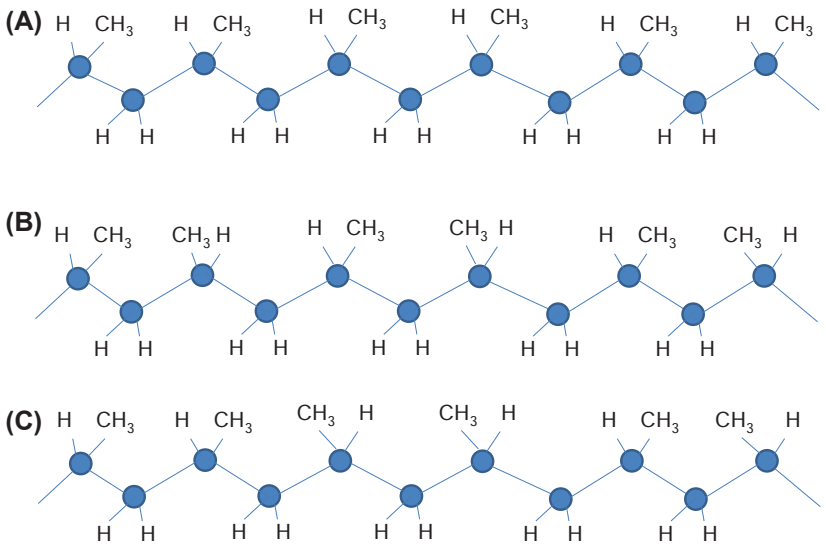


Figure 4.1 Isomerism of polypropylene: (A) isotactic, (B) syndiotactic, and (C) atactic.

translate into improved processibility which is described in greater detail in Chapter 5.

Polymers with a side group in the repeat structure can have different properties depending on the orientation of the side group (Fig. 4.1). An example is PP, which has a methyl side group. When the side groups are all arranged on the same side of the polymer chain the polymer is referred to as isotactic. If the methyl group alternates from side to side, it is called syndiotactic. If the side groups are randomly oriented, the polymer is atactic. Isotactic PP is highly crystalline, exhibits high stiffness and strength, and is the most important type used commercially. Atactic PP is amorphous and rubbery in nature.

Copolymers have more than one repeat unit. The distribution of the copolymer repeat units within the chain influences properties. The distribution of comonomers can range from purely random to purely alternating to blocks (Fig. 4.2). In block copolymers, the comonomers are arranged in groups. Examples of block copolymers are propylene–ethylene block copolymers where the blocks are EP rubber and various styrene copolymers such as styrene–ethylene–butene–styrene blocks. Alternating comonomer distributions are rather rare. One example is an alternating ECO copolymer [33]. Random copolymers include many ethylene copolymers made by free radical polymerization, such as EVA copolymers.

Manipulation of molecular architecture is often achieved through catalyst design. For example, the introduction of single site catalysts for producing LLDPE and PP copolymers has allowed resin manufactures to better control the MWD and comonomer distributions, resulting in unique structures. Examples include plastomers (uniform MWD and commoner distribution) and Dow Chemical's olefin block copolymers.

AAAAAABBBBBBBBBBBBBBAAAAAAA
block copolymer

ABABABABABABABABABABABABA
alternating copolymer

AAABAAAABAABAAAABABBAAABA
random copolymer

Figure 4.2 Copolymer types where A and B represent different comonomers or repeat units.

4.2.2 Polyethylene

Polyethylene is one of the most commonly used resins in flexible packaging due to its low cost, outstanding toughness, and flexibility. Polyethylene homopolymers have one of the simplest chemical structures of any polymer; they consist simply of carbon and hydrogen atoms as illustrated in Fig. 4.3. Yet polyethylene comes in a number of varieties, characterized by differences in crystallinity

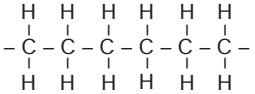


Figure 4.3 Chemical structure of polyethylene.

(as measured by density), long and short chain branching, MWD, comonomer, and comonomer distribution. Historically, PE was available in three general classes: LDPE, LLDPE, and HDPE. With the advancement of single site catalyst technology and reactor design, the LLDPE family of resins in particular has fractured into a number of different product types. Free radical polymerization has also yielded a variety of ethylene copolymers that are suitable for packaging applications.

4.2.2.1 Low Density Polyethylene

LDPE was developed by ICI in the 1930s and was the first type of PE to be commercialized. It is made by free radical polymerization on high pressure autoclaves and tubular reactors. A characteristic of the free radical polymerization process is that it contains long chain branching (LCB), which provides better processibility than LLDPE. The LCB contributes to greater shear thinning behavior in the melt (see Chapter 5) which results in lower pressure during extrusion. The LCB also contributes to better blown film bubble stability and less neck-in during extrusion coating. LDPE generally has lower ultimate seal strength, dart impact resistance, and transverse direction tear strength than LLDPE.

LDPE has a typical density between about 0.92 and 0.94 g/cc. LDPE is a homopolymer; density or crystallinity is controlled by the amount of short chain branching which arises from the free radical polymerization process. Density is controlled over a moderate range through changes in reactor synthesis conditions, namely reactor temperature and pressure.

There are subtle differences between LDPE produced on tubular and autoclave reactors. Historically, the tubular reactors produced a somewhat narrower MWD that is well suited to blown film applications, whereas autoclave polymers tend to be favored for extrusion coating. These distinctions have become blurred as technology has evolved. Differences in synthesis conditions and other considerations also play a role into how a particular grade of LDPE will process on a given converting process.

Some of the uses for LDPE in flexible packaging include the following:

- sealant or tie resin;
- adhesive or sealant in extrusion coating onto foil or paperboard;
- blending additive for LLDPE in blown film to improve processing (increase bubble stability to improve output) and reduce haze.

4.2.2.2 Linear Low Density Polyethylene

LLDPE, as its name implies, consists primarily of linear chains with no or little long chain branching. It is made via a coordination catalyst process. The original catalysts were developed by Ziegler and Natta and grades made with this technology are referred to as such. Ziegler–Natta LLDPE was commercialized in the 1970s. Chrome-based catalysts were developed by Phillips Petroleum in the 1950s. In the 1990s, LLDPE made with single site or metallocene catalysts were commercialized by Dow Chemical and ExxonMobil. These catalysts allow better control over MWD and comonomer distribution.

The density of LLDPE typically ranges from 0.90 to 0.94 g/cc and is controlled by introducing a comonomer during polymerization. Three comonomers are used commercially: butene, hexene, and octene. The catalysts only tolerate nonpolar comonomers, unlike the free radical polymerization process. Increasing comonomer content increases the number of short chains. Short chains disrupt crystallinity and lower the density. The size of the comonomer molecule determines the length of the short chain branch: butene produces a two-carbon branch, hexene a four-carbon branch, and octene a six-carbon branch. The length of the short chain branch influences properties. For example, films made from butene LLDPE generally have lower toughness than hexene or octene LLDPE [34,35].

Three types of processes are used commercially to make LLDPE:

- Gas phase-fluidized bed reactor. Ethylene is introduced in the gas phase and as the polyethylene polymerizes, it precipitates as a solid. The temperature is kept below 115°C to maintain the precipitate as a solid powder and the pressure is typically around 350 psi (2.4 MPa).
- Solution. The raw materials and polymer are in the liquid state in this process. The ethylene, hydrogen, comonomers, and catalyst are dissolved in a hydrocarbon fluid. Reactor temperature is >150°C and pressure typically around ~500 psi (3.4 MPa). The polymer solution

goes through a series of separators to remove the polymer and recycle the gases. Makeup ethylene helps cool the reactor.

- Slurry loop process. The raw materials are in the liquid state and the polymer in the solid state in this process. Ethylene, hydrogen, and comonomers are dissolved in a hydrocarbon fluid. The reactor temperature is kept below 90°C to keep the polymer solid. Pressure is typically <300 psi (2 MPa). The polymer is separated from the fluid in a flash tank and the ethylene recovered.

Each process is capable of producing a broad range of resin densities and molecular weights. A single catalyst or multiple catalysts, as well as multiple reactors in series, can be used to produce a wide variety of MWDs. Various additives to deactivate the catalyst and improve stability are added at the end of the process. Due to the differences in synthesis conditions and additives, there are often subtle differences between grades from different suppliers of nominally the same viscosity and density.

A number of manufacturing parameters influence the properties of LLDPE:

- Comonomer content. Higher levels of butene, hexene, or octene reduce the crystallinity and density. Lower density results in greater flexibility (lower modulus) and greater toughness.
- Comonomer type. Hexene and octene LLDPE generally has superior physical properties than butene LLDPE.
- Catalyst type. Chrome-based catalysts generally produce LLDPE with a very broad MWD but is more often used to produce high MW HDPE. Ziegler–Natta catalysts produce a heterogeneous MWD and comonomer distribution with more comonomer on low MW chains. Single site catalysts produce a more controlled MWD and comonomer distribution. The difference in chain structure is shown schematically in Fig. 4.4.
- Production process. The process (gas, solution, or slurry), number of catalysts, and number of reactors in series influence MWD and comonomer composition.

The comonomer (or short chain branching) distribution and MWD affects a number of properties of LLDPE. The PDI ranges from about 2 to 30 across all

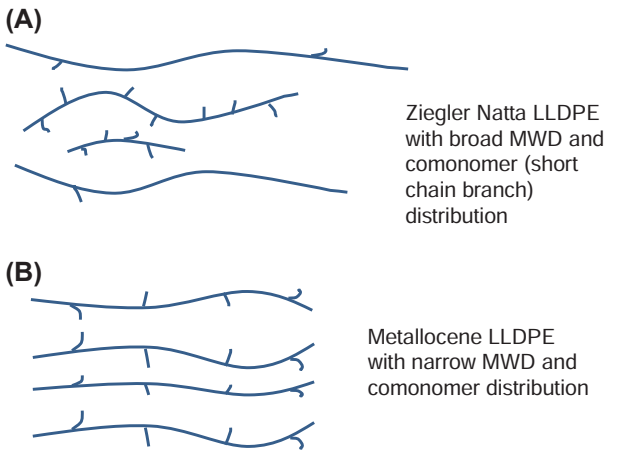


Figure 4.4 Differences in chain structure of (A) Ziegler–Natta and (B) metallocene catalyzed LLDPE.

LLDPE product families. Ziegler–Natta catalysts produce a broad MWD with the shorter chains more likely to have a higher amount of comonomer. A fraction of the long chains will have little or no comonomer or short chain branching and be HDPE-like. As a consequence, as the comonomer content is increased, the peak melting point of the polymer remains at about 125°C, despite a lower level of crystallinity (Fig. 4.5); the heat of fusion or the amount of energy needed to melt the polymer

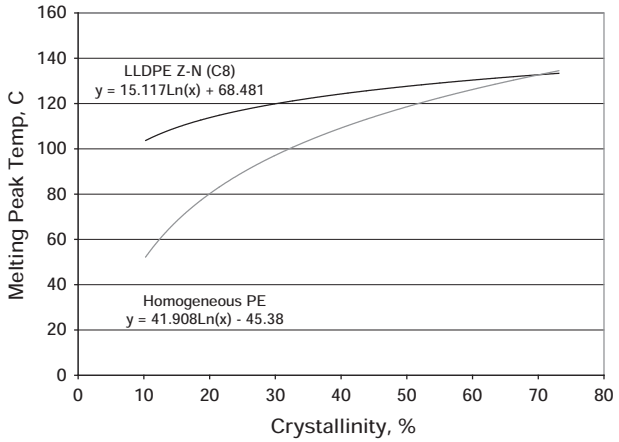


Figure 4.5 Peak melting temperature for homogeneous PE (single site catalyst) is compared to heterogeneous (Ziegler–Natta) LLDPE octene copolymers from a solution process.
Reproduced from Butler TI. PE processes. In: Wagner J, editor. Multilayer flexible packaging, technology and applications for the food, personal care and over-the-counter pharmaceutical industries. Oxford: Elsevier; 2010. p. 15–30, Figure 2-33.

decreases but the melt point is nearly constant. This influences sealing properties.

Metallocene catalysts allow the molecular weight and comonomer distributions to be more tightly controlled. The class of metallocene catalyzed LLDPE and VLDPE (very low density polyethylene) known as plastomers have a narrow MWD and comonomer distribution. As a consequence, as the comonomer content is increased, the peak melting point decreases since the polymer does not contain the long chain, no short chain branch, HDPE-like component found in Ziegler–Natta LLDPE. Benefits of the narrow MWD and comonomer distribution over Ziegler–Natta LLDPE include the following:

- fewer extractables, allowing VLDPE resins with higher comonomer content and lower density to comply with food contact regulations;
- higher tear strength;
- higher impact toughness;
- lower melting point and seal initiation temperature;
- higher hot tack strength;
- greater clarity.

The primary difference between LDPE and LLDPE lies in the molecular architecture. LDPE typically has a broad MWD and long chain branches. The chain structure of the different polyethylene types is illustrated in Fig. 4.6. Some of the property differences include the following:

- LLDPE typically draws down more readily, allowing thinner layers in extrusion coating.
- LDPE has greater melt strength, resulting in better bubble stability in blown film and edge stability in cast film/extrusion coating and lower neck-in in cast film and extrusion coating.
- LLDPE is generally tougher with a higher tear strength and dart impact strength than LDPE.
- Ziegler–Natta LLDPE has a higher melting temperature than LDPE (126 vs. 110°C), resulting in higher seal initiation temperature.
- Depending on its comonomer content, metallocene LLDPE may have a lower melting point than LDPE, resulting in lower seal initiation temperature.

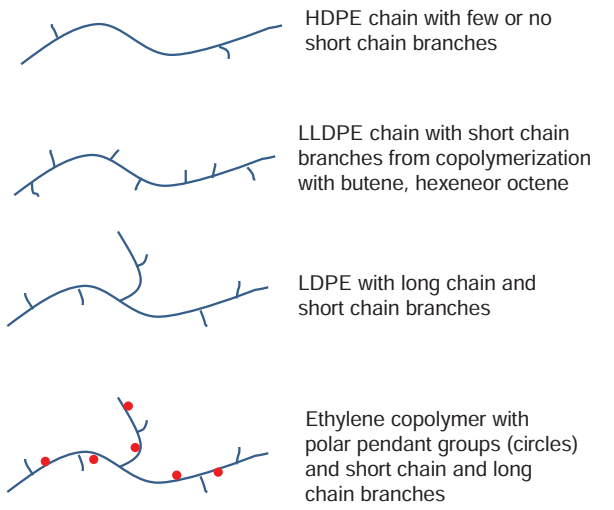


Figure 4.6 Chain structure differences between polyethylene types.

Some of the uses for LLDPE in flexible packaging include the following:

- sealants;
- components of tie resins;
- bulking layers;
- structural layers.

4.2.2.3 High Density Polyethylene

HDPE is a linear polyethylene with no or little comonomer content and density in the range of 0.95–0.96 g/cc. It is made via a coordination catalyst similar to the LLDPE process. Ziegler–Natta, chrome-based, and metallocene (single site) catalysts are all used to make versions of HDPE.

HDPE has the highest level of crystallinity of the polyethylenes, typically around 50–60%. The high crystallinity provides property benefits and trade-offs:

- greater stiffness (modulus in the range of 100–150 kpsi or 690–1030 MPa);
- higher melting temperature (135°C);
- high moisture barrier;
- excellent grease and oil resistance;
- lower clarity, higher haze.

In multilayer flexible packaging HDPE is typically used as a structural layer and for its moisture barrier.

Special grades of HDPE with ultrahigh MW have been developed that are often used for monolayer bags for their superior strength and downgaugability. Suppliers have optimized the processibility of these grades by using multiple reactors or catalysts to introduce bimodal MWD's.

4.2.2.4 Ethylene Copolymers

Ethylene copolymers are random copolymers of ethylene and polar monomers made on a high-pressure free radical process (LDPE process). The introduction of the polar comonomer

- Lowers the crystallinity (but typically increases the density due to the higher MW of the comonomer; unlike LDPE or LLDPE, density is not a good indicator of crystallinity in ethylene comonomers);
- Lowers the melting point, reducing the seal initiation temperature;
- Increases the polarity of the polymer, increasing adhesion to some substrates;
- Increases toughness;
- Reduces stiffness and increases flexibility;
- Increases optical transparency and reduces haze.

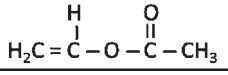
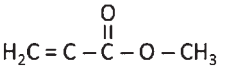
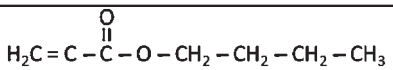
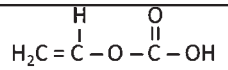
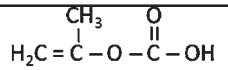
Typical comonomers used in flexible packaging are given in Table 4.4. The comonomer content typically ranges from about 3 to 30 wt%. The higher the comonomer content, the lower the crystallinity. At too high comonomer content, the polymer becomes tacky and difficult to handle.

Ethylene copolymers are made in the LDPE process and thus have similar molecular architecture: short chain branching and LCB (Fig. 4.6) and broad MWD. Thus they offer the same processing advantages as LDPE. Ethylene copolymers cannot be made using a coordination catalyst (LLDPE process) since the polarity of the monomer poisons the catalyst.

Ionomers are a special class of ethylene copolymer. These are copolymers of ethylene and methacrylic or acrylic acid that are partially neutralized with a metal salt. Their chemical structure is shown schematically in Fig. 4.7. The ionic interactions between the acid groups and metal salt form clusters within the polyethylene matrix as shown in Fig. 4.8. Like PE, ionomers have amorphous and crystalline regions. The presence of the ionic clusters enhances this morphology and gives rise to a unique balance of properties well suited for flexible packaging applications:

- In addition to covalent C—C bonds, and secondary dispersive bonds found in PE, ionomers have hydrogen bonding between acid groups and ionic bonding between the acid groups and metal salts. These additional forces act

Table 4.4 Typical Comonomers Used in Ethylene Copolymers in Flexible Packaging

Monomer	Typical wt%	Chemical Structure	Typical Use
Vinyl acetate (VA)	6—18% 20—28%		Sealant, Adhesive
Methyl acrylate (MA)	6—20%		Sealant, Adhesive, Blending component
Butyl acrylate (BA)	6—30%		Low temperature toughness, Blending component
Acrylic acid	3—9%		Tie resin (to aluminum), Sealant
Methacrylic acid	4—12%		Tie resin (to aluminum), Sealant

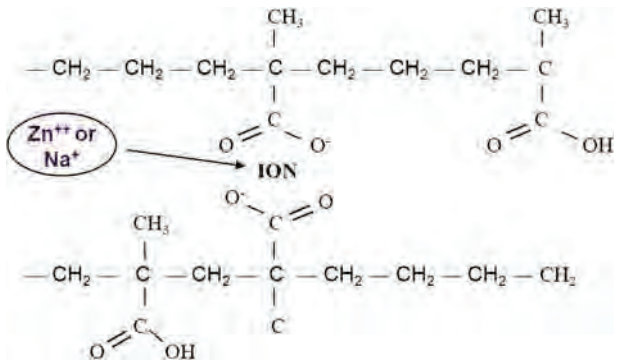


Figure 4.7 Chemical structure of an ionomer.

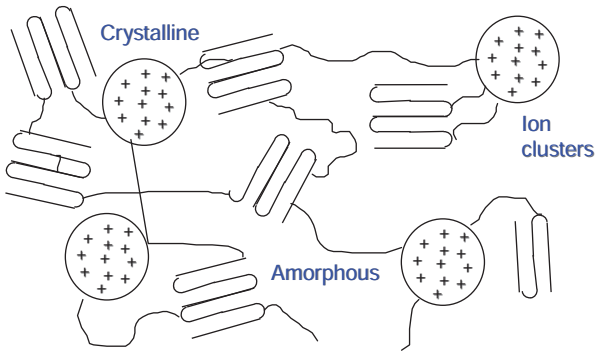


Figure 4.8 Ionomer morphology.
Reproduced with permission from E. I. du Pont de Nemours and Company.

like cross-links in the solid state, providing outstanding strength and toughness.

- The presence of the ionic clusters further impedes the movement of the polymer chains in the solid state, giving rise to higher stiffness than other ethylene copolymers. This is illustrated in Fig. 4.9.
- The formation of ionic interactions reduces the amount of primary crystallization. As a result, ionomers have exceptional clarity and low haze.
- The ionic domains are polar in nature, imparting excellent oil and grease resistance.
- The ionic "cross-links" are thermally reversible so that ionomers are melt processible. Like LDPE, they contain long chain branches which contributes to their overall processibility. But the ionic interactions, while weakened, persist into the melt state and impart exceptional melt strength. As a result, ionomers have outstanding bubble stability, thermoformability, and hot tack.

Ethylene copolymers are used in a wide variety of flexible packaging applications, primarily as sealants and adhesives or components of tie resins.

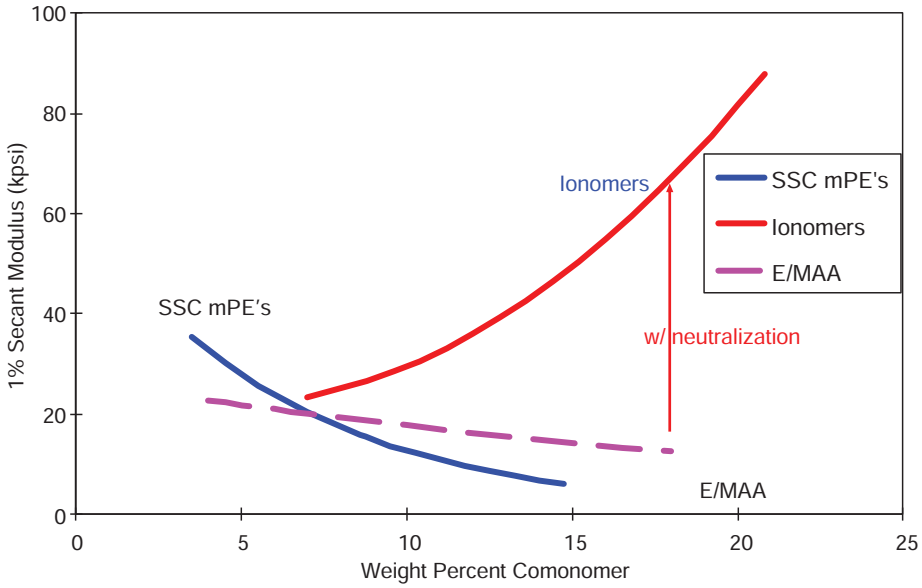


Figure 4.9 Effect of comonomer content on modulus (stiffness) for several ethylene copolymers.
Reproduced with permission from de Garavilla JR. Ionomer, acid copolymer, and metallocene polyethylene resins: a comparative assessment of sealant performance. TAPPI J 1995;78(6):191–203. Reproduced with permission from E. I. du Pont de Nemours and Company.

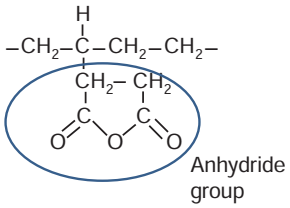


Figure 4.10 Chemical structure of maleic anhydride-grafted polyethylene.

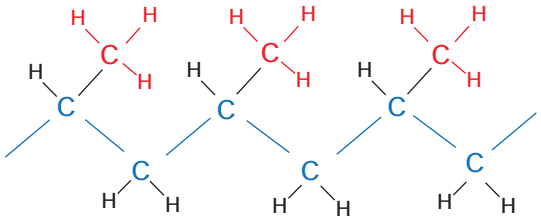


Figure 4.11 Chemical structure of isotactic polypropylene. Methyl side groups are highlighted in red (gray in print versions).

4.2.2.5 Grafted PE

Maleic anhydride is grafted onto polyethylene to impart chemical functionality. The chemistry is illustrated in Fig. 4.10. Many different types of polyethylene and ethylene copolymers have been grafted and are available commercially with HDPE, LLDPE, and PP being the most common. The grafting reaction is a postsynthesis reaction, typically done in a melt compounding process or by dissolving the polyolefin and reacting in solution. The level of anhydride functionality ranges from about 0.02 to 2 wt%.

In flexible packaging, maleic anhydride-grafted PE and PP are typically used as components of tie resins. The anhydride functionality bonds to the amine end groups on PA6 and to the OH groups on EVOH. It is also used as a compatibilizer for recycling multilayer packaging structures. Maleic anhydride-grafted PE is also used in nonpackaging applications such as toughening and compatibilizers for engineering polymers.

For Further Reading on Polyethylene and Ethylene Copolymers

1. Butler TI, editor. Film extrusion manual. Process, materials, properties. 2nd ed. Atlanta: TAPPI Press; 2005.
2. Bezigian T, editor. Extrusion coating manual. 4th ed. Atlanta: TAPPI Press.

4.2.3 Polypropylene

PP finds wide use in flexible packaging for its strength and high melting point. It comes in a variety of forms, depending on its tacticity, crystallinity, MW, MWD, and through the introduction of comonomers.

PP is derived from propylene (also called propene or methyl ethylene). A methyl group extends from the polymer chain on every other carbon atom as shown in Fig. 4.11. The position of this methyl group relative to its neighbors, known as tacticity, has a profound effect on properties. Only the isotactic form (where the methylene groups are aligned on the same side of the chain) is commercially important for film applications.

PP was initially made via a high-pressure free radical polymerization process but the technology produced a low MW oligomer that was not suited for flexible packaging [37]. In the 1950s and 1960s, coordinated catalyst technology was developed by Ziegler and Natta that produced high MW, predominately isotactic PP that was commercially viable and used today [38]. More recently, metallocene catalyst technology has been developed for PP.

PP is produced on slurry, solution, and gas phase processes similar to those described in Section 4.2.2.2 for LLDPE and HDPE.

Homopolymer isotactic PP is one of the most commonly used types of PP in flexible packaging. It has a high melting point (161°C) that is suitable for retort sterilization and other high temperature end uses. It has high stiffness (typically around 150 kpsi or 1030 MPa) and strength. It is typically used as a structural layer in rigid packaging (blow molded bottles and injection molded or thermoformed tubs or trays) and oriented or cast film, or as a structural layer in coextrusion blown film.

Random copolymers of propylene with ethylene and butene have lower melting points (ranging from 135 to 155°C) and are often used as sealant layers in multilayer cast or biaxially oriented PP films. In these copolymers, the comonomer comprises up to about 6 wt% of the total monomer content and is randomly distributed along the polymer chain. Block copolymers have higher levels of comonomer with blocks of ethylene–propylene rubber phases

embedded in the PP matrix. Block copolymers are not typically used in flexible packaging.

Similar to PE, the development of metallocene catalysts have allowed tighter control over the MWD and tacticity of PP.

PP by itself is subject to oxidative and thermal instability, and because of its crystalline structure, has a high level of haze. Antioxidants and thermal stabilizers, and clarifying agents are often added by the manufacturer to improve stability and enhance optical clarity.

PP films are used alone or as a substrate for lamination in multilayer flexible packaging. These films may be cast or biaxially oriented, in a tenter frame or double bubble process. PP films are often multilayer films themselves, made via coextrusion, with surface layers for heat sealing (random copolymer PP) or metallization. PP is typically used as a substrate for its strength, moisture barrier, and high temperature stability. Orientation of PP improves clarity, strength, and moisture barrier performance. OPP is used in a number of snack packages.

4.2.4 Specialty Polyolefins

4.2.4.1 Polybutene-1

Polybutene-1 (PB) is a polymer derived from butene. Its primary application in flexible packaging is as a blending resin for PE, EVA, or ionomers to create easy-open seals. More detail on this technology is described in Chapter 7.

4.2.4.2 Cyclic Olefin Copolymers

COCs are polymers of ethylene and norbornene. The structure is given in Fig. 4.12. These are amorphous polymers available with a variety of glass transition temperatures, ranging from about 30 to 180°C. They are stiff, transparent, and have a low MVTR. They find application in pharmaceutical packaging for their moisture barrier and as blending

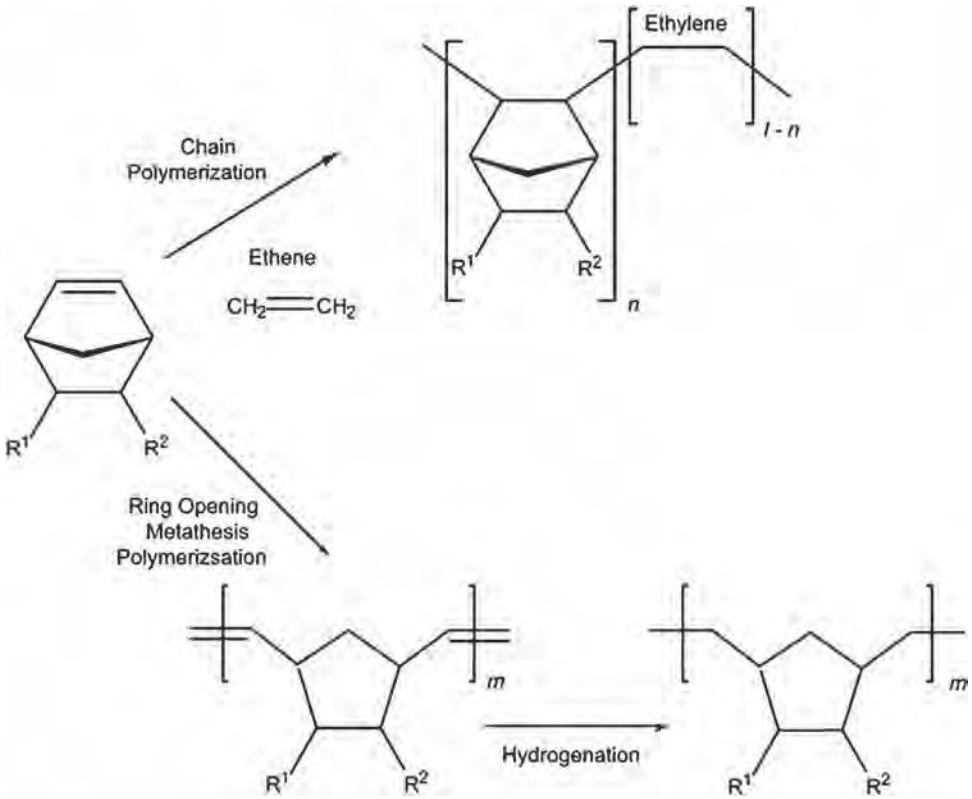


Figure 4.12 Chemical structure of cyclic olefin copolymers (COC).
Reproduced with permission from Shin JY, Park JY, Liu C, He J, Kim SC. Chemical structure and physical properties of cyclic olefin copolymers. IUPAC Technical Report. Pure Appl Chem 2005;77:801–14.

resins with polyolefins for downgauging and enhancing moisture barrier [39,40].

4.2.5 Polyamides

Polyamide or nylon was invented by Wallace Carothers at DuPont in the 1930s. Polyamides come in two types: those produced from the condensation reaction of diacids and diamines and those produced from addition polymerization of ring compounds that contain both acid and amine ends. An example of the former is PA66, which is derived from the reaction of adipic acid (six carbons) with hexamethylene diamine (six carbons) as shown in Fig. 4.13. The nomenclature for PA66 comes from the number of carbon atoms from the diamine (first six) and diacid (second six). Other PA types follow the same convention. For example, PA610 is derived from hexamethylene diamine (6) and sebacic acid (10).

PA6 is an example of the second type of polyamide. It is polymerized from ring opening caprolactam (six carbons) as shown in Fig. 4.14.

The two most important nylon types commercially are PA6 and PA66 with PA6 predominate in packaging. PA6 provides abuse resistance, strength, tear resistance, temperature resistance, clarity, and moderate oxygen barrier. Oriented PA6 is used as a substrate for some flexible packaging applications, but more often PA6 is found in coextruded cast or blown film structures. Meat and cheese packaging are two applications which often utilize one or more layers of PA6. Here, EVOH is often sandwiched between two layers of PA6 to improve the thermoformability of the structure.

PA66 is an engineering plastic more often used as fibers and injection molded parts, but sometimes is used in flexible packaging for outstanding temperature resistance. Its melting point of 255°C (vs. 230°C for PA6) makes it more difficult to process than PA6 in many coextrusion processes, especially with thermally sensitive polymers like EVOH. PA66 is sometimes used in high temperature applications such as boil-in-bag packaging.

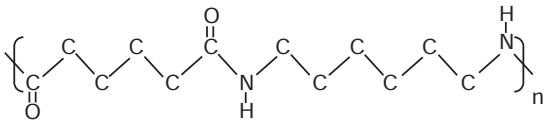


Figure 4.13 Chemical structure of PA66.

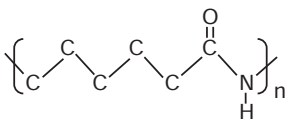


Figure 4.14 Chemical structure of PA6.

The longer chain polyamides (referring to the number of carbons in the repeat structure) such as PA610, 612, and 12 are specialty polyamides that are generally not used in packaging. As the chain length increases, the polymer becomes more linear and polyolefin-like (less polar). PA6 is highly polar and absorbs up to 2.8% water (at 23°C, 50% RH) [41]. The longer chain polyamides absorb less water (which is an advantage for injection molded parts) but their oxygen barrier suffers.

There are three specialty polyamides that bear mentioning for flexible packaging:

- PA6/66. This is a copolymer of 6 and 66 that has a lower melting point than PA6 (196 vs. 230°C). It is used in coextrusion applications where the melting or thermoforming temperature of PA6 is too high.
- PA6I/6T. This is an amorphous polyamide derived from hexamethylenediamine and a combination of aromatic diacids: isophthalic acid (6I) and terephthalic acid (6T). It is sold by DuPont (Selar PA) and EMS (Grivory). In flexible packaging, it is used primarily as a blending resin in PA6: 10–20% amorphous nylon improves the clarity, oxygen barrier, extrusion processibility, and thermoformability of PA6 [42].
- MXD6. This semiaromatic polyamide is derived from *m*-xylenediamine and adipic acid. Mitsubishi Gas is the predominate supplier. It has the best oxygen barrier performance of any of the commercial polyamides. While not typically used in flexible packaging, it is used in PET injection blow molded bottles as part of an oxygen scavenging technology (with iron) or as a separate oxygen barrier layer.

For Further Reading

1. Djordjevic D. Guide to nylon chemistry, equipment & processing (coating and casting). In: TAPPI polymers, laminations & coatings conference; 1997. p. 341–82.

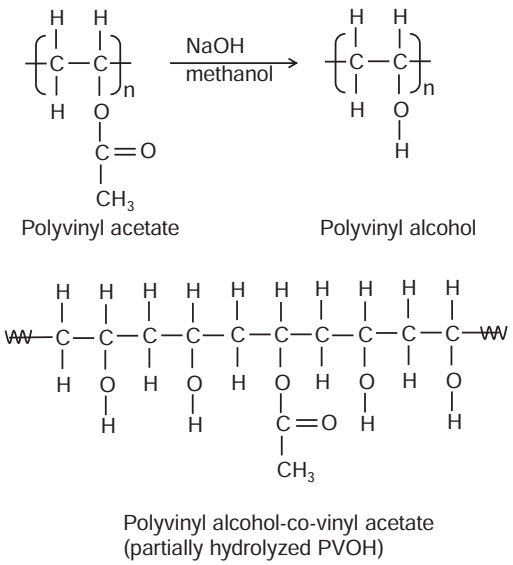


Figure 4.15 Chemical structure of PVOH.

4.2.6 Polyvinyl Alcohol

PVOH is a water-soluble polymer with excellent oxygen barrier at low RH. It is made by first polymerizing vinyl acetate and then hydrolyzing the acetate groups to −OH groups as shown in Fig. 4.15. There are three general types of PVOH: fully hydrolyzed (98% or higher), partially hydrolyzed (typically 87−89% hydrolyzed), and intermediate (89−98% hydrolysis). A number of copolymers have also been commercialized, the most prominent EVOH described in the next section.

PVOH is a challenge to melt process since its degradation temperature is close to its melting point of 230°C. Air Products Inc. introduced a copolymer with about 5 mol% comonomer that is reported to be melt processable and still water soluble [43]. Solution casting [44] has proven to be a commercially viable process for making water-soluble films from PVOH; Monosol (a subsidiary of Kuraray), a leading supplier of water-soluble PVOH films, uses a proprietary solution casting process [45].

Water-soluble films for hospital laundry bags, detergent bags, and other applications are the leading application for PVOH in flexible packaging. The temperature at which PVOH dissolves can be moderated by the level of hydrolysis: partially hydrolyzed grades can be dissolved in cold water whereas fully hydrolyzed grades only dissolve in hot water. Early versions of the technology were limited by a technical challenge: the ingredients being packaged can catalyze further hydrolysis of partially hydrolyzed PVOH. Over time the temperature at which the PVOH will dissolve increases. Various modification technologies have been developed to solve this problem [46].

Nippon Goshei makes a biaxially oriented PVOH film that is used in food packaging and other fields for its oxygen barrier, static resistance, and mold releasing performance [46,47].

For Further Reading

1. Finch CA, editor. Polyvinyl alcohol − developments. 2nd ed. England: John Wiley & Sons, Ltd.; 1992.

4.2.7 Ethylene Vinyl Alcohol

EVOH is one of the high oxygen barrier resins used in flexible packaging. It is derived from EVA copolymers where the vinyl acetate is completely hydrolyzed to hydroxyl (−OH) groups. Unlike EVA copolymers described in Section 4.2.2.4, these EVA copolymers have much higher levels of vinyl acetate in the range of 56−73 mol% (EVA used as sealants typically contain about 5 mol% vinyl acetate). EVOH is a random copolymer with a chemical structure that is a combination of ethylene and vinyl alcohol units as shown in Fig. 4.16.

EVOH is characterized by its mole percent ethylene and melt flow. Grades with ethylene contents ranging from 27 to 48 mol% are available commercially. The ethylene content represents a trade-off between ease of processing and barrier performance. As the mole% ethylene is decreased, the oxygen transmission rate (at low RH) decreases but processing becomes more difficult. An easy way to remember these effects is that the higher the ethylene content, the more like polyethylene and less like PVOH the molecule is.

The barrier performance of EVOH is highly influenced by the RH of the environment. This is

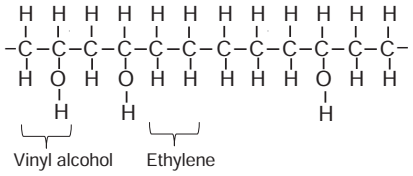


Figure 4.16 Chemical structure of EVOH.

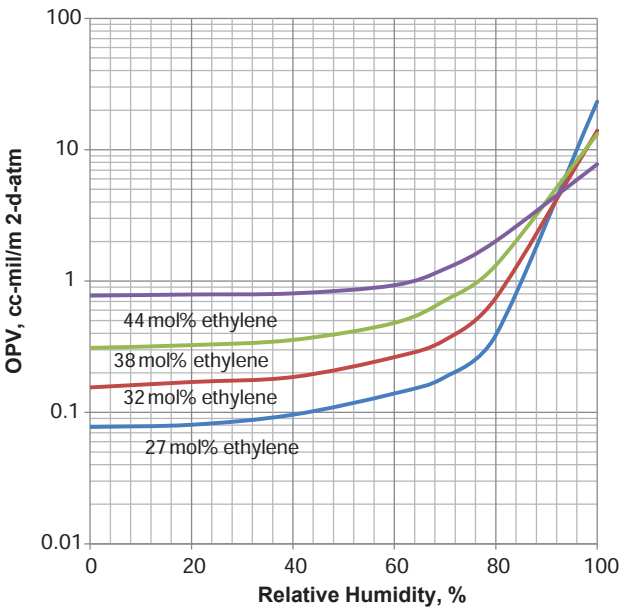


Figure 4.17 Oxygen transmission rate of EVOH as a function of relative humidity.
Data from Kuraray. Technical bulletin no. 110: gas barrier properties of resins. http://www.eval-americas.com/media/36916/tb_no_110.pdf.

explored in more detail in Chapter 8. Fig. 4.17 shows the relationship between oxygen transmission and RH. Above an RH of about 70%, the transmission rate increases rapidly. The lower ethylene content grades are more susceptible to changes in transmission rate with increasing RH.

EVOH comes in a variety of flow rates for processing on blown and cast film and extrusion coating processes. EVOH is transparent, stiff, and highly crystalline, and is an excellent oxygen barrier, but has a relatively high MVTR. EVOH is used primarily in coextruded structures for both rigid and flexible packaging. Because of its high crystallinity it can be difficult to thermoform or orient. A number of technologies have been developed to overcome these deficiencies, including

- sandwiching the EVOH layer between layers of PA6;
- blending in amorphous nylon [49–51] or ionomer [52–54];
- development of specialty grades by EVOH resin producers [55–57];
- splitting the EVOH layer into two or more thinner layers [58]. New microlayer technology reduces the crystallinity of EVOH, making the film more flexible and orientable [59,60] (see Section 8.5.2);
- using a rapid quench cast film or water quench blown film process, which suppresses crystallinity [61,62].

EVOH has become a ubiquitous barrier resin in transparent coextruded flexible packaging. It can be found in many applications where long shelf life is needed. Examples include processed meat and cheese packaging, instant coffee machine cups, lidding films, high barrier formable films for fresh pasta, barrier cereal liners, thermoformed cups and trays, extrusion-coated paper for soups, coffee and tea, and toothpaste tubes.

4.2.8 Polyvinylidene Chloride

PVDC is a clear barrier polymer made from vinylidene dichloride monomer (Fig. 4.18). Commercialized by Dow Chemical in the 1940s, PVDC is available as a powder for extrusion or solvent solutions, as an aqueous latex or emulsion, and as a solvent coating. It provides a unique combination of oxygen, moisture, and oil and grease resistance.

PVDC is sold commercially as a copolymer with other monomers such as vinyl chloride, acrylic or acrylates, and nitrile. The homopolymer decomposes near its melting point making melt processing a challenge. The addition of comonomer reduces the crystallinity and melting point, allowing the copolymer to be more easily melt processed, the typical vinylidene dichloride level is 70–90%. The lower levels of vinylidene dichloride, however, reduce the barrier performance. Even with the incorporation of comonomers, PVDC is difficult to melt process into a film, generally requiring temperature isolation and special materials of construction. Recent advances in

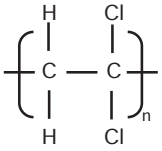


Figure 4.18 Chemical structure of vinylidene dichloride (or polyvinylidene chloride).

equipment design, such as improved temperature isolation and encapsulation, and new product offerings have expanded the application potential for PVDC [63–65].

PVDC brings a distinctive combination of performance attributes, including [64]

- moisture barrier;
- oxygen barrier;
- aroma barrier;
- grease and oil resistance;
- good seal performance;
- excellent transparency and gloss;
- good antifog properties;
- excellent printability;
- good scratch and abrasion resistance;
- flex crack resistance.

Other high-performance barrier polymers are sensitive to moisture or RH. PVDC uniquely has good moisture and oxygen barrier that does not significantly change with increasing RH.

PVDC is often coated as an aqueous latex or solvent coating onto BOPP or BOPET substrates, or as part of an adhesive formulation for adhesive lamination. Example applications include dry food packaging, retort pouches, transparent barrier stand-up pouches, and pharmaceutical blister packs. Coextrusions of EVA-PVDC-EVA have long been used for barrier shrink bags for meat packaging.

4.2.9 Polychlorotrifluoroethylene

The chemical structure of polychlorotrifluoroethylene (PCTFE) is given in Fig. 4.19. PCTFE film is sold commercially under the Aclar trade name by Honeywell. It has the best moisture barrier of any transparent thermoplastic film. It is often laminated with PET, PVC, or other substrates. Its largest application is for pharmaceutical blister packaging [66].

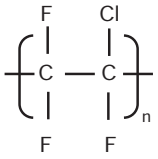


Figure 4.19 Chemical structure of PCTFE.

4.2.10 Tie Resins and Adhesives

Tie resins are adhesive polymers used to bond layers together in coextrusion or extrusion coating/lamination. Tie resins and adhesives are covered in more detail in Chapter 10. A few examples are highlighted here:

- LDPE is the workhorse resin used to bond to aluminum foil, paper, and other substrates in extrusion lamination. When extruded at temperatures above 300°C, oxidation occurs, producing polar groups such as aldehydes, acids, and ketones. These provide a moderate level of adhesion to polar substrates [67].
- For more demanding applications for bonding to aluminum foil, especially when product resistance is needed, acid copolymers are used [68].
- EVA and EMA are used to bond to PVDC, PET, and other polar substrates in coextrusion film and coating applications [69].
- Functionalized polyolefins, especially maleic anhydride-modified LLDPE, are used as tie layers to bond polyolefins to PA or EVOH in coextrusions [70,71].

Adhesives are solvent, aqueous or two part cured liquids that bond substrates together in adhesive lamination. Primers may also be applied to substrates to promote adhesion. Curing occurs through heat, UV, or e-beam radiation. Many chemistries are used as adhesives, including polyether imide, isocyanates, and polyurethanes. Some commonly used examples include the following [72]:

- solvent-borne two part urethane made up of polyester and or isocyanate;
- water-borne two part urethane using urethane/water dispersible isocyanate or polyfunctional aziridine/urethane;
- 100% solids two part urethane with polyol/isocyanate prepolymer;
- UV curable adhesive based on acrylic or cationic epoxy.

4.2.11 Polyester

The most commonly used polyester in flexible packaging is PET. The chemistry of this polymer is

described in Section 4.2.1 [Eqn. (4.4)]. Other versions of polyester include the following:

- Polybutylene terephthalate. This rigid polymer, used primarily in engineering plastics applications, is made from butylene glycol and terephthalic acid.
- Polytrimethyl terephthalate (PTT). This rigid polymer is used mostly for carpet fibers and some apparel applications. It is made from 1-3-propane diol and terephthalic acid. A biobased production route to making 1-3-propane diol was recently commercialized by DuPont and Tate & Lyle, making this polymer more economical. So far it has not found use in flexible packaging.
- Glycol modified PET (PETG). In this copolymer, some of the ethylene glycol is replaced by cyclohexane dimethanol (CHDM). Because CHDM is larger than ethylene glycol, its addition reduces the crystallinity of PET and lowers its melting point. It is a clear, transparent amorphous polymer that has not found general use in flexible packaging. One potential application is as a sealant with outstanding oil resistance.
- Polyethylene naphthalate. This polymer, made from ethylene glycol and naphthalene-2,6-dicarboxylate, has a higher barrier to oxygen than PET. Its high cost to performance ratio has limited its use in flexible packaging.

Most PET on the market today is derived from petrochemical feedstocks. A number of new developments are underway to commercialize partially and ultimately fully biobased versions of PET. In 2009, Coca-Cola introduced its PlantBottle [73], made from biobased ethylene glycol, which makes up about 30% of PET. They have announced plans with several companies to develop bio routes to terephthalic acid, which makes up the remaining 70%. Pepisco announced the development of a 100% biobased bottle in 2011 [74].

The two largest applications for PET in packaging are for injection stretch blow molded bottles and biaxially oriented film. While blow molded bottles lie outside the scope of this book, it should be noted that these bottles have undergone significant downgauging over the last several years. Some bottles have such thin walls they might be considered flexible.

Biaxially oriented PET film is typically produced on a tenter frame process (Chapter 3). PET crystallizes during orientation into small crystals, producing a strong, stiff, heat stable, transparent film. OPET has excellent abuse resistance and is a dimensionally stable substrate for printing. It also provides heat resistance during heat sealing. It has good oxygen barrier but can be coated with PVDC, PVOH, or metallized with aluminum to provide outstanding barrier. It is also used as a substrate for AlO_x and SiO_x coatings for transparent barrier applications. By itself it is has poor heat sealability; PET film is typically laminated to a sealant film or coated with a sealant.

As with any film substrate, dimensional stability and surface chemistry are important for subsequent converting and packaging processing. Dimensional stability is typically controlled by an annealing step after orientation; the oriented film is heat treated to prevent shrinkage. The surface chemistry may be modified by various treatments (corona, plasma, and so on) or by coatings (PVDC, primers, lacquers, heat seal coatings, and so on). Some of these treatments or coatings may be applied by the converter rather than the film manufacturer.

OPET film is used as a laminating layer in a variety of packaging applications including lidding films (structural layer), cheese packaging (abuse resistance) and standup pouches (printing surface and abuse resistance).

PET and PETG have been used in some coextrusion films, including multilayer-oriented films (Section 11.2.4.4). Two other packaging forms for PET are briefly discussed in Section 4.2.1. These are APET and CPET:

- APET takes advantage of the slow rate of crystallization of PET. A thin sheet is cast and quickly quenched against a cold roll. The resulting sheet is amorphous, transparent, and easily thermoformed. APET is used for clamshells, trays, and other packaging formats used for refrigerated foods or retail packaging.
- CPET (crystalline polyester) is formulated with a nucleating agent and typically a polymer modifier to improve low temperature toughness. Trays are produced via a two-stage thermoforming process that allows sufficient time for crystallization. The result is a temperature resistant, opaque tray or tub that is typically used for dual oven use (conventional and microwave oven).

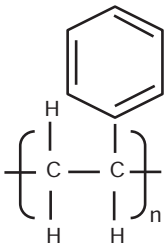


Figure 4.20 Chemical structure of polystyrene.

While not usually considered flexible packaging, APET and CPET trays are an integral part of many packages involving flexible lidding films. The chemistry and crystallinity of these trays play an important role in the adhesion and design of the lidding film structure.

4.2.12 Polystyrene

The chemical structure of polystyrene is shown in Fig. 4.20. The presence of the bulky phenyl group (benzene ring) prevents PS from crystallizing: PS is an amorphous polymer with a glass transition temperature of 100°C. At room temperature it is a stiff polymer that is often used in thermoformed cups and trays. It can also be easily foamed and is often used in clamshells for quick service restaurants and other applications. PS can also be oriented into films for various applications, although the clear film tends to be brittle.

General purpose PS is subject to crazing that leads to splitting and brittleness. To overcome these deficiencies, polybutadiene rubber is introduced during the polymerization process to make high impact polystyrene (HIPS). The rubber particles stop the cracks from propagating, improving its toughness.

4.2.13 Polyvinyl Chloride

Polyvinyl chloride is a widely used polymer with the chemical structure shown in Fig. 4.21. It comes in rigid and flexible varieties. Flexible PVC contains plasticizers. Some plasticizers in the phthalate family have become controversial in recent years and the industry has moved to replace them.

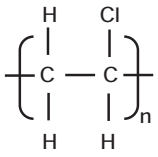


Figure 4.21 Chemical structure of PVC.

Flexible PVC can be made into a low cost, transparent flexible film suitable for wraps. It has a high oxygen transmission rate. One application in the United States has been for in-store packaging of beef cuts and ground beef on foamed PS trays. The high oxygen transmission rate helps retain the red color that is desired by many consumers.

4.2.14 Biobased Polymers

Biobased polymers are those polymers derived fully or partly from biobased resources such as plants. Biobased should not be confused with biodegradable or compostable, two end-of-life scenarios. Some biobased polymers are biodegradable or compostable but others are not. Likewise, some petroleum-based polymers are biodegradable or compostable. Biobased simply refers to the origin of the monomers or polymers.

A resurgence in development and introduction of biobased polymers occurred in the mid-2000s during a time of high petroleum costs and concern over impending shortages. Resourcing polymers from plants was thought to be a good strategy to even out the cyclic pricing of some commodity petroleum-based polymers and ensure long-term supply. Biobased polymers was also seen as a way to contribute to lower greenhouse gas emissions, although polymers represent only a tiny fraction of the consumption of petroleum products. In the intervening years, global petroleum reserves have increased, particularly with the development of horizontal drilling and fracking in the United States. It remains unclear if there is a sufficient driving force for biobased polymers in flexible packaging, as most surveys have shown that consumers are willing to use more "sustainable" packaging alternatives but are unwilling to pay for them. One reason for this is that the package is not seen as the product in the mind of the consumer, and so consumers have been unwilling to pay more for a product just because its package is bioderived. As discussed in Chapter 1, packaging helps prevent food waste, which may overwhelm any environmental benefit due to biosourcing of the package material. Finally, most biosourced polymers today use food crops such as corn and sugar cane as the starting point. As the world increases in population, crop land, water, and other resources diverted from food production may become an issue.

There are three general approaches for making biobased polymers:

- Use natural biobased polymers with some modification. An example is starch-based polymers.
- Make monomers from a biosource, such as fermentation of sugars, and use a conventional polymerization process to make the polymer. Examples include biopolyethylene and polylactic acid (PLA).
- Produce new polymers directly from bacteria. An example is polyhydroxyalkanoate (PHA).

These polymers can further be classified according to ease of adoption: those that are simply bioderived versions of polymers long used in flexible packaging (such as biobased PE and PET) and those that are new polymers or to flexible packaging [PLA, PHB (Poly-3-hydroxybutyrate), starch-based polymers]. The former enjoy an advantage of benefiting from many years of product evolution to meet the needs of the application.

4.2.14.1 Biosourced Monomer-Based Polymers

Braskem began making polyethylene from ethylene derived from sugarcane in 2010. The ethylene monomer is derived from ethanol, which in turn comes from the fermentation of sugar. Once the ethylene is made and purified, it is polymerized in the same process as conventional polyethylene. The advantage to this approach is that the properties of the polymer are the same as the petroleum-based analog. The biobased polymer takes advantage of the years of innovation and customizing that has taken place in polyethylene technology to tailor properties for flexible packaging.

Coca-Cola and Pepsico have both developed polyester packaging based on biobased monomers [74,75]. A number of other consumer goods companies have joined Coca-Cola and Pepsi to help drive this development.

The main disadvantage to this approach has been cost. The biobased monomers are considerably more expensive than the monomers they replace. A more successful approach was taken by DuPont in the development of its PTT resin. A key monomer for the production of PTT is 1,3 propane diol, which is very costly to produce from petroleum-based streams. DuPont and its development partner Tate & Lyle developed a biobased route to making 1,3 propane diol that is considerably less expensive. Once their production facility came on line, the existing petroleum-based process was shuttered. The resulting PTT is 37% biobased. Large-scale production of 1,3 propane diol has allowed the development of PTT into a number of applications, the most advanced as of this writing is carpet fibers [76]. Currently there are no flexible packaging applications for PTT, but such a strategy of developing biobased routes to monomers that are less expensive than their petroleum counterparts will likely be more successful in the marketplace.

4.2.14.2 New Biobased Polymers

4.2.14.2.1 Polylactic Acid

PLA is a high strength, high modulus polymer made from lactic acid. Bacterial fermentation is used to make lactic acid, which is then converted to the polymer as shown in Fig. 4.22. It is fully bioderived and is compostable in an industrial facility.

Due to the chiral nature of lactic acid, several forms of PLA exist. Table 4.5 shows the effect of L and D monomers on the thermal properties of PLA: the melting point decreases with increasing amounts of D. When made into a clear, transparent sheet for thermoformed trays and other packaging applications, it is in its amorphous state (PLA is slow to crystallize and crystallinity takes away from optical clarity). Because its glass transition temperature is just above room temperature PLA trays may lose stiffness when exposed to elevated temperatures during distribution. As a result, PLA is typically used for packaging refrigerated items. PLA sheet is also brittle; various additives have been developed to help improve toughness.

PLA also can be made into an oriented film. Typical properties of PLA biaxially oriented film are shown in Table 4.6. It has physical properties (tensile strength, % elongation, and modulus) approaching that of OPET but about an order of magnitude higher oxygen and moisture vapor transmission [77–79].

4.2.14.2.2 Polyhydroxyalkanoates

PHAs are a family of polyesters produced by bacterial fermentation. A variety of biological feedstocks, including cellulosics, vegetable oils, and organic waste, may be used depending on the

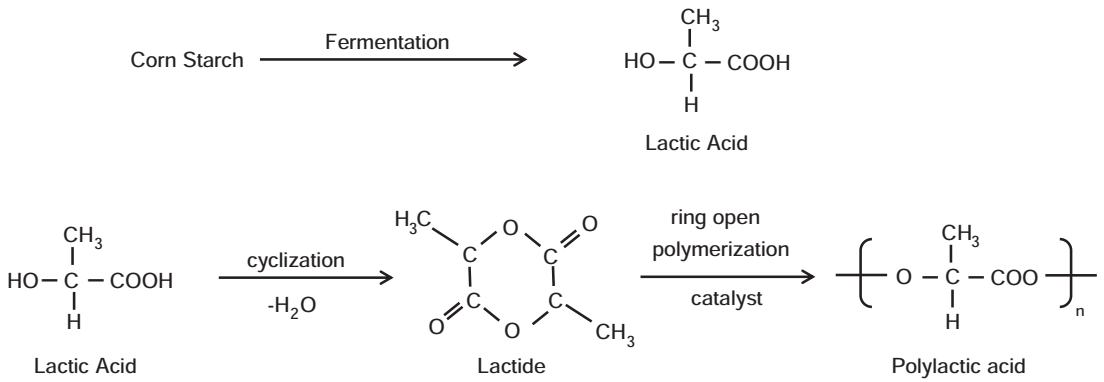


Figure 4.22 Chemical structure of PLA.

Table 4.5 Thermal Properties of PLA Copolymers

Copolymer Ratio *L*:*D* Monomer	Glass Transition (T_g, °C)	Melting Temperature (T_m, °C)
100:0	63	178
95:5	59	164
90:10	56	150
85:15	56	140
80:20	56	125

Data from Babu RP, O'Conner K, Seeram, R. Current progress on bio-based polymers and their future trends. Prog Biomater 2013;2:8. http://www.progressbiomaterials.com/content/2/1/8.

specific PHA. Microbes are engineered to produce particular PHA chemistries during the fermentation process. The PHA accumulates within the microbe cells, which is harvested by concentrating and drying the cells, followed by chemical extraction and purification. Hundreds of PHA polymers have been identified. Polyhydroxybutyrate (PHB) is one of the simplest and earliest to be developed and has physical properties similar to PS and PP. It has several shortcomings, however, including a slow rate of crystallization, a narrow processing window and a tendency to creep. Various copolymers of poly-3-hydroxybutyric acid and other monomers have been developed to overcome these deficiencies, including poly(3-hydroxybutyrate-co-3-hydroxyvalerate) or PHVB. PHVB has better toughness and increased tensile strength than PHB.

PHAs can be processed into films and sheet and have properties that may be suitable for flexible packaging.

Table 4.6 Typical Properties of PLA Biaxially Oriented Film

Property[a]	Typical Value
Melt temperature	160°C (320°F)
T_g	56.7–57.9°C (134–136°F)
Density	1.24 g/cc
Tensile strength	103 MPa MD, 144 MPa TD
Tensile modulus	3440 MPa MD, 3784 MPa TD
Elongation @ break	180% MD, 100% TD
Spencer impact strength	2.5 J
Elmendorf tear strength	17 g/mil MD, 14 g/mil TD
Haze	~2.0%
20 degrees gloss	90
O_2 transmission rate	550 cc-mil/m2/24 h atm
Moisture vapor transmission rate	325 g-mil/m2/24 h

[a] *1-mil biaxial-oriented film, oriented 3.5× in MD, and 5× in TD. Data from Natureworks. Natureworks PLA Polymer 4032D biaxially oriented films – high heat. http://www.turbocad.com/LinkClick.aspx?fileticket=3zQxvk4wJsU%3D&tabid=1941&mid=5097; n.d.*

4.2.14.2.3 Polybutylene Succinate

Polybutylene succinate (PBS) is an aliphatic polyester with properties somewhat similar to PET and polyethylene. It is synthesized from succinic acid and 1,4-butanediol. Bioroutes to succinic acid have been commercialized and several companies have announced development activities for biobased

butanediol. 1,4 butanediol has been produced commercially from hydrocarbon feedstocks for many years.

PBS is a semicrystalline polymer with a T_g of around −32°C and a T_m of around 115°C. The thermal, mechanical, and crystallization behavior is similar to PE. It is tougher than PLA and more flexible (lower modulus). It has relatively poor flex crack resistance and so is often blended with other polymers such as PLA or starch.

4.2.14.2.4 Starch Polymers

Starch is a biobased polymer that is the end product of plant photosynthesis. It is a natural carbohydrate that can be obtained commercially from a variety of sources including corn, rice, wheat, and potatoes. Starch contains linear polysaccharide amylose and highly branched polysaccharide amylopectin.

Starch alone does not melt process well and becomes brittle with age due to a phenomenon known as retrogradation. Several strategies have been developed to create "thermoplastic" starches [80,81].

- Destructuring or gelatinizing starch by exposing the starch to heat and pressure and blending with other polymers [82];
- Compounding with thermoplastic polymers such as PE as a filler. As such it does not bring much functionality other than lower cost;
- Compounding with a water-soluble polymer such as PVOH, plasticizers (typically a polyol such as glycerol) and water [83,84];
- Chemical modification of starch, such as esterification, etherification, and epoxidation [85−87];
- Compounding with a biodegradable polymer such as aliphatic polyesters [PLA, PBAT (Poly(-butylene adipate co-terephthalate)), PCA], typically adding polyol plasticizers and water [88−91];
- Compounding with a nonbiodegradable polymer such as PE [92−94].

Thermoplastic starches and hybrids are typically used in biodegradable/compostable garbage and grocery bags and various agricultural films. Their use in traditional flexible packaging so far has been limited.

4.2.14.2.5 Poly(Butylene Adipate co-Terephthalate)

BASF manufactures a petroleum-based compostable polymer called Ecoflex. They have announced their intention to develop biobased routes to one or more of the monomers. The polymer has LLDPE-like properties and is used in compostable bag applications. It is also used in blends with PLA and other compostable polymers.

4.2.15 Additives

Polymers by themselves often do not have all the properties needed for a given application. Additives have been developed by the industry to address issues in processing, handling, and stability, as well as provide product features such as improved flexibility. Some additives may be incorporated during the manufacturing process to aid in polymerization or isolation. These may include catalysts, emulsifiers, and processing lubricants. In addition, reaction by-products and residual monomers may be present. These are not the subject of this section, except to note that some additives are used to counter these residual components. The additives described here are purposely incorporated into the polymer by the resin supplier or the film converter to tailor properties. This section provides a brief introduction. The reader is referred to the references for further details. Good overviews of additives for flexible packaging can be found in King [95], Keck-Antoine [96], and Zweifel [97].

In general there are three classes of additives: stabilizers, modifiers, and fillers.

4.2.15.1 Stabilizers

Stabilizers include acid scavengers and other agents to neutralize residual catalyst or monomers left from the resin manufacturing process, as well as antioxidants, hydrolysis retardation agents, UV stabilizers, and UV blockers to prevent degradation with time.

Deactivation of catalysts and cocatalysts may result in acid residues such as hydrogen chloride (HCl). Residual HCl may result in corrosion issues and interfere with other additives. Acid scavengers are added to neutralize these acids. Examples include

zinc stearate, calcium stearate, zinc oxide, and dihydrotalcite [95].

Thermo and thermo-oxidative degradation is of concern for polyolefins, especially during processing. Oxidative degradation over long service times is also important for durable goods, but not as much for flexible packaging given the short shelf life of most packaging applications. Degradation proceeds along the pathways described in Fig. 4.23. Thermal energy from processing, UV light, catalyst residues, and other factors create alkyl radicals (R•). This in turn sets off autoformation of additional free radicals and radical precursors, including peroxy radicals (ROO•), hydroperoxide (ROOH), alkoxy radicals (RO•), and hydroxyl radicals (•OH). Here R refers to the main polymer chain. The creation of these free radicals results in cross-linking or scission of the polymer chain, leading to gels and other film defects (cross-linking) or embrittlement (scission).

There are two predominate chemistries used commercially to short circuit the degradation cycle: hindered phenols and phosphites. As depicted in Fig. 4.23, the phenolic antioxidants attack the degradation cycle by reacting with the RO• and •OH free radicals to yield inactive ROH and H_2O by-products. They also intercept the ROO• free radicals. The phosphite antioxidants react with hydroperoxides to yield inactive ROH. The use of one type of antioxidant over another often depends on the particular polymer being stabilized and the application. Phenolic antioxidants are frequently used to help stabilize the polymer both during processing and in the end use. Phosphite antioxidants tend to help more during polymer processing. Often a combination of phenolic and phosphite antioxidants is used. Typically the antioxidant system is added to the polymer by the resin supplier during their manufacturing process. Some of the commonly used antioxidants in polyolefins are described in Table 4.7.

Polyesters undergo hydrolysis, which causes chain scission and embrittlement. Drying is the most important method of preventing hydrolysis during processing, but epoxide, carbodiimide, and phosphorous acid ester additives may be used to help retard hydrolysis. Polyamides also undergo hydrolysis and thermal oxidative degradation. Copper salts, aromatic amines, and phenolic antioxidants are used to help stabilize polyamides [96].

UV stabilization is typically used for durable goods that are exposed outdoors for long periods of time. For packaging, the film itself will likely be stable enough without additives for the short duration of the use of the package. UV stabilizers and blockers, however, may be incorporated to help protect the product from UV exposure. The most effective way to block UV light is the use of opacifiers, such as metallization and pigments, for

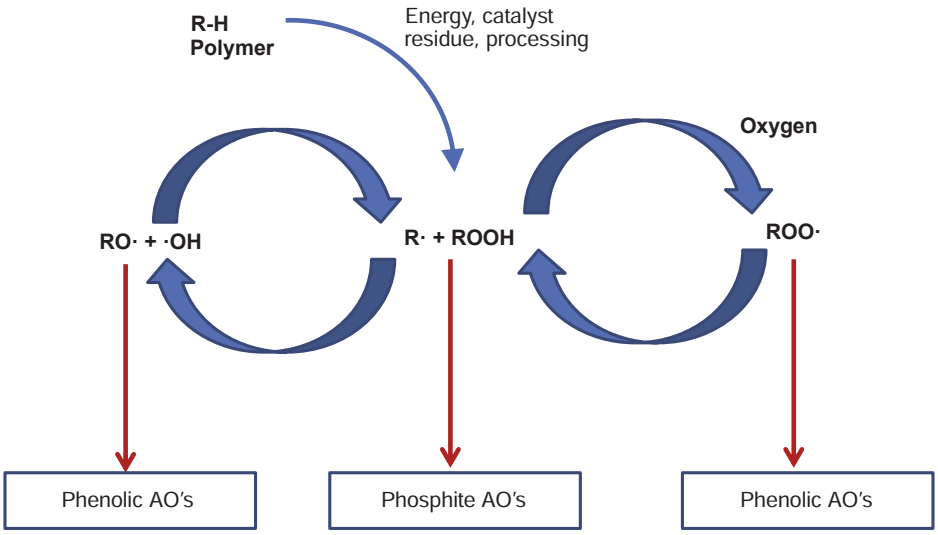
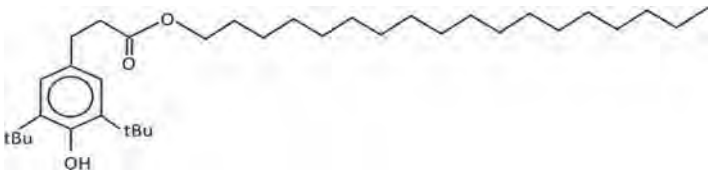
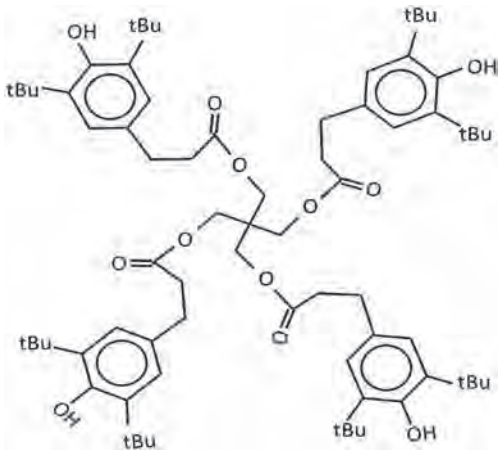
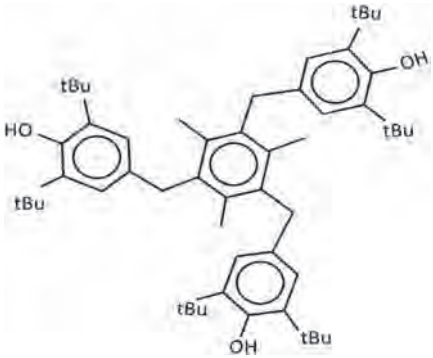
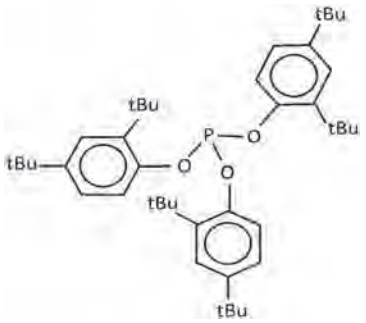
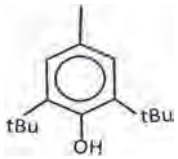
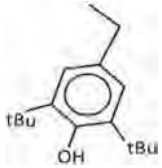


Figure 4.23 Autooxidative degradation of polyolefins and antioxidant intervention mechanisms.
Adapted from Stricker F, Horton M. New stabilizer solutions for polyolefin film grades. In: European TAPPI PLACE conference. http://www.tappi.org/content/enewsletters/eplace/2004/8-1stricker.pdf; 2003.

Table 4.7 Commonly Used Antioxidants for Stabilizing Polyolefins

Chemical Name	Chemical Structure	Grade	Supplier
Octadecyl-3-(3,5-di-tert-butyl-4-hydroxyphenyl) propionate		Irganox 1076 Anox PP18 Songnox 1076 Playox 1076	BASF Addivant Songwon Polymate
Tetrakis (methylene-3-(3,5-di-tert-butyl-4-hydroxyphenyl) propionate)methane		Irganox 1010 Anox 20 Songnox 1010 Wanox 1010	BASF Addivant Songwon Wanxing
1,3,5-trimethyl-2,4,6-tris-(3,5-di-tert-butyl-4-hydroxybenzyl) benzene		Ethanox 330 Irganox 1330 Anox 330 Sunox 555	Abemarle BASF Addivant Sunshow

Tris(2,4-di-tert-butlyphenhyl) phosphite		Irgafas 168 Songnox 1680 Wanox 168 Playox 168	BASF Songwon Wanxing Polymate
Butylated hydroxytoluene		BHT	Many
4-Ehtyl-2,6-di-tert-butylphenol		BHEP	Chevron Phillips Songwon

example, TiO_2. For transparent packaging, UV blockers such as hindered amine light stabilizers (HALS) and hydrobenzoates may be used. Antioxidants also help in stabilizing the film during UV exposure.

Discoloration of plastic films is known to occur as a result of complex interaction among additives and between additives and by-products in the resin. For example, discoloration of EVA encapsulant films in photovoltaic modules have been attributed to antioxidants, UV stabilizers, and peroxide by-products [99,100].

Most packaging films do not contain such additives, but overoxidation of phenolic antioxidants has caused discoloration issues, particularly in polyolefin films. Under harsh processing conditions or exposure to gaseous oxides of nitrogen (NO_x) from incomplete combustion of fossil fuels, a variety of colors from yellow to red and orange have been observed. The latter phenomenon is known as gas fading and often is associated with exposure of films to NO_x from propane powered fork lift trucks in warehouses. The color forms near the surface of the plastic and near the edges of rolls. Color formation increases with exposure time to NO_x and the amount of phenolic antioxidant in the resin. Some phosphites may also break down to low molecular weight phenols when exposed to heat and humidity, with subsequent color formation from the same pathway as for primary hindered phenol antioxidants [95]. Additionally, some pigments, such as some grades of TiO_2, also may contribute to the problem [101,102].

The mechanism for the color formation is thought to be the creation of quinone species, such as stilbenequinone [102]. Several techniques are used to try to control the problem [103]:

- Modifying the ratio of phosphite to phenolic antioxidant (toward more phosphite). Phosphites do not have the same functionality as phenolic antioxidants and so this approach can only be taken so far. Also, care must be taken in selecting the phosphite portion of the antioxidant system to ensure phenols are not created through hydrolysis reactions
- Using isocyanurate-type phenolic antioxidants that do not readily form quinone structures
- Improving ventilation in the warehouse and covering the film rolls to prevent NO_x from entering
- Adding acid neutralizers to buffer the pH
- Using different antioxidant chemistries, such as hydroxylamine, tocopherols (vitamin E), or HALS [104–108].

The last approach has been well studied in the literature but has been slow to be adopted except for special grades developed for applications that are most sensitive to the issue. For the most part, yellowing is not an issue and standard phenolic antioxidants are satisfactory.

4.2.15.2 Modifiers

4.2.15.2.1 Pigments and Opacifiers

Pigments and mineral fillers may be added to the polymer for light barrier or aesthesis. For white films with excellent light barrier, TiO_2 is often added. The amount of light barrier or opacity depends on the type of pigment (refractive index, particle size), loading, how well it is dispersed and thickness of the film [109]. TiO_2 in its raw form is highly reactive. Different coatings are applied by the manufacturer to make it suitable for use in plastics. The coating type may impact polymer stability as well as how easily it can be dispersed into the polymer matrix. Some polymers may be impacted more than others for a given grade of TiO_2. Consultation with the TiO_2 producer or masterbatch supplier is recommended.

Calcium carbonate ($CaCO_3$) is another inorganic often added to help opacify a film. Calcium carbonate brings other benefits to PE film, such as improved output and toughness, believed to be due to changes in heat conductivity and the crystalline morphology of the polyethylene [110,111]. In extrusion coating of PE, calcium carbonate is reported to increase output, adhesion, and printability [112,113].

Addition of mineral fillers is used to make white-oriented film through the creation of small air voids during orientation [114,115]. The particle size and dispersion of the cavitation agent is critical. Using such films may be less expensive than printing for creating a white background.

4.2.15.2.2 Slip Agents

A film needs a certain degree of slipperiness to run along rolls and other metal surfaces in high-speed packaging lines. The degree of slipperiness is measured as the coefficient of friction (COF). A higher COF means the film is tackier. Many sealant polymers, such as EVA or LLDPE, have COFs greater than about 1 and are too tacky to run on high speed lines. Slip agents have been developed to bring the COF of these resins down to the operable range of about 0.1−0.3.

Slip agents typically belong to a class of chemicals known as fatty acid amides [116]. They are added to the polymer either by the resin manufacturer or by the converter just prior to extruding into the film. Fatty acid amides are generally soluble in the polymer melt, but as the polymer is quenched into the solid film, the fatty acid amide is driven away from the crystallizing regions to the surface of the film. Once on the surface, they act as soaps to provide "slip." The effectiveness of a given fatty acid amide depends on the size and shape of the slip molecule, how much has bloomed to the surface and the bloom rate. Generally, once the surface of the film has a monolayer of slip molecules on it, the ultimate COF is achieved, which depends on the structure of the molecule. The bloom rate depends on the specific interactions between the polymer and slip agent. In some cases, it may take a few minutes but in others it may take days. The net effect is that a slip agent that works well in one polymer may not work as well in a second. Higher concentrations may be required to achieve the same COF in the same amount of time for LLDPE than LDPE, for example. Adding too much slip, however, can lead to problems with adhesion and aesthetic effects (chalking). A more in-depth discussion of slip agents and blooming rates is provided in Chapter 12.

Some of the more commonly used slip agents for polyolefins are described in Table 4.8.

4.2.15.2.3 Antiblock

Blocking refers to when a roll of film becomes difficult to unwind due to the film surfaces binding to one another. Some of the factors that influence blocking include the following:

- Softness and tackiness of the polymer: softer/tacky polymers tend to be more prone to blocking than harder polymers.
- Crystallinity of the polymer: higher crystallinity often reduces blocking of polyolefins.
- Glass transition temperature: amorphous polymers below their glass transition temperature are also less prone to blocking.
- Roll tension: high roll tension may increase blocking.
- Temperature: higher ambient temperatures may make blocking worse.

In addition to selecting the right polymer and controlling roll tension and temperature, antiblock additives are used to prevent blocking. There are two general types of antiblock agents: organic and inorganic. Examples of organic additives include some varieties of fatty acid amides, such as stearate, which helps reduce blocking of PE films. Like fatty acid amides used for slip agents, these organic additives bloom to the surface. The structure formed at the surface acts to reduce blocking of the films.

Examples of inorganic antiblock additives include diatomaceous earth, silica, and talc. These are dispersed throughout the bulk of the polymer. They are thought to reduce blocking by creating small bumps at the surface of the film. The small bumps reduce the surface contact between the films in the roll, reducing friction and blocking. The rougher surface also reduces friction at the surface. Often inorganic antiblock is added in conjunction with a fatty acid amide slip agent. The synergy between the two types of additives typically acts to reduce the COF more efficiently than either one alone.

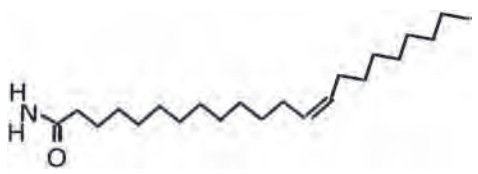
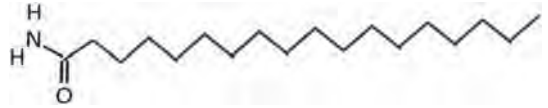
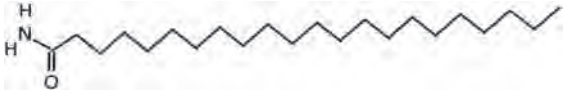
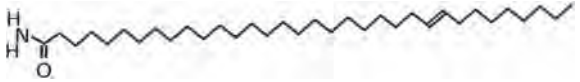
The particle size of the inorganic additive is important. If it is too large, it may create holes in the film rather than bumps. Optical clarity may also suffer, depending on the concentration. If the particle size is too small, the size of the bumps may be too small to prevent blocking. More detail on additive technology for preventing blocking can be found in Chapter 12.

4.2.15.2.4 Chill Roll Release

In cast film and extrusion coating, the melt curtain is cast directly onto a cold roll and quenched. The polymer may stick to the roll as it is drawn off. Factors that influence chill roll sticking include:

- The metallurgy of the roll surface. Chrome plating is often used to help prevent sticking;

Table 4.8 Commonly Used Slip Agents for Polyolefins

Slip Agent	Structure	Carbons	Saturation	Uses
Erucamide		22	Mono unsaturated	COF: PE, EVA
Oleamide		18	Mono unsaturated	COF: PE
Stearamide		18	Saturated	COF: EVA, ionomer; antiblock: PE
Behenamide		22	Saturated	Chill roll release and antiblock
n-Oleyl palmitamide		34	Monounsaturated	COF: Ionomer

- The roughness of the roll surface. The polymer often releases easier with a matted roll than a smooth one. Matting the roll surface, however, can affect the optical clarity of the film/coating;
- Chill roll temperature;
- Extrudate temperature;
- Polymer properties. Some polymers are tackier or adhere more strongly to the metal surface than others;
- Use of additives.

Additives for aiding in releasing the polymer from the chill roll must be fast acting. Typically fatty acid amides are used. For example, behenamide provides good chill roll release properties for acid copolymers and ionomers.

4.2.15.2.5 Lubricants

External lubricants serve to decrease frictional forces between the polymer and metal surfaces, or when compounding with fillers, between the filler and polymer. They are generally not used in polyolefins for film applications. They are more prevalent for processing of PVC or PA, particularly in injection molding. Some examples of external lubricants include polyethylene waxes, oxidized polyethylene waxes, paraffins, metal soaps (such as zinc stearate), esters, amides, and fatty acids [117].

4.2.15.2.6 Plasticizers

Plasticizers or internal lubricants act to reduce the bulk viscosity and increase the flexibility of a polymer. They are typically semisoluble in the polymer, opening up the polymer chain with the soluble portion and providing intermolecular lubrication with the less soluble portion [117,118]. Plasticizers also act to lower the glass transition temperature of polymers such as PVC. This makes the polymer more flexible, particularly at cold temperatures.

The most widely used plasticized polymer is flexible PVC [118]. The addition of a plasticizer completely transforms PVC from a very rigid polymer used in pipes to a flexible material suitable for flexible films. Most other polymers used in flexible packaging do not use plasticizers. Phthalate esters have been the predominate plasticizer used in PVC, the most common being di-2-ethylhexyl phthalate, also known as dioctyl phthalate. Some types of phthalate plasticizers have come under scrutiny due to concerns over their toxicity and potential to be endocrine disruptors. In response, the industry has shifted away from these plasticizers to alternatives for applications involving human health.

Water acts as a plasticizer for PA6. Some nylon films are "moisturized" in a post-fabrication step to help improve low temperature toughness and puncture resistance [119,120].

4.2.15.2.7 Antistats

Plastics are naturally nonconducting and are prone to static build up. This becomes an issue with high-speed windup of films, unwinding of films for packaging operations and in the end use. Dust attraction, electric discharge that may damage electronic components and electric shock are examples of end-use issues.

Three methods are typically used to reduce static buildup: addition of antistatic additives, addition of conductive fillers such as carbon black, and coating the surface with an antistatic agent. Fillers are often used in thick-walled parts where opacity is not an issue. In films, additives are more often used and can be divided into two categories: blooming and permanent [121].

Blooming additives, such as glycerol monostearate, diffuse to the surface during processing. They are generally added at 1−2% and are low in cost to use. Typically they are surfactants that are incompatible with the polymer matrix. Upon migrating to the surface of the film, they attract moisture. The charge is transferred from the polymer to the water layer on the surface for dissipation. Examples of blooming typing antistats are ethoxylated amines, glycerides, ammonia salts, phosphates, and sulfonamides [95]. Most do not work well at low RH and wear off with time. They can also cause delamination and adhesion issues.

Permanent additives are inherently dissipative or conductive polymers that are typically blended with polymers at 20−30% levels. They usually work at low RH and do not wear off with time. Polyether ester amides (such as Pebax) are one group of permanent antistatic polymer additives. They are relatively expensive to use, can cause some aesthetic issues in processing since they are often not compatible with polyolefins, and may yellow with aging. Potassium-based ionomers have also been

introduced as permanent antistat additives for polyolefin films [121,122]. They are more compatible with polyolefins, resulting in better aesthetics.

Two methods are typically used to measure the antistatic properties of films: surface resistivity and static charge decay time. Surface resistivity is evaluated by measuring the potential difference between set distances on the surface of the film when a charge is applied, as per ASTM D257. Polyolefins typically have surface resistivities of 10^{14} Ω/square or higher. Applications requiring antistats generally need values of around 10^{12} Ω/square or less. Static decay time is measured per U.S. Federal Test Standard 101C, Test Method 4046. The initial charge is +/−5000 V. Static decay times of less than 10 s and preferable less than 2 s are generally required. The RH and temperature are two key parameters that affect these measurements and should be specified.

4.2.15.2.8 Process Aids

Polymer processing aids are typically used to reduce melt fracture of polymers, especially of linear polyethylene. Melt fracture is a type of flow instability that begins as a roughening of the surface (shark skin) and at higher output can lead to severe distortion of the polymer. PPAs help extend the critical shear rate at which melt fracture occurs, allowing higher line speeds. The most common PPA's are based on fluoropolymers or fluoroelastomers [123]. They are inherently incompatible with the LLDPE matrix and coat out onto metal surfaces. The PPA forms a lubricating boundary layer at the surface of the flow channel. Advances in the understanding of the mechanisms and optimal compositions have occurred over the years [124−127], which has resulted in lower concentrations of additives needed. PPAs have also been found to help reduce die lip buildup and gel. The process is dynamic and the PPA must be continuously replaced. Various strategies are used, including adding the PPA to the resin during manufacture and precoating the die and flow channel surfaces by introducing a PPA masterbatch at the beginning of film production.

4.2.15.2.9 Nucleating and Clarifying Agents

Nucleating and clarifying agents help seed the formation of crystals, producing more crystals that are smaller and more uniform in size. The smaller crystals refract less light and reduce haze and increase transparency. Crystallization occurs at a higher temperature than it would normally, which provides some processing advantages.

When semicrystalline polymers cool from the melt, lamella organize into macrostructures called spherulites. These spherulites grow until they impinge on neighboring spherulites. Large spherulites can result in high levels of haze and affect physical properties. There are three types of nucleation: homogeneous, orientation-induced, and heterogeneous. Homogeneous nucleation occurs naturally as the polymer is supercooled below its crystallization temperature. Orientation-induced nucleation occurs when molecules align during orientation, typically during film fabrication. Heterogeneous nucleation involves the introduction of a foreign phase or surface, typically the nucleating agent, for the crystal to grow on. By introducing the nucleation agent, more crystals form at a higher temperature than would otherwise occur with pure homogeneous nucleation. More crystals result in small sizes as they impinge upon each other sooner.

Nucleation generally results in two types of advantages: better optical quality (lower haze and higher transparency) and crystallization at higher temperatures. The latter can have advantages in productivity, since quenching or cooling is often a limiting step of the film fabrication process. In injection molding, nucleating agents help reduce cycle time.

PP has been the most common polyolefin to nucleate. A subset of nucleating agents known as clarifying agents are added to PP to improve its optical clarity. PP is particularly amenable to nucleating agents due to its inherent slow rate of primary crystallization.

Polyethylene nucleation has been more difficult. Recently, Milliken introduced a nucleating agent for linear polyethylene [128]. Addition of the nucleating agent increases the peak crystallization temperature and reduces the crystalline half time. An increase in gloss and a reduction in haze have been measured for several types of linear polyethylene blown films. Improvements in physical properties, hot tack, and barrier are also noted.

Nucleating agents are typically small inorganic particles with melting points above that of the polymer. As the polymer melt cools, the solid particle forms the site around which the crystal forms. The most effective nucleating agents for PP are

derivatives of benzoic acid. The most widely used is sodium benzoate. Kaolin and talc are also commonly used [129].

Clarifying agents are typically organic molecules. Clarifying agents are nucleating agents, but not all nucleating agents are clarifying agents. Inorganic nucleating agents may actually increase haze. The most widely used clarifying agents for PP are derivatives of dibenzylidene sorbitol. Clarifying agents melt in the same temperature range as the PP. As the polymer cools from the melt, the clarifying agent solidifies, initiating crystallization of the PP at a higher temperature than it would with just homogeneous crystallization. Unlike inorganic nucleating agents, clarifying agents are transparent, aiding in the reduction of haze.

Care must be taken in the processing of clarified PP; high temperatures can degrade the clarifying agent, resulting in color and organoleptic issues.

4.2.15.2.10 Antifog

In certain types of packaging, particularly refrigerated packaging of foods, condensation may form on the inside surface of the film. Tiny droplets can form that detract from the clarity and aesthetics of the package. Antifog agents have been developed that change the surface tension of the film, allowing the water droplets to better wet the film. These types of additives are typically blended in with the resin and bloom to the surface with time. Examples include ethoxylated alkylphenols, polyethoxylated oleic acid esters, and sorbitan esters of fatty acids [95].

4.2.15.2.11 Tackifiers

Tackifiers may be added to change the cling, tack, or adhesive properties of a film. Often used in hot melt and pressure-sensitive adhesive formulations, tackifiers modify the viscous properties of polymers and elastomers, aiding in flow and tack. A common cling agent for stretch wraps is polyisobutylene. For hot melts, pressure-sensitive adhesives, and other adhesive polymers, there are hundreds of tackifiers to choose from. They are conveniently categorized by their basic raw material feed streams [130]:

- Rosin resins derived from wood rosin or gum rosin or the by-products of the paper making process (tall oil rosin).
- Hydrocarbon resins made from petroleum-based feedstocks that are either aromatic, aliphatic, or mixtures.
- Terpene resins derived from terpene feedstocks such as wood sources or citrus fruit. They have broad capability and impart adhesive properties to a wide range of polymer types but are limited in supply and high in cost.

4.2.15.2.12 Toughenners

Some polymers are inherently brittle. Modifiers have been developed to toughen the polymers. Although most often used for rigid applications, the basic concept is to add a rubbery component to the polymer. When designed properly, the rubbery phase helps stop cracks from propagating through the polymer, increasing its toughness. Some examples include the following:

- Copolymerization of butadiene with styrene (HIPS) to stop crazing of polystyrene;
- Blending in ethylene propylene rubber (EPR) or ethylene propylene diamine monomer (EPDM) rubber into PP, or creating impact block copolymers of PP and rubber with multiple reactors;
- Compounding nylon with maleic anhydride-modified rubber to form supertough nylon [131];
- Adding epoxy-functionalized ethylene copolymers to CPET to improve cold temperature toughness [19,22];
- Adding EMA to APET to improve refrigeration temperature toughness [19];
- Adding rubbery polymers to PLA to reduce brittleness [132].

The rubber modifier must be compatible with the polymer matrix to ensure good adhesion during impact events. Special compounding steps and chemical functionality is often used to obtain the optimum domain size and distribution of the modifier in the polymer, adding to the cost. In many cases, the size of the rubbery phase is greater than the wavelength of light, resulting in haze or even opacity. For these reasons, tougheners are not often used in flexible packaging.

4.2.15.2.13 Compatibilizers

When combining polymers with other polymers or inorganic fillers, good interfacial bonding is important to ensure mechanical integrity between the phases. Most polymer blends are immiscible (as is shown in Chapter 6), resulting in a discreet and continuous phase morphology. The minor or discreet phase forms droplets or ribbons within the major or continuous phase. Compatiblizers act to improve the adhesion between the phases or between the polymer and an inorganic filler. This can result in higher strength and integrity.

In multilayer flexible packaging, the individual layers are not always compatible with each other. Tie layers are used to bond the layers together. More and more often, scrap film is recycled. Sometimes compatibilizers are added to the recycle melt stream to improve the properties of the blend. An example is the use of maleic anhydride-modified polyolefins for compatibilizing PA or EVOH with PE or PP [133,134].

4.2.15.3 Fillers

Fillers are typically inorganic materials such as calcium carbonate, talc, mica, or glass fibers. Except for calcium carbonate, already discussed in Section 4.2.15.2.1, fillers are not typically used in flexible packaging. They increase stiffness at the expense of flexibility and clarity.

4.2.15.4 General Considerations

Additives may be synergistic or antagonistic when using more than one. For example, combining an inorganic antiblocking agent with a fatty acid amide slip agent can result in lower or higher COF than either one alone. Additives also may impact other properties such as adhesion or optical clarity. Care must be taken when selecting additives to test for all contingencies.

Some of the additives used in flexible packaging are designed to bloom to the surface. In coextrusion, migrating additives may diffuse to adjacent layers or interfaces as well as the free surface where it is intended. Often additional additive must be put into the adjacent layers to account for this. This is discussed with respect to COF and slip migration in more detail in Chapter 12.

4.3 Commonly Used Substrates in Flexible Packaging

Premade film, foils, and paper are commonly used as components of multilayer flexible packaging structures. This section highlights some of the commercially important substrates.

4.3.1 Oriented Polypropylene

This substrate is covered in Section 4.2.3.

4.3.2 Aluminum Foil

Aluminum foil has long been used as a barrier layer in flexible packaging. The production of aluminum foil begins with a series of cold roll steps where the thickness of an aluminum ingot is reduced in half with each step. In the final step below 60 μm, the foil is doubled over and sprayed with oil (for release). The foils are rolled together to the final thickness, separated, rerolled, slit into the desired width, and annealed. Annealing is a critical step to ensure the quality of the foil. The annealing

- removes the oil;
- creates a stronger, more uniform oxide crystalline structure;
- creates a wettable surface;
- provides a more homogenous surface;
- controls oxide crystal growth to prevent sticking between foil layers in the roll.

A number of quality issues can arise from the manufacturing process, including the following [135]:

- While most of the oil is removed during annealing, traces will remain. Residual oil is more likely to be near the center of the roll than the edges, causing differences in wettability across the width of the foil.
- There may be differences in wettability between the oil and non-oil sides of the foil.
- Less oxygen ingresses to the center of the roll during annealing; this may result in differences

in oxide structure and properties. Oxides form in two layers with the layer in contact with the foil providing barrier and the outer layer providing adhesion (surface properties). The nature and thickness of these layers change during annealing.

- Precipitates such as AlFeSi and Al_3Fe may form at the oxide surface causing defects, which may affect quality. While pure aluminum may have the best barrier (defect free), alloys and precipitates are needed to achieve the strength requirements for packaging applications. So there may be a trade-off between strength and defects.

Aluminum foil is available in a variety of thicknesses from about 6 μm and higher. Aluminum foil is often the most expensive layer in a multilayer flexible package, so the thinnest possible thickness is used. Since in theory aluminum foil is an impenetrable barrier, the minimum thickness is determined by defects that may occur during the foil manufacturing process, during handling by the converter and on the packaging line, and in the end use. Pinholes and flex cracking often lower the barrier performance of foil-based packaging [136].

Aluminum foil is typically coated with a lacquer- or water-based latex or laminated to a polymer film via adhesive or extrusion coating or lamination. Vinyl-based lacquer-coated aluminum foils are used in many lidding applications, particularly for dairy products such as yogurt. Laminations are used in many applications such as pharmaceutical packaging, aseptic liquid packaging, and condiment sachets.

4.3.3 Oriented Polyester

This substrate is covered in Section 4.2.11.

4.3.4 Metallized Film

Metallized film is used to provide moisture, oxygen and light barrier, and for aesthetics. A variety of substrate films for metallization are used in flexible packaging, including PET, PP, PA, and PE. Of these, oriented PET and PP are most common.

Metallized film is produced on a metallizing machine, which vacuum deposits a thin layer of aluminum (or other metals, but aluminum is the most common) onto the film substrate. The aluminum is melted, vaporized, and condensed onto the film surface. High vacuum is required to vaporize the aluminum [137].

As described by Mount [138], there are a number of manufacturing variables that affect film performance, including the following:

- vacuum level;
- conditions of the "boat" that holds the aluminum (temperature, wire feed rate);
- film formulation;
  - treatment level (surface energy),
  - presence of adhesion layer,
  - COF technology used (some technologies bloom to the surface and interfere with adhesion),
  - film dimensional stability (oriented films are typically used).
- web cooling conditions;
- tension levels;
- mechanical condition and cleanliness of the rolls.

These variables in turn influence the appearance, optical density, metal adhesion, and barrier properties of the metallized film.

The thickness of the metallization layer ranges from about 3 to 40 nm. As the thickness increases, the optical density (opacity) increases, as does the gas barrier performance. For oxygen and moisture barrier applications, typically around 30 nm are needed.

Metallized films are used in many packaging applications, including the following:

- bags for snack foods such as potato chips (met-BOPP for light barrier);
- coffee pouches (met-OPET or BON);
- candy wrappers (met-OPP or met-OPET);
- stand-up pouches (met-OPP or met-OPET);
- meat or cheese packages (met-OPET).

The metallized layer is typically turned inward in a laminate structure to protect the thin metal layer. Some example structures include OPP/print/

adhesive/met-OPP and print/OPET-met/adhesive/PE sealant film.

Metallized film has replaced aluminum foil in some barrier packaging applications. While in theory foil has superior barrier properties, handling and flex cracking can reduce its performance. An economic analysis by Lush and Ferrari shows that metallized films may provide a lower total cost in many applications when taking into account price per square meter, handling and processing [139].

Transparent barrier coatings of SiO_x and AlO_x onto film substrates are also available. These provide moisture and oxygen barrier but not opacity. They are useful for applications not requiring light barrier, where the product is meant to be seen, or when aluminum coatings interfere with online packaging metal detectors used to detect possible contamination in the product. Electron beam deposition or plasma-enhanced chemical vapor deposition processes are typically used to apply these coatings. At present these coatings are about two to three times more expensive than aluminum metallization [140].

4.3.5 Cellophane

Cellophane is a transparent film made from cellulose that has low permeability to oxygen, moisture, oil, grease, and bacteria. As described in Chapter 1, its introduction in the early 20th century allowed for the mass production and promotion of food items and changed the retail environment in the United States and elsewhere. It has largely been displaced by less expensive petrochemical-based films, such as OPET.

Cellophane is made from a rather complex process. Cellulose from wood or other sources is dissolved in alkali and carbon disulfide to form a viscose solution. The viscose is extruded through a slit into a bath of sulfuric acid and sodium sulfate to reconvert the viscose into cellulose. The film passes through a series of baths to remove excess sulfate and add softeners or plasticizers. Various mixtures of glycols, such as propylene, ethylene, or triethylene glycol, are typically used as the plasticizer to keep it from getting too brittle for packaging applications. After the film is dried, it is typically coated. Uncoated film has few packaging applications as it loses too much water and becomes brittle, or absorbs too much water, and loses its natural gas barrier properties. Nitrocellulose-based waterproof coatings were first developed by DuPont in the 1930s and are still used today. Other coatings have been developed, including ones based on PVDC, which provide additional functionality, such as heat resistance to heat seal jaws during heat sealing. Varying the plasticizer and coating technology allows the properties of cellophane to be tailored to a wide variety of application needs [141].

Cellophane is inherently stiff with a secant modulus in the range of 750 kpsi (5200 MPa), higher than OPET. It has high temperature resistance (typically up to 177°C), excellent moisture and oxygen barrier (depending on the coating), and oil and grease resistance.

Cellophane lost ground to lower cost petrochemical-based films such as BOPET and BOPP in the 1980s and 1990s. It has made somewhat of a resurgence in recent times due to the fact it is biosourced, compostable, and biodegradable. Its sustainability record is clouded by its energy-intensive manufacturing process and potential negative impact of some of the chemicals used, but significant progress in recent years has been made by leading manufacturers in reducing their environmental footprint [142].

4.3.6 Paper and Paperboard

Paper has been used as a packaging substrate for over two millennia. The main ingredient for making paper today is wood pulp. The properties of the paper vary depending on the type of wood and pulping process. Softwood pulp (from conifer trees) produces paper with good strength and tear resistance but with high porosity and roughness. Hardwood pulp (from deciduous trees) is suitable for making smooth paper for writing and printing. Often a blend is used [145].

Mechanical and chemical processes have been developed to make wood pulp. The mechanical process produces weak paper that is not suitable for packaging. The kraft (sulfate) process for the chemical pulping of paper is the dominate process used today. It produces higher yields and stronger paper, and the chemicals are more easily recovered than competing processes.

Unbleached paper is generally stronger, stiffer, and more course than bleach counterparts, but bleach paper is used for more applications.

While there is no official delineation between paper and paperboard, in general the cutoff is around 12 mils (300 μm): paper is below 12 mils thick and

paperboard above. Basis weight (weight per area) is a standard measurement used to specify papers. A standard ream of paper in the United States is based on 500 sheets of 24 × 36 in. paper or 3000 ft^2. The number of sheets and paper size that make up a ream may differ by region or application so it is important to pay attention to what is meant by a ream. The basis weight is often reported in lb/ream, kg/ream, or g/m^2 (gsm). The conversion factor to gsm (grams per square meter) is 1.6725 gsm per lb/ream for a ream of 3000 ft^2.

Typical packaging papers range from about 18 to 90 lb/ream (30−150 gsm) but may be as low as 10 lb/ream (17 gsm) and as high as 200 lb/ream (335 gsm). Paperboard generally starts at 150 lb/ream (250 gsm) but typically is in the range of 120−360 lb/ream (200−600 gsm) for packaging. Density can vary from about 2.2 to 4.4 g/cm^3 and so a wide range of thickness and strength is available.

Another classification is course versus fine papers. Course packaging papers are made from unbleached kraft softwood pulps. Fine papers are typically made from bleached pulps and used in demanding printing and barrier applications.

Some of the properties that differentiate one paper or paperboard from another include the following [146]:

- paper specifications;
  - basis weight,
  - specific volume,
  - thickness,
  - relative humidity,
  - porosity.
- optical properties;
  - opacity,
  - whiteness,
  - gloss.
- surface properties;
  - smoothness,
  - roughness,
  - surface energy/contact angle.
- strength;
  - tensile strength,
  - elongation at break,
  - tear strength,
  - stiffness.
- absorption;
  - moisture,
  - water vapor,
  - ink,
  - oil and grease.

TAPPI, ISO, and DIN test methods have been developed for these properties.

4.3.6.1 Common Paper Types Used in Packaging

4.3.6.1.1 Kraft

Kraft comes from the German word meaning strong. Kraft paper is made from at least 80% sulfate wood pulp. It is course and exceptionally strong, making it well suited for a packaging substrate. It is sometimes made with a rough surface to prevent bags from sliding off pallets. It accepts print from letterpress, flexography, and offset processes. It finds use in multiwall bags, shipping sacks, tape, sacks, envelops, and wraps.

4.3.6.1.2 Bleached

Bleached paper is used in applications that place a high value on printing, writing, or special functionality (such as barrier). It is generally not as strong as kraft paper but can be made with a good balance of strength and printability. Bleached pulps are generally white, bright, and soft. They are susceptible to chemicals used to impart special functionality. The whiteness helps in printing and they can be enhanced by clay coating on one or both sides.

4.3.6.1.3 Specialty Papers

"Greaseproof paper" is manufactured to have a pore-free structure to inhibit grease from penetrating. It is aided by the fact that cellulose is hydrophilic and so resists hydrophobic materials like grease. Chemical or mechanical refinements, as well as calendaring, are used to produce the structure.

Grease-resistant paper resists staining from oil and grease. This is achieved by a variety of methods, such as treatment with fluorochemicals or applying various coatings such as wax or PVDC. Oleophobic

chemicals have been developed to impart both grease and water resistance. Examples of these chemicals include alkylsuccinic anhydrides and alkylketene dimers. These may be added during the paper making process or as sizing in online coating processes. Specialty coatings have been developed for specific chemical resistance.

Grease and water resistance paper has many applications, including quick service restaurant food packaging, pet food packaging, and meat wraps.

Coated paper generally refers to clay-coated paper. Clay is often used to provide a smooth, glossy surface for printing. Other coatings include extrusion coatings and aqueous coatings for barrier and heat seal applications.

4.3.6.2 Paperboard for Packaging

Paperboard comes in a variety of structures, single and multiply. Single ply paperboard from bleached wood pulp is used where cleanliness and purity is important, together with good strength and printability. Multi-ply is used over a broader range of applications since quality outer plies can be combined with less expensive middle plies. They may be combined with plastic coatings or be used in laminations to extend their application range.

Examples of paperboard's use in flexible packaging include polyethylene-coated milk cartons, composite cans and laminations with foil, and polyethylene for aseptic juice boxes.

For General Reading

1. Sikora M. Paper. In: Bakker M, editor. Wiley encyclopedia of packaging technology. New York: John Wiley & Sons; 1986. p. 497–500.
2. Attwood BW. Paperboard. In: Bakker M, editor. Wiley encyclopedia of packaging technology. New York: John Wiley & Sons; 1986. p. 500–6.

4.4 Material Specifications

The manufacture of any material produces variability in composition and properties. Suppliers use a variety of tools to control this variation within a set of sales specifications. The sales specifications are set according to the needs of the users and the capabilities of the manufacturing unit. Sales specifications set too tight may result in low yields and poor economics for the supplier. Specifications set too wide may cause problems with the customer, resulting in loss of business. Hence, materials suppliers are continuously striving to improve their quality control to satisfy customer needs at the highest yields. Some of the tools used to achieve quality control include statistical process control, online or offline measuring of key properties, online monitoring of important process variables, established procedures, and standard operating conditions.

The nature of the manufacturing process determines the type and frequency of measurements for quality control. A continuous film process, for example, may have an online gauge for total thickness as well as video inspection for defects; measurements are made on a continuous basis. Other tests, such as heat seal or burst strength, are destructive tests and can only be made periodically, perhaps on samples taken at the end of each roll. A resin producer may have a continuous process but rely on monitoring and control of key process variables while taking samples periodically to measure properties for release to sales. The frequency of the sampling can be determined by statistics and depends on the variability of the process, run rate, and other considerations.

Many properties used for quality control are designed to ensure the composition is under control and may not be directly related to the end use. For example, melt index is often used as a quality control measurement for polyolefin production. Melt index is a measure of how much polymer melt flows through a standard orifice using a standard weight, time, and temperature. It is inversely related to viscosity, but the relationship is not exact. The deficiencies of relying on melt index for polymer processing are discussed in Chapter 5. Here it is important to note that melt index is used as a surrogate for molecular weight control. The higher the melt index, the lower the MW for a given polymer type. But other factors influence the melt index as well, such as melting point, branching, and MWD. Hence, two polymers with the same melt index from two different manufacturers may have very different flow characteristics in a film converting process. But for a given manufacturer and product, maintaining the melt index within a specified range is a good way to ensure the product is consistent from lot to lot. It is also important to note that typically melt index is not the

only parameter that is being tested or measured to ensure the process is under control. With experience, the manufacturer may have developed relationships between key process parameters such as reactor temperature or pressure and molecular weight. The combination of ensuring the process is under control as well as periodic testing is the bedrock of modern manufacturing.

Often properties that a manufacturer specifies differ from scientific measurements that may be conducted in a research environment. Returning to the example of melt index, in a laboratory environment gel permeation chromatography is typically used to characterize the MW and MWD. This test is time-consuming and not very robust for a manufacturing environment. The melt index test can be done in 10 min for the quick turnaround times needed for quality control. Similarly nuclear magnetic resonance spectroscopy may be the best scientific technique to determine molecular structure, but Fourier transform infrared spectroscopy (FTIR) is often used because it is faster. Or a simple density test with a density gradient column may be sufficient to ensure the comonomer content is within spec for an LLDPE. Cost, turnaround time for test results, and robustness in a manufacturing environment are all considered when developing quality control tests and specifications.

For quality control (QC) tests, the manufacturer will often make standards to correlate the QC test with a known laboratory test. From this data, the manufacturer can set reasonable specifications. Developing such tests is not always easy and may require substantial time and effort for new products. For example, IR is often used to measure the composition of the comonomer in copolymers, but the IR spectrum from different comonomers may interfere and obscure the presence of others, or change the quantitative relationship between peak size and composition. Subtractive techniques may help, where a baseline spectrum is subtracted from the measured spectrum to eliminate interference. But this may introduce other errors. The importance of developing quality control tests for new products should not be overlooked during the development process.

Properties that are specified by the manufacturer may also differ from what may be reported on a product data sheet. Product specifications are meant to ensure the process in under control and the product is consistent from lot to lot. Product data sheets often list "typical" properties. These are properties that are reasonable to expect from the product but may not be measured on every lot or used to determine if the product is fit for sale. Data sheet properties are meant to provide a starting point for product use and design.

Some typical properties that may be specified by resin manufactures are given in Table 4.9. Generally a resin supplier will specify four types of characteristics: rheology, composition, appearance, and additives. Rheology is the measurement of how the polymer flows. For PE, the melt index is the most commonly specified measurement of flow. Melt index is the weight in grams that flows from a specified orifice in 10 min under a weight of 2160 g at a temperature 190°C. Other weights and temperature may be specified, and the industry convention is to call this measurement melt flow rate. For example, for PP, 230°C is typically used. Intrinsic and inherent viscosities are solution viscosities and are typically used for polyamides and polyesters.

For the purposes of quality control, the rheology is used as a tool to ensure the molecular weight is within specification. The viscosity is related to the MW to the 3.4 power and so small changes in MW will have a large impact on viscosity. Viscosity is also impacted by MWD and branching. Some resin producers use online measurements of viscosity that they correlate to melt index or other specified rheological measurements.

For copolymers some sort of measurement of composition is typically specified. For LLDPE, the amount of butene, hexene, or octene is monotonically related to the polymer density. Therefore, density is measured and specified. For an ethylene copolymer such as EVA, the amount of VA is specified. FTIR is often used to measure the comonomer content of the polymer.

Film appearance is important in flexible packaging. Most polymers sold into the flexible packaging market will have a specification around film defects that may originate with the polymer manufacturing process, such as some types of gel or "fisheyes" and black specs. The resin manufacturer will extrude a sample into a film and measure defects per unit area. Visual standards may be used to rate film quality but in recent years most of this has been automated with cameras and digital defect counters.

Some resins may contain additives for specific functionality, such as slip and antiblock additives.

Table 4.9 Typical Properties Specified by Manufacturers

Category	Test	Comment
Rheology	Melt index Melt flow rate Intrinsic viscosity	These measurements are surrogates for MW
Composition	Density FTIR	For PE, density is an indication of comonomer content; FTIR and other spectroscopy techniques are used for measuring comonomer content
Appearance/contamination	Gel/fisheyes Black specs	Typically a count per standard area of film or weight of pellets (black specks) or a pass/fail versus a standard
Additives	Additive concentration	Some suppliers may provide data on measured amounts of additives, such as slip agents
Films	Thickness Surface energy Defects Optical properties	These are some of the properties that may be specified
Paper	Basis weight Thickness Density or specific volume Smoothness Porosity Absorption (water, and so on)	These are some of the properties that may be specified

The amount of the additive may be specified by some manufacturers, rather than a property such as COF. COF will depend on the slip additive concentration, thickness of the film, presence of adjacent layers in the film, and temperature. Converters often add to the amount of slip in the product for a given application. Hence, they need to know how much is in the product to begin with.

Substrates such as film, foil, and paper have their own set of specifications. Thickness uniformity is one of the most important properties. Surface characteristics may be another. For a film, the surface energy or dyne level may be specified. A foil may be classified by the class of finish (A, B, and so on). Film defects and optical properties may be specified. For paper, properties such as basis weight, porosity, and smoothness may be specified.

4.5 Regulatory Considerations

Compliance with appropriate government regulations for food, medical, and other packaging applications is an important consideration for material selection and structure design. The materials and additives that comply with food and medical packaging regulations is a small subset of the available materials and thus limit the choice of the packaging engineer. There are also materials, or components of materials, that may not be regulated but nevertheless be unsuitable due to public perception. Recent examples of chemicals that have come under public scrutiny due to possible health concerns include some types phthalate plasticizers used in PVC, bisphenol A found in polycarbonate and epoxies, and C8 fluorochemicals.

This introductory chapter will not go into detail about regulatory compliance. Good references on the subject include Ebnesajjad [147] and Knight and Creighton [148]. Since food packaging is the largest application of flexible packaging, the focus will be on describing the process for determining food packaging compliance in the United States and in Europe. The rest of the world tends to follow one of these, but other countries may have their own local regulations.

Special considerations for health-care packaging are also briefly described. Communication with regulatory agencies, study of the complete regulations, and obtaining sound legal advice is recommended for determining the compliance status of a package.

4.5.1 Food Packaging Regulatory Compliance in the United States

In the United States, every component of a food package must comply with the appropriate regulation for food packaging. For multilayer packaging, this means each layer must comply and if a layer comprises of more than one material (such as a blend), each component must comply. The individual substance that may reasonably be expected to migrate to the food in its intended use in the food contact material must be covered by one of the following:

- a regulation listed in Title 21 Code of Federal Regulations (CFR);
- a prior sanction letter;
- meeting the criteria for a generally considered safe status (GRAS);
- a threshold of regulation (TOR) exemption;
- an effective food contact notification (FCN).

An important difference between the United States and Europe is that the U.S. Food and Drug Administration (FDA) generally considers each polymer as a different material and subject to regulation, even if it is comprised of monomers used in already approved materials. In Europe, the regulatory process is built upon the status of the monomers; generally if the monomer is on the approved list, then any polymer made from that monomer is approved.

It is the responsibility of the manufacturer of the food packaging article to ensure that their article complies with the regulations. The regulations may set limitations on the use of materials depending on the application, such as temperature in use and the type of food being packaged. Extraction tests may be required to ensure the article meets the limitations set forth by the regulations. The regulations provide guidance for the type of testing required.

When determining whether a component used in a food package complies with the regulations, there are several places to begin:

- Consult the component manufacturer's product data sheet, which may have a statement regarding FDA compliance.
- Consult 21 CFR 174-179 to see if the component is appropriately regulated as an indirect food additive for the intended use.
- Consult 21 CFR 182-186 to determine if the component is GRAS or consult the GRAS notices.
- Consult 21 CFR 181 to see if the use of the component has been sanctioned for food contact.
- Consult the listing of Threshold of Regulation Exemptions.
- Consult the listing of Effective Food Contact Substance Notifications.

Be aware that Food Contact Notifications (FCNs) are for a specific manufacturer for a specific substance and conditions of intended use [Section 409(h)(2)(C) of the Federal Food, Drug and Cosmetic Act]. They may not be used for similar substances or different manufacturers. FCNs are proprietary to the manufacturer and must be obtained from that manufacturer.

Section 21 CFR 174−179 contains the list of indirect food additives for food packaging. It can be further broken down as follows:

- 21 CFR 175: Adhesives and Components of Coatings;
- 21 CFR 176: Paper and Paperboard Components;
- 21 CFR 177: Polymers;
- 21 CFR 178: Adjuvants, Production Aids and Sanitizers;
- 21 CFR 179: Irradiation in the Production, Processing and Handling of Food.

The regulations can be found on the FDA website: http://www.fda.gov/.

If one or more of the components in the article are not in the above lists, this does not mean the

material is inherently unsafe. It simply means no one has taken the material through the appropriate regulatory approval process. The options for getting a new material approved include submitting a Threshold of Regulation Exemption Request, submitting a Food Contact Substance Notification, or satisfying the criteria for GRAS. Consultation with attorneys who specialize in food regulations is often advisable.

4.5.2 Food Packaging Regulatory Compliance in the European Union

In May, 2011 the European Union Plastics Regulation went into effect in all the European states, replacing previously existing national laws. This new regulation was published in the Journal of the European Union on January 15, 2011 [149]. The complete regulation is beyond the scope of this chapter, but some highlights are selected below. Note that this regulation is for plastics; other substrates such as foil or paper are covered by other regulations.

- For synthetic macromolecules (which includes polymers and plastics), the starting monomers as well as the macromolecules should be assessed for risk.
- In macromolecules produced by natural means, such as fermentation, the final product may contain non- or incompletely reacted substances. The final product should be assessed for its health risk.
- Directive 2002/72/EC, which the Plastics Regulation supersedes, had separate lists of authorized monomers for additives and polymers. These have been merged into the new regulation.
- Polymers may be used as the main structural component of plastics, as well as additives. For the case of polymeric additives, if the monomers or starting substances are the same as a structural polymer, and the monomers have already been authorized, the additive is considered authorized. If not, an assessment of the additive is necessary.
- Substances used to manufacture polymers may contain impurities. During manufacture, reaction and degradation by-products may form. Main impurities and by-products, if they are relevant, should be considered in the assessment, but all impurities and by-products need not be considered.
- Aids to manufacture of polymers, such as catalysts, chain transfer agents, chain extending agents, and chain stopping agents, when used in minute amounts and not intended to be in the final product are not subject to the authorization procedure.
- The release of substances from food contact materials and articles should not bring about unacceptable changes to the food. According to good manufacturing practices, the upper limit for migration from the article to the food is 10 mg/dm^2. This is based on 60 mg/kg of food. For packaging of foods intended for infants and children, whose consumption per body weight is higher, special provisions should be set.
- The regulations allow for the concept of a functional barrier in multilayer food packaging. If a layer prevents the migration of substances, then nonauthorized substances may be used in layers on the nonfood side of the barrier layer, provided the migration is below a specified detection limit. The maximum limit is 0.01 mg/kg of food for the nonauthorized substances. Substances that are mutagenic, carcinogenic, or toxic to reproduction, as well as nanoengineered substances, are not covered by the functional barrier concept.
- For multimaterial layers within a multilayer package, each material should comply, and the concept of functional barrier also applies.
- Coatings, printing inks, and adhesives are not yet covered by a specific EU legislation. These may be covered by individual country regulations within the EU.

At the risk of being too general, the basic requirements for establishing whether an article is authorized for use in contact with food are as follows:

- The substances used to manufacture plastics used in the layers and as components of multicomponent layers must be on the authorized union list. The list contains monomers or other starting substances, additives excluding colorants, polymer production aids excluding solvents, and macromolecules obtained from microbial fermentation.

- Substances used in the manufacture of plastic layers in plastic materials and articles are subject to specific and overall migration limits, as set out in the regulations. The specific migration limits (SMLs) are expressed in milligram of substance per kilogram of food (mg/kg). For substances with no SML or other restriction, a generic SML of 60 mg/kg is used. The plastic article is subject to total or overall migration limits as well.
- In multilayer packaging, the functional barrier concept may be invoked, as described above.
- Formulas are given in the regulation for testing and computing limits for packaging.

The complete regulation should be consulted for a given application. This brief description is solely intended to give the reader an appreciation of the process and is not a substitution for reading the complete regulation.

4.5.3 Health-Care Packaging

For packaging of pharmaceuticals, medical devices, and other medical products, the package materials and structures must meet the appropriate regulations and expectations of the governing bodies and standards organizations. These include European Union Directives, U.S. Federal Drug Administration, and International Conference on Harmonization (ICH) regulations and guidances, European regulations and standards from groups such as the U.S. Pharmacopeial Convention (USP), Japanese Pharmacopeia (JP), European Pharmacopeia (EUP), and the World Health Organization (WHO). The issues that must be addressed by the material and package suppliers include the potential for migratory species in the flexible packaging structure, tolerance of the package to downstream processes such as sterilization, reliability of supply, notification of change, and requests for plant audits by the film converters and end users.

Even after meeting all of the relevant regulations, there is inherently an increased amount of liability and risk in these applications. Companies that can provide high quality packaging for improved health care, however, are meeting an important societal need that will only grow as the human population increases and more people gain access to quality health care.

References

[1] DuPont-Teijin Films. Mylar polyester film, physical-thermal properties. http://usa.dupontteijinfilms.com/informationcenter/downloads/Physical_And_Thermal_Properties.pdf; n.d.
[2] Breeze R. Economic benefits of utilizing MDO film in flexible packaging. In: TAPPI PLACE conference; 2007. http://www.tappi.org/content/events/07place/papers/breese.pdf.
[3] DuPont Teijin Films. Oxygen and water vapour barrier properties of flexible packaging films. http://usa.dupontteijinfilms.com/informationcenter/downloads/Oxygen_And_Walter_Vapour_Barrier_Properties_of_Flex_Pack_Films.pdf; n.d.
[4] McKeen LW. Film properties of plastics and elastomers. 3rd ed. Oxford: Elsevier; 2012.
[5] ExxonMobil Chemical. Exceed mLLDPE Exceed 1018CA. http://www.b2bpolymers.com/TDS/Exceed_1018CA.pdf; n.d.
[6] ExxonMobil Chemical. Exact 3128 ethylene based plastomer resin. http://exxonmobilchemical.ides.com/en-US/ds133765/Exact%E2%84%A2%203128.aspx?I=58933&U=1; n.d.
[7] ExxonMobil Chemical. LDPE LD 071. http://exxonmobilchemical.ides.com/en-US/ds76856/ExxonMobil%E2%84%A2%20LDPE%20LD%20071%20Series.aspx?I=58933&U=1; n.d.
[8] ExxonMobil Chemical. LLDPE LL 1001. http://exxonmobilchemical.ides.com/en-US/ds76881/ExxonMobil%E2%84%A2%20LLDPE%20LL%201001%20Series.aspx?I=58933&U=1; n.d.
[9] ExxonMobil Chemical. HDPE HD 7845.30. http://exxonmobilchemical.ides.com/en-US/ds75243/ExxonMobil%E2%84%A2%20HDPE%20HD%207845.30.aspx?I=58933&U=1; n.d.
[10] DuPont. Elvax® ethylene vinyl acetate resins, packaging grade selection guide. 1992.
[11] DuPont. Surlyn® ionomer resin selector guide. 1994.
[12] Blueridge Films, Inc. Cast PP film properties. http://www.blueridgefilms.com/cast_polypropylene_properties.html; n.d.
[13] Inteplast Group, Ltd. AmTopp − EM BOPP. http://www.inteplast.com/amtopp/bopp/bopp_datasheets/EM.pdf; n.d.

[14] Impex Global, LLC. Biaxially oriented polypropylene film (BOPP). http://www.impexfilms.com/products/pdf/USTD/TSYBOPP.pdf; n.d.
[15] Kuraray. EVAL EVOH resins. http://www.kuraray.eu/fileadmin/presse/publikationen/downloads_k_fair_2013/eval/EVAL_Technical_Brochure_English_version.pdf; n.d.
[16] Butler TI, Morris BA. PE based multilayer film structures. In: Wagner J, editor. Multilayer flexible packaging, technology and applications for the food, personal care and over-the-counter pharmaceutical industries. Oxford: Elsevier; 2010. p. 211.
[17] Dealy JM, Wissbrun KF. Melt rheology and its role in plastics processing, theory and applications. New York: Chapman & Hall; 1995. p. 370.
[18] Stehling FC, Meka P. Heat sealing of semicrystalline polymer films. II. Effect of melting distribution on heat-sealing behavior of polyolefins. J Appl Polym Sci 1994;51:105−19.
[19] Torradas J. Enhancing packaging performance, value and sustainability with modifiers. DuPont web site: http://www2.dupont.com/Packaging_Resins/en_US/assets/downloads/white_papers/Enhancing_Package_Performance_Value_Sustainability_wModifiers_Torradas_9262011.pdf.
[20] Saltman RP. Partially grafted thermoplastic compositions. U.S. Patent 5091478. 1992.
[21] McTaggart LS. Thermoformed polyester articles having impact resistance and high temperature stability. U.S. Patent 3960807. 1976.
[22] Deyrup EJ. Toughened thermoplastic polyester compositions. U.S. Patent 4753980. 1988.
[23] Keller A, Machin MJ. Oriented crystallization in polymers. J Macromol Sci (Phys) 1967;B1:41−91.
[24] Deleted in review.
[25] Billmeyer Jr FW. Textbook of polymer science. 2nd ed. New York: Wiley-Interscience; 1971. p. 320.
[26] Wikipedia. Ziegler Natta catalysts. http://en.wikipedia.org/wiki/Ziegler%E2%80%93Natta_catalyst; n.d.
[27] Demirors M. The history of polyethylene. In: Strom E, Rasmussen S, editors. 100+ years of plastics. Leo Baekeland and beyond. ACS symposium series. Washington (DC): American Chemical Society; 2011. p. 115−38.
[28] Billmeyer Jr FW. Textbook of polymer science. 2nd ed. New York: Wiley-Interscience; 1971. p. 255−79.
[29] Unknown. R7.1 polymerization. http://www.umich.edu/~elements/07chap/html/polymerization.pdf.
[30] Lai SY, Wilson JR, Knight GW, Stevens JC. Elastic substantially linear olefin polymers. U.S. Patent 5272236. 1993.
[31] Soares JBP, Hamielec AE. Semicrystalline polyolefins − narrow MWD and long chain branching: best of both worlds. In: SPE ANTEC conference; 1996. p. 2334−41.
[32] Kim YS, Chung CI, Lai SY, Hyun KS. Melt rheological and thermodynamic properties of polyethylene homopolymers and poly(-ethylene/α-olefin) copolymers with respect to molecular composition and structure. J Appl Polym Sci 1996;59:125−37.
[33] Drent E, Van Broekhoven JAM, Doyle MJ. Efficient palladium catalysts for the copolymerization of carbon monoxide with olefins to produce perfectly alternating polyketones. J Organomet Chem 1991;417:235−51.
[34] Gupta P, Wilkes GL, Sukhadia AM, Krishnaswamy RK, Lamborn MJ, Wharry SM, et al. Does the length of the short chain branch affect the mechanical properties of linear low density polyethylenes? an investigation based on films of copolymers of ethylene/1-butene, ethylene/1-hexend and ethylene/1-octene synthesized by a single site metallocene catalyst. Polymer 2005;46:8819−37.
[35] Butler TI. PE processes. In: Wagner J, editor. Multilayer flexible packaging, technology and applications for the food, personal care and over-the-counter pharmaceutical industries. Oxford: Elsevier; 2010. p. 15−30.
[36] de Garavilla JR. Ionomer, acid copolymer, and metallocene polyethylene resins: a comparative assessment of sealant performance. TAPPI J 1995;78(6):191−203.
[37] Calhoun A. Polypropylene. In: Wagner J, editor. Multilayer flexible packaging, technology and applications for the food, personal care and over-the-counter pharmaceutical industries. Oxford: Elsevier; 2010. p. 31−6.

[38] Moore Jr EP. Polypropylene handbook. New York: Hanser Publishers; 1996. p. 6–9.
[39] Jester R. Heat seal characteristics of cyclic olefin copolymer/polyethylene blends. In: TAPPI PLACE conference, Boston, MA; 2002. p. 1308–34.
[40] Jester R. Cyclic olefin copolymer enhances polyolefin blends for film packaging. Plastics Technology; 2011. http://www.ptonline.com/articles/cyclic-olefin-copolymer-enhanced-polyolefin-blends-for-film-packaging.
[41] Gerbig S. Polyamide moisture absorption. Relative dimensional change of various nylon products. UL IDES. http://articles.ides.com/polyamide-moisture-absorption.asp; n.d.
[42] DuPont. DuPont™ Selar® PA 3426 blends with nylon 6. http://www2.dupont.com/Selar/en_US/assets/downloads/selar_pa3426_nylon_blends.pdf; n.d.
[43] Tubbs RK. Polyvinyl alcohol acrylate and methacrylate copolymers. In: Finch CA, editor. 1992, Polyvinyl alcohol – developments. 2nd ed. England: John Wiley & Sons, Ltd.; 1992. p. 399.
[44] Brant GW. Polyvinyl alcohol casting solution. U.S. Patent 2491642 A. 1949.
[45] Monosol, A Kuraray Company. Film data sheet. 2012. http://www.monosol.com/resources.php?p=61.
[46] Masuda M. Recent advances in polyvinyl alcohol film. In: Finch CA, editor. 1992, Polyvinyl alcohol – developments. 2nd ed. England: John Wiley & Sons, Ltd.; 1992. p. 403–31.
[47] Nippon Goshei. Bovlon. http://www.nichigo.co.jp/pvohfilm/english/bovlon/; n.d.
[48] Kuraray. Technical bulletin no. 110: gas barrier properties of resins. http://www.eval-americas.com/media/36916/tb_no_110.pdf.
[49] Chou RT, Deak GI. Blends of ethylene-vinyl alcohol copolymer and amorphous polyamide, and multilayer containers made therefrom. EP Patent Application 380123 A1. 1990.
[50] Ofstein DE. Blends of amorphous nylon and ethylene-vinyl alcohol copolymer for oxygen barrier containers. U.S. Patent 500302. 1991.
[51] Chou R, Lee I-H. The behavior of ethylene vinyl alcohol amorphous nylon blends in solid-phase thermoforming. J Plast Film Sheeting 1997;13:74–93.
[52] Fetell AI. Ethylene-vinyl alcohol copolymer blends with balanced properties for laminates. WO 9709380 Patent Application. 1996.
[53] Fetel AI. Nylon-containing ionomer improves the performance of ethylene vinyl alcohol (EVOH) copolymers in multilayer structures. In: 1997 TAPPI polymers, laminations & coatings conference proceedings; 1997. p. 503–5.
[54] Gimenez E, Lagaron JM, Cabedo L, Gavara R, Saura JJ. Study of the thermoformability of ethylene-vinyl alcohol copolymer based barrier blends of interest in food packaging applications. J Appl Polym Sci 2004;91:3851–5.
[55] Eval Americas. EVAL™ SP – oriented for the future. http://eval.cms.dms-soft.be/media/38081/eval%E2%84%A2%20sp%20resin%20brochure%20(english).pdf; n.d.
[56] Ikko M, Onishi H, Yamamoto T, Ninomiya K. Study on orientable EVOH. In: European TAPPI PLACE conference; 2009. http://www.tappi.org/content/enewsletters/eplace/2004/10-3matsui.pdf.
[57] Nippon Gohsei. Soarnol® grade line up. 2013. http://www.soarnol.com/eng/grade/index.html.
[58] Chow E. High barrier forming films with EVOH. In: TAPPI/CETEA VII international conference on flexible packaging, Brazil; 2012.
[59] Medlock ED. Nanolayer film structures with ethylene vinyl alcohol resins. In: TAPPI PLACE conference; 2012.
[60] Lee PC, Dooley J, Robacki J, Jenkins S, Wrisley R. Flex barrier property enhancement in film structures using microlayer coextrusion technology. In: SPE ANTEC conference; 2013.
[61] Xiao K, Lee I-H, Armstrong R. Comparison of water-quench versus air-quench blown film processes – part I: flat film properties. In: SPE ANTEC conference, vol. 70; 2012. p. 972–7.
[62] Xiao K, Lee I-H, Armstrong R. Comparison of water-quench versus air-quench blown film processes – part II: thermoformability. In: SPE ANTEC conference, vol. 70; 2012. p. 978–83.
[63] Renard V. Saran PVDC barrier resin concepts for demanding coextrusion and lamination applications. In: TAPPI PLACE European conference; 2005. http://www.tappi.org/content/enewsletters/eplace/2004/13-1Renard.pdf.
[64] Paisley K. PVDC – new developments, new opportunities. In: TAPPI PLACE conference; 2007.

[65] Mueller TR. PVDC – past and current barrier material. In: TAPPI PLACE conference; 2007.
[66] Honeywell. Honeywell Aclar® films. https://www.honeywell-aclar.com/Documentation/Honeywell-Aclar-advantage-overview-brochure.pdf; n.d.
[67] Jerdee GD. Polyethylene for extrusion coating. In: Bezigian T, editor. Extrusion coating manual. 4th ed. Atlanta: TAPPI Press; 1999. p. 201–8.
[68] Vansant JD. Acid copolymers for extrusion coating. In: Bezigian T, editor. Extrusion coating manual. 4th ed. Atlanta: TAPPI Press; 1999. p. 235–9.
[69] Lee I-H. Bonding 'unjoinable' polymers. DuPont; 2011. http://www2.dupont.com/Packaging_Resins/en_US/assets/downloads/white_papers/Bonding_Unjoinable_Polymers_Lee_92011.pdf.
[70] Tanny SR. Tie layer adhesives. In: Butler TI, editor. Film extrusion manual. Process, materials, properties. 2nd ed. Atlanta: TAPPI Press; 2005. p. 403–12.
[71] Morris BA. Factors influencing adhesion in coextruded structures. TAPPI J 1992;75(8): 107–10.
[72] Rolando TE. Flexible packaging – adhesives, coatings and processes. Rappa Review Reports, Report 122. Rappa Technology, Ltd.; 2000.
[73] Plastics News. Coke's PlantBottle use swells globally. 2013. http://www.plasticsnews.com/article/20130607/NEWS/130609933/cokes-plantbottle-use-swells-globally.
[74] Pepsi to launch 100% biobased PET bottle. Plastics Today; March 16, 2011. http://www.plasticstoday.com/articles/pepsi-launch-100-biobased-pet-bottle-03179.
[75] Beresford M. Braskem freezes green plastics plans, focusses elsewhere. BNAmericas; February 7, 2013. http://www.bnamericas.com/news/petrochemicals/braskem-freezes-green-plastics-plans-focuses-elsewhere.
[76] Liu H, Xu Y, Zheng Z, Liu D. 1,3-Propane diol and its copolymers: research, development and industrialization. Biotechol J 2010;5(11): 1137–48.
[77] Natureworks. Natureworks PLA Polymer 4032D biaxially oriented films – high heat. http://www.turbocad.com/LinkClick.aspx?fileticket=3zQxvk4wJsU%3D&tabid=1941&mid=5097; n.d.
[78] Deleted in review.
[79] Babu RP, O'Conner K, Seeram R. Current progress on bio-based polymers and their future trends. Prog Biomater 2013;2:8. http://www.progressbiomaterials.com/content/2/1/8.
[80] Wojtowicz A, Janssen LPBM, Moscicki L. Blends of natural and synthetic polymers. In: Janssen LPBM, Moscicki L, editors. Thermoplastic starch. Wiley-VCH Verlag GmbH & Co.; 2009. p. 35–53.
[81] Averous L. Biodegradable multiphase systems based on plasticized starch: a review. J Macromol Sci C – Polym Rev 2004;C44: 231–74.
[82] Lay G, Rehm J, Stepto RF, Thoma M, Sachetto J-P, Lentz DJ, Sibiger J. Polymer compositions containing destructured starch. U.S. Patent 5,095,054. 1992.
[83] Mayer JM, Hepfinger MJ, Welsh EA. Method of producing biodegradable starch-based product from unprocessed raw materials. U.S. Patent 5322866. 1994.
[84] Yu L, Coombs S, Bruce G, Christie Y. Biodegradable polymer. U.S. Patent 7326743B2. 2008.
[85] Kiyotsuna T, Minematsu H. Carbonated starch derivative and its production method. Japanese Patent JP2004359737A. 2003.
[86] Neelam K, Vijay S, Lalit S. Various techniques for the modification of starch and the applications of its derivatives. Int Res J Pharm 2012;3(5):25–31.
[87] Demirgoz D, Elvira C, Mano JF, Cunha AM, Piskin E, Reis RL. Chemical modification of starch based biodegradable polymeric blends: effects on water uptake, degradation behaviour and mechanical properties. Polym Degrad Stab 2000;70(2):161–70.
[88] Loercks J, Pommeranz W, Schmidt H, Timmermann R, Grigat E, Schulz-Schlitte W. Thermoplastic starch utilizing a biodegradable polymer as melting aid. U.S. Patent 6472497. 2002.
[89] Bastioli C, Bellotti V, Montino A. Polymers of hydrophobic nature, filled with starch complexes. U.S. Patent 6962950. 2005.
[90] Bastioli C, Bellotti V, Tredici G, Guanella I, Lombi R. Complexed starch containing

compositions having high mechanical properties. U.S. Patent 6,348,524 B2. 2002.
[91] Bastioli C, Bellotti V, Cella GD, Giudice LD, Montino S, Perego G. Biodegradable polymeric compositions comprising starch and a thermoplastic polymer. U.S. Patent 7,176,251 B1. 2007.
[92] Flaris V, Alexander N, Bagrodia S. Morphological characterization of novel bio-based hybrid resin. In: SPE ANTEC conference proceedings; 2008. p. 803–6.
[93] Raj B, Udaya Sankar K, Siddaramaiah. Low density polyethylene/starch blend films for food packaging applications. Adv Polym Technol 2004;23:32–45. http://dx.doi.org/10.1002/adv.10068.
[94] Favis BD, Rodriquez F, Ramsay BA. Polymer compositions containing thermoplastic starch. U.S. Patent 6.605,657 B1. 2003.
[95] King III RE. Additive for film products. In: Butler TI, editor. Film extrusion manual. Process, materials, properties. 2nd ed. Atlanta: TAPPI Press; 2005. p. 547–68.
[96] Keck-Antoine K, Lievens E, Bayer J, Mara J, Jung D-S, Jung S-L. Additives to design and improve the performance of multilayer flexible packaging. In: Wagner J, editor. Multilayer flexible packaging, technology and applications for the food, personal care and over-the-counter pharmaceutical industries. Oxford: Elsevier; 2010. p. 211.
[97] Zweifel H, Maier R, Schiller M. Plastics additives handbook. 6th ed. Cincinnati: Hanser Plublications; 2009.
[98] Stricker F, Horton M. New stabilizer solutions for polyolefin film grades. In: European TAPPI PLACE conference; 2003. http://www.tappi.org/content/enewsletters/eplace/2004/8-1stricker.pdf.
[99] Ezrin M, Lavigne G, Klemchuk P, Holley W, Agro S, Thomas JGL, et al. Discoloration of EVA encapsulant in photovoltaic cells. In: SPE ANTEC conference; 1995. p. 3957–60.
[100] Pern FJ. Ethylene vinyl acetate (EVA) encapsulants for photovoltaic modules: degradation and discoloration mechanisms and formulation modifications for improved photostability. Die Angew Makromol Chem 1997;252:195–216.
[101] ExxonMobil Chemical. Tip from technology, discoloration. 2003.
[102] Tikuisis T, Ellis L, Chisholm S. Improving the gas-fading performance of polyolefin film resins by addressing the over-oxidation of phenolic antioxidants. In: TAPPI PLACE conference; 2005.
[103] Ye Y, King III RE. Phenol vs. phenol free stabilization and the impact of selected grades of TiO_2: can we make non-discolored white LLDPE film by adding phenol-free masterbatch to phenolic AO stabilized resin?. In: TAPPI PLACE conference; 2007.
[104] King III RE. Stabilization of a clarified gamma irradiated controlled rheology polypropylene random copolymer. In: SPE polyolefins RETEC conference, Houston; 1999. p. 479–504.
[105] King III RE. Discoloration resistant polyolefin films. In: TAPPI polymers, laminations, adhesive, coatings and extrusions conference, San Diego, August 2001; 2001.
[106] King III RE. Discoloration resistant polyolefin films – part 2. In: TAPPI polymers, laminations, adhesive, coatings and extrusions conference, Boston, September 2002; 2002.
[107] King III RE. Discoloration resistant polyolefin films – part 3. In: TAPPI polymers, laminations, adhesive, coatings and extrusions conference, Orlando, August 2003; 2003.
[108] King III RE. Discoloration resistant LLDPE; an overview of stabilization issues & opportunities. In: SPE polyolefins RETEC; 2006 [Houston, TX].
[109] DuPont. Polymers, light and the science of TiO_2. 2007. http://www2.dupont.com/Titanium_Technologies/en_US/tech_info/literature/Plastics/PL_B_Polymers_Light_Science.pdf.
[110] Roussel MD, Guy AR, Shaw LG, Cara JE. The use of calcium carbonate in polyolefins offers significant improvement in productivity. In: TAPPI PLACE conference; 2005.
[111] Ruiz FA. Film physical property effects on low-level calcium carbonate addition to LLDPE. In: TAPPI PLACE conference; 2004.
[112] Guy AR. Calcium carbonates for polyolefin extrusion coating applications. In: TAPPI polymers, laminations, and coatings conference proceedings, Indianapolis, IN; 2004.
[113] Ruiz FA. Mineral enhancement of extrusion coated polyethylene. In: TAPPI polymers,

laminations & coatings conference proceedings. TAPPI Press; 1994. p. 89–95.
[114] Mount III EM. Control of dispersed polymer domain size formation in melt processing. In: TAPPI PLACE conference; 2007. http://www.tappi.org/content/events/07place/papers/mount.pdf.
[115] Kong D-C, Larter JA, Mount III EM. Opaque polymeric films cavitated with PBT and polycarbonate. U.S. Patent 6500533 B1. 2002.
[116] Maltby AJ, Marquis RE. Slip agents. In: Butler TI, editor. Film extrusion manual. Process, materials, properties. 2nd ed. Atlanta: TAPPI Press. p. 569–76.
[117] Fulmer MS. Introduction to lubricants and additives for polymer compounds. Struktol. http://www.struktol.com/pdfs/lubricants.pdf; n.d.
[118] Cadogan DF, Howick CJ. "Plasticizers," Kirk-Othmer encyclopedia of chemical technology. John Wiley & Sons, Wiley Online Library; 2000.
[119] Noon E. Fundamentals of nylon for flexible packaging. In: TAPPI PLACE conference; 2004.
[120] Mollison A. Films from nylon blends. Canadian Patent CA1222086 A1. 1987.
[121] Maki N, Nakano S, Sasaki H. Development of a packaging material using non-bleed-type antistatic ionomer. Packag Technol Sci 2004;17:249–56.
[122] Morris BA. New developments in ionomer technology for film applications. J Plast Film Sheeting 2007;23(April):97–108.
[123] Blatz PS. Extrudable composition consisting of a polyolefin and a fluorocarbon polymer. U.S. Patent 3,125,547. 1964.
[124] Lavallee C. Advances in polymer processing additives. In: TAPPI PLACE conference; 2005. http://www.tappi.org/content/enewsletters/eplace/2006/09-5Lavallee.pdf.
[125] Meillon MG, Morgan D, Bigio D, Migler K, Oriani S. A description of the fluoroelastomer coating evolution as a polymer processing aid. In: SPE ANTEC tech. papers; 2005.
[126] Oriani SR. Optimizing process aid performance by controlling fluoropolymer particle size. J Plast Film Sheeting 2005;21(July): 179–98.
[127] Bigio D. Fluoropolymer process aids: the effect of processing conditions. In: SPE ANTEC conference; 2009. p. 1547–56.
[128] Dotson DL. A novel nucleating agent for polyethylene. In: TAPPI PLACE conference; 2007. http://www.tappi.org/content/events/07place/papers/dotson.pdf.
[129] Lyondell. Equistar technical tip: additives: nucleating and clarifying agents. http://www.lyondellbasell.com/techlit/techlit/Tech%20Topics/General/Nucleating%20and%20Clarifying%20Agents.pdf; n.d.
[130] Eastman. Tackifier center: resources for formulation. http://www.eastman.com/Markets/Tackifier_Center/Pages/introduction.aspx; n.d.
[131] Epstein BN. Tough thermoplastic nylon compositions. U. S. Patent 4,174,353A. 1979.
[132] Natureworks. Technology focus report: toughened PLA. 2007. http://www.natureworksllc.com/~/media/Technical_Resources/Properties_Documents/PropertiesDocument_Toughened-Ingeo_pdf.pdf.
[133] Weaver LB, Dalla Valle SF, Franca MP. Improving mechanical properties of polyethylene and polypropylene recycled streams using polyoefin elastomers and functionalized polyolefins. In: SPE ANTEC conference; 2011.
[134] Torradas JM. Polymer modifiers in flexible packaging. In: TAPPI PLACE conference; 2012.
[135] Shubert G. Adhesion of aluminum foil to coatings – stick with it. In: European TAPPI PLACE conference; 2004.
[136] Murray L. The impact of foil pinholes and flex cracks on the moisture and oxygen barrier of flexible packaging. In: TAPPI PLACE conference; 2005.
[137] Prince PE. Metallizing. In: Bakker M, editor. The Wiley encyclopedia of packaging technology. New York: John Wiley & Sons; 1986. p. 443–6.
[138] Mount III EM. Metallizing process parameters: impact on deposition and optimum film properties. In: TAPPI PLACE conference; 2004.
[139] Lush J, Ferrari D. An economic value model for converters comparing the total cost of metallized film vs. foil in flexible packages. In: TAPPI PLACE conference; 2006.

[140] Bishop CA, Mount III EM. Vacuum metallizing for flexible packaging. In: Wagner J, editor. Multilayer flexible packaging, technology and applications for the food, personal care and over-the-counter pharmaceutical industries. Oxford: Elsevier; 2010. p. 185–202.
[141] Taylor CC. Cellophane. In: Bakker M, editor. The Wiley encyclopedia of packaging technology. New York: John Wiley & Sons; 1986. p. 159–63.
[142] Innovia. Natureflex next generation packaging, sustainability and life cycle performance. http://www.innoviafilms.com/InnoviaFilms-Kentico5/media/PDFs/MARKET%20BROCHURES/NATUREFLEX/Natureflex-Prod-Life-Cycle-Assess.pdf; n.d.
[143] Deleted in review.
[144] Deleted in review.
[145] Shackford LD. A comparison of pulping and bleaching of kraft softwood and eucalyptus pulps. In: 36th international pulp and paper congress and exhibition, October 13–16, 2003, Sao Paulo, Brazil; 2003. http://www.celso-foelkel.com.br/artigos/outros/A%20Comparison%20of%20Pulping%20and%20Bleaching%20of%20Kraft%20Softwood%20and%20Eucalyptus%20Pulps.pdf.
[146] SAPPI Fine Paper. Paper standards and measurements. http://www.sappi.com/regions/sa/SupportAndSponsorships/Knowledge%20bank/Technical%20brochures/Paper%20-%20Standards%20and%20Measurements/20070709PaperStandards MeasurementsfinalversionENG.pdf.
[147] Ebnesajjad S. A survey of regulatory aspects of food packaging. In: Ebnesajjad S, editor. Plastic films in food packaging, materials, technology and applications. Amsterdam: Elsevier; 2013. p. 345–88.
[148] Knight DJ, Creighton LA. Regulation of food packaging in Europe and the US. Rappa Review Reports. Rappa Technology Limited; 2004.
[149] The Official Journal of European Union. http://eur-lex.europa.eu/LexUriServ/LexUriServ.do?uri=OJ: L:2011:012:0001:0089:EN: PDF; January 15, 2011.
[150] Shin JY, Park JY, Liu C, He J, Kim SC. Chemical structure and physical properties of cyclic olefin copolymers. IUPAC Technical Report Pure Appl Chem 2005;77:801–14.

5 Rheology of Polymer Melts

The term "rheology" is derived from the Greek word *rheo* or flow. It is the study of how materials flow, or more specifically, how materials deform under an applied force. Polymers exhibit many complex and interesting flow properties that impact film fabrication, coextrusion, heat sealing, and other aspects of flexible packaging.

5.1 Basic Terms

In engineering terms, materials deform or flow when a force is applied. The amount of deformation is known as *strain* and how fast the deformation occurs is known as the *rate of strain*. The applied force per unit area is the *stress*.

There are two general modes of strain: shear and elongation. Fig. 5.1 illustrates a simple shear flow. Here a fluid is sandwiched between two parallel plates. The bottom plate is stationary and a tangential force F is applied to the top plate. The fluid is sheared as the top plate moves. Fig. 5.2 illustrates an elongational flow where the fluid is stretched upon application of the force. Some examples of shear flow include pressure-driven flow down a circular pipe or rectangular channel, as in a transfer pipe or die and much of the flow in a single screw extruder. Examples of elongational flow include the drawdown of a film after it exits the die in blown or cast film, film orientation in a tenter frame or double bubble process, and flow in certain types of mixing devices in extrusion. Most polymer processes have a combination of shear and elongational flow, or are *rheologically complex*. Such complex flows are difficult to study and model, but insight can be gained from the analysis of simple shear and elongational flow.

In Fig. 5.1, the force F is known as the shear force, which acts over the area (A) of the top plate (normal to flow). F/A is the *shear stress*. The rate of strain or shear rate is equal to the change in velocity divided by the separation distance between the two plates, h. Since the bottom plate is stationary, the change in velocity is simply U, the velocity of the top plate. The Greek letters sigma (σ) [or in some texts, tau (τ)] and gamma dot ($\dot{\gamma}$) are used to designate the shear stress and shear rate, respectively. The viscosity is a material property that describes the resistance to deformation and is equal to the shear stress divided by the shear rate:

$$\eta = \frac{\sigma}{\dot{\gamma}} = \frac{F/A}{U/h} \tag{5.1}$$

where η is the shear viscosity.

Similarly for elongational flow, tensile or elongational stress and rate of strain are defined, as

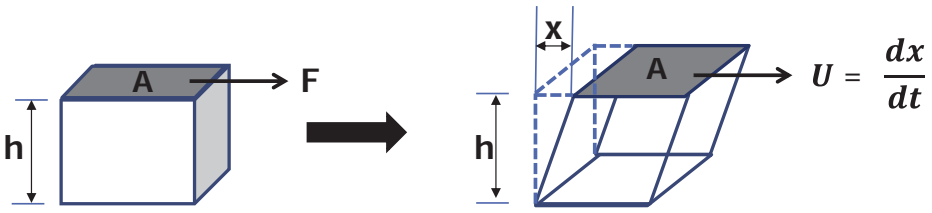


Figure 5.1 Simple shear flow. F, Force; U, velocity. *Inspired by M. Pottiger, DuPont.*

The Science and Technology of Flexible Packaging. http://dx.doi.org/10.1016/B978-0-323-24273-8.00005-8
Copyright © 2017 Elsevier Inc. All rights reserved.

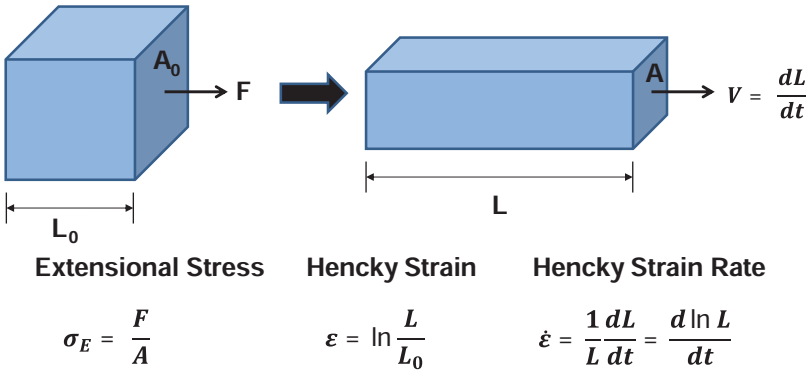


Figure 5.2 Extensional flow.
Inspired by M. Pottiger, DuPont.

illustrated in Fig. 5.2. The logarithm of the strain is used when the deformation is in increments. The *elongational* or *extensional viscosity* is the tensile stress divided by the strain rate:

$$\eta_E = \frac{\sigma_E}{\dot{\varepsilon}} \tag{5.2}$$

where η_E = extensional viscosity.

The extensional viscosity is sometimes associated with what is called the melt strength of the polymer. Melt strength is a subjective term that also may be related to elasticity and other properties of the polymer.

The stress is typically given in units of pounds force per square inch (psi) or Newtons per square meter (also known as Pascals, abbreviated as Pa). Shear rate has units of s^{-1}. Viscosity has units of Pa-s. Other units are given in Table 5.1. Viscosity of water and other small molecules are on the order of 10^{-2} Pa-s, whereas most polymer melts have viscosities in the range of $10-10^5$ Pa-s. Table 5.2 gives an order of magnitude value for the viscosities of several common materials that put the viscosity of polymers in perspective.

If the shear viscosity of a fluid does not change with shear rate, the fluid is known as a *Newtonian* fluid. Most polymers are *non-Newtonian*. A typical viscosity versus shear rate curve is given in Fig. 5.3. A key characteristic of the viscosity of many polymers is the decrease in viscosity with increasing shear rate, a phenomenon known as *shear thinning* behavior. Similarly, when subjected to a tensile stress, some polymers exhibit an increase in elongational viscosity as the rate of strain is increased. This is known as *strain hardening*. Other polymers *strain soften* with increasing rate of elongation. These are illustrated in Fig. 5.4.

If the material acts like a solid, the strain rather than the rate of strain is the appropriate value to describe how the material is deformed. Application of an applied stress will result in a given amount of strain. The *modulus* is the material parameter that describes the resistance of a solid to deformation and is defined as the ratio of the applied stress to the resulting strain:

$$E = \frac{\sigma_E}{\varepsilon} \quad \text{or} \quad G = \frac{\sigma}{\gamma} \tag{5.3}$$

where E = Young's modulus; ε = elongational strain; G = shear modulus; γ = shear strain.

Small molecules such as water in the liquid state are known as viscous liquids. Their deformation and

Table 5.1 Typical Units for Stress and Viscosity and Their Conversion Factors

Unit	Multiply by	New Unit
Force Per Area (Stress)		
Newton/m^2	1	Pascal (Pa)
lbf/in^2 (PSI)	6896	Pa
lbf/ft^2	47.88	Pa
Dyne/m^2	0.1	Pa
Atmosphere	1.01E+05	Pa
Kgf/cm^2	9807	Pa
Viscosity		
Centipoise	0.001	Pa-s
Poise	0.1	Pa-s
lbf-s/in^2	6895	Pa-s
lbf-s/ft^2	47.88	Pa-s

Table 5.2 Viscosity of Some Common Materials at Room Temperature

Liquid	Approximate Viscosity (Pa-s)
Glass	10^{40}
Molten glass (500°C)	10^{12}
Bitumen	10^{8}
Molten polymers	10^{3}
Liquid honey	10
Glycerol	1
Olive oil	10^{-1}
Water	10^{-3}
Air	10^{-5}

Adapted from Barnes HA, Hutton JF, Walters K. An introduction to rheology. Amsterdam: Elsevier; 1989. p. 13.

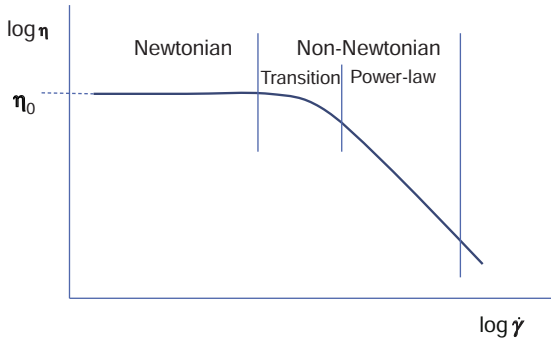


Figure 5.3 Typical viscosity versus shear rate curve.

flow can be described solely by viscosity. Simple elastic solids, known as Hookean solids, on the other hand, deform but do not flow under an applied stress. Their deformation can be described by the modulus. Polymers typically fall in between viscous fluids and elastic solids; they are known as *viscoelastic* fluids. A characteristic relaxation time can be described for a polymer that is related to how fast it responds to stress. Relaxation experiments and measurement of relaxation time are described in more detail in Section 5.5.1. To determine whether a polymer acts like a fluid, solid, or both, the relaxation time can be compared with the characteristic time scale for the process. A dimensionless number known as the Deborah number (De) is defined as the polymer relaxation time divided by the process time:

$$\mathrm{De} = \frac{\lambda}{t_f} \tag{5.4}$$

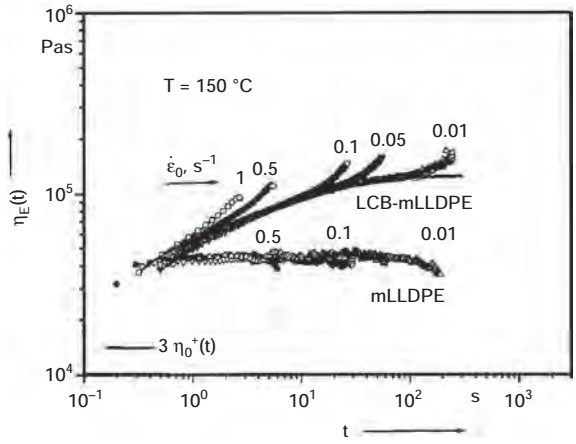


Figure 5.4 Examples of elongational viscosity behavior. Time-dependent elongational viscosity of a linear and a slightly long-chain branched metallocene linear low-density polyethylene (mLLDPE) of similar molecular mass distributions. The linear mLLDPE exhibits strain softening behavior whereas the slightly branched mLLDPE shows strain hardening behavior.
Reproduced with permission from Gabriel C, Munstedt H. Strain hardening of various polyolefins in uniaxial elongational flow. J Rheol 2003;47(3):619–30.

where De = Deborah number; λ = relaxation time of the polymer; t_f = characteristic process time.

If De » 1, the polymer will behave as an elastic solid. Conversely, if De « 1, it behaves like a viscous fluid.

The viscoelastic nature of a polymer arises from its molecular structure; polymers are long-chain molecules with long relaxation times compared to small molecules like water. The viscoelasticity of polymer melts give rise to *a normal force or stress*, as illustrated in Fig. 5.5. The normal forces act in the direction perpendicular to flow and are responsible for phenomenon such as the Weissenberg effect (where a viscoelastic fluid rises up a stirring rod when agitated), secondary flow patterns in polymer melts, and melt swell.

5.2 Importance of Rheology in Flexible Packaging

Rheology is a factor in almost every aspect of film extrusion, fabrication, and even in the end use. Fig. 5.6 shows the typical shear rate range for various processes superimposed on a shear

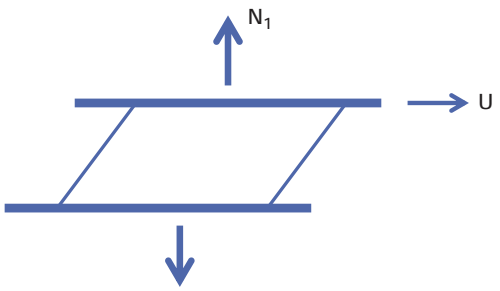


Figure 5.5 Illustration of normal force exerted on two parallel plates by a viscoelastic fluid in shear flow. The top plate is moved at velocity *U* and the bottom plate is stationary.

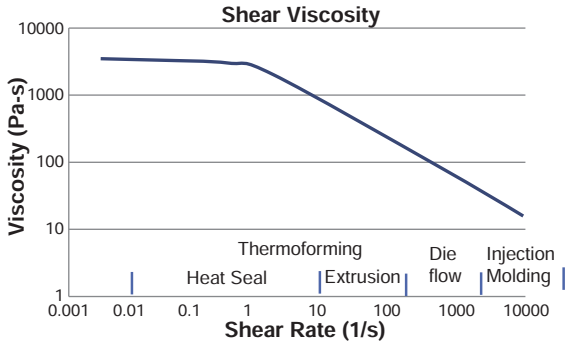


Figure 5.6 Typical shear rate ranges for commonly used processes in flexible packaging.

viscosity versus shear rate curve. Different portions of the curve are important for the different processes. At low shear rates, the viscosity curve is nearly horizontal; the viscosity is independent of shear rate. This is known as the Newtonian plateau, as shown in Fig. 5.3. The value of the viscosity in the plateau region is called the zero shear viscosity, η_0. At higher shear rates the viscosity decreases with increasing shear rate. This is the shear thinning regime. The amount of change can be several orders of magnitude and for this reason the log of the viscosity is typically plotted versus the log of the shear rate. On the log−log plot, the change in viscosity in this region is nearly linear. The viscosity in this region can be fit to a power-law model:

$$\eta = m\dot{\gamma}^{n-1} \tag{5.5}$$

Here n is the power-law exponent, and m is the consistency index. The value of n may be between 0 and 1. The closer n is to 1, the more Newtonian-like the fluid is. Fluids with lower values of n are said to be more shear thinning. The value of m can be obtained by looking at where the viscosity crosses the shear rate $= 1\ s^{-1}$ line. Factors that affect the values of m and n are discussed in Section 5.4.

At very high shear rates, the viscosity levels off again. This region is known as the second Newtonian plateau. The second Newtonian region is rarely reached in film extrusion, but sometimes is during the very high shear rates experienced in injection molding.

A Newtonian model (constant viscosity) can be used to fit the first part of the curve and the power-law model the second. Other models have been developed to fit the whole shear viscosity versus shear rate curve. Two popular models are the Cross model and the Carreau-Yasuda models. These are described in Table 5.3.

5.2.1 Extrusion and Film Fabrication

The shear thinning behavior of polymers is an important characteristic for extrusion. Greater shear thinning allows more output for a given pressure drop in the extruder. When linear low-density polyethylene (LLDPE) was first introduced, film fabricators struggled with processing it on their lines designed to process low-density polyethylene (LDPE). LLDPE is less shear thinning, resulting in higher viscosity at high shear rate than LDPE of the same molecular weight. Because of this, die

Table 5.3 Curve Fitting Models for Shear Viscosity

Model	Name
$\eta = \eta_0$	Newtonian model
$\eta = m\dot{\gamma}^{n-1}$ m = consistency index; n = power-law exponent	Power-law model
$\eta = \eta_0\left(1 + (\lambda\dot{\gamma})^a\right)^{\frac{n-1}{a}}$ η_0 = zero shear viscosity; λ, a, and n are fitted parameters	Carreau-Yasuda model
$\eta = \frac{\eta_0}{1+(\lambda\dot{\gamma})^{1-n}}$ η_0 = zero shear viscosity; λ and n are fitted parameters	Cross model

pressures became excessive. Processors had to slow their lines down to process it. Adding a small amount of LDPE substantially increases the shear thinning behavior and melt strength, allowing higher outputs [3–5].

The viscosity is also critical for helping melt the polymer in the extruder. Most single screw extruders rely on viscous heat generation to assist in melting the polymer (heat conduction from the heated barrels is not sufficient, particularly for large lines running at high output). The polymer generates heat as it is sheared. The amount of viscous heat generation is related to the product of the shear rate and shear stress:

$$D_{visc} = \sigma\dot{\gamma} = \eta\dot{\gamma}^2 \tag{5.6}$$

where D_{visc} = rate of viscous heat dissipation. Hence the viscosity plays a significant role in generating heat for melting. The adiabatic average temperature rise for polymer melts in an extruder is about 3°C for every 1000 psi (6.9 MPa) pressure drop, but local temperature rise near the wall can be greater since both the shear stress and shear rate are high in this region.

The viscosity of the polymer can also be important for mixing of polymers with other polymers or with mineral fillers. As discussed in detail in Chapter 6, matching the viscosities of the polymers in the blend often leads to the best blending. When dispersing pigments and other inorganic fillers, shear and elongational stresses act to break up the fillers into smaller particles.

The flow of polymers in an extruder and die is influenced by the shape of the viscosity versus shear rate curve. Table 5.4 gives stress, shear rate, and velocity profiles for flow in several simple shear flows for Newtonian and power-law fluids. The flow in the metering section of a single screw extruder, for example, is dominated by drag flow that is a form of simple shear flow shown in Fig. 5.1. In a simplification of the flow in the extruder, the screw flight is unwound into a rectangular channel, the screw is assumed to be stationary, and the barrel rotates. The top plate in Fig. 5.1 represents the moving barrel.

The flow in transfer pipes and the die is pressure-driven flow. The velocity profile in the channel is parabolic for a Newtonian fluid with a maximum at the centerline of the channel and zero at the channel wall. The classic assumption in fluid mechanics is to assume "no-slip" at the channel wall, meaning the fluid will take on the same velocity as the wall. There are situations where polymers exhibit some slip. The reader is directed to Vlachopoulis and Strutt [6] for details. Note that the shear rate and shear stress is zero along the centerline and maximum at the walls and that the shear stress is a linear function of the distance from the centerline. For shear thinning fluids ($n < 1$), the parabola becomes flatter as n decreases. The flow is said to be more "plug-like." This is illustrated in Fig. 5.7.

The elasticity of the polymer can give rise to normal stresses that produce recirculation flows in the corners of rectangular channels. An illustration of such a flow is shown in Fig. 5.8. These flows can result in stagnant areas in the extruder and die, leading to long hold-up times. This may lead to polymer degradation and contribute to film imperfections such as die lip build-up and gel. The elastic stress may also contribute to nonuniform film thickness and layer distribution in coextrusion. This is explored in Chapter 13.

Elasticity also contributes to swelling of the polymer as it exits dies. This phenomenon, known as *melt swell*, is illustrated in Fig. 5.9. A melt swell ratio can be defined as the ratio of the maximum diameter of the melt just after exiting the orifice to the orifice diameter. Melt swell is still not well understood. Newtonian fluids exhibit some swell, with a melt swell ratio of 1.13, due to streamline rearrangement at the die exit. Non-Newtonian polymers are known to exhibit ratios of up to 400%. Melt swell typically decreases as the die length increases, suggesting a memory effect. Melt swell can cause some problems with die lip build-up during film fabrication but is typically more of a problem with profile extrusion, where the final shape of the article can be affected by the amount of swell.

Melt fracture or extrudate distortion (Fig. 5.10) is an extreme example of a rheological phenomenon that affects productivity and quality. For linear polymers like LLDPE, as the throughput through a die is increased, at some point the surface takes on a rough appearance. This is known as sharkskin and typically occurs at a critical stress level of about 0.1–0.5 MPa [8]. It is generally thought that sharkskin is the result of rupturing of the melt at it accelerates near the die exit [9,10]. Addition of polymer processing aides, such as fluoroelastomers, which act to promote slip at the wall, helps delay the onset of sharkskin. Other techniques that have been proposed include heating the die lips to reduce the viscosity

Table 5.4 Equations for Simple Shear Flows (Q = volumetric flow rate, v = velocity)

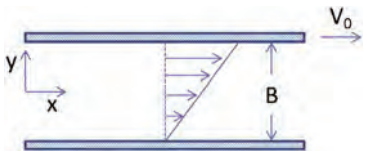
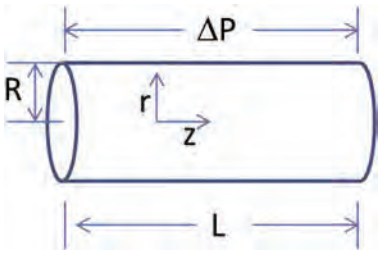
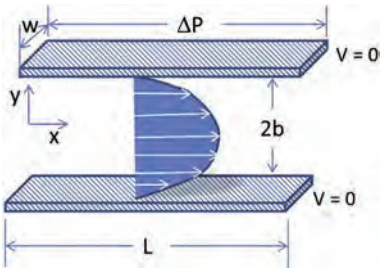
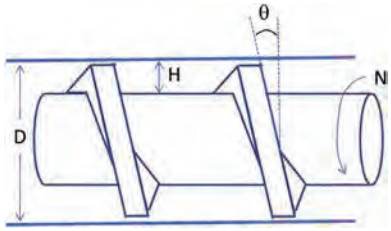
Flow	Equation	Picture of Flow
Drag flow between flat plates (Couette flow)	$v_x = \left(\frac{V_0}{B}\right)y$ $v_{avg} = \frac{V_0}{2}$ $Q = \frac{V_0 B w}{2}$ $\sigma_{yx} =$ constant $\dot{\gamma} = \frac{V_0}{B}$	
Pressure driven flow in circular channel (Poiseuille flow)	*Newtonian fluid* $v_z = v_{max}\left[1 - \left(\frac{r}{R}\right)^2\right]$ $v_{max} = \frac{R^2}{4\eta}\left(\frac{\Delta P}{L}\right)$ $v_{avg} = \frac{v_{max}}{2}$ $Q = \frac{\pi R^4}{8\eta}\left(\frac{\Delta P}{L}\right)$ $\Delta P = \frac{8Q\eta L}{\pi R^4}$ $\sigma_{rz} = -\frac{\Delta P}{2L}r$ $\sigma_w = -\frac{\Delta P}{2L}R$ $\dot{\gamma} = -\frac{2v_{max}}{R}\left(\frac{r}{R}\right)$ $\dot{\gamma}_w = -\frac{2v_{max}}{R} = \frac{4Q}{\pi R^3}$ *Power-law fluid* $v_z = v_{max}\left[1 - \left(\frac{r}{R}\right)^{\frac{n+1}{n}}\right]$ $v_{max} = \frac{n}{n+1}\left[\frac{R^{n+1}}{2m}\left(\frac{\Delta P}{L}\right)\right]^{\frac{1}{n}}$ $v_{avg} = \frac{n+1}{3n+1}v_{max}$ $Q = \pi\frac{n}{3n+1}\left[\frac{1}{2m}\left(\frac{\Delta P}{L}\right)\right]^{\frac{1}{n}}R^{\frac{1}{n}+3}$ $\Delta P = 2mR^{-(3n+1)}L\left[\left(3+\frac{1}{n}\right)\frac{Q}{\pi}\right]^n$ $\sigma_{rz} = -\frac{\Delta P}{2L}r$ $\sigma_w = -\frac{\Delta P}{2L}R$	

Table 5.4 Equations for Simple Shear Flows (Q = volumetric flow rate, v = velocity) (*Continued*)

Flow	Equation	Picture of Flow
	$\dot{\gamma} = -\frac{n+1}{n}\frac{v_{max}}{R}\left(\frac{r}{R}\right)^{\frac{1}{n}}$ $\dot{\gamma}_w = -\frac{n+1}{n}\frac{v_{max}}{R} = \left(\frac{3n+1}{4n}\right)\frac{4Q}{\pi R^3}$	
Pressure driven flow—rectangular channel	*Newtonian fluid* $v_x = v_{max}\left[1-\left(\frac{y}{b}\right)^2\right]$ $v_{max} = \frac{1}{2}\left[\frac{b^2}{\eta}\left(\frac{\Delta P}{L}\right)\right]$ $v_{avg} = \frac{2}{3}v_{max}$ $Q = \frac{2}{3}\frac{1}{\eta}\frac{\Delta P}{L}b^3 w$ $\Delta P = \frac{3\eta L}{2b^3}\frac{Q}{w}$ $\sigma_{yx} = -\frac{\Delta P}{L}y$ $\sigma_w = -\frac{\Delta P}{L}b$ $\dot{\gamma} = -\frac{2v_{max}}{b}\left(\frac{y}{b}\right)$ $\dot{\gamma}_w = -\frac{2v_{max}}{b} = \frac{3Q}{2wb^2}$ *Power-law fluid* $v_x = v_{max}\left[1-\left(\frac{y}{b}\right)^{\frac{n+1}{n}}\right]$ $v_{max} = \frac{n}{n+1}\left[\frac{b^{n+1}}{m}\left(\frac{\Delta P}{L}\right)\right]^{\frac{1}{n}}$ $v_{avg} = \frac{n+1}{2n+1}v_{max}$ $Q = \frac{2n}{2n+1}\left[\frac{1}{m}\frac{\Delta P}{L}\right]^{\frac{1}{n}} b^{\frac{1}{n}+2} w$ $\Delta P = \frac{mL}{b^{2n+1}}\left[\left(1+\frac{1}{2n}\right)\frac{Q}{w}\right]^n$ $\sigma_{yx} = -\frac{\Delta P}{L}y$ $\sigma_w = -\frac{\Delta P}{L}b$ $\dot{\gamma} = -\frac{n+1}{n}\frac{v_{max}}{b}\left(\frac{y}{b}\right)^{\frac{1}{n}}$ $\dot{\gamma}_w = -\frac{n+1}{n}\frac{v_{max}}{b} = \frac{2n+1}{n}\frac{Q}{2wb^2}$	
Single screw extruder, metering section • Newtonian fluid • 1st term drag flow • 2nd term pressure-driven flow	$Q = \frac{1}{2}\pi^2 D^2 HN \sin\theta\cos\theta - \frac{\pi D H^3}{12\mu}\sin^2\theta\frac{\Delta P}{L}$ where, Q = volumetric throughput; D = screw diameter; H = channel depth; N = speed of rotation; θ = helix angle; μ = viscosity; ΔP = pressure drop in metering section; L = length of metering section	

Vlachopoulos J. Introduction to polymer processing. 2nd ed. McMaster University; 1994.

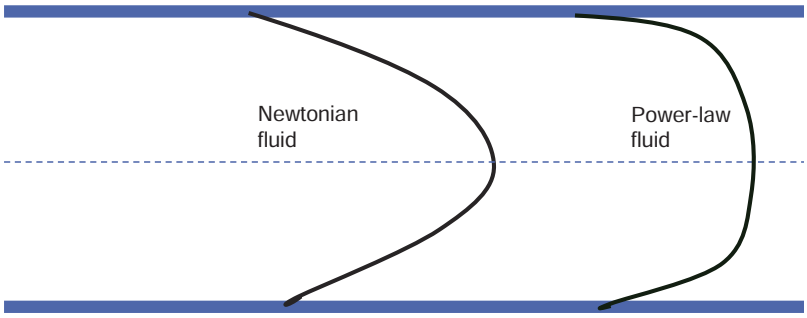


Figure 5.7 Velocity profile of pressure driven flow in a circular channel. The velocity of a Newtonian fluid is parabolic. A power-law fluid has more plug-like flow, depending on the value of the power-law exponent.

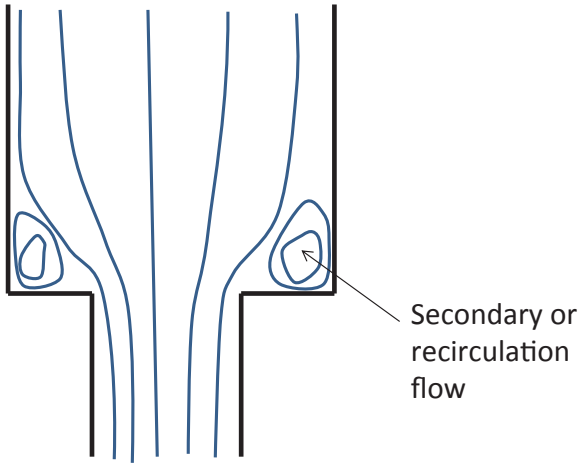


Figure 5.8 Example of recirculation secondary flows in the corners of a sudden contraction in a convergent flow channel. *Lines* represent streamlines or pathways of the flow through the channel.

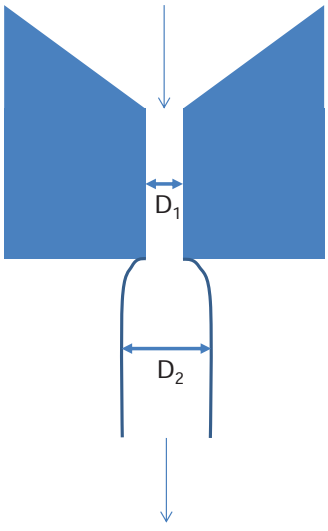


Figure 5.9 Illustration of melt swell.

and stress, flaring the exit angle of the die, and using special coatings on the metal surface [11,12].

Further increases in throughput may eventually lead to a flow regime where the extrudate is severely distorted as it exits the die, and wild pressure fluctuations occur. This is known as gross melt fracture or extrudate distortion. Such distortion results in poor appearance, nonuniform thickness, and other problems. A number of mechanisms have been proposed, including instabilities in the entry flow region (related to the secondary flows described earlier), elastic instabilities, and slip-stick phenomenon at the die wall. It is likely more than one mechanism may be involved [13–19].

In coextrusion, there are a number of flow instabilities that involve polymer rheology. These include the following:

- The layers may reorganize as they flow together down the channel. If the layers have different viscosities, the material with the lowest viscosity tends to migrate toward the high-shear rate region near the channel walls. This is the lowest energy state of the system. This reorganization or encapsulation can lead to layer nonuniformity. The channel dimensions are often contoured to counter this effect [20–22].
- If the stress at an interface in the die land region exceeds a critical value (typically around 40–80 kPa), a chevron pattern may develop in the film. This is known as zig-zap instability. Steps that reduce the interfacial stress, such as raising the temperature (to lower viscosity), increasing the thickness of the skin layer (to move the interface further away from the high-stress region near the die wall), and reducing the skin layer viscosity or reducing

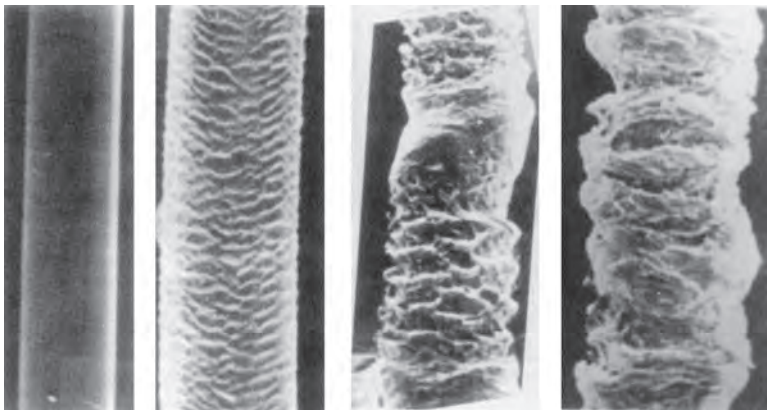


Figure 5.10 LLDPE extrudates obtained from a capillary at apparent shear rates of 37, 112, 750 and 2250 s^{-1}. *Reproduced with permission from Vlachopoulos J, Strutt D. Rheology of molten polymers. In: Wagner Jr JR, editor. Multilayer flexible packaging. Amsterdam: Elsevier; 2010. p. 68.*

output, help alleviate this type of instability [23–25].

- Wood grain and parabola-like patterns may develop in the film or sheet, an indication of "wave" type instability. This instability is believed to originate as the layers are first brought together in the feedblock or die. Differences in velocity, acceleration, and even elasticity are thought to be involved. Changes in die or feedblock design, resin types, and film structure may be needed to alleviate this type of instability [26–28].

These types of instabilities are discussed in more detail in Chapter 13.

Once the polymer melt exits the die, elongational flow predominates in film fabrication processes. The polymer is drawn down in thickness by impinging it onto a fast moving roll in cast film and extrusion coating, or in the case of blown film, by the combined action of blowing air inside the bubble to expand it laterally and the take-up roll which draws the film down in the machine direction. A number of instabilities and phenomenon can occur as the polymer is being drawn down and cooled that are influenced by the rheology of the polymer:

- In extrusion coating and cast film, the width of the melt curtain decreases as it is drawn down in thickness. This is known as neck-in. Neck-in reduces the thickness of the web, which can result in productivity issues. It also results in greater film or coating thickness near the edges, known as edge bead. Modern dies use inserts at the die edge to thin down the curtain before it exits the die to compensate. Increasing the melt strength of the polymer also helps. For example, LDPE with long-chain branching typically has less neck-in than LLDPE which has no long-chain branching. Ionomers and acid copolymers, which contain long-chain branching, as well as other chemical forces such as hydrogen bonding or ionic interactions, have even less neck-in. Broadening the molecular weight distribution (MWD) of PE typically reduces neck-in. Too little neck-in, however, can result in not enough of an edge-bead, which can lead to edge tear and line breaks [29,30].
- Drawing down the melt curtain at high speed can result in edge instability or draw resonance in extrusion coating or cast film. Also known as edge weave, this can result in line breaks or nonuniform coatings/films. The onset of the instability is related to the polymer rheology. Newtonian fluids have a critical draw ratio for the onset of draw resonance of 20:1. For non-Newtonian fluids, this may be higher or lower. Linear polymers, such as LLDPE, tend to draw down more than branched polymers. But for draw resonance, branched PE is more stable than LLDPE, and stability increases with increasing MWD and long-chain branching [16,31–34].
- In blown film, various modes of bubble instability may occur [32,35–37]. Such instability results in nonuniform thickness and ultimately lower line speeds. Melt strength and strain

hardening has been linked to improved bubble stability [3,32,35–44]. Linear polyethylene is known to have poorer bubble stability than branched polyethylene. Since the introduction of LLDPE and mLLDPE, blown film technology has evolved to better handle these materials, such as increasing the die gap and better cooling systems. Resin suppliers have tried to tweak the catalyst technology to allow the incorporation of long-chain branches. Processors often blend a small amount of LDPE into LLDPE to improve runnability and productivity, even though this negatively impacts properties.

These flow issues and instabilities are taken up in more detail in Chapter 13.

5.2.2 End Use

Some examples of how rheology affects the use of films include the following:

- Thermoforming: During forming, the polymer is heated and stretched into a cavity. Strain hardening is an important characteristic for the polymer to have to ensure uniform stretching and thickness in the final package. If an imperfection begins to occur where part of the film is drawn down more than another, the resistance to deformation in the thinned down region will increase in a strain hardening material. This self-correcting mechanism helps keep the thickness uniform throughout the forming process [44,45].
- Heat sealing: If the sealing pressure or temperature is too high, the sealant may flow too much during heat sealing, resulting in the sealant being squeezed out from the seal area. This can lead to poor seal strength. Depending on the geometry of the heat seal jaw, the shear rate during sealing may be quite small. Polymers with higher zero shear viscosity may have less squeeze out problems [46,47].
- Hot tack: After a heat seal is made but has not yet solidified, it may be subjected to opening forces such as the weight of the product in a vertical form fill seal packaging line. The resistance to seal failure from these opening forces is known as hot tack. Hot tack strength is a function of sealing temperature, and the temperature range over which hot tack strength is greater than the opening force is an important operational parameter. At low temperature, hot tack is controlled by the rate of intermolecular diffusion at the seal interface and other long range forces that act to create a good bond at the interface. At high temperatures, hot tack is dominated by the melt strength or viscosity of the polymer as it resists the opening stress (See Chapter 7 for details).
- Peel strength: The force required to pull a seal apart or to separate layers within a multilayer film structure is called the peel force or strength. The peel force is a complex function of the energy to irreversibly elongate the peel arm, the energy to bend the peel arm, and the energy to create new surface energy (called the fracture energy). The fracture energy is related to the bonding at the interface but is also influenced by local viscoelastic energy losses at the peel front as the specimen is pulled apart. As shown in Chapter 10, this viscoelastic energy contribution can be a significant portion of the measured peel strength.
- Physical properties: The stress–strain behavior of the film impacts the strength of the package. While typically outside the realm of melt rheology, factors such as modulus, elongation at yield, elongation at break, and tensile strength are important material properties that involve deformation of the polymer. An example is creep resistance of a pouch hanging on a peg in a store. The seal must not stretch and fail under the weight of the product. The change in strain under an applied stress is known as creep and is a fundamental rheological property of the material.

5.2.3 Polymer Characterization

Rheological measurements are often more sensitive to changes in polymer structure and molecular architecture than other analytical techniques. As such, rheology is used to characterize polymers. This can be useful during the development of new polymers, improving the properties of existing polymers or troubleshooting quality issues.

An example is small changes in MWD or branching that are not readily picked up in gel permeation chromatography, a commonly used method for measuring MWD. Some rheological measurements are very sensitive to the high MW

fraction in the polymer. For high-MW polymers above the entanglement MW, the viscosity is proportional to the MW raised to the 3.4 power. Small changes in MW can result in large changes in the viscosity.

At small deformations and slow rates of deformation, the rheological properties are typically linear. The rheological properties of polymers under such conditions are known as *linear viscoelasticity*. At larger deformations and fast rates of deformation, the rheological response becomes nonlinear. For characterizing molecular architecture (such as MWD), phase behavior, and polymer blends, linear viscoelasticity measurements are most useful. Methods such as dynamic rheology measurements (see Section 5.3.5), creep (Section 5.5.2), and stress relaxation (Section 5.5.1) experiments are often used. Deformation and rates of deformation during polymer processing, however, are typically in the nonlinear regime. Methods used to characterize fundamental polymer properties do not often translate to the nonlinear behavior found in film fabrication. A separate set of tools are used to measure properties in this regime, such as the capillary rheometer.

5.3 Rheological Measurements

5.3.1 Melt Index or Melt Flow Rate

The most commonly used rheological measurement for polyolefins is the melt flow rate (MFR). It is a measure of the mass of polymer that flows from an orifice under a given weight at a prescribed temperature. The melt indexer (the name of the instrument) consists of a heated tube, a piston for pushing the melted polymer, a weight that lies on top of the piston, and an orifice at the end of the tube. The dimensions of the orifice are specified in ASTM D1238 (ISO 1183) and fixed by the design of the instrument. The polymer pellets are introduced into the tube, and the piston is inserted to remove air from above the melting resin. After a prescribed amount of time to allow the polymer to melt and come to temperature, the weight is placed on top of the piston. The polymer that flows from the orifice in 10 min is weighed. The result is reported in grams per 10 min. The weight and temperature must also be reported. For polyethylene, the standard temperature and weight is 190°C and 2160 g, and the measurement is often called the melt index or MI. Higher temperatures are used for resins with higher melting points. For example, PP is typically measured at 230°C.

The MFR of a resin is inversely related to viscosity and molecular weight; high-MFR resins have lower MW and viscosity. The exact relationship between viscosity and MFR cannot be determined for several reasons:

- The shear rate is not controlled during the test. The stress (weight) is fixed rather than the shear rate (as is the case for a capillary rheometer). The shear rate will vary with the MFR. A crude calculation can be made for the shear rate in the capillary for a standard MFR test (2160 g):

$$\dot{\gamma} = \frac{1838}{\rho}\text{MFR} \tag{5.7}$$

  where $\rho =$ the melt density of the polymer. Assuming $\rho = 766$ kg/m^3 for a typical PE melt, $\dot{\gamma} = 2.4 \times$ MFR.
- The orifice length to diameter ratio (L/D) is zero, and entrance effects may result in significant errors. Corrections for capillary rheometry results are described in Section 5.3.3.
- Because of the short L/D, the flow is a combination of shear and elongational flow [48]. Capillary or cone and plate rheometry involves simple shear flow without any complications for elongational flow.

The MFR test is used as a quality control test by resin producers. For polymers of similar composition made on the same process, the MFR is a good control test. Over the years the MFR has been adopted by the industry as a surrogate for viscosity. As long as it is only used for general guidance, MFR is suitable for this purpose. Table 5.5 gives the typical MI range for various processes. It is important to note, however, that resins of the same MI can behave substantially different in a polymer process. This is because the MI only captures one point on the viscosity versus shear rate curve. Differences in shear thinning behavior, or other rheological phenomena, are not captured by the MI. This is illustrated in Fig. 5.11 where the viscosity curves for an LLDPE and LDPE for the same MI are shown. The LLDPE is less shear thinning and will extrude at higher pressure than the LDPE. This is not captured by the MI. Even within the same polymer family, grades with the same MFR can have

Table 5.5 Melt Index (MI) Ranges of Typical PE Grades by Process

Process	Typical MI range for PE, g/10 min (190°C/2160 g)
Blown film	1–5
Blown film (high stock UMW-high-density polyethylene)	0.01–1
Cast film	2–7
Extrusion coating	4–15

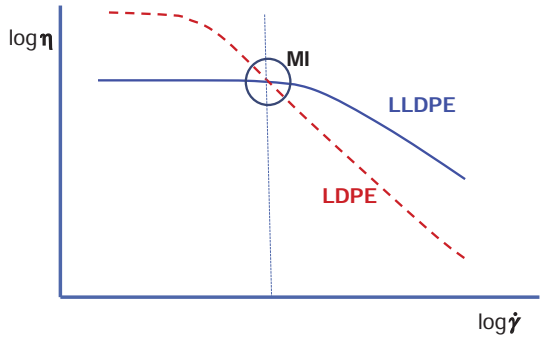


Figure 5.11 Comparison of viscosity versus shear rate curves for two types of polyethylene with the same MI. *LLDPE*, Linear low-density polyethylene; *LDPE*, low-density polyethylene; *MI*, melt index

significantly different processing behavior. For example, Clevenhag and Ovelby [49] screen many different grades of LDPE for suitability in a high-speed extrusion coating process. Even though all the grades have MIs in the typical range for extrusion coating, this is not enough to predict performance. They develop other screening measurements that predict suitability much better.

5.3.2 Solution Viscosity

Manufacturers of polyethylene terephthalate (PET) and PA 6 report a solution viscosity as a means of describing MW. The polymer is dissolved in a solvent at low concentrations and the viscosity measured either using a glass capillary viscometer (the time for the solution to flow through the capillary is related to the viscosity) or a rotational viscometer (such as a Brookfield viscometer). The solution viscosity is compared with the viscosity of the solvent; the ratio of the solution viscosity to the solvent viscosity is defined as the relative viscosity, η_r:

$$\eta_r = \eta/\eta_s \tag{5.8}$$

where η = solution viscosity; η_s = solvent viscosity.

The inherent viscosity (IV), η_{inh}, is the natural logarithm of the relative viscosity divided by the concentration:

$$\eta_{inh} = (\ln \eta_r)/C \tag{5.9}$$

where C is the concentration in g/100 mL in the United States and g/mL in Europe. Finally, the intrinsic viscosity, $[\eta]$, is defined as the limit of the IV as the concentration approaches zero:

$$[\eta] = \lim_{C \to 0} (\eta_{inh}). \tag{5.10}$$

The IV is found by measuring the solution viscosity at several concentrations, plotting η_{inh} versus C and extrapolating to zero concentration.

The IV is directly related to MW by the Mark–Houwink equation:

$$[\eta] = KM_v^a \tag{5.11}$$

where K = constant depending on the polymer solvent system; a = constant depending on the polymer solvent system; M_v = viscosity average molecular weight.

Values for K and a are tabulated in the literature [50–52]. The viscosity average molecular weight is related to the MWD in the following way:

$$M_v = \left(\sum_i w_i M_i^a \right)^{1/a} \tag{5.12}$$

where w_i = weight fraction of chain length M_i; M_i = molecular weight of chain with i repeat units.

M_v is typically about 80–90% of M_w and so the following approximation is often used:

$$[\eta] = kM_w^a \tag{5.13}$$

The PET industry typically uses IV, tested according the ASTM D4603. The polyester is dissolved in a solvent of 60% phenol/40% tetrachloroethane.

Bottle grades of PET have an IV of 0.70−0.85 dL/g. The viscosity of polyamide is typically reported as the relative viscosity. Formic acid, sulfuric acid, and *m*-creosol are commonly used solvents. Refer to ASTM D789 and D4878.

The IV and relative viscosity relate directly to the molecular weight of the polymer and are reported mostly for product design and quality control. The brittleness of PET, for example, is related to molecular weight and IV. For polymer processing, however, these values merely represent a benchmark. Processing conditions, and in particular the presence of moisture during processing, can significantly affect the melt viscosity. Furthermore, much like the MFR, these values only represent a portion of the viscosity versus shear rate curve. Shear thinning and other behaviors are not captured by the solution viscosity. For that, the melt viscosity must be measured.

5.3.3 Capillary Melt Shear Viscometry

Probably the most common viscometer used in industry for polymer melts is the capillary viscometer or rheometer. It is easy to operate, relative inexpensive, and captures viscosity data over a shear rate range of about 10−10,000 s^{-1}, which covers most polymer film and coating processes. Polymer pellets or powder are charged to a heated metal tube and allowed to melt. A piston pushes the polymer melt through a capillary die at a constant speed (shear rate). The pressure drop is measured, which is related to the stress. The ratio of the stress to shear rate is the viscosity. By taking measurements at several piston speeds, the viscosity over a range of shear rates is obtained.

Capillary viscometry differs from the MFR test in several important ways:

- Capillary viscometry controls the speed (shear rate) and measures the stress; the melt indexer uses a constant force (stress) and measures a flow rate. For reasons pointed out in Section 5.3.1, it is difficult to convert melt indexer data into a viscosity versus shear rate curve.
- Capillary viscometry allows the user to generate data over a wide shear rate range. The melt indexer generally captures data at only one stress, and shear rate varies with the molecular weight of the polymer being tested (see Eq. (5.7)).
- Capillary viscometry uses long dies that reduce entrance effects. The data can be corrected for entrance effect errors (see later discussion). The melt indexer uses a short *L*/*D* orifice that introduces entrance effect errors that cannot be corrected.

5.3.3.1 Basic Equations

The calculations for the capillary rheometer use equations that describe fully developed pressure-driven flow in a circular tube for a Newtonian fluid and then correct for non-Newtonian and entrance effects. As given in Table 5.4, the shear rate at the wall is related to the velocity:

$$\dot{\gamma}_w = \frac{2}{R} V_{max} \tag{5.14}$$

where $\dot{\gamma}_w$ = shear rate at the wall of the die; R = radius of die; V_{max} = maximum velocity in the channel.

It can be shown that

$$V_{max} = 2V_{avg} \tag{5.15}$$

and, therefore,

$$\dot{\gamma}_w = \frac{4}{R} V_{avg} \tag{5.16}$$

The average velocity, V_{avg}, is simply the piston speed. The volumetric flow rate, Q, is also related to the average velocity:

$$Q = V_{avg} \pi R^2 \tag{5.17}$$

Therefore, in terms of Q, the shear rate at the wall is

$$\dot{\gamma}_w = \frac{4Q}{\pi R^3}. \tag{5.18}$$

The shear stress is determined by the pressure drop:

$$\sigma = \frac{\Delta P}{2L} r. \tag{5.19}$$

where ΔP = pressure drop; L = length of the die; r = radial distance from the centerline.

Eq. (5.19) shows that the shear stress varies linearly with r and is greatest at the wall:

$$\sigma_w = \frac{\Delta P}{2L} R. \tag{5.20}$$

The shear rate and shear stress is calculated using Eqs. (5.18) and (5.20), knowing the dimensions of the die and the piston speed and measuring the pressure drop. Without any corrections, these are known as the apparent shear rate and apparent shear stress. The apparent viscosity, η_A, is simply the ratio of the shear stress to the shear rate:

$$\eta_A = \frac{\sigma_w}{\dot{\gamma}_w}. \tag{5.21}$$

Often times this is how the data will be reported from a resin supplier. The corrections described in the next section may change the absolute results by 20% or more and are important for scientific experiments, but are often not necessary to gain useful insight for polymer processing.

5.3.3.2 Corrections to Capillary Rheology Data

There are two corrections to capillary rheology data that are often applied. The first deals with the error associated with assuming the fluid is Newtonian and the second with entrance flow effects.

Even if the true nature of the flow is unknown, an elegant solution has been derived, often attributed to Rabinowitch, that allows the shear rate to be corrected for non-Newtonian effects. The procedure involves obtaining pressure drop data for a variety of flow rates, die lengths and die radii, and plotting $[4Q/\pi R^3]$ versus $[(\Delta P)R/2L]$. All should fall on the same line on a double log−log plot, the slope of which is b. The true shear rate at the wall is related to b:

$$\dot{\gamma}_w = \left(\frac{3+b}{4}\right)\dot{\gamma}_A \tag{5.22}$$

where

$$b = \frac{d(\log \dot{\gamma}_A)}{d(\log \tau_w)} = \text{slope of plot}. \tag{5.23}$$

For a power-law fluid, $b = 1/n$ and

$$\dot{\gamma}_w = \frac{3n+1}{4n}\frac{4Q}{\pi R^3}. \tag{5.24}$$

The pressure is measured from the reservoir on top of the die and represents the drop in pressure from the reservoir to the die exit, as shown in Fig. 5.12. This pressure drop includes contributions from the entrance to the capillary or die, the drop across the die itself, and the pressure drop at the exit of the die:

$$\Delta P = P_d - P_a = \Delta P_{entrance} + \Delta P_{die} + \Delta P_{exit} \tag{5.25}$$

where P_d = driving pressure; P_a = ambient pressure at die exit; $\Delta P_{entrance}$ = pressure drop in the entrance region to the die; ΔP_{die} = pressure drop through the die; ΔP_{exit} = pressure drop at the exit of the die.

The exit pressure drop is generally small but the entrance pressure drop can be significant. The entrance pressure drop is attributed to elastic effects since the value for a Newtonian fluid is small. Bagley proposed a method to correct for the entrance and exit effects by measuring the driving pressure at several values of L/R (by using several dies of constant radius but varying lengths). Plotting P_d versus L/R for a given piston speed (constant Q) yields a line

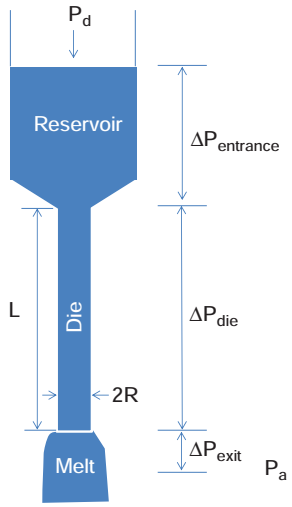


Figure 5.12 Contributions to pressure drop in a capillary viscometer.

that can be extrapolated back to $P_d = 0$ (here P_d is assumed to be the gauge pressure, $P_d - P_a$). The distance from this intercept and $L/R = 0$ is known as the Bagley end correction, e:

$$\sigma_w = \frac{P_d}{2\left(\frac{L}{R} + e\right)}. \tag{5.26}$$

The value of e for a Newtonian fluid has been shown to be 1.15 but can be near 20 for polymer melts near the onset of sharkskin [53]. More typically, the entrance effect may result in a 10–30% change in the calculated shear stress. As the L/R of the die is increased, the relative effect of the entrance pressure is diminished. Above L/R of about 50, the entrance effect becomes negligible.

A simple way to correct for entrance effects is to use a 2-bore capillary rheometer. This device has two bores that run off the same drive (and at the same piston speed). One bore has a die with a long L/R (typically 32), and the other one that has an L/R of 0, as shown in Fig. 5.13. Studies have shown that the P_a measured with the $L/R = 0$ die is equivalent to the entrance pressure drop [54], and

$$\sigma_w = \frac{\left(P_d^L - P_d^0\right)R}{2L} \tag{5.27}$$

where P_d^L = driving pressure measured in the bore with the long die; P_d^0 = driving pressure measured in the bore with the $L/R = 0$ die.

5.3.4 Cone and Plate Viscometry

The cone and plate viscometer, shown schematically in Fig. 5.14, is a type of rotational viscometer.

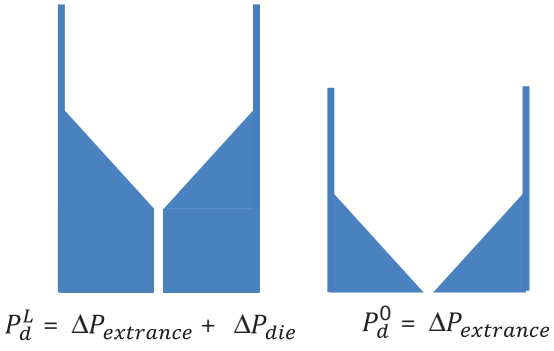


Figure 5.13 Dual bore capillary rheometer.

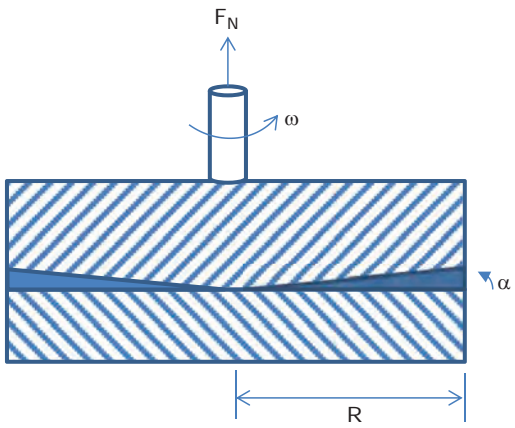


Figure 5.14 Cone and plate viscometer.

The angular speed and torque determine the shear rate and shear stress, as given in Eqs. (5.28) and (5.29):

$$\dot{\gamma} = \frac{\omega}{\alpha} \tag{5.28}$$

$$\sigma = \frac{3M}{2\pi R^3} \tag{5.29}$$

where ω = rate of rotation; α = cone angle (typically less than 5 degrees); M = torque; R = radius.

Rotational viscometers are typically used over a shear rate range of 10^{-2}–5 s^{-1}. At higher rotational speeds, flow instabilities and deviations from the simple shear flow assumed in Eqs. (5.28) and (5.29) occur.

5.3.5 Dynamic Rheology Measurements

Dynamic measurements are used to study the linear viscoelastic behavior of polymer melts. Linear behavior occurs at low levels of deformation. From the linear response, information about the structure and behavior of the polymer can be deduced. Nonlinear behavior, which often occurs in polymer processing, is more intractable to scientific analysis and prediction.

Dynamic measurements are conducted by imposing a sinusoidal strain on the polymer using a parallel plate or cone and plate rotational viscometer. A perfectly elastic material responds in phase

with the imposed sinusoidal strain $\gamma_0 \sin \omega t$. This is because the stress is directly proportional to the strain:

$$\sigma = G\gamma = G\gamma_0 \sin \omega t. \tag{5.30}$$

A perfectly viscous material responds 90 degrees out of phase since stress is proportional to the rate of strain rather than the strain:

$$\sigma = \eta\dot{\gamma} \tag{5.31}$$

$$\sigma = \eta \frac{d\gamma}{dt} = \eta \frac{d(\gamma_0 \sin \omega t)}{dt} = \eta\omega\gamma_0 \cos \omega t$$
$$= \eta\omega\gamma_0 \sin(\omega t + 90^\circ). \tag{5.32}$$

Viscoelastic materials have both elastic and viscous behavior, and measuring the in-phase and out-of-phase behavior provides useful insight into molecular structure and performance. The in-phase modulus, G', is known as the *storage modulus* and represents the elastic component. The out-of-phase modulus, G'', is known as the *loss modulus* and represents the viscous component:

$$G'(\omega) = \frac{\text{in-phase stress}}{\text{maximum strain}} \tag{5.33}$$

$$G''(\omega) = \frac{\text{out-of-phase stress}}{\text{maximum strain}} \tag{5.34}$$

where ω typically ranges from 0.01 to 10^3 rad/s. Furthermore, in-phase and out-of-phase viscosities are defined as:

$$\eta'(\omega) = \frac{G'}{\omega} \tag{5.35}$$

$$\eta''(\omega) = \frac{G''}{\omega}. \tag{5.36}$$

The magnitude of the viscosity is known as the complex viscosity, η^*:

$$\eta^* = \sqrt{\eta'^2 + \eta''^2} \tag{5.37}$$

An empirical relationship known as the Cox-Merz rule allows complex viscosity at a given frequency to be equated with steady state viscosity at a shear rate corresponding to that same frequency:

$$\eta(\dot{\gamma}) = \eta^*(\omega). \tag{5.38}$$

The Cox-Merz rule holds for most but not all polymers. This rule allows the viscosity to be measured over a broad shear rate range by combining the results of multiple measurements. While the steady state cone and plate viscometer goes up to about 5 s^{-1}, when operated in the dynamic mode, frequencies of up to about 500 s^{-1} can be achieved. This puts the data comfortably in the lower range of capillary viscometers, which can extend the range even further.

The dynamic modulus and viscosity of many polymers also obey time−temperature superposition. By operating the viscometer at different temperatures, the curves are shifted horizontally and vertically to create master rheology curves that span 8 decades, typically from 10^{-4} to 10^4 s^{-1}.

The elastic or storage modulus has been shown to be related to the first normal stress difference (a measure of the normal forces or elasticity of the polymer) in the limit as the frequency approaches zero:

$$2G' = N_1 \text{ as } \omega \to 0. \tag{5.39}$$

where N_1 = first normal stress difference. Since N_1 is difficult to measure by other means, dynamic measurements are often used.

5.3.6 Extensional Measurements

In the linear viscoelasticity regime of small deformations and rates of deformation, it can be shown that the extensional viscosity is three times the shear viscosity:

$$\eta_E = 3\eta. \tag{5.40}$$

Thus, shear measurements can be used to predict extensional properties at small deformations. For large, rapid deformations, there is no such relationship between extension and shear.

Extensional viscosity measurements are notoriously difficult to conduct in a controlled scientific

manner. Stretching a polymer above its softening point poses challenges in clamping, temperature control, and achieving sufficient strain and strain rates to be meaningful for polymer processing [55]. One method pioneered by Meissner uses rotary clamps to stretch a polymer ribbon in a hot oil bath [56,57]. Münstedt [58] has also developed devices. Besides the practical challenges mentioned earlier, these techniques are limited to strain rates of less than about $1\ s^{-1}$, making it difficult to study nonlinear behavior typical of polymer processing.

In more recent years, Sentamanat [59–61] has introduced an attachment to a rotational viscometer for extensional measurements. The device employs a dual drum wind-up mechanism to achieve rates of strain of up to $20\ s^{-1}$. It too is limited in its use. For example, a minimum zero shear viscosity of 10,000 Pa-s is recommended. Hence the device is restricted to higher MW polymers and lower temperatures. Test times are also very short at high rates of strain, and only transient measurements can be made. Andrade [62] reviews the pros and cons of a number extensional rheometer designs and proposes an updated version of the Meissner design that is said to achieve higher strain rates than the Sentamanat design.

These devices measure the start-up stress, usually expressed as the shear stress growth coefficient, $\eta_E^+(t)$. In start-up flow, the material is initially at rest and subjected to a steady extension at a rate $\dot{\varepsilon}$. The shear stress growth coefficient is defined as

$$\eta_E^+(t,\ \dot{\varepsilon}) \stackrel{\text{def}}{=} \frac{\sigma_E(t,\dot{\varepsilon})}{\dot{\varepsilon}} \tag{5.41}$$

At long times, the shear stress growth coefficient is assumed to approach a steady state elongational viscosity:

$$\lim_{t\to\infty} \eta_E^+(t,\dot{\varepsilon}) = \eta_E(\dot{\varepsilon}) \tag{5.42}$$

The shear stress growth coefficient is typically plotted versus time (see for example, Fig. 5.4). The relationship 3η is often superimposed on the plot so that deviations from linear viscoelasticity are obvious.

To characterize extensional behavior at the high rates of strain encountered during polymer processing, a pressure-driven converging flow measurement is sometimes used [63]. This method, often called the Cogswell method, uses measurements of the entrance pressure in a capillary rheometer (see Section 5.3.3.2). A dual bore capillary rheometer is often used. This method computes an average steady state elongational viscosity:

$$\dot{\varepsilon}_{avg} = \frac{4\dot{\gamma}^2\eta}{3(n+1)\Delta P_{entrance}} \tag{5.43}$$

$$\eta_{E_{avg}}(\dot{\varepsilon}) = \frac{9(n+1)^2(\Delta P_{entrance})^2}{32\dot{\gamma}^2\eta} \tag{5.44}$$

where η = shear viscosity; n = power-law index; $\Delta P_{entrance}$ = pressure drop in the entrance region to the die (as given by Eq. (5.25))

Cogswell makes several simplifying assumptions in his analysis that may or may not hold true for a given polymer melt. Several studies have tried to relate this method to the more rigorous stretching flow measurements with varying degrees of success [38,64–68].

Perhaps the most popular industrial test for elongational flow is the extrudate drawing test. Often known as the Rheotens test, this method uses the filament extruded from a capillary rheometer. The filament is drawn down by a set of motor-driven rolls. The vertical force or torque is measured. This is illustrated in Fig. 5.15. The method typically involves ramping up the speed of the rolls until the filament breaks. The force generally steadies out to a constant value and is recorded as the "melt strength or tension." The speed at break is converted into a maximum draw rate. This method simulates a number of industrially important processes, such as fiber spinning, film casting, and blowing (although film processes are biaxial extension processes). Because the temperature and strain are not held constant, the results do not correspond to well-defined rheological properties. Nevertheless, the method is useful for measuring differences in extensional behavior of materials and at strains and rates of strain representative of polymer processing. A number of studies have used the technique for this purpose [3,4,38,43,69–73].

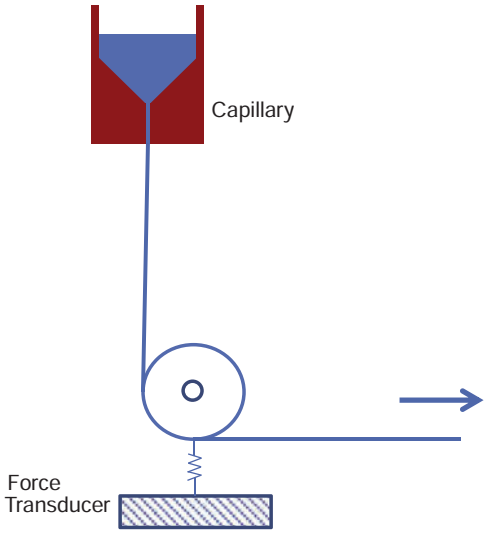


Figure 5.15 Extrudate drawing test.

5.4 Factors Influencing Polymer Rheology

5.4.1 Strain and Rate of Strain

It has previously been shown that the viscoelastic properties of polymer melts are a function of strain and rate of strain (see Fig. 5.3). The shear viscosity of most polymers is constant at low shear rates but decreases at higher shear rates (shear thinning behavior). Shear thinning behavior is beneficial for many polymer processes. For example, in blown film, it helps lower the pressure, allowing for higher throughput.

Similarly, polymers may be strain hardening or softening in extensional flows (see Fig. 5.4). Such behavior has been found to influence processability of polymers, such as drawability in cast film, bubble stability in blown film, and achieving uniform thickness during thermoforming.

Some of the molecular factors that influence these behaviors are explored in Section 5.4.5.

5.4.2 Temperature

Increasing the temperature generally decreases the viscosity, as illustrated in Fig. 5.16. On a molecular level, increasing the temperature provides more energy for the molecules to move, increasing the ability of the long chains to reptate or slide past one another. Increasing the temperature has a similar

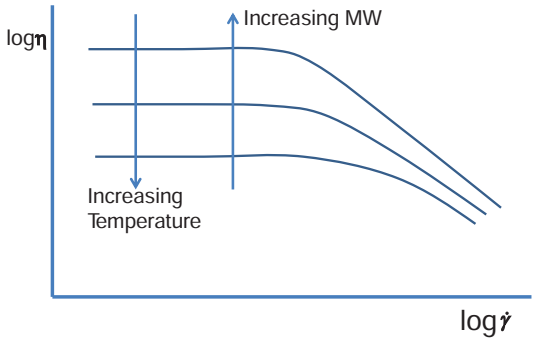


Figure 5.16 Effect of temperature and molecular weight (MW) on shear viscosity (η) of polymer melts.

effect as reducing the average molecular weight (see Section 5.4.5.1):

- The zero shear viscosity decreases.
- The critical value of the shear rate that delineates the transition between the Newtonian region and Power-law region increases.
- The slope of the power-law region (the power-law index, n) remains essentially unchanged.

For polymers that follow time−temperature superposition, the effect of temperature can be computed using a shift factor. "Reduced" variables are introduced to collapse viscosity versus shear rate curves onto a single master curve. From the master curve, the viscosity at any temperature and shear rate can then be computed:

$$\eta_r(\dot{\gamma}_r, T_0) = \frac{\eta(\dot{\gamma}, T)}{a_T} \tag{5.45}$$

$$\dot{\gamma}_r = a_T \dot{\gamma} \tag{5.46}$$

where η_r = reduced viscosity; T_0 = reference temperature; T = temperature.

$$a_T = \text{shift factor} = \frac{\eta_0(T)}{\eta_0(T_0)}. \tag{5.47}$$

For amorphous polymers, when $T > T_g + 100\text{K}$, the shift factor typically follows an Arrhenius-like or exponential dependence:

$$a_T = \exp\left[\frac{E_a}{R}\left[\frac{1}{T} - \frac{1}{T_0}\right]\right] \tag{5.48}$$

where E_a = activation energy of flow; R = ideal gas constant; T = temperature, in K; T_0 = reference temperature, in K.

For $T_g < T < T_g + 100\text{K}$, the so-called WLF equation typically holds:

$$\log a_T = \frac{-c_1^0(T - T_0)}{c_2^0 + (T - T_0)} \tag{5.49}$$

where c_1^0 and c_2^0 are constants.

For semicrystalline polymers, typically an Arrhenius relationship (Eq. (5.48)) is used for temperatures above the crystalline melting point ($T > T_m$).

The change in viscosity per degree of temperature change for a number of polymers is given in Table 5.6. For common polyolefin grades, an increase in temperature of 10°C decreases the viscosity by about 15%.

5.4.3 Pressure

Increasing pressure increases the viscosity. Generally an exponential model can be used:

$$\eta_0(P) = \eta_0(P_0)\exp(\alpha P) \tag{5.50}$$

where P = pressure; P_0 = reference pressure; α = constant.

A typical value of α for polymer melts is $2 \times 10^{-8}\ \text{Pa}^{-1}$ ($1.4 \times 10^{-4}\ \text{psi}^{-1}$). For a 1000 psi (6.9 MPa) pressure rise, the viscosity increases by about 15%.

5.4.4 Time

Changes in viscosity with time generally indicate a chemical reaction that is altering the MW of the polymer. Examples include cross-linking (increasing viscosity), reactions at interfaces (increasing viscosity), and chain scission (decreasing viscosity). For example, the MW of PET resin is very sensitive to moisture. During extrusion, moisture may cause chain scission, reducing MW and viscosity, and causing the polymer to become brittle in the solid state.

Table 5.6 Viscosity Change With Temperature for Some Common Polymer Melts

Polymer	Reference Temperature (°C)	Change in Viscosity (%/°C)
Polyethylene	190	-1.4
Polystyrene	190	-3.4
PA 6	280	-1.4
Polyethylene terephthalate	280	-2.8

Courtesy of E. I. du Pont de Nemours and Company.

5.4.5 Molecular Factors

The size (MW), size distribution (MWD), and architecture (branching) affect the ability of long chain polymers to flow.

5.4.5.1 Molecular Weight

Increasing the MW generally increases the viscosity as the polymer chains become more entangled and have less mobility to flow. This is illustrated in Fig. 5.16. Similar to decreasing the temperature, increasing MW:

- increases zero shear viscosity,
- decreases the critical shear rate where the Newtonian region ends and the power-law region begins, and
- has little effect on the slope of the power-law region.

Below the critical MW for entanglement (M_c), the zero shear viscosity is proportional to the MW:

$$\eta_0 = K_1 M_w \text{ for } M_w < M_c. \tag{5.51}$$

Above M_c, the effect of MW is much stronger:

$$\eta_0 = K_2 M_w^{3.4} \text{ for } M_w > M_c. \tag{5.52}$$

Here K_1 and K_2 are constants that depend on the polymer and temperature. M_c typically ranges from about 5000 to 30,000 g/mol and most commercial polymers used in flexible packaging are well above their M_c. For regions outside the Newtonian plateau, the power-law exponent is typically less than 3.4.

Elastic or normal forces are very sensitive to M_w, as shown in Eq. (5.53):

$$N_{1,0} \propto M_w^{7.0} \tag{5.53}$$

where $N_{1,0}$ = zero shear rate first normal stress difference.

Because G' is proportional to N_1 (Eq. (5.39)), dynamic measurements are a good tool for probing the presence of high MW components.

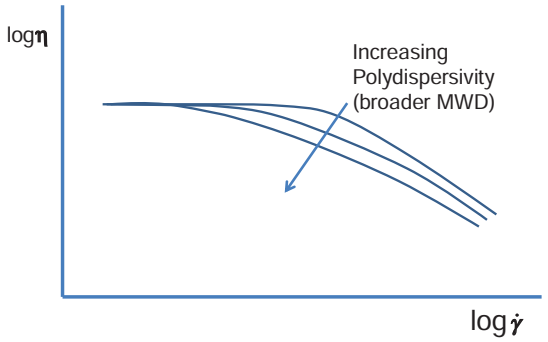


Figure 5.17 Effect of molecular weight distribution (MWD) on shear viscosity of polymer melts.

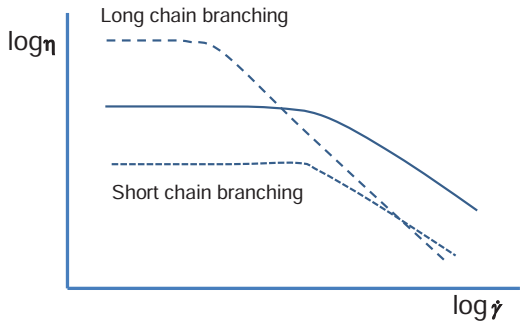


Figure 5.18 Effect of branching on shear viscosity of polymer melts.

5.4.5.2 Molecular Weight Distribution

As illustrated in Fig. 5.17, broader MWD or higher polydispersivity (M_w/M_n) generally:

- decreases the shear rate at which shear thinning begins,
- gives a more gradual transition region (from the Newtonian region to the shear thinning or power-law region), and
- decreases the viscosity at shear rates beyond the Newtonian region.

G' is particularly sensitive to changes in MWD. $N_{1,0}$ is proportional to high-order moments of the MWD that are heavily influenced by the highest MW chains in the polymer.

5.4.5.3 Branching

Short chain branching (SCB) generally has little effect on the shape of the shear viscosity versus shear rate curve; viscosity may decrease across the shear rate range with increasing SCB. Increasing the length of the short chain (eg, replacing butene with octene in LLDPE) may have some effect but MW and MWD often dominate.

Long-chain branching increases the zero-shear viscosity and gives more shear thinning behavior (steeper slope in the power-law region). This leads to lower viscosity at high shear rates. The combination of high viscosity at low shear rates and low viscosity at high shear rates has advantages in many polymer processes, as described earlier. The effect of branching on the shear viscosity versus shear rate curve is illustrated in Fig. 5.18.

MWD and long-chain branching effects are often confounded, especially in LDPE where it is difficult to separate the two effects. Decreasing the density of LLDPE (increasing short chain branching) generally has little impact on viscosity. With LDPE, decreasing the density typically results in a greater amount of short- and long-chain branches, and so the impact on viscosity can be more significant.

Long-chain branching has a substantial effect on extensional viscosity. LDPE is strain hardening while LLDPE is typically strain softening (see Fig. 5.4). Several studies of metallocene LLDPE show that introducing a small amount of long-chain branching changes the extensional viscosity behavior from strain softening to hardening [2,74].

5.4.5.4 Chemical Interactions

The presence of specific inter- (between molecular chains) and intrachain (within a chain) interactions can influence the rheology. A commercially important example in flexible packaging is ionomers. Introduced in Chapter 4, ionomers are partially neutralized acid copolymers. They are essentially LDPE but with acid—acid interactions (hydrogen bonding) and ionic bonding. Like LDPE, they contain long-chain branching. The hydrogen and ionic bonding tend to accent the effects of the branches. Compared with LDPE, ionomers typically have a higher activation energy to flow (their viscosity is more sensitive to changes in temperature), a higher zero shear viscosity (for a given MI), more shear thinning behavior, greater strain hardening, and higher melt strength [75,76].

5.4.5.5 Fillers and Additives

Inorganic fillers tend to increase the viscosity of polymer melts. The size, shape, and concentration of

the filler influence the rheological behavior. This is discussed in greater detail in Chapter 6. Additives such as plasticizers often decrease the viscosity. The specific effect will depend on the nature of the additive, its miscibility with the polymer, and its concentration.

5.5 Relaxation, Creep, and Constitutive Equations

The Newtonian and Power-law viscosity models introduced earlier relate the shear stress to the rate of strain for purely viscous fluids. For viscoelastic material responses, models that account for both viscous and elastic behavior are needed. It is often helpful to turn to mechanical analogies to represent these behaviors, as shown in Fig. 5.19. An ideal viscous fluid is represented by a dashpot; it deforms slowly (not instantaneous), its rate of deformation is related to the imposed stress through the viscosity, and when the imposed stress is removed, it does not return to its original length. An ideal elastic or Hookean solid is represented by a spring. The force exerted on a spring is proportional to the displacement, analogous to the stress being proportional to the strain. Ideal elastic solids deform instantaneously with the strain depending on the imposed stress and modulus. When the stress is removed, elastics solids return to their original length (An electrical analogy can also be used, where a capacitor represents the viscous fluid and a resistor the elastic solid.).

By combining these ideal elements, relationships between stress and strain known as constitutive equations can be developed. Constitutive equations are needed to solve the equations of motion and can be very complex for polymer flow. This approach is highlighted with two experiments that represent two of the extremes of viscoelasticity: stress relaxation and creep/recovery.

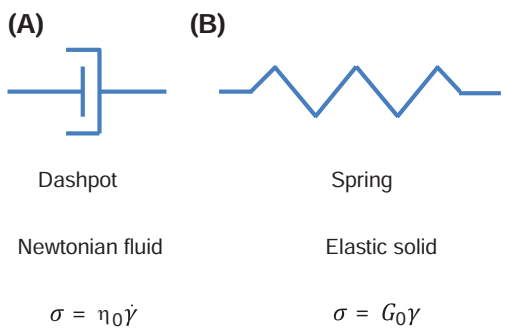


Figure 5.19 Mechanical representations of ideal viscous (A) and elastic materials (B).

5.5.1 Stress Relaxation

In a stress relaxation experiment, the polymer is subjected to a constant strain at time zero (Fig. 5.20(a)), and the resultant stress is measured as a function of time. The response typically looks like Fig. 5.20B where the stress initially spikes up and slowly decreases or relaxes. In the ideal case, the response can be represented as a dashpot and spring in series, as shown in Fig. 5.20C. The displacement initially stretches the spring, resulting in the stress. Over time, the force recedes as the dashpot moves. Mathematically, the force in both the spring and dashpot are equal. If Eq. (5.30) for the elastic solid is differentiated and combined with Eq. (5.31) for a viscous fluid, the following equation for the shear rate is obtained:

$$\frac{\dot{\sigma}}{G} + \frac{\sigma}{\eta} = \dot{\gamma} \tag{5.54}$$

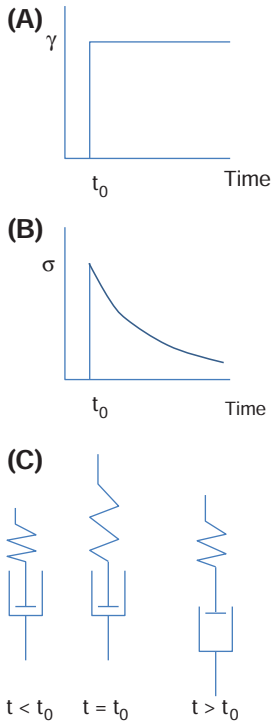


Figure 5.20 Stress relaxation experiment. (A) imposed strain, (B) stress response, (C) 2-element mechanical Maxwell model.

or

$$\sigma + \lambda\dot{\sigma} = \dot{\gamma} \tag{5.55}$$

The solution to Eq. (5.55) is

$$\sigma = \sigma_0 e^{-t/\lambda} \tag{5.56}$$

where

$$\lambda = \frac{\eta}{G} = \text{relaxation time.} \tag{5.57}$$

Eq. (5.55) is known as the Maxwell model. The solution results in exponential decay of the stress with time, similar to what is shown in Fig. 5.20. The parameter λ has units of time and can be thought of as a characteristic relaxation time. In real polymer responses, a single relaxation time is not sufficient. Instead, a spectrum of relaxation times best fit the data. It can be shown that λ is the longest relaxation time. A value for λ from dynamic rheology measurements can be obtained by letting $G = G'$ (the elastic modulus) and using Eq. (5.36) for η in the limit as the frequency approaches zero:

$$\lambda = \frac{G'}{G''\omega} \quad \text{for} \quad \omega \to 0. \tag{5.58}$$

Higher values of λ indicate greater elastic effects. Eq. (5.58) is perhaps the best method for determining a characteristic relaxation time for calculating the Deborah number in Eq. (5.4). Fig. 5.21 illustrates the concept of Eq. (5.58) in the context of dynamic modulus data. The relaxation time is the inverse of the frequency where the G' and G'' curves cross over. At frequencies or shear rates below this critical value of frequency, viscous effects dominate. At frequencies or shear rates above the critical value, elastic effects dominate

Some investigators use the λ parameter from the Cross equation (Table 5.3) for a characteristic relaxation time because it has units of time. This is generally a poor choice since it is not supported by theory or experimental evidence [77].

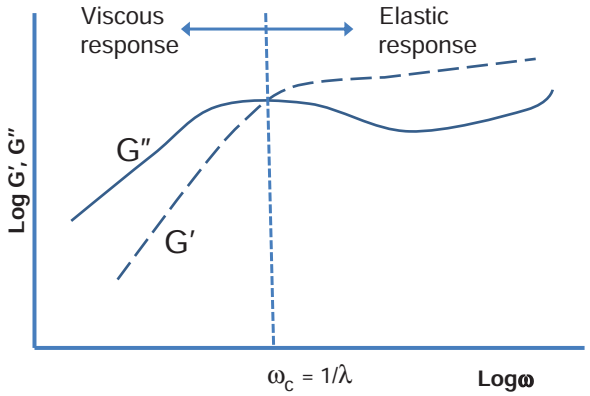


Figure 5.21 Relaxation time from dynamic modulus data.

5.5.2 Creep/Recovery

In a second type of experiment, the polymer is subjected to an applied load or stress at time zero, and the strain is measured as a function of time (Fig. 5.22A). The ideal response is shown in

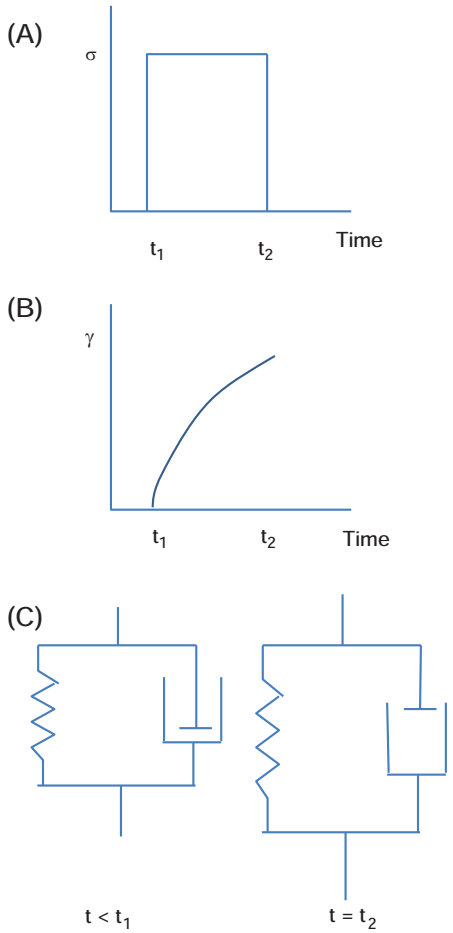


Figure 5.22 Creep experiment. (A) imposed stress, (B) strain response, (C) 2-element mechanical Voigt model.

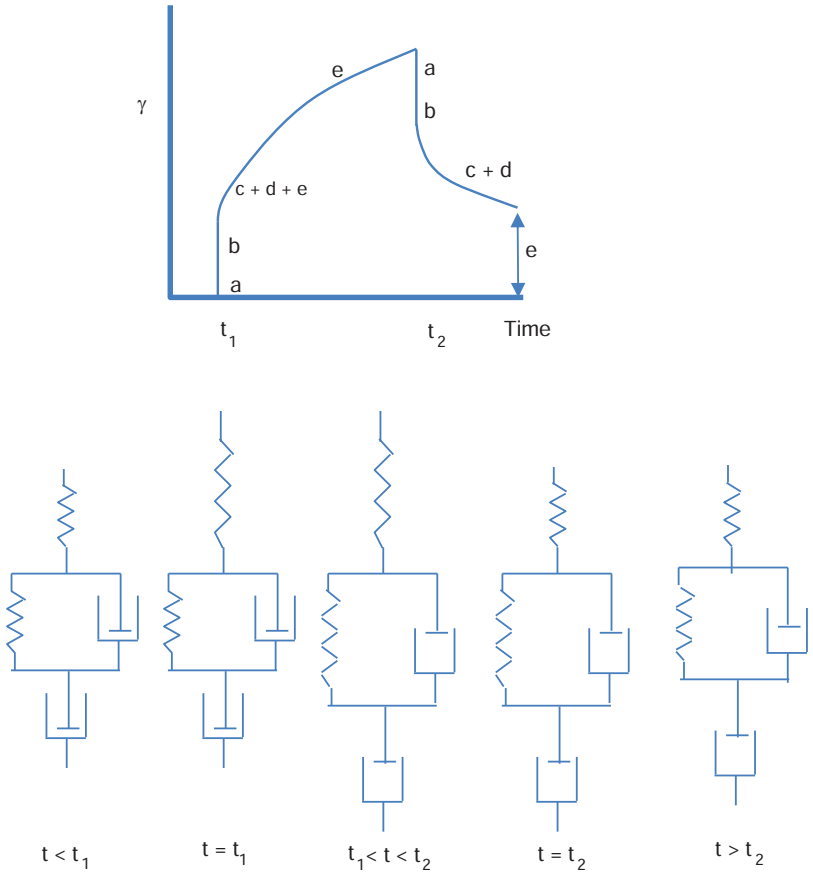


Figure 5.23 General creep behavior and the 3-element Maxwell–Voigt model.

Fig. 5.22B. The mechanical analogy is a dashpot and spring in parallel, as shown in Fig. 5.22C. The stress on each element is:

$$\sigma_1 = G\gamma \tag{5.59}$$

$$\sigma_2 = \eta\dot{\gamma} \tag{5.60}$$

For elements in parallel, the stress is additive:

$$\sigma = G\gamma + \eta\dot{\gamma} \tag{5.61}$$

Solving for the strain

$$\gamma = \frac{\sigma}{G}\left(1 - e^{-t/\lambda}\right) \tag{5.62}$$

where $\lambda = \eta/G =$ retardation time. This is known as the Voigt model. Retardation time refers to the delay in the response to the imposed stress. As λ approaches zero, the material behaves like an ideal elastic solid.

The Maxwell model can only handle viscoelastic fluid and the Voigt model viscoelastic solid behaviors. For more complex behavior, more elements are added. An example is given in Fig. 5.23 for a general creep response curve. Here a three-element model in series is used:

- Ideal elastic solid (spring)
- Retarded elasticity (spring and dashpot in parallel)
- Ideal viscous fluid (dashpot)

At time t_1 the stress is imposed. Prior to t_1 the polymer is in equilibrium. At t_1 the spring stretches instantaneously, but the retarded elastic and viscous components remain stationery. This corresponds to the rapid rise of the strain at t_1. Between t_1 and t_2 the strain increases as the dashpots increase in length. At t_2 the

stress is removed and the spring element responds instantaneously. Over time, the spring in the retarded elastic model relaxes, lowering the overall stress.

The elements of the model correspond to the physical changes occurring in the polymer, as shown in Fig. 5.23. Region (a) represents bending of bond angles and lengths and (b) the elastic distension of secondary bonds. This is analogous to the stretching of the spring. Region (c) involves short-range chain segment displacement, (d) uncoiling of the chain, and (e) chain−chain slip. These factors are responsible for the retarded elastic and ideal viscous behavior. Once the stress is removed at t_2, the strain from bending of the covalent bond angles and lengths and the ideal elastic distension of the secondary bonds recover instantly. The short-range chain segment displacement and uncoiling recover with time, but the chain−chain slip is permanent (as represented by the extended dashpot in the model) and is responsible for the unrecoverable strain.

Constitutive equations can be very complicated with complex derivatives and many parameters. For example, one of the most powerful constitutive equations is the K-BKZ model which uses over two dozen experimentally fit parameters. Other models are based on molecular motions such as the reptation models of De Gennes [78] and Doi and Edwards [79]. Many help in broadening our understanding of molecular motion but are too cumbersome or limiting in their assumptions to be of practical use in predicting polymer flow behavior. Indeed, the scientific literature is filled with papers on numerical simulation of viscoelastic fluids, yet one should use caution when interpreting the results. Most of the simulations use limiting assumptions because of the complexity of the behavior of these materials.

Further Reading

- Barnes HA, Hutton JF, Walters K. An introduction to rheology. Amsterdam: Elsevier; 1989.
- Dealy JM, Wissbrun KF. Melt rheology and its role in plastics processing, theory and applications. Chapman & Hall; 1995.
- Ferry JD. Viscoelastic properties of polymers. 3rd ed. New York: Wiley; 1980.
- Graessley WW. Viscoelasticity and flow in polymer melts and concentrated solutions. In: Physical properties of polymers. 2nd ed. Mark JE, editor. ACS Publishers; 1993.
- Gupta RK. Extensional rheometry of polymer melts. In: Lee L-H, editor. Adhesive bonding. New York: Plenum Press; 1991. p. 75−95.
- Vlachopoulos J, Strutt D. Rheology of molten polymers. In: Wagner Jr JR, editor. Multilayer flexible packaging. Amsterdam: Elsevier; 2010. p. 57−72.

References

[1] Barnes HA, Hutton JF, Walters K. An introduction to rheology. Amsterdam: Elsevier; 1989. p. 13.

[2] Gabriel C, Munstedt H. Strain hardening of various polyolefins in uniaxial elongational flow. J Rheol 2003;47(3):619−30.

[3] Ghijsels A, Ente JJSM, Raadsen J. Melt strength behavior of PE and its relation to bubble stability in film blowing. Intern Polym Process 1990;5(4):284−6.

[4] Ghijsels A, Ente JJSM, Raadsen J. Melt strength behavior of polyethylene blends. Int Polym Process 1992;7(1):44−50.

[5] Cunningham C, Savargaonkar N, Kardos L, karjala T. New low density polyethylene products for improved throughput. In: TAPPI PLACE Conference, Seattle, WA; 2012.

[6] Vlachopoulos J, Strutt D. Rheology of molten polymers. In: Wagner Jr JR, editor. Multilayer flexible packaging. Amsterdam: Elsevier; 2010. p. 62.

[7] Vlachopoulos J. Introduction to polymer processing. 2nd ed. McMaster University; 1994.

[8] Vlachopoulos J, Strutt D. Rheology of molten polymers. In: Wagner Jr JR, editor. Multilayer flexible packaging. Amsterdam: Elsevier; 2010. p. 68.

[9] Rutgers R, Mackley MJ. The correlation of experimental surface instabilities with numerically predicted exit surface stress concentrations and melt strength for linear low density polyethylene. J Rheol 2000;44:1319.

[10] Denn MM. Extrusion instabilities and wall slip. Ann Rev Fluid Mech 2001;33:265.

[11] Chaloupkova K, Zatloukal M. Theoretical and experimental analysis of the die drool phenomenon for metallocene LLDPE. Polym Eng Sci 2007;47:871−81.

[12] Musil J, Zatloukal M. Historical review of die drool phenomenon in plastics extrusion. Polym Rev 2014;54:139−84.
[13] Ramamurthy AW. Wall slip in viscous fluids and influence of materials of construction. J Rheol 1986;30:337−57.
[14] Yang X, Ishida H, Wang S-Q. Wall slip and absence of interfacial flow instabilities in capillary flow of various polymer melts. J Rheol 1998;42:63−80.
[15] Sukhadia AM. Sharkskin melt fracture behavior of medium and high molecular weight polyethylenes in film blowing. In: SPE ANTEC conference; 1997. p. 1059−66.
[16] Petrie CJS, Denn MM. Instabilities in polymer processing. AICHE J 1976;22:209−36.
[17] Bagley EB, Schreiber HP. Effect of die entrance geometry on polymer melt fracture and extrudate distortion. Trans Soc Rheol 1961;V:341−53.
[18] Vlachopoulos J, Alam M. Critical stress and recoverable shear for polymer melt fracture. Polym Eng Sci 1972;12:184−92.
[19] White JL. Critique on flow patterns in polymer fluids at the entrance of a die and instabilities leading to extrudate distortion. Appl Polym Symp 1973;20:155−74.
[20] Lee J, Allen JS, Gupta M. Observations from liquid-liquid encapsulation in coextrusion of inelastic Newtonian fluids. In: Annual Technical Conference of the Society of Plastics Engineers, 69th, vol. 2; 2011. p. 1360−6.
[21] Yue P, Zhou C, Dooley J, Feng J. Elastic encapsulation in bicomponent stratified flow of viscoelastic fluids. J Rheol 2008;52:1027−42.
[22] Han CD. Bicomponent coextrusion of molten polymers. J Appl Polym Sci 1973;17:1289−303.
[23] Schrenk WJ, Bradley NL, Alfrey T, Maack H. Interfacial flow instability in multilayer coextrusion. Polym Eng Sci 1978;18:620.
[24] Han CD, Shetty R. Studies on multilayer film coextrusion II. Interfacial instability in flat film coextrusion. Polym Eng Sci 1978;18:180−6.
[25] Zatloukal M, Kopytko W, Vlcek J, Saha P. Investigation of zig-zag type of interfacial instabilities in coextrusion. In: SPE ANTEC conference; 2005. p. 101−5.
[26] Ramanathan R, Shanker R, Rehg T, Jons S, Headley DL, Schrenk WJ. 'Wave' pattern instability in multilayer coextrusion − an experimental investigation. In: SPE ANTEC conference; 1996. p. 224−8.
[27] Zatloukal M, Vlcek J, Tzoganakis C, Saha P. Viscoelastic stress calculation in multilayer coextrusion dies: die design and extensional viscosity effects on the onset of "wave" interfacial instabilities. Polym Eng Sci 2002;42:1520−33.
[28] Martyn M, Spares R, Coates PD, Zatloukal M. Imaging and analysis of wave type interfacial instability in the coextrusion of low-density polyethylene melts. J Newt Fluid Mech 2009;156:150−64.
[29] Dobroth T, Erwin L. Causes of edge bead in cast films. Polym Eng Sci 1986;26:462−7.
[30] Kanning K, Co A. Edge effects in film casting. J Plastic Film Sheeting 2000;16:188−203.
[31] Bortner MJ, Doerpinghaus PJ, Baird DG. Effects of sparse long chain branching on the spinning stability of LLDPEs. Intern Polym Process 2004;19:236−43.
[32] Minoshima W, White JL. Instability phenomena in tubular film, and melt spinning of rheologically characterized high-density, low-density and linear low-density polyethylenes. J Newt Fluid Mech 1986;19:275−302.
[33] Zavinska O, Claracq J, van Eijndhoven S. Non-isothermal film casting: determination of draw resonance. J Newt Fluid Mech 2008;151:21−9.
[34] Co A. Draw resonance in film casting. Chem Ind (Dekker) 2005;103:287−319 (*Polymer Processing Instabilities*).
[35] Butler TI. Blown film bubble instability induced by fabrication conditions. In: TAPPI polymers, laminations & coatings conference, 2; 1999. p. 815−28.
[36] Laffargue J, Parent L, Lafleur PG, Carreau PJ, Demay Y, Agassant JF. Investigation of bubble instabilities in film blowing process. Intern Polym Process 2002;17:347−53.
[37] Tas P, Nguyen L, Marshall S, Kashanian M. Bubble stability and maximum output of Surpass sLLDPE resin in blown film. In: TAPPI PLACE conference; 2004. p. 320−34.
[38] Laun HM, Schuch H. Transient elongational viscosities and drawability of polymer melts. J Rheol 1989;33:119.
[39] Field GJ, Micic P, Bhattacharya SN. Melt strength and bubble stability of LLDPE/LDPE blends. Polym Int 1999;48:461−6.
[40] Munstedt H, Steffl T, Malmberg A. Correlation between rheological behavior in uniaxial elongation and film-blowing properties of various polyethylenes. Rheol Acta 2005;45:14−22.

[41] Meissner J. Basic parameters, melt rheology, processing and end-use properties of three similar low density polyethylene samples. Pure Appl Chem 1975;42:551−612.
[42] Winter HH. A collaborative study on the relation between film blowing performance and rheological properties of two low-density and two high-density polyethylene samples. Pure Appl Chem 1983;55:943−76.
[43] Vlachopoulos JND. Extensional viscosity and melt strength and their role in film blowing. In: SPE extrusion division consultants corner; 2015.
[44] Kurzbeck S, Munstedt H. Elongational properties of polymer melts and correlations with their processing behavior in blown film and thermoforming. In: Progress and trends in rheology V, Proceedings of the European rheology conference, 5th Potoroz, Slovenia; 1998. p. 402−3.
[45] Spence T, Hylton D. Rheological studies of commercial thermoforming materials. In: SPE ANTEC conference; 1998. p. 681−9.
[46] Morris BA, Scherer JM. Squeeze-out of sealant during hot bar sealing: modeling insights. In: SPE ANTEC conference; 2013.
[47] Morris BA, Scherer JM. Preventing squeeze-out of sealant during hot bar sealing: modeling and experimental insights. In: SPE ANTEC conference; 2014.
[48] Rohlfing DC, Janzen J. What's happening in the melt-flow plastometer: the role of elongational viscosity. In: SPE ANTEC conference; 1997. p. 1010−4.
[49] Clevenhag P-A, Oveby C. Rheological indicators to predict the extrusion coating performance of LDPE. In: TAPPI PLACE conference; 2003.
[50] Wagner HL. The Mark-Houwink-Sakurada equation for the viscosity of linear polyethylene. J Phys Chem Ref Data 1985;14:611−6.
[51] Kurata M, Stockmayer WH. Intrinsic viscosities and unperturbed dimensions of long chain molecules. Adv Polym Sci 1963;3:196.
[52] Kurata M, Tsunashima Y, Iwama M, Kamada K. In: Brandrup J, Imnmergut EH, editors. Chapter IV in Polymer handbook. 2nd ed. New York: John Wiley & Sons; 1975.
[53] Vlachopoulos J, Strutt D. Rheology of molten polymers. In: Wagner Jr JR, editor. Multilayer flexible packaging. Amsterdam: Elsevier; 2010. p. 61.
[54] Dealy JM, Wissbrun KF. Melt rheology and its role in plastics processing, theory and applications. Chapman & Hall; 1995. p. 322.
[55] Dealy JM, Wissbrun KF. Melt rheology and its role in plastics processing, theory and applications. Chapman & Hall; 1995. p. 241.
[56] Meissner J. Rheometer zur Untersuchung der deformationsmechanischen Eigenschaften von Kunststoff-Schmelzen unter definierter Zugbeanspruchung. Rheol Acta 1969;8:78.
[57] Meissner J. Dehnungsverhalten von Polyäthylen-Schmelzen. Rheol Acta 1971;10:230.
[58] Munstedt H. New universal extensional rheometer for polymer melts. Measurements on a polystyrene sample. J Rheol 1979;23:421−36.
[59] Sentmanat ML. Dual windup extensional rheometer. 2003. US patent 6578413.
[60] Sentmanat ML. Miniature universal testing platform: from extensional melt rheology to solid-state deformation behavior. Rheol Acta 2004;43:657−69.
[61] Sentmanat ML, Muliawan EB, Hatzikiriakos SG. Fingerprinting the processing behavior of polyethylenes from transient extensional flow and peel experiments in the melt state. Rheol Acta 2005;44:1−15.
[62] Andrade RJ, Harris P, Maia JM. High strain extensional rheometry of polymer melts: revisiting and improving the Meissner design. J Rheol 2014;58:869−90.
[63] Cogswell FN. Converging flow of polymer melts in extrusion dies. Polym Eng Sci 1972;12:64−73.
[64] Bersted BH. Refinement of the converging flow method of measuring extensional viscosity in polymers. Polym Eng Sci 1993;33:1079−83.
[65] Gotsis AD, Ke Q. Comparison of three methods to measure the elongational viscosity of polymer melts: entry flow, fiber spinning and uniaxial elongation. In: SPE ANTEC conference; 1999.
[66] Binding DM. An approximate analysis for contraction and converting flows. J Newt Fluid Mech 1988;27:173−89.
[67] Binding DM. Further considerations of axisymmetric constriction flows. J Newt Fluid Mech 1991;41:27−42.
[68] Gotsis AD, Odriozola A. The relevance of entry flow measurement for the estimation of extensional viscosity of polymer melts. Rheol Acta 1998;37:430−7.

[69] Goyal SK. The influence of polymer structure on melt strength behavior of PE resins. Plast Eng February 1995:25.
[70] La Manta FP, Acierno D. Influence of molecular structure on the melt strength and extensibility of polyethylenes. Polym Eng Sci 1985;25(5):279−83.
[71] Acierno D, Curto D, La Manta FP, Valenza A. Flow properties of low density/linear low density polyethylenes. Polym Eng Sci 1986;26(1):28−33.
[72] Wagner MH, Bernnat A. The rheology of the rheotens test. J Rheol 1998;42(4):917−28.
[73] Rauschenberger V, Laun HM. A recursive model for Rheotens tests. J Rheol 1997;41(3):719−37.
[74] Doerpinghaus PJ, Baird DG. Separating the effects of sparse long-chain branching on rheology from those due to molecular weight in polyethylene. J Rheol 2003;47(3):717−36.
[75] Takahashi T, Watanabe J, Minagawa K, Koyama K. Effect of ionic interaction on elongational viscosity of ethylene-based ionomer melts. Polymer 1994;35(26):5722−8.
[76] Tierney NK, Register RA. Ion hopping in ethylene-methacrylic acid ionomer melts as probed by rheometry and cation diffusion measurements. Macromolecules 2002;35:2358−64.
[77] Vlachopoulos J, Strutt D. Rheology of molten polymers. In: Wagner Jr JR, editor. Multilayer flexible packaging. Amsterdam: Elsevier; 2010. p. 67.
[78] De Gennes PG. Scaling concepts in polymer physics. Ithaca, NY: Cornell University Press; 1979.
[79] Doi M, Edwards SF. The theory of polymer dynamics. New York: Oxford University Press; 1986.

6 Polymer Blending for Packaging Applications

6.1 Introduction

Blending of polymers is becoming increasingly important in packaging applications to enhance properties, improve processing, or lower cost. Tailoring surface properties, such as coefficient of friction, adding color, promoting adhesion, increasing output, improving stability, and obtaining easy-opening features, are just a few of the attributes that can be achieved by blending.

The simplest blends can be made by mixing ingredients in the extruder used to convert the resin into a film or coating. For more complex blends, specialized screw designs or customized compounding equipment may be required to achieve the desired properties. These machines incorporate various mixing modes, such as flow rearrangement (distributive mixing) or high stress levels to break up particles (dispersive mixing). Complex shear and elongational flow fields may also be used to obtain optimum mixing.

The final blend properties will depend not only on the flow and stress history, which is process dependent, but also on the thermodynamics and the polymers' thermal and rheological properties. Most polymer blends are immiscible, resulting in the minor component forming a separate dispersed phase or domain within the major component. The major component forms a continuous phase or matrix. The phase size and shape is known as the blend morphology. Blend morphology has a profound effect on the final properties and is the subject of much study. Morphology is influenced by many factors, which include the following:

- interfacial tension (thermodynamics);
- dispersed to continuous phase viscosity ratio;
- elasticity of each phase;
- minor component concentration;
- mixing and melting order;
- stress and flow history.

A basic understanding of these complex relationships between polymer properties and processing can aid in optimizing blends for a given application.

This chapter highlights the fundamentals of blending polymers for packaging applications. The literature is too broad for a detailed review of polymer blending and alloying. The goal is to familiarize the reader with those aspects of polymer blending that are important for in-line mixing of resins and other ingredients during film converting. Some blend requirements, however, are too demanding for in-line mixing and are best left to a resin manufacturer or compounder. Some of the technology that may be used to design and produce such blends is also reviewed.

6.2 Why Blend?

Even with the flexibility of controlling properties by introducing specific functional layers within a multilayer film, blending can be critical for meeting package requirements. Blending may be needed to make the polymer stable enough to extrude or have the right surface properties after extrusion. Blending may be a way to tailor-specific properties into a layer, such as barrier or heat seal performance. The resin manufacturer often adds polymer additives, such as antioxidants, catalyst killers, and various processing aids, to the polymer. But the film manufacturer may add these and other additives, such as slip, antiblock, antifog, antistatic agents, or processing aids such as fluoroelastomers for reducing sharkskin and melt fracture. Typically, these additives comprise less than 1% of the final composition. They are usually in the form of a powder or liquid. Because of this, and their low concentrations, they are typically first made into a masterbatch, a highly concentrated blend of the additive with a carrier resin. Masterbatches are usually produced by companies with specialized compounding equipment. The film manufacturer blends the masterbatch into the resin at the extruder feed hopper used to make the film or sheet.

The Science and Technology of Flexible Packaging. http://dx.doi.org/10.1016/B978-0-323-24273-8.00006-X
Copyright © 2017 Elsevier Inc. All rights reserved.

Pigments such as titanium dioxide (TiO_2) and various colorants are typically added as a masterbatch. Since the additive or pigment is well dispersed in the masterbatch, blending can be done in a single screw extruder without special screw designs or compounding equipment.

Blending may be used to reduce the resin cost. For example, a metallocene polyethylene plastomer (mPE) may be diluted with standard linear low density polyethylene (LLDPE) or low density polyethylene (LDPE) to lower cost. Recycle may be incorporated back into the film structure. One form of recycle is in-house scrap, which may be ground up and introduced into the extruder hopper as "regrind."

Blending may also help improve resin processability. Two grades of the same resin with differing flow properties (such as melt index) may be blended together to achieve the proper flow for a given process. LDPE is typically blended into LLDPE to help increase output by reducing extruder pressure and torque and improving melt strength and bubble stability [1]. Other examples where blending improves processing include blending amorphous polyamide (nylon) into polyamide 6 (PA6) to increase extruder output and adding amorphous PA or ionomer to ethylene vinyl alcohol (EVOH) to improve thermoformability [2,3].

A polymer deficient in one property is often blended with another one to enhance that property. Blending in cyclic olefin copolymers (COC), for example, can enhance LLDPE stiffness [4]. Soft polymers are often blended into harder polymers to improve the toughness. Examples include blending ethylene vinyl acetate (EVA) into LLDPE, mPE into LLDPE, and ethylene-propylene-diene monomer (EPDM) rubber or mPE into polypropylene (PP) [5].

In the engineering polymer world, rubber is added to PA to improve low temperature toughness [6]. Adding polyethylene terephthalate (PET) to polycarbonate (PC) lowers cost and improves chemical resistance and processability. Blends of PC and acrylonitrile-butadiene-styrene (ABS) copolymer have lower cost than PC and higher heat deflection temperature and toughness than ABS [7].

Barrier properties may be enhanced by blending. High density polyethylene (HDPE) is blended into LLDPE or LDPE to improve moisture barrier performance. Amorphous polyamide, such as DuPont's Selar PA, is blended into PA6 to improve the oxygen barrier at high relative humidity [8]. DuPont invented a laminar barrier technology where PA is blended into HDPE forming large platelets that impede the migration of small molecules. The laminar morphology is accomplished by choosing specific resins and processing conditions [9–12].

Adhesion may be promoted by blending together several resins. For example, adding EMA or EVA to PE can improve adhesion to certain inks. Anhydride-modified polyolefins are blended with PE or EVA to improve adhesion to PA or EVOH in coextrusion (see section 10.4.2). An acid-based additive has been developed for enhancing the adhesion of LDPE to aluminum foil in extrusion coating (see section 10.4.1.4) [13].

Additives may also help control adhesion during the heat seal process. "Contaminants" are often blended into sealant resins to achieve easy openability. Examples include blends of polybutene-1 (PB) with LDPE, LLDPE, EVA, or ionomers, and EVA with ionomer [14–17]. The blend morphology and phase compatibility is important for these applications. For example, in the blends containing PB, the PB is the minor phase. It forms spherical particles that are stretched into fibers and ribbons during the film fabrication process. The poor compatibility between the PB and matrix resin results in failure along these fibers and ribbons near the sealant interface, lowering the seal strength.

6.3 Blending Processes

Blending requires that the ingredients be brought together in the right proportions and then homogeneously mixed. In polymer blending, the former is important because there is little back mixing in most continuous mixing devices used by the industry. This is particularly true of the single screw extruder, which is the primary device used by the film converting industry. For simple blends, such as those adding masterbatches, the pellets are premixed together and fed into the extruder hopper. In more sophisticated compounding devices, such as twin-screw extruders, ingredients can be added at various stages along the extruder.

Once the polymer enters the extruder or other mixing device, it is melted and the mixing mechanism depends on the specific device employed. Mixing in single screw extruders is the focus of this section. More sophisticated devices, however, are briefly introduced and compared and contrasted with single screw extruders. While specialty compounding devices, such as

twin-screw extruders, kneaders, and continuous mixers, have historically been used by the resin manufacturer or toll compounder and not by film converters, they are beginning to be used as in-line compounders for some large-scale film operations [18].

6.3.1 Pellet Premixing

Pellet mixers fit into two general types: off-line batch mixers and in-line feeders/mixers. Batch mixers can be as simple as a cement mixer. The ingredients are weighed and poured into the mixer, blended, and then transported to the extruder hopper. Batch mixers generally are less expensive and occupy less space than in-line mixers. They can be used to feed more than one extruder. Also, the ingredients' weight can be accurately measured, depending on the scale being used. On the other hand, they can be labor intensive, leave no automatic records, and open up the chance for human weighing errors and the possibility for pellet segregation during transport. Human weighing errors can be eliminated with automatic weighing that use either gravimetric or volumetric feed systems as described below.

In-line mixers generally are positioned above the extruder hopper. Each ingredient is fed by individual feeders. Fig. 6.1 shows a typical pellet blender. The ingredient feeders meter out a specific volume or mass over time, either by constant speed of an augur (volumetric feeders) or by an augur whose speed is controlled by the feed hopper loss in weight (gravimetric feeder). Volumetric feeders are less expensive but need to be manually calibrated for each ingredient since differences in density, bulk density, and compressibility affect the feed rate. Gravimetric feeders have become the most commonly used feeders. Their calibration is usually much simpler than volumetric feeders. For example, the feeder may measure the weight loss in 30 s of operation at 10% of the maximum feeder speed to compute a feed factor that takes into account the variation due to bulk density, density, and so on. The whole calibration process is usually done electronically and requires little operator interaction. Since the feed hopper weight is monitored by the computer control system, gravimetric feeders allow the individual feed rates to be recorded. Alarms can be set to ensure each ingredient is being fed to the extruder. Care must be taken when the feed hopper is refilled. Various control schemes are used to ensure feed continuity as the weigh cell is recalibrated, such as temporarily going into volumetric mode. Understanding how the gravimetric feeder handles refilling is helpful in ensuring a trouble-free operation.



Figure 6.1 Pellet blender.
Courtesy of AEC.

In-line mixers generally take up more space and are more expensive than batch mixers. They allow, however, for changing ingredient proportions during processing and can record the actual ingredient weights entering the extruder, which can be important for process control. They are also generally less labor intensive.

The ingredients in premixed pellet blends may segregate if they differ in density, size, or shape and are transported over a long distance. Keeping the transport distance as short as possible and avoiding mixing powders with pellets can minimize segregation.

Using properly sized feeders and augers is important to ensure ingredients are controlled to the correct proportions. An oversized feeder will likely have less precision and accuracy. There are also practical limits to pellet blending. A 1% pellet blend corresponds to blending one pellet in every 100.

When possible, it is best to strive for ingredients of 10% or higher for greater control and accuracy.

Care must be taken to clean thoroughly the feeders, mixers, and transport lines when changing over products. One wrong pellet in a product can cause film imperfections and other quality issues.

The film producer incurs extra risk when blending since the blend properties cannot be directly measured or controlled, especially if the blend is a thin layer in a multilayer film. Premade blends from a resin manufacture or compounder can be tested for properties to ensure they meet specifications. The error associated with premixing is directly related to the precision and accuracy of the pellet premixing system, how well it is maintained; and procedures that have been adopted to ensure the ingredients never run dry. Gravimetric pellet mixers typically have precisions ranging from about 0.1−1%, depending on hopper, feeder, and auger size.

6.3.2 Melt Blending

Once the ingredients have been fed in the correct proportions into the mixing device hopper, typically an extruder, the polymers and/or additives must be homogeneously blended together. This requires that the polymers be in the molten state. The mixing device melts the polymers, provides a means for mixing, and generates pressure for subsequent operations such as making film when in-line mixing and pelletizing when compounding.

Mixing is described as either distributive or dispersive and is illustrated in Fig. 6.2. In distributive mixing, the polymer is rearranged by deformation. Separation and rearrangement of flow and kneading are two examples of distributive mixing. In dispersive mixing, particles are broken up and dispersed within the polymer matrix. Shear stress is important for overcoming the yield stress of the material. Dispersing pigment particles in a masterbatch is an example of dispersive mixing.

The single screw extruder is the most commonly used device for film production. It efficiently melts the polymer and generates pressure for extruding the polymer through a flat or annular die. It is suitable for many blending applications but has its limitations, many of which can be overcome by optimizing the screw design. Single screw extruders rely on the difference in friction between the solid polymer pellets and the barrel and screw surfaces to propel the pellets forward. Slippery ingredients may impede the pellet flow and cause surging and other unwanted effects. Single screw extruders are typically flood fed, meaning the throughput is determined by the extruder screw speed, not how fast the ingredients are fed to the feed hopper. In more sophisticated compounding devices, such as twin-screw extruders, the throughput is decoupled from the screw speed. The output in these devices is determined by the feed rate and the screw speed can be increased or decreased to change the mixing intensity and energy input. Single screw extruders are also generally not well equipped to handle powder (due to potential problems with segregation in the feed hopper and nonuniform melting) and liquid feeds.

The melting mechanism for pellet blends with different melt points in a single screw extruder is not well understood. The standard melting model for uniformly melting pellets envisions a solid bed compressed against the trailing edge of the screw channel accompanied by an ever lengthening melt pool that results from the frictional heat near the

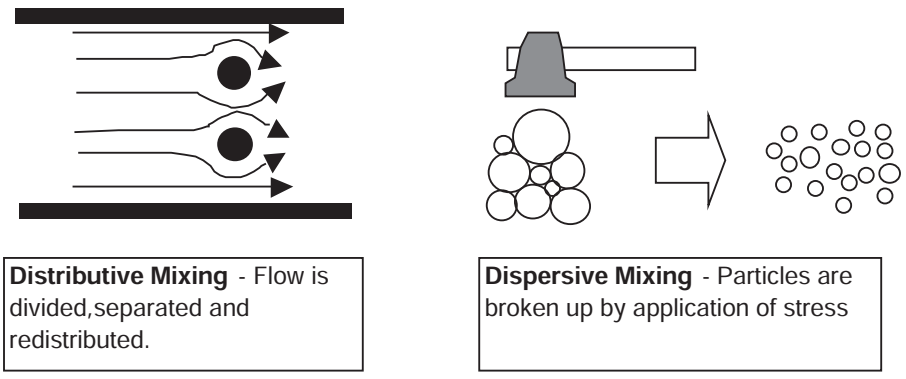


Figure 6.2 Distributive and dispersive mixing.

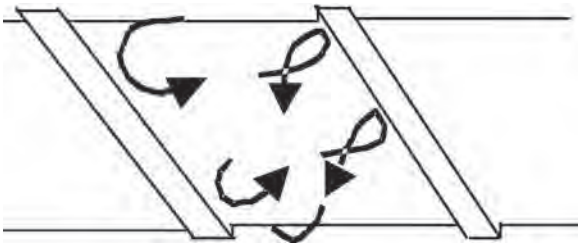


Figure 6.3 Illustration of circulatory flow patterns in the metering section of a single screw extruder.
Adapted from Middleman S. Fundamentals of polymer processing. New York: McGraw-Hill Book Company; 1977. p. 154.

barrel surface [19–21] (Fig. 6.23). Disruptions in the solid bed can result in poor melt quality; unmelted particles may exit the extruder, plugging screen packs, or appearing in the final film as "gel" particles [22]. A disruption in the solid bed can cause surging. Phase inversions and other aspects of blending of polymers that have different melt temperatures may cause disruptions in the solid bed and are not well documented in the literature. The polymer melting first may also act as a lubricant, impeding the melting of the higher melting point polymer since viscous heat generation from the friction between the polymer and barrel wall is one of the primary means for polymer melting.

Conversely, Morris and Kirschbaum [23] found that adding 1–2% of a low melting point ethylene copolymer to polylactic acid lowered power consumption by up to 30%, which may lead to higher output on extrusion lines limited by power. Baird [24] used a highly instrumented extruder to show that melting of the additive altered the frictional characteristics in the conveying section of the extruder as well as the melt film behavior in the melting zone. This resulted in less viscous energy dissipation and a more energy efficient process.

In a standard screw, the polymer melt is subject to nonuniform temperature and flow histories. There are circulatory flow patterns in the metering section of the screw (Fig. 6.3). These patterns aid distributive mixing and, as they are nonuniform, they may lead to uneven mixing. The shear stress and flow rates vary across the flow channel (Fig. 6.4). As a consequence, the temperature varies across the flow channel. The temperature nonuniformity exiting the extruder can cause film thickness variability. Mixing elements incorporated into the screw design or at the extruder exit (such as static mixers) help homogenize the melt temperature for proper control of film thickness. These same mixing devices also help blend polymers. Mixing elements that have been utilized over the years include pins, restriction rings, and more

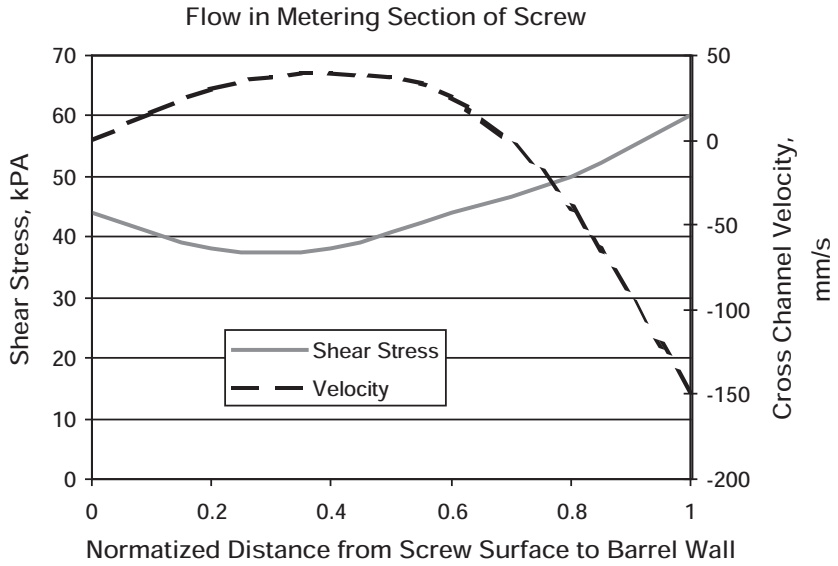


Figure 6.4 Example of stress and velocity distribution of polyethylene in the cross-channel direction of the metering section of a single screw extruder.
Calculations were done using commercial software from Polydynamics, Inc.

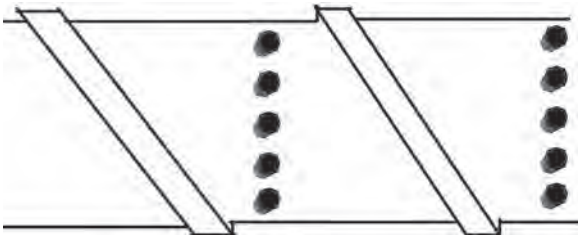


Figure 6.5 Pin mixing section.

specialized designs such as the pineapple, Dulmage, Saxton, and Maddock mixers [26].

Some mixing elements are characterized as distributive mixing elements—they achieve mixing by disrupting the flow. One of the easiest ways to do this is by inserting pins (Fig. 6.5), blisters, or other elements that impede the flow. Pins can cause problems, however, as stagnant flow zones are created behind the pins, setting up the potential for gel formation with some thermally sensitive polymers. More sophisticated designs, such as the Saxton mixer [27] (Fig. 6.6), eliminate the dead zones while dividing up the flow. Other elements are dispersive in nature, such as the well-known Maddock mixer (Fig. 6.7). In this design, the polymer flows down a fluted section and over a small clearance between the screw and barrel, which introduces high shear stresses to break up agglomerates. Its actual effectiveness at dispersive mixing is suspect, particularly compared to specialized compounding devices, such as twin-screw extruders, but it is often used for multipurpose mixing.

In recent years, several new high-performance screw designs have been developed that try to improve the mixing efficiency while increasing output. These screws generally work by having the polymer flow through a series of relatively tight clearances. The solid material is both entrapped and given time to melt or subject to high shear or elongational flow fields that aid in melting and mixing [26,28]. The high-performance section replaces the whole metering section of the screw. Some of the more commonly used high-performance screws include the energy transfer [29], variable barrier energy transfer [30,31], double wave [32,33], stratablend [34], unimix [35], and CRD [36] screws. An example of a variable barrier energy transfer screw element is shown in Fig. 6.8.

Although optimizing the screw design allows many polymer blends to be made on single screw extruders, in some cases, specialty compounding devices may be necessary. This is especially true when intensive dispersive mixing, reaction, or devolatilization is required. There are several compounder designs on the market. For general purpose compounding, corotating twin-screw extruders are often employed [37,38]. Kneaders provide good distributive mixing, easily allow the introduction of liquid feeds, and minimize temperature buildup, which is important for thermally sensitive polymers. Counterrotating twin-screw extruders are often used for reactive extrusion and devolatilization since they can have long *L*/*D*s (length to diameter ratios). The Farrel continuous mixer operates like a continuous Banbury mixer and is useful for making masterbatches with high filler loadings. Planetary mixers and other multiscrew devices are also available for specialty applications.

Of the specialty compounding devices, the corotating twin-screw extruder is the most often used. Corotating twin-screw extruders offer considerable versatility in design and operation. As described earlier, feeding is independent of extruder speed, which allows the mixing and energy intensity to be independently varied. Multiple feeding ports are common and screw designs can be changed from job to job to tailor the process. The screws are built from individual elements, which can be changed to suit the application. These elements come in several geometries with different mixing intensities. They provide good distributive and dispersive mixing and impart

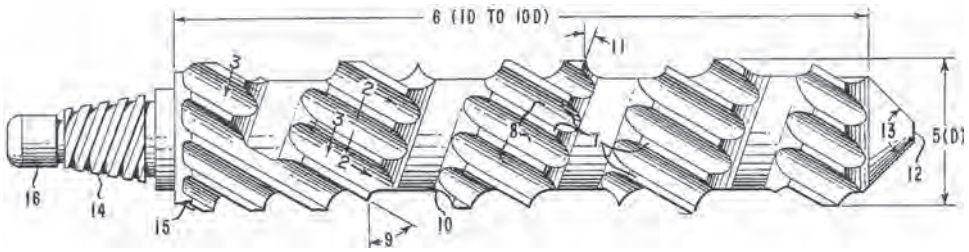


Figure 6.6 Saxton [27] mixing section.

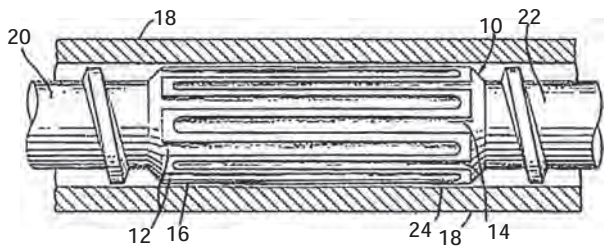


Figure 6.7 Maddock screw element. From B. Maddock, 1973, U.S. patent 3730492A.

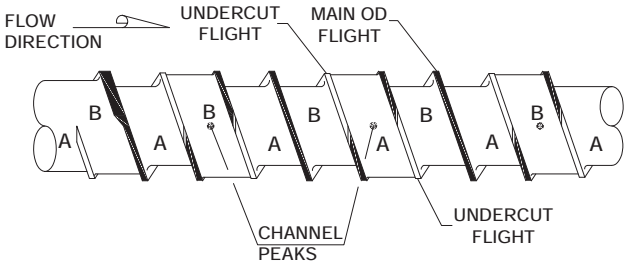


Figure 6.8 Illustration of a variable barrier energy transfer screw. Courtesy of Jeff Myers at BARR Inc.

both shear and elongational flow fields. Fig. 6.9 shows some twin-screw modular elements. Some twin-screw extruders have screws that are self-wiping, which results in a narrow residence time distribution for better mixing control. One drawback is that they are poor melt pumps. Because of this, temperatures can be difficult to control at the extruder exit. Twin screw extruders are not generally used alone for in-line compounding on a film line; a single screw extruder or gear pump is added to provide better melt pumping [18].

Twin-screw extruders and other specialty compounding devices are considerably more expensive than single screw extruders.

6.4 Physics of Blending

The properties of a polymer blend are influenced by specific interactions between the molecules (thermodynamics) and their response to deformation (rheology). The thermodynamics determine whether the blend forms a single phase (miscible) or multiple phases (immiscible). Miscible blends typically follow the rule of mixtures, namely the blend properties are directly proportional to the component ratio. Blends of different grades of the same polymer, such as two grades of LDPE, are typically miscible. Most polymer blends of different polymers are not miscible. There are only a few commercially important miscible blends on the market today. One is Sabic Noryl, which is a polyphenylene oxide and high impact polystyrene blend.

How does one determine whether a blend is miscible? One method is to look at transparency, either by microscopy or light scattering. An immiscible blend forms separate domains within the polymer matrix that may diffract light if they are large enough. Another technique is to measure the glass transition temperature (T_g) using differential scanning calorimetry or other thermal analyses. A miscible blend will have a single T_g, typically between that of the components. Both techniques use a fairly large

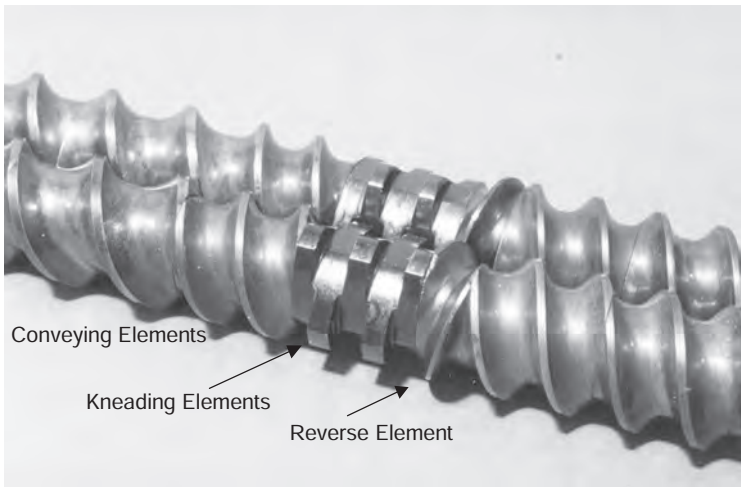


Figure 6.9 Twin-screw extruder modular elements.

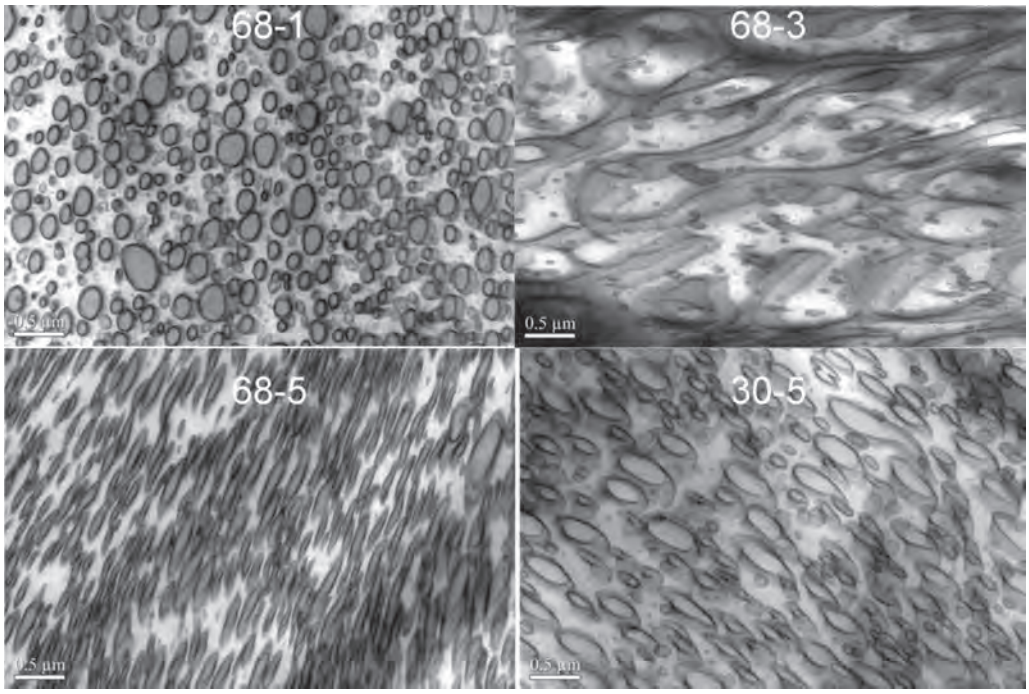


Figure 6.10 Transmission electron micrographs (TEMs) of immiscible polyethylene—styrene polymer blends of varying chemistries.

Courtesy of Barbara Wood and I-Hwa Lee, DuPont. Further examples of TEMs of immiscible blends can be found in Wood BA. Transmission electron microscopy of detection of rubber modifiers. In: 161st Technical meeting of the rubber division of the American Chemical Society, Savannah, GA, April 29–May 1, paper 45; 2002; Wood BA. Transmission electron microscopy of polymer blends. In: Finlayson K, editor. Advances in polymer blends and alloys technology, vol. 3. Lancaster (PA): Technomic Publishing Co., Inc.; 1992.

sample or probe size, which can at times be misleading. Sometimes blends appear to be miscible because the probe size is too large. Other techniques with smaller probe sizes are X-ray and neutron scattering and various spectroscopy techniques, such as infrared (IR) and nuclear magnetic resonance.

Occasionally, the word "compatibility" is used to describe the degree to which polymers interact. Miscibility can be thought of as the state of maximum compatibility. Compatibility is a subjective term and is not well defined. Miscibility has a specific definition—two polymers are miscible if they form a single phase over their entire composition range at a given temperature.

Immiscible blends, by definition, form multiple phases. In the simplest case, a two-component blend, the minor phase forms domains within a continuous major component matrix. The domain sizes, shapes, and distribution are known as the morphology. Fig. 6.10 shows some immiscible blend morphologies. The morphology is influenced by the concentration, thermodynamics, component rheology, and the flow and stress history during mixing and processing.

The morphology is critically important to the final blend properties, which often do not follow the rule of mixtures (Fig. 6.11). In many cases, blends

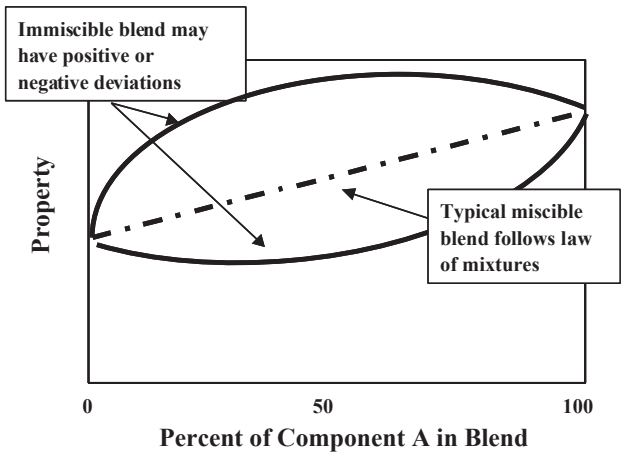


Figure 6.11 Properties versus percent of polymer A in polymer blends.

are designed to create a specific morphology to achieve certain property gains. An example is supertough polyamide (PA) or nylon, which is a PA66/rubber blend [6]. The rubber must achieve a certain domain size in order to stop cracks from propagating during impact. Another example is Selar RB laminar technology developed by DuPont. Here PA is dispersed in HDPE so that the PA phase forms platelets parallel to the surface. The platelets create a tortuous path for diffusion, resulting in improved barrier performance [8].

Once a specific morphology has formed, it may change with further processing. The domains may coalesce or be stretched through orientation (Fig. 6.10). Compatibilizers are frequently used to stabilize the blend morphology.

There is a third type of blend system, namely melt-miscible blends that are miscible in the melt state but phase separate in the solid state. An example is polyoxymethylene/polylactide (POM/PLA) [41]. This phenomenon may be important for ease of processing in order to obtain a fine dispersion of one component into another during melt blending.

6.4.1 Thermodynamics

When two materials are brought together, there must be a decrease in the free energy for them to transform into a single material or miscible blend. This can be expressed mathematically as:

$$\Delta G_m < 0 \text{ for miscibility} \tag{6.1}$$

where ΔG_m = Gibbs free energy of mixing.

The free energy includes enthalpy and entropic contributions:

$$\Delta G_m = \Delta H_m - T\Delta S_m \tag{6.2}$$

where ΔH_m = enthalpy of mixing; T = temperature; ΔS_m = entropy of mixing.

For most polymer blends, ΔH_m is positive and ΔS_m is nearly zero. Thus, it is rare that polymer blends are miscible.

Coleman [42] derived the following relationship for ΔG_m based on the work of Flory and Huggins:

$$\frac{\Delta G_m}{RT} = \left[\frac{\Phi_A}{N_A}\ln\Phi_A + \frac{\Phi_B}{N_B}\ln\Phi_B\right] + \chi\Phi_A\Phi_B\left(\frac{\Delta G_H}{RT}\right) \tag{6.3}$$

where ΔG_m = Gibbs free energy of mixing; R = ideal gas constant; T = temperature; Φ_A = volume fraction of polymer A; Φ_B = volume fraction of polymer B; N_A = degree of polymerization of polymer A; N_B = degree of polymerization of polymer B; χ = interaction parameter; ΔG_H = free energy of specific action between polymers, including hydrogen bonding.

The first term on the right side of Eq. (6.3) arises from combinatory entropy. Since N, which is related to molecular weight, is large for polymers, this term is nearly zero. The second term also arises from entropy and is always positive. The interaction parameter, χ, is defined by:

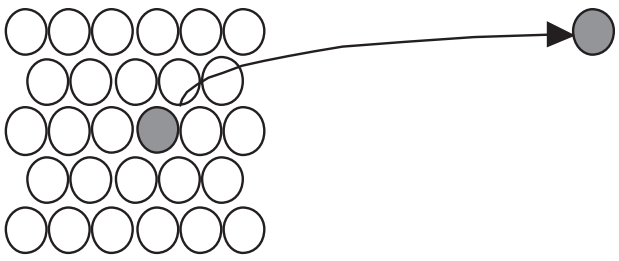
$$\chi = \frac{V_{ref}}{RT}[\delta_A - \delta_B]^2 \tag{6.4}$$

where V_{ref} = reference volume; δ_A = solubility parameter for polymer A; δ_B = solubility parameter for polymer B.

The final term, $\Delta G_H/RT$, is negative when specific interactions are present.

Eqs. (6.3) and (6.4) show that compatibility is improved by matching solubility parameters and miscibility is achieved only when specific interactions are present. Nonpolar polymer blends, such as PP—PE blends, have no specific interactions beyond weak dispersive forces. It will be shown that even though their solubility parameters are nearly equal, they are not miscible.

Eq. (6.4) introduces the solubility parameter. The solubility parameter is a measure of molecular attractiveness and arises from the energy per unit volume required to remove a molecule from a liquid or solid. This is known as the cohesive energy density and is illustrated in Fig. 6.12. The cohesive energy density is determined by the forces that hold the



Cohesive energy density is the energy needed to remove a molecule away from its environment and is the square of the solubilty parameter.

Figure 6.12 Illustration of cohesive energy density.

material together. The solubility parameter is the square root of the cohesive energy density. It contains contributions from both nonpolar (dispersive forces) and polar (dipole–dipole and hydrogen bonding) interactions.

Comparing solubility parameters is a way to quantify the "like dissolves like" principle of chemistry. For two polymers to be miscible, the difference in solubility parameters should be between 0.1 and 3 Hildebrands, depending on their interaction strength. Coleman [42] defines a critical solubility parameter difference, $\Delta\delta_c$, below which the polymers may be miscible. As shown in Table 6.1, the value of $\Delta\delta_c$ depends on what interactive forces are present.

Table 6.2 lists solubility parameter values for some polymers used in packaging films. Returning to the PE–PP blend example, the values from the table show that the difference in their solubility parameters is less than 1 ($\Delta\delta < 1$ Hildebrands). However, since only nonpolar dispersive forces are present, the critical solubility parameter difference ($\Delta\delta_c$) is less than 0.1. Thus, these polymers are not miscible.

It should be noted that there is some controversy around solubility parameters in the literature. They are exact for polymers with only physical interactions. There are errors associated with trying to extend the concept to polymer systems involving hydrogen bonding and other polar interactions and with the indirect methods used experimentally to measure them. These errors typically result in a broader range of values than is useful for predicting miscibility, hence matching solubility parameters is not an absolute condition for the miscibility of polymers. They are useful guides for compatibility, however, and since most polymer blends are not miscible, this may be their greatest strength. The solubility parameter difference has been related to the interphase thickness between immiscible polymers. Immiscible polymers with a solubility parameter difference of about 0.5 Hildebrands or less may still build up enough strength at the interface for good mechanical properties [47].

Returning to the PP–PE blends example, PE is often used to modify the properties of PP. For example, ethylene–propylene rubber (EPR) is blended with PP to improve PP impact toughness. The EPR forms a phase with sufficient adhesion to the PP that the properties are enhanced, as would be predicted by their close solubility parameters.

LDPE–LLDPE blends are perhaps the most commercially important blends used in flexible packaging applications. A distinguishing difference between LDPE and LLDPE is long chain branching in LDPE, which contributes to its relative processing ease. Typically, about 10–30% LDPE is added to LLDPE to improve melt strength, bubble stability, and other film production. Hussein [48–51] found that LDPE and LLDPE are not miscible over their

Table 6.1 Critical Solubility Parameter Difference Upper Limit

Specific Interactions Involved	Polymer Blend Examples	$\Delta\delta_{critical}$ Hildebrands
Dispersive forces only	Polybutadiene–polyethylene (PBD–PE)	<0.1
Dipole–dipole	Polymethylmethacrylate–polyethylene oxide (PMMA–PEO)	0.5
Weak	Polyvinyl chloride–butadiene acrylonitrile copolymer (PVC–BAN)	1.0
Weak to moderate	Polystyrene acrylonitrile–polymethylmethacrylate (SAN–PMMA)	1.5
Moderate	Polycarbonate–polyesters	2.0
Moderate to strong	Nylon–polyethylene oxide (nylon–PEO)	2.5
Strong	Poly vinyl phenol–poly vinyl acetate (PVPh–PVAc)	3.0
Very strong	Polymethacrylic acid–polyethylene oxide (PMMA–PEO)	>3.0

From Coleman M, Graf J, Painter P. Specific interactions and the miscibility of polymer blends. Lancaster (PA): Techonomic Publishing; 1991.

Table 6.2 Solubility Parameters for Some Polymers Used in Packaging

Polymer	Solubility Parameter $cal^{1/2}/cm^{3/2}$ (Hildebrands)	Sources
PE (polyethylene)	7.7–8.4	Van Krevelen [43]
PP (polypropylene)	8.2–9.2	Van Krevelen [43]
PS (polystyrene)	8.5–9.3	Van Krevelen [43]
PVC (poly vinyl chloride)	9.4–10.8	Van Krevelen [43]
PVDC (poly vinylidene chloride)	9.9–12.2	Van Krevelen [43]
PVOH (polyvinyl alcohol)	12.6–14.3	Van Krevelen [43]
EVOH (44 mol% ethylene) (ethylene vinyl alcohol)	17	Evalca literature [44]
EVOH (32 mol% ethylene)	19	Evalca literature [44]
PA 6 or Nylon 6	12.6	Evalca literature [44]
EVA(9% VA) (ethylene vinyl acetate)	8.1	DuPont calculation [45]
EVA(25% VA)	8.2	DuPont calculation [45]
EMA(20% MA) (ethylene methyl acrylate)	8.3	DuPont calculation [45]
PET (polyethylene terephthalate)	10.3	Wu [46]

entire composition range. Miscibility is favored for LLDPE-rich blends. The miscibility range increases by lowering the LLDPE molecular weight (MW) and by increasing the short chain branch length (replacing the butene comonomer with octene). At the same molecular weight and branch content, a Zeigler–Natta LLDPE is more miscible with LDPE than metallocene LLDPE (*m*-LLDPE), which has a narrow molecular weight and comonomer distribution. At the same molecular weight distribution (MWD) and molecular weight (MW), an *m*-LLDPE with higher branch content is more miscible with LDPE than an *m*-LLDPE with lower branch content. Comonomer type does not have an effect on miscibility of *m*-LLDPE with LDPE.

One can add specific interactions to promote miscibility. Coleman et al. [42] have developed software that uses group contribution theory to predict solubility parameters of polymers that, in many cases, agrees well with experimental results. This is illustrated in Fig. 6.13. Here, vinyl acetate (VA) and styrene (St) contents are varied in an EVA copolymer–styrene vinyl phenol (EVA–StVPh) copolymer blend. Increasing the VA and the vinyl phenol (VPh) content promotes polar interactions (ΔG_H) that drive ΔG_m below zero [Eq. (6.3)]. The experimental data are represented by the open and closed circles: the open circles represent miscible blends and the closed circles represent immiscible blends. The line demarking the region of miscibility comes from Eq. (6.3), using the software to predict the solubility parameters with specific interactions. The miscibility region depends on the comonomer percent in each polymer.

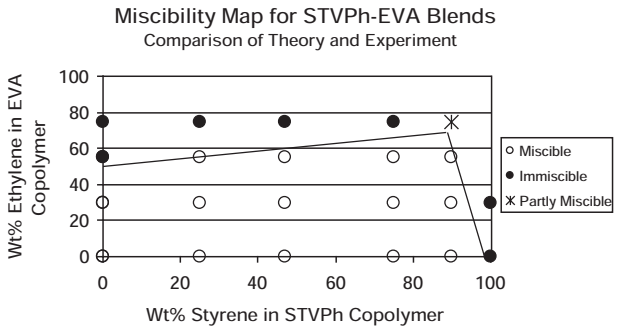


Figure 6.13 Example of using specific interactions between molecules to achieve miscible blends. *Taken from Coleman M, Graf J, Painter P. Specific interactions and the miscibility of polymer blends. Lancaster (PA): Techonomic Publishing; 1991.*

A practical note about compatibility and miscibility concerns masterbatches. The carrier resin in the masterbatch should be compatible and, ideally miscible, with the resin in which it is being blended. This way, the carrier resin will not harm the letdown resin properties. Poor compatibility can lead to poor

optical properties, reduced barrier performance, and, for sealants, poor seal performance. Benkreira and Britton [52] found that better dispersion occurs when the carrier resin is lower in viscosity and has a lower melting point than the host polymer, for reasons that will become clearer in the next section.

Solubility parameters may also prove useful for predicting miscibility of low molecular weight additives in polymers.

6.4.2 Morphology Development in Immiscible Blends

To understand how morphology develops in a polymer blend, the breakup of a single droplet suspended in a fluid during flow is first considered. The droplet is held together by interfacial tension, which arises from a nonuniform force distribution acting on the molecules at the interface (Fig. 6.14). Inside a material, a molecule is bound to its neighbors by attractive forces related to the cohesive energy density. At an interface, however, molecules are only partly surrounded by their own kind. The material across the interface may exert different attractive forces. The difference in these attractive forces gives rise to the interfacial tension. The more alike the materials are, the lower the interfacial tension, and the smaller the driving force holding the droplet together. If the droplet has a radius a, then this holding force, $F_{\text{interfacial}}$, is proportional to Γ/a, where Γ is the interfacial tension.

The interfacial tension can be related to solubility parameters introduced earlier. Wu [46] shows that the interfacial tension is related to the surface tensions of the two polymers:

$$\Gamma_{12} = \Gamma_1 + \Gamma_2 - 2\varphi\sqrt{\Gamma_1\Gamma_2} \tag{6.5}$$

where Γ_{12} = interfacial tension between polymers 1 and 2; Γ_1 = surface tension of polymer 1; Γ_2 = surface tension of polymer 2; φ = interaction parameter.

This is known as the Good and Girifalco equation. Wu tabulates the interaction parameter, φ, for several polymer combinations. They range from 0.79 to 0.98 for the polymers considered. The surface tension can be related to the solubility parameter:

$$\Gamma_1 = 0.2575\frac{\delta_1}{\sqrt[3]{\rho_1}} \tag{6.6}$$

where Γ_1 = surface tension (dynes/cm); ρ_1 = density of polymer 1 (g/mL); δ_1, polymer 1 solubility parameter $(\text{cal/mL})^{1/2}$.

Combining Eqs. (6.5) and (6.6), recognizing polymer densities are around 1 g/mL, and assuming $\varphi = 1$, the interfacial tension is found to be directly proportional to the square of the difference in solubility parameters:

$$\Gamma_{12} \cong 0.26(\delta_1 - \delta_2)^2. \tag{6.7}$$

As shown in Fig. 6.15, the flow field exerts a drag force that acts to break up the droplet. For shear flow, the drag force is equal to the viscosity of the continuous phase, η_c, times the shear rate, $\dot{\gamma}$ = acting over the area of the particle ($\approx a^2$):

$$F_{\text{drag}} \sim \eta_c \dot{\gamma} a^2.$$

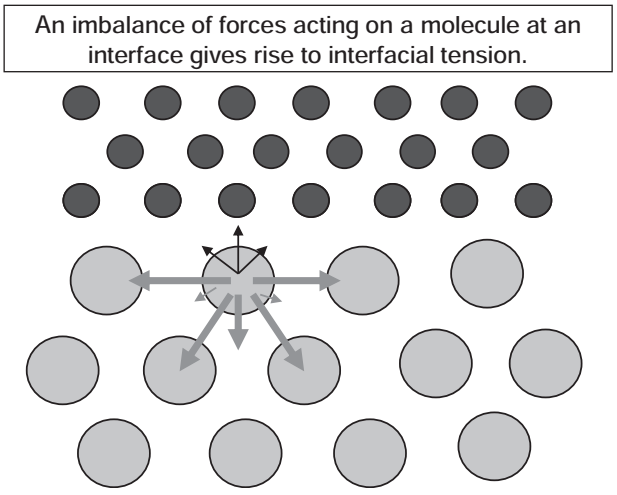


Figure 6.14 Illustration of the origins of interfacial tension.

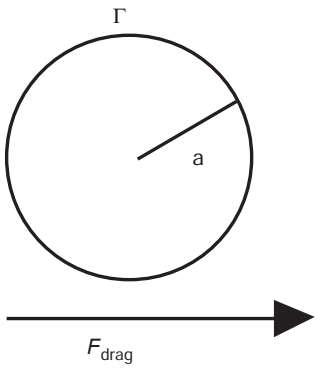


Figure 6.15 Balance of drag and interfacial forces on a spherical droplet in shear flow.

The dimensionless capillary number, Ca, is defined as the ratio of the drag force to the interfacial force:

$$\mathrm{Ca} = \frac{F_{\mathrm{drag}}}{F_{\mathrm{interfacial}}} = \frac{\eta_c \dot{\gamma} D_d}{2\Gamma_{12}} \tag{6.8}$$

where D_d = droplet diameter (= $2a$).

When Ca exceeds a critical value, $\mathrm{Ca}_{\mathrm{critical}}$, the droplet breaks up because the drag force exceeds the force holding the droplet together. This hydrodynamic instability was first proposed by G.I. Taylor [53]. Taylor found that $\mathrm{Ca}_{\mathrm{critical}}$ for a Newtonian droplet imbedded in a Newtonian fluid is a function of the viscosity ratio (the ratio of the droplet viscosity to the continuous phase viscosity): η_d/η_c. This has since been confirmed by other investigators and is illustrated in Fig. 6.16. In a shear flow, $\mathrm{Ca}_{\mathrm{critical}}$ reaches a minimum when the viscosity ratio is 1. When the viscosity ratio exceeds about 3.5, the droplet cannot be broken up in a shear flow as indicated by the rapid rise in $\mathrm{Ca}_{\mathrm{critical}}$. The bottom curve in Fig. 6.16 shows the relationship for $\mathrm{Ca}_{\mathrm{critical}}$ in elongational flow. Elongational flow is more effective for breaking up droplets than shear flow; $\mathrm{Ca}_{\mathrm{critical}}$ is lower and droplets can be broken up even at high viscosity ratios.

For transient flow, a different mechanism for drop breakup has been proposed by Tomotika [55] based on Rayleigh's instability theory. Here, the droplet becomes an elongated ellipse or cylinder that, upon cessation of flow, breaks up into small droplets due to capillary disturbances, provided that the wavelength of these disturbances is greater than $2\pi a$ [56,57].

The single droplet analysis provides considerable insight into the dispersion of polymer blends (Fig. 6.17). Typically, the minor component domain size (D_d) of the blend is desired to be small. For example, for good clarity, the dispersed phase should be less than the wavelength of visible light, or about 0.3 μm. For toughening, small soft rubber domains help prevent cracks from propagating. Eq. (6.8) shows that the droplet size decreases by increasing the continuous phase viscosity, increasing the shear rate or by decreasing the interfacial tension. The droplet size is also reduced by matching the polymer viscosities (a good guideline is to choose a viscosity ratio between 0.01 and 2) and using a mixing device that imparts elongational flow. The interfacial tension can be minimized by reducing the difference in solubility parameters [Eq. (6.7)] or by introducing specific interactions.

Compatibilizers are sometimes used to reduce the interfacial tension between polymers. Block or random copolymers often make good compatibilizers since they can be designed to contain two functionalities, each compatible with one of the polymers being blended. An example is using styrene–ethylene–butadiene–styrene (SEBS) copolymer to compatibilize HDPE and polystyrene (PS) blends [58]. Another approach is to add functional groups to the compatibilizer that react with one of the polymers. An example is using an ionomer to compatibilize PA (polyamide or nylon) and PE blends. The acid groups

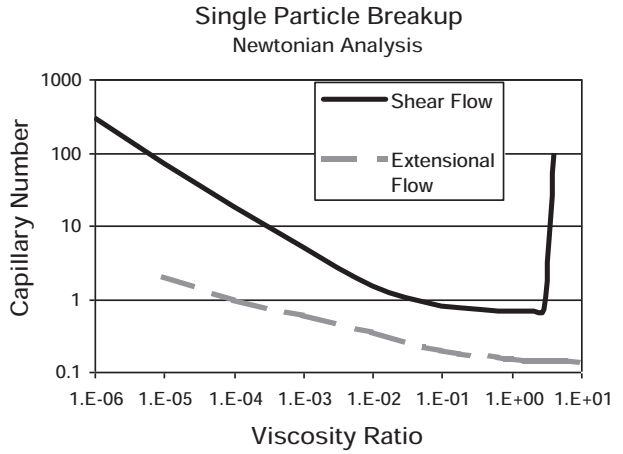


Figure 6.16 Critical Capillary Number for the breakup of Newtonian droplet in shear and elongational flow.
Data taken from Grace HP. Dispersion in high viscosity immiscible fluid systems and application of static mixers as dispersion devices in such systems. Chem Eng Commun 1982;14:225–77.

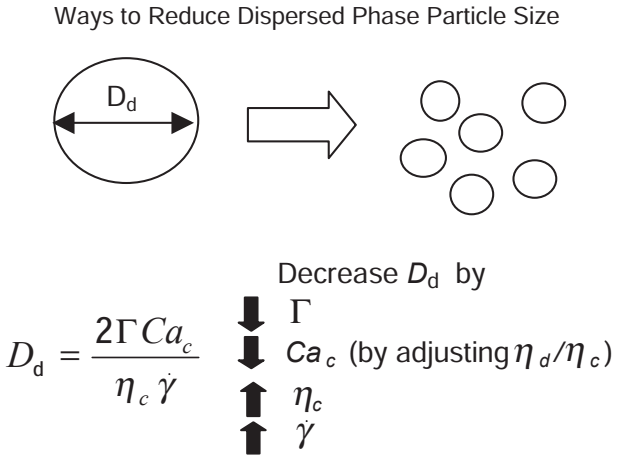


Figure 6.17 Learnings from single droplet mechanics.

in the ionomer interact with the PA amine end groups and the ethylene backbone is compatible with PE [59]. Another example is the use of maleated polyolefins to compatiblize PA or EVOH containing recycle streams [60].

While the breakup of a single Newtonian droplet in a Newtonian fluid is well understood, there are several difficulties in extending the analysis to polymer blends. The first is that polymer melts are typically non-Newtonian in their flow behavior (non-Newtonian fluids have viscosities that vary with shear rate and often exhibit elastic effects, such as normal stress differences and extrudate swell). Although several droplet breakup studies for non-Newtonian fluids have recently been published, this phenomenon is still not as well understood as the Newtonian case. Table 6.3 summarizes many of these studies. One aspect of non-Newtonian behavior is the polymer melt elasticity, characterized by the first and second normal stress differences (see Chapter 5 for an introduction to melt elasticity or consult a rheology text such as Dealy and Wissbrun [61] for a broader discussion). Some investigators have used the dynamic storage modulus, G', obtained from dynamic mechanical analysis, as a way to characterize elasticity. G' is proportional to the first normal stress difference but only at low shear rates. At higher shear rates typical of polymer processing, G' may underestimate the polymer elasticity. In general, it has been found that when the droplet is more elastic than the continuous phase, it is more difficult to disperse. An elastic force aids in holding the droplet together, resulting in larger $Ca_{critical}$ values and larger droplet sizes. Conversely, when the continuous phase is more elastic than the droplet, it is easier to break up the droplet because the matrix resin elasticity adds to the drag force on the droplet to break it up. Quantification and modeling of this behavior in flow regimes typical of polymer processing is still in its infancy.

Experimental studies with non-Newtonian fluids have also revealed different droplet breakup mechanisms. A Newtonian droplet immersed in a Newtonian fluid breaks up via Taylor [53] and Tomotika [55] instabilities (Fig. 6.18). Under some conditions, non-Newtonian fluids also break up in this manner, but other mechanisms have also been observed. In some cases, the droplet flattens in the flow direction and becomes elongated perpendicular to the flow [68,77]. The ends of highly elongated particles find themselves in different planes with respect to flow and are torn apart by the velocity differences. At very high viscosity ratios, greater than the cutoff of 3.5 for Newtonian droplets, Mighri and Huneault [77] observed breakup via attrition at the droplet surface.

As the droplet concentration increases, the breakup mechanism becomes more complex. Utracki and Shi [57] and Macosko [82] find that when the polymer concentration exceeds 0.5−1%, the droplet size after shearing is much greater than that predicted by the single drop experiments. As the concentration increases, the probability that droplets will collide and coalesce increases. The coalescence kinetics are not well understood and are thought to be critically important to the final blend morphology. Utracki and Shi [57] observe that the same factors that enhance droplet breakup, namely high shear rates and reduced droplet viscosity, favor coalescence. Several investigators [83,84,106] have proposed that compatibilizers act to inhibit coalescence by providing a protective shell around the droplet (Fig. 6.19). The shell acts to repulse other droplets. Thus, dispersion stabilization may be more important to the droplet size than reducing interfacial tension. Indeed, Mighri and Huneault [77] find that an EPR−PP droplet−matrix system with very low interfacial tension breaks up in a similar manner as a PS−PE system with an order of magnitude greater interfacial tension. They suggest that interfacial instabilities may not be required for non-Newtonian droplets to break apart.

As the minor component concentration is increased, the morphology may change. At high enough concentrations, the minor component becomes the continuous phase. Fig. 6.20 shows the different morphologies possible for HDPE/PS blends studied by Bourry and Favis [58]. At low PS levels, the PS forms droplets in the HDPE matrix. As the PS concentration is increased, fibers are formed. At about 70% PS, the morphology becomes cocontinuous; the HDPE and PS phases form an interpenetrating network structure where both phases are continuous. Higher PS levels result in HDPE droplets in a PS matrix. Note how the SEBS compatibilizer decreases the domain size.

Another concern in applying single droplet studies directly to polymer blends is uncertainties about the flow field in the mixing device and how to calculate the appropriate viscosity ratio. Polymer-mixing devices, such as extruders, have complex flow fields involving both shear and elongational flow. The flow fields are typically nonuniform; the shear rate varies

Table 6.3 Summary of Studies of Viscoelastic Droplet Deformation in a Viscoelastic Matrix Under Shear or Elongational Flow

Sources	Experimental or Theoretical	Droplet	Matrix	Flow	Result
Flumerflet [62]	Experimental	Newtonian	Viscoelastic	Shear	Minimum droplet size and critical shear rate for breakup increases with matrix elasticity
Tavgav [63]	Experimental	Viscoelastic	Viscoelastic	Shear	Effect of elastic matrix depends on the viscosity ratio: • when ratio is small, matrix elasticity stabilizes the droplet • when ratio is high, elasticity helps break up the droplets
Gauthier [64]	Experimental	Viscoelastic	Newtonian	Shear	Small viscosity ratio: similar to Newtonian drop in Newtonian matrix High viscosity ratio: $Ca_c > Ca_{c-Newtonian}$
Parabodh and Stroeve (in Utracki and Shi) [57]	Experimental	Viscoelastic	Newtonian	Shear	For viscosity ratio <0.5, droplet viscoelasticity has a stabilizing effect For viscosity ratio >0.5, droplet viscoelasticity has a destabilizing effect
DeBruijn [65]	Experimental	Viscoelastic	Newtonian	Shear	$Ca_{critical}$ for elastic droplet is slightly higher than for Newtonian droplet
Elmendorp and Maalcke [66]	Experimental	Viscoelastic	Viscoelastic	Shear	Viscoelastic drop deformation in Newtonian matrix decreases with increasing drop elasticity Newtonian drop deformation in viscoelastic matrix increases with increasing matrix elasticity Problems with quantifying the behavior due to fluid shear thinning
Varanasi [67]	Experimental	Viscoelastic	Newtonian	Shear	At any viscosity ratio $Ca_{critical}$ increases with increasing droplet elasticity
Levitt et al. [68]	Experimental	Viscoelastic	Viscoelastic	Shear	Studied PP droplets in PS matrix at different viscosity and elasticity ratios Shear flow at 1 s^{-1}. For high elastic matrix found that the droplet widened in the direction perpendicular to the flow. The width of the flattened drops depended on the differences in second normal stress differences between the phases
Han and Funatsu [69]	Experimental	Viscoelastic	Viscoelastic	Elongation	Viscoelastic drops are more stable than Newtonian drops in both Newtonian and viscoelastic matrices
Milliken and Leal [70]	Experimental	Viscoelastic	Newtonian	Elongation	Viscoelastic drops with viscosity ratios less than 1 have smaller deformation and $Ca_{critical}$ than Newtonian drops. For viscosity ratio >1 the viscoelastic drop deformation behavior is similar to Newtonian drops
Delaby et al. [71]	Experimental	Viscoelastic	Viscoelastic	Elongation	For negligible interfacial tension, viscoelastic drops deform less than the surrounding media when the viscosity ratio is less than 1 and more when the viscosity ratio is greater than 1

(*Continued*)

Table 6.3 Summary of Studies of Viscoelastic Droplet Deformation in a Viscoelastic Matrix Under Shear or Elongational Flow (*Continued*)

Sources	Experimental or Theoretical	Droplet	Matrix	Flow	Result
Meijer and Janssen [72]	Experimental	Not disclosed	Not disclosed	Elongation	At small viscosity ratios, the droplet deformation in planar elongational flow resembles that for the matrix
Chin and Han [73]	Experimental	Viscoelastic	Viscoelastic	Elongation	Higher droplet elasticity results in less deformation compared to the matrix
Shanker et al. [74]	Experimental	Viscoelastic	Viscoelastic	Elongation	Higher droplet elasticity results in less deformation compared to the matrix
Mighri et al. [75]	Experimental	Viscoelastic	Viscoelastic	Elongation	Used Boger fluids which have elasticity and nonshear thinning viscosity behavior For a given elastic matrix fluid, increasing the droplet elasticity decreased droplet deformation relative to the surrounding media. Droplet deformation increases with increasing matrix elasticity. Defined k' as first normal stress difference ratio divided by the viscosity ratio. When $k' < 0.2$, the matrix elasticity has a greater effect on deformation than the drop elasticity. The opposite is true with $k' > 0.2$. The study was conducted over a fairly narrow viscosity ratio range (0.5–1.1); shear rates were not disclosed.
Mighri et al. [76]	Experimental	Viscoelastic	Viscoelastic	Shear	Used Boger fluids, which have elasticity and constant viscosity versus shear rate behavior. Shear rates not disclosed; viscosity ratios ranged from 0.2 to 1.1. Defined k' as first normal stress difference ratio divided by the viscosity ratio For high matrix elasticity ($k' < 0.37$), the elastic drop deformation in an elastic matrix was higher than for the Newtonian case with same viscosity ratio and interfacial tension. In some cases, droplet widening in the direction perpendicular to flow was observed. For $k' > 0.37$, elastic drops deform less than the Newtonian case. The critical shear rate for droplet breakup increases with increasing k'. For $k' < 4$, $Ca_{critical}$ increases rapidly with k'; for $k' > 4$, $Ca_{critical}$ levels off at 1.75
Mighri and Huneault [77]	Experimental	Viscoelastic	Viscoelastic	Shear	Studied model systems and PS/PE system with viscosity ratio between 5 and 20 under relatively high shear rate ($1–20\ s^{-1}$) in shear flow. In PS/PE system, the PS drop widened in the direction perpendicular to flow, which contributed to droplet breakup (the ends of the highly elongated droplet are in different flow planes). At high shear, a second breakup mechanism different from the Newtonian case was observed: attrition from the surface. An EPR/PP system had similar breakup mechanisms as the PS/PE system despite a 10× difference in interfacial tension

Van Oene [78]	Theoretical	Viscoelastic	Viscoelastic	Shear	Developed an expression for the dynamic interfacial energy to account for viscoelasticity: $\Gamma_{12} = \Gamma^{o}_{12} + D_d/12 \times [(N_{11} - N_{22})_d - (N_{11} - N_{22})_m]$ where Γ^{o}_{12}, the interfacial tension in quiescent flow, $(N_{11} - N_{12})$, the first normal stress difference Droplet elasticity greater than the matrix stabilizes the droplet; matrix elasticity greater than the droplet destabilizes the droplet.
Greco [79]	Theoretical	Viscoelastic	Viscoelastic	Shear and elongation	Assumed the materials are simple second-order fluids, which includes elastic effects for slow flows. Used a perturbation method to analyze the first normal stress difference effect on droplet shape for small drop deformations
Maffettone and Greco [80]	Theoretical	Viscoelastic	Viscoelastic	Shear and elongation	Developed a phenomenological model for the dynamics of a drop immersed in an immiscible fluid. Assumed the drop is ellipsoidal. Either or both fluids may have elasticity. Found that elastic drops deform less than Newtonian drops. Elastic drops in Newtonian matrix under shear are forbidden to break up at lower viscosity values than the Newtonian case. In elongational flow, the drop breakup is easier when the matrix is elastic and more difficult when the droplet is elastic
Lerdwijitjarud et al. [81]	Experimental	Viscoelastic	Newtonian	Shear	Studied deformation and breakup of viscoelastic drops (Boger fluids) in a nearly Newtonian matrix. Viscosity ratio controlled to around 1.0. Shear rates up to 5 s^{-1} used The deformation decreases for isolated drops at constant Ca as the drop elasticity increases. They did not observe droplet widening in the transverse to flow direction and suggest widening is influenced by factors other than first normal stress difference (such as second normal stress difference, shear thinning, or a shift of the critical condition to lower Ca when the matrix is elastic). $Ca_{critical}$ increases with increasing droplet elasticity. For a 10% blend, the steady state Ca is less than $Ca_{critical}$ for an isolated drop (they suggest this may be due to flow differences in concentrated suspensions). The steady state Ca was found to increase monotonically with the dispersed phase first normal stress difference.

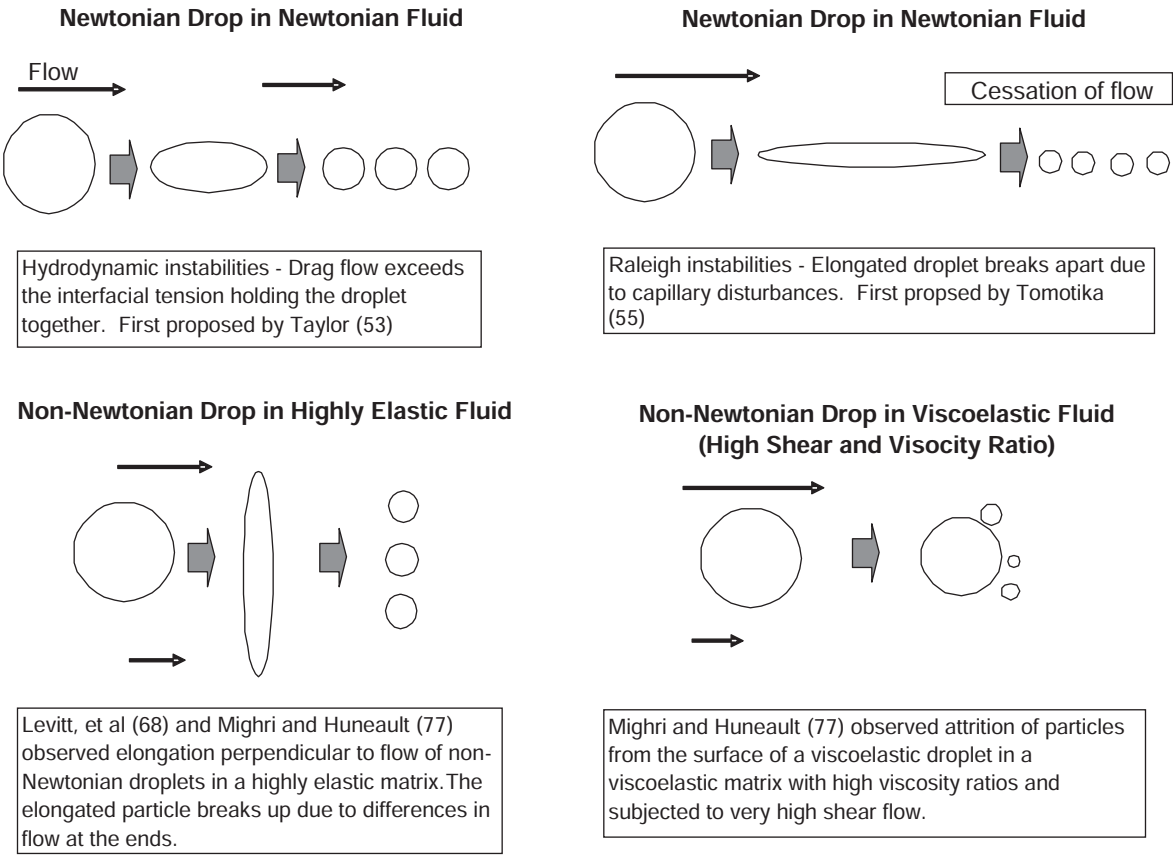


Figure 6.18 Single droplet breakup mechanisms in shear flow.

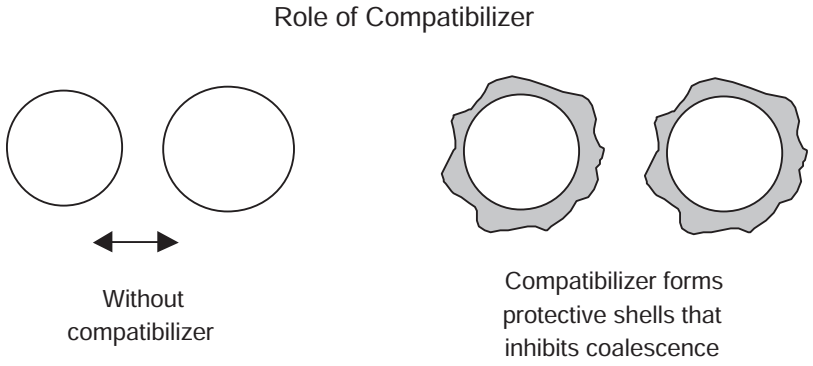


Figure 6.19 Role of compatibilizers in reducing coalescence in polymer.

across the screw channel (Fig. 6.4). Further complicating matters are temperature changes along the extruder. Given these complexities, Lyngaae-Jorgensen [85] proposes measuring the $Ca_{critical}$ versus viscosity ratio curve for the given device.

One must also consider the fact that the polymer melt viscosity varies with temperature and shear rate. Generally, there are two schools of thought on calculating the viscosity ratio. Some argue that the zero shear viscosities should be used. Others suggest using the viscosity at a representative shear rate for the process. However, it is stress, not shear rate, that drives dispersion and droplet break up. Stress is determined by the flow field and is continuous across an interface, whereas the shear rate is discontinuous. A better method is to plot the viscosity as a function

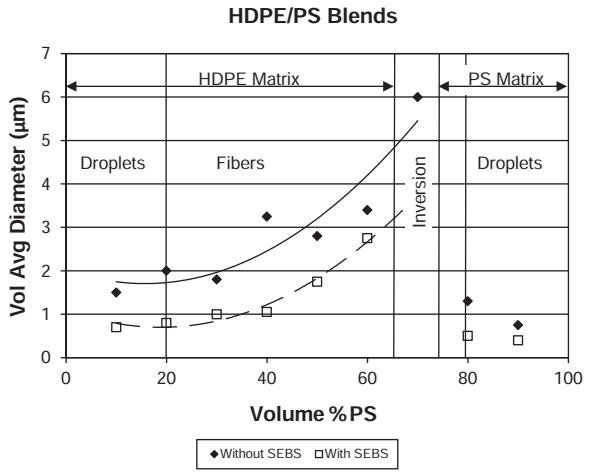
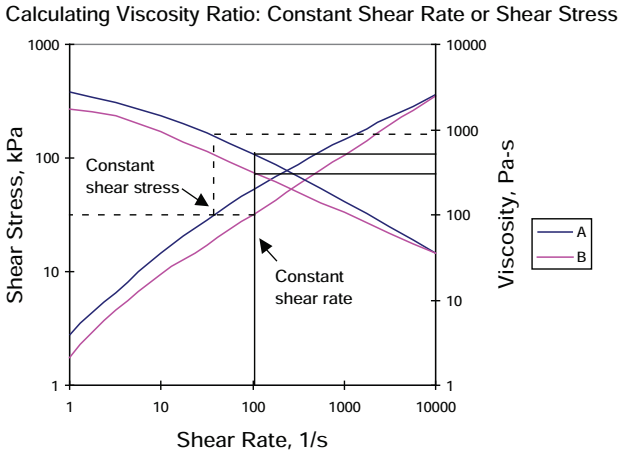


Figure 6.20 Blend morphology as a function of concentration.
PS–HDPE blends from Bourry D, Favis B. Co-continuity and phase inversion in HDPE/PS blends: the role of interfacial modification. In: SPE ANTEC conference; 1995. p. 2001.



	Viscosity, Pa-s		Ratio
	A	B	A/B
Constant Shear Rate	520	320	1.6
Constant Shear Stress	840	320	2.6

Figure 6.21 Calculating viscosity ratio.

of stress (stress is equal to the viscosity times the shear rate) and compare the blend components at a representative stress for the process. This is illustrated in Fig. 6.21. Here, polymers A and B are the minor and major components, respectively. At a constant shear rate equal to 100 s^{-1}, the viscosity ratio is 1.6. But, at constant stress, the ratio is 2.6, very close to the 3.5 cutoff for shear flow.

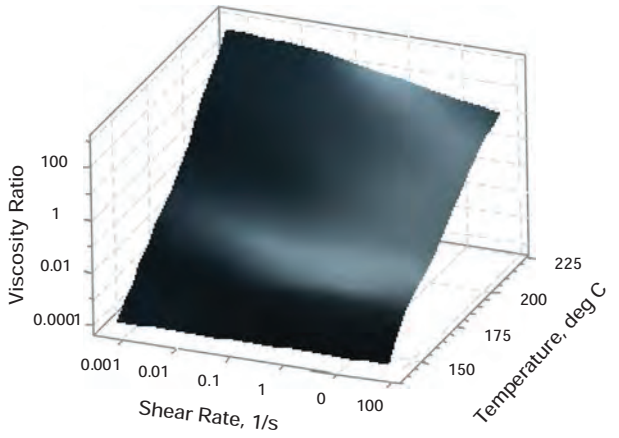


Figure 6.22 HDPE–PS blend viscosity ratio variation as a function of shear rate and temperature. Based on Huneault [86].

The polymer temperature changes along the extruder as the polymer becomes molten and is conveyed to the exit. Huneault [86] shows that, for a PS/HDPE blend, the viscosity ratio varies by six orders of magnitude depending on the temperature (Fig. 6.22). Computing the viscosity ratio just at the final extrusion temperature may be misleading. They find that, for this blend, the mixing is much better than what they expected just by looking at the viscosity ratio at the final temperature (200°C). Notice in Fig. 6.22 that the viscosity ratio is sometimes less than 1 and other times greater than 1. This indicates that, for the two polymers, the viscosity temperature dependence is not the same, another complication in computing the viscosity ratio.

So far in this discussion, the polymers have been assumed to both be molten at the time they are mixed. This is generally not the case as mixing can begin during melting. Ghosh [87] studies the softening/mixing of two similar amorphous polymers and finds that laminar sheets or striations form that subsequently break up into droplets. Lindt and Ghosh [88] show that the striations come from the single screw extruder melting process. A thin molten layer forms between the pellet solid bed and the barrel or screw surface caused by frictional heat and heat transferred from the barrel (Fig. 6.23 for the solid bed melting model). The high stress and deformation rates in this region transform the molten polymer into laminar morphologies as the pellets melt. The domain size decreases from a few millimeters (pellets) to about 50–100 μm due to the melting process. They make measurements as well as calculations that confirm these striations and abrupt domain thickness changes

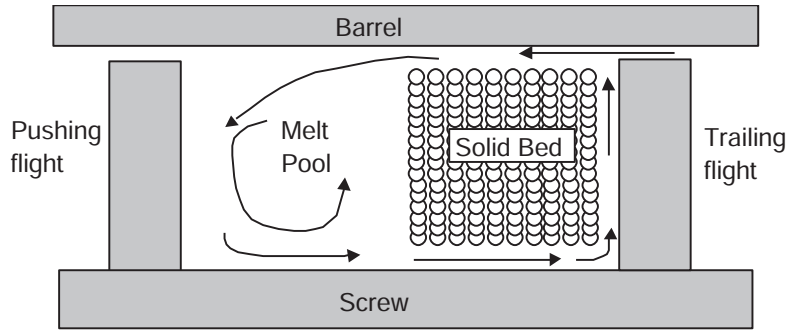


Figure 6.23 Single screw extrusion solid bed melting model. Melting above and below the solid bed causes the minor component to form thin layers or striations in a two-component polymer blend.
After Lindt JT, Ghosh AK. Fluid mechanics of the formation of polymer blends. Part I: formation of laminar structures. Polym Eng Sci 1992;32:1802–13.

for blends of both rheologically similar and dissimilar resins. Huang [89] study blends of two semicrystalline polymers (PP and PA6) by sampling along the length of an extruder. They observe striations followed by droplet formation, the nature of which depend on the viscosity ratio.

Benkreira [90] find that, when mixing a masterbatch into a host polymer, most of the mixing occurs during melting and little thereafter. They propose a laminar mixing model where the striation stretching during melting leads to a reduction in dimensions. Scott and Macosko [91] describe how component melting and softening in a batch mixer leads to the domain size reduction. They find sheets and ribbons are formed first, which become unstable due to flow and interfacial tension effects. Holes form, then a lace-like structure followed by irregular-shaped particles and finally spheres (Fig. 6.24). Breakup is driven by interfacial instabilities. Burch and Scott [92] show similar behavior for miscible polymers during the initial mixing stages and propose instabilities due to dynamic interfacial tension as the cause. Willemse [93] finds that sheets or striations form during single screw extrusion and that the final droplet size depends on the striation dimensions at the start of breakup rather than the capillary number. The sheet to droplet breakup during shear is very effective at dispersing the minor phase, more so than the elongated droplet to subdroplet mechanism found in single drop experiments.

In a single screw extruder, Tyagi and Ghosh [94] follow a PP–EVA blend as it develops its morphology using freeze experiments pioneered by Maddock [19]. In these experiments, after the extruder has reached steady state, the screw is stopped and the polymer is quickly quenched. The screw is pulled and samples from the screw channels are analyzed. Tyagi and Ghosh find that striations form in the feed zone. The

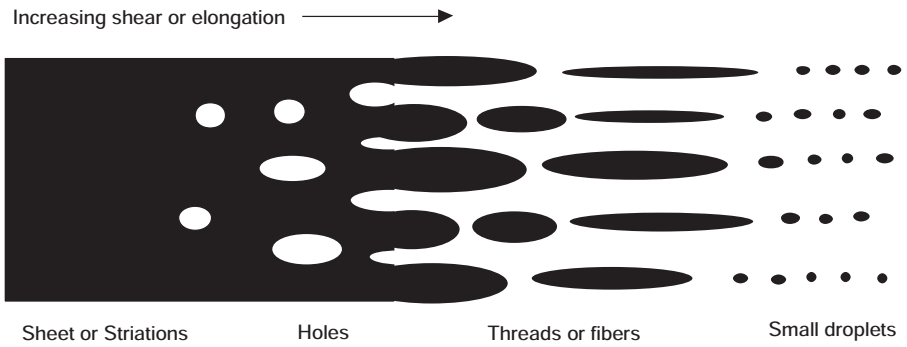


Figure 6.24 Morphology development during melting and subsequent shear in an extruder. Striations or sheets form during melting. Shear and stress cause holes to form, followed by threads and particle breakup. This process leads to large changes in the minor phase morphology.

dimensions quickly diminish along the channel length. In the compression zone, the shear and elongation increase, causing the striations to break up. The droplets that form are an order of magnitude smaller in size than the striation thickness prior to breakup. The breakup into droplets requires a step-up in shear and stretching. They conclude that, for an extruder to be an effective mixer, periodic flow reorientations should occur. This concept is used in high-performance screw designs where the polymer is forced to flow through tight clearances.

Li [95] find that the minor phase melts faster during mixing when a compatibilizer is present. They attribute this to faster heat transfer between the phases due to their intimate contact. Faster melting can affect the final blend morphology.

Shih [96] study the solid−melt transition for many polymer blends in a batch mixer equipped with a glass window. They find that blends go through four stages from solid to melt:

- Elastic solid pellets. Below the glass transition temperature (T_g) or melting point (T_m) the solid pellets are observed sliding in the mixer. Torque is low.
- Deformed solid pellets. As the temperature is increased, some components begin to soften and deform. The torque starts to rise.
- Transition material. This can take on several different forms including:
  - a fluid with suspended solid particles;
  - fractured or semifluid material;
  - a dough-like material.

  This is the transition zone between solid and liquid. Different blends took on different transition phases. The temperature increases sharply and then remains constant near the polymer melt temperature (T_m) if it was crystalline. Torque rises sharply.
- Viscoelastic material. The typical liquid appearance is observed. Temperature rises to about 20−50°C above the matrix resin T_m or T_g and the torque decreased.

During the transition phase they observe several phase transitions that aided in the mixing process. Shih [97] and others [98,99] find that phase inversions are to be expected when the minor component melts first. The molten minor component surrounds the still solid major component. As the major component melts, it becomes the continuous phase. This inversion is accompanied by a spike in the mixer torque and dramatically reduces the minor component phase size. They also describe how phase inversion can explain some unique morphologies, such as major component regions imbedded within the minor component domains.

The phase inversion onset is a function of the volume fraction ratio and viscosity ratio. A simple expression is given by Bourry [58] and Steinmann [100].

$$\frac{\eta_1}{\eta_2} \sim \frac{\Phi_1}{\Phi_2} \tag{6.9}$$

where $\Phi =$ volume fraction.

Two polymers with the same viscosity will undergo a phase inversion when the minor component reaches about 50% of the blend composition. If the minor component viscosity is substantially less than the major component, the minor component can become the continuous phase. This is the case when the minor component melts first. As the major component melts and its viscosity decreases, then conditions no longer favor the minor component as the continuous phase and the phase inversion occurs.

6.5 Morphology Development in Blown Film

Several morphologies have been described for immiscible blends in blown film, including elongated particles, such as fibrils and ribbons [101−105]. The factors influencing this morphology are covered in Chapter 14.

6.6 Dispersion of Rigid Particles and Nanocomposites

Dispersing inorganic and other particles in polymers is not well studied. As White [37] explains, this may be because breaking up agglomerates is hard to quantify, particularly since most fillers have a particle size distribution. Generally, it is thought that high stresses are needed to achieve dispersive mixing. Such stresses are typically not found in a single screw

extruder. Hence, most mineral-filled polymers are manufactured in specialized compounding equipment as described earlier. In packaging applications, blending fillers is generally limited to letting down masterbatches. Here, the filler, pigment, or additive have been predispersed and simple distributive mixing is all that is required.

One noteworthy aspect of dispersing rigid particles into polymers is particle attrition. Fillers, such as glass fibers, mica, and clay, may have large aspect ratios that are important for the blend properties. For a rod-like particle, the aspect ratio is defined as the length divided by the diameter. Too much dispersive mixing can reduce their aspect ratio, degrading performance. Filler abrading the mixing device surfaces can also cause excessive wear. Adding mineral filler at a downstream location where the polymer is molten rather than to the feed hopper with the solid pellets can significantly reduce abrasion and attrition.

A key question when dealing with pigments is how do you know if good mixing has been achieved? One commonly used method is to compare a sample against a visual standard. Spectroscopic techniques have also been used, as well as microscopic image analyses [90]. Various indices, such as striation thickness, variance in minor component concentration, and segregation scales, have been used, as discussed by McKelvy [107]. More recently, computer image analysis (red−green−blue correlations) has been used. Translating such color analysis to a quantitative distributive mixing index has been difficult. Alemaskin [108,109] has made progress in developing such an index by employing Shannon entropy. They use both computer simulation and experiments to verify the method. They simulate mixing two ABS colors in a conventional single screw extruder metering section using a numerical particle tracer analysis. The results are compared with extrusion experiments under similar conditions using the extruder freezing procedure described earlier. The color homogeneity evolution is measured using digital computer imaging. Color homogeneity indices based on entropic considerations computed for both the simulations and digital images qualitatively agree. This approach can potentially be used for scale-up, control, and process design optimization.

A polymer filled with nanoparticles is a special case. These blends are typically with inorganic particles that have nanometer dimensions (less than 0.1 μm). At levels between 3 and 5 wt%, they have been found to be effective in improving stiffness, mechanical strength, barrier, electrical conductivity, and flame retardancy. Although nanotechnology is still in its infancy, two nanofillers have received the most attention, carbon nanotubes, and clay. Carbon nanotubes have been found to impart good electrical properties for shielding and other potential applications. Because of their cost, except for some specialty electronics applications, carbon nanotube composites are not suited for packaging applications.

Of greater interest are clay nanocomposites [110−116]. Most work to date has been done with montmorillonite clay, initially at Toyota. In its natural state, each montmorillonite particle is an agglomeration of many layers of nanosized platelets. The platelet length and width range from a few tenths of a micron to about 1.5 μm. Their thickness is only about 1 nm and is the reason they are considered nanomaterials. Their high aspect ratios give them their unique properties.

The platelets are hydrophilic and are held together at a distance of about 3.5 Å by attractive forces. Clay suppliers add surfactants to the clay to promote interplatelet expansion to about 20 Å. To obtain the best properties, the platelets must be completely separated from each other. This complete dispersion into the polymer matrix is known as exfoliation and is illustrated in Fig. 6.25. There are two typical ways to accomplish this. One is to introduce the clay during the polymerization process. The monomer is absorbed into the spaces between platelets. As the monomer polymerizes, the platelets separate. This process is only amenable to certain polymers where the clay can be introduced during polymerization. Most often it has been applied to PA.

The second method is to compound the clay particle with an already polymerized polymer and rely on the stress generated during mixing to separate the platelets. The surfactant selection is critically important; it must help turn the hydrophilic environment between the platelets into one that is compatible with the monomer or polymer. In some cases, compatibilizers are used to aid in the exfoliation. For example, in PP−montmorillonite nanocomposites, maleic anhydride-grafted PP is often added as a compatibilizer. Nevertheless, so far it has proven difficult to fully exfoliate montmorillonite in a compounding process and is the focus of continued R&D. The first approach of polymerizing in the presence of the clay has been more successful.

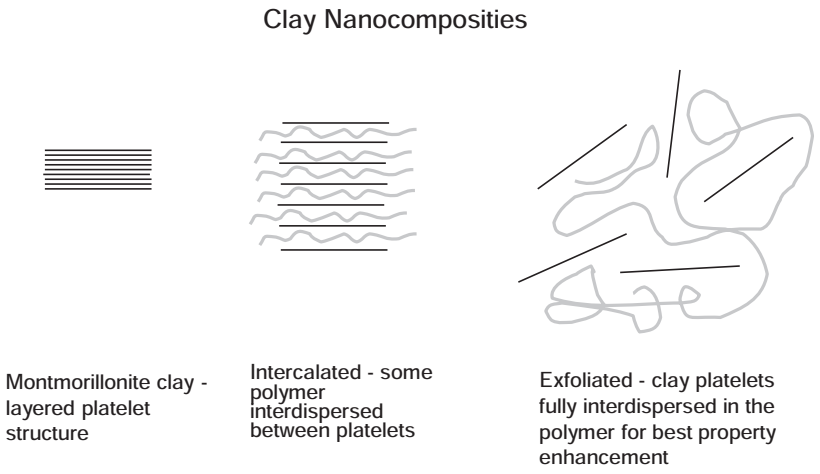


Figure 6.25 Illustration of states of clay nanocomposites.

Adding nanosized particles to the polymer restrains the molecule's movement, more so than in conventional fillers because of the extremely high surface area that is generated. The restrained motion enhances stiffness and heat deflection temperature. Because the individual platelets are small, toughness, and optical properties do not suffer. Of particular importance for packaging applications is the potential for increased barrier performance, especially oxygen barrier. The orientation of the platelets is flexible and their longer dimensions line up in the extrusion and orientation direction. The resulting platelet network structure creates a more tortuous path for gas molecules to diffuse through. Reductions in gas permeability of 60–80% for PA or EVOH nanocomposites have been reported [105,110].

Nanoparticles have been used to change or stabilize the morphology of immiscible polymer blends. For example, Bose [117] multiwalled carbon nanotubes compatiblized cocontinuous blends of PA6 and ABS. Tiawari and Paul [118] show that organo-nanoclay particles stabilize and reduce the dispersed phase size of PP–PS blends. The nanoparticle shape (aspect ratio) has been found to influence which phase the particle ends up in and its ability to stabilize the interface [119].

6.7 Rheology of Polymer Blends

Utracki [120] provides a good review of the rheology of polymer–polymer blends. Miscible blends are easier to characterize than immiscible ones. Often a log mean rule is used to estimate the miscible blend viscosity, although there may be some positive deviation:

$$\log(\eta_{\text{blend}}) = X_A \log(\eta_A) + X_B \log(\eta_B) \qquad (6.10)$$

where X_A = weight fraction of polymer A in the blend; X_B = weight fraction of polymer B in the blend.

Eq. (6.10) is useful for estimating the viscosity or melt flow index (MI) for two grades of the same polymer. For example, a 70–30 wt%, LDPE1–LDPE2 blend where the LDPE1 MI is 4 and LDPE2 MI is 12 g/10 min, yields:

$$\log(\text{MI}_{\text{blend}}) = 0.7 \log(4) + 0.3 \log(12)$$

$$\text{MI}_{\text{blend}} = 5.6 \frac{g}{10 \text{ min.}}$$

For immiscible blends, Lyngaae-Jorgensen [85] points out that steady-state data, such as capillary rheometry data, look superficially like homogeneous polymers. Unless they have been compatibilized [120], however, their behavior may be complex. These blends typically do not follow time–temperature superposition and mixing rules since the individual phases may behave differently. Their transient behavior and die swell may also be complicated. The immiscible blend morphology is the driving force for this complex behavior.

Reactive polymer blends are a special case. Typically, the reactive blend viscosity increases due to the formation of cross-links that effectively

increase the polymer molecular weight. An example is blending maleic anhydride-modified PE with PA. The PA viscosity can increase by an order of magnitude. The viscosity rise is related to the amount of new interfacial area created; the smaller the domain size of the dispersed PE phase, the higher is the viscosity.

Some additives can cause gels and other problems when blended with a polymer. For example, the acid groups in acid copolymers and ionomers can react with a coupling agent used in some TiO_2 grades, causing gel and other problems. Most masterbatch suppliers have learned how to deal with this through the design of the masterbatch. On the other hand, adding wax, tackifiers, and other low molecular weight additives to polymers will reduce their viscosity.

How rigid fillers effect viscosity can also be complex. For very dilute solutions of rigid spheres in a Newtonian fluid, Albert Einstein derived the following result:

$$\eta = \eta_f(1 + 2.5\phi) \tag{6.11}$$

where η = viscosity of the suspension; η_f = viscosity of the suspending fluid; ϕ = volume fraction of the rigid spheres.

The assumptions for this equation break down quickly for filled polymers: the filler loading is not typically dilute, the filler is not spherical, and the polymer matrix is non-Newtonian. Dealy and Wissbrun [61] describe the following complexities:

- non-Newtonian effects caused by particle concentration and aspect ratio;
- buoyancy effects;
- particle migration and agglomeration.

A number of equations have been proposed, including the following by Maron and Pierce [121]:

$$\eta = \frac{\eta_f}{[1 - (\phi/A)]^2} \tag{6.12}$$

Here, A is a constant that is a function of the filler. Dealy and Wissbrun propose that it can be thought of as the maximum filler packing fraction. For example, the value for A for spheres is 0.68, close to the theoretical maximum packing fraction of 0.637. The value for A decreases with the increasing filler aspect ratio (0.44 and 0.16 for L/Ds equal to 8 and 30, respectively). The value of A for filler with a nonuniform particle size distribution is greater than that for a uniform particle size. A nonuniform filler size distribution, therefore, can reduce the concentrated suspension viscosity.

There are other complications. One is the viscosity to choose when dealing with polymers, since η_f varies with shear rate. Dealy and Wissbrun point out that plotting the viscosity versus shear stress rather than shear rate, as noted earlier for polymer–polymer blends, gives the best results. At low shear rates, the filled polymer may exhibit a yield stress, below which the material behaves like a solid (and does not flow). The yield stress increases with filler concentration.

6.8 Conclusion

Blending is an important aspect of polymer/property design for many packaging applications. Achieving a consistent quality blend with the desired properties requires proper attention to both process and product design. The polymer blend properties are a complex function of the stress history imposed by the process and the rheological and thermodynamic properties of the components. Based on experience and science, several guidelines are proposed for reducing these complexities to practice:

- Careful control of the blend components fed to the mixing device feed hopper is important since most continuous mixers, such as extruders, do not have very good back mixing.
- All things being equal, target 10% or more for the minor component for better accuracy and control.
- Single screw extruders can be used for many blending applications where only simple distributive mixing is required. For more demanding applications, high-performance screws or ultimately specialty compounding devices, such as twin-screw extruders, may be required.
- When using a masterbatch concentrate, make sure the masterbatch carrier resin is compatible with the resin it is being blended into.
- Very few polymer blends are miscible. For miscible blends, the viscosity can be approximated using the log mean rule [Eq. (6.10)].

- The immiscible blend morphology influences the properties, which generally deviate from the mixing rule. Some examples include using small domains of a soft resin to improve toughness without detracting from optical clarity and laminar morphologies to help improve barrier performance.
- The immiscible blend morphology is influenced by the following:
  - the component concentrations;
  - stress history imposed by the compounding device;
  - the viscosity and mutual attractiveness (thermodynamics) of the components.
- The minor component domain size of an immiscible blend can be reduced by the following:
  - increasing the stress (by increasing the viscosity of the matrix phase and the shear rate or rate of elongation during mixing);
  - matching phase viscosities (a viscosity ratio in the range of 0.01−2 is preferred, particularly for shear flow);
  - lowering the interfacial tension by matching solubility parameters;
  - minimizing coalescence.
- Compatibilizers reduce interfacial tension and coalescence thus reducing domain size. They also reduce the minor phase melt time, which can affect domain size.
- Elongational flow is generally more efficient than shear flow for dispersing the minor component of an immiscible blend. The flow in single screw extruders is typically dominated by shear flows unless special mixing elements are used. Both shear and elongational flow can be found in twin-screw extruders.
- Most mixing in a single screw extruder occurs as the polymers melt, forming sheets or striations that break up into holes and droplets as the shear and elongation are increased along the extruder. Increased shear and stretching in the compression zone or high-performance metering zones (such as energy transfer screws) promote sheet breakup.
- For immiscible blends, orientation during the blown film process often elongates the minor component domains within the matrix resin.
- Dispersive mixing may be required to break up agglomerates when blending mineral fillers or pigments with polymers. For this reason, these blends are often made as masterbatches using specialized compounding equipment and let down using a single screw extruder by the film manufacturer.

References

[1] Ghijsels A, Ente JJSM, Raadsen J. Melt strength behavior of polyethylene blends. Int Polym Process 1992;7(1):44−50.
[2] Fetel AI. Nylon-containing ionomer improves the performance of ethylene vinyl alcohol (EVOH) copolymers in multilayer structures. In: TAPPI polymers, laminations & coatings conference proceedings; 1997. p. 503−5.
[3] Fetel AI. Amorphous nylon improves the performance of EVOH copolymers in multilayer structures. Future-Pak; 1977.
[4] Jester R. Heat seal characteristics of cyclic olefin copolymer/polyethylene blends. In: Tappi place conference, Boston, MA; 2002. p. 1308−34.
[5] Qiu G, Zhang P, Pan J, Xie Y, Zhoa S. Mechanical properties and morphology of polypropylene toughened with metallocine polymerized polyethylene elastomers. Polym Plast Technol Eng 2003;42(1):33−44.
[6] Epstein BN. Tough thermoplastic nylon compositions. US patent 4174358; 1979.
[7] Encyclopedia of polymer science and technology. 2nd ed. New York: Wiley & Sons; 1987.
[8] DuPont. DuPont Selar® PA blends with nylon 6. http://www2.dupont.com/Selar/en_US/assets/downloads/selar_pa3426_nylon_blends.pdf.
[9] Subramanian PM. Permeability barriers by controlled morphology of polymer blends. Poly Eng Sci 1985;25:483−7.
[10] Kamal MR, Garmabi H, Hozhabr S, Arghyris L. The development of laminar morphology during extrusion of polymer blends. Can Polym Eng Sci 1995;35:41−51.
[11] Garmabi H, Kamal MR. Improved barrier and mechanical properties of laminar polymer blends. J Plast Film Sheeting 1999;15(2):120−30.
[12] Huang H-X, Huang Y-F, Yang S-L. Developing laminar morphology in higher-viscosity ratio polyblends by controlling flow fields in a single-screw extruder. Polym Int 2005;54:65−9.

[13] Morris BA. Improving the adhesion of LDPE to aluminum foil through blending. In: SPE ANTEC tech. papers; 2004. p. 1101–5.
[14] Soutar AM. Polymer combinations for peel/seal applications. In: TAPPI seminar notes, coextrusion; 1986. p. 31–43.
[15] Pirtle S, Mergenhagen L, Wooster J, Cotton R. The effects of resin selection and extrusion variables on peelable seal performance. In: TAPPI PLACE conference; 2004.
[16] Hwo CC. Polybutylene blends as easy open seal coats for flexible packaging and lidding. J Plastic Film Sheeting 1987;3(4):245–60.
[17] Mergenhagen LK, Pope TJ, Timper CA. Polyolefin plastomer-based peelable seal formulations. In: TAPPI polymers, laminations & coating conference, vol. 1; 1996. p. 63–71.
[18] Martin C. Evolution of direct extrusion using high speed twin screw extruders. In: SPE ANTEC technical papers; 2002.
[19] Maddock BH. A visual analysis of flow and mixing in extruder screws. SPE J May 1959:383–9.
[20] Tadmor Z, Duvdevani I, Klein I. Melting in plasticating extruders theory and experiments. Poly Eng Sci 1967;7:198.
[21] Mount E. A review of melting mechanisms in single screw extrusion. In: SPE ANTEC conference; 2005. p. 304–10.
[22] Spalding MA, Hyun KS. Troubleshooting mixing problems in single-screw extruders. In: SPE ANTEC tech. papers; 2003. p. 229.
[23] Morris BA, Kirschbaum D. Modification of PLA for improved processing and properties. In: Bioplastics processing conference, Charlotte, NC; 2007.
[24] Baird JC, Christiano JP, Morris BA. An extrusion study: examination of the improved processing characteristics of a PLA impact modified blend. In: SPE ANTEC conference, Chicago, IL; 2009.
[25] Middleman S. Fundamentals of polymer processing. New York: McGraw-Hill Book Company; 1977. p. 154.
[26] Rauwendaal C. Polymer extrusion. New York: Hanser; 1986.
[27] Saxton R. Extruder mixer screw. US patent 3006029; 1961.
[28] Schut J. Single-screw compounding is learning new tricks. Plastics Technology; July 1999. At: http://www.plasticstechnology.com/articles/199907fa2.html.
[29] Somers SA, Spalding MA, Dooley J, Hyun KS. An experimental study of the flows in an energy transfer screw. In: SPE ANTEC tech. papers; 2002. p. 307.
[30] Hogan TA, Spalding MA, Kim EK, Barr R, Meyers J. Performance analysis of a variable barrier energy transfer screw. In: SPE ANTEC tech. papers; 2003. p. 92.
[31] Myers JA, Barr RA. Improved screw design for maximum conductive melting. In: SPE ANTEC tech. papers; 2002. p. 154.
[32] Kruder GA, Calland WN. Fundamentals of wave screw extrusion. In: SPE ANTEC tech. papers; 1990. p. 74.
[33] Fan P, Vlachopoulos J, Smith N, Sheth H. Computer simulation of melt flow in wave screws. In: SPE ANTEC tech. papers; 1998. p. 97–101.
[34] Somers SA, Spalding MA, Hughes KR, Frankland JD. Performance of a Stratablend mixing screw for single-screw extrusion. In: SPE ANTEC tech. papers; 1998. p. 272.
[35] Myers JA. Feedscrew for injection molding and extrusion. US Patent 5,342,125; 1994.
[36] Rauwendaal C, Ponzielli G. Performance characteristics of elongational mixing screws. In: SPE ANTEC tech. papers; 2004. p. 178–82.
[37] White JL. Twin screw extrusion, technology and principles. Munich: Hanser Publications; 1990.
[38] Curry JE. Practical aspects of processing blends. In: Folkes MJ, Hope PS, editors. Polymer blends and alloys. London: Blackie Academic & Professional; 1993.
[39] Wood BA. Transmission electron microscopy of detection of rubber modifiers. In: 161st Technical meeting of the rubber division of the American Chemical Society, Savannah, GA, April 29–May 1, paper 45; 2002.
[40] Wood BA. Transmission electron microscopy of polymer blends. In: Finlayson K, editor. Advances in polymer blends and alloys technology, vol. 3. Lancaster (PA): Technomic Publishing Co., Inc.; 1992.
[41] Ohme H, Kumazawa S, Kumaki J. Resin composition and molded article, film and fiber each comprising the same. US Patent application 2007/0260019A1; 2007.

[42] Coleman M, Graf J, Painter P. Specific interactions and the miscibility of polymer blends. Lancaster (PA): Techonomic Publishing; 1991.
[43] Van Krevelen DW. Properties of polymers: their estimation and correlation with chemical structure. Amsterdam: Elsevier Scientific Publishing Co.; 1976.
[44] Kuraray. Eval properties. At: http://www.eval-americas.com/us/eval-properties.aspx.
[45] McBride E. DuPont internal memo. 1993.
[46] Wu S. Polymer interface and adhesion. New York: Marcel Dekker, Inc.; 1982.
[47] Walsh DJ. Personal communication. 2005.
[48] Hussein IA, Williams MC. Rheological study of heterogeneities in melt blends of ZN-LLDPE and LDPE: influence of M_w and comonomer type, and implications for miscibility. Rheol Acta 2004;43(6):602−14.
[49] Hussein IA, Williams MC. Rheological study of the miscibility of LLDPE//LDPE blends and the influence of T_{mix}. Can Polym Eng Sci 2001;41(4):696−701.
[50] Hameed T, Hussein IA. Rheological study of the influences of M_w and comonomer type on the miscibility of m-LLDPE and LDPE blends. Polymer 2002;43(25):6911−29.
[51] Hussein IA, Hameed T, Sharkh B, Mezghani K. Miscibility of hexane-LLDPE and LDPE blends: influence of branch content and composition distribution. Polymer 2003;44:4665−72.
[52] Benkreira H, Britton R. The optimization of masterbatch formulations for use in single screw machines. Intern Polym Process 1994;9:205−10.
[53] Taylor GI. The formation of emulsions in definable fields of flow. Proc R Soc Ser A 1934;146:501.
[54] Grace HP. Dispersion in high viscosity immiscible fluid systems and application of static mixers as dispersion devices in such systems. Chem Eng Commun 1982;14:225−77.
[55] Tomotika S. On the stability of a cylindrical thread of a viscous liquid surrounded by another viscous fluid. Proc R Soc Ser A 1935;150:322.
[56] Kang J, Bigio D, Smith T. Study of breakup mechanisms in cavity flow. In: SPE ANTEC conference; 1995. p. 1988−93.
[57] Utracki LA, Shi Z. Development of polymer blend morphology during compounding in a twin-screw extruder. Part I: droplet dispersion and coalescence − a review. Poly Eng Sci 1992;32:1824−33.
[58] Bourry D, Favis B. Co-continuity and phase inversion in HDPE/PS blends: the role of interfacial modification. In: SPE ANTEC conference; 1995. p. 2001.
[59] Sinthavathavorn W, Nithitanakul M, Magaraphan R, Grady BP. Blends of polyamide 6 with low-density polyethylene compatibilized with ethylene-methacrylic acid based copolymer ionomers: effect of neutralizing cations. J Appl Polym Sci 2008;107:3090−8.
[60] Torradas J, Pimentel RO, Dean DM. "Additives to improve regrind utilization and recycling of high barrier blow molded containers. In: SPE ANTEC conference; 2013.
[61] Dealy J, Wissbrun K. Melt rheology and its role in plastics processing: theory and applications. London: Chapman & Hall; 1995. p. 392−400.
[62] Flumerfelt RW. Drop break-up in simple shear fields of viscoelastic fluids. Ind Eng Chem Fundam 1972;11:312−8.
[63] Tavgav T. Drop deformation and breakup in simple shear fields [Ph.D. thesis]. Houston (TX): Chemical Engineering, University of Houston; 1972.
[64] Gauthier F, Goldsmith H, Mason S. Particle motions in non-Newtonian media. II: Poiseuille flow. Trans Soc Rheol 1971;15:297−330.
[65] De Bruijn R. Deformation and breakup of drops in simple shear flow [Ph.D. thesis]. Eindhoven (The Netherlands): Eindhoven University of Technology; 1989.
[66] Elmendorp J, Maalcke R. A study on polymer blending microrheology: part I. Poly Eng Sci 1985;25:1041−7.
[67] Varanasi P, Ryan M, Stroeve P. Experimental study on the breakup of model viscoelastic drops in uniform shear flow. Ind Eng Chem Res 1994;33:1858−66.
[68] Levitt CL, Macosko CW, Pearson S. Influence of normal stress difference on polymer drop deformation. Poly Eng Sci 1996;36:1647−55.
[69] Han CD, Funatsu K. An experimental study of droplet deformation and break-up in pressure-driven flows through converging and diverging channels. J Rheol 1978;22:113−33.
[70] Milliken W, Leal L. Deformation and breakup of viscoelastic drops in planar extensional

flows. J Non-Newtonian Fluid Mech 1991;40:255−379.
[71] Delaby I, Ernst B, Muller R. Droplet deformation in polymer blends during uniaxial elongational flow: influence of viscosity ratio for large capillary numbers. J Rheol 1994;38:1705−20.
[72] Meijer HEH, Janssen JMH. Mixing of immiscible liquids. In: Tadmor Z, editor. Mixing and compouding of polymers, Manas-Zloczower. Germany: Hanser Publishers; 1994. p. 85−147.
[73] Chin H, Han C. Studies on droplet deformation and breakup: droplet deformation in extensional flow. J Rheol 1979;23:557−90.
[74] Shanker R, Spradling R, Pham H, Namhata S, Bosnyak C. Effect of viscoelasticity on transient drop dispersion. In: SPE ANTEC conference; 1996. p. 2596−600.
[75] Mighri F, Ajji A, Carreau P. Influence of elastic properties on drop deformation in elongational flow. J Rheol 1997;41:1183−201.
[76] Mighri F, Carreau P, Ajji A. Influence of elastic properties on drop deformation and breakup in shear flow. J Rheol 1998;42:1477−90.
[77] Mighri F, Huneault MA. Drop deformation and break-up mechanisms in viscoelastic model fluid systems and polymer blends. Can J Chem Eng 2002;80:1028−35.
[78] Van Oene HJ. Modes of dispersion of viscoelastic fluids in flow. J Colloid Interface Sci 1978;40:448.
[79] Greco F. Drop deformation for non-Newtonian fluids in slow flows. J Non-Newtonian Fluid Mech 2002;107:111−31.
[80] Maffettone P, Greco F. Ellipsoidal drop model for single drop dynamics with non-Newtonian fluids. J Rheol 2004;48:83−100.
[81] Lerdwijitjarud W, Sirivat A, Larson R. Influence of dispersed-phase elasticity on steady-state deformation and break-up of droplets in simple shearing flow of immiscible polymer blends. J Rheol 2004;48:843−62.
[82] Macasko C. Morphology development and control in immiscible polymer blends. Macromol Symp 2000;149:171−84.
[83] Uttandaraman S, Macosko CW. Drop breakup and coalescence in polymer blends: the effects of concentration and compatibilization. Macromolecules 1995;28:2647−57.
[84] Milner S, Xi H. How copolymers promote mixing of immiscible homopolymers. J Rheol 1996;40:663−87.
[85] Lyngaae-Jorgensen J. Rheology of polymer blends. In: Folkes MJ, Hope PS, editors. Polymer blends and alloys. London: Blackie Academic & Professional; 1993.
[86] Huneault M, Champagne M, Daigneault L, Dumoulin M. Blend morphology development during compounding in a twin-screw extruder. In: SPE ANTEC tech. papers; 1995. p. 2020.
[87] Ghosh AK, Ranganathan S, Lindt JT, Lorek S. Blend morphology development in a single screw extruder. In: SPE ANTEC tech. papers; 1991. p. 232−6.
[88] Lindt JT, Ghosh AK. Fluid mechanics of the formation of polymer blends. Part I: formation of laminar structures. Polym Eng Sci 1992;32:1802−13.
[89] Huang H-X, Huang Y-F, Li X-J. Detecting blend morphology development during melt blending along an extruder. Polym Test 2007;26:770−8.
[90] Benkreira H, Shales R, Edwards M. Mixing on melting in single screw extrusion. Intern Polym Process 1992;7:126−31.
[91] Scott C, Macosko C. Morphology development during the initial stages of polymer−polymer blending. Polymer 1995;36(3):461−70.
[92] Burch H, Scott C. Evolution of structure in the softening/melting regime of miscible polymer mixing. Polym Eng Sci 2001;41(6):1038−48.
[93] Willemse RC, Ramaker E, van Dam J, Posthuma de Beor A. Morphology development in immiscible polymer blends: initial blend morphology and phase dimensions. Polymer 1999;40:6651−9.
[94] Tyagi S, Ghosh AK. Morphology development during blending of immiscible polymers in screw extruders. Polym Eng Sci 2002;42:1309−21.
[95] Li H, Hu G-H, Sousa JA. Morphology development of immiscible polymer blends during melt blending: effects of interfacial agents on the liquid-solid interfacial heat transfer. J Polym Sci B Polym Phys 1999;37:3368−84.
[96] Shih C, Tynan D, Denelsbeck D. Rheological properties of multicomponent polymer systems undergoing melting or softening during compounding. Poly Eng Sci 1991;31(23): 1670−3.

[97] Shih C. Fundamentals of polymer compounding: the phase inversion mechanism during mixing of polymer blends. Adv Polym Tech 1992;11(3):223−6.
[98] Ratnagiri R, Scott C. Phase inversion during compounding of polycaprolactone/polyethylene blends. In: SPE ANTEC conference; 1996. p. 59.
[99] Sundararaj U, Macosko C, Shih C-K. Evidence for inversion of phase continuity during morphology development in polymer blending. Poly Eng Sci 1996;36(13):1769−81.
[100] Steinmann S, Gronski W, Friedrich C. Cocontinuous polymer blends: influence of viscosity and elasticity ratios of the constituent polymers on phase inversion. Polymer 2001;42:6619−29.
[101] David C, Trojan M, Jacobs R, Piens M. Morphology of polyethylene blends: I. From spheres to fibrils and extended co-continuous phases in blends of polyethylene with styrene-isoprene-styrene triblock copolymers. Polymer 1991;32(3):510.
[102] David C, Getlichermann M, Trojan M. Morphology of polyethylene blends. II: formation of a range of morphologies in blends of polyethylene with increasing content of styrene-isoprene-styrene triblock copolymers during extrusion-blowing. Poly Eng Sci 1992;32(1):6.
[103] Getlichermann M, David C. Morphology of polyethylene blends: III. Blend films of polyethylene with styrene-butadiene or styrene-isoprene copolymers obtained by extrusion-blowing. Polymer 1994;35(12):2542.
[104] Ronzalez-Nunez R, Favis B, Carreau R. Factors influencing the formation of elongated morphologies in immiscible polymer blends during melt processing. Poly Eng Sci 1993;33(13):851.
[105] Lee S-Y, Kim S-C. Morphology and oxygen barrier properties of LLDPE/EVOH blends. Intern Polym Process 1996;XI:238.
[106] Basell Product Literature. Polybutene-1 for use in seal-peel applications, customer presentation aid. 2001.
[107] McKelvy JM. Polymer processing. New York: John Wiley; 1967.
[108] Alemaskin K, Camesasca M, Manas-Zloczower I, et al. Entropic mixing characterization in a single screw extruder. In: SPE ANTEC conference; 2004. p. 167−72.
[109] Alemaskin K, Manas-Zloczower I, Kaufman M. Color mixing in single screw extruder: simulation & experimental validation. In: SPE ANTEC conference; 2005. p. 255−9.
[110] Lan T. Nanocomposite materials for packaging applications. In: SPE ANTEC conference; 2007. Online: http://www.nanocor.com/tech_papers/Antec-Nanocor-Tie%20Lan-5-07.pdf.
[111] Leaversuch R. Nanocomposites broaden roles in automotive, barrier packaging. Plast Technol October 2001:64.
[112] Sherman L. Chasing nanocomposites. Plast Technol November 2004:56.
[113] Manias E, Strawhecker K, Wu L, Kuppa V. Concurrent enhancement of various materials properties in polymer/clay nanocomposites. Proc Am Chem Soc Compos 2001;16:236−46.
[114] Dahman S. Melt processed polymer-clay nanocomposites: properties and applications. SPE ANTEC Conf 2000;58(2):2407−11.
[115] Akkapeddi K, Socci E, Kraft T, Facinelli J, Worley D. A new family of barrier nylons based on nanocomposites and oxygen scavengers. In: SPE ANTEC conference, vol. 61(3); 2003. p. 3845−8.
[116] Krook M, Hedenqvist M. Polymer-clay nanocomposities: one way to improve the barrier properties of polymers used in packaging. In: TAPPI PLACE conference; 2002. p. 194−7.
[117] Bose S, Bhattacharyya AR, Bondre AP, Kulkarni AR, Potschke P. Rheology, electrical conductivity, and the phase behavior of cocontinuous Pa6/ABS blends with MWNT: correlating the aspect ratio of MWNT with the percolation threshold. J Polym Sci B Polym Phys 2008;46:1619−31.
[118] Tiawari RR, Paul DR. Effect of organoclay on the morphology, phase stability and mechanical properties of polypropylene/polystyrene blends. Polymer 2011;52:1141−54.
[119] Goldel A, Marmur A, Kasaliwal GR, Potschke P, Heinrich G. Shape-dependent localization of carbon nanotubes and carbon black in an immiscible polymer blend during melt mixing. Macromolecules 2011;44:6094−102.
[120] Utracki LA. Polymer alloys and blends: thermodynamics and rheology. New York: Hanser Publishers; 1989.
[121] Marion S, Pierce P. Application of Ree-Eyring generalized flow theory to suspensions of spherical particles. J Coll Sci 1956;11:80.

PART IV: FILM PROPERTIES

This section provides detailed descriptions and analysis of the key properties of packaging films from an engineering and science perspective. Each chapter begins with why the property under discussion is important, how to measure it and typical values. This is followed by a discussion of the science behind how materials influence these properties. The effect of the converting process and end use conditions on these properties is covered in more detail in Parts V and VI.

7 Heat Seal

Heat sealing is one of the primary unit operations of flexible packaging. Different methods of heat sealing are covered in Section 3.2.5. In this chapter, heat sealing is described from a science and engineering perspective: why it is important, how to measure it, and factors that influence performance, as well as the scientific fundamentals of heat sealing with an eye toward understanding how to troubleshoot heat seal issues. The technology of easy-open seals and reclosable technology is highlighted. Hot bar heat sealing, the most common method used in flexible packaging, is the focus but ultrasonic sealing is introduced. This chapter ends with a comparison of sealant attributes that may be important for selecting one sealant over another for a specific application.

7.1 Why It Is Important

Heat sealing in flexible packaging involves the fusion of one film to another or to a rigid container to create a hermetic seal. An example of the former is the creation of a pouch or bag where the film is sealed to itself. The latter typically involves lidding films used to seal rigid containers such as tubs or trays. Sealing helps keep product in the package until the consumer or user opens it and protect the product from the outside environment. A good heat seal helps the package provide one of its primary functions of protecting the product as described in Chapter 1. For the packaging of food, the seal helps ensure product freshness.

In multilayer flexible packaging the inner most layer (the outside film layer closest to the product) provides the sealing functionality. Specialized sealant materials have been developed to optimize the sealing function, which often warrants its own layer. This is because the properties of a polymer needed to provide good sealing may be the opposite of what is needed for other key attributes of the package, such as barrier, stiffness, and strength. These functions can be provided by other layers. The sealant layer has a number of characteristics including the following:

- low seal initiation temperature for high-speed packaging operations and to prevent the distortion of other layers of the film;
- the ability to seal around or through product contamination;
- low extractables and minimum effect on food quality (scalping or impartation);
- tamperproof or tamper evidence (especially for medical packaging);
- seal integrity (strength);
- ease of opening (specific seal strength);
- resistance to premature opening during the packaging operation (hot tack strength).

Even in multilayer packaging the sealant layer often is called upon to provide other attributes to the package beyond sealing. These may include the following:

- transparency;
- toughness (impact resistance, tear resistance, puncture resistance);
- oil or chemical resistance;
- moisture resistance;
- stiffness;
- thermoformability;
- adhesion;
- reclosability.

Of special importance is the ability to resist opening forces during packing while the seal is still molten. This is critical since it can take several seconds before the seal area cools and the seal solidifies. During this time, the seal may be stressed by several external forces as illustrated in Fig. 7.1. In vertical form fill seal operations, the weight of the product

The Science and Technology of Flexible Packaging. http://dx.doi.org/10.1016/B978-0-323-24273-8.00007-1
Copyright © 2017 Elsevier Inc. All rights reserved.

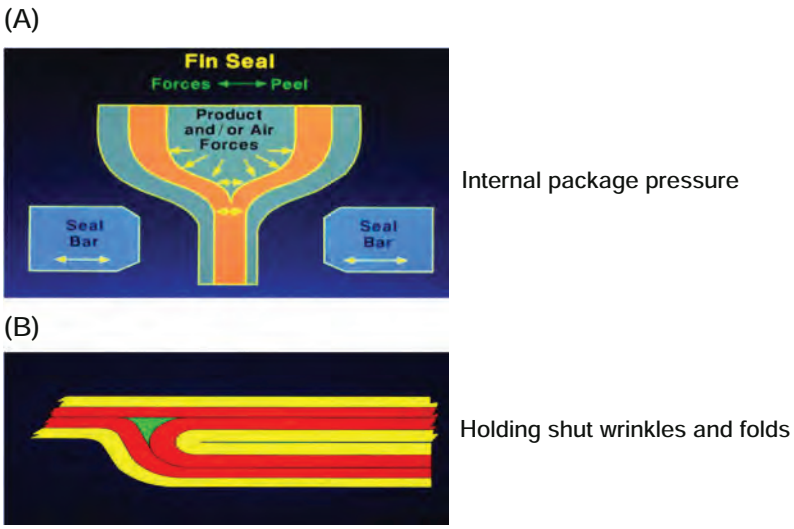


Figure 7.1 Examples of why hot tack is important. (A) Internal pressure from the weight of the product or air in a vertical form fill seal operation. (B) Holding shut wrinkles and folds in a horizontal form fill seal operation. *Reproduced with permission from E. I. du Pont de Nemours and Company.*

puts a burden on the seal immediately after filling. In horizontal filling operations, the gusseted areas tend to spring back, putting stresses on the seal. The quality of the seal to withstand these stresses is known as hot tack.

A sealant requires a balance of properties to ensure good performance:

- Low melting point to allow the molecular chains enough mobility to diffuse and build strength across the interface. High enough crystallinity to help aid in the buildup of that strength.
- Sufficient flow to fill or caulk voids in the seal area. High enough viscosity to avoid being squeezed out from the seal area during sealing.
- Low molecular weight to speed diffusion across the interface. High molecular weight and branching to provide melt strength for hot tack.
- High polarity to provide good oil and grease resistance. Low polarity to bond to adjacent layers.

Typical sealants used today include low density polyethylene (LDPE), linear low density polyethylene (LLDPE), metallocene LLDPE (including lower density plastomers), ethylene vinyl acetate (EVA) copolymer, acid copolymers (ACR), and ionomers. Random polypropylene (PP) copolymers and polyesters are also used in some applications.

7.2 How to Measure

7.2.1 Seal Strength of Packages: The Peel Test

Seal strength is a measure of the force required to pull open a package or a sealed film. In the lab this is typically measured using a peel test. The peel test is generally performed on a tensile tester. The specimen is cut into strips, typically 1-in. (25.4 mm), 25 mm, or 15 mm wide. The tabs or ends of the strip that have not been sealed are placed into the jaws of the tensile tester. These tabs are known as the peel arms. The jaws are separated at a fixed rate, typically in the range of 200–300 mm/min (8–12 in./min), and the force measured as a function of time. A schematic of the peel test is shown in Fig. 7.2. The peel force typically goes through a maximum as the peel is initiation and then settles down to a steady plateau value as shown in Fig. 7.3. The maximum or plateau value may be reported as the seal strength, whichever is more appropriate for the application. The maximum value is most often used [1].

The angle, speed, and temperature of the pull can all be important and affect the measurement result. As is described in more detail in Section 7.5.6, the peel test is a measure of the energy to pull the specimen apart which involves bending and stretching the peel arm and the creation of new interfacial area. The angle of pull directly affects the bending

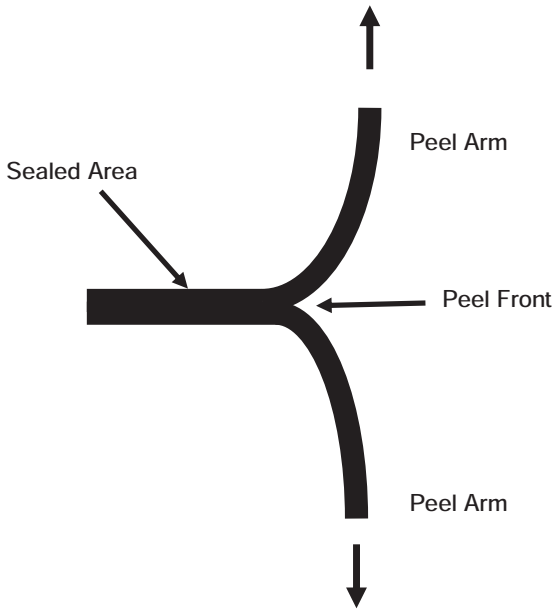


Figure 7.2 T-peel test.

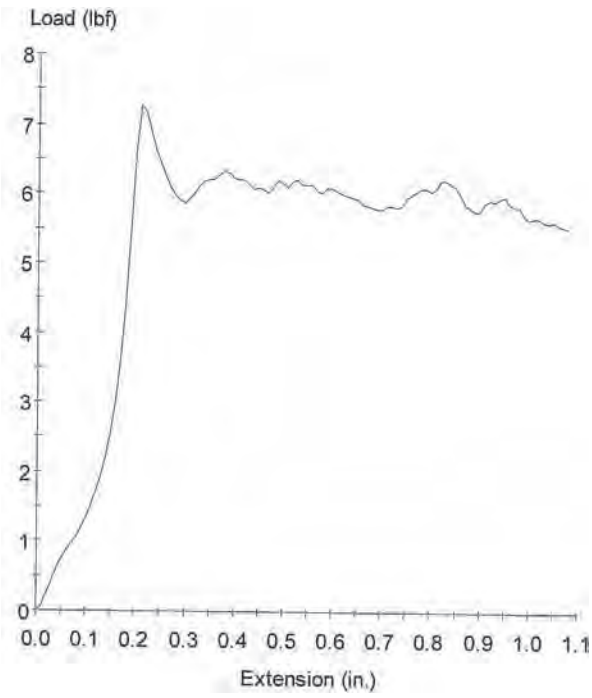


Figure 7.3 Example of peel force during a peel test.

energy, but this contribution is often small. More important, the angle can influence the concentration of stresses at the peel front, which can affect peel strength. In most controlled peel tests in the lab, the angle is fixed at 180 degrees in either a "T-peel" configuration (Fig. 7.2) or pulled completely back on itself. These typically give different results.

The speed of the pull affects the viscoelastic properties of the film, which can have a significant effect on the measured seal strength. As the seal is pulled apart, local resistance to deformation near the peel front can impact the energy to create new surfaces. This gives rise to greater resistance to peel. Tear strength and other properties can also be important.

Temperature also plays a role through its effect on the viscoelastic energy of deformation near the peel front as well as bulk properties of the peel arm such as elongation and stiffness.

The result of the heat seal measurement is typically reported as the seal strength or force divided by the width of the specimen. Some of the common units and their conversions are given in Table 7.1. It is also helpful to record how the specimen fails with descriptive language such as "peel followed by delamination," "peel followed by tear," "elongation," and "cohesive failure." The mode of failure can be important for troubleshooting (see Section 7.10).

7.2.2 Laboratory Heat Seal Tests

Heat seal tests are often conducted in the lab under controlled conditions to compare materials and film structures. Several ASTM methods describe heat seal or peel tests, including F88, F2029, and F2824 [1—3]. The heat seal test generally involves the following steps:

- conditioning the films for a prescribed amount of time at a fixed temperature and relative humidity (typically 23°C and 50% RH);
- cutting strips to a standard width, typically 25 or 15 mm;
- sealing the films on a laboratory hot bar sealer under a fixed set of conditions:
  - bar width;
  - sealing temperature;
  - sealing time (known as the dwell time);
  - sealing pressure;
  - top and/or bottom bar heated.
- Conditioning the sealed films for a prescribed amount of time at a fixed temperature and relative humidity. For lab testing, the time is often 24 h;
- Measuring the heat seal strength, as described in Section 7.2.1. Typically five or more specimens are measured for a given sample, or enough to ensure the accuracy of the measurements.

Table 7.1 Some Common Units and Their Conversion Factors for Peel Strength

	Multiply Current Value in Row Units by Factor to Get Column Units					
	lb/in	**g/25 mm**	**g/15 mm**	**N/15 mm**	**N/25 mm**	**N/m**
lb/in	1	454	757	7.42	4.45	178
g/25 mm	0.0022	1	1.67	0.0163	0.0098	0.392
g/15 mm	0.00132	0.599	1	0.0098	0.00587	0.235
N/15 mm	0.135	61.3	102	1	0.600	24
N/25 mm	0.225	102	170	1.67	1	40
N/m	0.00562	2.55	4.25	0.0417	0.025	1

Conditioning of the samples prior to heat sealing is important as the performance of some materials and films change with moisture and other effects of aging (Section 7.10.2.5). For materials with suspected aging effects, conducting experiments with different aging times and conditions may be warranted.

There are no standard set of heat seal settings and these are known to vary from one investigator to the next. Some typical ranges are given below:

- Seal bar width: ½ to 1 in. (12.7−25.4 mm) with 15 or 25.4 mm the most common.
- Sealing temperature: Usually varied over a range to construct a heat seal curve of seal strength versus sealing temperature.
- Dwell time: 0.25−3 s, with 0.5 s being most common. This is often set to match the sealing time on a packaging line. For example, a packaging machine operating at 60 packs/min (1 per second) with half the cycle time devoted to sealing would have a dwell time of 0.5 s.
- Sealing pressure: 20 to 70 psi (0.14−0.48 MPa). This is generally set at the minimum needed to ensure good contact.
- One or both bars heated. This is up to the investigator and should be noted.

Some heat sealers will have a Teflon film or tape covering the seal bar or the investigator will insert a high temperature film (such as Teflon or polyethylene terephthalate (PET)) between the seal bar and the sample to prevent the sealant from sticking to the seal bar during sealing. This should be noted since it affects the heat transfer between the heated bar and the test specimen.

Conditioning the sealed specimens after heat sealing is important to ensure the seal has cooled to room temperature and crystallization has occurred. Cooling can take several seconds, much longer than the heat-up portion of the heat seal. This is because during heat-up the hot bar is in direct contact with the film surface whereas during cooldown the film may only be in contact with air. Heat transfer is much more efficient for direct contact than it is in air. The polymer may undergo various changes over the first 24 h, such as secondary crystallization and moisture absorption. Hence, waiting 24 h before conducting the peel test is more representative of what the seal strength may be in a package. Some seals are known to age over several weeks, especially some types of peel−seal or easy-open seals (Sections 7.7.3 and 7.10.2.5). Longer conditioning times may be needed to study these systems.

7.2.3 Laboratory Hot Tack Measurement

A number of home-grown hot tack testing techniques were developed in the early days of flexible packaging, several of which are reviewed by Soutar [4,5] and Brodie [6]. One device was developed by the Dow Chemical company [7] as shown in Fig. 7.4 [8]. It measures the peel strength of a sample along a temperature gradient. A sample of the film, sealant side up, is clamped onto a heated temperature bar that is hot on one end and cold on the other. A second sample, sealant side down, is placed on top of the first and clamped at the cold end. After the temperature has time to equilibrate, the bonded films are pulled apart from the hot end. The peel force is measured and plotted versus distance of pull, which

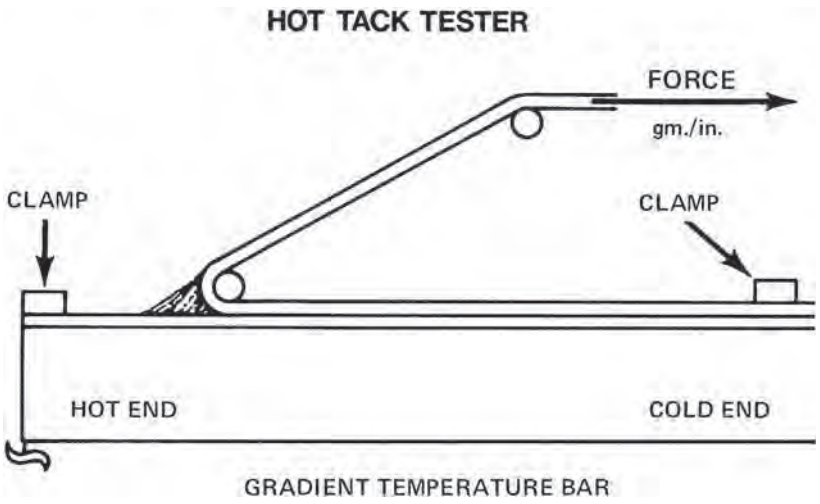


Figure 7.4 Dow chemical hot tack tester (c.1960's).
Reproduced with permission from DuPont Literature, Hot tack strength. Surlyn® update, vol. 1. 1970, issue 4, E. I. du Pont de Nemours and Company.

corresponds to a temperature profile measured by thermocouples along the length of the bar. The film requires a temperature resistant outside layer for the clamps to hold onto and was used primarily for the testing of polyethylene-coated paper in the late 1960s.

Deadweight tests where developed by DuPont to showcase their sealant resins at tradeshows [8]. A clip is attached to one peel arm to which a weight is attached. As the seal jaws are released, the seal is exposed to the force of the weight as shown in Fig. 7.5. Soutar [4,5] suggests that this technique is mostly a measure of the creep behavior of the polymer.

Frito-Lay developed a version of a deadweight test. A frame is used to control the distance and angle of the film extending from a standard bar heat sealer. A weight is hung from the frame so that when the seal jaws are released, a force is applied to the hot seal. The distance the seal has opened is measured and if it is above a critical value (typically 3/16 in.), the test is deemed a failure at that temperature and weight. If the seal creep is less than the critical value, the test is repeated with a higher weight [6].

The DuPont Sprint Test was used well into the 1990s. Spring steel is cut in the shape of a tensile bar; the width of the bar at its narrowest point and thickness determine the spring force. The spring is bent into a U shape and inserted into the structure to be tested as shown in Fig. 7.6. The ends of the film are placed into a standard heat sealer. The films are

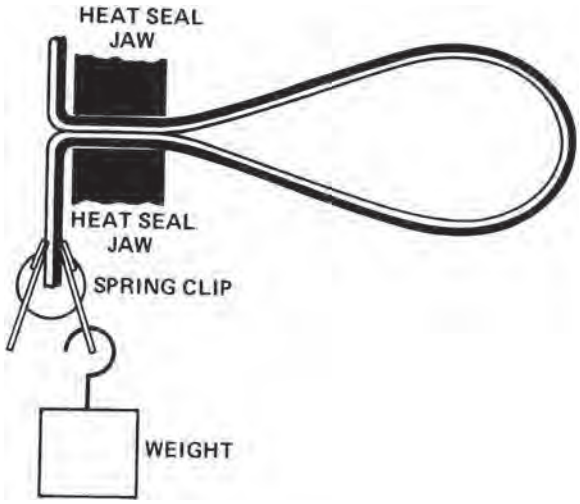


Figure 7.5 Deadweight hot tack test.
Reproduced with permission from DuPont Literature, Hot tack strength. Surlyn® update, vol. 1. 1970, issue 4, E. I. du Pont de Nemours and Company.

sealed under standard conditions. DuPont used a dwell time of 3 s to ensure the seal was complete and to accurately measure the interfacial temperature with a thermocouple. As the seal jaws are released, the spring immediately exerts a force on the molten seal. The sample is allowed to cool down and the separation of the seal to the nearest 0.1 in. is measured. Different springs representing different forces are used to measure several seal separations ranging from 10% to 90% separation. The results are

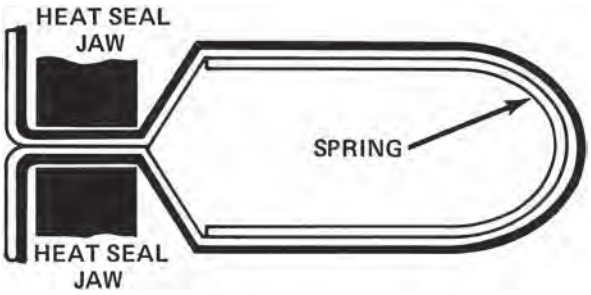


Figure 7.6 DuPont spring test for hot tack.
Reproduced with permission from DuPont Literature, Hot tack strength. Surlyn® update, vol. 1. 1970, issue 4, E. I. du Pont de Nemours and Company.

plotted and interpolated to find the force required for 20% separation, which is deemed the hot tack strength for that sealing temperature. The process is repeated for different sealing temperatures to generate a hot tack curve.

In 1979, The Swedish Packaging Research Institute introduced the Packforsk hot tack testing device [4,9], an automated device that measures the force to pull the specimen apart. Later known as the DTC hot tack tester, this device consists of two heated sealing jaws: clamps to hold the test sample with the lower clamp dropping to pull the seal apart, a transducer to measure the force, and controls for setting the dwell time, temperature, pressure of the heat seal, peel speed, and the delay time between when the seal is completed and when the force is measured (Fig. 7.7). A sample with a high heat resistant outer layer, such as paper or PET, is generally required to prevent distortion during the measurement. Various versions of this basic design have come out over the years, some of which are cam driven and others motor driven [10,11]. These quickly became the preferred method of measuring hot tack.

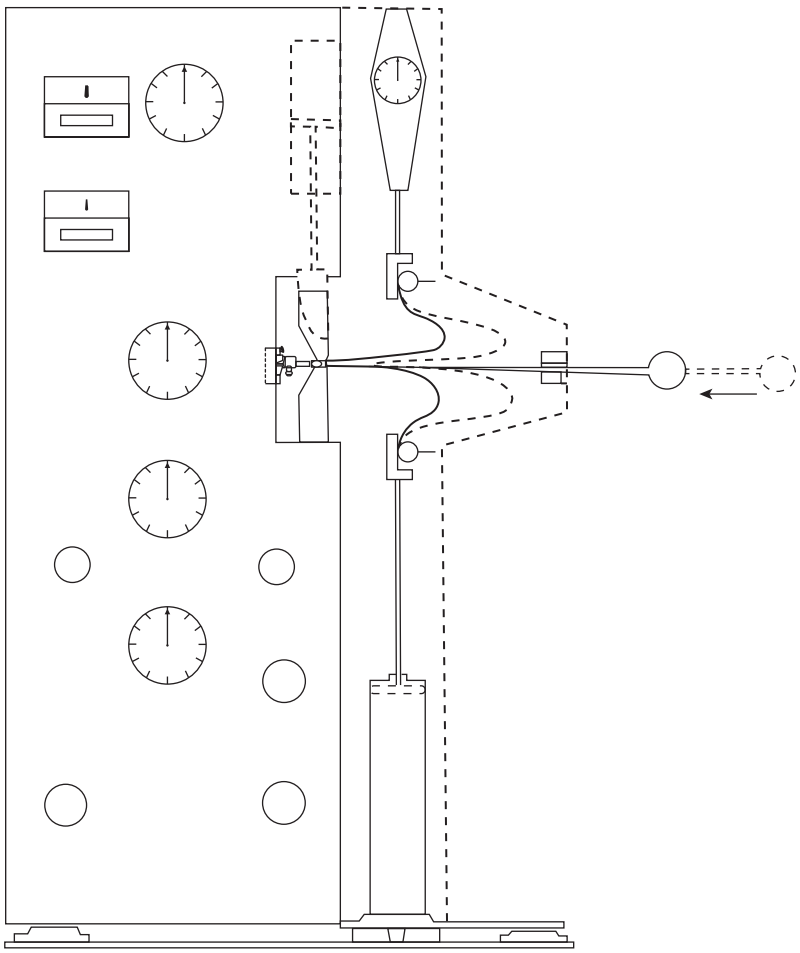


Figure 7.7 Packforsk hot tack tester.
Courtesy of DuPont.

Soutar [4,5] discusses the pros and cons of the DuPont Spring Test versus automated tests such as the Packforsk test. The spring test exerts the separation force immediately after the seal jaws are released, closely representing what typically occurs on a packaging line. The automated tests usually have a delay of 0.05−2 s following the seal before the force is measured. Cooling during this delay time was registered as a concern. Both methods are quantifiable, although the automated tests tend to only record the maximum force prior to full separation, whereas the spring method gives a wealth of information regarding the force for partial to full separation of the seal (an automated device introduced by Theller [11] removes this negative.).Theller [11] suggests that the speed of pull in automated hot tack testers is not representative of the dynamics of packaging operations. Indeed, the speed is two orders of magnitude greater than the heat seal test. The spring method is less expensive in terms of initial capital outlay but does require more time (to conduct each test, as well as to calibrate the springs prior to each test) and is subject to variability due to operator experience. Hence, the chief advantages of the automated hot tack devices are their speed and reproducibility.

ASTM F1921 [12] provides guidance around measuring hot tack but does not specify the equipment or conditions. Key variables for the automated hot tack testers include the following:

- seal bar width;
- seal dwell time;
- sealing pressure;
- delay time;
- pull speed.

Falla [10] surveys the literature of major resin suppliers and lists a range of typical values used for these parameters. The seal bar width is 5 mm and the seal time is typically 0.5 s. Pressure ranges from 0.21 to 0.69 MPa. Delay time is 0.02−0.5 s and pull speed ranges from 33 to 500 mm/s.

Berger [13] finds that sample width, temperature, and pressure are key factors influencing hot tack measurements. They use a Theller device. The method for preparing and cutting the sample is not found to be significant. Falla [10] compares a 45° cam driven with a 90° motor-driven hot tack tester for measuring hot tack of polyethylene films and concludes the motor-driven device gives more consistent and reliable results. Close examination of their results, however, suggests that differences in delay time may have influenced the results. Falla went on to study factors that influence the variability on the motor-driven device:

- Hand cut versus punch die cut specimens. They find significantly more variation in the specimen width with the hand cut specimens. Whether this translates into more variation in hot tack strength is not discussed. Berger [13] examines the shape of the cut (straight vs. sinusoidal) and finds it has no statistically significant effect on the hot tack strength.
- Teflon tape. They recommend the use of Teflon tape on the seal bars to prevent sticking to an all-polyolefin film.
- Film tension. The amount of slack in the film after the sample is loaded into the seal jaws is varied. Using a slight tension gives better consistency in the hot tack measurements.
- Pressure across seal bar. They recommend testing the uniformity of the pressure across the seal bar using a pressure indicating sensor film.
- Seal time. They cite literature sources that show the hot tack plateaus at around 0.5 s for polyolefin films and use this throughout their work. Hocking [9] shows that the onset of the plateau depends on the structure of the film being tested with a thicker paper/LDPE/Al/LDPE film taking longer than a thinner Al/LDPE structure.
- Peel speed. They test pull speeds ranging from 100 to 500 mm/s. As the pull speed is decreased, the hot tack initiation temperature (HTIT, which they define as the temperature at which 1 N/25 mm is achieved) and the maximum hot tack strength decreases. They find a pull rate of 200 mm/s results in the most differentiation between the different films tested.
- Delay time. Falla uses a delay time of 0.5 s. Hocking shows data varying delay time from 0.1 to 3 s for several structures. Hot tack strength is shown to increase and then level off with increasing delay time. He attributes the initial rise to cooling of the interface, increasing the viscosity of the sealant. The leveling off is explained as radiant heat deforming the film, resulting in nonuniform peeling and lower

values. Hocking states that the delay time in production packaging machines is of the order of 0.1 s and they use this time for routine testing. Berger [13] shows data for delay times (or cooling time on the Theller instrument) of 0, 0.125, and 0.25 s for a (HDPE (high density polyethylene)—EVA) film. Hot tack strength increased monotonically from 0 to 0.25 s. Soutar [4] questions the use of long delay times, citing cooling as a concern.

- Sealing pressure. Hocking recommends a sealing pressure of 0.1—0.5 MPa, which is typical of most heat sealing operations. Falla uses a pressure of 0.28 MPa (40 psi). Berger uses a range of 0.69—2.1 MPa.

7.2.4 Relating Lab Results to Packaging Line Studies

Care must be taken when comparing hot tack or heat seal results from the literature. The film structure (thickness, layers), heat seal test parameters and hot tack test parameters, and even preparation methods are likely to be different from one investigator to another. For example, Schubert [14] found that foil-containing structures had higher hot tack than non-foil structures with the same sealant. They also showed that the extrusion temperature in extrusion coating has a substantial impact on hot tack performance.

Even when looking at results from a single study comparing different sealants one should be cautious. The investigator may pick test conditions that are optimum for one type of sealant but not for another, skewing the results. For example, ionomers give excellent hot tack results under conditions of long seal times and very short delay times whereas metallocene plastomers give good results for shorter seal time but long delay times. Neither condition may be representative of a commercial packaging line. Studies on monolayer films may be useful for screening sealants, but in actual multilayer structures interlayer adhesion and the tensile properties of the other layers may impact sealing performance. Indeed, laboratory heat seal and hot tack tests should be regarded as just a first step in qualifying materials. Ultimately, the structure needs to be tested on the actual packaging line. Lab tests do not always correlate with packaging line experience. Several examples are given by Wooster [15], Bilgen [16], and Kapur [17] where sealant films with the best hot tack performance in the lab did not provide the best hermicity on a vertical form film seal line. Factors such as caulkability may also play a role on the real packaging line.

Analysis of failures can be instrumental in finding the underlying cause of sealing problems. This subject is taken up in detail in Section 7.10. The ultimate test is the measure of leaker rates on actual package lines. A common method is to select a sampling from the run and test for hermicity by immersing the sealed package in water and looking for bubbles. The location of the bubbles can be examined to try to determine the cause of the failure. An even more sensitive test is to inject helium into the sealed package and use a helium detector along the seal to find channel leakers.

7.3 Typical Values

7.3.1 Heat Seal Curves

A plot of seal strength versus seal bar temperature is known as the heat seal curve. It provides information about performance and operating window of the film. An example is shown in Fig. 7.8. At low seal bar temperature, this is no tack or seal strength. As the temperature is increased, the heat seal reaches the heat seal initiation temperature (HSIT) where the seal strength rises rapidly. The actual definition of the onset of sealing varies in the literature and throughout the industry. Some define HSIT as the temperature at which the seal strength first becomes nonzero. Others define it as the temperature at which the seal strength reaches an arbitrary seal strength threshold, such as 100 g/in or 1 N/25 mm. Because of the rapid rise in seal strength in this region, both approaches give similar results.

As the seal bar temperature is increased further, the seal strength will reach a plateau. The temperature at which the plateau begins is known as the plateau initiation temperature, T_{pi}. The seal strength at the plateau is known as the ultimate seal strength. Ultimate seal strength values vary with sealant type and structure (tear strength, tensile strength, and heat distortion often limit the value of the ultimate seal strength, which may depend on other layers in the structure). Typical values are in the range of 400—1200 g/25 mm for easy-open seals and above 1200 g/25 mm for standard hermetic seals.

The practical heat seal temperature window is defined by the HSIT on the lower end and by

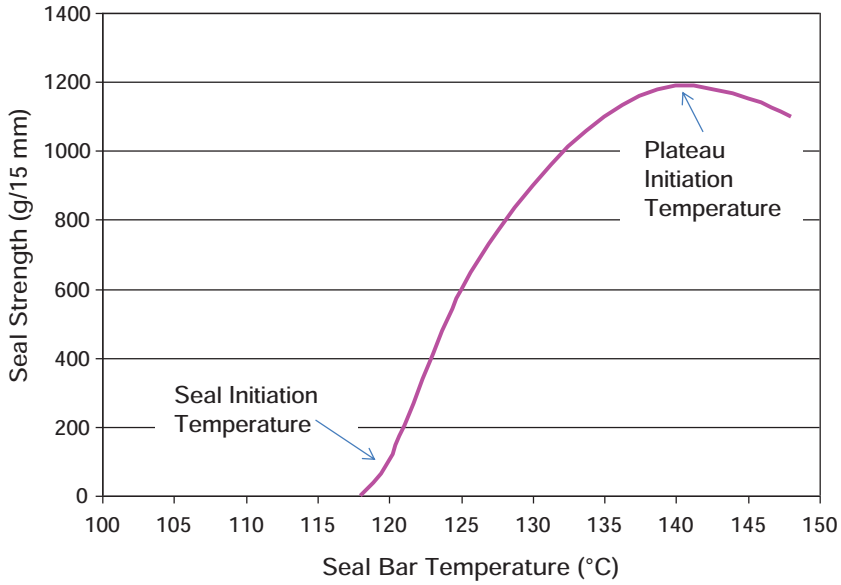


Figure 7.8 Typical heat seal curve.

distortion and other limitations on the upper end. This is illustrated in Fig. 7.9. Section 7.5 shows that HSIT is related to the melting point of the sealant. Operating near the HSIT is not wise since in this region the seal strength varies greatly with small changes in temperature. This may result in variable seal strength, poor sealing, and channel leakers. At the upper end, excessive temperature may result in the sealant becoming too fluid and being squeezed out from the seal area, resulting in poor seal performance. Also, the heat may distort the structural layers, such as HDPE, oriented polypropylene (OPP), or polyethylene terephthalate (PET), resulting in poor aesthetics and functionality. High temperatures can also result in the seal bar cutting through the film resulting in tearing and failure. The middle region is the sweet spot where the seal strength has reached its maximum performance level, there is sufficient flow to caulk voids in gussets and wrinkles and seal around contamination, and the film is not distorted.

To ensure a good operational temperature window, the sealant and structural layers should be matched for performance. For example, when using a high temperature structural layer such as OPET, an LLDPE sealant may work well. But if the structural

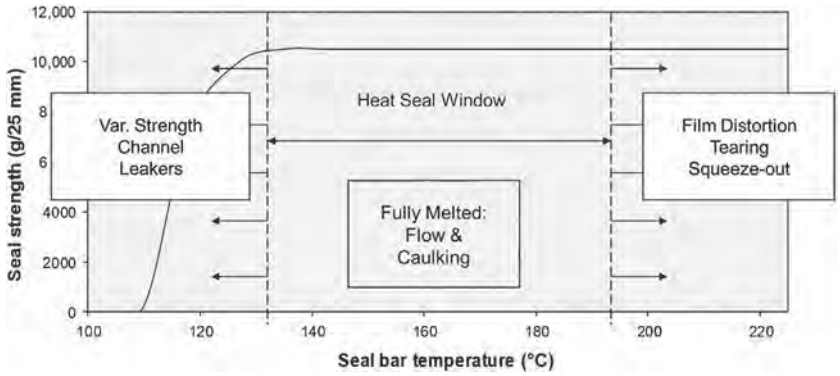
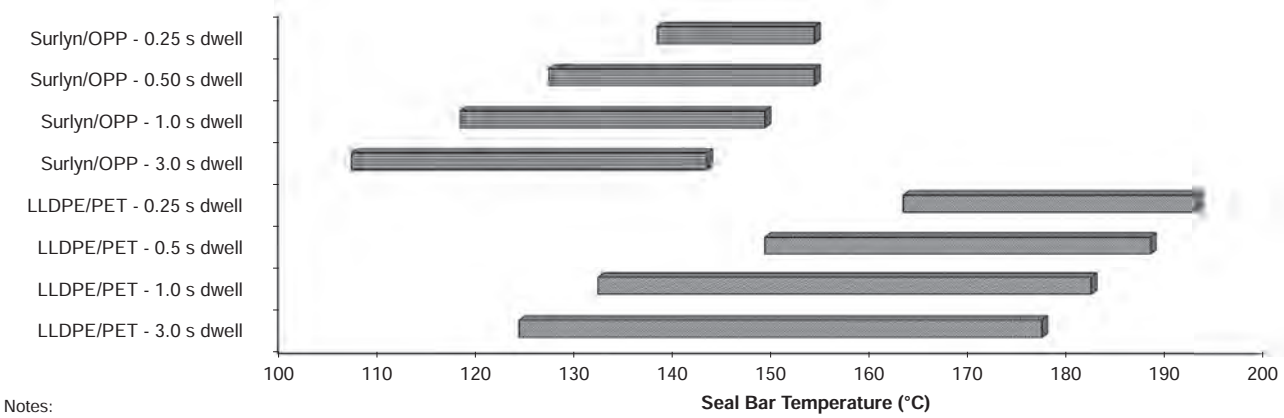


Figure 7.9 Illustration of heat seal temperature window.
Reproduced with permission of E. I. du Pont de Nemours and Company.



Notes:
1) OPP/Surlyn - (75 ga OPP/0.5 mil LPDE/35 ga met PET/0.5 mil LDPE/1.5 mil Surlyn coex)
Upper temperature limit is set by distortion due to melting of the OPP.
2) PET/LLDPE - (48 ga PET/0.7 mil LDPE/35 ga met PET/0.7 mil LDPE/1.5 mil coex (LDPE/LLDPE))
Upper temperature limit is set by distortion due to melting of the LDPE inside the structure.

Figure 7.10 Heat seal window of some packaging film structures.
Reproduced with permission of E. I. du Pont de Nemours and Company.

layer is OPP, LLDPE may not be a good choice since the melting point of the LLDPE is near the distortion temperature of the OPP. Here a lower melting sealant, such as EVA, plastomer, ACR, or ionomer is preferred to extend the operational temperature window. This is illustrated in Fig. 7.10 for LLDPE/PET and ionomer/OPP. The OPP structure is 19-µm OPP/12.7-µm LPDE/8.9-µm met-OPET/(12.7-µm LDPE-38-µm ionomer) and the upper heat seal temperature limit is a result of distortion of the OPP. The PET structure is 12-µm OPET/17.8-µm LDPE/8.9-µm met-OPET/17.8-µm LDPE/38-µm (LDPE/LLDPE). Here the upper temperature limit is the result of melting of the LDPE inside the structure. Since both film structures have about the same thickness, the lower seal temperature limit is governed by the sealant layer. Especially at short dwell times, there is very little overlap in the seal temperature windows of the two structures, indicating the LLDPE sealant would not be suitable for the OPP structure since its HSIT would be higher than the distortion temperature (for 0.25 s dwell).

Fig. 7.10 shows the effect of four different sealing dwell times for each structure. As the seal dwell time is decreased, the seal initiation temperature must increase to compensate for the reduced time available to heat and build strength at the seal interface. Thus, the seal temperature window is a function of both the design of the film structure and the sealing conditions.

7.3.2 Hot Tack Curves

A plot of hot tack strength versus seal bar temperature is known as the hot tack curve. An example is given in Fig. 7.11. Like the heat seal curve, the hot tack curve has an initiation region of rapidly rising hot tack strength, the onset of which is known as the HTIT. This is due to the buildup of strength at the interface and corresponds to the same region in the heat seal curve. The HTIT and HSIT temperature

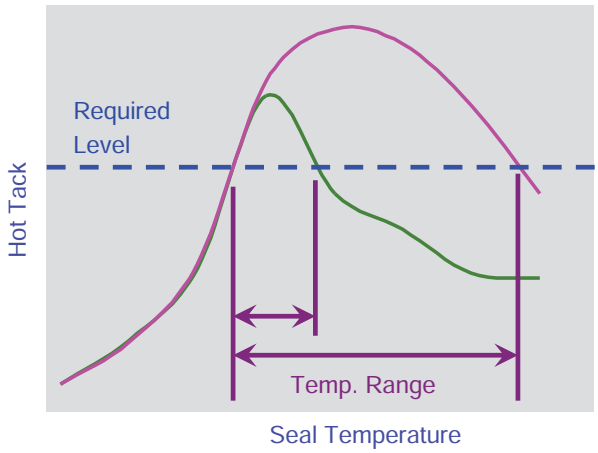


Figure 7.11 Hot tack versus seal bar temperature curves for two films illustrating differences in the breadth of the hot tack temperature window.
Reproduced with permission of E. I. du Pont de Nemours and Company.

may differ due to differences in sealing conditions (dwell time and so on) as well as the nature of the adhesion at the interface (melt adhesion for hot tack and solid state adhesion for heat seal). Unlike the heat seal curve which plateaus, the hot tack curve typically goes through a maximum followed by a decrease in hot tack as the temperature is increased further. This is the result of a reduction in melt strength of thermoplastic polymers with increasing temperature.

In addition to the HTIT there are three other parameters of note. One is the temperature at which the maximum hot tack occurs. For most polyolefins, this occurs near the melting point of the polymer. The second is the peak or maximum hot tack strength. The third is the breadth of the hot tack curve or hot tack temperature window. This is generally determined for a given hot tack strength and may be related to the force exerted on the seal during packing. For example, in a vertical form fill seal operation, the weight of the product acts as an opening force exerted on the molten seal. Gusset areas exert opening forces due to the numerous folds and the springback nature of polymer films. Once the package is filled, it may see forces due to handling or secondary packaging. For example, cereal is often packaged in a bag liner that is inserted into a cardboard box. The filled bag is stuffed into the box shortly after sealing; the stuffing force can be significant and the seal may still be molten.

The breadth of the hot tack temperature range is perhaps more important than the peak hot tack strength since it provides information regarding the operational window. Changes in packaging machine line speed, nonuniformity of the temperature across the seal bar, and other operational factors favor the use of structures with broad temperature windows to ensure good seal performance.

While the hot tack curve provides useful information, it is difficult to quantitatively translate the measurement to actual field experience. One reason is that calculating the opening force can be challenging, especially for a gusset. Also, most hot tack measurements today test to failure, whereas partial failure or "mooning" of seals may be what is important from a consumer perspective. The old spring method, now mostly out of favor, produced results for 20% of seal area failure. The maximum force that is measured today may not relate to actual field issues. Still, the hot tack curve is a useful means to compare different sealants and structures.

7.4 Factors That Influence Heat Seal Performance

7.4.1 Heat Seal Operation

7.4.1.1 Dwell Time

Since heat sealing is a melt fusion process, time and temperature are the two most fundamental parameters affecting seal performance. Time and temperature are interrelated. For shorter dwell times, higher temperature is typically needed to achieve the same performance. Conversely, for lower sealing temperatures, longer dwell times may be required. The sealing dwell time on a packaging machine is the time the sealing bars are in actual contact with the film. The dwell time is determined by the line speed and the fraction of the registration cycle that involves sealing. For example, if a machine is packaging 60 packages per minute and half the cycle time is devoted to heat sealing, the dwell time is 60 pkg/min $\times$ min/60 s $\times$ 1/2 = 0.5 s.

Given that the dwell time is fixed by the machine parameters and line speed and that it takes a finite amount of time for heat to conduct through the thickness of the film once the seal bars contact the outer surface, the need for low seal initiation temperature sealants becomes apparent. The lower the HSIT, the faster the line speed can be for a given film structure.

7.4.1.2 Temperature

Temperature is important during the sealing operation as well as in the end use. Time and temperature impact the melting of the sealant during sealing. This is critical for wetting, diffusion, and flow (caulking). Too much temperature, however, can lead to distortion of the film and squeeze-out of the sealant. Oriented films, such as OPP and PET, are prone to shrinkage when the temperature is raised above their thermal setting temperature. Other films may melt and shrink. The viscosity of a polymer melt decreases with increasing temperature. Squeeze-out occurs when the sealant becomes too fluid and is pushed away from the seal area by the pressure on the

seal. Some flow is desirable to fill voids and seal around contamination, but too much flow results in thinning down the sealant layer and loss of strength. Squeeze-out is further discussed in Section 7.6.3.

Nonuniform temperature across the seal bar can cause variability in seal strength and lead to leakers. Without proper control and maintenance, the temperature differential can be quite large. Even in a laboratory environment, significant temperature differences were found across the seal bars on packaging equipment as is described in Section 3.2.5.4 and pictured in Figure 3.9. Temperature may also vary throughout the day as a packaging line is slowed and sped up for various reasons.

The temperature at which the package is exposed to during its use can also influence seal strength. Hot fill and retort temperatures can put stress on the bond that has formed during sealing, especially if the exposure temperature exceeds the melting point of the sealant (and hot tack becomes an important predictor of package performance). Cold temperature may embrittle the film and cause seal failures.

Even the temperature at which the seal strength is measured can impact the result. Temperature affects the stiffness and other viscoelastic properties of the sealant and other layers in the structure, which can affect the dynamics of the peel test (see Section 7.5.6).

7.4.1.3 Pressure

Pressure is required to bring the films into intimate contact to allow bonding to take place. But too much pressure can result in squeeze-out of the sealant, especially at elevated temperatures. A general guideline is to use just enough pressure to ensure good contact and no more. Operators sometimes mistakenly increase the sealing temperature and pressure to try to resolve a sealing issue. This often results in worse seals rather than better ones.

7.4.1.4 Seal Bar Design

The crimper design and its effect on heat sealing is described in Section 3.2.5.3. Lengthening the seal (wider bars) is one approach to increasing hot tack as the separation distance is longer before seal failure. Crimping may also help. Wider bars also help prevent squeeze-out. Wider seals, however, require more film, which can result in higher cost.

Covering the seal bar with Teflon or other high temperature-resistant material can help prevent the hot bar from sticking to the film. This may be necessary if the outside layer of the film is not temperature resistant.

Some sealing operations heat just one bar whereas others heat both bars. This depends on the design of the packaging line. For example, in a lidding operation, it makes sense to only heat the film side since the substrate may be too thick for the heat to reach the interface within the time frame of the sealing operation.

7.4.1.5 Product Contamination

There is no industry-accepted standard method for measuring how a sealant will perform in the presence of product contamination. Most references in the literature focus on food-based contaminants, both solid and liquid. In laboratory tests, liquid contaminants such as various oils are often painted on to the seal area with a brush. These usually cover the entire seal area, which generally does not represent the type of splattering that may occur on a packaging line. Solid contaminants include various powders, such as flour meal. These are often dusted on, again covering the entire seal area. It should not be surprising that most laboratory studies show that the presence of product contamination increases the seal initiation temperature, sometimes substantially. In some cases the ultimate seal strength is also reduced.

Hahm [18] took a different approach, studying the effect of a liquid marinade sauce on sealing. She postulates that the liquid contaminant is squeezed across the seal surface during sealing, resulting in leakers and channels across the entire seal width. Sealants that are able to encapsulate a liquid droplet should perform better. Using films of OPET/sealant (12/51 μm), she puts a droplet of controlled size (2.5 mm) onto the seal area and heat seals the films at 40 psi (0.28 MPa) pressure and 1 s dwell time. The sealants include LLDPE, EVA, mPE plastomer, and ionomer (zinc and sodium). She measures the final droplet size and describes the seal. Each sealant is found to have an optimum sealing temperature. At low temperatures the sealant is not fluid enough to flow around the droplet. At high temperature, the marinade and sealant are too low in viscosity. The ionomers perform best, containing the droplet and preventing its expansion across the seal. The ionomer seals tightly even after venting steam. All the other

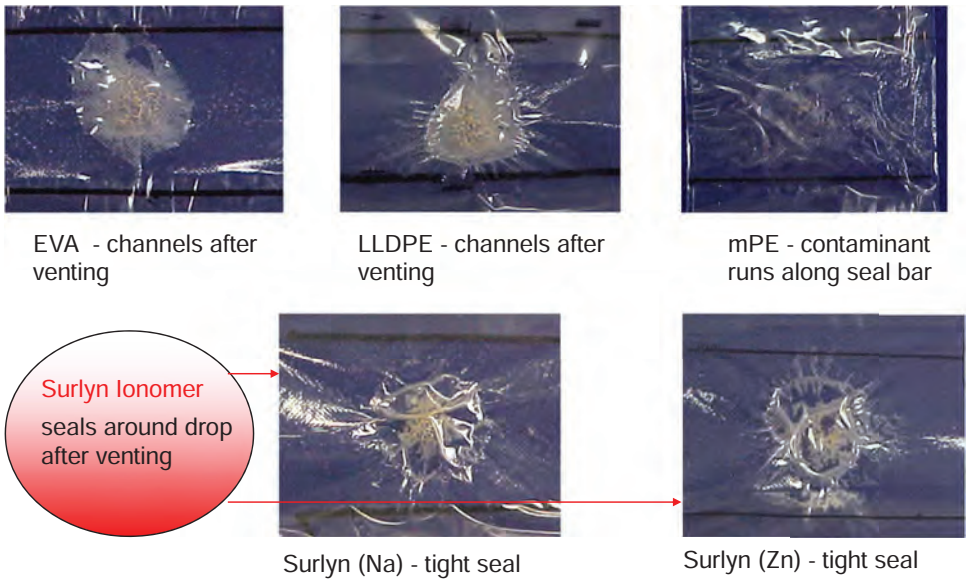


Figure 7.12 Examples of sealing in the presence of a liquid marinade sauce.
Reproduced with permission from Hahm DM. Sealing study with meat marinades on seal surface. In: American Meat Institute conference, October 1999, E. I. du Pont de Nemours and Company.

sealants leave channels. Some examples from her study are shown in Fig. 7.12.

The methods are still unsatisfying and seem to be subject to manipulation. Most of the studies have been conducted by resin manufacturers and show their resin to be better than a competitive resin [18–22]. Competing manufactures counter with studies showing their product performs best. Until a more definitive test is developed, some general concepts can be considered:

- When dealing with a powder product, it helps to minimize static attraction between the sealant and the product. This helps prevent contamination. For example, DuPont recommends an amide (slip agent) containing ionomer for situations where static is an issue [23].
- The chemical affinity of the sealant to the contaminant can be important, as is shown in the Hahm study. Ionomers and ACRs are more polar than PE and may be better suited for containing oily contaminants.
- The presence of long range intermolecular attractive forces such as hydrogen bonding and ionic interactions may aid in sealing through contamination, helping the sealant to lock onto the opposing sealant surface. These types of forces are found in acid copolymers and ionomers.
- The rheology of the sealant may be important, especially for sealing around and encapsulating solid contaminants. Linear polyethylene often has more flowability during sealing than branched ones. Sadeghi [24], however, shows that greater shear thinning behavior can lead to better caulking, which would favor branched polymers like LDPE, EVA, ACR, and ionomers.
- Hot tack can help the sealant encapsulate the particle or droplet [25].
- Increasing jaw pressure can help push contaminants out of the seal area or assist in flow around them [26]. Too much pressure can result in problems as previously discussed.
- Ultrasonic sealing works well for sealing through some bulk product contamination. The vibration of the horn helps push contaminants away from the seal area [27].

7.4.2 Film Fabrication and Package Design

7.4.2.1 Film Thickness

The time for heat to conduct through the thickness of a film is related to the square of the thickness. The thicker the film structure, the longer the dwell time needs to be for the sealant interface

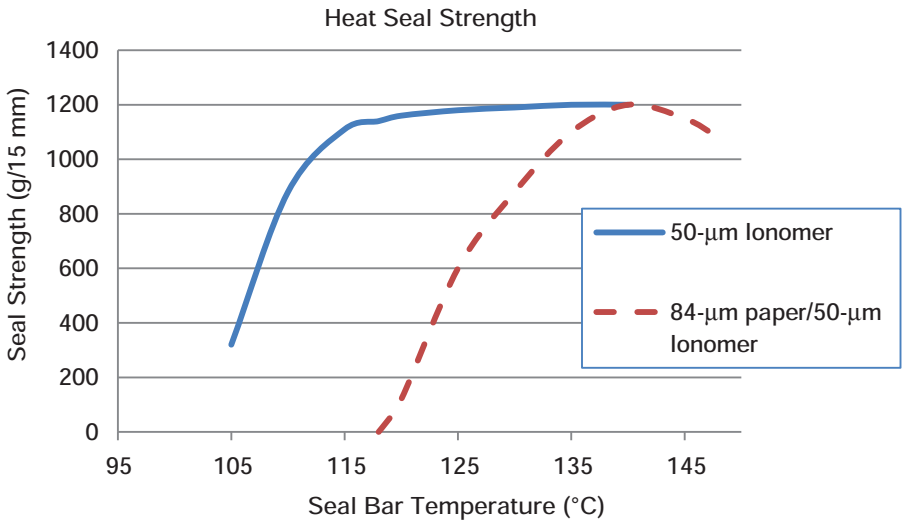


Figure 7.13 Heat seal curves for two structures of different thickness.
Reproduced with permission from E. I. du Pont de Nemours and Company.

to reach the bar temperature. For some high speed processes, the dwell time is too short and the thickness of the film is too great for the interfacial temperature to actually reach the bar temperature. In these situations the bar temperature is set above the desired interfacial temperature to achieve sufficient performance. The limit to this approach is the dimensional stability of the film structure; if the sealing temperature is too high, the film may get distorted and other sealing methods may need to be used.

Fig. 7.13 shows an example of the effect of thickness on the heat seal curve. Here the sealant is the same ionomer resin. In the thin structure the sealant is a monolayer film, whereas in the thick structure the sealant is laminated to paper. The dwell time is constant at 0.5 s. The HSIT of the thick structure is about 25°C higher than the thin structure. Section 7.6 on modeling of heat seal performance revisits this example in more detail.

The thickness of the film structure may affect the seal strength measurement through changes in the bending stiffness of the peel arm. This may affect the peel strength directly through a change in the energy to bend the peel arm and indirectly by changing the local angle of failure and stress concentration. The thickness of the sealant also affects the amount of local viscoelastic energy dissipation as new interfacial area is created during the peel tests. These factors are taken up in greater detail in Section 7.5.6.

7.4.2.2 Sealant Resin

As is described in more detail in Section 7.5, heat sealing involves melting and fusion of the sealant at the interface. Semicrystalline polymers that are commonly used as sealants do not have a single melting point like small molecules do. Rather they melt over a temperature range. A common method used to measure melting behavior is by differential scanning calorimetry (DSC), which measures the heat flux while heating or cooling a sample compared to a reference. Primary transitions such as melting and crystallization show up as peaks. A typical DSC curve plotting heat flux versus temperature is shown in Fig. 7.14. The melting point typically reported in a technical data sheet is the value at the peak of melting. Some of the crystals will melt well before the peak temperature, allowing for some tack. Others will melt after the peak, especially those associated with longer chains. Stehling and Meka [28] conduct a comprehensive study of the melting behavior of polyolefins used as sealants and correlated their DSC melting behavior with heat seal strength. They find that the temperature of the onset of the plateau or ultimate seal strength (T_{pi}) correlates with the temperature at which all the crystals have melted and the HSIT corresponds to a certain fraction of melting. Hence the melting point of the sealant is a key parameter that can be used to predict seal initiation temperatures. Table 7.2 gives the melting points of some common sealant resins. In general, the lower the melting point, the lower the HSIT.

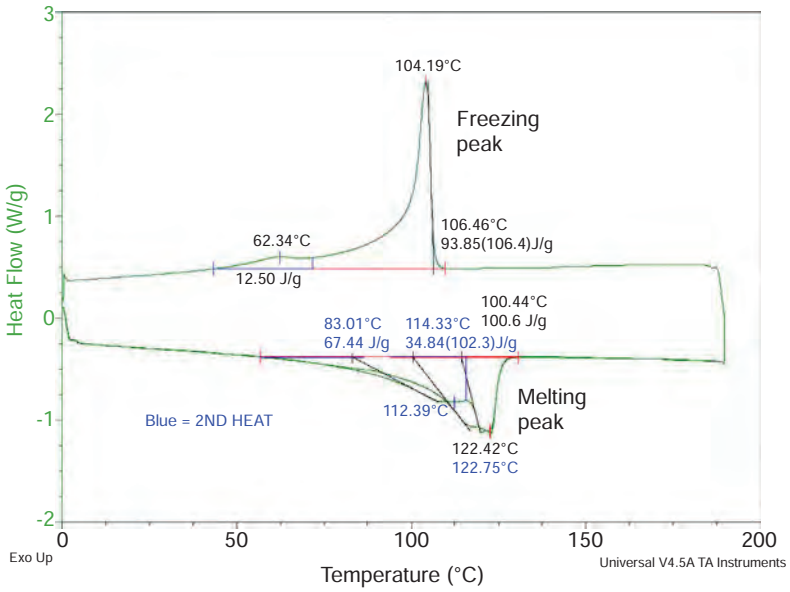


Figure 7.14 DSC curve for PE.
Courtesy of E. I. du Pont de Nemours and Company.

As described in Section 4.2.2.2, one of the factors affecting melting behavior of LLDPE is their molecular weight distribution (MWD) and comonomer distribution. Single site or metallocene-catalyzed LLDPE has a much narrower MWD and comonomer distribution than their Ziegler–Natta counterparts. This results in lower peak melting points as well as narrower temperature ranges over which melting takes place. A comparison of the melting points of the two technologies is given in Figure 4.4.

The molecular architecture also influences the ultimate seal strength. Linear polyethylene (LLDPE, HDPE) generally has higher ultimate seal strength than polyethylene and ethylene copolymers containing long chain branching or LCB (LDPE, EVA, ionomers, and so on). This is likely due to differences in ultimate tensile strength as well as tear strength behavior.

7.4.2.3 Substrate Adhesion

For lidding and other applications where the sealing film must bond to a different substrate (as opposed to heat sealing of a pouch where the sealant seals to the same material), the affinity or adhesion of the sealant to the substrate becomes important. In many lidding applications, the tray or cup is made of a polymer with a high melting point, such as PET, or even a nonpolymer material such as paperboard or aluminum. The substrate may not melt during the sealing operation and development of seal strength relies on the sealant wetting and adhering to the surface of the substrate. A number of factors play a role including the ability of the sealant to flow, tackiness, and polarity. See Chapter 10 for more detail.

7.4.2.4 Package Design

The film structure ideally suited for hot bar sealing has an outer layer that is temperature resistant and an innermost layer that has a low seal initiation temperature. This provides the greatest sealing temperature window for operations, allowing, for example, higher seal bar temperatures to be used to achieve strong seals at shorter dwell times. This allows for faster cycle times and line speeds.

Gussets or folds in the film in the corners of pouches are prone to sealing problems due to the difference in thickness compared with the rest of the seal area. This presents challenges in pressure distribution and the transfer of heat within the many interfaces within the gusset region. The folds provide springback forces that can lead to seal failure.

Hot bar sealing of lidding films onto thick trays or cups can be a challenge; the thick flange of the tray can act as a heat sink and reduce the temperature of the interface.

Table 7.2 DSC Peak Melting Temperature for Common Sealants

Polymer	DSC Peak Melting Temperature (°C)
EVA	
4% VA	101–105
7.5% VA	88
12% VA	95
18% VA	89
EMA	
6% MA	102
18% MA	81
23% MA	75
27% MA	64
Acid Copolymer	
7% AA	102
9% AA	97
4% MAA	109
9% MAA	103
12% MAA	97
Ionomer	88–100
PE	
HDPE	135
MDPE	126–130
LLDPE (Ziegler–Natta)	118–125
LDPE	98–115
mLLDPE, 0.900 g/cc	91–100
mLLDPE, 0.87–0.88 g/cc	60
PP	
Homopolymer	161
Random copolymer	145–155

As flexible packaging structures become more sophisticated with more and more layers, care must be taken to ensure the sealing performance is maintained. Factors such as interlayer adhesion and the hot tack performance of layers next to the sealant become important, especially as the sealant layer is downgauged. This is brought out in a study by Vansant [25], which examines the effect of coextrusion on the hot tack performance of an ionomer, a sealant known for its broad hot tack window. Vansant coextrusion coats three layers onto 50-μm aluminum foil: Al/(ACR-B-ionomer) and measures hot tack and heat seal performance. The goal is to understand the effect of downgauging the sealant layer by adding a less expensive bulking layer (layer B). The ACR (acid copolymer resin) is chosen to ensure good adhesion to the aluminum foil. Three different resins for the B layer are studied: the ACR, an LDPE, and a metallocene plastomer (mPE). For controls, all ACR (ACR-ACR-ACR) and ionomer (Ion-Ion-Ion) coatings are also run. The total thickness of the coating is 25-μm and the ratio of the B to ionomer layer is varied.

Selected hot tack results are shown in Fig. 7.15. The ratio of ionomer to B layer and composition of the B layer has a substantial impact on the performance:

- The ionomer control gives the highest hot tack over a broad temperature range.
- The (ACR-ACR-Ion) structure approaches the hot tack performance of the ionomer when the ACR layer is thin compared to the ionomer. Thinner layers of ionomer result in poorer hot tack. Vansant attributes this to cohesive or internal failure within the ACR. The thinner the ionomer layer, the easier it is for a crack to break through this layer and reach to ACR, lowering hot tack.
- With LDPE as the core layer, the hot tack is good until the LDPE reaches its melting point. Below Tm (around 120°C), interfacial adhesion seems to dominate; failure occurs at the LDPE–ionomer interface. Above 120°C, enough LDPE is melted to transfer failure to within the LDPE layer and the hot tack approaches that of LDPE.
- With mPE as the core, the hot tack resembles that of the ACR alone. The melting point of the mPE is similar to that of the ionomer, increasing the likelihood that the core layer will flow with the ionomer layer to help seal and caulk wrinkled and gusseted areas.

Vansant points out that this work involves measuring hot tack on a lab tester, which measures the force to completely pull the specimen apart. This may be too severe for some sealing situations. In some circumstances, such as seal around

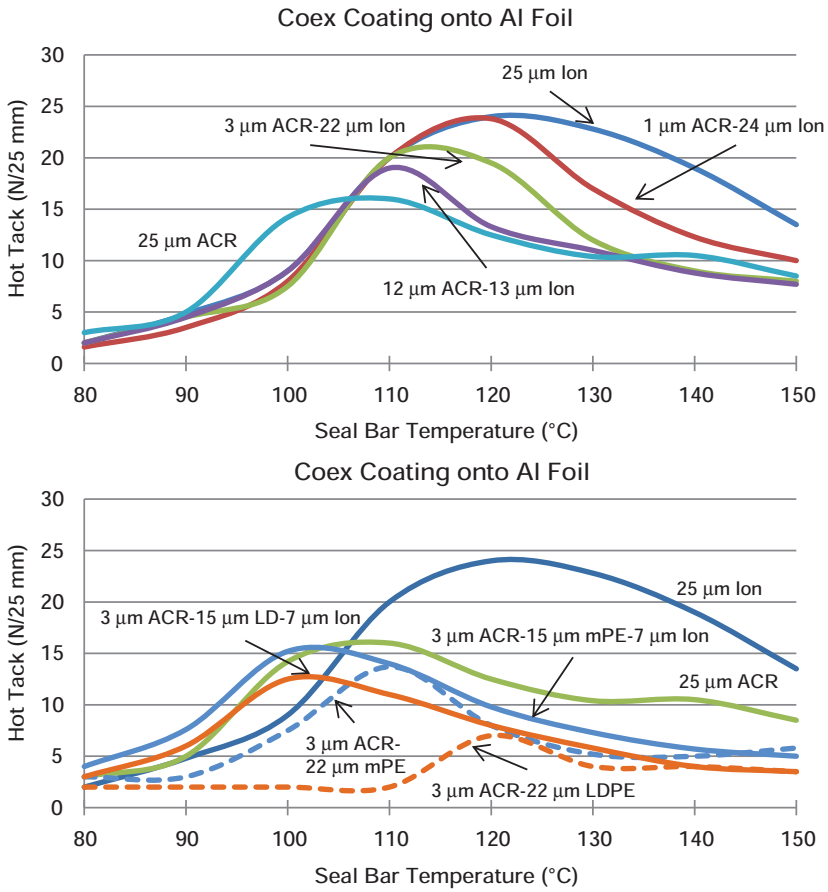


Figure 7.15 Hot tack of coextruded structures. Top graph is ACR–Ionomer coextrusion coatings onto Al foil. Bottom graph is ACR–PE–Ionomer coextrusion coatings.
From Vansant JD. The effect of coextrusion on the hot-tack performance of a common ionomer resin. In: TAPPI PLC conference, 1998, p. 743–54. Reproduced with permission from E. I. du Pont de Nemours and Company.

contamination and preventing channel leakers in gussets and wrinkled areas, "surface hot tack" may be all that is needed to obtain good seal integrity. These applications may be able to tolerate a sublayer that has poorer hot tack than the surface sealant layer.

7.4.2.5 Additives and Treatments

Tackifiers and plasticizers are sometimes added to promote adhesion. The former may alter the surface chemistry and change the viscoelasticity of the sealant. Plasticizers generally help increase the mobility of rigid polymer chains, aiding in diffusion. They may also act as lubricants, reducing adhesion by increasing intermolecular slippage.

Low molecular weight fatty acid amides are often added to control the coefficient of friction (COF) of the film. These "slip agents" bloom to the surface to create a low friction coating. They typically do not interfere with heat seal performance unless too much is used, which results in a "chalking" effect on the surface. At normal levels, they are thought to revert back into the polymer as the sealant melts.

Various lubricants and processing aids such as silicone oils can interfere with seal performance by acting as contaminants or weak boundary layers at the interface.

Inert fillers such as calcium carbonate or talc may reduce seal performance by decreasing the amount of polymer–polymer contact and increasing the viscosity, which affects spreading, wetting, and caulking.

Farley and Meka [29] found that corona treatment increases HSIT and reduces ultimate seal strength of LLDPE. Corona treatment is usually used to promote adhesion (to ink or coatings) and is typically not applied to the sealant side of the film. Some treatment

may inadvertently expose the sealant side in what is called back side treatment. In these cases, sealing may be an issue. Interestingly, at very low levels of treatment, seal strength is enhanced. The enhancement is negated if a slip agent is added. At higher levels, the HSIT increases by 5−17°C. They compare the effect with cross-linking the surface with e-beam or chemical cross-linking and conclude that the negative effect of corona treatment on heat seal is due to cross-linking of the PE.

Cross-linking can occur with excessive thermal history in the film fabrication process. This is especially true in high temperature processes such as extrusion coating and cast film.

7.5 Science of Heat Sealing

Heat sealing involves the formation of an adhesively bonded interface through melting, flowing, wetting, and diffusion or the creation of attractive chemical interactions. For a successful heat seal, mechanical work must be able to be transferred across the sealed interface. The resulting seal typically either has a diffuse or a sharp interface. The diffuse interface is the result of substantial movement of molecular segments across the interface over time. This type of seal typically occurs in film to film heat seal applications involving a common sealant on each side of the interface. To be consistent with the literature the term "auto adhesion" is used here to describe this type of sealing. It is also sometimes called "self-adhesion." With sufficient penetration across the interface, the interface becomes diffuse and given enough time disappears (and becomes part of the bulk polymer). Long range chemical interactions such as covalent, ionic, or electrostatic forces are not necessary; weaker secondary intramolecular forces build up as penetration proceeds. Nonpolar polymers such as polyethylene lack chemical functionality for such long range forces but work well under this scenario.

Sharp interfaces often occur in lidding applications where the sealant film bonds to a rigid tray or bowl. Here the tray material may not melt during the sealing process. The sealant melts and wets the surface of the tray material but cannot penetrate the surface of the tray substrate that is still crystalline or glassy. The seal forms almost instantaneously due to intermolecular attractive forces across the interface and its strength is strongly influenced by the chemical nature of the surfaces.

This section focuses primarily on the diffusion mechanism of heat sealing since it predominates in flexible packaging. The bonding of dissimilar substrates is described in Section 7.7.4 (peelable seals) and adhesion more generally in Chapter 10.

The modern view of auto adhesion during hot bar sealing is shown schematically in Fig. 7.16.

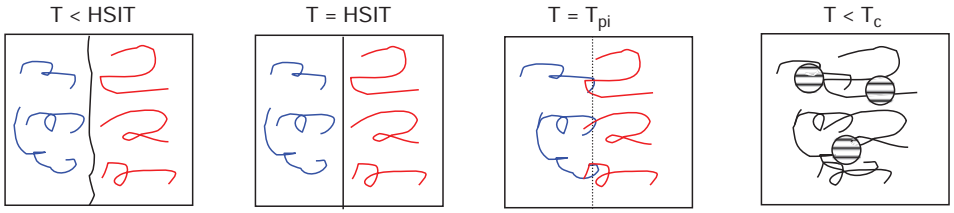


Figure 7.16 Mechanisms of auto-adhesion during heat seal. *HSIT*, heat seal initiation temperature, T_{pi}, plateau initiation temperature, T_c, crystallization temperature.
Adapted from Stehling FC, Meka P. Heat sealing of semicrystalline polymer films. II. Effect of melting distribution on heat-sealing behavior of polyolefins. J Appl Polym Sci 1994;51:105−19.

The two films are brought together and heat and pressure is applied from the outside. Initially the surfaces of the films are rough on a microscopic scale and little molecular contact is made. As the heat transfers through the film and begins to melt (or soften in the case of amorphous polymers) the interface, the surfaces of the films become smoother, allowing more intimate contact and wetting. The partial melting also produces tack. Further melting of the sealant results in molecular motion and the start of diffusion across the interface. This accounts for the sharp rise in seal strength with increasing temperature in the seal initiation region of the heat seal curve. Stehling and Meka [28] studied a number of polyolefins and found seal initiation occurs when the temperature reaches the point where, on average, 77% of the polymer is amorphous, as determined by DSC (Fig. 7.14). This accounts for differences in the initial crystallinity of the polymer; a sealant with a lower level of crystallinity to begin with will reach the point of 77% amorphous at a lower temperature. Indeed, semicrystalline polymers with low levels of crystallinity, polyethylene and ethylene copolymers in particular, have long been used as sealants for their low seal initiation temperatures.

Stehling and Meka, and van Alsten [30] found that the onset of the plateau region of the heat seal curve corresponds with the temperature at which all the crystals have melted (the temperature where the melting peak completely disappears on the DSC curve). Van Alsten found this also corresponds to the peak hot tack temperature for polyethylene. The crystals that melt at the highest temperature are associated with the longest molecules in the polymer. It is only after the longest chains are freed from the confines of the crystals that they are able to migrate across the interface. The longest chains are needed to build maximum strength at the interface [31].

The diffusion and strength buildup at the interface is influenced by the molecular forces present in the polymer. The strength and reach of these forces determines how much molecular penetration is needed to achieve the ultimate seal strength. With enough time and temperature, the interphase region will disappear, leaving a continuous bulk polymer. Further strength builds as the polymer crystallizes and the interpenetrating chains participate in the crystalline structure.

7.5.1 Early Theories of Auto Adhesion

By the early 1960s the diffusion model of auto adhesion of high molecular weight polymers was gaining acceptance as the primary mechanism for heat sealing. McKelvey [32] describes heat sealing along the lines depicted in Fig. 7.16. Voyutskii [33] reviewed the literature on auto adhesion in his monogram in 1963, arguing that the diffusion model best explains the experimental results of the day. While most of his examples do not involve heat sealing and packaging, they provide the basis for our understanding today.

One of the early theories is the adsorption theory. Here the adhesion is thought to be due to secondary interactions between the surface molecules of the adhesive and substrate; the nature and magnitude of the chemical interaction is unimportant since secondary interactions are present in all polymers. Secondary bonds, also called intermolecular forces or van der Waals forces, are described in Section 4.2.1.5.2. These are weaker bonds that do not include covalent, ionic, or electrostatic forces that make up the polymer chain. Wetting was thought to be the key. The stages of adhesion according to this theory include migration of the polymer chain to the surface followed by the establishment of an adsorption equilibrium that brings the distance between the molecules of the adhesive and substrate to less than 5 Å needed for secondary forces to be important. This theory may play a role in adhesion of polymers to solid substrates such as glass but early proponents may have fallen victim to thermodynamic arguments showing wetting alone gives very high work of adhesion. Wu [34] discounts this since the work of adhesion due to wetting is an equilibrium calculation for reversible fracture. Almost all adhesion applications, however, involve irreversible fracture and large viscoelastic deformation of the polymer. The calculated ideal adhesion due to wetting is often two orders of magnitude larger than actual measurements due to the presence of defects and stress concentration. For sharp interfaces, secondary forces alone are not sufficient to overcome these defects. For diffuse interfaces, where the polymer segments have migrated sufficiently across the interface, secondary forces can provide good adhesion. This gives credence to the diffusion theory for auto adhesion.

The electrical theory of adhesion was proposed by Deryagin and Krotova [35–38] and is based on

the phenomena of two dielectrics. The adhesive substrate is compared with a condenser and the double electric layer produced at the interface of two polymers is analogous to the plates of the condenser. When stripping the adhesive from the substrate a potential difference develops that increases with separation distance. Some observations of electronic emissions during stripping were observed that gave credence to the theory. Voyutskii gives a number of arguments against this theory including that it does not explain adhesion between nonpolar polymers or conductive polymers and calculates that any electric contribution is dominated by molecular diffusion.

7.5.2 Bonding at the Interface

There are three primary factors that influence bonding at the interface:

1. wetting;
2. diffusion; and
3. interfacial bond strength and molecular ordering (crystallinity).

The wetting of solid substrates is dealt with in more detail in Chapter 10. The thermodynamic driving force for wetting can be described by a spreading coefficient:

$$\lambda_{12} = \gamma_2 - \gamma_1 - \gamma_{12} \tag{7.1}$$

where λ_{12} = spreading coefficient of substance 1 onto substance 2, γ_1 = surface tension of substance 1 (adhesive), γ_2 = surface tension of substance 2 (adherend), γ_{12} = interfacial tension of substance 1 and 2.

For spontaneous wetting, $\lambda_{12} \geq 0$. For auto adhesion, the two substances are the same. Therefore, $\gamma_1 = \gamma_2$ and $\gamma_{12} = 0$ so that $\lambda_{12} = 0$. For the case of dissimilar sealant and substrate (eg, lidding applications) matching solubility parameters, first introduced in Chapter 6, to minimize interfacial tension can help improve wetting and adhesion.

In auto adhesion, wetting is not instantaneous. The surface is rough, at least on a microscopic scale, and sufficient time (and temperature) is needed to smooth out the surface for wetting. The development of a wetted interface proceeds as wetted pockets randomly form and radiate outwardly as the polymer melts and flows. The fraction of wetted contact area, $\Phi(t)$, can be modeled as a two-dimensional nucleation and growth process [38]:

$$\Phi(t) = 1 - \exp(-\mathrm{k}t^{\mathrm{m}}) \tag{7.2}$$

where Φ = fraction of interface wetted, t = time, k, m = constants.

The application of pressure helps ensure interfacial contact and heat transfer for melting of the sealants and subsequent flow and wetting. The time dependence of viscous flow for wetting and for diffusion are similar since they depend on the same molecular dynamic process. Hence, it is difficult to isolate the importance of each mechanism. Some investigators have proposed that wetting alone is sufficient for adhesion (as in the adsorption theory described in Section 7.5.1) but the preponderance of evidence suggests diffusion is also important for developing strength at the interface [34,38].

For nonpolar sealants like polyethylene, wetting and diffusion are the primary mechanisms for adhesion development. These molecules contain no polar or chemical functionality and rely on very short range secondary forces for their cohesive strength. Significant penetration and interdiffusion across the interface is required for enough of these secondary bonds to form. The rate of diffusion is thus critical and is influenced by molecular architecture, thermal motion (temperature), and time.

With polar sealants, additional forces come into play such as hydrogen bonding and ionic interactions. These forces may hinder the diffusion rate, but because they are longer range forces, cohesive strength can build with less penetration than for sealants relying solely on secondary interactions.

Polar sealants are also ideally suited to wet and adhere to dissimilar substrates found in lidding applications, especially if the substrate is polar in nature, such as PET. Here a sharp interface is typically created and dispersion forces alone are not sufficient for good adhesion development. This topic is further explored in Section 7.5.4.

7.5.3 Diffusion at the Interface

Diffusion involves the movement of molecular segments. The transfer of whole chains across the interface has the effect of erasing the interface and transforming interfacial properties into bulk ones. Such complete movement and erasure of the interface is difficult in the timescales of heat seal

operations and may not be necessary. Ends or small segments can move more readily across the interface and Wool [43] shows that these are responsible for strength development. To build strength, sufficient penetration is required for the creation of molecular bridges and entanglements and possibly cocrystallization. For polar molecules, longer range attractive forces may also be important.

The polymer needs to be in the melt state (or amorphous state for amorphous polymers) so that the molecules have enough thermal energy for movement and are not constrained by the crystalline domains. As described earlier, Stehling and Meka [28] found that seal initiation only takes place once most of the polymer is in the amorphous state.

The modern theory of molecular dynamics, developed by de Gennes [39], Rouse [40], Doi and Edwards [41,42], among others, has brought theoretical grounding to the proposals of Voyutskii and others. Wool [43] nicely summarizes the current thinking. In the bulk amorphous polymer, the chains are constrained by the entangled network structure. These constraints confine the movement of the chain to a tube-like region defined by the instantaneous location of the entanglements and the chain. The chain can wiggle within the tube due to thermal fluctuations (Brownian motion). This results in random movement of the chain along the contour of the tube. As the head of the chain extends out from the tube by a chain segment length, the tail of the tube disappears, and a new tube is formed. In this way the chain "snakes" its way through the network structure. This is known as reptation theory, coined and first proposed by de Gennes and refined by Doi and Edwards.

Wool [43] defines five time regions associated with diffusion that occur in order:

- Short range Fickian diffusion of monomers. By monomers, Wool is referring to the diffusion of individual repeat units on the polymer chain;
- Rouse relaxation of entanglements. (P.E. Rouse [40] developed the molecular dynamic model for dilute solutions of polymers from which the reptation model for concentrated polymer solutions or melts is based.);
- Rouse relaxation of the whole chain;
- Reptation;
- Long range Fickian diffusion of the polymer chains.

There are three important time scales for diffusion, again defined by Wool:

- τ_e, Rouse relaxation time between entanglements, characteristic of the wiggling motion;
- τ_{RO}, Rouse relaxation time of the whole chain, characteristic of the movement along the tube;
- T_r, reptation time, also known as the tube renewal time. This is the time required for the chain to escape its initial tube. It is the characteristic relaxation time for the chain and refers to 70% escaping (complete escape occurs at $1.94T_r$). At $t > T_r$ the interfacial region disappears and behaves like the bulk.

The important time for heat sealing is $\tau_{RO} < t < T_r$. In this region, chain segments can diffuse across the interface and strength develops. Times less than τ_{RO} may be important for bonding of dissimilar surfaces. T_r is typically much larger than τ_{RO} since T_r scales as M^3 (where $M =$ molecular weight) and τ_{RO} as M^2 and the molecular weight for sealant polymers is large.

Wool computes the time dependence of the average segment penetration distance across the interface as

$$\langle l \rangle \approx 2(Dt/\pi)^{1/2} \tag{7.3}$$

where $\langle l \rangle =$ average minor segment length as it escapes the tube, $D =$ diffusion coefficient.

Eq. (7.3) is valid up to the point where t approaches T_r (where $T_r \cong L^2/(2D)$) and $M > M_e$. Here L is the tube length from the reptation model and M_e is the molecular entanglement molecular weight. The diffusion coefficient relates the diffusive flux to the concentration gradient (Fick's first law):

$$J = -D\frac{\partial c}{\partial x} \tag{7.4}$$

where $J =$ diffusion flux (amount of chain segments per unit area per time), $c =$ concentration, $x =$ dimension of diffusion (perpendicular to interface).

The average penetration distance at an interface, X (defined for only one side of the interface; the total interface width is $2X$), is found to scale with the square root of the average segment penetration distance:

$$X \approx \langle l \rangle^{\frac{1}{2}}. \tag{7.5}$$

Scaling relationships such as the ones presented in this section are helpful for understanding relationships between physical properties and fundamental molecular and physical parameters. Most of these molecular dynamic models, such as the Rouse model, are too difficult to use for estimating the exact relationships but nevertheless provide key insight into relationships.

The equilibrium penetration distance is found to be $0.8R_g$, where R_g is the radius of gyration of the polymer chain (a characteristic length scale of the chain in its relaxed coiled state) and scales as $M^{1/2}$. The scaling law for the interface thickness becomes

$$X(t) = X_\infty (t/T_r)^{1/4} \sim t^{1/4} M^{-1/4} \text{ at } t < T_r \quad (7.6)$$

$$X(t) = X_\infty (t/T_r)^{1/2} \sim t^{1/2} M^{-1} \text{ at } t > T_r \quad (7.7)$$

where X = average interpenetration distance (half of interfacial thickness), X_∞ = equilibrium monomer interdiffusion distance at T_r, T_r = reptation time, M = molecular weight of polymer chain, t = time.

At T_r the scaling relationship switches from reptation to Fickian diffusion, where $X^2 \sim Dt$.

Wool presents scaling laws for a number of mechanical properties at the interface. Most important for this discussion is the fracture energy, the energy to create new interfacial area, which is related to the seal strength (Section 7.5.6). The fracture energy is found to scale with the minor segment penetration distance across the interface, $\langle l \rangle$:

$$G_a \approx t^{1/2} M^{-1/2} \quad (7.8)$$

where G_a = fracture energy, t = time, M = molecular weight.

Wu [44] reports that experimental data show the fracture strength often develops as $t^{1/4}$ rather than $t^{1/2}$, and that the $t^{1/4}$ behavior is predicted by kinetic theory. This suggests that G_a may scale with X rather than with $\langle l \rangle$. Heat seal results for PE films in Section 7.5.3.2.2 from several investigators, however, show a $t^{1/2}$ behavior.

The molecular weight dependence given in Eq. (7.8) is suspect since the mechanics of polymer welds, particularly heat seals, are highly complex, involving more than the deformation of the first few hundred angstroms at the interface. Experimental studies indeed show a complex relationship between molecular weight and peel strength, underscoring the competing effects of reduced diffusion and increased strength when the molecular weight is increased.

7.5.3.1 Heat Seal Process Effects: Time, Temperature, and Pressure

Seal dwell time, seal bar temperature, and pressure are controlled parameters for the heat seal process, which influence the heat history at the interface and the extent of diffusion that occurs. As shown in Eq. (7.6), the amount of molecular diffusion or penetration increases with the fourth root of time up to the reptation time, after which Fickian center-to-mass diffusion best describes the molecular motion.

The diffusion coefficient increases with increasing temperature. An Arrhenius relationship is often used to describe this relationship:

$$D = D_0 \exp\left(\frac{-E_d}{RT}\right) \quad (7.9)$$

where D = diffusion coefficient, D_0 = constant, E_d = activation energy for diffusion, R = ideal gas constant, T = temperature (K).

Wu [44] tabulates values of E_d for several polymers (4–15 kcal/mol) and comments that the activation energies for diffusion and viscous flow are in the same range, making it difficult to distinguish between these two mechanisms.

The temperature at the interface can be modeled by simple heat conduction models. Meka and Stehling [45] develop a finite element model that agrees well with experimental measurements with microthermocouples. Morris [46] uses a finite difference algorithm to compute temperature profiles at the sealant interface for different thickness films. For the thicker structure investigated, the interface temperature never reaches the seal bar temperature in the time frame of the heat seal operation. This model is developed in more detail in Section 7.6.

Increasing the sealing pressure may reduce the volume available for segmental motion (depending on the compressibility of the polymer) [47]. This may decrease the diffusion coefficient. In practice, the seal jaw pressure needs to be large enough to ensure good contact to allow wetting and diffusion to take place but not too large as to cause excessive flow from the seal area.

7.5.3.2 Polymer Properties

7.5.3.2.1 Thermal Properties

The polymer chains must be mobile for diffusion to take place. In semicrystalline polymers the crystalline structure constrains the movement of the molecules. Enough thermal energy must be transferred to the polymer to at least partially melt the crystals for appreciable movement to take place. Amorphous polymers must be well above their glass transition temperature for effective diffusion.

For many ethylene copolymers, the crystalline melting point (Tm) decreases with increasing comonomer content. This is true for metallocene LLDPE, EVA, ethylene methyl acrylate (EMA), ethylene acrylic acid (EAA), ethylene methacrylic acid (EMAA), and ionomers. One exception among the commonly used sealant resins is standard LLDPE made with Ziegler–Natta catalysts. These are heterogeneous in MWD and comonomer distribution. The longer chains in these polymers tend to have little comonomer content, even as the overall comonomer content is increased. The peak Tm is determined by the crystallization of the longest chains. As a result, the peak Tm of Z-N LLDPE remains almost constant as total comonomer content is increased, even though the amount of crystallinity decreases (see Figure 4.5).

7.5.3.2.2 Molecular Architecture

Eqs. (7.6)–(7.8) show that as the molecular weight increases, the amount of chain diffusion decreases. The reptation model shows that the interfacial thickness scales with M^{-1} (Eq. (7.6)) and the center of mass diffusion scales with M^{-2} [42]. This agrees with experimental evidence.

Long chain branching (LCB) also slows diffusion. The branching entangles the polymer network resulting in less chain movement. Of the common ethylene-based sealant resins, LDPE, EVA, EMA, EAA, EMAA, and ionomer contain LCB. The linear polyethylenes (LLDPE and mPE plastomers) do not. Some metallocene-catalyzed plastomers have a sparse amount of LCB for improved bubble stability in blown film. The diffusion coefficients for these materials lie somewhere between linear LLDPE and LDPE.

The molecular weight and comonomer distribution of LLDPE has a significant effect on diffusion and the buildup of seal strength. Schuman et al. [48,49] use layer multiplier technology to produce film structures with 32 alternating layers of LLDPE and HDPE with an average layer thickness of 17 and 25 μm, respectively. They anneal the films at 200°C for up to 10,000 min, periodically running a DSC scan. Since these two polymers are miscible, as the interface disappears through interdiffusion the two melting peaks merge into a single peak. By following this change with annealing time, they calculate the rate of diffusion. They find that the rate of disappearance of the layers (interface) depends on the MWD and especially the longer chain molecules. The boundaries between the layers remain stationary during the characteristic diffusion time of the main components and only move at long times associated with diffusion of the high molecular weight fraction.

Mueller [31] studies the heat seal behavior of a heterogeneous Ziegler–Natta LLDPE with a polydispersivity (Mw/Mn) of 5.1. The resin is made into a blown film and heat sealed over a temperature range of 100–130°C for 1–100,000 s. DSC shows that complete melting takes place at 130°C. Long dwell times are used to characterize diffusion since the short time scales of the commercial heat seal process are of the same order as the time for the interface to reach the seal bar temperature. Over the temperature range of 100–125°C, and especially near 115°C, there is a strong dependence of temperature and sealing time on heat seal strength. The development of seal strength is found to increase as $t^{1/2}$ in agreement with Wool's scaling analysis. Wool [50] suggests that to build strength in a polymer melt, the chain segments form bridges across the interface (entanglements). For melts the minimum number of bridges required is three and the scaling goes as $t^{1/2}$. Mueller finds this to be true for semicrystalline LLDPE polymers with the presence of crystals as an anchoring point.

Mueller finds that the seal times needed to reach the ultimate seal strength are always longer than the characteristic diffusion time based on theory. They consider a number of possibilities for this behavior. The change in diffusion coefficient with temperature is not sufficient to explain the results. In the narrow range of 113–117°C where the greatest change in peel strength takes place, the amorphous fraction only changes from 70% to 75%. They conclude that this is not likely a major factor. Looking at the MWD and comonomer distribution of the polymer, they propose that at temperatures below 115°C, only the shorter MW, high comonomer content chains

melt and diffuse. These chains make poor tie molecules and weak crystals. It is only when the longer, less branched chains melt and move that the peel strength can approach good seal strength. This results in a considerable increase in the entanglement time.

Qureshi [51] studies the hot auto-adhesion of three Ziegler–Natta LLDPE resins that are polydisperse in MWD and heterogeneous in comonomer distribution. Fifty micron monolayer blown films are laminated to OPET: OPET/adh/LLDPE. Sealing is done within a controlled temperature chamber on a tensile tester so that the peel strength is measured at the sealing temperature (the temperatures are well below the distortion temperature of the OPET so that the films can be grasped by the tensile tester even if the LLDPE is completely molten). The seal time is varied from 0.5 to 25 s.

The measured peel strength increases with total time (seal time plus the peel time) and curves produced at different seal times overlap. This shows that diffusion continues during the peel (when the polymers are in the melt). This observation comes up again with respect to the delay time in hot tack (Section 7.6.2). Peel strength increases with $t^{1/2}$ at short contact times but saturates or levels out at longer times (when the time-independent value is reached). The time for saturation is T_r in Wool's analysis: the time for the chain to completely diffuse out of the tube and when the interphase region begins to behave like the bulk. As described in the development of Eq. (7.6), T_r is related to the time for the polymer to diffuse the distance R_g, the radius of gyration of the polymer chain. Qureshi calculates T_r and finds it to be two orders of magnitude less than the measured time to reach the ultimate seal strength. This is similar to the findings of Mueller.

Qureshi explains the discrepancy by the presence of an inert surface layer made up of predominately low MW, high comonomer content chains. This layer is approximately 100 nm thick. Both enthalpic and entropic forces drive this segregation of chains. One is flow-induced segregation due to higher shear rates at the wall of the flow channels during film fabrication, favoring low molecular weight (lower viscosity) chains to move toward the wall. Another driving force favors the amorphous fraction (high comonomer content) to be near the surface [52,53]. This is consistent with the high comonomer content chains being near the surface since the comonomers in LLDPE act as short chain branches that disrupt crystallinity. In a second paper, Qureshi et al. [54] present AFM (atomic force microscopy) evidence showing the presence of this amorphous surface layer.

As soon as the two films are joined in the melt, the low MW, high comonomer chains at the surface quickly diffuse but cannot generate good adhesion in the melt (they disentangle at the same rate as they entangle). But once the surfaces are joined, they become part of the bulk and the thermodynamics for segregation no longer exist. Homogenization of the interphase by mutual interdiffusion brings long chains to the interface. This interdiffusion process has a $t^{1/2}$ dependence. Not only do the long chains have lower diffusion coefficients than the short chains, they have a longer distance to travel, moving through the former amorphous surface layer, before diffusing across the interface.

In a follow-up paper, Qureshi et al. [54] compare the three Ziegler–Natta LLDPE with a metallocene hexene–LLDPE. All have similar molecular weight (MW) but the mPE has a narrower MWD and comonomer distribution. The seal strength of the Z-N LLDPE increases with $t^{1/2}$, whereas the seal strength of the mPE shows no dependence on time (t^0). This indicates the mPE diffusion rate is much faster than the Z-N LLDPE. This is consistent with the narrower MWD of the mPE and its lack of the high MW fraction contained in the Z-N LLDPE. Furthermore, AFM shows no presence of an amorphous surface layer on the mPE blown film as is found with Z-N LLDPE.

Qureshi et al. [54] also studied blends of two octene mPE resins with two different densities, 0.87 and 0.91 g/cc. These densities correspond to different comonomer contents with the 0.87 g/cc grade having considerable more comonomer than the 0.91 g/cc grade. When they blend 5–20% of the 0.87 g/cc grade into the 0.91 g/cc grade, they observe heterogeneous behavior: $t^{1/2}$ dependence. At levels greater than 20% the behavior reverts back to the t^0 dependence observed for the hexene mPE.

7.5.3.2.3 Chemistry

The chain rigidity influences diffusion rates. Polymers that contain aromatic groups typically are stiffer and slower to diffuse. The presence of bulky side groups can also impede movement of the chains. Polar forces such as hydrogen bonding and specific chemical interactions also generally increase rigidity and change the diffusion behavior [33,55].

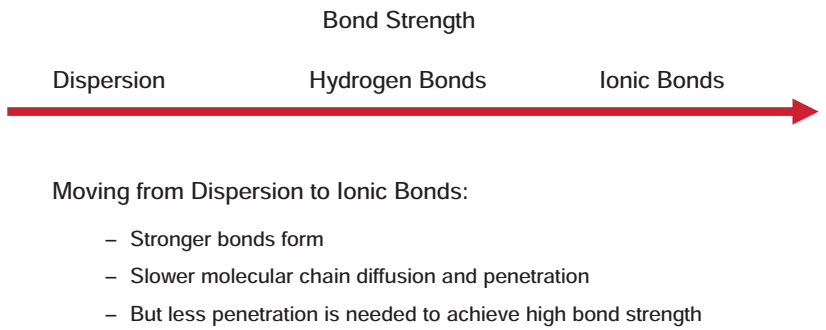


Figure 7.17 Continuum of molecular forces.

Cross-linking of the polymer also impedes molecular mobility and hinders diffusion.

For bonding of dissimilar polymers, compatibility is important. Small chain segments diffuse across the interface but this may not be enough to build strength [63]. A significant number of bridges are required; the formation of such bridges is not thermodynamically favored for incompatible polymers. Chemical means to promote adhesion at an interface when the polymers are not compatible are described in Chapter 10.

7.5.4 Interfacial Bond Strength and Crystallization

Once sufficient wetting and diffusion takes place, the strength of the interface builds as the polymer chains bridge across the interface and come close enough for intermolecular forces to take hold. The adhesive strength of the interface is determined by the nature of the molecular forces that are present. For common sealants used in flexible packaging, these range from dispersion to hydrogen bonding to ionic interactions. These forces can be thought of as a continuum as shown in Fig. 7.17. Moving from left to right, the molecular forces increase in strength and stronger bonds form. These same forces can impede the movement of the chains resulting in slower diffusion and less penetration, but less penetration is needed to build strength.

The types of intermolecular forces present in some of the commonly used sealant resins are given in Table 7.3. For nonpolar molecules like PE, only weak dispersion forces are present. The relatively weak dispersion forces are compensated by their number. A high level of penetration is needed to essentially erase the interface and achieve the strength of the bulk.

The polar ethylene copolymers such as EVA and the acrylate copolymers contain relatively polar side groups. These are particularly helpful in wetting and bonding to dissimilar substrates such as PET or PP for lidding applications. In auto adhesion, the polar groups likely help in establishing bond strength. It is difficult to separate out this effect from the influence the comonomer has on the melting point. The lower melting point allows the chains to diffuse at lower temperature and provides low HSIT.

Table 7.3 Types of Molecular Forces Present in Some Common Sealant Resins.

Sealant	Dispersion	Polar	Hydrogen Bonding	Ionic
LLDPE, mPE, LDPE	X			
PP	X			
EVA	X	X		
EMA, EEA, EBA	X	X		
EAA, EMAA	X		X	
Ionomer	X		X	X

Ionomers and their acid copolymer precursors have hydrogen bonding between the oxygen atom in one molecule and hydrogen atom in another. These are stronger than dispersion forces and act over a longer distance. In addition to helping with auto adhesion, the acid groups bond well to aluminum foil and enhance melt strength.

Ionomer sealant bonds involve dispersion, hydrogen bonding, and ionic interactions. As described previously, the ionic bonding provides many of the favorable attributes of ionomers for flexible packaging: high melt strength and hot tack, low seal initiation temperature, toughness, and transparency. van Alsten [26] shows that the ultimate heat seal strength occurs only after the polymer has fully melted. He and others [52] have shown that the metal ions diffusion several orders of magnitude faster than the polymer chains. Hence, van Alsten concludes that the development of strength at the seal interface involves the diffusion of large chains, similar to what happens in polyethylene. Morris [46], however, shows that ionomers only need penetration on the order of about $0.1R_g$ to reach the ultimate seal strength, 10 times less that needed for polyethylene.

In the heat seal process, once the seal bars are removed, the interface begins to cool. Whereas heating of the interface takes on the order of a second or less, cooling takes much longer: several seconds or more. This is because heat transfer from direct contact with the hot bar is much faster than convective cooling from air. A typical temperature profile is shown in Fig. 7.18 based on the modeling of Morris [46] which is described in Section 7.6. The long times at temperatures above the freezing point underscore the importance of hot tack.

As the interface cools, the molecular mobility decreases, reducing the rate of diffusion. For semicrystalline polymers, the chains organize into crystalline structures as the temperature drops to the crystallization temperature. The ability of sealants to crystallize at the interface contributes to interfacial strength.

The influence of crystallization of two incompatible semicrystalline polymers is complex. The shrinkage of the first polymer to crystallize may cause an influx of the other polymer across the interface if the second polymer is still molten. As it solidifies, this may create mechanical interlocking between the two polymers and add to the interfacial strength. The interfacial strength is dependent on a number of factors including the compatibility of the two polymers, their crystallization temperatures, their crystallization rates, and the rate of quenching. The nature of the influxes and the effect of cocrystallization of incompatible polymers are still not well understood [57].

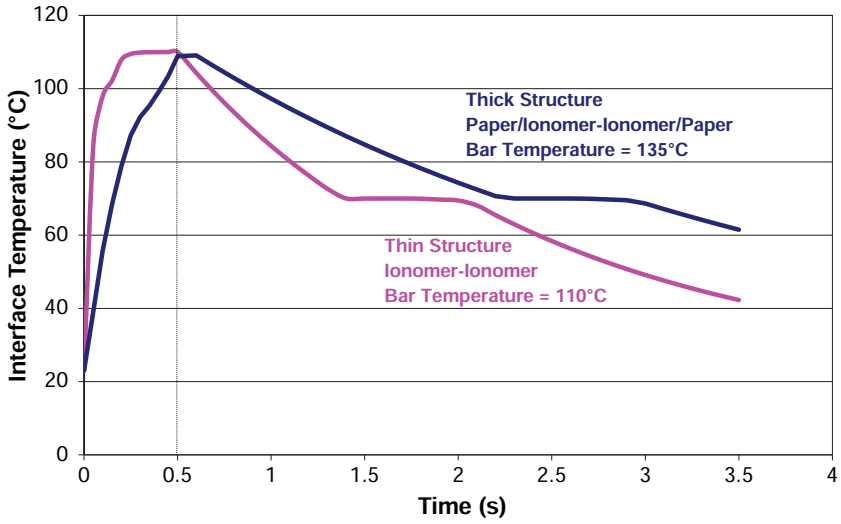


Figure 7.18 Model calculation of temperature of the interface during hot bar sealing for the two film structures as shown in Fig. 7.13. Each film is sealed at its respective plateau initiation temperature (110 and 135°C for the thin and thick structure) for 0.5 s.

Reproduced with permission from Morris BA. Predicting the heat seal of ionomer films. J Plast Film Sheeting 2002;18:157–67.

7.5.5 Hot Tack

Hot tack is a function of interfacial bonding and melt strength. The hot tack versus sealing temperature curve, introduced in Fig. 7.11, goes through a maximum due to the competing effects of temperature on chain diffusion and melt strength: diffusion increases with temperature and melt strength decreases. The maximum or peak hot tack temperature is typically near where the heat seal strength reaches its plateau value. These may not exactly be the same due to differences in measurement. In the heat seal test, there may be significant diffusion that occurs during the initial stages of cooling, which shifts the curve to the left. In the hot tack experiment, long delay times may mimic this effect but may not be representative of the actual sealing operation.

The initial stages of the hot tack test are similar to the heat seal test. The films are brought together with pressure but initially are not in intimate contact due to the microscopic roughness of the surfaces. As the heat from the seal jaws transfers through the film and melts the interface, polymer chain segments become mobile, wet the surface, diffuse across the interface, and build strength through entanglements and molecular interactions. As described in Section 7.2.3, most commercial hot tack testers today have a programmed delay time between when the seal bars are released and the specimen is pulled apart. During the delay, further chain diffusion may occur as well as cooling. Following the delay, the force to separate the films is measured, typically at much higher pull rates than those used in the heat seal test. This force is not only a function of the hot adhesion at the interface but also the resistance to elongational stress, which is related to the melt strength or elongational viscosity.

Diffusion is described in detail in Section 7.5.3. This discussion pertains to hot tack as well. One difference is that the amount of chain penetration, bridging, and entanglement needed to build hot adhesion strength may be greater than for cold adhesion (heat seal). This is because the hot tack measurement is done while the sealant is molten, whereas in the heat seal measurement the sealant has solidified and crystallized. Hot adhesion is also more heavily influenced by strong molecular forces than cold adhesion because of the lack of crystallinity in hot adhesion. The presence of stronger bonds such as hydrogen and ionic bonding not only helps with interfacial adhesion but also increases the melt strength.

Melt strength is related to elongational viscosity and decreases with increasing temperature, typically in an exponential manner. Several factors influence melt strength including molecular forces and chain architecture. In general the presence of longer range molecular forces increases melt strength and hot tack. The strength and range of these forces are in the following order: dispersion < hydrogen bonding < ionic or covalent bonds. Cross-linking, for example, increases melt strength but runs the risk of rendering the polymer difficult to seal since this also impedes diffusion. Ionomers have outstanding melt strength due to the presence of ionic interactions and clusters, which act like cross-links but still allow for flow and sealing.

The molecular architecture also has a substantial impact on melt strength as described in Chapter 5. Increasing MW, introducing LCB, and broadening the MWD tend to increase melt strength. Just as strong molecular forces impede chain movement and diffusion, so to do these factors. A recurring theme in hot tack is that factors that help the left side of the curve often negatively affect the right side of the curve (and vice versa) making sealants with broad hot tack temperature windows rare.

Some of the resin design strategies for improving hot tack are shown in Fig. 7.19. These include the following:

- Broadening the hot tack temperature window by lowering the sealant melting point (to lower the HTIT) and increasing the sealant melt strength (through changes in chemistry or architecture). The melting point for ethylene copolymers can often be lowered by increasing the comonomer content.
- Increase the peak hot tack strength by increasing the melt strength, increasing the hot adhesion between the layers (by increasing chain diffusion and entanglement or introducing long range molecular forces), or inducing crystallization.
- Decrease the peak hot tack temperature by lowering the sealant melting point or increasing the rate of diffusion (lower MW, narrower MWD, less LCB, and so on).

Some typical hot tack curves for PE and ethylene copolymers are shown in Fig. 7.20. The two families of ethylene-based sealants with the best hot tack

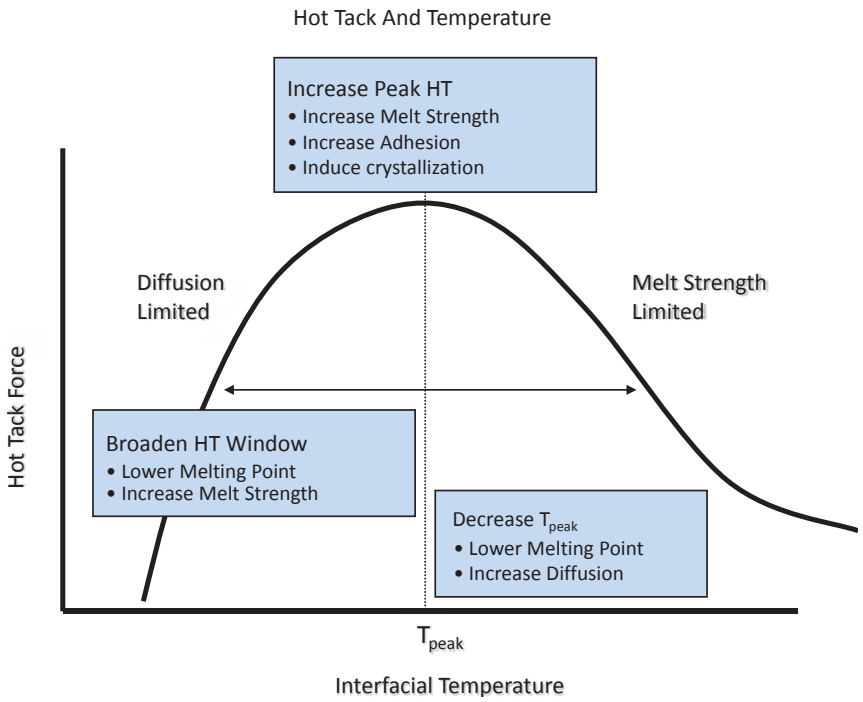


Figure 7.19 Resin design strategies for hot tack performance.

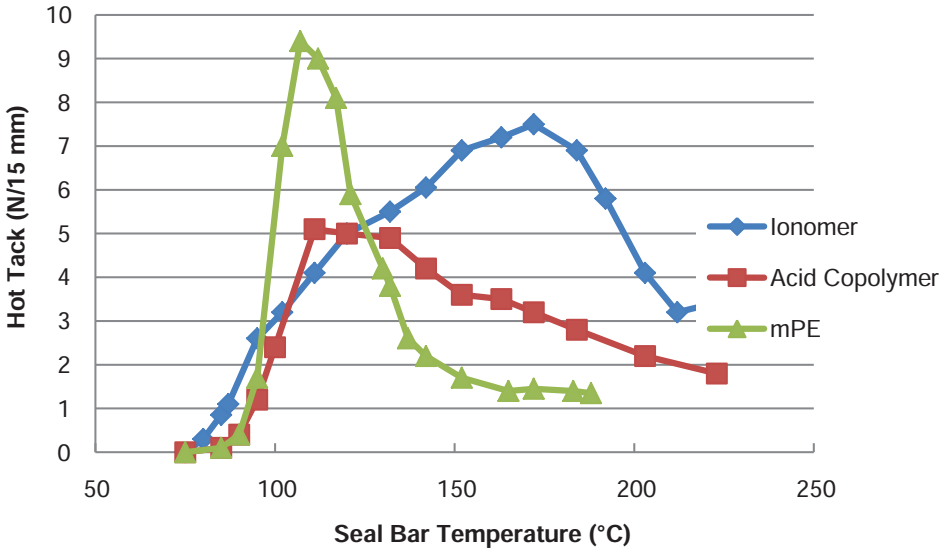


Figure 7.20 Comparison of hot tack performance of different ethylene-based sealants. Packforsk hot tack tester, 0.5 s dwell time, 0.1 s delay time.
Data from E. I. du Pont de Nemours, Inc.

performance are the metallocene or single site catalyst plastomers and ionomers. They achieve their performance in substantially different ways.

The mPE plastomers typically have very high hot tack strength over a narrow temperature range. The peak hot tack temperature occurs at the temperature where the final crystals melt [21,30]. This exceptionally high hot tack is likely due at least in part to strain-induced crystallization. Normally the crystallization rate is zero at the melting point. Extensional flow causes the chains to line up in the direction of extension, enabling crystallization. Metallocene PE

is more likely to undergo strain-induced crystallization than Ziegler–Natta PE due to its more uniform comonomer and chain size distribution. The comonomers do not participate in the crystals. In heterogeneous Z-N LLDPE, the shorter chains have a high comonomer content that is not conducive to crystallization. The longer chains have lower comonomer content but are more constrained and less likely to form crystals in the time frame of the test.

Sentmanat and Hatzikiriakos [58] use uniaxial extensional rheometry and DSC to study the behavior of a metallocene plastomer with a peak melting point of 92°C, the onset of melting at 87°C, density 0.900 g/cm^3, PDI of 2.0, MI of 1.2 g/10 min, and MW of 80 kg/mol. Their study focuses on a narrow temperature range near the peak melting point where the maximum hot tack is typically observed. In the solid state (<87°C) the polymer exhibits classic plastic yielding. At 95°C and above, there is no strain hardening typical of LLDPE melts. When the temperature ranges between 89 and 93°C the polymer is partially molten and exhibits strain-hardening behavior as shown by the steeply rising transient elongational viscosity in Fig. 7.21. DSC of rapidly quenched samples show evidence of an increase in crystallinity in the samples stretched at 91 or 93°C. This strain-induced crystallinity may explain the exceptional hot tack performance of these resins. Note that under quiescent conditions, the mPE has a crystallization temperature of 73°C, nowhere near the melting point.

Qureshi [51] observes an overshoot in hot tack strength at the beginning of hot tack measurements. They propose this is due to strain-induced crystallization since the strain rate at initiation is higher than the steady strain rate. While they observe overshoot at high peel rates, none is observed at low peel rates, which supports the hypothesis. In a second study, Qureshi et al. [54] compare metallocene- and Ziegler–Natta-catalyzed (heterogeneous) polyethylene of similar densities and molecular weights. At high peel speeds (500 m/min), the metallocene LLDPE gives substantially higher peel strength than the heterogeneous LLDPE. As described

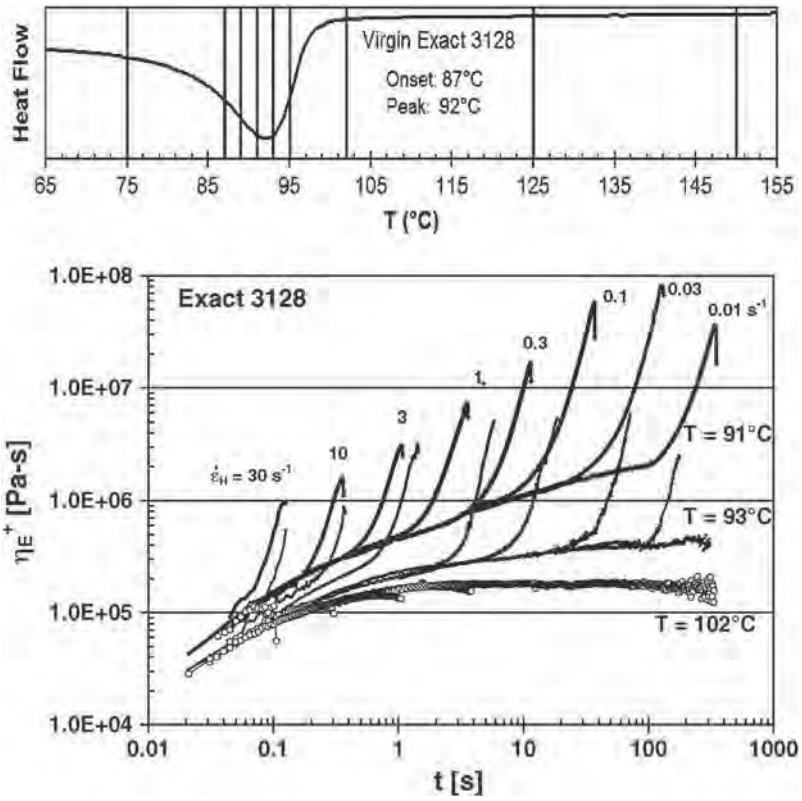


Figure 7.21 DSC (top) and transient elongational viscosity (bottom) of a mPE.
From Sentmanat M, Hatzikiriakos SG. Flow induced crystallization of polymers in extension. In: SPE ANTEC conference, 2010, p. 51–5.

in Section 7.5.3.2.2, they conduct their measurements in a heated chamber so the peel strength is essentially a measure of hot tack. At 50 m/min, there is no difference in hot tack between the two polymers. They attribute the change in behavior to strain-induced crystallization in the mPE at the higher peel rate.

The scientific explanation for the high peak hot tack strength of mPE reveals how laboratory hot tack measurements may not represent actual performance in a commercial packaging operation. Most commercial hot tack testers use a high peel rate that is more characteristic of the registration speed of the packaging line than the pulling force acting on the hot seal. High peel rates favor strain-induced crystallization. Many users of hot tack testers set the delay time for 0.1−0.5 s when the opening force in many applications occurs almost instantaneously. While the heat transfer is slow during the delay time there is nevertheless a small amount of cooling that takes place (see, Fig. 7.18, for example). Early work with standard grades of polyethylene show that delay time has a minimal effect on the hot tack curve [9], but these materials are not sensitive to strain-induced crystallization. The work of Sentmanat and Hatzikiriakos shows that for the newer metallocene LLDPEs and plastomers, even small changes in temperature can greatly increase the potential for strain-induced crystallization.

For acid copolymers and ionomers, the presence of LCB, hydrogen bonding, and for the case of ionomers, ionic interactions imparts strain-hardening behavior in the melt. This is depicted in Fig. 7.22. The amount of strain hardening increases in the following order: LDPE < ACR < ionomers. The strain hardening arises from chain entanglements and molecular interactions rather than from strain-induced crystallization. As a result the strain-hardening behavior of ACR and ionomers persists over a very broad temperature range. The measurements shown in Fig. 7.22 are conducted at 140°C, well above the peak melting point of around 95°C.

mPE is characterized by a sharp melting peak over a narrow temperature range, rapid self-diffusion across the interface, strain-induced crystallization within a few degrees of the melting point and a swift reduction in melt strength with further temperature increases. Ionomers are slower to diffuse across the interface due to their broader melting point range, long chain branches, and strong ionic intermolecular forces. Because of the longer range forces present, chain penetration at the interface is not as critical.

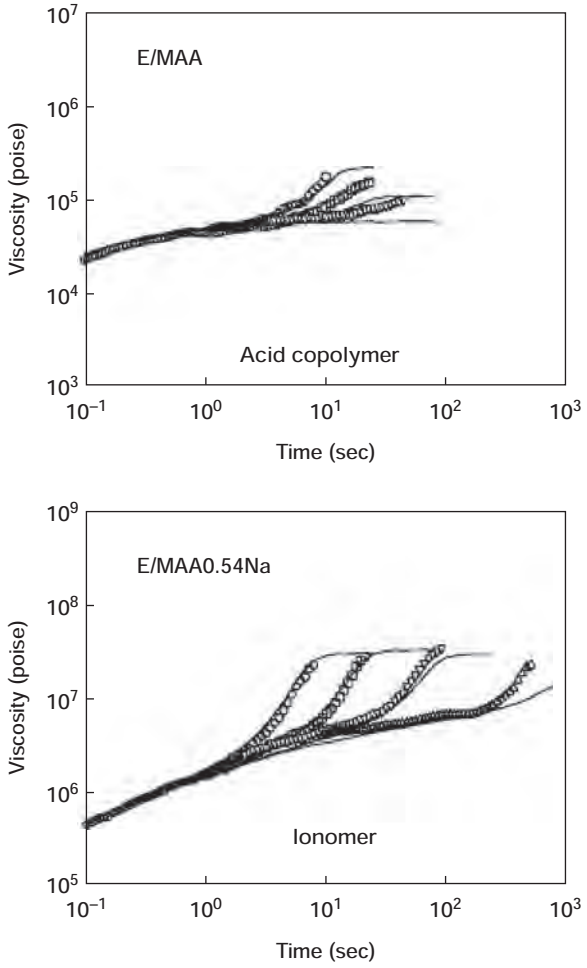


Figure 7.22 Transient elongation viscosity of an ionomer and acid copolymer.
Reprinted with permission from Takahashi T, Watanabe J, Minagawa K, Koyama K. Effect of ionic interaction on elongational viscosity of ethylene-based ionomer melts. Polymer 1994, 35:5722−8.

Once the ultimate hot tack strength is achieved, its magnitude persists over a much broader temperature range than mPE due to its outstanding melt strength.

7.5.6 Fracture Mechanics

The measurement of seal strength, whether in a controlled manner in the lab, or in an uncontrolled manner by the consumer, is essentially a peel test. The peel test, introduced in Section 7.2.2, measures the energy or force needed to pull the specimen apart. During the test a peel front moves through the specimen, which can be thought of as a crack propagating through the length of the seal. The engineering discipline that studies crack propagation and

failure of materials is known as fracture mechanics. A fracture mechanics analysis of the peel test helps provide insight into the factors that influence it.

A detailed analysis of the peel test is developed in Chapter 10. Here basic concepts are introduced and a discussion of the insights the analysis provides for heat seal strength is provided.

The peel force is not simply the bond strength; many other factors are involved. As the peel arms are separated and pulled apart, they may stretch irreversibly depending on the stiffness and yield strength of the materials in the peel arm. The peel arms are bent to an imposed angle, typically 180 degrees for a T-peel test, although the actual local angle may differ depending on the stiffness of the arms. New interfacial area is created as the peel front advances. The measured force is a function of the energy required to bend the peel arms (E_b), the energy to irreversibly stretch the peel arms (E_e), and the energy to create new interfacial area, known as the fracture energy (G_a):

$$\text{Peel Strength} = f(E_b, E_e, G_a) \tag{7.10}$$

Often E_b and E_a are small compared to G_a for flexible packaging. So far the bond strength has not been explicitly mentioned. This is introduced through G_a. G_a is a function of the work of adhesion (W_a) times the local viscoelastic energy dissipation at the peel front (Φ):

$$G_a = W_a(1 + \Phi(R, T)) \tag{7.11}$$

W_a includes bonding due to wetting, diffusion, and chemical interaction. The local viscoelastic energy dissipation, Φ, can be significant compared with the bond strength and has a substantial impact on the measured peel strength. Φ is a function of the pull rate (R) and temperature (T).

Insights from fracture mechanics into factors that affect seal strength include the following:

- The peel strength is rate dependent. The pull speed can significantly change the measured seal strength. This is a consequence of Eq. (7.11).
- The peel strength is temperature dependent through changes in Φ and in the bulk properties of the film. For example, an increase in temperature typically decreases the modulus, which affects bending angles and irreversible elongation.
- Changing the angle of pull changes seal strength through a number of effects. The imposed peel angle has a direct effect on E_b. Changing the angle will likely change the actual angle at the interface; this may change how stress is concentrated and impact the separation dynamics.
- Changing the modulus of the sealant changes the local viscoelastic energy dissipation, the bending energy, and the energy to irreversibly elongate the peel arm, each of which may affect seal strength.
- Increasing sealant thickness may increase seal strength. Fracture mechanics predicts that increasing thickness will increase peel strength up to a point and then level off. At the front of the crack tip, there is a region of local deformation. At very small sealant thickness, the size of the deformation zone is constrained by the thickness of the sealant. As the thickness increases, the size of the deformation zone increases; peel strength is raised through an increase in Φ. At some critical thickness, the zone of deformation reaches its natural size and is no longer constrained by the thickness of sealant. At thicknesses greater than the critical thickness no further increase in fracture energy occurs.
- Other layers in the film structure besides the sealant can influence the measured peel strength. Poor interlayer adhesion can reduce seal strength as described in Section 7.7 for peelable seal technology. Elongation and stretching of the peel arm during testing can lead to higher peel strength values; elongation is impacted by all the layers in the structure. The stiffness of the layers can influence the actual local angle at the interface.

An example of the last point is illustrated by work done by DuPont researchers a number of years ago. They developed special copolymers for bonding to aluminum foil. They made a series of polymer compositions that had the same chemical functionality (for bonding to the foil surface) but differed in stiffness as measured by the tensile modulus. Their screening test was to make heat seals of the polymer sandwiched between two layers of aluminum foil: Al/film/Al. They found that the peel strength increased substantially as they decreased the modulus of the film. The actual application involved extrusion coating the polymer onto the foil with the final structure: Al/coating. When they conducted

trials on a pilot-coating line, they found the change in modulus had no effect on the peel strength between the coating and foil. After some investigation they concluded that the difference was due to the local angle at the interface. In the Al/film/Al structure, the local angle is controlled by the stiff foil layers and does not change when the modulus of the film is decreased. The observed increase in peel strength is attributed to greater local viscoelastic deformation (Φ). For the Al/coating structure, as the modulus of the coating was decreased, the local angle of pull also increased, concentrating more of the stress on the interface and counteracting the effect of greater Φ.

One final example is used to illustrate the concepts of fracture mechanics and the influence of factors beyond bond strength on peel strength. Suppose a person walks down the street on a hot summer day and steps on some old chewing gum. The gum is very difficult to remove from the shoe. It stretches as it is pulled. If the shoe is put in a freezer and the gum is allowed to cool down, it becomes easy to remove. The gum no longer stretches. The bond strength of the gum to the shoe is the same for the two cases. What has changed is the elongational properties of the gum. It is the total energy, not just the bond strength that determines how hard it is to remove the gum.

7.6 Modeling Heat Seal and Hot Tack

7.6.1 Heat Seal

De Gennes, Wool, and others have developed the theoretical framework for understanding diffusion and scaling of strength buildup at the interface as described in Section 7.5.3. Predictive modeling based on this framework, however, remains challenging [60]. For example, Wool gives a relationship for the penetration distance as a function of time and diffusion coefficient, but ambiguities regarding the value of the diffusion coefficient make this approach impractical. The reptation-based models are still lacking; while describing a power law dependence of the weld strength on time and MW, they are incomplete, failing for example to account for the thermal history. On the other hand, purely empirical-based models lack a scientific basis. Hybrid models, combining scientific and empirical modeling, is one approach, such as that employed by Ezekoye [60] for the weld strength of polymers. Here, two models by Moffitt [61–64] and Morris [46] based on fundamental considerations are highlighted. These show how, despite the limitations, modeling can provide useful insight into practical sealing applications.

Moffitt [61–64] develops a mathematical model for heat sealing of linear, semicrystalline polymers such as LLDPE based on reptation theory. The model includes transient heat transfer with phase change to accomplish amorphous contact, interfacial wetting kinetics, and chain interdiffusion via reptation. The kinetics of wetting is described by the model of Wool and O'Conner [65] and De Gennes reptation scaling concepts are used. The model does not include any contributions to the seal strength from cooling or crystallization.

The model predictions are compared with the experimental results reported by Stehling and Meka [28]. The model shows that interfacial melting, wetting, and chain interdiffusion are all important. The wetting and interdiffusion times are similar in magnitude; the inclusion of noninstantaneous wetting is needed to get good agreement with the experimental results. The model also shows good agreement with Stehling and Meka on the amount of melting (amorphous fraction) needed for seal initiation. Moffitt constructs curves of relative heat seal strength versus melt index (MI) for a given sealing dwell time and temperature. He finds the optimum MI is in the range of 2–10 g/10 min for dwell times of 0.5–1 s. This range of MIs is what is typically used in heat seal applications in industry.

Morris [46] develops a heat seal model for ionomers that includes heat transfer. Most laboratory experiments on seal performance are done under somewhat long dwell times using standard structures. Changing the design of the film structure or the dwell time can significantly alter the transfer of heat to the interface. This can have a substantial impact on plateau initiation temperature, T_{pi}. The thicker the structure or shorter the dwell time, the higher the value of T_{pi} since less heat gets transferred to the interface. An example is shown in Fig. 7.13. Here a thin (50-μm ionomer) and thick (84-μm paper/50-μm ionomer) film structure with the same ionomer sealant is compared. (The ionomer in this example is a sodium ionomer with an MI of 1.3 g/10 min.) The thin and thick structures have T_{pi}s of 110 and 135°C, respectively. Both values are considerably above the peak melting point of the ionomer (95°C).

Presumably, T_{pi} is directly related to the penetration distance of chain segment diffusion across the seal interface. If the penetration distance of one structure

can be related to T_{pi}, the T_{pi} for any other structure can be computed from heat transfer modeling. An obvious explanation for the difference between the curves in Fig. 7.13 is that it takes a longer time for heat to transfer through the thicker structure. This necessitates the use of higher seal bar temperatures to achieve equivalent molecular penetration during the short duration of the heat seal experiment. To determine if heat transfer considerations alone are sufficient to make predictive calculations, Morris uses a heat transfer model to compute the temperature of the interfaces as a function of time. The heat conduction equation simplifies to one dimension (in the direction perpendicular to the surface or across the thickness of the film) since the thickness is so much thinner than the lateral dimensions of the film. Several investigators have applied the solution of the one-dimensional heat conduction equation to the heat sealing process of single layer films [32,45,61]. Morris uses a finite difference technique. The model handles multiple layers by assuming constant heat flux at each interface. An enthalpy approach is used to take into account the latent heat of fusion as the polymer changes from solid to melt [70]. Initially the film is at room temperature. For boundary conditions, he assumes that one surface is at the seal bar temperature (T_{pi}) and the other surface is insulated (rubber bar). This computation is run for a sealing time of 0.5 s after which the boundary conditions are changed to reflect cooling in air (by using a convective heat transfer coefficient).

The results are given in Fig. 7.18. Here structure 1 (thin) has a bar temperature of 110°C and structure 2 (thick) has a bar temperature of 135°C. These are the plateau initiation temperatures from Fig. 7.13. If heat transfer considerations alone can be used to predict equal performance, the curves in Fig. 7.18 should be equivalent. The results show:

- During the heat-up portion of the sealing process, when the seal bars are in contact with the films, the interfacial temperatures are substantially different. The interface of the thin structure reaches its seal bar temperature (110°C) in 0.2 s, whereas the interface of the thick structure barely reaches 110°C (and never 135°C) during the 0.5 s of the sealing process.
- Cooling of the thick structure is much slower than cooling of the thin structure.
- If the whole process from heat-up to cooldown is considered, then the heat history of the interface may be equivalent. But this is difficult to determine from this calculation. A better way to quantify the equivalency of these two curves is needed.

These results suggest that the molecular chain segment penetration across the interface needs to be included in the model. Morris assumes the penetration can be modeled as Fickian diffusion in a semi-infinite slab:

$$W = 4\sqrt{Dt} \tag{7.12}$$

where W = penetration distance, D = diffusion coefficient, t = time.

The penetration distance is assumed to be proportional to the interfacial strength. In Section 7.5.3, it is found that the diffusion is not Fickian up until the reptation time and that penetration of chain segments is actually proportional to $t^{1/4}$. The fracture energy (G_a), however, scales as $t^{1/2}$ (Eq. (7.8)), and so the approach is valid.

Rather than computing a diffusion coefficient, Morris uses an approach originated by Register [66] for modeling hot tack (Section 7.6.3) involving the terminal relaxation time. The terminal relaxation time, t_d, is the time it takes a polymer chain to diffuse a distance characteristic of its own size in the melt. The characteristic size is the radius of gyration, R_g, the size of the coiled chain. Assuming a Fickian diffusion model, the penetration is related to the square root of the diffusion coefficient times the time (Eq. (7.12)), thus

$$R_g = 4\sqrt{Dt_d} \tag{7.13}$$

where R_g = radius of gyration or characteristic size of the coiled chain, D = center of mass diffusion coefficient, t_d = terminal relaxation time.

The terminal relaxation time can be determined from rheological measurements. It is related to the product of the recoverable compliance and zero shear viscosity:

$$t_d = J_e^0 \eta_0 \tag{7.14}$$

where J_e^0 = recoverable compliance (strain/stress) and η_0 = zero shear viscosity.

Vanhoorne and Register [67] and Tierney [56,68] measure the zero shear viscosity of several ionomers using a constant stress cone and plate rheometer

with shear rates ranging from 10^{-5} to 1 s^{-1}. The recoverable compliance is obtained from creep relaxation experiments on the cone and plate rheometer. They compute the terminal relaxation time and relate it to the compositional variables of the ionomer such as acid level, cation, and percent neutralization.

Combining Eqs. (7.12) and (7.13) yields an expression for the dimensionless penetration distance, W^*:

$$W^* = \frac{W}{R_g} = \sqrt{t/t_d}. \tag{7.15}$$

An Arrhenius equation similar to Eq. (7.9) is used to fit the temperature dependence of the terminal relaxation time:

$$t_d = A \exp\left[\frac{E_a}{R}\left(\frac{1}{T_i} - \frac{1}{408}\right)\right] \tag{7.16}$$

where t_d = terminal relaxation time, A = factor related to polymer chemistry and architecture, E_a = activation energy, R = ideal gas constant, T_i = temperature at the interface at increment time i.

The heat transfer model uses a finite difference algorithm where the time is divided into small increments for the purposes of the computation. At the end of each time increment the interface temperature is computed. This is fed into Eq. (7.16) to compute the incremental t_d. By summing over all past t_d, the average t_d over that time period is obtained:

$$\frac{1}{t_d^{avg}} = \frac{1}{n}\sum_{i=1}^{n}\frac{1}{t_d^i} \tag{7.17}$$

The dimensionless penetration distance becomes:

$$W^* = \sqrt{t\Big/t_d^{avg}} \tag{7.18}$$

Results of the W^* computation for the thin and thick structures at their respective T_{pi}s are given in Fig. 7.23. Both structures now have the same penetration as would be expected from the heat seal results. It is encouraging that model results using terminal relaxation times derived from independent measurements give excellent results when applied to this sealing application. Key learnings from the analysis include the following:

- The results suggest that W^* can be used as a parameter for predicting heat seal performance. As W^* increases, the seal strength should increase due to increasing chain bridging and entanglement at the interface. At some point the increase in strength levels off either because the interface has been erased or the solid state yield strength exceeds the tear strength. The penetration at this point is identified as the

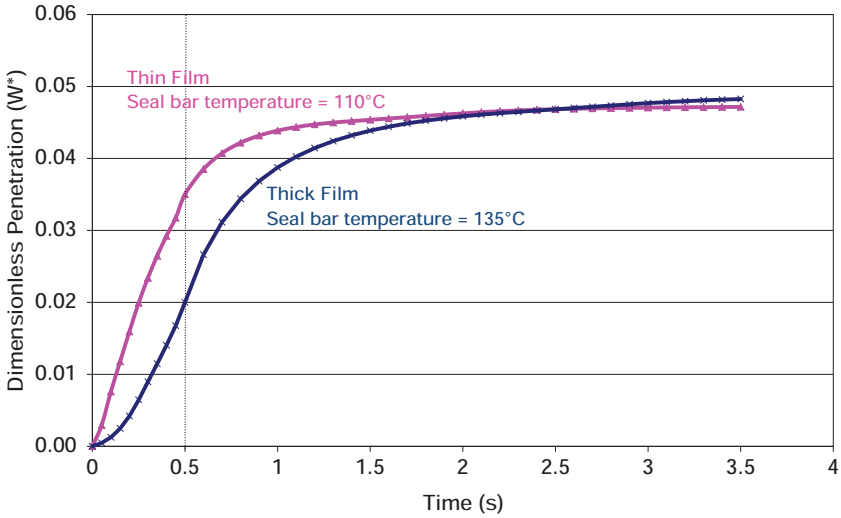


Figure 7.23 Model calculation of dimensionless penetration during heat sealing for two structures.
From Morris BA. Predicting the heat seal of ionomer films. J Plast Film Sheeting 2002;18:157–67.

critical dimensionless penetration, Wc^*, and is directly related to T_{pi}. Once Wc^* is known for a given sealant structure, the model can be used to predict whether similar structures of differing thickness, heat seal bar temperature, and dwell time will be on the seal strength plateau by comparing W^* with Wc^*.

- Both the heat up and cooldown phases of the process need to be included. During the heat up phase the thin structure reached about 70% of the ultimate penetration and the thick structure about 40%. A significant amount of penetration occurs during the cooling phase.
- Penetration of only a small fraction (around 5%) of the coiled size of the molecular chain (R_g) is needed for the ionomer to achieve maximum seal strength. The scaling laws described earlier suggest for PE to achieve maximum peel strength its chains need to diffuse a distance on the order of R_g. The ionic interactions in ionomers act over longer distances than the dispersive forces in PE, suggesting that less entanglement is necessary for the ionomers.
- The model has limitations. In particular, the penetration at temperatures near the melting point may not be accurately portrayed by the Arrhenius relationship given in Eq. (7.16). Also, the computed value of the penetration depends on the assumptions made in the heat transfer model. The ability to translate results from a lab experiment to a high-speed packaging line will depend on how accurately the heat seal conditions are portrayed.

Morris tests the model by comparing the results with laboratory heat seal measurements on two cast films of ionomer 63-μm and 102-μm thick. The films are heat sealed at dwell times ranging from 0.25 to 1.0 s (at 0.28 MPa pressure, 25-mm seal bar width, top bar heated only). OPET films of about 13-μm are placed on top of the films to protect the seal bar. The measured value of T_{pi} for each dwell time is plotted in Fig. 7.24 along with results from the model. The model predictions agree well with the data for both films, confirming the utility of the model. At long dwell times, thickness has little impact on T_{pi}. At short dwell times, thicker films require much higher seal bar temperatures to achieve the ultimate heat seal strength.

Morris also compares model predictions with the results of a trial run on a Doboy Super Mustang horizontal packaging line. Such lines package candy bars, crackers, cookies, baseball cards, and other items at speeds up to about 300 packages per minute. In the trial the quality of the seal at several seal bar

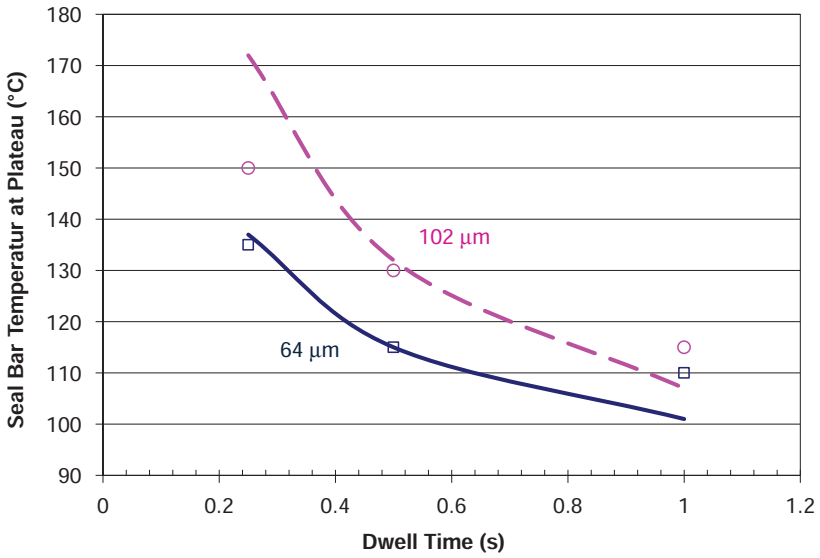


Figure 7.24 Comparison of experimental measurement and model prediction of heat seal plateau initiation temperature. Structure is 13-mm OPET/ionomer with two different thicknesses of ionomer film. *Symbols* are experimental data points and *solid lines* model results for $Wc^* = 0.081$.
From Morris BA. Predicting the heat seal of ionomer films. J Plast Film Sheeting 2002;18:157–67.

temperatures at line speeds ranging from 50 to 150 packages per minute is evaluated without packaging any product. The seal area on the front and back seals comprises 26-mm out of the total packaging length of 190-mm. Thus, the dwell time ranges from 0.168 to 0.056 s. The packaging structure is 13-μm OPET/25-μm Surlyn 1652, a zinc ionomer with an MI of 5 g/10 min.

In Fig. 7.25, the open circles represent weak seals and closed circles represent good seals. The modeling of laboratory heat seal data gives a value for Wc^* of 0.1. Using this value for Wc^* overpredicts the transition from good to bad seals as shown by the solid curve in Fig. 7.25. A better fit is found using a value of $Wc^* = 0.04$, suggesting either the temperature on the packaging line is reading too low or the heat seal plateau does not have to be reached in order to achieve good seals. Also, the slope of the transition curve is too shallow if it is assumed the seal cools in air, the standard assumption used in the model. It is likely that the seal area cools faster because the bottom of the film comes into contact with a cold surface after the heat seal has been made. Assuming a faster cooling rate achieves better agreement between the model and experimental results.

The results point to how laboratory heat seal experiments can help predict seal performance on high speed lines but at the same time underscore several limitations. These include the proper selection of heat transfer parameters and what constitutes a good heat seal (plateau strength or otherwise). In practice, data from an existing film structure run on the high speed line can be used to determine Wc^* and the heat transfer coefficients, rather than relying on laboratory data. Once these parameters are determined for a given line, the model should be useful for predicting the performance of other structures and line speeds on that line.

7.6.2 Hot Tack

Register [66], in some unpublished work supported by DuPont, develops a model for hot tack of ionomers. There are two fundamental issues for optimizing hot tack performance:

- What is the ultimate hot tack (at long contact times at a given seal temperature after interdiffusion has completely erased the interface)? This should be related to bulk elongational viscosity.

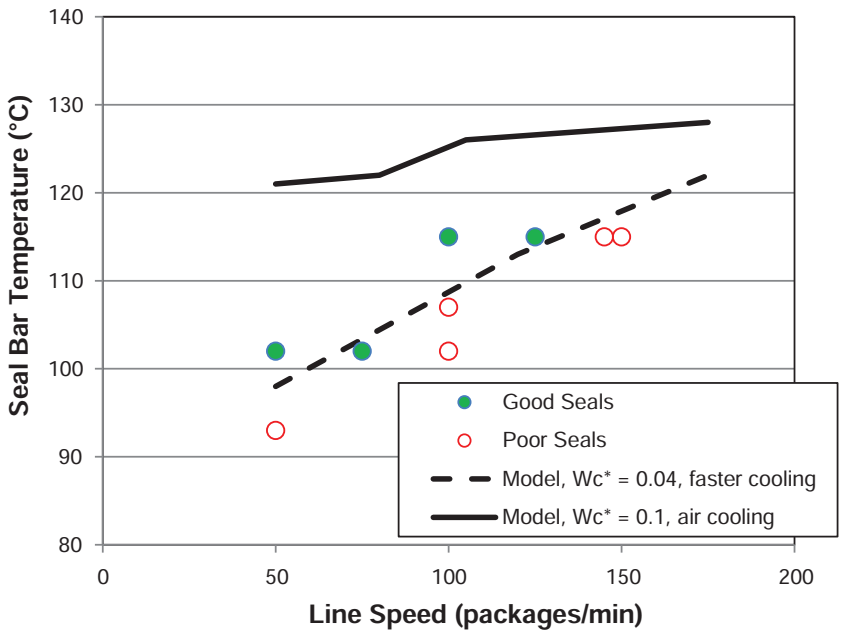


Figure 7.25 Results of horizontal form fill seal trial. *Open circles* represent experimental results of poor seals, *closed circles* represent good seals. *Solid lines* are model predictions. Packaging structure is 13-μm OPET/25-μm ionomer 2.

Reproduced with permission from Morris BA. Predicting the heat seal of ionomer films. J Plast Film Sheeting 2002;18:157–67.

- How long does it take to develop this ultimate hot tack at a given sealing temperature? This should relate to polymer diffusivity, D.

The goal of the work was to establish what rheological properties will yield maximum hot tack within the constraints of the process (sealing temperature (T_s) and dwell or contact time (t_c)).

J. Paul [69] and J.R. de Garavilla at DuPont prepared blown films of a series of ionomers of the same base resin (MW and acid level) at different neutralization levels. The films are laminated to paper and the hot tack measured over a range of 1−15 s and 120−220°C. Register plots hot tack force versus contact time for several temperatures, as shown in Fig. 7.26. The plateau hot tack strength is the "ultimate hot tack force." The measurement process exerts a baseline force, which is subtracted out, yielding the net ultimate hot tack (NUHT). This is what is used in the analysis.

An Arrhenius plot of NUHT versus 1/T gives unique curves for each ionomer. The slope is related to the activation energy and differs from the activation energy for shear flow (Eq. (5.48)) by more than a factor of two: 45 versus 80 kJ/mol for zinc and 35 versus 100 kJ/mol for sodium ionomers for hot tack versus shear flow, respectively. This means that with increasing seal temperatures, ionomers retain their hot tack better than they retain their shear viscosity. The difference is likely due to differences in deformation. It is suggested that NUHT may correlate better with elongational viscosity or melt strength.

Register creates a master hot tack curve by scaling the hot tack at a given temperature by NUHT and t_c by t_d (here t_d is the terminal relaxation time, the time for the polymer to diffuse one random coil distance). The determination of t_d from rheological measurements is described in Section 7.6.1. One such master curve is shown in Fig. 7.27. Note that the x-axis is related to W^{*2} per Eq. (7.18). The data are expected to collapse onto a single sigmoidal shaped curve with the center at $t_c/t_d < 1$ since ionomers do not need to diffuse a whole coil size to erase the seal interface. Indeed, the data show t_c/t_d is centered around 0.12 for this particular grade of ionomer. The data also show that 80% of the hot tack develops in a narrow range of t_c/t_d of less than a decade (8× to go from 10% to 90% of the ultimate hot tack). Since the midpoint is around 0.12, 80% of the NUHT is achieved at $t_c/t_d = 0.3$. If $t_c \ll 0.3t_d$, then no hot tack develops. If $t_c \gg 0.3t_d$, all the hot tack develops but the value is too low since the viscosity or melt strength is too low.

From a polymer design perspective, the above relationship can be reversed to tailor the resin for a given sealing process. The dwell or contact time is dictated by the packaging line speed. Thus, to achieve good hot tack, the rheology of the ionomer should be adjusted so that $t_d = 3t_c$ to $5t_c$. For

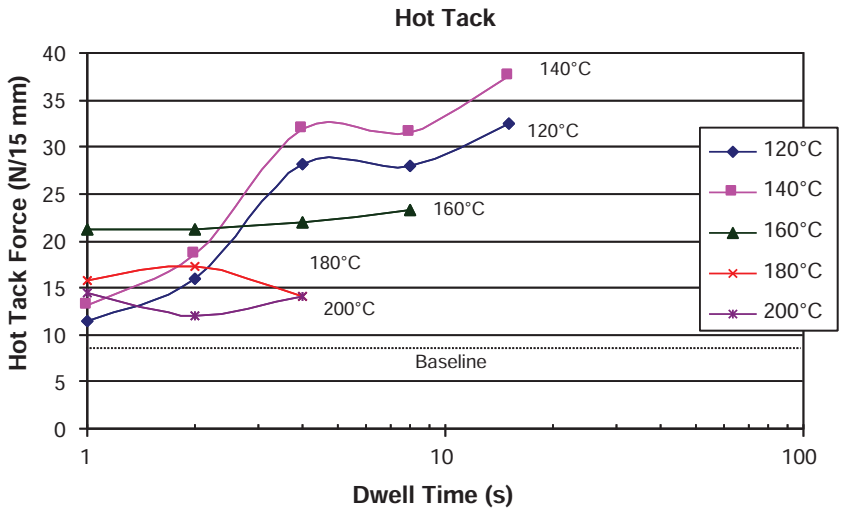


Figure 7.26 Hot tack force as a function of seal contact time (dwell time) and seal bar temperature for one ionomer.

Reproduced with permission from Register RA. Optimizing hot tack in packaging sealing operations. 1999. Presentation to DuPont. E. I. du Pont de Nemours and Company.

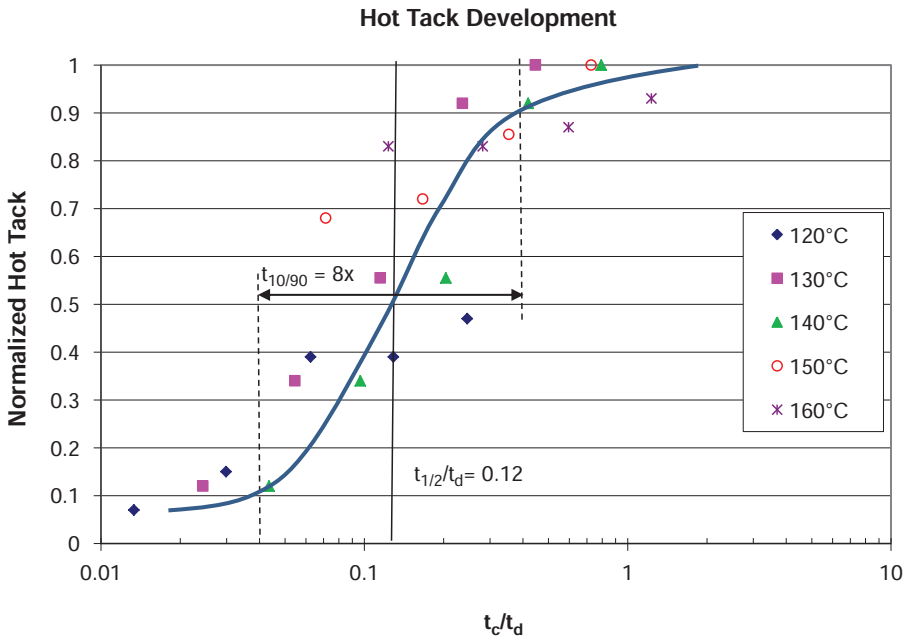


Figure 7.27 Master hot tack curve.
Reproduced with permission from Register RA. Optimizing hot tack in packaging sealing operations, 1999. Presentation to DuPont. E. I. du Pont de Nemours and Company.

ionomers, this can be accomplished by changing the amount of neutralization of the acid groups. Register compares his model's prediction for peak hot tack temperature at a given dwell time with data on grades of ionomer used commercially for heat seal applications. The model shows good agreement.

Moffitt uses his model to determine a design range for the melt index of LLDPE for optimum heat seal at a given dwell time. The same can be done with Register's hot tack model. As shown in Eq. (7.14), t_d is related to the zero shear viscosity, which in turn generally correlates with the inverse of the melt index. The result predicts that ionomers with MIs in the range of 1−10 g/10 min have good hot tack, which is in agreement with Moffitt's study of LLDPE and what is used commercially. While these models may merely validate what has long been known in the industry about suitable sealants, they provide the theoretical basis for this performance. Such scientific understanding may allow the development of other chemistries with good heat seal performance.

In some unpublished work, Morris extends the hot tack model of Register by coupling it with his heat transfer model. This allows for the prediction of the whole hot tack curve. Results of the model compared with experimental measurements by J.R. de Garavilla at DuPont are shown in Figs. 7.28 and 7.29 at two different sealing dwell times. The model correctly predicts the shape of the curve but has difficulty in predicting the onset of hot tack at short dwell times.

The model can be used to gain insight on the effect of delay time on hot tack of ionomers. Fig. 7.30 shows that the influence of delay time is insignificant at long dwell times with good agreement between experiment and model prediction. At short dwell times, a substantial increase in hot tack is measured as the delay time is increased. The model correctly captures this difference but fails to predict the onset of hot tack. Nevertheless, the model can be used to discern the underlying mechanism for higher hot tack at longer delay times at short dwell times. Fig. 7.31 shows the model predictions for the interfacial temperature and molecular penetration (W^*) profiles during the heat seal and subsequent delay time of the hot tack experiment. Many have hypothesized that cooling of the seal area is responsible for the increased hot tack at long delay times. These results show that the cooling is insufficient to significantly affect the strength of the interface; the temperature only decreases by 9°C and is well above the freezing point of the ionomer. Also, ionomers do not undergo strain-induced crystallization at these temperatures. Furthermore, the model reveals that substantial

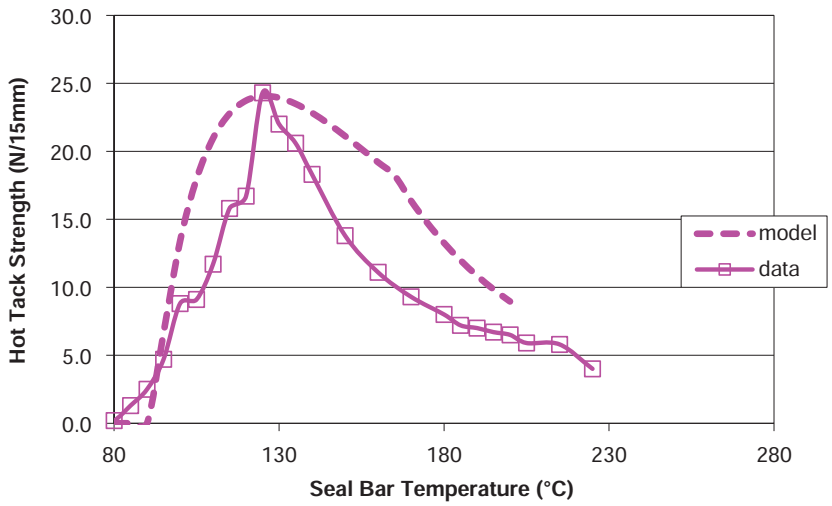


Figure 7.28 Comparison of hot tack model with experimental data for an ionomer film at long seal dwell time. 3.3-mil kraft paper/2-mil Ionomer, 3-s dwell.
Reproduced with permission from E. I. du Pont de Nemours and Company.

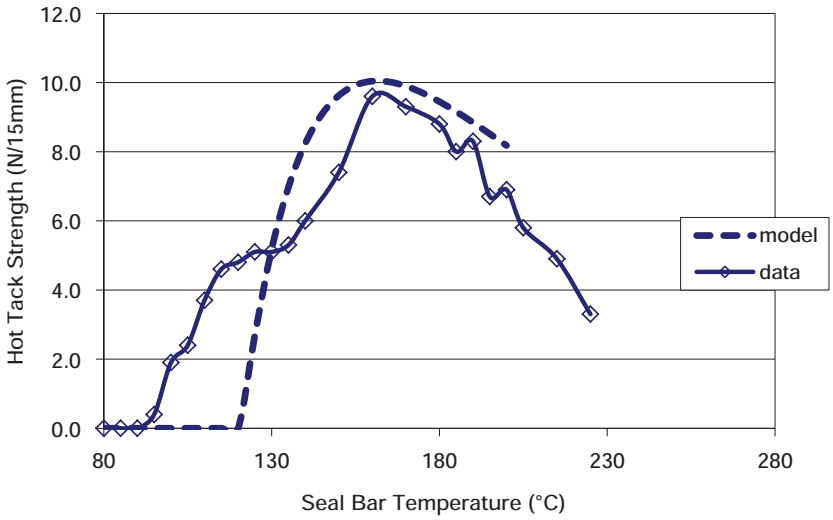


Figure 7.29 Comparison of hot tack model with experimental data for an ionomer film at short dwell time. 3.3-mil kraft paper/2-mil Ionomer, 0.5-s dwell.
Reproduced with permission from E. I. du Pont de Nemours and Company.

molecular penetration occurs during the delay. This is likely the source of the increased hot tack. At longer dwell times, sufficient penetration occurs during the heat seal so that the influence of delay time is minimal.

Recall in Section 7.5.5 that mPE plastomers undergo strain-induced crystallization near their melting point. A 9°C reduction in interfacial temperature, therefore, may have a substantial impact on hot tack performance for these materials. It is likely both cooling and penetration influence the impact of delay time on the hot tack performance of mPE.

7.6.3 Squeeze Flow

In Section 7.3.1 the concept of the heat seal temperature window is introduced. Excessive flow of the sealant may occur at the high end of the temperature range. Morris and Scherer [71,72] model

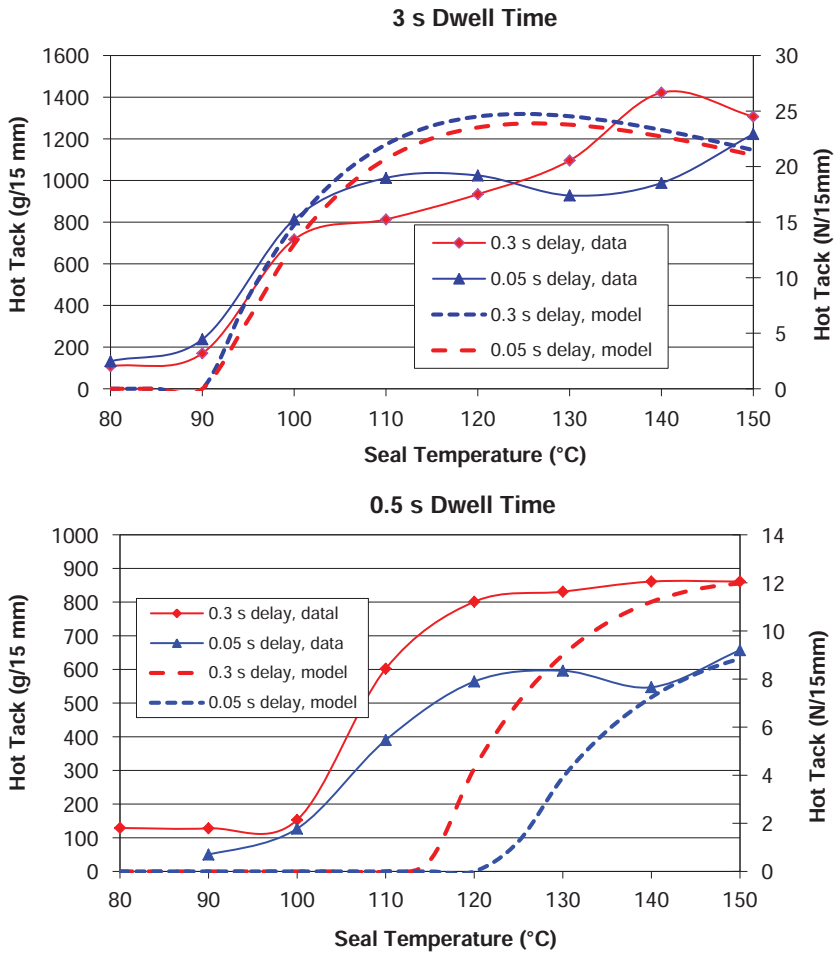


Figure 7.30 Effect of delay time on hot tack of an ionomer. 3.3-mil kraft paper/2-mil Ionomer. Top: 3 s dwell time. Bottom: 0.5 s dwell time.
Reproduced with permission from E. I. du Pont de Nemours and Company.

this behavior by adapting an approach originally developed for predicting the squeeze flow between flat plates found in the rheology literature [73]. Their work is summarized here.

7.6.3.1 Model Development

The film area under the sealing bars can be represented by two parallel flat plates under a constant applied force (Fig. 7.32). A rectangular coordinate system is defined, originating at the center point between the plates with z in the direction of plate separation, x in the width direction, and y in the length direction. The following assumptions are made:

- The initial film thickness is much less than the seal area half width ($h_o \ll w$), so the flow is mostly in the x direction.
- Seal length is much greater than the width ($L \gg 2w$), so the flow in the y direction is ignored.
- Inertia and gravity effects are negligible.
- Flow is quasi steady state.
- Flow is Newtonian.
- There is no slip at the surface of the plates.
- The process is isothermal.

Details of the model derivation are found in Morris and Scherer [71]. The equations of continuity and motion are solved with the following results:

$$v_x = \frac{3}{2}\frac{\left(-\dot{h}\right)}{h}x\left(1-\left(\frac{z}{h}\right)^2\right) \qquad (7.19)$$

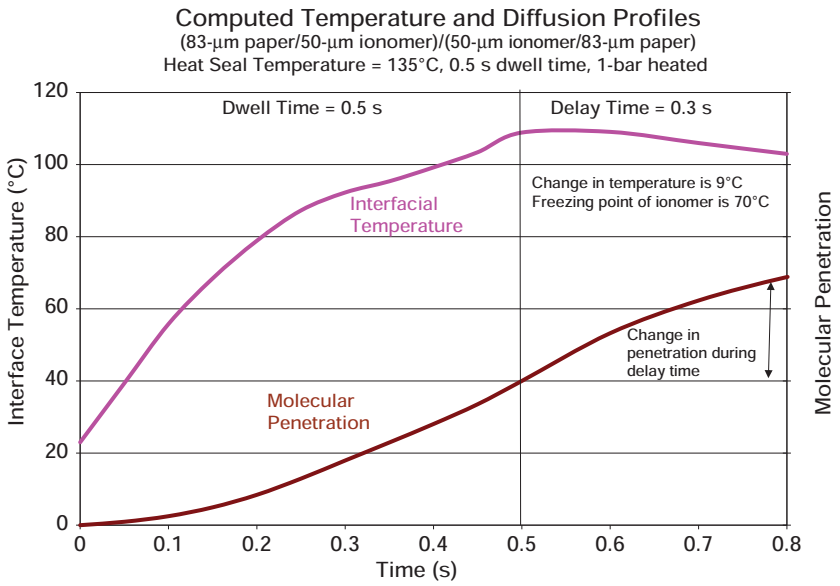


Figure 7.31 Model prediction of temperature and penetration profiles of an ionomer sealant.
Reproduced with permission from E. I. du Pont de Nemours and Company.

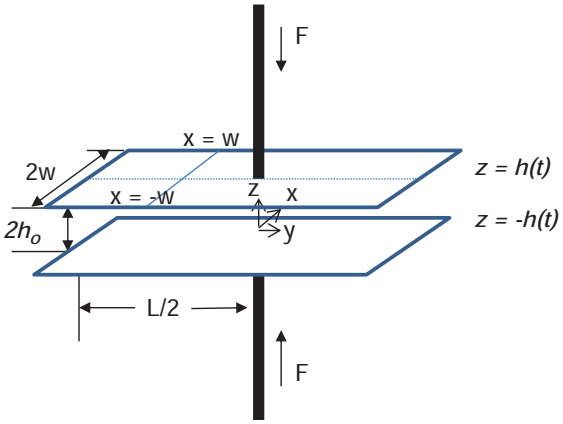


Figure 7.32 Squeeze flow between flat plates.
Reproduced with permission from Morris BA, Scherer JM. Squeeze-out of sealant during hot bar sealing: modeling insights. In: SPE ANTEC conference, 2013.

$$v_z = \frac{3}{2}\dot{h}\left(\frac{z}{h} - \frac{1}{3}\left(\frac{z}{h}\right)^3\right) \tag{7.20}$$

$$p - p_a = \frac{3}{2}\frac{\left(-\dot{h}\right)}{h^3}\mu w^2\left(1 - \left(\frac{x}{w}\right)^2\right). \tag{7.21}$$

where v_x = velocity in x direction, v_z = velocity in z direction, p = pressure, μ = viscosity, h = half distance between moving plates, w = half width of the plates, p_a = atmosphere pressure.

The change in separation between the plates is found to be [71]

$$\frac{1}{h^2} - \frac{1}{h_o^2} = \frac{2Pt}{w^2\mu} \tag{7.22}$$

where h_0 = initial half distance between the plates and $P = F/2wL$. This is the key result that is used to model squeeze-out during hot bar sealing.

An expression equivalent to Eq. (7.22) for circular disks is [73]

$$\frac{1}{h^2} - \frac{1}{h_o^2} = \frac{16Pt}{3R^2\mu} \tag{7.23}$$

where R = radius of the circular disk; $P = F/\pi R^2$.

This is a form of Stephan's equation and may be useful for analyzing the squeeze flow near the long edge of the seal bar (in the rectangular plate analysis the flow is assumed to be far away from the length edge of the bar). Bird, Armstrong, and Hassager [73] also derive expressions for squeezing flow between disks for power law fluids (Scott's equation) and for fluids following the Criminale–Ericksen–Filbey constitutive equation.

The viscosity must be known to use the model. In the derivation, the viscosity is assumed to be independent of shear rate (Newtonian), yet the viscosity of most polymers decreases with increasing

shear rate. This is accounted for by choosing a representative viscosity at a shear rate characteristic of the sealing process.

Morris and Scherer [71] derive the following expression for average shear rate near the edge of the plates:

$$\dot{\gamma}_{\text{avg}} = \frac{3Ph}{2w\mu}(x = \pm w, w \gg h). \tag{7.24}$$

Table 7.4 gives some typical values for the variables and their effect on the average shear rate given by Eq. (7.24).

From a mass balance, the amount of polymer squeezed out from the plates is equal to the negative of the change in separation distance. The percent squeeze-out is defined as the volume of polymer squeezed out from the seal area divided by the total volume of polymer:

$$\%\ \text{Squeeze} - \text{Out} = 100(h_{\text{o}} - h)/h_o. \tag{7.25}$$

7.6.3.2 Experimental Results

Morris and Scherer conduct experiments to compare with the model predictions. Films with the structure (PA-tie-PA-EVOH-PA-tie-sealant) with (25/8/13/8/13/8/25 vol%) and total thickness 100-μm are produced on a nine-layer blown film line. Two sealants described in Table 7.5 are used. The adjacent tie layer is Bynel 41E687, an anhydride-modified LLDPE-based resin with an MI of 1.7 g/10 min and manufactured by DuPont.

The sealants, an ionomer and a metallocene polyethylene plastomer, are chosen to study the effect of molecular architecture on performance. Ionomers contain long chain branches (LCB) and ionic interactions. Plastomers are essentially linear polymers with a nearly uniform molecular weight and comonomer distribution.

The viscosity of the sealant resins is measured using a TA Instruments ARES LS2 controlled strain parallel plate rheometer. The frequency is varied from 0.01 to 100 radians per second at 130, 150, and 170°C. Results are found to follow time temperature superposition. The master curve is fit to a Carreau–Yasuda model:

$$\eta_{\text{r}} = \frac{\eta_{\text{o}}}{\left[1 + (\lambda\dot{\gamma}_{\text{r}})^{\text{a}}\right]^{(1-n)/\text{a}}} \tag{7.26}$$

where η_{r} = reduced viscosity ($=b_{\text{T}}\eta/a_{\text{T}}$); η = viscosity; a_{T} = horizontal shift factor; b_{T} = vertical shift factor; $\dot{\gamma}_{\text{r}}$ = reduced shear rate$(a_{\text{T}}\dot{\gamma})$; $\dot{\gamma}$ = shear rate; η_{o}, λ, n, a = model parameters.

Table 7.4 Typical Shear Rate Values Near the Edge of the Seal Bar as Computed by Morris and Scherer [71]

P (Pa)	h_{o} (mm)	*h* (mm)	Squeeze Out (%)	*w* (mm)	*t* (s)	Viscosity (Pa-s)	Shear Rate (s^{-1})
275,000	0.025	0.025	0	6.35	1	20,000	0.08
275,000	0.025	0.025	0.55	6.35	1	2000	0.81
620,000	0.025	0.020	21.5	1.25	1	2000	7.5

Table 7.5 Description of Sealant Polymers Used in Squeeze Flow Study

Resin	Grade	Manufacturer	Manufacturing Process	Density (g/cc)	MI (g/10 min)
Ionomer	Surlyn 1601	DuPont	Free radical	0.95	1.3
Plastomer	Affinity PL1881G	Dow	Single site catalyst	0.906	1

Reproduced with permission from Morris BA, Scherer JM. Preventing squeeze-out of sealant during hot bar sealing: modeling and experimental insights. In: SPE ANTEC conference, 2014, p. 1452–9.

Table 7.6 Carreau–Yasuda Rheology Model Parameters for the Two Sealant Polymers Used in the Squeeze-Out Study

Parameter	Units	Ionomer	Plastomer
η_o	Pa-s	774,000	37,700
λ	S	4.339	6.895
n		0.419	0.589
a		0.530	0.977
T_o	K	423.15	423.15
E_a	kJ/mol	98	59
E_b	kJ/mol	5.87	10.13

The shift factors follow an Arrhenius relationship:

$$a_T = \exp\left[\frac{E_a}{R}\left(\frac{1}{T} - \frac{1}{T_o}\right)\right] \tag{7.27}$$

$$b_T = \exp\left[\frac{E_b}{R}\left(\frac{1}{T} - \frac{1}{T_o}\right)\right] \tag{7.28}$$

where E_a and E_b = activation energies, T = temperature (K), T_o = reference temperature (K).

The rheology model parameters for the sealants are given in Table 7.6. Fig. 7.33 shows the viscosity versus shear rate data. The shape and temperature dependence of the viscosity curves differ due to the differences in molecular architecture and chemistry. The ionomer sealant has a higher low shear rate viscosity, which decreases substantially as the shear rate is increased. This shear thinning behavior is due to the presence of LCB and ionic interactions. The viscosity decreases more rapidly with an increase in temperature than the linear plastomer, as indicated by the ionomers higher E_a. Consequently, as the temperature is increased, the low shear rate viscosity of the ionomer and plastomer becomes closer in value. At even higher temperatures, the low shear rate viscosity of the ionomer crosses over that of the plastomer and is the lower viscosity polymer.

Heat seals are made on a Sentinel heat sealer at several temperatures. Pressure, dwell time, and seal bar width are held constant at 0.345 MPa (50 psi), 3 s, and 12.7 mm (0.5-in.), respectively. Both top and bottom seal bars are heated. The sealed samples are allowed to cool to room temperature, cross sectioned, and examined under an optical microscope.

The experimental procedure involves cutting a cross section from the seal edge of each sample. Next the samples, with a polyester slip sheet placed between the films to allow for a more defined squeeze-out area, are placed into the holder of the

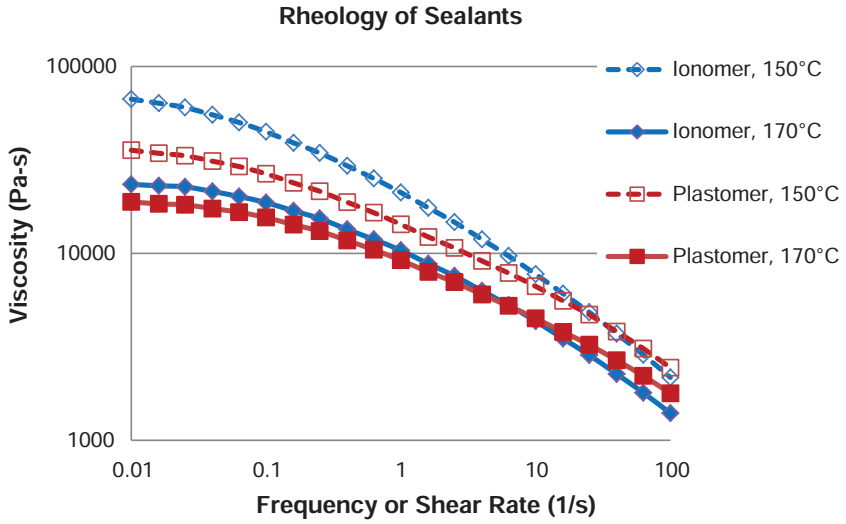


Figure 7.33 Complex viscosity of sealant resins as measured by a parallel plate rheometer.
Reproduced with permission from Morris BA, Scherer JM. Preventing squeeze-out of sealant during hot bar sealing: modeling and experimental insights. In: SPE ANTEC conference, 2014, p. 1452–9.

microscope and viewed at 40–63X magnification. Pictures and measurements of the squeeze widths are taken under the microscope. An example of severe squeeze-out from the edge of the seal area is shown in Fig. 7.34. The darkest layer is EVOH and the two dark layers next to the EVOH are PA6. The region between the dark layers is the tie and sealant.

Calculated percentage squeeze-out results from the microscopy results are given in Table 7.7 and plotted in Fig. 7.35. They show the ionomer having very low squeeze-out until around 200°C. This is consistent with the model predictions discussed below. The plastomer has a higher amount of squeeze-out until the ionomer crosses over at around 200°C.

Table 7.7 Percentage of Sealant Squeeze-Out From Experimental Results. Seal Conditions: 0.345 MPa, 3 s Dwell, and 12.7 mm bar Width, Two-Side Heated Seal Bars

Seal	Squeeze-Out	
Temperature (°C)	Plastomer	Ionomer
121	6%	7%
149	12%	7%
177	10%	6%
204	16%	33%

Reproduced with permission from Morris BA, Scherer JM. Squeeze-out of sealant during hot bar sealing: modeling insights. In: SPE ANTEC conference, 2013.

7.6.3.3 Model Results

Eq. (7.22) is used to explore the effect of heat seal parameters and sealant rheology on squeeze-out. The film structure used in the experiments is used as the basis, where the initial separation distance, h_o, is taken to be the thickness of the sealant and adjacent tie resin. The next layer in a PA layer is assumed to not melt or flow during the heat seal process since it has a much higher melting point than the sealing temperature.

To use Eq. (7.22) some of the parameters must be defined with respect to the experiment. The values for P and w are straightforward: the seal bar pressure and half width of the seal bar, respectively. The time parameter, t, is taken as the sealing process dwell time. As is discussed in Section 7.6.3.4, there is a time lag for the temperature of the sealant to reach the bar temperature. The time lag will depend on the film thickness and whether one or both bars are heated. The time lag can be predicted with standard heat transfer models [32,45,46] but is ignored in these calculations.

Eqs. (7.26)–(7.28) are used to predict the viscosity of the fluid. For simplicity the rheology of the tie resin is ignored and only the viscosity of the

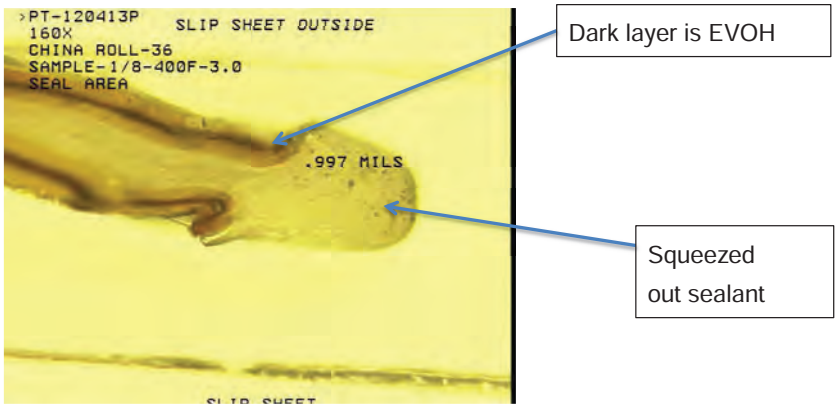


Figure 7.34 Photo of squeeze-out of sealant taken from an optical microscope. Seal conditions are 204°C seal bar temperature, 3 s dwell, 0.345 MPa (50 psi) bar pressure, 3.2 mm bar width.
Reproduced with permission from Morris BA, Scherer JM. Squeeze-out of sealant during hot bar sealing: modeling insights. In: SPE ANTEC conference, 2013.

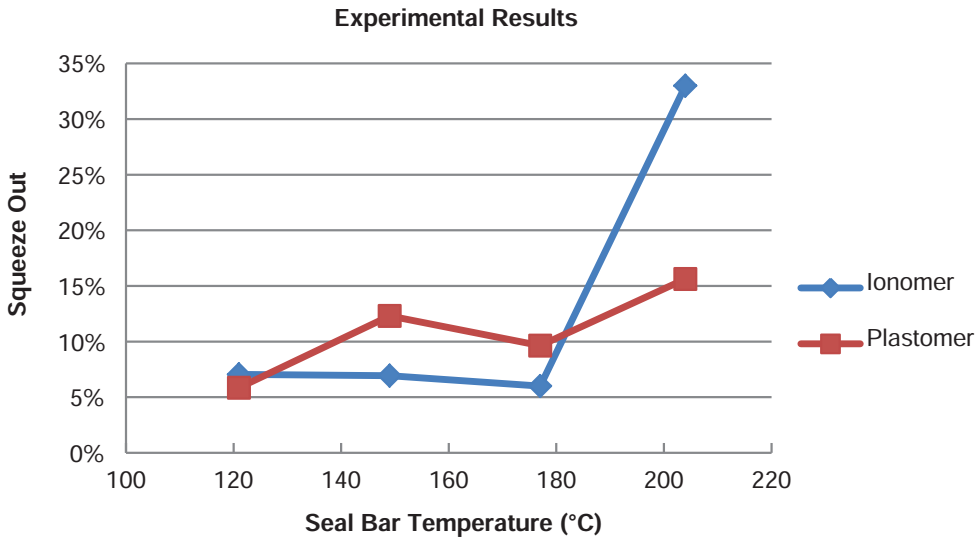


Figure 7.35 Experimental results of squeeze-out plotted versus seal bar temperature.
Reproduced with permission from Morris BA, Scherer JM. Squeeze-out of sealant during hot bar sealing: modeling insights. In: SPE ANTEC conference, 2013.

sealant is used in the calculations. Given that the thickness of the sealant layer is typically much larger than the tie layer, this is thought to be a good assumption.

The viscosity is a function of temperature and shear rate for a given sealant. The temperature is assumed to be the seal bar temperature (subject to the time lag limitation described earlier). The average shear rate at the edge of the seal bar is used for the shear rate (Eq. (7.24)). Eq. (7.24) shows that the shear rate is a function of the final separation distance, h, being computed. An iterative process is used. An initial value for the shear rate is assumed (typically 1 s^{-1}), the viscosity computed using the rheology model for the sealant (Eqs. (7.26)–(7.28)), h computed from Eq. (7.22), and the average shear rate computed with Eq. (7.24). This value for the shear rate is then compared with the assumed shear rate. If they do not agree, the newly computed value for the shear rate is used to repeat the calculation. Usually the two shear rates agree after three iterations. Typical shear rates range from about 0.01 to 10 s^{-1}, depending on the amount of squeeze-out.

A factor analysis is shown in Figs. 7.36–7.40 for the ionomer sealant, where each of the input parameters to Eq. (7.22) is varied one at a time. The results show the following:

- Squeeze-out increases almost linearly with increasing pressure (Fig. 7.36).
- As expected, squeeze-out increases nearly linearly with dwell time (Fig. 7.37). Some nonlinearly is introduced due to the change in shear rate and its effect on the viscosity.
- As seal temperature increases (Fig. 7.38), the amount of squeeze-out increases exponentially. This is due to the exponential decrease in viscosity with increasing temperature (Eqs. (7.27) and (7.28)).
- As the seal bar width increases, squeeze-out decreases (Fig. 7.39); more squeeze-out is expected in seal designs involving thin serrations, which can concentrate the force on the seal.
- As sealant thickness (h_o) is increased, squeeze-out increases (Fig. 7.40).

Fig. 7.41 highlights the effect of the sealant type on squeeze-out. The sealant type has the greatest impact on the temperature dependence of the squeeze-out due to the differences in rheology (Fig. 7.33). The ionomer has the least amount of squeeze-out at low sealing temperatures, where it is most often used. This is consistent with its very high viscosity at low shear rates at these

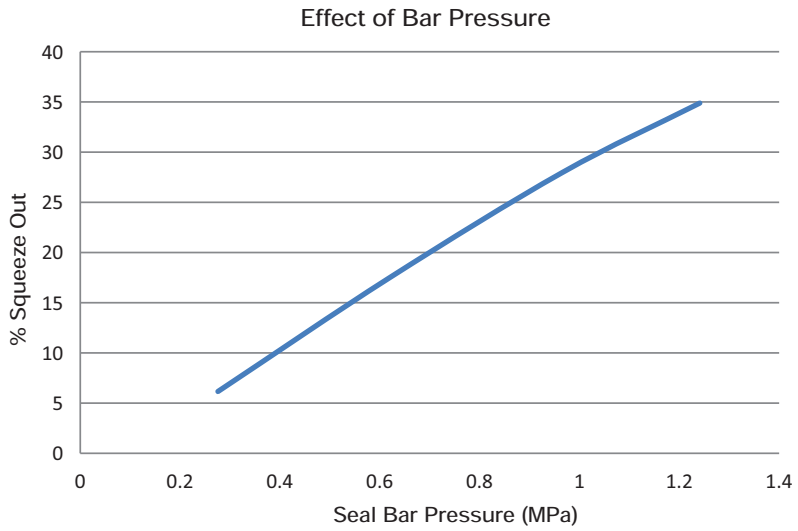


Figure 7.36 Model prediction (Eq. (7.22)) of percentage squeeze-out of an ionomer as a function of sealing pressure. Seal temperature = 175°C, bar width ($2w$) = 2.5 mm, dwell time = 1 s, sealant thickness = 0.05 mm.
Reprinted with permission from Morris BA, Scherer JM. Preventing squeeze-out of sealant during hot bar sealing: modeling and experimental insights. In: SPE ANTEC conference, 2014, p. 1452–9.

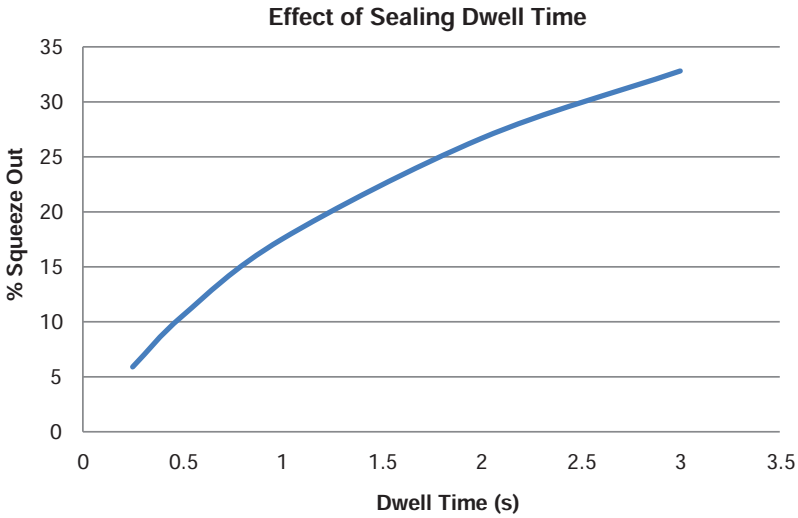


Figure 7.37 Model prediction (Eq. (7.22)) of percentage squeeze-out of an ionomer sealant as a function of sealing dwell time. Seal temperature = 175°C, bar width ($2w$) = 2.5 mm, seal bar pressure = 0.6 MPa, sealant thickness = 0.05 mm.
Reprinted with permission from Morris BA, Scherer JM. Preventing squeeze-out of sealant during hot bar sealing: modeling and experimental insights. In: SPE ANTEC conference, 2014, p. 1452–9.

temperatures. The plastomer also has low squeeze-out, although not as low as the ionomer. The amount of squeeze-out of the ionomer increases with temperature faster than the plastomer, so that at about 170°C the two curves crossover. This again is consistent with the higher activation energy (Ea) of the ionomer.

7.6.3.4 Insights and Limitations

The model parameters used to construct Fig. 7.41 were chosen to simulate the experimental conditions in Fig. 7.35. Comparing the two figures, the model correctly predicts the experimental trends. In both cases, the ionomer has lower squeeze-out than the

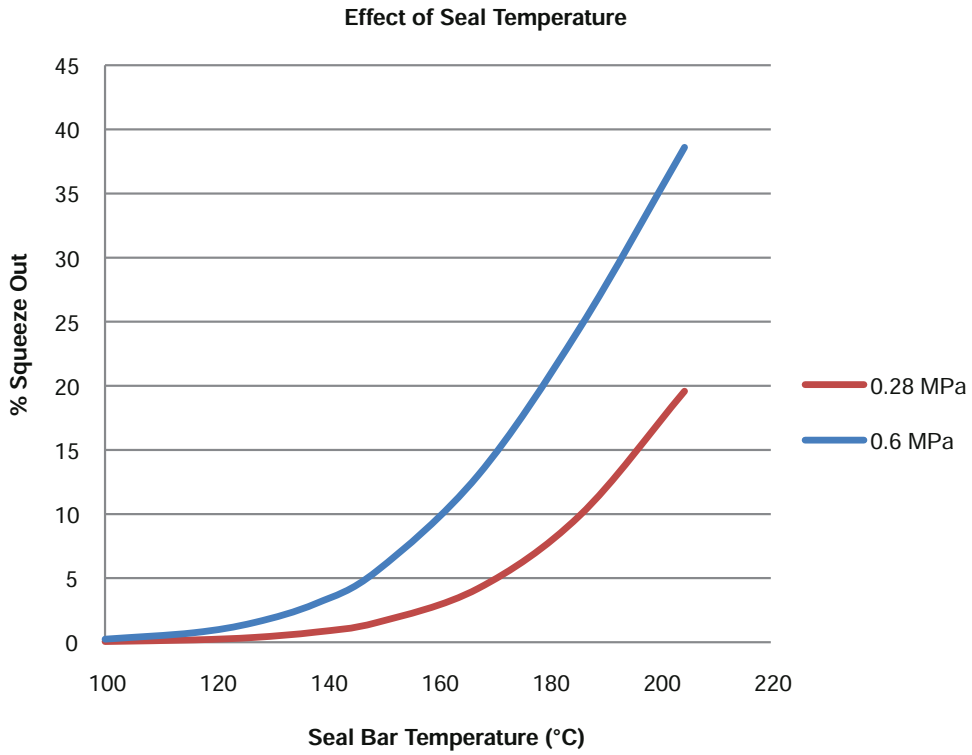


Figure 7.38 Model prediction (Eq. (7.22)) of percentage squeeze-out of an ionomer sealant as a function of sealing temperature at two sealing bar pressures. Sealing dwell time = 1 s, bar width ($2w$) = 2.5 mm, sealant thickness = 0.05 mm.

Reprinted with permission from Morris BA, Scherer JM. Preventing squeeze-out of sealant during hot bar sealing: modeling and experimental insights. In: SPE ANTEC conference, 2014, p. 1452–9.

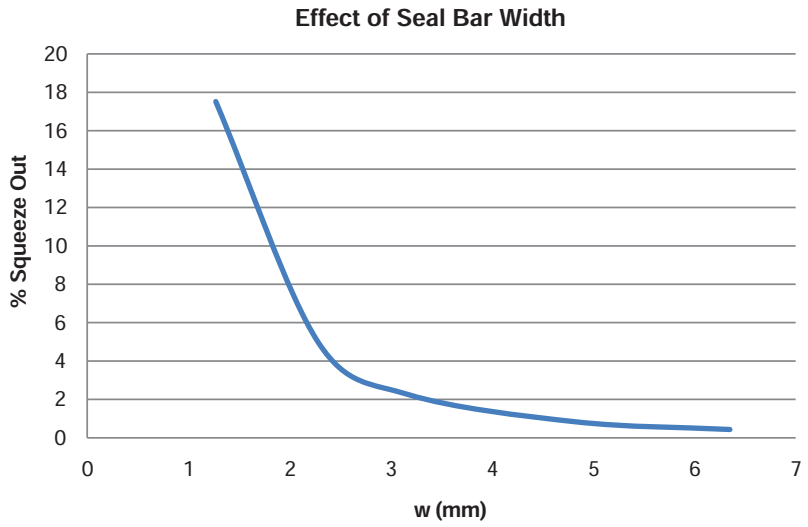


Figure 7.39 Model prediction (Eq. (7.22)) of percentage squeeze-out of an ionomer sealant as a function of sealing bar half width (w). Seal temperature = 175°C, seal bar pressure = 0.6 MPa, dealing dwell time = 1 s, sealant thickness = 0.05 mm.

Reprinted with permission from Morris BA, Scherer JM. Preventing squeeze-out of sealant during hot bar sealing: modeling and experimental insights. In: SPE ANTEC conference, 2014, p. 1452–9.

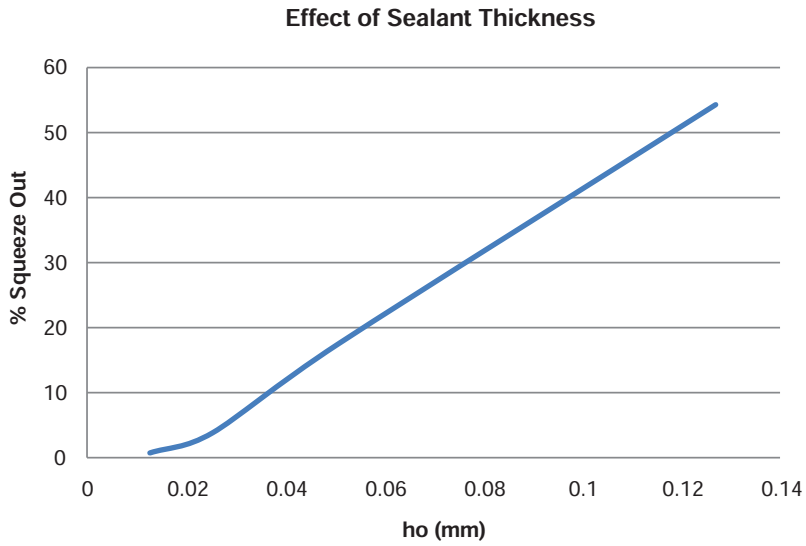


Figure 7.40 Model prediction (Eq. (7.22)) of percentage squeeze-out of an ionomer sealant as a function of initial sealant thickness (h_o). Seal temperature = 175°C, seal bar pressure = 0.6 MPa, dealing dwell time = 1 s, seal bar width ($2w$) = 2.5 mm.
Reprinted with permission from Morris BA, Scherer JM. Preventing squeeze-out of sealant during hot bar sealing: modeling and experimental insights. In: SPE ANTEC conference, 2014, p. 1452–9.

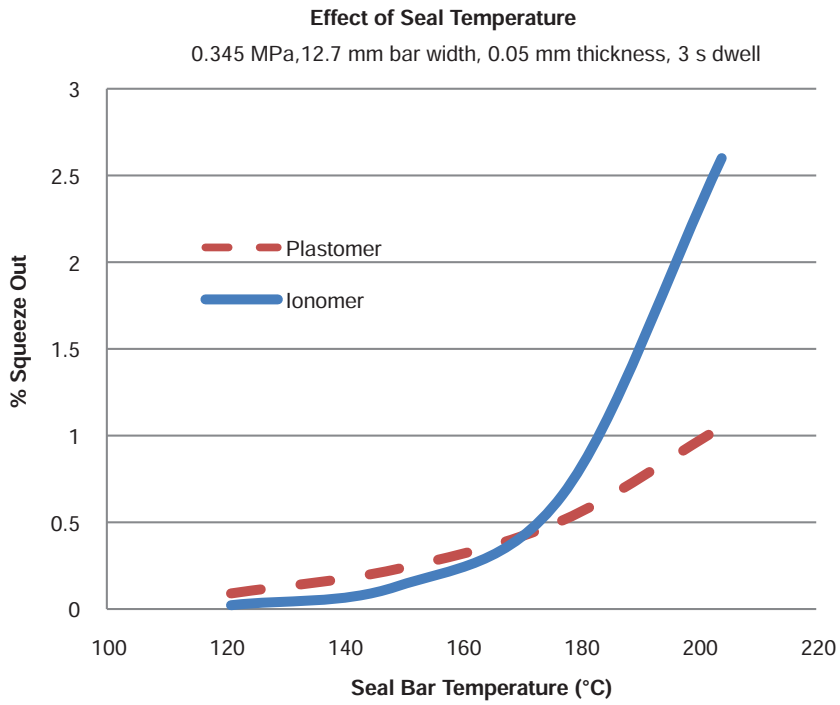


Figure 7.41 Model prediction (Eq. (7.22)) of percentage squeeze-out of different sealants as a function of seal bar temperature. Sealing dwell time = 3 s, bar width ($2w$) = 12.7 mm, sealant thickness = 0.05 mm.
Reprinted with permission from Morris BA, Scherer JM. Preventing squeeze-out of sealant during hot bar sealing: modeling and experimental insights. In: SPE ANTEC conference, 2014, p. 1452–9.

plastomer, despite having a higher MI, until the temperature reaches 170–200°C. At that point the squeeze-out of the ionomer begins to take off.

While the model predicts the correct trends, the actual values differ by about an order of magnitude. More work needs to be done to bring the model predictions in line with the experimental observations. Several factors may be involved, including the following:

- Possible errors in the experimental technique and measurements.
- Non-Newtonian flow effects. The model assumes Newtonian flow and quasi steady state. At the low shear rates characteristic of the heat seal process, many polymers are near the Newtonian plateau region of the viscosity versus shear rate curve. For these polymers, the Newtonian assumption may be a good representation. Other polymers, such as the ionomer used in this analysis, undergo a transition from the Newtonian plateau to the power law region over the range of shear rates found in heat sealing. One consequence is that the velocity in the x direction will be less parabolic with respect to z and more like plug flow since the viscosity will be lower in the higher shear rate region near $z = h$. Future work should help determine if the iterative approach used here to estimate the viscosity is sufficient to get good agreement with experimental results.
- Heat transfer effects. The model assumes the temperature is constant, yet it takes time for the heat to transfer through the film and bring the sealant up to the seal bar temperature [45]. The heat-up time will take longer with thicker films [46]. Lower temperatures during part of the sealing time will result in higher viscosities and less squeeze-out than calculated by the model. Shortening the sealing time or lowering the effective temperature may compensate for this in the model.
- The temperature gradient in the z direction during heat up will also affect the velocity profile. Since the heat is applied at the outside surface of the film, the outside portion of the sealant ($z = h$) will be hotter than the sealant–sealant interface ($z = 0$) until the temperature comes to equilibrium. This lowers the viscosity at the outside of the sealant, resulting in more plug-like flow (similar to the effect of non-Newtonian flow behavior for the higher shear rates near $z = h$). The heat profile at different snap shots in time, as computed using a heat conduction model, is shown in Fig. 7.42. For the film structures used in these experiments, the model computations show it takes about 0.15 s for the sealant interface to reach the seal bar temperature.

Even without quantitative agreement between the model and experimental results, the model is useful

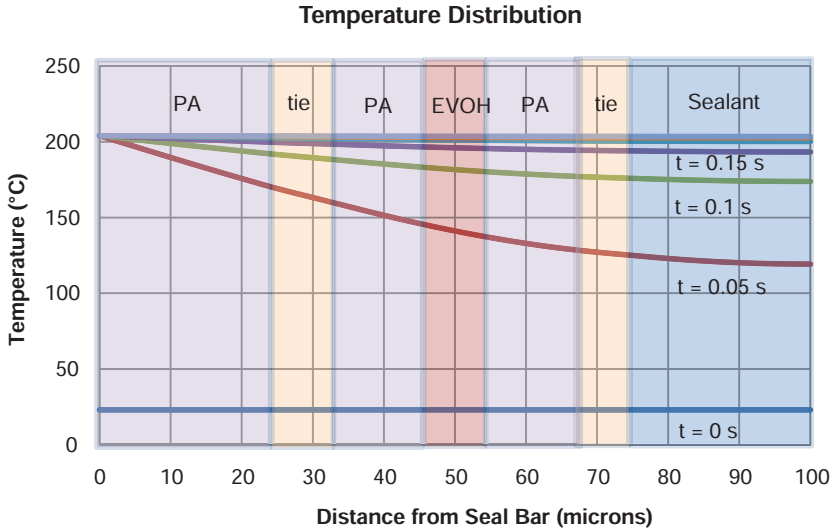


Figure 7.42 Heat transfer analysis of the seal area during squeeze flow. Results from the solution of the unsteady state heat conduction equation in one dimension for 100 μm thick film with bar temperature of 204°C. *Courtesy of E. I. du Pont de Nemours and Company.*

for better understanding the factors that increase the chances for squeeze-out problems during heat seal. These include the following:

- higher temperature;
- higher pressure;
- longer time;
- lower viscosity at low shear rates;
- narrow seal width;
- thicker sealant layers.

The development of the model also provides insight into the flow patterns within the seal area. Eqs. (7.19) and (7.20) describe the velocity in the x and z directions. These are shown schematically in Fig. 7.43. Starting at the center ($x = 0$), the velocity in the z direction is small at the surface of the plate and decreases to zero at the centerline between the plates. The velocity in the x direction increases as x increases, reaching a maximum at the bar edge ($x = w$). The flow in the x-direction is parabolic, similar to pressure-driven flow through a rectangular channel or pipe.

The model confirms what is known in the field: squeeze-out should not be a problem if the seal temperature is controlled within the operating temperature range of the sealant. It is only when the seal temperature or pressure is set too high that significant squeeze-out occurs. In the case of the plastomer and ionomer, both provide very low squeeze-out over the typical seal temperature range for which they are designed to be used.

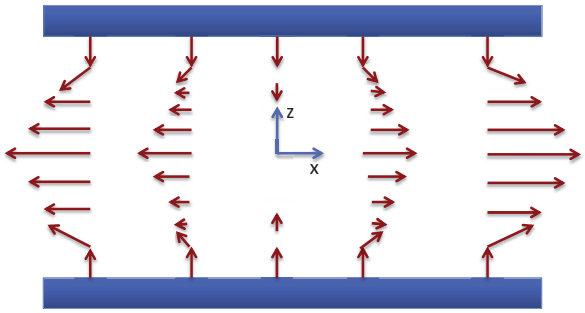


Figure 7.43 Schematic of flow patterns in the heat seal area during squeeze from based on Eqs. (7.19) and (7.20). Note the flow patterns in the z and x directions are not at scale.
Courtesy of E. I. du Pont de Nemours and Company.

One consequence of the model predictions is that squeeze-out may be a particular challenge in ultrasonic sealing. There the heat is generated at the sealant–sealant interface through friction. This can generate high temperatures in a very short amount of time. Squeeze-out may occur if the horn pressure is too high. Further discussion of ultrasonic sealing is provided in Section 7.9.

7.7 Easy-Open Seal Technology

7.7.1 Introduction

The definition of "easy open" depends on the application but generally corresponds to a seal strength that falls in the range of about 250–700 g/15 mm (400–1200 g/25 mm). Above 700 g/15 mm the seal is known as a lockup seal. Below about 250 g/15 mm the seal may fail during handling and shipping (eg, altitude changes during shipping are known to put stress on seals). Film-to-film seals within the easy-open range are often called peel seals. Most film-to-film seals are lockup unless specific technology has been introduced to control the seal strength within the peel seal range.

There are three main methods used to control seal strength as illustrated in Fig. 7.44:

- Interfacial or adhesive. Here there is a clean failure along the sealant–sealant or sealant–substrate (lidding) interface. Interfacial failure often occurs in standard heat seals at low sealing temperatures and is difficult to control since it typically occurs on the fast rising portion of the heat seal versus temperature curve. Typically cohesive or delamination technology is used for sealant to sealant applications. The interfacial mechanism is often used when sealing to a dissimilar substrate as in a lidding application. Here the adhesion to the substrate is primarily due to wetting and polar interactions and not interdiffusion (if the substrate does not melt during sealing). The sealant can be cleanly peeled away from the substrate.
- Cohesive. Failure occurs within a layer, usually the sealant layer. This is typically accomplished by "contaminating" the sealant with an incompatible polymer. The incompatible polymer forms a separate domain within the sealant resin, which is the continuous phase. At the

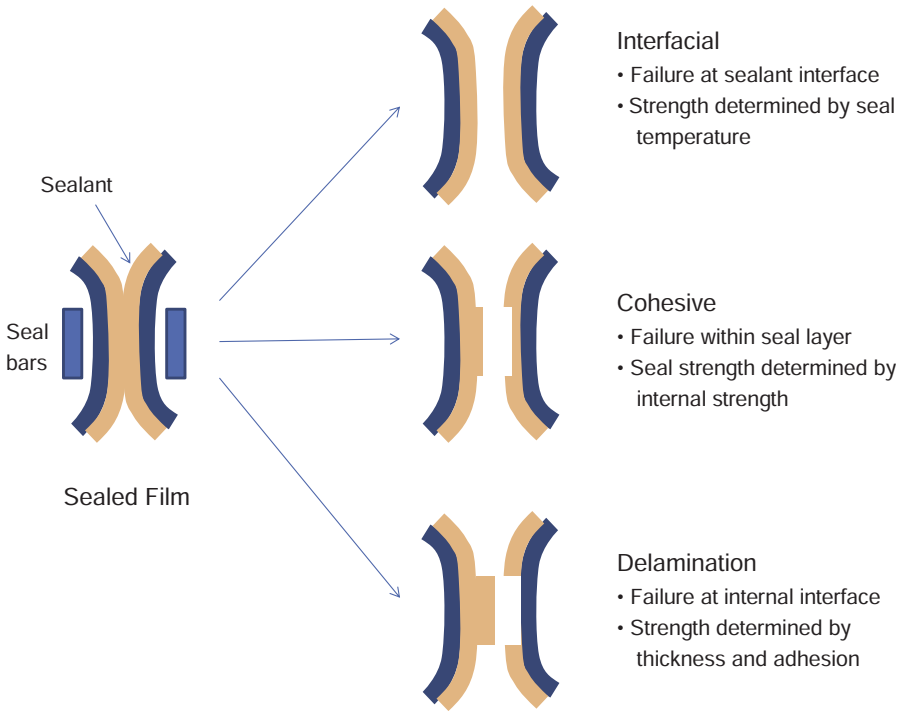


Figure 7.44 Mechanisms of easy-open seals.
Courtesy of Diane Hahm, DuPont. Reproduced with permission from E. I. du Pont de Nemours and Company.

sealant to sealant interface, the sealant bonds to the sealant on the other side, providing a hermetic seal. As the peel arms are pulled apart, the stress separates the sealant from the contaminating polymer since this is the weakest interface, propagating a crack that opens the seal. The size and shape of contaminating polymer domains, their position relative to the interface, and their adhesion to the sealant resin influence the seal strength. Compatibility, mixing, dispersion, and orientation all play a role.

- Delamination. Failure occurs at an interface adjacent to the seal layer in a multilayer film. Here the seal to seal interfacial strength is greater than the sealant to adjacent layer bond strength. The adjacent layer or the sealant itself is often modified to control the adhesion between the layers. During the peel, an initial burst or force is need for the peel front to propagate through the sealant layer to reach the adjacent interface. This initial opening force is influenced by the tear strength of the sealant and can be controlled by changing the thickness of the sealant layer.
- Combinations are possible. For example, Hayden [74] describes a peel seal system where failure occurs cohesively in the layer adjacent to the sealant: Sealant/cohesive peel layer/backing layer. During the peel, the peel front propagates through the sealant like the delamination method, but instead of relying on the adhesion between the sealant and adjacent layer the failure is within the adjacent layer.

Creating an easy tear feature is another method to provide ease of opening of a flexible package. Since this is not necessarily a function of the sealant or sealant technology, it will not be covered in this chapter. Notching, scoring and perforation are sometimes used to achieve easy tear. Directional tear properties of films are covered in Section 9.4.4.2.

7.7.2 Examples

The interfacial peel seal mechanism is most often used in lidding applications, which is taken up in Section 7.7.4.

There are numerous examples of cohesive peel seals involving blends of incompatible polymers. Many involve blends of polybutene-1 (PB-1) with polyolefins or ethylene copolymers. These include blends of PB-1 with EVA or LDPE [75–81], EMA

[80], tie resins [80], EAA [81], ionomers [82,83], and mPE [84]. Since PB-1 blends are so common, this technology is discussed in greater detail in Section 7.7.3. Other blends include EAA with EVA [81], ionomer with EVA [75], ionomer with PP [85,86], and mPE with PP [81]. Typically the minor component is added in the range of 10–30% but higher levels may be needed if the compatibility between the two polymers is good.

One delamination-type peel seal involves the use of ionomers in combination with HDPE. This technology is often used in snack packages where the HDPE provides moisture barrier and strength. The ionomer chemistry can be tailored to control the adhesion to HDPE either directly through the synthesis of the polymer (DuPont offers a special grade designed for this purpose called Surlyn E185SB) or by blending zinc- and sodium-based ionomers. Sodium ionomers have a lower affinity toward HPDE than zinc ionomers and the blend can be used to adjust the adhesion. Earlier versions of this technology used blends of ionomer and EVA to control the adhesion to HDPE [75,87].

Busche [88] describes a delamination system involving a sealant layer and controlled adhesion of the sealant layer to a tie layer adjacent to the sealant layer. The adhesion of the tie layer to a third layer is stronger than the adhesion to the sealant so that failure occurs along the tie–sealant interface. The adhesion of the tie layer to the sealant may be controlled by adding PB-1 to the tie layer. Hwo [77] teaches that PB-1 blends really fail cohesively near the interface, so the concept of Busche [88] and Hayden [74] are similar: the sealant is unaltered so it can perform its sealing function, but failure is programed to fail either by delamination or cohesively within the adjacent layer.

Delamination and cohesive peel seal technologies each have their pros and cons. Delamination peel seals allow for the use of unaltered sealants; adding incompatible polymers may affect sealing and other properties important to the application. Delamination peel seals typically have a broader temperature window for the easy-open seal strength range. This is because the seal strength is determined by the adhesion between the sealant and adjacent layer rather than the complex morphology and melting behavior of the blend. Delamination seals also typically do not change with time. Some peel seals, particular those containing PB-1, are prone to aging due to changes that take place in the crystalline form of the PB-1 [77]. Cohesive peel seals tend to turn white (stress whitening) as they are peeled, providing tamper evidence. Cohesive peel seals also can be designed to be less "stringy"; in the delamination peel seal, the initial tearing through of the sealant layer to reach the adjacent interface can leave some polymer strings behind. Cohesive seals are not altogether immune to stringiness, however. Improper control of the morphology of the discontinuous phase can lead to stringiness [81].

A variation on peel seal technology is the peel–lock seal. For example, a pouch may require lockup seals around three sides and an easy-open seal on top. Alternatively, a frangible seal may be desired in the interior of a pouch to provide easy open between two compartments. These concepts are shown in Fig. 7.45. Here it is desirable to have a sealant that is a hybrid between a peel seal and lockup as shown in Fig. 7.46. At low sealing temperatures, the seal has low seal strength over a wide temperature range. At high seal strength, the seal strength increases to the lockup range. Such seals are typically formed by blending different polymers or heat sealing dissimilar surfaces [89]. Standard cohesive type peel seal blends do not lockup at high seal temperatures and special technologies have been developed for this purpose, such as ionomer/propylene copolymer blends [89,90]. Frangible seals can also be assisted by the design of the seal geometry. DuPont used finite element modeling to optimize the seal geometry for a dual compartment pouch [90].

7.7.3 PB-1 Blends

Since blends with polybutene-1 are one of the most commonly used and well-documented technologies for cohesive-failure peel seals, they are considered here in detail. Many of the issues encountered with this system are also prevalent in other blend systems.

The chemical structure of polybutene-1 is similar to isotactic polypropylene with a butyl group (2-carbon) protruding from the polymer backbone instead of a methyl group (Fig. 7.47). The extra polarity makes it less compatible with most types of polyethylene but it adheres well to PP. It has a melting temperature similar to PE. Homopolymers and copolymers with alpha olefins are available.

When dispersed in a PE or EVA matrix, the poor adhesion between the PB and matrix results in low

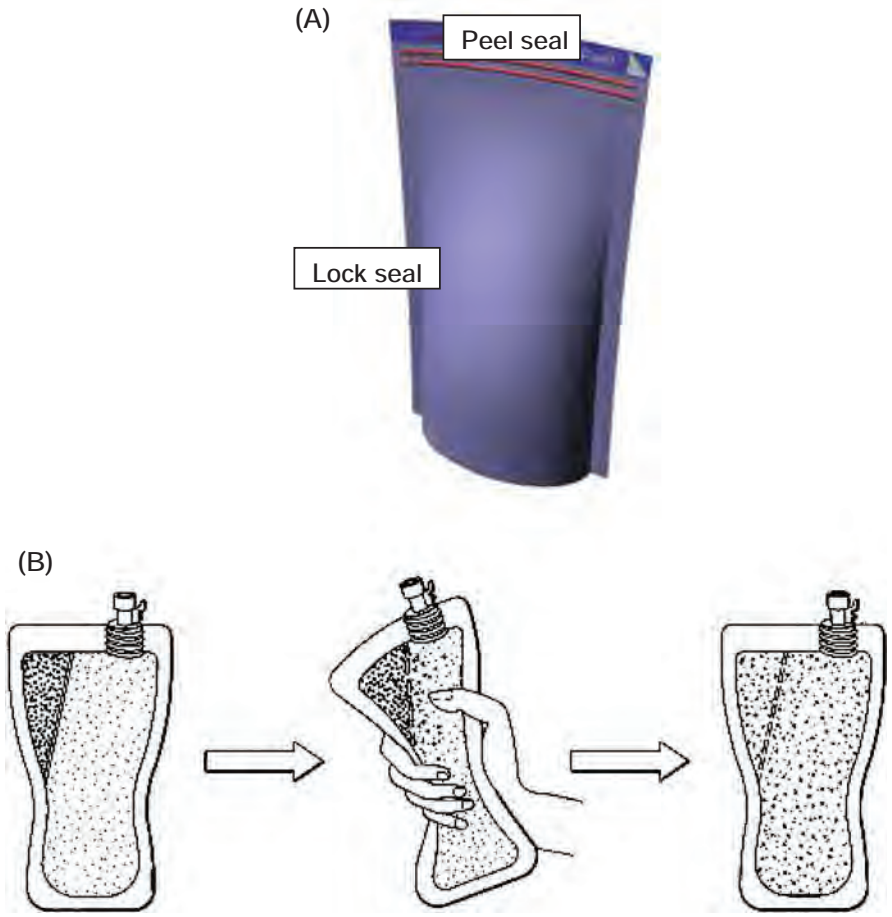


Figure 7.45 Peel–lock seal packaging concepts. (A) Single compartment pouch with top peelable seal and side lockup seals *(Reproduced with permission from E. I. du Pont de Nemours and Company.)*. (B) Dual compartment pouch with interior frangible seal for mixing compartments *(Reproduced from Bourque RA, et al. Multiple compartment pouch and beverage container with frangible seal. U.S. Patent 7306095 B1, 2007.)*.

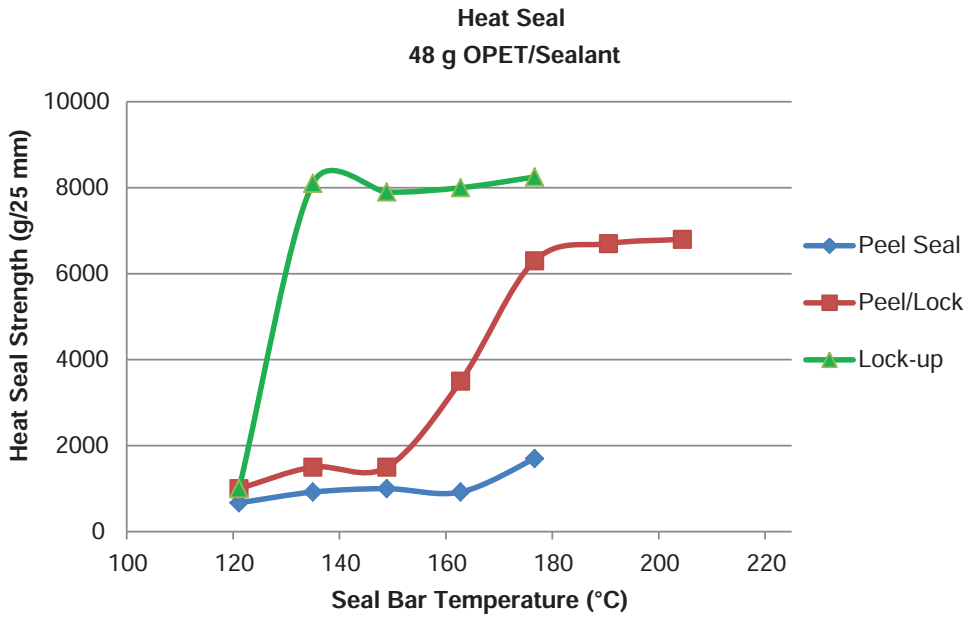


Figure 7.46 Peel–lock heat seal curves.
Reproduced with permission from E. I. du Pont de Nemours and Company.

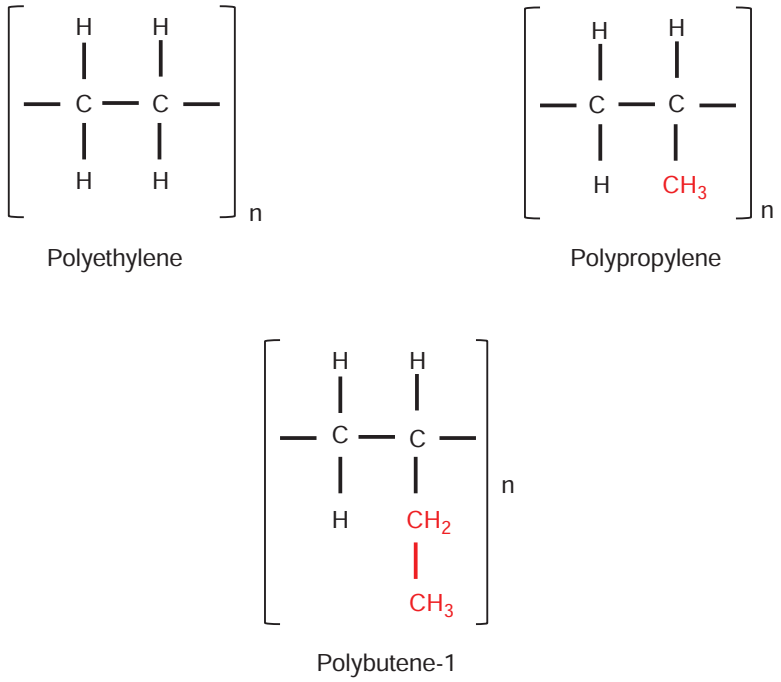


Figure 7.47 Comparison of the chemical structures of polyethylene, polypropylene, and polybutene-1.

cohesive strength necessary for peel-seal behavior. Some advantages of PB-based easy-open systems include the following [79]:

- broad seal temperature range;
- consistent and reproducible peel force;
- tailorable seal strength;
- initiation seal force similar to the propagation seal force;
- processable on conventional film fabrication equipment;
- no effect on hot tack.

Concentration, compatibility, and dispersion are the key factors influencing seal strength. These factors control the interfacial area, which in turn influence the seal strength. Generally the higher the concentration the lower the seal strength as more weak interfacial area is created. Typical concentrations are 8–20 wt% for LDPE and EVA [77] and higher for LLDPE and mPE (around 35% according to Mergenhagen [84]). If the concentration is too low, the seal becomes stringy upon opening.

The order of increasing compatibility is EVA (VA $<$ 18%) = LDPE $<$ HDPE $<$ LLDPE $<$ mPE. Resins with good compatibility, such as mPE, typically require much higher concentrations of PB-1 to achieve peelable seal strengths. Higher compatibility increases the interaction between the PB and matrix, increasing interfacial adhesion. The PB copolymers tend to have greater compatibility with PE. Increasing VA content of EVA beyond about 18 wt% increases seal strength of PB-EVA blends. In theory, increasing VA content should reduce the compatibility with PB-1 since the EVA becomes more polar. Increasing VA content also decreases the crystallinity, however, which may be responsible for the rise in peel strength. Most EVA sealants contain 18% VA or less so this effect is not a hindrance for using EVA–PB peel seal blends.

The dispersion of the PB-1 in the sealant is critical, influencing domain size and distribution. All things being equal, smaller domain size results in lower and more uniform seal strengths since more weak interfacial area is created. As discussed in Chapter 6, however, the domain size is influenced by interfacial adhesion; greater adhesion tends to produce smaller domain size. Therefore, the effect of domain size can be complex.

The film fabrication process can influence the PB-1 domain size and shape. High shear rates near the die wall can result in smaller domain sizes and

lower seal strength. Orientation during film blowing or casting can result in elongated domains. De Clippelier suggests that greater orientation may be better (lower seal strength), whereas Pirtle [81] suggests the opposite, and that a more oval shape is preferred. Pirtle suggests increasing the frost line height, lowering the draw down ratio, and maintaining a layer distribution consistent with the die design to minimize stress and orientation to obtain the optimum morphology. It is likely that these factors are important but may vary in the way they affect the seal strength depending on specific circumstances. The effect of blown film processing on dispersed phase morphology is explored in more detail in Section 14.3.

Matching the viscosities of the PB-1 and matrix resin is important for minimizing the domain size. PB-1 is more shear thinning than many of the polymers it is blended with. So simply matching melt indexes is not sufficient—careful attention to the whole rheology curve is a better approach.

Cast film generally gives higher seal strength than blown film with the same composition. Higher levels of PB-1 are added to cast film peel−seal blends to compensate. Hwo [77] attributes the increased seal strength in cast film to the PB-1 being in a different crystalline form and more amorphous (due to the rapid quench rate) than in blown film. This form of PB-1 has a lower melting point and stronger adhesion to PE.

The angle of the pull during the peel test affects the mechanism of failure and seal strength. Nase [91,92] found that the mode of failure changes with peel angle. Interlaminar failure occurs parallel to the interface, whereas translaminar failure occurs perpendicular to the interface (propagating through the thickness of the sealant). For angles less than 120°, failure was interlaminar with a minimum peel strength occurring at 120°. For angles 140°−180°, failure was translaminar and higher peel strengths were measured.

Seal strength of blends of PE or EVA with PB-1 ages down with time after the film has been fabricated (prior to sealing) as well as after heat sealing (Fig. 7.48). Reductions in seal strength of 40% or more have been reported [77,79]. PB-1 has four crystalline forms and some of these forms can change from one to another over time. These crystalline forms have different adhesion characteristics, which affect seal strength. Hwo [77], for example, describes the transition of Type II crystals to Type I crystals and correlates this with the age-down in seal strength. The user of PB-1 blend peel seal formulations needs to establish correlations for seal strength measured off the packing line with seal strength when the package is opened by the consumer, which may be several weeks later.

One method to reduce or eliminate the age-down issue is to pick a matrix resin that requires less PB-1 addition to achieve a peel seal. The lower the level of addition, the less effect aging has on the overall performance of the film. Ionomers are one such sealant. Brodie [83] shows that less than 10% PB-1 can to be added to some grades of ionomer to achieve a cohesive peel seal. This is considerably less than the amount required for LDPE or EVA blends (15−20%), much less LLDPE (20−25%), or mPE (25−35%) blends.

7.7.4 Lidding Films

There are two general types of sealing technologies used for lidding applications: sealant coatings and sealant resins. Both are designed to bond to the tray or cup stock, typically made from PP, PET, PS, PE, or PVC.

7.7.4.1 Heat Seal Coatings

A heat seal coating is essentially a water- or solvent-based adhesive that is applied as a nonblocking layer to a flexible substrate. The adhesive is activated with heat and pressure to provide a peelable adhesive bond to another rigid or flexible substrate. The adhesive formulation may contain a number of components, including the following [93]:

- resins;
- tackifiers and additives;
- lubricants, waxes, and slip modifiers;
- antioxidants and fillers;
- antibock and heat stabilizing agents;
- solvents and diluents;
- water, dispersants, pH control additives, defoamers, and surfactants.

EVA-based formulations have long been used as heat seal coatings. Gel lacquer is one of the oldest technologies. This solvent-based technology is

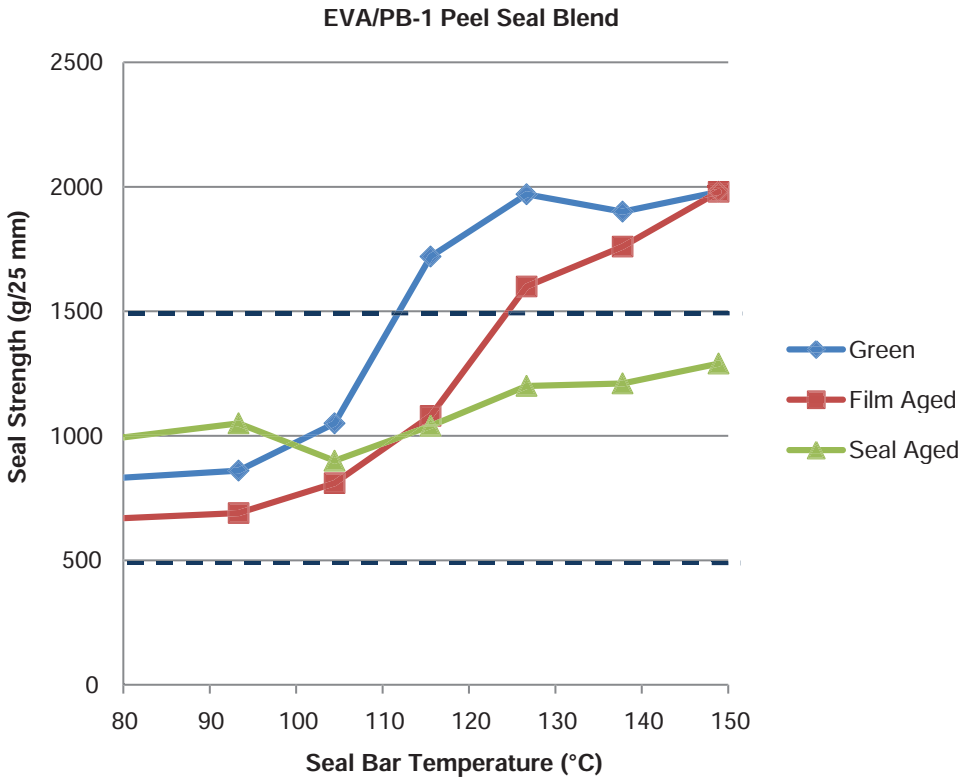


Figure 7.48 Heat seal curves for an 80% EVA (18% VA), 20% PB-1 blend. Film structure is (56-μm HDPE—8-μm sealant) blown film. The three curves show the effect of aging. "Green" measurements are for heat seals made and measured within a day of making the film. "Film aged" represents film stored at 22°C (72°F), 50% RH for 14 days before sealing and measuring. "Seals aged" designates film sealed within a day of making the film but the seal strength was measured after the sealed film had been stored at 22°C, 50% RH for 14 days. *Dashed horizontal lines* represent the typical range for easy-open seals.
Reproduced with permission of E. I. du Pont de Nemours and Company.

supplied as a gel that requires heating to 38°C (100°F) or higher for application. Solvents such as toluene also are added. Despite the challenges, they provide a number of useful benefits, including the following:

- bonding to a broad range of substrates, including PET, PP, PS, and PVC;
- good product resistance;
- ability to be used in hot fill food and autoclave medical applications;
- relatively low activation temperature.

Newer formulations with EVA have been developed that can be applied at ambient temperatures. These formulations tend to be more specific for the substrates they bond to but have better product resistance. Drawbacks include more expensive solvents and lower percentage solids.

Another category of solvent-based heat seal coatings involve true solutions at room temperature. A number of chemistries are available for specific applications:

- Vinyl/acrylics. These formulations have better chemical resistance than EVA coatings, excellent clarity, and heat resistance (for hot fill and autoclave). They do not work for PET or polyolefin substrates and require higher heat seal temperatures (121—177°C or 250—350°F).
- Polyesters. These high temperature-resistant coatings can be used for retort or ovenable applications. They are coated onto PET or aluminum foil and bond to CPET, APET, PVC, and PVDC-coated PS. These coatings are easy to apply; have excellent clarity; can be modified with fillers to provide specific seal strengths; have excellent chemical resistance to grease,

oil, and fats; and have high hot tack strength and temperature resistance. They are higher priced than other coatings and generally only adhere to PET or foil films.

- Polypropylene dispersions. These are used for foil and PP containers, typically in retort pouches, medical device packages, and aseptic pouches requiring excellent product or chemical resistance. They have specific adhesion to aluminum foil and require high processing temperatures to drive off the solvent.

Water-based coatings are made from EVA, EMA, and EAA chemistries. They are aqueous dispersions formulated for broad use. Benefits of these technologies include the following [93]:

- no volatile organic compounds;
- minimal health and safety issues;
- lower seal temperatures;
- adhesion to a wide range of film substrates;
- seal to a wide range of cup substrates including PP, PS, PVC, and PET;
- formulated for peel seal and hot tack characteristics.

Their main drawbacks derive from being water based; the coatings are susceptible to freezing and may have drying and foaming issues.

One advantage of heat seal coatings over heat seal resins is that they can be pattern coated. This allows the coating to be applied just in the seal area of the container. This minimizes food exposure and the potential for contamination, reduces cost and avoids membraning of the seal layer during opening.

Lacquers and other heat seal coatings often fail by rupture, which can be an advantage [75].

7.7.4.2 Peelable Seal Resins

There are a number of requirements for extrudable lidding structures, including the following [94]:

- easy-open peeling;
- reliable sealing over a wide temperature range;
- versatility;
- compliance with regulations;
- good machinability;
- good processability at extrusion stage.

Factors that influence sealing force include the following:

Sealant composition. Many lidding sealant resins are EVA or EMA based. These copolymers have a good balance of polarity and softness to bond to a number of substrates. Soutar [75] describes a blend of an EVA-based tie resin and an ionomer for bonding to PVC. DuPont offers a variety of EMA- and EVA-based single bag (preblended) lidding sealants in its Appeel product line [95]. Pascal [94] describes an EMA-based composition. EVA or EMA by themselves often lack the versatility to bond to a number of different substrates or provide the right level of seal strength. They are typically modified with other resins, tackifiers, softeners, or elastomers to achieve the desired performance [94].

Substrate chemistry. Eq. (7.1) shows that the substrate surface tension must be greater than the adhesive for good wetting. This is often accomplished by surface treatment such as corona treatment. Eq. (7.1) also shows that the interfacial energy should be small. In Chapter 6, the concept of the solubility parameter was introduced. Eq. 6.7 shows that the interfacial tension is minimized when the solubility parameters closely match. One of the reasons EVA and EMA work well as lidding sealants is that their solubility parameters more closely match those of common substrates such as PET or PVC [96].

The geometry of the seal area. Pascal [94] describes how the geometry can influence the initiation force independent of the sealant characteristics. One influence is the concentration of stress, as was highlighted in Section 7.7.2 for the two-compartment pouch.

Peel angle and speed. As described in Section 7.5.6, the angle and speed in any peel test influences the measured peel force. Care should be taken to mimic the end use when running peel tests in the lab for screening lidding sealant candidates.

Thickness of the sealant layer. This is especially important when flow or caulking may be needed to fill in voids or to seal around contamination.

Thermal conductivity and thickness of the lidding structure. Thinner structures seal faster (or seal at lower seal temperatures) than thicker ones. The same is true for foil structures, which have a higher thermal conductivity than paper or polymer substrates.

Plasticity of the sealant and structure. Pascal [94] provides an example of three structures with the same sealant and tie resin bonding to a PS substrate: (1) Al/tie/sealant, (2) paper/tie/OPET/tie/sealant, and (3) OPET/tie/sealant. The order of seal strength is $1 > 2 > 3$ with fairly significant differences. He attributes this to differences in the peel dynamics (fracture mechanics).

Soutar [75] compares field studies with lab results and shows that lab heat seals are a good starting point for screening lidding sealant candidates. Pascal [94] describes a lab method for studying initiation and propagation of the seal strength.

Some of the advantages of extrudable lidding sealants over lacquers and other sealant coatings include the following [97]:

- A well-designed extrudable sealant resin is very versatile, providing peelable seal functionality with multiple substrates. This may allow for a reduction in the number of materials inventoried (stock keeping units or sku's).
- Extrudable sealants can be used with multiple converting processes, such as extrusion coating and coextrusion blown or cast film.
- Extrudable sealants can be converted with higher coat weights (thickness), which provide better caulking and improved sealing in the presence of contaminants such as milk solids.
- Some versions of extrudable sealants have better product resistance.
- Extrudable sealants may have lower seal initiation temperatures.
- Extrudable sealants are solvent free.

As described in the proceeding section, some of the advantages of heat seal coatings are their low coat weight and ability to be pattern coated just in the seal area.

7.8 Reclosable Seal Technologies

Some of the methods used to create a reclosable flexible package include the following:

- Zippers;
- Pressure-sensitive strips that the consumer can apply after rolling up the end of the opened package to keep it from unrolling;
- Pressure-sensitive adhesives (PSAs) incorporated into the body of package that are exposed when the package opened.

Zipper technology has been around for several decades and is probably the most widely used technique for incorporating a reclosable feature into a flexible package. Zippers have been incorporated into a wide variety of package forms, adapted to many different packaging machine formats, and used across most food types from shredded cheese to deli meats and snacks. They come in a variety of styles such as press-to-close and sliders. The most widely used press-to-close zippers typically consist of integral profiles and flanges made by profile extrusion [98].

Zippers are normally added to the package on the packaging line while the pouch is being formed. The zipper is a separate entity usually in the form of a tape that is heat sealed to the package. The zipper material must be compatible with the sealant on the package film for proper bonding.

Anzini [98] discusses some of the challenges and opportunities for zipper technology:

- Providing easy-to-open and recloseabilty. Zipper packaging often requires scissors to get into. Why not combine easy-to-open features with zippers? Perforations allow for easy tearing but without an additional seal are not hermetic, which rules it out for many products. Laser scoring or linear tear film technology works for some package formats but is particularly difficult to implement in a vertical form fill seal operation where the tear is in the transverse direction. Combining an easy open seal technology, as described in Section 7.7, with the zipper seems to be a viable solution.
- Market research shows consumers are often frustrated with trying to reclose packages with zippers. The ultimate cause is misalignment of the zipper profiles when the consumer attempts to close the package. The double profile zipper and multialign closures [99] have been developed to help address this issue.
- With the newer double or multialign zippers, the ability to incorporate tactile or auditory signals become possible. For example, the consumer may hear a snapping sound or receive a tactile signal when the zipper has been successfully closed.

The use of PSAs in flexible packaging has grown in recent years but the concept dates back at least until the 1990s. Straus [100] describes a reclosable flexible package with a tacky adhesive layer and a thin skin layer on a substrate such as polyester film. The thin skin (sealant) layer fractures when opened, exposing the adhesive layer to form a resealable seal surface. The tacky adhesive is preferably a PSA and typically contains 40−80% of a thermoplastic elastomer (such as styrene butadiene, polyurethane, or EVA), 20−60% tackifier, and up to 15% other components.

Timm [101] describes a multilayer film with the structure: Substrate/PSA/cold seal//cold seal/substrate. Adhesion of the cold seal to the PSA and substrate is stronger than the adhesion of the PSA to the substrate so that when the seal is pulled apart, the PSA is exposed for resealing.

Exner [102] discloses structures involving a cold seal under a sealing layer. Selective adhesion allows the cold seal to be partially exposed after opening, allowing for reclosability.

Trouilhet [103] and Haedt [104] describe polyester seal layers in contact with a PSA layer that are exposed upon opening.

Cruz [105] describes a multilayer film with the structure: Tie layer (anhydride-modified polyolefin)/EVOH/PSA. The interface between EVOH and PSA provides a peelable/reclosable seal.

Ranganathan [106] discloses a tray with a liner comprising a sealant, which is at least 80% ionomer and a laminated lidding film sealed to the tray liner. The lidding film consists of a substrate film and a coextruded film. The substrate film contains a high modulus thermoplastic (BOPET, BOPP, or BOPA) outer layer and a barrier inner layer. The coextruded film has the structure (sealant−PSA) where the sealant is a blend of 80% ionomer and 20% polyolefin. The barrier layer of the substrate film is laminated to the PSA layer of the coextruded film, and the lidding film is sealed to the tray liner. When the package is opened, at least part of the PSA is exposed and can be reclosed by adhering to part of the sealant layer of the coextruded film that remains sealed to the tray.

Trouilhet [107] found that an ionomer and PSA can be coextrusion coated onto a variety of substrates including BOPP-met, paper, Al-foil, and BOPET/tie/Al. The seal strength can be adjusted from 5 to 20 N/15 mm by changing the PSA layer thickness. The resulting package can be reclosed up to 10 times with steady seal strength of 1.5 N/15 mm. The ionomer works well since it has low elongation at break to allow for easy tear through the sealant to expose the PSA during opening. The ionomer also brings other known attributes as a sealant such as low HSIT, oil resistance, seal through contamination, and stiffness.

These are just a sampling of the many patents and publications in the field. Most involve an extrudable PSA disclosed by Bardiot [108].

7.9 Ultrasonic Sealing

Ultrasonic sealing involves the use of a horn to impart an oscillatory force on the films (or film and substrate), which generates frictional heat to melt and seal the interface. Some of the reported advantages of ultrasonic sealing (US) over hot bar or conductive sealing (CS) include the following:

- Lower operating expense since less energy is consumed during sealing (the ultrasonic horn is only engaged during the sealing process, whereas energy to heat the bars in CS is continuous).
- Ability to seal heat-sensitive products. In US the heat is generated from the heat seal interface outward rather than from the outside of the film inward, reducing the amount of heat transferred to the product.
- Smaller film footprint since the seal area is typically narrower for US.
- The ability to seal through contamination. The sonic force pushes many powders and other products out of the seal area during sealing [109]. Bach [27], however, notes that US only has a marginal advantage with bulk materials such as wheat flour and CS was better for other materials in their study.
- The ability to seal-oriented films without distorting them.
- The ability to seal poor conducting films such as paperboard, or thick films in a shorter amount of time, increasing packaging line speeds.

Despite these advantages ultrasonic sealing is not widely used in flexible packaging. Some of the

disadvantages that have kept it from overtaking conductive sealing include the following:

- higher capital expense;
- higher maintenance cost;
- inability to seal some geometries, such as fin seals. US is mostly designed for flat surfaces;
- difficulty in maintaining barrier due to squeeze-out;
- lower seal strength [27,110,111].

A number of studies have been conducted on ultrasonic welding of thermoplastic parts that are relevant to heat sealing [112–114]. These studies reveal that:

- Amorphous polymers generally weld better than semicrystalline polymers.
- The temperature at the interface rises quickly, which is attributed to asperities at the surface which concentrate the stress. The interfacial temperature levels off above Tg or Tm.
- The temperature of the bulk also rises, although not as fast as the interface, which is attributed to viscous dissipation of the bulk molecules from the oscillations rather than to conduction of heat from the interface. The rise in the temperature in the bulk is too fast for conduction to be the major factor.
- When a tie layer or sealant is used, substantial squeeze-out can occur from the seal area once the bulk temperature of the sealant reaches its melting point.

Bach [27,110] studied the differences between US and CS, sealing the same film structure with the two processes. Seal seam strength is often lower for US than for CS. In one example with a commercial PA/PE laminate, the seal strength of the US is only 40% of CS. They find a number of differences between the two processes, including:

- Pressure is more important for US than for CS. In CS, only sufficient pressure to ensure the films are in contact is needed. For US, higher pressures help transmit the vibrations to the interface for melting.
- The temperature is generated from the outside in for CS and from the inside out for US. This creates a more uniform temperature profile in the seal area for CS. Hot spots were observed in US. Also, cooling is more rapid near the edges of the seal area in US than for CS. This impacts flow and crystallization.
- Melt is squeezed out from the seal area in both processes, but in US a melt bubble with a double notch at the edge of the seam forms (Fig. 7.49). Infrared thermal images and transmission electron microscopy (TEM) images show a higher level of orientation in the seam area for US. As a result, a different crystalline orientation structure forms; the interlamellar chains are stretched and molecular diffusion is constrained.
- For the US seals, failure is often along the morphological interface where flow has occurred. This depends on the seal force. At low force, no squeeze-out is observed but the seal strength is weak. Failure occurs along the seal to seal interface, presumably due to insufficient melting and diffusion. At high seal force, the interface heats up to well above the melting point and a significant amount of squeeze-out occurs. Failure is along the flow interface and seal strength is reduced. Optimum seal strength occurs with a small amount of squeeze-out. For strong bonds to form, $T >> Tm$, but this sets up conditions for squeeze flow and failure along flow lines.
- The double notch at the edge of the US seal area also tends to concentrate the stress during peeling and reduces seal strength.
- In CS, failure is clean along the sealant interface at low temperatures. At high temperatures, failure occurs by breakage (tearing) along the seam side. If squeeze-out occurs, the profile is concave rather than the convex melt bubble found in US and likely has little effect on the seal strength other than thinning of the sealant in the seal area.

Van Dun [111] compares different polyethylene sealants with the goal to optimize seal performance in ultrasonic sealing. They measure seal performance of 50-μm sealant films laminated to OPET or OPP

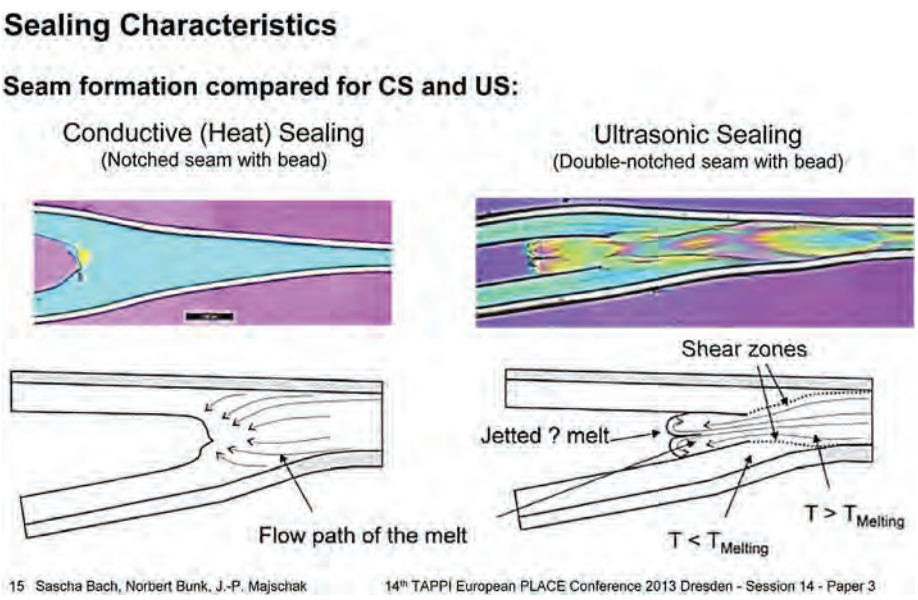


Figure 7.49 Picture of area near seal edge in ultrasonic and conduction sealing.
Courtesy of Bach S, Bunk N, Majschak J-P. Effect of laminate structure and morphology on fracture mechanics and seam strength of sealed seams. In: European TAPPI PLACE conference, 2013.

film. In one study, they compare various linear polyethylenes of different densities. The ultimate seal strength develops at lower seal force as the density of the LLDPE is decreased. This is analogous to lower seal initiation temperature in hot bar sealing. Reducing the density also increases the ultimate seal strength. Thus, an ultra low density polyethylene (ULDPE) outperforms an LLDPE.

van Dun relates this behavior to the linear elastic behavior of the polymers. The viscoelastic heat generation for small cyclic deformations is given by Eq. (7.29):

$$\dot{Q} = \pi f \gamma^2 G'' \tag{7.29}$$

where $\dot{Q}$ = heat generation, f = frequency, γ = strain amplitude, G'' = loss modulus.

The horn frequency is 20 kHz. Measurements at this frequency are difficult so they use time–temperature superposition to translate this to measurements at 10 Hz. They assume 20 kHz at 25°C is equivalent to 10 Hz at 10°C. Plotting G″ at these conditions for the different sealants, they find G″ decreases with decreasing density, in the opposite direction for increased heat generation according to Eq. (7.29). With LLDPE, however, the applied sealing force produces a larger deformation which increases the strain amplitude. Since the heat generation is a function of the strain amplitude squared, this overwhelms the effect of decreasing loss modulus. At higher densities, apparently there is less heat generation to fully melt the crystals, resulting in lower seal strength.

They also compare several other commercial sealant polymers including EAA, mPE plastomer, ionomer, and LDPE resins. The plastomer performs the same as the ULDPE of the same density. The EAA performs exceptionally well, and this corresponds to its higher G″. The ionomer and LDPE give lower seal strength. They also compare the performance of these sealants with their hot bar (CS) seal strength. The plastomer and ionomer give comparable seal strength as found in conductive heat seal tests, EAA higher, and LDPE lower.

In other studies, they find:

- A propylene–ethylene copolymer (Versify from Dow Chemical) outperforms the ULDPE and LLLDPE.
- A ULDPE outperforms an LLDPE when sealing a four-layer seals (to simulate a gusset region).
- A coextruded structure gives more complex performance than a monolayer structure with the same sealant. The coextruded structure (40 μm LLDPE + LDPE − 10 μm sealant) is compared

with a 50 μm monolayer sealant film. At low sealing force the seal strengths are the same, but as the sealing force is increased, the monolayer outperforms the coextruded film. Layers outside of the seal participate in the heat generation, deformation, and flow.

To date, only a few studies have been published elucidating the factors that influence sealant selection and optimization for ultrasonic sealing. This technology remains a ripe area for further research and development.

7.10 Failure Analysis and Troubleshooting

The performance of heat seals does not always conform to expectations. A number of factors may be involved. By understanding the symptoms and their root causes, the packaging professional can identify what corrective actions to take. This section borrows heavily from the collective experience at DuPont.

7.10.1 Types of Seal Failures

The first step in a failure investigation is to understand how the seal is failing. This will help determine what the root cause may be. There are three types of failure:

- interfacial;
- delamination; and
- cohesive.

It is not a coincidence that these failure modes are the same as for creating peelable seals described in Section 7.7.1. In peelable seals, the failure mode is carefully and purposely controlled. In the failure of heat seals, these modes may be undesired and the cause of poor performance.

A seal fails interfacially if it cleanly peels at the sealant−sealant or sealant−substrate. It is as if the seal was never made or was only tacked together. As described below, failure in this mode may point to too low sealing temperature or time or contamination.

In delamination, the failure occurs along the interface between adjacent layers. The seal-to-seal or seal-to-substrate strength is greater than the interlayer adhesion so that when the sealed film is pulled apart, the peel front tears through the sealant layer and failures at the adjacent interface. This may suggest a poorly cured adhesive, a problem with a tie layer, or perhaps chemical attack of the bond strength by a product ingredient.

Cohesive failure occurs when the seal fails within the seal layer (not at the interface). This is an indication of poor cohesion that may be the result of poor mixing, migration of additives to near the surface, or degradation near the seal surface.

7.10.2 Common Causes of Failure

In this section, a number of root causes of seal failures are described along with their symptoms and actions that can be taken to eliminate the cause. Table 7.8 provides this information in the reverse form, listing the symptoms followed by the causes and corrective action. The reader is referred to Section 7.4 for further discussion on factors that affect seal performance.

7.10.2.1 Sealing Variables

The three primary variables in the hot bar sealing process are time, temperature, and pressure. Improper settings or control over these variables can negatively impact seal performance.

If the sealing temperature is too high, the film may shrink, causing wrinkles and channel leakers. High temperatures may distort one or more layers and cause loss of orientation. In extreme conditions, the seal bar will burn through the film, causing holes in the seal area.

If the sealing temperature is too low, not enough heat will transfer to the sealant interface for bonding. The film will delaminate interfacially.

Solutions to these issues involve first checking to make sure the bar temperature is set to a temperature appropriate for the film structure. The film structure may have to be redesigned. For example, if the sealant seal-initiation temperature is greater than the distortion temperature of one of the layers either the sealant or the other layer will need to be changed. The film thickness must also be taken into account. The bar temperature set point should be higher for a thicker film with the same sealant and seal time to compensate for the longer time it will take for the heat to transfer to the sealant interface.

Table 7.8 Troubleshooting Guide to Heat Seal Issues

Symptom	Root Cause	Action
• Shrinkage of entire structure, wrinkles • Distortion of outside layer • Loss of orientation • "Burn-through"	• Seal temperature too high • Seal time too long	• Reduce temperature set point • Check thermocouple placement • Check heating elements • Reduce seal time
• Interfacial failure	• Seal temperature too low • Not enough contact pressure • Seal time too short	• Increase bar temperature set point • Check thermocouple placement • Check heating elements • Increase pressure • Increase seal time
• Squeezing sealant out of seal area	• Seal temperature too high • Seal pressure too high • Inconsistent pressure • Misaligned crimp teeth	• Reduce temperature set point • Check thermocouple placement • Check heating elements • Reduce seal pressure • Check pressure profile with carbon paper impressions • Align crimp teeth
• Cohesive failure	• Poor mixing during extrusion • Poor purging during extrusion • Too much release, slip, lubricant, etc. • Carrier resin for additive incompatible with sealant • Degradation of polymer during extrusion • Gel	• Optimize extrusion process • "Disco" purge procedure (vary rpm during purging) • Practice good purge procedures • Reduce additive level • Check composition of carrier resins for additives • Eliminate dead zones and hot spots in extruder
• Poor seal strength	• Product contamination in seal area	• Look for evidence of dust, powder, oils, and so on in seal area • Eliminate static charge that attracts powdery contaminates to the seal area • Select sealant optimized for sealing through the type of contamination encountered • Adjust packaging line operation to minimize the contamination of seal area
• Poor seal strength	• Substances transferred to seal areas	• Check for source of contaminates from contact with other layers in roll (backside transfer) • Check for sources of known troublemakers: silicones, stearates, slips, release sprays, residual solvent

(*Continued*)

Table 7.8 Troubleshooting Guide to Heat Seal Issues (*Continued*)

Symptom	Root Cause	Action
• Peelable seal blend too high or low in seal strength	• Poor mixing of incompatible polymers • Too much stress or orientation	• Adjust level of polymers in blend • Adjust mixing in extruder • Adjust orientation
• Channel leakers	• Poor caulking of wrinkles, gusset areas • Poor hot tack • Contamination	• Select sealant for better flow and/or hot tack • Check for sources of contamination • Note: Higher pressure may not improve caulking and just thin out sealant layer
• Seal strength changes with time	• Product ingredient degrades bonding • Low end-use temperature embrittles sealant • Low atmospheric pressure during shipping	• Select sealant that resists product migration and loss of adhesion • Select sealant for low temperature toughness
• Weak surface layer or cohesive skin layer failure	• Corona treatment • Backside corona treatment exposing sealant surface	• Check dyne levels for evidence of treatment
• Interlayer delamination	• Incomplete cure of adhesive	• Check for insufficient drying (too much residual solvent) • Check for incorrect recipe • Increase curing time
• Partial seal failure	• "Mooning" due to lack of hot tack strength • Hot seals pulling apart due to film sticking to seal jaws or high COF	• Select sealant with higher hot tack • Select outside surface layer with higher temperature resistance or protect seal bars with Teflon • Decrease COF of film

If the set temperature is OK, then the next step is to check to make sure the actual bar temperature is within a few degrees of the set point. There may be a hot or cold spot from a broken heater or the thermocouples controlling the temperatures may be in the wrong location to properly control the temperature.

If the sealing pressure is too high, the sealant may be squeezed from the seal area. Examining a cross-sectioned sample of the seal area near the seal edge may reveal this. Solutions include reducing the pressure set point, checking to make sure the pressure is uniform across the seal bar by making carbon paper impressions and ensuring the crimper teeth are aligned. If the pressure is too low, not enough contact is being made and the seal will fail interfacially. In this case, try increasing the pressure.

If the dwell time is too short, the seal will not be made and it will fail interfacially. If the dwell time is too long, there may be degradation of the polymer in one or more layers and distortion. Time and temperature go hand in hand; increasing time is equivalent to increasing temperature.

7.10.2.2 Contamination

There are a number of potential sources of contamination that may affect seal performance. One

involves the introduction of foreign matter during extrusion. The addition of an incompatible polymer may reduce seal strength by creating a second phase with weak adhesion between the phases, the same concept purposely used to create peelable seals. Additives or contaminants may migrate to the surface and form a weak boundary layer. These types of issues may be caused by a variety of problems including poor purging; addition of too much slip, release agent, lubricant, filler, antiblock, and so on; degradation of the polymer; and creation of gel that cannot be melted or sealed.

Corrective action may include choosing the carrier resin for an additive masterbatch to be compatible with the sealant resin so that an inadvertent peel seal is not created. Using proper purge procedures such as varying the screw speed randomly up and down during purging can help dislodge hung up resin (see Section 13.1 for details). Streamlining dead spots in the extruder, transition pipe, and die may also help.

Product contamination is another source of seal issues. Dust and powders attracted by static charge to the seal area are a challenge. Examples include cereal, powdered products, starch, coffee, and shredded cheese. Oil and greasy foods such as meat are another challenge. Liquids are sometimes purposely sealed through to eliminate headspace gases. Corrective action includes taking steps to prevent or discharge static charge and selecting sealants that excel at sealing through the type of contamination being encountered.

Foreign substances may be transferred to the sealant surface from contact with the outside layer in the roll (known as backside transfer), from additives migrating from adjacent layers in the film or from various processing aids used in the manufacturing area [115,116]. These may include silicones, stearates, slip agents, release sprays, and residual solvent. Silicones and fluorocarbon sprays are particularly problematic for sealing and should be avoided.

7.10.2.3 Film Converting

Surface treatments, such as corona, flame, ozone, or plasma treatment, are generally detrimental to heat sealing performance. These are used primarily to increase the surface energy of films to improve adhesion to coatings and inks. They promote oxidation of the surface and their effectiveness can be evaluated by measuring the surface energy using dyne solutions or other surface techniques. Oxidation may reduce the molecular weight of the surface molecules, decreasing the strength of the interface. In other cases, oxidation may promote cross-linking at the surface, which impedes molecular diffusion during heat sealing and reduces seal strength. Overtreatment can create a skin layer that readily delaminates from the bulk.

Surface treatment of the seal layer is normally avoided for these reasons. But backside treatment can inadvertently treat the front side of the film (the sealant) if the treatment station is not working properly. When treatment is suspected as a cause for poor heat seal performance several corrective actions can be taken, including the following:

- Measure the surface energy of the sealant surface to see if it is higher than expected. This may be a tip off for backside treatment.
- Try turning off the treatment to see if this improves the seal strength.
- Carefully examine seals to see if some of the symptoms of over treatment are present.
- Check to make sure the treater is not causing the backside (sealant side) to be treated with the front side.

Another potential problem is incomplete curing of solvent- or water-based adhesives. Interlayer delamination may occur during the seal strength measurement due to too much residual solvent, using the incorrect formulation, or not providing enough curing time.

7.10.2.4 Package Design: Channel Leakers and Gussets

Channel leakers are capillaries that run across the width of the seal area creating a pathway for leakage of product from the package or ingress of gasses from the external environment. These often form from wrinkles or around product contamination. A contributor to channel leakers is not having enough sealant resin, or a sealant resin with the right flow properties, to flow into the channels to caulk them shut.

Gussets are multi-ply regions of the seal area, such as where the film is folded or where a fin seal meets the end seal. These areas can be particularly

challenging to seal since there is often a gap between the single and multi-ply regions. Like channel leakers, selecting a sealant that has the ability to flow into and caulk the gap is important.

Increasing the hot tack of the sealant can also help prevent channel leakers and improve seal integrity in gusseted seals. In both cases, the resilience of the film in the gusset or wrinkle act to open up the hole after sealing if hot tack is not sufficient.

7.10.2.5 Aging Effects

Seal strength may age up or down with time. In some situations the film may change prior to sealing in a way that affects its ability to be sealed. Physical changes, such as changes in crystallinity or moisture absorption, may take place in the roll during storage. This may be influenced by storage conditions such as temperature and relative humidity. Many semi-crystalline polymers undergo secondary crystallization in the first few days or weeks after fabrication into a film. This is a process where even at room temperature the molecular chains may be able to form imperfect ordered structures (hence the name secondary crystals) over time. This may cause shrinkage in one or more layers and put stress on interfaces, causing changes in adhesion and seal strength. Crystallization increases stiffness, which may impact bending and stretching of the peel arm during peeling. The presence of crystals may also increase the time/temperature needed to melt the polymer for sealing.

Other aging effects may occur after the seal has been made while the package is stored. Filling, storage, and end-use conditions should be considered. For example, hot fill or retort may distort the film or melt the seal, weakening the seal. Internal bonds may also weaken over time, which may affect seal strength. Changes in the crystal form may also affect seal performance. The example of the different forms of PB-1 and its effect on peelable seals is discussed in Section 7.7.3.

A special form of aging involves product migration. Some components of the product being packaged may diffuse through the sealant layer and attack the adhesion to an adjacent layer. A well-known example is acetic acid in condiments such as ketchup and salad dressings. These products have been packaged in sachets and pouches that use aluminum foil as the barrier and LDPE as the sealant. The adhesion of LDPE to aluminum foil relies on the formation of oxidative by-products such as acid groups during extrusion coating. The acid groups bond to the oxides on the aluminum surface. But these bonds are rather weak and susceptible to attack by the acetic acid that readily migrates through the PE. A solution is to use an acid copolymer tie layer. The high acid level in these copolymers provides better adhesion that is more resistant to attack from the acetic acid, as well as slows down the diffusion of the acetic acid through the layer.

Aging and product migration effects are discussed in greater detail in Chapter 16.

7.10.2.6 Environmental Conditions

There are a number of environmental factors that the package may be subjected to during packaging, sterilization, or the end use that can affect seal strength. Examples include the following:

- Too high temperature. Retort or hot fill conditions may exceed the melting point of the sealant or other layers in the structures, weakening seal strength or interfacial adhesion.
- Too low temperature. The seal area may become embrittled if the temperature gets too low. Blast freezing can be problematic for some package structures.
- Low atmospheric pressure found during shipment of packages over mountains can cause the interior of gas flushed or modified atmosphere packaging to expand and stress the seal.
- High internal pressure, such as cooked-in deli meats during cooking. The combination of high pressure and temperature puts stress on the seal.

7.10.2.7 Low Hot Tack Strength

Partial seal failure, often referred to as mooning, results from the seal being pushed open by the product due to low hot tack strength. On horizontal form fill seal lines, this can be the result of high line speeds exerting forces from registration and product filling. In vertical form fill seal operations, the product falling on the newly created seal provides the opening force. The weight and drop height of the product are key factors. Lowering the seal temperature generally increases hot tack strength but this can

only be safely done if the sealing temperature is well above the onset of the seal plateau region. Otherwise the seal strength may be affected. Equipment modifications may also help with reducing opening forces or cooling the seal during packing. Short of this, switching to a sealant with better hot tack is the best way to deal with this problem. As described in Section 7.4, interlayer adhesion and the hot tack of layers adjacent to the seal layer may also impact hot tack; adjustments to the film structure may help improve hot tack.

Hot seals can also be pulled apart from the jaw sticking on the outside of the film. Coating the seal bar with Teflon can help, but the thickness of the Teflon layer must be taken into account when considering the time needed for the heat to transfer to the sealant interface. Higher seal bar temperatures may be needed to compensate. Changing the film structure so that the outside layer has greater temperature resistance can also help.

High COF of the film/metal surfaces of the packaging line can act to pull hot seals apart. Fatty acid amide slip agents are often less effective at the elevated temperatures present just after sealing. These agents act by blooming to the surface. At elevated temperatures they are more soluble in the polymer; some of the slip may migrate back into the polymer leaving less on the surface to control COF. Using nonmigratory slip agents or adding additional migratory slip agents may help. Adding too much migratory slip agent, however, can cause other problems such as chalking of the surface. Changing the outside layer to a more temperature resistant one may help. Increasing the hot tack strength of the sealant also can help.

7.10.3 Analytical Techniques

There are a number of analytical tools that can be used to help identify the cause of heat seal problems. These include the following:

- Microscopy. This can be very useful for identifying the location and type of the failure. Optical and electron microscopy may be worthwhile.
- Fourier transform infrared analysis (FTIR). This is useful for making sure the correct sealant is being used and for identifying the composition of any obvious contaminants that may be in the seal area.
- Electron spectroscopy for chemical analysis (ESCA) [also known as X-ray photoelectron spectroscopy or XPS] and time of flight secondary ion mass spectroscopy (TOF-SIMS). These are two complementary techniques for identifying chemical and molecular species near the surface of films. They have a much finer resolution than FTIR. Where the measurement size of FTIR is in microns, the effective measurement size for these techniques is in nanometers ($<$100 nm lateral resolution and $<$1 nm depth resolution). Thus they are useful for identifying trace contaminants near the surface that may affect heat seal performance. ESCA uses electrons and TOF-SIMS larger ions to bombard the surface under vacuum. Detectors sense the atoms and molecules that are knocked off from the bombardment.
- Differential scanning calorimetry (DSC). This technique can determine the melting points and crystallinity of the sealant. It may also be useful for detecting changes in crystallinity with age. More sophisticated techniques such as wide and small angle X-ray scattering can provide more detail on crystalline structure and orientation, which may prove useful in identifying problems.
- Thermal−mechanical analysis (TMA) and atomic force microscopy (AFM). Van Ness [116] showed how TMA can be used to detect cross-linking at the surface that may occur during film fabrication or extrusion coating. AFM is a more modern technique that is more sensitive and versatile. It can be used to detect soft and hard regions on the surface of the film, which may be helpful for understanding seal strength variability.

7.10.4 Troubleshooting Checklist

DuPont put together the following checklist for systematically troubleshooting heat seal problems:

1. How did the seal fail?
   - Interfacial, delamination, cohesive
2. Are the sealing conditions optimized?
   - Time, temperature, pressure
3. Compare problem material with a control
   - Use lab testing for comparison

4. Are correct surfaces being sealed?
    - FTIR for identification
    - Roll wound incorrectly may put seal surface on outside
5. Can seal be made if surface is cleaned with a solvent (mineral spirits, alcohol)?
    - Removes possible contamination
6. Check for surface treatment
    - Dyne level measurement
7. Does material seal on a different packing line?
    - Check condition of seal bars/jaws
8. Has anything changed?
    - Product
    - Film
    - Equipment
    - Product storage/transportation
9. Call suppliers! Provide as much information as possible, including samples of good and bad seals.

7.11 Selecting Sealant Resins

Many factors go into selecting a sealant. Some, which have been touched upon in preceding sections, involve sealing performance such as seal initiation temperature, ultimate seal strength, hot tack, sealing temperature range, and seal through contamination. Often times, however, the sealant contributes to other features of the package such as clarity, puncture resistance, abrasion resistance, tear strength, moisture barrier, and oil and grease resistance. The sealant may also need to contribute to the ease of making the structure into a film, such as melt strength for bubble stability in blown film and drawability for extrusion coating. Thermal resistance may be important during converting as well as in the end use (as in cook-in or pasteurization processes).

At the same time, the sealant needs to be the most cost-effective solution. Cost, however, is not just the price of the resin but involves ease of processing into a film (and its effect on yields), packaging efficiencies (line speed), and package quality (leaker rates). Sometimes a higher priced sealant will yield a lower cost package when total cost is considered. Total cost modeling is discussed in Chapter 16 and 17.

Polyethylene and ethylene copolymers are the most common sealant resins used in multilayer flexible packaging. In the sections that follow, qualitative rankings for a number of attributes are provided for a representative set of ethylene-based sealant resins. These resin families are described in detail in Table 7.9. The rankings are summarized in Table 7.10. These rankings represent qualitative comparisons based on the author's experience and should only be used as a rough guide. The performance of individual grades within a polymer family may vary greatly.

For this discussion, PP-based sealants are ignored. It is simply noted that random copolymers of propylene and ethylene are commonly used as the sealant layer in oriented PP films. The rPP provides good adhesion to the homopolymer structural layer of OPP and melts at 10–20°C lower so provides an adequate seal temperature window. It also has excellent high temperature resistance, making it suitable for retort applications. More recently, propylene–ethylene copolymers and elastomers such as Versify from Dow Chemical and Vistamaxx from ExxonMobil have found use as sealants (or in blends for sealants) in PP structures. These have even lower seal initiation temperature than traditional propylene random copolymers.

7.11.1 Seal Initiation Temperature

HSIT follows the melting point of the polymer. The order of increasing seal initiation temperature is (lower HSIT allows for higher packaging line speeds):

EVA, mPE < ACR, Ionomer < LDPE < VLDPE < LLDPE

7.11.2 Ultimate Seal Strength

Linear polymers have higher ultimate seal strength than those with LCB:

mPE, VLDPE, LLDPE > EVA, Ionomer, ACR, LDPE.

7.11.3 Peak Hot Tack Strength

mPE > Ionomer > ACR > VLDPE > LLDPE > EVA > LDPE.

Table 7.9 Description of Some Common Ethylene-Based Sealant Resin Families

Resin	LDPE	LLDPE	VLDPE	mPE	EVA	ACR	Ionomer
Name	Low density polyethylene	Linear Low density polyethylene	Very low density polyethylene	Metallocene polyethylene (plastomers)	Ethylene vinyl acetate	Acid copolymer resin	Acid copolymer resin partially neutralized with a metal cation
General characteristics as a sealant	Good processing in extrusion coating and blown film due to its high melt strength (via long chain branching). Excellent clarity in blown film. Moderate adhesion to foil in extrusion coating.	Better toughness than LDPE in film applications. More difficult to process than LDPE.	Lower melting point range, broader hot tack, lower seal initiation temperature than LLDPE.	Lower melting point, better clarity, and greater toughness than LLDPE. More difficult to process. Low seal initiation temperature and high hot tack. Excellent organoleptics.	Lower melting point, better clarity, and greater toughness than LDPE. Low seal initiation temperature.	Lower melting point, better clarity, and toughness than LDPE. Excellent adhesion to metal in extrusion coating. Low heat seal initiation and broad hot tack window.	Low melt point; excellent clarity; low seal initiation temperature; very broad hot tack temperature window; excellent oil and grease resistance; excellent optical properties; good adhesion to metal; excellent formability; excellent abrasion resistance; and depending on the grade higher stiffness than ACR, mPE, and EVAs.
Polymerization process	High pressure, free radical initiated	Low pressure (1000 psi), catalyst	Low pressure (1000 psi), catalyst	Low pressure (1000 psi), catalyst	High pressure, free radical initiated	High pressure, free radical initiated	High pressure, free radical initiated
Comonomer	None	Butene, hexene, octene	Butene, hexene, octene	Butene, hexene, octene	Vinyl acetate	Acrylic acid (AA) or methacrylic acid (MAA)	Acrylic acid (AA) or methacrylic acid (MAA)
MWD	Very broad	Broad	Broad	Narrow	Very broad	Very broad	Very broad
Comonomer distribution	None	Broad	Broad	Narrow	Random	Random	Random
Long chain branching	Yes	No	No	No or limited	Yes	Yes	Yes
Density (g/cc)	0.915–0.93	0.915–0.935	0.89–0.91	0.89–0.91	0.94–0.95	0.94–0.95	0.94–0.95
Typical melting point (°C)	108	123	115–123	95–99	87 (18% VA)	97–103	87–100
Modulus, kpsi (MPa)	30 (207)	30–40 (207–275)	10–20 (69–138)	9–13 (62–89)	7 (48)	20 (138)	7–70 (48–480)

Table 7.10 Summary of Qualitative Assessment of Common Ethylene-Based Sealant Polymers

Attribute	LDPE	LLDPE	VLDPE	mPE	EVA	ACR	Ionomer
Low seal initiation temperature	◆◆◆	◆	◆◆	◆◆◆◆◆	◆◆◆◆◆	◆◆◆◆	◆◆◆◆
Ultimate seal strength	◆◆◆	◆◆◆◆◆	◆◆◆◆◆	◆◆◆◆◆	◆◆◆	◆◆◆	◆◆◆
Peak hot tack strength	◆	◆◆	◆◆	◆◆◆◆◆	◆	◆◆◆	◆◆◆◆
Hot tack temperature window	◆	◆◆	◆◆◆	◆	◆	◆◆◆◆	◆◆◆◆◆
Seal through contamination	◆◆	◆◆	◆◆	◆◆◆◆	◆◆	◆◆◆◆	◆◆◆◆◆
Grease and oil resistance	◆◆◆	◆◆◆	◆	◆	◆	◆◆◆◆	◆◆◆◆◆
Adhesion to PE	◆◆◆◆◆	◆◆◆◆◆	◆◆◆◆◆	◆◆◆◆◆	◆◆◆◆◆	◆◆◆◆	◆◆◆
Adhesion to Al foil	◆◆					◆◆◆◆◆	◆◆◆◆
Low MVTR	◆◆◆	◆◆◆◆	◆◆	◆◆	◆◆	◆◆	◆◆
Transparency	◆◆	◆	◆◆	◆◆◆	◆◆◆◆◆	◆◆◆◆	◆◆◆◆◆
Melt strength	◆◆◆	◆◆	◆	◆	◆◆◆	◆◆◆◆	◆◆◆◆◆
Tear strength	◆◆◆◆	◆◆◆◆◆	◆◆◆◆◆	◆◆◆◆◆	◆◆◆◆◆	◆◆◆	◆◆
Abrasion resistance	◆◆◆	◆◆◆	◆◆	◆◆	◆◆	◆◆◆◆	◆◆◆◆◆
Puncture resistance	◆◆◆	◆◆◆	◆◆	◆◆	◆◆	◆◆	◆◆◆◆◆
Stiffness	◆◆◆	◆◆◆◆	◆	◆	◆	◆◆	◆◆◆◆◆

The greater the number of diamonds, the better the performance is for a given attribute.

7.11.4 Breadth of Hot Tack Temperature Window

Ionomer > ACR > VLDPE > LLDPE > mPE > EVA > LDPE.

7.11.5 Seal Through Contamination

There is a lot of disagreement in the literature on the ranking of the sealants on this attribute as is discussed in Section 7.4.1.5. Ionomers and ACRs have historically been used in applications involving sealing of greasy products such as processed meats. PE and EVA still find their way into many meat applications, and so the suitability of a given sealant depends on the severity and type of contamination.

7.11.6 Grease and Oil Resistance

The oil resistance of polyethylene is a strong function of its density; the higher the density, the greater the crystallinity, and the better the oil resistance. Ionomers and ACRs, because of the polar nature of their comonomers, have excellent oil resistance:

Ionomer > ACR > LLDPE, LDPE > VLDPE, mPE, EVA.

Fig. 7.50 compares the oil resistance of several sealant resins. These results are obtained using the ground glass technique where the time for an oil to penetrate through the film is measured. Here corn oil is used and the test is accelerated by using a temperature of 40°C. Nevertheless, the test was stopped before the penetration through the ionomer films occurred.

7.11.7 Adhesion to Polyethylene

Adhesion to PE is important in many coextruded flexible packaging films. The adjacent layer to the sealant layer is often a PE-based tie resin or a PE structural or bulking layer. Good adhesion helps improve heat seal strength and hot tack. Lower adhesion can be an advantage for the design of delamination peelable seals.

mPE, LLDPE, VLDPE, EVA, LDPE > ACR > Ionomer.

7.11.8 Adhesion to Aluminum Foil

Adhesion to foil is important for some extrusion coating applications. The order of performance, highest to lowest:

ACR > Ionomer > LDPE.

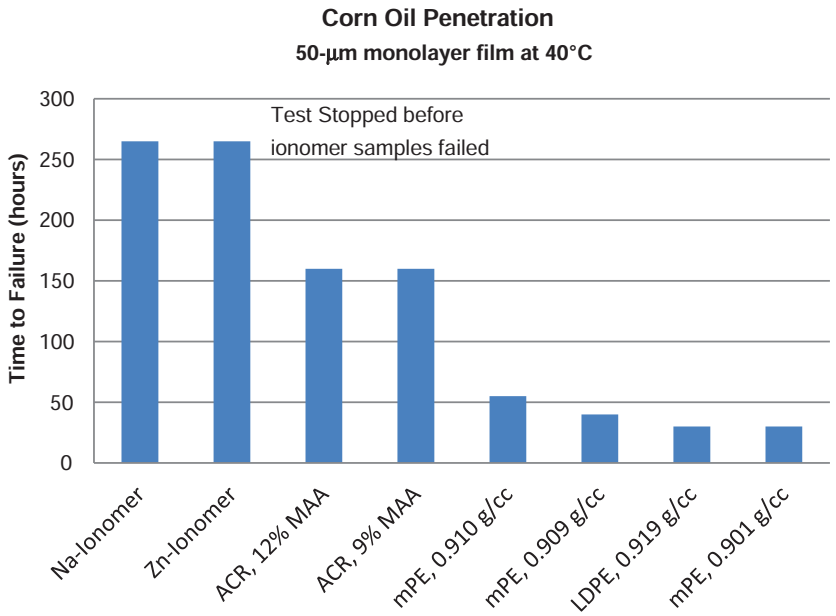


Figure 7.50 Oil resistance of some common sealant resins. Penetration of corn oil through 50-μm film at 40°C. *From De Garavilla JR. Ionomer, acid copolymer, and metallocene polyethylene resins: a comparative assessment of sealant performance. TAPPI J 1995;78(6):191–203. Reproduced with permission from E. I. du Pont de Nemours and Company, Inc.*

7.11.9 Moisture Vapor Transmission Rate

The higher the crystallinity, the lower is the MVTR, and the better the moisture barrier. The order of increasing MVTR:

LLDPE < LDPE < VLDPE, mPE, EVA, ACR, Ionomer.

7.11.10 Oxygen Barrier

None of the polyethylene or ethylene copolymer sealants have good oxygen barrier performance compared with high barrier polymers such as EVOH, PVDC, or even medium barrier polymers such as PA6 or PET.

7.11.11 Clarity and Transparency (Low Haze)

The order from highest clarity to lowest:

EVA, Ionomer > ACR > mPE > VLDPE > LDPE > LLDPE.

7.11.12 Melt Strength

Melt strength is important for hot tack, bubble stability, thermoforming, and low neck-in (extrusion coating). The order of melt strength from the highest to lowest:

Ionomer > ACR > LDPE, EVA > LLDPE > VLDPE > mPE.

7.11.13 Tear Strength

Linear PE has high tear strength in the transverse direction but low tear strength in the machine direction. The opposite is true for branched PE and ethylene copolymers.

EVA, LLDPE, VLDPE, mPE > LDPE > ACR > Ionomer.

7.11.14 Abrasion Resistance

Ionomer > ACR > LDPE, LLDPE > mPE, EVA, VLDPE.

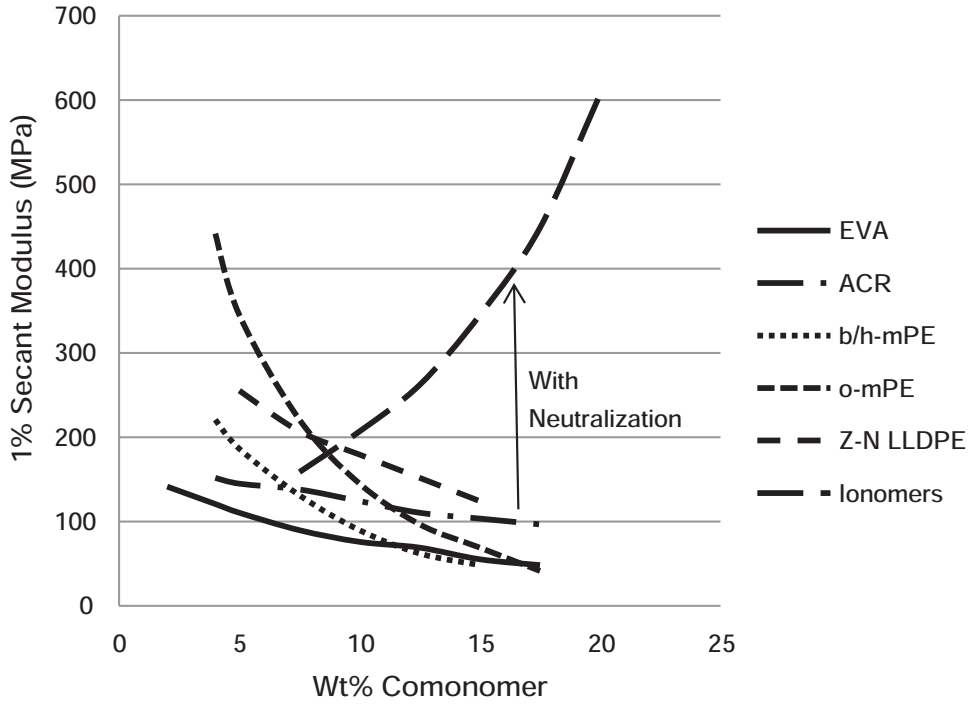


Figure 7.51 Film stiffness (secant modulus) as a function of comonomer content for several classes of ethylene-based sealant resins.

From De Garavilla JR. Ionomer, acid copolymer, and metallocene polyethylene resins: a comparative assessment of sealant performance. TAPPI J 1995;78(6):191–203. Reproduced with permission from E. I. du Pont de Nemours and Company, Inc.

7.11.15 Puncture Resistance

Puncture resistance is important for protecting products with sharp features such as bones or noodles.

Ionomer > LDPE, LLDPE > ACR, mPE, EVA, VLDPE.

7.11.16 Stiffness

The stiffness of the sealant can have a disproportionate effect on the bending stiffness of a package, allowing the structure to be downgauged [117]. A model of bending stiffness is described in Chapter 9. Most premium ethylene-based sealant resins have low stiffness. This is because the high comonomer content needed to achieve low HSIT also reduces stiffness (Fig. 7.51). Stiffness is directly related to crystallinity; crystals restrict the movement of nearby molecular chains making the polymer less flexible. Crystallinity (and HSIT) decreases with increasing comonomer content. An exception is ionomers. The ionic interactions in ionomers constrain molecular movement, raising the stiffness.

The order of stiffness from highest to lowest:

Ionomer > LLDPE > LDPE > ACR > VLDPE = EVA = mPE.

Resin suppliers can supply comparisons and help in selecting grades from their portfolio. In Chapter 17 the development of tools to help select resins is described. One such tool was developed by DuPont [118] that allows the user to input attributes and assign importance factors for a given application. The tool then assesses which family of sealant resins provide the most benefit based on the attributes chosen.

References

[1] ASTM International. Standard test method for seal strength of flexible barrier materials (F88/F88M-09). 2009.
[2] ASTM International. Standard test method for making heatseals for determination of heatsealabilitiy of flexible webs as measured by seal strength (F2029−08). 2008.
[3] ASTM International. Standard test method for mechanical seal strength testing for round cups and bowl containers with flexible peelable lids (F2824−10). 2010.
[4] Soutar AM. Hot testing: or is it?. In: TAPPI polymers, Laminations and coatings conference; 1994. p. 383.
[5] Soutar AM. Hot tack testing: a review. J Plast Film Sheeting 1996;12:304−34.
[6] Brodie III V. Hot tack of sealant resins. In: Tappi polymers, laminations and coatings conference; 1986. p. 187−96.
[7] Cooper BA, Wharton WH. Adhesion testing method and apparatus. U.S. Patent 3412606. 1968.
[8] DuPont Literature. Hot tack strength. Surlyn® update, vol. 1; 1970. issue 4.
[9] Hocking C. Latest findings on hot tack show worth of test unit. Package Engineering; February 1983.
[10] Falla D, Li M. Reliable hot tack testing of polyolefin films. In: SPE ANTEC conference; 2014.
[11] Theller HW. Hot tack tester. U.S. Patent 5847284. 1998.
[12] ASTM International. Standard test methods for hot seal strength (hot tack) of thermoplastic polymers and blends comprising the sealing surfaces of flexible webs (F1921/F1921M-12). 2012.
[13] Berger KR, Knoelke M, Welt B. Influence of sample preparation and instrument settings on hot tack measurements of thin sealant films. J Plast Film Sheeting 2004;20:55−63.
[14] Schubert G, Plassmann O, Husch S. Hot tack of extrusion coatings on aluminum foil and paper − does the process always lead to the same result?. In: TAPPI PLACE conference; 2010.
[15] Wooster JJ, Mergenhagen LK. Assessing real-life sealant performance in flexible packaging. In: TAPPI polymers, Laminations & coatings conference; 2000. p. 617−30.
[16] Bilgen M, Van dun J, Patel R, Garnett J, Bafna A. Insuring seal integrity and broad operating window. In: TAPPI PLACE conference; 2012.
[17] Kapur M, Bilgen M, O'Connell P. Importance of application representative sealant test methods. In: SPE ANTEC; 2014. p. 1393−9.

[18] Hahm DM. Sealing study with meat marinades on seal surface. In: American Meat Institute conference; October 1999.
[19] Mesnil P, Arnaunt J, Halle R, Rohse N. Seal through contamination performance of metallocene plastomers. In: TAPPI PLC conference; 2000.
[20] Cooper J, Moreno AP. Metallocene copolymers for extrusion coating applications designed specifically for exceptional ultimate hot tack and high temperature hot tack strength. In: TAPPI PLC conference; 2000.
[21] De Garavilla JR. Ionomer, acid copolymer, and metallocene polyethylene resins: a comparative assessment of sealant performance. TAPPI J 1995;78(6):191−203.
[22] Hausmann K. All you want to know about hot-tack. DuPont literature; 1997.
[23] Surlyn® Update. Sealing through product residue, vol. 1. n.d., issue 6.
[24] Sadeghi F, Ajji A. Application of single site catalyst metallocene polyethylenes in extruded films: effect of molecular structure on sealability, flexural cracking and mechanical properties. Can J Chem Eng 2014;9999:1−8 (published online).
[25] Vansant JD. The effect of coextrusion on the hot-tack performance of a common ionomer resin. In: TAPPI PLC conference; 1998. p. 743−54.
[26] Mihindukulasuriya S, Lim L-T. Effects of liquid contaminates on heat seal strength of low-density polyethylene film. Packag Technol Sci 2012;25:271−84.
[27] Bach S, Thurling K, Majschak J-P. Ultrasonic sealing of flexible packaging films − principle and characteristics of an alternative sealing method. Packag Technol Sci 2011;25:233−48.
[28] Stehling FC, Meka P. Heat sealing of semicrystalline polymer films. II. Effect of melting distribution on heat-sealing behavior of polyolefins. J Appl Polym Sci 1994;51:105−19.
[29] Farley JM, Meka P. Heat sealing of semicrystalline polymer films. III. Effect of corona discharge treatment of LLDPE. J Appl Polym Sci 1994;51:121−31.
[30] Van Alsten JG. Ionic and chain interdiffusion and interfacial strength development in ionomers of poly(ethylene-co-methacrylic acid). Macromolecules 1996;29:2163−8.
[31] Mueller C, Capaccio G, Hiltner A, Baer E. Heat sealing of LLDPE: relationships to melting and interdiffusion. J Appl Polym Sci 1998;70:2021−30.
[32] McKelvey JM. Bonding operations. Polymer processing. New York: John Wiley & Sons; 1962. p. 356−71.
[33] Voyutskii SS. Autoadhesion and adhesion of high polymers. New York: Interscience Publishers; 1963.
[34] Wu S. Polymer interface and adhesion. New York: Marcel Deker; 1982. p. 338.
[35] Deryagin BW, Krotova NA. Adhesion. Izd. Akad. Nauk, M-L; 1949 (cited in Voyutskii, 1963).
[36] Deryagin BW, Krotova NA. Doklady Akad, vol. 61. Nauk SSR; 1948. p. 849 (cited in Voyutskii, 1963).
[37] Deryagin BW, Krotova NA. Usphekhi Fiz, vol. 36. Nauk; 1948. p. 387 (cited in Voyutskii, 1963).
[38] Wool RP. Polymer interfaces, structure and strength. New York: Hanser Publishers; 1995. p. 278.
[39] de Gennes PG. Scaling concepts in polymer physics. Cornell University Press; 1979.
[40] Rouse PE. A theory of linear viscoelastic properties of dilute solutions of coiling polymers. J Chem Phys 1953;21:1272.
[41] Doi M, Edwards SF. The theory of polymer dynamics. Oxford University Press; 1986.
[42] Doi M. Introduction to polymer physics. Oxford: Clarendon Press; 1996. p. 97.
[43] Wool RP. Polymer interfaces, structure and strength. New York: Hanser Publishers; 1995. p. 40−82.
[44] Wu S. Polymer interface and adhesion. New York: Marcel Deker; 1982. p. 388−95.
[45] Meka P, Stehling F. Heat sealing of semicrystalline polymer films. I. Calculation and measurement of interfacial temperatures: effect of process variables on seal properties. J Appl Polym Sci 1994;51:89−103.
[46] Morris BA. Predicting the heat seal of ionomer films. J Plast Film Sheeting 2002;18:157−67.
[47] Wool RP. Polymer interfaces, structure and strength. New York: Hanser Publishers; 1995. p. 286.
[48] Schuman T, Stepanov EV, Nazarenko S, Capaccio G, Hiltner A, Baer E. Interdiffusion of

linear and branched polyethylene in microlayers studied via melting behavior. Macromolecules 1998;31:4551−61.
[49] Schuman T, Nazarenko S, Stepanov EV, Maganov SN, Hiltner A, Baer E. Solid state structure and melting behavior of interdiffused polyethylenes in microlayers. Polymer 1999;40:7373−85.
[50] Wool RP. Polymer interfaces, structure and strength. New York: Hanser Publishers; 1995. p. 225.
[51] Qureshi NZ, Stepanov EV, Capaccio G, Hiltner A, Baer E. Self-adhesion of polyethylene in the melt. I. Heterogeneous copolymers. Macromolecules 2001;34:1358−64.
[52] Scheffold F, Budkowski A, Steiner U, Eiser E, Klein J, Fetters LJ. Surface phase behavior in binary polymer mixtures. II. Surface enrichment from polyolefin blends. J Chem Phys 1996;104:8795−806.
[53] Brant P, Karim A, Douglas JF, Bates FS. Surface composition of amorphous and crystallizable polyethylene blends as measured by static SIMS. Macromolecules 1996;29:5628−34.
[54] Qureshi NZ, Rogunova M, Stepanov EV, Capaccio G, Hiltner A, Baer E. Self-adhesion of polyethylene in the melt. 2. Comparison of heterogeneous and homogeneous copolymers. Macromolecules 2001;34:3007−17.
[55] Bulacu M, van der Giessen E. Effect of bending and torsion rigidity on self-diffusion in polymer melts: a molecular-dynamics study. J Chem Phys 2005;123:114901.
[56] Tierney NK, Register RA. Ion hopping in ethylene-methacrylic acid ionomer melts as probed by rheometry and cation diffusion measurements. Macromolecules 2002;35:2358−64.
[57] Wool RP. Polymer interfaces, structure and strength. New York: Hanser Publishers; 1995. p. 395.
[58] Sentmanat M, Hatzikiriakos SG. Flow induced crystallization of polymers in extension. In: SPE ANTEC conference; 2010. p. 51−5.
[59] Takahashi T, Watanabe J, Minagawa K, Koyama K. Effect of ionic interaction on elongational viscosity of ethylene-based ionomer melts. Polymer 1994;35:5722−8.
[60] Ezekoye OA, Lowman CD, Fahey MT, Hulme-Lowe AG. Polymer weld strength predictions using a thermal and polymer chain diffusion analysis. Polym Eng Sci 1998;38:976−91.
[61] Moffitt RD. A mathematical model for the heat sealing of linear, semi-crystalline polymers. In: SPE ANTEC conference; 2006. p. 1027−32.
[62] Moffitt RD. Industrial applications of heat sealing modeling. In: SPE ANTEC conference; 2007. p. 2312−7.
[63] Wool RP. Polymer interfaces, structure and strength. New York: Hanser Publishers; 1995. p. 336−9.
[64] Moffitt RD. Heat seal design and optimization. Polym Prepr 2007;48:735−6.
[65] Wool RP, O'Conner KM. A theory of crack healing in polymers. J Appl Phys 1981;52:5953.
[66] Register RA. Optimizing hot tack in packaging sealing operations. Presentation to DuPont. 1999.
[67] Vanhoorne P, Register R. Low shear melt rheology of partially neutralized ethylene methacrylic acid ionomers. Macromolecules 1996;29(2):598−604.
[68] Tierney NK, Register RA. The role of excess acid groups in the dynamics of ethylene-methacrylic acid ionomer melts. Macromolecules 2002;35:6284−90.
[69] Register RA. Letters to J. W. Paul, DuPont. 1996−1997.
[70] Shamsundar N, Rooz E. Numerical methods for moving boundary problems. In: Minkowycz WJ, et al., editors. Handbook of numerical heat transfer. New York: John Wiley & Sons; 1988.
[71] Morris BA, Scherer JM. Squeeze-out of sealant during hot bar sealing: modeling insights. In: SPE ANTEC conference; 2013.
[72] Morris BA, Scherer JM. Preventing squeeze-out of sealant during hot bar sealing: modeling and experimental insights. In: SPE ANTEC conference; 2014. p. 1452−9.
[73] Bird RB, Armstrong RC, Hassager O. Dynamics of polymeric liquids. Fluid mechanics. 2nd ed., vol. 1. New York: John Wiley & Sons; 1987. p. 20. 189, 539.
[74] Hayden A. A novel peel-seal system. In: TAPPI PLACE conference; 2004.
[75] Soutar AM. Polymer combinations for peel/seal applications. In: 1986 coextrusion conference; 1986. p. 31−43.

[76] Hwo CC. Peel seals. U.S. Patent 4882229 A. 1989.
[77] Hwo CC. Polybutylene blends as easy open seal coats for flexible packaging and lidding. J Plast Film Sheeting 1987;3:245–60.
[78] De Clippeleir J. PE/PB blends for film applications. Specialty plastic films '97. 1997. Zurich, Switzerland.
[79] De Clippeleir J, Hirata S, Roucourt I. Easy-opening packaging technology. A technical perspective from Basell Polyolefins. In: TAPPI PLACE conference; 2004.
[80] Tickner WG. Heat sealable resin blends. U.S. Patent 4189519. 1980.
[81] Pirtle SE, Mergenhagen L, Wooster J, Cotton R. The effects of resin selection and extrusion variables on peelable seal performance. In: TAPPI PLACE Conference CD, paper PLA0468; 2004.
[82] Yanidis, A.., 1996, Blend of polybutylene and ionomer forming easy-open heatseal," U.S. Patent 5547752 A.
[83] Brodie III V. Packaging films capable of being heat-sealed closed and thereafter peeled open. U.S. Patent 5891500. 1999.
[84] Mergenhagen LK, Pope TJ, Timper CA. Polyolefin plastomer-based peelable seal formulations. In: TAPPI PLC conference proceedings; 1996. p. 63–71.
[85] Hoh GL. Blends of ionomer with propylene copolymer and articles. U.S. Patent 4539263A. 1985.
[86] Hoh GL. Blends of ionomer with propylene copolymer. U.S. Patent 4550141A. 1985.
[87] Cook SO. Flexible packaging films of high density polyethylene capable of forming easy openable seals. U.S. Patent 4188441. 1980.
[88] Busche DA, Bostian DH. Easy open package. U.S. Patent 4944409 A. 1990.
[89] Bourque RA, et al. Multiple compartment pouch and beverage container with smooth curve frangible seal. U.S. Patent 7055683. 2006.
[90] Bourque RA, et al. Multiple compartment pouch and beverage container with frangible seal. U.S. Patent 7306095 B1. 2007.
[91] Nase M, Zangel A, Langer B, Baumann HJ, Grellmann W, Poelt P. Investigation of the peel behavior of polyethylene/polybutene-1 peel films using *in situ* peel tests with environmental scanning electron microscopy. Polymer 2008;49:5458–66.
[92] Nase M, Langer B, Grellmann W. Fracture mechanics on polyethylene/polybutene-1 peel films. Polym Test 2008;27:1017–25.
[93] Mueller TR. Lidding applications for peelable seal roll applied coatings. In: TAPPI PLACE conference; 2004.
[94] Pascal J. Peelable structures for PP, PS, PET and PVC. Understanding how multilayer construction influences seal and peel properties. In: TAPPI PLACE conference; 2008.
[95] DuPont. DuPont™ Appeel® lidding sealant resins. 2008. viewed on July 26, 2014, from: http://www.dupont.com/content/dam/assets/products-and-services/packaging-materials-solutions/assets/L-14227_Appeel_brochure_dupont_09-03-2011_BD.pdf.
[96] Zhang DD. Peelable seals applications to dissimilar surfaces. In: Tappi polymers, laminations & coatings conference; 1998. p. 341–50.
[97] Kendig T. DuPont Appeel® lidding sealant resin, concepts for easy open packaging. Pack Expo; 2010.
[98] Anzini DJ. Creating the next generation of flexible recolosable packages. In: SPE FlexPackCon conference/AIMCAL conference; 2014.
[99] Christoff PB. Reclosable bag, material, and method of and means for making the same. U.S. Patent 4,617,683. 1986.
[100] Straus SJ, Zuscik EJ, Bower WB, Yanidis A. Resealable packaging material. U.S. Patent 5089320. 1992.
[101] Timm LS, Bublitz TE. Resealable packaging system. U.S. Patent 5993962. 1996.
[102] Exner R, Dagestad O. Recloseable package. U.S. Patent 8596867. 2013.
[103] Trouilhet YM, Roulin J. Multilayer films for recloseable packaging. U.S. Patent 8617677. 2013.
[104] Haedt EL, Sheridan PJ, Michaels JJ, Nett LM. Peelable/resealable packaging film. U.S. Patent 7422782 B2. 2008.
[105] Cruz TK. Easy-open reclosable films having an interior frangible interface and articles made from them. U.S. Patent 8329276 B2. 2011.
[106] Ranganathan SS, Westmoreland BL, Moehlenbrock AW, Frost AJ, Shaver VA, Karam DC. Easy-open, reclosable package. U.S. Patent 8541081 B1. 2013.

[107] Trouilhet Y. Recloseable structures produced by co-extrusion coating PSA/ionomer. In: TAPPI European PLACE conference; 2011.
[108] Bardiot A, Sajot N, Gerard P, Notteau C. Hot-extrudable pressure-sensitive hot-melt adhesives and their use in multilayer films. U.S. Patent 7622176. 2009.
[109] Reade L. Sound method: ultrasonic sealing. Film & Sheet Extrusion; 2014. June 2014, p. 23–7, viewed July 27, 2014 from, www.filmandsheet.com.
[110] Bach S, Bunk N, Majschak J-P. Effect of laminate structure and morphology on fracture mechanics and seam strength of sealed seams. In: European TAPPI PLACE conference; 2013.
[111] Van Dun J, Bensason S, Thurling K. Polyolefins for ultrasound sealing. In: European TAPPI PLACE conference; 2013.
[112] Suresh KS, Roopa Rani M, Prakasan K, Rudramoorthy R. Modeling of temperature distribution in ultrasonic welding of thermoplastics for various joint design. J Mater Process Technol 2007;186:138–46.
[113] Tolunay MN, Dawson PR, Wang KK. Heating and bonding mechanisms in ultrasonic welding of thermoplastics. Polym Eng Sci 1983;23:726–33.
[114] Tateishi N, North TH, Woodhams RT. Ultrasonic welding using tie materials. Part I: analysis of process operation. Polym Eng Sci 1992;32:600–11.
[115] Brebner DL. Troubleshooting heat seal layers of Surlyn® ionomer resin. Precautionary measures in developing coextruded structures with heat seal layers of Surlyn®, DuPont technical literature, n.d.
[116] Van Ness RT. Heat seal performance. The role of contaminates and processing variables. TAPPI J 1979;62:79–82.
[117] Morris BA, Vansant JD. The influence of sealant modulus on the bending stiffness of multilayer films. In: TAPPI polymers, laminations and coatings conference; 1997. p. 165.
[118] DuPont. Sealant selector, viewed on August 2, 2014, from: http://www2.dupont.com/Packaging_Resins/en_US/Modeling_Tools/Sealant_Selector_Guide/index.html; n.d.

8 Barrier

Protecting the product is a critical function of packaging. Often this requires the inclusion of special barrier layers or coatings within a multilayer structure to manage gas permeation, provide oil and grease resistance, prevent loss or impartation of organic molecules affecting taste and aroma, and block light. This chapter examines the importance of barrier packaging, especially with respect to food packaging, describes methods for measuring barrier performance, and provides typical permeation properties of commonly used barrier materials. The science of permeation is highlighted with an emphasis on factors that control permeation. The chapter concludes with a critical review of four emerging technologies: oxygen scavenging, layer multiplier technology, barrier nanocomposites, and advanced coatings.

8.1 Why It Is Important

As described in Chapter 1, protecting the product is a fundamental function of a package. Packaging plays an important role in preserving the freshness of food by helping manage:

- oxygen ingress
- moisture (ingress or egress)
- carbon dioxide (for modified atmosphere packaging)
- light
- loss of flavorants, nutrients, and oils from the product to the package (known as scalping) or external environment
- loss of aromas from the product
- impartation of off-flavors, aromas, oils, or deleterious compounds to the food from the package or external environment

In pharmaceutical packaging, protecting active ingredients from moisture has been the primary barrier need, although oxygen barrier is increasingly becoming important for biological medicines.

The importance of barrier to food freshness is covered in detail in the food chemistry literature [1–4]. Only a brief overview is given here along with a summary of common barrier needs. There are many factors that influence the shelf life of food, which can be grouped into two categories (Table 8.1). Intrinsic factors are inherent to the food itself and extrinsic factors relate to the environment. Packaging is designed to mitigate many of the external factors.

Interactions between the intrinsic and extrinsic factors increase the likelihood of adverse reactions that limit shelf life. These include chemical/biochemical, microbiological, and physical interactions.

One of the most important chemical interactions that affect food quality is oxidation. Foods high in

Table 8.1 Factors Affecting Food Quality

Intrinsic Factors	Extrinsic Factors
• Water activity (water availability) • pH, type of acid • Microbes present in the product • Availability of oxygen • Redox potential • Natural chemistry of the product • Added preservatives • Product formulation • Packaging interactions	• Time temperature history during processing • Temperature, RH, and light exposure during storage and distribution • Gas composition inside package • Consumer handling

Adapted from Brown H, Williams J. Packaged product quality and shelf life. In: Coles R, McDowell D, Kirwan MJ, editors. Food packaging technology. Boca Raton (FL): Blackwell Publishing, CRC Press; 2003. p. 65–95.

The Science and Technology of Flexible Packaging. http://dx.doi.org/10.1016/B978-0-323-24273-8.00008-3
Copyright © 2017 Elsevier Inc. All rights reserved.

fats, especially unsaturated fats, are susceptible to oxidation and rancidity. There are three chemical routes to oxidation of fatty acids [1]:

- free radical oxidation in the presence of metal ion catalysts, heat, or light;
- photooxidation where photosensitizers such as chlorophyll or myoglobin affect the energetic state of oxygen; and
- enzymic oxidation catalyzed by lipoxygenase.

Once oxidation has been initiated by any of these routes, the reaction proceeds along the same lines. Hydroperoxide intermediates are formed, which then react to form aldehydes, ketones, and alcohols which give the off-flavor or odor associated with stale, rancid products.

The role of light, especially UV light found in fluorescent lighting in many retail stores, in the oxidation of foods has been well studied. Dairy products such as milk [5−13], cheese [14−16], yogurt [17] and sour cream [18], various oils [19−26], cookies [27], meat [28], and juices [29−31] are susceptible. These studies typically combine sensory panel and analytical testing to ascertain degradation mechanisms that result in off-flavor, color formation, and loss of food quality. Riboflavin (vitamin B2) is particularly prone to photooxidation and often contributes to the degradation of other components [32−35]. Korman [33] uses it as a model compound to study the ability of different packaging structures to block UV light and slow degradation. Other investigations compare the effectiveness of different package forms using actual food products [8,10,11,14,17,23,24,27]. Generally, the more light the package blocks, the longer is the shelf life, as determined by sensory panel or color change. Lennersten [23] determines the specific wavelength of light that is most deleterious to color change of mayonnaise. Since different polymers absorb light at different wavelengths, such studies may lead to better packaging structures, although none of the materials used by Lennersten completely prevents color change.

Successful strategies for limiting oxidation include lowering the oxygen level to less than 1%, limiting light exposure, and adding antioxidants. Packaging that provides oxygen barrier or scavenging, light barrier, and enables modified atmosphere packaging (MAP) is used. Examples include the following:

- using nitrogen flushed packaging for nuts to extend the time until the onset of rancidity;
- providing light barrier for packaging of dairy products, oily food, and juices, as described previously;
- vacuum packaging of fatty fish;
- MAP for fresh red meat to extend shelf life over simple plastic overwrap. MAP preserves the red color of meat longer. Vacuum packaging with a barrier film can be used for even greater shelf life but turns the meat purple. This low-oxygen state is the freshest state of a complex oxidation process of meat known as the myoglobin cycle. Consumer perception that red meat is freshest, however, has been difficult to change.

Fresh fruits and vegetables are living and respiring. Respiration can lead to a depletion of reserves, metabolic collapse, and disruption of tissue. Respiration can be slowed by lowering temperature or by controlling the atmosphere. Modified atmosphere packaging is often used to extend shelf life; optimal gas environments specific to each fruit or vegetable have been determined and can be found in the literature [3,37]. Ethylene scavengers are also sometimes used to slow the ripening process.

Microbial growth in food can consume nutrients, give off by-products such as gases or acids, and release enzymes. These may affect the texture, flavor, odor, and appearance of the food. Some enzymes persist after the death of the microorganism and contribute to spoilage. Deleterious pathogens such as *Listeria monocytogenes* and *Clostridium botulinum* can cause food poisoning. Under ideal conditions, bacteria populations double every 20 min and can reach $10^6/cm^2$ in 8 h. The minimum number of microorganisms before food quality in compromised depends on the intrinsic and extrinsic factors. These need to be carefully controlled to limit or prevent the impact of microoganisms. Counts of 10^6−$10^8/cm^2$ microorganisms per gram or square centimeter are often used as the upper limit, 10^5 when dealing with pathogenic bacteria [2].

Packaging technology can be used to control or kill microbes. Examples include retort or in-package pasteurization to sterilize and MAP and vacuum

packaging to exclude oxygen and/or introduce CO_2 which can retard growth of some microbes. Packaging structures that enable these processes contribute to the shelf life of the product.

Considerable research has been conducted on antimicrobial packaging [36] but with few commercial adoptions. One challenge is that it generally requires the package to be in direct contact with the food to be effective. (See Section 16.2.3 for more details on active packaging.)

Physical processes that limit shelf life include material damage during storage, transportation and distribution; insect infestation; and moisture effects. Packaging can play a role in each of these:

- Vibration, handling, and compressive loads during stacking may cause packages to burst or open. Structural integrity of the package is important.
- Insect penetrators bore holes into the package; having a good aroma barrier can help prevent this. Insect invaders enter through holes already present, such as in poor seals.
- Moisture ingress can affect the texture of dry foods such as cereals or crackers. Moisture loss can affect food quality; examples are changes in the color of fresh red meat and dehydration and freezer burn in frozen foods. Moisture loss also can result in serious economic consequences for products sold on a weight basis. Proper choice of packaging materials helps control moisture.

Migration of molecules from the outside environment or from the package itself into the food can result in poor food quality. Similarly, migration of components of the food into the package, known as scalping, can affect flavor or nutrient value. These molecules are typically larger than gas molecules and their migration in plastic packaging has not been well studied. Complex interactions may occur between the ingredients and the package, resulting in swelling or plasticization of the polymers that make up the package. This in turn may affect migration rates of the ingredients or other components in the food.

The barrier needs of several food types are summarized in Tables 8.2 and 8.3. This is based on data compiled by Petersen [37] and Robertson [3]. These are presented merely as starting points and derive from work in the 1970s by Salame [38]. Changes in food formulation, preparation, and packaging technology influence shelf life. The use of modified atmosphere packaging, for example, has grown. Robertson [2,3] reviews accelerated shelf-life testing, modeling, and other tools for helping determine barrier needs.

8.2 How to Measure

8.2.1 Definitions

A permeant is a gas or liquid molecule that migrates through the package film. Permeation is the amount of permeant that is transported through a unit area of film in a given time. The permeation coefficient, P, is normalized to a constant thickness and a given temperature and pressure. Typically, the pressure and temperature is standard temperature and pressure, STP, which unfortunately varies depending on the standard being considered; for example, IUPAC uses 0°C, 100 kPa and NIST uses 20°C, 101.325 kPa.

For gases, P has the following units:

$$P = \frac{(\text{Quantity of permeant})(\text{Film thickness})}{(\text{Area})(\text{Time})(\text{pressure drop across film})} \tag{8.1}$$

The quantity of the permeant may be in volume, mass, or molar units. There are many different units used in the scientific literature for P. For barrier packaging, the most common units for oxygen permeation are cm^3-mil/(100 in^2-day-atm) or cm^3-25-μm/(m^2-day-atm). Some conversion factors are given in Table 8.4. Note that the film thickness is in the numerator. A common mistake in converting units is to divide by the film thickness instead of multiplying. For example, suppose one measures the oxygen permeation of a 2-mil film to be 2 cm^3/(m^2-day-atm). To put this into standard units for P, the value needs to be normalized to a 1-mil film. Rather than dividing by 2, one must multiply by 2; $P = 4$ cm^3-mil/(m^2-day-atm). A way to remember this is to recognize that a 1-mil film should let more gas permeate through than a 2-mil film; hence the value for P should be higher than the measured results for the 2-mil film.

For oxygen permeation, P is typically called OPV or oxygen permeation value.

Table 8.2 Barrier Needs by Food Type

Food	Typical Time/ Temperature	Required Gas Composition	Optimum Barrier Properties				
			O_2	CO_2	H_2O	Light	Other
Animal Products							
Red meats	0–5°C, 6 –14 days	High oxygen (70–80%), high carbon dioxide (30–20%)	High	High	High		
	0–5°C, 1–4 days	No controlled atmosphere	Low		High		
Other meats	0–5°C, 1 day to 6 weeks	Low oxygen, high carbon dioxide	High	High	High		
Cured meat products	5°C, 4 weeks	No oxygen	High	High	High	High	
Cured fish products	5°C, 4 weeks	High carbon dioxide	High	High	High	High	
Fish, high fat	0–5°C, 1–7 days	Carbon dioxide (40%), oxygen (30%), nitrogen (30%)	High	High	Low		Odors
Fish, low fat	0–5°C, 1–7 days	Carbon dioxide (40–60%), nitrogen (60–40%)	High	High	Low		Odors
Eggs	2–12°C, 25 days to 4 weeks						Aroma
Fluid milk	2–5°C, 2 days to 8 months		High		High	High	Aroma
Fermented milk	2–5°C, 16 –18 days		High	High	High	High	Aroma
Fresh cheese	<5°C, 1–8 weeks		High	High	High	High	
Semi soft and hard cheese	<5°C, 1 –18 weeks		High	Low	High	Low or high	
Mold ripened cheese	<5°C, 1–8 weeks		High	High	High	High	

Butter, oil, dairy spreads, etc.	<5°C, 6 weeks or more		High		High	High	Odors, grease
Pasta (fresh)	2–5°C, 4 weeks	Low oxygen	High	High	High	High	
Fruits and Vegetables							
Root crops	0–25°C, from 1 week	No oxygen, no carbon dioxide	High	High	High	High	Odors
Most vegetables	0–25°C, from 1 week	Oxygen (1–5%), no carbon dioxide	High	High	High	High	Odors
Most fruits and some vegetables	0–18°C, from 1 week	Oxygen (1–5%), carbon dioxide (0–5%)	High	High	High	High	Odors
Dry Products							
Flour/grains	2°C—room temperature, 3 years				High		
Powders, high fat	Room temperature, 1 year	Low oxygen	High		High	High	
Powders, low fat	Room temperature, >1 year	Low oxygen	High		High	High	
Breakfast cereals	Room temperature, 1 year	Atmospheric/low oxygen	High	Low	High		
Pastas (dried)	Room temperature, 1–6 months				High		
Spices and herbs	Room temperature, from 6 months		High		High	High	
Snack foods	Room temperature, 1 year	Low oxygen	High		High	High	
Coffees/teas	5°C—Room temperature, 1 year	Low oxygen	High	Low	High	High	

(*Continued*)

Table 8.2 Barrier Needs by Food Type (*Continued*)

Food	Typical Time/ Temperature	Required Gas Composition	Optimum Barrier Properties				
			O_2	CO_2	H_2O	Light	Other
Breads	5°C—Room temperature, 1 day to 12 weeks	Low oxygen, high carbon dioxide	High	High	High		
Cakes	5°C—room temperature, 1 day to 4 months	Atmospheric/low oxygen, high carbon dioxide	High	High	High	High	
Crackers and cookies	Room temperature, 4 months				High		
Chocolates	2°C—room temperature, 6 −12 months					High	
Beverages							
Water	Room temperature, 1 year				High		Aroma
Juice	5°C—room temperature, 5 days to 1 year	Atmospheric, low oxygen	High		High	High	
Carbonated drinks (beer and soft drinks)	5 °C—room temperature, 6 months to 1 year	High carbon dioxide, low oxygen	High	High	High	High	
Frozen Foods							
High fat products	−18°C, 1 year	Low oxygen	High		High	High	
Low fat products	−18°C, 2 years	Low oxygen	High		High	High	
Others							
High fat products (dressing, sauce, etc.)	5°C—room temperature, 1 year	Low oxygen	High		High	High	Aroma, grease
Ready meals	2−5°C, 3 −21 days	Low oxygen, high carbon dioxide	High	High	High		

Adapted from Petersen K, Nielsen PV, Bertelsen G, Lawther M, Olsen MB, Nilsson NH, et al. Potential of biobased materials for food packaging. Trends Food Sci Technol 1999; 10:52−68 with permission.

Table 8.3 Degree of Protection Required by Various Foods Assuming 1-year Shelf Life at 25°C

Food/Beverage	Max O_2 Gain (ppm)	Other Gas Protection Needed?	Maximum Water Gain or Loss	High Oil Resistance Needed?	Good Barrier to Volatile Organics Needed?
Canned milk and flesh foods	1–5	No	3% loss	Yes	No
Baby foods	1–5	No	3% loss	Yes	Yes
Beers and wine	1–5	<20% CO_2 or SO_2 loss	3% loss	No	Yes
Instant coffee	1–5	No	2% gain	Yes	Yes
Canned soups, vegetables, and sauces	1–5	No	3% loss	No	No
Canned fruits	5–15	No	3% loss	No	Yes
Nuts and snacks	5–15	No	5% gain	Yes	No
Dried foods	5–15	No	1% gain	No	No
Fruit juices and drinks	10–40	No	3% loss	No	Yes
Carbonated soft drinks	10–40	<20% CO_2 loss	3% loss	No	Yes
Oils and shortenings	50–200	No	10% gain	Yes	No
Salad dressings	50–200	No	10% gain	Yes	Yes
Jams, jellies, syrups, pickles, olives, vinegars	50–200	No	10% gain	Yes	No
Liquors	50–200	No	3% loss	No	Yes
Condiments	50–200	No	1% gain	No	Yes
Peanut butter	50–200	No	10% gain	Yes	No

Adapted from Robertson GL. Shelf life of foods. In: Food packaging. Principles and practice, 3rd ed. Boca Raton (FL): CRC Press; 2013. p. 329–366. Reprinted with permission.

The transmission rate, TR, is defined as the amount of permeant that is transported through a film of unit area per time:

$$\mathrm{TR} = \frac{(\mathrm{Vol\ or\ mass})}{(\mathrm{Area})(\mathrm{Time})} \tag{8.2}$$

For different gases, TR may take on a specific descriptor such as oxygen transmission rate, OTR. Other acronyms in use include O2TR (oxygen transmission rate) and OGTR (oxygen gas transmission rate). The TR is a property of a package and permeant under the specific conditions of the test [pressure, temperature, thickness, package structure, relative humidity (RH), etc.] These should be specified when reporting data. An equation for calculating TR for a multilayer film from individual layer permeation values and thicknesses is given in Section 8.4.

Another important parameter governing gas or liquid diffusion and permeability is the solubility parameter, S, which relates the concentration of a gas to its partial pressure through Henry's law:

$$c = Sp \tag{8.3}$$

where c = concentration of permeant; S = solubility coefficient; p = partial pressure of the permeant.

The diffusion coefficient, D, relates the flux of the permeant, J, to the concentration gradient. This relationship is known as Fick's first law:

$$J = -\mathrm{D}\frac{dc}{dx} \tag{8.4}$$

Table 8.4 Conversion Factors for Several Units Used to Report Permeation of Gases

Unit	Multiply by This Factor to Get cm^3-mil/m^2-d-atm
cm^3-mil/m^2-d-atm	1
ml-mil/m^2-d-atm	1
cm^3-25 μm/m^2-d-atm	1
cm^3-mil/100 in^2-d-atm	15.5
Barrier [10^{-10} ml-cm/cm^2-s-(cm Hg)]	2587
ml-μm/m^2-d-atm	0.0394
m^3-μm/m^2-d-atm	39,370
in^3-mil/100 in^2-d-atm	254.2
ml-mm/m^2-d-atm	39.4
ml-mm/cm^2-d-atm	3.94E+05
ml-mm/cm^2-s-atm	3.40E+10
ml-mm/cm^2-d-Pa	3.99E+10
ml-mm/m^2-d-kPa	3989
m^3-μm/m^2-d-kPa	3,989,173
ml-μm/m^2-d-kPa	3.99

where J = flux of permeant (amount of permeant transporting through a unit area of film per time); D = diffusion coefficient; c = concentration of permeant (amount per unit volume); x = dimension normal to the surface of the film (thickness direction).

Here dc/dx is the concentration gradient or the difference in concentration across the film of thickness X:

$$\frac{dc}{dx} = \frac{c_{\text{outside}} - c_{\text{inside}}}{X} \tag{8.5}$$

where c_{outside} = concentration of permeant on the outside of the film; c_{inside} = concentration of permeant on inside of the film; X = thickness of the film.

The value of D relates to how fast the permeant will diffuse through the film at a given concentration gradient. Higher values of D indicate faster diffusion.

Section 8.4 shows that P is the product of D and S ($P = DS$) and is a steady-state value. The importance of these parameters is explored in Section 8.4. This section describes how to measure P, the parameter most relevant for determining barrier in flexible packaging. Once P is known for each layer in a multilayer package, the TR can be calculated. The TR multiplied by time yields the amount of permeant that will be transported into the package, which can be related to shelf-life performance.

8.2.2 Gas Permeation

A number of standards have been developed for measuring gas permeation through films. These are summarized in Table 8.5. Robertson [40] outlines four general methods for measuring gas permeability:

- Pressure increase. As described in ASTM D1434, a flat film is clamped to a chamber with the test gas introduced on one side and the pressure on the other side measured with a mercury manometer. The pressure drop is related to the TR.
- Volume increase. Also described in ASTM D1434, the change in volume at constant pressure is measured. Although not used as much as other methods, rapid measurements can be made for high TR films.
- Concentration increase. ASTM D3985, F1307, and F1927 describe methods to measure the TR by maintaining a constant total pressure on both sides of a film clamped in a cell. On one side, a partial pressure of the permeant gas is swept continuously across the film while an inert gas is maintained on the other side into which the permeant gas diffuses. The concentration of the permeant is measured by one of several techniques including chemical analysis, gas chromatography (GC), thermal conductivity, or special electrodes. The RH can be controlled. This method is probably the most commonly used method today given its speed and accuracy. Several companies sell test equipment including Mocon, Labthink Ltd., and OxySense.
- Detector film. A detector film is sealed between two pieces of test film. The detector film is coated with a reagent that changes its absorption spectra as the gas is absorbed. The TR is measured using a photospectrometer.

OPV results are typically reported in units of cm^3-mil/(100 in^2-day-atm) or cm^3-mil/(m^2-day-atm). Here the atm in the denominator is the total pressure drop across the film. For food packaging, air is on the outside of the package. Since air only contains 21% oxygen, the OPV should be multiplied by 0.21 to

Table 8.5 Summary of Standard Methods for Measuring Gas Permeation

Method	Title	What is Measured?
Oxygen Permeation		
ASTM D3985	Method for determination of oxygen transmission rate	Measurement of O_2 transmission through films,sheets,laminates,etc.
ASTM F1307	Method for determination of oxygen transmission rate through dry packages using a coulometric sensor	Measurement of steady-state rate of transmission of oxygen gas into packages
ASTM F1927	Method for determination of O_2GTR, permeability,and permeance at controlled relative humidity through barrier materials using ac coulometric detector	Determination of the rate of Transmission of O_2 gas, at steady state, at a given temperature, and %RH level, through film, sheeting, laminates, etc.
JIS K 7126	Method for determining the gas transmission rate of any plastic material in the form of film, sheeting, laminate, etc.	Determination of the gas transmission rate of any plastic material in the form of film, sheeting, laminate, etc.
DIN-53380 Part 3	Testing of plastics—Determination of gas transmissions rate	Oxygen-specific carrier gas method for testing of plastic films and plastics moldings
ISO-14663-2	Determination of steady-state rate of transmission of oxygen	Determination of steady-state rate of transmission of oxygen gas through ethylene/vinyl alcohol copolymer in the form of film
Water Vapor		
ASTM F1249	Test method for determination of O_2GTR, permeability, and permeance at controlled RH through barrier materials using a coulometric detector	Obtain reliable values for the water vapor transmission rate (WVTR) of plastic film and sheeting. The WVTR is an important property of packaging materials and can be directly related to shelf life and packaged product stability
ASTM D6701	Test method for determining WVTRs through nonwoven and plastic barriers (withdrawn)	Covers a procedure for determining the rate of water vapor transmission (WVT) ranging between 500 and 100,000 g/m2/day through nonwoven and plastic barrier materials. The method is applicable to films, barriers consisting of single or multilayer synthetic or natural polymers, nonwoven fabric, and nonwoven fabrics coated with films up to 3mm (0.1in.) in thickness
ASTM E398	Test method for determination of O_2GTR, permeability, and permeance at controlled RH through barrier materials using a Coulometric detector	Covers a procedure for determining the rate of WVT ranging between 500 and 100,000g/m2/day through nonwoven and plastic barrier materials. The method is applicable to films, barriers consisting of single or multilayer synthetic or natural polymers, nonwoven fabric, and nonwoven fabrics coated with films up to 3 mm (0.1 in.) in thickness

(*Continued*)

Table 8.5 Summary of Standard Methods for Measuring Gas Permeation (*Continued*)

Method	Title	What is Measured?
JIS K-7129	Plastics—film and sheeting—determination of WVTR by instrumental method	Specifies an instrumental method for determining the WVTR of plastic film, plastic sheeting, and multilayer structures including plastics that have smooth surfaces without any embossed portions, using a humidity detection sensor method, infrared detection sensor method, and gas chromatographic sensor method
ISO-15106-2	Plastics—film and sheeting—determination of WVTR—Part2: infrared detection sensor method	Specifies an instrumental method for determining the WVTR of plastic film, plastic sheeting, and multilayer structures including plastics, using an infrared detection sensor. The method provides rapid measurement over a wide range of WVTRs
TAPPI T-557	WVTR through plastic film and sheeting using a modulated infrared sensor	Covers a procedure for determining the rate of WVT through flexible barrier materials. The method is applicable to sheets and films up to 2.54 mm (0.1 in.) in thickness, consisting of single or multilayer synthetic or natural polymers and foils, including coated materials. It provides for the determination of (1) WVTR, (2) the permeance of the film to water vapor, and (3) for homogeneous materials, water vapor permeability coefficient
Carbon Dioxide		
ASTM F2476	Method for the determination of CO_2TR through barrier materials using an infrared detector	Determination of the steady-state rate of transmission of carbon dioxide gas through plastics in the form of film, sheeting, laminates, coextrusions, or plastic-coated papers or fabrics. It provides for the determination of (1) CO_2TR, (2) the permeation of the film to carbon dioxide gas (PCO_2), and (3) carbon dioxide permeability coefficient ($PvCO_2$) in the case of homogeneous materials.

Taken from Fereydoon M, Ebnesajjad S. Development of high-barrier film for food packaging. In: Ebnesajjad S, editor. Plastic films in food packaging. New York: Elsevier; 2013. p. 71–92.

obtain the OTR for the package. To avoid confusion, once this factor has been applied, the "atm" should be dropped from the units.

8.2.3 Moisture Vapor Transmission Rate

ASTM E96 describes what is often called the cup method. A desiccant is placed in a standard cup and the flat film sealed on top with wax. The container is placed in a controlled environment (typically 25°C, 75% RH or 38°C, 90 or 100% RH), and the weight gain is tracked over time. Moisture vapor transmission rate (MVTR) is equal to the slope of the weight versus time curve divided by the area of the film. While simple and inexpensive, this technique is labor intensive, takes several days to complete and cannot handle films with very low TRs. The partial pressure inside the cup may also change as the desiccant absorbs water. This is particularly true of silica gel [40].

An alternative is to use the desiccant weight gain method on the actual package, which may provide results that correlate better to a packaging application. This method is described in ASTM D3079.

More rapid methods, such as ASTM F1249, have been developed using infrared (IR) detectors to measure changes in RH on the dry side of a film located in a test cell. The film is positioned in the cell so that it divides the cell into two chambers, top and bottom. Water is placed in the bottom chamber to create a 100% RH atmosphere. The top side of the cell is swept with dry air and the change in RH measured with the IR detector. One disadvantage of this method

is that the RH is limited to 100% unless special equipment is used that allows for control over RH.

8.2.4 Permeation of Organic Molecules

Relatively little data have been published in the scientific literature for the permeation of organic molecules through plastic films. Organic molecules such as flavor or aroma molecules are large and complex. Their permeation often depends on their concentration and the presence and concentration of other permeants. Most gases are noninteracting with the polymer, and the diffusion coefficient is independent of concentration. This allows relatively simple Fickian diffusion equations to be used to interpret and predict behavior. Experimental results with pure gases can be extrapolated to low concentrations typical of real packages. For organic molecules, diffusion is often non-Fickian. Interactions between the permeant and the polymer may swell the polymer, creating more free volume and faster diffusion. The permeant may also plasticize the polymer, allowing polymer chains to move and more readily open temporary holes for the transport of the permeant molecules. Even if the permeant does not cause swelling or plasticization, other organic molecules may be present that do, allowing the permeant to diffuse more rapidly.

Organic molecule permeation experiments are often done with pure components to facilitate detection of the permeant. This has several drawbacks. One is that the presence of co-permeants may open up free volume through swelling or plasticization effects that would not be accounted for in an experiment looking at pure components one at a time. Secondly, food quality frequently suffers with just a small loss or gain of a flavorant molecule. Extrapolating from a high-concentration experiment to low concentration is problematic with non-Fickian diffusion since the diffusion coefficient is a function of concentration. Finally, odor/taste issues are often very difficult to attribute to a specific molecule, and if one is implicated it often is at very low concentrations compared to other molecules that may be present. Headspace GC or other methods may reveal a plethora of candidate species that are present, and the temptation is to pick a molecule that is present in abundance. Designing packaging film structures to minimize the permeation of that molecule may be counterproductive since the factors that influence its permeation rate may be totally different than the actual culprit molecule.

There is no standard method for measuring permeation of organic molecules. Methods typically involve one of the following, often with pure compounds with the limitations described previously [41]:

- measuring sorption into the polymer by following weight gain with time
- determining the amount of permeant released from the polymer once it has been saturated
- measuring the loss of permeant molecule from the aroma/flavor source.

Vaha-Nissi [41] uses a two-cell device with automatic sampling for GC analysis. They use a dilute blend of four aroma molecules to circumvent the concentration and co-permeant issues. Stevens [42] describes work at Mocon to measure aroma/flavor barrier. They create a three to five component aroma/flavor molecule "soup" using multidimensional GC. They test the permeation of the soup through the test material using an isostatic cell to measure individual and total permeation rates. They also couple human olefactory and analytical techniques to identify the key compounds to study.

8.3 Typical Permeation Values

8.3.1 Gas Barrier

Typical OPVs for high barrier polymers are given in Table 8.6, and OTRs for substrates in Table 8.7. Of the high oxygen barrier polymers, the most commonly used resins are ethylene vinyl alcohol (EVOH), polyvinylidene chloride (PVDC), and polyamide 6 (PA 6). These resins are described in Chapter 4. Here a few of the key attributes of these resins for barrier applications are highlighted.

8.3.1.1 Ethylene Vinyl Alcohol

- EVOH comes in a variety of compositions, usually designated by the mol% ethylene in the polymer backbone, ranging from about 27 to 48 mol%. The remainder of the polymer chain contains vinyl alcohol groups which are responsible for its oxygen barrier performance. The lower the percentage of ethylene, the lower the OPV. The limiting case of 0% ethylene is

Table 8.6 Typical Oxygen Permeation Value (OPV) and Moisture Vapor Transmission Rate (MVTR) Values for High Barrier Polymers

Resin	OPV 23°C/0% RH cc-mil/m^2-d-atm	MVTR 38°C/90% RH g-mil/m^2-d	References
LDPE/LLDPE	6500–7800	12–19	Robertson [40] and Butler [43]
HDPE	1600–2300	4–12	Robertson [40] and Butler [43]
EAA	3100–7750	15.5–25	Butler [43]
EMAA	3100–7750	15.5–25	Butler [43]
Ionomer	3100–7750	15.5–25	Butler [43]
EPE	7750–12,400	14–19	Butler [43]
EVA	9300–15,500	15.5–85	Butler [43]
EMA	9300–15,500	15.5–139	Butler [43]
ULDPE	9300–14,725	19–23	Butler [43]
POP/POE (mPE)	9300–31,000	20–31/31–46	Butler [43]
COC	1000	1–2	Constant [185]
PVDC	1.2–14	0.6–3.2	Robertson [40] and Butler [43]
PET	55–70	20–50	Robertson [40] and Butler [43]
PA 6	40–60	155–310	Robertson [40] and Butler [43]
aPA (6I/6T)	54	22	DuPont [44] and Kuraray [45]
MXD6	2.5–8	50	Mitsubishi Gas [46] and Kuraray [45]
EVOH (32 mol% ethylene)	0.3	60	Robertson [40], Butler [43] and DTF [47]
EVOH (44 mol% ethylene)	1.2	23	Robertson [40], Butler [43] and DTF [47]
Polyacrylonitrile	12	95	Kuraray [45]
PLA	465	620.00	Butler [43]
PS	5425	109–155	Butler [43]
PB-1	5970	15.5–19	Butler [43]

COC, *cyclic olefin copolymers;* EAA, *ethylene acrylic acid;* EMA, *ethylene methyl acrylate;* EMAA, *ethylene methacrylic acid;* EPE, *enhanced polyethylene;* EVA, *ethylene vinyl acetate;* EVOH, *ethylene vinyl alcohol;* HDPE, *high-density polyethylene;* LDPE/LLDPE, *low-density polyethylene/linear low-density polyethylene;* PA, *polyamide;* PB-*1, polybutene-1;* PET, *polyethylene terephthalate;* PLA, *polylactide;* POP/POE, *polyolefin plastomer/polyolefin elastomer, also known as mPE or metallocene plastomer;* PS, *polystyrene;* PVDC, *polyvinylidene chloride;* ULDPE, *ultralow-density polyethylene.*

polyvinyl alcohol (PVOH) which has excellent oxygen barrier but is not melt processable.

- The oxygen permeation of EVOH is sensitive to RH. As the RH increases above 60%, the OPV increases substantially. The OPV of EVOH with lower mol% ethylene changes more rapidly as RH is increased. This is shown in Fig. 8.1.
- EVOH is a transparent, melt processable resin. The processability improves with increasing mol% ethylene although the barrier performance decreases.
- EVOH is stiff, prone to flex cracking and difficult to thermoform. It is often sandwiched between layers of polyolefin or PA to improve performance.

Table 8.7 Typical Oxygen Transmission Rate (OTR) and Moisture Vapor Transmission Rate (MVTR) Values for Barrier Substrates

Substrate	OTR 23°C/0% RH cc/m^2-d-atm	MVTR 38°C/90% RH g/m^2-d	References
OPET	55–70	20	Robertson [40] and DTF [47]
OPET, PVDC coated	3–8	8.5	Robertson [40] and DTF [47]
met-OPET	0.65	0.5–1	Robertson [40] and DTF [47]
PP cast	3000–4200	8–12	Robertson [40] and DTF [47]
OPP	1550–1700	5	Robertson [40] and Jindal [48]
met-BOPP	25	<1	Robertson [40] and Jindal [48]
PCTFE—Aclar	5.4	0.24	Honeywell [49]
Cellulose (cellophane), PVDC coated	8	6–9	Robertson [40] and DTF [47]

Film thickness is 25 μm (1-mil). BOPP, *biaxial orientated polypropylene;* met, *metalized;* OPET, *oriented polyester;* OPP, *oriented polypropylene;* PCTFE, *polychlorotrifluoroethylene;* PP, *polypropylene;* PVDC, *polyvinylidene chloride.*

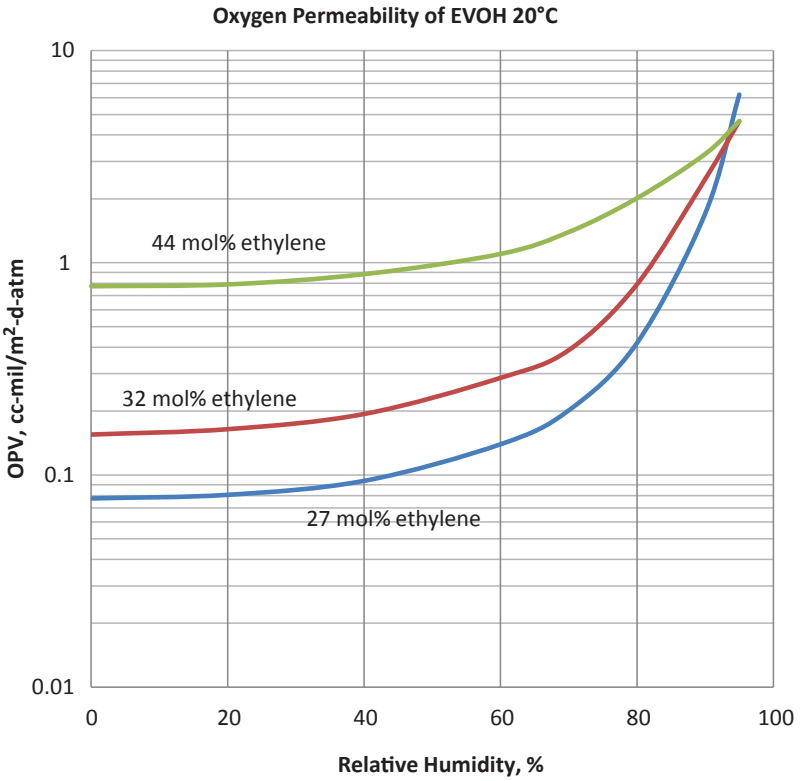


Figure 8.1 Oxygen permeation value (OPV) of ethylene vinyl alcohol (EVOH) as a function of relative humidity. *Data from Kuraray. Gas barrier properties of resins, Tech Bulletin No. 10, viewed 12 November 2014, from http://www.eval.eu/media/36916/ea%20-%20technical%20bulletin%20no%20110.pdf; 2007.*

- EVOH is used in coextruded barrier films for a wide variety of applications. Some example structures are given in Appendix B.

8.3.1.2 Polyvinylidene Chloride

- PVDC is used as a barrier coating or as a coextruded resin.
- PVDC is challenging to melt process since its decomposition temperature is close to its melting point. Temperature isolation and other equipment technologies have been developed to help process it.
- PVDC is one of the few barrier polymers that is not sensitive to RH. In addition to excellent oxygen barrier, it has low MVTR.

8.3.1.3 Polyamide

- PA 6 and PA 6/6,6 are the primary polyamides used in flexible packaging. PA 6/6,6 has improved flexibility, better clarity and gloss, improved dimensional stability, lower moisture sensitivity, and lower processing temperatures than PA 6, but is more expensive. They have similar oxygen permeation performance.
- Longer-chain polyamides, such as PA 12, absorb less water than PA 6 but have poorer oxygen barrier performance.
- Amorphous 6I/6T copolyamides are often blended with PA 6 to improve processibility, clarity, and oxygen barrier performance.
- MXD6 polyamide has lower oxygen permeability than PA 6 but is not used very much in flexible packaging due to cost and poor flex crack performance.
- The OPV of PA 6, 6/6,6 and MXD6 increases with increasing RH; the OPV of 6I/6T amorphous PA decreases with increasing RH.

8.3.1.4 Other Resins and Substrates

- Liquid crystal polymers generally have low oxygen permeability but have not found much use in flexible packaging due to their high cost and poor processability. They have very low molecular weight (MW) and viscosity, and most have very high melting point (T_m), making them difficult to match with other polymers in coextrusion. In films they exhibit highly anisotropic physical properties without the use of special rotating dies that have proven difficult to scale-up to commercial production.
- Polyethylene terephthalate (PET) is only a moderate oxygen barrier. Oriented PET has lower permeation but is still not sufficient for many high barrier applications. Oriented polyester (OPET) is often coated with PVDC or PVOH or metalized to achieve high barrier performance.
- Polyethylene naphthalate (PEN) is a polyester resin with about 3× the oxygen barrier of PET. The high cost and insecure supply of the monomer has limited its use.
- Aluminum foil has long been used in flexible packaging as a barrier layer. Gas permeability is essentially zero except for defects or cracks that may occur during manufacturing, handling, or flexing of the package during use.
- High barrier substrates are typically coated with a barrier material such as aluminum, SiO_x, AlO_x, or PVDC. The inorganic coatings are often susceptible to flex cracking and other abuse, resulting in pinholes and cracks that let gas permeate through. These films are typically laminated with other polymers to protect the barrier coating.

8.3.2 Moisture Vapor Barrier

Typical MVTRs for various polymer films and substrates are provided in Tables 8.6 and 8.7. The high moisture barrier polymers are hydrophobic and typically have a high level of crystallinity. Many of the high oxygen barrier polymers have poor barrier to moisture vapor. A quick guide to moisture and oxygen barrier can be found in Fig. 8.2.

8.3.2.1 Polychlorotrifluoroethylene

Polychlorotrifluoroethylene (PCTFE) film has the highest moisture barrier of any clear thermoplastic film. It is sold by Honeywell/Allied Signal under the tradename Aclar. It is used primarily in pharmaceutical blister package applications and in military ration packaging; its relative high cost compared to functional alternatives such as

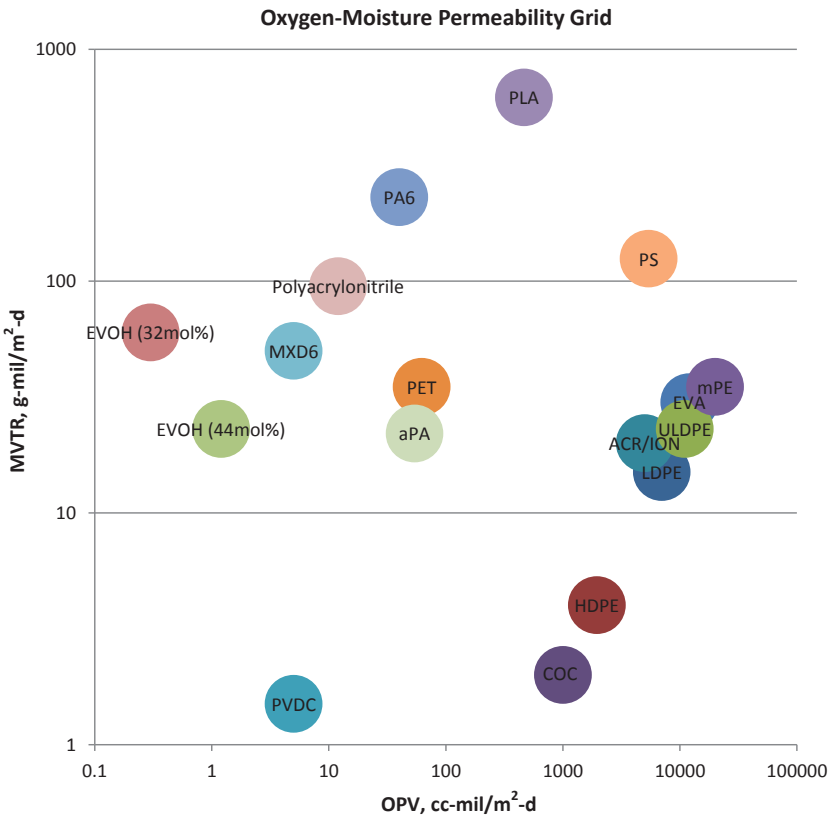


Figure 8.2 Moisture vapor transmission rate (MVTR) (38°C, 90% RH) and oxygen permeation value (OPV) (23°C, 0% RH) of common packaging resins. *ACR*, acid copolymer resins; *COC*, cyclic olefin copolymers; *EVA*, ethylene vinyl acetate; *HDPE*, high-density polyethylene; *LDPE*, low-density polyethylene; *PA*, polyamide; *PET*, polyethylene terephthalate; *PLA*, polylactide; *PS*, polystyrene; *PVDC*, polyvinylidene chloride; *RH*, relative humidity; *ULDPE*, ultralow-density polyethylene.

polyolefins keeps it out of most other flexible packaging applications.

8.3.2.2 Polyolefins

Of the commonly used polymers in flexible packaging, polyolefins have the highest moisture barrier. Isotactic polypropylene homopolymer and high-density polyethylene (HDPE) have the best moisture barrier properties within the standard polyolefin family of resins due to their high crystallinity. Crystalline regions are generally thought to be impermeable to gases or vapors and their presence also restricts the mobility of nearby molecules. The higher the level of crystallinity in the polymer, therefore, the better is the moisture barrier.

Cyclic olefin copolymers (COC) have excellent moisture barrier and are increasingly being used in pharmaceutical blister packaging.

8.3.2.3 Polyvinylidene Chloride

Of the high oxygen barrier polymers, PVDC is the only one that also has excellent moisture barrier. It is used as a barrier layer in coextruded films or as a coating onto PET or polypropylene (PP) substrates. Other high oxygen barrier polymers, such as EVOH or PA, swell in the presence of water, opening up voids on a microscale that allow water to permeate. In PVDC, the halogen groups more strongly interact with themselves than water, making the permeation insensitive to water or RH [50].

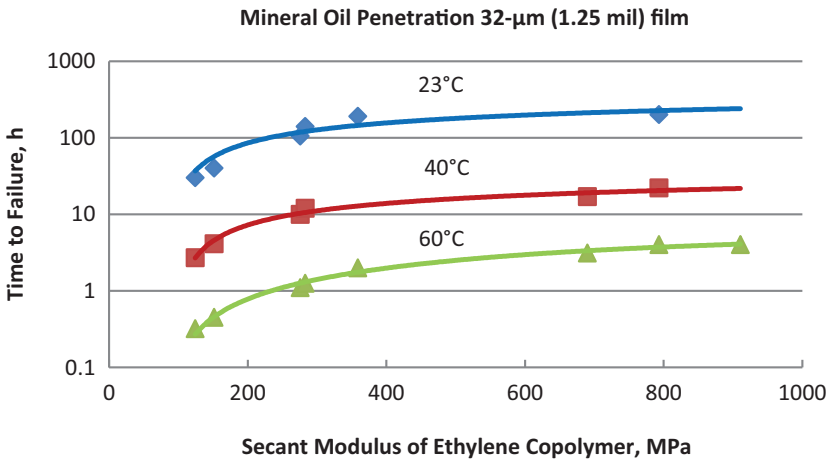


Figure 8.3 Penetration of mineral oil through polyolefin films.
Reproduced with permission from E. I. du Pont de Nemours and Company.

8.3.2.4 Other Substrates

Metalized oriented polypropylene (OPP) and aluminum foil also make excellent moisture barriers and are used as components of laminations used in flexible packaging.

8.3.3 Grease and Oil Resistance

Most of the high oxygen barrier polymers such as EVOH, PA, PVDC, and even PET have excellent oil and grease resistance due to their high level of crystallinity and polarity. The oil and grease resistance of polyolefins vary with their crystallinity and polarity. Based on an old chemistry adage of "like dissolves like" this is not surprising since oils are simply low MW polyolefins and generally nonpolar. In the following sections, the oil resistance of polyolefins is discussed based on work done at DuPont [51–53].

8.3.3.1 Polyethylene

The oil resistance of polyethylene (PE) is strongly affected by its crystallinity. In general, if the PE has lower crystallinity, the oil resistance is reduced. Crystallinity, in turn, is influenced by the density of the resin and film fabrication conditions (particularly quench conditions). For polyolefins and ethylene alpha-olefin copolymers like linear low-density polyethylene (LLDPE) the crystallinity increases with increasing density. For polar ethylene copolymers like ethylene vinyl acetate (EVA) the opposite is true due to the higher MW of the comonomer. One way to normalize the effect of crystallinity is to plot the oil resistance versus the secant modulus of the film.* Typical data for the penetration of mineral oil in PE are given in Fig. 8.3. Here the time to failure in a ground glass patch test (ASTM F-119-70) is plotted. In this method, a longer time indicates greater oil resistance. A change in slope occurs at around 350 MPa (50 kpsi), equivalent to about 0.935 g/cc density for a PE. The oil resistance levels off above this level of crystallinity. This suggests that an HDPE resin has about the same oil resistance as a medium-density polyethylene resin.

Similar results are found for peanut oil and are plotted in Fig. 8.4. Here grades of ionomer and a grade of PP are included for comparison.

EVA copolymer is expected to have comparable oil resistance to a PE with similar crystallinity. Again, secant modulus can be used as a common parameter. One of the data points in Figs. 8.3 and 8.4 is from a 5% VA copolymer (secant modulus equals 110 MPa or 16 kpsi); it fits on the same curves as the PE grades.

*Modulus increases with crystallinity; VLDPE and EVA's typically have a modulus in the range of 34–140 MPa (5–20 kpsi), LDPE and LLDPE 140–410 MPa (20–60 kpsi), and HDPE 690–970 MPa (100–140 kpsi). Cast films typically have a lower crystallinity and modulus than blown films of the same composition.

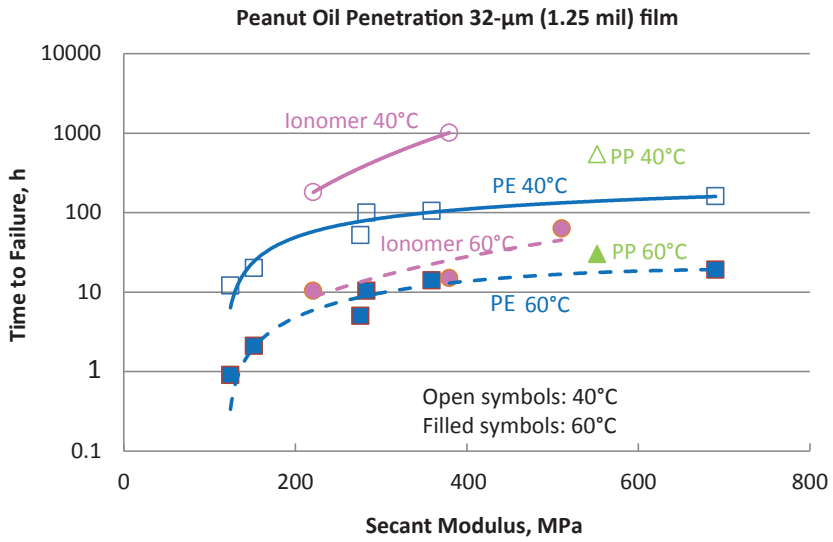


Figure 8.4 Penetration of peanut oil through polyolefin films.
Reproduced with permission from E. I. du Pont de Nemours and Company.

As the temperature is increased, the oil resistance decreases. The greater the density of the PE, the less sensitive the oil resistance is to changes in temperature. This may reflect the differences in melting points. Polyolefins melt over a temperature range with HDPE having a peak melting point of 135°C and low-density polyethylene (LDPE) 110°C. Some of the less perfect crystals melt at a temperature well below the peak melting point. At 60°C, some of the crystals in LDPE have begun to melt whereas very few crystals of HDPE have. It should be noted that this observation is based on a study done before the introduction of metallocene PE, which have much narrower melting point ranges.

8.3.3.2 Acid Copolymers

The oil resistance of acid copolymer resins (ACR) increases with increasing acid level. As the acid level is increased, the crystallinity decreases. This contrasts with PE where decreasing crystallinity reduces oil resistance. This suggests that hydrogen bonding among the acid groups in the copolymer is important for oil resistance.

Fig. 8.5 shows the effect of acid level on the resistance to mineral oil penetration. Most grades of acid copolymer have an acid level in the range between 4 and 12 wt% methacrylic acid (MAA) or between 3% and 9.5% acrylic acid (AA). At 12 wt% MAA, the oil resistance is substantially better than a standard LLDPE grade or metallocene plastomer, but not as good as HDPE (see Fig. 8.2). Data for EAA are not generated in this study, but EAA is expected to have similar performance as EMAA at equivalent mole % acid. Because AA has a lower MW than MAA, the wt% AA must be multiplied by 1.2 to convert from wt% AA to wt% MAA at the same mol%. Thus a 10 wt% AA EAA resin has about the same amount of acid on a molar basis as a 12 wt% MAA EMAA resin.

8.3.3.3 Ionomers

Partially neutralizing an acid copolymer typically improves its oil resistance. The greater the acid level and percent neutralization, the better is the resistance. Sodium ionomers typically give better resistance than equivalent zinc ionomers. In DuPont's Surlyn ionomer product line, Surlyn 1707 (sodium, 0.9 MI) and 1605 (sodium, 2.8 MI) have the best oil resistance. Surlyn 1652 (zinc, 5 MI) has the least oil resistance, but is still better than standard acid copolymers and LDPE.

Ionomers typically have better oil resistance than LDPE, LLDPE, and in many cases HDPE. See Fig. 8.4 for a comparison of peanut oil penetration. DeGaravilla [52] compares the corn oil penetration resistance of several polyolefins. His results, shown in Fig. 8.6, show that ionomers have substantially better oil resistance than other premium sealants such as very low-density polyethylene (VLDPE),

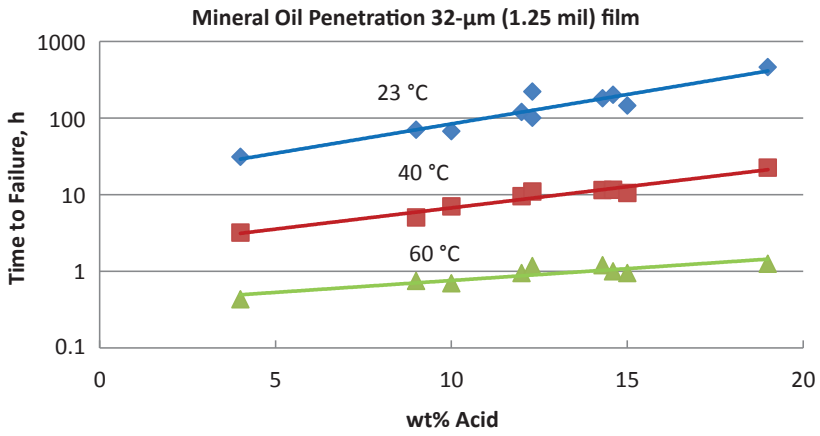


Figure 8.5 Mineral oil resistance of acid copolymers as a function of acid content (methacrylic acid) and temperature.
Reproduced with permission from E. I. du Pont de Nemours and Company.

metallocene polyethylene plastomer (mPE), and EVA. The oil resistance of Surlyn ionomers is sensitive to temperature; like PE, the higher the temperature, the poorer the oil resistance. The temperature dependence of the penetration of vegetable oils is illustrated in Fig. 8.7.

8.3.3.4 Polypropylene

One grade of PP is included in the DuPont study [51]. PP is found to have better oil resistance than HDPE and is comparable to the best ionomer grades. The sensitivity of the oil resistance of PP to temperature changes is greater than HDPE but about the same as ionomers. See Fig. 8.4.

8.3.3.5 Film Thickness

The DuPont study finds that the oil resistance of polyolefin films is non-linear with respect to film thickness. A doubling of the thickness results in a more than doubling of the oil resistance. (No

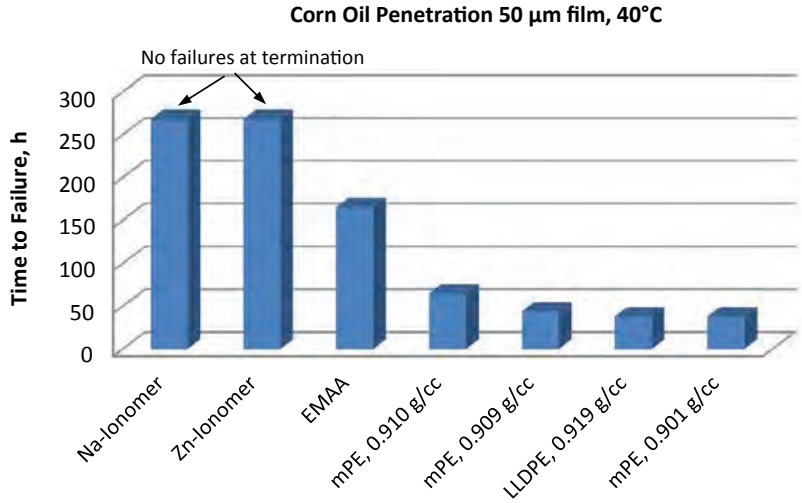


Figure 8.6 Oil resistance of several premium sealant resins. 50-µm film exposed to 40°C corn oil in ground glass test. Test terminated at 268 h (before ionomer samples failed). *EMAA*, ethylene methacrylic acid; *LLDPE*, linear low-density polyethylene.
From deGaravilla J. Ionomer, acid copolymer, and metallocene polyethylene resins: a comparative assessment of sealant performance. Tappi J 1995;78(6):192. Reproduced with permission from E. I. du Pont de Nemours and Company.

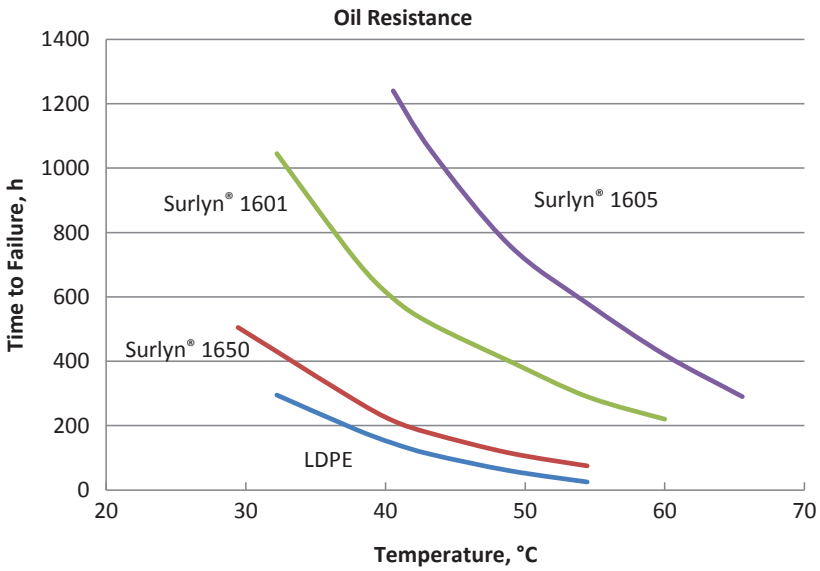


Figure 8.7 Oil resistance of several grades of Surlyn ionomer as a function of temperature. Samples from 25-μm extrusion coatings on paper. Tested in vegetable oil using ground glass test. *LDPE*, low-density polyethylene. *Composite data taken from Ref. [53]. Reproduced with permission from E. I. du Pont de Nemours and Company.*

explanation was given at the time. Subsequent studies have shown that the crystallinity at the surface of a blown film may be lower than the bulk. Thus, one explanation is that the thicker the film, the less impact the surface regions have on permeation.)

8.3.3.6 Oil Type

Most of the study by DuPont was done with mineral and vegetable (primarily peanut) oils. For mineral oil, it was found that the MW of the oil can have a substantial impact on oil resistance. A low MW oil, such as No. 2 fuel oil (similar to kerosene), will permeate through the film much faster than a standard mineral oil.

Vegetable oils are composed mainly of triglycerides and these can normally be expected to behave similarly regardless of the source. For example, it is found that soy oil and peanut oil give similar permeation rates. Other studies show peanut oil, corn oil, cottonseed oil, and olive oil give similar results. However, vegetable oil can contain various levels of free fatty acid that can greatly alter the permeation rate and even the comparison between ionomers and PE. In one such case, the permeation rate of rice oil containing 18% free fatty acid is found to be considerably faster through an ionomer than through LDPE. (For comparison, the peanut oil used in the study has only 0.14% free fatty acid.) Consequently, the oil resistance of the ionomer to rice oil is poorer than an LDPE with density 0.922 g/cc.

8.3.4 Organic Molecules

The migration of aroma and flavor molecules into or through packaging films is a challenge to measure due to interactions between the molecules and package, as is discussed in Section 8.2.4. What little data that exist in the literature should be viewed with caution; studies may be conducted at concentration ranges that do not reflect real packaging applications or in absence of other molecules that may affect the migration rates.

Many packaging engineers assume that barrier to organic molecules correlates with oxygen barrier. While high barrier polymers such as EVOH, PA, and even PET often provide good barrier to aroma and flavor molecules, this is not always the case.

d-limonene is one of the most studied molecules. Polymers that have shown to be good barriers include acrylonitrile (Barex), PET, amorphous PA (DuPont Selar PA), EVOH, and polylactic acid (PLA) [54,55].

The permeation of flavor and aroma molecules is discussed in more detail in Chapter 16, where product–package interactions in the end-use are considered.

8.3.5 Chemical Resistance

Chemical resistance can be important for some packaging applications, such as in the packaging of chemicals, cleaning agents, reagents, and alcohol towelettes. Chemicals can affect the strength, flexibility, impact resistance, appearance, dimensions, and weight of packaging films. For plastics, chemicals may attack the polymer chain through oxidation reaction to functional groups on the chain or depolymerization. Chemicals may swell or soften the polymer. Some chemicals may also cause stress cracking.

The chemistry of the polymer that makes up the package and the product are two prime factors affecting chemical resistance, but a number of other factors are important. In general the chemical resistance will decrease with increasing temperature, higher concentration of the chemical, higher pressure, longer exposure time, and higher residual stress. Mixtures of chemicals may also affect resistance in ways single chemicals do not. For example, one chemical may swell the polymer, allowing another to permeate and react with the polymer.

There are a number of references on chemical resistance of polymers. A good general reference is the *Chemical Resistance of Plastics and Elastomers* [56]. A number of tables can be found online [57–61]. Most of the data used in these references are generated using thick plaques and may not represent what may occur in a thin film. Because of this and the many factors outlined above that affect chemical resistance, these references should only be used as a guide. Testing the actual package under conditions of its actual use and environment is always warranted.

8.3.6 Light Barrier

More opaque films are better light barriers. Some transparent films, however, will preferentially absorb certain wavelengths of interest, blocking them from the product. For example, amorphous nylon (PA 6I/6T) absorbs light in the UV wavelength that is often used in supermarkets and is deleterious to a number of foods [62].

Aluminum foil, some types of paper, and metalized films provide good light barrier. Pigments and fillers are also used to create opacity. Rutile titanium dioxide, TiO_2, is a particularly effective additive for light barrier because of its high refractive index [63]. To create a good barrier to light, the film must bend the light wave. One way is to add an inorganic material that has a higher refractive index than the plastic film. Calcium carbonate, clay, and barium carbonate have refractive indices too close to most plastics to scatter much light. Rutile, followed by anatase, TiO_2 is very effective. Particle size also affects scattering and opacity. The optimal particle diameter depends on the wavelength of light being scattered:

$$\mathcal{D} = \frac{2\lambda}{\pi(\varepsilon_1 - \varepsilon_2)} \tag{8.6}$$

where $\mathcal{D}$ = optimal particle size for a given wavelength; λ = wavelength of light being scattered; $\varepsilon_1 - \varepsilon_2$ = refractive index difference between the polymer and particle.

For scattering of visible light, a range of particle sizes works best.

Opacity increases with increasing concentration of the pigment and film thickness [64].

$$\text{Scattering} \propto \varepsilon lc \tag{8.7}$$

where ε = refractive index; X = thickness of polymer film layer thickness; c = concentration of pigment in polymer.

Increasing the concentration by two times is equivalent to increasing the film thickness by two times. It is the total amount of pigment that controls scattering. Splitting the pigment layer into separate layers separated by clear layers has no effect on the opacity.

8.4 Science of Permeation

The permeation of gas or liquid molecules through flexible packaging films generally follows one of two modes:

- Sorption of the permeant onto the film, diffusion through the film, followed by desorption on the other side. This is the mode for most polymer films.
- Permeation or effusion through pinholes, cracks, or other defects in the film. This mode explains the behavior of aluminum foil, metalized films, and glass-coated films.

8.4.1 Permeation Through Polymer Films

The mechanism for permeation through a polymer film is illustrated in Fig. 8.8. The permeant is absorbed onto the surface, diffuses through the film, and desorbs on the other side. The driving force for

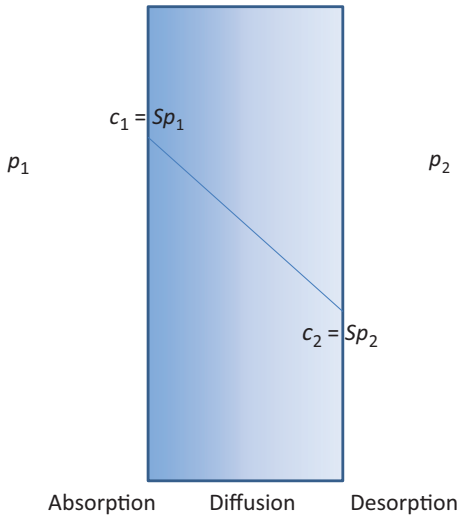


Figure 8.8 Mechanism for permeation through a polymer film.

flow of a permeant through a polymer film is the concentration gradient, or the difference between the concentrations on each side of the film divided by the film thickness, as given by Eq. (8.5).

Fick's first law, given by Eq. (8.4), relates the diffusive flux to the concentration gradation through the proportionality constant D. D is known as the diffusion coefficient and has units of [length^2/time]. Larger values of D indicate greater diffusion. If D is independent of concentration then the diffusion is known as Fickian. If D changes with concentration it is known as non-Fickian. The diffusion of most inert gases through polymer films is Fickian. The diffusion of larger organic molecules, as well as moisture, for some polymers may be non-Fickian.

Fick's second law relates the change in concentration with time to the derivative of the concentration gradient. For thin films it is assumed that the diffusion is only in the thickness dimension:

$$\frac{\partial c}{\partial t} = \mathrm{D}\frac{\partial^2 c}{\partial x^2} \tag{8.8}$$

Here D is assumed to be independent of concentration (Fickian).

If the diffusion is at steady state, the diffusive flux is constant and Eq. (8.4) can be integrated over the thickness:

$$JX = -\mathrm{D}(c_2 - c_1) \tag{8.9}$$

Substituting the definition of J ($= Q/At$) into Eq. (8.9) gives the following relationship for Q:

$$Q = \frac{\mathrm{D}(c_2 - c_1)At}{X} \tag{8.10}$$

where Q = quantity of permeant; A = film area; t = time; and X = film thickness.

For gases it is convenient to use partial pressures rather than concentration. The concentration of a dilute gas is equal to the product of the partial pressure and the solubility coefficient of the permeant in the polymer (S). This relationship is known as Henry's law and is introduced in Eq. (8.3).

Substituting Eq. (8.3) into (8.10):

$$Q = \frac{DS(p_2 - p_1)At}{X} \tag{8.11}$$

The product DS is known as the permeability coefficient, P:

$$P = DS. \tag{8.12}$$

Eq. (8.11) becomes

$$Q = \frac{P(p_2 - p_1)At}{X}. \tag{8.13}$$

Since the permeability is a fundamental quantity of a polymer and is often used to compare and select polymers for barrier applications, reviewing the assumptions used in deriving P and their limitations is in order:

- Diffusion is at steady state. For most gases this turns out to be a good assumption. Ylvisaker [58] shows that steady state is reached when $t > 0.5X^2/D$. Since most flexible packaging films are thin, steady state is reached within hours. For example, Ylvisaker calculates the time to reach steady state for moisture transport through an OPP film to be 15 min. For large molecules, the diffusion is slower, particularly if there is any interaction between the permeant and polymer. Unsteady-state calculations may need to be considered for these permeants [40,65].
- Diffusion is one-dimensional. The thickness dimension of flexible packaging films is typically orders of magnitude smaller than either of the planar dimensions. This assumption is

usually valid.

- Diffusion is Fickian, and the diffusion coefficient is independent of concentration. This is true for most gases such as oxygen, nitrogen, and carbon dioxide. It fails to be true for water in some polymers, as well as some large organic molecules that interact with the polymer.

By definition, P is independent of thickness and is a material property rather than a package property. On the other hand, the TR is a package property that relates the amount of permeant that is transported through a package film with a particular structure subject to a given environment (pressure, RH, etc.). For a monolayer film, TR is related to P is the following manner for gases:

$$\mathrm{TR} = \frac{P\Delta p}{X} \tag{8.14}$$

When the film thickness is halved, the TR doubles.

8.4.1.1 Permeation Through Multilayer Films

For multilayer films a total permeation coefficient can be computed. Fig. 8.9 shows the key parameters for permeation through a three-layer film. At steady state, the amount of permeation, Q, through each layer is equal:

$$Q = Q_1 = Q_2 = Q_3 \tag{8.15}$$

Also, the area of each layer is the same:

$$A = A_1 = A_2 = A_3 \tag{8.16}$$

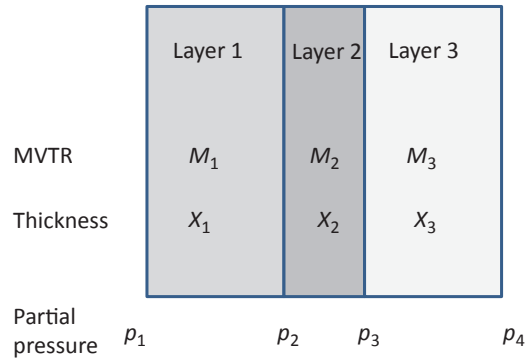


Figure 8.9 Permeation through three-layer film. *MVTR*, moisture vapor transmission rate.

The pressure drop across the multilayer film is the sum of pressure drops across each layer:

$$p_1 - p_4 = (p_1 - p_2) + (p_2 - p_3) + (p_3 - p_4) \tag{8.17}$$

Rearranging Eq. (8.13):

$$\Delta p = \frac{QX}{tPA}. \tag{8.18}$$

Substituting into Eq. (8.15):

$$\frac{QX_\mathrm{T}}{tP_\mathrm{T}A} = \frac{QX_1}{tP_1A} + \frac{QX_2}{tP_2A} + \frac{QX_3}{tP_3A} \tag{8.19}$$

where X_i = thickness of layer i; X_T = total thickness of the multilayer film; P_i = permeability coefficient of layer i; P_T = permeability of multilayer film.

Factoring out Q/tA:

$$\frac{X_\mathrm{T}}{P_\mathrm{T}} = \frac{X_1}{P_1} + \frac{X_2}{P_2} + \frac{X_3}{P_3} \tag{8.20}$$

Extending to n layers yields the general relationship for permeation through a multilayer film:

$$\frac{X_\mathrm{T}}{P_\mathrm{T}} = \sum_{\mathrm{i}=1}^{n} \frac{X_\mathrm{i}}{P_\mathrm{i}}. \tag{8.21}$$

In terms of TRs:

$$\frac{1}{\mathrm{TR}_\mathrm{T}} = \sum_{\mathrm{i}=1}^{n} \frac{1}{\mathrm{TR}_\mathrm{i}}. \tag{8.22}$$

A consequence of Eq. (8.21) is that if one of the layers has a much lower P than the other layers, the other layers do not contribute much to the overall permeability of the film. For example, in a coextruded film with the structure (PE-tie-EVOH-tie-PE), the PE and tie layers do not contribute much to the oxygen barrier—it almost all comes from the EVOH layer. Functionally, however, the other layers may contribute to the barrier of the structure by reducing pinholes or flex cracks in the EVOH, or by helping to maintain layer continuity during thermoforming.

8.4.1.2 Factors that Affect Permeability Through Polymer Films

The chemistry and structure of the polymer film, the permeant molecule, and the external environment affect the rate of permeation through a polymer film. Although *P* is the product of diffusion and solubility, *P* generally trends with D. The solubility coefficient varies by about two orders of magnitude for various polymers and permeants, whereas the diffusion coefficient may vary over six orders of magnitude [66].

8.4.1.2.1 Polymer Factors

The diffusion of permeant molecules through polymer films can be thought of as a series of hops through temporary voids in the polymer microstructure. These voids are related to the free volume of the polymer, which is defined as the difference in molar volume at the system temperature and at 0 K. The voids are due to imperfections in packing for polymers above their Tg and vibration and rotation of molecular segments for both rubbery and glassy polymers [50]. *P* generally increases with increasing free volume, as is shown in Fig. 8.10 based on the work of Lee [66].

Factors that decrease free volume (and gas permeation) include the following:

- Absence of bulky side groups on the polymer chain.
- Narrower molecular weight distribution (MWD) and less long-chain branching.
- Higher cohesive energy density (CED). CED is introduced in Chapter 6. It is a quantitative measure of how strongly the polymer molecules interact with one another. Stronger interactions generally result in higher packing densities.
- More rigid polymer chains. Chain stiffness hinders molecular movement, reducing the creation of temporary voids for permeant molecules to hop into.
- Higher crystallinity. Crystals are generally impermeable and so by themselves they reduce permeation to the surrounding amorphous

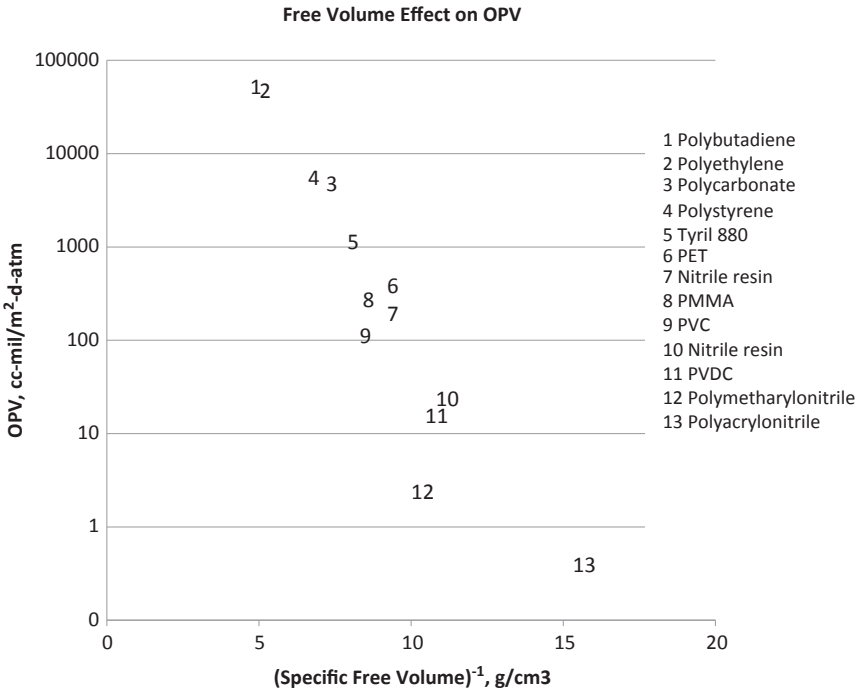


Figure 8.10 Influence of polymer free volume on permeability of oxygen. *OPV*, oxygen permeation value; *PET*, polyethylene terephthalate; *PMMA*, polymethyl methacrylate, *PVC*, polyvinyl chloride; *PVDC*, polyvinylidene chloride.

Based on work of Lee WE. Selection of barrier materials from molecular structure. Polym Eng Sci 1980;20:65–69. Printed with permission.

regions. Their orientation and morphology may create a tortuous path for the permeant molecule to pass through. Crystals can also inhibit the movement of nearby molecules in the amorphous regions of the polymer, affecting free volume.

- Higher polarity. Polarity generally increases chain stiffness and CED. An example of the effect of polymer functional group chemistry on oxygen permeation is given in Table 8.8. The side groups with the greater polarity have the lowest permeation. Polarity also may increase the interaction with polar permeant molecules. Increased interaction slows down diffusion.
- Higher Tg. The solubility of permeants in glassy polymers ($T < \text{Tg}$) may be greater than in rubbery polymers ($T > \text{Tg}$) due to the presence of unrelaxed voids that may form during quenching [50]. The lower chain mobility in the glassy region, however, reduces free volume and diffusion, and typically outweighs the solubility effect.
- Higher orientation. Orientation aligns the molecules and can increase packing density, which reduces free volume. Orientation may also induce crystallization and morphologies that are conducive to lower permeation. Orientation processes, such as tenter frame and double bubble processes, typically decrease the permeability but the effect varies with the polymer.

Table 8.8 Effect of Vinyl Functional Group on Oxygen Permeability

Functional Group R in $(-CH_2-CHR-)_n$	Oxygen Permeation Value cc-mil/m^2-d-atm
−OH	1.6
−CN	0.62
−Cl	124
−F	233
$-COOCH_3$	259
$-CH_3$	2328
$-C_6H_5$	6468
−H	7502

With permission from Robertson GL. Optical, mechanical and barrier properties of thermoplastic polymers. In: Food packaging. Principles and practice, 3rd ed. Boca Raton (FL): CRC Press; 2013. p. 91−130.

- Absence of plasticizers and lubricants. Plasticizers and lubricants increase the flexibility and molecular mobility of the polymer chains, increasing free volume. Plasticized versions of polyvinyl chloride (PVC), for example, may have OPV values of that are 200 times greater than unplasticized PVC [40].
- Interaction between polymer chains. Beyond hydrogen bonding, ionic, and other chemical interactions that influence CED and packing density, cross-linking reactions may take place. Cross-linking limits mobility of polymer chains, reducing free volume. Robertson provides an example where one cross-link out of 30 monomers leads to a 50% reduction in D [40].

8.4.1.2.2 Thickness

Permeability is normalized for thickness of the film and so in theory is independent of thickness. This is true if the polymer itself is unchanged by thickness. The stress and cooling conditions in the film manufacturing process, however, may change as the thickness is altered. This may affect the orientation and crystalline morphology of the polymer. This in turn may affect the permeability [67,68]. Haley and Borke [68] provide an example for the MVTR of HDPE. They measure the MVTR of blown films ranging in thickness from 30 to 75 μm for 11 different grades of HDPE. The grades are manufactured with a variety of catalyst technologies and have a range of MW and MWD characteristics. The characteristics of a selected set of resins from their study are shown in Table 8.9. These resins are selected to highlight the differences in their permeation behavior, which are plotted in Fig. 8.11. The MVTR of some of the resins are independent of thickness, whereas others show an increase in MVTR with decreasing film thickness. The authors conclude that polydisperse HDPE grades with Mz greater than about 400,000−500,000 g/mol are more susceptible to morphological changes during film blowing and exhibit an increase in MVTR with decreasing thickness. (Mz is a version of MW that is weighted toward the high MW fraction of the polymer.) They correlate the change in MVTR with overall crystallinity.

8.4.1.2.3 Permeant Factors

The size, shape, chemistry, and, in some cases, the concentration of the permeant influences P. The

Table 8.9 Characteristics of High-Density Polyethylene Grades Used in Haley and Borke [68] Study

Sample	Type	Catalyst	Process	Density g/cc	MI g/10 min	Mn g/mol	Mw g/mol	Mz g/mol
CC-1	Ethylene −butene	Chrome		0.949	0.3	12,000	140,000	568,000
SH-4	Homopolymer	Vanadium/ titanium	Solution	0.960	1.0	24,000	121,000	380,000
ZC-1	Ethylene −butene	Ziegler−Natta	Slurry cascade	0.949	0.1	10,000	296,000	1,574,000
ZH-2	Homopolymer	Ziegler−Natta	Slurry cascade	0.957	1.3	22,000	123,000	407,000

MI, *melt index;* Mn, *number average molecular weight;* Mw, *weight average molecular weight.*

relative diffusion, solubility, and permeation factors for several gas molecules are given in Table 8.10.

Larger and bulkier molecules will diffuse more slowly, although they may have greater solubility and condense more readily onto the surface of the film. Molecules with eight or more carbons are sorbed more easily than smaller molecules. Branched molecules are sorbed more easily than linear molecules. Larger molecules are more likely to condense on the surface of the film [69].

The polarity of the permeant and the polymer affects the diffusion rate. The greater the affinity of the permeant to the polymer, the slower is the diffusion. Cooksey [69] provides the example of carvone ($C_{10}H_{14}O$) and limonene ($C_{10}H_{16}$). Both have 10 carbons. Limonene is less polar and permeates faster through nonpolar films. The solubility parameter, introduced in Chapter 6, is a way to estimate polarity differences. The solubility parameter is related to the square root of the CED and can be found tabulated in various references [71−73]. The solubility parameters for several polymers can be found in Table 6.2. In general, small differences in solubility parameters of the permeant and polymer indicate an affinity that may result in greater interactions. Auras [55] provides a good grounding on the use of solubility parameters for flavor−polymer interactions as well as an example. They study the sorption of ethyl acetate and d-limonene by several polymers including PLA, polystyrene (PS), PET, PP, and PE. The difference in

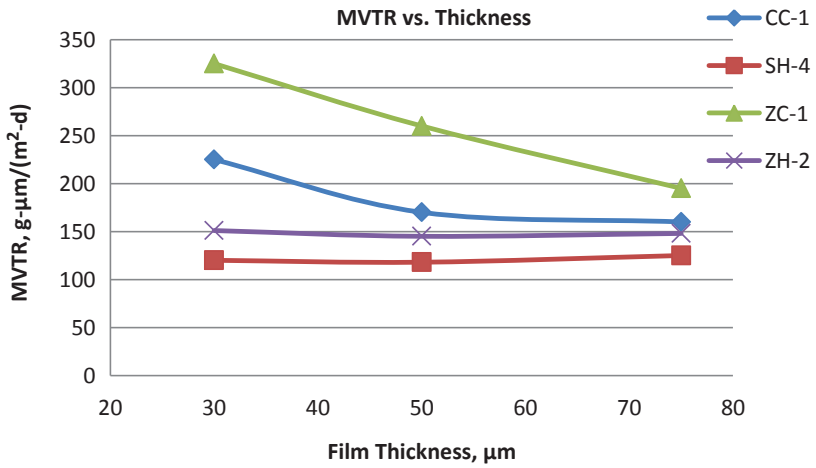


Figure 8.11 Moisture vapor transmission rate (MVTR) (normalized for thickness) as a function of blown film thickness.

Data from Haley JC, Borke JS. The interplay between polymer polydispersity and film gauge in HDPE barrier films: how polydispersity controls gauge dependence of film barrier properties. In: SPE ANTEC conference; 2009. p. 231−235.

Table 8.10 Effect of Gas Molecule on Permeation, Diffusion, and Solubility

Gas	Permeation	Diffusion	Solubility
N_2 (=1)	1	1	1
CO	1.2	1.1	1.1
CH_4	3.4	0.7	4.9
O_2	3.8	1.7	2.2
He	15	60	0.25
H_2	22.5	30	0.75
CO_2	24	1	24
H_2O	550	5	10

Nitrogen value is 1; others values are relative to nitrogen.
From Van Krevelen DW, te Nijenhuis K. Properties of polymers. Amsterdam: Elsevier Science; 2009. p. 655–702.

solubility parameters between the flavor molecule and polymer correlates fairly well with sorption (S) but not very well with permeability (P). They conclude that the solubility parameter method is useful for predicting S but does not account for specific interactions such as swelling, dissolution, or immiscibility. This may account for the poor correlation with permeability.

Interaction between the permeant molecule and the polymer can lead to swelling or plasticization effects. This results in greater free volume and higher permeation, not only for the permeant molecule causing the effect, but for other molecules that may be present. Such interactions are often more pronounced at higher permeant concentrations, leading to non-Fickian diffusion behavior. Moisture vapor permeation has this effect on some polar polymers which is discussed in more detail in Section 8.4.1.2.4.3.

8.4.1.2.4 Environmental Effects

8.4.1.2.4.1 Temperature

$\mathcal{D}$, S, and P all tend to increase with increasing temperature, following an Arrhenius relationship:

$$P = P_0 e^{-\frac{E_p}{RT}} \tag{8.23}$$

where P_0 = permeability coefficient at reference temperature; E_p = activation energy; R = ideal gas constant; T = temperature (K).

The activation energy is made up of contributions from $\mathcal{D}$ and S:

$$E_p = E_d + \Delta H_s \tag{8.24}$$

where E_d = activation energy for diffusion; ΔH_s = heat of sorption.

E_d is always positive; diffusion increases with increasing temperature. ΔH_s is generally positive for gases but negative for vapors: solubility increases with increasing temperature for gases and decreases for vapors. P may increase or decrease with temperature depending on the relative contributions of S and D. As a result, the order of performance of barrier films may change with temperature [40].

The glass transition temperature impacts the temperature dependence of P. Cooksey [69] reports that for gas permeation, P increases by about 9%/°C at temperatures above the Tg of the polymer and about 5%/°C at temperatures below Tg.

8.4.1.2.4.2 Pressure

Pressure has little impact on permeability unless the permeant has a strong interaction with the polymer (then P increases with pressure). It is important to note that for gas permeation, it is the partial pressure of the permeant, not the total pressure, that is the driving force for diffusion. Robertson [40] reports on studies of high-pressure pasteurization, citing the work of Juliano [74] and Guillardo [75]. These studies show that at the high pressures experienced in this process (300–600 MPa), gas transmission is more affected by distortion of the film that may result in leakers than by the effect of pressure on permeability.

8.4.1.2.4.3 Relative Humidity

The permeability of some polymers is sensitive to water. Examples include PVOH, EVOH, PA6, PA6,6/

6, and acrylonitrile. In these polymers water acts as a plasticizer or lubricant, increasing the mobility of the polymer chains and increasing free volume. At higher RH, the permeability increases, as is shown in Fig. 8.12.

The permeability of nonpolar polymers such as polyolefins is generally not sensitive to water. This is because the solubility of water in these polymers is too low to have a plasticizing effect. Highly polar polymers containing halogens (Cl or F atoms), such as PVDC and fluoropolymers, more strongly interact with each other than to water [50]. Their barrier properties are insensitive to RH.

One interesting exception in the polyamide family of resins is PA 6I/6T or amorphous nylon (sold as Selar PA by DuPont and Grivory by EMS). The oxygen permeation of this polyamide decreases with increasing RH. Studies show that this is due to the presence of both aliphatic and aromatic units along the polymer chain. Longer aliphatic chains increase the overall permeability, but are responsible for the drop in permeability with higher RH. The studies conclude that water molecules compete with gas molecules for pathways through the polymer, decreasing the permeability of the gas [50].

In flexible packaging, water-sensitive high-oxygen barrier polymers such as EVOH are typically sandwiched between other polymers, especially polyolefins. Many mistakenly believe that by placing the EVOH between good moisture barrier resins like PE that the EVOH is protected from water. This is only true during the first few minutes of exposure until the transport of moisture reaches a steady state. For thin films, steady state can be reached in a few hours [58,184]. Granger [184] measures the OPV of EVOH monolayer and symmetric coextruded films of (LDPE-tie-EVOH-tie-LDPE) over a range of RH from 0% to 100%, where the RH is controlled to be the same on both sides of the film. The OPV results from the mono and coextruded structures fit on top of one another, indicating that the LDPE is offering no protection from the moisture once steady state is reached.

In a multilayer film, the RH of the EVOH layer falls somewhere between the RH on the inside and outside of the package. The composition and

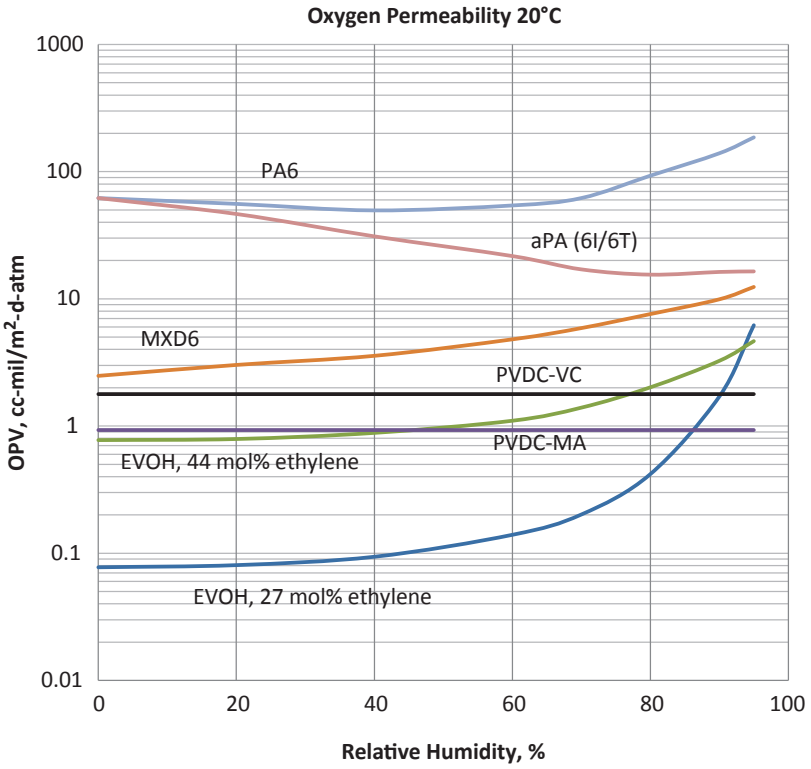


Figure 8.12 Effect of relative humidity on the oxygen permeability of some common barrier polymers. *OPV*, oxygen permeation value.

thickness of layers surrounding the barrier layer never fully protect the barrier layer from seeing moisture, but can influence the RH within this range. This can be important since the OPV of EVOH rapidly rises when the RH is raised above about 70%. Moving the barrier layer toward the side of the package that is exposed to lower humidity may be advantageous.

For a quick estimate of what RH to use in calculating the permeability for the barrier layer, the change in RH throughout the package thickness can be considered to be linear and the RH of the barrier layer can be determined by its location:

$$\%\mathrm{RH_B} = \%\mathrm{RH_{outside}} - \frac{x_B}{X_T} \times (\%\mathrm{RH_{outside}} - \%\mathrm{RH_{inside}}) \quad (8.25)$$

where x_B = distance from the outside film surface to the centerline of the barrier layer, X_T = total thickness of the film.

For example, if the RH on the outside of the package is 70% and the RH on the inside is 30%, the barrier layer would see an average RH of 50% if it were placed in the middle of the film structure. As the barrier layer is moved closer to the inside of the film structure, the effective RH that it sees will become closer to that of the inside of the package. Snack foods and other dry foods such as crackers and cereal generally have a low RH inside the package. Liquids and moist food have a high RH inside the package (100% RH for water-based liquids). Barrier films for packaging such products will experience high RH in the barrier layer. Most refrigerated and freezer environments are at high RH (but at colder temperatures, which generally reduces gas permeation.)

Eq. (8.25) can be used for a quick estimate. A more accurate estimation needs to include the relative moisture TRs of each of the layers in the analysis. Consider a three-layer structure shown in Fig. 8.9 where the center layer is a moisture sensitive oxygen barrier polymer such as EVOH and the outer layers are PE: (PE-EVOH-PE). In reality there will be tie layers but these are left out (considered part of the PE layers) to simply the analysis. The tie layers are typically thin and made up of similar resins as the layers they are bonding to so this is a good assumption. By calculating the effective RH of the barrier layer, one can select a representative permeability for that layer using data from the literature for P versus RH, such as that found in Fig. 8.12. Normally the temperature is constant across the multilayer film, and the partial pressure of water vapor is directly related to the RH:

$$p = \frac{\%\mathrm{RH}}{100} p_s \quad (8.26)$$

where p_s = saturated water vapor pressure at the given temperature.

In the following analysis the partial pressure, p, will be used with the understanding that the partial pressure can be replaced with RH at any time using Eq. (8.26). The saturated water vapor pressure for air is tabulated in many standard engineering handbooks [76,77].

The partial pressure of moisture vapor in the center (barrier) layer is the average of the partial pressure at each interface (see Fig. 8.9):

$$p_c = \frac{p_2 + p_3}{2}. \quad (8.27)$$

The mass flow rate of moisture, Q/t, through an area of film, A, is related to the MVTR of that layer. Since MVTR is generally measured at a particular pressure (based on the RH and temperature of the measurement) and film thickness, the MVTR is corrected to account for these differences:

$$\frac{Q}{t} = A\left(\frac{M\Delta p}{X}\right) \quad (8.28)$$

where M = MVTR; X = thickness; Δp = partial pressure difference. At equilibrium

$$\frac{Q_1}{t} = \frac{Q_2}{t} = \frac{Q_3}{t} \quad (8.29)$$

Substituting Eq. (8.28) into Eq. (8.29):

$$\frac{M_1(p_1 - p_2)}{X_1} = \frac{M_2(p_2 - p_3)}{X_2} \quad (8.30)$$

$$\frac{M_2(p_2 - p_3)}{X_2} = \frac{M_3(p_3 - p_4)}{X_3} \quad (8.31)$$

Solving Eqs. (8.27), (8.30), and (8.31) simultaneously yields

$$p_c = \frac{p_1\left[\frac{X_2}{M_2} + \frac{2X_3}{M_3}\right] + p_4\left[\frac{X_2}{M_2} + \frac{2X_1}{M_1}\right]}{2\left[\frac{X_1}{M_1} + \frac{X_2}{M_2} + \frac{X_3}{M_3}\right]}. \quad (8.32)$$

The MVTR of O_2 barrier polymers like EVOH is much greater than that of polyolefin layers and the thickness of the barrier layer is small. Under these conditions, the term X_2/M_2 in Eq. (8.32) is small compared to the other terms and can be ignored. The equation simplifies to:

$$p_c = \frac{p_1\left[\frac{X_3}{M_3}\right] + p_4\left[\frac{X_1}{M_1}\right]}{\left[\frac{X_1}{M_1} + \frac{X_2}{M_2} + \frac{X_3}{M_3}\right]} \tag{8.33}$$

Table 8.11 reveals that when M_1 and M_2 are small, such as when the inside and outside layers are polyolefins, the RH essentially varies linearly across the thickness of the film and Eq. (8.25) is a good estimation of the RH of the barrier layer. This is illustrated in Fig. 8.13.

When the moisture permeability of the outside layer (M_1) is large and the inside layer (M_3) is small, the structure acts as if the outside layer is not present. The RH of the barrier layer is nearly that of the outside of the package. This is typical of a (PA-EVOH-PE) barrier film. The reverse is true: if $M_3 >> M_1$ then the barrier layer RH is nearly that of the inside of the package. By optimizing the thickness and composition of the layers of the structure, the barrier layer can be better protected from the moisture.

The math gets rather tedious when extending Eq. (8.32) to more than three layers. When dealing with four or more layers, one can group the layers to the left of the barrier layer into a single layer using Eq. (8.21) as an approximation for layer 1 in Eq. (8.32). Similarly, the layers to the right of the barrier layer can be grouped into layer 3.

8.4.1.2.4.4 Retort Sterilization

Retort sterilization is a particularly demanding process for high barrier plastic packaging, combining elements of elevated temperature, pressure, and RH. Conditions vary with the specific application but a typical retort process involves exposing the packaged product to 121°C for 30 or more minutes in a pressurized steam environment. Under these conditions, EVOH is particularly prone to loss of barrier performance. Most structures using EVOH surround the barrier layer with layers of polyolefins such as PP or PE that at room temperature provide effective moisture barrier. Temporary swings in ambient RH would not impact the EVOH performance since it typically takes on the order of an hour or more for the moisture permeation to reach a new steady state. At the elevated temperature found in retort, however, polyolefins readily transmit water to the EVOH. The EVOH becomes saturated and its oxygen permeation increases substantially.

Following retort, the EVOH layer eventually dries out to the equilibrium moisture content associated with the ambient RH and temperature (through Eq. (8.32)). This can take considerable time since once the package cools down, the polyolefin layers once again become good moisture barriers and impede the drying process. Even after drying, however, the permeability of the EVOH never fully recovers. This is shown in Fig. 8.14 for a (PP-tie-EVOH-tie-PP) plastic can. The OPV of cans exposed to retort (top and middle curves) never converge to the steady-state OPV of an untreated can (bottom curve) even after 700 days of storage. This phenomenon is known as retort "shock." Tsai and Jenkins [78] attribute this to a permanent change in the free volume that cannot be overcome under normal storage conditions.

Lopez-Rubi [79] explores the effect of exposing monolayer EVOH film to elevated temperature and/or humidity. They use a variety of analytical techniques such as wide-angle X-ray scattering, small-angle X-ray scattering, Raman spectroscopy, Fourier transform infrared spectroscopy (FTIR), and differential scanning calorimetry. They find the following:

- Thermal exposure alone results in an increase in crystallinity, which should decrease oxygen permeability, although it is not measured in this study.
- Exposure to high humidity at room temperature essentially "melts" some of the imperfect crystals of the EVOH. These crystals do not return when the film dries out.
- Exposure to a combination of high temperature and humidity (120°C for 20 min to simulate retort) show significant change in the crystallinity and crystalline morphology. Visual inspection reveals damage from water vapor exiting the amorphous phase as well as partial melting of the crystalline phase. Retort appears to result in a more heterogeneous crystalline structure with small-sized crystals. The crystalline structure itself is more defective, especially for grades of EVOH with low levels of ethylene.

Table 8.11 Effect of Layer Composition and Thickness on Relative Humidity of Barrier Layer (RH_c)

Example Structure	Outside RH_1 %	Inside RH_4 %	X_1 μm	M_1 g/m^2-d	X_2 μm	M_2 g/m^2-d	X_3 μm	M_3 g/m^2-d	RH_c %
(PE-EVOH-PE)	50	100	45	18	10	70	45	18	75
(PE-EVOH-PE)	50	100	25	18	10	70	65	18	64.2
(PE-EVOH-PE)	50	100	65	18	10	70	25	18	85.8
(PE-EVOH-PE)	50	100	65	18	5	70	30	18	84.1
(PA-EVOH-PE)	50	100	45	200	10	70	45	18	55.2
(PA-EVOH-PE)	50	100	25	200	10	70	65	18	52.5
(PA-EVOH-PE)	90	30	25	200	10	70	65	18	87.0
(PE-EVOH-PLA)	50	100	45	18	10	70	45	600	97.3
(PE-EVOH-PLA)	50	100	25	18	10	70	65	600	94.5
(PE-EVOH-PLA)	50	100	65	18	10	70	25	600	98.5

EVOH, *ethylene vinyl alcohol;* PA, *polyamide;* PE, *polyethylene;* PLA, *polylactide.*
Calculated from Eq. (8.32).

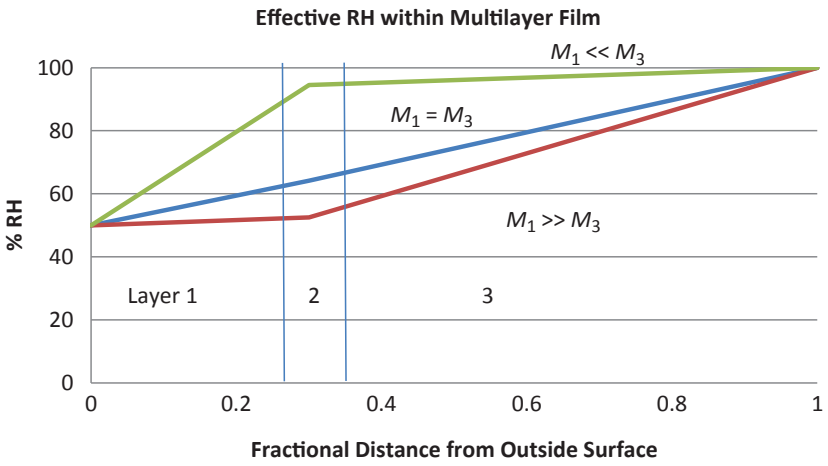


Figure 8.13 Effect of structure composition on relative humidity (RH) of barrier layer. Assumes 100 μm film with three layers, with individual layer thicknesses 24, 10, and 65 μm, respectively. Inside RH is 50% and outside RH is 100%.

In a follow-up study [80], multilayer films are tested. The structure is (PP-tie-EVOH-tie-PP) with thickness (90/10/10/10/90 μm). Grades of EVOH ranging from 26 to 48 mol% ethylene are used. The film samples are dried at 70°C for 1 week prior to conditioning. Conditioning states include no treatment, retort (120°C for 20 min in a steam autoclave), retort followed by drying in an oven at 70°C for 1 week, and thermal annealing (at low humidity). OTR is measured at 45°C and 0% RH, conditions chosen to speed up the drying process following retort. For the retorted samples, the testing is done continuously to generate curves similar to Fig. 8.14. The results show the following:

- A substantial increase in OTR immediately following retort followed by a decline over 30 or so hours due to drying. The recovery time

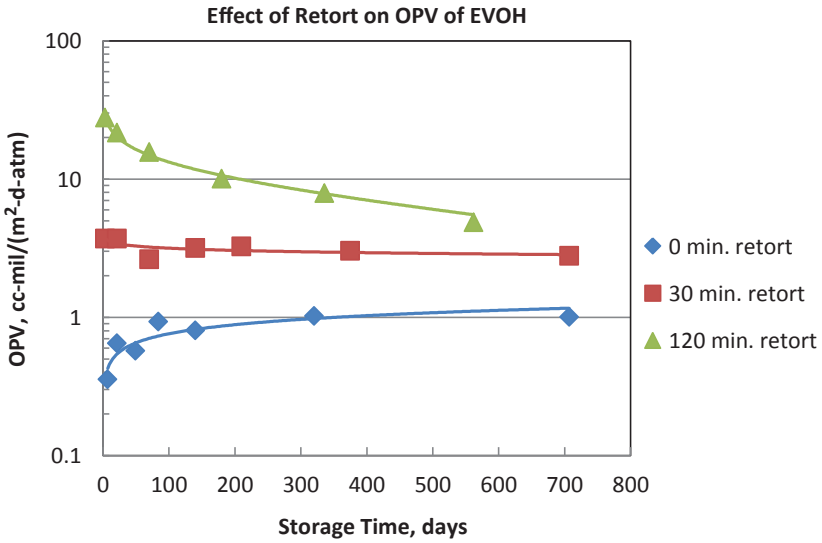


Figure 8.14 Effect of retort on oxygen permeability of ethylene vinyl alcohol (EVOH). Structure storage: (PP-tie-EVOH-tie-PP) with thickness (355/25/50/25/355 μm). Retort temperature: 121°C. Conditions: 21°C, 100% RH outside, 75% RH inside. *OPV*, oxygen permeation value.
From Tsai BC, Jenkins BJ. Effect of retorting on the barrier properties of EVOH. J Plast Film Sheeting 1988;4:63–71.

would likely be considerably longer if the testing had been done at room temperature.

- A permanent offset in OTR after retort for grades of EVOH with high vinyl alcohol content. This is similar that found by Tsai and Jenkins for 32 mol% ethylene EVOH.
- For grades of EVOH with 44 mol% ethylene and higher, no permanent offset in OTR. The OTR returned to the value found for the untreated sample.
- Films that are dried at 70°C for a week after retort show a reduction in OTR compared with untreated samples. They attribute this to higher levels of crystallinity as shown by FTIR and scanning electron microscopy (SEM). They note that this is not a practical solution to retort shock.
- Annealing the films prior to retort (160°C for grades with less than 44 mol% ethylene and 140°C for grades with 44 or 48 mol% ethylene) for 20 min prevented some of the loss in crystallinity in the low ethylene samples.

A number of ideas have been proposed to reduce the impact of retort shock of EVOH, including the following:

- Using higher ethylene content grades of EVOH. Grades with 32 and 38 mol% ethylene are probably the most used grades in film applications. As shown by Lopez-Rubio [80], switching to a 44 mol% grade essentially eliminates retort shock. The higher OPV of these grades, however, often make them unsuitable for many high barrier applications. These grades also will still exhibit the temporary increase in OPV immediately after retort.
- Preannealing the film at 140–160°C [80]. This would likely be challenging to do on a commercial scale.
- Postdrying at 70°C [80]. This is impractical for packaged foods.
- Adding a desiccant to the tie layers [81]. Farrell developed technology that was used in plastic retorted cups for many years. A desiccant was selected that absorbs water at the elevated temperatures of retort, just when the PP layers have their highest moisture transmission. The addition of the desiccant reduces the amount of water the EVOH layer sees during retort and significantly reduces oxygen ingress and retort shock. In a thin film this may be impractical since the desiccant may run out of absorption capacity during the retort recycle. Addition of desiccant also reduces optical clarity.
- Adding nanoparticles such as nanoclay (kaolinite) [82]. Largon shows that oxygen and moisture permeation decrease with addition of 4% clay and note that there is less damage after retort when the clay is added.
- Adding other polymers such as amorphous nylon, ionomer, or polyolefin [83–85].

None of these approaches have proven to be highly successful. In most cases, the film structure must be designed with higher levels of EVOH to compensate for the change in performance during and after retort. Other barrier materials such as foil are often used for retort flexible packaging.

8.4.2 Permeation Through Defects, Pinholes, and Perforations

High barrier flexible packaging structures containing aluminum foil, vacuum deposited metal coatings or "glass" oxide coatings (such as SiO_x and AlO_x) are impermeable except in regions where defects, cracks, or pinholes may be present. The amount of permeation is governed by the number and size of the pinholes, as well as the permeation properties of the rest of the film structure. In modified atmosphere packaging, holes or perforations are sometimes introduced to control the atmosphere inside the package, especially for fruits and vegetables that transpire during storage. Here the holes penetrate through the entire package structure and the amount of permeation is governed by the number and size of the holes and the diffusion coefficient of the permeant in air. The analysis for perforations can also be used to understand the effect of channel leakers in the seal area.

8.4.2.1 Permeation Through Pinholes: High Barrier Packaging

Defects resulting in pinholes in aluminum foil and metalized film can arise from the foil manufacturing process or from handling and use. Table 8.12 shows

Table 8.12 Specifications for Number of Pinholes for Various Aluminum Foils From a Major Supplier

Foil Gauge	Foil Caliper, μm	Average Number of Pinholes	Maximum Number of Pinholes
28.5	7	423	1584
35	9	211	1056
50	13	85	528
75	18	21	106
100	25	0	0

Reproduced with permission from Murray L. The impact of foil pinholes and flex cracks on the moisture and oxygen barrier of flexible packaging. In: TAPPI PLACE conference; 2005.

data provided by Murray [86] for the number of pinholes specified by an aluminum foil manufacturer. The number of defects increases with decreasing foil thickness. According to Murray "the number and size of the pinholes will depend on the filtration of inorganic materials from the molten aluminum, the casting process and the rolling conditions such as lubricant type and lubrication function." Weis [87] and Yializis [88] discuss how the process for metalizing OPP and OPET films can result in cracks and pinholes.

Lush [89] provides data, shown in Table 8.13, on the effect of flexing on the OTR of foil and metalized OPP film. Flexing generally increases permeation through the creation of cracks. Weis [87] conducts a number of mechanical stress tests on metalized films and finds that stress has little impact on oxygen barrier unless the film is elongated by more than 5% in the process. For the most part, in flexible packing structures, foil and metalized films are protected by laminating them with other polymer layers. The adhesion and toughness of the polymer affects its ability to protect against flex cracking. For example, acid copolymers generally provide better flex crack protection for foil than does LDPE [90].

Besides flexing, the package may be subjected to other stresses during storage or the end use that may affect pinholes and barrier performance. Weis found metalized films stored for 3 years have greater permeation than when originally tested. He attributes this to elevated pinhole density caused by moisture and corrosion at key points on the surface.

Weis shows that the permeability of oxygen through metalized films is determined by the number of pinholes and is inversely proportional to the film thickness. Murray concludes that even with the pinholes, the permeation through the pinholes is smaller than through the edges of the film (heat seals) and that flexed packages with foil provided better barrier than those without foil.

Rossi [91] finds that the transmission of permeants through a defect in a barrier coating is complex. They consider a film structure as shown in Fig. 8.15 where the permeant flows through a hole of diameter d in a thin coating on top of a film of thickness L. Here the term "film" is used to denote the substrate that is coated by the barrier layer. The coating is assumed to be impermeable and the diffusion through the film is characterized by a diffusion coefficient $\mathcal{D}$. They develop the equations for a circular hole but later generalize their arguments for any shape hole characterized by a single dimension. They find that the amount of permeant crossing the hole per unit time, Q, is given by two expressions, depending on the

Table 8.13 Oxygen Transmission Rates of Two Flexed and Unflexed Foils and Films

Substrate	Unflexed	Flexed
9-μm aluminum foil three-ply structure	0.47	50
12-μm met-OPET two-ply structure	1.5	10.8

Units are cm^3/m^2-day at 23° C/50% relative humidity. OPET, *oriented polyester.*
Based on data from Lush J, Ferrari D. An economic value model for converters comparing the total cost of metallized film vs. foil in flexible packages. In: TAPPI PLACE conference; 2006.

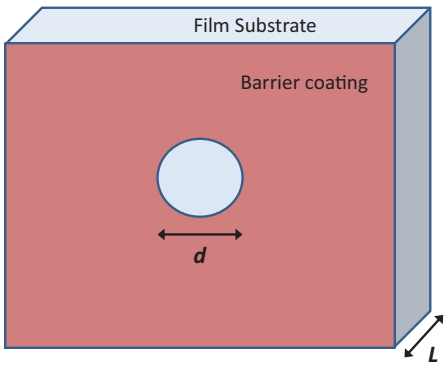


Figure 8.15 Structure of film with hole in barrier coating considered in analysis by Rossi [91].

relative size of L with respect to d:

$$Q \propto \mathrm{D}d \quad \text{for} \quad L \gg d \tag{8.34}$$

$$Q \propto \mathrm{D}\frac{d^2}{L} \quad \text{for} \quad L \ll d \tag{8.35}$$

where Q = amount of permeant passing through the hole in the barrier layer per unit time; d = diameter of hole in barrier layer; L = thickness of film backing up barrier layer; D = diffusion coefficient of permeant in film.

The two regime solution is a consequence of two different types of boundary conditions: zero flux at the surface where the barrier layer is intact, and a steady-state flux at the hole boundary. These results, along with numerical simulations by Rossi and Hanika [92], provide the following insights into the effect of substrate and defect on permeability in these systems:

- Permeation increases with increasing number of defects and defect area.
- Defects are more important when the permeation of the permeant through the film is high.
- For large holes, permeation increases with hole area and decreasing film thickness.
- For small holes, permeation is independent of film thickness and increases with the diameter of the hole.
- Many small defects lead to a higher permeability than a few large defects with the same area fraction of defects.
- Permeation increases with increasing spacing between defects, up to the point where the average spacing between defects is three times the diameter.

Hanika develops a formula for predicting transmission through a film with a distribution of defects in the barrier layer based on numerical simulations:

$$\frac{Q_{\text{coated film}}}{Q_{\text{film}}} = \sum_{\text{all defects}} \left(\frac{\frac{A_D}{l^2}}{1 - \exp\left(-0.507 \frac{\sqrt{A_D}}{L} \right) + 0.01 \frac{A_D}{l^2}} \right) \tag{8.36}$$

where A_D = area of defect; l = distance between defects; L = thickness of film.

They determine the defect size distribution of a metalized OPP film using optical microscopy, SEM, and atomic force microscopy. Optical microscopy is found to be sufficient to measure the defect distribution. Their prediction of oxygen permeation using Eq. (8.36) agrees well with their experimental permeation results. Agreement is not as good for moisture permeation, which they attribute to a large number of domain boundaries on the metalized surface.

8.4.2.2 Permeation Through Perforations or Channels

When the hole or channel extends through the whole package film, diffusion and convection of molecules through the hole must be considered. Solubility and Henry's law are no longer factors. A number of approaches have been used to model the mass transport through a hole in a film, including modified Fick's law, the Maxwell–Stefan equation, and Knudsen diffusion [93]. For the diffusion of oxygen the problem can be simplified by treating the gas phase as a pseudobinary gas (O_2 and N_2) since the binary diffusion coefficients are similar [94,95]. Other gases such as CO_2 can be treated in turn. This avoids the complications of the more rigorous Maxwell–Stefan equation.

Following the approach of Paul [95], the diffusion of gas from the outside to the inside of the package can be divided into three zones, as shown in Fig. 8.16. Diffusion to and from the hole is

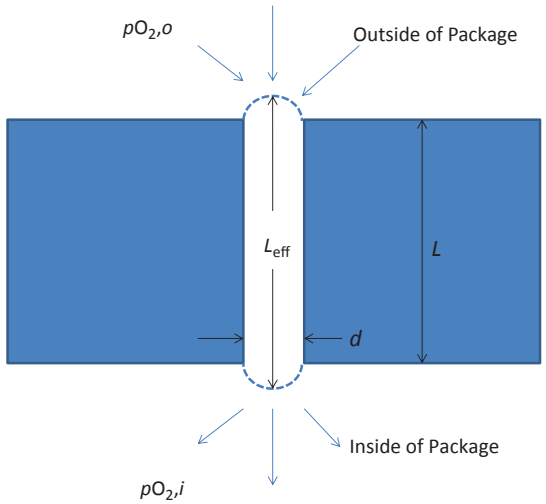


Figure 8.16 Schematic of hole diffusion model.
From Paul DR, Clarke R. Modeling of modified atmosphere packaging based on designs with a membrane and perforations. J Membr Sci 2002;208:269–283.

considered in a hemisphere extending from the hole. An effective length of the hole is derived to account for the diffusion in these regions:

$$L_{\text{eff}} = L + \frac{7}{6}d \tag{8.37}$$

where L = length of hole (thickness of film for the case of perforations, or length of channel in seal area); d = diameter of the hole.

The factor 7/6 varies depending on the assumptions used in the entrance and exit of the hole. DelValle [94], for example, finds the factor to be $^1/_2$. For the case of oxygen, the molar transport through the hole is given by

$$Q = n_{\text{holes}}\left(\frac{\pi d^2}{4}\right)\frac{\mathrm{D}_{\mathrm{O}_2,\text{air}}\left(p_{\mathrm{O}_2,o} - p_{\mathrm{O}_2,\,i}\right)}{L_{\text{eff}}RT} \tag{8.38}$$

where Q = molar transport rate through the holes; n_{holes} = number of holes; d = diameter of hole; $\mathrm{D}_{\mathrm{O}_2,\text{air}}$ = diffusion coefficient of oxygen in air; $p_{\mathrm{O}_2,o}$ = partial pressure of oxygen on outside of package; $p_{\mathrm{O}_2,i}$ = partial pressure of oxygen on inside of package; R = gas constant; T = temperature (absolute).

For other gases or gas mixtures, these are simply substituted for oxygen and air in Eq. (8.38). In deriving this equation, Paul assumes the pressure inside the package is nearly the same as on the outside so that the convective flow is small.

The diffusion coefficient used in Eq. (8.38) differs by several orders of magnitude from the diffusion through most polymer films. For example, $\mathrm{D} = 0.18\ \mathrm{cm}^2/\mathrm{s}$ for oxygen in air at STP (298 K, 1 atm). For diffusion of oxygen through LDPE, $\mathrm{D} = 5 \times 10^{-5}\ \mathrm{cm}^2/\mathrm{s}$. Graham's law of effusion states that the rate of transport of a gas through a pinhole is inversely related to the square root of its molar mass. Therefore,

$$\mathrm{D} \propto \frac{1}{\sqrt{\widetilde{M}}} \tag{8.39}$$

where $\widetilde{M}$ = molar mass of gas molecule. Hence, the permeability of gases through perforations has some selectivity based on the molar mass of the molecules. Lee [96], for example, finds that longer pinholes with smaller diameters accelerates the formation of higher CO_2 and lower O_2 concentration within a modified atmosphere package.

Eq. (8.38) shows that the amount of transport of gas through the hole increases with

- increasing number of holes
- increasing hole diameter
- decreasing hole length
- increasing diffusion coefficient (in the gas mixture)
- increasing partial pressure difference between the inside and outside of the package

A number of investigators [94–98] have coupled models of gas transport through holes in modified atmosphere packaging with models of product transpiration and the like. A general conclusion is that the number of holes and their dimensions along with the permeability of different films can be used to optimize MAP performance. Chung [99] models the permeation due to small leaks and concludes that pinholes and channel leakers have a significant impact on high barrier packaging and should not be ignored.

8.5 Emerging Technologies

8.5.1 Oxygen Scavenging

The concept of actively scavenging oxygen from a package dates back to the 1920s [100]. Combined with a passive barrier structure, scavenging can significantly extend shelf life of oxygen sensitive products. Most applications have been inserts, such as sachets or labels, to flexible packaging or liners for closures of rigid packaging. Using the technology in the flexible film structure itself has had limited commercial success.

Rooney [100] provides a good review of oxygen scavenging technology, and the reader is referred to his work for details. Here a few of the technologies are highlighted [100,101]:

- Powdered iron or other oxidation species such as sulfites. The oxygen is consumed by oxidation of the iron. The reaction is fast and very effective with enough concentration of the iron. It is mostly used in sachets, such as Mitsubishi Gas Chemical's Ageless sachets. Color and scavenging capacity issues have made it difficult to apply to a packaging film structure.

- Polydiene and cobalt. There have been numerous patent applications on this type of technology but limited commercial applications. One issue is the creation of aldehyde by-products that can result in poor organoleptics.
- MXD6 nylon and cobalt. Cobalt cations form a complex with the benzylic groups of *meta*-xylene. This complex traps oxygen and/or causes the oxygen to oxidize the benzylic groups. MXD6 provides some passive barrier as well.
- Cyclohexene and cobalt. Chevron Phillips developed technology based on polyethylene methacrylate with cyclohexenyl groups that reportedly gives off few by-products. [102]

Some of the potential issues to consider when evaluating scavenging technology include the following:

- Regulatory compliance of additives for food packaging. Many of the technologies involve new chemistries or reactions. These chemistries must be in compliance with global food packaging regulations.
- Capacity/shelf life of the scavenger. The inability of a thin film to hold enough of the scavenger and still provide the other requirements of the package (strength, clarity, etc.) is one reason adding the scavenging technology to the film has only had limited commercial success. Sachets and rigid packaging have more capacity. Another aspect of shelf life of the scavenger is marrying the scavenger technology with a good passive barrier. This will reduce the amount of oxygen coming into the film from the outside, extending the shelf life.
- Initiation of the scavenging reaction. Given the limited capacity of the film to hold the scavenger, ideally the scavenging reaction should be turned on only when it is needed. Some technologies are initiated by moisture. Others use UV light. Understanding the technology and matching it to the type of product being packaged (moisture initiation may not be a good approach for a dry food, for example) and the facilities is an important consideration.
- Organoleptics. Many of the technologies have failed due to the poor taste/odor of by-products that are given off during the scavenging reaction. This should be tested with the product to be packaged.
- Color. Some of the technologies, such as iron, impart color to the plastic. Iron works well when hidden in a sachet insert, but not so well in a clear film.
- Scavenging rate. The rate of scavenging must match the speed of oxidation of the packaged food. If a food product spoils before the scavenger has even been initiated, the active barrier is wasted.

8.5.2 Layer Multiplication

Splitting and recombining layers in coextrusion has been used to create film structures with hundreds and even thousands of layers. Sometimes referred to as micro- or nanolayer technology due to the thickness dimension of the layers, this technology has recently been evaluated for potential barrier applications. A schematic of the process is shown in Fig. 8.17. Much of the original development was done by Schrenk and coworkers at Dow Chemical [103–109] using a feedblock and a series of multipliers. In each multiplier, two or more layers are split down the middle and then stacked on top of each other, multiplying the number of layers by a factor of two. Adding additional multipliers increases the

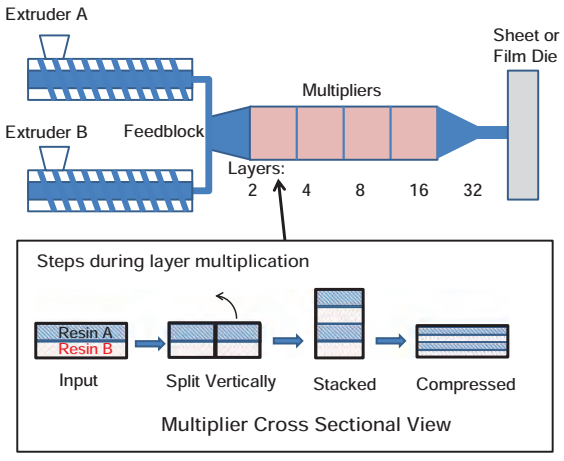


Figure 8.17 Schematic of layer multiplication technology

number of layers by a factor of 2^n, where n is the number of multipliers.

Most of the early applications for layer multiplication technology were for optical films [110–116]. Various optical effects can be achieved through proper selection of refractive indices of the polymers used in adjacent layers. Such films can be used as optical filters and reflectors. Electrical capacitor films have also been fabricated.

When the original patents expired in the 2000s, several feedblock and flat die manufactures, including EDI/Nordsen and Cloeren [117], came out with versions of the technology, opening it up to potential use by a broader group of converters. Schirmer [118–120] developed a blown film process that involves flow through a series of thin plates to create up to about 30 thin layers. Schirmer is working with Alpha Marathon to bring the technology to market. Dow Chemical [121] introduced annual die technology for blown film that uses the feedblock/layer multiplier technique combined with a crosshead style die. The multilayer composite formed in the multipliers flows around the mandrel and combines on the other side. To deal with this weld line, Dow designs the die to overlap the flow, doubling the number of layers in the region. Zumbrunnen [122] at Clemson University has developed blown film technology based on chaotic advection to create microlayers in a controlled manner.

Layer multiplication has proven useful for studying the fundamentals of polymer flow, crystallinity and orientation in confined layers, polymer diffusion, and interfacial adhesion and reactivity. Dooley [123–125] at Dow Chemical uses the technique to show how the elastic behavior of polymer creates complex flow patterns in dies. Macosko's group at the University of Minnesota finds the technique to be useful for its ability to amplify interfacial effects through the creation of hundreds of interfaces. They use it to study polymer interlayer adhesion and other interfacial phenomenon [126–132]. Hiltner and Baer's group at Case Western Reserve University (CWRU) also use the technique to study interfaces, such as polymer diffusion and adhesion [133,134]. The focus of the CWRU group, however, is on the effect that confined micro- and nanolayers has on film properties. They find that the crystalline structure of PE and PP, when confined between layers of PS or other polymers in which they are immiscible, changes as the layers become thinner and approach the molecular dimension [135–138]. Typically, the amount of crystallinity decreases. For HDPE they find crystallinity decreases from 60% to 33% in one case and from 56% to 40% in another. A 3× increase in oxygen permeability is reported, which they attribute to the reduced crystallinity. A decrease in PET crystallinity and greater orientation of crystalline domains is also reported when confined to thin layers [139].

Schrenk and Alfrey [108] show that sandwiching a high modulus, low elongation material between layers of low modulus, high elongation material may result in a film that undergoes much larger ductile deformation before failing than what the stiffer material would do alone. The high elongation material acts to stop the propagation of cracks across the brittle layers, allowing the stress in the brittle materials to reach their ductile yield point. All the layers can be stretched to large elongations; the composite has both high modulus and high elongation. They give several examples which are explored in more detail in Chapter 9.

CWRU also report an increase in ductility of brittle layers sandwiched between other polymers. For example, polycarbonate (PC)/styrene acrylonitrile copolymer (SAN) and PC/polymethyl methacrylate (PMMA) structures show improved toughness as the layer thickness is decreased. They attribute this to a change in deformation from crazing to shear yielding as the layers get thinner. Of critical importance is the interaction between the craze opening and the microlayer bands in the PC. Adhesion between the layers is also important. [133,140,141]

Reports on the barrier properties of micro- and nanolayer films have been mixed. Schrenk and Alfrey [108] show that films with 125 alternating layers of PS and PE or PP have MVTR properties that can be predicted by Eq. (8.22). The MVTR decreases with increasing amount of PE or PP in the structure and has a value similar to a structure with all the PP or PE in a single layer. At least for PE and PP, the thinness of the layers does not affect the permeability. As discussed previously, CWRU found that the crystallinity of HDPE decreases with decreasing thickness, which increases MVTR.

Studies by Hiltner and Baer's group at CWRU [142–146] find that when polyethylene oxide (PEO) or caprolactone (PCL) is confined to nanolayers, the oxygen barrier improves by two orders of magnitude. In the original experiments, PEO was sandwiched between layers of ethylene acrylic acid copolymer or PS. Layer multiplier technology is used to create

films with 1000 or more layers, with the thickness of each layer in the nanometer realm. As the thickness dimension is reduced, the crystalline morphology changes to a single large crystal to which they attribute the 100× improvement in gas barrier. So far the technology does not seem to have been commercialized. One factor is that PEO is water soluble and so the OPV is likely to be strongly influenced by RH, although data by the CWRU show only a 2−3× increase in OPV at 85% RH compared with 0% RH. Another is that PEO can be difficult to process and matching of viscosities to prevent flow instabilities is critical when creating hundreds or even thousands of layers. (Flow instability in coextrusion is described in Chapter 13.) Scaling up the technology may prove difficult. More importantly, even with a 100× reduction in OPV, the OPV of PEO and PCL is still not as good as commercial barrier polymers such as EVOH or PVDC.

Layer multiplier studies using conventional barrier polymers such as PA 6 or EVOH have not found significant reductions in OPV when reducing the layer thickness to the micro- or nanometer regime [147−151]. Oliver [147] found some reduction in OPV with thinner layers compared with thicker layer controls in sheet but not in films. In many investigations the permeability is actually higher than conventional coextrusion of the same total amount of EVOH. Reduction in crystallinity and layer nonuniformities due to flow instabilities have been suggested as possible reasons. The nature of the tie resin has been shown in some studies to affect flow instability; development of tie resin technology to allow nanolayered films may be needed.

Two advantages have been reported for EVOH films. Both involve a reduction in brittleness of EVOH. EVOH is a very stiff polymer at room temperature, making it prone to flex cracking and difficult to draw or thermoform. Several studies have found that by splitting the EVOH into tens or hundreds of layers, the flex crack resistance is improved. Medlock [150] compares a conventional 7-layer cast film structure with a 21-layer structure made with Cloeren's layer multiplier technology. Two 130 μm conventional films are made as controls:

1. (58 μm LDPE-4 μm tie-7 μm EVOH-4 μm tie-58 μm LDPE)
2. (58 μm LDPE-4 μm PA-7 μm EVOH-4 μm PA-58 μm LDPE)

In structure 2, each LDPE layer is comprised of two separate layers, the one closest to the PA layer contained a tie resin concentrate. Twenty-one layer counterparts are made of each of these structures by splitting the tie-EVOH-tie or PA-EVOH-PA core into 17 layers. Each layer is less than 1 μm thick. The sum of the thicknesses of each of the EVOH layers totals that of the conventional controls so that the barrier properties can be directly compared. OPV measurements show that the 21-layer structures have essentially the same permeation as the 7-layer conventional structures, within experimental error. The films are subjected to Gelbo flex cycles and remeasured. The nanolayer film structures show superior flex crack resistance. After 500 flexes, the conventional films experience a substantial increase in OPV and pinholes. The tie-EVOH-tie (structure 1) nanolayer films show little change in OPV even at 1000 flexes. The PA-tie-EVOH nanolayer structure give mixed results depending on the grade of EVOH used. The authors conclude that the lower modulus PE-based tie resin stops the propagation of cracks better than the stiffer PA.

Lee [151] conducts a similar study using the Dow layer multiplier technology, making cast film structures with up to 35 layers and use statistical analysis to confirm the effect of the number of layers on the barrier performance after flexing. They make 5-, 17-, and 35-layer structures of (PE-[tie-EVOH-tie]-PE) where the core [tie-EVOH-tie] is split and recombined to achieve the desired number of layers. The ratio of PE to core is kept constant at 80−20%. Within the core, the EVOH to tie ratio is varied from 30:70 to 70:30. The films are subjected to Gelbo flex cycles. In addition to OPV measurements, the number of pinholes is measured by using a dye test. The number of pinholes is found to decrease with increasing number of layers (and decreasing layer thickness). They attribute the improved flex crack resistance of the nanolayer structures to (1) greater flexibility of the EVOH layer when coextruded into thinner layers and (2) a more tortuous path for the gas molecules to travel if some of the EVOH layers are broken.

Investigators [148,149] have also reported that nanolayer barrier films are more ductile and easier to draw and orient. This is due to lower crystallinity and changes in orientation and crystalline morphology, as well as the synergistic effects when ductile materials are coextruded with brittle ones (see Chapter 9).

So far most of the applications for layer multiplication for packaging films have been taking

advantage of the improved mechanical properties of the film, particularly for stretch films for pallet wraps and the like [149,152,153]. For example, Apeldoorn Flexible Packaging uses microlayer technology to make a stretch film that increases pallet stability at elevated temperatures, uses 30% less material, and reduces product damage during transportation by 80% [152]. An early adopter of layer multiplier technology is Nike [154,155] which uses it to make flexible cushioning membranes for athletic shoes. Structures containing microlayers of alternating gas barrier (EVOH) and elastomers (thermoplastic polyurethane) provide superior barrier for the pressurized nitrogen as well as flexibility and strength. Up to 1000 microlayers are used with layer thicknesses as thin as 0.01 μm.

8.5.3 Nanocomposites

Nanocomposites are blends of polymer and nanosized inorganic particles. They have received considerable attention in recent years dating from work done at Toyota [156] in the 1980s with PA 6. Conventional inorganic fillers such as calcium carbonate, glass fibers or beads, or talc are micron-sized and are typically added to polymers at levels of 20% and higher to impart stiffness or strength. The addition of the filler typically detracts from optical clarity and toughness. Nanoparticles have at least one dimension less than 100 nm. They are added at much lower levels, typically around 5% or less. At such levels and dimensions they have little negative impact on optical clarity (because of the small size, light is not diffracted) and toughness, yet have been reported to impart improvements in stiffness, strength, flame retardancy, electrical conductivity, and gas barrier.

Most of the early work on gas barrier was with clay-nylon nanocomposites and that continues to be the dominant system in the literature. The nylon is mostly PA 6, with some work on MXD6 and amorphous PA such as DuPont's Selar PA. Other polymers include PET, PP, PE, and ionomers. The nanoparticle is most often montmorillonite (MMT) clay. Other particles include kaoline, metal oxides, sepiolite, and layered silicates.

Dispersing the particles in the polymer matrix is critical for enhancing performance. Various surface treatments and coupling agents are used to enhance the dispersion of the nanoparticles [157–164]. As described in Chapter 6, MMT has a layered structure with the individual platelets bound to one another by attractive forces with a separation distance of about 3.5 Å. Manufacturers add surfactants that separate the platelets to about 10 Å. For the best properties, fully separating the platelets is required. This is called exfoliation. Partial separation of the layers into smaller domains is called intercalation. In terms of barrier performance, intercalation is better than no separation, and exfoliation gives the best results. Unfortunately, achieving a true exfoliated state is difficult. There are three methods that are typically used to disperse the particles. One is in situ polymerization of the polymer with the nanoclay [156,165]. The monomer can diffuse between the platelets and cause further separation as the polymer chain grows. This only works for certain polymers, such as PA 6, that can be polymerized in the presence of the nanoclay. Other methods of dispersing the nanoparticle in the polymer include melt compounding and making aqueous dispersions. The latter process is used for coatings onto the surface of a film or other substrate.

Oxygen and carbon dioxide permeation have received most of the attention from investigators studying barrier performance of nanocomposites. Most authors report decreases in gas permeation of about 67% or less (or 3× increase in barrier performance) for films made of nanocomposites [161,165–170]. Chaiko [157–159] reports a decrease in OPV of LDPE of 95% by optimally selecting the surfactant. They attribute this to an increase in crystallinity of the PE due to nucleating effects of the clay (as well as the more traditional mechanism of the clay particles creating a more tortuous path for the permeant). Choi [165] measures an 11× reduction in OPV for a PET-MMT nanocomposite formed in situ during polymerization. Layered deposition of nanoparticles from dispersions has reported to yield improvements in barrier of up to about 20× [171,172].

The reduction in permeability is generally thought to be due to the creation of a more tortuous path for the gas molecule through the film due to the alignment of the clay platelets parallel to the surface of the film. Many investigators [173–175] have derived models of the gas permeability of a nanocomposite as a function of the nanoparticle concentration, aspect ratio, and orientation, such as Eq. (8.40):

$$P_{\text{nanocomposite}} = \frac{\phi_{\text{matrix}} P_{\text{matrix}}}{1 + 0.5\phi_{\text{clay}}\alpha_{\text{clay}}^{\frac{2}{3}}\left(s + \frac{1}{2}\right)} \quad (8.40)$$

where P = permeability; ϕ = volume fraction; α_{clay} = aspect ratio of clay particle; s = orientation factor (s = 1 for particles parallel to surface, −0.5 for particles perpendicular to surface and 0 for randomly oriented particles. Here the aspect ratio is defined as the ratio of the dimension of the face of the platelet to its thickness.

Eq. (8.40) shows that permeability decreases with increasing aspect ratio, volume fraction of the clay particle, and orienting the particles parallel to the film surface, all consistent with a more tortuous path mechanism. These effects are highlighted in Figs. 8.18 and 8.19. Bhunia [175] also finds that increasing the length of the particle decreases the permeability.

Lan [166] uses Eq. (8.40) to compute the aspect ratio and volume concentration needed to achieve a 50% reduction in gas permeation assuming the platelets are aligned parallel to the film surface ($s = 1$). The results, given in Table 8.14, show that with a particle aspect ratio of 200, only 1 vol% is needed to achieve a 50% reduction in permeability. The high aspect ratio of these particles is responsible for their barrier enhancing properties. The aspect ratio is determined by the natural dimensions of the clay and its dispersion in the polymer matrix. If there is no separation of the platelets, then the particle is nearly spherical and the aspect ratio is approximately 1. Intercalation reduces the average thickness and increases the aspect ratio. Fully exfoliated clay exposes the nanometer thickness of the individual platelets and has the highest aspect ratio. Aspect ratios of 400 and higher are possible for exfoliated clay. Attrition during processing may reduce the aspect ratio of the particles by shortening their length. The difficulty in achieving full exfoliation and minimizing attrition help explain why in practice it is challenging to achieve increases in barrier performance greater than 3×.

A 3× improvement in barrier may not be enough to bring a moderate barrier resin like PA 6 into the high-performance barrier category. High barrier polymers like EVOH and PVDC have O_2 permeability (cc-mil/m^2-day-atm) of 0.3 (dry) and 2.5, respectively. PET (30−80 oriented) and PA6 (30−80 dry) are at least an order of magnitude higher. Polyolefins range from about 3100 to 15,500 and so are a couple of orders of magnitude even higher. Therefore, a 3× reduction in OPV does not bring PA 6 to the next level of performance needed to displace incumbent materials such as EVOH and PVDC.

Adding nanoparticles to more expensive barrier polymers such as EVOH or MXD6 has been reported [166,176]. By starting with higher-priced polymers, however, the improved barrier performance may not be cost-effective. Nanocomposites of these materials have also suffered from performance issues. For example, Aleperstein [176] finds that adding nanoclay to EVOH reduces the mechanical properties of the EVOH. They attribute this to a reduction in the crystallinity of the EVOH.

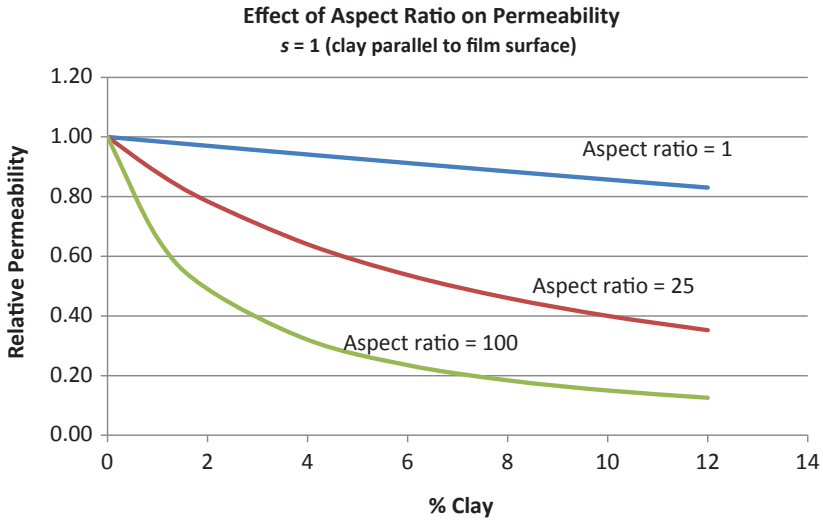


Figure 8.18 Model prediction of reduction in permeability as a function of nanoclay content and aspect ratio. *From Eq. (8.40) [174].*

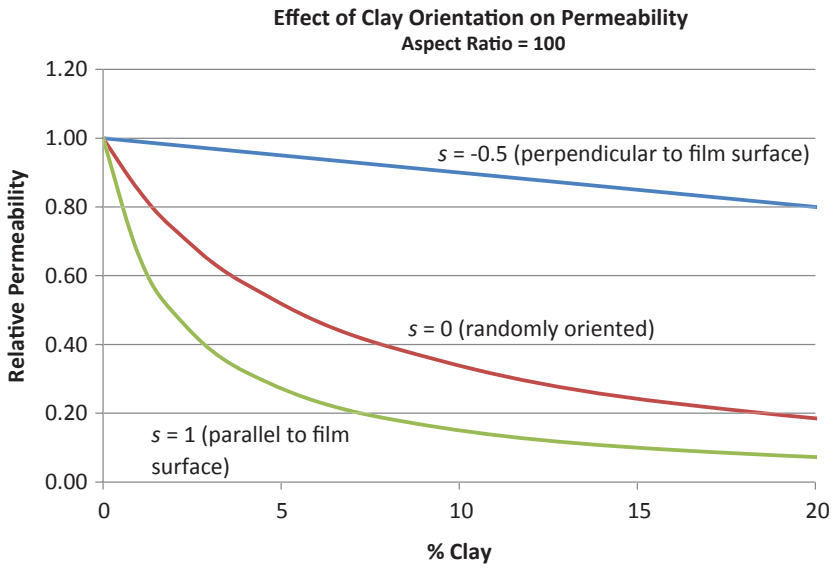


Figure 8.19 Model prediction of reduction in permeability as a function of nanoclay particle orientation and volume percent.
From Eq. (8.40) [174].

Nevertheless, there are some applications where a 3× improvement could be significant. The one that gets the most attention is PET bottles where a somewhat small improvement in barrier may allow PET to capture new markets (eg, beer, smaller bottles for carbonated beverages). Any solution, however, must be very cost competitive as multiple technologies are pursuing this large market opportunity.

Cost and performance are the biggest hurdles for the adoption of nanocomposites into mainstream barrier packaging applications. Another is color. Even if the optical transparency is not negatively affected, many of the nanoparticles are natural clays and the like. They tend to impart a brownish tint to the film that may detract from the appearance of the package. Synthetic clays and nanoparticles are available but typically at higher cost.

Table 8.14 Nanoparticle Volume Percent and Aspect Ratio Relationship to Provide a 50% Reduction in Gas Diffusivity Through a Film

Aspect Ratio	Volume %
20	9
200	1
400	0.5

Nanocomposite barrier coatings have also been slow to be adopted commercially. PVOH-based nanocomposite coatings [172] are sensitive to moisture. Coatings are also susceptible to scratching and abrasion if they are on the outside of a package. Coated films, therefore, are typically laminated to other films so that the coating is protected in the interior of a package film structure.

Finally, nanomaterials are subject to increased scrutiny for potential health issues. Not enough research has yet been conducted to make definitive claims around health effects. One concern is if the nanoparticles become airborne. Their size makes it difficult for the human body's natural defenses to prevent them from getting into the lungs. When properly dispersed in polymers they should be protected from becoming airborne, although their fate in the environment is still uncertain. Nanocomposites have garnered considerable attention in the R&D community and these challenges are the subject of ongoing research.

8.5.4 Advanced Coatings

In addition to nanocomposite coatings, a number of other coating technologies are in various stages of development or commercialization. Standard techniques to produce metalized and SiOx coatings are

described in Chapter 4. Here two emerging technologies are briefly discussed: atomic layer deposition (ALD) and "diamondlike carbon (DLC)" coatings made by plasma-enhanced chemical vapor deposition (PECVD). One of the driving forces is the desire by some end users to eliminate metalized films so that metal detectors can be used on packaging lines to divert inadvertent metal from getting into the package.

8.5.4.1 Atomic Layer Deposition

ALD uses sequential gas-phased chemical reactions to deposit a very thin coating, typically in the nanometer thickness realm, onto a substrate [177]. ALD is based on self-terminating reactions. The cyclical self-limiting reactions allows for controlled, very thin coatings to be made. Most of the work directed at reducing gas permeability involves depositing thin layers of aluminum dioxide coatings.

The main advantage of ALD over chemical vapor deposition and physical vapor deposition techniques is the ability to produce very thin coatings. Disadvantages include its slow speed. Most of the work to date has been with batch processes. Challenges remain to scale-up the process to high-speed continuous roll-to-roll processes necessary to produce quantities for packaging applications. It has found use primarily in the semiconductor and energy conversion (solar cells) markets.

Hirvikorpi [178,179] and Groner [180] demonstrate that, at least on a lab scale, ALD provides a reduction in gas permeation in a range suitable for packaging applications. In one study they coat AlOx onto various uncoated paper and polymer-coated paper. Oxygen transmission decreases by 50−90% with coatings of 25−100 nm. In a second study they compare ALD with three other barrier coating technologies: electron beam evaporation, magnetron sputtering, and sol-gel. They coat PE and PLA substrates and find ALD gives the best overall reduction in gas permeability. They admit that this is just a feasibility study and that ALD is still a time-consuming and expensive process.

8.5.4.2 Diamondlike Coatings

PECVD can be used to produce a DLC coating. Such coatings are hard, scratch resistant, and have good barrier properties. The advantages of PECVD over chemical vapor deposition include lower temperatures (coatings can be made at room temperature so that the polymer substrate is not distorted), chemical stability, fewer toxic by-products, quick processing time, and high deposition rates [181].

Several companies have introduced technology to coat the inside of PET bottles with DLC, including Mistubishi Heavy Machinery and Sidel. DLC has been used by Kirwin Brewery for PET beer bottles [182]. One of the limitations for using this technology for flexible films is that cracks form in the coating when the coated film is stretched by only a few percent [183]. Cracks increase the gas permeability. Abbasa introduces Si during the coating process to reduce internal stress and pinholing. They claim that this produces films with similar barrier performance as metalized films. Indeed, a competing technology introduced by several firms, including Toyo Seikan Kaisha, Ltd., Toppan Printing Co., Ltd., and SIG Corpoplast GmbH Co., uses SiOx in a PECVD method to produce barrier coatings for PET bottles.

Another drawback to DLC coatings is that they typically produce an off-color.

While PECVD is scalable to high-speed coating suitable for packaging films, it still has its challenges. Both DLC and ALD are technologies to monitor to see if they develop into a viable technologies for barrier packaging films.

References

[1] Brown H, Williams J. Packaged product quality and shelf life. In: Coles R, McDowell D, Kirwan MJ, editors. Food packaging technology. Boca Raton (FL): Blackwell Publishing, CRC Press; 2003. p. 65−95.

[2] Robertson GL. Deteriorative reactions in food. In: Food packaging. Principles and practice. 3rd ed. Boca Raton (FL): CRC Press; 2013. p. 293−328.

[3] Robertson GL. Shelf life of foods. In: Food packaging. Principles and practice. 3rd ed. Boca Raton (FL): CRC Press; 2013. p. 329−66.

[4] Blakistone B. What suppliers need to know: a brief course in food chemistry. In: TAPPI polymers, laminations and coatings conference; 1998. p. 153−61.

[5] Webster JB, Duncan SE, Marcy JE, O'Keefe SF. Effect of narrow wavelength bands of light on the production of volatile and aroma-active

compounds in ultra-high temperature treated milk. Int Dairy J 2011;21:305−11.
[6] Webster JB, Duncan SE, Marcy JE, O'Keefe SF. Controlling light oxidation flavor in milk by blocking riboflavin excitation wavelengths by interference. J Food Sci 2009;74:S390−8.
[7] Whited LJ, Hammond BH, Chapman KW, Boor KJ. Vitamin A degradation and light-oxidized flavor defects in milk. J Dairy Sci 2002;85:351−4.
[8] Cladman W, Scheffer S, Goodrich N, Griffiths MW. Shelf-life of milk packaged in plastic containers with and without treatment to reduce light transmission. Int Dairy J 1998; 8:629−36.
[9] Saffert A, Pieper G, Jetten J. Effect of package light transmittance on vitamin content of milk. Part 2: UHT whole milk. Packag Technol Sci 2008;21:47−55.
[10] Moyssiadi T, Badeka A, Kondyli E, Vakirtzi T, Savvaidis I, Kontominas MG. Effect of light transmittance and oxygen permeability of various packaging materials on keeping quality of low fat pasteurized milk: chemical and sensorial aspects. Int Dairy J 2004;14:429−36.
[11] Karatapanis A, Badeka AV, Riganakos KA, Savvaidis IN, Kontominas MG. Changes in flavour volatiles of whole pasteurized milk as affected by package material and storage time. Int Dairy J 2006;16:750−61.
[12] Dalsgaard TK, Otzen D, Nielsen JH, Larsen LB. Changes in structure of milk proteins upon photo-oxidation. J Agric Food Chem 2007; 55:10968−76.
[13] Becker EM, Cardoso DR, Skibsted LH. Deactivation of riboflavin triplet-excited state by phenolic antioxidants: mechanism behind protective effects in photooxidation of milk-based beverages. Eur Food Res Technol 2005;221:382−6.
[14] Mortensen G, Sorensen J, Stapelfeldt H. Effect of light and oxygen transmission characteristics of packaging materials on photo-oxidative quality changes in semi-hard Havarti cheeses. Packag Technol Sci 2002;15:121−7.
[15] Deger D, Ashoor SH. Light-induced changes in taste, appearance, odor, and riboflavin content of cheese. J Dairy Sci 1987;70:1371−6.
[16] Wold JP, Veberg A, Lundby F, Nilsen AN, Moan J. Influence of storage time and color of light on photooxidation in cheese: a study based on sensory analysis and fluorescence spectroscopy. Int Dairy J 2006;16:1218−26.
[17] Frederiksen CS, Haugaard VK, Poll L, Becker EM. Light-induced quality changes in plain yoghurt packed in polylactate and polystyrene. Eur Food Res Technol 2003;217:61−9.
[18] Larsen H, Tellefsen SBG, Dahl AV. Quality of sour cream packaged in cups with different light barrier properties measured by fluorescence spectroscopy and sensory analysis. J Food Sci 2009;74:S345−50.
[19] Thron M, Eichner K, Ziegleder G. The influence of light of different wavelengths on chlorophyll-containing foods. Lebensm Wiss Technol 2001;34:542−8.
[20] Hicks CL, Adbullah C. Photooxidation of cinnamon oil. J Food Sci 1987;52:1041−6.
[21] Psomiadou E, Tsimidou M. Stability of virgin olive oil. 2. Photo-oxidation studies. J Agric Food Chem 2002;50:722−7.
[22] Kim JY, Choi DS, Jung MY. Antiphoto-oxidative activity of sesamol in methylene blue- and chlorophyll-sensitized photo-oxidation of oil. J Agric Food Chem 2003;51:3460−5.
[23] Lennersten M, Lingnert H. Influence of wavelength and packaging material on lipid oxidation and colour changes in low-fat mayonnaise. Lebensm Wiss Technol 2000;33:253−60.
[24] Kanavouras A, Coutelieris FA. Shelf-life predictions for packaged olive oil based simulations. Food Chem 2006;96:48−55.
[25] Kanavouras A, Hernandez-Munoz P, Coutelieris FA. Shelf life predictions for packaged olive oil using flavor compounds as markers. Eur Food Res Technol 2004;219: 190−8.
[26] Ramirez G, Hough G, Contarini A. Influence of temperature and light exposure on sensory shelf-life of a commercial sunflower oil. J. Food Qual 2001;24:195−204.
[27] Lu L-X, Xu F. Effect of light-barrier property of packaging film on the photo-oxidation and shelf life of cookies based on accelerated tests. Packag Technol Sci 2009;22:107−13.
[28] Larsen H, Westad F, Sorheim O, Nilsen LH. Determination of critical oxygen level in packages for cooked sliced ham to prevent color fading during illuminated retail display. J Food Sci 2006;71:S407−13.

[29] Manzocco L, Kravina G, Calligaris S, Nicoli MC. Shelf life modeling of photosensitive food: the case of colored beverages. J. Agric Food Chem 2008;56:5158−64.
[30] Haugaard VK, Weber CJ, Danielsen B, Bertelsen G. Quality changes in orange juice packed in materials based on polylactate. Eur Food Res Technol 2002;214:423−8.
[31] Solomon O, Svanberg U, Sahistrom A. Effect of oxygen and fluorescent light on the quality of orange juice during storage at 8°C. Food Chem 1995;53:361−8.
[32] King JM, Minn DB. Riboflavin photosensitized singlet oxygen oxidation of vitamin D. J Food Sci 1998;63:31−4.
[33] Korman N, Orbey N, Ozilgen M. A simple procedure for assessing the protective effect of transparent polymer films used for packaging foods containing light−sensitive nutrients. Polym Int 1991;25:163.
[34] Ahmad I, Fasihullah Q, Noor A, Ansari IA, Nawab Manzar Ali Q. Photolysis of riboflavin in aqueous solution: a kinetic study. Int J Pharm 2004;280(1−2):199−208.
[35] Kanner JD, Fennema O. Photooxidation of tryptophan in the presence of riboflavin. J Agric Food Chem 1987;35:71−6.
[36] Han JH. Antimicrobial packaging systems. In: Ebnesajjad S, editor. Plastic films in food packaging, materials, technology and applications. New York: Elsevier; 2013. p. 151−80.
[37] Petersen K, Nielsen PV, Bertelsen G, Lawther M, Olsen MB, Nilsson NH, et al. Potential of biobased materials for food packaging. Trends Food Sci Technol 1999;10:52−68.
[38] Salame M. The use of low permeability thermoplastics in food and beverage packaging. In: Hopfenberg HB, editor. Permeability of plastic films and coatings to gases vapours and liquids. New York: Plenum Press; 1974. p. 275.
[39] Fereydoon M, Ebnesajjad S. Development of high-barrier film for food packaging. In: Ebnesajjad S, editor. Plastic films in food packaging. New York: Elsevier; 2013. p. 71−92.
[40] Robertson GL. Optical, mechanical and barrier properties of thermoplastic polymers. In: Food packaging. Principles and practice. 3rd ed. Boca Raton (FL): CRC Press; 2013. p. 91−130.
[41] Vaha-Nissi M, Hjelt T, Kokko A, Kokkonen R, Mikkelson A. Tool for measuring diffusion of aromas through packaging materials. In: TAPPI PLACE conference; 2008.
[42] Stevens M. Aroma/flavor barrier measurement. In: TAPPI PLACE conference; 2004.
[43] Butler TI, Morris BA. PE-based multilayer film structures. In: Ebnesajjad S, editor. Plastic films in food packaging, materials, technology and applications. New York: Elsevier; 2013. p. 21−52.
[44] DuPont. DuPont™ Selar® PA3426 blends with nylon 6. 2005. viewed 12 November 2014, from, http://www.dupont.com/content/dam/assets/products-and-services/packaging-materials-solutions/assets/selar_pa3426_nylon_blends.pdf.
[45] Kuraray. Gas barrier properties of resins. 2007. Tech Bulletin No. 10, viewed 12 November 2014, from, http://www.eval.eu/media/36916/ea%20-%20technical%20bulletin%20no%20110.pdf.
[46] Mitsubishi Gas Chemical Company, Inc., ND, Nylon-MXD6, superior performance in barrier packaging, viewed 10 November 2014, from http://www.idspackaging.com/Common/exhib_349/Mxd6bro.1.pdf.
[47] DuPont Teijin Films. Oxygen and water vapour barrier properties of flexible packaging films. 2001. viewed 10 November 2014, from, http://usa.dupontteijinfilms.com/informationcenter/downloads/Oxygen_And_Walter_Vapour_Barrier_Properties_of_Flex_Pack_Films.pdf.
[48] Jindal Poly Films, Ltd., BOPP films, viewed 10 November 2014, from http://jindalpoly.com/products/bopp-films/86.html.
[49] Honeywell International, Inc. Honeywell Aclar films. 2011. viewed 10 November 2014, from, https://www.honeywell-aclar.com/Documentation/Honeywell-Aclar-films-Overview-metric.pdf.
[50] Singh A, Koros WJ. Permeation processes in barriers and membranes: differences and similarities. In: TAPPI polymers, laminations and coatings conference; 1998. p. 361−71.
[51] Powell RJ. DuPont internal report. 1968.
[52] deGaravilla J. Ionomer, acid copolymer, and metallocene polyethylene resins: a comparative assessment of sealant performance. Tappi J 1995;78(6):192.
[53] DuPont. Surlyn® Update. Barrier properties − oil resistance, vol. 1(9); 1973.

[54] Sajilata MG, Savitha K, Singhal RS, Kanetkar VR. Scalping of flavors in packaged foods. Compr Rev Food Sci Food Saf 2007;6:17−35.
[55] Auras R, Harte B, Selke S. Sorption of ethyl acetate and d-limonene in poly(lactide) polymers. J Sci Food Agric 2006;86:648−56.
[56] Woishnis W, editor. Chemical resistance of plastics and elastomers. 4th ed. St. Louis: William Andrew; 2007.
[57] Sabic EuroPetrochemicals BV. Chemical resistance of polyethylenes. 2005. viewed 26 June 2014, from, http://polymers.sabic-europe.com/technical/_media/chemical_resistance_pe.pdf.
[58] Lati High Performance Thermoplastics. Chemical resistance data. 2002. viewed 26 June 2014, from, http://www.lati.com/en/technical_data/chemical_resistance_03.html.
[59] Plastics International, Unknown, Chemical resistance chart, viewed 26 June 2014, from http://www.plasticsintl.com/plastics_chemical_resistence_chart.html.
[60] Burkle GmbH. Chemical resistance. 2014. viewed 27 June 2014, from, http://www.buerkle.de/media/files/Downloads/Chemical_resistance_EN_2014.pdf.
[61] ThermoScientific, Unknown, Labware chemical resistance, viewed 26 June 2014, from http://www.thermoscientific.com/content/dam/tfs/LPG/LCD/LCD%20Documents/Product%20Manuals%20%26%20Specifications/Filtration%20Products/Filter%20Units%20and%20Bottletop%20Filters/Filter%20Units/D20480～.pdf.
[62] Graham BM, Luisa F, Cezar MA. Transparent container. 2003. Patent application WO2003022699 A1.
[63] Niedenzu PM. Choices of light attenuation in plastic film applications. In: TAPPI PLACE conference; 2008.
[64] Niedenzu PM. Review of titanium dioxide ability to scatter light. In: AIMCAL conference, Myrtle Beach, SC; 2014.
[65] Ylvisaker J. Mass transfer analysis of film barrier materials. In: TAPPI polymers, laminations and coatings conference; 1998. p. 1181−9.
[66] Lee WE. Selection of barrier materials from molecular structure. Polym Eng Sci 1980;20:65−9.
[67] Todd WG, Podborny WR, Krohn JV. Maximize barrier performance of reduced-gauge HDPE films. In: SPE ANTEC conference; 1999.
[68] Haley JC, Borke JS. The interplay between polymer polydispersity and film gauge in HDPE barrier films: how polydispersity controls gauge dependence of film barrier properties. In: SPE ANTEC conference; 2009. p. 231−5.
[69] Cooksey K. Important factors for selecting food packaging materials based on permeability. In: Flexible packaging conference; 2004.
[70] Van Krevelen DW, te Nijenhuis K. Properties of polymers. Amsterdam: Elsevier Science; 2009. p. 655−702.
[71] Barton AFM. Handbook of solubility parameters and other cohesion parameters. New York: CRC Press LLC; 1999.
[72] Hansen CM. Hansen solubility parameters: a user's handbook. New York: CRC Press LLC; 1999.
[73] Van Krevelen DW, te Nijenhuis K. Properties of polymers. Amsterdam: Elsevier Science; 2009. p. 189−227.
[74] Juliano P, Koutchma T, Sui Q, Barbosa-Cánovas GV, Sadler G. Polymeric-based food packaging for high-pressure processing. Food Eng Rev 2010;2:274−97.
[75] Guillarda V, Mauricio-Iglesiasa M, Gontarda N. Effect of novel food processing methods on packaging: structure, composition, and migration properties. Crit Rev Food Sci Nutr 2010;50:969−88.
[76] Genskow LR, et al. Psychrometry, evaporative cooling, and solids drying. In: Green DW, Perry RH, editors. Perry's chemical engineering handbook. 8th ed. McGraw Hill; 2008. pp. 12−11.
[77] Avallone EA, Baumeister III T, Sadegh AM, editors. Marks' standard handbook for mechanical engineers. 11th ed. New York: McGraw Hill; 2006. p. 4−45.
[78] Tsai BC, Jenkins BJ. Effect of retorting on the barrier properties of EVOH. J Plast Film Sheeting 1988;4:63−71.
[79] Lopez-Rubio A, Lagaron JM, Gimenez E, Cava D. Morphological altercations induced by temperature and humidity in ethylene-vinyl alcohol copolymers. Macromolecules 2003; 36:9467−76.

[80] Lopez-Rubio A, Hernandez-Munoz P, Gimenez E, Yamamoto T, Gavara R, Lagaron JM. Gas barrier changes and morphological alterations induced by retorting in ethylene vinyl alcohol-based food packaging structures. J Appl Polym Sci 2005;96:2192−202.
[81] Farrell CJ, Tsai BC, Wachtel JA. Drying agent in multi-layer polymeric structure. 1983. U. S. patent 4,407,897.
[82] Lagaron JM, Nunez E. Nanocomposites of moisture-sensitive and biopolymers with enhanced performance for flexible packaging applications. J. Plast Film Sheeting 2011; 28:79−89.
[83] Largaron JM, Gimenez E, Altava B, Del-Valle V, Gavara R. Characterization of extruded ethylene-vinyl alcohol copolymer based barrier blends with interest in food packaging applications. Macromol Symp 2003;198:473−82.
[84] Lee SA, Kim SC. Laminar morphology development using hybrid EVOH-nylon blends. J Appl Polym Sci 1998;67:2001−104.
[85] Yeo JH, Lee CH, Park C-S, Lee K-J. Rheological, morphological, mechanical, and barrier properties of PP/EVOH blends. Adv Polym Tech 2001;20:191−201.
[86] Murray L. The impact of foil pinholes and flex cracks on the moisture and oxygen barrier of flexible packaging. In: TAPPI PLACE conference; 2005.
[87] Weis J. Factors affecting barrier properties of metallized films. Verpack Rundsch 1993; 44:23−9.
[88] Yializis A, Ellwanger RE, Harvey J. Loss of barrier in aluminum metalized polypropylene. In: Proc. Int. Conf. Vac. Web Coat 10th; 1996. p. 276−83.
[89] Lush J, Ferrari D. An economic value model for converters comparing the total cost of metallized film vs. foil in flexible packages. In: TAPPI PLACE conference; 2006.
[90] Vansant JD. Acid copolymer for extrusion coating. In: Bezigian T, editor. Extrusion coating manual. 4th ed. Atlanta: TAPPI Press; 1999. p. 235−9.
[91] Rossi G, Nulman M. Effect of local flaws in polymeric permeation reducing barriers. J Appl Phys 1993;74:5471−5.
[92] Hanika M, Langowski H-C, Moosheimer U, Peukert W. Inorganic layers on polymeric films − influence of defects and morphology on barrier properties. Chem Eng Technol 2003;26: 605−14.
[93] Del-Valle V, Almenar E, Lagarón JM, Catalá R, Gavara R. Permeation through porous polymeric films for modified atmosphere packaging. Food Addit Contam 2003; 20:170−9.
[94] Del-Valle V, Hernandez-Munoz P, Catala R, Gavara R. Optimization of equilibrium modified atmosphere packaging (EMAP) for minimally processed mandarin segments. J Food Eng 2009;91:474−81.
[95] Paul DR, Clarke R. Modeling of modified atmosphere packaging based on designs with a membrane and perforations. J Membr Sci 2002;208:269−83.
[96] Lee DS, Renault P. Using pinholes as tools to obtain optimum modified atmospheres in packages of fresh produce. Packag Technol Sci 1998;11:119−30.
[97] Hirata T, Makino Y, Ishikawa Y, Katsuura S, Hasegawa Y. A theoretical model for designing modified atmosphere packaging with a perforation. Trans ASAE 1996;39:1499−504.
[98] Rennie TJ, Tavoularis S. Perforation-mediated modified atmosphere packaging. Part I. Development of a mathematical model. Postharvest Biol Tech. 2009;51:1−9.
[99] Chung D, Papadakis S, Yam KL. Simple models for evaluating effects of small leaks on the gas barrier properties of food packages. Packag Technol Sci 2003;16:77−86.
[100] Rooney MJ. Oxygen-scavenging packaging. In: Ebnesajjad S, editor. Plastic films in food packaging, materials, technology and applications. Elsevier; 2013. p. 139−49.
[101] Xu J, Uradnesheck J, Morris BA. DuPont internal report. 2009.
[102] Ching TY, Katsumoto K, Current S, Theard L. Ethylenic oxygen scavenging compositions and process for making same by esterification nor transesterification in a reactive extruder. 1995. PCT Application PCT/US1994/07854.
[103] Schrenk WJ, Chisholm DS, Cleereman KJ, Alfrey Jr T. Multilayered iridescent plastic articles. 1971. U.S. patent 3576707.
[104] Alfrey Jr T, Schrenk WJ. Highly reflective thermoplastic bodies for infrared, visible or ultraviolet light. 1973. U. S. patent 3711176.

[105] Schrenk WJ. Apparatus for multilayer coextrusion sheet or film. 1975. U. S. patent 3884606.
[106] Alfrey Jr T, Schrenk WJ. Multilayer coextrusion process for producing selective reflectivity. 1978. U. S. patent 4094947.
[107] Schrenk WJ, Shastri RK, Roehrs HC, Ayres RE, Barger MA, Bremmer JN. Method and apparatus for producing multilayer plastic articles. 1997. U. S. patent 5628950.
[108] Schrenk WJ, Alfrey Jr T. Some physical properties of multilayered films. Polym Eng Sci 1969;9:393−9.
[109] Im J, Schrenk WJ. Coextruded multilayer sheet and film. J Plast Film Sheeting 1988;4:104−15.
[110] Tangirala R, Baer E, Hiltner A, Weder C. Photopatternable reflective films produced by nanolayer extrusion. Adv Funct Mater 2004;14:595−604.
[111] Kazmierczak T, Song H, Hiltner A, Baer E. Polymeric one-dimensional photonic crystals by continuous coextrusion. Macromol Rapid Commun 2007;28:2210−6.
[112] Lai C-Y, Baer E. The interdiffusion of polymeric gradient refractive index (GRIN) lens materials. In: SPE ANTEC conference; 2011.
[113] Mackey M, Wolak M, Shirk J, Flandin L, Hiltner A, Baer E. Enhanced dielectric properties of micro and nanolayered films for capacitor applications. In: SPE ANTEC conference; 2011.
[114] Ponting M, Hiltner A, Baer E. Gradient multilayered films by forced assembly coextrusion. In: SPE ANTEC conference; 2009.
[115] Tai HT, Hiltner A, Baer E, Wiggins M, Sandrock M, Shirk J. Tunable reflective polymeric nanolayered films. In: SPE ANTEC conference; 2005.
[116] Pointing M, Hiltner A, Baer E. Gradient multilayer films by forced assembly. In: SPE ANTEC conference; 2009.
[117] Cloeren PF. Interface control. 2005. U. S. patent 6905324 B2.
[118] Schirmer HG. For extrusion of resin to form modular assembly of thin disks. 1998. U.S. patent 5762971 A.
[119] Schirmer HG. Modular disk coextrusion die. 2002. U. S. patent 6413595.
[120] Schirmer HG, Jester R, Medlock GD, Schell T. Nano-layer effects in blown barrier films. In: SPE international polyolefins conference; 2010.
[121] Dooley J, Robacki J, Jenkins S, Lee P, Wrisley R. Producing microlayer blown film structures using layer multiplication and unique die technology. In: SPE ANTEC conference; 2011.
[122] Zumbrunnen ML, Zumbrunnen DA. A new blown film die for controllably forming and extruding microlayers, polymer blends and composites. In: SPE ANTEC conference; 2009.
[123] Dooley J, Hughes K. Coextrusion layer thickness variation − effect of polymer viscoelasticity on layer uniformity. In: SPE ANTEC conference; 1995. p. 69−74.
[124] Dooley J, Hyun KS, Hughes K. An experimental study on the effect of polymer viscoelasticity on layer rearrangement in coextruded structures. Polym Eng Sci 1998;38:1060−71.
[125] Dooley J. Viscous and elastic effects in polymer coextrusion. J Plast Film Sheeting 2003;19: 111−22.
[126] Zhao R, Macosko CW. Polymer-polymer mutual diffusion via rheology of coextruded multilayers. AIChE J 2007;53:978−85.
[127] Levitt L, Macosko CW, Schweizer T, Meissner J. Extensional rheometry of polymer multilayers: a sensitive probe of interfaces. J Rheol 1997;41:671−85.
[128] Zhao R, Macosko CW. Slip at polymer-polymer interfaces: rheological measurements on coextruded multilayers. J Rheol 2002;46:145−67.
[129] Zhang Z, Lodge TP, Macosko CW. Interfacial slip reduces polymer-polymer adhesion during coextrusion. J Rheol 2006;50:41−57.
[130] Schultz JS, Lodge TP, Macosko CW. The reactive formation of diblock copolymer at a polymer/polymer interface and its effect on interfacial structure. Mat Res Soc Symp 2000;629:FF2.2.1−2.2.6.
[131] Saito T, Macosko CW. Interfacial crosslinking and diffusion via extensional rheometry. Polym Eng Sci 2002;42:1−9.
[132] Macosko CW, Jeon HK, Hoye TR. Reactions at polymer-polymer interfaces for blend compatibilization. Prog Polym Sci 2005;30: 939−47.

[133] Hiltner A, Nazarenko S, Ebeling T, Schuman T, Baer E. Novel microlayered structures for adhesion and interdiffusion studies. Polym Mater Sci Eng 1996;75:471–2.
[134] Baer E, Jarus D, Hiltner A. Microlayer coextrusion technology. In: SPE ANTEC conference; 1999.
[135] Bernal-Lara TE, Masirek R, Hiltner A, Baer E, Piorkowska E, Galeski A. Morphological studies of multilayered HDPE/PS systems. J Appl Polym Sci 2006;99:597–612.
[136] Bernal-Lara TE, Liu RYF, Hiltner A, Baer E. Structure and thermal stability of polyethylene nanolayers. Polymer 2005;46:3043–55.
[137] Pan SJ, Im J, Hill MJ, Keller A, Hiltner A, Baer E. Structure of ultrathin polyethylene layers in multilayer films. J Polym Sci Part B Polym Phys 1990;28:1105–19.
[138] Jin Y, Rogunova M, Hiltner A, Baer E, Nowacki R, Galeski A, et al. Structure of polypropylene crystallized in confined nanolayers. J Polym Sci Part B Polym Phys 2004;42:3380–96.
[139] Balta Calleja FJ, Ania F, Orench IP, Baer E, Hiltner A, Bernal T, et al. Nanostructure development in multilayer polymer systems as revealed by X-ray scattering methods. Prog Colloid Polym Sci 2005;130:140–8.
[140] Bernal-Lara TE, Ranade A, Hiltner A, Baer E. Nano- and microlayered polymers: structure and properties. In: Michler GH, Balta-Calleja FJ, editors. Mechanical properties of polymers based on nanostructure and morphology. Baco Raton: Taylor & Francis; 2005. p. 629–81.
[141] Kerns J, Hsieh A, Hiltner A, Baer E. Mechanical behavior of polymer microlayers. Macromol Symp 1999;147:15–25.
[142] Pethe VV. Oxygen and carbon dioxide permeability of EAA/PEO blends and microlayers [Masters thesis]. Case Western Reserve University; 2008.
[143] Wang HP, Keum JK, Hiltner A, Baer E, Freeman B, Rozanski A, et al. Confined crystallization of polyethylene oxide in nanolayer assemblies. Science 2009;323:757–60.
[144] Baer E, Hiltner A. Confined crystallization multilayer films. 2010. U. S. patent application 2010/0143709 A1.
[145] Wang H, Keum JK, Hiltner A, Baer E. Confined crystallization of PEO in nanolayered films impacting structure and oxygen permeability. Macromolecules 2009;42:7055–66.
[146] Pointing M, Keum J, Freeman B, Hiltner A, Baer E. Substrate effects on the confined crystallization of polycaprolactone in coextruded nanolayered films. In: SPE ANTEC conference; 2011.
[147] Oliver G. Performance packaging utilizing layer multiplication. In: AMI barrier conference, Germany; 2009.
[148] Oliver G. Micro-layer coextrusion methods and applications. In: TAPPI PLACE conference; 2012.
[149] Catherine O. Sub-micron coextrusion technology and application examples. In: TAPPI PLACE conference; 2012.
[150] Medlock G, Dolgovskij. Barrier performance of nanolayer EVOH film. In: TAPPI PLACE conference; 2012.
[151] Lee PC, Dooley J, Robacki J, Jenkins S, Wrisley R. Flex barrier property enhancement in film structures using microlayer coextrusion technology. In: SPE ANTEC conference; 2013.
[152] DuPont. 23rd DuPont packaging awards: sustainability and waste reduction drive winners. DuPont Packaging and Industrial Polymers; 2011. viewed 18 October 2014, from, http://www2.dupont.com/Packaging_Resins/en_US/whats_new/23rd_packaging_awards_winners.html.
[153] Schirmer H. Nano-layers create thinner and wider tubular films. In: SPE FlexPackCon conference; 2014.
[154] Plastics Technology. Microlayer films: new uses for hundreds of layers. 2006. viewed 18 October 2014, from, http://www.ptonline.com/articles/microlayer-films-new-uses-for-hundreds-of-layers.
[155] Bonk HW, Goldwasser DJ, Mitchell PH. Flexible membranes. 2000. U. S. patent 6082025 A.
[156] Okada A, Fukushima Y, Kawasumi M, Inagaki S, Usuki A, Sugiyama S, et al. Composite material and process for manufacture same. 1988. U. S. patent 4,739,007.
[157] Chaiko DJ. Nanocomposite packaging. In: Landgrebe AR, editor. Power sources for transportation applications: proceedings of the international symposium. The Electrochemical Society; 2004. p. 205–12. ISBN: 1566774098, 9781566774093.

[158] Chaiko DJ, Leyva AA. Thermal transitions and barrier properties of olefinic nanocomposites. Chem Mater 2005;17:13−9.
[159] Chaiko DJ. Thermally stable surfactants and compositions and methods of use thereof. 2008. US Patent 7420071B2.
[160] Osman MA, Rupp JEP, Suter UW. Effect of non-ionic surfactants on the exfoliation and properties of polyethylene-layered silicate nanocomposites. Polymer 2005;46:8202−9.
[161] Sirousazar M, Yari M, Achachlouei BF, Arsalani J, Mansoori Y. Polypropylene/montmorillonite nanocomposites for food packaging. e-Polymers 2007;(1):305−13.
[162] Ali Dadfar SM, Alemzadeh I, Reza Dadfar SM, Vosoughi M. Studies on the oxygen barrier and mechanical properties of low density polyethylene/organoclay nanocomposite films in the presence of ethylene vinyl acetate copolymer as a new type of compatibilizer. Mater Des 2011;32:1806−13.
[163] Shafiee M, Ahmad Ramazani SA, Danaei M. Investigation of the gas barrier properties of PP/clay nanocomposite films with EVA as a compatibilizer prepared by the melt intercalation method. Polym Plast Technol Eng 2010;49:991−5.
[164] Hosseinkhanli H, Sharif A, Aalaie J, Khalkhali T, Akhlaghi S. Oxygen permeability and the mechanical and thermal properties of (low-density polyethylene)/poly (ethylene-co-vinyl acetate)/organoclay blown film nanocomposites. J Vinyl Addit Technol 2013;19:132−9.
[165] Choi WJ, Kim H-J, Yoon KH, Kwon OH, Hwang CI. Preparation and barrier property of poly(ethylene terephthalate)/clay nanocomposite using clay-supported catalyst. J Appl Polym Sci 2006;100:4875−9.
[166] Lan T. Nanocomposite materials for packaging applications. In: SPE ANTEC conference; 2007. viewed 15 October 2012, from, http://www.nanocor.com/tech_papers/Antec-Nanocor-Tie%20Lan-5-07.pdf.
[167] Goldman AY. Barrier liner material with nanocomposite for packaging applications. In: SPE ANTEC conference; 2005. p. 1468−71.
[168] Bonner S, Sabandith D, Swannack C, Zhou W. Nanocomposite film technology. In: SPE ANTEC conference; 2001.
[169] Meneghetti P, Qutubuddin S. Synthesis, thermal properties and applications of polymer-clay nanocomposites. Thermochim Acta 2006;442:74−7.
[170] Shah RK, Krishnaswamy RK, Paul DR. Blown films from LDPE-organoclay and ionomer-organoclay nanocomposites. In: SPE ANTEC conference; 2006. p. 597−601.
[171] Sherman LM. Nanocomposites: less hype, more hard work on commercial viability. Plast Technol May 2007. viewed 04 November 2014, from, https://www.princeton.edu/∼cml/assets/publicity/Nanocomposites200705.pdf.
[172] Kravitz HS, Levitt F. Barrier coatings for films and structures. 2011. US patent 8080297 B2.
[173] Neilson LE. Models for the permeability of filled polymer systems. J. Macromol Sci (Chem) 1967;A1(5):929−42.
[174] Abbott S, Holmes N. Nanocoatings: principles and practice. DesTech Publications; 2013. spreadsheet viewed 15 November 2014, from, http://www.destechpub.com/links/catalogs/bookstore/advanced-materials-sciencetechnology/nanomaterials-and-nanotechnology-2/nanocoatings-principles-and-practice/.
[175] Bhunia K, Dhawan S, Sablani SS. Modeling the oxygen diffusion of nanocomposite-based food packaging films. J Food Sci 2012;77:N29−30.
[176] Aleperstein D, et al. Experimental and computational investigations of EVOH/clay nanocomposites. J Appl Polym Sci 2005;97:2060−6.
[177] Johnson RW, Hultqvist A, Bent SF. A brief review of atomic layer deposition: from fundamentals to applications. Materials Today 2014;17:236−46.
[178] Hirvikorpi T, Vähä-Nissi M, Mustonen T, Iiskola E, Karppinen M. Atomic layer deposited aluminum oxide barrier coatings for packaging materials. Thin Solid Films 2010;518:2654−8.
[179] Hirvikorpi T, Vähä-Nissi M, Harlin A, Karppinen M. Comparison of some coating techniques to fabricate barrier layers on packaging materials. Thin Solid Films 2010;518:5463−6.
[180] Groner MD, George SM, McLean RS, Carcia PF. Gas diffusion barriers on polymers using Al_2O_3 atomic layer deposition. Appl Phys Lett 2006;88:51907.
[181] Abbasa GA, Papakonstantinoua P, Okpalugoa TIT, McLaughlina JA, Filikb J, Harkin-Jonesc E. The improvement in gas

barrier performance and optical transparency of DLC-coated polymer by silicon incorporation. Thin Solid Films 2005;482:201−6.
[182] Shirakura A, Nakaya M, Koga Y, Kodama H, Hasebe T, Suzuki T. Diamond-like carbon films for PET bottles and medical applications. Thin Solid Films 2006;494:84−91.
[183] Asakawa R, Nagashima S, Nakamura Y, Hasebe T, Suzuki T, Hotta A. Combining polymers with diamond-like carbon (DLC) for highly functionalized materials. Surf Coat Technol 2011;206:676−85.
[184] Granger VM, Tigani MA. Permeation properties of moisture sensitive barriers materials under end use conditions. TAPPI J 1993;76:98−102.
[185] Constant DR. Cyclic olefin copolymer, A primer on basic structure, polymer attributes and barrier properties in films for flexible packaging. In: TAPPI PLACE conference; 2004.

9 Strength, Stiffness, and Abuse Resistance

The structural integrity of the package is critical for protecting the product from packing through distribution and use. In multilayer flexible packaging, often one or more layers are specifically incorporated to bear the load when it comes to strength and integrity, but the other layers play a role as well. This chapter looks at various aspects of structural integrity, including tensile strength; flexural stiffness; and tear, scratch, puncture, and impact resistance. The importance of these attributes, how they are measured, and how they are impacted by the design of the multilayer film are explored.

9.1 Why It is Important

9.1.1 Strength

The package needs to be able to hold the product and withstand any stress that occurs throughout the life of the packaged good. An important stress factor is the mass and density of the product being packaged. A film structure for packaging cement will require greater strength than one for packaging feathers. If the weight of the product exceeds the tensile strength of the film, then the package will likely fail. Even before the ultimate strength is exceeded, the film may yield and deform, which may be undesirable. Stiff, high yield strength layers such as oriented polyethylene terephthalate (OPET), paperboard or woven polypropylene are often incorporated into the package design to bear the load.

Other stresses may also be important. For example, some deli meats are cooked in the package. During cooking, the elevated temperatures lower the tensile strength of the film. As the cooking proceeds, pressure may buildup inside the package as water and other components volatilize, exerting a stress on the package. This combination of higher stress and lower strength must be factored into the design of the film.

Forces experienced during shipping may cause a package to fail. An example is illustrated in Fig. 9.1 where a package filled at sea level is transported over a mountain pass. The lower ambient pressure at the higher elevation causes the package to bulge outward and puts a stress on the film. If this stress exceeds the yield strength of the film, then the film will elongate; when the package returns to lower elevation it may look distorted and aesthetically unpleasing. Higher stress may result in failure. In this example, the mountain pass is at 3660 m (12,000 ft) and the pressure differential is 0.038 MPa. For the given dimensions of the package film, this results in a stress of 388 MPa [1]. If the yield strength of the film is lower than this, it will yield.

The tensile strength of the film is not the only consideration. If the film is heat sealed, the strength of the seal must be considered. The reader is referred to Chapter 7 for a discussion on heat seal and hot tack strength. Puncture resistance, flex cracking, and other abuse factors are considered below.

9.1.2 Stiffness

The bending or flexural stiffness of a packaging film is important for a number of reasons. In some packages, it is a critical part of the package form. The standup pouch, for example, needs stiffness for the package to maintain its rigidity. The bending stiffness is also important for handling of the film on automated packaging lines. If it is too stiff it may not form around shaping mandrels in form-fill-seal operations. If it is too flexible, it may not maintain its shape during filling and other operations.

Bending stiffness is related to the "hand" or feel of the film and package. The consumer may associate a "flimsy" package with an inferior product. Downgauging (reducing the thickness) of a packaging film without maintaining the bending stiffness may be perceived by the consumer. McKenna et al. [2] and Bunker [3] found that consumers can detect a difference in film thickness of 15% in films of the same bending stiffness but that increasing stiffness while downgauging may allow further thickness reduction without consumer awareness. As is discussed below, the design of a multilayer film structure can have a substantial impact on its bending stiffness.

The Science and Technology of Flexible Packaging. http://dx.doi.org/10.1016/B978-0-323-24273-8.00009-5
Copyright © 2017 Elsevier Inc. All rights reserved.

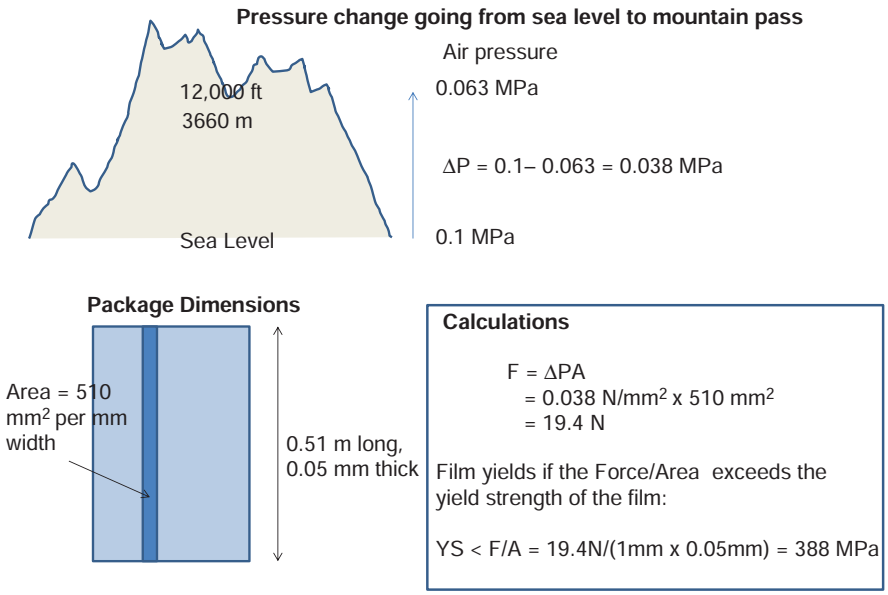


Figure 9.1 Example of shipping a flexible package over a mountain pass. The package will experience a stress as the ambient pressure decrease with the elevation gain. If this stress exceeds the yield strength of the film, the film will elongate.

Bending stiffness should not be confused with tensile stiffness or elastic modulus. Tensile modulus (also known as the elastic or Young's modulus) is obtained from tensile tests and is a fundamental property of a material. When combining multiple materials in a multilayer film, however, the tensile modulus is a simple average of the component moduli. Bending stiffness is a package property that is a complex function of the tensile moduli, thickness, and location of the individual layers.

9.1.3 Abuse Resistance

Abuse can come from the product within the package or from external factors. Some examples include the following:

- Puncture of the film from bones in meat products or sharp noodles in dry foods. This is generally a slow puncture process that occurs during distribution.
- Puncture of the film as the product is dropped into the package during a vertical filling operation. This often involves high speed impact and scratching of the film by the product.
- Abrasion of the film from the product within. This often results from vibrations that occur during shipping and handling. Examples include coffee grinds and snack products.
- Abrasion of the film from outside the package. This may occur as packages rub against each other during shipping.
- Failure of a package during dropping. The package may be dropped during handling, for example, as the filled package is placed into a secondary package for shipping. Dropping often involves high speed impact.
- Tearing of the film. Tear resistance can be an important aspect of many abuse events such as puncture and abrasion. Poor tear resistance can propagate cracks generated during these events, contributing to failure. In some cases, however, low tear strength is desirable; directional tear properties, where the film tears easily in a particular direction, may be used as an easy-open feature for a package.
- Distortion of the film at elevated temperatures. Processes such as heat sealing can distort the film or cause the film to stick to the seal bar. Hot fill, retort sterilization, cook-in the package, and in-package pasteurization expose the film to elevated temperatures and pressures that may distort the film.

- Cold temperature impact failure. Some food products are exposed to blast freezing after packaging, which can put stress on the film. Some polymers have good toughness at room temperature but become brittle at cold temperatures.

9.2 How to Measure

9.2.1 Mechanical Properties

ASTM D882 [4] provides a standard method for measuring the tensile properties of film. Strips are cut from the sample and placed in the gripping jaws of a tensile testing machine. The load is measured as the gripping jaws are pulled apart at a constant speed. At the same time, the distance between the jaws is measured. The load vs displacement data allows for the calculation and plotting of stress vs strain and the tensile properties. A common specimen width is 1-inch (25.4 μm) and test speed ranges from about 1 to 10 inches/min (25−250 mm/min).

A typical stress vs strain curve for a ductile plastic is shown in Fig. 9.2. At low strain, the stress increases linearly. The deformation is elastic; the slope of the curve in this region is known as the elastic modulus and is related to the stiffness. The yield point represents the transition from elastic to plastic deformation. Below the yield point, the plastic will recover to its original shape once the strain is removed. Deformations above the yield point are not recoverable. The test specimen may neck-in at the yield point, giving a local maximum in the stress. Further increases in strain eventually result in rupture of the specimen.

The stress vs strain curve differs from one polymer to next but generally takes on one of the characteristic shapes as shown in Fig. 9.3. Brittle plastics typically have a steep initial slope but fail at low strains and do not exhibit plastic deformation. Stiff and strong plastics have a steep slope, exhibit a yield point, have a high maximum or ultimate stress at break, but fail at a relatively low stain. Softer, tough polymers generally have a gentler slope but fail at much higher strains. Their maximum stress is lower but their high elongation before failure often translates into greater toughness. Representative curves for several polymers are shown in Fig. 9.4.

The stress vs strain curve is used to calculate or define a number of mechanical properties of the film:

Strain or elongation. The change in length as the specimen is stretched between the moving grips of the tensile tester is known as the engineering or Cache strain or elongation:

$$\varepsilon = \frac{\Delta L}{L_0} \tag{9.1}$$

where ε = engineering strain, ΔL = change in length $= L - L_0$, L_0 = initial length of the specimen (or distance between grips), L = length of specimen during the tensile test.

When ε is expressed as a percentage, it is known as the % elongation.

Strain ratio. Sometimes the tensile curve is plotted vs the strain ratio rather than the strain or elongation.

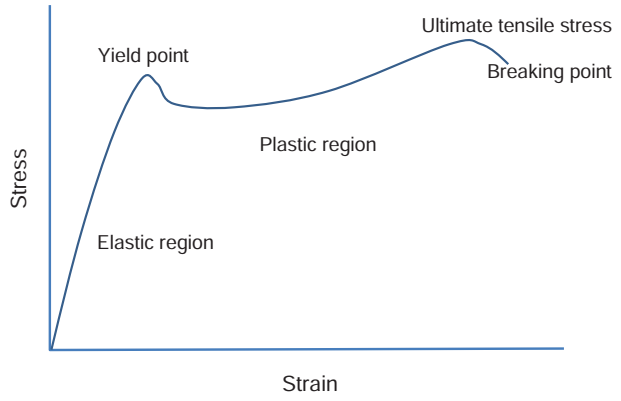


Figure 9.2 Characteristic stress vs strain curve for a plastic.
Adapted from McKeen LW. Film properties of plastics and elastomers. 3rd ed. Amsterdam: Elsevier; 2012. p. 27–34.

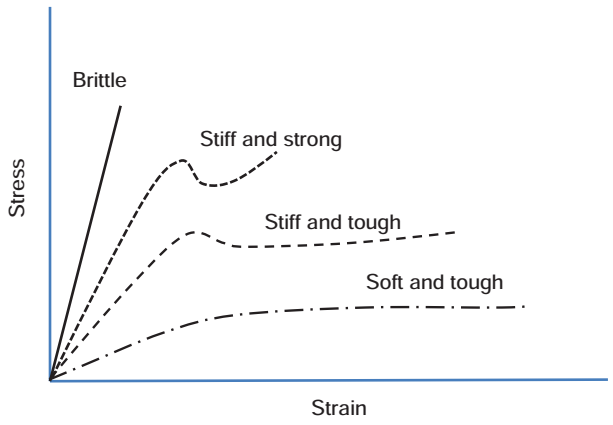


Figure 9.3 Characteristic stress vs strain curves for various polymer types.
Adapted from McKeen LW. Film properties of plastics and elastomers. 3rd ed. Amsterdam: Elsevier; 2012. p. 27–34.

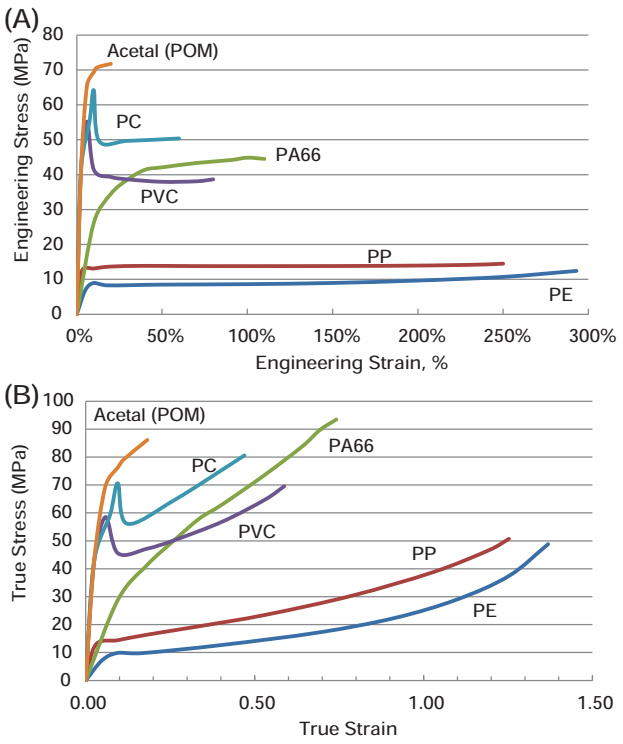


Figure 9.4 Representative stress vs strain curves for several polymers. (A) Engineering stress and strain. (B) True stress and strain.
From Bahadur S. Strain hardening equation and the prediction of tensile strength of rolled polymers. Polym Eng Sci 1973;13:266–72.

The strain ratio is the ratio of the instantaneous length to the initial length:

$$\lambda = \frac{L}{L_0} \tag{9.2}$$

where λ = strain ratio, L = length, L_0 = initial length.

True strain. The engineering strain is useful for small strains but as the strain becomes greater than about 5% the logarithmic strain, known as the true or Hencky strain, is a better representation of the strain. This takes into account the incremental stretching of the specimen.

$$\varepsilon_T = \ln(\lambda) = \ln(1 + \varepsilon) \tag{9.3}$$

where ε_T = true strain.

Engineering stress. The load measured by the tensile tester divided by the initial cross-sectional area (specimen width times thickness) is known as the engineering or nominal stress. The engineering stress is used to report most tensile properties in accordance with ASTM D882.

True stress. The true stress is the load divided by the instantaneous cross-sectional area. The true stress (σ_T) is related to the engineering stress (σ_E) in the following manner:

$$\sigma_T = \sigma_E \lambda = \sigma_E \exp(\varepsilon_T) \tag{9.4}$$

Yield stress or strength. As a viscoelastic material is stretched, initially the elongation is reversible; when the strain is released, it returns to its original length. At some critical strain, however, the material begins to deform plastically. Beyond this point, the material does not return to its original shape. This typically shows up as an inflection point on the stress vs strain curve. The engineering stress at this point is known as the yield stress or yield strength.

Elongation at yield. This is the engineering strain or elongation where the material yields or begins or plastically deform.

Tensile strength. The maximum engineering stress is known as the tensile stress or strength. This is also known as the ultimate tensile strength.

Tensile strength at break. The engineering stress at the point where the specimen breaks is known as the tensile strength or stress at break.

Elongation at break. The engineering strain at which the specimen breaks is known as the elongation at break. It is often expressed as a percentage.

Elastic modulus. The slope of a tangent drawn parallel to the initial linear portion (before the yield point) of the stress vs strain curve is known as the elastic modulus, tensile modulus, or Young's modulus. The modulus is related to the stiffness of the material.

Secant modulus. For many films, it is difficult to accurately determine the slope of the initial portion of the stress–strain curve. Rather than approximating a slope, a line is drawn from zero to the engineering stress at a specified strain (such as 1%). The slope of this line is the secant modulus at that strain, such as the 1% secant modulus.

Strain hardening parameter. The plastic deformation behavior of many ductile polymers can be represented by a two-parameter model [5]:

$$\sigma_T = \sigma_0 \exp(m\varepsilon_T) \tag{9.5}$$

where σ_T = true stress, ε_T = true strain, σ_0 = constant, m = strain hardening parameter.

The strain-hardening parameter is the slope of a line drawn through the yield stress and the ultimate tensile strength.

9.2.2 Stiffness

The bending stiffness of a film is only partly related to the elastic or tensile modulus obtained from the tensile tests described in Section 9.2.1. For a monolayer film, the bending stiffness is proportional to the modulus times the cube of the thickness of the film:

$$E_b \propto EX^3 \tag{9.6}$$

where E_b = bending stiffness, E = elastic or tensile modulus, X = thickness of film.

For a multilayer film, the relationship is more complex as is described in Section 9.4.2. The geometry of the test frame also plays a role, so measuring the bending stiffness directly is preferable to relying on the tensile modulus of the film.

Lange [7] describes several types of test methods for measuring the bending stiffness of films, some borrowed from the paper industry and some home grown:

9.2.2.1 Bend Under Own Weight

In this type of test, a length of film is extended over a ledge and the angle of the bend is measured. The extension is increased until a characteristic bending angle is achieved. The length of extension is related to the bending stiffness. One such method is described in DIN 53 362 [8]. In their tests, Lange finds this method gives values lower than other methods, which they attribute to large plastic deformation that underestimates the elastic stiffness. They also find that it does not work for curled films.

9.2.2.2 Cantilever Tests

These tests apply a load or weight to the free end of the film specimen that is anchored on the other end. The amount of deflection of the film at a given load is measured, which is related to the stiffness. Standard methods include ASTM D5342 [9], ASTM D747 [10], and ISO 2493 [11]. Cantilever tests usually work best for stiff films. Lange reports that this method gives reliable and accurate results for the films they tested.

9.2.2.3 Three-Point Flex

These tests typically involve measuring the force to push a film through a slot. The slope of the force vs displacement is related to a bending modulus. Standard methods include ASTM D2923 [12] and BS 2782: Part 3, Method 332A [13].

Many of these methods use homegrown equipment, such as the DuPont method described by Morris and Vansant [14,15]. Fig. 9.5 shows conceptually how the test is performed. A 10 × 10 cm film specimen is placed on a slotted flat plate, the dimensions of which are shown in Fig. 9.6. The slot has Teflon tape applied to both sides to minimize friction. The slotted plate is rigged on a tensile testing machine such that it rises toward a stationery beam as the crosshead moves at a fixed speed of 12.7 mm/min (0.5 inches/min). See Fig. 9.7 for a schematic of the rig. As the crosshead rises, the film contacts the beam and is forced into the slot. The force is recorded by the tensile tester. The force vs displacement curve is plotted. The slope of the force vs displacement curve is computed using the same method for computing the secant modulus (ASTM D882). This slope is called the stiffness factor, which is a bending modulus.

To obtain the most accurate results, DuPont takes the following precautions:

- The stiffness factor is taken as the average of measurements of multiple specimens of the film with the film facing down and oriented in the machine direction (MD) (perpendicular to the slot), facing down with transverse direction (TD) orientation, facing up with MD orientation and facing up with TD orientation.

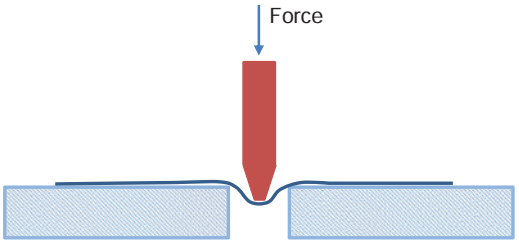


Figure 9.5 Schematic of three-point flex bending test.
Adapted from Morris BA, Vansant JD. The influence of sealant modulus on the bending stiffness of multilayer films. In: TAPPI polymers, laminations and coatings conference; 1997.

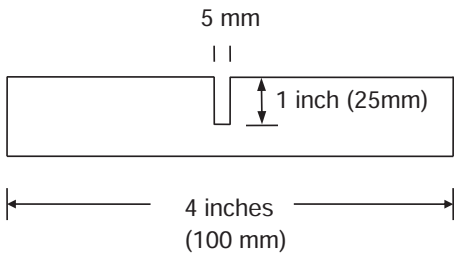


Figure 9.6 Side view of slotted plate used in DuPont bending stiffness test method.
Courtesy of E. I. du Pont de Nemours and Company.

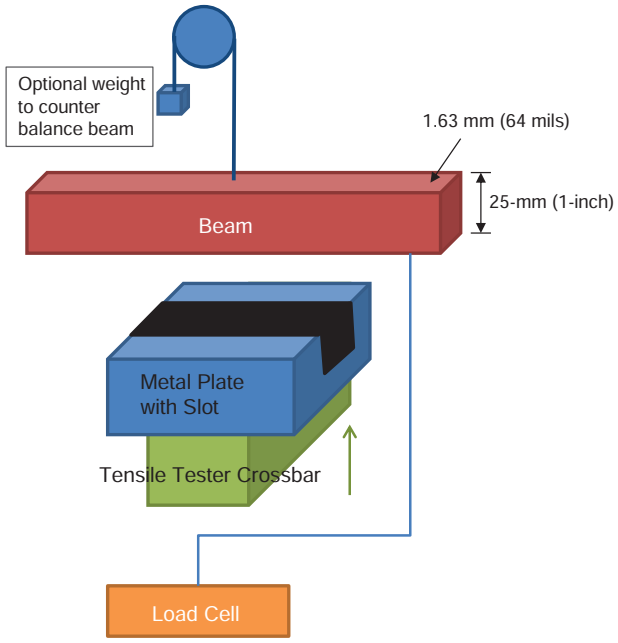


Figure 9.7 DuPont bending test. Slotted plate sides on crossbar of tensile tester. As the crossbar moves upward, the film is pushed against the beam. The load cell measures the force. The slope of the force vs displacement curve is the stiffness factor.
Courtesy of E. I. du Pont de Nemours and Company.

- The slope of the force vs displacement curve is used rather than just the force.
- The specimen width is kept constant when comparing data; the film specimen width directly effects the force measurements.
- Some films (such as polyolefins) are dusted with talc to reduce the error from surface friction. Tack, low slip, or static laden films will give erroneously high readings because of the added force required to overcome these factors.
- A lead weight is used on top of the tensile tester to reduce vibration effects.
- Other factors that may alter the results are minimized, including variations in surface slip of the samples or sides of the instrument slot, improper machine alignment, incorrect full-scale load adjustment, incorrect sample size, wrinkled samples, and excessive film curl.

Morris and Vansant find that the DuPont method gives consistent results that agree well with their model predictions. Lange finds that the version of the three-point flex test they evaluate works well but is sensitive to misalignment errors. For this reason, they prefer the cantilever test.

A common element of all the test methods is that they depend on the test geometry. To compare among the different tests, the results should be normalized against a standard.

9.2.3 Tear Strength

The Elmendorf tear resistance test is the most commonly used method for measuring the tear strength of packaging films. The method is described in detail in ASTM D1922 [16] and ISO 6383-2 [17]. The Elmendorf method is a high-speed notched tear test. The specimen is cut to a specified size and mounted to the test machine. A knife in the machine cuts a slit in the film where the tear will initiate. A weighted pendulum is released that swings through the specimen, propagating a tear. The machine measures the loss in kinetic energy of the pendulum as it tears through the specimen. This loss in energy is related to the tearing force. The tear resistance is reported in units of force divided by the thickness of the film. Typically 10 specimens are tested and the results averaged.

The trouser tear method is a slow speed tear resistance test and is described in ASTM D1938 [18] and ISO 6338-1 [19]. A standard tensile tester is used with a crosshead speed of 200 or 250 mm/min (8−10 inches/min). The rectangular tear specimen is precut on one end in what resembles a pair of trousers (Fig. 9.8). The two sides of the precut region are placed in the grips of the tensile tester and the force needed to propagate the tear is measured. The tear resistance is the force divided by the specimen thickness.

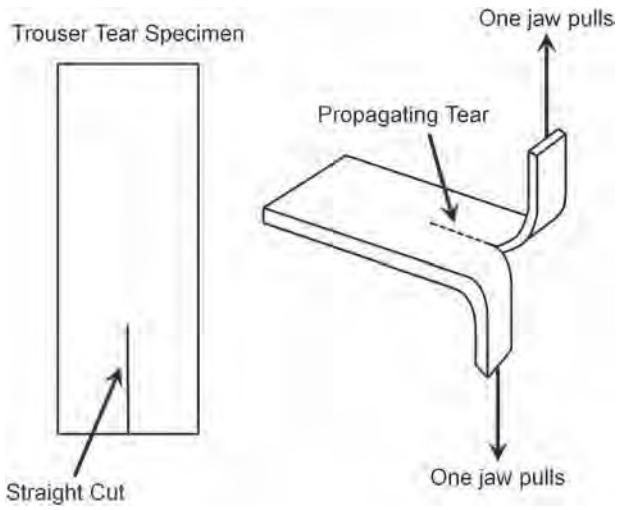


Figure 9.8 Trouser tear test sample configuration.
Reprinted with permission from McKeen LW. Film properties of plastics and elastomers. 3rd ed. Amsterdam: Elsevier; 2012. p. 27–34.

9.2.4 Puncture and Impact Resistance

A number of tests are used in the packaging industry to measure puncture resistance. No one test represents all the types of failures that may be experienced by a package in the field. Indeed, some package puncture failures do not correlate with any lab test; packaging engineers have sometimes resorted to homegrown tests, such as drop tests with packages filled with screws, to try to simulate real-world issues. The standard laboratory tests can be categorized as slow puncture or high-speed impact/puncture tests.

9.2.4.1 Slow Puncture

The integrity of some packages is compromised by puncture from sharp objects in the package, such as bones or dry noodles. Slow puncture laboratory tests try to mimic the conditions that cause this type of failure. One such method is ASTM D1306 [20]. A specimen is cut from the sample and clamped into a frame mounted to a universal test machine (tensile tester). The mounted specimen is positioned perpendicular to and below a vertical probe that punctures the film during the test. The standard recommends the probe tip be hemispherical with a radius of 3.2 mm. The probe is forced into the specimen at a constant speed of 25.4 mm/min (1 inch/min). The test machine measures the peak force, displacement, and energy to penetrate the film (area under the force vs displacement curve).

Other probe geometries and speeds are sometimes used. Lange [21] reviews several methods and probe designs. Other homegrown methods have been developed. One such method developed by DuPont [22] is shown schematically in Fig. 9.9. Here the film specimen is mounted on a test rig and a vertical needlelike probe, 2 mm in diameter with a 45 degree tip angle, is placed on top. A weight is placed on top of the probe to exert a known force. The time for the probe to penetrate the film is measured by recording when the probe hits a metal plate underneath the film and completes an electric circuit.

9.2.4.2 High Speed Puncture

The falling dart impact test is a noninstrumented test that is simple to use but can be time-consuming and labor intensive. The test is described in detail in ASTM D1709 [23] and ISO 7765-1 [24]. A film specimen is clamped horizontally into a test ring at the base of a drop tower. The dart is positioned above the specimen and dropped at a specified distance (method A calls for a 38-mm (1.5-inch) diameter dart dropped at 0.66 m (26-inch) and method B calls for a 51-mm diameter dart dropped at 1.5 m (60-inch)). The result is pass or fail. If the dart penetrates through the film, the test is repeated with a fresh specimen with a higher weight dart. If the dart fails to penetrate the film, the test is repeated with a lower

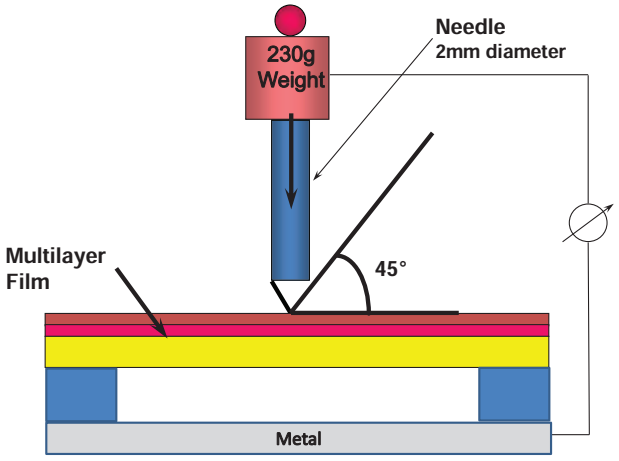


Figure 9.9 Schematic of DuPont Static Puncture Test.
Reproduced with permission of E. I. du Pont de Nemours and Company.

weight dart. The results from a series of determinations are used to calculate the weight at which 50% of the test specimens will fail known as the impact failure weight.

An instrumented version of the dart impact test, described in ASTM D4272 [25], measures the total energy of impact for rupturing the film. The velocity of a free falling dart of a specified shape that has passed through the film specimen is measured by using a photoelectric speed trap. The kinetic energy is calculated and compared with the kinetic energy of the free falling dart when no film is present. The loss in kinetic energy due to the impact and rupture of the film is used as an index of impact resistance. Special speed-sensing sensors are needed for this test method.

ISO 7765-2 [26] covers a similar instrumented falling dart test but differs from ASTM D4272, so their results cannot be directly compared. The ISO method uses an instrumented impactor head with a load cell to measure the energy of impact directly. The ASTM method computes the kinectic energy from the velocity of the dart.

A pendulum impact test is described by ASTM D3420 [27]. A film is clamped vertically in a holder with a circular aperture. A pendulum swings a hemispherical probe (25.4 mm in diameter) through the film. The energy needed to burst through the film is measured by the loss in kinetic work from the expenditure of kinetic energy by the pendulum. There are two methods that differ by the size of the diameter of the aperture: method A uses a 60 mm diameter sample size, whereas method B uses 89 mm. Method B is commonly known as the Spencer impact test. The pendulum hits the film at a maximum velocity of 74 m/min and a maximum energy of 5 J. The impact strength is reported in units of energy (J). There is no equivalent ISO test.

ASTM makes a note in each of these test methods that the results are not necessarily equivalent, especially ASTM D1709 and ASTM D4272, which measure different aspects of the energy (initiation of failure for the former and initiation plus completion to failure energy for the latter). Also, ASTM cautions that impact measurements are not linear with film thickness. Results should be compared only for specimens that differ by no more than ± 15% in thickness.

A high-speed puncture test for plastic films is described in ASTM D7192 [28] and by McKeen [6]. The film specimen is clamped into a ring horizontally, exposing a circular area to the puncture probe. The probe consists of a 12.7 mm diameter rod with a hemispherical end of the same diameter positioned perpendicular to the circular area. A hydraulic actuator forces the probe into the specimen. Load cells and displacement sensors record the load vs displacement as the probe contacts and breaks through the specimen under what is essentially multiaxial deformation. The load vs displacement curve, such as that given in Fig. 9.10, provides information that can be used to calculate the puncture strength (load required to break the specimen divided by the cross-sectional area of the film) and the energy to puncture (related to the area under the curve). The test is often performed at several speeds, ranging from 2.5 to 250 m/min, to determine the rate sensitivity of the film to impact.

The development of a new high speed, reverse impact laboratory test by Carbajal [64] that better simulates impact events during vertical-form-fill-seal filling operations is described in Section 9.4.3.2.

9.2.5 Scratch and Abrasion Resistance

Several scratch tests have been developed for the automotive industry to measure the scratch and mar resistance of coatings. These include ISO 1518 [29] and the five-finger scratch test (Ford BN 108-13; General Motors GMN3943; Daimler-Chrysler LP-463DD-18-01 and PF-10,938; and Nissan NEW M0159 Supplement U01-1) [30]. These methods apply a constant force to a scratch pin as it is traversed across the specimen. Different weights or forces are applied. The samples are examined for evidence of scratching. The force at which the

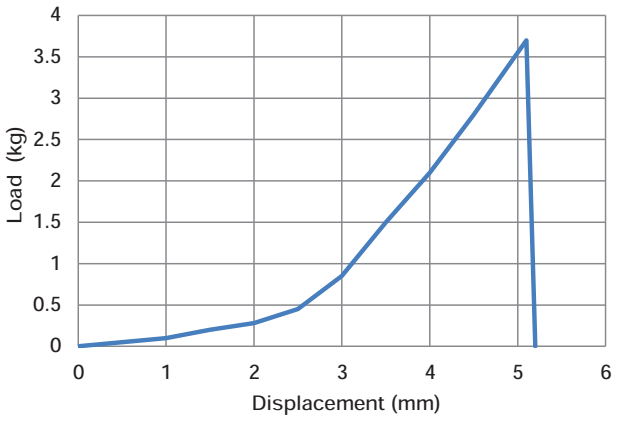


Figure 9.10 Typical output of high-speed puncture test: Load vs displacement curve.

scratch first becomes evident is recorded. These methods generally penetrate too deeply for most packaging films and typically have not been used for that purpose. Other scratch test devices include pencil hardness, scratching machine, Taber test, single-pass pendulum sclerometer, scratch apparatus, Revetest scratch tester, and needle test [31]. These also have not found widespread use in flexible packaging.

A method developed at Texas A&M university [31,32] incorporated into ASTM 7027 [33] has recently been applied to packaging films [34,35]. An instrumented scratch machine is used that consists of a stage and clamping system for holding the specimen, a load generator and a horizontal motion servo system. Load and position sensors, data acquisition, and computer-recording devices may also be used. The machine uses a stylus-type scratch indenter with a 1 mm diameter spherical tip. The specimen is usually a plaque or tensile bar at least 3 mm thick but thinner films can be tested with appropriate backing [34,35].

Two test modes are specified. In test mode A, the scratch is imparted on the specimen with a linearly increasing normal load from 2 to 50 N over a distance of 0.1 m at a speed of 0.1 m/s. This mode allows for the determination of the critical normal load for failure. The onset of failure is noted as the point where damage to the surface is first considered unacceptable. Preferably a quantitative method is used to determine the onset of failure. The depth of the scratch is one indication, but measuring the width of the scratch has been found to be more accurate. This is done by using a flatbed scanner or more accurately with a microscope. Generally a criterion for the width of the scratch that represents unacceptable damage is determined in advance for the test. The test is run and the sample examined. The location of the point where the width of the scratch reaches the failure point is noted. The normal load for failure is then determined by calculating the load at that location knowing that the load varies linearly along the length of the scratch. The scratch deformation of many polymers recovers partially over time. It is recommended to measure the scratch width/depth after the scratched specimen has aged for 24 h.

In test mode B, a constant load is applied over the same distance and speed as in mode A. This mode measures the constant load response and can be used to compute a scratch coefficient of friction.

Different loads, speeds, and stylus geometries may be used. Similar "nano" scratch tests that use stylus diameters of around 1 μm [36–39] have also been developed to evaluate the material response to scratch and mar. One of the advantages of the linear load technique is that it allows one to study the different damage mechanism that may occur during a scratch event.

Blom [39] reviews abrasion testing for flexible packaging. As of this writing no ASTM method has been published for abrasion testing of flexible packaging films, although one is under review by the standards committee. In his study, Blom uses a Taber linear abrasion tester fitted with a flexible materials kit. A weighted probe with a 1.5 mm tip is rubbed across the surface for a cycle length of 25.4 mm (1 inch) at 30 cycles per minute. The cycles to failure is recorded. Different weights can be attached to the probe depending on the nature of the sample.

A number of other abrasion tests are used in other industries but most are not easily adapted to flexible packaging. A common test is a rotary abrasion test where a roughened surface of a wheel is rubbed across the surface. One problem with this method is that many of the softer polymers used in packaging tend to quickly "gum" up the roughened surface, which skews the results.

9.2.6 Flex Fatigue

Flexing of packaging films can lead to the formation of pinholes. ASTM F392 [40] describes a method for subjecting film samples to a standard cycle of twisting motion. The test is generally referred to as the Gelbo flex test after one of the manufacturers of the test equipment. The method involves mounting the film specimen in the testing device and subjecting the specimen to a prescribed number of cycles. The specimen is removed and tested for pinholes.

9.2.7 Shipping Tests for Package Durability

Blom [39] describes a number of tests for simulating shipping and transportation of packages. These include the following:

- ASTM D4169-09, Standard Practice for Performance Testing of Shipping Containers and Systems;

- ASTM D7386-12, Standard Practice for Performance Testing of Packages for Single Parcel Delivery Systems;
- ISTA Method 3A, Packaged-Products for Parcel Delivery System Shipments 70 kg (150 lb) or Less (standard, small, flat, or elongated);
- ISTA Method 3E, Unitized Loads of Same Product;
- ISTA Method 4AB, Enhanced Simulation Performance Tests.

These methods require testing of actual packages and are typically done in the final stages of new product development. They are time-consuming, expensive, iterative, and do not yield results that are predictive (or suitable for modeling). As a result, they often lead to over engineered packages.

9.3 Typical Values

Table 4.3 provides typical values of mechanical, tear, and impact resistance properties of monolayer films. Many of these properties can be found on product datasheets provided by the material supplier or in compiled databases online, such as Campus [41], Prospector [42], Matweb [43], or Plastics Technology [44]. Examples with properties of multilayer flexible films are discussed in Section 9.4.

9.4 Engineering Principles for Multilayer Films

A starting point for the prediction of the physical properties of multilayer films is the rule of mixtures. This rule simply states that the property of the multilayer film is sum of properties of its individual layers, normalized for the relative thickness of each. For a two-layer film the relationship is:

$$S = \varphi_1 S_1 + \varphi_2 S_2 \tag{9.7}$$

where S = property of the multilayer film, S_1 = property of layer 1, S_2 = property of layer 2, φ_1 = volume fraction of layer 1 (thickness of layer 1/total film thickness), φ_2 = volume fraction of layer 2.

Generalizing for more than two layers:

$$S = \sum_{i=1}^{n} \varphi_i S_i. \tag{9.8}$$

The rule of mixtures assumes that the properties of the composite are a linear combination of each of its components and that there are no interactions between the layers. In many packaging situations the rule of mixtures is sufficient. There are a number of deviations, however. Some of the reasons for these deviations include the following:

- Certain properties, such as bending stiffness and abrasion resistance, are nonlinear with respect to thickness. Bending stiffness is taken up in detail in Section 9.4.2 and abrasion resistance in Section 9.4.3.4.
- Adhesion or changes in crystallization behavior at the interface between layers may provide reinforcing effects.
- A neighboring ductile layer may block the propagation of cracks initiated in a brittle layer.
- The load may be transferred to a stronger layer.
- Neighboring layers may confine the local deformation in a ductile layer, increasing the tendency of a crack to propagate. This explains why many multilayer films containing PE have lower tear strength than PE alone.
- The stress history imparted during film fabrication may differ between monolayer films and coextruded films, resulting in differences in properties. This topic is taken up in more detail in Chapter 14.

There is no comprehensive theory to know when there will be a deviation from the rule of mixtures. Indeed, identical structures with layers made from different grades of the same generic resin may display different behavior. Table 9.1 provides an overview of the literature that is reviewed in the following sections. Many of the properties are found to follow the rule of mixtures in these studies (labeled L in the table), although many more deviate (labeled N). There is some bias in this list, however, since the goal of the ensuing sections is to highlight some of the factors that cause such deviation.

9.4.1 Mechanical Properties

A number of investigators have studied the properties of multilayer polyethylene (PE) films [45–52], comparing them with monolayer films of the component resins, as well as blends with the same volume ratio. Several studies evaluate (A-B-A)

Table 9.1 Summary of Structure and Property Studies From the Literature

Study	Structures	Yield Strength	Tensile Strength	Elongation at Break	Elastic Modulus	Bending Stiffness	Puncture	Impact (Spencer or Dart)	Scratch	Elmendorf Tear	Flex Failure	Abrasion
Siegmann, 1987	(LLDPE-LDPE-LLDPE)	L	L	L				N		N		
Martinez, 1990	(LLDPE-LDPE-LLDPE)	L	N	L	L		N	L		N		
Beagan, 1999	(LDPE-mPE$_A$-LDPE)		N		L							
Elkoun, 2003	(LDPE-mPE$_B$-LDPE)		L		N							
	(bLLDPE-mLLDPE-bLLDP-mLLDPE)							N		N		
	(oLLDPE-mLLDPE-oLLDP-mLLDPE)							L		L		
Butler, 2013	(LLDPE-LDPE-LLDPE)							L				
	(LLDPE-HDPE-LLDPE)							N				
Borse, 2014	(mLLDPE-LLDPE-mLLDPE)									N		
	(LLDPE-mLLDPE-LLDPE)									L		
Guillotte, 1969	(Ionomer-LDPE)		L					N		N	N	
	(PA66-ionomer)		L					N		N	N	
Gaucher-Miri, 2002	(EVA-EVOH-EVA)	L										
Timm, 2005	OPET (48 g)/adh/PE sealant OPET (48 g)/adh/Al (38 g)//PE sealant		N	N	L			N		N		
Wu, 1994	BOPP/OPET									L		
	BOPP/cPP									L		
	BOPP/LLDPE									N		
Huang, 2004	(PA6-tie-PE)	L			L							
Schrenk, 1969	OPET/adh/Al/adh/OPET	N	N	N								
	(LDPE-PS-LDPE)		N	N	L							
	(PP-PS-PP)		L	N	L							
Blom, 2014	OPET/EVA											N
	OPA or cPA/EVA											N
Hu, 1973	OPET/Al/PE OPET/Al/PVC							N			N	N

(*Continued*)

Table 9.1 Summary of Structure and Property Studies From the Literature (*Continued*)

Study	Structures OPET/Al/PP OPET/Al/PA	Yield Strength	Tensile Strength	Elongation at Break	Elastic Modulus	Bending Stiffness	Puncture	Impact (Spencer or Dart)	Scratch	Elmendorf Tear	Flex Failure	Abrasion
Lange, 2002	Paper/Al/PE or PET/Paper/Al/PE						N					
	PET/Al/PE or OPP/Al/Ion						N					
Carbajal, 2015	(HDPE-tie-PA-tie-sealant)							N				
Hare, 2012	OPET-met/adh/PE								N			
	OPET-met/adh/(PA-tie-PE)								N			
Hare, 2014	OPET-met/adh/(PE sealant) OPET-met/extr/(PE-sealant)								N			
Morris, 1997	OPP/sealant OPET/EVA/sealant					N						
Lange, 2002	OPET-met/adh/PE					N						
McKenna, 2010	PE/PE/PE					N						
Morris, 2011	(LLDPE-tie-PA-tie-LLDPE)					N						
Morris, 2013	(HDPE-tie-PA-tie-sealant)					N						

Properties labeled L follow the law of mixtures (linear behavior), whereas properties labeled N do not (nonlinear behavior).
adh, adhesive*; Al,* aluminum foil*; bLLDPE,* butene LLDPE*; BOPP,* biaxially oriented polypropylene*; cPP,* cast polypropylene*; EVA,* ethylene vinyl acetate copolymer*; EVOH,* ethylene vinyl alcohol*; HDPE,* high density polyethylene*; Ion,* ionomer*; LDPE,* low density polyethylene*; LLDPE,* linear low density polyethylene*; mLLDPE,* metallocene LLDPE*; mPE,* metallocene polyethylene plastomer*; oLLDPE,* octene LLDPE*; OPET,* oriented polyethylene terephthalate*; PA,* polyamide or nylon*; PP,* polypropylene*; PS,* polystyrene*; PVC,* polyvinyl chloride*; tie,* tie resin.

or (A-B-A-B) coextruded blown film structures with the volume percent of B varying over the range of 0–100%. Different compositions of A and B are studied, such as low density polyethylene (LDPE) and linear low density polyethylene (LLDPE) [51], LDPE and metallocene polyethylene plastomer (mPE) [48,49], and Ziegler–Natta LLDPE and metallocene linear low density polyethylene (mLLDPE) [50]. Some of the mechanical properties of the coextruded structures follow the rule of mixtures and others show significant deviation as summarized in Table 9.1. An example is shown in Figs. 9.11 and 9.12 taken from the work of Beagan [48]. Here two different mPE grades are coextruded with LDPE skin layers. The tensile strength of the coextruded film structures with mPE resin A shows substantial positive deviation from the rule of mixtures, whereas those with mPE B show a slight negative deviation. The opposite is true for secant modulus (Fig. 9.12) where resin A shows a slight deviation from the rule of mixtures and resin B

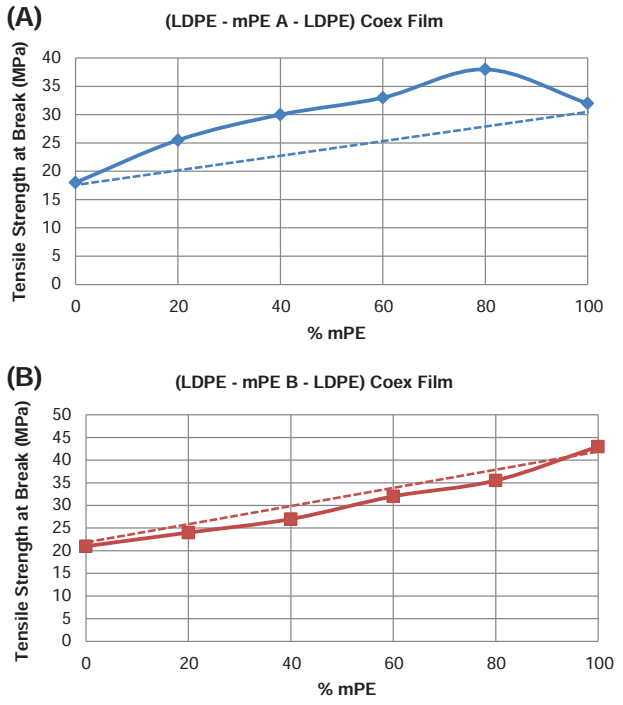


Figure 9.11 Tensile strength at break of coextruded films with different amounts of a core mPE layer. Top graph is for mPE A and bottom graph for mPE B. *Dashed curves* represent the values predicted by the rule of mixtures.

Adapted from Beagan CM, McNally GM, Murphy WR. The blending and coextrusion of metallocene catalyzed polyethylene in blown film applications. In: SPE ANTEC conference; 1999.

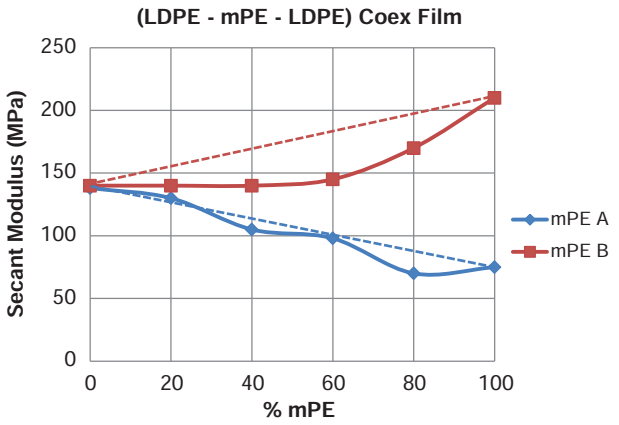


Figure 9.12 2% Secant modulus of coextruded films with different amounts of a core mPE layer. *Dashed curves* represent the values predicted by the rule of mixtures.

Adapted from Beagan CM, McNally GM, Murphy WR. The blending and coextrusion of metallocene catalyzed polyethylene in blown film applications. In: SPE ANTEC conference; 1999.

shows a substantial negative deviation. The crystallinity of the two mPE grades differ, as is indicated by the lower modulus of resin A. The two grades are not produced by the same manufacturer and so may have other differences as well.

Several investigators have suggested that co-crystallization at the interface of some polyethylenes is responsible for the deviations from the simple rule of mixtures. Differences in crystalline morphology have been reported. For example, Elkoun [50] finds that coextruded films with layers of Ziegler–Natta butene LLDPE (B) and a single-site LLDPE (S) deviate more from the rule of mixtures than one containing Z-N octene-LLDPE (O) and S. They attribute the improved performance of the B-S coextrusion to the formation of transcrystalline regions at the interface between the dissimilar B and S (and less formation for the similar O and S).

Zhang and Ajji [53,54] study polypropylene-LLDPE blends and coextrusions. A homopolymer (hPP) and random copolymer (rPP) polypropylene are tested. The PE is an octene-LLDPE made by a Ziegler–Natta catalyst. A five-layer coextrusion blown film with the structure (PP-LLDPE-PP-LLDPE-PP) is compared with a blend of the same volume ratio of PP to PE (50:50). The film is made under conditions to impart high draw in the MD (high draw down ratio (DDR) and low frost line height). The coextruded film generally has a higher

% elongation to break than the blend. Wide angle X-ray scattering (WAXS) measurements and scanning electron microscopy (SEM) show differences in the crystalline morphology and orientation. Two types of oriented lamellae crystalline structure may form at the PE-PP interface: an epitaxial structure where the PE crystallizes on the PP and a transcrystalline structure where the PP, with its higher crystallization temperature (T_c), induces an oriented crystalline structure on the polymer with the lower T_c (PE in this case). The homopolymer PP-LLDPE blend exhibits epitaxial structure whereas the random copolymer PP-LLDPE blend and coextrusion show transcrystalline behavior. The difference in crystalline morphology may influence adhesion at the interface.

Gaucher-Miri [55] evaluate coextruded films of ethylene vinyl acetate-ethylene vinyl alcohol-ethylene vinyl acetate (EVA-EVOH-EVA). The films are 500-μm thick with the EVOH core ranging from 1% to 20% of the structure. The skin layers are a blend of EVA (9% VA) and very low density polyethylene (VLDPE) (10% of the blend). There is no mention of a tie layer. They conduct dynamic mechanical analysis and tensile tests (mostly at 100 in/min [2500 mm/min] or 10,000%/min) at 55−95°C.

Monolayer control films are first evaluated. The EVA deforms homogeneously in the tensile tests and exhibits strain-hardening behavior. The EVOH control film exhibits neck-in at the yield point. The elongation at break increases with temperature, the opposite of what occurs with EVA, but breaks just after yielding at 55°C. The strain-hardening parameter for EVOH is independent of temperature but decreases at high strain rates and increases with increasing relative humidity. Gaucher-Miri manipulate the data to compare EVOH and EVA at the same true strain rate (to account for the necking of the EVOH). They find that EVOH has higher yield stress and a lower strain-hardening parameter than EVA. By measuring the stress vs strain curve at strain rates ranging from 0.254 to 254 mm/min they show that the EVOH transitions from homogeneous to heterogeneous (necking) deformation when the strain-hardening parameter changes from being less than one to greater than one. This occurs between 2.54 and 25.4 mm/min.

The (EVA-EVOH-EVA) coextruded film deforms homogeneously (no necking) over the temperature range tested; the EVA layers control the deformation. Yield stress increases and strain-hardening parameter decreases with increasing fraction of EVOH in the structure. The rule of mixtures works well and can be used to predict under what conditions the coextruded film will neck: when the strain-hardening parameter drops below one, neck-in occurs.

Huang [56] make (PA6-tie-PE) coextruded films with different layer ratios. They provide a good discussion of engineering vs true stress and strain and fitting or modeling the data with a two-parameter model (yield stress and strain hardening parameter). Yield stress, strain-hardening parameter, and tensile modulus are found to follow the rule of mixtures.

Schrenk and Alfrey [57] describe mutual mechanical reinforcement of multilayer films. When thin layers of high modulus low elongation material is sandwiched between thin, adhering layers of low modulus, high elongation material, the stress at break for the laminate is much higher than for either material alone. The high modulus material undergoes higher elongation in the laminate than as a monolayer film. The low modulus material acts to stop cracks from propagating laterally. These materials exhibit high elongation and high modulus and have much higher energy to break than the single materials.

In one study, they make OPET/adh/Al/adh/OPET laminates and vary the adhesive strength. Good adhesion produces the reinforcement effect, allowing the foil to reach the plastic yield region by inhibiting cracks that form transverse to the direction of pull. Poor adhesion results in a breakup of the foil layer into shorter segments during the tensile test.

They describe experiments with LDPE-PS-LDPE films with 3 or 125 layers. Adhesion is poor between LDPE and polystyrene (PS), but as the thickness of the layers get smaller separating the layers becomes more difficult. Despite the poor adhesion, the three layer films show mutual reinforcement when the tensile test is done in the MD. Here the PS layer is the high modulus, low elongation layer. In the transverse direction, the three layer films show mutual destruction with failure of all the layers at low elongation.

The 125-layer films of LDPE and PS are biaxially stretched on a lab stretcher to 25-μm (1-mil) thickness. The ultimate tensile strength obeys the rule of mixtures in both directions with no mutual reinforcement. Elongation at break is low for all the compositions. The thin PE layers are too weak to stop cracks from propagating.

Films with 125-layers of PP and PS are also made and biaxially stretched to 1-mil. Tensile strength increases linearly with increasing PP content. The

elongation is 100% or more—much higher than for the PE-PS films—indicating mutual reinforcement is occurring.

They conclude the following:

- Mutual reinforcement depends on the adhesion between the layers—better adhesion makes reinforcement more likely.
- Mutual reinforcement depends on the orientation of the brittle layer.
- The high elongation layer must be strong enough to stop the propagation of cracks in the brittle layer in order for mutual reinforcement to occur.
- Tensile strength in some structures can be predicted from the volume fractions of the components using the rule of mixtures.

When no mutual reinforcement exists, Hu [58] explains how the tensile strength may be less than the sum of its components. Consider the two-layer structure as shown in Fig. 9.13. As the laminate is stretched axially, a stress develops in each layer that is the product of its modulus and the strain. In equilibrium, the stress on the laminate, σ_L, is simply the sum of the stress on each layer:

$$\sigma_L = \sigma_1 + \sigma_2. \tag{9.9}$$

When stretched, the layer with the higher modulus carries more of the load until it reaches its ultimate tensile strain and breaks. When the first layer breaks, this puts more stress on the second layer, which then breaks when it reaches its ultimate tensile strength. Because of the combination of modulus and tensile strengths, the tensile strength of the laminate is never greater than the sum of its components.

Timm [59] studies the tensile properties of two laminate structures: OPET (13-μm)/adh/PE sealant and OPET (13-μm)/adh/Al (10-μm)//PE sealant. Six different sealant films are tested with varying stiffness and thickness (25−125 μm). He asks the question, are the properties the sum of its parts? The answer depends on the test method failure mode and dynamics. He provides a conceptual model as to why this is so:

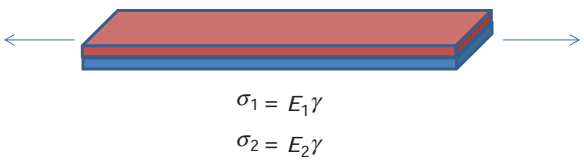


Figure 9.13 Multilayer film being stretched.

- *Single ply polymers*: crystals bear most of the load in a tensile test, especially in the MD. Weaker amorphous regions are shielded from the load until cracks develop. The TD is less predictable—both amorphous and crystalline regions bear the load.
- *Laminate*: adhesion is critical. The stiffer/stronger layer bears more of the load initially in both MD and TD. The TD properties are more consistent.

The results show that the tensile strength of the OPET film dominates until the sealant film thickness reaches about 100 μm (4 mils) where the sealant film starts to become as important as the OPET film. The elongation to break is dominated by the OPET film. The secant modulus, however, follows the rule of mixtures. Results of impact and tear tests from this study are discussed in Sections 9.4.3 and 9.4.4.

These examples show that the mechanical properties of multilayer films often follow the rule of mixtures and can be estimated by the linear sum of the properties of the component layers. There are many exceptions, however, that arise when mutual reinforcement or destruction occurs at the interface. Changes in crystallization, adhesion, and the ability of the adjacent layers to stop the propagation of cracks are some of the mechanisms for these deviations.

9.4.2 Bending Stiffness

The bending stiffness of multilayer films is not a simple linear combination of the stiffness or modulus of the component layers. Instead, it is a complex function of the elastic modulus, location, and thickness of each of the layers. A brief analysis is presented here, based on Morris and Vansant [14], followed by several examples of how it applies to flexible packaging.

To describe the bending stiffness of a thin film, it is assumed that the film or sheet can be modeled as a beam, such as an I-beam. As a beam is bent, one side of the beam is in compression and the other is in tension as shown in Fig. 9.14. The tensile or compressive stress is at a maximum at the outer surfaces and zero at a point within the beam. This

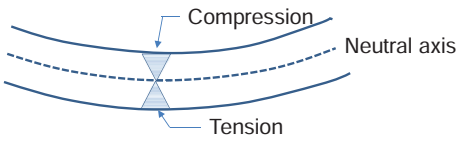


Figure 9.14 Beam under bending motion, rectangular cross section of single material.

zero stress point is called the neutral axis. A beam (film, sheet, and so on) is stiffer than another if it bends less under a given amount of stress.

For calculation purposes, the modulus in compression is assumed to be represented by the elastic modulus and equal to the modulus in tension. Compression moduli are difficult to measure and making this assumption makes the computation easier. The assumption is validated by the good agreement between the experimental work of Morris and Vansant and the model results.

The deflection, D, of a beam under an applied force, F (Fig. 9.15) is described by Eq. (9.10):

$$D = \frac{F}{\sum_{i=1}^{n} E_i I_i}\left[\frac{L^3}{24}\right] \tag{9.10}$$

where E_i = modulus of layer i, I_i = contribution to the total moment of inertia from layer i, n = number of layers, and L = length of the beam.

Here the term in brackets is independent of the beam design (or film structure), but rather is a function of the way it is held and how the force is applied. Rearranging Eq. (9.10) and renaming the term in brackets H and its inverse H' yields

$$\frac{F}{D} = \left(\sum_{i=1}^{n} E_i I_i\right) H'. \tag{9.11}$$

Eqn. (9.11) is in the same form as that for a spring, where EIH' is the spring constant describing the relationship between applied force and deflection. $\Sigma E_i I_i$ represents a "stiffness factor" describing the composite stiffness of the beam, film, sheet, and so on. H' describes how the force is applied. $\Sigma E_i I_i$ is calculated by first locating the neutral axis. The moment of inertia term for a given layer, I_i, is related to the cube of distance of that layer from the neutral axis. For a more detailed analysis, see Jones [60].

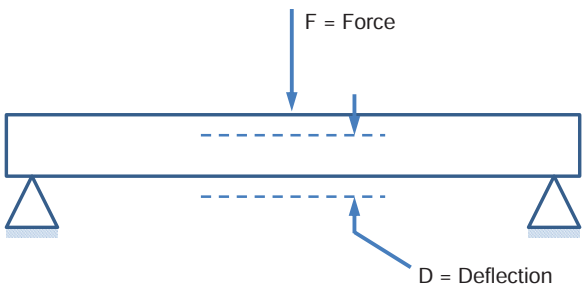


Figure 9.15 Force and deflection of a beam.

Morris and Vansant develop a computer model based on Eqn. (9.11). The model input includes the elastic modulus, thickness, and location of each layer. They validate the model by comparing the calculated stiffness factor to experimental measurements of bending stiffness using the DuPont three-point bending method described in Section 9.2.2. Two types of structures are tested, a three-layer coextrusion of (HDPE-tie-sealant) and a proprietary laminate. The results comparing the test results with the model are plotted in Fig. 9.16. The statistically determined trend line through the results has a R^2 value of the curve is 0.96, indicating an excellent fit. Lange [7] develops a similar model and also reports good agreement between model and experimental results.

There is an offset in the prediction (the slope of Fig. 9.16 is not equal to 1) due to the effect of the geometry of the test (H' in Eq. (9.11)). The model, therefore, is most useful for computing changes in bending stiffness vs a control. The model is very helpful for understanding how material selection and

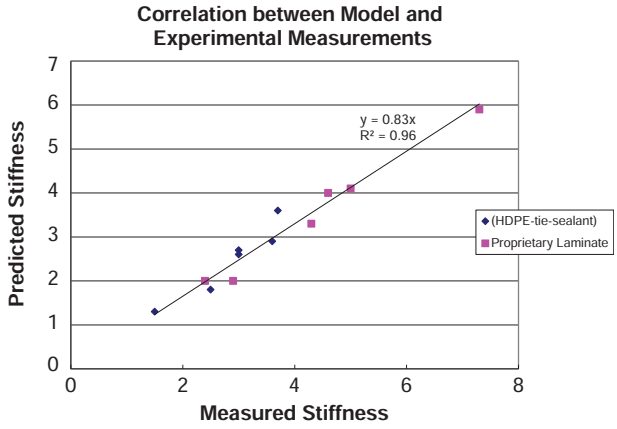


Figure 9.16 Comparison of model prediction and experimental results.
Adapted from Morris BA, Vansant JD. The influence of sealant modulus on the bending stiffness of multilayer films. In: TAPPI polymers, laminations and coatings conference; 1997.

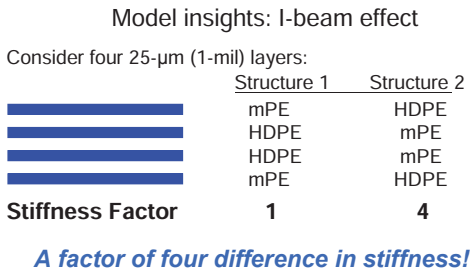


Figure 9.17 Example of the effect of layer arrangement on bending stiffness of a multilayer film. Assumptions: HDPE modulus = 690 MPa, mPE modulus = 69 MPa.
From Morris BA, Vansant JD. The influence of sealant modulus on the bending stiffness of multilayer films. In: TAPPI polymers, laminations and coatings conference; 1997. With permission from E. I. du Pont de Nemours and Company.

structure design influence stiffness. An example is shown in Fig. 9.17. Here four 25-μm thick layers are combined to make a film. Two of the layers are made from a relatively stiff HDPE resin and two are made from a flexible polymer such as EVA or mPE plastomer. If the layers are arranged so that two stiff layers make up the core, the stiffness factor is 1. Simply rearranging the layers so that the stiff layers make up the skin increases the bending stiffness by a factor of 4! This is what Morris and Vansant call the I-beam effect. Separating stiff layers can be very effective for building in bending stiffness into a structure. Note that in a tensile test, these two structures would have the same elastic modulus. It is only in bending that the layer location makes such a difference.

In engineering terms, the further apart from the neutral axis and stiffer the skin layer, the stiffer is the structure. Many food packaging applications involve the combination of a stiff protective or barrier layer (such as nylon, OPET, OPP, foil, or EVOH) and a sealant. In such structures, frequently the neutral axis resides in the stiff barrier or protective layer. Thus the material of highest modulus has the smallest contribution to the bending stiffness of the structure. The sealant layer is always on the outside of the structure, often away from the location of the neutral axis. As a result, the modulus and location of the sealant layer can have a disproportionate effect on the overall bending stiffness. Understanding this effect can aid in anticipating potential problems with substituting relatively stiff sealant materials with ones with lower modulus. It also points to opportunities for down-gauging and cost reduction without loss of stiffness by using relatively stiff sealants such as ionomers (see Figure 4.9 for a comparison of the stiffness of various sealant resins).

The I-beam effect often comes in play when dealing with lamination of films. An example is given in Table 9.2 where laminations made by adhesive and extrusion lamination are compared. The structure involves bonding OPP to a sealant film. The base case (A) is for when the generic sealant film, such as a 25-μm (1-mil) LLDPE or ionomer film, is adhesively laminated to the OPP. Extrusion laminating the two films, case B, substantially increases the bending stiffness, even though the LDPE adhesive has a lower modulus than the chemical adhesive. This is because the extruded adhesive is thicker and separates the two films further, enhancing the "I-beam" effect. This is confirmed in case C where the LDPE adhesive thickness is increased to 25-μm (1-mil). The OPP must be increased from 18 to 38-μm (70−150 gauge) in the adhesive lamination (case D) to achieve the

Table 9.2 Comparison of Adhesive and Extrusion Laminated Films

Case	OPP Thickness Microns (gauge)	Adhesive Type	Adhesive Modulus MPa (kpsi)	Adhesive Thickness μm (mil)	Predicted Stiffness Factor
A	18 (70)	Adhesive	690 (100)	2.5 (0.1)	0.39
B	18 (70)	LDPE	138 (20)	12.7 (0.5)	0.70
C	18 (70)	LDPE	138 (20)	25.4 (1)	1.25
D	38 (150)	Adhesive	690 (100)	2.5 (0.1)	1.38

Structure is OPP/adh/sealant film. Assumptions: OPP modulus is 1590 MPa (230 kspi), sealant modulus is 275 MPa (40 kspi), and sealant thickness is 25 μm (1 mil).
Adapted from Morris BA, Vansant JD. The influence of sealant modulus on the bending stiffness of multilayer films. In: TAPPI polymers, laminations and coatings conference; 1997.

same increase in stiffness as extrusion laminating with 25-μm (1-mil) of LDPE. Lange [7] obtains similar results with a PET/adh/PE-film lamination and concludes that the thickness of the adhesive layer overwhelms the effect of its modulus. The designer can use the model results to weigh the relative material and fabrication costs of the two processes to achieve the desired increase in stiffness.

The model can also be used to look at the effect of material substitution and downgauging on stiffness. Table 9.3 shows an example of a capping web for a meat package that has the structure OPET/EVA/ionomer with thicknesses 11.9/22.9/33 μm (0.47/0.9/1.3 mils). Such combinations of a high modulus film with a sealant are prevalent in the snack industry as well. Using typical values for the moduli of these materials, Morris and Vansant compute a stiffness factor (case 1 in Table 9.3). Case 2 shows the effect of substituting a lower modulus mPE sealant for the ionomer. The bending stiffness is reduced by 67%. Case 3 shows that the thickness of the mPE layer would have to be increased to 63.5-μm (2.5 mils) to achieve the same stiffness as case 1. This not only increases the cost but also may slow the transfer of heat to the interface during heat sealing, slowing packaging line speeds. Case 4 looks at substituting the ionomer with a higher modulus one. The sealant can be downgauged by 7.6-μm (0.3 mils) and still achieve the same stiffness as the base case. In case 5, the sealant is further downgauged by bulking up the EVA layer. This effectively moves the stiff sealant layer away from the neutral axis, resulting in a structure with potentially lower cost. As with any of these cases, the model only predicts what will happen to bending stiffness. Reducing sealant layer thickness may diminish the sealing properties and must be thoroughly tested under conditions simulating its actual use.

McKenna [2] varies the PE type and thickness of three layer polyethylene films. Using a model as a guide, they design structures with lower thickness and a range of bending stiffness. A consumer panel perceives the stiffest films to be the thickest, independent of their actual thickness. The tests show that consumers can distinguish between films differing in bending stiffness of about 10−15%. By judicious material selection and layer arrangement, film structures can be significantly downgauged while maintaining performance and consumer perception by matching the bending stiffness of the incumbent film.

These concepts are used by Morris, Vansant, and Hausmann [15] to redesign a package for meat products such as smoked ham. Fig. 9.18 shows the typical structure of a conventional forming web. The sealant layer placed to the inside of the film is 56 μm thick, while a layer of only 24 μm of the significantly stiffer ionomer (Surlyn from DuPont, shown on the right) provides the same mechanical properties. As part of this optimization, they propose additional changes to the structure in order to reduce thickness and costs. This includes shifting the second stiff component, a polyamide 6 (PA6) barrier layer, to the outside of the structure so that the I-beam effect can be used to further raise the flexural stiffness. Additionally the concept provides improvements to the thermoformability through blending amorphous polyamide (Selar PA from DuPont) into the PA6 layer. Because this material increases the oxygen barrier, this step also allows the PA thickness to be

Table 9.3 Model Results, OPET//(EVA-Sealant)

Case	Sealant	Sealant Modulus MPa (kpsi)	Sealant Thickness μm (mils)	EVA Thickness μm (mils)	Total Thickness μm (mils)	Predicted Stiffness Factor	Stiffness Change
1	IONOMER1	276 (40)	33 (1.3)	22.9 (0.9)	67.8 (2.67)	1.49	
2	mPE	69 (10)	33 (1.3)	22.9 (0.9)	67.8 (2.67)	0.49	−67%
3	mPE	69 (10)	63.5 (2.5)	22.9 (0.9)	98.3 (3.87)	1.48	−1%
4	IONOMER2	483 (70)	25.4 (1)	22.9 (0.9)	60.2 (2.37)	1.49	0%
5	IONOMER2	483 (70)	10.2 (0.4)	45.7 (1.8)	67.8 (2.37)	1.48	−1%

Assumptions: OPET modulus is 3450 MPa (500 kpsi), OPET thickness is 11.9 μm (0.47 mil), and EVA modulus is 69 MPa (10 kpsi).
Adapted from Morris BA, Vansant JD. The influence of sealant modulus on the bending stiffness of multilayer films. In: TAPPI polymers, laminations and coatings conference; 1997.

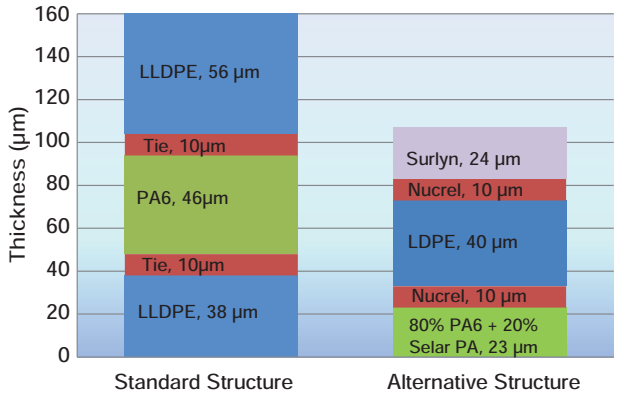


Figure 9.18 Redesign of thermoforming web for meat package using principles from bending stiffness model.

Reproduced with permission from Morris BA, Vansant JD, Hausmann K. More structural strength for thin films. Kunstoffe International; May 2011. p. 42–46.

reduced. At the same time, the amorphous PA adds to the stiffness of the PA layer. Finally the new concept calls for an inner layer of low cost LDPE, which has the effect that both of the stiff layers (Surlyn and PA) lie further from the neutral axis. This additionally optimizes the I-beam effect and overall helps to achieve the minimum thickness for the thermoforming sheet. Nucrel acid copolymer resin from DuPont has proven to be an ideal tie layer for such structures.

In total the new film concept is more than 30% thinner than the original structure at slightly lower cost. The material costs are reported as being reduced by 4%, and if the structure is used in Europe, further savings can be obtained from a reduction in packaging levies. The switch to the ionomer sealant has additional advantages: an expected 25% higher film puncture resistance, greater packaging integrity, because the high hot tack provided by the ionomer sealant can reduce the danger of leakers, and the possibility of raising productivity due to the low temperature at which sealing begins.

9.4.3 Puncture, Scratch, and Abrasion Resistance

The abuse resistance of multilayer films, whether measured by puncture, scratch, or abrasion tests, often deviates from the rule of mixtures. Some of the deviation is due to nonlinear thickness effects. For example, if the abuse resistance increases with the square of the thickness, combining two layers of the same material and thickness will quadruple the abuse resistance whereas the rule of mixtures predicts a mere doubling. As will be illustrated in the examples below, other factors also play a role, such as the orientation of the film toward the indenter. Here the presence of a soft sealant layer or a hard structural layer on the surface can affect the deformation of the film as it is contacted by the probe, changing the forces and puncture or scratch resistance. Other factors include interlayer adhesion, load transfer, changes in crystalline morphology, and blunting of crack propagation by adjacent ductile layers.

9.4.3.1 Puncture Resistance of Polyethylene Films

A number of studies have examined the impact resistance of multilayer polyethylene films. Butler and Morris [61] provide an example of two three-layer coextruded films with an LLDPE skin layer and either LDPE or HDPE as the core. As shown in Fig. 9.19, dart impact strength of the (LLDPE-LDPE-LLDPE) follows the rule of mixtures but the (LLDPE-HDPE-LLDPE) film shows a negative deviation. LLDPE is a highly elastic resin that absorbs high levels of the impact energy. LDPE, while not as elastic, does not detract from the impact strength. HDPE is more brittle than LLDPE and tends to form

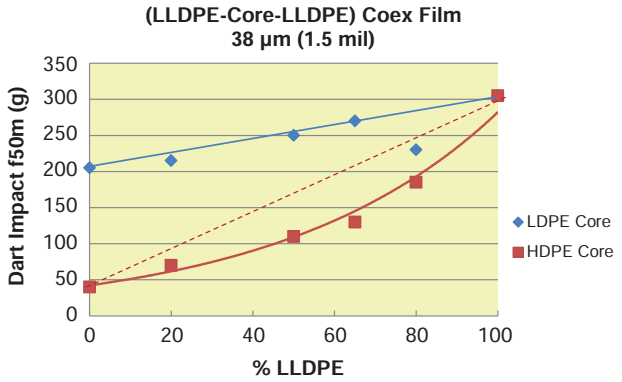


Figure 9.19 Dart impact of coextruded three-layer film. Core layer is either LDPE (0.918 g/cc, 2.0 g/10 min MI) or HDPE (0.965 g/cc, 0.7 MI). Outside layers are LLDPE (0.920 g/cc, 1 MI). *Dashed curve* is what would be predicted from the rule of mixtures for the HDPE-core structure.

From Butler TI, Morris BA. PE-based multilayer film structures. In: Ebnesajjad S, editor. Plastic films in food packaging, materials, technology and applications. New York: Elsevier; 2013. p. 21–52.

localized stress concentration sites that result in lower impact strength for the structure.

Siegman and Nir [45] compare blown films of 100% LDPE, 100% LLDPE (octene, Ziegler–Natta), a 50/50 blend, and a coextrusion of (25% LLDPE—50% LDPE—25% LLDPE). The LLDPE monolayer control film has superior tensile strength, yield strength, % elongation at break, dart drop impact, and Elmendorf tear compared with the LDPE monolayer film. For the high speed tests (dart drop, and Elmendorf tear), the coextruded film outperforms the blend and approaches the values of LLDPE, suggesting a positive deviation from the rule of mixtures. Martinez [51] also compares LLDPE-LDPE blends with (LLDPE-LDPE-LLDPE) coextrusions over a composition range of 0–100% LLDPE. Dart impact follows the rule of mixtures fairly well but puncture resistance of the coextruded films shows a positive deviation from the rule of mixtures at LLDPE concentrations above 50%, and has considerably higher resistance than the blend. As described in Section 9.4.1, Siegman and Nir ascribe the deviations from the rule of mixture and differences between coextruded structures and blends to crystalline morphology changes. They show microscopy evidence of the formation of a row-nucleated crystalline structure in the coextruded films at the LLDPE-LDPE interface, which they attribute to layer orientation during the film blowing process. Taylor [52] observes similar property advantages of coextrusion vs blends of LLDPE and LDPE.

Elkoun [50] evaluated blends and coextruded films of three different types of LLDPE: a butene Ziegler–Natta LLDPE (B), an octene Zielger–Natta LLDPE (O), and an octene single site catalyst LLDPE (S). Films with the construction (A-B-A-B-A) are made on a five-layer coextrusion blown film line. S is blended or coextruded with B or O. The dart impact strength of the (B-S-B-S-B) coextrusion shows some negative deviation from the rule of mixtures, whereas the (O-S-O-S-O) coextrusion follows the rule of mixtures fairly well. The deviation from the rule of mixtures for tear strength is more pronounced and is described further in Section 9.4.4.1. The B-S coextrusion has significantly better dart impact strength than the blend of the same composition, whereas both the O-S coextrusion and blend follow the rule of mixtures. They attribute this to the formation of transcrystalline regions at the interface between the dissimilar B and S (and less formation for the similar O and S resins).

9.4.3.2 Puncture Resistance of Laminates

Combining polyolefin films with stiffer layers such as PA or PET can be less straightforward. Hausmann [22] evaluates three-layer blown films of (PA6-tie-sealant) with layer thicknesses (50/20/40 μm). The tie layer is an acid copolymer. Three sealants are tested, an LLDPE, a mPE plastomer, and an ionomer. The ionomer is Surlyn 8140, an especially stiff grade of ionomer with a modulus of around 480 MPa (70 kpsi). The films are tested according to DIN 53373 (similar to ASTM D1306 described in Section 9.2.4.1), using a 2-mm diameter probe with a 90 degree angle and a test speed of 100 mm/min. Surprisingly, the sealant selection made a significant contribution to the penetration resistance as is shown in Fig. 9.20. The nylon layer, known for its toughness, was expected to dominate. The mPE plastomer performs better than the LLDPE, but the stiff grade of ionomer performs the best. Similar results are found when the DuPont static puncture test is used as is shown in Fig. 9.21. Here the time for failure for the coextruded film containing Surlyn as the sealant is five times that of the film with mPE as the sealant.

The toughness of Surlyn is attributed to its stiffness and strain-hardening behavior. In relative terms, the stiffness of Surlyn 8140 is 10–15 times that of the mPE plastomer. The soft plastomer does not strain harden (see Chapter 5). It exhibits a high amount of creep elongation and fails quickly in a slow puncture test, which is essentially a measure of creep resistance. The stiff ionomer has a high degree of strain

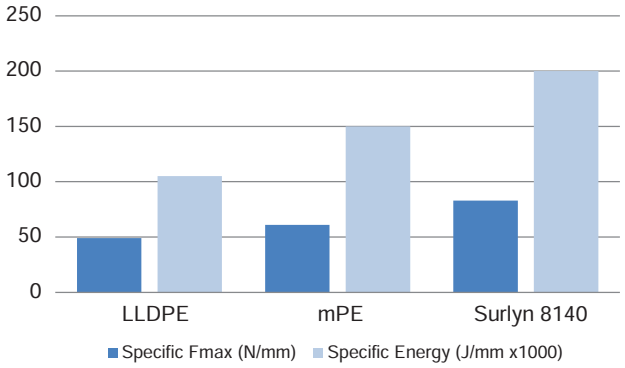


Figure 9.20 Penetration resistance of (PA6-tie-sealant) multilayer film. 2-mm probe diameter with 90 degree tip angle, 100 mm/min.
Reproduced with permission from E. I. du Pont de Nemours and Company.

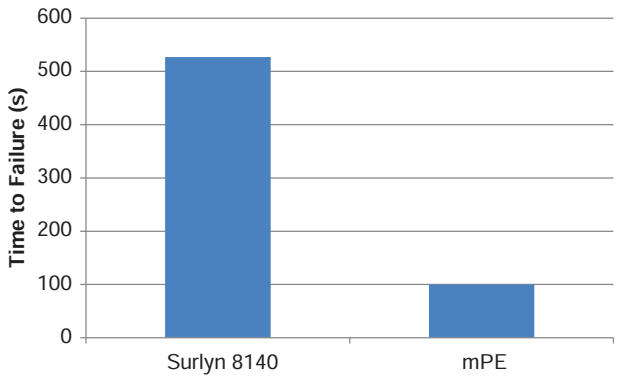


Figure 9.21 DuPont static puncture test of (PA6-tie-sealant) multilayer film. Weight of probe is 230 g. Tested from sealant side.
Reproduced with permission from E. I. du Pont de Nemours and Company.

hardening due to its long chain branching and ionic interactions. This results in a low level of elongation and higher puncture energy.

Many in the industry believe that lower interlayer adhesion increases the puncture resistance of multilayer films by dissipating some of the energy through delamination. Darby [62] finds this is not true for slow puncture tests. They adhesively laminate films and measure puncture resistance as a function of curing time. Two structures are studied: 25 μm foil/adh/12-μm OPET and 12-μm OPET/50-μm LDPE film. ASTM F1306-90, a slow speed test described in Section 9.2.4.1, is used to measure puncture resistance. They use two probes, one specified in the standard (needle with a 3-mm diameter tip) and the other hemispherical [21].

Peel tests and puncture tests are conducted on samples as a function of adhesive cure time. In an initial experiment, they apply the adhesive by hand with a Mayer rod and due to equipment limitations test adhesion and puncture resistance on separate specimens exposed to the same cure time. A second experiment uses a pilot scale laminator. Testing for puncture and peel strength is done at the same time intervals on the same specimens. Both experiments give similar results. Control films and films with zero adhesion (using shampoo as the adhesive) are also tested.

The results show that with good bonding, the laminate behaves like a single material. Puncture resistance is similar to the PET alone. With poor bond strength, there are two peaks on the force vs displacement curve, one associated with separation of the layers followed by puncture of the foil and the second to the puncture of the PET. The foil punctures at lower load than the PET. The laminate fails at higher deformation but with about the same puncture force as the PET. The peel strength is found to increase with curing time, as expected. The puncture force, however, only slightly increases with cure time and the change is small enough that it may not be statistically significant. They conclude that at least in their tests, bond strength is not a factor for puncture resistance. No data are collected at high speed and so no conclusions can be drawn regarding high-speed puncture tests.

Lange [21] provides a good transition toward high speed testing of laminate structures. They evaluate a number of different test methods, settling on a penetration probe method similar to ASTM 1306. They test six different probe geometries and test speeds ranging from 1 to 1000 mm/min. The ranking of test structures remains the same over this speed range. Force to puncture, energy to puncture (area under force vs displacement curve), and puncture resistance factor (PRF, force times work or energy to puncture) are compared with field experience for several structures. Energy to puncture and PRF give the best agreement with field experience. A set of test conditions are selected for the remaining tests based on these results.

For paper laminates Lange finds the penetration resistance is limited by the paper; it fails first (along with foil if that is in the structure) followed by the polymer. Failure of the laminate is defined with the first layer that fails. Polymer layers fail quickly afterward due to stress concentration created by the failure of the paper layer. Puncture resistance is somewhat lower when tested from the polymer side of the paper laminates. Seyler [63] also reports slow puncture resistance depends on which side of an asymmetric multilayer film is facing the probe. Lange explains this with beam theory, which says the stress will be uneven during penetration, with higher stress on the side furthest away from the probe. When the probe comes from the polymer side, the stress in the paper is higher and breaks sooner. Lange finds some benefit from putting the paper in the middle of the structure, which results in higher puncture resistance due to the whole structure failing, not just the paper. This suggests structure design plays a role.

Structures without paper (only polymer) show a one-step rupture mechanism in Lange's experiments. All the layers fail at the same time—any improvement

in one layer directly translates into an improvement for the laminate. Puncture resistances of two to six times that of structures with paper are achieved. Direction of penetration still makes a difference for all-polymer structures. Puncture resistance is lower when the probe penetrates from the side with the stiffest side (such as OPP or OPET). This is consistent with scratch tests reported by Hare who provides an explanation involving differences in deformation behavior (see Section 9.4.3.3 for details).

Timm's [59] study of OPET/adh/PE film laminates, introduced in Section 9.4.1, includes measurements of dart drop. They find that the impact resistance is not a simple sum of the impact resistance of the component films. Increasing the thickness of the PE film increases the dart drop resistance. The composition of the PE film also gives some variation in the results.

Laboratory puncture tests such as dart impact, Spencer, and slow puncture often do not correlate very well with actual field experience [33,64]. Empirical tests, such as screw drop tests, have been developed in an ad hoc fashion by package engineers to screen new film structures. Such tests may provide rankings among film candidates but lack the rigor to compare structures among different labs or the quantitative output that can be used to validate predictive models. The lack of good lab tests has necessitated conducting expensive trial by error field testing on actual packing lines, often cutting into production to test new structures.

A well-documented early attempt to develop meaningful lab tests and correlate the results with field tests was made by Hu [58] at the US Army Natick Laboratories. Hu describes the development of foil-based packaging structures for military rations. Many factors are important for foil laminate packaging such as good sealing. This study focuses on abuse resistance and specifically pinholes. Two types of pinholes are described—those that only puncture the foil layer and those that completely puncture through the whole package, which they call complete-puncture pinholes. The latter are the most important for vacuum packaging (such as freeze-dried food) and the focus of the study.

Puncture, flexure, and abrasion are the three modes of failure. Puncture can occur when sharp food such as a freeze-dried carrot pierces the package. Flexural issues arise in folds or the seal area that are bent during transportation. Abrasion occurs when the package rubs against another during transportation. Hu notes that most lab tests do not simulate these modes of failure.

For puncture resistance, Hu observes that previous work by Furno [65] and others use a probe size (0.25-inch or 6-mm) that is much larger than the typical pinholes they observe in the actual packages. Hu settles on a slow puncture test, similar to ASTM 1306, with a needlelike probe with a 0.14—0.16 mm diameter and a test speed of 5 mm/min. For flexure resistance, Hu uses a MIT Folding Endurance tester with a specially designed vacuum box. The film is flexed for a given number of cycles and then mounted on the vacuum box to test for pinholes (using a dye technique). Abrasion resistance is tested by cutting a square specimen from the film and folding it twice into a triangle. The tip of the triangle is subjected to an abrasive material on a rotating turntable. After a given number of rotations, the sample is removed and tested for pinholes.

Hu tests a number of film samples to select the best for field tests. In addition to the above-mentioned lab tests on the films and laminates, Hu also fills packages in the lab and tests for puncture by vacuum packaging them and testing for loss of vacuum after 2 weeks. Abrasion is tested on the filled packages with a modified belt abrasion machine. A good test of flexure is not found. Field testing is conducted on the US. Army base with freeze-dried vacuum-packaged food carried by soldiers while maneuvering an obstacle course.

An attempt is also made to correlate the package failure results to food texture and hardness. Maximum force (during compression), force of rupture, ultimate strain, and work of rupture measurements are made on the food, depending on the food product.

The results of the lab puncture testing of various laminates show that the puncture resistance increases with thickness. Hu observes different results depending on which side the puncture is initiated (inside—for heat seal side or outside). He finds no definitive relationship for which side gives the highest puncture resistance and concludes that it may depend on the structure components and design. The puncture resistance of the laminates is less than the sum of the puncture resistance of its components. Hu explains this by relating it to how a laminate fails when stressed axially as described in Section 9.4.1.

The lab flexure tests show that increasing film thickness decreases the flex resistance. This is true of the laminates as well. The laminate flex resistance

falls in between the flex resistance of its component films. Aluminum foil has poor flex resistance as expected; adding an OPET layer increases it appreciatively.

Increasing thickness increases the abrasion resistance. The laminate abrasion resistance is much higher than the sum of the individual components.

Varying the test speed within the limited range of the lab tests does not change the rankings of the laminates. In general the laminates perform well on one or two tests but not all three. Compromises have to be made depending on which mechanisms are believed to be most important for the application.

Tests on the lab-filled packages show the following:

- Higher hardness foods result in a greater number of package failures in the puncture and abrasion tests.
- Vacuum packaging creates more pinholes than air packaging.
- The rank correlation between the lab tests on the laminates and the filled packages is good, ranging from 0.715 to 0.99.

Hu subjects 10 states (2 food types and 5 package structures) to the field test. The field failures correlate better with the product of puncture force and puncture energy (the PRF mentioned earlier when describing the study by Lange) rather than either one alone. Hu suggests that the PRF may correlate better because some layers may have higher force than energy, while other layers may have higher energy than force. Field failures correlate well with the instrumented PRF and the abrasion resistance lab tests but not well with flex resistance. This suggests that puncture and abrasion are the two main failure mechanisms for this application.

Carbajal [64] recently developed a puncture test to simulate pinholes created during the filling operation of a snack food vertical-form-fill-sealing line. They recognize that food packaging has unique characteristics that are not captured in standard lab tests: the speed of the falling food, the diameter of punctured holes, and low stiffness and strength of the food product that may result in deformation during the event. To create a test that better represents the conditions of a real filling operation, they conduct a preliminary study of the dynamics of single crackers falling onto a suspended horizontal film. They use high speed photography to examine the puncture event. A sequence of photos from the study is shown in Fig. 9.22. For a particular commercial nonwoven cracker impinging onto a film, they find the cracker does not significantly deform during the puncture event and pinholes form at a critical speed of 6.1 m/s. These last data are obtained by varying the speed of the cracker by adjusting the drop height and checking for pinholes by using a dye technique. This provides the basis for the test method, where a speed of 4.2 m/s (speed of cracker dropped 3 feet or about 1 m) is used.

The reverse impact test developed by Carbajal is shown in Fig. 9.23, where a moving hydraulic frame with the mounted film contacts a stationary needle probe at a constant velocity (4.2 m/s). The probe is a hardened steel needle with a 1 mm diameter hemispherical tip and designed to simulate the size of the pinholes found in the cracker drop tests. The film is mounted horizontally on the hydraulic frame for ease of testing (tests conducted at different angles give the same ranking of results). The needle is attached to a force transducer that measures the force vs displacement during the impact event. The platform moves rather than the needle to reduce noise in the measurement. Noise is further reduced by computing the energy (work) vs displacement by integrating the area under the force curve. The ultimate work of puncture is used to correlate with puncture resistance. The puncture event during the test is monitored with two high-speed video camera (50,000 frames/s).

There are several features of this test that make it well suited to the study impact puncture of foods. One is the dimensions of the needle probe is similar to the small dimensions found in the cracker drop tests and much smaller than standard laboratory dart drop tests. Second, the speed of the test mimics that found in the drop tests and is much higher than standard lab tests such as dart drop and Spencer impact. Finally, specific steps are taken to reduce the noise of the measurement to obtain reliable data.

The method is tested on a series of barrier snack films with the structure (HDPE-tie-PA-tie-sealant). The PA layer thickness, total thickness, sealant (ionomer or EVA-ionomer blend), and adhesion of the tie layer to the outside PA layer are varied. The results show an increase in puncture resistance with increasing PA layer thickness (shown in Fig. 9.24); this is consistent with what is known from field studies. The results are also compared with a bullet drop test. This is similar to a screw drop test that is

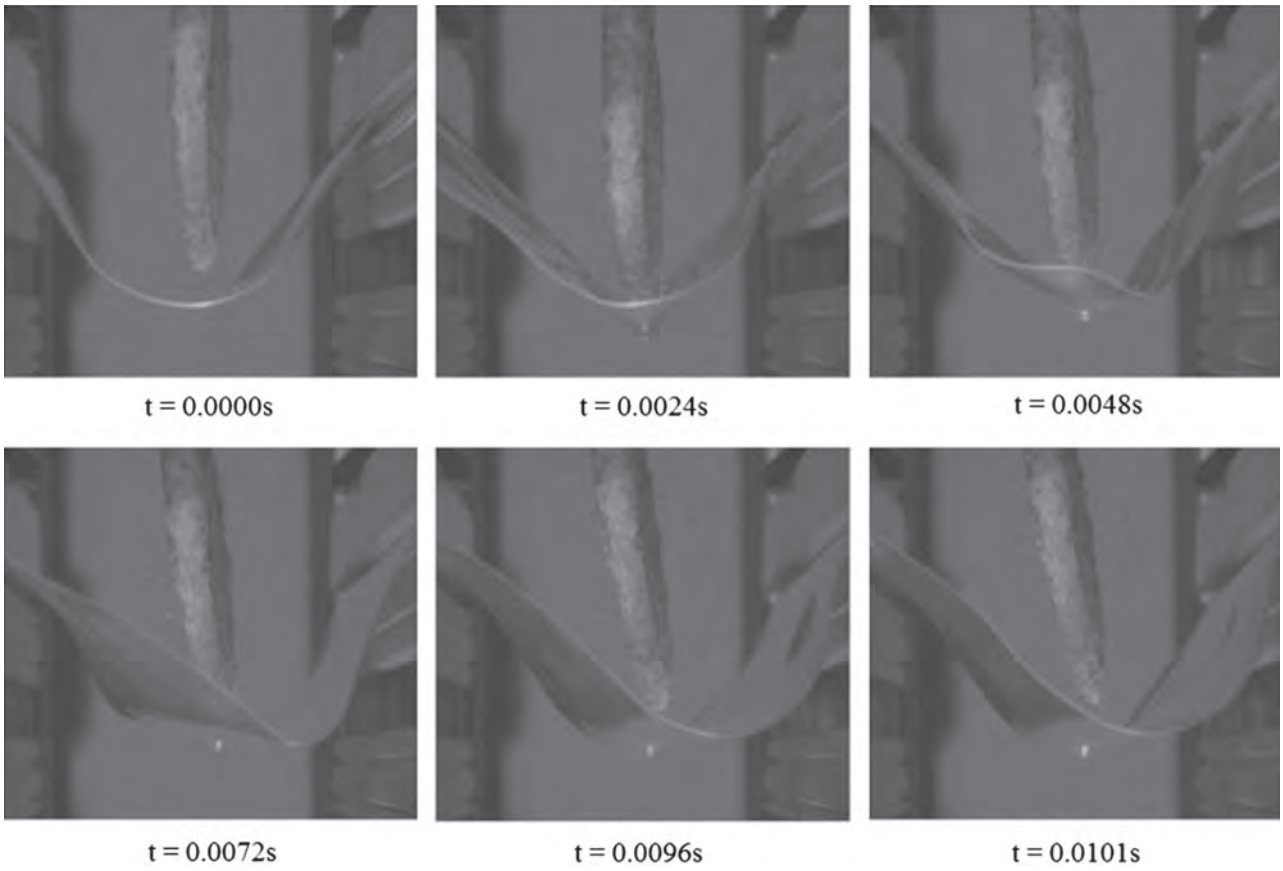


Figure 9.22 Photos from high speed photography of cracker dropped onto a film.
Reprinted with permission from Carbajal LA, Jio R, Hahm DM, Morris BA, Kendzierski RR. Impact puncture resistance of multilayer flexible food packages. In: SPE ANTEC conference; 2015.

sometimes used to rank films; the projectiles simulate the falling food product. Bullets are selected over screws due to their better flying stability, closeness to the weight of a cracker, and similar tip diameter as measured pinholes from the earlier cracker impact tests. Excellent agreement between the puncture test and the ranking of the bullet drop test is found. The test method can be used to validate numerical models to predict puncture resistance and study design features such as toughening individual layers, interlayer adhesion, splitting layers, and sealant selection (Section 17.2).

9.4.3.3 Scratch Resistance

Scratch resistance tests have been proposed for improving the correlation between laboratory tests and field package failure studies. Many package failures originate from scratching from either the inside or outside of the package, as for example when a sharp food product is dropped into the bag on the filling machine, a bone or sharp product rubs against the inside of the package during shipping, or the outside of the package is subjected to sharp objects during handling or shipping. Hare [34,35] and coworkers use a scratch tester with a linearly increasing load to analyze damages in packaging films. As described in ASTM D7027 and Section 9.2.5, a probe is moved across the specimen at a constant velocity with a linearly increasing force and the resulting scratch is examined. In one study [34], two 75-μm (3-mil) laminates are tested: (1) OPET-met/adh/(PE—PE) and (2) OPET-met/adh/(PA-tie-PE). A probe with a 1-mm diameter steel tip is used with a testing speed of 1 mm/s over a force range of 0—40 N. The films are mounted onto a hard surface (PMMA). The tests are run until the probe penetrates through the entire sample.

Hare reports that structure 2 requires a higher scratch force before it punctures, agreeing with field trials. Structure 1 delaminates between the layers during the scratch test, contributing to the lower force for failure. Structure 2 maintains structural integrity throughout the test, distributing the stress more

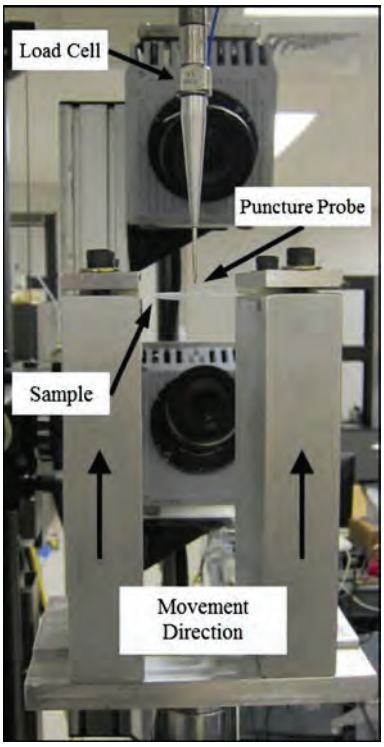


Figure 9.23 Reverse impact test.
Reprinted with permission from Carbajal LA, Jio R, Hahm DM, Morris BA, Kendzierski RR. Impact puncture resistance of multilayer flexible food packages. In: SPE ANTEC conference; 2015.

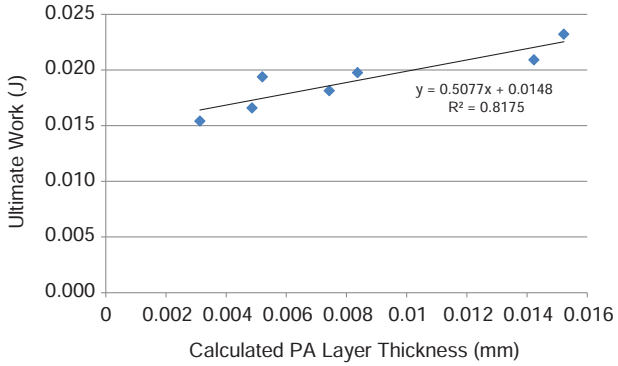


Figure 9.24 Effect of nylon layer thickness on high-speed puncture resistance from DuPont study.
Reprinted with permission from Carbajal LA, Jio R, Hahm DM, Morris BA, Kendzierski RR. Impact puncture resistance of multilayer flexible food packages. In: SPE ANTEC conference; 2015.

uniformly. Superior adhesion contributes to higher scratch resistance.

The scratch progresses through several modes of deformation as the load increases from smooth deformation to slip-stick. Modes of deformation during scratching are discussed by a number of investigators [31,66,67]. Examination of the progression under a steadily progressive load can be useful in understanding damage mechanisms.

Scratching from the sealant side results in higher force to puncture than from the OPET side of the laminate. Hare cites earlier work by Jiang [68] to explain this. When a soft coating (or film in this case) lies on top of hard surface the probe deforms the soft film but the deformation does not disturb the hard surface beneath. This is illustrated in Fig. 9.25. It is only after the soft surface is fully penetrated that the hard surface starts to see deformation and damage. When a hard coating lies on a soft surface the probe deforms the hard surface, which in turn deforms the soft film beneath, resulting in damage of both layers. Failure occurs at lower forces. Hare shows microscopy evidence that bears this out.

In a second test using the same test procedure, Hare [35] tests a laminate structure put together by two different methods, adhesive and extrusion lamination:

1. OPET-met/adh/(PE sealant film) [98 μm total]
2. OPET-met/LDPE (extrusion)/(PE-sealant film) [106 μm total]

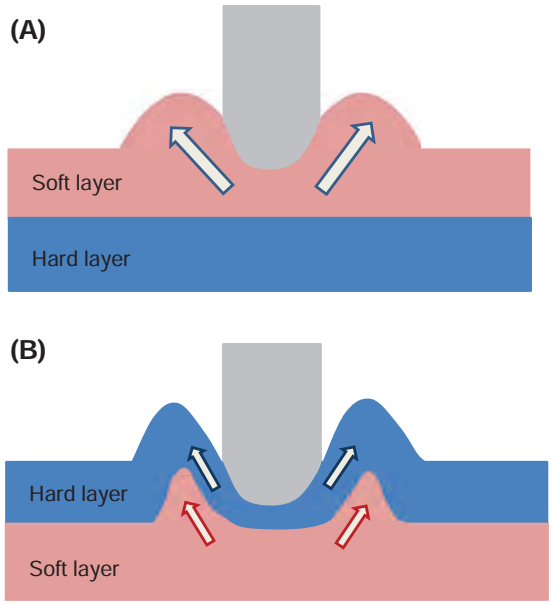


Figure 9.25 Illustration of deformation of (A) soft film on top of a hard film and (B) a hard film on top of a soft one.
Adapted from Hare BA, Moyse A, Sue H-J. Analysis of scratch-induced damages in multi-layer packaging film systems. J Mater Sci 2012;47:1389–98.

Scratch tests are conducted on the OPET side of the structure. The results show that the extrusion-laminated structure has higher scratch resistance than the adhesive-laminated structure. Microscopy indicates that the adhesive-laminated structure delaminates, concentrating the stress and causing failure at lower loadings. The extrusion-laminated structure maintains its integrity with no localized delamination throughout the test, helping to distribute the stress over a wider area.

Factors that affect the linear load scratch test include the following:

- Hardness of the surface that the film is mounted on during the scratch test. Fig. 9.25 illustrates the effect this has on the deformation of layers within the film.
- Probe shape. Like puncture tests, the size and shape of the probe influence the force of scratching.
- Film orientation (which layer is exposed to the probe). This is discussed earlier and illustrated in Fig. 9.25.
- Method for fixing the film to the surface (Hare uses vacuum).
- Interlayer adhesion. This is a factor in both of the Hare studies. Some investigators use the scratch test as a way of measuring adhesion [69].

The scratch test is most applicable to damage caused by scratch-related events, such as puncture or tearing. It is probably best suited for abrasion and scratch damages such as sliding and vibration during transportation. It may not be well suited for investigating the mechanical integrity of seals where a peel test may be more appropriate.

9.4.3.4 Abrasion Resistance

Not many studies of abrasion resistance of packaging films are reported in the literature. As is described in Section 9.4.3.2, Hu [58] uses an abrasion test method to evaluate foil-based laminates for the packaging of military rations. The lab method involves cutting a square specimen from the film and folding it twice into a triangle. An abrasive material attached to a rotating turntable is rubbed against the tip of the triangle. After a given number of rotations, the sample is removed and tested for pinholes. Hu finds that this and a puncture test correlates well to field testing of vacuum-packaged freeze-dried food subjected to soldiers carrying the packages while maneuvering an obstacle course.

Blom [39] uses a Taber test described in Section 9.2.5. A probe is rubbed across the surface. Different weights can be attached to the probe depending on the nature of the sample. Blom runs the test until the sample fails and records the number of cycles to failure. The test results are variable and Blom recognizes more work is needed to understand the source of the variability (test method, material, and so on). Nevertheless, his work provides interesting observations and insights into the abrasion resistance of packaging films:

- Measurements in the TD of monolayer film often give higher values (cycles to failure) than the MD. Biaxially oriented films have a fairly balanced abrasion resistance in TD and MD.
- Abrasion resistance is inversely related to applied load, but it is not linear. The relationship is more exponential in nature. Some films are more sensitive to changes in applied load than others.
- Abrasion resistance increases with film thickness. The relationship is not linear. When plotted on a log—log plot, the cycles to failure vs thickness curves for monolayer films are fairly linear, indicating a power law type of relationship. For OPET and PA films, the power law exponent is around 4; for an E/5% VA film, it is around 3.7. This means that the cycles to failure increases with the thickness raised to the fourth power.
- Multilayer films have much higher abrasion resistance than the simple sum of the components as is shown in Fig. 9.26. (Note that the vertical scale in this figure uses a logarithmic scale.) The nonlinear nature of the effect of thickness plays a role in this behavior, but it is more complex; applying the power law model to the total thickness of the laminate overpredicts the cycles to failure. Blom suggests adhesion plays a role—stacked films without the adhesive have lower abrasion resistance, but no data are provided.

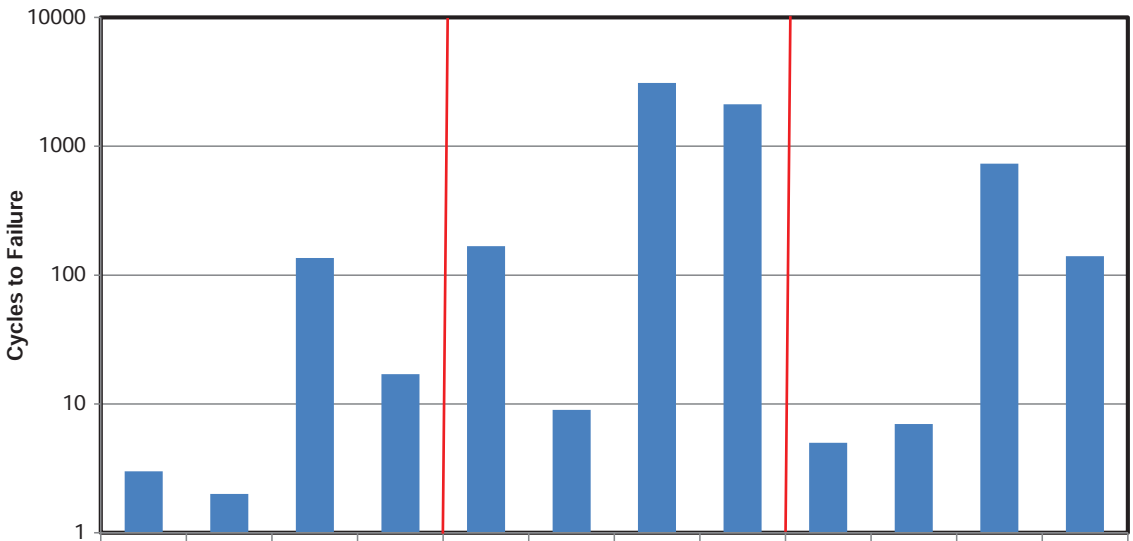


Figure 9.26 Abrasion resistance of packaging films and their laminations. *EVA,* ethylene vinyl acetate copolymer; *LDPE,* low density polyethylene; *OPET,* oriented polyethylene terephthalate.
Adapted with permission from Blom H. Flexible packaging durability studies. In: SPE FlexPackCon conference; 2014.

- The orientation of the multilayer film (sealant or nonsealant side facing the abrader) has an effect for some films. In general, the film failed in fewer cycles when the sealant side was facing the abrader. This differs from the puncture and scratch results of Lange and Hare described in Sections 9.4.3.2 and 9.4.3.3 where the nonsealant side facing the probe produced the lower results.

Blom proposes an abrasion coefficient as a material parameter:

$$A = \frac{\log(\text{cycles to failure}) \times \text{Applied Load}}{\text{thickness}} \quad (9.12)$$

Stiffer materials (PET, PA) have higher A than soft ones like EVA and PE. The coefficient of friction may also play a role. Values for A reported by Blom are given in Table 9.4.

9.4.4 Tear Resistance

The tear resistance of multilayer films made up of only stiff materials such as OPET or OPP generally follows the rule of mixtures. Most flexible packaging film structures, however, contain a ductile polyethylene or ethylene copolymer sealant layer. These materials have some of the highest tear strength of films used in packaging due to plastic yielding as the tear propagates through the sample. Combining a ductile layer with a stiff layer typically results in tear

Table 9.4 Abrasion Coefficient (Eq. (9.12)) of Some Common Packaging Materials

Material	Abrasion Coefficient
OPET	39.3
OPA	21.3
Cast PA	14.4
Cast PP	7.6
EVA, 6% VA	4.1
EVA (5% VA)/LLDPE blend	2.9

From Blom H. Flexible packaging durability studies. In: SPE FlexPackCon conference; 2014.

strength that is considerably lower than a simple addition of the two layers. This section begins with a discussion of the tear resistance of polyethylene films and the special consideration of directional tear properties. The case of multilayer flexible film structures combining stiff and ductile layers is then addressed.

9.4.4.1 Polyethylene Films

Polyethylene has a low yield strength, which results in a large zone of plastic deformation that precedes the propagation of a crack as the film is torn. This zone of deformation gives rise to high tear strength. The size of this zone of deformation can be predicted from fracture mechanics. Kinloch and Young [70] show that the radius of the zone of deformation in front of a crack tip is

$$r_y = \frac{1}{2\pi}\frac{G_a E}{\sigma_y^2} \tag{9.13}$$

where r_y = radius of zone of deformation, G_a = fracture energy or toughness, E = elastic or Young's modulus, σ_y = yield stress.

Values of r_y for some common polymers used in flexible packaging are computed in Table 9.5 from parameters compiled by Wu [71]. The value of r_y for LLDPE is particularly high due to its high fracture toughness (for which Wu cites several sources) and low yield strength. In their experiments, Wu measures the width of the yield zone for an LLDPE film to be around 20 mm, somewhat lower than the calculated value in Table 9.5 but of the right order of magnitude. Chang [72] also measured the yield zone width for a number of films made from LLDPE and blends of LLDPE and PP. These fall within a range of 10–22 mm for LLDPE and much lower for the blend. They find that the measured trouser tear resistance is directly proportional to the width of the yield zone.

Most polyethylene films exhibit a certain degree of anisotropy in the tear strength. Generally, the different classes of polyethylene behave as follows:

- LDPE: moderate tear resistance with MD tear strength > TD tear strength;
- LLDPE: high tear resistance with TD tear strength > MD tear strength;
- HDPE: very high tear strength in TD, very low in the MD.

These differences is tear anisotropy can be explained by differences in molecular architecture, crystalline morphology, and orientation. Key molecular parameters include the molecular weight distribution and amount of short and long chain branching. The crystalline morphology relates to the ordered structures that form as the polymer chains organize into crystals. This is a function of the stress the polymer is under during quenching, as well as the

Table 9.5 Fracture Mechanics Parameters for Some Common Polymers Used in Flexible Packaging

Polymer	Tensile Yield Stress, σ_y (MPa)	Young's Modulus, E (GPa)	Fracture Energy, G_a (kN/m)	Theoretical Radius of Deformation Zone, r_y (mm)
LLDPE (high MW)	8	0.2	120	60
HDPE	30	1.0	6	1.1
PP	35	1.2	8	1.2
PC	65	2.8	1	0.1
PVC	50	3.5	4	0.9
PET	50	2.8	8	1.4
PA (66)	60	3.0	3	0.4
PMMA	75	3.4	0.4	0.04
PS	70	3.4	0.3	0.03

Parameter values are taken from Wu [71] and computation of r_y from Eq. (9.13).

time available for crystallization. Since most films are quenched while being uniaxially or biaxially stretched, orientation of both the crystalline and amorphous regions may take place. Hence, the film fabrication process plays an important role in the ultimate shape of the crystals, the orientation of the polymer, and the tear strength.

A number of investigators have studied the crystalline morphology of polyethylene film using X-ray scattering, birefringence, electron microscopy, and other techniques [72–84]. A complete review of the literature is beyond the scope of this book. A number of structures have been proposed, including the following:

- Low stress Keller–Machin row-nucleated structure [72]. As the longest chains are extended in flow and cooled, stress-induced crystallization provides nucleation sites for the formation of lamella or plate-like structures of folded chains extending radially from the primary orientation direction, typically the MD. This is illustrated in Fig. 9.27. Because of the nearness of the nucleation sites, the lamella extends radially or nearly perpendicular from the direction of orientation. The lamella twists as they grow outward. They resemble twisted ribbons that extend perpendicular to the main chains. This is one of the most commonly reported structures for polyethylene blown films.

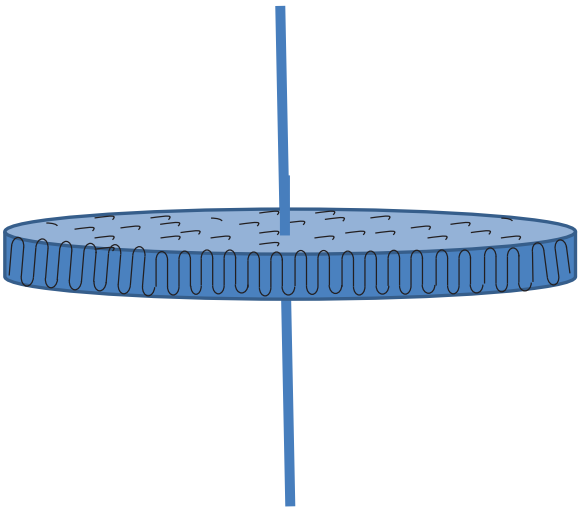


Figure 9.27 Illustration of plate-like lamellae structure of folded chains extending radially from a primary extended chain.

- High stress Keller–Machin row-nucleated structure. This is similar to the low-stress structure, except that the lamellae do not grow as long and extend radially outward without twisting; the folded chains that make up the lamella structure remain parallel to the primary chain orientation. This structure has been reported primarily for high molecular weight HDPE films, although Lee [85,86] has reported it for ionomers. The difference between the high and low stress morphologies is illustrated in Fig. 9.28.
- Spherulite-like superstructure. Spherulites are crystalline structures that extend radially from a single point, forming spherical domains. Boundaries between spherulites can sometimes lead to weakness or brittleness. Zhang [87] found spherulitic-like regimes with randomly oriented lamella in LLDPE films, while others have observed row-nucleated morphologies. Subtle differences in molecular architecture and processing conditions can lead to different morphologies.

Two studies are highlighted here that reveal the role that crystalline morphology, orientation, and molecular architecture have on tear strength anisotropy in polyethylene films. The first is Zhang [87]. Their study includes one grade of LDPE, three grades of LLDPE (a Ziegler–Natta butene copolymer, a Z-N octene copolymer, and metallocene octene copolymer), and one HDPE resin. Blown films are made from each of the resins keeping the output, blow-up

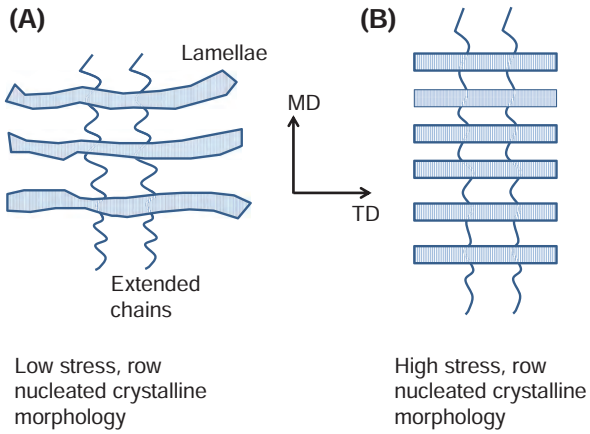


Figure 9.28 Comparison on low and high stress Keller–Machin row-nucleated lamellae morphologies.

ratio (BUR) and die gap constant while varying the DDR. DDR (also known as the take-up ratio) and BUR are defined in equations 2.3 and 2.4. As is described in Chapter 2, the thickness ratio, BUR, and DDR are interrelated (see equation 2.7), so that as they increase the DDR, the thickness decreases. The thickness of their films ranges from 25 to 100 μm. The frost line height is minimized. FTIR trichroism and scanning electron microscopy (SEM) are used to determine the orientation and crystalline structure of the films. The tear strength is measured following ASTM D1922 (Elmendorf tear).

The HDPE film exhibits the low stress Keller–Machin structure but without twisting of the lamella. The LDPE film also has a low stress Keller–Machin lamella structure, but it becomes more twisted and intertwined as the DDR is increased. The LLDPE films exhibit spherulitic structures with relatively random lamellae arrangements. All three LLDPE types exhibited the same type of structure with evidence of regional orientation. Low DDR favors transcrystalline morphology (in the thickness dimension). The metallocene LLDPE shows the least amount of orientation.

In order for a lamella crystal structure to form, polymer chains must extend during flow to create nucleation sites (fibril crystals) that initiate the growth of the lamella outward. This is favored for polymers with high MW fractions or long chain branching and long relaxation times. Zhang measures the relaxation time for the polymers used in the study and finds they have the following order: LLDPE < LDPE < HDPE. Both the HDPE and LDPE have long relaxation times. In addition, the HDPE has a high zero shear viscosity (high MW) and the LDPE has long chain branching, which contribute to chain entanglement and strain hardening. These setup conditions for the formation of oriented fibril nuclei followed by lamellae growth. The short relaxation time of the LLDPE allows the extended chains to relax prior to crystallization, making row nucleation or lamella formation less likely.

Zhang computes the ratio of the TD to MD tear strength for each of the films and relates this to the film structure. The HDPE shows very high tear resistance in the TD and extremely low tear strength in the MD. The LDPE film shows the reverse: high tear strength in the MD and low in the TD, with the TD:MD tear strength ratio decreasing with increasing DDR. The LLDPE films are more balanced but with a predominance of tear strength in the TD. For LDPE, the twisted lamellae favors tear in the TD (between stacks of lamellae). For HDPE, the nontwisted lamellae result in weak columns of crystals and tear propagates in the MD between the stacks. The lack of row-nucleated structure in LLDPE gives a fairly balanced tear resistance but with preference in the MD due to local orientation of lamellae in the TD. This model for the tear resistance of polyethylene films is illustrated in Fig. 9.29.

Zhang also measures the tensile strength of the films in the TD and MD. The tensile strength of the HDPE and LLDPE films is higher in the MD than

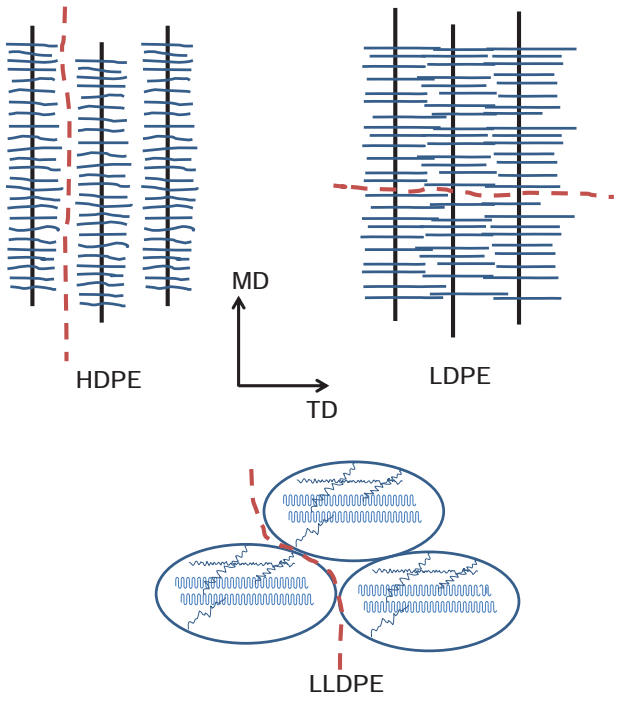


Figure 9.29 Model of tear resistance of HDPE, LDPE, and LLDPE blown film. HPDE has short lamella perpendicular to the main orientation of the long nucleating chains in the MD. Tear propagates along the interface between columns (*red* (light gray in print versions) *dashed line*). LDPE has long, intertwined lamellae perpendicular to the main orientation in MD. Tear propagates between lamellae. LLDPE in Zhang's experiments showed spherulitic structures with local orientation. Tear is fairly isotropic with some preference in the MD.
Adapted from Zhang XM, Elkoun S, Ajji A, Huneault MA. Oriented structure and anisotropy properties of polymer blown films: HDPE, LLDPE and LDPE. Polymer 2004;45:217–29.

TD, which they attribute to the presence of the long fibril structure.

Lee [88] also examines the crystalline morphology and orientation of different families of polyethylene blown films and relates this to the tear strength. They use a grade of LDPE, two grades of LLDPE (a Ziegler–Natta octene copolymer and a metallocene hexene copolymer), and one grade of HDPE. These are blown into film using a conventional process (short stalk). Thickness (50-μm) and the frost line height are held constant. The BUR is varied, which changes the DDR accordingly (see equation 2.7). The films are tested for Elmendorf tear strength (ASTM D1922) and characterized by wide and short angle X-ray scattering (WAXS and SAXS).

WAXS and SAXS show that all the films have a Keller–Machin low stress crystalline morphology: row nuclei are aligned in the MD and lamellae grow along the TD and twist as they grow. A Herman's orientation function, which is a measure of crystal orientation, is computed from the results, which confirm that all the films have the same structure. This simplifies the interpretation of the tear strength. For the mPE, only isotropic patterns are found for the range of BUR investigated. The authors explain that the mPE is isotropic since it contains very few long chains. The long chains contribute the most to orientation.

As orientation is increased in the MD (BUR decreased), the tear strength of mPE and LLDPE remains isotropic, the LDPE films tear more readily in the TD (MD tear strength > TD tear strength), and the HDPE films tear predominately in the MD (MD tear strength < TD tear strength). The results are shown in Fig. 9.30. Here the isotropic base line for MD/TD tear strength is around 0.6 rather than the expected 1. Lee explains that this is due to an artifact of the laboratory blown film line used, which produces nonuniform thickness in the hoop direction that favors MD tear. The trends, however, agree with those reported by Zhang and others.

Lee argues that the tear results are consistent with the morphology and number of tie molecules. Tie molecules are polymer chains that connect crystalline lamellae together through the amorphous regions [89]. They bear the load, contributing toward the mechanical strength. This is a refinement on the model proposed by Zhang. Because of its long chain branching, LDPE has a lower density of tie molecules than LLDPE and HDPE. For LDPE, tear prefers to propagate in the TD (between lamellae) since the density of tie molecules is low. For LLDPE and HDPE, tear propagates between the lamellae columns or breaks up crystals (breaking van der Waals forces rather than the stronger covalent bonds) since the tie molecule density is much higher. This is illustrated in Fig. 9.31.

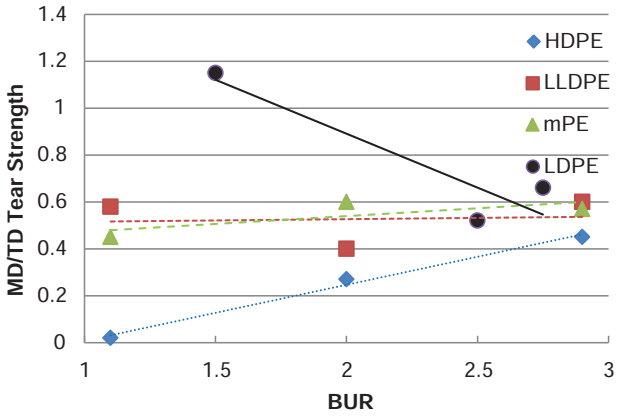


Figure 9.30 Results of blown film trial by Lee [88] showing differences in MD/TD tear strength ratio as a function of blow-up ratio (BUR). As BUR increases, orientation in the machine direction decreases. Results originally reported as a function of Herman's orientation factor but are replotted here in terms of BUR.

Lee also notes that the high tear strength of LLDPE often leads to other deformation that contributes to the tear strength. LDPE and HDPE exhibit much less plastic deformation, simplifying the analysis of their tear strength.

Several studies of multilayer polyethylene films reveal that tear strength is not additive. Siegman and Nir [45] and Martinez [51] find that (LLDPE-LDPE-LLDPE) films deviate from the rule of mixtures. Elkoun [50] finds different combinations of LLDPE either give linear or nonlinear behavior as described in Section 8.4.3.1 for impact toughness. A coextrusion of b-LLDPE and *m*-LLDPE deviates from the rule of mixtures, whereas a coextrusion of *o*-LLDPE and *m*-LLDPE agree well with the rule of mixtures. The distinctions are attributed to differences in the crystalline structure.

Borse [47] makes three layer structures of (A-B-A) with a butene-LLDPE and a metallocene LLDPE. When the b-LLDPE comprises the skin layers, the film follows the rule of mixtures. Placing the mLLDPE on the outside and b-LLDPE in the core creates synergies above that of the rule of mixtures.

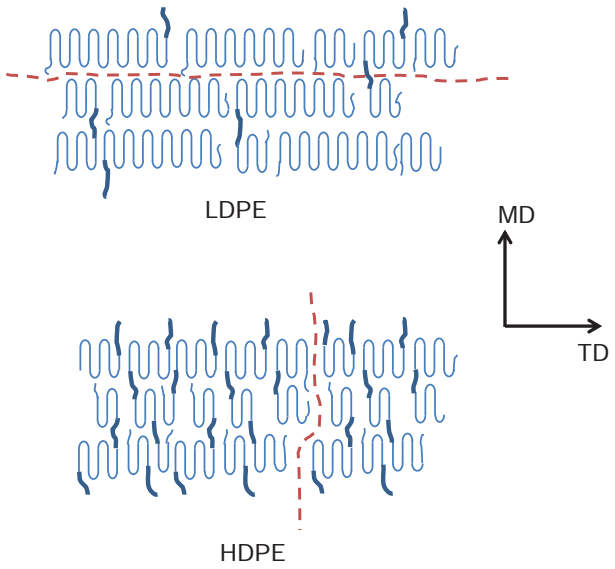


Figure 9.31 Model of tear resistance of LDPE (top) and HDPE (bottom). Top illustration shows few tie molecules spanning the gap between lamella. Tear propagates between lamellae stacks in the TD (*red* (light gray in print versions) *dashed line*). Bottom illustration shows many tie molecules linking the individual lamellae. Tear propagates between lamellae columns in the MD.
Adapted from Lee L-BW, Register RA, Dean DM. Tear anisotropy in films blown from polyethylenes of different molecular architectures. J Polym Sci Part B: Polym Phys 2005;43:413–20.

Guillotte [117] tests coextruded films of ionomer and LDPE and finds the tear strength to be lower than either the PE or ionomer alone and does not change as the percent of ionomer is increased. He attributes this to less orientation in the ionomer layer during coextrusion since the LDPE freezes first and dictates the stretching of the polymer. The ionomer is molten while it is extended, reducing its orientation. This effect is explored in more detail in Chapter 14.

9.4.4.2 Directional Tear Technology

Some packages are designed to be torn open. While perforations and laser scoring are often used to facilitate easy tear performance, the choice of materials and the film fabrication process can sometimes be manipulated to provide a directional tear function. Directional tear refers to the ability of the film to tear in one direction, typically the machine or transverse film direction, no matter how the tear is initiated. For the tear to propagate readily in the TD, the MD tear strength needs to be substantially greater than the TD tear strength and the TD tear strength needs to be low. The reverse is true for directional tear performance in the MD.

Most applications requiring directional tear performance need the tear to propagate in the TD. This is due to the orientation of most packaging films on packaging equipment. For example, on a pouch machine, the opening is sealed in the transverse direction. A notch may be incorporated into the package to help the consumer initiate the tear in the transverse direction. As is described in Section 9.4.4.1, linear polyethylene, such as LLDPE and HDPE, typically has much higher tear strength in the TD than the MD. This makes it difficult to use these materials for TD directional tear applications. A better starting point is LDPE, which typically has weaker tear strength in the TD than MD. The TD to MD tear strength ratio of LDPE can be minimized through the selection of fabrication conditions. Studies dating back to the early 1960s [90] show that the TD to MD tear ratio decreases as the orientation in the MD is increased. This can be accomplished by increasing the DDR, decreasing BUR, and minimizing the frost line height.

The TD tear strength of LDPE can still be too high for effective directional tear due to plastic deformation as described by Eq. (9.13). Meilhon and Wollak [91–93] propose the use of ionomers, either alone or in a coextruded blown film structure with LDPE. Typical film structures involve (A-B-A) coextrusion with ionomers as either the skin layers (for greater gloss) or as the core (for lower COF). The LDPE should be a high-pressure, low density resin, not an LLDPE or metallocene polyethylene.

Ionomers are ethylene–acid copolymers whose acid groups have been partially neutralized with a metal salt such as zinc or sodium. They are similar to LDPE in that they are made by free radical polymerization, which introduces long chain branching along the polymer chains. Therefore, they have similar property trends. For example, ionomers have the same preference toward TD tear propagation as LDPE. Ionomers, however, typically have lower tear strength than LDPE, which makes them ideal for directional tear applications.

On the simplest level, the origin of the lower tear strength of ionomers likely arises from the glassy amorphous regions in ionomers. The acid–metal salt interactions tend to associate into nanometer-sized clusters or domains within the amorphous phase of

the polyethylene matrix. Ionomers, therefore, have crystalline and amorphous regions like PE, but also ionic domains, as illustrated in Figure 4.8. In the solid state, the molecular chains are restrained by the ionic interactions within the domains, as well as for some distance surrounding these domains, creating a pseudoglassy amorphous state. Longworth [94] proposes that the notched sensitivity of ionomers may be due to a stress concentration effect. The radius of the propagating crack is small and may be of the same order of magnitude as the distance between ionic clusters. The ionic phase is glassy and non-deformable. As the crack propagates, greater strain is put on the polyethylene phase surrounding the ionic domains than when the ionic domains are not present. As a result, failure occurs at a lower stress. This is consistent with a theory for tear strength put forward by Rohn [95], which assumes that tear resistance is related to the amount of molecular mobility available to respond to the formation of a tear or crack. The lower the mobility, the lower is the tear strength.

Meilhon and Wollak find that ionomers are even more responsive to changes in blown film processing parameters than LDPE. Directional tear in the TD direction is favored by running the film line at high DDR, low BUR, and low frost line height. Lee [85,86] conducts fundamental studies to understand the origins of the directional tear. They study six polymers, a high and low melt index (approximately 1 and 10 g/10min) grade of LDPE, ethylene methacrylic acid (EMAA) copolymer (a precursor to ionomer), and ionomer. Blown films from each of the grades are made on a lab line, varying the BUR (1.5−3.5) and frost line height (8−50 cm), keeping the film thickness constant (50-μm). The take-up speed is adjusted to keep the film thickness constant so that as the BUR is increased, the DDR decreases (as per equation 2.7). Elmendorf tear strength in the MD and TD is measured and the film crystalline morphology is characterized using SAXS and WAXS.

The LDPE film exhibits Keller−Machin low stress orientation with lamellar stacking along the MD and twisting as they grow (Fig. 9.27). The ionomers and EMAA have a structure corresponding to the Keller−Machin high stress structure, which up to this point had only been reported in the literature for HDPE. EMAA and ionomers crystallize more slowing than LDPE and have a higher density of crystalline nuclei (since they freeze at a lower temperature where crystallization rapidly occurs). Lee suggests that this results in the high-stress crystalline structure.

The low MI ionomer shows a rotation of the crystalline lamellae when the film is made at high BUR. The authors say they are not aware of LDPE exhibiting this behavior. The rotation corresponds to a change in directional tear from TD to MD. Thus, ionomers under the right processing conditions can be made to have directional tear in either the TD or MD directions.

Lee computes the Herman's orientation function (f), an indication of crystalline orientation, and finds it correlates with preferred tear direction and ratio of MD to TD tear strength (negative f gives preferred MD tear and positive f preferred TD tear for the ionomer and EMAA). The LDPE tear is either isotropic or in the TD direction. Lower MI grades of all three resins have a steeper slope of f vs BUR indicating more orientation. There is not a perfect correlation between 1/MI and MD/TD tear strength ratio since 1/MI is a melt property, whereas Herman's orientation function is a solid state value.

Of the three processing variables, only BUR shows a significant effect on tear. Since take-up velocity (MD strain) is decreased as BUR (TD strain) is increased, the MD/TD strain ratio increases rapidly as BUR is increased.

Based on the X-ray analysis, Lee proposes that the least resistance to tear propagation is between the lamellae—perpendicular to the nucleating lines and to the direction of laminar stacking as is shown for LDPE in Fig. 9.28. As the BUR is increased, the crystalline orientation of the ionomer and EMAA flips 90 degree so that the extended polymer chains are in the TD and the parallel stacks of lamellae are in the MD, the new preferred direction of tear. Tear propagation is still between lamellae.

Sometimes, direction tear is needed in the MD rather than TD. As shown in Section 9.4.4.1, linear polyethylenes such as HDPE and LLDPE tend to preferentially tear in the MD. But these polymers have their drawbacks. HDPE has poor heat seal performance and the overall tear strength of LLDPE may be too high for directional tear. As shown above, ionomers can be flipped to tear preferentially in the MD direction by running at high BUR. Alternatively, blends of ionomer and LDPE can be used to achieve MD tear [96]. These blends may be used as monolayer or in coextrusions with other layers that would not typically have linear tear properties on their own.

Translating direction tear from an ionomer or polyolefin film to a laminate can be challenging. In general, good adhesion is needed between the layers to transfer the tear propagation across the laminate. Loss of adhesion during the tear event can dissipate the tear force and cause the structure to become more resistant and less likely to tear in the preferred direction.

9.4.4.3 Multilayer Films

Polyethylene films have some of the highest tear strengths found in flexible packaging, yet laminations of PE film to stiffer substrates such as OPET or OPP typically have much lower tear strength [59,71]. Wu [71] provides insight into this phenomenon. They begin by developing a theoretical model for the tear strength of multilayer films. They find that the tear strength of the composite is the sum of the tear strength of the individual layers; tear strength is predicted to follow the rule of mixtures. They conduct experiments with laminates of LLDPE film with biaxially oriented polypropylene (BOPP) using a two-sided adhesive tape (based on BOPP). The tear strength of the BOPP-LLDPE laminates is much lower than the LLDPE film alone. They also conduct tear strength measurements on BOPP-OPET and BOPP-cPP (cPP is polypropylene cast film) laminates and find that these follow the simple rule of mixtures, as predicted by their model. This is illustrated in Fig. 9.32.

As noted in Section 9.4.4.1, the tear strength of polyethylene, and LLDPE in particular, is enhanced by a large zone of deformation in advance of the crack tip. When the LLDPE film is laminated to the stiff OPP, the OPP constrains the deformation, limiting the zone of deformation. Wu conducts experiments confining the lateral dimension of the zone of deformation by applying the double-sided tape to each side of the notch in the LLDPE-film test specimen. This leaves a well-defined width through which the tear can propagate. They measure the tear strength at several confined zone widths, the results of which are shown in Fig. 9.33. For large zone widths, the tear strength is the same as that of the unconfined specimen. As the zone width is constrained, the tear strength begins to decrease in a linear manner, as predicted by fracture mechanics. By extrapolating to zero width, they obtain a value for the "limiting tear resistance" or LTR. By using LTR in their model for the BOPP-LLDPE laminates, the predicted tear resistance of the laminate agrees well with the measured values.

This mechanism of the deformation of the PE layer being confined by stiffer layers in a laminate is confirmed in work by Timm [59]. Timm measures the tear strength of an OPET/LLDPE laminate and finds that the tear strength to be considerably less than the LLDPE alone. Increasing the thickness of the LLDPE sealant layer is more effective in increasing the tear strength of the laminate than changing the composition of the LLDPE sealant film to one with stronger tear strength. This is consistent with Wu's explanation since the thicker LLDPE film would allow a larger zone of deformation to form.

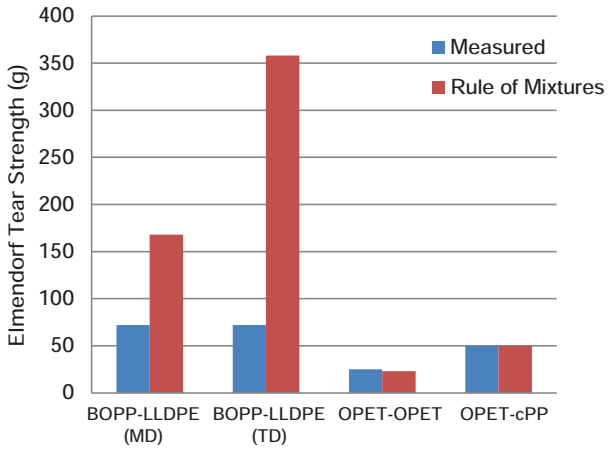


Figure 9.32 Elmendorf tear measurements of laminates.
Data from Wu [71].

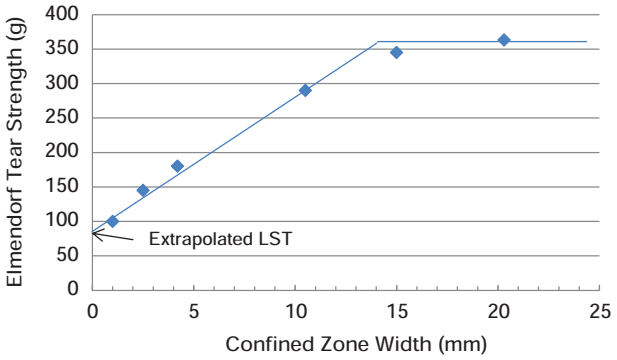


Figure 9.33 Results of Wu [71] confined tear resistance measurements on an LLDPE film. The edges on both sides of the test specimen are taped to confine the zone of deformation to a predetermined value. Curves are fits provided by Wu.
Wu R-Y, McCarthy LD, Stachurski ZH. Tearing resistance of multi-layer plastic films. Intern J Fract 1994;68:141–50.

9.4.5 Essential Work of Fracture

Tear strength is not an intrinsic material property as it varies with test geometry and other factors. Fracture toughness and stress intensity factors often used in the study of the fracture failure of bulk polymers fall short for thin ductile films used in flexible packaging. Recently the concept of essential work of fracture (EWF) has been applied to films in the academic literature as a way to measure fracture toughness [97–104].

The concept of work of fracture involves dividing the fracture into two zones, an inner region corresponding to the fracture process zone and an outer region corresponding to yielding, as illustrated in Fig. 9.34. The work of fracture (W_f) is partitioned into two components, the EWF (W_e) and the nonessential (plastic) work of fracture (W_p). These two components correspond to the two regions. W_e and W_p can be interpreted as the energy to initiate the crack and the energy for propagation, respectively. The EWF is an intrinsic material property, whereas the non-EWF depends on the geometry.

The work of fracture test typically involves using a tensile tester to measure the force vs displacement of a double notched specimen as shown in Fig. 9.34. The horizontal distance between the notches is the ligament length, l. The work of fracture is given by Eq. (9.14):

$$W_f = W_e + W_p = w_e l X + w_p \beta l^2 X \qquad (9.14)$$

where W_f = work of fracture, W_e = EWF, W_p = nonessential or plastic work of fracture, w_e = specific EWF (per unit ligament length), l = ligament length, X = thickness of specimen in the ligament region, w_p = specific non-EWF (per unit ligament length), β = plastic zone shape factor.

In terms of the specific work of fracture, W_f is divided by the cross-sectional area of the ligament, Xl:

$$w_f = \frac{W_f}{Xl} = w_e + \beta w_p l \qquad (9.15)$$

Specimens are double notched to different ligament lengths and the force vs displacement measured. A typical outcome is shown in Fig. 9.35. The area under the force vs displacement curve is equal to w_f. The plot of w_f vs l yields a straight line with intercept w_e and slope βw_p.

The applicability of using the ESF analysis for thin films is subject to certain conditions described in detail in various references [105,106]. Three of these conditions are the following [102]:

- The ligament must be fully yielded prior to crack propagation;
- The load vs displacement curves must be self-similar as is shown in Fig. 9.35; and
- The ligament must be in pure plane stress.

Academia is starting to use this technique to relate the fundamental mechanics of crack initiation and propagation to orientation and crystalline morphology of films. For example, Maspoch [105] finds that the EWF, w_e, is independent of film thickness but sensitive to orientation, whereas the reverse is true for the non-EWF. Rennert [102] applies the technique to a series LDPE blown films with thickness ranging from 15 to 400 μm made by varying the DDR. The fracture mechanics parameters obtained from the work of fracture testing are related to the crystalline morphology and orientation found from X-ray diffraction studies. Such studies should ultimately enhance the basic understanding of impact toughness, tear strength, and peel strength in

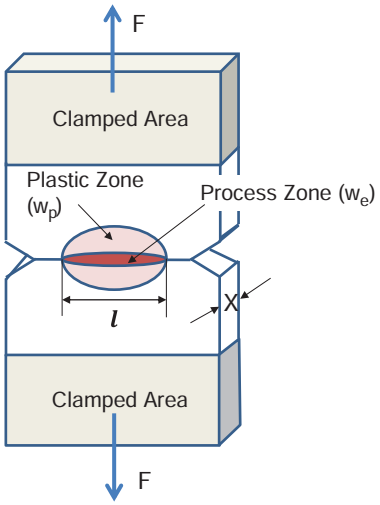


Figure 9.34 Illustration of double notched specimen during work of fraction test.
Adapted from Maspoch ML, Henault V, Ferrer-Balas D, Velasco JI, Santana OO. Essential work of fracture on PET films: influence of the thickness and the orientation. Polym Test 2000;19:559–68.

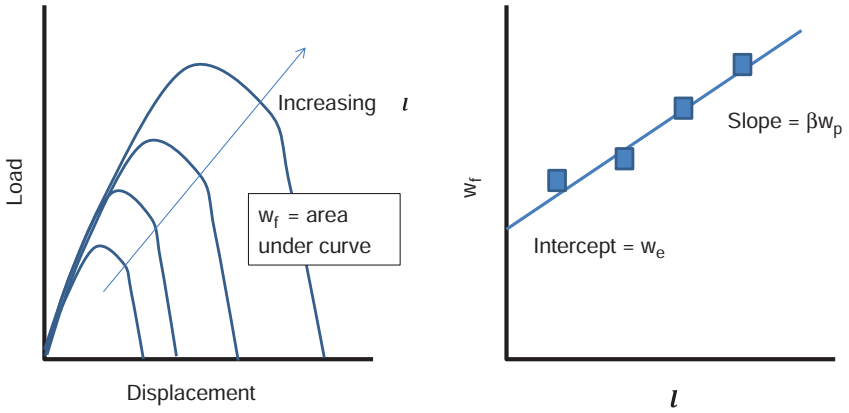


Figure 9.35 Example force vs displacement curves produced during work of fracture measurements. Area under the curve is the work of fracture, which when plotted vs the ligament length (right) yields a line with intercept w_e and slope βw_p.

packaging films and lead to better models for predicting performance.

9.4.6 Microlayer Technology

Section 8.5.2 describes layer multiplication technology that allows for the creation of tens, hundreds, or even thousands of layers in a coextruded film. This is accomplished by systematically doubling the number of layers by splitting the flow stream and recombining the layers, as is shown in Figure 8.17. Typically this is done with two or three layers repeatedly being "multiplied," creating a core region with many thin layers of A/B/A/B… As the number of layers increases, their individual thicknesses decrease. Films with layer thickness in the submicron and even nanometer dimension have been reported. As the layer dimension decreases, there may be changes in the physical properties brought on by changes in crystallinity, crystalline morphology, orientation, and other factors.

As described in Section 9.4.1, Schrenk and Alfrey [57] show that the mechanical properties of thin layers of stiff and ductile polymers are mutually reinforced as the layer dimensions decrease. This occurs when there is good adhesion between the layers and the ductile material can stop cracks initiated in the brittle layer from propagating.

The research group of Hiltner and Baer [107–115] at Case Western Reserve University has published several papers exploring the effect of forced assembly of micro- or nanolayers in coextruded film structures. Some of their findings include the following:

- Improved toughness of polycarbonate/styrene acrylonitrile (PC-SAN) and polycarbonate/polymethyl methacrylate (PC-PMMA) microlayer structures which they attribute to a change in deformation from crazing to shear yielding. They note that differences in interlayer adhesion may explain some of the dissimilarities found between the two systems [107–109].
- Greater ductility of talc-filled PP. Microlayers of talc-filled PP are made by compression molding and by coextrusion (using the process illustrated in Figure 8.17). The coextruded structures of alternating layers of talc-filled PP have better ductility than compression-molded versions. They explain that the talc particles are more oriented in the coextrusion process, providing greater cross-sectional area for the load bearing PP. The ductility of alternating layers of unfilled PP and filled PP go through a maximum with increasing number of layers [110,111].
- Reduction in crystallinity of HDPE sandwiched between layers of PS. As the HDPE layers become thinner (from 300 μm to 10 nm), % crystallinity decreases from 60% to 33%. The peak Tm decreases from 134 to 130°C. The decrease in crystallinity is accompanied by a change in crystalline morphology. Nucleation occurs from the interface—bulk nucleation becomes insignificant as thickness

decreases. Edge-on lamella form at low thickness as opposed to discoids (flattened spherulites due to the thickness dimension being less than the spherulite dimension). As a result of the changes in crystallinity and morphology, the gas transmission rate increases with increasing number of layers [109,112−114].

- Change in crystalline structure of PET. Films with 1056 layers of PET-PET or PET-PC were coextruded with layer thickness ranging from micro- to nanometer dimensions. After extrusion the PET layers are amorphous. The samples are annealed at various temperatures to crystallize the PET. The nonconfined PET crystals in the PET-PET structures start to form at 117°C. Crystallization of PET confined between the layers of PC does not begin until 132°C. The confined PET exhibits lower percentage crystallinity and greater orientation in the crystalline domains. [109,115]
- Change in crystalline morphology of PP. Films with alternating layers of PP and PS are coextruded with layer dimensions ranging from 650 to 10 nm. As the confined dimension of the PP layer is decreased, the crystalline morphology changes from spherulitic to flatted spherulitic (discoids). As the dimension approaches 10 nm, further distortions are found. [116]

Section 8.5.2 discusses improvement in ductility of PE-tie-EVOH coextrusion films by using layer multiplication technology. Improvements in physical properties by utilizing microlayer technology have found their way into commercial stretch and shrink films, as is described in Sections 8.5.2 and 11.2.4.6.

Layer multiplication technology is a good example of how the structure design and fabrication process influence film properties and may lead to deviations from the simple rule of mixtures. As the layer dimensions decrease and the layers are confined between other layers, changes in the crystalline morphology and orientation may arise that positively or negatively impact performance. The design of the structure (layer composition, layer placement, and layer dimension) cannot be done in isolation of the process. Chapter 14 deals with processing effects in more detail.

References

[1] Vansant JD. Internal communication. 2012.

[2] McKenna J, Bunker G, Fry T, Savargaonkar N, Wooster J. Change the package, keep the feel. In: TAPPI PLACE conference; 2010.

[3] Bunker G. Tips and techniques: how to downgauge film without losing the 'feel' of quality. Plastics Technology; 2010. viewed December 30, 2014 on: http://www.ptonline.com/articles/tips-and-techniques-how-to-downgauge-film-without-losing-the-feel-of-quality.

[4] ASTM International. Standard test method for tensile properties of thin plastic sheeting. D882-12. West Conshohocken, PA: ASTM International; 2012.

[5] Bahadur S. Strain hardening equation and the prediction of tensile strength of rolled polymers. Polym Eng Sci 1973;13:266−72.

[6] McKeen LW. Film properties of plastics and elastomers. 3rd ed. Amsterdam: Elsevier; 2012. p. 27−34.

[7] Lange J, Pelletier C, Wyser Y. Modeling and measuring the bending stiffness of flexible packaging materials. In: PFFC Peer reviewed paper, March; 2002.

[8] German Institute for Standardization. Determining the flexural rigidity of plastic film and woven textile fabrics with or without plastic coating by the cantilever method (DIN 53 362). German Institute for Standardization; 2003.

[9] ASTM International. Standard test method for resistance to bending of paper and paperboard (Taber type tester in basic configuration) (D5342-97). West Conshohocken, PA: ASTM International; 1997.

[10] ASTM International. Standard test method for apparent bending modulus of plastics by means of a cantilever beam (D747-10). West Conshohocken, PA: ASTM International; 2010.

[11] International Organization for Standardization. Paper and board - determination of bending resistance (ISO 2493). Geneva, Switzerland: International Organization for Standardization; 2010.

[12] ASTM International. Standard test method for rigidity of polyolefin film and sheeting (D2923-13). West Conshohocken, PA: ASTM International; 2013.

[13] British Standards Institution. Method of testing plastics. Mechanical properties. Stiffness of

plastics film,(BS 2872, Part 3, Method 332A). London, England: BSI; 1976.
[14] Morris BA, Vansant JD. The influence of sealant modulus on the bending stiffness of multilayer films. In: TAPPI polymers, laminations and coatings conference; 1997.
[15] Morris BA, Vansant JD, Hausmann K. More structural strength for thin films. Kunstoffe International; May 2011. p. 42–6.
[16] ASTM International. Standard test method for propagation tear resistance of plastic film and thin sheeting by pendulum method (D1922-09). West Conshohocken, PA: ASTM International; 2009.
[17] International Organization for Standardization. Plastics – film and sheeting – determination of tear resistance – Part 2: Elmendorf method (ISO 6383–2). Geneva, Switzerland: International Organization for Standardization; 1983.
[18] ASTM International. Standard test method for tear-propagation resistance (trouser tear) of plastic film and thin sheeting by single-tear method (D1938-14). West Conshohocken, PA: ASTM International; 2014.
[19] International Organization for Standardization. Plastics – film and sheeting – determination of tear resistance – Part 1: trouser tear method (ISO 6383–1). Geneva, Switzerland: International Organization for Standardization; 1983.
[20] ASTM International. Standard test method for slow rate penetration resistance of flexible barrier films and laminates (F1306–90(2008E1)). West Conshohocken, PA: ASTM International; 2010.
[21] Lange J, Mokdad H, Wyser Y. Understanding puncture resistance and perforation behavior of packaging laminates. J. Plastic Film Sheeting 2002;18:231–44.
[22] Hausmann K, Fleiger D. New sealants and peelable film concepts. In: Specialty plastic films '98, 14th Annual world Congress, October 19–21, 1998, Dusseldorf, Germany; 1998.
[23] ASTM International. Standard test method for impact resistance of plastic film by the free-falling dart method (D1709-09). West Conshohocken, PA: ASTM International; 2009.
[24] International Organization for Standardization. Plastics film and sheeting – determination of impact resistance by the free-falling dart method, part 1: staircase methods (ISO 7765–1). Geneva, Switzerland: International Organization for Standardization; 1988.
[25] ASTM International. Standard test method for total energy impact of plastic film by dart drop (D4272-14). West Conshohocken, PA: ASTM International; 2014.
[26] International Organization for Standardization. Plastics film and sheeting – determination of impact resistance by the free-falling dart method, part 2: instrumented puncture test (ISO 7765–2). Geneva, Switzerland: International Organization for Standardization; 1994.
[27] ASTM International. Standard test method for pendulum impact resistance of plastic film (D3420-14). West Conshohocken, PA: ASTM International; 2014.
[28] ASTM International. Standard test method for high speed puncture properties of plastic films using load and displacement sensors (D7192-10). West Conshohocken, PA: ASTM International; 2010.
[29] International Organization for Standardization. Paints and varnishes – determination of scratch resistance, Part 1: constant-loading method (ISO 1518–1). Geneva, Switzerland: International Organization for Standardization; 2011.
[30] Taber Machines Inc., 2015. Multi-finger scratch/mar tester, viewed online on June 28, 2016 from: http://www.testingmachines.com/pdf/10-45-multi-finger-scratch-tester.pdf
[31] Wong M, Lim GT, Moyse A, Reddy JN, Sue H-J. A new test methodology for evaluating scratch resistance of polymers. Wear 2004;256:1214–27.
[32] Browning RL, Lim G-T, Moyse A, Sue H-J, Chen H, Earls JD. Quantitative evaluation of scratch resistance of polymer coatings based on a standardized progressive load scratch test. Surf Coatings Technol 2006;201:2970–6.
[33] ASTM International. Standard test method for evaluation of scratch resistance of polymeric coatings and plastics using an instrumented scratch machine (D7027-13). West Conshohocken, PA: ASTM International; 2013.
[34] Hare BA, Moyse A, Sue H-J. Analysis of scratch-induced damages in multi-layer packaging film systems. J Mater Sci 2012;47:1389–98.

[35] Hare BA, Sue H-J, Liang LY, Kinigakis P. Scratch behavior of extrusion and adhesive laminated multilayer food packaging films. Polym Eng Sci 2014;54:71−7.
[36] Lin L, Blackman GS, Matheson RR. A new approach to characterize scratch and mar resistance of automotive coatings. Prog Org Coatings 2000;40:85−91.
[37] Lin L, Blackman GS, Matheson RR. Quantitative characterization of scratch and mar behavior of polymer coatings. Mater Sci Eng 2001;A317:163−70.
[38] Consiglio R, Randall NX, Bellaton B, von Stebut J. The nano-scratch tester (NST) as a new tool for assessing the strength of ultrathin hard coatings and the mar resistance of polymer films. Thin Solid Films 1998;332:151−6.
[39] Blom H. Flexible packaging durability studies. In: SPE FlexPackCon conference; 2014.
[40] ASTM International. Standard practice for conditioning flexible barrier materials for flex durability (F392/F392M-11). West Conshohocken, PA: ASTM International; 2011.
[41] Campus website, viewed on January 09, 2014, from: http://www.campusplastics.com/.
[42] Prospector website, viewed on January 09, 2014, from: http://www.ulprospector.com/en/na.
[43] Matweb website, viewed on January 09, 2014, from: http://matweb.com/.
[44] Plastics Technology website, viewed on January 09, 2014, from: http://www.ptonline.com/.
[45] Siegmann A, Nir Y. Structure-property relationships in blends of linear low- and conventional low-density polyethylene as blown films. Polym Eng Sci 1987;27:1182−6.
[46] Baldizonne R, Carianni G, Mariani P. A new Ziegler-Natta octene LLDPE for high performance blown film applications: benefits of coextruded vs. blended LDPE/LLDPE films. In: European TAPPI PLACE conference; 2005.
[47] Borse N, Aubee N. Developing cost effective co-extruded film structures for flexible packaging. In: SPE ANTEC conference; 2014. p. 1304−8.
[48] Beagan CM, McNally GM, Murphy WR. The blending and coextrusion of metallocene catalyzed polyethylene in blown film applications. In: SPE ANTEC conference; 1999.
[49] Beagan CM, McNally GM, Murphy WR. The blending and coextrusion of metallocene catalyzed polyethylene in blown film applications. J Plastic Film Sheeting 1999;15:329−40.
[50] Elkoun S, Huneault MA, Zhang XM, McCormick K, Puterbaugh F, Kale L. LLDPE blown films property enhancement through coextrusion. In: SPE ANTEC conference; 2003. p. 1396−400.
[51] Martinez F, Mazuera GE, Parikh DR. Comparative analysis of thick gauge blended and coextruded polyethylene films. J Plastic Film Sheeting 1990;6:44−62.
[52] Taylor J, Baik JJ. Benefits of coextruded LLDPE/LDPE film vs. blended LLDPE/LDPE film. J Plastic Film Sheeting 2000;16:223−35.
[53] Zhang X, Ajji A. Polypropylene-polyethylene multilayer films. In: SPE ANTEC conference; 2005. p. 2947−51.
[54] Zhang X, Ajji A. Oriented structure of PP/LLDPE multilayer and blends films. Polymer 2005;46:3385−93.
[55] Gaucher-Miri V, Jones GK, Kaas R, Hiltner A, Baer E. Plastic deformation of EVA, EVOH and their multilayers. J Mater Sci 2002;37:2635−44.
[56] Huang C-H, Wu J-S, Huang C-C. Predicting the permeability and tensile properties of multilayer films from properties of individual component layers. Polym J 2004;36:386−93.
[57] Schrenk WJ, Alfrey Jr T. Some physical properties of multilayered films. Polym Eng Sci 1969;9:393−9.
[58] Hu KH. Measurements on the resistance of flexible packaging materials to puncture, abrasion, and flexure and the relationship of these measurements to the performance of packages subjected to conditions causing pinhole formation. U.S. Army Natick Laboratories; 1973. Technical Report 73-32-GP.
[59] Timm D. How sealant film choice can affect a laminated structure's properties. In: TAPPI PLACE conference; 2005.
[60] Jones RM. Mechanics of composite materials. New York: McGraw-Hill Book Co.; 1975.
[61] Butler TI, Morris BA. PE-based multilayer film structures. In: Ebnesajjad S, editor. Plastic films in food packaging, materials, technology and applications. New York: Elsevier; 2013. p. 21−52.
[62] Darby D, Cooksey K, Kaas R, Gerard P, Cheruvathur R. Studying the relationship of

adhesive bond strengths and puncture resistance of flexible packaging laminations. In: SPE FlexPackCon conference; 2014. p. 37−43.
[63] Seyler RJ. Slow rate penetration of packaging films. J Plastic Film Sheeting 1990;6:191−224.
[64] Carbajal LA, Jio R, Hahm DM, Morris BA, Kendzierski RR. Impact puncture resistance of multilayer flexible food packages. In: SPE ANTEC conference; 2015.
[65] Furno FJ, Webb RS, Cook NP. High speed puncture testing of thermoplastics. J Appl Polym Sci 1964;8:101−10.
[66] Wong M, Moyse A, Lee F, Sue H-J. Study of surface damage of polypropylene under progressive load. J Mater Sci 2004;39:3293−308.
[67] Jardret V, Zahouani H, Loubet JL, Mathia TG. Understanding and quantification of elastic and plastic deformation during a scratch test. Wear 1998;218:8−14.
[68] Jiang H, Browning R, Whitcomb J, Ito M, Shimouse M, Chang T, et al. Mechancial modeling of scratch behavior of polymer coatings on hard and soft substrates. Tribol Lett 2010;37:159−67.
[69] Seo T-W, Weon J-I. Influence of weathering and substrate roughness on the interfacial adhesion of acrylic coating based on an increasing load scratch test. J Mater Sci 2009;47:2234−40.
[70] Kinloch AJ, Young RJ. Fracture behavior of polymers. London: Elsevier Applied Science Publishers; 1985.
[71] Wu R-Y, McCarthy LD, Stachurski ZH. Tearing resistance of multi-layer plastic films. Intern J Fract 1994;68:141−50.
[72] Keller A, Machin MJ. Oriented crystallization in polymers. J Macromol Sci (Phys) 1967;B1:41−91.
[73] Maddams WF, Preddy JE. X-ray diffraction orientation studies on blown film polyethylene films. I. Preliminary measurements. J Appl Polym Sci 1978;22:2721−37.
[74] Maddams WF, Preddy JE. X-ray diffraction orientation studies on blown film polyethylene films. II. Measurements on films from a commercial blowing unit. J Appl Polym Sci 1978;22:2739−49.
[75] Maddams WF, Preddy JE. X-ray diffraction orientation studies on blown film polyethylene films. III. High-stress crystallization orientation. J Appl Polym Sci 1978;22:2751−9.
[76] Lindenmeyer PH, Lustig S. Crystalline orientation in extruded polyethylene film. J Appl Polym Sci 1965;9:227−40.
[77] Kwak TH, Han CD, Vickers ME. Development of crystalline structure during tubular film blowing of low-density polyethylene. J Polym Sci 1988;35:363−89.
[78] Haber A, Kamal MR. Morphology and orientation in polyethylene tubular blown films. In: SPE ANTEC conference; 2001. p. 446−50.
[79] Gilbert M, Hemsley DA, Patel SR. Effect of processing conditions on the orientation and properties of polyethylene blown film. Br Polym J 1987;19:9−23.
[80] Gupta A, Simpson DM, Harrison IR. Crystalline morphology in oriented HDPE blown films. Plastics Engineering; November 1993. p. 33−6.
[81] Fatahi S, Ajji A, Lafleur PG. Structure-property correlations for PE blown films. In: SPE ANTEC conference; 2005. p. 1766−70.
[82] Patel RM, Butler TI, Walton KL, Knight GW. Investigation of processing-structure-properties relationships in polyethylene blown films. Polym Eng Sci 1994;34:1506−14.
[83] Godshall D, Wilkes G, Krishnaswamy RK, Sukhadia AM. Processing-structure-property investigation of blown HDPE films containing both machine and transverse direction oriented lamellar stacks. Polymer 2003;44:5397−406.
[84] Sukhadia AM. The effects of molecular structure, rheology, morphology and orientation of polyethylene blown film properties. In: SPE ANTEC Conference; 1998.
[85] Lee L-BW, Register RA, Dean DM. Origin of directional tear in blown films of ethylene copolymers. Polym Mater Sci Eng 2000;83:482−3.
[86] Lee L-BW, Register RA, Dean DM. Origin of directional tear in blown films of ethylene/methacrylic acid copolymers and ionomers. J Polym Sci, Part B: Polym Phys 2005;43:97−106.
[87] Zhang XM, Elkoun S, Ajji A, Huneault MA. Oriented structure and anisotropy properties of polymer blown films: HDPE, LLDPE and LDPE. Polymer 2004;45:217−29.
[88] Lee L-BW, Register RA, Dean DM. Tear anisotropy in films blown from polyethylenes of different molecular architectures. J Polym Sci, Part B: Polym Phys 2005;43:413−20.

[89] Keith HD, Padden Jr FJ, Vadimsky RG. Intercrystalline links in polyethylene crystallized from the melt. J Polym Sci, Part A-2 Polym Phys 1966;4:267−81.
[90] Huck ND, Clegg PL. The effect of extrusion variables on the fundamental properties of tubular polyethylene films. In: SPE ANTEC conference; 1961. p. 18−22.
[91] Meilhon D, Wollak HF. Shrinkable thermoplastic packaging films. 1994. US patent 5356677.
[92] Meilhon D. Ready-tear packaging. 1996. US patent 5556674.
[93] Wollak HF, Rioux B. Thermoplastic film for packaging. 2003. US patent 6572979 B1.
[94] Longworth R. The physical structure of Surlyn® ionomer resins. DuPont internal report. 1967.
[95] Rohn CL. Tear strength theory of semicrystalline polymer. J Appl Polym Sci 1983;28:3011.
[96] Otten NJ, Presnell EJ. Polymer film having linear tear properties. 1978. US patent 4098406.
[97] Nottez M, Chaki S, Soulestin J, Lacrampe MF, Krawczak P. Mechanical behavior and essential work of fracture of starch-based blown films. In: International polymer processing society conference, 30; 2014. S07−597.
[98] Wong JSS, Ferrer-Balas D, Li RKY, Mai Y-W, Maspoch ML, Sue H-J. On tearing of ductile polymer films using the essential work of fracture (EWF) method. Acta Mater 2003;51:4929−39.
[99] Martínez AB, Segovia A, Gamez-Perez J, Maspoch ML. Essential work of fracture analysis of the tearing of a ductile polymer film. Eng Fract Mech 2010;77:2654−61.
[100] Bárány T, Czigány T, Karger-Kocsis J. Application of the essential work of fracture (EWF) concept for polymers, related blends and composites: A review. Prog Polym Sci 2010;35:1257−87.
[101] Mai Y-W, Cotterell B. On the essential work of ductile fracture in polymers. Int J Fract 1986;32:105−25.
[102] Rennert M, Nase M, Lach R, Reincke K, Arndt S, Androsch R, et al. Influence of low-density polyethylene blown film thickness on the mechanical properties and fracture toughness. J. Plastic Film Sheeting 2013;29:327−46.
[103] Maspoch ML, Gamez-Perez J, Gordillo A, Sanchez-Soto M, Velasco JI. Characterization of injected EPBC plaques using essential work of fracture (EWF) method. Polymer 2002;43:4177−83.
[104] Ferrer-Balas D, Maspoch ML, Martinez AB, Ching E, Lie RKY, Mai Y-W. Fracture behavior of polypropylene films at different temperatures: assessment of the EWF parameters. Polymer 2001;42:2665−74.
[105] Maspoch ML, Henault V, Ferrer-Balas D, Velasco JI, Santana OO. Essential work of fracture on PET films: influence of the thickness and the orientation. Polym Test 2000;19:559−68.
[106] Lach R, Schneider K, Weidisch R, et al. Application of the essential work of fracture concept to nanostructured polymer materials. Eur Polym J 2005;41:383−92.
[107] Kerns J, Hsieh A, Hiltner A, Baer E. Mechanical behavior of polymer microlayers. Macromol Symp 1999;147:15−25.
[108] Bernal-Lara TE, Ranade A, Hiltner A, Baer E. Nano-and Microlayered Polymers: Structure and Properties. In: Michler GH, Balta-Calleja FJ, editors. Mechanical properties of polymers based on nanostructure and morphology. Baco Raton: Taylor & Francis; 2005. p. 629−81.
[109] Hiltner A, Nazarenko S, Ebeling T, Schuman T, Baer E. Novel microlayered structures for adhesion and interdiffusion studies. Polym Mater Sci Eng 1996;75:471−2.
[110] Mueller C, Kerns J, Ebeling T, Nazarenko S, Hiltner A, Baer E. Microlayer coextrusion: processing and applications. Polym Process Eng 1997;97:137.
[111] Baer E, Jarus D, Hiltner A. Microlayer coextrusion technology. In: SPE ANTEC Conference; 1999.
[112] Bernal-Lara TE, Masirek R, Hiltner A, Baer E, Piorkowska E, Galeski A. Morphological studies of multilayed HDPE/PS systems. J Appl Polym Sci 2006;99:597−612.
[113] Bernal-Lara TE, Liu RYF, Hiltner A, Baer E. Structure and thermal stability of polyethylene nanolayers. Polymer 2005;46:3043−55.
[114] Pan SJ, Im J, Hill MJ, Keller A, Hiltner A, Baer E. Structure of ultrathin polyethylene

layers in multilayer films. J Polym Sci, Part B: Polym Phys 1990;28:1105−19.
[115] Balta Calleja FJ, Ania F, Orench IP, Baer E, Hiltner A, Bernal T, et al. Nanostructure development in multilayer polymer systems as revealed by X-ray scattering methods. Progr Colloid Polym Sci 2005;130:140−8.
[116] Jin Y, Rogunova M, Hiltner A, Baer E, Nowacki R, Galeski A, et al. Structure of polypropylene crystallized in confined nanolayers. J Polym Sci, Part B: Polym Phys 2004;42:3380−96.
[117] Guillotte JE. Co-extrusion of blown film laminates. SPE J 1969;25:20−4.

10 Adhesion

Combining different materials into a multilayer film is a useful way to achieve packaging performance needs, but without sufficient interlayer adhesion the film will fail. Many combinations of polymers and substrates used in flexible packaging do not adhere well to one another. Adhesive and tie resin technology is used to enhance the adhesion between these layers. This chapter provides an introduction to adhesion in multilayer films, including how adhesion is measured, the fundamental science and engineering of bonding surfaces, and a guide to tie layer technology for extrusion coating/lamination and coextrusion processes.

10.1 Why Adhesion is Important

The concept of combining different materials into a common film structure rests on the premise that those layers will adhere to one another. Without sufficient adhesion, the layers will delaminate and not provide the function required. Tensile strength, stiffness, and other physical properties of the film require good interlayer adhesion. Puncture, impact, tear, and scratch resistance are influenced by the transfer of stress between layers, which is influenced by adhesion. The question becomes, how much adhesion is sufficient? In some snack structures, 50 g/25 mm is deemed sufficient. In other rigid packaging applications, 4000 g/25 mm may be specified. The requirement varies with the film structure and application. Even within a film structure, adhesion between some layers may be more demanding than others. For example, in a barrier film structure, the layers on the outside of the barrier layer may have lower adhesion requirements than those on the inside; preventing layer delamination between the barrier layer and the product may be critical for stopping oxygen or moisture from penetrating into the package.

In some applications, "inseparable" adhesion is not the best adhesion. Instead, controlling the adhesion within a certain range may be important. For example, delamination peel–seal technology (Section 7.7) relies on controlled adhesion between the sealant layer and the adjacent layer to provide an easy-open feature. In some cases, films may provide better resistance to tear or puncture if their layers delaminate during the event. In other instances, a film may be laminated onto a substrate to protect it during transportation but must be easily stripped off for retail use; adhesion in such cases is required to be fairly low.

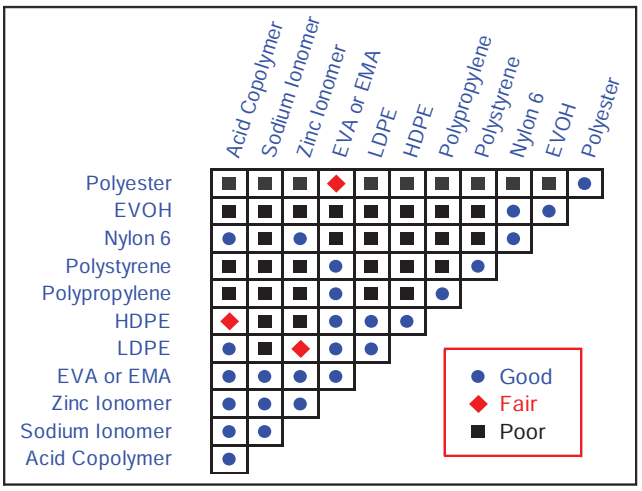
Adhesion depends on the fabrication method, the chemistry of the layers, and the relative configuration of the layers to each other. If the multilayer film is fabricated from premade films or substrates, these films will require an adhesive or glue to bond them to one another. This is typically accomplished using an adhesive or extrusion lamination process. When bonding a polymer melt to a solid substrate, as in extrusion coating and lamination, the coating parameters such as temperature, line speed, air gap, and draw down are important. In coextrusion blown or cast film where the polymers are joined in the melt, temperature, contact time, and quench conditions are important. The influence of processing on adhesion is explored briefly in Section 10.4 and in greater detail in Chapter 15.

Many combinations of resins used to make coextrusion films for flexible packaging do not naturally bond to one another. This is illustrated in Table 10.1 where combinations that have poor adhesion are represented by a square. For these combinations, tie resins have been developed to provide adhesion; the tie resin is sandwiched between the two incompatible layers. Tie layer technology is described in Section 10.4. While the tie layer technology is critical, other factors influence adhesion in coextrusion, including the structure design (what is being bonding to what, layer thicknesses), the fabrication process, and the end-use.

Polymer coatings onto solid substrates depend on the chemistry as shown in Table 10.2. Oxidation is often used to impart sufficient polarity to LDPE to achieve adhesion to polar substrates such as paper and aluminum foil. This is not sufficient to obtain good

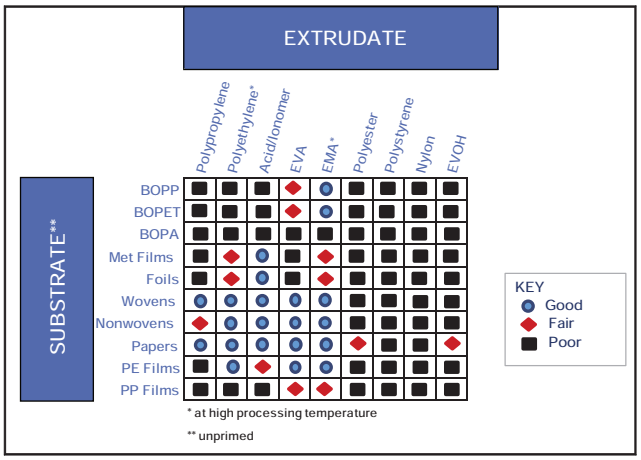
The Science and Technology of Flexible Packaging. http://dx.doi.org/10.1016/B978-0-323-24273-8.00010-1
Copyright © 2017 Elsevier Inc. All rights reserved.

Table 10.1 Adhesion of Various Polymers in Coextrusion



EMA, ethylene methyl acrylate; *EVA,* ethylene vinyl acetate; *EVOH,* ethylene vinyl alcohol; *HDPE,* high density polyethylene; *LDPE,* low density polyethylene.
Reproduced with permission from E. I. du Pont de Nemours and Company.

Table 10.2 Adhesion of Various Polymers (Extrudates) to Solid Packaging Substrates



BOPA, biaxially oriented polyamide (nylon); *BOPET,* biaxially oriented polyethylene terephthalate; *BOPP,* biaxially oriented polypropylene; *EMA,* ethylene methyl acrylate; *EVA,* ethylene vinyl acetate; *EVOH,* ethylene vinyl alcohol; *Met films,* metallized films; *PE,* polyethylene; *PP,* polypropylene.
Reproduced with permission from E. I. du Pont de Nemours and Company.

bonds to OPET or OPP as is highlighted in Table 10.2. Acrylates, vinyl acetate, acid, anhydride, and other functionalities can be incorporated into the polymer, through copolymerization or grafting, to enhance adhesion to specific substrates. Even with such functionality, additional methods may be needed to achieve good adhesion. These include ozone treatment of the melt curtain (especially for LDPE); corona, ozone, flame, or plasma treatment of the substrate; and the use of chemical primers on the substrate.

10.2 How to Measure Adhesion

10.2.1 Peel Test

The peel test is the most commonly used method for measuring adhesion in flexible packaging. The peel test comes in a variety of forms, varying in angle and apparatus. Mount [1] counted 23 different procedures listed in the ASTM index plus another 40 under the term "adhesive bonding." Other organizations, such as the Association of Industrial Metallizers, Coaters and Laminators (AIMCAL), have additional procedures. Perhaps the most often used procedure is the "T-peel" test described in ASTM D1876 [2]. In this procedure, a rectangular specimen 25.4 by 305 mm is cut from the film. The layers are separated at the interface the adhesion is to be

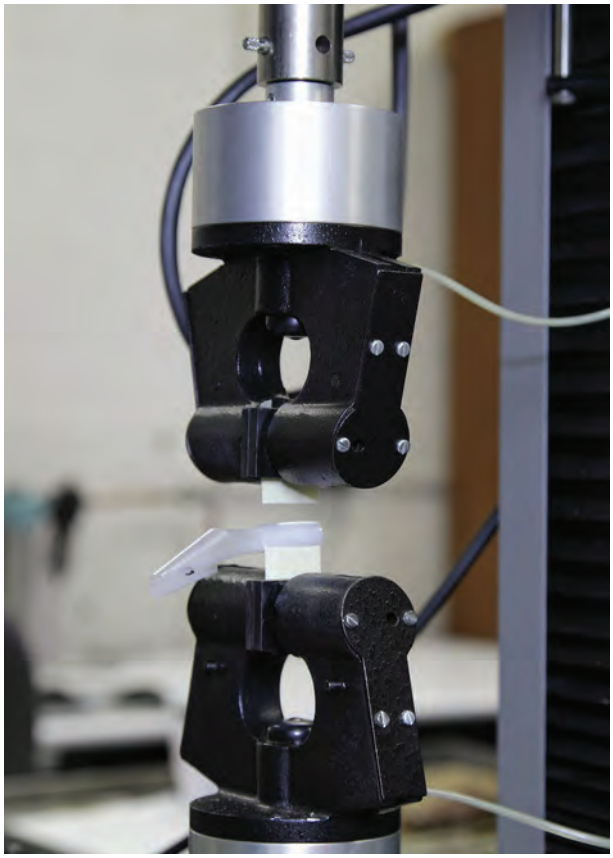


Figure 10.1 Photo of peel test. Picture by Vladimir Antonov.
Reproduced with permission from E. I. du Pont de Nemours and Company.

Table 10.3 Unit Conversion Factors for Peel Strength

	g/in	g/25 mm	g/15 mm	lb/in	N/25 mm	N/15 mm	J/m^2 (N/m)
g/in	1	1	0.6	0.0022	0.0098	0.0059	0.392
g/25 mm	1	1	0.6	0.0022	0.0098	0.0059	0.392
g/15 mm	1.67	1.67	1	0.0037	0.0163	0.0098	0.654
lb/in	454	454	272.4	1	4.44	2.67	178
N/25 mm	102	102	61.2	0.225	1	0.6	40
N/15 mm	170	170	102	0.375	1.67	1	66.7
J/m^2 (N/m)	2.55	2.55	1.53	0.0056	0.025	0.015	1

Multiply by the factor to convert from the unit in the first column to the corresponding unit in the first row. For example, 1 g/25 mm = 0.0098 N/25 mm.

measured. The separated ends become what are known as the peel arms. These peel arms are clamped in the jaws of a tensile tester (Fig. 10.1) and pulled apart at a constant speed. The force to pull the peel arms apart is recorded. Peel strength is reported as the peel force divided by the specimen width, such as g/25 mm. Conversion factors for commonly used units are given in Table 10.3. The mode of failure is also recorded along with any descriptors as to how the specimen failed. These may include terms such as cohesive, adhesive, partial tear, and so on. These descriptors can be important for determining why adhesion may have changed from one measurement or structure to another.

The angle, peel speed, specimen width, and temperature all influence the peel strength result. ASTM D1876 calls for a peel speed of 254 mm/min (10 inches/min). Other commonly used test speeds include 50.8 mm/min (2-inch/min) and 25.4 mm/min (1-inch/min). Specimen width is 25.4 mm in the standard, but 15 and 10 mm are often used, especially in Europe and Japan. Standard conditions of 23°C and 50% RH are specified in the standard.

Converting results based on different specimen widths is fairly straightforward; the peel strength varies linearly with width. So if a result is reported as 100 g/15 mm, the result for 25 mm width should be proportionally higher: 100 g/15 mm × 25/15 = 167 g/25 mm.

Results run at different test speeds and temperatures cannot be directly compared. The effect of these parameters on peel strength is examined in detail in Section 10.2.3. The peel angle is an another important parameter. ASTM D1876 calls for placing the peel arms into the tensile tester jaws; the two peel arms form a 180° angle relative to one another. The actual angle between the peel arms and the substrate is not controlled; it is allowed to establish whatever angle is dictated by the forces on the peel arms and substrates. The actual angle during the pull is important since it affects the amount of energy expended during the pull on bending and stretching the peel arms. The angle influences the concentration of stress as the peel front moves through the specimen. In scientific investigations of peel strength, the angle is typically controlled. This may be done simply by manually holding the peel tab during the pull so that it maintains a 90° angle with the peel arms (a true "T"). A variation is to hold or mount the specimen so that the peel tab forms a 180° angle with one of the peel arms. This is known as a 180° peel test. These configurations are illustrated in Fig. 10.2. Special sleds have been designed to explore other angles so that as the peel progresses, the angle remains constant. A variation on this is the German

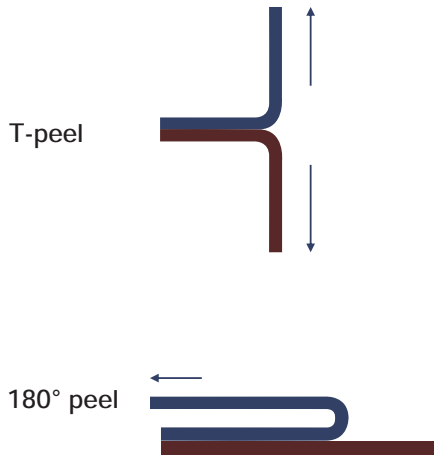


Figure 10.2 Peel angle configurations during peel tests.

wheel, usually used to test rigid structures, described in DIN 53357 [3]. Here the specimen is mounted to the circumference of a large wheel that freely rotates. The peel arm is clamped to the jaw of the tensile tester above the wheel. As the jaw pulls the peel arm from the substrate, the wheel rotates, keeping the angle at a constant 90°.

10.2.2 Adhesion of Coatings

Adhesion of thin coatings or ink on films is difficult to measure using a peel test. Various tape tests have been developed [4–6], where a pressure-sensitive tape is applied to the surface of the coating. When the tape is removed, the amount of area of the coating that is pulled from the substrate is recorded. A variation on this test involves scoring a grid pattern in the coating prior to applying the tape. When the tape is removed, the number of grids that have been removed can be counted for an accurate measurement of the surface area removed.

The specific type of tape, and how it is applied and removed can affect the results of these types of tests. They generally are more useful as a go/no-go quality control test rather than a quantitative measurement of adhesion.

AIMCAL [1] has developed a laboratory test for measuring the adhesion of the metallized layer from the film substrate in metallized films. The test involves constructing a specified structure by heat sealing an adhesive film to the metallized surface along with a backing layer. The adhesive film and backing layer are then pulled from the metallized film using a T-peel test. The test is designed to mimic the failure mode in a real packaging laminate, although the results are only good enough for quality control purposes. The actual adhesion in a real laminate will differ due to differences in lamination technique, structure, and so on.

10.2.3 Fracture Mechanics Analysis of Peel Test

Peel strength is a measure of the force required to separate the peel arms from each other or from a substrate. On a fundamental level, it involves propagating a crack along the interface as new interfacial area is created. The engineering discipline of fracture mechanics, introduced in Section 7.5.6, can be used to analyze the peel test and gain insight on how the peel test parameters (imposed angle and rate) and viscoelastic properties of the peel arms affect

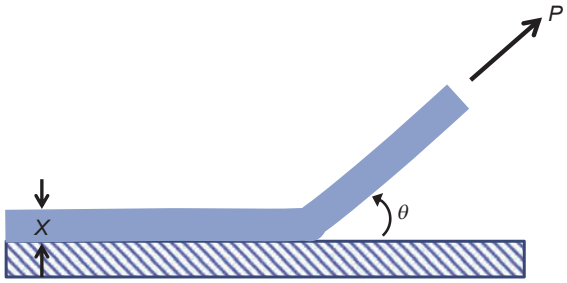


Figure 10.3 Peel test with peel force P, peel arm thickness X, peel arm width b; and peel angle θ.

the result [7,8]. Fig. 10.3 shows a schematic of the peel test where a force P is imposed at an angle θ, causing the peel arm to delaminate over a distance a. The width of the peel arm is b and thickness X. The external work imposed on the interface is equal to the peel force times the distance traveled as given by Eq. (10.1):

$$W_{\text{ext}} = Pd \tag{10.1}$$

where W_{ext} = external work, P = peel force, d = travel distance of the peel force.

After peeling, the length of the peel arm is simply the original length of the peel arm, L_0, plus the peeled distance a, plus any extension of the peel arm during peeling:

$$L = L_0 + a(1 + \varepsilon_a) \tag{10.2}$$

where L = length of peel arm after peeling, L_0 = initial length of peel arm, ε_a = inelastic extension of peel arm ($= \Delta a/a$), a = peeled distance.

Referring to Fig. 10.4, due to geometric considerations, the peel force travel distance is given by Eq. (10.3):

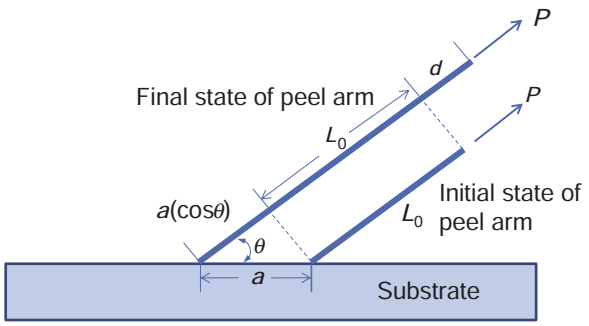
$$d = (1 + \varepsilon_a - \cos\theta)a \tag{10.3}$$

Substituting Eq. (10.3) into Eq. (10.1) yields

$$W_{\text{ext}} = P(1 + \varepsilon_a - \cos\theta)a \tag{10.4}$$

An energy balance shows that the external work is equal to the sum of the energy of creating new interfacial area, the energy of extending the peel arm, and the energy of bending the peel arm:

$$W_{\text{ext}} = U_a + U_e + U_b \tag{10.5}$$



Length of peel arm after peeling:

$$L_o + a(1+\varepsilon_a) = a(\cos\theta) + L_0 + d$$

$$\therefore d = a(1+\varepsilon_a - \cos\theta)$$

Figure 10.4 Geometry of peel test force displacement.

where W_{ext} = external work,

$$U_a = \text{energy of fracture} = G_a ab, \tag{10.6}$$

$$U_e = \text{energy of elongation} = G_e ab, \tag{10.7}$$

$$U_b = \text{energy of bending} = G_b ab, \tag{10.8}$$

G_a = fracture energy = energy to create new surfaces per unit area of peel propagation, G_e = energy dissipated during peel arm elongation per unit area of peel propagation, G_b = energy dissipated during bending of the peel arm per unit area of peel propagation, a = peel distance, b = peel arm width.

Substituting Eqs. (10.4), (10.6), and (10.7) into (10.5) and rearranging gives the following general equation for peel strength:

$$\frac{P}{b} = \frac{G_a + G_e + G_b}{1 + \varepsilon_a - \cos\theta}. \tag{10.9}$$

The fracture energy is the energy needed to create new interfacial area as the peel arms are pulled away from each other. This involves breaking bonds as well as overcoming local deformation during the creation of the new area at the peel front. The local deformation gives rise to viscoelastic energy dissipation, which can be significant for many polymers used in flexible packaging. The fracture energy is often written as the product of these two factors:

$$G_a = W_a(1 + \Phi(R, T)) \tag{10.10}$$

where W_a = work of adhesion, Φ = local viscoelastic energy dissipation, R = rate of pull, T = temperature.

The work of adhesion encompasses wetting and bonding at the interface. This term is often smaller than Φ but since it has a multiplying effect, it is very important. The effect of peel test pull rate and temperature enter through their effect on local viscoelastic dissipation.

If the peel arms have infinite tensile stiffness (no extension or $\varepsilon_a = 0$) and zero bending stiffness (zero modulus), the material takes on the behavior of an "infinitely rigid string." This essentially ignores stretching and bending of the peel arm and Eq. (10.9) reduces to:

$$G_a^{\infty E} = \frac{P}{b}(1 - \cos\theta) \tag{10.11}$$

where $G_a^{\infty E}$ = fracture energy of an infinitely rigid string.

In this case, the measured peel strength (P/b) is directly related to the fracture energy. Often the elongation and bending of the peel arm are ignored in flexible packaging, but as is described below this is generally not a good assumption.

If the peel arm undergoes tensile deformation but the bending stiffness is still zero, Eq. (10.9) becomes:

$$G_a^{eb} = \frac{P}{b}(1 + \varepsilon_a - \cos\theta) - X\int_0^{\varepsilon_a} \sigma d\varepsilon \tag{10.12}$$

where G_a^{eb} = fracture energy of an elastic peel arm with zero bending modulus, X = thickness of peel arm, σ = stress, ε = strain.

Here the integral term is simply the area under the stress–strain curve in a tensile test of the peel arm and represents the energy to elongate the peel arm.

The bending energy contribution to Eq. (10.9) can be significant if there is plastic yielding of the peel arm. Gent and Hamed [9] studied the plastic yielding of OPET film during bending. They note that peel strength often has been observed to go through a maximum at intermediate thickness. Gent and Hamed conclude that at low thickness, plastic yielding occurs, but the total dissipated energy is small. As thickness increases, more energy is dissipated and peel strength increases with G_b. Eventually, the peel arm gets too stiff and less yielding occurs, which leads to a reduction in G_b and peel strength. At high thickness, no yielding occurs and G_b is small.

Kinloch, Lau and Williams [8] use a beam theory approach to compute G_b. The peel arm goes through a loading and unloading cycle as the crack propagates and the peel arm is straightened out afterward. Bending with large displacements can occur which they describe with beam theory. Both elastic and plastic deformation is considered. They derive a set of equations that can be easily solved iteratively using standard software tools. Their results are highlighted here but the reader is referred to the original paper for the appropriate equations.

Kinloch's model allows for the rotation of the "beam" representing the peel arm; the local angle at the peel front, θ_0, may differ from the imposed angle, θ. At the extremes, if $\theta_0 = 0$ then all the energy for delamination is transmitted during bending of the peel arm. If $\theta_0 = \theta$ then the peel arm has zero bending modulus and acts as a string; all the energy is transmitted directly to the interfacial region. For most laminates $0 < \theta_0 < \theta$ and energy is transmitted both directly and through bending of the peel arm. Of particular interest is how the local bending angle is influenced by the stiffness and thickness of the peel arm since the local angle can affect the concentration of stress at the interface. For example, Pascal [10] shows that the coating thickness in extrusion coating affects the bending angle and peel strength.

As described by Eq. (10.9), the measured peel force, P, is dependent of the test geometry; it will vary with test angle, speed, and the laminate structure. The fracture energy, G_a, is a better parameter for adhesion since it is less dependent on these factors. While computing G_a is often a useful exercise, the peel force measurement is sufficient in practice if its limitations are clearly understood. These limitations are explored in more detail later, using the experimental work of Kinloch, Lau and Williams as an illustration.

10.2.3.1 Peel Angle

Kinloch [8] measures peel strength of four laminate structures characteristic of those found in flexible packaging:

1. 6 μm Al//PE1. PE is extrusion coated onto the aluminum foil (Al). The PE thickness ranges from 30 to 250 μm. For the peel measurement, the Al is bonded to a rigid support and the PE peeled away from it: Al is the substrate and PE the peel arm.
2. 6 μm Al//PE2. PE2 differs from PE1 in molecular weight distribution and orientation, resulting in different physical properties. Al is the substrate and PE the peel arm.
3. 12 μm OPET//(10 μm Tie1−20 μm PE1). This structure is made via coextrusion coating of the tie and PE onto the OPET film. During the peel test, the PE is mounted and becomes the substrate from which the OPET is peeled away (as the peel arm).
4. 12 μm OPET//(10 μm Tie2−20 μm PE1). This is the same as structure 3 except a different tie resin is used. Both tie resins are modified polyethylene. The PE is the substrate and the OPET is the peel arm.

Kinloch uses a special sled to control the angle and test speed during the peel tests. The angle is varied from 30 to 180 degrees. Peel speed is 5 mm/min. Tensile tests are conducted on the peel arms to obtain parameters for their model. Optical microscopy is used to measure the local peel angle, θ_0, during peeling. $G_a^{\infty E}$ is computed using Eqn. (10.11) and G_a using their model, taking into account both extension and bending of the peel arm.

The local peel angle, θ_0, is plotted vs the imposed peel angle, θ, in Fig. 10.5. There is a good agreement between the measured values (shown in the figure) and the model calculation for θ_0 (not shown). For all four structures $0 < \theta_0 < \theta$ indicating the peel force is transferred to the interface directly and through bending as described earlier. The two structures with PE as the peel arm (1 and 2) give similar results, as do the two structures with OPET as the peel arm (3 and 4). The initial peel angle with PE as the peel arm is significantly higher at a given imposed angle than when OPET is the peel arm. This reflects the greater stiffness of the OPET. Structure 2 has somewhat higher θ_0 than structure 1. Structure 2 also has substantially higher G_a than structure 1 (Table 10.4).

Fig. 10.6 shows peel strength (P/b), $G_a^{\infty E}$, and G_a as a function of imposed peel angle for structures 1 and 3. Structures 2 and 4 behaved similarly to structures 1 and 3, respectively, and are not shown. Peel strength decreases with increasing angle, as is expected from the $(1-\cos\theta)$ dependence from geometric considerations. Yet the simple form of Eq. (10.11) is not sufficient to account for the angular effect as is shown by the rise in $G_a^{\infty E}$ with increasing angle. As the angle increases, more elongation and

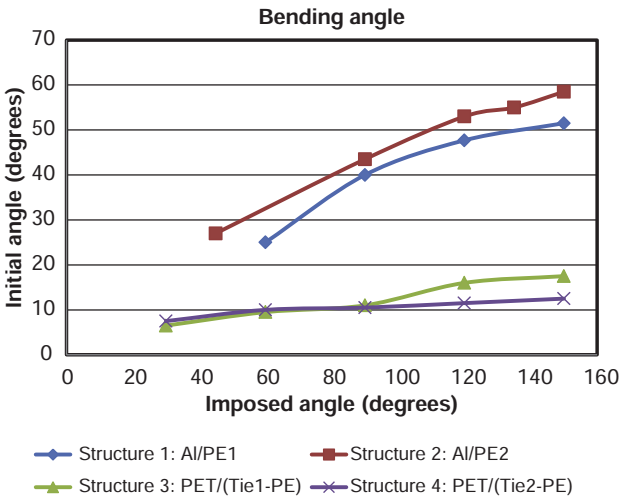


Figure 10.5 Effect of peel test angle (imposed angle) on the local angle near the peel front, θ_0. Peel speed is 5 mm/min.
Data from Kinloch AJ, Lau CC, Williams JG. The peeling of flexible laminates. Int J Fract 1994;66:45–70.

Table 10.4 G_a for the Four Structures

Structure	Structure	Peel Arm	G_a (J/m^2)
1	Al/PE1	PE	133 ± 6
2	Al/PE2	PE	228 ± 7
3	OPET/(Tie1-PE1)	OPET	46.7 ± 8.1
4	OPET/(Tie2-PE1)	OPET	24.1 ± 3.0

Data from Kinloch AJ, Lau CC, Williams JG. The peeling of flexible laminates. Int J Fract 1994;66:45–70.

bending occurs, which must be taken into account. Kinloch's model provides values for G_a, which are nearly independent of angle. So while the measured peel strength varies with peel angle, the fracture energy is independent of angle if computed correctly. It is often challenging to compute the fracture energy from raw peel strength data. For the most part the industry simply uses peel strength and so care must be taken to ensure the angle is specified.

Values for the average value of G_a for the four structures are given in Table 10.4. G_a for structures 1 and 2 (PE peel arm) is considerably higher than that for structures 3 and 4 (PET peel arm). This reflects differences in bond strength but also differences in viscoelastic properties of the peel arm. The flexible PE peel arm likely has greater local viscoelastic dissipation (Φ) than the OPET peel arm in structures 3 and 4. Comparing structures 1 and 2, G_a is considerably higher for structure 2. The bond strength of PE1 and PE2 is likely similar since both grades rely on oxidation during coating to create polar species for adhering to the metal oxides on the foil. The substantial difference in G_a, therefore, likely reflects differences in viscoelastic dissipation.

10.2.3.2 Peel Rate, Temperature, and Viscoelasticity

The effect of peel rate and temperature on peel strength is complicated due to a number of transitions the polymer may go through. For a detailed discussion, the reader is referred to Wu [7]. In general, as the temperature is increased at a constant peel rate, peel strength decreases and the failure mode may transition from cohesive to interfacial. As peel rate is increased at constant temperature, peel strength typically increases, but decreases sharply when the failure mode changes from cohesive to interfacial. These transitions generally correspond to viscoelastic transitions in the bulk adhesive and can be thought of as equivalent. Indeed, investigators have constructed master curves for G_a by using appropriate shift factors for the peel rate and temperature.

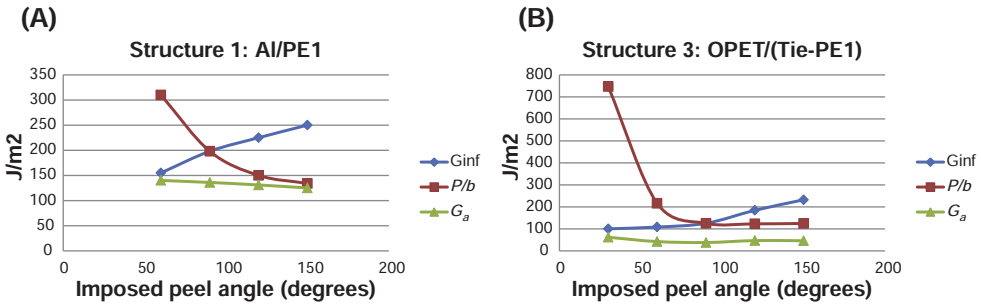


Figure 10.6 Effect of peel strength (P/b), fracture energy of an inelastic string ($G_a^{\infty E}$), and fracture energy from Kinloch model [8] (G_a). Peel speed is 5 mm/min.
Data from Kinloch AJ, Lau CC, Williams JG. The peeling of flexible laminates. Int J Fract 1994;66:45–70.

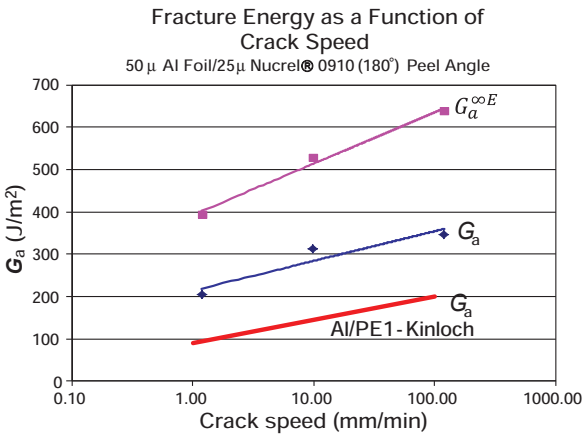


Figure 10.7 The effect of peel rate on peel strength. Bottom curve is G_a data from Kinloch [8] from measurements on the structure Al//35 μm PE1. The top and middle curves are data from DuPont on the structure Al//25 μm EMAA; the top and bottom curves are $G_a^{\infty E}$ and G_a, respectively.
Courtesy of E.I. du Pont de Nemours and Company and reproduced with permission.

One way the peel rate affects the peel test measurement comes in through the local viscoelastic energy dissipation at the crack tip, Φ, as described in Eq. (10.10). Kinloch [8] plots G_a for structure 1 (Al/PE1, as described in Section 10.2.3.1) as a function of the crack speed, which is the test peel rate divided by $(1 + \varepsilon_a - \cos\theta)$. The PE thickness is 35 μm and data for several peel angles are superimposed onto a single curve reproduced in Fig. 10.7. Included in Fig. 10.7 is data for the structure 51 μm Al//25 μm EMAA, where the EMAA (ethylene methacrylic acid copolymer) is Nucrel 0910, a 10 wt % MAA grade from DuPont. These DuPont measurements were conducted with a 180° peel angle. From Eq. (10.11), $G_a^{\infty E}$ is simply $2(P/b)$ at this peel angle. $G_a^{\infty E}$ and G_a results are both plotted, where G_a is computed using the Kinloch model that accounts for both bending and stretching of the peel arm.

The results presented in Fig. 10.7 provide a number of insights into peel strength performance, which include the following:

- The positive slope indicates that higher peel rate increases the local viscoelastic energy dissipation at the crack tip (Eq. (10.10)). If the curves were extrapolated to zero speed, the result theoretically would be W_a. Kinloch notes that in previous work investigating styrene–butadiene rubber bonding to various polymer substrates, the curve extrapolated to values of around 0.05 J/m^2, which is the order of magnitude for secondary van der Waals forces. Whether these curves would actually extrapolate to such a low value is undetermined with the limited data provided, and the value of W_a is likely higher due to the presence of chemical interaction between polar oxidative species on the PE formed during extrusion coating and the aluminum oxide on the surface of the foil. The slope, however, shows that the measured energy is at least an order of magnitude greater than the bond strength, underscoring the importance of the deformation zone at the peel front and the viscoelastic properties of the peel arm from which it arises.
- Comparing G_a for PE and EMAA gives an indication of the effect of bonding strength. Both curves have similar slopes and both peel arms have similar physical properties. Hence, the shift upward from PE to EMAA reflects the stronger bonds formed by the acid groups in EMAA to the oxides on the aluminum surface.
- The difference between G_a and $G_a^{\infty E}$ for EMAA reflects the impact of bending and stretching the peel arm. Roughly half the measured peel strength for this structure is due to these factors.

The viscoelastic nature of the adhesive influences the peel strength. Consider the three adhesive materials illustrated in Fig. 10.8 taken from Wu [7]. Materials I, II, and III are rubbery, liquid-like, and strain-hardening, respectively. The dashed horizontal lines represent two scenarios for the maximum interfacial stress. When the stress measured during peel testing exceeds the maximum interfacial stress of the structure, failure occurs. This happens where the stress–strain curve intersects the horizontal line. If the maximum interfacial stress is represented by the bottom line, then all three materials fail adhesively (or interfacially) with about the same peel strength. If the maximum interfacial stress is represented by the top line, then material I fails first (adhesively). Materials II and III have a large deformation energy contribution that is given by the area under their stress–strain curve. Material II eventually fails cohesively and III adhesively. In this case, the measured peel strength of II and III will be considerably higher than material I.

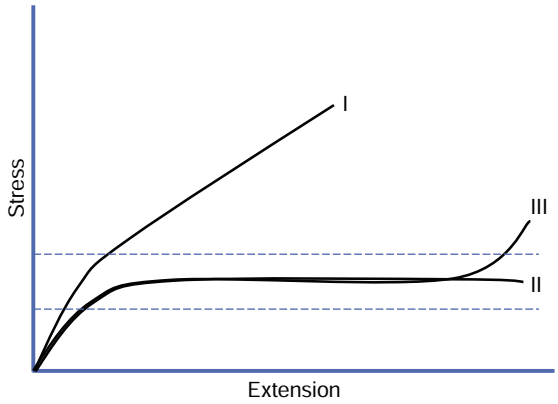


Figure 10.8 Illustration of stress–strain curves for rubbery (I), liquid-like (II), and strain-hardening (III) materials and their influence on peel strength. *Dashed horizontal lines* represent two scenarios for the maximum interfacial strength as described in the text.
Adapted from Wu S. Fracture of adhesive bond. In: Polymer interface and adhesion. New York: Marcel Dekker, Inc.; 1982. p. 475–569.

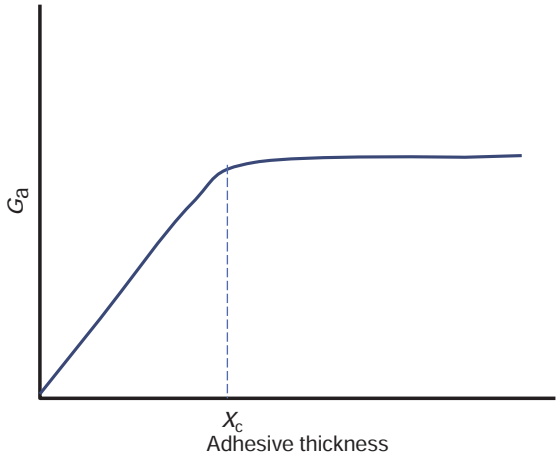


Figure 10.9 Effect of adhesive thickness on G_a.

The molecular structure influences the shape of the stress–strain curve but so does the rate and temperature. Decreasing the temperature or increasing the rate may change the material from II to I, which changes the peel failure mode from cohesive to adhesive and decreases the peel strength.

In multilayer structures with adhesives, both the adhesive and the adjoining layers that make up the peel arm influence the peel strength. Gent [9] shows that the bending angle and thickness of OPET films affect the bending energy, which goes through an abrupt increase when the film yields. This bending force affects the measured peel strength, as is mentioned earlier. Gent finds, however, when the adhesion of the OPET to the substrate is strong, the peel strength is much higher than the bending mechanics of the OPET layer would suggest. They conclude that deformation in the adhesive layer makes up the difference.

10.2.3.3 Thickness

Fracture mechanics predicts that the fracture energy, G_a, increases with increasing thickness up to a critical thickness, X_c, after which G_a is constant. This is illustrated in Fig. 10.9. The zone of deformation in front of the peel, which gives rise to Φ extends across the entire thickness of the adhesive when the thickness is small. Indeed, the size of the zone of deformation is constrained by the adhesive thickness as is illustrated in Fig. 10.10A. As the thickness is increased, the size of the zone of deformation increases along with Φ. When the thickness of the adhesive equals the critical thickness, the zone of

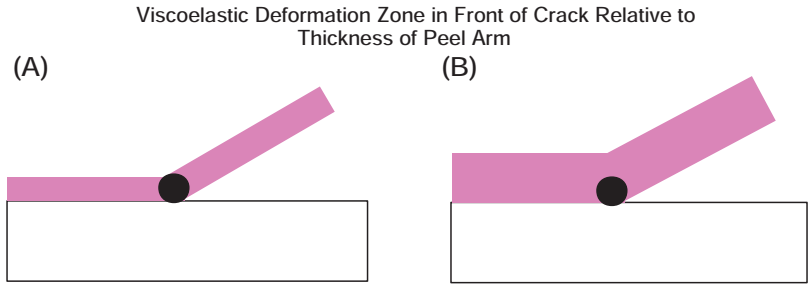


Figure 10.10 Cartoon of the influence of the thickness on the size of the zone of deformation in front of the advancing peel or crack. (A) thickness is less than natural size of zone of deformation, (B) thickness is greater than natural size of deformation.
Reproduced with permission from Morris BA. Understanding why adhesion in extrusion coating decreases with diminishing coating thickness. J Plastic Film Sheeting 2008;24:53–88.

deformation has reached its natural size. Further increases in the adhesive thickness result in no further increase in the size of the zone of deformation and G_a is constant (Fig. 10.10B).

The critical thickness of the adhesive is the radius of the plastic zone at the peel front (or crack tip in the language of fracture mechanics), r_y. From Kinloch and Young [12], a stress analysis for plane stress gives:

$$r_y = \frac{1}{2\pi}\left(\frac{K_I}{\sigma_y}\right)^2 \tag{10.13}$$

where r_y = radius of plastic zone at crack tip, K_I = stress intensity factor, σ_y = yield strength.

The stress intensity factor comes from an analysis of the stress on the advancing peel front. It is defined as the maximum stress at the crack tip divided by the imposed stress and is typically >1. It is used to account for the fact that failure generally occurs at loads considerably less than the idealized strength of the interface. The stress is thought to be amplified at the crack tip. When the stress analysis is equated with the energy analysis previously introduced, K_I is found to be directly related to G_a and E (modulus):

$$K_I^2 = EG_a. \tag{10.14}$$

Combining Eqs. (10.13) and (10.14) and letting $X_c = r_y$:

$$X_c = \frac{1}{2\pi}\frac{G_a E}{\sigma_y^2}. \tag{10.15}$$

Eq. (10.15) shows that the critical thickness increases with increasing modulus and decreasing yield strength. It also increases with increasing G_a, which is a circular argument: the size of the zone of deformation depends on the fracture energy, which depends on the amount of deformation. This makes sense if one considers that anchoring the peel arm to the substrate more strongly will allow for more deformation to occur as the peel arm is pulled away. The same argument can be made for bending and stretching the peel arm. If the adhesion is stronger, the peel arm can be pulled away at a steeper angle, resulting in more bending and possible yielding of the adhesive and adherend. Similarly, more stretching of the peel arm may occur when it is more firmly attached to the substrate.

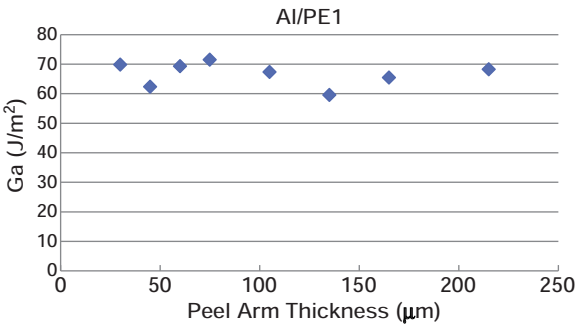


Figure 10.11 G_a as a function of PE1 thickness for the structure Al//PE1. Peel angle is 180 degrees and rate 1 mm/min.
Data from Kinloch AJ, Lau CC, Williams JG. The peeling of flexible laminates. Int J Fract 1994;66:45–70.

Kinloch [8] measures G_a for Al/PE1 (structure 1 introduced in Section 10.2.3.1) with the peel arm (PE1) thickness ranging from 30 to 215 μm. The peel angle is 180 degrees and peel rate 1 mm/min. The results are plotted in Fig. 10.11. G_a is mostly constant. A calculation of X_c yields a value of 15–20 μm, suggesting that the thickness range explored by Kinloch is on the plateau region of the curve. Wu [7] reviews several studies that show an increase in fracture energy with increasing thickness similar to that shown schematically in Fig. 10.8.

The effect of thickness is further explored in Sections 10.4.2.2.3 and 15.1.4.

10.3 Fundamentals

Adhesion is the state in which two dissimilar materials are in such intimate contact that mechanical force or work can be transferred across their interface. The interfacial bonding forces may arise from thermodynamics, mechanical interlocking, chemical bonding, or electrostatic attraction. The mechanical strength of the adhered system is a function of interfacial attraction, the strength of the interface, and the cohesive strength of the two bulk phases.

The adhesion at an interface predicted from theoretical considerations is generally much greater than what is measured. Fracture mechanics, introduced in Section 10.2.3, resolves this discrepancy by introducing the concept of defects. The fracture energy involves the propagation of these defects or cracks and the generation of new interfacial area. As described by Eq. (10.10), the fracture energy has contributions from the work of adhesion and viscoelastic deformation. The adhesion component arises

from the reversible work of adhesion (thermodynamics), diffusion, and chemical interaction. This section briefly explores each of these contributions to adhesion performance. The terms "adhesive" and "substrate" will be used in this section to describe bonding between layers. The adhesive may be a specially formulated material for bonding, such as a liquid adhesive used in lamination or a polymeric tie layer in coextrusion, or it may simply be one of the two layers at the interface. The substrate may be a solid substrate such as OPET film, paper, or aluminum foil, or it may designate a molten polymer layer in a coextrusion, depending on the context of the discussion.

10.3.1 Thermodynamics of Adhesion

10.3.1.1 Surface and Interfacial Tension

When two materials are joined, they form a region of finite thickness between them over which the composition and energy vary continuously from one bulk phase to the other. This is known as the interface. A tension is created at the surface of a material due to the energy difference between the material and the medium at the surface (such as air). When two materials are joined by an interface, an interfacial tension develops. The concept of interfacial tension at a polymer–polymer interface is introduced in Section 6.4.2 and Figure 6.14.

The surface tension (also known as the surface energy) of solids is not determined directly, but rather is typically measured by the response of a liquid or liquids on the surface, usually in the presence of air or a saturated vapor of the test liquid. Two techniques are commonly used. The practical test is the dyne test [13,14], which uses calibrated formulations of 2-ethoxyethanol and formamide. A test solution (often in the form of a marker pen) is applied onto the surface to estimate the surface energy. The second approach is to measure contact angles, which requires laboratory equipment. The contact angle is the angle a droplet forms on the surface of a solid as shown in Fig. 10.12. Young's equation relates the cosine of the contact angle to the interfacial tensions at the solid–liquid–vapor interface:

$$0 = \gamma_{SV} - \gamma_{SL} - \gamma_{LV}\cos\theta_c \qquad (10.16)$$

where γ_{SV} = interfacial tension between the solid and vapor phases, γ_{SL} = interfacial tension between the solid and liquid phases, γ_{LV} = interfacial tension between the liquid and vapor phases, θ_c = contact angle.

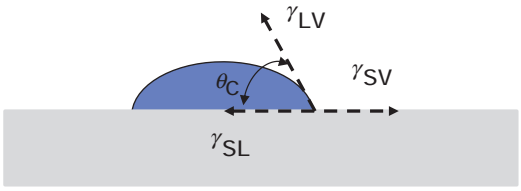


Figure 10.12 Contact angle and associative surface tensions.

In a method known as the Zisman plot, $\cos\theta_c$ is plotted vs γ_{LV} for a series of homologous liquids. The value of γ_{LV} at a point extrapolated to $\cos\theta_c = 1$ is known as the critical surface tension of the solid. Other methods involve measuring the contact angle of a polar (water) and nonpolar (methylene iodide) liquid on the substrate, from which the surface energy can be calculated by various averages. These methods tend to yield more accurate values according to Wu [15]. The critical surface tension from the Zisman plot is often smaller than the surface tension measured by other techniques. The surface tension and critical surface tension of several polymer substrates are given in Table 10.5.

A pendant drop method is often used to measure the surface tension of polymer melts. The surface tension of polymer melts decreases linearly with increasing temperature. A series of measurements at different temperatures can be used to extrapolate a

Table 10.5 Surface Tension of Solid Polymer Films at 20°C

Polymer	Surface Tension (dynes/cm)	Critical Surface Tension (dynes/cm)
Polyethylene	35.7	31
Polypropylene	30.1	32
Polystyrene	40.7	33
Polyvinyl chloride	42.9	39
Polyethylene terephthalate	42.1	43
Polyamide 66	44.7	46

Data from Wu S. Interfacial and surface tensions of polymer melts and liquids. In: Polymer interface and adhesion. New York: Marcel Dekker, Inc.; 1982. p. 67–132.

Table 10.6 Surface Tension of Polymer Melts

Polymer	Temperature (°C)	Surface Tension (dynes/cm)
Linear polyethylene	180	26.5
Branched polyethylene (LDPE)	180	24.6
Ethylene vinyl acetate (17.7 wt% VA)	180	25.5
Ethylene vinyl acetate (26.6 wt% VA)	180	25.4
Polypropylene	180	20.8
Polystyrene	180	29.2
PET	300	26.4
PA 66	300	28.3

Data from Wu S. Surface tension and polarity of solid polymers. In: Polymer interface and adhesion. New York: Marcel Dekker, Inc.; 1982. p. 169–214.

value for the polymer solid. This method typically agrees well with the liquid homolog methods. Surface tensions of several polymer melts used in flexible packaging are given in Table 10.6.

The surface tension of a polymer decreases with decreasing density. Thermal transitions that change the density can affect the surface tension. During the glass transition, the surface tension undergoes a continuous change and the slope of the surface tension vs temperature curve changes. For semicrystalline polymers, as the polymer is cooled from the melt crystallization increases the density, resulting in a discontinuous increase in the surface tension. Most polymer films have an amorphous region at the surface; as the polymer cools and solidifies, polymer chain segments not participating in forming crystals are pushed toward the surface. Thus, typical measurements of solid polymers reflect the surface tension for the amorphous phase (and have good agreement with extrapolations from the melt). Schonhorn [17] shows, however, that if the polymer is quenched against a nucleating surface, different degrees of crystallinity form at the polymer surface changes the surface tension. Table 10.7 provides data on polyethylene molded against different surfaces. The test method involves placing 250 μm thick polyethylene film against a thin metal

Table 10.7 Effect of Mold Surface on Surface Tension and Surface Crystallinity of Polyethylene

Mold Surface	Surface Crystallinity (%)	Surface Tension at 20°C (dynes/cm)
Nitrogen	0	36.2
Polytetra-fluoroethylene	0	36.2
Polyethylene terephthalate	0	36.2
Copper	5.1	37.4
Nickel	53.3	51.3
Tin	60.1	53.8
Aluminum	63.2	54.9
Glass	63.2	54.9
Chromium	66.2	56.1
Mercury	86.4	64.8
Gold	96.3	69.6
Tantalum	78.5	61.4
NaCl	86.4	64.8
KBr	86.4	64.8
KCl	86.4	64.8
CaF_2	91.4	67.3

Data from Schonhorn H. Heterogeneous nucleation of polymer melts on high-energy surfaces. II. Effect of substrate on morphology and wettability. Macromolecules 1968;1:145–51 and adapted from Wu S. Surface tension and polarity of solid polymers. In: Polymer interface and adhesion. New York: Marcel Dekker, Inc.; 1982. p. 169–214.

or salt surface, exposing the sample to 200°C for 30 min under nitrogen, cooling, and chemically dissolving away the metal or salt. The surface tension is calculated from contact angle measurements. The surface crystallinity of the PE was calculated based on the values for amorphous and crystalline surface tensions. The results show PE molded against surfaces that provide no nucleating such as nitrogen and PET have a surface tension of 36.2 dyn/cm, consistent with amorphous PE. Molding surfaces comprising of various metals and salts promote crystallinity at the surface of the PE; surface tensions greater than 60 dyn/cm are measured, which correspond to surface crystallinity of greater than 90%. Wu [15] tabulates data for other polymers, such as PP and PA 66, which have similar behavior when molded against nucleating surfaces.

Note that Table 10.7 shows that chromium has a nucleating effect on PE. In practice, however, commercial films of PE made by casting onto a chromium-plated chill roll do not have the high surface tensions found in the table. The rate of quenching in a commercial cast film process is very fast, which suppresses crystallization. Furthermore, Schonhorn makes the point that good wetting is required for surface nucleation to occur. Chrome plating is used to minimize wetting and chill roll sticking. These factors conspire to suppress the crystallinity at the surface.

Wu [16] describes methods for measuring interfacial tension and tabulates values for several pairs of polymers. An approximate relationship for the interfacial tension of polymer pairs (Eq. 6.7) is derived in Chapter 6 based on the Good and Girifalco equation. This equation relates the interfacial tension to the difference in solubility parameters:

$$\gamma_{12} \cong 0.26(\delta_1 - \delta_2)^2 \qquad (10.17)$$

where γ_{12} = interfacial tension, δ_I = solubility parameter of material i.

The interfacial tension is strongly influenced by the polarity of the polymer, which is reflected in the solubility parameter. Values for solubility parameters for polymers commonly used in flexible packaging are given in Table 6.2 and more extensive data are found in the literature [18,19].

10.3.1.2 Wetting and Work of Adhesion

The ability of the polymer or adhesive to spread across a substrate is known as wetting. In Section 7.5.2, the concept of the spreading coefficient is introduced:

$$\lambda_{12} = \gamma_2 - \gamma_1 - \gamma_{12} \qquad (10.18)$$

where λ_{12} = spreading coefficient of substance 1 onto substance 2, γ_1 = surface tension of substance 1 (adhesive), γ_2 = surface tension of substance 2 (substrate), γ_{12} = interfacial tension of substance 1 and 2. For spontaneous wetting, $\lambda_{12} \geq 0$.

The thermodynamic work of adhesion, W_a, is the reversible work required to separate two surfaces in a direction perpendicular to their interface. W_a is related to the surface energies in the following manner:

$$W_a = \gamma_2 + \gamma_1 - \gamma_{12}. \qquad (10.19)$$

There are two competing theoretical models of adhesion as it relates to wettability. In the interfacial defect model, loss of adhesion is thought to be due to stress concentration around defects, which may be considered to be micro unwetted voids. Improving wetting reduces defects. To maximize adhesion, the spreading coefficient is maximized. From Eq. (10.18), this can be accomplished by minimizing γ_1 and γ_{12}.

In the fracture energy model, the energy to propagate fracture (G_a) is proportional to W_a (Eq. (10.10)). Adhesion is maximized by maximizing W_a. This can be done by minimizing γ_{12} and maximizing γ_1.

The two models agree on minimizing the interfacial tension, γ_{12}, but disagree on the direction to move the adhesive surface tension, γ_1. Combining the two approaches, the following generalizations can be made for the conditions for optimal adhesion:

1. The first condition for optimum adhesion is to minimize the interfacial tension. This can be done by matching the polarity of the adhesive or coating to the substrate. By Eq. (10.17), matching solubility parameters is a way to do this.
2. To further optimize adhesion, the spreading coefficient can be driven to zero by matching surface tensions. Thermodynamically, the spreading coefficient does not need to be maximized; spontaneous wetting still occurs at $\lambda_{12} = 0$. Letting $\gamma_1 = \gamma_2$, W_a can be maximized while still maintaining $\lambda_{12} = 0$.

These models just consider the thermodynamics of adhesion. Irreversible contributions to the work of adhesion can be achieved through chemical bonding at the interface, which can overwhelm the thermodynamic contribution.

The viscosity is also important—the coating or adhesive must be able to flow to wet the surface. Increasing temperature reduces the viscosity and helps with spreading. Increasing the contact time provides more time for spreading and adhesion.

10.3.1.3 Practical Guidelines

A general guideline for good wetting is for the surface tension of the substrate to be about 10 dyn/cm greater than the coating. Often the surface is corona, plasma, flame, or ozone treated to clean the surface and raise the surface tension to promote good

wetting, especially of inks. Gilbertson [20] provides the following typical surface energies for inks:

- Solvent-based inks: 27−30 dyn/cm;
- Water-based inks: 35−40 dyn/cm;
- UV ink monomers and oligomers: 30−36 dyn/cm.

Following the guideline, the substrate surface tension needs to be in the range of 37−50 dyn/cm for ink adhesion. Comparing this with the values in Table 10.5, most films need to be treated for good adhesion. Similarly, most polymer substrates (Table 10.5) must be treated for bonding with polymer melts (Table 10.6).

Usually OPET, OPP, and PA are corona treated by the film manufacturer to promote adhesion. The treatment level may age down with storage time. A second treatment is often applied in-line prior to coating to get the best results. Too much treatment can cause problems if the treatment breaks down the molecules at the surface. Primers are sometimes used to prepare the surface for subsequent adhesion.

Aluminum foil is classified according to its wettability. When water forms a continuous layer across the width of the coil with no beading the foil is given a Class A rating. This corresponds to a surface energy of >72 dyn/cm and is the best rating for foil wettability. Class B foil wets with a solution of 90% water, 10% alcohol (47 dyn/cm), and Class C with a solution of 80% water, 10% alcohol (38.5 dyn/cm). The wettability may vary across the width of the coil (roll) due to the manufacturing process. Foil less than 60 μm thick is rolled to its final thickness by squeezing two layers together separated by oil. The coiled product is usually annealed to refine its crystalline grain structure, remove the oil, and promote a homogeneous oxide layer. This is called soft annealing. The oxide layer forms immediately after rolling but is refined in the annealing step. The oxide can be considered as having two layers, a bottom "barrier" layer next to the aluminum that provides moisture barrier and corrosion protection, and a top layer that must bond to the coating. During annealing, the bottom layer becomes thicker and the top layer more compact as it loses water. Since annealing is done on the coil, the oxide layers are typically thicker near the edges of the coil than in the middle (along the width) since more oxygen can diffuse near the ends. Also, not all the oil is removed during annealing—about 10% remains. More oil is concentrated near the center—so wettability may be better near the edges than the center of the web [21−23].

Corona treatment of foil can help with adhesion by helping to burn off the oil and raise the energy level, especially for unannealed foil [24]. Flame treatment is also often used to help clean the surface of the foil.

The smoothness, porosity, and chemical composition of paper and paperboard influences its ability to be wet and bonded to. These are impacted by a number of factors in the paper-making process such as calendering, softness of the wood pulp, openness of the fiber structure, basis weight of the paper, and chemical treatments and coatings.

The quality of the surface of the substrate is important for good bonding. Solid substrates should be free of contaminates that may affect adhesion. Contaminates may arise from a number of sources, which include the following:

- Oils left from the manufacturing process, such as in the rolling of aluminum foil;
- Various processing or slip agents that bloom to the surface with time. These low molecular weight components sometimes interfere with adhesion;
- Breakdown of molecules from excessive treatment of the surface;
- Silicone sprays sometimes used to prevent chill roll sticking and other processing issues. These are particularly problematic for good adhesion and should be avoided;
- Reverse-side transfer, where the coating surface picks up contaminates from the adjoining layer in the roll.

Films of polar ethylene copolymers such as ethylene vinyl acetate (EVA), ethylene methyl acrylate (EMA), ethylene acrylic acid (EAA), and ionomers typically have surface tensions similar to nonpolar LDPE. One factor for this behavior is that these polymers are mostly polyethylene in character. They are random copolymers with typically up to about 20 wt% of the polar monomer. On a molar basis, less than 10% of the repeat units contain the polar monomer. Another factor is the polarity of the medium the film is exposed to. Studies [25−28] show that the surface tension of modified PE increases when immersed in water, a polar medium. Schultz [27]

measures the contact angle of acrylic acid-grafted polyethylene (PE-g-AA) films immersed in water or formaldehyde (which is less polar than water). The grafted PE has about 1 wt% AA. The measurement uses a liquid droplet technique that allows the calculation of the polar and nonpolar contributions to the surface tension. For the PE control, the polar surface tension does not change when immersed in the liquid. The PE-g-AA surface energy does change, which Schultz attributes to the AA groups reorienting to the surface. At 20°C this takes several days (12 days to level off) but at 90°C it takes about an hour. The ratio of the polar surface tension of the PE-g-AA to the liquid is constant; the surface tension is lower in the less polar formaldehyde than it is in water.

Schultz conducts adhesion experiments with the PE-g-AA by pressing films against aluminum foil. The PE-g-AA gives about 11 times the peel strength as the PE control. They attribute this to the AA groups reorienting to the interface with the polar aluminol on the surface of the foil. They show that a commercially made coating of PE-g-AA onto foil gives lower adhesion than their model system. They relate this to the short contact time for the commercial process—seconds vs 1 min for their process. Putting the commercial laminate through their process raises the adhesion to the same levels found in their model system.

Cho [28] measures contact angles of films pressed from EAA copolymers and their blends with LDPE in both air and water. From this they compute the polar contribution to the surface tension. Their results are plotted in Fig. 10.13. The EAA ranges in AA content from 3 to 20 wt%. The percent of EAA in the blends ranges from 5% to 83% so that the %AA in the blend ranges from 1 to 7 wt%. When measured in air, the polar contribution of the surface tension of all the EAA copolymers is 0, the same as for an LDPE control. For the water measurements, they immerse the films for 1 h at 80°C in octane-saturated water prior to the measurement. The films are then placed in distilled water and, while immersed, the contact angle measured for a droplet of octane. The polar surface tension increases with increasing acid level of the copolymer. When in contact with a polar medium, the acid groups reorient to the surface.

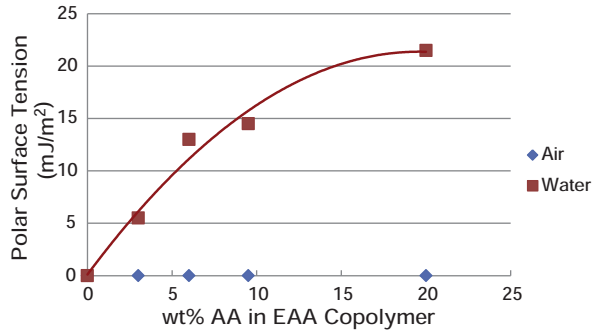


Figure 10.13 Effect of acrylic acid (AA) level on polar contribution to surface tension for EAA films tested in air or water.
Reproduced with permission from Cho CK, Cho K, Park CE. Relationship between surface rearrangement and adhesion strength of poly(ethylene-co-acrylic acid)/LDPE blends to aluminum. J Adhes Sci Technol 1997;11:433–45.

The EAA-LDPE blends show similar behavior. The polar surface tension measured in water increases with increasing wt% AA in the blend until about 6–8 wt% AA (in the blend), after which it plateaus to the pure EAA value. Peel strength is measured on laminates made by hot pressing the films to aluminum foil for 30 min at 170°C. Peel strength increases with increasing % AA in the blend, suggesting that the reorientation shown in the water immersion experiment simulates the reorientation that must occur when the film wets the polar aluminum surface.

The discussion so far has been about wetting a liquid adhesive or coating onto a solid substrate. In coextrusion, two molten polymers are combined. Wetting is typically not a limiting factor for adhesion in coextrusion. This is because the surface tensions of molten polymers are fairly similar (Table 10.6) so that the thermodynamics for spreading are favorable. Also, the flow geometry in coextrusion forces the melt into intimate contact.

The adhesion of many inks and coatings to films is driven by wetting and thermodynamics, but for interlayer adhesion in coextruded films, wetting is a necessary but typically not a sufficient condition for good adhesion. Without good wetting, other mechanisms such as diffusion and chemical interaction that build strength at the interface cannot take place.

10.3.2 Mechanical Interlocking

Mechanical anchoring of the adhesive or coating to the substrate can be utilized to create a strong interface if the substrate has sufficient cavities and microscopic undercuttings. An example is bonding to paper and paperboard, where flow into the pores and around the fibers creates a mechanical interlocking network.

Factors that favor mechanical interlocking include high surface roughness and porosity of the substrate, and good wetting and sufficient flow of the bonding layer. In flexible packaging, porous substrates such a paper, paperboard, and nonwovens (such as DuPont Tyvek) may take advantage of this mechanism. Mechanical adhesion is widely utilized in other industries, such as chemical and mechanical etching of metals for adhesion.

10.3.3 Diffusion

Once sufficient contact between the layers is obtained through wetting, diffusion of molecular chains across the interface may occur if the layers have sufficient compatibility and mobility. Diffusion builds strength at the interface by providing further intimate contact between chains, enabling short range attractive forces (such as dispersive forces), entanglement, and cocrystallization. The interface becomes more diffuse as penetration proceeds and ultimately the interface disappears. The mechanism of diffusion and buildup of strength at the interface for dissimilar materials is the same as for autoadhesion, explored in detail in Section 7.5.3.

In self-adhesion or autoadhesion, the two bonding layers are the same and so compatibility is not an issue. For dissimilar materials, the molecules must have enough chemical affinity for diffusion to take place. One way to quantify this is with solubility parameters: polymers with similar solubility parameters will be more compatible and likely to interdiffuse. Wu [29] derives the following relationship from a fracture energy balance:

$$\sigma_f = p \ \exp[-q(\delta_1 - \delta_2)] \tag{10.20}$$

where σ_f = fracture strength; p, q = constants; δ_i = solubility parameter of layer i.

The validity of this relationship is shown in Fig. 10.14 where the peel strength of a series of polymers melt bonded to polyethylene terephthalate (PET) is plotted against their solubility parameter. The solubility parameter of PET is 10.3 $(cal/mL)^{1/2}$, where the maximum peel strength is observed.

Ward [30] uses a heat seal test to measure peel strength of 16 grades of polyethylene, ethylene copolymers, and tie resins to two styrene copolymers (a styrene methyl acrylate copolymer and a styrene maleic anhydride copolymer). He finds that the results correlate with the difference in solubility parameters, but that the polymer mechanical properties are also important. EVA resins give the best performance.

Section 7.5.3 shows that diffusion and the resulting bond strength increases with increasing time and temperature and decreasing molecular weight. Increasing time allows more molecular penetration, up to the point where the interface disappears in the case of autoadhesion. Increasing temperature increases the thermal motion of the molecular chains, speeding up diffusion. Lower molecular weight increases the amount of diffusion but reduces cohesive strength: the experimental data on the effect of molecular weight are

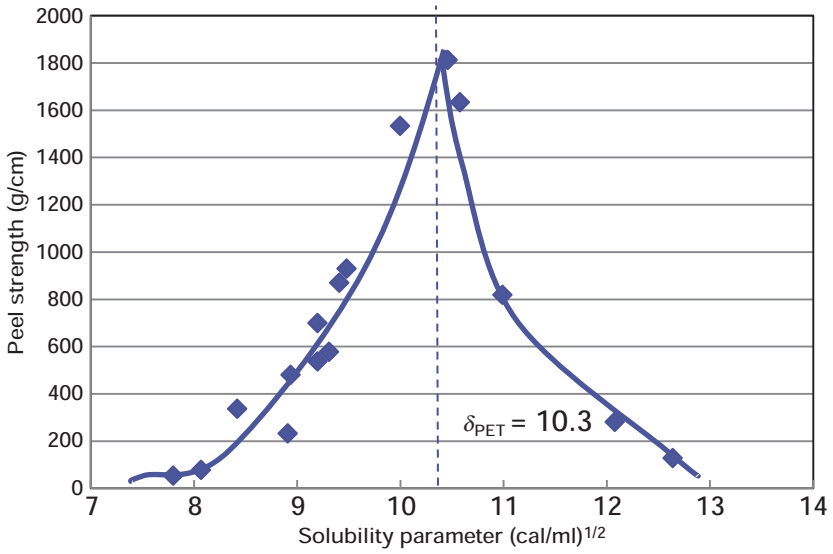


Figure 10.14 Peel strength vs solubility parameter for various adhesives on polyethylene terephthalate. Peel strength measured at 90° angle at 5 cm/min.
Adapted from Wu S. Formation of adhesive bond. In: Polymer interface and adhesion. New York: Marcel Dekker, Inc.; 1982. p. 359–447.

not definitive. In some cases, higher MW increases peel strength due to an increase in mechanical strength.

Diffusion and strength buildup when chemical reactions occur at the interface are constrained by the formation of bond sites. Lee and Wool [31–33] study a model polymer/substrate system: carboxylated polybutadiene bonding to an amine-functionalized aluminum substrate. Both the carboxylate and amine densities are controlled. The adhesion of some of their structures ages up over a period of 41 days. Their explanation is that initially the polymer has strong bonds to the solid surface but the density of chains near the surface is sparse compared to the bulk of the polymer. The cohesive strength between the chains attached to the surface and the nearby chains is weak since there is not much chain entanglement. With time, if the surface energetics is right, the near-surface region can fill in: nearby chains entangle, increasing the cohesive strength and hence the peel strength. The timescale for the near-surface diffusion of polymer chains is 100–10,000 times greater than the terminal relaxation time for bulk diffusion. Near the surface the polymer chains are constrained in their movement by the bond sites with the surface. Hence diffusion is considerably slower at the interface. In the model system, the terminal relaxation time is 2 s but the timescale for diffusion near the interface is many days.

They vary the amine concentration on the surface and find that the adhesion goes through a maximum at an intermediate level of surface functionality. The higher the amine level, the higher is the surface tension. So they find that the highest surface tension does not necessarily give the best adhesion. They propose that this is due to competing mechanisms. As the surface functionality is increased, there is more bonding between the polymer and substrate: the polymer wets the surface better. This increases the adhesive strength at the interface. On the other hand, as the surface wetting is increased, the density of chains nearby is depleted, reducing the cohesive strength. If the surface energetics is right, over time these depleted regions can fill-in and peel strength will increase, as described above. They argue, however, that for a high surface energy situation, there are so many polymer surface interactions that the molecular structure near the surface is permanently altered. The chains become ordered near the surface and cannot entangle as readily, resulting in lower cohesive strength. This results in the peel strength (at long times) being higher at an intermediate level of surface wettability.

10.3.4 Chemical Interaction

Bond strength can develop at the adhesive–substrate interface through specific chemical interactions. Chemical bonding as it relates to the bulk polymer is reviewed in Section 4.2.1.5. These same types of bonds can be used to promote adhesion at the interface between two dissimilar materials. The relative strength of these bonds is summarized in Table 10.8. The dispersive and polar bonds are collectively known as van der Waals forces. They are relatively weak and act over very short distances. They can be very numerous as atoms along the polymer chain can interact with other atoms of neighboring chains to collectively provide strength at an interface. Polymers that form a diffuse interface through molecular diffusion often rely upon these types of forces. Examples include the following:

- heat sealing of polyethylene to itself;
- bonding HDPE to an LLDPE (linear low density polyethylene) or EVA sealant in coextrusion;
- bonding of PE-based tie resins to PE in coextrusion;
- bonding of EAA tie resins to LDPE in coextrusion coating.

If conditions do not favor diffusion then specific chemical interactions must be promoted at the interface to achieve good bond strength. This may be accomplished by modifying the substrate,

Table 10.8 Bond Energies

Type of Bond	Range (kcal/mol)
Dispersive	0.02–10
Polar	
Dipole–dipole	1–5
Dipole–induced dipole	<0.5
Hydrogen bond	2–6
Chemical	
Covalent	15–150
Ionic	150–250
Donor–Acceptor	
Bronsted acid/base	Up to 250
Lewis acid/base	Up to 20

incorporating specific chemical functionality into the adhesive or both. In general, the stronger and most durable bonds involve covalent, ionic, or acid/base interactions, although van der Waals forces are also used. Some examples include the following:

- Heat sealing an EVA-based lidding film to a PET tray. Little intermolecular diffusion can occur since the T_g and T_m of PET is high. The polar vinyl acetate groups on the EVA bond with the polar groups on the PET through dipole−dipole and other polar van der Waals forces.
- Bonding of EVA to PVDC in coextrusion. This involves dipole−dipole interactions.
- Bonding of EMAA to PA6 in coextrusion. The acid groups in EMAA react with the amine end groups of the PA6 to form a covalent bond (imide or amide) or an ionic salt.
- Bonding maleic anhydride containing tie resins to EVOH in coextrusion. The anhydride reacts with the hydroxyl (OH) groups on the EVOH to form a covalent bond (ester).
- Bonding EAA tie resin to aluminum foil in coextrusion coating. The acid group in the EAA reacts with the aluminum oxide to form an acid/base interaction.
- Oxidizing LDPE during extrusion coating to bond to aluminum foil. Oxidation forms polar species on the LDPE, such as acids, aldehydes, and ketones, which interact with the aluminum oxide. The oxidation is typically accomplished through heat or by ozone treatment.
- Priming OPET, OPP, or PA film with a polyethylene imide (PEI) primer to promote adhesion to oxidized LDPE in extrusion coating. The imide group on the PEI provides an anchor to the film (which may be treated) and the oxidized PE (carboxyl groups formed during oxidation form amide linkages with the PEI).

In extrusion coating, adhesion of LDPE is generally improved by pretreating the substrate. When functional polymers are used, pretreatment may not be necessary. Leclere [34] considers the effect pretreating paper has on bonding to maleic anhydride-functionalized polyethylene. The functionalized polyethylene is made via either copolymerization or by chemical grafting and the amount of functionality is varied. Corona, ozone, and flame treatment are studied. They find that low levels of anhydride functionality respond favorably to pretreatment but higher levels do not.

Allen [35] and Bodine [36] show that adhesion of a tie layer (with anhydride functionality) to various substrates (PET, PP, paper, and aluminum) can be improved by first priming the substrate with PEI. Alternatively, the adhesion of PE, PP, or EVA in monolayer extrusion coating can be improved by adding a tie layer concentrate to the resin and priming the substrate. Other performance properties may also be enhanced, such as the water resistance of the bond.

For chemical interaction to occur, the reactants must be accessible to each other at the interface with sufficient time and temperature. The reacting functional groups must be able to find each other. This requires that they be present in sufficient concentration. They also must be mobile enough to reach the interface and have enough energy and time to react. Higher processing temperature favors greater chain mobility and faster reaction rates. Longer contact times at temperature allow for more diffusion of reactants to the interface and for more bonding to take place. Chain mobility and surface energetics also play a role. For example, maleic anhydride-functionalized tie resins bond very well to PA6 in the melt but poorly to solid PA films. The amine end groups on the PA6 are accessible to the anhydride in the melt but not in the solid state. The amines may be buried beneath the surface of the PA in the solid state. Steric hindrance and other factors may also affect accessibility. An example that is described more fully in Section 10.4 is the difference in performance of anhydride-grafted polyethylene and anhydride copolymers. When the anhydride is copolymerized in the polymer chain, it is less accessible and reactive than when it dangles from the chain, as it does when it is grafted. The grafted polymer performs well with only a fraction of the anhydride concentration of the copolymer.

Molecular weight is an another factor. If the functional group is on the end of the chain, reducing the molecular weight increases the number of functional groups (by decreasing the average chain length and increasing the number of chains). Lowering molecular weight also reduces the viscosity and increases the diffusion rate, which may help get the functional group to the interface. If the MW is too low, however, the strength of the interfacial region may be weakened.

Evidence of chemical interaction at the interface in coextrusion of polymer melts is found in a number of

studies. Botros [37–39] examines the reaction of maleic anhydride-grafted polyolefins to EVOH through melt blends and coextrusion. Fourier transform infrared spectroscopy (FTIR) studies on melt blends show a complete disappearance of the peaks associated with anhydride after 1 min in an extruder, indicating the reaction is fast enough for industrial processes. Melt viscosity of the blends also increases suggesting interfacial reactions. Scanning electron microscopy (SEM) of peeled interfaces from coextruded films show local regions with adhesive residue suggesting cohesive and adhesive failure at the interface. They conclude that the tie resin forms strong covalent bonds in local regions. They also find the evidence of rupture of the EVOH layer in places, again suggesting strong bonds. This is confirmed with electron spectroscopy chemical analysis (ESCA) and FTIR. In a second study, the complex viscosity and dynamic modulus of blends of maleic anhydride grafted polypropylene (PP-g-MAh) and EVOH and their components are measured. The complex viscosity and dynamic moduli (G' and G'') correlate with peel strength in coextrusion. Stronger interactions between the PP-g-MAh and EVOH increase the viscosity and modulus and also peel strength. FTIR spectra of the blends show the creation of an ester peak when the anhydride reacts with EVOH. They find that the tie resin with the greatest adhesion in coextrusion has the highest viscosity and modulus and the largest ester peak in the blends.

Macosko's group at the University of Minnesota uses rheology of multilayer structures to study interfacial interactions. Through compression molding or coextrusion layer multiplier technology, they create hundreds of layers, which amplify the interfacial area, creating a sensitive system to study different types of interactions. Levitt [40] uses multilayer stacks and extensional viscosity measurements to study nonreactive pairs (PS-PP, PS-aPA), graft reactions where the reaction just occurs at the end of the PA chain (aPA/PS-co-MAH), and cross-linking where multifunctional polymers react (PS-MAH and PS-oxazoline). They make films of the pure polymers and then compression mold multilayer stacks of the pairs with 20, 50, and 100 layers. A Meissner-type extensional rheometer (Section 5.3.6) with elongations of >20 (Hencky strain of 3) at 0.1 s^{-1} and 220°C is used to measure the force to stretch the laminates under controlled conditions. The sensitivity can be increased simply by increasing the number of layers. The increase in measured force over the bulk average is related to the interfacial tension. For the ungrafted polymer pairs, the interfacial tension increases with extension rate. The grafting interaction produces a substantially different rheology response with a much larger increase in interfacial tension than for the nonreactive pairs. Cross-linking pairs show strain-hardening behavior with the apparent viscosity increasing by a factor of 200 over the homopolymer average.

Saito and Macosko [41] use coextrusion layer multiplier technology to create 256-layer sheets, which they pull in a uniaxial extensional rheometer. The sheet contains alternating layers of ethylene-co-glycidyl methacrylate (E/GMA) copolymer and maleic anhydride-grafted polyethylene (PE-g-MAh). The EGMA contains 8 wt% GMA (an epoxy group) and the PE-g-MAh contains 4 wt% MAh. Maleic anhydride opens up to form a diacid, which reacts readily with the epoxy group on the EGMA. The extension force increases substantially from which the interfacial stress is extracted and correlated with the amount of interfacial cross-linking.

Song [42] studies the reaction of HDPE-g-MAh with PA6, a commercially important combination in flexible packaging, using both a lab press (thermal lamination) and coextrusion. The anhydride reacts with the amine end group on the PA6 chain to form an imide [113]. They coextrude bilayer sheet with different levels of anhydride (by blending down the HDPE-g-MAh with HDPE). Two dies are used, one that compresses the melt as it flows and another that does not. The bilayers have equal volume flow rate so that the interface is near the centerline of the flow channel where the shear rate and stress is zero. Laminations of similar compositions are also separately prepared with a laboratory press at different holdup times. They use the asymmetric dual cantilever beam method to measure adhesion. This involves inserting a wedge (razor blade) between the layers and measuring the crack length that forms in front of it (after allowing the sample to equilibrate for 24 h). The stiffness of the layers separated by the wedge acts as the driving force for crack propagation, which decreases as the crack propagates. The facture energy (critical fracture release rate, G_c) is calculated from the crack length, modulus and thickness of the layers, and thickness of the razor blade. X-ray photoelectron spectroscopy (XPS or ESCA) is used to measure the density of the PE-g-PA chains that are formed at the interface, after first dissolving and washing away the free PA chains.

Their results show the following:

- G_c increases with increasing reaction time and concentration of PE-g-MAh in the blend with HDPE. G_c also increases with increasing temperature.
- The extent of the chemical reaction at the interface, as measured by the interfacial grafted chain (PE-g-PA) concentration, Σ, increases with increasing reaction time and temperature.
- The fracture energy increases with increasing interfacial chain concentration as is shown in Fig. 10.15. $G_c \propto \Sigma$ for small Σ and $G_c \propto \Sigma^2$ for larger Σ. They cite literature that G_c is proportional to Σ if simple chain scission or chain pull-out is the cause of the interfacial failure. If a small amount plastic deformation becomes involved (as in glassy polymers), then G_c is proportional to Σ^2. They show that this is also true for semicrystalline polymers.
- Σ is a linear function of C_o (initial concentration of MAh) at the beginning of the reaction. Therefore, $G_c \propto C_o$ in the initial stages of the reaction.

This work directly shows that chemical interaction at the interface is responsible for enhanced peel strength. The paper goes on to report on acceleration of the reaction rate during coextrusion; the reaction rate is two orders of magnitude faster than that found in the thermal lamination experiments. Botros [38] reports similar behavior for an anhydride-functionalized tie resin and EVOH. Song [43] reports acceleration of peel strength between polyurethane and an amine-modified polyethylene during coextrusion. Song relates this to chain alignment during compression in the die. This phenomenon is discussed further in Chapter 15.

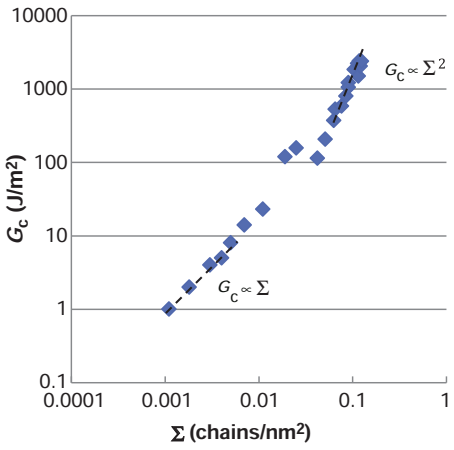


Figure 10.15 Fracture energy as a function of the surface concentration of reactive pairs (interfacial copolymer density, Σ) for thermal lamination or coextrusion of HDPE-g-MAh to PA 6.
Adapted from Song J, Baker AM, Macosko CW, Ewoldt RH. Reactive coupling between immiscible polymer chains: acceleration by compressive flow. AIChE J 2013;59:3391–402.

10.3.5 Boundary Layer

The strength of the interface is critical to good adhesion. If a weak layer forms near the interface, even if the bond strength is high, the peel strength may be poor due to cohesive failure within the "boundary" layer. Weak boundary layers can form for a number of reasons. Some examples include the following:

- Low molecular weight polymer. If the adhesive or substrate contains a low molecular weight component, this may create poor cohesive strength. Even if the low MW component contains functional groups that securely bond to the substrate, the lack of chain entanglement near the interface will cause the chains to be pulled away from the interface when stressed. One contributor to loss in molecular weight is chain scission brought on by polymer degradation from too much heat exposure during processing, excessive oxidation (typically in extrusion coating), or overtreatment. Low molecular weight may also be caused by insufficient curing of a primer or adhesive.
- Surface contamination. Oils, blooming agents, and various processing aids can interfere with adhesion and create a weak boundary layer. These may be by-products of the substrate or polymer manufacturing process, such as oils from the rolling of aluminum foil. They may be slip, antiblock, or chill roll release agents purposely added to modify the surface of the film or polymer. These act by blooming to the surface. Chapter 12 describes blooming agents in detail. Excessive amounts can form a "chalk" like appearance on the surface of film and cause adhesion problems, especially during printing. Various lubricating agents, such as stearates, can interfere with adhesion. Surfaces can pick up contamination from the reverse side of a

multilayer film while wound in the roll. This is known as reserve-side transfer. Contaminates may also come from outside the film, such as lubricating sprays used during lamination or coating to prevent chill roll sticking. Silicone sprays are especially problematic toward adhesion. Contaminates may act to block wetting, diffusion, or chemical interaction directly or by creating a weak boundary layer near the interface due to their low MW.

10.4 Tie Resin Technology

Obtaining good adhesion between polymer melts (coextrusion) or between a molten polymer and solid substrate (extrusion coating and lamination) can be challenging, depending on the specific substrates involved. As described in Section 10.1, often specialized tie resins or coating resins are needed to achieve the desired results. The chemistry of the tie resin is important, as is the chemistry of the substrate, the design of the structure, and the end-use environment. Solid substrates may need to be cleaned, treated, or even primed to be receptive to the coating. In coextrusion, layers need to have similar flow properties to avoid instabilities. This section discusses the chemistry of tie resins, factors that influence their performance and selection criteria.

10.4.1 Extrusion Coating and Lamination

In extrusion coating and lamination, the molten polymer bonds to a solid substrate by wetting, chemical interaction, and in some case by mechanical interlocking. This section discusses the critical properties of the substrate and polymer for effective bonding. The coating process can have a significant impact on the adhesion through its influence on the chemistry and stress. These are taken up in detail in Chapter 15. How the structure is ultimately used—the temperature and chemical environment is it exposed to—also affects the adhesion. This is described in Chapter 16.

10.4.1.1 Substrate

Film, foil, and paper substrates can be thought of as three-dimensional structures with both surface and bulk properties. On a microscale, the surface is generally not molecularly homogeneous. Polymer films have molecular chain length variations (MWD), chain end variation, branching, additives, catalyst residues, and degradation products. Most films are amorphous at the surface but changes in surface crystallinity can affect surface energy (Section 10.3.1). Metal foils often have multiple morphologies, additives, process contaminates, and oxides (Section 10.3.1.1). Paper has fiber length variation, fiber thickness variation, fiber orientation, porosity, binders, and additives. On a macroscale, the surface has both a distinct surface energy and topography that influence adhesion.

The surface and bulk properties of the substrate are important for peel strength performance. Key aspects of the surface include the following:

- Contact angle/surface energy or tension. A general guideline used by practitioners (Section 10.3.1.1) is for the substrate to have a surface energy of about 10 dyn/cm higher than the coating for good wetting. Since most coating resins are polyolefin based with surface energies of around 30 dyn/cm, substrate surface tensions of 40–45 dyn/cm are typically used. Often this requires treatment with corona, ozone, flame, or plasma [20,24,44–49]. Films treated by the manufacturer may lose some of their surface energy during storage; in-line treatment is typically used to ensure that the energy level is sufficient and to help clean the surface of the film.
- Chemical functionality. For a durable bond, the substrate needs a "hook" for the polymer to latch onto. The hook needs to match with the chemical functionality on the polymer. Some substrates naturally have functional groups that can be used to attach to the polymer. An example is the oxides on the surface of aluminum, which can interact with the acid groups of oxidized polyethylene or acid copolymers. For other substrates, treatment or chemical primers [50,51] may be required to provide the functional groups for bonding. A summary table of general guidelines for primers presented by Bentley and Singer [50] is reproduced in Table 10.9.
- Cleanliness. Contamination at the surface can interfere with chemical bonding or create weak boundary layers. Sources of contamination

Table 10.9 General Guidelines on Chemical Primers

Primer Type	Substrate			Property		
	Paper	Metal	Plastic Film	Heat Resistance	Moisture Resistance	Chemical Resistance
Shellac	Poor	Excellent	Poor	Poor	Poor	Poor
Organic titanate	Good	Good	Good	Fair	Fair	Fair
Polyurethane	Very good	Excellent	Excellent	Excellent	Excellent	Excellent
Polyethylene imide	Very good	Good	Excellent	Excellent	Poor	Poor
Ethylene acrylic acid	Excellent	Excellent	Fair	Fair	Excellent	Good
Polyvinylidene chloride	Excellent	Fair	Excellent	Good	Very good	Fair

Reproduced with permission from Bentley Jr DJ, Singer FM. Chemical primers to enhance adhesion and other properties. In: Bezigian T, editor. Extrusion coating manual. 4th ed. Atlanta: TAPPI Press; 1999. p. 185–200.

include oils from the substrate-manufacturing process, catalyst residues, lubricants, processing aids, and other low molecular weight species. Some additives, such as slip agents, migrate to the surface (Chapter 12); the surface may change with time. One effective method for ensuring a clean surface is in-line treatment, such as flame or corona treatment. The high energy treatment burns off most contamination.

- Pore structure and roughness. The surface topology influences how much polymer penetration and mechanical interlocking can take place. Although not typically used in flexible packaging, chemical etching and physical abrasion can be used to create a roughened surface for bonding. In flexible packaging, porous substrates such as paper, paperboard, and nonwovens take advantage of the ability of the polymer to flow into the pores and around the fibers. Many applications using paper or paperboard look for evidence of fiber tear when evaluating adhesion. This occurs when the polymer takes the fibers with it as the coating is peeled away from the substrate. This happens when there is a sufficient mechanical interlocking. Some papers, however, have been designed with poor cohesive strength near the surface so that fiber tear can be more easily obtained. This is a case of purposely creating a weak boundary layer, which may be appropriate for some applications but not for others.

Some of the important properties of the bulk include the following:

- Dimensional stability. The substrate needs to withstand the temperature during coating without shrinking or distorting. Dimensional changes can cause stress, which reduces peel strength. Trouilhet and Morris [52] give an example of a coextrusion coating of two layers of LDPE onto OPET: OPET/primer/(LDPE-LDPE). The initial structure has poor adhesion between the OPET and LDPE. The layer of LDPE that contacts the OPET is extruded at 310°C and the outer layer at 280°C to reduce taste and odor issues. The authors use a heat transfer model to calculate the temperature of the OPET layer during coating. They find that the OPET never melts but it does get above the temperature at which the OPET starts to shrink. By switching to an OPET film with a higher shrinkage temperature and better dimensional stability, the peel strength improved. Troulihet and Morris hypothesize that the shrinkage imparts a stress on the interface, reducing the peel strength.

  A similar problem occurs when extrusion coating of hot LDPE onto a metallized film such as met-OPP. If the supporting film shrinks when exposed to the hot polymer, the induced stress may crack or craze the thin metal layer. This is more of an issue with metallized PP than for OPET.

- Physical properties. The thickness, stiffness (modulus), and yield strength of the substrate can affect the peel dynamics, as discussed in Section 10.2.3. Yielding can result in stretching of the peel arm during the peel test, contributing to higher peel strengths. The thickness and stiffness of the substrate may change the local angle at the peel front, affecting the peel energy.

10.4.1.2 Polymer

A number of characteristics of the coating polymer are important, which include the following:

- Type of chemical functionality. Chemical functionality is often added to the polymer, the substrate, or both to achieve the desired bond strength. LDPE is the most common coating resin used in extrusion coating and lamination. It is inexpensive and has good thermal stability and processes well at high line speeds. By itself, however, it lacks chemical functionality for bonding to polar substrates such as aluminum foil. To overcome this, LDPE is purposely oxidized during the process by running hot (above 300°C), increasing the time in the air gap, and in some cases applying ozone treatment [53,54] to the melt curtain. The oxidation creates polar species such as acids, aldehydes, and ketones on the surface that help with bonding to polar substrates. These bonds can be variable since they rely on the coating process to form the oxidative species. Specific functionality can be built into the polymer chain through copolymerization or grafting reactions. Table 10.10 gives some examples of functional groups that bond to various substrates and commonly used ethylene copolymers that have these functional groups. Co- and terpolymers of ethylene with acid [55–62], anhydride [10,63], and acrylates [64–70] are the most commonly used specialty copolymers in extrusion coating for their wide range of adhesion performance. EVA [71,72] is used but requires low temperature processing to avoid thermal degradation. Silanes [73,74] have also been studied but have not gained widespread adoption for flexible packaging.
- Amount of chemical functionality. Generally, higher amounts of functionally give better peel strength. The amount of functionality on oxidized LDPE is fairly small. By some measurements [75], it is equivalent to about 1 wt% acrylic acid. Commercial grades of EAA copolymers range in acid level from about 3 to 10 wt %. High acid levels tend to have better product resistance, which can lead to longer shelf life for packaged goods. There are trade-offs. For example, higher acid results in less compatibility with LDPE. EAA is often used as a tie layer to coextrusion coat LDPE onto foil: Al// (EAA-LDPE). High acid gives better foil adhesion but lower adhesion to the LDPE. Intermediate levels are often used as a compromise.
- Flow characteristics. The polymer must wet the substrate in a short amount of time between first contact with the substrate and solidification. This requires low viscosity. If the viscosity is too low, however, neck-in and other processing problems may develop. Also, since viscosity is related to molecular weight, low viscosity may cause the cohesive strength of the coating to be too weak for high peel strength performance. As described in Chapter 5, the melt index (MI) is not the best measure of flow, but for reference a typical range for polyethylene extrusion

Table 10.10 Examples of Chemical Functional Groups That Bond to Various Substrates and Ethylene Copolymers That Contain These Groups

Substrate	Functionality	Example Polymers
Al foil	Acid, anhydride, acrylate	Oxidized PE, EAA, EMAA, Ionomer, E/MAH/MA, EMA
OPET	Acrylate, vinyl acetate	EMA, EVA
OPP	Acrylate, vinyl acetate	EMA, EnBA, EVA, VLDPE
Paper	Acid	Oxidized PE, EAA, EMAA, Ionomer
Inks	Acrylate, vinyl acetate, acid	EMA, EnBA, EVA, E/BA/MAA

Reproduced with permission from E. I. du Pont de Nemours and Company.

coating grades is from 4 to 12 g/10 min (190°C/2160 g).

- Thermal stability. The polymer is often run hot to achieve good flow characteristics and to provide heat for chemical interaction at the interface. LDPE is also run hot to promote oxidation. The polymer must have the thermal stability to be run at the desired temperature without significant degradation. Degradation can cause off-gassing; taste and odor issues in the final product; and gel and blackspecs. Degradation can also cause the polymer chains to either cross-link (increasing viscosity) or scission (reduce MW and strength). The use of antioxidants can improve thermal stability but must be used with caution if oxidation is desired for adhesion. Gregory [76], for example, shows that adding 50 ppm of an antioxidant to LDPE drops the peel strength to Al from about 250 to 50 g/15 mm. One of the reasons LDPE is the mainstay of the extrusion coating industry is that it has excellent thermal stability without the use of antioxidants and good melt strength.
- Additives. Chill roll release, slip agents, antiblock, lubricants, processing aids, antioxdiants, and other additives may affect adhesion. For example, Gregory [76] reports a 50% drop-off in adhesion of LDPE to foil when 3000 ppm of calcium stearate is added. Additives can affect adhesion in a number of ways. One is that they may interfere or react with the functional groups in the polymer. The effect of adding antioxidants to LDPE is one such example. Some additives are designed to bloom to the surface, such as chill roll release and slip agents. They may change the surface properties or block the wetting and bonding at the interface, although normal amounts generally do not cause problems. Low molecular weight additives may preferentially bond to the substrate and create a weak boundary layer. It is advisable to test the effect of additives on adhesion to ensure that they do not have an undesirable affect.

10.4.1.3 Examples From the Literature

A few examples from the scientific literature are provided here to illustrate these factors. Ulren and Hjertbert [77] study the effect of functional group chemistry on the adhesion to aluminum. They prepare laminates by solution casting or hot pressing films to the aluminum. They measure peel strength and correlate the results with FTIR measurements of the interaction at the interface. Three types of ethylene copolymers are tested: poly(ethylene-co-vinyltrimethoxysilane), EAA copolymer, and ethylene butyl acrylate (EBA). Three levels of BA (0.7−3.7 mol%) and AA (1.2−3.7 mol%) are used. The strength of the interfacial interactions (as measured by FTIR and peel strength) correlate with the concentration and acidity/basicity of the group: AA being more efficient than BA. Silane functionality provides strong adhesion to the aluminum at much lower concentrations than the acid or ester groups. Silanols as well as Al-O-Si linkages are detected at the interface.

It should be noted that silanes are typically not used commercially in flexible packaging due to their thermal stability issues. Acid copolymers are used commercially and provide good adhesion to a number of polar substrates [55]. Schultz [27] studies the adhesion of PE-g-AA to aluminum foil and finds that the acrylic acid interacts with the aluminol on the surface of the foil leading to the formation of carboxylates.

Several investigators report an increase in peel strength when Al/EAA or Al/EBA laminates are immersed in boiling water [27,78]. They attribute this to hydration of the oxides, forming a layer of pseudoboehmite (an altered form of oxide) on the surface of the foil. The growth of this oxide layer occurs mostly in the interfacial cavities, increasing the contact area between the foil and polymer.

Schulz and Lavielle [79] describe the peel strength to aluminum foil of three acid/anhydride-functionalized polymers: HDPE-g-AA (1% AA) (bulk grafted), EVA terpolymer (12.7% VA, 0.39% MAH, 1.8% grafted AA), and a blend of PP + PP-g-MAH. The PP-graft concentrate has a low MW due to chain scission that occurs during grafting. Laminates of films of the polymers to Al foil are made by hot pressing for 15 min. They measure contact angles in water to different alkanes to get polar and nonpolar surface energies. An EVA control does not bond to the foil; the presence of the AA and MAH groups on the EVA provides adhesion. They find the acid groups reorient to the polar foil interface as is described in Section 10.3.1.1. The PP blend gives poor adhesion, underscoring the fact that chemical interaction is not sufficient for good peel strength. Here the low MW-grafted molecules create a weak cohesive boundary layer near the interface.

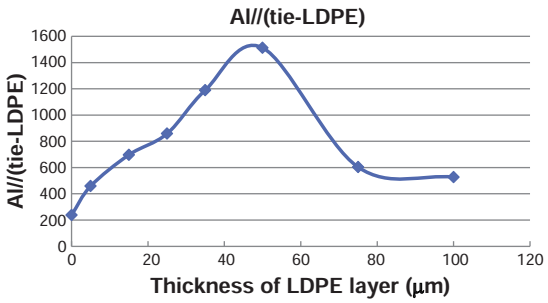


Figure 10.16 Peel strength as a function of LDPE thickness.
Adapted from Pascal J. Ultraversatile adhesives to broaden the possibilities of extrusion lamination. In: TAPPI Place conference. Cincinnati, OH; 2006.

Pascal [10] provides an example of how the mechanical properties and thickness of the coating affect peel strength. He coextrusion coats LDPE onto 37-μm aluminum foil using 10-μm of a tie resin: 37 μm Al//(10 μm tie−LDPE). The thickness of the LDPE is varied from 0 to 100 μm. The peel strength to the foil is shown in Fig. 10.16. The peel strength increases with increasing LDPE thickness until the thickness reaches about 50 μm, after which it decreases sharply. He attributes this change to a change in the peel geometry during the peel test. In the zone below 50 μm, the local peel angle is more acute and plastic deformation dominates. Starting at 50 μm the angle becomes less acute and the peel strength is more dependent on the interfacial strength. The effect of coating thickness is explored with more depth in Section 15.1.4.

The effect of the bulk properties of the polymer can be seen when comparing the peel strength of LDPE, EBA, and EAA tie resins to aluminum foil [80]. Laminates are made by first creating an OPET/EAA/Al laminate and subsequently extrusion laminating it to a PE film: 13 μm OPET/19 μm EAA/9μmAl//18 μm Tie//50 μm LLDPE film. The lamination temperature is 321°C. Table 10.11 shows the results of peel strength measurements. A T-peel configuration is used with a pull rate of 300 mm/min. The samples are separated at the tie-Al interface. The order of peel strength performance is EBA > EAA > LDPE. The EAA is generally believed to provide the best adhesion to the foil. Indeed, high AA is needed to maintain adhesion to the foil in the presence of chemical attack from acid foods, as is described in Chapter 16. As described above, the AA forms a carboxylate with the oxides on the surface of the foil. LDPE relies on oxidation during the coating process to provide adhesion. At lower coating temperatures, the peel strength drops to zero. As mentioned earlier, the amount of acid functionality that forms during oxidation is equivalent to only about 1 wt% AA. The peel strength of LDPE to aluminum foil is sensitive to processing conditions and typically has a lower value than the peel strength of EAA. EBA generally has poor adhesion to aluminum foil at lower coating temperatures. It too relies on oxidation. In addition, some of the BA groups can convert to AA groups, liberating ethyl alcohol, during extrusion. The amount of conversion is small and the level of AA is expected to be considerably less than the 7% AA on the EAA copolymer. So why does the EBA give higher peel strength performance than the EAA? The explanation lies in the failure mode. The EBA structure elongates as it peels from the aluminum. This creates substantially more energy for failure. The elongation relates back to the bulk properties of the polymer. The EBA is a much softer molecule, with a much lower tensile modulus, than the LDPE and EAA.

10.4.1.4 Choosing a Coating Adhesive Resin

When choosing among coating polymers, a number of factors must be taken into account including cost, performance, mode of failure, processibility, regulatory status, and organoleptics. Table 10.12 provides a selector guide for choosing among various

Table 10.11 Peel Strength of LDPE, EAA, and EBA to Aluminum Foil in Structure OPET/EAA/Al//Tie/LLDPE Film. Lamination temperature is 321°C

Polymer	Wt% Comonomer	Modulus (MPa)	Peel Strength (g/25 mm)	Peel Failure Mode
LDPE	0	210	240	Peel
EAA	7	180	750	Peel
EBA	27	35	1470	Elongation/peel

Data from Morris BA, Trouilhet YM. Lamination adhesion of foil to thermoplastic polymers; 2004. US patent 8137776 B2.

Table 10.12 Relative Ratings of Some Commonly Used Ethylene Copolymers for Extrusion Coating/Lamination to Aluminum Foil

Attribute	LDPE	LLDPE	EAA, EMAA, Ionomer	EMA, EBA, EEA
Low price	◇◇◇◇	◇◇◇◇	◇	◇◇
Green peel strength	◇◇	◇	◇◇◇	◇◇◇◇
Chemical resistance/shelf life	◇	◇	◇◇◇◇	◇
General processibility	◇◇◇◇	◇	◇◇◇	◇◇
Ability to run at low temperatures to reduce off-flavor/odor			◇◇◇◇	
Ability to run at high line speed and maintain adhesion	◇	◇	◇◇◇	◇◇
Regulatory status	◇◇◇◇	◇◇◇◇	◇◇◇◇	◇◇◇

A higher number of diamonds indicates better performance.
EAA, ethylene acrylic acid copolymer; *EBA,* ethylene butyl acrylate copolymer; *EEA,* ethylene ethyl acrylate copolymer; *EMA,* ethylene methyl acrylate copolymer; *EMAA,* ethylene methacrylic acid copolymer; *LDPE,* low density polyethylene; *LLDPE,* linear low density polyethlene.

ethylene copolymers for bonding to aluminum foil. Depending on the application, one polymer type may be favored over another. If the peel strength performance is not demanding, shelf life and organoleptics are not issues, and line speeds are not too high, then LDPE is an excellent choice. LDPE has its limitations, however. LDPE relies on oxidation from the extrusion process to achieve bonding to aluminum foil. Oxidization can be inconsistent at high line speeds and can result in off-flavor and odor issues. The bonds formed with the oxidized species are more susceptible to chemical attack from demanding products. If any of these issues are important to the application, an ethylene copolymer may be a consideration. EMA or EBA may be well suited where high peel strength but little chemical resistance is required. EAA and EMAA have often been used for the packaging of ketchup, salad dressing, orange juice, and toothpaste where acetic acid or other product components attack the foil bond over time. In even more demanding applications, such as alcohol wipes and condoms, ionomer has been used. Acid copolymers and ionomers can be run at lower temperatures than LDPE to avoid oxidative byproducts and higher line speeds while maintaining consistent adhesion.

Table 10.2 provides an additional information on the relative adhesion performance to various substrates of some commonly used polymers in extrusion coating and lamination. These are merely starting points. Actual results will depend on the processing conditions and overall structure design. Processing considerations are taken up in detail in Chapter 15. Some substrates, such as PA film, require chemical primers for lasting bonds.

Cost is an important consideration when selecting the coating polymer. It is important to consider all aspects of the cost and not just the price of the resin. LDPE is usually the lowest price resin used in extrusion coating and for many applications it is the best choice. Since the adhesion of LDPE to polar substrates is dependent on oxidation, its performance is susceptible to variations in the extrusion coating process, especially at high line speed. Oxidation of LDPE produces by-products that contribute to odor and off-flavor issues for some food products. Hence, LDPE may be limited in yield and productivity, two key components of cost. One way to overcome these challenges is to use ozone treatment, which allows the LDPE to be run at lower temperatures and faster line speeds. Some of the organoleptic issues remain, however.

A second approach is to coextrude LDPE with an acid copolymer. This allows more consistent adhesion at high line speeds and the ability to run at lower temperatures to reduce the negative aspects of

oxidation. For demanding applications using an acid copolymer or ionomer tie layer and sealant will be required, but coextrusion with LDPE is often used to minimize cost, especially on the sealant side of a foil or metallized film lamination where organoleptics and product resistance is most important.

A third approach for enhancing the performance of LDPE while minimizing cost is to modify the LDPE by blending it with a polar ethylene copolymer such as E/MAH/BA [62,63], EEA [70], or acid copolymer [81,82]. Morris [81,82] shows that compatibility between the modifier and the LDPE is important. He tests a series of blends of LDPE with acid copolymers with different acid functionality and finds that the lower acid content blends provide the greatest boost in adhesion to foil over LDPE alone. To test the compatibility, he makes blown films from blends of the same polymers and measures the film haze. The haze correlates with the inverse of the peel strength to foil. Film haze will decrease as the minor component of the blend is better dispersed (smaller domain size), which occurs as the compatibility between the components increases. A finer dispersion of the acid copolymer within the LDPE provides more acid functionality at the interface for bonding to the foil. While initially counterintuitive, copolymer with lower acid functionality is better dispersed in the LDPE matrix and provides higher functionality at the interface where it is needed. Based on this finding, Morris developed a modifier which DuPont commercialized as Nucrel AE.

The performance of a 20% Nucrel AE and 80% LDPE blend is shown in Fig. 10.17. Here 50-μm aluminum foil is coextrusion coated with 8-μm of the tie layer and 38-μm of LDPE. The performance of an LDPE control is poor, indicating the conditions were not favorable for oxidation. As is described in Chapter 15, the time in the air gap is an important parameter governing oxidation and adhesion. The value here, while fairly typical for commercial operations, is on the low side for good oxidative adhesion. The AE blend substantially improves the peel strength to around 600 g/25 mm. While not as good as a standard acid copolymer, which in this experiment gives a value of 1200 g/25 mm, this represents a significant gain in performance. To better understand how this boost in performance may play out in improved operational efficiency, Morris conducts a statistically designed experiment, varying the % AE in the blend (0−20%), processing temperature (293−327°C),

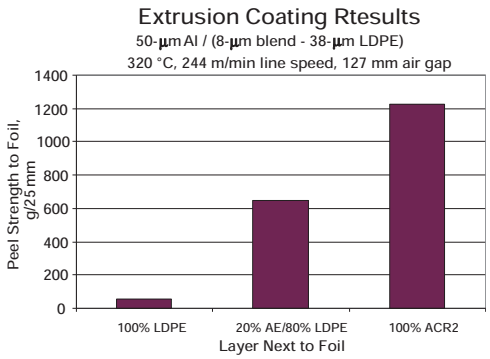


Figure 10.17 Performance of LDPE, LDPE modified by blending 20% Nucrel AE, and an acid copolymer in coextrusion coating. Peel strength is to the aluminum foil.
Adapted from Morris BA, Thai HT. Modifying LDPE for improved adhesion to aluminum foil. In: TAPPI PLACE conference; 2004. Reproduced with permission from E. I. du Pont de Nemours.

thickness of the coating (20−45 μm), and time in the air gap (60−100 ms). A quadratic response surface model is used to design and analyze the results. A statistical model is developed from the peel strength results.

All four variables are found to be statistically significant. Peel strength increases with increasing level of AE modifier in the blend, increasing temperature, increasing thickness, and increasing time in the air gap. The effect of temperature and TIAG is similar to that found with LDPE, suggesting an oxidation or stress mechanism [54]. The effect of thickness is discussed in detail in Section 15.1.4.

The benefits of adding Nucrel AE to the LDPE can be illustrated using the output from the statistical model. The model predictions from the statistically designed experiment are mapped on a contour plot as shown in Figs. 10.18 and 10.19. Such a plot is similar to a topographical map where each line represents a line of constant elevation. Here each line represents a constant region of peel strength. Moving along the line is like walking along a ridge of a hill. Moving perpendicular to the line is like walking up or down a hill. The closer the lines are together, the steeper the hill.

The lower left corner of Fig. 10.18 represents the case of running at 90 m/min with pure LDPE (0% AE). Here the coating temperature and thickness are set at the midpoint of the range investigated. Under these conditions, the peel strength is 450 g/25 mm. The effect of increasing line speed can be seen by

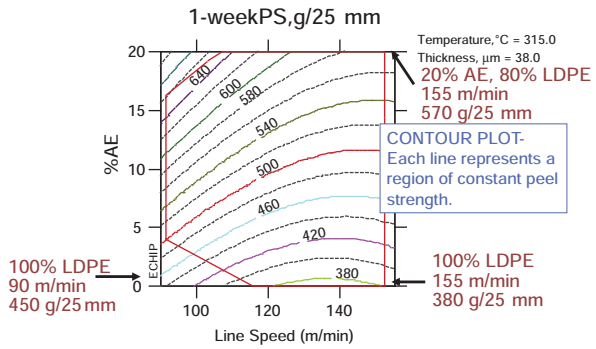


Figure 10.18 Contour plot of peel strength to aluminum foil showing effect of varying % AE and line speed.

Adapted from Morris BA, Thai HT. Modifying LDPE for improved adhesion to aluminum foil. In: TAPPI PLACE conference; 2004. Reproduced with permission from E. I. du Pont de Nemours and Company.

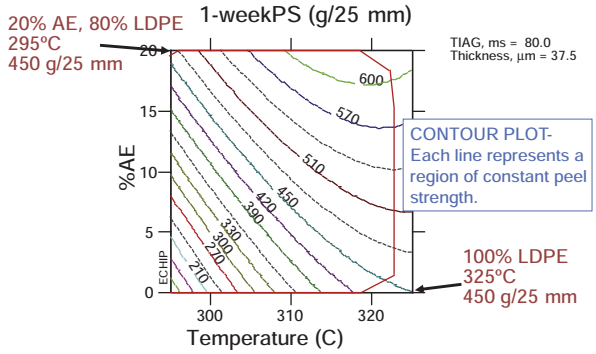


Figure 10.19 Contour plot of peel strength to aluminum foil showing effect of varying % AE and temperature.

Adapted from Morris BA, Thai HT. Modifying LDPE for improved adhesion to aluminum foil. In: TAPPI PLACE conference; 2004. Reproduced with permission from E. I. du Pont de Nemours and Company.

moving horizontally across the plot. Increasing the line speed to 150 m/min reduces the peel strength to 380 g/10 min (lower right corner). The effect of adding AE is found by moving vertically on the plot. At 20% AE and a line speed of 150 m/min (upper right corner), the peel strength is 580 g/25 mm. The productivity can be improved while maintaining the peel strength performance by adding AE.

Fig. 10.19 shows the effect of lowering the coating temperature, which may help reduce odor and off-flavors. Beginning in the lower right corner, the peel strength for 100% LDPE at 325°C is 450 g/25 mm. Moving along the 450 g/25 mm contour line to the upper left corner shows that adding 20% AE modifier will allow the temperature to be reduced to 293°C while maintaining peel strength. Lowering the coating temperature the same amount with 100% LDPE will reduce the peel strength to 150 g/25 mm (lower left corner).

Morris and Thai [81] went on to describe the benefits demonstrated during a trial at a converter. The converter produced a standard foil laminate for a dry food application. They had a quality specification of 250 g/25 mm for the peel strength to aluminum foil and were having trouble meeting it using LDPE. Control charts for three conditions are shown in Fig. 10.20. The top chart shows the preexisting situation using LDPE alone. None of the 15 production lots charted here met the 250 g/25 mm specification. The yield is only 4% or there are 960,000 defects per million opportunities (DPMO).

The middle chart shows the case of adding 20% AE to the LDPE, keeping the line speed and temperature constant. The mean peel strength increases from 166 to 308 g/25 mm. Except for one data point (lot 14), all the results meet the 250 g/25 mm specification. The poor adhesion with lot 14 was found to be due to special causes—poor foil quality. Statistical analysis shows that by adding 20% AE, the yield increases from 4% to 86% (139,000 DPMO).

The lower chart shows the case for adding 20% AE as well as increasing the temperature by 5°C. Now the mean is 384 g/25 mm, yield 99.6%, and defects only 4400 per million opportunities. The process reliability has been improved by four sigma.

This demonstrates that the use of a modifier can be a cost-effective approach for many applications. Situations where product resistance or very high line speeds are needed will still require specialty polymers used at full strength, such as acid copolymers and ionomers.

10.4.2 Coextrudable Adhesives

10.4.2.1 Coextrudable Tie Resin Technology

As described in Section 10.1, many combinations of polymers used in coextrusion do not bond well to each other. Resin suppliers have responded by developing tie resins that are sandwiched between the polymers to provide good adhesion. The general strategy is shown in Fig. 10.21. Frequently, a polyolefin such as polyethylene is being bonded to a polar polymer such as polyamide or ethylene vinyl alcohol. The bonding mechanisms of diffusion and chemical

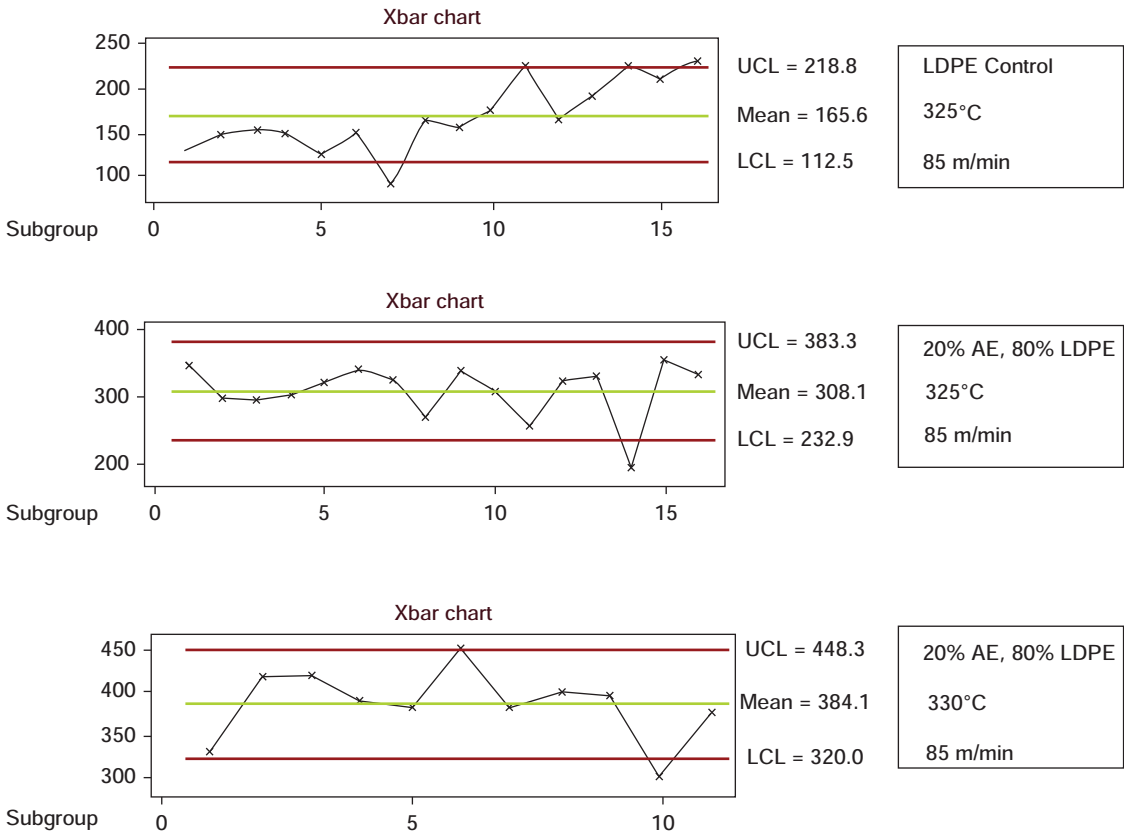


Figure 10.20 Control charts of peel strength performance at a converter run under three conditions.
Adapted from Morris BA, Thai HT. Modifying LDPE for improved adhesion to aluminum foil. In: TAPPI PLACE conference; 2004. Reproduced with permission from E. I. du Pont de Nemours and Company.

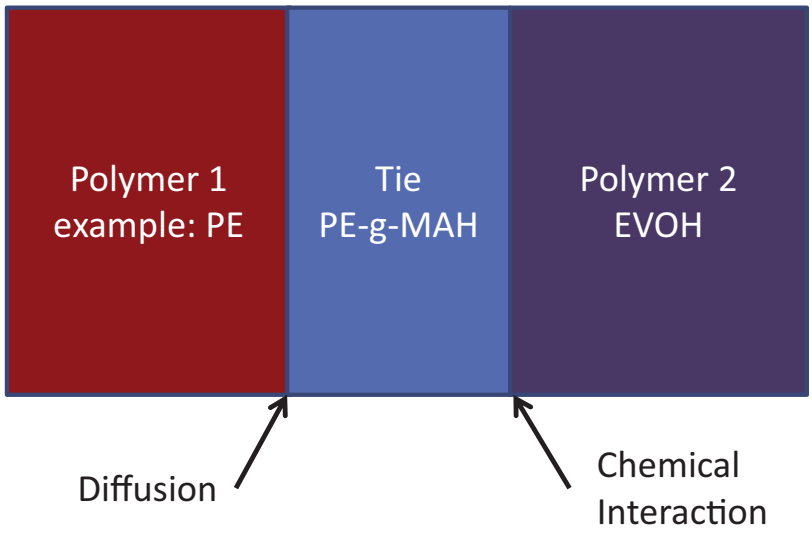


Figure 10.21 Design strategy for tie resins in coextrusion.

Table 10.13 Common Functional Groups Used in Coextrudable Tie Resins

Functional Group	Bonds to
Acid	PA, ionomers
Anhydride	PA, EVOH
Vinyl acetate	PVC, PVDC, PETG, PS, PP, ionomers
Acrylate (MA, EA, BA)	PET, PS, PP, ionomers

BA, butyl acrylate; *EA,* ethyl acrylate; *EVAOH,* ethylene vinyl alcohol; *MA,* methyl acrylate; *PA,* polyamide; *PET,* polyethylene terephthalate; *PETG,* polethylene terephthalate glycol; *PP,* polypropylene; *PS,* polystyrene; *PVC,* polyvinyl chloride; *PVDC,* polyvinylidene chloride.

interaction are primarily utilized. The tie resin is typically comprised of a matrix or base resin to which chemical functionality has been added. The matrix resin provides bonding to one side of the structure via diffusion and the chemical functionality provides adhesion on the other side via chemical interaction.

Most commercial tie resins are based on polyolefins. This is to take advantage of the diffusion mechanism for bonding to polyolefin substrates. Polyolefins have no chemical functionality in which to interact and so diffusion is the primary way to achieve adhesion at the polyolefin-tie interface. Good compatibility is required. As is discussed in Section 10.3.3, matching polarities and solubility parameters is one way to ensure good compatibility and diffusion at the interface. In practice, if the substrate is polyethylene or an ethylene copolymer such as EVA or ionomer, the tie resin is based on polyethylene or an ethylene copolymer that is most compatible. Similarly, if the substrate is polypropylene then a polypropylene-based tie resin is usually chosen.

The polyolefin-based tie resin is typically modified so that it contains functional groups that can bond to polar substrates. A list of common coextrusion tie resin functional groups is given in Table 10.13. Some of these are the same as for solid substrates (Table 10.10). The main difference is that in coextrusion both the tie resin and the substrate are molten. Reactivity and accessibility of reactive species is higher in coextrusion. The functional group can be incorporated into the tie resin by direct copolymerization, chemical grafting, blending, or any combination of these methods. Acid copolymers are examples of direct copolymerization where acrylic or methacrylic acid is incorporated into the polyethylene backbone via free radical polymerization. Grafting maleic anhydride onto a polyolefin chain is an example of the second approach. This is accomplished either in a reactive extrusion or solution process. A peroxide creates a free radical on the polymer chain to which the anhydride group attaches. The anhydride dangles from the polymer chain rather than being directly incorporated into the backbone of the polymer. For this reason, grafted functional groups are typically more reactive than the same group directly polymerized into the chain. The blending approach is often employed by tie resin manufacturers or film converters who use tie resin concentrates. For economic reasons, it is less expensive to graft polymer and let it down in a base resin. Furthermore, most tie resins are formulated for specific adhesion attributes, in some cases using all three approaches. For example, a formulated anhydride-modified EVA-based tie resin contains a base resin with vinyl acetate groups incorporated by direct polymerization. The anhydride may be grafted onto a polyethylene or EVA polymer and then blended with the EVA and other ingredients to create the final formulation.

Tie resins can be further formulated with various modifiers such as rubber and tackifiers [83–87]. While these modifiers provide some level of compatibility or chemical interaction, in many cases they impact peel strength performance by increasing the viscoelastic dissipation, bending energy, or elongation of the peel arm. These factors are discussed in detail in Section 10.2.3.

10.4.2.2 Factors Affecting Peel Strength in Coextrusion

The chemistry of the tie resin and the substrates it bonds to are critical for adhesion performance, but the design of the entire multilayer film structure, how it is fabricated and the environment it is subjected to in its ultimate use are also important.

10.4.2.2.1 Tie Resin Matrix and Adherend Chemistry

Diffusion is the primary mechanism for adhesion of tie resins to nonpolar substrates such as polyethylene and polypropylene. Polyethylene and ethylene copolymers come in a number of varieties as is described in Section 4.2.2. In general, polyethylene homopolymers (LDPE and HDPE) will bond well to each other and to linear alpha-olefin copolymers,

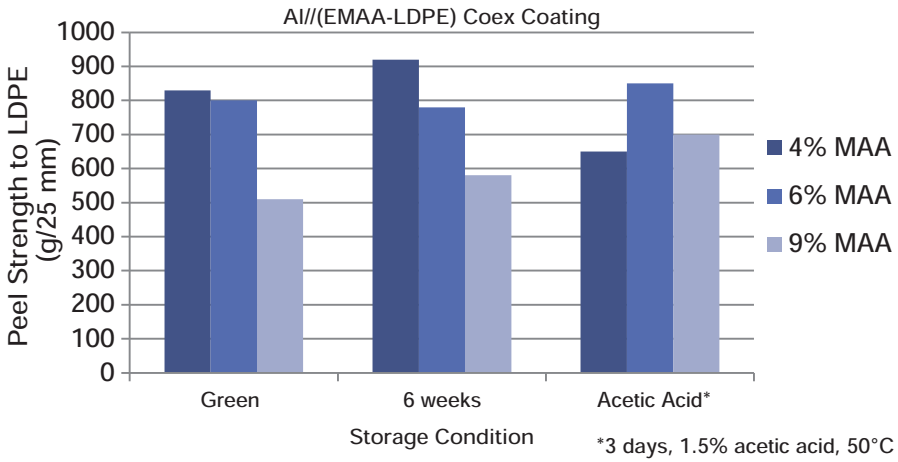


Figure 10.22 Peel strength performance of ethylene methacrylic acid copolymers to polyethylene in coextrusion coating.
Adapted from Hester DL, Sadik SA, Trouilhet Y. Using acid copolymers as coextrusion tie layers. In: TAPPI polymers, laminations and coatings conference; 1989. p. 459–63. Reproduced with permission from E. I. du Pont de Nemours and Company.

commonly known as LLDPE. These are all nonpolar polymers. While metallocene-catalyzed polyethylene generally provides better adhesion than Ziegler–Natta-catalyzed LLDPE, both types will bond well to other types of polyethylene.

When it comes to polar ethylene copolymers, the type of copolymer and level of functionality affect adhesion. Most grades of EVA will bond well to polyethylene, as will EMA copolymers. Bonding to the more polar acid copolymers and ionomers can be more challenging. The adhesion of acid copolymers to LDPE decreases with increasing acid content. This is illustrated in Fig. 10.22 with data from a study by Hester [88]. The peel strength of the laminates as made (green) and after storage for 6-weeks at 50% RH, 23°C decreases as the acid content increased from 4 to 9 wt%. After exposure to acetic acid to simulate the packaging of acetic food products such as ketchup, salad dressings, and orange juice, the peel strength shows the opposite effect. The effect of end-use environment is discussed in more detail in Section 10.4.2.2.5. Here it is sufficient to note that the selection of an acid copolymer for this application is often a compromise: high acid is favored for the best product protection and shelf life performance but low acid is favored to prevent delamination to the PE. Acid copolymers with approximately 7–9 wt% acrylic or methacrylic acid are often used.

Ionomers are often more polar than acid copolymers. Their adhesion to polyethylene decreases with increasing acid content and neutralization. Some grades are more compatible with polyethylene than others and are used as tie resins to bond PE to PA. The type of polyethylene also affects the adhesion. HDPE has poor adhesion to many grades of ionomer; indeed, this property is used to an advantage for designing easy-open peel seal packages that delaminate between the ionomer sealant and HDPE core (Section 7.7.2). In the LLDPE family of resins, lower density generally improves adhesion to ionomer, and metallocene LLDPE provides better adhesion than Ziegler–Natta. Ziegler–Natta LLDPE, because of its broader comonomer distribution, typically has a fraction of chains that have little comonomer content. In effect, these chains act like islands of HDPE embedded in the LLDPE, negatively impacting the adhesion to ionomer.

Section 10.3.3 describes how solubility parameters can be used as a guide to compatibility and diffusion. The smaller the difference in solubility parameters, the more alike the polymers are, and the more likely they will interdiffuse. One example where this has historically not been a good indicator is bonding polyethylene to polypropylene. Section 6.4.1 shows that the solubility parameters of these two nonpolar resins differ by less than 1 Hildebrand. Because there are no polar interactions between the molecules, this small difference in solubility parameters is not enough for miscibility. They should still be compatible, however. Yet in most coextrusion films, the adhesion between PE and PP is poor. The advancement of metallocene LLDPE has shed new light as to why. Research [89–92] shows that an amorphous layer forms at the surface of Ziegler–Natta LLDPE films. This is due to the broad MWD and comonomer distribution of these polymers: a fraction of the polymer contains relatively short chains with an abundance of comonomer. These low

molecular weight chains are excluded from the crystals and are forced toward the surface. The low MW amorphous region serves as an impediment to building strength at the interface. The longer PE chains most responsible for strength development must first diffuse through the weak amorphous region before entangling and cocrystallizing with the PP polymer chains (see Section 7.5.3.2.2 for a discussion of this phenomenon and its effect on heat sealing performance). Chain entanglements formed in the amorphous region are weak and unanchored.

Metallocene-catalyzed LLDPE has been found to bond well to PP. The proposed explanation is that because of its uniform MWD and comonomer distribution, low MW amorphous regions do not form at the interface. Diffusing polymer chains become entangled and can participate in the PE or PP crystals. This creates an anchoring effect that builds strength at the interface.

EVA bonds well to PP in coextrusion. EVA is made via a free radical polymerization process and generally has a very uniform comonomer distribution. This may help prevent the formation of the amorphous region at the interface. Also, EVA has a slightly higher solubility parameter than LDPE that is more of a match for PP.

One method to build strength between two incompatible polymers is to use a block copolymer. Block copolymers (Section 4.2.1.6) have long sequences of a single repeat unit along the chain. They are most often found commercially in the styrene family, such as styrene–butadiene–styrene copolymers. These have long sequences of styrene and butadiene along the chain. If an appropriate copolymer can be synthesized such that one block is compatible with one polymer and the other block with another polymer, block copolymers can be used as tie resins. Cole [93] found, however, that miscibility of the blocks with the polymers to be adhered to is not sufficient for good adhesion. They synthesized block copolymers for bonding PP or PE to PS. One of the copolymers did not participate in the polyolefin crystalline structure while the other one did. They found that cocrystallization gives better adhesion performance and actual reaction at the interface performs even better.

Olefin block copolymers (OBCs) have shown good affinity between PE and PP in several studies. Developed by The Dow Chemical Company, these are polymers with blocks of different olefinic compositions on the same polymer chain by a unique catalyst technology involving chain shuttling [94]. Ayyer [95] compares the adhesion performance of a polyethylene-based OBC with two mVLDPE plastomers with density 0.855 and 0.876 g/cc, respectively. The OBC has soft segments with density 0.855 g/cc and an overall density of 0.876 g/cc. Coextruded sheet of 2 mm thick with repeated microlayers of (HDPE-tie-PP) are tested using the three polyethylene grades as tie resins. The OBC provides higher peel strength than either of the two plastomers. Hu [96] evaluates a PP-PE OBC consisting of 50% iPP and 50% LLDPE blocks as tie resins for bonding PE to PP in coextrusion cast films. The polymer outperforms a number of LLDPEs and polythene OBCs, giving good adhesion to both the PE and PP layers. Adding a maleic anhydride-grafted HDPE to the PP-OBC provides good adhesion of PE and PP to PA, which is maintained at 85°C. Good adhesion before and after retort at 121°C is also obtained.

Using block copolymers as modifiers in tie resins may be less promising. Macosko [97] reports that when blended with other polymers, already formed block copolymers take too long to get to the interface to be effective tie resins in coextrusion. A better strategy is to form block copolymers in situ at the interface via chemical reactions [93,98].

As described in Section 10.4.2.1, many tie resins designed to bond to EVOH or PA comprise a polyolefin matrix resin to which anhydride and other functionality is added. The matrix resin is selected primarily to bond to the polyolefin side of the film

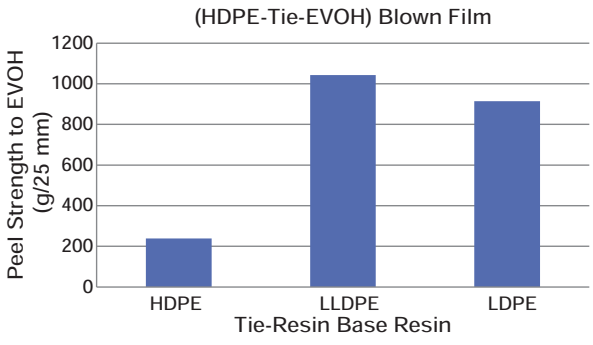


Figure 10.23 Peel strength to EVOH as a function of tie resin base resin type. All the tie resins are anhydride-modified polyethylene tie resins with the same general formulation except for the change of the matrix resin. Data are for blown film.
Reproduced with permission from E. I. du Pont de Nemours and Company.

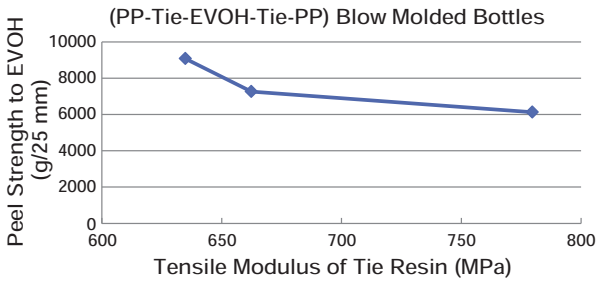


Figure 10.24 Effect of tie resin matrix resin modulus on peel strength to EVOH in extrusion blow molded bottles. Tie resins are anhydride-modified PP resins with the same general formulation except the base resin.

Adapted from Morris BA. Factors influencing adhesion in coextruded structures. TAPPI J 1992;75:107–10. Reproduced with permission from E. I. du Pont de Nemours and Company.

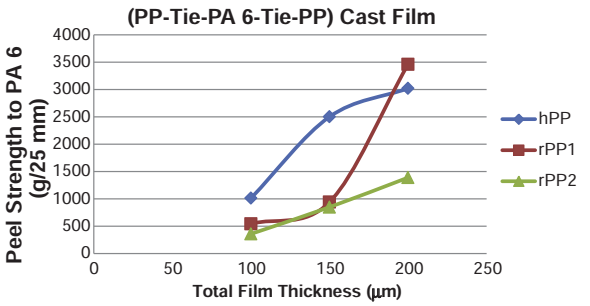


Figure 10.25 Effect of PP tie resin matrix resin on peel strength to PA6 in cast sheet. *hPP*, Homopolymer polypropylene; *rPP*, random PP-E copolymer polypropylene.

Reproduced with permission from Kamykowski GW. Factors affecting adhesion of tie-layers between polypropylene and polyamides. J Plastic Film Sheeting 2000;16:237–46.

structure, as described above, but can also affect the peel strength to EVOH and PA. Fig. 10.23 shows an example of the effect of matrix resin for one tie resin formulation developed by DuPont. LLDPE-based tie resins often outperform their LDPE and HDPE counterparts. The effect of PP matrix resin on peel strength is shown in Figs. 10.24 and 10.25. Fig. 10.24 shows peel strength to EVOH decreasing with increasing modulus of the base resin. Since homopolymer PP has a greater modulus than a random copolymer PP, this indicates a progression of higher peel strength with greater comonomer content. The opposite is shown in Fig. 10.25 where adhesion to PA for the tie resin with homopolymer PP as the matrix resin gives the best peel strength performance. All of

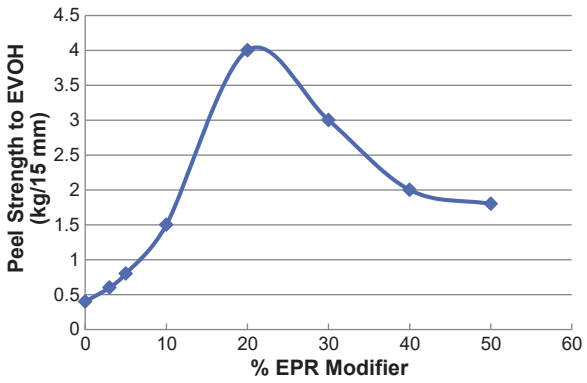


Figure 10.26 Effect of rubber modification of a PP-based tie resin on peel strength to EVOH. The tie resin formulation contains PP, PP-g-MAh, and an ethylene–propylene rubber (EPR). The amount of PP-g-MAh is held constant at 10% and the amount of EPR varied.

The data is from Inoue T, et al. Process for preparing laminated resin product; 1977. US patent 4058647.

these examples are anhydride-modified polyolefin formulations and within each set the same grafted polyoelfin is used as the source of the anhydride. The key takeaway is that the matrix resin upon which the tie resin is based upon can have a significant impact on the peel strength performance even though the actual bond strength comes from the anhydride. The performance may depend on the physical properties of the matrix polymer (such as modulus), chemical compatibility between the grafted letdown resin and the matrix resin, and other formulation details. This is important for film converters who blend their own tie resins from tie resin concentrates. Fully formulated grades produced by a tie resin manufacturer have been optimized for matrix resin, graft source, and other additives. When the converter does their own blending, they take on the responsibility for understanding and testing the effect the matrix resin has on the performance in their structure.

The matrix resin can be modified through copolymerization or melt compounding. Rubber modification is often used to toughen polymers, such as the addition of an ethylene–propylene rubber (EPR) to toughen PP. Tougheners act by stopping cracks from propagating. Rubber modification is also sometimes used in tie layer formulations. Fig. 10.26 shows an example from Inoue [86] where an EPR is added to an anhydride-modified PP tie resin formulation. The amount of anhydride is held constant. The peel strength to EVOH steadily increases with increasing

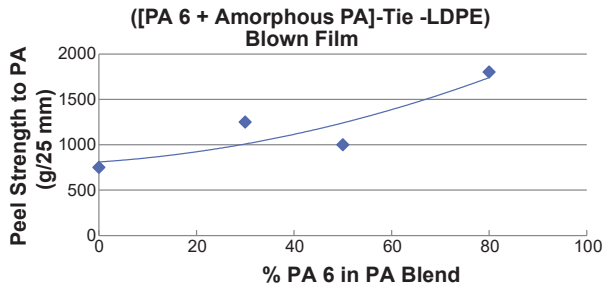


Figure 10.27 Effect of PA type on peel strength of an anhydride-modified ethylene copolymer tie resin. *Adapted from Morris BA. Factors influencing adhesion in coextruded structures. TAPPI J 1992;75:107–10. Reproduced with permission from E. I. du Pont de Nemours and Company.*

EPR content until about 20 wt% and then decreases. As described earlier, the patent literature is full of examples of different modifiers used in tie resins. The type of modifier and its level of addition affect the peel strength performance.

The chemistry of the adherend (what the tie layer is bonding to) is also important. The type of functionality on the adherend chain, whether the reactive group is located at the chain end or in the backbone, the concentration of the functional groups, and the ability for the functional group to get to the interface can all be important. Fig. 10.27 shows an example of the peel strength of a maleic anhydride-functionalized polyolefin to a blend of amorphous PA and PA6 in a coextruded blown film. Increasing the amount of PA6 in the nylon blend increases the peel strength. Presumably the end group chemistry is more favorable at higher levels of PA6 in the blend for greater reactivity and bond strength.

The physical properties of the adherend can also influence the peel strength performance. An example is the evaluation of tie resin formulations for bonding to PA6 in a three-layer blown film. Initially films with the structure (PA6—tie—LDPE) were made and the peel strength between the tie and PA6 layers tested. The results showed no discrimination among the tie resin compositions. This is because the adhesion exceeded the yield strength of the LDPE; all the peel arms elongated during the peel test. The peel test was measuring the tensile properties of the LDPE rather than the peel strength to PA. When the PE layer was switched to HDPE, the peel arm no longer stretched during the test and differences in tie resin performance could be assessed.

Another example can be found in Fig. 10.28. Here four different tie resin compositions are compared for their peel strength to EVOH. A three-layer blown film structure is used: (EVOH—tie—sealant). In one structure an ionomer is the sealant and the other is an EVA. In all cases, the peel strength to the EVOH layer is reported. The ionomer containing structure has lower peel strength, in general, than in the EVA structure. This is because the ionomer is stiffer than the EVA. The EVA yields and elongates more during the peel test. The actual bond strength to the EVOH is the same, but the peel strength is higher with the EVA structure due to the energy to elongate the peel arm. As a consequence, the choice of the sealant may affect the choice of the tie resin. In this set of data, Tie 1 gives the best performance for the ionomer sealant but Tie 2 provides the best peel strength when the EVA is the sealant.

10.4.2.2.2 Tie Resin Functionality

Choosing the appropriate chemical functionality to bond to the adherend is an important consideration in selecting tie resins. Table 10.13 provides a list of

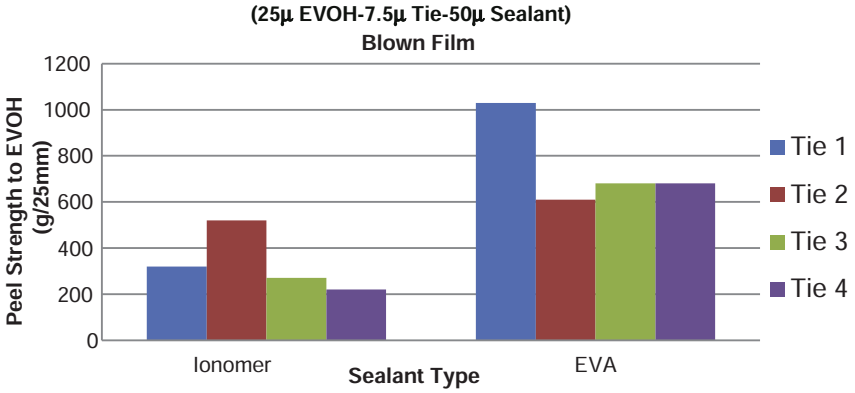


Figure 10.28 Effect of sealant type of peel strength of tie resins to EVOH. *Reproduced with permission from E. I. du Pont de Nemours and Company.*

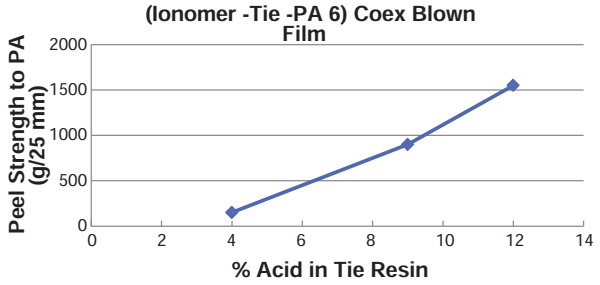


Figure 10.29 Effect of acid level on adhesion to PA6 in blown film. Tie layers are EMAA copolymers with wt% MAA ranging from 4 to 12 wt%.
Data from Hester DL, Sadik SA, Trouilhet Y. Using acid copolymers as coextrusion tie layers. In: TAPPI polymers, laminations and coatings conference; 1989. p. 459–63.

common functional groups and the polymers they bond to. Of particular interest in flexible packaging are tie resins that bond polyolefins to PA and EVOH. Historically, acid copolymers and ionomers were used to bond to PA6 in the early days of coextrusion. Lightly neutralized zinc ionomers gave the best adhesion to nylon in internal studies at DuPont [101,102]. As shown in Fig. 10.29, weight percent acid in the 6–12% range is needed to give good adhesion.

Anhydride-modified polyolefins have become the mainstay of tie resin technology for bonding to PA6 and EVOH [103–108]. The anhydride group reacts with the amine end groups of PA6 to form an imide [113] and with the hydroxyl group of EVOH to form an ester. These reactions are shown in Fig. 10.30.

Anhydride is typically grafted onto the polymer chain in a separate process after the polymer has been synthesized, rather than via copolymerization.

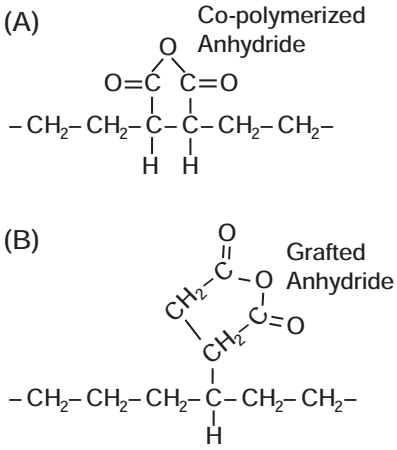


Figure 10.31 Chemical structure of ethylene-co-maleic anhydride copolymer (A) and maleic anhydride-grafted polyethylene (B).

Anhydride grafts tend to be much more reactive than copolymers. For example, the patent literature teaches that anhydride levels in the range of 0.1–0.5 wt% are used to bond to PA and EVOH when the anhydride is grafted onto a polyethylene backbone. This is an order of magnitude less than the amount of acid needed in an EMAA copolymer to bond to PA as shown in Fig. 10.29. Arkema makes an ethylene–acrylate–maleic anhydride copolymer with 3 wt% MAh but sells anhydride-grafted polymers for use as tie resins for PA or EVOH in coextrusion, presumably because they are more effective at one-tenth the functionality. The difference is explained in Fig. 10.31 where the grafted anhydride group is less restricted than an anhydride group incorporated into the polymer chain via

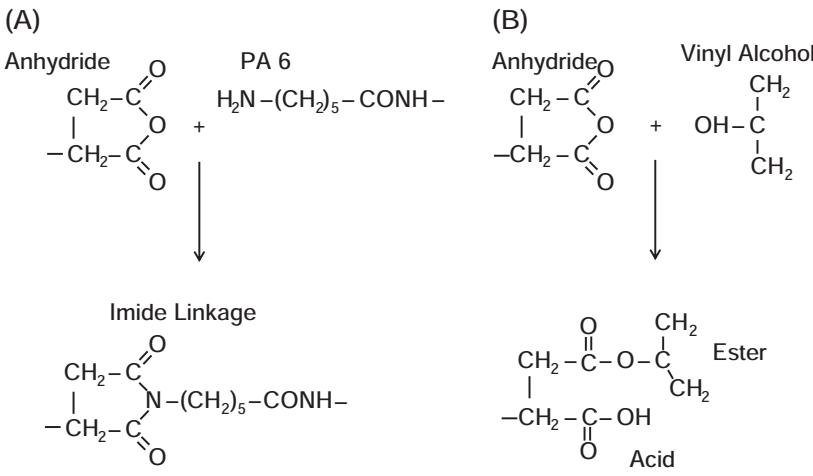


Figure 10.30 Chemical coupling of anhydride with (A) PA6 and (B) EVOH.

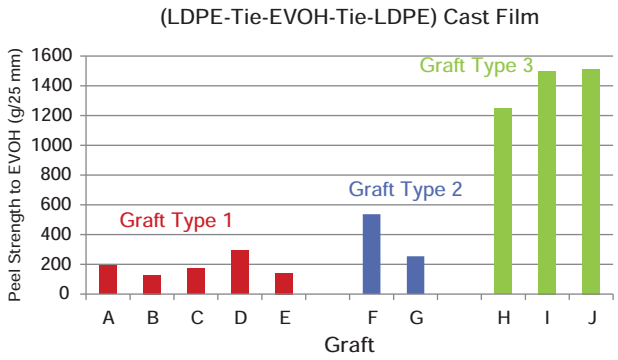


Figure 10.32 Influence of grafting technology of anhydride-functionalized tie resins.
Reproduced with permission from E. I. du Pont de Nemours and Company.

copolymerization. The greater mobility of the grafted anhydride group contributes to its enhanced reactivity.

Not all anhydride grafts are the same. Tie resin manufactures often have several technologies to choose from for optimizing peel strength for a given application. Fig. 10.32 shows an example from DuPont of three different graft technologies evaluated in a cast film structure. Clearly, graft type 3 gives the best performance in this structure. In other applications, graft 1 or 2 may be better.

The amount of chemical functionality is an important parameter. Fig. 10.29 shows that increasing the acid content of an acid copolymer tie resin increases the peel strength to PA6. Fig. 10.33 shows a similar effect for anhydride. Here a PP-g-MAh concentrate is blended with PP as the tie resin.

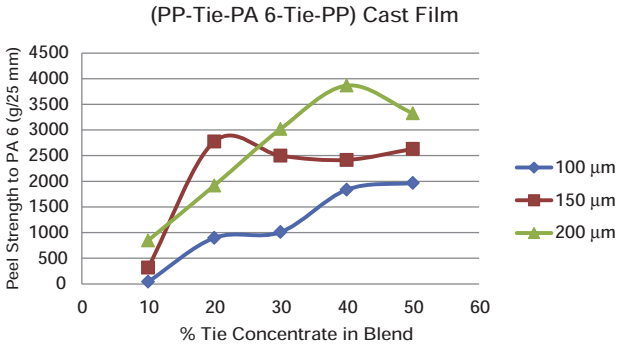


Figure 10.33 Effect of tie layer anhydride level on peel strength to PA. The tie layer is a blend of PP and a PP-g-MAh concentrate.
Data from Kamykowski GW. Factors affecting adhesion of tie-layers between polypropylene and polyamides. J Plastic Film Sheeting 2000;16:237–46.

An increase in concentrate corresponds to an increase in anhydride content and greater peel strength. As described in Section 10.3.4, Song [42] directly measures the amount of anhydride–imide linkages in a coextrusion of HDPE-g-MAh and PA6 by dissolving away the free PA and measuring the imide groups with XPS. The surface concentration of linkages at the interface is found to correlate with the initial concentration of anhydride.

Increasing chemical functionality has its limits. At some point diminishing returns or economics take their toll. Eventually the bond strength may exceed the cohesive strength of the tie resin or adherend and further increases do not yield improved performance. Or the target peel strength is achieved and further increases just add cost to the tie resin. In some cases the peel strength reaches a maximum and decreases with further increases in functionality. An example is PP-based tie resins. Grafting maleic anhydride onto PP generally reduces the molecular weight of the PP due to the susceptibility of PP to chain scission. Adding too much low MW graft to a tie resin formulation can reduce its cohesive strength to the point where peel strength suffers.

10.4.2.2.3 Film Structure

In addition to the chemistry of the tie resin and layers it bonds to, the thickness and mechanical properties of the film structure can influence the peel strength. Figs. 10.25 and 10.34 show the effect of total structure thickness on peel strength. Here the structure is (PP-tie-barrier-tie-PP) with each tie layer

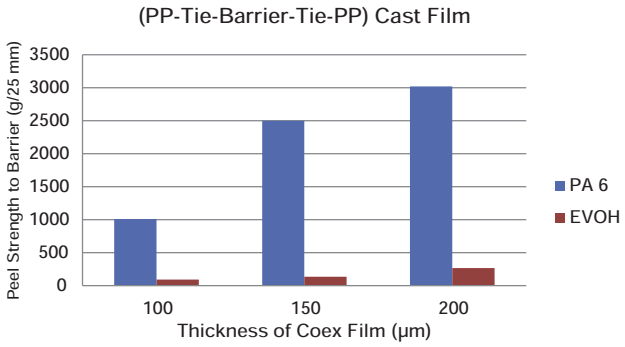


Figure 10.34 Effect of total film thickness on peel strength between a tie layer and barrier. Cast film of (PP-tie-barrier-tie-PP) with thicknesses of (38/4/16/4/38%).
Data from Kamykowski GW. Factors affecting adhesion of tie-layers between polypropylene and polyamides. J Plastic Film Sheeting 2000;16:237–46.

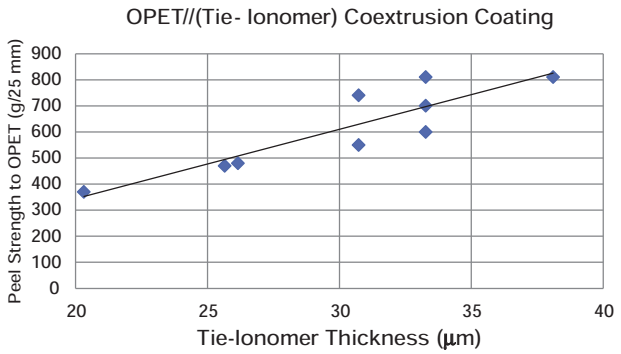


Figure 10.35 Effect of coextrusion coating thickness on peel strength to OPET film.
Reproduced with permission from E. I. du Pont de Nemours and Company.

being 4% of the structure [100]. The tie is an anhydride-modified PP and the barrier is PA6 or EVOH. The thickness is controlled by changing the line speed while keeping the output constant. The results show an increase in peel strength with increasing thickness. One explanation for this behavior comes from the fracture mechanics of the peel test (Section 10.2.3): as the peel arms become thicker and stiffer, the energy to bend the peel arms gets greater. A second explanation involves an increase in stress as the sheet is drawn down to thinner gauge. The effect of processing and stress is explored in detail in Chapter 15.

Fig. 10.35 shows the effect of varying the thickness of a (tie—ionomer) coating onto an OPET film. As the thickness increases, the peel strength to the OPET increases. Since the (tie—ionomer) is thin and flexible, the energy to bend the peel arm is likely not contributing much to the overall peel strength. The effect shown here is more likely a result of the mechanism described in Section 10.2.3.3 and Fig. 10.10 where increasing the thickness increases the zone of viscoelastic deformation at the peel front, increasing the fracture energy. Using typical values for the modulus and yield strength of ionomers, Eq. (10.15) predicts the critical thickness is around 150 μm. Since the (tie—ionomer) thickness is well below this value, the peel strength is on the rising portion of the peel strength vs thickness curve (Fig. 10.9).

How thin is too thin for the tie layer thickness? This depends on the total structure, the strength of the chemical interaction at the interface, and the target peel strength needed for the application. Often times it is limited by how well the converting equipment can control the thickness uniformity. Two to four percent of the structure is often the lower limit, but some structures have stretched this limit.

Ayyer [95] finds that when the tie layer thickness becomes very thin the mode of failure changes and the peel strength decreases faster than is predicted by the change in viscoelastic deformation. They make coextruded tapes with a repeat structure of (PE-tie-HDPE) using layer multipliers to divide and stack the layers. For films with tie layer thickness in the range of 2—14 μm, 65 layer structures are made. To study the regime of tie layer thickness from 0.1 to 2 μm, films with 257 layers are created. The results for a mVLDPE tie resin with a density of 0.855 g/cc is shown in Fig. 10.36. As the tie layer thickness decreases from 14 to 1 μm, the fracture toughness (which is related to peel strength) decreases linearly as expected from the fracture mechanics theory described in Section 10.2.3.3. The fracture toughness

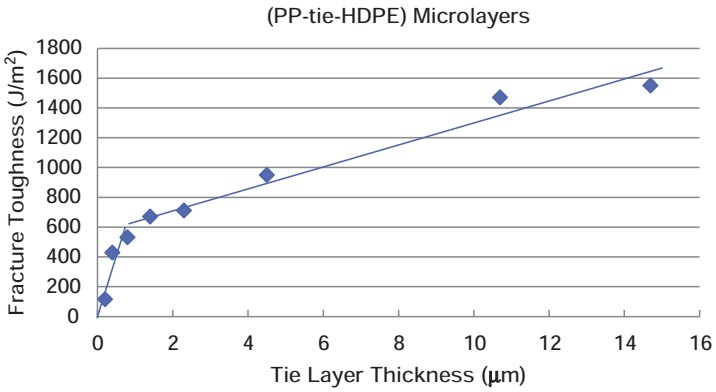


Figure 10.36 Effect of tie layer thickness on fracture toughness. Structure is repeated layers of (PP-tie-HPDE) where the tie is a metallocene plastomer with density 0.855 g/cc.
Data from Ayyer RK, Kamdar AR, Lin YJ, Dias PS, Poon BC, Hiltner A, et al. Effect of tie layer thickness on the adhesion of ethylene based copolymers to polyolefins. In: SPE ANTEC conference; 2009. p. 428—32.

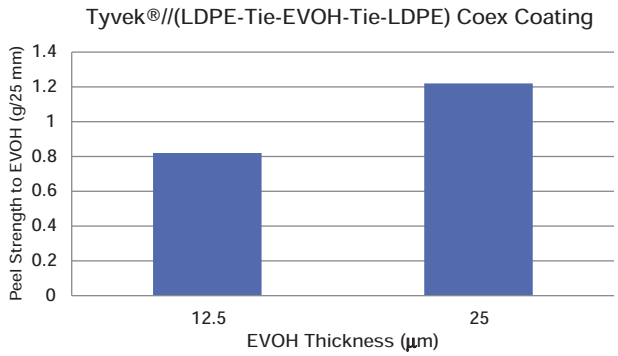


Figure 10.37 Effect of EVOH layer thickness on peel strength to EVOH in a coextrusion coating.
Reproduced with permission from E. I. du Pont de Nemours and Company.

correlates with the measured and calculated zone of deformation length. Below 1 μm they find that the change in fracture toughness decreases faster than expected. Scanning electron microscopy reveals that continuous plastic deformation in the thick tie layers gives way to fibril character as the tie layer thickness drops below 1 μm.

The thickness and stiffness of other layers in the structure also affect peel strength. Some examples of the effect of stiffness of the tie resin are presented in Section 10.4.2.2.1. Fig. 10.37 shows an example where increasing thickness of the adherend, in this case EVOH, increases the peel strength. Here the structure is a coextrusion coating of (LDPE-tie-EVOH-tie-LDPE) onto Tyvek, a spun-bond nonwoven PE fabric. The adhesion between the anhydride-modified polyolefin-based tie resin and EVOH is shown for two EVOH thicknesses. Stiffness of the peel arm may be one factor for the higher adhesion of the thicker EVOH layer. Another factor may be slower cooling of the molten web when it contacts the chill roll during coating due to the thicker extrudate.

Fig. 10.16 in Section 10.4.1.3 gives an example from Pascal [10] showing the effect of LDPE thickness on the adhesion of a tie resin to aluminum foil. Pascal [109] provides another example of how the structure design can affect peel strength. Heat seal strength of three structures each with the same sealant and tie resin is shown in Fig. 10.38. The seal strength varies considerably among the three structures even though they have the same sealant. Differences in the adhesion of the tie resin to foil and PET film (which is likely primed, but this is not revealed in the paper) may account for some of the differences in performance. More than likely, however, the observed differences are due to variation in energy dissipation due to bending and yielding of the peel arms.

10.4.2.2.4 Processing

The converting process can have a substantial impact on peel strength performance. Contact time, temperature, area creation, and stress are determined by the converting process. Often these can be varied to optimize adhesion.

Anhydride-containing tie resins have a special temperature consideration. The anhydride group can convert to a diacid with the addition of water. This is an equilibrium reaction with the anhydride form favored at high temperatures typical of extrusion. During transportation and storage the resin pellets absorb enough water to drive some of the anhydride

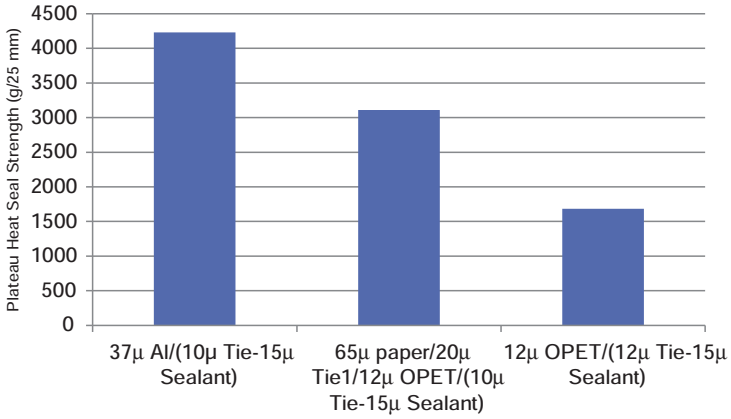


Figure 10.38 Effect of film structure on seal strength.
Data from Pascal J. Peelable structures for PP, PS, PET and PVC. Understanding how multilayer construction influences seal and peel properties. In: TAPPI PLACE conference; 2008.

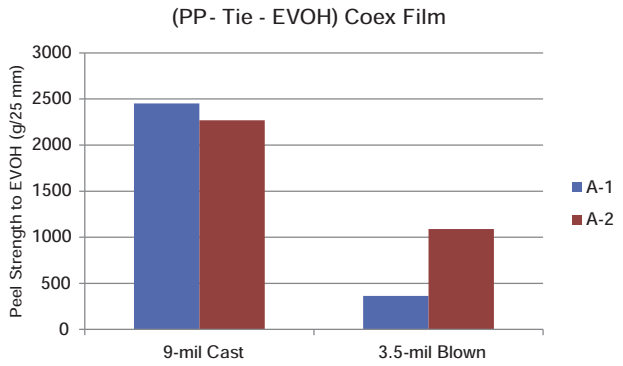


Figure 10.39 Effect of converting process on tie layer selection.
Reproduced with permission from E. I. du Pont de Nemours and Company.

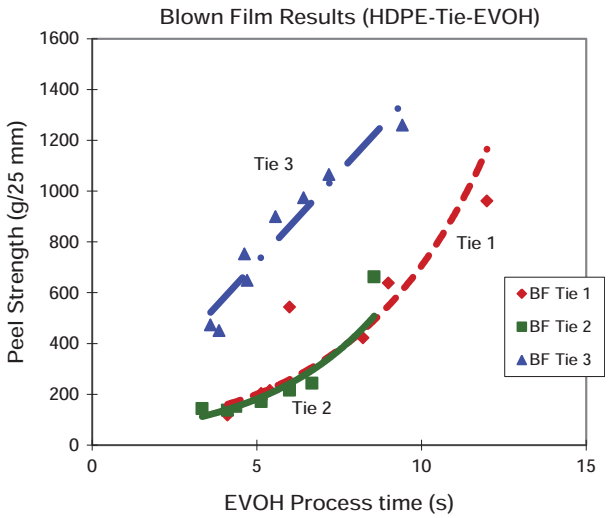


Figure 10.40 Effect of processing variables on peel strength to EVOH in blown film. Process time is the time the polymer spends in the bubble between the die exit and the frost line. It is defined by Eq. 2.14 and is directly proportional to the contact time prior to crystallization in the bubble and inversely related to the stress.
Reprinted with permission from Morris BA. The effect of coextrusion blown film processing variables on peel strength performance. In: SPE ANTEC conference; 1996.

to the diacid form. The diacid form does not bond well to PA or EVOH. The anhydride can be reformed in the extruder. Tie resin suppliers generally recommend a starting temperature of 210°C or higher to ensure the reaction is complete. Once good adhesion performance is established, the temperature can be incrementally reduced to determine the best temperature for that particular process.

The performance of tie resins may differ from one process to another. An example is shown in Fig. 10.39 comparing the results of peel strength measurements on a series of cast and blown films. The structure is the same for each: (PP—tie—EVOH). Two tie resins are evaluated. The cast film gives higher peel strength for both tie resins than the blown film, which may be due to the greater thickness of this film. In the cast film, both tie resins give the same performance, but in the blown film tie A-2 substantially outperforms tie A-1. This underscores the importance of testing tie resins in the same process and structure as the commercial process.

In general, less orientation and longer contact times at higher temperatures favor greater adhesion. Many processing parameters influence these characteristics and can be used to help optimize adhesion:

- Adhesion is favored at higher temperatures, within the bounds of the thermal stability of the polymers. Higher temperature increases the diffusion rate of the polymer chains and enhances the rate of chemical reactions at the interface.
- Increasing contact time in the die after the layers has been combined and in the air gap between when the polymer leaves the die and is quenched also improves adhesion. For example, Morris [110] finds that increasing the time between the die exit and the frost line in blown film increases peel strength by up to 10 times as is shown in Fig. 10.40. Similar effects are found for coextrusion coating and cast film [111]. Compressive flow has been found to accelerate reaction rates at the interface [42,43]. These effects can be substantial and are described in detail in Chapter 15.
- Increasing line speeds reduces contact time, which can reduce peel strength.
- Increasing the quench rate or heat transfer rate can reduce the time the polymers remain in contact at elevated temperatures, reducing peel strength. Decreasing chill roll temperature in coextrusion coating, lamination, or cast film or using inner bubble cooling in blown film increases the quench rate. An example of the effect of chill roll temperature is provided in Fig. 10.41. The peel strength to EVOH at two chill roll temperatures is shown with the higher chill roll temperature providing greater peel strength.

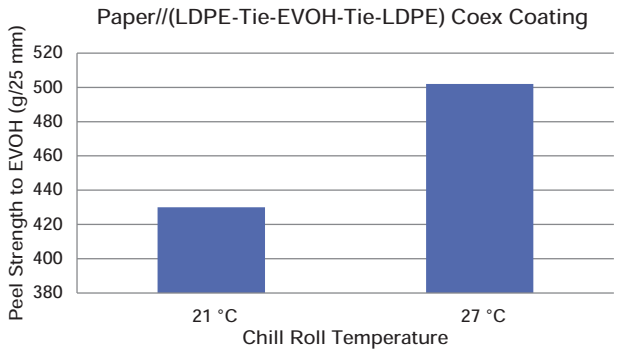


Figure 10.41 An example of the effect of chill roll temperature on peel strength to EVOH in coextrusion coating.
Reproduced with permission from E. I. du Pont de Nemours and Company.

- Orientation generally lowers peel strength by increasing the amount of interfacial area, which can reduce the density of bonding sites at the interface, as well as impose stress on the existing bonds. Increasing blow-up ratio or draw down ratio in blown film or increasing line speed and draw down ratio on flat film or coextrusion coating increases orientation and may reduce peel strength. Peel strength measured in the direction of orientation is often less than in the transverse direction. Film orientation processes such as tenter frame, double bubble, and machine direction orientation (MDO) often result in lower peel strength. An example of this effect for MDO is shown in Fig. 10.42 where peel strength of a tie layer to EVOH decreases with increasing draw ratio.
- The effect of thermoforming on peel strength is similar to orientation. As the film is stretched into its final shape, new interfacial area is created and stress is imparted at the interface, negatively affecting peel strength. An example is shown in Fig. 10.43 for (PA6—tie—ionomer) blown film where thermoforming decreases the peel strength by a factor of three. Increasing the thermoforming temperature can help improve the peel strength, as is illustrated in Fig. 10.44 for a PP-based structure. As the forming temperature is increased, less stress is imparted on the interface and the molecules have more mobility to relax.

All processing effects have limitations from an operation or performance perspective. For example,

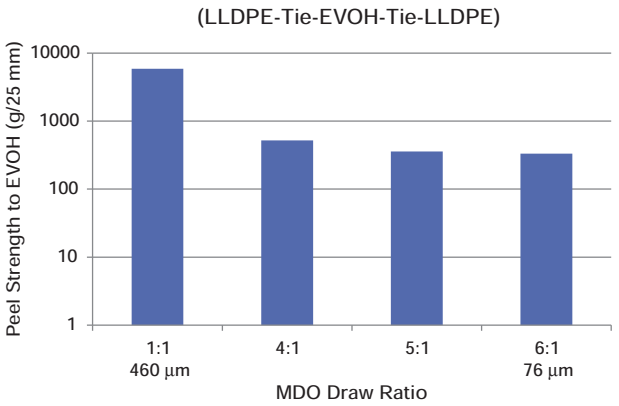


Figure 10.42 An example of the effect of machine direction orientation (MDO) on peel strength. Plotted results are for peel strength of an anhydride-modified polyethylene tie resin to EVOH. Initial sheet thickness is 0.5 mm and the orientation temperature is 115°C.
Adapted from Lee CD, Strebel JJ, Goudelock JD. Higher tie layer adhesion in machine direction oriented (MDO) barrier films. In: TAPPI PLACE conference; 2007.

increasing extrusion temperature may cause gel and black specs, increasing chill roll temperature may result in chill roll sticking and blocking, increasing air gap in extrusion coating/lamination increases neck-in, decreasing line speed reduces productivity and output, and decreasing orientation may reduce the physical properties. By understanding the fundamentals of why these parameters affect peel strength in the way that they do and the limits of the polymer involved, optimizing the process can often

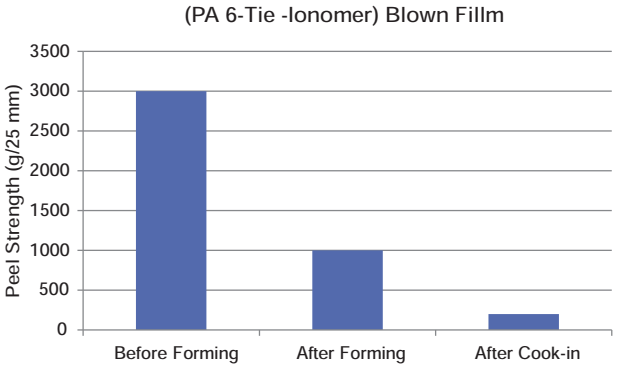


Figure 10.43 An example of the effect of orientation and end-use temperature on the adhesion of a tie resin to PA in a three layer coextrusion. After thermoforming the film is subjected to cook-in the package conditions.
Reproduced with permission from E. I. du Pont de Nemours and Company.

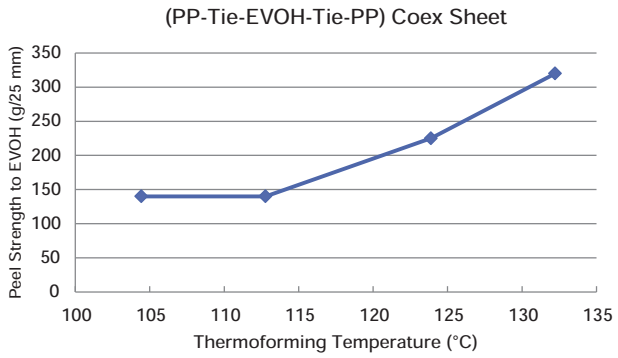


Figure 10.44 The effect of thermoforming temperature on the peel strength of an anhydride-modified PP-based tie resin to EVOH after forming.
Adapted from Morris BA. Factors influencing adhesion in coextruded structures. TAPPI J 1992;75:107–10. Reproduced with permission from E. I. du Pont de Nemours and Company.

bring a boost in adhesion performance. Sometimes this cannot be done within the limits of the process and changes in material selection or film design are required to meet the specifications for film performance and interlayer adhesion. Fig. 10.45 shows an example of how this may play out. The graph plots the data from Fig. 10.40 in terms of output (keeping the frost line height constant). As the output of the converting line is increased, the peel strength decreases. By changing the tie resin from a standard grade to a high-performance grade, peel strength can be designed back into the film at high output. Similar plots can be produced for other processes such as coextrusion cast film [111].

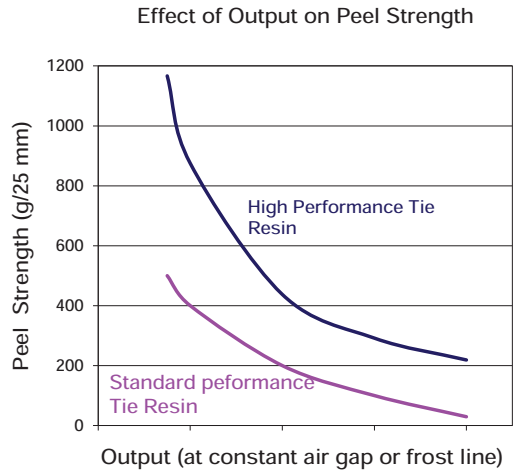


Figure 10.45 The effect of output on tie resin selection. Curves are replotted from data in Fig. 10.40. As output is increased, the peel strength decreases for a given tie resin. To maintain peel strength performance at higher output, sometimes a higher performance tie resin needs to be used.
Reproduced with permission from E. I. du Pont de Nemours and Company.

10.4.2.2.5 End Use

How the film is ultimately used—the environment and conditions it is subjected to—affects adhesion performance. Stresses from temperature, humidity/moisture, and chemical attack (from inside or outside the package) can reduce peel strength performance. These factors should be considered when selecting a tie resin.

Both cold and hot temperatures can affect adhesion performance. Polymers undergo thermal transitions that can affect their physical properties such as modulus, which affect peel strength performance. The best tie layer at room temperature may not be the best choice at the temperature of use. An example is shown in Fig. 10.46 where the peel strength of three tie resins to polycarbonate (PC) is shown. At room temperature tie 2 has the best performance but at −25°C, tie 1 has the best performance.

Elevated temperature often decreases the peel strength. An example is shown in Fig. 10.43 for a (PA−tie−ionomer) coextruded blown film used in cook-in of deli meats. As discussed earlier, the peel strength to PA decreases due to thermoforming. The meat slurry is cooked at 80−90°C for several hours in the package. During this time the temperature and stresses can reduce the peel strength performance as is shown by the third bar in the figure.

In some cases, peel strength can increase when exposed to elevated temperatures due to relaxation of stresses. An example of this is shown in Fig. 10.47 for a (PP-tie-EVOH-tie-PP) thermoformed cup. Two anhydride-modified PP tie resins are evaluated under conditions simulating retort sterilization. In the initial cups, the peel strength of both adhesives is relatively low, presumably due to stresses imposed on the interface during solid phase pressure forming. Both tie resins give about the same performance. Test strips cut from the cup are put on a tensile tester with an environmental chamber and heated up to 121°C to simulate retort. The peel strength measured at 121°C is shown in the middle set of bars. At this temperature the tie resins are below their melting points but the molecular chains become more mobile. The peel strength increases for both tie resins. This may be due

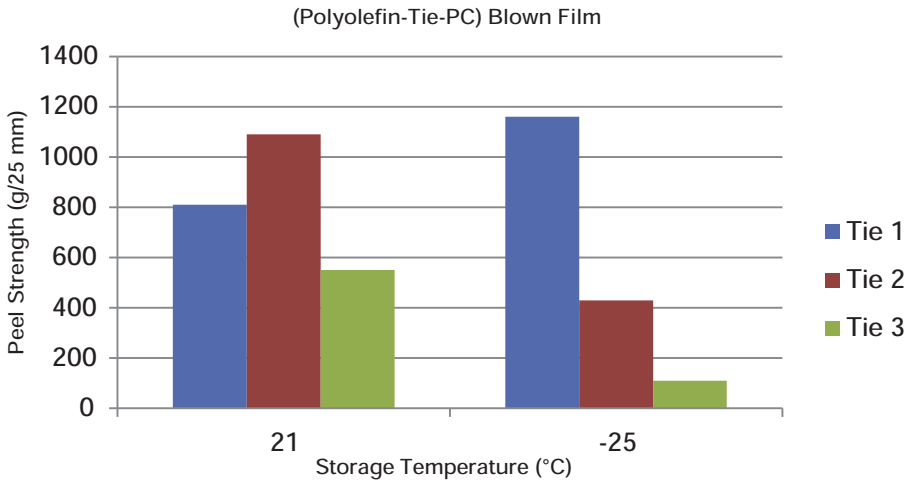


Figure 10.46 Effect of end-use temperature on tie resin selection. Peel strength of a coextruded blown film measured at room temperature after stored at the 21 or −25°C.
Adapted from Morris BA. Factors influencing adhesion in coextruded structures. TAPPI J 1992;75:107−10. Reproduced with permission from E. I. du Pont de Nemours and Company.

to relaxation of the stresses from thermoforming. The test strips are cooled back to room temperature and remeasured. The peel strength of tie 2 remains high but the peel strength of tie 1 drops. The performance of the two tie resins responds differently to the heat history imposed by the retort process.

Moisture can have an effect on bond strength. Section 10.4.1.3 describes the effect of boiling water on adhesion of EAA to aluminum foil where the form of the metal oxide on the surface of the foil changes. In coextruded structures, one or more of the layers may be plasticized or softened by moisture, which can affect peel strength through changes in the physical properties of the peel arms. Chemical interactions between some polymers may be negatively affected by water if the water outcompetes with the functional groups on the polymer for the bond site.

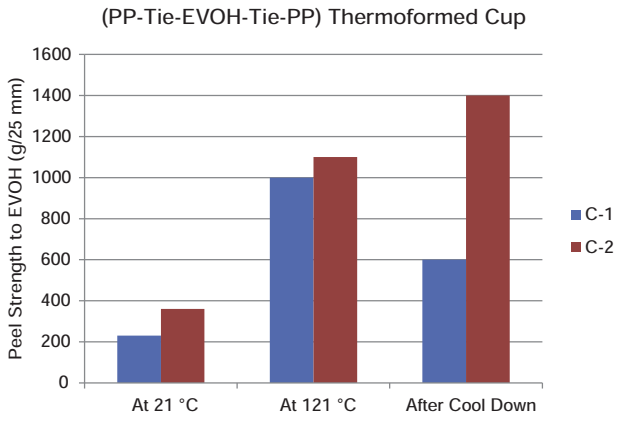


Figure 10.47 Effect of retort sterilization conditions on peel strength.
Reproduced with permission from E. I. du Pont de Nemours and Company.

Sometimes the bonds at the interface can undergo chemical attack from species in the product being packages or from the outside. An example of the former is shown in Fig. 10.22. Here (LDPE-tie) is coextrusion coated onto aluminum foil. At room temperature, the dry peel strength to LDPE decreases with increasing acid level due to the decreasing compatibility between the acid copolymer and LDPE. But when the structures are subjected to acetic acid to simulate migration from acidic food products such as ketchup or salad dressing, the higher acid EMAA copolymers provide the best peel strength and hence self-life performance.

End-use considerations are taken up in greater detail in Chapter 16. The important takeaway is that the tie layer selection depends on the end-use requirements and conditions the package will be subjected. Care should be taken when selecting a tie resin to test it under the actual conditions of use.

10.4.2.3 Choosing a Coextrudable Tie Resin

Table 10.14 outlines many of the factors that should be considered when selecting a tie resin. The first is the peel strength performance: will the tie resin provide the desired amount of adhesion to the two polymers? This depends on the tie resin formulation—the base resin and chemical functionality

Table 10.14 Coextrudable Tie Resin Selection Criteria

Selection Criteria	Resin Parameters
Peel strength	Adhesion (bonding, diffusion) Stress dissipative properties
Processing	Rheology Thermal stability Melt stability
End-use performance	Regulatory compliance MVTR Clarity Oil resistance Toughness Stiffness
Cost	Price Density Layer thickness Quality

Reproduced with permission from E. I. du Pont de Nemours and Company.

and any modifiers as described in Section 10.4.2.1. For common situations, such as bonding polyethylene to polyamide or EVOH, there are often a number of choices. For other situations, there may be only a few choices to consider. Most tie resin manufactures provide selector guides and other product literature to help their customers find grades that bond to the substrates. This provides a starting point for fine-tuning the selection based on the overall needs of the packaging films. Often a discussion with the tie resin manufacturer's technical service group will help with this process.

The tie resin must be compatible with the process in which it will be used. To prevent flow instabilities during coextrusion, it helps to try to match the viscosity of the tie resin to the other layers in the structure. This is one reason tie resin manufacturers have multiple grades for bonding the same combination of resins. These grades may differ in their rheology to run on different converting equipment, such as a 1 or 2 g/10 min melt index resin for blown film and a 4−8 g/10 min grade for cast film or extrusion coating. A description of flow instabilities, strategies for minimizing flow instability, and limitations that these place on resin selection is provided in Chapter 13.

The tie resin must also have sufficient thermal stability for the converting process at the processing temperatures needed to run the substrate resins. For example, an EVA-based tie resin may run well in a blown film operation but may not have enough thermal stability for some extrusion coating or cast film operations running at temperatures above 230°C. EVA manufacturers generally recommend that EVA be run at temperatures below 240°C in coextrusion (230°C for mono extrusion). For high temperature processes, EMA- or PE-based tie resins may be more suitable due to their greater thermal stability. This sometimes is dictated by the substrate. For example, an EVA may be suitable for bonding to polyethylene terephthalate glycol but not as suitable for use with PET homopolymer ($T_m = 260°C$), which must be run hotter.

The tie resin can contribute to melt strength of the coextrusion, which is important for maintaining bubble stability in blown film and preventing edge weave and neck-in in extrusion coating. Tie resins based on LDPE or polar ethylene copolymers generally have better melt strength than linear polymers like LLDPE.

The performance of the film in the end use is the ultimate goal, and even though the tie resin is often a small component of the overall film thickness, it can contribute, or at least not takeaway, from this goal. Most tie resins take on properties similar to that of the resin they are based on. This can be used to help screen potential grades to use for a given application. Factors that may enter into the tie resin selection criteria may include the following:

- Compliance with appropriate government regulation such as the U.S. FDA and European Union food packaging regulations.
- Moisture vapor transmission rate. Some packages require low moisture permeation (high barrier) and the tie layer can contribute. In this case a tie based on a medium or high density polyethylene may be favored over one base on EVA or EMA.
- Clarity. The tie resin should not detract from the clarity of the package if transparency is an important criterion. This involves selecting tie resins that are based on polymers with high clarity and low haze. An EVA-based tie resin may be favored over an HPDE-based one. Rubber modification and other additive technologies may take away some of the tie resin's clarity. These should be kept in mind when selecting the tie resin grade.

- Oil resistance. For polyolefins, the greater the density, the better the oil resistance. For situations where this is critical and the tie resin can be the difference, higher density PE-based tie resins or even ionomers may be used.
- Toughness. The tie resin may help contribute to the toughness of the film in concert with the other layers of the structure. Depending on the failure mode, this may involve selecting tie resins with very soft base resins such as EVA, EMA or plastomer, or very stiff base reins such as HDPE or PP.
- Stiffness. As is described in Chapter 9, bending stiffness of a multilayer film is important for runnability on packing lines and for consumer perception. The bending stiffness is highly influenced by layer modulus or stiffness, thickness, and location. Sometimes using a stiffer tie resin, such as one based on HDPE, can help increase the bending stiffness.

Finally there is cost. The overall system cost should be considered, not just the price of the resin. The cost of using a higher priced resin may be offset by a lower density, the ability to downgauge the thickness of the tie layer or increase line speed. Quality is also an important consideration. Fewer line breaks and less defects and product loss during film production can have significant payback. Inventory costs can also influence grade choice; a tie resin grade that can be used for multiple applications at the same plant may allow for reductions in inventory of raw materials and cost savings.

To help reduce costs, tie resin manufacturers have introduced tie resin concentrates for some applications, such as bonding PE to PA or EVOH. The concentrates are typically anhydride-modified PE with a high level of maleic anhydride. They are blended into a polyolefin letdown resin on the film extruder at anywhere from 5% to 40% depending on application and concentrate. This cuts out a compounding step typically done by the tie resin manufacturer. The film converter essentially becomes the tie resin manufacturer and takes on the responsibility for formulating and increased risk for quality. It is important to understand the special challenges when using tie resin concentrates. These include the following:

1. The composition of the letdown resin (resin that is blended with the concentrate). As described in Section 10.4.2.2.1, the generic type (LDPE, LLDPE, HDPE, PP, and so on) as well as the specific grade (MWD, branch distribution, comonomer type, comonomer content, additives, and so on) can affect the peel strength performance. The base or matrix resin of a tie resin fully formulated by the tie resin manufacturer is often carefully chosen after many trials to ensure robust performance across a number of customers and applications. A converter who uses just what is on the plant floor as the letdown resin may have a suboptimum formulation. As described in the previous Section 10.4.2.2.5, the physical, optical, chemical resistance, and other key properties of the tie resin are dictated by the base resin. These same properties need to be considered when choosing the letdown resin.
2. Anhydride source. There are a number of tie resin concentrate grades on the market. These may differ by the base resin used in the grafting process, the grafting process, the amount of anhydride, and other factors. The compatibility of the anhydride concentrate and the letdown resin may be important for adhesion. More demanding converting processes, such as cast film or extrusion coating, may require a more robust anhydride source. Most suppliers keep details of their concentrates confidential, so it can be difficult to compare concentrates from different suppliers prior to testing on the actual film line.
3. Anhydride level. The amount of anhydride needed depends on the substrate being bonded to. The tie resin should be formulated for robustness. Fig. 10.48 shows a typical anhydride vs peel strength curve for the combination of concentrate and letdown resin. The shape of this curve may differ considerably from one concentrate and letdown resin to the next. As the anhydride level is increased, the peel strength generally increases until it reaches a plateau where further increases do not change the peel strength appreciably. The ideal target anhydride level is somewhere on the plateau far enough away from the onset of the plateau that typical quality fluctuations keep the peel strength within specifications. If the amount of concentrate used is too low and the peel strength is on the rapidly rising section, the resulting peel strength can be highly variable. A good practice is to run a trial with several different levels of concentrate in

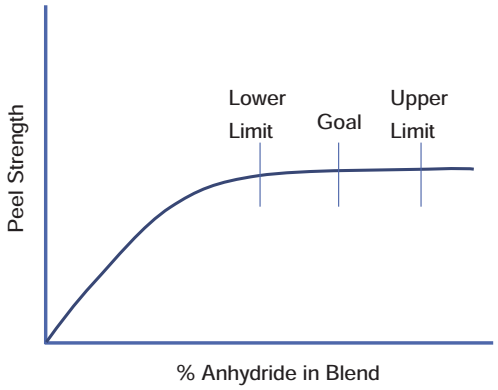


Figure 10.48 Theoretical effect of anhydride level on peel strength performance and ideal region to set specifications to avoid large variability in peel strength performance.

the blend and test the peel strength performance to generate the curve. From this, the optimum blend concentration can be established based on quality and cost.

4. Anhydride level consistency. Consistency in peel strength performance is directly dependent on the consistency of the anhydride level of the final blend. Tie resin manufactures make pellets that can be directly tested for anhydride using FTIR and other analytical methods. They can use this data to ensure the process is under control and the product is within specifications. A converter making its own tie resin by blending with a concentrate does not isolate the tie resin as a pellet. Rather the tie resin ends up in a coextruded film structure where measuring the amount of anhydride is usually not possible. The converter must rely upon mass balance to control the process. The amount of variability will depend on the variability of the amount of anhydride in the concentrate and the error associated with the blending:

$$\begin{aligned} \%\ \text{Anhydride} &= (B + e_b)(C + s_c) \\ &= B(C + s_c) + e_b(C + s_c) \end{aligned} \quad (10.21)$$

where B = target % of concentrate in blend, e_b = error associated with blending, C = amount of anhydride in concentrate, s_c = standard error of anhydride in concentrate.

The last term on the right side of the equation, $e_b(C + s_c)$, represents the extra risk the converter takes on when blending rather than using a fully formulated tie resin. Modern loss-in-weight feeders and blenders help minimize e_b (Chapter 6). The variability of the anhydride level in the concentrate, s_c, depends on the manufacturing capability of the concentrate supplier. This may vary by grade and among suppliers. The converter should ask for quality control specification ranges if they are not already provided by the manufacturer.

5. Blending. The quality of blending is important to ensure uniform distribution of the anhydride throughout the tie layer and to minimize local variation in anhydride functionality. Factors affecting the blend quality are described in Chapter 6. These include matching the shape, size, and density of the concentrate and letdown resin so that the pellets do not segregate prior to entering the extruder, using appropriate-sized feeders and blenders to ensure good accuracy, minimizing the transfer length of pellet blends from the blender to the extruder, and using an extruder screw design sufficient for the task of melt blending. The percentage of the blend made up of concentrate can also be important. Very low blend percentages may hinder the ability of the blending system to adequately mix and distribute the anhydride uniformly. For example, a 1% blend represents just 1 pellet out of 100 pellets entering the feed hopper to the extruder. Small variations can create rather large deviations from the target composition, especially since single screw extruders have little ability for back mixing. The concentrate supplier may have less concentrated grades for use at intermediate concentrations up in the 20–40% range. Alternatively, sometimes fully formulated grades can be used as the concentrate.
6. Processing. All the processing issues described in Section 10.4.2.2.4 that affect peel strength also apply to concentrate formulations.
7. Patents. The tie resin intellectual property space is fairly crowded. It is up to the converter to ensure they have freedom to operate.
8. Quality complaints. Quality complaint handling becomes less straightforward when using concentrates. The tie resin supplier does not have control over what the converter does in their plant to properly blend the concentrate into the letdown resin. Often it is difficult to troubleshoot and find the root cause of adhesion issues when

concentrates are used. This becomes a challenge for converters and tie resin suppliers alike.

9. Safety. Functionalized polymers may contain skin irritants and other health hazards. As the concentration increases, the potential for safety and health issues may increase. Care should be taken to read the safety data sheet and consult with the manufacture about proper handling.
10. Testing. Since there is no intermediate quality control tests on the tie resin itself to ensure consistency and quality, the converter may need to increase the frequency of quality control tests on the coextruded film.

A final note on choosing a tie resin is to test the candidates under conditions that simulate actual production and use. This includes running trials in the commercial structure on the production film line at production rates. Running a structure at low output to "get it right" may result in higher peel strength than once the process is ramped up to full production rates (Fig. 10.45). It also means testing the film structure under conditions that simulate the end use, such as thermoforming, or cold or hot temperatures. Lab tests can help screen candidates but ultimately the structure needs to be made and tested under actual conditions of manufacture and use.

References

[1] Mount III EM. Adhesion testing. November 2005. p. 66–8. pffc-online.com.
[2] ASTM International. Standard test method for peel resistance of adhesives (T-peel test) (D1876-08). West Conshohocken, PA: ASTM International; 2008.
[3] Deutsches Institut fur Normung. Testing of plastic sheet; adhesion test (DIN 53357), Berlin, Germany; 1982.
[4] ASTM International. Standard test methods for measuring adhesion by tape test (D33590-09e2); 2009.
[5] ASTM International. Standard test methods for assessing the adhesion of metallic and inorganic coatings by the mechanized tape test (B905-00). West Conshohocken, PA: ASTM International; 2010.
[6] ASTM International. Standard practice for evaluating ink or coating adhesion to flexible packaging materials using tape (F2252/F2252M-13e1). West Conshohocken, PA: ASTM International; 2013.
[7] Wu S. Fracture of adhesive bond. In: Polymer interface and adhesion. New York: Marcel Dekker, Inc.; 1982. p. 475–569.
[8] Kinloch AJ, Lau CC, Williams JG. The peeling of flexible laminates. Int J Fract 1994;66:45–70.
[9] Gent AN, Hamed GR. Peel mechanics for an elastic-plastic adherend. J Appl Polym Sci 1977;21:2817–31.
[10] Pascal J. Ultraversatile adhesives to broaden the possibilities of extrusion lamination. In: TAPPI PLACE conference, Cincinnati, OH; 2006.
[11] Morris BA. Understanding why adhesion in extrusion coating decreases with diminishing coating thickness. J Plastic Film Sheeting 2008;24:53–88.
[12] Kinloch AJ, Young RJ. Fracture behavior of polymers. London: Elsevier Applied Science Publishers; 1985.
[13] ASTM International. Standard test method for wetting tension of polyethylene and polypropylene films (D2578-09). West Conshohocken, PA: ASTM International; 2009.
[14] Diversified Enterprises, 2016. Accu dyne test, introduction and overview, viewed on July 1, 2016, https://www.accudynetest.com/adt_introduction.html.
[15] Wu S. Surface tension and polarity of solid polymers. In: Polymer interface and adhesion. New York: Marcel Dekker, Inc.; 1982. p. 169–214.
[16] Wu S. Interfacial and surface tensions of polymer melts and liquids. In: Polymer interface and adhesion. New York: Marcel Dekker, Inc.; 1982. p. 67–132.
[17] Schonhorn H. Heterogeneous nucleation of polymer melts on high-energy surfaces. II. Effect of substrate on morphology and wettability. Macromolecules 1968;1:145–51.
[18] Coleman M, Graf J, Painter P. Specific interactions and the miscibility of polymer blends. Lancaster, PA: Techonomic Publishing; 1991.
[19] Van Krevelen DW. Properties of polymers: their estimation and correlation with chemical structure. Amsterdam: Elsevier Scientific Publishing Co.; 1976.
[20] Gilbertson T. Adhering flexo inks to flexible packaging substrates... The surface energy solution. In: SPE FlexPackCon Conference; 2014.

[21] Schubert G. Adhesion of aluminum foil to coatings – stick with it. In: European TAPPI PLACE Conference; 2004.
[22] Schubert G. Adhesion of coatings to aluminum foil. PFFC; September 2003. p. 148–50.
[23] Schubert G, Plassmann O. Adhesion to foil – more than just a one-sided story. In: TAPPI PLACE conference; 2008.
[24] Schubert G, Plassmann O. Shedding new light on corona-treated alu-foil. In: TAPPI PLACE conference; 2004.
[25] Andrade JD, Ma SM, King RN, Gregonis DE. Contact angles at the solid-water interface. J Colloid Interface Sci 1979;72:488–94.
[26] Ko YC, Ratner BD, Hoffman AS. Characterization of hydrophilic-hydrophobic polymeric surfaces by contact angle measurements. J Colloid Interface Sci 1981;82:25–37.
[27] Schultz J, Carre A, Mazeau C. Formation and rupture of grafted polyethylene/aluminum interfaces. Int J Adhes Adhes 1984;4:163–8.
[28] Cho CK, Cho K, Park CE. Relationship between surface rearrangement and adhesion strength of poly(ethylene-co-acrylic acid)/LDPE blends to aluminum. J Adhes Sci Technol 1997;11:433–45.
[29] Wu S. Formation of adhesive bond. In: Polymer interface and adhesion. New York: Marcel Dekker, Inc.; 1982. p. 359–447.
[30] Ward DR. Thermodynamic parameters for predicting adhesion between functional polyethylenes to polystyrene copolymers. In: TAPPI PLACE conference; 2006.
[31] Lee I, Wool RP. Optimum polymer solid interface design for adhesion strength. J Adhes 2001;75:299–324.
[32] Lee I, Wool RP. Polymer adhesion vs substrate receptor group density. Macromolecules 2000;33:2680–7.
[33] Gong L, Friend AD, Wool RP. Polymer-solid interfaces: influence of sticker groups on structure and strength. Macromolecules 1998;31:3706–14.
[34] Leclere IN, Dinelli B, Kuusipalo J. Keys to good adhesion in coextrusion coating: interactions between tie resin nature and pre-treatments. In: TAPPI polymers, laminations & coatings conference; 1997. p. 203–9.
[35] Allen R. Using primers in combination with adhesive tie-layer resins or their blends to make structures with unique performance. In: TAPPI PLACE conference; 2005.
[36] Bodine J, Tanny SR. Improved bonding performance of low temperature extrudate on primed substrates. In: SPE FlexPackCon Conference; 2006.
[37] Botros MG. Investigation of adhesion and failure mechanisms in tie-layer adhesvies/EVOH stystems. In: TAPPI polymers, laminations & coatings conference; 1995. p. 331–47.
[38] Botros MG. Investigation of adhesion and failure mechanisms in tie-layer adhesive/EVOH systems. J Plastic Film Sheeting 1996;12:195–211.
[39] Botros M, Lee C, Ward D, Schloemer T. New developments of Plexar® tie-layer adhesives in flexible and rigid applications. In: European TAPPI PLACE conference; 2005.
[40] Levitt L, Macosko CW, Schweizer T, Meissner J. Extensional rheology of polymer multilayers: a sensitive probe of interfaces. J Rheol 1997;41:671–85.
[41] Saito T, Macosko CW. Interfacial crosslinking and diffusion via extensional rheometry. Polym Eng Sci 2002;42:1–9.
[42] Song J, Baker AM, Macosko CW, Ewoldt RH. Reactive coupling between immiscible polymer chains: acceleration by compressive flow. AIChE J 2013;59:3391–402.
[43] Song J, Ewoldt RH, Hu W, Silvis HC, Macosko CW. Flow accelerates adhesion between functional polyethylene and polyurethane. AIChE J 2011;57:3496–506.
[44] Markgraf DA. Corona treatment enhanced adhesion for extrusion coating. In: Bezigian T, editor. Extrusion coating manual. 4th ed. Atlanta: TAPPI Press; 1999. p. 65–74.
[45] Laiho E, Ylänen. Flame, corona, ozone – do we need all pretreatments in extrusion coating? In: Bezigian T, editor. Extrusion coating manual. 4th ed. Atlanta: TAPPI Press; 1999. p. 89–98.
[46] DiGiacomo JD. Flame plasma surface treatment. In: Bezigian T, editor. Extrusion coating manual. 4th ed. Atlanta: TAPPI Press; 1999. p. 121–30.
[47] Wolf RA. Advances in adhesion with CO_2-based atmospheric plasma surface modification. In: TAPPI PLACE conference; 2008.
[48] Hansen MH, Finlayson MF, Castille MJ, Goins JD. The role of corona discharge treatment on improving polyethylene/aluminum –

an acid/base perspective. In: TAPPI polymers, laminations & coatings conference; 1992. p. 311.
[49] Eckert W. Corona and flame treatment of polymer film, foil and paperboard. In: TAPPI PLACE conference; 2004.
[50] Bentley Jr DJ, Singer FM. Chemical primers to enhance adhesion and other properties. In: Bezigian T, editor. Extrusion coating manual. 4th ed. Atlanta: TAPPI Press; 1999. p. 185–200.
[51] Mica Corp, 2006. Primer technology: converting with water, viewed on March 07, 2015, http://www.tappi.org/content/06asiaplace/pdfs-english/converting.pdf.
[52] Trouilhet Y, Morris BA. Prediction of temperature profiles across coating and substrate in the nip. In: TAPPI polymers, laminations and coatings conference; 1999.
[53] Sherman PB. Ozonation of polymer melt for improved adhesion. In: Bezigian T, editor. Extrusion coating manual. 4th ed. Atlanta: TAPPI Press; 1999. p. 75–88.
[54] Morris BA, Suzuki N. The case against oxidation as a primary factor for bonding acid copolymers to foil. In: TAPPI polymers, laminations & coatings conference; 2000.
[55] Smarook WH, Bonotto S. Adhesion of carboxyl-containing polyolefins. Polym Eng Sci 1968;8:41–9.
[56] Bernacki RF. Adhesive polymers for extrusion coating and laminating. In: TAPPI polymers, laminations and coatings conference; 1985. p. 311–8.
[57] Shah BA. The effect of interfacial chemical interactions in inter-layer adhesion of packaging structures. In: TAPPI polymers, laminations and coatings conference; 1989. p. 789–92.
[58] Hoh G, Sadik SA, Gates JA. Aluminum foil adhesion of ethylene/methacrylic acid copolymer extrusion coatings. In: TAPPI polymers, laminations and coatings conference; 1989. p. 361–6.
[59] Finlayson MF, Shah BA. The influence of surface acidity and basicity on adhesion of poly(ethylene-co-acrylic acid) to aluminum. J Adhes Sci Technol 1990;5:431–9.
[60] Charboneau DB, Domine JD. Acid terpolymers for extrusion coating and laminations. In: TAPPI polymers, laminations and coatings conference; 1991. p. 281–8.
[61] Vansant JD. Acid copolymers for extrusion coating. In: Bezigian T, editor. Extrusion coating manual. 4th ed. Atlanta: TAPPI Press; 1999. p. 235–9.
[62] Vansant JD. Ionomer resins for extrusion coating. In: Bezigian T, editor. Extrusion coating manual. 4th ed. Atlanta: TAPPI Press; 1999. p. 241–7.
[63] Couturier LL, Schultz J. Adhesion das les multicouches polymere-metal (Adhesion in polymer-metal multi-layers). Vide, Les Couches Minces – Suppl 1990;251:87–9.
[64] Baker GL, Buesinger RF. The ethylene methyl acrylate copolymer. J Plastic Film Sheeting 1987;3:112–7.
[65] Henn B. It's time to get to know n-butyl acrylate copolymers. Plastics Technology; June 1992. p. 71–4.
[66] Davis DS. EnBA: expanding the portfolio. In: SPE ANTEC conference; 1995. p. 2115–9.
[67] Laiho E, Kuusela S. Specialities for extrusion coating – high pressure copolymers. In: TAPPI polymers, laminations and coatings conference; 1995. p. 613–23.
[68] Trouilhet Y. New acrylate based resins for extrusion coating. In: TAPPI European place conference; 2003.
[69] Baker GL. Ethylene methyl acrylate copolymers for extrusion coating. In: Bezigian T, editor. Extrusion coating manual. 4th ed. Atlanta: TAPPI Press; 1999. p. 231–4.
[70] Walther B, Falla D, Niemann D, Zudercher C. Adhesion properties and performance of ethylene-ethylacrylate copolymers. In: European TAPPI place conference; 2003.
[71] Van Ness RT. Ethylene vinyl acetate in extrusion coating. TAPPI J 1976;59:114–6.
[72] Cheney GD. Ethylene vinyl acetate resins for extrusion coating. In: Bezigian T, editor. Extrusion coating manual. 4th ed. Atlanta: TAPPI Press; 1999. p. 227–30.
[73] Hjertberg T, Lakso JE. Functional group efficiency in adhesion between polyethylene and aluminum. J Appl Polym Sci 1989;37:1287–97.
[74] Ulren L, Hjertberg T. Adhesion between aluminum and copolymers of ethylene and vinyltrimethoxysilane. J Appl Polym Sci 1989;37:1269–85.
[75] Hansen MH, Finlayson MF, Vaughn MH. Characterizing aluminum adhesion for low density

polyethylene. In: TAPPI polymers, laminations & coatings conference; 1991. p. 349.
[76] Gregory BH. Extrusion coating, a process manual. 2005. p. 73–92. Trafford, Victoria, Canada.
[77] Ulren L, Hjertberg T. An FT-IR study on interfacial interactions in ethylene copolymers/ aluminium laminates in relation to adhesion properties. J Adhes 1990;31:117–36.
[78] Stralin A, Hjertberg T. FTIR study on interfacial interactions between hydrated aluminium and polar groups in ethylene copolymers. Surf Interface Anal 1993;20:337–40.
[79] Schultz J, Lavielle L. Adhesion mechanisms of grafted polyolefins. Makromol Chem, Macromol Symp 1989;23:343–53.
[80] Morris BA, Trouilhet YM. Lamination adhesion of foil to thermoplastic polymers. 2004. US patent 8137776 B2.
[81] Morris BA, Thai HT. Modifying LDPE for improved adhesion to aluminum foil. In: TAPPI PLACE conference; 2004.
[82] Morris BA. A blend of low density polyethylene and a copolymer of low acid-ethylene copolymer (such as acrylic acid or methacrylic acid); high speed coating. 2005. US patent 6903161 B2.
[83] Lee I-H. Ethylene-vinyl acetate copolymer blend, graft polymer. 1989. US patent 4861677 A.
[84] Hattori M, et al. Adhesive resin composition. 1997. US patent 5591792.
[85] Lee I-H. Adhesive compositions based on blends of grafted polyethylenes and non-grafted polyethylenes and styrene container rubber. 2001. US patent 6184298 B1.
[86] Inoue T, et al. Process for preparing laminated resin product. 1977. US patent 4058647.
[87] Matsumoto H, Niimi H. Grafted with an unsaturated carboxylic acid or derivative thereof. 1980. US patent 4198327 A.
[88] Hester DL, Sadik SA, Trouilhet Y. Using acid copolymers as coextrusion tie layers. In: TAPPI polymers, laminations and coatings conference; 1989. p. 459–63.
[89] Chaffin KA, Knutsen JS, Brant P, Bates FS. High-strength welds in metallocene polypropylene/polyethylene laminates. Science 2000;288:2187–90.
[90] Sherman LM. Metallocene PP & PE weld strongly to each other. Plastics Technology; April 2001. p. 45.
[91] Poon B, Chang A, Chum SP, Tau L, Volkenburgh WR, Hiltner A, et al. Adhesion of polyethylene to polypropylene in multi-layer films. In: SPE ANTEC conference; 2001. p. 1668–72.
[92] Poon B, Chum SP, Hiltner A, Baer E. Adhesion of polypropylene to metallocene/Ziegler-Natta polyethylene blends in microlayers. In: SPE ANTEC conference; 2002. p. 1849–53.
[93] Cole PJ, Macosko. Polymer-polymer adhesion in melt-processed layered structures. J Plastic Film Sheeting 2000;16:213–22.
[94] Arriola DJ, Carnahan EM, Hustad PD, Kuhlman RL, Wenzel TT. Catalytic production of olefin block copolymers via chain shuttling polymerization. Science 2006;2006(312): 714–9.
[95] Ayyer RK, Kamdar AR, Lin YJ, Dias PS, Poon BC, Hiltner A, et al. Effect of tie layer thickness on the adhesion of ethylene based copolymers to polyolefins. In: SPE ANTEC conference; 2009. p. 428–32.
[96] Hu Y, Bonekamp J, Garcia-Meitin E, Marchand G, Walton K, Patel R. Polypropylene based olefin block copolymers as tie layers for multilayer packaging. In: SPE ANTEC conference; 2014.
[97] Macosko W. Flow accelerates interfacial reaction in coextrusion and compatibilization of polymer blends. In: SPE ANTEC conference; 2015.
[98] Macosko CW, Jeon HK, Hoye TR. Reactions at polymer-polymer interfaces for blend compatibilization. Prog Polym Sci 2005;30:939–47.
[99] Morris BA. Factors influencing adhesion in coextruded structures. TAPPI J 1992; 75:107–10.
[100] Kamykowski GW. Factors affecting adhesion of tie-layers between polypropylene and polyamides. J Plastic Film Sheeting 2000;16: 237–46.
[101] Powell RJ. DuPont internal report. 1971.
[102] Smith MS. DuPont internal report. 1979.
[103] Ashcraft CR, Kerr ML. Adhesion by molecular orientation. 1987. US patent 6650721 A.
[104] Moriarty Jr JW. Ethylene-maleic anhydride tie layer between polyamide and polyolefin layer. 1987. US patent 4668571 A.
[105] Bivens DA, Duncan GL. Maleic-anhydride modified polymer lager coated with polymeric composition derived from vinylidene chloride. 1977. US patent 4064315 A.

[106] Krueger DA, Odorzynski TW. An adhesive of a blend of maleic anhydride propylene graft polymer and polypropylene. 1986. US patent 4617240.
[107] Krueger DA, Odorzynski TW. Coextruded film of polypropylene, polypropylene blend, and nylon. 1982. US patent 4361628 A.
[108] Deyrup EJ. Plastic composite barrier structures. 1990. US patent 4973625 A.
[109] Pascal J. Peelable structures for PP, PS, PET and PVC. Understanding how multilayer construction influences seal and peel properties. In: TAPPI PLACE conference; 2008.
[110] Morris BA. The effect of coextrusion blown film processing variables on peel strength performance. In: SPE ANTEC conference; 1996.
[111] Morris BA. Effect of process and material parameters on interlayer peel strength in coextrusion coating, film casting and film blowing. J Plastic Film Sheeting 2010;26:343−76.
[112] Lee CD, Strebel JJ, Goudelock JD. Higher tie layer adhesion in machine direction oriented (MDO) barrier films. In: TAPPI PLACE conference; 2007.
[113] Marechal P, Coppens G, Legras R, Dekoninck J-M. Amine/anhydride reaction versus amide/anhydride reaction in polyamide/anhydride carriers. J Polym Sci Part A Polym Chem 1995;33:757−66.

11 Thermoforming, Orientation, and Shrink

Many packaging films undergo thermoforming or orientation. During thermoforming, the film is stretched into a mold or cavity to form a package of desired shape. Such stretching involves biaxial and planar orientation of the film typically below the melting point of one or more of the layers. In orientation processes such as the tenter frame, double bubble, and machine direction orientation (MDO) processes, the film is stretched under similar conditions to enhance physical properties or impart shrink. Both processes are covered in this chapter, with a focus on the process and material parameters that affect performance. This chapter concludes with a description of oriented multilayer film technology.

11.1 Thermoforming

Thermoforming is an important packaging fabrication process used in both flexible and rigid packaging. In flexible packaging, forming is used to create cavities, such as in horizontal form fill seal machines, for the product to lie in. The film is heated to the forming temperature and forced into a cavity or mold with vacuum or the positive force of a plug or both. The temperature, material properties, and process parameters (rate of draw, draw ratio, and so on) influence the ability of the film to be successfully thermoformed. Most of the thermoforming literature involves sheet processes with very little on films and even less on multilayer films. There is no single material or processing parameter that characterizes good and bad thermoformability. This section describes the important features of thermoforming and the factors that influence the ability of films to be thermoformed, borrowing from the sheet literature where appropriate.

11.1.1 Thermoforming Part Testing

Some of the properties of the thermoformed part that are critical to quality include the following:

- Uniformity of the layers after forming. Uniformity of the draw, especially in the corners of the cavity is often a challenge. Thin areas can result in greater gas permeation and lower strength.
- Integrity of the layers after forming. This is particularly important for barrier layers. If the barrier layer breaks up or is stretched too thin during forming, the shelf-life of the package may suffer. The strength of the materials and package also requires integrity of the layers.
- Low residual stress. High stress frozen into the formed package can result in what is sometimes referred to as "suck back" where the final shape of the cavity is not the same as the dimensions of the mold.

During the forming process, the forming force (vacuum or plug) and the surface temperature of the film or sheet is measured, usually with an IR thermometer. The force and temperature are two key parameters to control for consistent quality of the formed parts.

After forming, the thickness distribution in the formed part is typically measured on a representative set of samples. The total thickness can be measured by a number of devices. Some of the most commonly used in the literature include the following:

- sonic techniques: eg, MagnaMike, Panametrics 25DL;
- magnetic flux: eg, Electro Physik Minitest F44000;
- digital micrometer;
- spiral micrometer;
- optical microscope;
- electron microscope.

The thickness is measured at several fixed locations on the part, such as near the lip, along a side wall, along the bottom and in the corners. The results are typically reported as the standard deviation divided by the mean. The greatest variation is typically in the corners where the highest elongation has occurred.

The Science and Technology of Flexible Packaging. http://dx.doi.org/10.1016/B978-0-323-24273-8.00011-3
Copyright © 2017 Elsevier Inc. All rights reserved.

For multilayer films, the layer distribution of the individual layers is also important to measure. This is typically done using an optical or electron microscope on cross-sectioned specimens. Depending on the structure, other techniques such as interferometry or IR spectroscopy may be able to distinguish the thickness of one or more of the critical layers, such as the barrier layer [1,2].

11.1.2 Material Properties and Testing

A number of material properties have been shown to influence forming, which include the following:

- Crystallinity. Lower crystallinity generally improves formability. The ideal material for forming is a rubbery elastic solid that deforms or flows uniformly with applied stress. Above their glass transition temperature (T_g), amorphous polymers exhibit this behavior often over a broad temperature range. Semicrystalline polymers usually have a much narrower thermoforming window that is dependent on the degree of crystallinity, the crystalline morphology, and the thermal properties. Formability is generally improved with lower degree of crystallinity and smaller crystal size. The use of nucleating agents, for example, may help improve formability by reducing the size of the crystals. The addition of a rubbery phase can improve formability. An example is impact copolymers of polypropylene (PP) where an ethylene–propylene rubbery phase is copolymerized into the PP homopolymer backbone. The resulting product has superior hot strength for greater sag resistance, improved formability, and better low temperature toughness but maintains most of its high temperature performance since the homopolymer PP remains the continuous phase [3].
- Hot strength. Higher strength at the forming temperature provides better sag resistance in the film or sheet. Higher molecular weight (MW) generally improves hot strength.
- Yield stress. Low yield strength helps give uniform orientation during forming. The temperature and speed of the process needs to be adjusted to reach the yield point to achieve uniform thickness distribution [4].
- Recoverable strain (from creep tests, see Section 5.5.2). High recoverable strain makes it more difficult for the polymer to conform to mold shapes and increases residual stress (which affects physical properties) [5].
- Strain hardening (after yielding). Materials that strain harden exhibit higher stress as the strain is increased (see Chapter 5 for a discussion on strain hardening in the melt). Strain hardening helps control the uniformity of the thickness during forming through a "self-healing" effect. A region that locally experiences higher elongation than adjacent regions will experience higher stress. This acts to impede further stretching of that region, allowing the adjacent regions to catch up. High strain-hardening behavior is thus self-correcting. As described in Chapter 5, incorporating long chain branching (LCB) and broadening the molecular weight distribution (MWD) are two ways to increase strain-hardening behavior of a polymer.

Since thermoforming involves nonlinear biaxial deformation of the film at elevated temperatures, it is generally difficult to measure polymer properties that simulate the thermoforming process. Several lab tests are used but each has its limitations:

- Hot tensile test. This involves measuring the tensile properties (stress vs. strain) at the forming temperature using a tensile tester with an environmental chamber. This test is generally easy to perform and so probably is the most commonly used test for formability. The deformation is uniaxial rather the biaxial and Throne [6] warns about the danger of extrapolating uniaxial data to biaxial: "no current analytical model can be used a priori to predict the thermoformability of a given polymer. Practical methods of comparing the performance of one material with another must remain relatively empirical for the time being." The strain rate ($0.3–0.6\ s^{-1}$) is at the low end of the thermoforming process ($0.1–10\ s^{-1}$). Hot tensile tests have been used to fit model parameters, but some authors warn the fit is not generally applicable. There are also practical measurement issues that affect the reproducibility: grip slip and stretching not confined to neck-down region [7].
- Hot creep test. The creep test is described in detail in Section 5.5.2. A load or stress is applied and the

resulting strain measured as a function of time. This is another commonly used test for formability. The hot creep test allows higher shear rates than the hot tensile test but like the tensile test, the deformation is uniaxial. The creep experiment yields a characteristic retardation time, λ, which corresponds to the delay in response to the imposed stress. When the process time of the thermoforming process is less than 0.1λ, the material behaves like an elastic membrane, making it suitable for snap-back forming. When the process time is greater than 10λ, the material behaves like a viscous fluid, ideal for pressure forming [6].

- Dynamic mechanical (thermal) analysis (DMA or DMTA). This test is described in Section 5.3.5. The sample is subjected to an oscillatory stress in the linear viscoelastic regime and the response measured. The elastic (G') and loss (G'') modulus are two responses recorded by the test. The test can be either run at constant temperature, varying the frequency, or constant frequency varying the temperature. DMA is very repeatable and is useful for obtaining model parameters, but as a direct indication of thermoformability it has several deficiencies. The test uses small deformations in the linear regime whereas thermoforming involves highly nonlinear deformations. DMA also does not duplicate the stretching and orientation found in thermoforming.
- Melt strength (Rheotens). This test is described in Section 5.3.6. It measures the melt tension on a filament extruded from a capillary rheometer at elevated temperatures drawn down between rotating rolls. This test is conducted in the melt, whereas thermoforming is done in the rubbery plateau region below the melting point. As such, the Rheotens test does not mimic the thermoforming process very well, although it can provide relative rankings for hot strength and sag resistance.
- Extensional viscosity. Several techniques used to measure this melt property are described in Section 5.3.6. Most are uniaxial measurements in the melt state, but some indication of strain hardening can be obtained with these measurements. To better simulate thermoforming and biaxial stretching, several investigators have devised a membrane inflation rheometer [8–11].
- Differential scanning calorimetry (DSC). The glass transition temperature, melt point, crystallization temperature, and heat of fusion are important attributes that can be measured with DSC. The fraction of molten resin at a given temperature can be computed by dividing the area under the melting peak up to that temperature by the total area under the peak (the heat of fusion).
- Optical or scanning microscopy. These techniques can be used to examine the crystalline size and morphology.
- Instrumented lab scale former. Dharia [7,12] developed a small-scale thermoformability analyzer that mimics the forming process. The device heats, forms, and cools a single sheet under controlled conditions similar to a production thermoformer. Plug, vacuum, or vacuum with plug-assisted thermoforming modes can be used. The sheet temperature (monitored by an IR thermometer), soak time, plug speed, cooling time, maximum plug force, and maximum draw depth can all be controlled. The force to form is measured as a function of draw depth and time. Force vs depth plots provide useful information about the formability of the material. The thickness distribution in the final part can also be measured. The device can be used for materials development, process engineering, and quality control. The test is rapid, repeatable and represents the thermoforming process. One limitation is the cost of the machine [13].

11.1.2.1 Predictive Criteria

Just as there is no single test for formability, there is no single criteria or test result that predicts performance. Many investigators have tried to correlate results from lab tests to lab or field forming experience. Some of the criteria proposed by these investigators are highlighted here.

Wang [14] and Ho [15] use the difference in the area draw ratio (width times thickness after drawing divided by the initial width times thickness of the specimen, Eq. (11.4)) in the machine and transverse direction of a hot tensile test as a guide for thermoformability. They define a dimensional thermoformability index (DTI) related to this difference:

$$\mathrm{DTI} = 100 \sum_{i=1}^{n} \mathrm{Abs}\left(\tilde{y} - y_i\right)/n \qquad (11.1)$$

where

$$y_i = \mathrm{ADR}_i(\mathrm{TD}) - \mathrm{ADR}_i(\mathrm{MD}) \tag{11.2}$$

$$\widetilde{y} = \sum_{i=1}^{n} y_i/n \tag{11.3}$$

$$\mathrm{ADR}_i = \frac{W_i X_i}{W_0 X_0} \tag{11.4}$$

i = location of ith position on the tensile bar, n = number of positions or specimens, ADR = area draw ratio, W_i = width of specimen at the ith position after drawing, W_0 = initial width of specimen, X_i = thickness of specimen at the ith position after drawing, X_0 = initial thickness of specimen.

In Eq. (11.1), Abs stands for absolute value. Multilayer films containing polyamide (PA) and polyethylene (PE) were tested for DTI using a hot tensile test at 95°C. Lower values of DTI (smaller difference between the TD and MD draw ratios) correlate with better formability based on experience and lab forming results. For example, a film containing a nylon copolymer has a lower DTI than one with PA 6, as do films containing more PA at the expense of PE. This is consistent with industry experience and lab forming trials showing better formability with PA copolymer and greater PA content vs PE.

Ho [15] uses a hot tensile test to evaluate strain hardening. Using the slope of the true stress vs strain curve at two locations, they compute two moduli, one at low strain (0.3−0.5) and one at high strain (2). Multilayer films with lower low-strain modulus and higher high-strain modulus are expected to thermoform well. Lower low-strain modulus is associated with ease of filling the mold and higher high-strain modulus helps resist blow outs. This is borne out, at least qualitatively, in their experiments with multilayer films.

Kurzbeck [16] uses transient elongational melt viscosity measurements to predict formability. Two grades of PP are compared, a standard linear PP and a PP containing LCB induced by e-beam irradiation. The branched PP exhibits strain-hardening behavior in the transient elongational rheometer, whereas the linear PP does not. A laboratory thermoforming test shows that the branched PP has more uniform thickness after forming than the linear PP.

Spence [5] varies the applied stress and time in a hot creep test to simulate different parts of the forming process. A low stress (1916 Pa) and long time (10 s) test correlates with sag, and high stress (10 kPa) for a shorter time (5 s) is used to simulate part forming. Long retardation times in the first experiment correspond with long sag times on a commercial sheet line for polystyrene (PS), high density polyethylene (HDPE), and PP sheet.

DMA is used by several investigators in different ways:

- In the frequency sweep mode, G'' is initially greater than G', indicating the viscosity dominates over elasticity at low frequencies (long times). G' increases faster than G'' with increasing frequency and the crossover point represents the point where elasticity starts to dominate. Elasticity is needed for sag resistance and viscous flow for part formation. Spence and Hylton [5] relate the crossover frequency (ω) to sag resistance. Materials with a crossover frequency near the sag frequency ($<0.1\ \mathrm{s}^{-1}$) have good sag resistance. The sag frequency is simply the inverse of the heat soak time of the sheet (10 s in this example). The crossover frequency relationship is borne out in their experiments on a sheet line: PS and PP has good and poor sag resistance with crossover frequencies of 0.034 and $10\ \mathrm{s}^{-1}$, respectively.
- The width of the viscoelastic plateau in the temperature sweep mode is related to the temperature window for forming [4]. The modulus is high at temperatures below the T_g or T_m (melting temperature) and decreases once it reaches the amorphous region. Many investigators [15,17,18] have proposed that the temperature at which the elastic modulus (G') measured at a frequency of $1\ \mathrm{s}^{-1}$ drops below 10 MPa is a good estimate for the minimum forming temperature. This is based on practical experience.
- DiRaddo [19] compute a deformation sensitivity ratio ($= G''(\omega)/G'(\omega)$). The greater the ratio, the more viscous (and less elastic) is the material. DiRaddo also compute a temperature sensitivity ratio ($= G(T_1)/\mathrm{G}(T_2)$ at constant ω; $T_2 > T_1$); a higher ratio indicates greater sensitivity to process temperature. These ratios can be useful for understanding thermoforming issues.

Wang [14] shows that formability increases as the total crystallinity of the film structure decreases, as measured by the total heat of fusion using DSC. The formability is found to improve as the fraction of molten polymer at the forming temperature decreases. One way this is accomplished is by incorporating more high-melting PA6 into the film structure. Ho [15] proposes that reducing the fraction of molten polymer at the forming temperature reduces blow outs.

Ward [20] suggests using the inflection point of the crystallization peak from DSC results to correlate with formability. This is illustrated in Fig. 11.1. Monolayer films of various PE grades, ionomer, ethylene vinyl acetate copolymer (EVA), PA, and ethylene vinyl alcohol copolymer (EVOH) are thermoformed using a laboratory single cavity former. The films are evaluated for completeness of filling the cavity, presence of film breaks, and uniformity and gauge reduction at various points in the formed parts. The results show the following:

- Ionomer has the best forming characteristics with the most uniform gauge reduction and cell definition.
- Butene-LLDPE, PA, and LDPE do not form completely (at 105°C).
- Octene-LLDPE form well but with slightly more thinning at edges.
- EVOH and EVA form completely but cell definition and gauge thinning are not as good.
- Formability correlates with inflection point of the DSC crystallization peak. When the sheet temperature is varied, if the surface temperature is above this point the film formed well. The approach is also extended to multilayer coextruded films.

11.1.3 Factors that Affect Thermoforming

Some of the key factors that affect the performance include the following:

11.1.3.1 Material Parameters

These are discussed in Section 11.1.2.

11.1.3.2 Film Structure

The composition, placement, and thickness of layers as well as how the film is fabricated may influence formability. As discussed in Section 11.1.3.3, the thermoforming temperature window of each of the materials in a multilayer structure must overlap. Careful selection of the layers is sometimes needed, especially for deep draw applications. Locating more formable layers next to difficult to form ones can help. For example, EVOH is often sandwiched between layers of PA6 to improve formability. The method used to fabricate the film, such as blown film, cast film, or lamination, can influence the

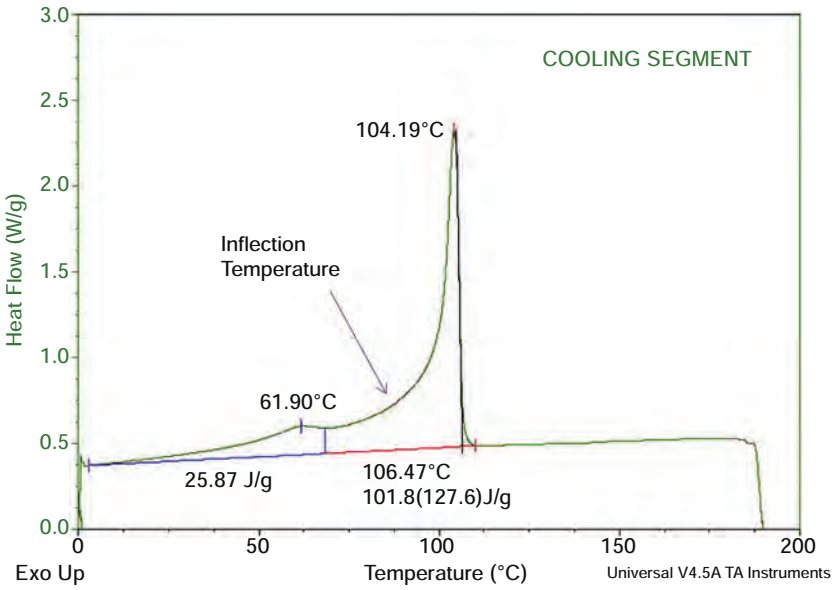


Figure 11.1 Cooling inflection temperature as defined by Ward [20]. DSC cooling curve for LLDPE. *Courtesy of Russ LaFon, DuPont.*

formability. A rapid quench process such as cast film or water-quenched blown film reduces the crystallinity of films containing semicrystalline polymers and improves formability [21]. The film fabrication process also affects the balance of orientation and properties in the machine and transverse directions. Anisotropy can contribute to nonuniformities during forming.

11.1.3.3 Film Temperature

The forming temperature and its uniformity across the film have a pronounced effect on thermoformability. The uniformity of the temperature depends on the heater type, heater profile, and heat up time, which are all crucial variables for quality control. The target-forming temperature will depend on the thermoforming temperature windows of each of the layers. For a material to deform, it must be soft enough, yet not too soft that it causes sagging and other issues. Table 11.1 provides typical thermoforming temperature ranges for a variety of polymers. These are based on sheet melt forming processes. Some of the factors affecting this window include the intrinsic orientation of the sheet, hot strength, sag, thermal sensitivity and stability of the polymer, sheet geometry and thickness, uniformity of the heating, depth of draw, mold geometry, plug rate, and plug temperature [22]. The temperature must be hot enough to soften the polymer so that it can deform under vacuum or plug assist, yet not too hot that it suffers blow outs.

In packaging, solid phase pressure forming (SPPF) is sometimes used. This process was developed for PP sheet by Shell in the 1980s [3,23]. It involves forming at a temperature just when the resin starts to soften. As shown in Fig. 11.2, this occurs at around 160°C for PP. In this region the complex viscosity starts to decrease. The forming window given in Table 11.1 reflects this since most PP sheet is solid phase pressure formed to avoid excessive sag. Melt forming processes for PP operate at around 180–190°C. Chou [25] and Chow [26] provide typical forming ranges for EVOH and common polymers coextruded with EVOH. These are summarized in Table 11.2.

The forming temperature window for EVOH is particularly narrow since it is highly crystalline, crystallizes rapidly, and contains strong inter- and intramolecular interactions due to hydrogen bonding between –OH groups. The ease of forming and orienting EVOH improves as the mol% ethylene is increased, but at the expense of higher oxygen permeation. One way to visualize the challenge with forming multilayer structures containing EVOH is to look at the crystallization half time as shown in Fig. 11.3. Here the half time represents the time for half the crystals to form at the given temperature. These results are for crystallization under quiescent conditions. In reality, crystallization is much faster due to stress-induced crystallization during forming: the stretching of the polymer chains speeds up the crystallization. Nevertheless, the data show how narrow the temperature window can be.

Table 11.1 Thermoforming Temperature Ranges for Some Common Polymers

Polymer	Thermoforming Temperature (°C)	Maximum Areal Draw Ratio
Polystyrene (PS)	150–190	8:1
High-impact polystyrene (HIPS)	160–205	8:1
Acrlonitrile butadiene styrene (ABS)	150–205	10:1
Flexible or plasticized polyvinyl chloride (PVC)	110–150	10:1
Low density polyethylene (LDPE)	125–175	6:1
High density polyethylene (HDPE)	140–190	8:1
Polypropylene (PP)	140–165	6:1
Polycarbonate (PC)	175–230	8:1
Amorphous polyethylene terephthalate (PET)	125–165	6:1

Data from Ashter SA. Thermoforming of single and multilayer laminates: plastics films technologies, testing, and applications. Walthan, MA: Elsevier; 2014 and Throne JL. Thermoforming. Munich: Hanser Publishers; 1986.

The shaded region on the far left represents the forming window for PP in the SPPF process. Only the 44 and 38 mol% ethylene grades crystallize slowly enough to form in the same temperature window as PP. If the crystallization is too fast, as it is for the 32 and 27 mol% ethylene grades, local deformation occurs that leads to neck-in and breaks during forming.

Thermoforming EVOH containing films often requires judicious selection of the other layers that match up well with the forming window of EVOH. Common practices include using high ethylene grades (44 and 38 mol%) and limiting the draw to shallow depths. The high ethylene grades have wider thermoforming windows but also have poorer gas barrier. EVOH suppliers have introduced special grades of EVOH with wider forming windows [26–28]. These are usually less crystalline and so the barrier performance may suffer. Film fabricators often blend grades of EVOH, such as blending a 32 mol% grade with a 38 mol% grade. This improves the forming window somewhat but also results in a reduction in barrier performance. Chou [25,29] and others [30–32] show that blending about 20% of an amorphous PA (Selar PA, a 6I/6T copolymer from DuPont) with EVOH improves the forming window

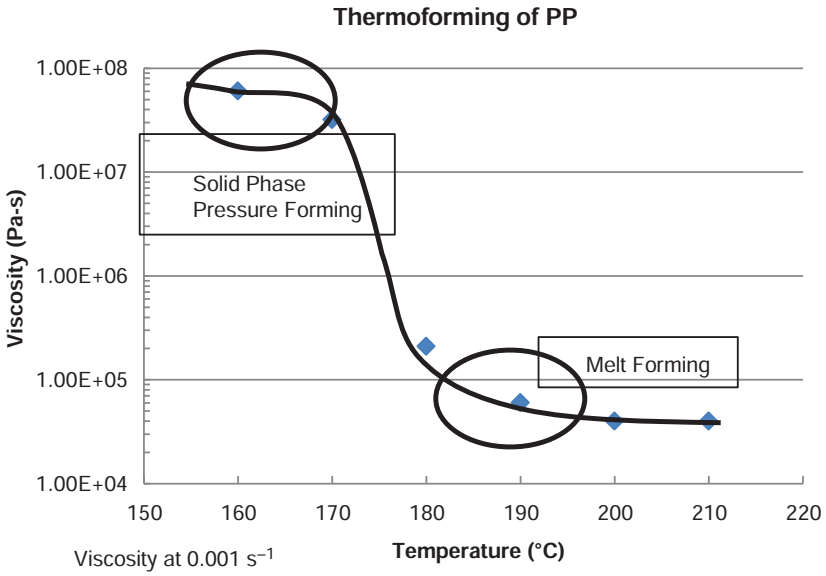


Figure 11.2 Complex viscosity of PP as a function of temperature from oscillatory rheology measurements highlighting thermoforming temperature regions.
Data from Shell Development Company. Polypropylene technology seminar; 1987.

Table 11.2 Thermal Properties and Typical Thermoforming Temperatures for EVOH and Common Resins Coextruded With EVOH.

Resin	T_g (°C)	T_c (°C)	T_m (°C)	Thermoforming Temperature Range (°C)	
				SPPF	Melt
EVOH	40–60	130–170	160–191	70–90	155–210
PS	100–120			110–135	135–210
PP	−10–0	120–145	165–175	140–160	170–210
PA 6	50	160–170	225–235	80–120	205+
PET	80	160–180	250	80–120	

Data from Kuraray Technical Bulletin No 150. Thermoforming of EVAL® resin containing structures, viewed May 31, 2015 from: http://eval-americas.com/media/36418/tb_no_150.pdf; 2000; Chou R, Lee IH, Behavior of ethylene vinyl alcohol (EVOH) amorphous nylon blends in solid-phase thermoforming. J Plastic Film Sheeting 1997;13:74–93 and Chow E. High barrier forming films with EVOH. In: VII International TAPPI/CETEA conference on flexible packaging; 2012.

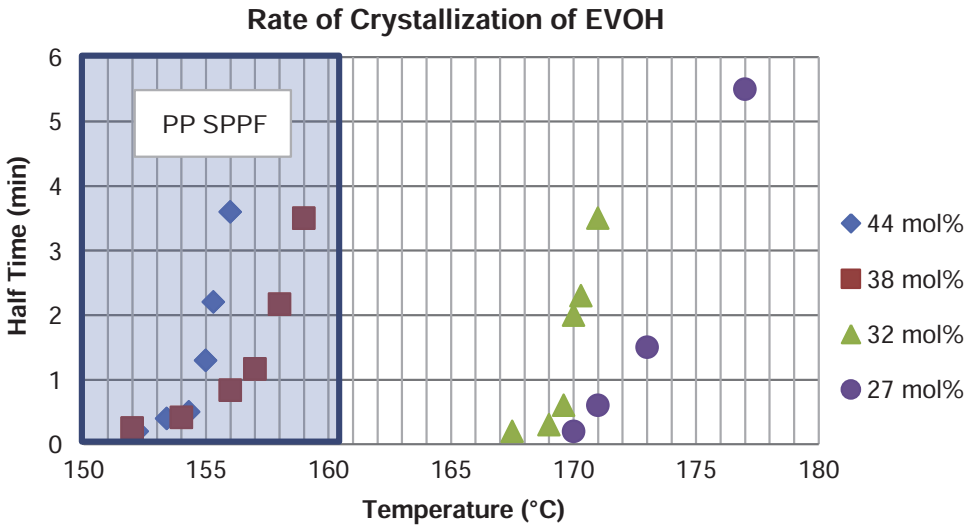


Figure 11.3 Crystallization half times for EVOH. *Shaded rectangle* represents typical forming temperature range for PP in solid phase pressure forming (SPPF).
Data from Kuraray Technical Bulletin No 150. Thermoforming of EVAL® resin containing structures, viewed May 31, 2015 from: http://eval-americas.com/media/36418/tb_no_150.pdf; 2000; Chou R, Lee IH, Behavior of ethylene vinyl alcohol (EVOH) amorphous nylon blends in solid-phase thermoforming. J Plastic Film Sheeting 1997;13:74–93.

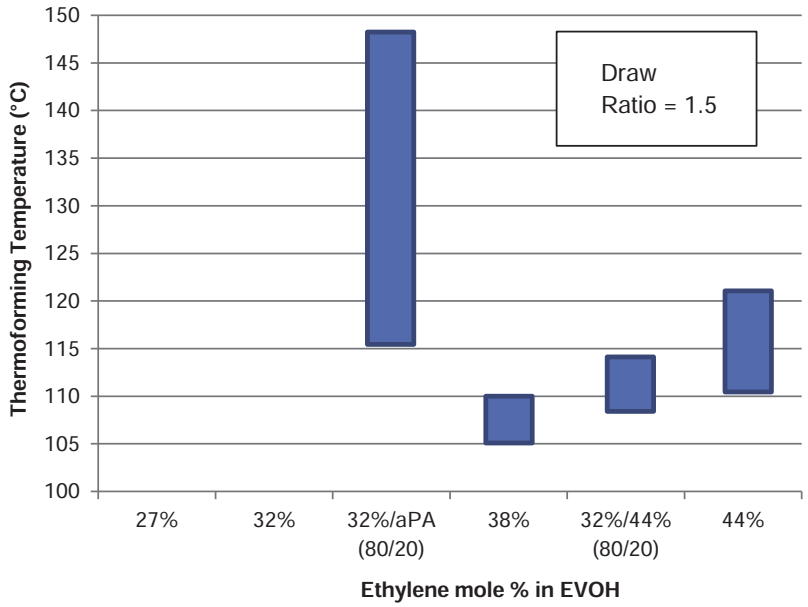


Figure 11.4 Temperature range over which a (PP-tie-EVOH-tie-PP) with layer thicknesses [660/50/100/50/660 μm] can be thermoformed without defects.
Reproduced with permission from Chou R, Lee IH. Behavior of ethylene vinyl alcohol (EVOH) amorphous nylon blends in solid-phase thermoforming. J Plastic Film Sheeting 1997;13:74–93.

substantially without a loss in barrier and allows the film to be drawn to much greater depths. One example is illustrated in Fig. 11.4 for a (PP-tie-EVOH-tie-PP) sheet with a draw ratio of 1.5. The sheet with unmodified 27 and 32 mol% ethylene grades of EVOH cannot be drawn without substantial neck-downs and breaks. Structures with 38, 32/44 blends, and 44 mol% ethylene can only be drawn over a 5–10°C window. Addition of 20% aPA to the 32 mol% ethylene grade of EVOH increases the

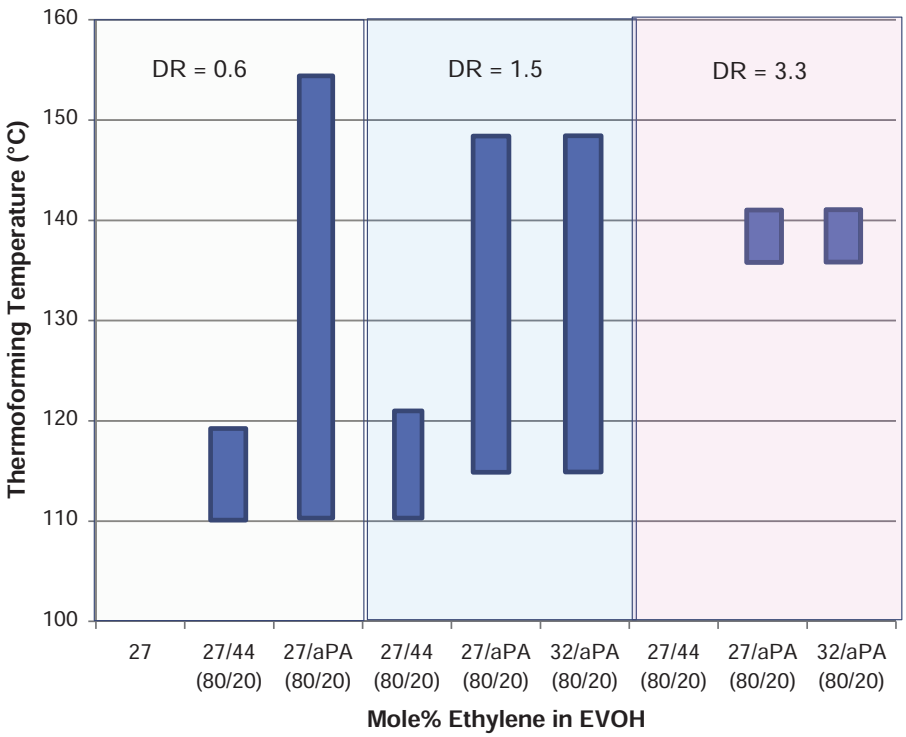


Figure 11.5 Temperature range over which a (PP-tie-EVOH-tie-PP) can be thermoformed without defects. For 1.5 and 3.3× draw ratio, the layer thickness is the same as in Fig. 11.4. For 0.6× draw, the layer thicknesses are [280/25/50/25/280 μm].
Reproduced with permission from Chou R, Lee IH, Behavior of ethylene vinyl alcohol (EVOH) amorphous nylon blends in solid-phase thermoforming. J Plastic Film Sheeting 1997;13:74–93.

forming window to 33°C. Fig. 11.5 shows the effect of draw ratio. Blending 20% of the 44 mol% ethylene grade with the 27 mol% grade allows the structure to be thermoformed over a 10°C window for 0.6 and 1.5× draw ratios but is not sufficient for large draw ratio. The addition of amorphous polyamide (aPA) provides a much greater forming range for the shallow and moderate draw and allows the sheet to be formed, albeit over a narrow temperature range, for deep draw (3.3×).

Adding aPA to EVOH increases the haze. Fetell and others [31–35] show that adding a special PA–ionomer alloy (Surlyn AM7927 from DuPont) improves the thermoforming window and drawability without a loss in clarity. The barrier performance, however, decreases by about the same as switching to a grade of EVOH with one level higher ethylene. For example, adding the ionomer to a 32 mol% ethylene grade of EVOH provides barrier properties about the same as a 38 mol% ethylene but with better formability.

Small differences in film temperature can affect thickness distribution in the final part. Temperature affects strain hardening and elongational viscosity, as well as the friction between the film and mold or plug. For complex shapes, nonuniform heating of the film may be optimal; increasing the temperature in regions where the polymer is stretched more may help with thickness distribution [36].

11.1.3.4 Processing Parameters

For plug-assisted thermoforming, the plug shape/geometry (height, width, and depth), plug speed and plug timing affect thermoforming [37]. For example, increasing the plug depth increases the draw ratio. The maximum draw ratio depends on the materials in the film structure, but in general, as the draw ratio is increased a critical draw ratio is reached above which breaks occur. The plug speed and timing may also affect breaks. In addition, the plug material is important: the material of construction affects how much the plug heats up during forming and its temperature, which in turn affects frictional properties and the film temperature.

For vacuum/pressure forming, the level and rate of change of the vacuum or pressure are significant factors.

In snap-back forming, the prestretch height, mold temperature, and sheet temperature are important [38].

The mold temperature and its surface properties affect the friction between the film and tooling, which influences film thickness uniformity after forming.

11.1.3.5 Interlayer Adhesion After Forming

As described in Section 10.4.2.2.4, thermoforming tends to reduce interlayer adhesion. This is illustrated in Figure 10.43 for a (PA 6—tie—ionomer) coextruded film. Orientation during forming increases the interfacial area and decreases the density per unit area of bonds. Orientation also puts stress on the bonds that have formed. Improved adhesion can be obtained after forming and orientation by the following:

- Increasing the number of functional groups. For example, the amount of chemical functionality on a tie resin can be increased. Tanaka [39] provides an example for a (LDPE—tie—EVOH) film, where the peel strength to EVOH after a 3×3 orientation at 80°C increased from about 10 g/15 mm to 30 g/15 mm by increasing the grafting ratio of the tie layer by a factor of 10.
- Decreasing the stiffness of the tie layer. An example for Tanaka's (LDPE-tie-EVOH) film is shown in Fig. 11.6. Decreasing the modulus increases the peel strength after orientation by a factor of two.
- Lowering the crystallization and crystallization temperature of the tie resin. Like decreasing the modulus, this decreases the stress during orientation. Switching from a PE-based tie resin to one based on VLDPE, EVA, or EMA may be advantageous. If the end use can tolerate it, selecting a tie resin whose freezing point is below the forming temperature often improves the peel strength after forming.

Tie resin suppliers often have special grades that work better for thermoforming. Consulting with the supplier can be helpful.

11.1.4 Modeling

A number of investigators [10,40—63] have developed numerical models to better understand the thermoforming process and predict performance. The deformation during thermoforming is large, nonlinear, rapid and complex, being primarily planar to equi-biaxial. Hyperelastic or viscoelastic constitutive models are typically used to simulate the rubbery polymer near its glass transition temperature (amorphous polymers) or melting point (semi-crystalline polymers). Hyperelastic models include the Ogden and Mooney—Rivlin models. The Christensen and K-BKZ models are often used for the viscoelastic models. Hyperelastic models generally work well for vacuum assist forming but not as well for plug-assisted thermoforming, where the need to take into account the strain history makes the viscoelastic models more suitable [45,48].

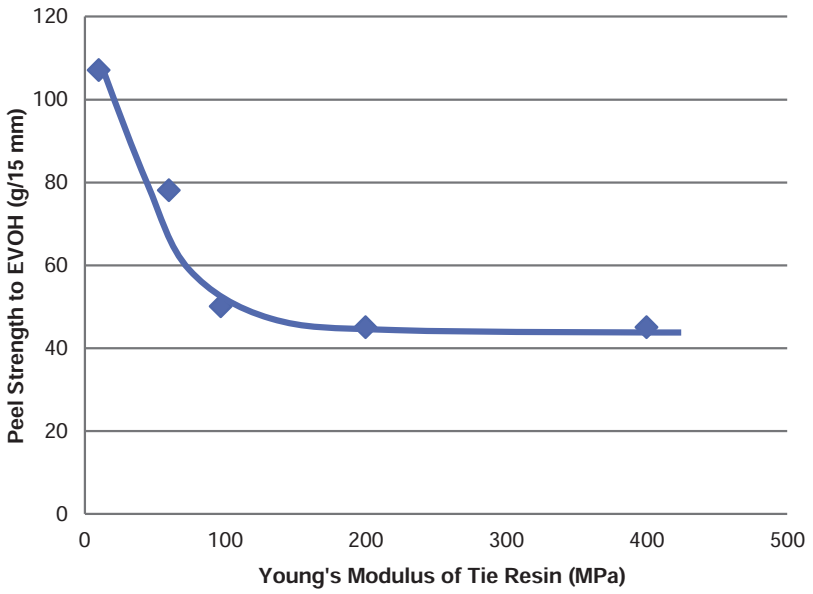


Figure 11.6 Effect of tie layer modulus on peel strength to EVOH after thermoforming. Structure is (LDPE—tie—EVOH) with thickness [160/40/40 μm]. Orientation is 3×3 at 80 C. *Data from Tanaka H, Shigemoto H, Hawachi H. Adhesive resin for multi-layer films used for shrink or thermoforming processes. J Plastic Film Sheeting 1996;12:278—86.*

Obtaining material parameters for the models is challenging [43,44,50,53]. The difficulties of testing under conditions similar to thermoforming have already been highlighted in Section 11.1.2. High temperatures, high strain rates, and complex deformations are problematic. Uniaxial tests are most often used, even though biaxial stresses found in thermoforming are often more than two times higher.

Most models use complex finite element analysis grids and algorithms. A membrane approximation is typically used, where the stresses in the thickness dimension are ignored. This typically agrees well with full 3D analysis if the width/thickness ratio is >100 [40]. A drawback of the membrane approximation is the difficulty of correctly modeling the boundary conditions. Most of the studies reported in the literature further simplify the problem by assuming the temperature is constant (isothermal), although a few studies have coupled the thermal and flow analysis [41,46,47,56,60,62,63]. The model results show good agreement with experimental results for some examples and not so good agreement for others. In general, the models are not truly predictive yet, but do offer insight into material parameters and process conditions that influence thermoforming behavior and performance.

An example of how modeling can be used to screen new film structures is presented by Christopherson and Briere [64]. They apply modeling to predict the puncture resistance of medical forming webs for a syringe packaging application. The acceptable failure rate during a simulated transit test is <0.2%. Fifty percent of the failures typically come from abrasion of the film from the flanges of the syringe. Another 30% comes from puncture at the end. Typically films with thickness of 65−150 μm are used to package a 10-mL syringe. After forming, the thickness in the corners is 15−35 μm. They compare two film structures with testing and modeling:

- (35-μm EVA(4.5%VA) −80-μm Surlyn Ionomer−35-μm EVA)
- (30-μm PA−5-μm tie−65-μm LLDPE).

The films are formed with a 0.7-s cycle time at 14 packs per minute. The thickness at different locations on the formed package is measured using a Magna-Mike accurate to ± 1 μm. The formed pack is cut at the flange and the force to puncture the end of pack at a 45 degree angle to the main axis of symmetry is measured using a 6.5-mm diameter metal probe at 508 mm/min (20 in/min).

To obtain the material parameters for the model, tensile tests are conducted on the films at 70, 80, and 90°C. Uniaxial stretching is conducted at 10, 50, and 100 mm/min. The results are fit to a KBKZ model with WLF (Williams−Landel−Ferry) temperature dependence.

A finite element model is used to simulate forming and puncture. Post-forming shrinkage (reversion) is not accounted for by the model (see Xu [61] and Song [41] for discussions on warpage and shrinkage modeling). The shrinkage generally occurs at the top of the package where the film is thicker and has not yielded during forming. Since the puncture is measured in the corner away from the top flange area, the errors associated with this are expected to be small.

The model prediction of the thickness distribution and puncture agree well with the experimental results. The Surlyn film thickness distribution is in better agreement with the model, suggesting less reversion. Both film structures give similar puncture results (and both are used commercially). The authors conclude that the model is a good tool to screen structures.

11.2 Orientation and Shrink

Orientation involves stretching and aligning molecular chains during polymer processing. Polymer chains generally favor a random coil configuration as depicted in Fig. 11.7. When stretched, the force aligns the molecular chains in the direction of the imposed strain. If the film is rapidly quenched, this orientation is frozen in place, which influences many film properties as described in Section 11.2.1. If the orientation stress (force per area) has not been allowed to relax, the chains may exhibit a memory effect. When heated above the T_g or crystalline melting point, the chains may relax back toward their preferred random coil configuration, causing the film to shrink. This is the basis of shrink films and bags. If dimensional stability is desired, the oriented film is often annealed at an elevated temperature while under the imposed strain to allow the chains to relax while retaining their oriented configuration.

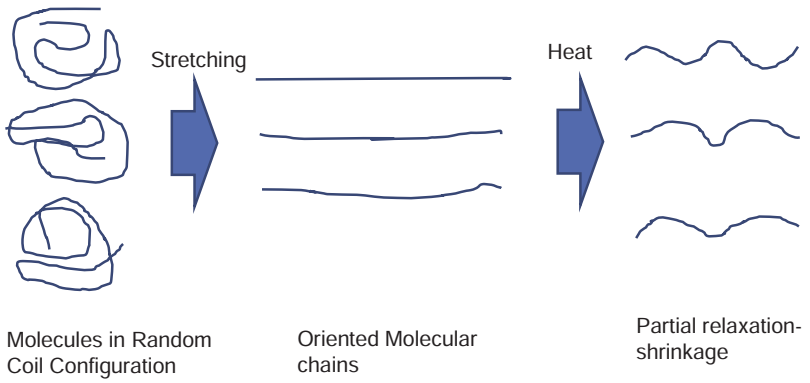


Figure 11.7 Stretching of polymer chains.

The terms stretching and orientation, while often used together, should be differentiated. Stretching is the amount of strain imposed by the polymer process. In blown film and double bubble processes, it is related to the draw down ratio and blow up ratio. In MDO, it is determined by the difference in roll speeds of the orientation rolls. In a tenter frame process, it is determined by the chain draw ratio. The direction of the stretching is generally in either one (mono) or two (biaxial) directions. These directions are typically designated the machine direction (MD) and transverse direction (TD), although the orientation in a blown film or double bubble process is really in the hoop or circumferential direction.

Orientation refers to the alignment of the molecules, which affects the film properties. The amount of orientation depends on the amount of imposed stretch, the rate of stretching, orientation temperature, annealing temperature (if the film is annealed after orientation), and the molecular chemistry and architecture of the polymer (chain stiffness, MW, MWD, amount of LCB, hydrogen bonding, and so on). Processes that stretch the polymer from the melt, such as cast film and blown film, generally provide less orientation than those that impose stretch from the solid state, such as double bubble, tenter frame, and MDO processes.

11.2.1 Why It Is Important

Orientation is important for a number of commercial package forms, especially those involving shrink. These include:

- Shrink film, such as Cryovac and Clysar film, used in a variety of retail bundling and other applications.
- Barrier shrink bags, such as (EVA—PVDC (polyvinylidene chloride)—EVA), used for packaging of raw meat.
- Retail skin packaging, an alternative to clam shell packaging. In carded skin packaging, polyvinyl chloride (PVC), PE, or ionomer film is heated and draped over the product. Vacuum is applied through the card, forming the film over product. The film shrinks as it solidifies, holding the product in place.
- Shrink labels.

Orientation is also used to improve the properties of nonshrink films. Examples include biaxial oriented polypropylene (BOPP), biaxial oriented polyester (BOPET), and coextruded barrier films. These are oriented and then annealed to fix the orientation and prevent shrinkage. Some of the property enhancements include the following:

- An increase in optical transparency of semicrystalline polymers. Orientation often changes the crystalline structure, reducing the size or amount of large spherulites that refract light and cause haze. The overall amount of crystallinity may actually increase as strain helps induce crystallization. Because the size of the crystals is smaller, the transparency is improved.
- An increase in tensile strength and modulus as the molecules are more aligned. At low levels of orientation, properties such as strength and modulus correlate with both amorphous and crystal phase orientation. After the crystals become fully oriented, the amorphous phase may continue to orient, increasing the properties further [67].

- A decrease in oxygen and moisture permeation due to changes in crystalline morphology.

Orientation does not come for free. There are some trade-offs, which include the following:

- a decrease in elongation at break and slow puncture resistance, depending on the materials and process;
- a decrease in transverse direction tear strength, but this depends on the specific material and process;
- a decrease in interlayer adhesion of multilayer films due to a reduction in the number of bonds per unit area (due to the increase in interfacial area) and an increase in residual stress.

Another important class of films involves orientation during the packaging process. These include stretch films, pallet wraps and hoods, and cling films.

11.2.2 How to Measure

11.2.2.1 Orientation

A number of analytical techniques are used to measure the molecular orientation in films. These include the following:

- Birefringence [65–69]. Birefringence is related to changes in polarized light as it passes through a specimen. The difference in the refractive index of light polarized in parallel and perpendicular directions is an indication of the anisotropy of the material. This difference can be measured using polarized light optical microscopy. Birefringence correlates with orientation in both the amorphous and crystalline phase of polymer films.
- Dichroism or FTIR [67–69]. Dichroism is a measure of absorption of electromagnetic waves by the specimen. In the most widely used method, polarized infrared light is used. The simplest representation of anisotropy is given by the dichroic ratio:

$$D = \frac{A_1}{A_2} \tag{11.5}$$

where D = dichroic ratio, A_1 = absorption of polarized light in the direction parallel to stretching of the polymer, A_2 = absorption of polarized light in the direction perpendicular to stretching.

Dichroism is a more powerful technique than birefringence since birefringence measures mean values over all components present. Specific frequencies or absorption bands using FTIR can be used in dichroism that relate to different groups on the molecule, different segments, or even different polymers in polymer blends. Reviews of dichroism for oriented polymers are provided by Read and Ward [70] and Jasse and Koenig [71].

- X-ray diffraction [67,68]. X-ray diffraction is a common technique for studying crystal structures and atomic spacing. X-rays are generated in an X-ray tube and directed at the sample. The diffracted rays are collected with the angle between the incident and diffracted rays being important. The wide angle technique is useful for determining the orientation of the unit cell (generally noted as the a, b, and c axes) of the crystalline regions of a polymer. The results are often presented in the form of pole plots, which are stenographic projections of the intensities of the normals to the crystallographic planes [67].
- Shrinkage. Unrestrained linear thermal shrinkage of a film is related to the molecular orientation (see Section 11.2.2.2 for a description of this method).

Often more than one technique is applied due to challenges in measurement and interpreting results. For example, Ajji and Zhang [68] compare orientation of PE and PP films using birefringence, FTIR (dichroism), and X-ray diffraction. They find that the FTIR measurements overestimate the a-axis orientation and in some cases can be wrong. They also question the FTIR results for amorphous phase orientation.

11.2.2.2 Shrink and Shrink Force

The unrestrained linear thermal shrinkage of a film is related to molecular orientation. Ajji [65] finds that shrinkage correlates with birefringence; both the amorphous and crystalline phase orientation is important.

ASTM D2732 [72] describes a method for measuring shrinkage by immersing the film in a liquid bath. The liquid is chosen so that it does not

plasticize the film. A PE glycol–water mixture is often used. The liquid is controlled to a specified temperature ± 0.5°C. A 100 × 100 mm film specimen is placed onto a holder that allows free movement in the lateral directions but ensures the film is immersed in the bath. Specifics of the holder are given in the standard. The specimen is immersed in the liquid bath at a specified temperature for a given length of time. The film is removed and placed in a liquid bath at room temperature to quickly cool. The sample is removed and the linear dimensions in the machine and transverse directions measured.

The percent-free shrinkage is given by Eq. (11.6):

$$\text{Unrestrained linear shrinkage, \%} = \left[\frac{L_0 - L_f}{L_0}\right] \times 100 \tag{11.6}$$

where L_0 = initial length of side (100 mm), L_f = length of side after shrinking.

If the sample elongates, the % shrinkage will be negative in the direction of elongation.

Some investigations use an air or vacuum oven to expose the film to the specified temperature. Specimens are sometimes hung vertically (clipped to the upper edge) to ensure free shrinkage, or placed horizontally on a surface roughened with sand, corn meal, or other granular medium to help ensure the film has the freedom to shrink laterally. In general, an oven takes longer to heat the film and the temperature may not be as uniform as a liquid bath. Curl also can be a problem with oven heating of specimens.

The *shrink force* is defined by ASTM D2838 as the force per original unit width in a specified direction developed by a film under restraint while attempting to shrink at a given temperature. The *shrink tension* is the shrink force per unit original cross-sectional area. The *orientation release stress* is the maximum shrink tension developed in a specified direction throughout its range of shrink temperatures while totally restrained from shrinking [73].

ASTM D2838 describes a test method that involves clamping a 1-inch (25.4 mm) wide film specimen in a shrink tension holder, one arm of which contains a strain gauge. The holder is immersed in a hot liquid bath and the force exerted by the film is measured by the strain gauge. Two methods are described. In Procedure A, the film is totally restrained from shrinking. In Procedure B, the film is allowed to shrink by a predetermined amount before being restrained.

Shrink tension affects the appearance and performance of a film or package. It may also be used as a measure of orientation and is influenced by the film fabrication conditions. Procedure A is useful for determining the amount and direction of orientation, the orientation release stress, and the maximum stress the film can exert at a given temperature. Procedure B better represents a packaging application since the film is seldom totally restrained. The procedure can be used to estimate the force that will be exerted on the packaged item and to predict the appearance of the package after shrinkage.

The orientation release stress is determined by carrying out shrink tension measurements using Procedure A at several temperatures and plotting the results. The maximum tension is the orientation release stress. Generating the full shrink tension vs temperature curve is typically only carried out to characterize a particular film made under an established set of processing conditions. For quality control and product development purposes, running the test at one or two temperatures is often sufficient.

ASTM D2838 works well for measuring the shrink force of high shrink films, such as those made on a double bubble process. Many applications require low shrink forces, such as when the product being packaged is deformable. Jin [74] describes blown films of blends of LLDPE and LDPE that are used for this purpose. The LLDPE provides strength and LDPE shrinkage (due to LCB). The shrink force tester described in ASTM D2838 is not sensitive enough to measure the shrink force of low shrink films or the shrink in the transverse direction. Jin develops a low shrink tension test that uses a solids dynamic mechanical analyzer (TA Instruments RSA III). The DMA device is used in the strain-controlled dynamic temperature ramp mode. The strain and tension are set so that the clamp distance remains constant as the temperature is ramped from room temperature to the melting temperature of the film. The measured force is related to the shrink tension.

They find that unlike a double bubble film which shows a shrink force from the outset (as the sample is heating up from room temperature), a low shrink force film first undergoes an expansion. The expansion is due primarily to thermal expansion but is complex. They find that they cannot compensate for this by preloading the film, so they end up subtracting it out as a baseline to calculate the shrink force near

the melting point. They provide results for a series of LLDPE–LDPE monolayer films, which show that increasing the LDPE content increases the shrink force and reduces the temperature at which the maximum shrink occurs.

11.2.3 Factors that Affect Orientation and Shrink

11.2.3.1 Polymer Characteristics

MW, MWD, and LCB influence orientation and shrinkage behavior. In general, linear polymers draw down and orient more easily but generate less shrinkage than polymers with LCB. As mentioned in Section 11.2.2.2, LDPE is often blended with LLDPE to increase shrinkage. Broader MWD and higher MW (for chain entanglement) also tend to provide a wider processing window and increase shrinkage. Typical PP grades suitable for biaxial orientation have melt flow rates (MFRs) ranging from 1 to 5 g/10 min [75]. This is a lower MFR, or higher MW, than grades generally used in injection molding or fiber spinning. The polydispersivity index, a measure of MWD (Section 4.2.1.2), of standard Ziegler–Natta PP used in orientation is typically in the range of 8–12. DeMeuse [75] found that narrower MWD grades made via single site catalysis provide better mechanical properties upon orientation, but the stretching temperature window is very narrow.

One consequence of increased chain entanglement is strain-hardening behavior, described in Chapter 5 and mentioned in Section 11.1 as an important parameter for thermoforming. Strain hardening increases the stress generated during stretching, which may result in more residual stress after quenching. The relaxation of residual stress results in shrinkage once the film is reheated.

The chemistry of the polymer also plays a role. Hydrogen bonding results in greater shrinkage and shrink force. Polymers with a high level of hydrogen bonding, such as PVC, PVDC, PA6, acid copolymers, and ionomers, generally provide a high level of shrink. As an example, consider the family of acid copolymers and ionomers. Higher acid levels provide greater hydrogen bonding. Ionomers, which are acid copolymers whose acid groups have been partially neutralized with a metal salt, contain hydrogen and ionic bonding. Increasing the acid level increases the shrinkage of blown film as shown in Fig. 11.8. Here the shrinkage of two grades of ionomer with differing acid levels is plotted versus draw ratio. Increasing neutralization of the ionomer also increases shrinkage as shown in Fig. 11.9. Both increasing acid and neutralization increases strain-hardening behavior as is described in Chapter 5.

The degree of crystallinity, rate of crystallization, and crystalline morphology influence drawability and orientation. In two-stage orientation processes, such as the tenter frame and double bubble processes, the sheet or tube is typically rapidly quenched in the first stage. For slow crystallizing polymers such as PET, the rapid quench results in an amorphous sheet or tube. For more rapidly crystallizing polymers such as PE, PP, and PA6, the rapid quench gives rise to smaller spherulites. Nonuniform cooling can result in regions of differing crystallinity or crystalline morphology, which will affect the uniformity of the film after stretching [76].

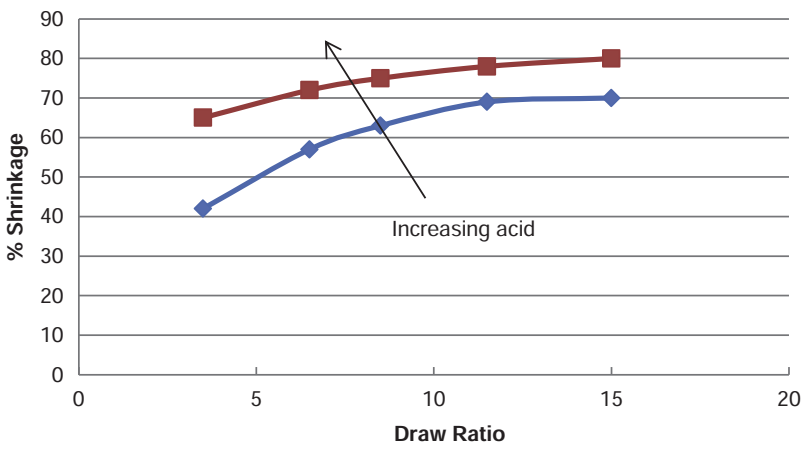


Figure 11.8 Effect of acid level and draw ratio on shrinkage of ionomer strands drawn in the melt. Shrinkage is measured at 95°C, which is above the melting point of the ionomers.
Reproduced with permission from E. I. du Pont de Nemours and Company.

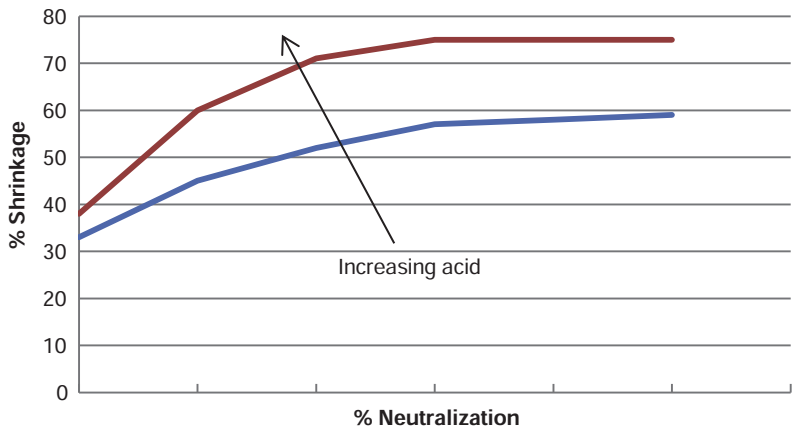


Figure 11.9 Effect of neutralization of acid groups on shrinkage of ionomer strands drawn in the melt. Shrinkage is measured at 95°C, which is above the melting point of the ionomers.
Reproduced with permission from E. I. du Pont de Nemours and Company.

DeMeuse [75] reviews the literature for stretching of PP, showing that lower density of the sheet prior to orientation makes stretching easier. Lower density corresponds to lower crystallinity.

EVOH is particularly difficult to orient due to its high level of crystallinity, which confines the mobility of its polymer chains. It crystallizes very rapidly as described in Section 11.1.3.3 and Fig. 11.3 and undergoes further crystallization during stretching. Drawing of the crystal regions leads to local deformation and tearing. Sequential (MD and TD) orientation is particularly problematic since it crystallizes too fast during the first orientation step. Simultaneous orientation has been more successful [77]. As described in Section 11.1.3.3, special grades of EVOH as well as various modifiers have been developed that help improve the drawability of EVOH.

PET and PA6 are slower to crystallize and have been sequentially oriented commercially, starting with a rapidly quenched sheet. Ajji [78] finds that strain-induced crystallization of a PET film does not occur until the draw ratio is greater than 2×2 on a lab tenter frame stretcher. PA6,66 is often blended with PA6 to reduce crystallinity to improve the drawability [79].

11.2.3.2 Processing

A number of processing factors influence the orientation and shrinkage of polymer films, including the stretch temperature, stretch ratio, stretch rate, annealing temperature (and time), whether the stretching occurs from the melt (cast and blown film) or the solid (tenter frame, double bubble, MDO), and whether the stretching occurs sequentially or simultaneously in the MD and TD.

11.2.3.2.1 Stretching Temperature

The stretching temperature should be above the T_g for amorphous polymers and near the Tm for semi-crystalline ones. For multilayer films, the temperature needs to be above the T_g of the layer with the highest T_g and below the melting temperature of the highest melting point layer; the stretching temperature is determined by the layer with the highest stretching temperature even if it is not the thickest layer [80,81]. A few examples from the patent literature put some further bounds on this:

- Nishamoto [82] teaches that for a multilayer barrier shrink bag with PVDC as the core and polyolefin skins, the film can be stretched at 110°C provided the intermediate layers have melting points from 70 to 100°C. The stretch window is about 15°C. Furthermore, for good stretchability, the laminate must have at the stretch temperature a tensile strength of 5−25 kg/cm^2 and greater than 500% elongation.
- Ciocca [83] shows that the orientation temperature for a (PE−tie−EVOH−tie−PE) film is between 110 and 125°C. The PE layer was a blend of three different density PE grades.
- Lustig [84] teaches that the stretching temperature must be below the melting temperatures of the outer layers and preferably between about 10 and 20°C below the lower of the melting points of the outer layers. Structures containing (PA−tie−LLDPE) layers have stretching temperatures ranging from 100 to 110°C.
- Forloni [85] reports that the stretching temperature for a multilayer barrier film is 120−135°C.

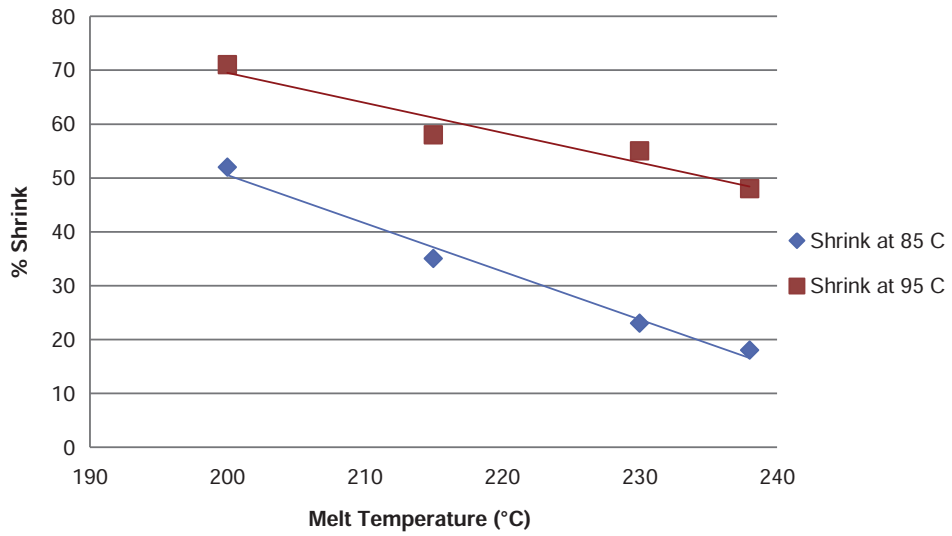


Figure 11.10 Shrinkage of ionomer blown film as a function of melt temperature and shrinkage temperature. DDR = 7.
Reproduced with permission from E. I. du Pont de Nemours and Company.

An example is given for the structure (LLDPE–tie–EVOH–tie–LLDPE) on a sequential tenter frame. The MD stretching is conducted at 110°C and the MD at 125°C.

- Tanaka [86] teaches the use of a stretching temperature from 70 to 130°C for PP compositions.

Generally, lowering the stretching temperature increases the stress and orientation. This translates to greater shrinkage.

In the blown film process the stretching occurs as the polymer begins to freeze (near the frost line). Lowering the melt temperature at the die exit has been found to increase shrinkage, as illustrated in Fig. 11.10 for an ionomer. In coextrusion blown film, the stretching temperature is controlled by the first layer to freeze, which may have consequences for the orientation and properties of the other layers. This is described in detail in Section 14.1.2.

11.2.3.2.2 Stretch Ratio

The amount of stretch is typically characterized by a stretch ratio. In blown film the stretch in the machine direction is often calculated by the ratio of the haul off speed to the velocity of the polymer as it exits the die, known as the takeoff ratio or draw down ratio. In the transverse direction, the blow up ratio is used, which is the ratio of the final bubble diameter to the die diameter. Formulas used to calculate each of these are provided in Section 2.2.1.3.

In cast film, the orientation is primarily in the machine direction as characterized by the draw down ratio (Section 2.2.2.3). Similarly for MDO processes, the amount of stretching can be represented by a single number, either the ratio of the linear speeds of the rolls in the stretching chamber [see Eq. (11.7)] or the ratio of the initial thickness of the film or sheet to the final thickness. For biaxial stretching, the stretching ratio is typically given in both directions, such as 2×2, meaning the stretch is 2:1 in the MD and 2:1 in the TD.

In general, increasing the stretching or draw ratio will increase the orientation and shrinkage. This is demonstrated for ionomer blown film in Fig. 11.8. As the stretching increases, the amorphous and crystalline regions (if they are present) orient. At high stretch ratios, the crystals become fully oriented, but the amorphous phase may still continue to be oriented [67].

11.2.3.2.3 Stretch Rate

The rate of stretching affects the stress that develops; the greater the rate of stretching or rate of elongation, the higher is the stress and orientation. For blown and cast film, the process time introduced in Chapter 2 is a good surrogate for the rate of stretching: the rate of stretching is inversely proportional to the process time. The process time here is

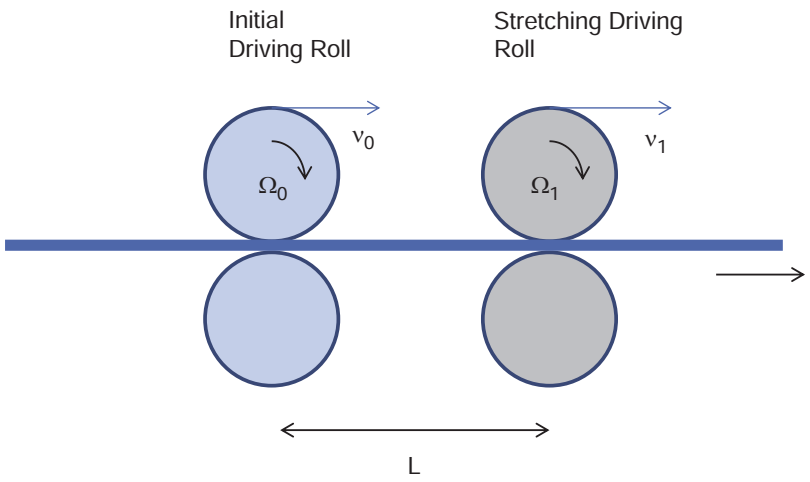


Figure 11.11 Schematic of roll-driven MDO process. The differential speed and distance between the two sets of rolls determines the draw ratio and draw rate as given in Eqs. (11.7) and (11.8).

defined as the time the polymer spends between the die exit and when it begins to freezes off. It is in this region of melt orientation processes where the stretching occurs, so it makes sense that the shorter the process time, the faster the rate of stretching. The importance of process time is described in more detail in Chapters 14 and 15.

For an MDO process, the stretch rate is inversely related to distance between the stretching rolls (Fig. 11.11):

$$\text{Stretch Ratio} = \frac{v_1}{v_0} = \frac{D_1\Omega_1}{D_0\Omega_0} \qquad (11.7)$$

$$\text{Stretch Rate} = \frac{v_1 - v_0}{L} = \frac{\pi D_1\Omega_1 - \pi D_0\Omega_0}{L} \qquad (11.8)$$

where v_1 = linear velocity of driving roll imparting the stretch, v_0 = linear velocity of the initial driving roll, D_1 = diameter of the driving roll imparting the stretch, D_0 = diameter of the initial driving roll, Ω_1 = rotational speed (eg, rpm) of driving roll imparting stretch, Ω_0 = rotation speed of initial driving roll, L = distance between rolls.

For a tenter frame process, the stretch rate is determined by the speed of the clips.

11.2.3.2.4 Annealing Temperature

Annealing is an important part of the film-stretching process. Most films require dimensional stability. BOPP and BOPET films used for lamination and other nonshrink applications are heat set or annealed following orientation. This involves exposing the film to elevated temperature for a given amount of time to relax stress [76]. For polyolefin films, the annealing temperature is typically between T_g and T_m [87,89,90]. Annealing is usually done while the film is constrained to preserve the orientation, although some amount of shrinkage may be allowed [80,90]. In addition to reducing shrinkage, annealing reduces shrink tension [88].

Annealing may be done on hot rolls, or in the case of the double bubble process in a third bubble where the temperature and tension can be carefully controlled. For example, Hausmann [80] describes a double bubble orientation process for making dimensionally stable multilayer-oriented film with a low temperature sealing layer, such as the structure (PET−tie-PP−tie−ionomer). The polymers are coextruded into a tube and quenched in a 15°C water bath (1st bubble). The tube is reheated in a water bath at 92°C for 5 s and inflated (second bubble) with a draw ratio of 3.5 in the TD and 2.6 in the MD. The bubble is collapsed and then reinflated (third bubble) for annealing. Here it is exposed to 300°C air and a stretch ratio of 0.72. They provide general guidelines for the stretching and annealing temperature:

- The stretching temperature should be above the T_g of the polymer layer with the highest T_g and less than the melting point of the polymer with the highest melting point.

- The annealing temperature (third bubble) should be above the stretching temperature in the second bubble and generally needs to be above the T_g of the polymer layer with the highest T_g and less than the melting point of the polymer with the highest melting point.

Annealing is also often used during the production of shrink films. Annealing relaxes the stress introduced by the stretching process up to the annealing temperature. The temperature of the shrink tunnel must exceed the annealing temperature for shrinkage to occur.

Tabatabaei [87] finds that the modulus of MDO HDPE film increases with increasing annealing temperature. They attribute this to an increase in crystallization. Barham [90] mentions that when oriented polyolefin films are allowed to shrink during the annealing process, the stiffness decreases, just the opposite of Tabatabaei. The annealing temperature can be one of many variables that are tricky to get right. Schut [91] cites this as one reason why the use of MDO has not taken off as fast as some have predicted. She cites an example of PA−EVOH films where MDO increases barrier performance, but if it is not done right the film becomes brittle.

11.2.3.2.5 Melt vs Solid State Stretching

Conventional blown and cast film processes impose some amount of orientation with blown film typically providing a more balanced orientation in the MD and TD than cast film (mostly MD). In these processes, the stretching occurs primarily in the melt, although in blown film most of the stretching occurs at temperatures near the point where the polymer begins to freeze. This is explored in more detail in Chapter 14. While the amount and rate of stretching can be quite high, the stress that develops is limited because the polymer is fluid. As described in Chapter 5, polymers are viscoelastic. The amount of stress that develops is characterized by the modulus times the stretch ratio (elastic component) and viscosity times the rate of stretching (viscous component). The modulus and viscosity undergo a rapid decrease as the polymer transitions from the "solid" to liquid state: above the T_g for amorphous polymers and the Tm for semicrystalline polymers. Hence, substantially greater stress can be generated if the stretching is done while the polymer is in the "solid" state. Higher stress results in greater polymer orientation and property enhancement when the orientation begins in the solid state, as in the double bubble, MDO, and tenter frame processes.

11.2.3.2.6 Sequential vs Simultaneous Orientation

For biaxial orientation processes, the order in which the sheet or tube is stretched in the MD and TD may have advantages. In the double bubble and blown film processes, the stretching occurs simultaneously. Early tenter frame processes were sequential, but newer technologies have been developed that simultaneously stretch the sheet in both directions [76,77,92]. In sequential orientation, the MDO is typically done first, followed by TDO. The orientation after the first orientation must be low enough so that the film can be stretched in the second direction. Often the film will need to be heated to a higher temperature for the second stretch. BOPP is typically made sequentially; high throughput and good quality can be achieved [92]. Some polymers, however, cannot be stretched sequentially. For example, EVOH crystallizes too fast during the first orientation to be oriented in the second direction. Simultaneous orientation is the only way to make biaxially oriented films with these polymers [77].

The simultaneous stretch tenter frame process has a higher capital cost than double bubble processes but can have higher throughput. The tenter frame process has greater temperature control over double bubble, which may allow for increased orientation [76]. The tenter frame process also has flexibility for profiling the stretch—linear, exponential, logarithmic, and so on.

Briel [92] provides some examples of how changing the stretch protocol can influence properties. In one experiment, polyolefins are stretched in a two-stage process: simultaneous MD and TD followed by MDO at a cooler temperature. The cooler second stage stretching provides greater shrinkage. McLeod [93] varies the stretching protocol for a sequential−biaxial PP orientation process. In one experiment the area draw ratio is kept constant at 6×6 and the TDO draw speed is varied. Increasing the TD draw speed increases the amount of shrinkage without changing the mechanical properties, which remain isotropic. In a second set of experiments, the draw ratios are varied. Anisotropic mechanical properties (as well as lower permeability) are achieved when the draw ratios are not equal (such as 5×8) but the shrinkage is the same as the 6×6 film.

11.2.3.2.7 Irradiation

Shrink films are often irradiated with electron beams either before or after orientation. Irradiation prior to orientation helps provide stability during orientation, allowing for greater draw ratios. Irradiation after stretching helps retain the orientation [94]. Irradiation is also used to improve mechanical properties (such as resistance to piercing and abrasion), increase shrinkage, and obtain higher seal strength [95]. Biddle [96] provides a history of two early approaches to shrink films:

- Cryovac used irradiation before blowing the film. The irradiation cross-links the PE, so that it is less fluid (higher viscosity) at the melting temperature. Tensile strength, shrink tension, and shrink percent are improved over nonirradiated film.
- DuPont used a different approach for Clysar. HDPE is typically not used for shrink film because it crystallizes too fast and so cannot be stretched very much. Blending in LDPE slows the rate of crystallization, making it act like a cross-linked film (crystals act like cross-links).

Zhang [94] finds that varying the radiation sequencing (before or after orientation) changes the shrinkage and shrink force characteristics. They evaluate commercial shrink films provided by a major supplier that have different e-beam sequences: NonIrr (no irradiation), PreIO (prior to orientation), and PostIO (after orientation). The three layer films are made from blends of LLDPE and LDPE and are 0.6 mil (15 μm) thick and biaxially oriented 400% at draw ratio 5×5. Zhang measures shrink force and shrinkage as a function of temperature. By plotting the force vs shrinkage at each temperature they create what they call "fictitious" stress−strain curves. By fictitious they mean that the data come from two different experiments and so are not true stress−strain curves. Nevertheless, they conclude the approach is promising for better understanding how the manufacturing conditions affect shrinkage, but a more systematic study is needed on monolayer films.

11.2.4 Oriented Multilayer Films

11.2.4.1 Laminations

Multilayer films used in flexible packaging often contain one or more oriented layers. OPP, oriented polyester (OPET), and oriented polyamine (OPA) films are typically used as the structural layer in multilayer laminates. Here the OPP, OPET, or OPA is first formed and subsequently additional layers (such as sealing or barrier layers) are added by adhesive or extrusion lamination. Many oriented films are also coated for sealing or to improve barrier. Examples include PVDC-coated OPET for improved barrier and EVA-coated OPET for sealing. Metallization can also be thought of as a form of coating. In each of these examples the base film is oriented first and additional nonoriented (or oriented) layers are subsequently added. Details on lamination and coating can be found in Chapter 10.

11.2.4.2 Base Films

Commercial OPP or OPET film is often made up of multiple layers, all of which have been oriented. For example, OPP may have a core layer made from homopolymer PP and an outer layer made from a propylene−ethylene random copolymer for sealing, or an outer layer made from a modified PP for improving the adhesion to metal during metallization. Further examples and a more detailed description of OPP technology can be found in Breil [97]. These films are made via coextrusion followed by orientation. Since the polymers used in these films are similar to each other, the techniques and challenges of orientation are similar to that of monolayer films.

11.2.4.3 Multilayer Barrier Shrink Film and Bags

Multilayer barrier shrink bags are used for a variety of meat and cheese applications. PVDC was one of the earliest polymers used for barrier shrink bags. One of the first applications was to protect poultry from freezer burn, taking advantage of its ability to shrink at 100°C. The poultry was placed in a blown film bag, the bag evacuated and sealed, and then immersed in boiling water. The bag shrank around the product for protection [96]. PVDC is still the primary barrier resin used for barrier shrink bags for subprime meats and many other applications [98]. Typically it is coextruded with EVA and oriented in a double bubble process. Common structures include (EVA−PVDC−EVA) and (PE−EVA−PVDC−EVA−PE) with about 10% of the structure PVDC [79,99]. PVDC provides excellent barrier to oxygen, moisture, aroma, and flavors and shrinks up to 40−50% at 85°C [79,98].

PVDC has a number of limitations due to its poor thermal stability. It is prone to gel and black spec formation during high temperature extrusion, evolves corrosive by-products, which require special materials of construction and good ventilation, and is known to discolor when exposed to radiation. Hence special care must be taken to process PVDC into films [100]. Other barrier structures have been developed using PA and EVOH. EVOH alone does not process well on a double bubble process. In general, grades with higher ethylene content process easier but at the expense of barrier performance. EVOH suppliers have made progress in developing special grades with improved stretching characteristics by lowering the level of crystallinity [27,98,100]. One approach has been to manipulate the head-to-head adjacency of hydroxyl groups along the polymer chain [100]. Polymer blending has also been used to improve the stretchability of EVOH, such as those described in Section 11.1.3.1 for improving the formability of EVOH. Sandwiching EVOH between layers of PA also helps stretchability. Most commercial non-PVDC barrier shrink bags use PA or a combination of PA−EVOH−PA. Copolymers of PA6, such as PA6/66, generally stretch better than PA6 due to their lower crystallinity [101]. Addition of PA6I/6T aPA (such as DuPont's Selar PA) to PA6 is also used to improve stretchability [84,95,102] Structures include (PE−tie−PA−tie−PE) and (PE−tie−PA−EVOH−PA−tie−PE) [98]. In general the non-PVDC barrier bags do not shrink as much as the PVDC bags, tend to be stiffer, and as a result hold a small share of the overall barrier shrink bag market. Alternative structures continue to be developed, such as the incorporation of an ionomer layer to improve shrinkage and reduce stiffness [100].

PA is used in barrier shrink bags for sausage casings and some cheese packaging. Example structures include (PA−tie−PE), (PA−tie−PA), (PA−tie−PA−tie−PE), or (PA−tie−EVOH−tie−Ionomer) [79]. The PA is often a blend of PA6 and PA6,66 for improved stretching. The PA provides moderate oxygen barrier, good aroma and flavor barrier, excellent temperature resistance, and good abuse resistance.

11.2.4.4 Multilayer Nonshrink Barrier Films

In recent years a number of investigators have looked at MDO, double bubble, and tenter frame processes to orient coextruded barrier films for improved performance with the objective to reduce cost. An in-line orientation process following the production of the coextruded sheet or tube has two inherent advantages over standard multilayer laminates. The first is the elimination of the lamination step by producing the structure in a single step. Rather than first producing an oriented substrate film, such as OPET, and subsequently adhesive or extrusion laminating it to a sealant film, these two processes can be consolidated into a single processing step. Second, the improved strength, barrier, and other properties of the oriented film hold the prospect of decreasing the thickness of the film, reducing material usage while still meeting performance specifications.

Several studies show improved barrier and mechanical strength performance of coextruded barrier films following MDO. Tabatabaei [87] finds that orientation of HDPE generally improves its moisture barrier. Breese [103] evaluates MDO of high molecular weight high density polyethylene (HMW−HDPE) films and finds reductions in moisture vapor transmission rate (MVTR) and oxygen permeation value (OPV) correlates with increasing draw ratio and orientation as measured by birefringence. Froio [104] presents results from oriented (LDPE−tie−EVOH−tie−HDPE) films that show a 33% reduction in OPV, a 600% increase in MD tensile strength, and a 75% increase in modulus.

Hatfield [105] orients (LLDPE−LLDPE−tie−EVOH−tie−LLDPE−LLDPE) blown film using a Collins MDO unit. The blown film has a 2:1 BUR. The EVOH is a standard 38 mol% ethylene grade and the LLDPE is a hexene copolymer. The total blown film thickness is 8 mils (200 μm) with individual layer thicknesses of [17/25/4/8/4/25/17%]. During MDO, the film is preheated, drawn, and annealed, all at 100°C. Draw ratio is varied from 1 to 6.5. The results of oxygen permeation measurements show a reduction in OPV (measured at 50% relative humidity [RH]) of 40% when the draw ratio is increased from 1 to 6.5. The OPV also becomes less sensitive to relative humidity, normally a limitation with EVOH. As described in Chapter 8, the OPV of EVOH increases substantially as the RH is increased from 50% to 100%. Hatfield finds that the reduction in OPV with MDO orientation is greater at higher humidity. In the RH range of 0−50%, the OPV decreases by 40% with orientation. At 90% RH, the reduction is 67% and the OPV is about the same as PVDC.

Hatfield also measures the optical properties of the MDO film. The haze decreases by 35% to a value of 10%. The gloss increases from 50% to 80% with orientation.

Lawrence [106] studies the effect of MDO on multilayer sealant films. Three layer blown films are prepared with the general structure (A−B−C) with a fixed layer ratio of (20/60/20%). Layer A is the sealant layer, a 0.916 g/cc density mLLDPE. C is the backing layer, an LLDPE (0.920 g/cc). The B layer is an LLDPE whose density is varied over a range of 0.917−0.936 g/cc. The blown films are made at their maximum thickness for the film line, ranging from 13 to 18 mils (330−460 μm) depending on the resins used. The MDO draw ratio is increased until the samples fail with samples collected for property testing at 3 mil [76 μm] and the maximum draw ratio. Conventional blown films of the same thickness are made as controls.

The results show the following:

- Normalized dart drop impact increases with increasing orientation. This runs counter to conventional wisdom, but previous work has shown that the film design impacts this. Increasing the density of the core layer reduces the effect of orientation on the dart drop strength.
- Secant modulus substantially increases with increasing orientation. They cite literature that attributes this to changes in crystalline morphology from a laminar to a fibrillar structure.
- MD tear is substantially lower in the oriented samples than the standard blown film counterparts. The magnitude of the difference is not as great at the highest draw ratios—so some of the tear strength is recovered with further orientation. They attribute this to neck-in changing the crystalline morphology.
- Film haze decreases with increasing orientation.
- Ultimate heat seal strength is substantially increased with orientation. The oriented films do not elongate as much as the blown films during the heat seal measurement. The heat seal initiation temperature is increased with orientation. They attribute this to the crystalline structure becoming more perfect during orientation, increasing the melting temperature. These effects are illustrated in Fig. 11.12.
- OPV and MVTR decrease with increasing orientation. The effect is more pronounced for oxygen and for the lower density core structures.

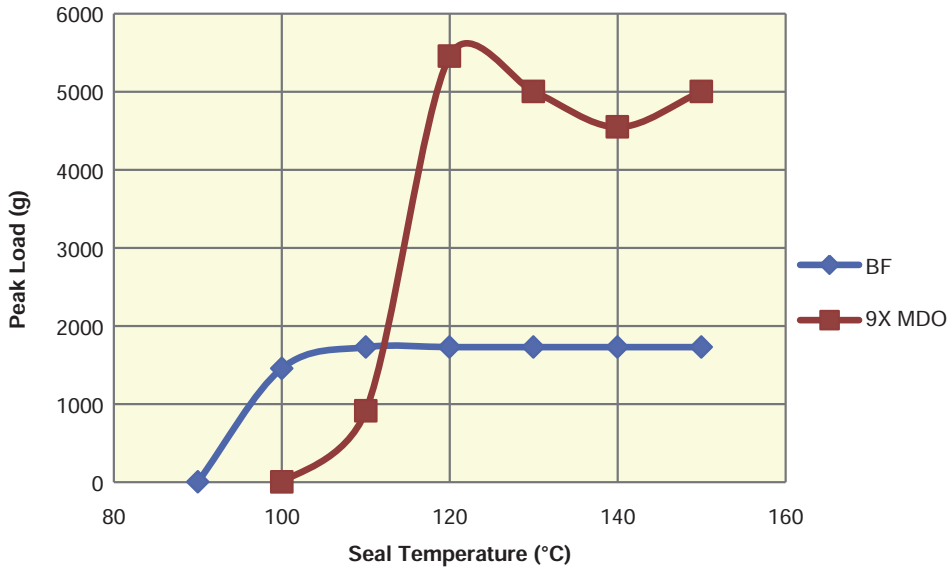


Figure 11.12 Heat seal strength for an LLDPE three-layer film with thickness 1.5 mil. The "BF" film is fabricated on a conventional blown film process (state 4). The MDO film has a draw ratio of 9.
Adapted from Lawrence C, Forziati Jr KT, Garnett J. Machine direction orientation and its effect on multilayer sealant film. In: SPE FlexPackCon conference; 2013.

The impact resistance and tear strength are often negatively impacted by MDO, in addition to the increase in seal initiation temperature. These drawbacks can often be lessened through changes in the design of the structure and the processing conditions. For example, changing the sealant layer to a lower crystalline copolymer may help retain the seal initiation temperature.

Breese [107,108] provides several examples of how MDO can reduce cost:

- Source reduction. The increase in modulus and strength allows for downgauging (reducing thickness) without sacrificing package integrity. An example of a heavy duty shipping sack is provided. A conventional 5-mil (127 μm) hexene−LLDPE blown film provides the right combination of properties to meet specifications. A specially formulated MDO film meets the requirements with 10% lower thickness.
- Material burden—replacing less desirable materials. An example is the replacement of a 48 gauge (12.5 μm) OPET film with a 60 gauge (15 μm) polyolefin MDO film. Despite the higher gauge, the yield of the polyolefin film is higher because of its lower density. The MDO also brings advantages in MD break strength, anisotropic tear, heat sealability, and resistance to moisture. Disadvantages include lower thermal stability, higher haze, higher oxygen permeability, and lower TD properties.
- Reduce processing steps. Replacing a laminate with a coextrusion can reduce processing steps. Breese provides an example of replacing a high barrier laminate with a coextruded MDO film but does not provide details of the structures.

Schut [91] observes that MDO of multilayer films has not been widely adopted despite the potential advantages. The process remains tricky. Beyond monolayer stretch film it is difficult to get right. Several companies in the early 2000s invested heavily only to abandon their lines. Lines for specific applications, such as breathable hygienic films for diaper liners, self-adhesive labels, synthetic paper, PET strapping, PVC food wrap, and fibrous HDPE ribbon for weaving sacks were adopted by the 1990s. These lines were not very flexible and lab lines too small for development of wide products. Newer lines allow more flexibility for product development on production lines, but the number of variables is huge: number and temperature of preheat rolls, type of roll heating, size of gap in draw rolls, number of times the film is drawn, temperature, dwell time for annealing, annealing temperature, temperature, and number of cooling rolls. Annealing conditions are particularly important to achieve dimensional stability. The sheer number of variables may be inhibiting the use of the process.

Resin suppliers have become more interested in MDO, which bodes well for the future. Some properties can be achieved that are not possible with biaxial orientation. For example, EVOH can be oriented in one direction but breaks up when oriented biaxially. HDPE provides good dead fold properties when machine direction oriented, but not when biaxial oriented. Bimodal grades of HMW−HDPE have been developed that provide better drawability. Resins filled with minerals such as calcium carbonate impart breathability through hole formation after stretching: after orienting in the MD, the film is rapidly quenched and then MD oriented a second time to open up the holes behind the mineral particles.

Dimensionally stable biaxial-oriented multilayer barrier films can be made with the double bubble or tenter frame processes with the proper annealing or heat setting following the orientation. Hausmann [80] provides some of the details for annealing, which is covered in Section 11.2.3.2.4. Alexy [109] gives several examples of oriented coextruded barrier films made on a double bubble process that can replace thicker laminates due to their superior physical and barrier properties. Further cost savings come from eliminating processing steps. Examples include:

- Lidding film. A conventional film has the structure OPET/adh//(PO−tie−PA−EVOH−PA−tie−PO) [12 μm/2 μm//40−65 μm]. Important features include puncture resistance and barrier. A proposed replacement structure is a biaxial-oriented coextruded film with the structure (PET−tie−PO−tie−PA−EVOH−PA−tie−PO) with a total thickness of only 20−25 μm
- Metallized balloon film. The conventional structure is BOPA/adh//PE/met [6−12/2//10/1 μm]. The proposed replacement structure is a double bubble film with the structure (PA−tie−PO−tie−PA−EVOH−PA−tie−PO), 18−20 μm.
- Coffee package. The conventional structure is OPET−met/PE [12/1/70−110 μm] with total

thickness ranging from 80 to 120 μm. The proposed replacement is a 40–50 μm biaxial oriented film with the structure (PET–tie–PO–tie–PA–EVOH–PA–tie–PO).

The PET coex structure in the coffee package example is also proposed for stand up pouches. Similar structures are reported by Hausmann [80] and Shiffmann [110,111].

Breil [77] discusses oriented multilayer barrier films made on a simultaneous linear stretcher (tenter frame). One example of a PP film has the structure (coPP–hoPP–tie–EVOH–tie–hoPP–coPP) with thicknesses [0.7/8.5/0.4/1.3/0.4/8.5/0.7 μm] after orientation. Here hoPP and coPP are homopolymer and copolymer PP, respectively. The oxygen transmission rate (OTR) is reported to be 2.08 cm^3/m^{2-}d-bar, which is in line with metallized films and barrier laminates. The film has low cost, is transparent, and provides enhanced shelf life.

11.2.4.5 Shrink Films and Labels

Shrink films are used for overwraps and a variety of retail and food packaging applications. PVDC was one of the first materials used in shrink films. Other polymers include LDPE, irradiated LDPE, PE copolymer, PP, PET, and PVC [96]. A performance comparison of these materials is provided in Table 11.3. Up until the early 2000s, LDPE was preferred over LLDPE for shrink films because LLDPE did not shrink enough in the transverse direction. LLDPE resin suppliers adjusted the MW and MWD distribution to introduce grades for the application [112]. Currently a variety of PEs are used in shrink films, including LLDPE, LDPE, blends of LLDPE and LDPE, coextrusions of LLDPE and LDPE, blends of HDPE and LDPE, and blends of HDPE, LDPE and LLDPE [74,94,96,113,114].

Shrink films are typically fabricated using blown film, double bubble, or tenter frame processes. The performance depends on the processing conditions as described in Section 11.2.3. Obi [115] describes the fundamental features of shrink films. In a shrink film packaging process, the heat and time in the shrink tunnel provides the thermal exposure to relax the orientation stress in the film, resulting in the shrinkage. For PE films, the typical oven temperature is from 180 to 215°C and time in the oven 10 s. When the film heats up, the oriented polymer chains partially revert back toward their random coil configuration. As a result, the film shrinks against the product. As the film cools, the polymer contracts due to crystallization and normal thermal contraction (as described by the thermal expansion coefficient). This is shown in Fig. 11.13 where the specific volume vs temperature is plotted for a semicrystalline polymer like PE or PET. The specific volume is the inverse of density and increases as the temperature increases; as more thermal energy is provided, the molecules move more, expanding the volume they occupy. The specific volume rises rapidly near the melting point of the polymer as the crystals lose their ordered structure and the chains expand. Conversely, as the film cools, the contraction gives rise to the shrink force. If the tunnel temperature is too low, not enough shrinkage occurs and the contraction force is too small. If the tunnel temperature is too high, the shrinkage will occur but the shrink force will decline as the orientation relaxes. If the temperature is excessive the film will melt, leading to burn holes.

Semicrystalline polymers retain much of their stiffness or modulus at temperatures above their T_g until the melting point is reached. This is because the crystals act as reinforcements. Once the crystals melt, the modulus drops precipitously. The polymer melts over a temperature range with the smaller crystals melting first. The larger crystals have the greatest reinforcing effect. In general, the heat tunnel is set below the peak melting point of the polymer so that all the crystals do not melt. If the temperature is too high, the polymer will end up as a viscous puddle.

DSC measurements can be used to calculate the cumulative percent melting at a given temperature. Obi shows for a particular LLDPE-based shrink film, the shrink tension rapidly rises as the oven temperature increases above 109°C. DSC shows that 55% of the crystals have melted. The tension peaks at 115°C where 69% of the crystals are melted. By 120°C, 86% have melted, leaving 14% of the crystals (the largest) to reinforce the film. Obi concludes that the polymer should have a broad melting temperature range to work well as a shrink film.

The shrink tension is a key parameter. The shrink tension generally decreases with decreasing crystallinity. For instance, films made from EVA and ionomers have lower shrink tension than LDPE or LLDPE and may be used in coextrusions or blends to produce shrink films for packaging fragile products. The work of Babovitch [116] illustrates this. Five layer films with the structure (LLDPE–EVA–

Table 11.3 Comparison of Shrink Film Types

Film Type	Advantages	Disadvantages
LDPE	Strong heat seals	Narrow shrink temperature range
	Low temperature shrink	Low stiffness
	Medium shrink force	Poorer optical properties
	Low cost	Sealing wire contamination
Irradiated LDPE	Higher tensile strength, shrink tension and percentage shrinkage than LDPE. Retains shrink tension for longer times than LDPE.	May have lower tear strength
LLDPE	High seal strength	Lower shrinkage than LDPE Higher shrinkage temperature
PP	Good optical appearance	High shrink temperature
	High stiffness	High sealing temperature
	High shrink force	Brittle seals
	Good durability	High shrink force—not suitable for fragile products
PVC	Lowest shrink temperature range Wide shrink temperature range Excellent optical appearance Controlled stiffness (by plasticizer content) Lowest shrink force for wrapping fragile products	Weakest heat seals Least durable after plasticizer lost Toxic and corrosive gas emissions from heat seal process Plasticizer health issue perceptions Durability issues at low temperatures Low shrink force hinders use as a multiple-unit bundling film Low film slip causes machine wraps
Multilayer coextrusion	Excellent balance of properties as determined by the layer construction	No significant performance disadvantages if the structure is designed well—the strengths of one ply compensates for the deficiencies of another

Adapted from Biddle G. Films, shrink. In: Bakker M. editor. The Wiley encyclopedia of packaging technology. New York: John Wiley & Sons, Inc.; 1986. p. 335–38.

LLDPE–EVA–LLDPE) and thickness [10/20/40/20/10%] are made on a double bubble process. The stretch ratio is 5:1 in both MD and TD. Three different grades of EVA are used with 4, 12, and 19 wt% VA. Fig. 11.14 shows the results of shrink tension measurements. As the VA content in the EVA layers is increased, the shrink tension decreases. Increasing VA content decreases the crystallinity of the EVA. These results are consistent with internal studies at DuPont for EVA resins. Ionomers are also known for their low shrink force allowing them to be used in skin packaging of fragile materials.

Shrink labels and sleeves have the ability to shrink and conform to the shape of the container. Key attributes include the ability to maintain shape and shrink under the application of heat, shrink force, shrink geometry, and printability. Commonly used polymers in shrink labels include PVC, polyolefins, polyethylene terephthalate glycol (PETG), styrene polymers, and cyclic olefin copolymers (COCs) [117]. PVC is low in cost but because of its high density it does not float in recycle separation systems. Halogens are also an issue. PETG has a high growth rate but is the most expensive, has shrink properties that are very sensitive to temperature, and does not float. Oriented PS is primarily used in Japan. It is less stiff than PVC or PETG and due to temperature sensitivity, logistics can be

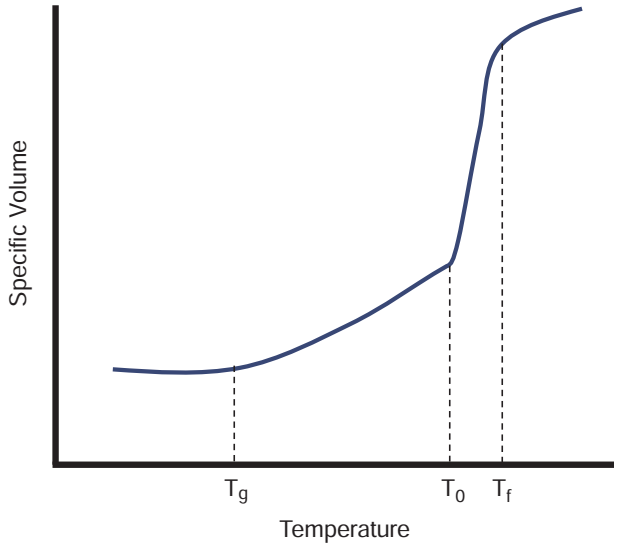


Figure 11.13 Specific volume change with temperature for a semicrystalline polymer.
Adapted from Obi BE, Leano M. Correlating the melting of semi-crystalline polymers to the shrink wrapping process in shrink-film packaging applications. In: SPE ANTEC conference; 2015.

challenging. OPP is not generally used because it does not shrink enough and is not stiff enough [118].

Recycling has been a driving force toward polyolefin-based shrink labels. With their density less than water, polyolefin labels float when ground and put into a water floatation separation system. Enhanced polyolefin systems are described by Jester [118]. They are typically multilayer, achieve medium shrink (around 50%), and are recycle friendly (they float). COCs may be blended or used as a separate layer. One structure is a (A−B−A) coextrusion with A being COC-rich and B being a PE-rich core. The COC adds stiffness and printability, and because it is amorphous, helps with orientation.

11.2.4.6 Stretch and Cling Films

Stretch films are extendable, elastic−plastic films that when stretched around a product, generate residual tension that contracts the film to the contour of the product. Stretch films and hoods have increasingly replaced tapes, shrink films, and metal banding for palletization and bundling. Some advantages of stretch films in these applications include the following [119]:

- lower handling costs;
- labor savings;
- transportation savings;
- protection;

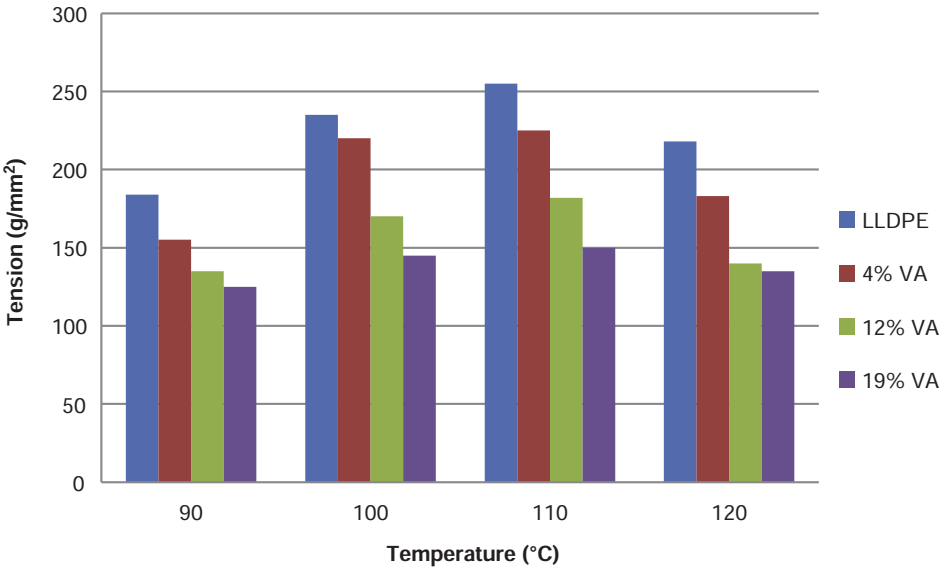


Figure 11.14 Shrink tension of (LLDPE−EVA−LLDPE−EVA−LLDPE) films as a function of VA content and temperature.
Results from Babovitch AL, Sagron A, Unigovski Y, Jarashneli A, Gutman EM. Stress relaxation in low-shrink-force polyolefin films. Poly Eng Sci 2004;44:1716−20.

- inventory control (easier identification of the product due to the clarity of the film).

A stretch film is stretched and oriented by the user at room temperature. The cold draw increases strength and if the stretch occurs in the elastic range of the polymer, the molecules attempt to recoil back to their original configuration once the strain is released [120]. This contrasts with shrink films where the film is stretched by the film producer at an elevated temperature with the residual stress frozen in place. This stress is relieved when the film is exposed to elevated temperature by the user, resulting in shrink.

Stretch films and stretch hoods are typically made from polyolefins such as EVA, LLDPE, VLDPE and metallocene LLDPE and plastomers. Some typical structures can be found in Table B.14 in Appendix B.

Cling films have historically been made from LDPE, EVA, and PVC. Metallocene LLDPE is starting to be used due to its higher mechanical properties (tear, impact, tensile strength). PE requires additives, such as polyisobutylene (PIB), for cling whereas EVA is naturally tacky. The tackiness of EVA increases with increasing VA content but the VA content has limits. In blown film, high VA (above about 18 wt%) causes blocking; in cast film it causes chill roll sticking, which can lead to line tension variability and differential cooling and mechanical performance [120]. Metallocene LLDPE provides greater strength and dart impact resistance over conventional LLDPE, allowing for down gauging [119].

Stretch and cling film have moved from mono- to multilayer (3, 5, 7, and 9 layers). Blends and coextrusions are increasingly being used to optimize and customize the performance of stretch and cling films for a variety of applications. For example, coextruded films can be made with cling on one side and slip on the other or with different colors [119]. A typical three-layer coextrusion has the layer ratio 1:3:1 with the core an elastic layer (EVA or thermopolastic olefin) and skins a polyolefin such as mLLDPE (with slip and antiblock) [121].

Both cast and blown films are used to make stretch films, with about 70% in cast film as of 2001. The cast film process provides high clarity [119]. Some of the properties that are important for stretch films include strength, puncture resistance, tear resistance, stretch percentage at break, load retention, haze, gloss, and cling [119].

Shelley [121] evaluates three layer blown films for stretch hood applications. The core layer is made from blends of a reactor made PP-based thermoplastic olefin (TPO) with EVA (6.6% VA) or LDPE. The ratio of TPO to EVA or LDPE ranges from 100:0 to 0:100. The film is blown at 3:1 BUR with thickness 100 or 80 μm. They propose using a residual stress (ASTM D5748) test over stress relaxation to better simulate the strains imposed during pallet wrapping. The test involves imposing an initial extension of 100%, reducing the strain to 75%, and measuring the change in stress after 180 s. They use an elastic recovery test as an indication of snap back, important once the stretch hood is released (so it can hold in the product). This test involves measuring the stress after imposing an initial strain of 100% for 10 s and releasing it to zero. Increasing the TPO content, and switching from LDPE to EVA in the blend, increases the elastic recovery. Elmendorf tear resistance and dart impact resistance also increase with increasing amount of TPO in the core layer blend. The authors postulate that these properties may correlate with the amount of amorphous phase in the core.

Small [122] studies the effect of PIB concentration, extrusion conditions, storage temperature and aging on mechanical properties, crystallinity, and surface tack. PIB migrates to the surface after extrusion to provide cling. This migration is similar to slip additive migration and is affected by many of the same factors: compatibility between the additive and polymer, film morphology, extrusion variables, and film conditioning. Further discussion of slip migration is provided in Chapter 12. Small makes blown and cast films of a 70/30 blend of LLDPE and LDPE containing 0–4% PIB. For the blown film, three different blowup ratios (1.5, 2, and 2.5) are used. Results show that at these low levels of PIB there is little effect on the mechanical properties of the film. Tack increases with PIB level as expected. Tack also increases with storage time (up to about 20 days) and storage temperature.

Small finds that the cast film does not have greater tack than the blown film. Previous investigators propose that the small PIB molecules migrate through the amorphous regions. Since cast film has more amorphous regions than blown film, Small expected the tack to be greater for the cast film. They suggest that cocrystallization between the LLDPE and LDPE in the cast film may explain their observation. Evidence for cocrystallization shows up in DSC measurements. Other factors, not considered by Small, may also be involved, such as loss of additive due to temperature (cast film typically is produced at

higher temperatures than blown film), differences in polymer surface roughness, and crystallinity effects (cast film typically has a lower level of crystallinity than blown film, which affects the solubility of the additive in the polymer.) These factors are discussed in Chapter 12.

In a second study, Small [120] compares (EVA−mLLDPE−EVA) [2.5/20/2.5 μm] cast films with monolayer mLLDPE films. The EVA ranges from 6 to 18 wt% VA. Zero to twenty percent of a PIB masterbatch (52% PIB in LLDPE) is added to the EVA layers. The VA content and PIB level have only a small effect on most of the tensile properties of the film, but the modulus is found to decrease with increasing VA in the EVA layer. Higher PIB levels increases elongation at break and decreases modulus. Increasing VA level also increases elongation at break. The (EVA−mLLDPE−EVA) films give better tack and comparable mechanical properties to mLLDPE monolayer films. By adding PIB just in the surface layer there is a potential for cost reduction using the coextruded structure. Tack development is also faster. A trade-off is the lower modulus of the coextruded film.

In a third study Small [123] considers the effect of varying the LLDPE type (comonomer, density, and melt flow rate) on mechanical and tack properties of monolayer cast films. The PIB level is fixed at 8% addition of the masterbatch. Measurements include DSC for crystallinity, FTIR for crystalline orientation, trouser tear, film tack, and tensile properties. They find that the crystalline orientation decreases with decreasing MFR. As orientation decreases, modulus, percent crystallinity, and tear resistance decrease. Octene LLDPE has higher tear resistance than hexene LLDPE. Tack is influenced both by crystallinity and orientation: decreasing crystallinity increases tack due to more migration of the PIB to the surface and higher orientation results in less tack. In some cases, orientation dominates crystallinity.

Microlayer technology, described in Sections 8.5.2 and 9.4.6, has been adopted for stretch films for pallet wrapping and other applications. AEP commercialized a 27-layer structure with a split sandwich structure of 11 microlayers on each side of a core and intermediate skin layers. They had reportedly considering buying a 9- or 11-layer line but found that the microlayer technology gave stronger films. The two microlayer sections are each 10% of the structure, the LLDPE core 40%, skin layers 10%, and intermediate layers 10%. So each microlayer is about 1% of the overall structure. A 70 gauge (17.8 μm) film stretched 250% has layers only 0.057 μm thick. Putting the same material through all the extruders creates a plywood effect, strengthening the film. AEP found using the process for an all LLDPE film gave the same strength as a multimaterial film (9000 psi [62 MPa] vs 6000 psi [41.4 MPa]) for a typical stretch wrap film. The big gains with the multimaterial film are in holding strength and tear resistance [124].

Going to multilayers enhances stretchability, tear resistance, and puncture resistance. Equipment supplier Nordson EDI reports 34% greater stretch with a 48 microlayer LLDPE stretch film over conventional films. Productivity can also be enhanced as gels are less likely to cause line breaks due to the other layers encapsulating them [125].

11.2.4.7 Adhesion

Stretching and orientation of multilayer films can substantially reduce interlayer adhesion. Up to 90% of the preorientation bond strength can be lost during MDO of barrier films with conventional maleic anhydride-based tie resins. There are a number of factors that have been implicated or postulated for this loss of adhesion, which include the following:

- the creation of new interfacial area during stretching, reducing the number of chemical bond linkages (created prior to orientation) per unit area;
- the thinning of the structure, resulting in lower tensile strength and stiffness;
- strain hardening of some tie resins during stretching, reducing their elasticity and ability to absorb and dissipate interfacial stress;
- strain hardening during stretching due to bonds formed between the tie and barrier resin;
- increasing crystallinity, contributing to less elasticity of the tie and barrier;
- a change in crystalline morphology during stretching, influencing mechanical properties that affect peel strength;
- frozen-in stress created during orientation and rapid quenching;
- differential stress between the polyolefin and barrier during stretching, concentrating the stress at the interface.

An example of loss of adhesion in (LLDPE−tie−EVOH−tie−LLDPE) film during orientation in an MDO process is given in Figure 10.42. This is taken from Lee [126] who found evidence for a number of these factors in their study. Many of these factors can be mitigated through the design of the tie resin. Close consultation with the tie resin manufacturer is important when dealing with oriented structures. Further discussion of the factors that influence adhesion is provided in Chapter 10.

References

[1] Joseph G, McGowan C. Near infrared sensor technology & the modern approach. In: TAPPI PLACE conference; 2004.

[2] Blalock T, Heveron-Smith S. Multi-layer film measurement using dual-light interferometry. In: TAPPI PLACE conference, Indianapolis, IN; 2004.

[3] Hilton C. Thermoforming polypropylene: an overview. In: SPE polyolefins conference; 2002. p. 219−33.

[4] MaCauley N, Harkin-Jones E, Murphy W. Dynamic mechanical thermal analysis: a method for assessing the thermoformability of plastic sheeting. In: IChemERes. Event-Eur Conf. Young Res. Chem. Eng., 1st, 2; 1995. p. 677−6799.

[5] Spence T, Hylton D. Rheological studies of commercial thermoforming materials. In: SPE ANTEC conference; 1988. p. 681−9.

[6] Throne JL. Thermoforming. Munich: Hanser Publishers; 1986.

[7] Dharia A, Hylton D. Novel method for rapid determination of thermoformability. In: SPE ANTEC conference; 2005. p. 1214−9.

[8] Joye DD, Pohlein GW, Denn CD. A bubble inflation technique the measurement of viscoelastic properties in equal biaxial extensional flow. Trans Soc Rheol 1972;16:421.

[9] Joye DD, Pohlein GW, Denn CD. A bubble inflation technique the measurement of viscoelastic properties in equal biaxial extensional flow II. Trans Soc Rheol 1973;17:287.

[10] Derdouri A, Connolly R, Verron E, Peseux B. Material constants identification for thermoforming simulation. In: SPE ANTEC conference 56th; 1998. p. 672−5.

[11] Schmidt LR, Carley JF. Biaxial stretching of heat-softened plastic sheets: experiments and results. Polym Eng Sci 1975;15:51−62.

[12] Dharia A. Applications of thermoformability analyzer. In: SPE ANTEC conference; 2006. p. 2605−9.

[13] Grande JA. A simple, repeatable, realistic test of thermoformability. Plastics Technology Magazine; October 2005. p. 55−7.

[14] Wang XC, Boparai M. Identification of thermoform-ability indicators for multilayer films. In: SPE ANTEC conference; 2010. p. 2055−9.

[15] Ho K, Ward D, Kuklisin K, Murphy A. Multilayer blown films for thermoformed food packaging applications. In: SPE ANTEC conference; 2011.

[16] Kurzbeck S, Munstedt H. Elongational properties of polymer melts and correlations with their processing behavior in blown film and thermoforming. In: Progress an trends in Rheology V, Proceedings of the European Rheology conference, 5th Portoroz, Slovenia, September 6−11; 1998. p. 402−3.

[17] Yu TC. Thermoforming behavior of olefinic instrument panel skins. In: SPE ANTEC conference; 1999.

[18] Baird DG, Collias DI. Polymer processing: principles and design. Boston: Butterworth-Heinemann; 1995. p. 286−91.

[19] DiRaddo R, Meddad A. Sensitivity of operating conditions and material properties for thermoforming process. Plastics, Rubber Compos 2000;29:163−7.

[20] Ward D. The importance of thermal transfer and heat retention in designing thermoformable coextruded film structures. In: TAPPI PLACE conference; 2010.

[21] Xiao K, Lee I-H, Armstrong R. Comparison of water-quench versus air-quench blown film processes − Part II: Thermoformability. In: SPE ANTEC conference; 2012.

[22] Ashter SA. Thermoforming of single and multilayer laminates: plastics films technologies, testing, and applications. Walthan, MA: Elsevier; 2014.

[23] Shell Development Company. Polypropylene technology seminar. 1987.

[24] Kuraray Technical Bulletin No 150. Thermoforming of EVAL® resin containing structures. 2000. viewed May 31, 2015 from: http://eval-americas.com/media/36418/tb_no_150.pdf.

[25] Chou R, Lee IH. Behavior of ethylene vinyl alcohol (EVOH) amorphous nylon blends in

solid-phase thermoforming. J Plastic Film Sheeting 1997;13:74–93.
[26] Chow E. High barrier forming films with EVOH. In: VII International TAPPI/CETEA conference on flexible packaging; 2012.
[27] Matsui I, Onishi H, Yamamoto T. Study on orientable EVOH. In: TAPPI PLACE conference; 2003.
[28] Eval Americas, Eval™ SP – oriented for future, Kuraray ; n.d., viewed May 31, 2015 from: http://www.docstoc.com/docs/79126600/EVAL-SP-Oriented-for-the-future.
[29] Chou RT, Deak GI. Blends of ethylene vinyl alcohol copolymer and amorphous polyamide, and multilayer containers made. 1991. US patent 4990562.
[30] Oberle WA. Process for thermoforming EVOH barrier sheets and products relating hereto. 1998. EP0699125 B1.
[31] Giménez E, Lagarón JM, Cabedo L, Garava R, Saura JJ. Study of thermoformability of ethylene-vinyl alcohol copolymer based barrier blends of interest in food packaging applications. J Appl Polym Sci 2004;96:3851–5.
[32] Giménez E, Lagarón JM, Maspoch LM, Cabedo L, Saura JJ. Uniaxial tensile behavior and thermoforming characteristics of high barrier EVOH-based blends of interest in food packaging. Polym Eng Sci 2004;44:598–608.
[33] Fetell AI. Nylon-containing ionomer improves the performance of ethylene vinyl alcohol (EVOH) copolymers in multilayer structures. In: TAPPI polymers, laminations & coatings conference; 1997. p. 503–5.
[34] Fetell AI. Ethylene vinyl alcohol copolymer blends. 1997. WO 1997009380 A1.
[35] Shelat KJ, Dutta NK, Choudhury NR. Interfacial interaction and morphology of EVOH and ionomer blends by scanning electron microscopy and its correlation to barrier characteristics. Langmuir 2008;24:5464–73.
[36] Lee JK, Virkler TL, Scott CE. Influence of initial sheet temperature on ABS thermoforming. Polym Eng Sci 2001;41:1830–44.
[37] Harron GW, Harkin-Jones EMA, Martin PJ. Influence of thermoforming parameters on final part properties. In: SPE ANTEC conference; 2000.
[38] Bordonaro C, Virkler T, Galante P, Pineo B, Scott C. Optimization of processing conditions in thermoforming. In: SPE ANTEC conference, 56th; 1988. p. 696–700.
[39] Tanaka H, Shigemoto H, Hawachi H. Adhesive resin for multi-layer films used for shrink or thermoforming processes. J Plastic Film Sheeting 1996;12:278–86.
[40] Nam G, Hah K-H, Lee J. Three-dimensional simulation of thermoforming process and its comparison with experiments. Polym Eng Sci 2000;40:2232–40.
[41] Song Y, Zhang K, Wang Z, Diao F, Yan Y, Zhang R. Coupled thermomechanical analysis for plastic thermoforming. Poly Eng Sci 2000;40:1736–46.
[42] Laroche D, Erchiqui F. Experimental and theoretical study of the thermoformability of industrial polymers. J Plastic Film Sheeting 1999;15:287–96.
[43] Novotny P, Saha P, Kouba K. Fitting of K-BKZ model parameters for the simulation of thermoforming. Intern Poly Process 1999;14:291–5.
[44] Novotny P, Kouba K, Saha P. The role of material in the simulation of the thermoforming process. In: Progress and trends in Rheology V, Proceedings of the European Rheology conference, 5th Portoroz, Slovenia, September 6–11; 1998. p. 367–8.
[45] Novotny P, Saha P. Optimization of thermoforming. In: SPE ANTEC conference, 57th; 1999. p. 841–3.
[46] DiRaddo R, Laroche D, Bendada A, Ots T. Optimization of thermoforming with process modeling. In: SPE ANTEC conference, 57th; 1999. p. 844–9.
[47] DiRaddo R, Girard P, Chang S. Model-based control of material distribution in thermoformed parts. In: SPE ANTEC conference, 60th; 2002.
[48] Lappin J, Harkin-Jones E, Martin P. Finite element modeling of the plug-assisted thermoforming process. In: SPE ANTEC conference, 57th; 1999. p. 826–30.
[49] Nam G, Rhee H, Lee J. Finite element analysis of the effect of processing conditions on thermoforming. In: SPE ANTEC conference, 56th; 1998. p. 690–769.
[50] Laroche D, Erchiqui F. Experimental and theoretical study of the thermoformability of industrial polymers. In: SPE ANTEC conference, 56th; 1998. p. 676–80.

[51] Debbaut B, Homerin O. 3-D numerical simulation of thermoforming: prediction of thickness and extensions. In: SPE ANTEC conference, 55th; 1997. p. 720–5.
[52] Koziey B, Procher J, Tan J, Vlachopoulos J. New results in finite element analysis of thermoforming. In: SPE ANTEC conference, 55th; 1997. p. 714–9.
[53] Martin N, Harkin-Jones E, Martin P. Characterizing the biaxial properties of materials used in thermoforming and blow molding. In: SPE ANTEC conference, 60th; 2002. p. 732–6.
[54] Nam G, Ahn K, Lee J. Numerical and experimental studies of 3-dimensional thermoforming process. In: SPE ANTEC conference, 57th; 1999. p. 836–40.
[55] Christopherson R, Debbaut B, Rubin Y. Simulation of pharmaceutical blister pack thermoforming using a non-isothermal integral model. In: SPE ANTEC conference, 58th; 2000. p. 773–7.
[56] Wang C-H, Nied H. Solution of inverse thermoforming problems using finite element simulation. In: SPE ANTEC conference, 58th; 2000. p. 768–72.
[57] Rachik M, Roelandt J. A unified approach for thermoforming numerical simulation. In: SPE ANTEC conference, 57th; 1999. p. 831–5.
[58] Tshai KY, Harkin-Jones EMA, Martin PJ, Menary G. A unified approach of modeling polypropylene for thin-gauge solid-phase thermoforming applications. In: SPE ANTEC conference; 2004. p. 919–23.
[59] Van Mieghem B, Desplentere F, Van Bael A, Ivens J. Improvements in thermoforming simulation by use of 3D digital image correlation. eXPRESS Polym Lett 2015;9:119–28.
[60] Throne JL. Parametric study of extrusion and thermoforming conditions for CPET. J Plastic Film Sheeting 1989;5:222–40.
[61] Xu H, Kazmer DO. Thermoforming shrinkage prediction. Polym Eng Sci 2001; 41:1553–63.
[62] Yousefi A, Bendada A, Diraddo R. Improved modeling for the reheat phase in thermoforming through an uncertainty treatment of the key parameters. Polym Eng Sci 2002;42: 1115–29.
[63] O'Conner C, Martin P, Menary G, Sweeney J, Caton-Rose P, Spencer P. Development of a constitutive model of polypropylene for thermoforming. In: AIP conference proceedings, 1353 (Part 1); 2011. p. 874–9.
[64] Christopherson R, Briere M. Simulation of the puncture resistance of a thermoformed syringe pack. In: SPE ANTEC conference; 2001.
[65] Ajji A, Zhang X. Correlations between orientation and some properties of polymer films and sheets. J Plastic Film Sheeting 2002;18: 105–16.
[66] Chambon F, Srinivas S. Orientation analysis of cast and blown polyethylene films. J Plastic Film Sheeting 1999;15:297–307.
[67] White JL, Cakmak M. "Orientation," Encyclopedia of polymer science and technology. John Wiley & Sons; 2010.
[68] Ajji A, Elkoun S, Zhang X. Biaxial orientation characterization in PE and PP using WAXD X-ray pole figures, FTIR spectroscopy, and birefringence. J Plastic Film Sheeting 2005;21:115–26.
[69] Zhang X, Ajji A, Jean-Marie V. Processing-structure-properties relationship of multilayer films. I. Structure characterization. Polymer 2001;42:8179–95.
[70] Read BE, Ward IM. Structure and properties of oriented polymers. New York: Wiley-Interscience; 1975.
[71] Jasse B, Koenig JL. Orientation measurements in polymers using vibrational spectroscopy. J Macromol Sci Rev Macromol Chem 1979;C17:61–135.
[72] ASTM International. Standard test method for unrestrained linear thermal shrinkage of plastic film and sheeting. West Conshohocken, PA: ASTM International; 2014 (D2732-14).
[73] ASTM International. Standard test method for shrink tension and orientation release stress of plastic film and sheeting. West Conshohocken, PA: ASTM International; 2009 (D2838-09).
[74] Jin Y, Hermel-Davidock T, Karjala T, Demirors M, Wang J, Leyva E, et al. Shrink force measurement of low shrink force films. In: SPE ANTEC conference; 2008. p. 1364–8.
[75] DeMeuse MT. Biaxial stretching of film, principles and applications. Oxford: Woodhead Publishing; 2011. p. 37–40.
[76] Hanschen TP. "Films, orientation," Encyclopedia of polymer science and technology. John Wiley and Sons, Inc.; 2002. p. 559–77.

[77] Breil J. Speciality oriented films: new markets, new applications, new developments. Specialty Plastic Films; 2004. 2004.
[78] Ajji A, Zhang X. Biaxial orientation of multilayer LDPE/PET films: structure and properties. In: SPE ANTEC conference; 2004. p. 2112–6.
[79] Strobie J. Producing co-extruded high barrier heat shrinkable packaging films. In: TAPPI PLACE conference; 2002.
[80] Hausmann K, Trouilhet YM, Schiffman J. Low temperature sealing films. 2013. US patent application 2013/0164516 A1.
[81] Mount III EM. Uniformly stretching polymer sheets and multilayer films. 2011. Converting Quarterly "Substrate Secrets" blog, viewed June 7, 2015 from: http://www.convertingquarterly.com/blogs/substrate-secrets/id/2271/uniformly-stretching-polymer-sheets-and-multilayer-films.aspx.
[82] Nishamoto Y, Yamazaki K. Heat-shrinkable laminate film. 1984. US patent 4424243.
[83] Ciocca P, Forloni R. Multilayer oxygen barrier packaging film. 2001. US patent 6221470 B1.
[84] Lustig S, Vicik SJ. Oriented multilayer film and process for making same. 1991. US patent 5077109.
[85] Forloni R. Heat-shrinkable multilayer thermoplastic film. 2001. US patent 6299984 B1.
[86] Tanaka H, Kawachi H. Adhesive polypropylene composition and multi-layer laminate layer body using the resin composition. 1997. US patent 5695838 A.
[87] Tabatabaei SH, Parent L, Cigana P, Ajji A, Carreau PJ. Effect of machine direction orientation conditions on properties of HDPE films. J Plastic Film Sheeting 2009;25:235–49.
[88] Pakula T, Trznadel M. Thermally stimulated shrink forces in oriented polymers: 1. Temperature dependence. Polymer 1985;26:1011–8.
[89] Gillette PC. Biaxially oriented polyolefin film is post-treated by annealing to improve dimensional stability in limited temperature range for various time periods. 1992. US patent US 5152946 A.
[90] Barham PJ, Odell JA, Willmouth FM. Heat-treating polyolefin films. 1981. UK patent application, GB 2055855 A.
[91] Schut JH. MDO films: lots of promise, big challenges. Plastics Technology; 2005. February 2005, viewed June 07, 2015 at: http://www.ptonline.com/articles/mdo-films-lots-of-promise-big-challenges.
[92] Breil J. New developments for biaxially stretched polyolefin film with linear motor driven simultaneous stretching technology. In: SPE ANTEC conference; 2002.
[93] McLeod MA. Drawing forces and film properties in semi-sequentially stretched polypropylene. In: SPE ANTEC conference; 2005. p. 1752–6.
[94] Zhang W, Yang H, Moffitt R, Tung J. Characterization of crosslinked, heat-shrinkable packaging films. In: SPE ANTEC conference; 2007. p. 537–42.
[95] Zanella M, Gini A, Prandi P. A multilayer heat-shrinkable plastic film with barrier characteristics. 2001. WO 2001003922 A1.
[96] Biddle G. Films, shrink. In: Bakker M, editor. The Wiley encyclopedia of packaging technology. New York: John Wiley & Sons, Inc.; 1986. p. 335–8.
[97] Breil J. Multilayer oriented films. In: Wagner JR, editor. Multilayer flexible packaging, technology and applications for the food, personal care and over-the-counter pharmaceutical industries. Oxford: Elsevier; 2010. p. 231–7.
[98] Medlock G. Enhanced EVOH for improved orientability and shrink. In: TAPPI PLACE conference; 2010.
[99] Lind KD, Eckstein J, Blemberg RJ, Kaas RL, Walbrun GH. Heat shrinkable barrier films. 2000. US patent US 6074715 A.
[100] Lee I-H, Schenck HE. Heat shrinkable multilayer film or tube that exhibits shrink stability after orientation. 2012. US patent 8202590 B2.
[101] Ube. Ube nylon extrusion application. Ube Industries, Ltd; 2005. viewed July 26, 2015 from: https://www.ube.es/archivos/pdfs/extrusion.pdf.
[102] Ueyama T, Itoh T. Heat-shrinkable multilayer film. 2002. European patent EP 1190847 A1.
[103] Breese R, Beaucage G. Effects of machine direction orientation (MDO) on the moisture and oxygen barrier properties of HMW-PE films. In: TAPPI PLACE conference; 2005.
[104] Froio D, Schirmer S, Ratto JA, Burke M, Pigeon G. The effect of machine direction orientation on multilayer high barrier films. In: SPE ANTEC conference; 2012.
[105] Hatfield E, Breese DR. Step change improvements in EVOH barrier using MDO. Equistar;

2006. viewed June 07, 2015 at: http://www.lyondellbasell.com/techlit/techlit/Tech%20Topics/Equistar%20Industry%20Papers/EVOH_Barrier_Using_MDO.pdf.
[106] Lawrence C, Forziati Jr KT, Garnett J. Machine direction orientation and its effect on multilayer sealant film. In: SPE FlexPackCon conference; 2013.
[107] Breese R. Economic benefits of utilizing MDO films in flexible packaging. In: TAPPI PLACE conference; 2007.
[108] Breese R. Benefits of machine direction-oriented (MDO) films in flexible-packaging applications. 2011, quarter 2. Converting Quarterly; 2011. p. 32–6. viewed June 07, 2015 at:, http://www.convertingquarterly.com/magazine/back-issues.aspx.
[109] Alexy F. Replacing aluminum in high barrier packaging with Triple Bubble® blown film extrusion. In: Multilayer packaging films 2012 conference; 2012.
[110] Schiffmann J. Multi-layered two-dimensional or tubular food casing or food film. 2014. US patent application US 2013/0044980 A1.
[111] Shiffmann J. Multilayer sheet- or tube-type food casing or food film. 2014. US patent application US 2014/0044902 A1.
[112] Chiu DY, Ealer GE, Moy FH, Bühler-Vidal JO. Unipol II LLDPE – gas phase LLDPE for the shrink market. J Plastic Film Sheeting 1999;15:153–78.
[113] Torres A, Colls N, Méndez F. Properties predictor for HDPE/LDPE/LLDPE blends for shrink film applications. J Plastic Film Sheeting 2006;22:29–37. Also 2005, *SPE ANTEC conference*, pp. 2986–2989.
[114] Werlang MM. Effect of polymer processing conditions on shrinkability of LDPE and LLDPE films, and on optical properties of LLDPE films. In: SPE ANTEC conference; 2003. p. 3271–4.
[115] Obi BE, Leano M. Correlating the melting of semi-crystalline polymers to the shrink wrapping process in shrink-film packaging applications. In: SPE ANTEC conference; 2015.
[116] Babovitch AL, Sagron A, Unigovski Y, Jarashneli A, Gutman EM. Stress relaxation in low-shrink-force polyolefin films. Poly Eng Sci 2004;44:1716–20.
[117] Chen C-W, Pham HT, Poslinski AJ. Understanding of shrink films through viscoelastic behavior of films. In: SPE ANTEC conference; 2013.
[118] Jester R. COC enhanced polyolefin films for shrink label sleeves and labels. In: SPE polyolefins and flexible packaging conference; 2011.
[119] Wainer MW. Stretch film properties – effects of equipment and process variables. J Plastic Film Sheeting 2002;18:279–86.
[120] Small CM, McNally GM, Murphy WR, Garrett G. The effect of vinyl acetate concentration and polyisobutylene concentration on the properties of metallocene polyethylene/ethyl vinyl acetate co-extruded film for stretch and cling film applications. In: SPE ANTEC conference; 2003. p. 3167–71.
[121] Shelley C, Kokel N. Elastic recovery behavior of three layer film structures comprised of TPO and various ethylene copolymers. In: SPE ANTEC conference; 2009. p. 2775–80.
[122] Small CM, McNally GM, Marks A, Murphy WR. The effect of extrusion processing conditions and polyisobutyene concentration on the properties of polyethylene for stretch and cling film applications. In: SPE ANTEC conference; 2002.
[123] Small CM, McNally GM, Murphy WR, Garrett G. The effect of polymer properties on the mechanical behavior and morphological characteristics of cast polyethylene film for stretch and cling film applications. In: SPE ANTEC conference; 2003. p. 3266–70.
[124] Naitove M. First microlayerd commodity films. Plastics Technology; 2009. viewed June 12, 2015 at: http://www.ptonline.com/articles/firstmicrolayeredcommodityfilms.
[125] AIMCAL. MicroLayer cast film process yields stretch wrap with properties and potential to save on wrapping. AIMCAL; 2008. viewed June 12, 2015 at: http://www.aimcal.org/membernews/articles/id/910/microlayercastfilmprocessyieldsstretchwrapwithpropertiesandpotentialtosaveonwrapping.aspx.
[126] Lee CD, Strebel JJ, Goudelock JD. Higher tie layer adhesion in machine direction oriented (MDO) barrier films. In: TAPPI PLACE conference; 2007.

12 Frictional and Optical Properties

The slipperiness or tackiness of a packaging film impacts its ability to be handled on high-speed packaging lines. The incorporation of low-melting sealant layers, which are naturally tacky, into multilayer flexible packaging films brings challenges for controlling the frictional properties. As in single layer films, migrating additives are typically used to control the surface properties of multilayer films. But special consideration must be taken for how the presence of adjacent layers influences migration and performance. While frictional properties are the subject of this chapter, the principles are similar for other migrating additives such as antifog and antistat additives.

Similarly, the optical properties of multilayer films can be more than the simple sum of the properties of the constituent layers. The interfacial properties must be taken into account, whether they are positive or negative.

This chapter explores the frictional and optical properties of films with a focus on how multilayer constructions may differ from single layer films.

12.1 Frictional Properties

In many flexible packaging applications, the film must easily slide over film and metal surfaces. This ease of sliding is generally characterized by the coefficient of friction (COF), which is the ratio of the force required to slide a film over a surface to the total force perpendicular to that surface. The COF is typically measured by sliding a weighted sled over the film as described in Section 12.1.2. A COF of around 0.2 is often desired for running on high-speed packaging lines. Many common polymers used in packaging have inherently high COF values, including polyethylene (PE). The problem can be even more severe with low-melting polymers, such as mVLDPE (plastomers), ethylene vinyl acetate (EVA) copolymers and ionomers. It is a common practice in the industry to add fatty acid amides to polyolefins to reduce and control the COF. These low molecular weight (MW) additives bloom to the surface to form a lubricating layer. The amount and rate at which these additives migrate to the surface affects the performance of films. If too little of the additive ends up on the surface, the COF may be too high. If too much comes to the surface, adhesion, appearance, and heat seal performance may suffer.

Nonmigrating additives have also been developed to help control the COF of films but due to the higher additional levels these additives typically require, they have not been cost-effective for many packaging applications. With the ability to make multilayer structures, placing these additives in a thin surface layer may make this technology more attractive.

Films that have been wound into a roll must be able to be unwound. Some polymers, particularly soft or tacky ones, tend to bind to each other in the roll. The inability to unwind the film is known as film blocking. Migrating and nonmigrating additives are used to help prevent blocking of films.

12.1.1 Why Frictional Properties Are Important

The frictional properties of films affect their ability to be handled in packaging operations. Two related but independent properties are important: COF and antiblocking behavior. The first relates to how easily the film slides past other films or metal surfaces. The second relates to how easy it is to unwind a roll. Often polymers that have high COF also tend to block, but this is not always the case. The types of additives used to control COF are not usually the same utilized for preventing blocking, and the two may be synergistic or antagonistic.

The COF of films are often categorized into ranges:

- high slip: 0.1−0.2;
- medium slip: 0.21−0.4;
- low slip: 0.41−0.7;
- no slip: >0.7.

The Science and Technology of Flexible Packaging. http://dx.doi.org/10.1016/B978-0-323-24273-8.00012-5
Copyright © 2017 Elsevier Inc. All rights reserved.

Some applications require low slip, others medium to high slip. For example, films run on vertical form fill seal lines require a low COF on the sealant side and a medium to high COF on the outside. The film needs to slide easily along the metal forming mandrel on one hand but needs some film-to-film friction to help with feeding of the film [1].

At the extreme, a roll that cannot be unwound cannot be used. But even limited blocking can distort the film as it is removed from the roll if the film is stretched. Blocking forces may also result in increased static buildup and resulting problems.

12.1.2 How It Is Measured

12.1.2.1 Coefficient of Friction

The frictional characteristics of a film may be measured on a specimen sliding over itself, usually called film-to-film, or to another substrate. Typically film-to-film and film-to-metal properties are measured. ASTM D1894 [2] describes a method for determining the COF of plastic films by measuring the force to pull a weighted sled across the film. A characteristic of the sliding force is that often the initial or starting force is higher or lower than the ongoing force needed to move the sled. The *static* COF is defined as the force required to slide the film over the surface divided by the force applied normal to the surface (as determined by the weight of the sled), the moment the motion starts. The *kinetic or dynamic* COF is that ratio once that motion is in progress.

The test comprises of two surface specimens, one mounted to the sled and one to the plane so that during the test the specimen mounted to the sled slides across the specimen mounted to the plane. The method provides for a number of apparatuses that can be used, one of which is reproduced in Fig. 12.1. Here the apparatus is mounted to a tensile tester so that when the jaws separate the sled moves across the plane at a constant speed. The force transducer of the tensile tester measures the sliding force. The normal force is simply the weight of the sled. The COF is calculated using Eqs. (12.1) and (12.2):

$$\mu_s = \frac{F_s}{B} \tag{12.1}$$

$$\mu_k = \frac{F_k}{B} \tag{12.2}$$

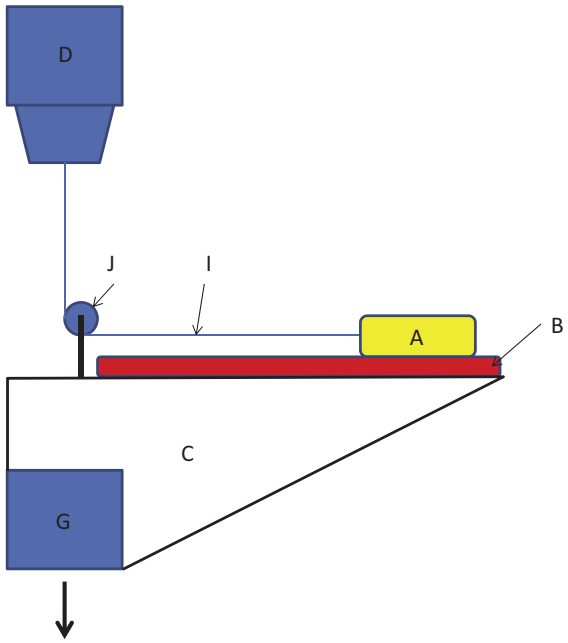


Figure 12.1 Schematic of COF measurement apparatus. The sled (A) moves across the plane (B) as the crosshead of the tensile tester (G) moves downward. The stationary force gauge (D) measures the sliding force. The sled is attached to the gauge with a nylon monofilament (I) that loops around a low friction pulley (J). The plane is attached to a supporting base (C).
Adapted from ASTM International. Standard test method for static and kinetic coefficients of friction of plastic film and sheeting, (D1894-14). West Conshohocken (PA): ASTM International; 2014.

where μ_s = static COF; F_s = initial force reading (g); B = weight of sled (g); μ_k = kinetic COF; F_k = average force reading during uniform sliding of the surfaces (g).

The test is usually carried out at room temperature but can be carried out at elevated temperature by heating the plane.

As described in Section 12.1.4, many plastic films use migrating additives to control the surface frictional properties. The performance of these additives is sensitive to temperature and aging effects. When making measurements of films containing these types of additives, care must be taken to control the temperature of the test and storage history of the specimen.

Maltby [3] shows that the sled weight can affect the COF results for tacky polymers. The ASTM D1984 standard calls for a sled weight of 200 g, whereas BS 824, a British standard, uses a 700 g

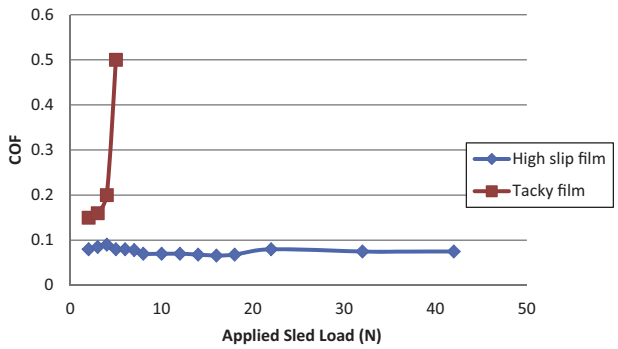


Figure 12.2 Effect of sled weight on COF measurement.
Reproduced with permission from Maltby A. The effects of polyolefin formulation and processing variables on slip agent performance (I). In: TAPPI polymers, laminations & coatings conference; 1998. p. 1241–50.

weight. Neither may represent the load in an actual application. Maltby presents the results for a series of films with different levels of a slip additive using the two test standards. The high sled weight gives on average a COF that is about 40% higher than the lower sled weight, but the differences are fairly small and both methods provide the same trends. More interesting are the results of tests comparing the COF versus sled weight for a "slippery" film and a "tacky" film. The COF of the slippery film is unaffected by the sled weight as shown in Fig. 12.2. The tacky film, while showing low COF under the standard weight, shows a rapid increase in COF with increasing weight. The important lesson here is that the COF measurement will not always mimic the real application.

12.1.2.2 Blocking

ASTM D3354 [4] describes a method for measuring the blocking force between two films. The method uses two metal flat plates with rigid adaptors mounted in parallel to a universal testing machine (tensile tester). A specimen of two unblocked films is cut so that the films extend 40 mm from the front and back sides of the plates. The specimen is placed between the two plates. The free ends are carefully separated and taped to the top and bottom plates with double-sided tape. The configuration is illustrated in Fig. 12.3. The plates are moved away from each other by the motion of the tensile tester at a constant speed of 5 mm/min until the films are completely separated or the distance between the plates reaches 19 mm.

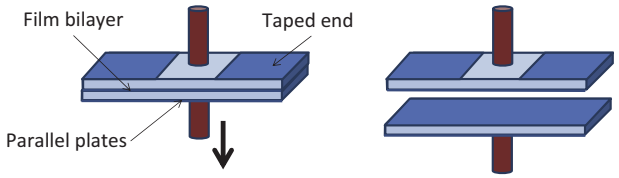


Figure 12.3 Blocking force measurement.

The force of separation is recorded. A similar method is described for a constant rate of load device.

12.1.3 Additive Technology

12.1.3.1 Why Friction Arises and How Additives Work

The surface of any material is never truly smooth—there are always asperities or protrusions from the surface present that are larger than the size of individual molecules. Collectively, these asperities give rise to surface roughness. When two surfaces are brought together, they touch only on the asperities; the real area of contact is governed by the deformation properties of the asperities (Fig. 12.4). This area is influenced by the load or normal force (W) exerted on the surfaces and the yield pressure (p) or hardness of the surface:

$$A = \frac{W}{p} \tag{12.3}$$

where A = real area of contact; W = applied load; p = yield pressure of the material.

As the load is applied, a high unit pressure is exerted over the asperities, causing adhesion or junction formation at the asperity interfaces. These junctions give rise to the resistance to sliding or friction and are sheared during the sliding action.

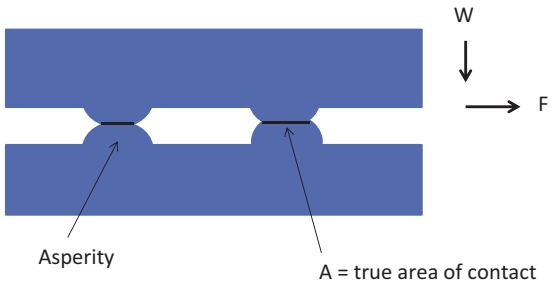


Figure 12.4 Illustration of true area of contact between surfaces. The area is determined by the deformation behavior of asperities that make actual contact.

If these adhesive junctions have a shear strength, s, the force to shear the junctions is given by

$$F = As \tag{12.4}$$

where F = sliding force; A = true contact area; s = shear strength of junctions.

Combining Eqs. (12.3) and (12.4),

$$F = Ws/p. \tag{12.5}$$

Since the COF is defined as the sliding force divided by the normal force or load,

$$\mu \equiv F/W, \tag{12.6}$$

it follows that

$$\mu = \frac{s}{p}. \tag{12.7}$$

The COF is equal to the shear strength of the interface divided by the interfacial hardness, two material parameters. This turns out to be sufficient to describe the behavior of metals; for polymer films the load and surface roughness also play a role as described below.

Eq. (12.7) suggests several strategies for reducing COF as illustrated in Fig. 12.5 [5]. One is to interpose a low shear strength lubricating layer between the asperities [decreasing the numerator of Eq. (12.7)]. This is one of the reasons why fatty acid amides are effective as slip additives: their low surface energy reduces the adhesion between the asperities, effectively lowering the shear strength.

Another strategy is to increase the hardness of the surface [increasing the denominator of Eq. (12.7)]. Lubricants that can crystallize, such as the longer chain fatty acid amides, have been found to be more effective than liquid lubricants for reducing the COF of polymer films; the crystalline structure helps increase the hardness of the surface [5]. Even partial coverage of the surface can reduce COF [5–7]. Inorganic additives, such as talc or diatomaceous earth, as well as thermoset silicone powders employ this strategy. These nonmigrating additives also increase the number of asperities and surface roughness, which helps reduce COF and blocking.

This last effect arises from the viscoelastic nature of polymers. Owens [8] finds that the effect of load and surface roughness on the frictional behavior of

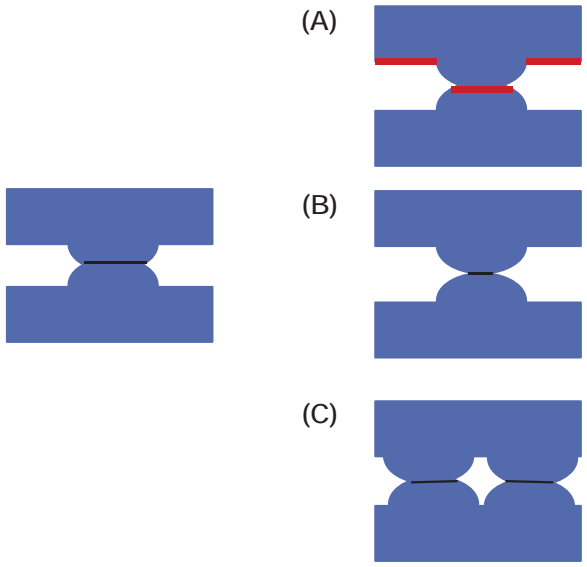


Figure 12.5 Illustration of strategies to reduce COF: (A) Introduce a lubricant at the interface [red (gray in print versions)] with weak shear strength or adhesion, (B) increase the hardness of the asperities, thereby reducing the real contact area, and (C) increase the number of asperities (surface roughness).

polymer substrates can be related to a single material parameter, the deformation index. This parameter describes the manner in which the area of real contact varies with the load and roughness. He proposes the following relationships:

$$\mu = k_1 W^{\left(\frac{2}{m}\right)-1} \tag{12.8}$$

$$\mu = k_2 N^{\left(\frac{2}{m}\right)-1} \tag{12.9}$$

where W = load; N = number of asperities (related to surface roughness); m = deformation index; k_1, k_2 = constants.

The value for m varies from 2 for plastic materials to 3 for purely elastic ones. Metals deform plastically and therefore the COF of metal against metal is independent of load and surface roughness [the exponent in Eqs. (12.8) and (12.9) reduce to 0 when $m = 2$]. Rubbers have been experimentally found to have a deformation index of 3, conforming to the theory. For cellophane coated with a copolymer of vinylidene chloride–acrylonitrile (the K coating developed in the 1920s to make cellophane moisture proof), Owens measures the value of m to be 2.35, consistent with a viscoelastic material. From

Eq. (12.9), the COF of the K-film is proportional to $1/N^{0.65}$. Other polymer films should have values of m that fall between 2 and 3, which in practice means that as the surface roughness increases, the COF will decrease.

12.1.3.2 Migrating Additives

The most commonly used slip agents are fatty acid amides with chain lengths ranging from about 16 to 24 carbon atoms. Several of the more commercially important varieties are listed in Table 12.1. There are three general classes of amides used as slip agents: primary amides, secondary amides, and N,N-ethylene bisamide structures. Table 12.1 shows the chemical structures of these classes of amides. The primary amides are further categorized as saturated and unsaturated amides. Saturated amides have no carbon double bonds. Unsaturated amides have one or more carbon double bonds, which are more reactive or thermally unstable than single bonds. The commercially important unsaturated amides all have only one double bond; more than one results in too much instability. Erucamide and oleamide are unsaturated primary amides that are commonly used as slip agents for polyolefins but are more volatile and less thermally stable than many of the other amides. Stearamide and behenamide are examples of primary saturated amides. They typically do not provide very good slip performance but are used as release and antiblock agents.

Secondary amides include oleyl palmitamide and stearyl erucamide. These have better thermal stability than the primary amides but are slower to migrate and give higher COF. Ethylene-bis-stearamide and ethylene-bis-deamide are examples of N,N-ethylene bisamides. They too are more thermally stable than primary amides. The selection of the amide will depend on the polarity of the polymer (which affects migration rate), the processing temperature (which determines the need for thermal stability) and the ultimate COF needed (which is determined by the amide crystalline structure).

Fatty acid amides are derived from natural sources, typically vegetable oils or tallow (animal fat). The oils contain a mixture of acids of different chain length and saturation. These must be purified, typically using fractional distillation, and converted to amides to produce commercially viable slip agents. For example, erucamide is derived from rapeseed oil. The raw oil contains about 50% erucic acid. After purification, the fraction of erucic acid or its derivative erucamide ranges from about 80–94% [9]. Higher levels of purity are not economically viable. Walp [9] finds that the COF of linear low density polyethylene (LLDPE) with two grades of erucamide, one with 80% purity and the other with 93%, are the same. Maltby [10] reports similar results. Nevertheless, it is important to understand that the composition may vary with manufacture and source of the plant oil or animal fat.

Fatty acid amide slip agents are typically added into the polymer at 200–2000 ppm either by the resin manufacturer or by the converter using a masterbatch. They are soluble in the polymer melt but not in the solid crystals. As the polymer crystallizes, the polymer crystals push the slip molecules away from the bulk toward the surface. The affinity or solubility of the slip agent with the polymer influences how fast the additive will migrate to the surface. Fatty acid amides are more soluble in polar polymers (such as EVA) and polymers with low levels of crystallinity

Table 12.1 Examples of Commercially Important Fatty Acid Amides and Their Classifications

Type	Chemical Structure	Examples
Primary, saturated	R–CO–NH2 where R is –C–C–C–…	Stearamide (C18:0) Behenamide (C22:0)
Primary, unsaturated	R–CO–NH2 where R is …–C=C–C–…	Oleamide (C18:1) Eurcamide (C22:1)
Secondary	R′–CO–NH–R	Oleyl palmitamide (C18:1 C16:0) Stearyl eurcamide (C18:0 C22:1)
N,N-ethylene bisamide	R′–CO–NH–CH2–NH–CO–R	Ethylene-bis-stearamide (C18:0) Ethylene-bis-oleamide (C18:1)

R and R′ represent carbon chains of a general length. The nomenclature CXX:Y used in the examples indicates XX carbons in the molecule and Y double bonds.

(such as plastomers); they take longer to migrate to the surface in these polymers than standard low density polyethylene (LDPE). Some slip additives that migrate quickly in nonpolar polyethylene are too soluble in polar polymers and take too long to migrate. For these polymers, less polar amides, such as secondary amides and bis-stearamides, are often used instead of primary amides. Once on the surface, the slip molecules organize into bilayers and, with sufficient quantity, crystals. The crystalline structure of the amide has a substantial impact on COF. Some have favorable structures, such as erucamide, leading to lower COF. Others like monosaturated primary amides are poor slip agents but help reduce blocking.

Fatty acid amides are the most economical slip additives. They provide low-cost control of the frictional properties of the film when used optimally. They do have several drawbacks, however, which include the following:

- The COF takes time to develop due to the migrating action of the additive.
- Too much amide on the surface can lead to adhesion issues for subsequent printing or lamination steps.
- Too much amide can affect film appearance (described as chalking) and sealing properties.
- Slip can be lost to adjacent layers in coextrusion, making it difficult to predict COF performance.
- Slip agents can transfer to the adjacent surface in the wound roll, causing adhesion or COF issues on the opposite side of the film.

Despite these issues, fatty acid amides are the most widely used slip additives in flexible packaging. Factors affecting their performance are described in greater detail in Section 12.1.4.

Other migrating additives include antifog agents (eg, ethoxylated alkylphenols, polyethoxylated oleic acid esters, and sorbitan esters of fatty acids), antistats (eg, glycerol monostearate), and cling additives (eg, polyisobutylene).

12.1.3.3 Nonmigrating Additives (Slip and Antiblock)

Inorganic additives such as talc, diatomaceous earth, and silica (natural and synthetic) are often used as antiblock agents. They are typically added at levels ranging from 1000 to 10,000 ppm (0.1−1 wt%). They reduce blocking by providing a rough surface to the film, which reduces the contact area when films are brought together in the roll. The size, shape, and hardness of the additive and how well it is dispersed in the polymer influence the antiblocking performance. Larger particles may be more efficient at preventing blocking but generally increase the film haze. Irregular-shaped particles may be more effective at providing a bumpy surface than more regular-shaped particles. These inorganic additives typically do not reduce the COF of a film on their own but may allow a migrating slip agent to be more effective; in some cases the combination of a slip agent and antiblock may provide lower COF at lower concentration than the slip agent alone. Other factors influencing the selection of antiblocking additives include the following:

- Particle hardness, which affects machine wear.
- Film clarity needs. Film clarity is a function of antiblock loading, film gauge, and the difference in refractive indices (RI) of the polymer and particle. If the RIs are closely matched, light will not bend as it moves from polymer to particle, reducing film haze, and improving transparency. Higher loadings and film thickness act to increase haze simply because there are more particles for the light to encounter as it travels through the film.
- Iron content. Iron may degrade some organic additives and cause color formation.

Talc is one of the most cost-effective inorganic antiblock additives and has the greatest usage for packaging films. Diatomaceous earth is perhaps the most effective at low concentrations and is used where optical clarity is important [11].

Glass spheres significantly reduce COF in polyolefin films [12]. They are most effectively used in thin skin layers that are less than 1-μ thick, such as in oriented polypropylene (PP) film. They can reduce the COF to 0.35−0.45.

Thermoset silicone powders are also used as nonmigrating slip additives. They are utilized like glass spheres but are more effective, reducing the COF to 0.25−0.35. These are considered the premier nonmigratory slip additives. The COF can be further reduced by adding migratory fatty acid amide slip additives.

Thermoplastic silicones are also used as slip additives, particularly in skin layers in coextrusion. There are differing accounts as to their effectiveness and their impact on sealing and printing performance. Ryan [13] describes masterbatches of ultra high MW siloxane in LLDPE, which produce COF values in LLDPE film of around 0.25 when added at a 2% loading (4% of a 50% masterbatch). Sarargaonkar and McKinley [14] describe similar results with a nonmigratory masterbatch. They claim no effect on heat sealability of a 50-μm LDPE cast film when 10% or 20% of the masterbatch (containing 10% or 20% slip additive) is added.

Constant [12] finds that cyclic olefin copolymers (COCs) impart medium slip performance. Adding 10−20% of COC into LDPE reduces the COF from 0.6 to around 0.3. Increasing the COC concentration lowers COF but increased the haze, as does increasing the T_g of the COC.

The advantages of nonmigratory slip additives include the following:

- The COF does not change with time. Migratory additives require time to bloom to the surface after fabrication.
- COF does not change with storage temperature. The performance of migratory additives changes with temperature (Section 12.1.4.6).
- The additive is thermally stable, nonvolatile, and can be used in high temperature processes such as cast film or extrusion coating.
- Cost can be mitigated somewhat by using the additive in only an outside layer in a multilayer film.

Despite these advantages, most of the industry uses migratory additives today.

12.1.4 Migratory Slip Additive Performance Factors

COF performance depends on the nature of the polymer surface, the amount of additive that migrates to the surface and the properties of the resulting surface (particularly the amide itself).

12.1.4.1 Polymer Surface

The roughness of the polymer surface is shown to be important from a fundamental perspective in Section 12.1.3 [Eqn. (12.9)]: a smooth surface provides greater real contact area between the surfaces, resulting in higher friction. This has been observed in practice:

- In general, films with higher gloss may require a higher slip concentration or longer time to achieve a desired COF value. DuPont shows this to be true for ionomer films [15].
- In some cases, using migrating slip agents in combination with inorganic antiblock additives such as diatomaceous earth can improve COF performance, either allowing less slip to be used or by achieving faster COF development [15−17].
- Using a matted chill roll in extrusion coating provides lower COF than one with a mirror finish; the surface texture with the matted finish contributes to surface roughness [18,19].

Some of the improved performance may be due to the direct effect of increased surface roughness on reducing the real contact area. Slip migration may be another factor. There is a thermodynamic driving force for the slip to come to the surface to minimize free energy (the slip lowers the surface energy of the film). This driving force is eliminated if the film surfaces are so tightly bound in the roll that the interface disappears. Roughening the surface helps preserve this interface, facilitating the migration of the slip additive.

Polymer surface crystallinity is an another factor. Sakhalkar and Hirt [20] use electron microscopy to show that the surface region of a Ziegler−Natta LLDPE blown film is amorphous. The slip is more soluble in this amorphous region than in the bulk, contributing to accumulation of the slip at the surface. The amount and morphology of crystals at the surface is influenced by the polymer chemistry and molecular structure, as well as how the film is made. Sections 7.5.3.2.2 and 10.4.2.2.1 discuss how the molecular architecture of LLDPE affects the surface crystallinity. Blown films of metallocene LLDPE, with its uniform comonomer distribution, do not have the surface amorphous region found in Ziegler−Natta LLDPE blown film. The Ziegler−Natta catalyst technology produces polymer chains with a broad molecular weight distribution (MWD) and comonomer distribution with the shorter chains having an abundance of comonomer. The comonomer creates short chain branches that do not participate in the

crystalline structure. As crystals form during quenching, these short chains are pushed toward the surface, forming the amorphous surface region. mLLDPE films typically require higher levels of slip than ZN-LLDPE films. The lack of the amorphous surface region to help accumulate the slip at the surface is one factor contributing to this.

The film fabrication process can also contribute to differences in surface and bulk crystallinity. Kitchel [21] observes that slip in a multilayer LLDPE blown has a tendency to migrate toward the outside of the bubble; the COF is lower on the outside surface than the inside surface if slip is added to all layers uniformly. No explanation is given, but disparate cooling conditions on each side of the bubble may be contributing to crystallinity differences. Section 10.3.1 describes how contact with surfaces of different surface energy during quenching can induce changes in surface crystallinity. This suggests a cast film made in contact with a chrome chill roll may have a different surface crystallinity than a blown film whose contact surface is air. However, the reduction in overall crystallinity due to the much faster quench rate in cast film may overwhelm this effect.

12.1.4.2 Migration of Slip Additives

The thermodynamic driving force for additive migration and accumulation at the surface is threefold [20]. The first is the solubility of the slip additive in the polymer; if the slip is not soluble, it is forced to the surface. It is widely accepted that amides are not soluble in the crystalline regions of polymers. Thus, as the polymer melt crystallizes, the slip additive is forced toward the surface. Sharma and Beard [6] report that after solvent stripping of the slip on the surface of a PE blown film, no additional slip migration occurs, suggesting that solubility of slip in the bulk of the PE is low. Work by Hirt and his students at Clemson University, however, suggests that for LLDPE, the solubility limit is high enough in the amorphous regions that solubility is not a significant driving force [28–33].

The solubility of the additive is a function of its chain length, functional groups and saturation, and the chemistry of the polymer. The classes of fatty acid amides are described in Section 12.1.3.1. The primary amides tend to be more polar than the secondary amides and ethylene bisamides and so are less soluble in nonpolar polymers such as polyolefins. Oleamide and erucamide, two primary amides, are the two most commonly used slip additives in polyolefins. But even among the polyolefins, there are differences in the migration of these amides. In general, LLDPE requires higher slip levels and more time to reach the ultimate COF than does LDPE. PP takes even higher levels of slip to achieve the same COF [3,22–25]. Metallocene plastomers require very high levels of slip [26]. At such high levels, heat seal properties may be affected [27].

For polar ethylene copolymers such as EVA, EMA, acid copolymers, and ionomers, the solubility of oleamide and erucamide is higher, reducing the driving force for migration to the surface. The migration rate in these polymers can be several times slower than for LDPE. For example, erucamide in an EVA containing 3.8% VA migrates three to five times slower than in a polyethylene of the same crystallinity. Alternative slip additives are used in acid copolymers and ionomers since the interaction with erucamide is too great for effective modification. Higher levels of slip are also required. Even so, the development of low COF in ionomer films can take several days versus hours for LDPE. Resin suppliers can offer advice on the type of slip agent and amount to use for a given resin.

The second driving force for surface accumulation of the slip additive is a reduction of surface tension of the system favoring the formation of slip at the surface. This occurs as the amide forms a polar network structure on the surface.

The third driving force is related to morphological differences between the bulk and surface of the polymer. As described in Section 12.1.4.1, the surface of Ziegler–Natta LLDPE blown film has been found to have an amorphous region near the surface. Sakhalkar and Hirt [20] calculate that the greater solubility of the slip in the amorphous surface region than in the bulk is a significant driving force for slip accumulation at the surface.

The rate of migration of the slip additive is of particular concern for processors and is a function of the thermodynamic driving force and the diffusion coefficient. Several investigators have found the diffusion of slip in polymers to be Fickian or nearly Fickian, meaning the diffusion coefficient is independent of concentration. This simplifies the analysis considerably. The diffusion coefficient relates the diffusive flux to the concentration gradient, in a relationship known as Fick's first law. This is introduced in Chapter 8, where the diffusive flux is the

amount of the permeant transporting through a unit area of film per time:

$$J = -D\frac{dc}{dx} \tag{12.10}$$

where J = diffusion flux = Q/At; Q = amount of permeant; A = area normal to flow, in this case the surface area of film; t = time; D = diffusion coefficient; dc/dx = concentration gradient in thickness dimension (x). The larger the value of D, the greater is the diffusion.

The diffusion coefficient is a function of the MW of the slip additive, the molecular shape of the additive, and the percent crystallinity of the polymer. Higher MW of the additive decreases the diffusion coefficient. Oleamide (C18:1),[1] for example, is known to migrate faster to the surface of LDPE than erucamide (C22:1) [24,34]. Foldes [35] finds that additives with linear structures diffuse more slowly that spherical molecules, but the rate of change with temperature is more pronounced. Some authors state that the higher the percent crystallinity of the polymer, the slower the diffusion since crystals block the path of the slip molecule [36]. Others have found, however, that higher crystallinity (brought about by slower quench rates) increases the diffusion rate [33,37]. Klein [37] proposes a theory that explains this behavior in terms of entanglements in the disordered amorphous regions between the polymer crystalline lamellae. Tie molecules and fixed entanglements between adjacent lamellae are less abundant in the higher crystalline polymer, resulting in more slip mobility. This mobility overwhelms the effect of more crystals (fewer diffusion paths), which results in higher diffusion rates. Once again, the polymer molecular architecture (MW, MWD, long chain branching, % crystallinity, and crystalline morphology) is seen to influence properties.

Several authors relate the diffusion rate to free volume theory [38–40]. The theory, introduced in Section 8.4.1.2.1, describes temporary "voids" that form and allow the slip molecules to pass through. These voids or "free volume" are due to imperfections in the packing of polymer molecules and rotational and vibrational motions. Free volume is influenced by molecular architecture (MWD, long chain branching), presence of bulky side groups, chain rigidity, polarity, crystallinity, and orientation. External factors may also influence the free volume. Muire and Hirt [41] show that externally applied pressure (as in a tightly wound roll) reduces the diffusion rate. They attribute this to a reduction in free volume for diffusion. Schumann [42] also shows that less slip makes it to the surface when the roll tension is higher in a wound roll. Many observers attribute this to a disappearance of the interface, reducing the driving force for accumulating at a surface that no longer exists. It is likely both affects contribute to the decrease in effectiveness of slip agents in tightly wound rolls.

There are two general methods for measuring the diffusion coefficient of slip additives in polymers. One involves measuring the mass absorption of a film or plaque exposed to an additive at the surface, the so-called "diffusion-in" experiment. A variation of this technique is to measure the diffusion through a stack of films. Several authors describe work with a variety of additives using these techniques [31,33,37–39,43,44]. Gagliardi [32] describes the difficulties with these techniques: they require measurement of longtime equilibrium additive concentrations, they introduce possible handling errors and, specifically for the film stack technique, they introduce a number of polymer–polymer interfaces.

The second technique is the "diffusion-out" experiment, usually done with FTIR microspectroscopy on the cross section of a film. With this technique, the polymer is mixed with the slip additive and then made into a film, much like in commercial film applications. The slip additive distribution is measured as a function of time. A number of authors describe work using this technique [29,30,32,40,45–49]. Many investigators use FTIR to measure the slip concentration. It can be challenging, however, to associate a specific IR peak to the slip [47]. Rawls [45] uses a surface washing technique to measure the surface concentration of erucamide on LLDPE films, followed by a bulk extraction to measure the remaining erucamide in the bulk. The technique involves washing the surface for 5–20 s in ethyl ether. The washings are analyzed by gas chromatography to determine the amount of erucamide on the surface. The surface concentration is plotted versus wash time and extrapolated back to zero. This provides a value for

[1]The nomenclature CXX:Y refers to XX carbon atoms and Y double bonds. Oleamide has 18 carbon atoms, with one C=C double bond, or level of unsaturation.

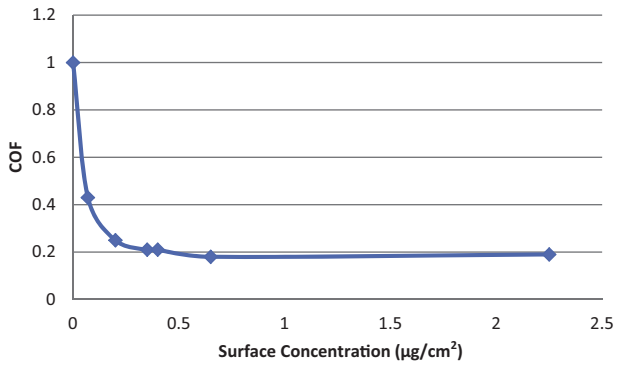


Figure 12.6 Correlation of kinetic COF with surface concentration of erucamide on an LLDPE film.
Adapted from Ramirez MX, Walters KB, Hirt DE. Relationship between erucamide surface concentration and coefficient of friction of LLDPE film. J Vinyl Addit Technol 2005:9–12.

the surface concentration that has not been affected by the solvent.

The surface concentration of slip additive can be directly related to the COF. Fig. 12.6 provides an example from the work of Ramirez [50]. The concentration of erucamide on the surface of an LLDPE film is measured and plotted against the COF. The COF is found to monotonically decrease until a concentration of around 0.5 μg/cm^2, after which further accumulation of slip at the surface has no effect.

The results of diffusion experiments typically show a partitioning of the slip additive between the bulk and surface. With time, the concentrations reach equilibrium. Table 12.2 shows data from Rawls [45] for the portioning of erucamide in an LLDPE film after 168 h (7 days) using the surface washing technique. Twenty-five to fifty percent of the erucamide ends up on the surface.

The diffusion and accumulation of slip agents is described by the one-dimensional diffusion equation (assuming Fickian diffusion) with an accumulation boundary condition:

$$\frac{\partial C}{\partial t} = D\frac{\partial^2 C}{\partial x^2} \tag{12.11}$$

where C = concentration of additive in the bulk; t = time; D = diffusion coefficient; x = spatial dimension normal to the surface of the film.

Eq. (12.2) is subject to the following initial and boundary conditions (see Fig. 12.7 for a diagram of the variables).

Initial Condition

Initially, the concentration of the slip additive is uniform throughout the bulk of the film and zero at the surface:

$$C = C_0 \quad \text{at } t \le 0,\ 0 < x < X \tag{12.12}$$

$$\Gamma = 0 \quad \text{at } x = 0,\ X,\ t \le 0 \tag{12.13}$$

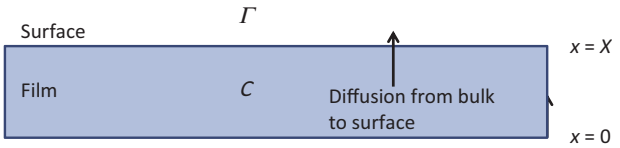


Figure 12.7 Diffusion in a film.

Table 12.2 Fraction of Erucamide in the Bulk and on the Surfaces of LLDPE Film.

Film Thickness (μm)	Wt% Added	Bulk Concentration (μm/cm^2)	Surface Concentration[a] (μm/cm^2)	% of Total on Surfaces (Both Sides)
27	0.6	3.7	3.8	51
27	1.2	8.3	6.7	45
27	1.8	15.5	6.5	30
27	2.5	22.5	9.5	30
50	1.8	32	10	24

Bulk and surface concentrations are reported as the mass divided by the total surface area (both major faces, ignoring the edges).
[a]*Both surfaces.*
Data taken from Rawls A, Hirt DE, Havens MR, Roberts WP. Evaluation of surface concentration of erucamide in LLDPE films. J Vinyl Addit Technol 2002;8:130–8.

where C_0 = initial bulk concentration; Γ = surface concentration (μg/cm^2); X = film thickness.

Boundary Conditions

At the surfaces, the change in surface concentration is balanced by the diffusive flux. This results in an accumulation of slip at the surface [51].

$$\frac{\partial \Gamma}{\partial t} = D\frac{\partial C}{\partial x} \quad \text{at } x = 0 \tag{12.14}$$

$$\frac{\partial \Gamma}{\partial t} = -D\frac{\partial C}{\partial x} \quad \text{at } x = X. \tag{12.15}$$

To solve the equations, the surface concentration must be related to the bulk concentration. The simplest way is to assume a linear relationship:

$$\Gamma = MC = \frac{m}{S_g \rho_s} C \tag{12.16}$$

where ρ_s = solid density (mass/volume) of polymer; S_g = surface area/unit mass of polymer; m = partition coefficient of additive between the surface and bulk.

For a smooth surface,

$$S_g \rho_s = \frac{1}{X} \tag{12.17}$$

so that

$$\Gamma = mXC. \tag{12.18}$$

For a rough surface

$$S_g \rho_s = \frac{a}{X}, \quad \text{where } a > 1. \tag{12.19}$$

In Eq. (12.19), the parameter "a" is a roughness factor.

These equations can be solved numerically for the concentration of the surface and in the bulk as a function of time and location within the film. The input parameters are the following:

C_0 (g/cm^3), initial bulk concentration of slip;

X (microns), film thickness;

D (cm^2/s), diffusion coefficient;

m, partition coefficient;

a, roughness coefficient.

Joshi and Hirt [51] solve these equations using a finite difference method and get reasonable agreement between the model predictions and experimental results for the portioning of the slip between the bulk and surface. To build upon Joshi's work, the finite difference model developed for heat transfer (Sections 7.6.1 and 15.1.3) is repurposed to handle diffusion; the basic equations are the same and only the boundary conditions have to be modified. Fig. 12.8 shows the effect of varying the diffusion coefficient: higher D at constant m results in the surface reaching its equilibrium surface concentration faster. Fig. 12.9 shows the effect of increasing m at constant D. The equilibrium surface concentration increases. Fig. 12.10 illustrates the effect of increasing the film thickness at constant D and m. The equilibrium surface concentration is proportional to the film thickness.

The utility of the model is that it allows one to predict the level of slip accumulating at the surface as a function of time, polymer thickness, and initial slip concentration. Presumably, one then could correlate slip surface concentration with COF, using empirical relationships such as the example in Fig. 12.6. While the model provides insight into slip migration and COF development, it has limitations for predicting actual COF in packaging films. Some of the challenges that still need to be resolved include the following:

- Measurements of D and m are tedious and influenced by a number of factors, such as storage

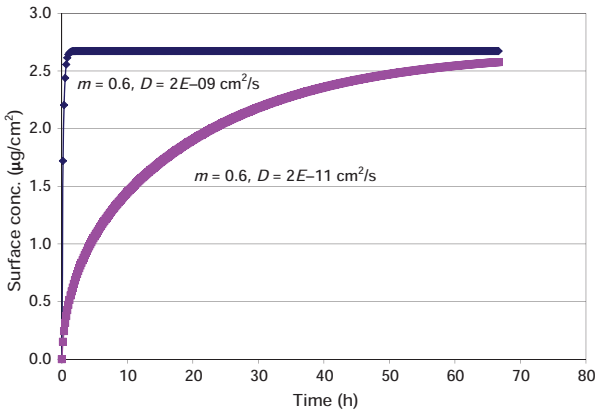


Figure 12.8 Model calculation of the migration of slip molecules to the surface of a 50 μm film. The partition coefficient (m) and initial additive concentration (C_0) are held constant.
Reproduced with permission from E. I. du Pont de Nemours and Company.

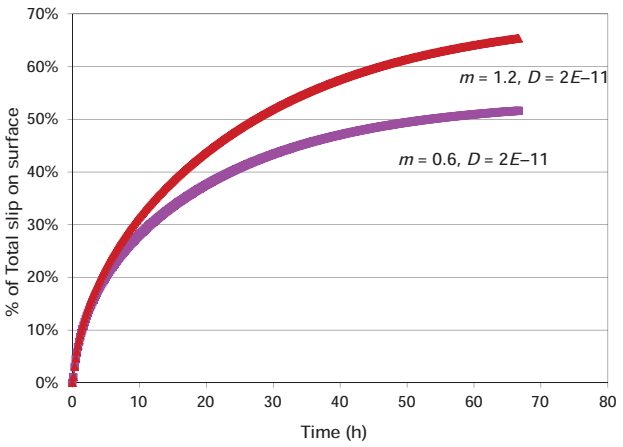


Figure 12.9 Model calculation of the migration of slip molecules to the surface of a 50 μm film. The diffusion coefficient (D) and initial additive concentration (C_0) are held constant.
Reproduced with permission from E. I. du Pont de Nemours and Company.

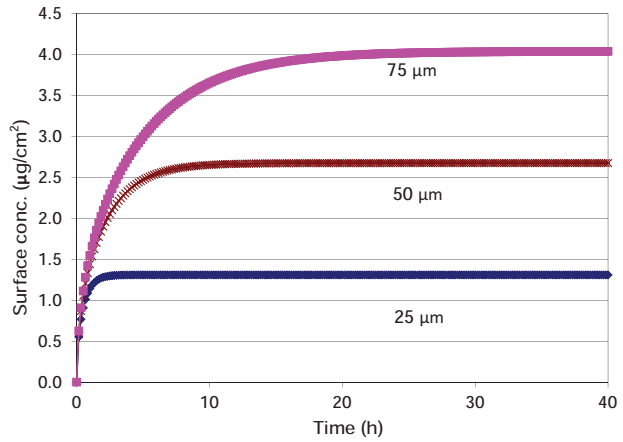


Figure 12.10 Model calculation of the migration of slip molecules to the surface of a film as a function of film thickness. $m = 0.6$ and $D = 2 \times 10^{-10}$ cm^2.
Reproduced with permission from E. I. du Pont de Nemours and Company.

temperature, polymer chemistry, film fabrication process, and so on.

- The correlation of COF with slip additive surface concentration will differ with each polymer and slip additive.
- The effect of surface roughness has not been explicitly considered. Subtle changes in process conditions may change the surface roughness and completely change the COF versus surface concentration relationship.
- The effects of coextrusion have not been worked out. For example, what is the proper boundary condition for interfaces between dissimilar materials? Does slip accumulate near the interface?

12.1.4.3 Amide Structure

The structure of the amide on the surface determines the ultimate COF. Allen [52] uses electron microscopy to directly image the formation of slip regions on the surface of LDPE with time and correlates the observations with previous measurements of COF. Initially, very small discrete concentrations of slip appear on the surface. With time, the number and size of the regions increase. The regions eventually coalesce and form a more or less continuous lubricating layer. The concentration at which coalescence occurs corresponds to the onset of low COF. Owens [5] observes the crystalline structure of fatty acid amides that migrate to the surface of PVDC-coated cellophane. Ramirez [50] uses atomic force microscopy (AFM) to probe the surface of LLDPE films after erucamide has bloomed to the surface. They find the surface may not be completely covered even at high concentrations of additive. The AFM study shows evidence of crystals and discreet patches on the surface. Poison [53] reports similar behavior for PE-coextruded films. Chen [7] examines LLDPE film with erucamide as the slip additive stored at room temperature (RT) and at 60°C. Initially the samples aged at RT have complete coverage of erucamide with crystal heights of around 10 nm. After greater than 1 year of RT aging, large crystals with heights of around 100 nm have formed, with bare PE between; islands of crystals on top of the bare PE have formed.

Sharma and Beard [6] use XPS (X-ray photoelectron spectroscopy) to characterize the surface structure of LDPE blown films containing stearamide or oleamide. The oleamide is found to have a complete structure or coverage, whereas the stearamide is only partially complete on the surface. This is consistent with the performance of the two additives: for oleamide, the complete layer corresponds to good surface lubrication and slip properties. For stearamide, the partial layer that forms is sufficient to reduce large-scale surface interactions and, hence, reduce blocking. Maltby [3] uses molecular modeling to show why some fatty amides are better than others for slip performance. The very regular

crystalline structure of behenamide may inhibit its slip performance. Partial disruption of the crystalline structure, as occurs with monounsaturated erucamide, may produce better slip properties.

Since the structure of the amide dictates the COF value once enough slip has migrated to the surface, it can be very challenging to obtain a medium value of COF using a low-COF amide like erucamide. If midrange values of COF are needed for an application, the best approach may be to switch to another type of fatty acid amide that provides such performance.

12.1.4.4 Film Fabrication

Fatty acid amides are susceptible to degradation by oxidation, especially the unsaturated types. The high temperatures of some converting processes, such as extrusion coating and cast film, may affect the performance of these additives. Fatty acid amides generally melt in the range of 80–110°C and can become volatile at polymer processing temperatures. This can result in loss of additive.

As described in Section 12.1.4.1, the film fabrication process can affect the roughness of the surface. A matted chill roll will typically provide lower COF than a polished chill roll. Conditions favoring high gloss in blown film may negatively affect COF performance.

The rate of quenching affects the amount of crystallinity. Fast quench process such as cast film and water-quench blown film may have lower levels of crystallinity than the same structure made on a conventional air-quench blown film process. Higher levels of crystallinity affect the solubility of the slip additive. Similarly, orientation during film making may induce crystallization or change the crystalline morphology (Chapter 11), which can influence slip additive solubility and diffusion.

The tension on the roll during windup affects slip migration. Muire [41] attributes this to a reduction in polymer-free volume, which hinders slip migration. Others [42] attribute this to a loss of a well-defined interface between film layers in the roll, reducing the driving force for surface accumulation.

12.1.4.5 Film Thickness and Additive Level

For a monolayer film, decreasing the film thickness while keeping the initial additive concentration constant decreases the reservoir of additive that can migrate to the surface. At equilibrium or long times, the amount of slip that accumulates on the surface increases in proportion to the film thickness. For example, if the film thickness is halved, the weight percent of slip that needs to be added to achieve the same COF is doubled. This result arises from a simple mass balance (Fig. 12.11):

$$\text{Initial Mass} = (\text{Mass on Surface} + \text{Mass in Bulk})_{\text{at equilibrium}}$$

$$C_0 V = 2\Gamma_\infty A + C_\infty V \qquad (12.20)$$

where C_0 = initial additive concentration (g/cm^3); V = volume ($=XA$); X = film thickness; A = film

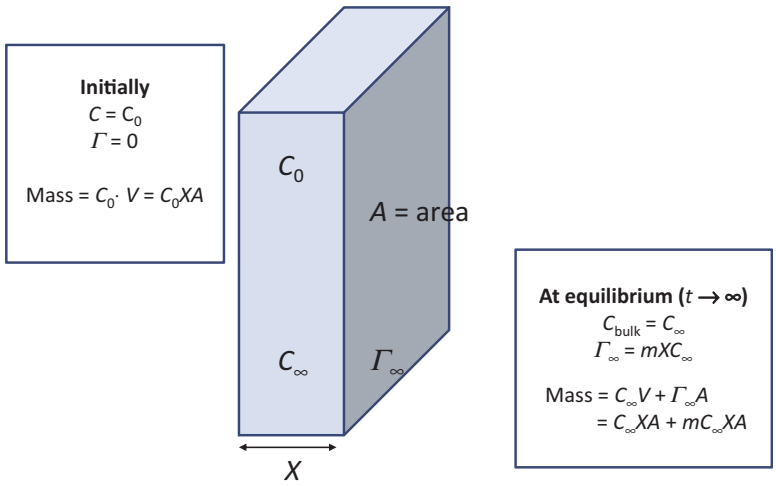


Figure 12.11 Mass balance for slip redistribution between bulk and surface over time. Conservation of mass is assumed.

surface area (one side); Γ_∞ = surface concentration of additive (g/cm^2) at equilibrium; C_∞ = additive concentration in bulk at equilibrium (g/cm^3).

Substituting Eq. (12.18) into Eq. (12.20):

$$C_0XA = 2mXC_\infty + C_\infty XA \tag{12.21}$$

By rearranging Eq. (12.21), the relationship between the initial and equilibrium concentration in the bulk is found to be simply related to the partition coefficient:

$$C_\infty = C_0/(1+2m). \tag{12.22}$$

The equilibrium surface concentration is found by substituting Eq. (12.22) into Eq. (12.18):

$$\Gamma_\infty = mXC_0/(1+2m). \tag{12.23}$$

If the partition coefficient, m, is assumed to be constant for a given film type and additive, then

$$\Gamma_\infty \propto XC_0. \tag{12.24}$$

Eq. (12.24) shows that the surface concentration increases with increasing thickness or initial additive concentration. Since the COF is determined primarily by the surface concentration of the additive, two similar films with the same surface concentration (Γ_∞) should have the same COF. For equal surface concentration, Eq. (12.24) becomes:

$$X_1C_{0,1} = X_2C_{0,2}. \tag{12.25}$$

Eq. (12.25) can be rearranged to calculate the amount of additive ($C_{0,1}$) that should be put into a film of new thickness (X_2) to achieve the same COF as a reference film of known thickness (X_1) and additive level ($C_{0,1}$):

$$C_{0,2} = C_{0,1}(X_1/X_2). \tag{12.26}$$

Eq. (12.26) shows that if the film thickness is halved, the initial slip concentration must be doubled to achieve the same COF.

The utility of Eq. (12.26) is illustrated in Fig. 12.12. Here the COF is plotted for a series of films of different thickness made from three LDPE resins. The resins have the same density (0.922 g/cc) and three levels of slip (C_0). The top curve (290 ppm)

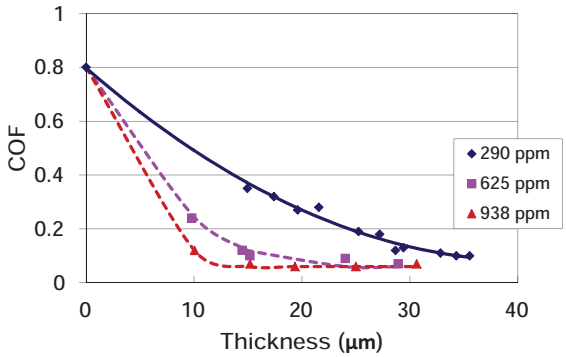


Figure 12.12 Effect of film thickness and slip additive level on COF of LDPE blown film with three levels of slip additive. *Solid curve* is a curve fit of the data points. *Dashed curves* were computed using Eq. (12.27).
Data courtesy of E. I. du Pont de Nemours and Company.

was fitted to a curve and used as a reference. Once the reference curve is known (film 1), the COF of any other film (film 2) with a different concentration of additive can be calculated. Eq. (12.26) is rearranged to compute an "effective" thickness, X_1:

$$X_1 = X_2\left(C_{0,2}/C_{0,1}\right) \tag{12.27}$$

X_1 represents the thickness on the reference curve that has the same COF as the point on the film 2 curve (X_2, $C_{0,2}$). The COF for film 2 is read off the reference curve at thickness X_1. The two dashed curves for the 625 and 928 ppm data points are computed in this way. The agreement with the actual measured COF is excellent.

A number of investigators [45,54] have reported experimental data for the effect of film or coating thickness on COF that agree with Eq. (12.25). The relationship, however, does not always hold true in practice. For example, Edwards [18] analyzes COF measurements from extrusion coating of LDPE onto kraft paper and finds the COF was inversely proportional to the square of the initial slip concentration ($1/C_0^2$), rather than $1/C_0$ given in Eq. (12.25).

As described in Section 12.1.4.2, once the surface concentration of additive reaches a critical value, the COF reaches its ultimate value and further increases in surface slip concentration have no effect on the COF. Increasing the initial additive concentration, however, may help speed up the time for the film to reach this ultimate value. Adding too much slip additive, though, can cause problems, which are discussed in Section 12.1.4.9.

12.1.4.6 Storage Temperature

Many have observed that film stored at elevated temperatures, such as might be encountered in a warehouse during the summer months, has higher COF. One polymer supplier noted that they get more complaints on COF in the summer than any other time of the year. Several explanations for this have been investigated:

- A widely expressed rationale for this behavior is that the slip additive becomes more soluble in the film at elevated temperatures. As a result, some of the slip migrates from the surface back into the film, increasing the COF. Soutar [17] describes an incident where the COF is recovered by placing the film in cold storage for 10 days. Shuler [55] investigates the fate of erucamide on the surface of trilayer LLDPE films with a plastomer skin layer during storage. Storing the films at 55°C for several days results in a significant reduction in the erucamide surface concentration as measured by both FTIR and surface washing techniques. After investigating several of the possibilities mentioned here, they conclude that migration back into the PE is the most reasonable explanation. Interestingly, the COF in these experiments actually decreases, which Shuler hypothesized is due to a change in the crystalline morphology of the erucamide.
- Rawls [45] suggests slip additives may evaporate when films are stored at elevated temperatures. Rawls claims LLDPE film stored at 60°C show significant loss of erucamide due to sublimation or evaporation, even though the melting point is around 80°C. About 10% is lost over a 7-day period whereas substantially none is lost at room temperature. Shuler [55], however, concludes that evaporation loss of samples stored at 55°C is insignificant. Chen [7] draws a similar conclusion that evaporative loss of erucamide in their LLDPE films at 60°C storage conditions is negligible.
- Chemical changes in the slip additive on the surface or in the bulk are investigated by Shuler. They conclude that a small portion of the erucamide on the surface of their films degraded and outline the potential chemical pathways. Chen [7], however, cites previous work showing the decomposition of erucamide at 60°C is negligible.
- Chen [7] investigates the concentration and morphology of erucamide on the surface of LLDPE stored at room temperature for up to a year, and at 60°C in a nitrogen environment for 72 h. XPS is used to measure the surface concentration of erucamide. The morphology is measured with AFM. Initially the samples aged at room temperature have complete coverage of erucamide with crystal heights of around 10 nm. After greater than 1 year of room temperature aging, large crystals with heights of around 100 nm have formed, with bare PE between; islands of crystals have formed on top of the bare PE. After annealing at 60°C for 72 h, the large crystals have melted. The erucamide does not appear to recrystallize on the PE surface (even after remaining at RT for 2 weeks). XPS shows a substantial increase in erucamide on the surface following the annealing. They postulate that the annealing unlocks the migration of erucamide in the bulk of the PE that had been trapped by the PE crystals.

Based on these investigations, the change in COF during storage at elevated temperatures is complex and still not completely understood. For the practitioner, the important thing to note is that the COF may change during storage.

12.1.4.7 Effect of Other Additives

Slip additives are often not the only additive used in the film. Other additives are described in Chapter 4 and include antioxidants, antiblocks, antifog agents, chill roll releases, and antistat agents. Some of these, such as antifog, chill roll release, and antistat additives, may bloom to the surface much like slip additives. The slip additive must compete with the other additives for surface coverage. Reinecke [56], for example, studies the migration of erucamide and co-additives in a three-layer film with the structure (PE−PE−PE), where the additives are all added to the third layer. The co-additives are ethylene oxide oligomers. The hydrophilic nature of the co-additive impedes the migration of erucamide to the surface. The MW and number of polar groups of the co-additive are the important factors.

Inorganic antiblock additives are often used in films with marginal blocking performance. Soutar [17] and Zahedi [16] cite several studies showing synergy between adding silica and amide slip agents; adding silica not only reduces blocking but allows less slip to be added to achieve the target COF. Radosta [57] shows similar results for treated talc. Most suppliers of resins requiring low COF provide grades with both.

Some types of additives, such as calcium carbonate, have been found to absorb slip agents, increasing COF [34].

High levels of silica and other inorganic additives can result in high haze. This can be alleviated by confining the inorganic to a thin skin layer. Inorganic additives have also been reported to react with some slip agents, resulting in degradation by-products with color or odor/taste issues [58].

12.1.4.8 Coextrusion and Multilayer Structures

COF development in multilayer films containing migrating slip additives can be complex. The additives can migrate into adjacent layers or be transferred to the back side of films while wound in the roll. This leaves less of the additive for blooming to the desired low COF surface. The amount of adjacent layer migration is influenced by the solubility of the additive in the layers; fatty acid amide slip additives are more soluble in polar polymers such as tie layers and ionomers than PE. Further complicating matters is the effect of temperature on amide solubility and diffusion. The conclusion is that slip additives placed in one layer are not likely to stay in that layer. This needs to be accounted for when deciding how much additive to use and in which layers to place it.

Sankhe and Hirt [59] measure the erucamide concentration across a 50-μm bilayer film of LLDPE. The structure is (25-μm LLDPE−25 μm LLDPE); only one layer contains erucamide (at 1% loading). The erucamide concentration profile across the thickness of the film is measured using synchrotron-based FTIR microspectroscopy in order to get sufficient spacial resolution for the films. Previous work [60] measuring erucamide profiles had been limited to thick films (600 μm) due to the limited resolution of conventional FTIR spectroscopy. In the previous work, significant concentration gradients were found when slip was added to only one layer compared with adding equal amounts of slip to all layers. In the thin film work, they find that the concentration is nearly uniform across the entire thickness of the bilayer film, even at 1 day after fabrication. They postulate that the slip migrates into the adjacent layer during coextrusion; the characteristic diffusion time increases with the square of the film thickness so it is not surprising that the concentration evens out quickly in thin films. The surface concentration of erucamide is measured using ATR. Both sides of the bilayer film see an almost equal rise in surface concentration with storage time (up to 3 days) that coincides with a reduction in the bulk concentration.

Kitchel [21] tests a series of three-layer LDPE blown films with 500 ppm erucamide added to different layers. The total film thickness is 50 μm with layer percentages of (20/60/20). The COF is measured on the front and back side of the film with the goal to maximize the difference. The greatest differential in COF is obtained when all the slip is added to the outside skin layer (with respect to the blown film bubble). In a second experiment, the overall film thickness is varied from 25 to 150 μm. Increasing the thickness helps increase the COF differential.

Glover [54] extrusion coats LDPE containing a fatty acid amide slip additive onto two different substrates, kraft paper and aluminum foil. The COF of the coating is higher for the paper coatings, which he attributes to the porous paper absorbing some of the slip, leaving less to migrate to the surface of the LDPE.

Bryant [61] measures the COF as a function of time on a series of three-layer blown films containing different layer combinations of LLDPE and a sodium ionomer. Each layer is 25 μm thick for a total film thickness of 75 μm. The amide is placed in one or more of the layers to study the effect of migration between the adjacent polar (ionomer) and nonpolar (LLDPE) layers. Higher levels of slip additive are needed to achieve low COF when at least one of the layers is an ionomer, reflecting the greater solubility of the amide in the ionomer. Interestingly, lower COF is obtained when the slip is added to the ionomer layer than when only added to an LLDPE layer. The presence of a polar layer also affects the response of the COF with increasing storage temperature (from 23 to 38°C). The COF changes with temperature are more pronounced with the nonpolar LLDPE film than with those containing ionomer. Bryant attributes this to differences in solubility.

Soutar [17] provides a number of anecdotes regarding migrating slip in multilayer films. Tie

resins in particular are shown to have an effect on COF, presumably due to their polar nature. He hypothesizes that the chemical functionality of the tie resin attracts the amide molecules. In one example, the layers are peeled apart and no accumulation of amide is found at the interface between the tie and polyethylene layers. This suggests the slip resides in the bulk of the tie layer.

Soutar also discusses issues with backside transfer of amides or other additives from the front surface of the film to the adjacent back surface of the film wound in a roll. This has led to contamination issues involving poor printing or heat sealing.

Poisson [53] examines three-layer barrier blown films with the structure (Polyamide 6,66—tie—PE). The tie is a maleic anhydride-modified polyethylene. To this base case structure, several variations are considered by adding 50% by weight EVA (VA = 9 wt%) to the tie layer, sealant, or both. The layer thicknesses are (30/10/50 μm). Erucamide or oleamide is added to the sealant layer at concentrations ranging from 0 to 2500 ppm. AFM and FTIR are used to measure the slip concentration profile across the thickness of the film and the surface concentration. IR could not be used to measure the slip level in the polyamide (PA) layer since the IR peaks of the PA and amide overlap. The amount of slip in the PA layer is estimated by subtracting the measured amounts on the surface, in the sealant and in the tie layer from the total amount added.

Erucamide gives the best COF performance of the two slip additives tested. The oleamide shows some surprising COF results, such as increasing initially with time, which may be due to the polarity of the EVA. The COF with erucamide reaches the 0.2 goal quickly, even at 500 ppm concentration. Heat seal performance is not affected until high levels of erucamide are added; at 2500 ppm the heat seal initiation temperature increases by 30°C.

In Poisson's experiments with erucamide most of the slip ends up near the surface after the samples age for 1000 h. COF correlates with the fraction of the total slip on the surface. The presence of EVA increases the COF at all levels of slip, but the difference is not substantial and is overcome by adding a small amount of additional erucamide. With oleamide not as much slip ends up near the surface, and surface concentration does not correlate with COF.

Poisson presents data on how much slip ends up in each layer. When EVA is added to the tie or PE layer, this substantially affects the concentration of slip in each of the layers and at the surface. A significant amount of slip is found in the polar tie layer and PA layers, although the amount reported for the PA layer seems unrealistic. It is likely this is due to the measurement technique. The FTIR may lack the resolution to accurately measure the concentration in the thin PE and tie layers. This error in turn is compounded by the subtraction method used to arrive at the PA layer concentration. Nevertheless, the tie layer measurements do confirm what others have surmised about the tie layer absorbing slip.

As the complexity of coextruded film structures increases, a better understanding of slip migration between layers and to the surface will be needed.

12.1.4.9 Problems With Too Much Slip

Too much fatty acid amide slip accumulating at the surface can have consequences, which include the following:

- The film may take on a chalky or hazy appearance.
- The film may become difficult to adhere to or print.
- The slip additive may interfere with corona treatment. Treatment often attracts more slip to the surface (due to its polarity), causing COF to decrease, but contributing to loss of treatment and adhesion issues.
- Odor issues from degradation by-products may increase due to the higher concentration.
- In some cases, high slip leads to poor heat seal performance [27,46,53]. This is particularly true of grades of polyethylene where high levels of slip are needed, such as for metallocene plastomers [27]. For example, Wooster [27] finds seal initiation temperatures increase by as much as 11°C for a metallocene plastomer blown film. More polar polymers, such as ionomers, have been found to tolerate high levels of slip without negative effects on heat seal [15,61].

In some polymers, especially polar ones, the slip additive can take a long time to come to the surface. It is tempting to add higher levels of additive; this may reduce the time to reach the desired COF but may also bring on problems over time as more slip comes to the surface.

12.1.4.10 Tips and Classic References

Some practical tips for dealing with COF issues include the following:

- Working with your resin supplier to find the best additive and level for your application. Many resin suppliers have grades with slip and antiblock additives already incorporated or sell masterbatches for this purpose.
- Trying to control the COF to a medium level with a high-slip migrating-type additive can be very challenging. The slope of the COF versus slip additive concentration is very steep at low concentrations as illustrated in Fig. 12.6. It is difficult to control the amount of slip on the surface in this region. Once a sufficient amount of the slip additive has reached the surface, the COF is determined primarily by the crystalline structure of the amide. Consider switching to another amide that provides the intermediate COF at equilibrium.
- Using only as much slip agent as needed—too much can lead to adhesion and printing problems.
- Combining an inorganic antiblock and a fatty acid amide-type slip agent may provide the targeted COF at lower loadings. Some combinations may cause color or odor issues, however.
- Extruding at high temperatures can volatilize or degrade fatty acid amide slip additives. Select additives with the appropriate thermal stability when using high temperature processes like extrusion coating.
- Increasing the film surface roughness can improve the effectiveness of migrating slip additives. Reducing the film gloss or the smoothness of the chill roll may help reduce COF.
- Storing film at elevated temperatures, such as in a warehouse, can cause the COF to increase. Consider controlling the temperature swings the film may experience during storage and transport, particularly during summer months.
- Fatty acid amide slip additives can migrate between layers in coextruded films or be transferred from the backside of adjacent layers in a wound roll. Consider adding slip additives to more than one layer if migration is an issue.
- Considering the use of permanent slip additives if changes in COF due to coextrusion or storage, or adhesion performance are issues with migrating additives.
- Polar polymers such as EVA or ionomers require higher levels of fatty acid amide slip additives and the COF takes longer to develop than for polyethylene.
- When selecting a masterbatch, make sure the carrier resin is compatible with the polymer it is being blended into. For example, if the polymer is LLDPE, use a carrier that is PE or EMA based. If the polymer is an ionomer, use a carrier that is acid copolymer based. Poor compatibility can lead to heat seal problems and increased haze.

Slip concentrations are typically reported in the units of ppm (parts of slip additive per million parts of polymer). To convert to wt%, use the conversion 1000 ppm = 0.1 wt% (10,000 ppm = 1 wt%). Most of the time the converter will be adding slip to the polymer using a masterbatch. To calculate the wt% masterbatch to add, Eq. (12.28) can be used:

$$\text{wt\% MB} = \frac{\text{Goal Slip Concentration (ppm)}}{100 \times \text{ wt\% Slip in MB}} \tag{12.28}$$

For example, if the goal is to add 1000 ppm of slip into LDPE, and if the masterbatch contains 10% slip, then the amount to add is $1000/(100 \times 10) = 1\%$.

Fatty acid amide technology for lowering the COF of polyolefin and other plastic films has been around for over 50 years. There are a number of classic references that provide more detailed examples and practical observations of performance, many of which have been cited in this chapter. These include the following:

- Owens [5,8,62] in a series of papers describes work done at DuPont on the use and understanding of fatty acid amide slip agents in PVDC-coated cellophane. Many of the observations and analysis are relevant to any plastic film.
- Tabor et al. [52,63] review early work on slip additives and describes performance of oleamide and stearamide in polyethylene.
- Thompson [34] provides a good overview of COF control for PE films.

- Itzkoff and Woodell [19] describe the effect of extrusion coating processing parameters on COF.
- Edwards and Foster [18] provide simple calculations to predict COF performance in extrusion coating.
- Glover [54] provides a good overview of slip additive technology in extrusion coating of LDPE.
- Soutar [17] provides examples of the complexity of COF in multilayer films and the effect of storage temperature.
- Breuer et al. [22,23] provide a good introduction to fatty acid amides for polyolefin films.
- Maltby et al. [3,10,24,26,64] provide additional information on slip agents for polyolefin films.
- Hirt et al. [20,28–32,37,41,45,47,50,51,55,59,60] provide sound fundamental work on migration of erucamide in LLDPE film.

12.2 Optical Properties

The ability to see through a film and the sparkle or gloss reflected from a film's surface are part of the set of properties collectively known as optical properties. This chapter deals primarily with high clarity films, which are important in many packaging applications where the product is meant to be seen. Some applications call for a light barrier, which is usually achieved by incorporating an opaque layer (such as aluminum foil) into the structure, metallization of a surface of the film or incorporating pigments. Light barrier technology is reviewed in Chapter 8. Likewise, printing, glossy coatings, and pigmented films are not covered in this chapter. Optical films such as polarizers, reflectors, diffusers, and light filters generally fall outside the realm of packaging; however, one of the techniques used to make optical filters is briefly described at the end of this chapter as an example of where technology from other markets may bring new ideas to packaging.

12.2.1 Definitions and Measurement

The transmittance or clarity of a film refers to its ability to pass through light. This is sometimes known as "see through clarity," referring to the ability of a person to see far objects through a handheld sample of the film. ASTM D1746 [65] provides a method for measuring the transparency of plastic film. The sensitivity of the measurement decreases as the angle between the incident light beam and detector decreases. To provide accurate results, the method calls for using a device that controls this angle to within 0.1 degree. The results are reported as a percent transmittance on a scale of 0–100.

Haze refers to the scattering of light, which is observed as "smokiness" in the film. ASTM D1003 [66] defines haze as the percent of transmitted light that is scattered so that it deviates from its intended direction by more than a specified angle (2.5 degrees in the standard). This method is for low-haze films. If the haze is greater than 30%, ASTM E2387 or D1044 may be more appropriate. An equivalent method is ISO 14782 [67]. The ASTM method has two procedures, one using a hazemeter and the other using a spectrophotometer. Results are reported as percent transmittance that has been scattered.

Haze can originate in the bulk of the film or from surface roughness. To help separate the two effects, some investigators mask the surface of the film by applying oil, such as mineral oil or silicone oil, which has a refractive index similar to the plastic film. This results in a measurement of just the internal haze. The surface haze is then calculated by subtracting the internal haze from the total haze (measured on the specimen with no oil on the surface).

Gloss is a measure of surface reflectance or the shininess of the surface when observed at a specified angle. It is strongly influenced by surface roughness. A glossmeter (ASTM D2457 [68]) measures the specular reflectance of white, unpolarized light at a specific angle from the incident beam. Several angles are used for gloss measurements with the most common for films being

- 20 degrees—high gloss surface;
- 45 degrees—medium gloss surface;
- 60 degrees—medium gloss surface;
- 85 degrees—low gloss surface.

For transparent packaging films, 20 degrees gloss is the most often used. Results are reported as the specular reflectance, in percent. Because transparent films have two reflecting surfaces, gloss values can exceed 100%.

12.2.2 Haze and Transparency

In general haze and transparency are inversely related—an increase in haze reduces transparency. Most studies have focused on haze of film, especially on the haze of polyolefin films.

Haze in a polymer film arises from interior or bulk effects (internal haze) and surface roughness (surface haze). Crystallinity, gel, voids, phase separation of blends, and various additives or fillers increase internal haze by providing sites for light to refract and scatter. In general, any disparity greater than the wavelength of light (400−700 nm) and a refractive index different from the polymer will refract light and contribute to internal haze. Surface haze is caused by surface roughness. Crystallinity, certain additives, and flow instabilities are known to contribute to surface roughness and haze. The film fabrication process may affect both internal and surface haze.

12.2.2.1 Monolayer Polyethylene Film

Studies have conclusively shown that the haze of monolayer polyethylene blown and cast films is dominated by surface haze. Huck and Clegg [69] propose that the surface roughness of polyethylene film is due to two mechanisms: extrusion haze due to flow instabilities such as sharkskin and crystallization haze from stress-induced crystallization near the surface. Many investigators since Huck and Clegg have confirmed their hypothesis and refined the general knowledge of the origins of surface haze. Stehling [70] shows that the extrusion haze is related to the elasticity of the polymer, which can be related to the MWD, especially the presence of a high MW component. Ashizawa [71] shows that haze correlates directly with surface roughness of a series of high density polyethylene (HDPE), LLDPE, and LDPE blown films, with the HDPE films having the highest roughness and haze. Patel [72] later confirms this relationship with more sophisticated AFM measurements.

Johnson [73−75] finds that elasticity also influences the crystalline morphology near the surface of LLDPE films. Comparing a mLLDPE that has high haze with a ZN-LLDPE that has lower haze, they find that the crystalline morphologies differ. The mLLDPE has what they call a spherulitic superstructure, which results in a high level of surface roughness. The ZN-LLDPE has a fibrillar or lamellar morphology with lower surface roughness. They propose that the narrower MWD of the mLLDPE results in short relaxation times, allowing for the superstructure morphology to develop. The broader MWD of the ZN-LLDPE, and in particular the high MW fraction, increases the elasticity and relaxation time, impeding the development of the superstructure morphology. Using a series of polymers, they correlate surface haze with recoverable shear strain from stress relaxation experiments (Chapter 5), which is a measure of elasticity. When this parameter is small, the relaxation time is short and the spherulitic superstructure morphology forms. At intermediate values, the spherulitic structure gives way to row nucleated lamellar structures and haze decreases. At even higher values, extrusion haze takes over and surface roughness and haze increase.

Other studies described in Sections 7.5.3.2.2, 10.4.2.2.1, and 12.1.4.1 show that blown film of ZN-LLDPE has an amorphous region near the surface due to the polymer's broad comonomer and MWD distribution. The shorter chains with an abundance of comonomer and short chain branches are more pronounced near the surface, creating an amorphous region not found in metallocene LLDPE blown films. This region influences heat seal, adhesion, and slip migration. It is not clear how to reconcile these two different observations except that they both suggest differences in crystallinity or crystalline morphology contribute to surface roughness and haze.

Several approaches have been explored to reduce the haze of polyethylene films. LDPE generally has lower haze than ZN-LLDPE blown film, likely due to its higher level of elasticity. EVA copolymers have lower levels of haze than LDPE due to their lower level of crystallinity. Blending a small amount of LDPE into some types of LLDPE has lowered haze, presumably by increasing the elasticity of the LLDPE [76−79]. Similarly, Cooke [79] shows that adding a small amount of a high MW HDPE to LLDPE reduces haze. Various blends of LLDPE with other grades of LLDPE or rigid polymers, and manipulating the molecular architecture by adding a small amount of long chain branching has also reduced haze [80−85].

Polymer processing also affects haze. When crystallinity is the dominate mechanism for surface roughness, reducing overall crystallinity is important. For polyethylene blown film, increasing the cooling

rate by reducing the frost line height reduces haze [69,71,86]. Ashizawa [71] finds that increasing draw down ratio or blowup ratio decreases internal haze but increases surface haze somewhat. Cast film typically has lower haze than blown film due to the faster quench rate (and lower overall crystallinity) of the cast film process, although the haze of PE cast films is still dominated by surface roughness effects [73,87]. Water-quench blown films also have lower haze than air-quench blown films [88]. When elasticity or extrusion haze dominates, lowering output or decreasing the rate of cooling helps. Ionomers, for example, have a lower level of crystallinity than LDPE but higher elasticity. The haze of ionomer films is almost always dominated by elastic flow irregularities rather than crystallinity. Increasing the melt temperature and the frost line height generally helps lower the haze and increase the gloss of ionomers, just the opposite of what is typically done for polyethylene. The slower cooling rate allows more time for the surface irregularities caused by elasticity to relax.

12.2.2.2 Coextrusion

Since surface haze is the primary cause of haze in polyethylene film, burying the high haze resin in a multilayer coextrusion is often an effective strategy for reducing the haze of a film. The same surface roughness that develops on the free or outer surface of the film may not develop at an interior interface of a coextruded film. One explanation for this is that the level of stress may be different. The outside of the film experiences a high level of stress in the die channel since stress is at its maximum at the die wall. At the die exit, the polymer on the outside must accelerate from essentially no flow to the average draw speed of the molten web. This may give rise to strain-induced crystallization. The stress on the polymer is smaller away from the outside of the film since the amount of acceleration is not as great. A polymer–polymer interface may also induce the formation a different crystalline structure than a polymer–air interface due to differences in free energy and physical constraints on chain movement.

Several investigators have shown that coextruded structures with the same overall material composition but with different layers on the surface may have lower haze [87,89–92]. An example from Elkoun [89] is shown in Fig. 12.13. Five-layer blown film with

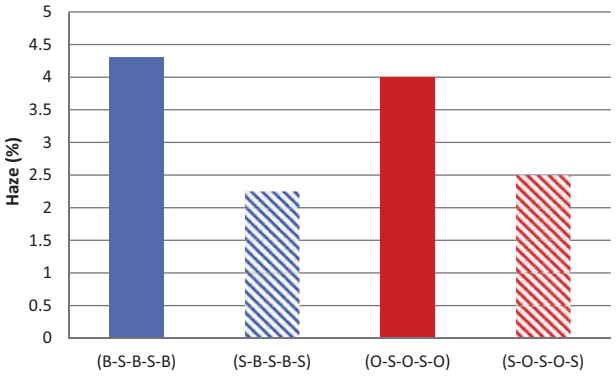


Figure 12.13 Effect of film structure on coextruded blown film haze. *B*, bLLDPE; *O*, oLLDPE; *S*, mLLDPE. Each film structure contains 50% S split equally among two or three layers.
Adapted from Elkoun S, Huneault MA, Zhang XM, McCormick K, Puterbaugh F, Kale L. LLDPE blown films property enhancement through coextrusion. In: SPEANTEC conference; 2003. p. 1396–400.

different layer combinations of three LLDPE resins is tested. One resin is a conventional Ziegler–Natta butene-LLDPE (0.918 g/cc, 1 g/10 min MI), labeled B. Another is an advanced Ziegler–Natta octene-LLDPE (0.920 g/cc, 1 g/10 min MI), labeled O. The final grade is a metallocene LLDPE (0.917 g/cc, 1 g/10 min MI), labeled S. The typical haze for these three grades in a monolayer 25-μm blown film is 3.5%, 8.5%, and 2.5% for B, O, and S, respectively. The five layer films contain alternating layers of S with either O or B, with the amount of S comprising 50% of the total structure. As shown in Fig. 12.13, when the lower haze S grade is on the outside of the film, the haze is lower than when the higher haze O or B grade is on the outside. The haze of coextruded films with the S skin layers also is similar to the typical value for a 100% S film.

Coextrusion does not always produce predictable results based simply on the haze of the outside layers. Fig. 12.14 shows results of haze and gloss measurements on three-layer blown film structures from Borse [90]. They evaluate combinations of a Ziegler–Natta butene-LLDPE (0.921 g/cc, 0.8 g/10 min MI), labeled L, and a single site-catalyzed LLDPE (0.916 g/cc, 0.65 g/10 min MI), labeled M. The first two sets of bars represent the control monolayer films. The next three sets of bars show data for a coextrusion with the M resin on the outside, with different layer ratios. The haze is significantly lower and gloss higher than the two controls; having M on the outside has a positive

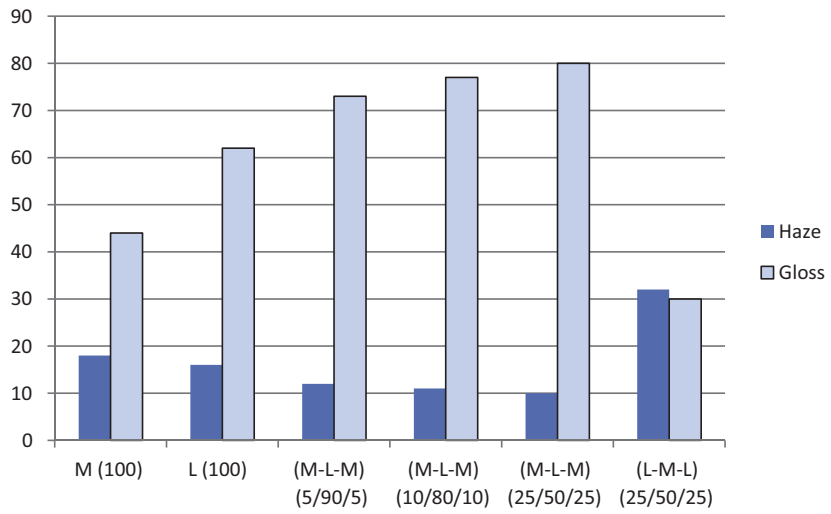


Figure 12.14 Example of synergistic and antagonistic effects of coextrusion on optical properties of a blow film. *L*, Ziegler–Natta butene-LLDPE; *M*, single site-catalyzed LLDPE.
Adapted from Borse N, Aubee N. Developing cost effective co-extruded film structures for flexible packaging. In: SPE ANTEC conference; 2014. p. 1304–8.

synergistic effect on the optical properties. The final set of bars shows the case where the L resin is on the outside. Here the haze is higher and the gloss is lower than either of the controls.

Another example of synergic and antagonistic effects is shown in Fig. 12.15. Zhang [91] evaluates five-layer blown film with different combinations of PP and LLDPE. The LLDPE is a Ziegler–Natta octene-LLDPE. The results for two PP grades are shown in the figure, a clarified random copolymer (coPP) and a homopolymer (hoPP). The bars on the far left and right represent the results for monolayer controls. The bars in the middle represent different combinations of layers of PP (P) and LLDPE (L). In each case, 50% of the total composition is PP and 50% LLDPE. As expected, the coPP control film has significantly lower haze than the hoPP control. This due to the lower crystallinity of the coPP as well as the addition of the clarifier additive. The coPP also has somewhat lower haze than the LLDPE control. All the coPP–LLDPE multilayer structures (graph A) have lower haze than either of its component control films. In contrast, graph B shows that the multilayer structures with hoPP on the surface have higher haze than either the hoPP or LLDPE control, whereas the structures with LLDPE on the surface have haze similar to the LLDPE control.

12.2.2.3 Other Factors

Many other factors influence the haze and transparency of blown or cast film, which include the following:

- Tie resin selection for coextruded films. Every layer in a coextrusion can detract from the optical clarity of the structure, even a thin tie resin. For many common barrier films involving bonding PE to PA or EVOH, there are many different tie resins to choose from. These are functionalized polymers typically based on different types of PE (HDPE, LLDPE, or LDPE) or ethylene copolymers (EVA or EMA) (see Chapter 10 for details). If clarity is a critical attribute, then selecting a tie resin based on its clarity should be a consideration. Tie resins generally have similar clarity as the polymer on which they are based. For good clarity, an EVA-based tie resin may be a better choice than an HDPE-based one, as long as it meets all the other requirements of the structure (such as barrier or temperature resistance).
- Antiblock and other additive selection. As described in Section 12.1.3, antiblock additives are typically inorganic particles such as silica

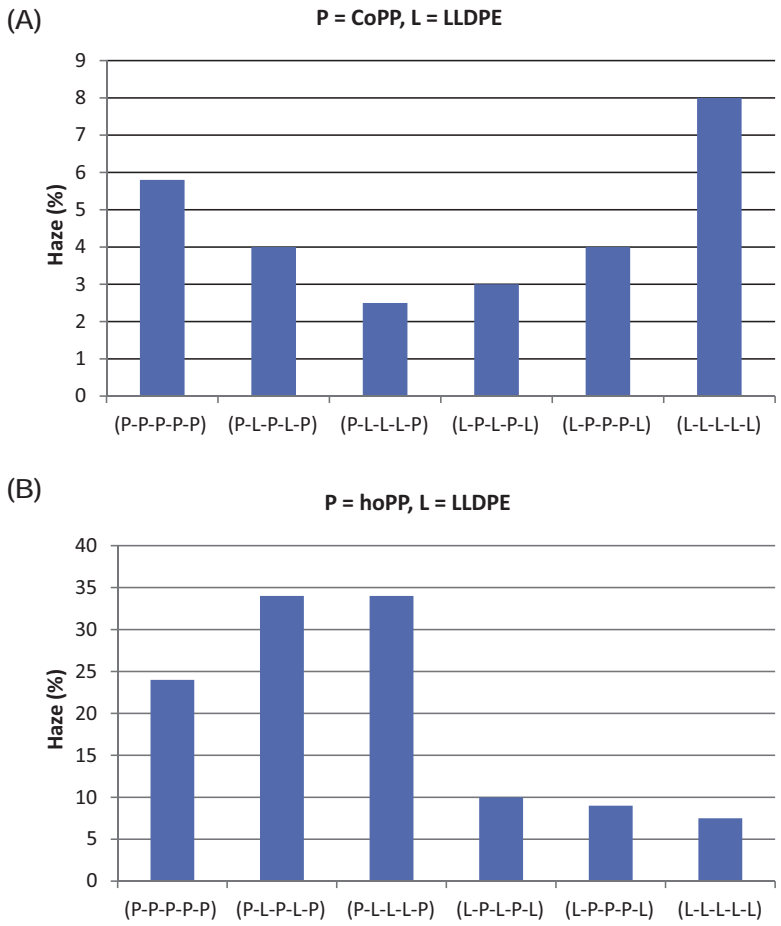


Figure 12.15 Effect of coextrusion blown film layer composition and structure on haze. *L*, octene LLDPE; *P*, random copolymer PP (Graph A) or homopolymer PP (Graph B). Structures with both PP and LLDPE layers contain a total of 50% PP and 50% LLDPE distributed among the individual layers.
Adapted from Zhang X, Ajji A. Polypropylene-polyethylene multilayer films. In: SPE ANTEC conference; 2005. p. 2947–51.

(diatomaceous earth) or talc. Their size, shape, and concentration can affect haze and transparency [93]. They are generally in the size range where they diffract light, so optimizing compositions for minimal usage can be important for minimizing haze. Coextrusion may allow them to be used in a thin skin layer, decreasing their effect on haze.

- Nucleating or clarifying agents. Nucleating agents seed the crystallization process so that when the polymer cools from the melt, more crystals form (nucleate). With many more crystals growing, individual crystals cannot become as large. If the crystal size is limited to below the wavelength of light (400–700 nm), then haze is reduced. The most successful nucleating agents have been for PP.
- Orientation. Orientation can induce crystallization but often the crystalline morphology that develops favors lower haze. Biaxially oriented polypropylene (BOPP) and polyester (OPET) are highly crystalline yet very transparent.
- Polymer blends. Chapter 6 describes blending technology for flexible packaging. Most polymer–polymer blends are immiscible so that one of the polymers forms a separate phase or domain within the other. If these domains are larger than the wavelength of light and their refractive index does not match that of the continuous polymer phase, they will contribute to haze. The domain size is a complex function of viscosity ratio, surface energy, and mixing. It is very challenging to obtain domain sizes that are small enough to maintain transparency.

Therefore, it is important to consider the compatibility of polymers being blended into film layers, such as masterbatch carrier resins. Even polymers of the same product class, such as LLDPE and LDPE, may be immiscible depending on their composition.

- Refractive Index. If two materials have refractive indices that are the same, their blends will be transparent to light even if they are immiscible. Unfortunately, it is very rare that the refractive indices of two immiscible polymers, or a polymer and an inorganic additive, match sufficiently to avoid haze issues.

12.2.3 Gloss

Gloss is highly dependent on the surface roughness; smoother surfaces typically have higher gloss. Factors for minimizing surface haze in polyolefins are discussed in Section 12.2.2. These same factors generally will help maximize gloss, which include the following:

- Reducing surface imperfections due to flow instability (such as sharkskin and melt fracture) and elastic effects. The rheology of the polymer contributes to this behavior. For LDPE, selecting a grade with a narrower MWD or less long chain branching may help. Processing is also a factor: changes in melt temperature, frost line height, and output may have an impact. As discussed in Section 12.2.2, different polymers may respond in opposite ways, so understanding the dominant mechanism for low gloss will help guide the approach.
- Reducing overall crystallinity of the polymer. Surface crystallinity is an another contributor to surface roughness and low gloss. Reducing the overall crystallinity of the polymer may help. Ionomers, for example, have low levels of crystallinity and very high gloss. Faster quench rates also generally help reduce crystallinity of polymers, which may help increase gloss. Cast film generally has higher gloss than blown film. When casting film, the surface of the chill roll can impact gloss—a polished mirror surface will generally provide higher gloss than a matted one.
- Minimizing other surface imperfections such as gel.
- Optimizing the use of inorganic antiblock additives, which by design roughen the surface.

12.2.4 Specialty Microlayer Films

Microlayer film technology is described in Sections 8.5.2, 9.4.6, and 11.2.4.6. It involves combining two or more layers and repeatedly spitting and recombining them to produce film structures with tens to hundreds of layers. The concept is illustrated in Fig. 8.17. Some of the earliest commercial adoptions of this technology were for films for optical filters. By selecting polymers with the right combination of refractive indices or other properties, specialty films can be made that selectively reflect certain wavelengths of light or have specific dielectric properties for use as optical filters, components for LCD displays, capacitors, and other electronic devices [94–102].

One intriguing application for this technology that may have application for flexible packaging is described by Im and Schrenk [94]. They made a film with 400-alternating layer of PP and PC, which blocked 80% of UV light while retaining good transparency of visible light. A two-layer control film of the same total thickness and PP and PC content does not block the UV light. They develop the theoretical basis for this effect based on the difference in refractive indices of layers, layer thickness, and number of layers.

References

[1] Clark TA, Wagner Jr JR. Film properties for good performance on vertical-form-fill-seal packaging machines. J Plast Film Sheet 2002;18:145–56.
[2] ASTM International. Standard test method for static and kinetic coefficients of friction of plastic film and sheeting (D1894-14). West Conshohocken (PA): ASTM International; 2014.
[3] Maltby A. The effects of polyolefin formulation and processing variables on slip agent performance (I). In: TAPPI polymers, laminations & coatings conference; 1998. p. 1241–50.
[4] ASTM International. Standard test method for blocking load of plastic film by the parallel plate method (D3354-15). West Conshohocken (PA): ASTM International; 2015.

[5] Owens DK. Friction of polymer films. I. Lubrication. J Appl Polym Sci 1964;8:1465−76.
[6] Sharma A, Beard B. Mode of action of surface active slip and antiblocking additives. In: SPE ANTEC conference; 1997. p. 3019.
[7] Chen J, Pham H, Savargaonkar N, Ge S. Aging dependent slip agent surface morphology of LLDPE films. In: SPE ANTEC conference; 2011.
[8] Owens DK. Friction of polymer films. II. Effects of deformation properties. J Appl Polym Sci 1964;8:1477−82.
[9] Walp L, Tomlinson H. Effect of erucic acid percentage on slip properties of erucamide. J Plast Film Sheeting 2004;20:275−87.
[10] Maltby A. Effect of amide composition on performance as a plastics additive. In: TAPPI PLACE conference; 2002.
[11] Rosato D. Advanced slip & antiblock friction control in packaging film. SpecialChem; 2008. http://polymer-additives.specialchem.com/tech-library/article/advanced-slip-antiblock-friction-control-in-packaging-film.
[12] Constant DR. Cyclic-olefinic copolymers as non-migrating, polymeric slip additives in LDPE cast film. In: SPE ANTEC conference; 2002.
[13] Ryan KJ, Lupton KE, Pape PG, John VB. Ultra high molecular weight functional siloxane additives in polymers: effect on processing and properties. Dow Corning; 2001. http://www.dowcorning.com/content/publishedlit/26-036-UHMW-Siloxane-Additives-in-Polymers_-_Masterbatches.pdf.
[14] Savargaonkar S, McKinley B. Slip agents: extended performance range for polyolefins. Plastics Technology; 2006. http://www.ptonline.com/articles/slip-agents-extended-performance-range-for-polyolefin-films.
[15] DuPont. Processing and properties of Surlyn® ionomer resins by blown and cast film processes. STL from TSL, 70−4 (Revised October 1979). 1979.
[16] Zahedi AR, Ranji A, Asiaban S. Optimizing COF, blocking force, and printability of low density polyethylene. J Plast Film Sheeting 2006;22:163−76.
[17] Soutar AM. The fugitive slip. In: TAPPI polymers, laminations and coatings conference; 1994.
[18] Edwards R, Foster B. Coefficient of friction in polyethylene extrusion coatings: an analysis. In: TAPPI polymers, laminations and coatings conference; 1993.
[19] Itzkoff ML, Woodell GL. Effect of production parameters on COF of extrusion coated substrates. In: TAPPI paper synthetics conference; 1983. p. 111−6.
[20] Sakhalkar S, Hirt D. Surface segregation of erucamide in LLDPE films: thermodynamic analysis and experimental verification. In: SPE ANTEC conference; 1998.
[21] Kitchel F. Differential C.O.F. in coextruded blown films. In: TAPPI polymers, coatings and laminations conference; 1988.
[22] Breuer T, Martin N, Tomlinson H, Leonard E. Effect of oleochemical additive lubricants on surface properties of polyolefin films. In: SPE ANTEC conference; 1983. p. 896.
[23] Breuer T, Martin N, Tomlinson H, Gloyer S, Crawford H. Fatty amide slip and antiblock additives in polypropylene and linear low density polyethylene. In: SPE ANTEC conference; 1984. p. 141.
[24] Maltby A, Marquis R. Slip additives for film extrusion. J Plast Film Sheeting 1988;14:111.
[25] Patel P, Savargaonkar N. COF & blocking in mLLDPE film: 'Why don't my recipes work?'. In: TAPPI polymers, laminations and coatings conference; 1999. p. 1071.
[26] Coupland K, Maltby A. Modification of the surface properties of polyethylene plastomer films by the use of additives. J Plast Film Sheeting April 1997;13:142.
[27] Wooster J, Simmons B. Optimizing COF, seal performance, and optical properties of polyolefin plastomers. In: TAPPI polymers, laminations and coatings conference and 1996 SPE ANTEC conference; 1995.
[28] Sankhe S, Hirt D, Roberts W, Havens M. Evaluation of additive concentration profiles in multilayer films. In: SPE ANTEC conference; 1999.
[29] Rawls A, Joshi N, Sakhalkar S, Hirt D. Evaluation of surface concentration of additives in LLDPE films. In: SPE ANTEC conference; 1997. p. 3029.
[30] Joshi N, Hirt D. Evaluating bulk-to-surface partitioning of erucamide in LLDPE films using

FT-IR microspectroscopy. Appl Spectrosc 1999;53:11 (Erratum 1999;53:261A).
[31] Joshi N, Hirt D. Studying additive diffusion in polymer films using FTIR microspectroscopy. In: SPE ANTEC conference; 1998.
[32] Gagliardi C, Murie L, Hirt D. Measuring the diffusivity of additives in polymer films using in situ FTIR-ATR spectroscopy. In: SPE ANTEC conference; 1999.
[33] Klein J, Briscoe B. Diffusion of long molecules through solid polyethylene. II. Measurements and results. J Polym Sci 1977;15:2065−74.
[34] Thompson KI. Coefficient of friction testing and factors that affect the frictional behavior of polyethylene films. TAPPI J September 1998;71:157−61.
[35] Foldes E. Mobility of additives in ethylene polymers. Polym Bull 1995;34:93−9.
[36] Coupland K, Malty A, Parker D. In: AddCon Asia, paper 15; 1997.
[37] Joshi N, Sakhalkar S, Hirt D. Mass transfer of slip and antifogging agents in LLDPE films. In: SPE ANTEC conference; 1996. p. 2406.
[38] Hu S, Lin-Vien D, French R. Probing the concentration profiles of additives in polymers in IR microspectroscopy: the diffusion of Cyasorb UV531 in polypropylene. Appl Spectrosc 1992;46:225.
[39] Quijada-Garrido I, Barrales-Rienda J, Frutos G. Diffusion of erucamide (13-cis-docosenamide) in isotactic polypropylene. Macromolecules 1996;29:7164−76.
[40] Foldes E. Transport of small molecules in polyolefins. II. Diffusion and solubility of Irganox 1076 in ethylene polymers. J Appl Poly Sci 1993;48:1905−13.
[41] Muire L, Hirt D. Effect of applied external pressure on the surface concentration of erucamide in LLDPE films. In: SPE ANTEC conference; 1999.
[42] Schumann B, Wooster J, Murray S. The effect of film winding tension and melt temperature on COF and other properties of PE blown film. In: TAPPI polymers, laminations and coatings conference; 1998. p. 633.
[43] Passiniemi P. General theory for determination of diffusion coefficients of solvents and gases in polymers. Polymer 1995;36:341.
[44] Fieldson GT, Barbari TA. The use of FTIR-ATR spectroscopy to characterize penetrant diffusion in polymers. Polymer 1993;34:1146.
[45] Rawls A, Hirt DE, Havens MR, Roberts WP. Evaluation of surface concentration of erucamide in LLDPE films. J Vinyl Addit Technol 2002;8:130−8.
[46] Foldes E, Szigeti-Erdei A. Migration of additives in polymers. In: SPE ANTEC conference; 1997. p. 3024.
[47] Ramirez M, Hirt DE, Roberts B, Havens M, Miranda N. COF of LLDPE films as a function of erucamide surface concentration. In: SPE ANTEC conference; 2000.
[48] Silverwood RJ, Sadeghi F, Ajji A. Study of kinetic of slip agent migration in polyethylene sheets. In: SPE ANTEC conference; 2012.
[49] Chang S-S. Migration of low molecular weight components from polyolefins. Macromol Symp − Intern Union Pure Appl Chem 1982;28:734−5.
[50] Ramirez MX, Walters KB, Hirt DE. Relationship between erucamide surface concentration and coefficient of friction of LLDPE film. J Vinyl Addit Technol 2005:9−12.
[51] Joshi N, Hirt D. Theoretical analysis of additive distribution in polymer films. In: SPE ANTEC conference; 1994. p. 2798−802.
[52] Allen D, Briscoe BJ, Tabor D. Lubrication of polymers by oleamide and stearamide. 2. Wear 1973;25:393−7.
[53] Poisson C, Hervais V, Lacrampe MF, Krawczak P, Falher T, Gondard C, et al. Optimization of polyethylene/binder/polyamide extrusion blow-molded films. III. Slippability improvement with fatty acid amides. J Appl Polym Sci 2010;115:2332−45.
[54] Glover JH. Slip migration in extrusion coating of LDPE. In: TAPPI polymers, lamination and coatings conference; 1987. p. 231−9.
[55] Shuler CA, Janorkar AV, Hirt DE. Fate of erucamide in polyolefin films at elevated temperature. Polym Eng Sci 2004; 44:2247−53.
[56] Reinecke H, Navarro R. How to control migration of slip agents in polyethylene films. Plastics Research Online, Society of Plastics Engineers; 2011.
[57] Radosta JA, Riley WD. Treated talc as an effective anti-block for LDPE blown film. J Plast Film Sheeting 1991;7(3):247−58.
[58] Peloso CW, O'Connor MJ, Bigger SW, Scheirs J. Characterizing the degradation of the polymer slip additive erucamide in the presence

of inorganic antiblock agent. Polym Degrad Stab 1998;62:285−90.
[59] Sankhe SY, Hirt DE. Studying additive migration in LLDPE and POP films using synchrotron-based FTIR microspectroscopy. In: SPE ANTEC conference; 2002.
[60] Sankhe SY, Hirt DE. Evaluation of additive concentration profiles in multilayer films. In: SPE ANTEC conference; 1999.
[61] Bryant K. Understanding coefficient of friction in coextruded films. In: TAPPI polymers, laminations and coatings conference; 1998. p. 969.
[62] Owens DK. Friction of polymer films. III. Migration of lubricants. J Appl Polym Sci 1970;14:185−92.
[63] Briscoe BJ, Mustafaev V, Tabor D. Lubrication of polythene by oleamide and stearamide. Wear 1972;19:399−414.
[64] Maltby A, Read M. Effect of temperature on the slip and blocking of polyolefins containing various fatty acid amides. In: TAPPI polymers, laminations and coatings conference; 1999. p. 1079.
[65] ASTM International. Standard test method for transparency of plastic sheeting (D1746-15). West Conshohocken (PA): ASTM International; 2015.
[66] ASTM International. Standard test method for haze and luminous transmittance of transparent plastics (D1003-13). West Conshohocken (PA): ASTM International; 2013.
[67] International Organization for Standardization. Plastics − determination of haze for transparent materials (ISO 14782). Geneva (Switzerland): International Organization for Standardization; 1999.
[68] ASTM International. Standard test method for specular gloss of plastic films and solid plastics (D2457-13). West Conshohocken (PA): ASTM International; 2013.
[69] Huck ND, Clegg PL. The effect of extrusion variables on the fundamental properties of tubular polyethylene film. In: SPE ANTEC conference, 18-2; 1961. p. 1−14.
[70] Stehling FC, Speed CS, Westerman L. Causes of haze of low-density polyethylene blown films. Macromolecules 1981;14:698−708.
[71] Ashizawa H, Spruiell JE, White JL. An investigation of optical clarity and crystalline orientation in polyethylene tubular film. Polym Eng Sci 1984;24:1035−42.
[72] Patel R, Ratta V, Saavedra P, Ji J. Surface haze and surface morphology of blown film compositions. J Plast Film Sheeting 2005;21:217−31.
[73] Johnson MB, Wilkes GL, Sukhadia AM, Rohlfing DC. Optical properties of blown and cast polyethylene films: surface versus bulk structural considerations. J Appl Polym Sci 2000;77:2845−64.
[74] Wilkes GL, Johnson MB, Sukhadia AM, Rohlfing DC. Optical haze properties of polyethylene blown films: part 1 − surface versus bulk structural considerations. In: SPE ANTEC conference; 2001.
[75] Sukhadia AM, Rohlfing DC, Johnson MB, Wilkes GL. Optical haze properties of polyethylene blown films: part 2 − the origins of various surface roughness mechanisms. In: SPE ANTEC conference; 2001.
[76] Lue CT, Kwalk TH, Li D, Davey CR, Chiu DY. "Haze improvement with addition of HP-LDPE or HDPE. Part I − blown film property comparison. In: SPE ANTEC conference; 2004. p. 2140−3.
[77] Chen HY, Li J, Sammler RL, Lue CT, Kolb R, Kwalk TH. Haze improvement with addition of HP-LDPE or HDPE. Part II − mechansitic understanding. In: SPE ANTEC conference; 2004. p. 2117−21.
[78] Jordens K. The influence of small amounts of LDPE on the morphology and resulting haze of LLDPE blown films. In: SPE ANTEC conference; 2002.
[79] Cooke DL, Tikuisis T. Addition of branched molecules and high molecular weight molecules to improve optical properties of LLDPE film. J Plast Film Sheeting 1989;5:290−307.
[80] Liu L, Karjala T, Ge S, Demirors M. Relationship between surface haze and crystalline morphology of polyethylene blown films. In: SPE ANTEC conference; 2012.
[81] den Doelder J, Karjala T, Demirors M. The relationship between tubular low-density polyethylene (LDPE) blown-film optics and molecular structure. In: SPE ANTEC conference; 2009. p. 2806−10.
[82] Cran MJ, Bigger SW. The effect of metallocene-catalyzed polyethylene on the physicomechanical properties of film blends with

conventional linear low-density polyethylene. J Plast Flim Sheeting 2006;22:121−32.
[83] Mavridis H. Blending of high-performance LLDPEs with butene-LLDPEs and LDPEs. J Plast Film Sheeting 2001;17:253−65.
[84] Chinsirikul W, Fuongfuchat A, Kerddonfag N, Phiboonkulsumrit S, Winotapun C, Khumsang P. Preventing film blocking and optimizing haze of metallocene PE blown films through blending with rigid polymers. Intern Polym Process 2004;XXIII:152−60.
[85] Butler TI, Lai SY, Patel R. A blown film comparison between conventional LLDPE and POP. J Plast Film Sheeting 1994;10:248−61.
[86] Werlang MM. Effect of polymer processing conditions on shrinkability of LDPE and LLDPE films, and on optical properties of LLDPE films. In: SPE ANTEC conference; 2003. p. 3271−4.
[87] Scarfato P, Di Maio L, Garofalo E, Incarnato L. Three-layered coextruded cast films based on conventional and metallocene poly(ethylene/α-olefin) copolymers. J Plast Film Sheeting 2014;30:284−99.
[88] Xiao K, Lee I-H, Armstrong R. Comparison of water-quench versus air-quench blown film processes − part I: flat film properties. In: SPE ANTEC conference, vol. 70; 2012. p. 972−7.
[89] Elkoun S, Huneault MA, Zhang XM, McCormick K, Puterbaugh F, Kale L. LLDPE blown films property enhancement through coextrusion. In: SPE ANTEC conference; 2003. p. 1396−400.
[90] Borse N, Aubee N. Developing cost effective co-extruded film structures for flexible packaging. In: SPE ANTEC conference; 2014. p. 1304−8.
[91] Zhang X, Ajji A. Polypropylene-polyethylene multilayer films. In: SPE ANTEC conference; 2005. p. 2947−51.
[92] Baldizonne R, Carianni G, Mariani P. A new Ziegler-Natta octene LLDPE for high performance blown film applications: benefits of coextruded vs. blended LDPE/LLDPE films. In: European TAPPI PLACE conference; 2005.
[93] Davidson DL, Swartz D. Unique antiblocks for high clarity polyethylene film. In: SPE ANTEC conference; 2004. p. 1111−6.
[94] Im J, Schrenk WJ. Coextruded microlayer sheet and film. J Plast Film Sheeting 1988;4:104−15.
[95] Hiltner A, Nazarenko S, Ebeling T, Schuman T, Baer E. Novel microlayered structures for adhesion and interdiffusion studies. Polym Mater Sci Eng 1996;75:471.
[96] Tangirala R, Baer E, Hiltner A, Weder C. Photopatternable reflective films produced by nanolayer extrusion. Adv Funct Mater 2004;14:595−604.
[97] Kazmierczak T, Song H, Hiltner A, Baer E. Polymeric one-dimensional photonic crystals by continuous coextrusion. Macromol Rapid Commun 2007;28:2210−6.
[98] Lai C-Y, Baer E. The interdiffusion of polymeric gradient refractive index (GRIN) lens materials. In: SPE ANTEC conference; 2011.
[99] Mackey M, Wolak M, Shirk J, Flandin L, Hiltner A, Baer E. Enhanced dielectric properties of micro and nanolayered films for capacitor applications. In: SPE ANTEC conference; 2011.
[100] Ponting M, Hiltner A, Baer E. Gradient multilayered films by forced assembly coextrusion. In: SPE ANTEC conference; 2009.
[101] Tai HT, Hiltner A, Baer E, Wiggins M, Sandrock M, Shirk J. Tunable reflective polymeric nanolayered films. In: SPE ANTEC conference; 2005.
[102] Pointing M, Hiltner A, Baer E. Gradient multilayer films by forced assembly. In: SPE ANTEC conference; 2009.

PART V: EFFECT OF THE CONVERTING PROCESS ON PROPERTIES

Part IV focuses primarily on how the resin or substrate properties affect film properties. Such properties cannot be isolated from the process used to make the film. The process has profound effects on orientation, crystallization, interlayer adhesion, and other aspects of product performance. While process—structure—property relationships have been well studied in the literature for monolayer films, coextruded films have received much less attention. This section describes in detail the effects the converting process has on film properties with a focus on coextrusion blown and cast film and extrusion coating and lamination.

The properties of polymer films are dependent upon the process by which they are made. A polymer has inherent characteristics determined by its chemical make-up: length of its molecules, presence of bulky side groups, nature of bonds that form between molecules, and so on. These characteristics, in response to the stress and temperature history imposed by the process, create macroscopic features that determine the film properties. These features include ordering of the molecules into crystals, the distribution or morphology of these crystals, the strength or density of tie molecules that bind the crystalline regions to each other, and orientation of molecular chains.

The stress imposed by the process is a function of the strain, strain rate, and the temperature at which the strain is imposed. A process that stretches the polymer near the melting temperature imposes more stress than a process that imposes the same strain at higher temperature where the polymer can flow. The timescale of the process where the stress is applied must be compared with the fundamental timescales of the polymer. These include the following:

- relaxation time of the polymer versus process time (Deborah number)
- crystallization versus process time (quench rate)
- adhesion versus process time (kinetics of reaction and diffusion vs. new area generation).

The fundamental flow characteristics must also be considered, especially for coextrusion of dissimilar materials. Flow instabilities may arise if the polymers are not well matched. Such instabilities directly affect what materials can be successfully coextruded and may limit the choice of materials or the design of the coextruded structure.

This section is organized into three chapters. Chapter 13 describes how the process affects film quality and properties. Thermal instability gives rise to gel, flow instability produces surface imperfections (“wood grain”) and other appearance issues, and differences in shrinkage and crystallinity produce curl. These issues are scrutinized as they are vital to making functional film. The stress—strain history and quench rate influence film properties through their effect on orientation and crystallinity. These factors are illustrated in Chapter 14 by examining features of the blown film process:

- differences in stress history between monolayer and coextrusion processes and their effect on properties;
- differences between air- and water-quench blown film;
- the development of elongated morphology in polymer blends.

Chapter 15 provides a comprehensive look at how the process affects adhesion in coextrusion.

13 Effect of Processing on Quality

The film fabrication or coating process affects product quality in a number of ways. Quality issues can arise when the process is not under control: surges in output or variability in processing parameters such as temperature or draw rates, to name a few, can affect product quality. A number of references deal with troubleshooting of polymer processes that the reader is referred to for methods to ensure good extrusion, film fabrication, and coating operations [1–9]. This chapter focuses on some of the unique processing issues that are encountered in coextrusion: thermal stability issues that may occur when coextruding resins of different melting points, flow maldistribution and instability issues when polymers of different rheological characteristics are brought together, and curl of multilayer film comprised of layers that shrink by different amounts during quenching. These issues may limit the use of certain combinations of materials in the fabrication of flexible packaging films and should be understood by processors and film designers alike.

13.1 Thermal Stability

Processing polymers above their thermal stability temperature limit can create gel, black specs, and organoleptic issues (from oxidative and thermal degradation by-products). Butler [9] and Spalding and Campbell [3,10] provide good overviews of gel issues. Thermal stability problems in coextrusion are sometimes encountered when combining polymers with substantially different melting points. For example, coextruding an ethylene vinyl acetate (EVA)-based tie resin with polyethylene terephthalate (PET) is problematic since the PET must be processed at greater than 280°C to melt the polymer. Suppliers of EVA recommend not processing EVA above about 230°C due to its limited thermal stability. The fundamental stability issue can be addressed by either using an ethylene methyl acrylate (EMA)-based tie resin, which has greater stability or substituting the PET with a lower melting copolymer such as polyethylene terephthalate glycol copolymer (PETG).

Determining the source of gel can be a challenge in coextrusion, particularly if it is large enough to distort the layers around it or affects more than one layer. Microscopy can be used to try to identify the layer. FTIR is useful for identifying the composition of the gel, although this can be difficult if the gel particle is grossly decomposed. Hot stage microscopy can help determine if the gel particle is cross-linked or simply unmelt.

Sources of gel and film defects include the following:

- Unmelted particles of the same composition as the layer. The extrusion screw design and processing conditions may need to be optimized if this is the case.
- Foreign contamination, such as fibers, insects, and other particles.
- Foreign contamination from other resin particles/pellets. This is sometimes called particle cross-contamination. This may arise from contamination at the resin manufacturer or the converter and typically occurs when pellets of one polymer inadvertently mix with another. Pellets of the same product family but significantly different in molecular weight (MW) may have difficulty in melting completely and cause this type of gel. Pellets from resins of differing chemistry may not melt completely if they have a higher melting point, thermally degrade if they have poor thermal stability, or in extreme cases react with the main pellets to cause cross-linked resin. Valves on blenders, hoppers, and transfer devices are notorious for hang-ups where polymer from several runs prior may be present and slough off into the main stream.
- Fines, angle hair, and longs. These are typically generated during transport of the polymer pellets through transfer pipes. Because they have

The Science and Technology of Flexible Packaging. http://dx.doi.org/10.1016/B978-0-323-24273-8.00013-7
Copyright © 2017 Elsevier Inc. All rights reserved.

different shapes, they may process differently resulting in unmelt, gel, or black specs.

- Degraded polymer. This can occur anywhere along the manufacturing process from resin manufacturer to converter. Degradation is generally due to long holdup times at high temperatures. Oxidation is often involved.

The gel can be present in the incoming resin as received from the resin supplier or be created during the converting operation. Some questions to answer to determine the source of the gel include the following:

- Does the gel occur randomly or is it steady? A steady stream of gel particles coming out of the die may indicate a hang-up somewhere in the extruder or die.
- Is the gel distributed uniformly throughout the melt curtain or bubble or in a single location? Uniform or random location of the gel may indicate the gel was in the resin prior to extrusion. If the gel is in a single location, however, it is more likely to have originated in the extruder or die.
- Does the amount of gel increase when the polymer throughput is increased? If the gel is in the incoming resin, increasing throughput should increase the amount of gel that comes through.
- Does the gel stop when a different lot is introduced into the extruder? To definitively determine if there is a bad lot, reintroduce the trouble lot and see if the gel returns.

Thoroughly cleaning hoppers and transfer lines when switching resins is critical for preventing gel. Good purging practices are also important. Functional polymers such as acid copolymers, ionomers, and tie resins often have an affinity to stick to metal surfaces, making purging more challenging. They also tend to react with polymers that may have hung up from previous runs, pushing them out in a shower of gel. Because of this, they may be blamed for a past problem.

Some tips for efficient purging include the following:

- Empty the hopper prior to introducing the new resin, but do not allow the extruder to run empty while running at production speed. The heat from the process is carried away by the polymer. If the polymer feed is reduced while the extruder is still operating at full speed, the energy will be absorbed by less polymer mass, causing the temperature of the remaining polymer to spike higher. This can cause degradation. In severe cases, off-gassing may cause pressure to build up inside the extruder, which can be dangerous.
- Introduce the new resin [or an inert purge resin such as polyethylene (PE) or polypropylene (PP)].
- If the new resin is run at higher temperature settings than the old one, allow the new polymer to be completely introduced before raising the temperature settings. This helps the prior resin from seeing too much temperature. (If the new resin has a higher melting point than the operating temperature of the old resin, this will have to be modified. Slowing down the line before raising the temperature is recommended in this case.)
- Likewise, if the new resin is run at a colder temperature than the old resin, lower the temperature first before introducing the new resin.
- Vary the speed of the extruder in random intervals for 1−5 min each. The variable speed is important for dislodging hang-up resin. By changing the screw speed, the shear rate is varied and with it the viscosity. A higher viscosity helps push out a lower viscosity resin. Different polymers respond differently to changes in shear rate; by varying the screw speed the chances of hitting upon a favorable shear rate for dislodging the incumbent resin is increased. DuPont calls this the disco purge procedure (after the 1980s dance craze). An illustration of the DuPont disco purge method is given in Fig. 13.1. This procedure has been found to be more efficient than running the purge resin at a constant screw speed [11].
- Repeat the procedure if necessary. More than one iteration of the disco purge procedure may be required, especially for more complex dies such as those found in blown film.
- Purge compounds can be effective for cleaning the extruder. These compounds often contain foaming agents, inorganic scrubbing additives such as silica, and reactive compounds to help remove degraded polymer deposits. Carefully follow the instructions from the supplier. Purging

Worksheet for Disco Purge Procedure

MAXIMUM EXTRUDER RPM = _____ RPM

1st min: 30% of MAX = 0.30 x _____ RPM = _____RPM

2nd min: 90% of MAX = 0.90 x _____ RPM = _____RPM

3rd min: 50% of MAX = 0.50 x _____ RPM = _____RPM

4th min: 15% of MAX = 0.15 x _____ RPM = _____RPM

5th min: 70% of MAX = 0.70 x _____ RPM = _____RPM

Minutes 6-10: 15 to 20% of MAX =

0.15 x _____ RPM = _____RPM

to 0.20 x _____ RPM = _____RPM

Minutes 11 to 15: Repeat the cycling steps of the first 5 min.

Figure 13.1 Worksheet for DuPont "disco" purge procedure. *From DuPont. The disco purge procedure for extrusion coaters, http://www.dupont.com//content/dam/dupont/products-and-services/packaging-materials-and-solutions/packaging-materials-and-solutions-landing/documents/disco_purge_procedure_.pdf; 2005. Reprinted with permission from E. I. du Pont de Nemours and Company.*

these compounds out can be difficult and may take more resin than normal purging. The use of purge compounds, however, is warranted when polymer has degraded in the extruder or die and when a particularly thorough cleanup is needed.

Degradation of some polymers can create by-products that are detrimental to equipment or human health. PVDC, for example, can degrade into corrosive chlorine compounds. Coextrusion lines running PVDC are typically designed to isolate the temperature the PVDC layer sees to help prevent degradation. Thermal degradation of polymers may evolve fumes containing carbon monoxide, acrolein, and other by-products. Proper ventilation is required [12].

13.2 Die Drool

Die drool, also known as die lip buildup, die drip, and plate-out, is the unwanted deposit and accumulation of material on the die face during extrusion. The material can slough off onto the film or coating resulting in product defects or line breaks. Increased machine down time to clean the die of accumulated drool hurts productivity. Die drool is a problem with monolayer and coextrusion processes and has been reviewed by Gander and Giacomin [13] and Musil and Zatloukal [14,15]. Many factors influence die drool; Zatloukal [15] provides an extensive list shown in Table 13.1.

The root causes of die drool are not completely understood and are likely due to multiple mechanisms, some specific to particular polymer systems. Musil categorizes die drool into internal and external origins. External die drool is related to the die exit region only and is more easily rectified; flaring of the exit angle generally reduces this type of drool. Internal die drool is related to the die exit as well as flow channels upstream of the die exit, such as the extruder screw, barrel, transition pipes, and die.

Flow-induced fractionation of the polymer is one of the proposed mechanisms. As polymers flow, low MW components tend to migrate toward the high shear rate region near the die wall. Musil [16,17] shows that for high density polyethylene (HDPE) significant fractionation only occurs very near the die wall, and that fractionation and die drool increase with increasing linear chain length. Increasing the polymer chain length is associated with increasing melt elasticity and shear viscosity. Long chain branching is found to reduce die drool. These polymer characteristics also influence slip-stick flow behavior, which they conclude is associated with die drool for this polymer. Slip-stick is a phenomenon where the flow changes from zero velocity at the die wall to a finite velocity (known as the slip velocity) and back. Musil also find that thermal degradation of HDPE inside the processing equipment upstream of the die exit can increase melt elasticity and die drool [18].

Table 13.1 Factors Influencing Die Drool

Category	Factors
Die design	Abrupt corners at die lips "Dead corners" inside extrusion die (thermal degradation) High-surface energy die wall materials High surface roughness Short die land length
Polymer material	Low molecular weight fractions Multimodal polymers (low molecular weight tail) High elasticity of polymer Linear architecture of polymer High filler content High concentration/incompatible additives or pigments High concentration of volatiles (eg, moisture) Dissimilar material properties in blends High content of stearates, ester lubricants, extending oils, or waxes Chemical reactions between polymer and metal barrel/screw/die (PVC or PVDC resins)
Processing conditions	High processing temperature (thermal degradation) Draw down Intensive cooling of die exit
Other factors	Melt swell Shark skin Wall slip Vortices (thermal degradation) Slip-stick flow Pressure fluctuations in screw Excessive screw/barrel wear

Adapted from Zatloukal M, Musil J. Die drool phenomenon in polymer extrusion. In: SPE ANTEC conference; 2014. p. 1048–54.

Hogan [19] investigates whether melt swell is related to die drool. Melt swell (also known as die swell) is the expansion of the polymer as it exits the die; it increases with increasing elasticity of the polymer but is present even in nonelastic (Newtonian) materials. In a series of experiments with capillary dies, they find that as the length to diameter ratio (L/D) is increased the melt swell decreases (as expected) but die drool increases. Their experiments with different shear rates and residence times provide further evidence that shear-induced migration of low MW species toward the die wall contributes to die drool.

Holtzen and Musiano [20] study the effect of pigments on die drool. The addition of pigments such as TiO_2 is known to exacerbate die drool. They conclude that plate-out can originate at flow disturbances upstream of the die lips, typically in a region of abrupt change, such as the entrance region of the die. Viscoelastic polymers have a tendency to form vortices or dead zones behind flow disturbances. Holtzen's experimental studies show that the vortices that form behind burrs or even degraded polymer can give rise to plate-out. They postulate that polymer trapped in the vortices can degrade over time into more polar species (through oxidation) that adhere to the die walls and eventually come out as die drool. Their experiments show streaks of degraded polymer working their way up the die channel in accordance with this theory.

The tendency for vortices to form depends on the channel geometry and the viscoelastic nature of the polymer. They use the Deborah number (De) as a way to characterize the viscoelastic nature of the flow. The Deborah number is the ratio of the characteristic relaxation time of the polymer to the characteristic time of the process:

$$De = \frac{\lambda}{t_p} \tag{13.1}$$

where De = Deborah number; λ = polymer relaxation time; t_p = process time.

Increasing polymer throughput (decreasing t_p) increases De. Increasing the polymer MW and amount of long chain branching (which increase λ) also increases De. Vortices will form more readily in flows with high De. By varying the throughput in their experiments, they find that increasing De increases the amount of die drool.

Their work suggests two reasons why pigment particles tend to be implicated in die drool problems. The first is that the particles bind to some of the polymer molecules, reducing the polymer's mobility. This increases the relaxation time of the polymer and increases De. The ability of the pigment particle to bind to the polymer depends on the surface coating on the pigment. Holtzen's study finds the surface coating on TiO_2 has a significant impact on die drool. Secondly, some pigments reduce the thermal stability of the polymer; polymer caught up in the vortex is more likely to degrade and cause die buildup.

Another implication of Holtzen's work is that the entrance geometry of the die channel is important: more streamlined flow will reduce the tendency for dead zones to form. Elbows and sudden expansion of flow channels should be avoided. Elimination of burrs and other protrusions in the flow channel is also essential. Paying attention to the materials of construction, specifically the surface finish, may help reduce die drool. Lowering processing temperatures to help prevent polymer degradation may also help minimize die drool.

The die exit region has garnered considerable attention for both the origin of die drool and the means to mitigate it. As the polymer emerges from the die, the flow at the die wall transitions from no-flow to free-surface flow. This is illustrated in Fig. 13.2. This sudden acceleration has been implicated in causing die drool. Gander [13] shows that this boundary between the solid wall, liquid polymer, and air is a high stress region; they suggest high stress may fractionate or rupture the polymer, releasing low MW components. Zatloukal [21] and Chaloupkova [22] use finite element modeling to show that this acceleration creates a negative pressure that extends inside the die. They propose that the negative pressure may suck low MW species toward the wall and surfaces of the die at the exit.

Flaring or chamfering the die exit region has been found to be an effective means to reduce die drool [23]. Gander explains this in terms of stress. In a converging flow channel the stress will overshoot, exacerbating the die drool (causing more fractionation). In a flared or diverging channel, the stress will undershoot, reducing the fractionation. Zatloukal [15] shows that chamfering reduces the negative pressure at the die exit with a 45 degrees angle having the best results.

Addition of polymer processing aids (PPAs), particularly fluoroelastomers, has been shown to reduce die drool [13]. Modifying the die surface with a low surface energy coating (such as a fluoropolymer) has also proven successful [24]. These techniques reduce the adhesion between the polymer and

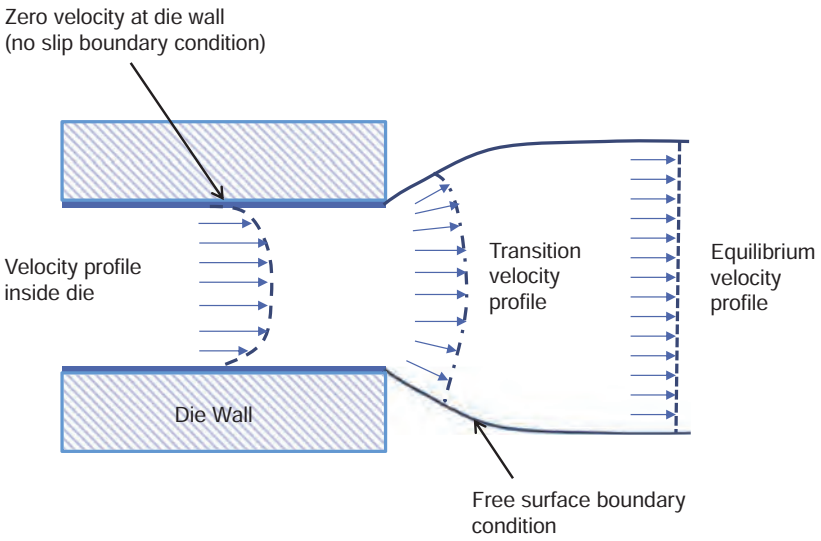


Figure 13.2 Illustration of flow rearrangement at the die exit.

channel wall. This relaxes the no-slip condition at the die wall; slip flow along the wall reduces the shear rate at the wall and the driving force for fractionation. Furthermore, the presence of slip flow reduces the amount of flow rearrangement and acceleration at the die exit. This reduces the stress and the negative pressure, further decreasing the driving force for migration of low MW species to the die surfaces.

Moisture entrained with the polymer, or generated during extrusion, can contribute to plate-out. Most polyolefins contain negligible moisture due to their hydrophobic nature, but various mineral fillers, pigments, or other additives may absorb moisture that can be volatilized during extrusion. Polar polymers, such as acid copolymers and ionomers, also have the ability to pick up moisture if not handled properly prior to extrusion. Acid copolymers can also generate moisture during extrusion when adjacent acid groups react to form anhydride groups; higher acid grades are more prone to moisture evolution due to the greater probability that acid groups will come into contact. As the polymer exits the die, the pressure drops and allows the water vapor (and other volatiles) to escape. As it does, the polymer may rupture or small bits of polymer may be entrained and impinge upon the external die surface. Avoiding moisture issues can be as easy as ensuring open boxes of hydrophilic resins are kept closed during operations, or in the case of acid copolymers, using the proper screw design, processing at optimal conditions, and selecting a grade that is less prone to problems.

Many other factors have been implicated in die drool as delineated in Table 13.1. More than one may be involved in a specific problem and a systematic approach to resolving issues is recommended. The reader is referred to the review articles mentioned at the beginning of this section for more ideas on how to address the problem.

13.3 Moisture-Related Issues

Condensation polymers such as polyester and polyamide (PA) are susceptible to chain scission if moisture is present during extrusion. This reduces the MW and can make the polymer brittle. Also, lower MW reduces the melt viscosity, which can lead to flow instability issues during coextrusion (Section 13.4). Most polyester resins need to be dried prior to extrusion. The resin supplier can provide guidance as to the proper drying conditions. PA resins are packaged dry in moisture-resistant packaging; they generally can be used without drying if they are processed immediately after opening the bag or box and care is taken to keep moisture out during processing.

As described in Section 13.2, moisture absorbed by the polymer prior to extrusion can contribute to die drool. Moisture can also show up as a bubble pattern in the film known as lace curtain. The water molecules are soluble in the molten polymer under pressure in the die. When the pressure is released at the die exit, the water expands, forming bubbles. Generally there is a threshold temperature and water concentration at which this occurs; as the processing temperature is increased, the maximum amount of water than can be entrained with the polymer without generating bubbles decreases. Resin moisture tends to present more problems in higher temperature processes such as extrusion coating compared to lower temperature processes.

13.4 Flow Maldistribution and Instability Issues

The fabrication of coextruded films and coatings involves complex flows at high elongation and shear rates. These give rise to various flow issues that affect product quality. The specific issues described below have their origins in the viscoelastic nature of polymers or in the hydrodynamics of the process. Perhaps the largest cause of quality issues in film and coating is extruder instability and should not be overlooked. Most flow issues arise from poor melt quality to the feedblock or die. This is true for coextrusion or monolayer extrusion. The pressure variation should be less than one percent and the temperature uniform to ensure good film converting. This can generally be achieved through proper screw design and processing conditions. The reader is referred to a number of useful books that cover this topic [1–7].

13.4.1 Sharkskin and Extrudate Distortion

This family of defects has a variety of names and causes, some of which are still unknown or debated in the scientific community. They have been studied for well over 50 years and subject to periodic reviews, including those by Koopmans [25] and Vergnes [26]. These defects have dramatically different characteristics for linear and branched

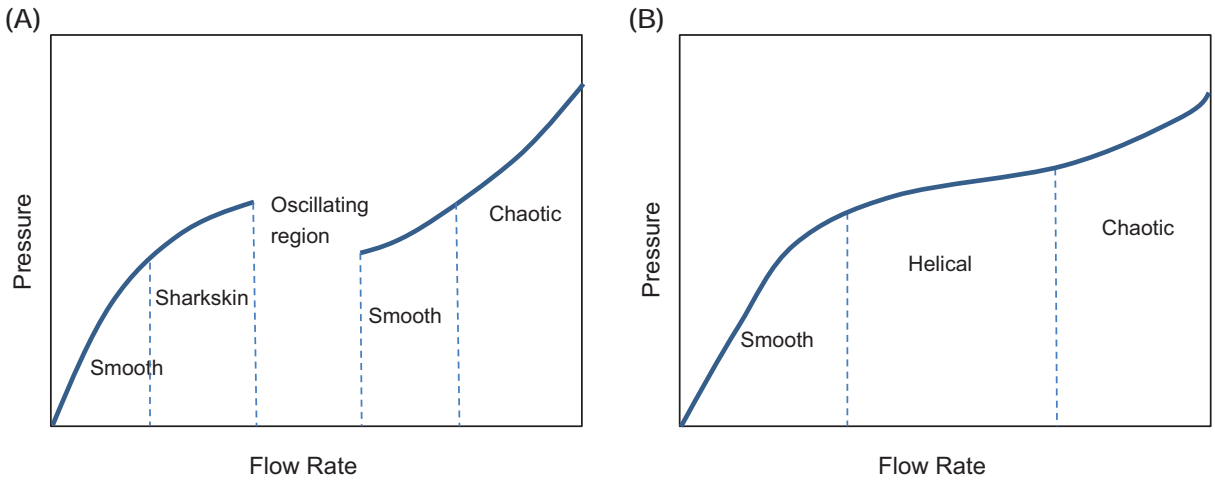


Figure 13.3 Extrudate distortion flow curves for linear (A) and branched (B) polymers.
Adapted from Vergnes B. Extrusion defects and flow instabilities of molten polymers. Intern Polym Process 2015;XXX:3–28.

polymers. One way to characterize these defects is to consider the behavior of the extrudate emanating from a die as the flow rate is increased. As depicted in Fig. 13.3, the extrudate of linear polymers such as HDPE and linear low density polyethylene (LLDPE) at low flow rate is smooth. As the flow rate is increased, the surface starts to become rough. This is typically seen as a loss of gloss and transparency. With higher flow, the surface defect takes on a regular pattern of ridges on the surface perpendicular to the flow. This surface texture is commonly called sharkskin.

Sharkskin originates at the die exit. It is associated with the abrupt transition from the confined flow in the die to the free surface flow at the die exit described in Section 13.2 and illustrated in Fig. 13.2. There are two explanations still being debated in the literature. One involves slip-stick behavior at the die wall. The other involves rupture of the skin of the extrudate due to the elongational stresses arising from the acceleration in velocity of the polymer as it changes from parabolic flow to plug flow at the die exit.

With further increases in flow rate, the pressure becomes unstable with regular oscillations. The flow curve, depicted in Fig. 13.3A, is discontinuous: the flow switches between regions of smooth flow and sharkskin. This is known as oscillatory or slip-stick flow. The latter describes what has been experimentally observed as the mechanism for the behavior. As the pressure oscillates, the flow at the wall jumps from the traditional no-slip condition to a finite slip velocity. The cause of this seems to be an entanglement–disentanglement transition of polymer chains adsorbed onto the wall [26].

At higher flow rates, the flow may become stable and smooth before eventually, at still higher flow rates, it becomes chaotic. The chaotic flow is known as extrudate distortion or gross melt fracture. This severe distortion in many polymer systems appears to originate in the die entrance region.

Branched polymers like low density polyethylene (LDPE), as well as polystyrene (PS) and some polypropylene (PP) grades, do not exhibit sharkskin or slip-stick flow. Instead, they transition to helical flow, where the extrudate has a regular screw-like appearance. As shown in Fig. 13.3B, at higher flow rate, the flow becomes chaotic, exhibiting behavior similar to the linear polymers at high flow rates.

The phenomenon that is responsible for these defects may be specific to each polymer. There are a number of factors that have been found to influence these defects, which include the following [27]:

- chemical nature of the polymer;
- polymer MW and molecular weight distribution (MWD);
- polymer branching;
- die entrance geometry;
- length to diameter ratio (L/D) of capillary or die;
- material of construction of the capillary or die;
- temperature;
- flow rate.

As stated previously, long chain branching prevents the formation of sharkskin. Indeed, when LLDPE was first introduced in the 1970s, it could only be run on blown film equipment designed to run LDPE at severely reduced rates due to sharkskin and bubble instabilities. Several methods used to eliminate or postpone the onset of sharkskin include the following:

- Reducing the output. This is not a desirable fix but can be a short-term solution while other methods are evaluated.
- Increasing the die gap. This can cause some cooling issues, which have been resolved by equipment design improvements over the years. LLDPE is typically run commercially today with a wider die gap than LDPE. It also may lead to some property changes.
- Heating the die lips. This reduces the viscosity and stress at the wall.
- Increasing the MWD or decreasing the MW of the linear polymer. This can result in loss of film strength and other property changes.
- Utilizing coextrusion to add lower viscosity skin layers. This lowers the stress at the wall to reduce sharkskin while maintaining a higher MW core layer to retain film physical properties.
- Lowering the surface energy of the metal surface. Brass and some other metals have been found in the lab to suppress sharkskin but Vergnes comments that this is not done commercially. Coating with fluoropolymer or other techniques to enhance slip at the wall has also been proposed.
- Using PPAs. These are described in Section 13.2. Typically made from fluoroelastomers, these are added in small amounts to the polymer. After an induction time of several minutes, the PPA coats the die walls. The PPA is continuously added with the polymer to replenish the coating that is sloughed off during flow. The generally accepted mechanism is that the coating aids in the slip of the polymer flow along the die wall (known as slip flow). This helps reduce the magnitude of flow acceleration at the die exit. Ramamurthy [28] proposes, however, that the PPA works by increasing the adhesion at the die wall.

The use of PPAs is also the most practical method to postpone slip-stick or oscillatory flow to higher throughput. Other methods have been tried in the lab but are not practical for commercial operations.

For both linear and branched polymers the helical instability and chaotic or gross melt fracture have been shown to originate in the entrance region of the die. The main method for reducing the onset of these instabilities is to reduce the entrance angle. Vergnes [26] reports that the use of a smooth convergent entrance whose angle varies continuously between the reservoir and the die land increases the throughput (at the onset of gross melt fracture) by a factor of six over an abrupt 90 degrees entry. For a long time it was thought that the disruption of eddies or secondary flow at an abrupt entrance was responsible for these instabilities; but it has been shown that such eddies do not exist for linear polymers and are not needed for gross melt fracture to occur. Extensional stresses may be involved; Vergnes finds evidence for a critical extensional stress above which distortion develops.

Another method that has been successful for reducing extrudate distortion is increasing the temperature. The lower viscosity reduces the stress. A longer die land can also sometimes help.

13.4.2 Draw Down Instabilities in Extrusion Coating/Lamination and Cast Film

13.4.2.1 Neck-In and Edge Bead

As the molten polymer is drawn from the die exit to the chill roll in extrusion coating and cast film, the width of the web decreases. This is known as neck-in and is illustrated in Fig. 13.4. It arises from the contraction that must occur in the transverse directions (TDs) as the polymer is stretched in the machine direction (MD). Neck-in affects productivity since the processer does not have the ability to utilize the full width of the die. It also contributes to a thickening of the web near the outside edge of the web. This is known as edge bead and is sometimes referred to as a dog bone profile. This too affects productivity since the edges that fall out of specification must be slit and removed (edge trim). Examples of neck-in and edge bead are shown in Figs. 13.5 and 13.6 for an LLDPE and LDPE resin, respectively.

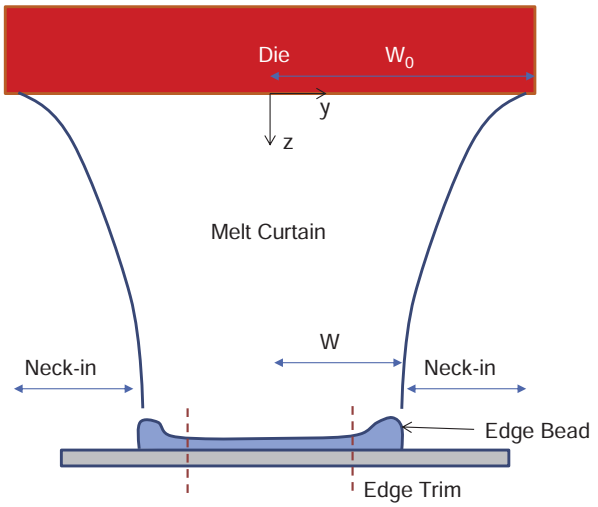


Figure 13.4 Definition of neck-in, edge bead, and coordinate variables in extrusion coating and cast film.

Neck-in is influenced by both the melt strength of the polymer and processing parameters. This is seen in the numerical simulation work of Debbaut [30]. Fig. 13.7 shows the width or neck-in ratio as a function of draw ratio (the ratio of the line speed to the velocity at the die exit and can be estimated by the ratio of the die gap to the final film or coating thickness—Eq. 2.16) for a Newtonian and a Giesekus fluid. A Newtonian fluid is purely viscous whereas a Giesekus fluid includes elasticity (shear thinning and strain hardening in extension) that generally gives rise to melt strength. The viscoelastic fluid has less neck-in. Canning and Co [121] study the neck-in of an LDPE and two LLDPE resins. The LDPE exhibits extensional hardening behavior and its neck-in decreases with increasing draw ratio, in agreement with the Giesekus fluid of Debbaut's model. The neck-in of the LLDPE resins increases with increasing draw ratio, agreeing with Debbaut's analysis of a Maxwell fluid, which exhibits shear thinning but not extensional hardening. Other investigators have found similar results [123–126].

Fig. 13.8 shows the simulation for constant draw ratio but different Deborah numbers (De) [Eq. (13.1)]. $De = 0$ corresponds to a Newtonian fluid and increasing values of De represent greater elasticity or melt strength. As De increases, the neck-in decreases (neck-in ratio increases), as indicated by the longer lines along the $y/2W_0$ axis. Also, as De increases, the shape of the thickness profile changes; the thickness remains steady over a wider swatch (until the very edge of the melt curtain). This is important for product quality and productivity as less of the edge will need to be trimmed. Note that the actual thickness ratio (X/X_0) at the edge of the web is about the same for the different Deborah numbers. In industry, the Rheotens melt tension measurement (Section 5.3.6) is often used as a measure of melt strength. Polymers with higher melt tension generally have lower neck-in. Polymers with higher MW, broader MWD, or long chain branches typically have higher melt strength. Ionomers, with their ionic interactions, have exceptionally high

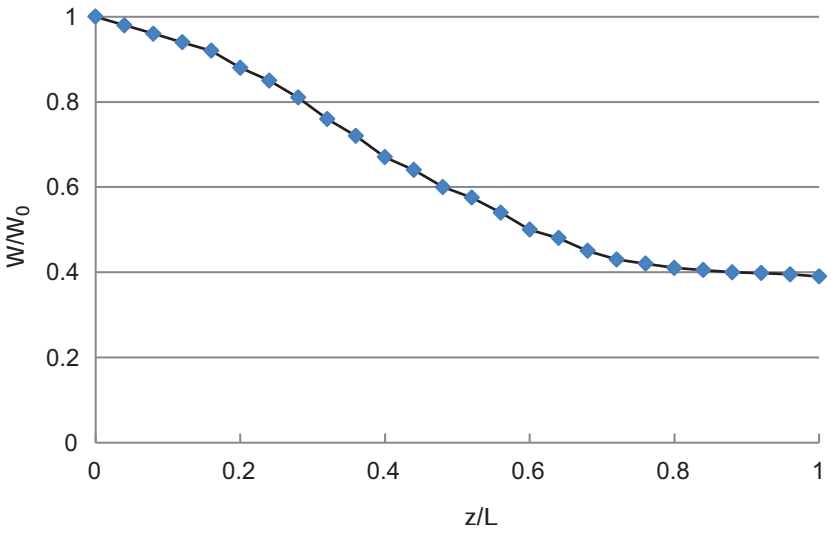


Figure 13.5 Change in width ($2W$) of an LLDPE extrusion cast film as a function of distance from the die exit. $2W_0$, die width; L, distance from die exit to chill roll (air gap); z, distance from die exit.
Experimental data from Silagy D, Demay Y, Agassant JF. Stationary and stability analysis of the film casting process. J Non-Newtonian Fluid Mech 1998;79:563–83.

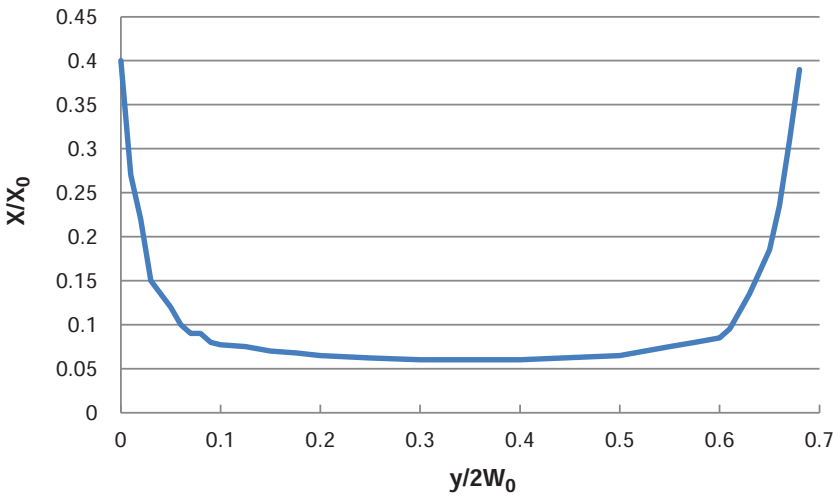


Figure 13.6 Thickness profile across a cast film of LDPE illustrating edge bead. $2W_0$, die width; y, distance from left edge to position along the width of the web; X, thickness; X_0, thickness of die gap.
Experimental data from Silagy D, Demay Y, Agassant JF. Stationary and stability analysis of the film casting process. J Non-Newtonian Fluid Mech 1998;79:563–83.

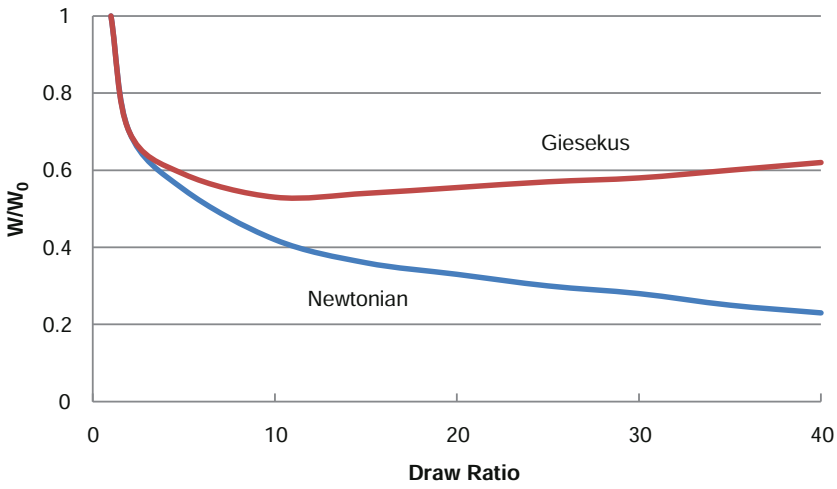


Figure 13.7 Effect of draw ratio and polymer viscoelasticity on neck-in. The Newtonian fluid is purely viscous whereas the Giesekus fluid has viscous and elastic behavior.
From numerical simulations of Debbaut B, Marchal JM. Viscoelastic effects in film casting. In: Theoretical, experimental, and numerical contributions to the mechanics of fluids and solids. Z. Angew Math Phys 1995;46(Special Issue):S679–98.

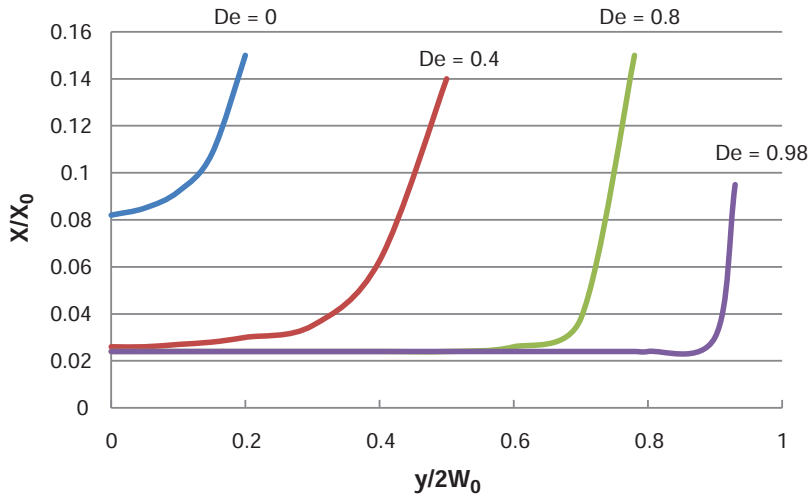


Figure 13.8 Effect of Deborah number (*De*) on neck-in and edge bead. Here y is the distance in the width dimension from centerline (differs from Fig. 13.6). Thickness ratio is taken at the chill roll. Draw ratio is constant at 40.
From numerical simulations of Debbaut B, Marchal JM. Viscoelastic effects in film casting. In: Theoretical, experimental, and numerical contributions to the mechanics of fluids and solids. Z. Angew Math Phys 1995;46(Special Issue):S679–98.

melt strength for polyolefins. Increasing the melt temperature reduces melt strength and increases neck-in.

Figs. 13.7 and 13.8 also show how processing affects neck-in. Draw ratio is directly related to the ratio of the die gap to the coat weight or film thickness. If the die gap is kept constant, increasing the coating or film thickness will decrease the draw ratio. Fig. 13.7 shows that this will increase the amount of neck-in (depending on the elasticity of the polymer). Likewise, the Deborah number in Fig. 13.8 is proportional to the line speed and inversely proportional to the air gap. At constant draw ratio and coating or film thickness, Fig. 13.8 indicates that increasing the line speed or decreasing the air gap will reduce neck-in. This is shown more explicitly in Table 13.2, which shows some unpublished data by Foederer and Morris [31] collected while conducting a temperature in the air gap study. LDPE is extrusion coated onto paper at a melt temperature of 324°C. The die width and gap are kept constant at 91 cm (36 in.) and 760 μm (30 mils), respectively. The coat weight (final thickness) is varied from 6.4 to 25.4 μm (0.25−1 mil), the air gap from 17.8 to 28 cm (7−14 in.), and line speed from 152 to 457 m/min (500−1500 fpm). The neck-in is recorded as the total reduction in width from both edges at the chill roll. For example, if the final coating width was 81 cm, the neck-in was recorded as 10 cm (91 cm die width—81 cm final width).

The results are plotted in Fig. 13.9 as a function of line speed. The plot of main effects from a statistical analysis (Fig. 13.10) shows that increasing air gap and reducing coat weight substantially increase the neck-in. The effect of line speed is less pronounced in this study. The results are consistent with the numerical analysis of Debbaut.

Neck-in can be reduced by the following actions:

- Increasing the melt strength of the polymer. Polyolefins with long chain branching (LDPE, EVA, EMA, EAA, EMAA, and ionomers) exhibit less neck-in than linear polymers such as LLDPE and HDPE. Broader MWD and higher MW (lower MI) may also help.
- Decreasing the melt temperature. This increases the melt strength.
- Decreasing the air gap or increase the line speed (at constant draw ratio, which occurs when the die gap and final film or coating thickness are held constant). This reduces the characteristic process time, which for this process is the time in the air gap, and increases the Deborah number. Higher *De* is an indication of higher elasticity and melt strength.

Table 13.2 Neck-In Data From an Extrusion Coating Trial. LDPE was Coated at 324°C Using a Cloeren Edge Bead Reduction Die (57 mm Plug and 32 mm Flag Settings). The LDPE had a Density of 0.923 g/cc and Melt Index (190°C/2160 g) of 4.5 g/10 min. Deckled Die Width was 91 cm and Die Gap 760 μm

Line Speed (m/min)	Coat Weight (μm)	Air Gap (cm)	Neck-In (cm)
152	6.4	18	11
152	6.4	28	16
152	12.7	18	9
152	12.7	28	14
213	12.7	28	12
213	12.7	18	8
152	25.4	18	8
152	25.4	28	12
305	25.4	28	11
305	25.4	18	7
457	25.4	18	7
457	25.4	28	11

Data courtesy of Foederer BM, Morris BA. Use of IR technology to model temperature loss in the air gap. In: TAPPI PLACE conference; 2014.

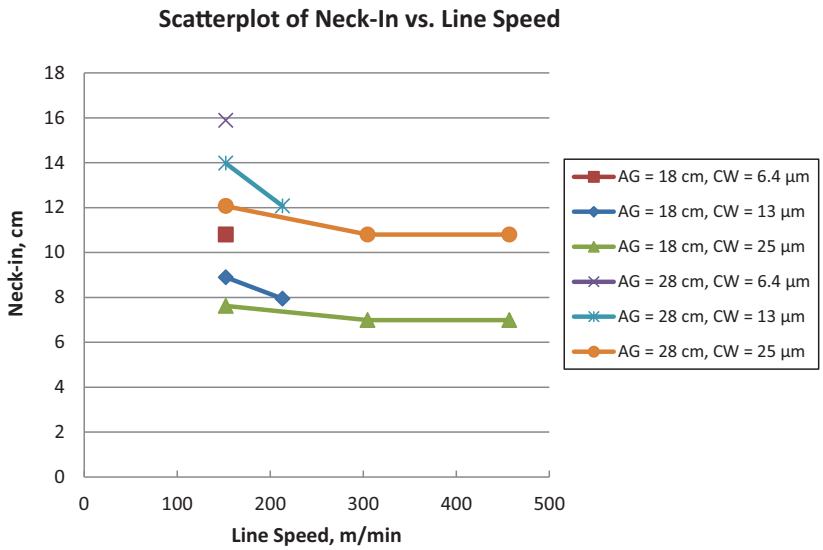


Figure 13.9 Scatterplot of neck-in experimental results from Table 13.2.
Data courtesy of Foederer BM, Morris BA. Use of IR technology to model temperature loss in the air gap. In: TAPPI PLACE conference; 2014.

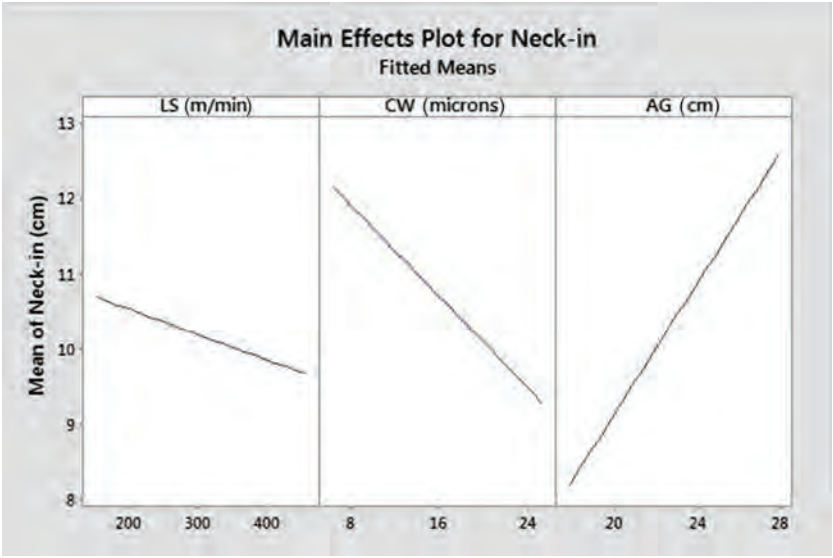


Figure 13.10 Main effects of plot from statistical analysis of neck-in data from Table 13.2. *LS*, line speed; *CW*, coat weight; *AG*, air gap.

- For linear polymers, increasing the coating or film thickness (at constant die gap). This decreases the draw ratio.
- For linear polymers, decreasing the die gap (at constant coating or film thickness). This decreases the draw ratio.
- For highly elastic polymers, reducing the stress in the die exit region by modifying the die design to allow for more relaxation. Zatloukal and Barborik [125] shows that greater stress at the die exit increases neck-in for polymers with long relaxation times (which is typical for polymers with long chain branching).

Edge bead arises from an unbalance of forces at the edge of the melt curtain due to the free surface [32]. This is illustrated in Fig. 13.11. As the melt curtain is stretched in the MD, it contracts in the transverse and thickness dimensions; the draw

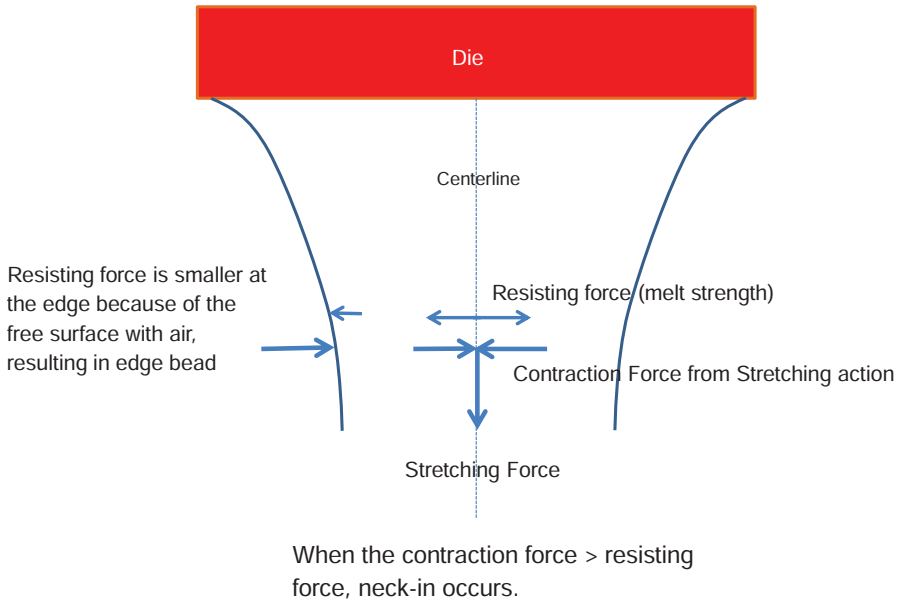


Figure 13.11 Forces on melt curtain leading to edge bead.

down in the air gap gives rise to a contraction force. Near the centerline, the contraction force is opposed by the melt tension of the web. Adjacent molecules along the width help to resist the contraction in the width dimension. This resistance is related to the elasticity or melt strength of the polymer. Dobroth and Erwin [33–35] recognize that the extension of the melt curtain near the centerline behaves like planar extension, where the width is fixed and the contraction occurs only in the thickness dimension:

$$X_L = X_0 \frac{v_0}{v_L} = X_0/\mathrm{DR} \tag{13.2}$$

where X_L = thickness near centerline at the chill roll; X_0 = thickness at die exit (die gap); v_0 = velocity at die exit; v_L = velocity at chill roll (or line speed); DR = draw ratio.

At the edges, the resisting force is unbalanced. On one side is polymer that can help transfer the tension across the web, but on the other side the contraction is only opposed by the air pressure. As a result, the polymer beads up in response to the contracting force. At the edge, the extension resembles tensile extension:

$$d_L = X_0 \sqrt{v_0/v_L} \tag{13.3}$$

where d_L = thickness of the edge bead.

Combining Eqs. (13.2) and (13.3) yields an equation for the bead ratio (ratio of the edge thickness to the centerline thickness):

$$\frac{d_L}{X_L} = \sqrt{\frac{v_L}{v_0}} = \sqrt{\mathrm{DR}} \tag{13.4}$$

Dobroth and Erwin measure the bead ratio for an LDPE and find it agrees well with Eq. (13.4). Canning and Co's [121] study of LDPE and LLDPE resins shows similar agreement with Eq. (13.4).

Edge bead and neck-in usually go hand-in-hand and so the actions described above for reducing neck-in also apply to edge bead. The effect of draw ratio is more explicit as described by Eq. (13.4). Increasing the coating or film thickness and decreasing the die gap reduce DR. Increasing melt strength by changing the polymer or decreasing temperature, or increasing *De* by increasing line speed and reducing the air gap may shorten the length of the edge that needs to be trimmed, as shown in Fig. 13.8.

Modern extrusion coating and cast film dies utilize edge bead reduction technology to minimize the edge bead [36,37]. This technology involves thinning the flow at the edges to compensate for thickening during draw down. Several versions exist, each with their pros and cons. In one version, plugs

are inserted at the ends to contour the flow at the edges. These can be adjusted for different polymers and operating conditions. Other designs use flexible die lips. Leakage flow should be considered when considering the design and operation of these types of dies.

13.4.2.2 Edge Weave, Draw Resonance, and Edge Tear Instabilities

Instabilities in the drawn molten web can occur at high draw ratios. One type is often called edge weave or draw resonance. These may have different origins and characteristics depending on the process and polymer. Examples include the following:

- Weaving of the coating. If the edge of the melt curtain moves beyond the substrate, it may stick to the nip roll and cause line breaks and wrap-ups.
- Periodic variation of the polymer output when the draw ratio exceeds a critical threshold. This is known as draw resonance and is a common problem in high-speed fiber spinning and film/coating operations. For films and coatings, the thickness, width, or both may periodically vary. It is a hydrodynamic phenomenon and even occurs for Newtonian fluids. The critical draw ratio for Newtonian fluids is around 20 and can be higher for non-Newtonian fluids [38].

These instabilities are more severe for linear polymers such as LLDPE and HDPE. Long chain branching improves things considerably, which corresponds to higher melt strength. Strategies for minimizing this type of instability include the following:

- Ensuring the extruder is producing a good quality melt. Pressure fluctuations should be minimized and the temperature uniform across the die width. Thermocouples in the extruder or transfer pipes can be unreliable. IR thermometry can be used to get an accurate reading of the temperature profile in the melt curtain. Hot spots at the edges can result in loss of melt strength, leading to edge weave issues [39].
- Reducing temperature. Lower temperature increases melt strength. In some cases, excessive temperature may cause cross-linking or other changes in the polymer that contribute to instabilities.
- Decreasing the die gap. This reduces the draw ratio, although as with any of these tactics, care should be taken to ensure the change does not cause other issues such as excessive pressure, high stress, or sharkskin.
- Increasing the film or coating thickness. This also reduces the draw ratio.
- Decreasing the take-up speed, but this reduces output.
- Switching to a higher melt strength polymer. Higher MW (lower MI), long chain branching, polar interactions (as in ionomers and acid copolymers) and broader MWD may help.
- Coextruding with a high melt strength resin such as LDPE or ionomer. Bain and Co [40] show that coextruding thin extensional hardening resin (LDPE) skin layers with a linear (LLDPE) core improves the stability of the process.
- Blending with a higher melt strength polymer such as LDPE. Frey [41] shows data for edge weave of linear PE and blends of linear PE with LDPE. The addition of LDPE reduces the edge weave considerably.
- Managing the air flow in the air gap. This is mostly for extrusion coating where the die gap is often fairly long. As the melt curtain is accelerated through the air gap it entrains air. The air is forced down onto the chill roll and has nowhere to go but up or out. This can cause air circulation patterns that cool the web unevenly.
- Encapsulating the core resin with a high melt strength polymer. New die technology allows a material to be fed to the edge of the die via a satellite extruder. This allows the encapsulation material to help stabilize the core resin. Frey [41] reports mixed results when applying this to linear polyethylene.

Another type of instability is edge or curtain tear. Tears can initiate at the edge of the melt curtain as it

is drawn down. This may cause line breaks and loss of productivity. Many of the remedies for this instability are the opposite of those for edge weave and draw resonance:

- Change the temperature. Lower viscosity may be needed to help draw the polymer down. Some polymers, however, may cross-link at high temperatures. Increasing their temperature may actually worsen the problem, as cross-linking tends to increase the likelihood of tearing. So as a general guideline, try raising the temperature and if that does not help, try lowering the temperature.
- Reduce the draw ratio (this is the same for both types of instability). This can be achieved by decreasing the die gap or increasing the coating or film thickness. Lowering the line speed may also help, although this reduces output.
- Lower the melt strength. Narrower MWD, lower MW (higher MI), and less long chain branching may help.
- Use an IR thermometer to check the temperature distribution across the curtain width. Air circulation patterns created as air is entrained by melt curtain as it is drawn down in the air gap may suck in cooler air at the edges. This may cause the edges to be cooler than the rest of the web. If this is the case, try heating up the die near the edges or better managing the air flow.

In extrusion coating, it can be a balancing act between edge weave and edge tear issues. Look for the sweet spot where both are acceptable.

13.4.3 Bubble Instability in Blown Film

As the output is increased on a blown film line, the bubble can become unstable, causing gauge variation, and ultimately line breaks and downtime. Butler [42] reviews the bubble stability literature and proposes six types of instability:

- periodic oscillations of bubble diameter;
- helical motion;
- bubble tears at die;
- bubble flutter;
- bubble sits down on air ring;
- variation in frost line height.

These are illustrated in Fig. 13.12. The first is particularly prevalent when processing linear polymers such as LLDPE.

A number of investigators have studied the effect of processing conditions on bubble stability. Factors that improve stability include decreasing the melt temperature [44,45], increasing the blowup ratio (BUR) [43], changing the frost line height [42], improving equipment design or operation [42], and modifying the rheology of the resin

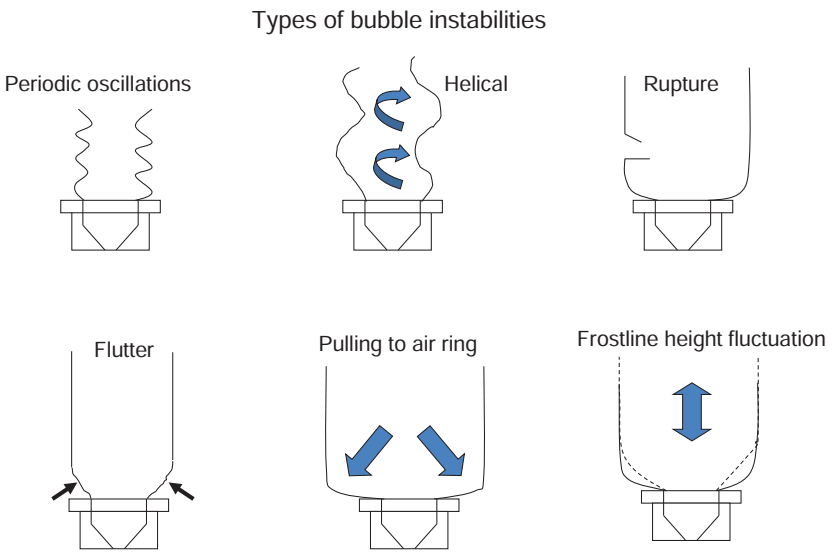


Figure 13.12 Types of bubble instability as categorized by Butler. *Adapted from Tas P, Nguyen L, Marshall S, Kashanian M. Bubble stability and maximum output of SURPASS sLLDPE resin in blown film. In: TAPPI PLACE conference; 2004. p. 320–34.*

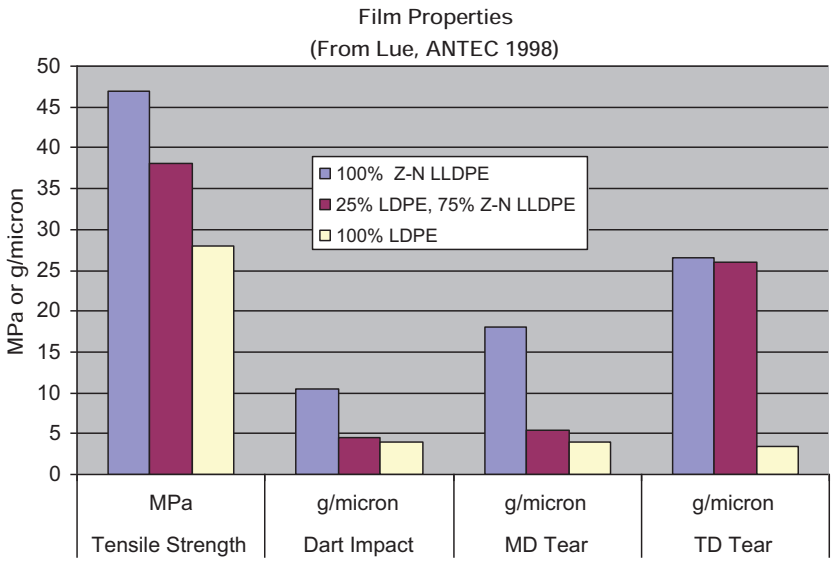


Figure 13.13 Effect of adding 25% LDPE to a hexene Ziegler–Natta LLDPE on blown film properties. *Adapted from Lue CT. Easy processing metallocene polyethylene. In: SPE ANTEC conference, vol. 56(2); 1998. p. 1816–9.*

[46–48]. Some of these approaches are limited by practical or physical considerations. For example, lowering the melt temperature of the polymer may be limited by the design of the extruder screw [42] and has been shown to negatively impact film properties [49].

The rheology and structure of the polymer is considered by many investigators. Han and Park [44] find that the presence of long chain branching improves stability. Broader MWD and increasing comonomer length [47] (butene < hexene < octene) has been shown to increase bubble stability. Field [50] shows explicitly that bubble stability improves with increasing melt strength of the polyethylene, as measured by the Rheotens method (Chapter 5).

A common technique used in the blown film industry to improve bubble stability and increase output is to blend a minor amount of LDPE into LLDPE [48–51]. This increases the melt strength of the LLDPE but can negatively impact film properties. One study by Lue [52] on 50-μm (2-mil) blown film shows reductions in tensile strength, dart impact strength, and MD Elmendorf tear resistance of 19%, 62%, and 87%, respectively, when 25% of a 0.6 MI LDPE resin is added to a hexene Z-N LLDPE (1.0 MI). This is shown in Fig. 13.13.

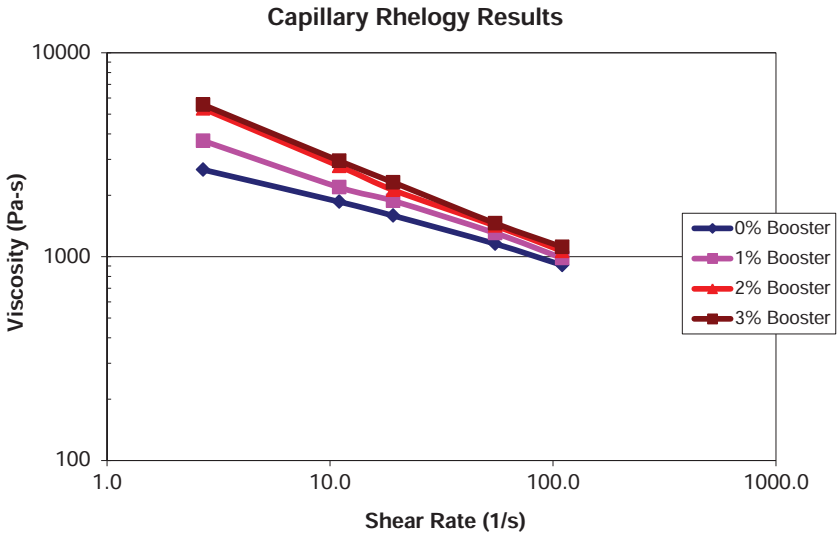


Figure 13.14 Effect of Booster addition to LLDPE rheology. *Reproduced with permission from Morris BA. Modifier for increasing output and reducing gauge variation in LLDPE blown film. In: SPE polyolefins conference; 2008.*

Table 13.3 Melt Strength Measurements of Blend of LLDPE With Booster

Resin	Melt Strength (g/3 min)
LLDPE control	0.2
LLDPE + 1.5% Booster	1.0
LLDPE + 3% Booster	2.5
LLDPE + 4.5% Booster	3.5

Reproduced with permission from Morris BA. Modifier for increasing output and reducing gauge variation in LLDPE blown film. In: SPE polyolefins conference; 2008.

Additives that enhance the melt strength of LLDPE have been developed. Although they are not widely used, they offer the processer a different set of trade-offs. Morris [53] describes a product offered by DuPont called Booster. This is a masterbatch that is added at 1–3 wt% during extrusion by the film converter.

This melt strength additive (MSA) can be thought of as a chain extender. It acts to create long chain branching, which, in turn, modifies the resin rheology. Fig. 13.14 shows the effect of adding small amounts of MSA to an LLDPE resin. The viscosity at low shear rates increases substantially whereas the viscosity at high shear rates is relatively unchanged. The effect of adding MSA is to make the viscosity behave more like high pressure LDPE; that is, the increase in viscosity at low shear rate is an indication of increased elasticity and melt strength and is not accompanied by increased power consumption at high shear rates. This is further illustrated in Table 13.3, showing an increase in melt strength, as measured by a DuPont Canada test that determines the mass of an extrudate that hangs from an orifice of a melt indexer for 3 min. Higher values indicate greater melt strength.

The increased melt strength translates directly into improved bubble stability. Trials at various converters in the 1980s, when the product was developed, showed improvements in output as a result of greater bubble stability of 10–50%. The benefits help in the manufacture for very thin (10–20 μm or 0.4–0.8 mils) or very thick (200–800 μm or 5–20 mils) films at high production rates without the need for special bubble support systems.

The improved melt strength can also contribute to a reduction in gauge variation. During draw down, the MSA increases the resistance of the melt to localized draw thinning around the die circumference. This is especially beneficial with die gaps larger than 1.5 mm (60 mil). Gauge uniformity is thus improved, permitting downgauging of up to 20% without loss of physical properties.

Most LLDPE film properties, including dart impact, puncture resistance, and tensile properties, are unchanged when using MSA. There is a moderate decrease in MD tear strength and an increase in haze. Both are believed to be related in an increase in molecular relaxation time due to the chain extension.

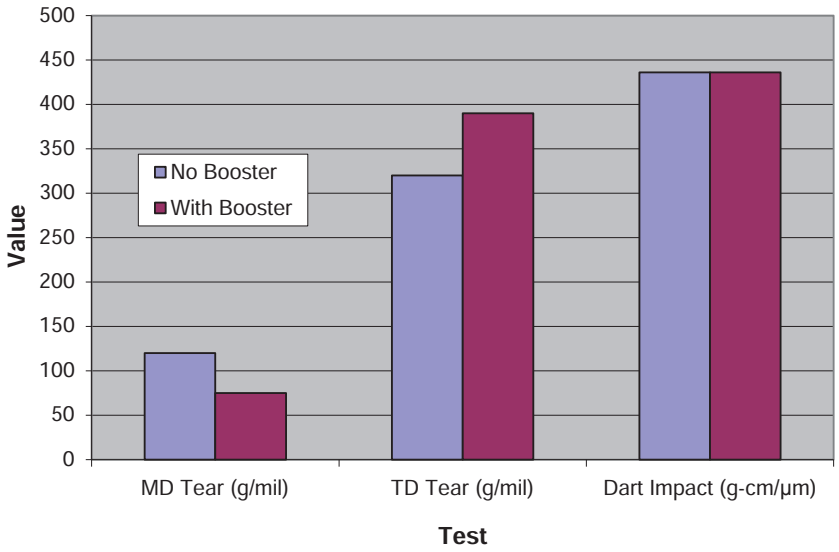


Figure 13.15 Effect on Elmendorf tear resistance and dart impact resistance of adding Booster to a 50 μm butene LLDPE blown film.

Reproduced with permission from Morris BA. Modifier for increasing output and reducing gauge variation in LLDPE blown film. In: SPE polyolefins conference; 2008.

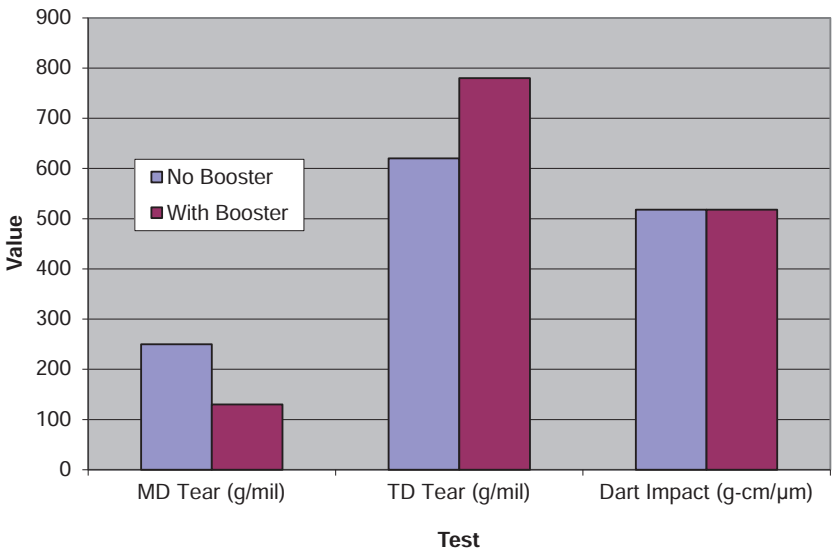


Figure 13.16 Effect of adding Booster to a 50 μm octene LLDPE blown film. *Reproduced with permission from Morris BA. Modifier for increasing output and reducing gauge variation in LLDPE blown film. In: SPE polyolefins conference; 2008.*

This results in an increase in MD orientation, causing the reduction in MD tear strength. The increase in haze is a consequence of surface roughness due to unrelaxed stress. Figs. 13.15 and 13.16 show the reduction in tear strength of b-LLDPE and *o*-LLDPE blown films, respectively. Some of the reduction in tear strength can be compensated by increasing the frost line height or by blending in a tougher resin such as mLLDPE. Fig. 13.17 shows the effect of MSA on haze.

MSA technology is not suitable for every situation. It only improves output when production is limited by melt strength considerations such as bubble stability. The extruder must have enough power to run LLDPE. MSA does not improve the melt strength of LDPE or HDPE. It also does not reduce melt fracture of LLDPE or act as a lubricant to reduce power requirements, but it can be used with other processing aids that do so. MSA also creates trade-offs, mainly in MD tear strength and clarity, which differ from blending with LDPE. Using MSA may allow the film producer to retain the outstanding puncture resistance and tensile properties of LLDPE while gaining operational benefits.

Resin producers continue to improve the performance of LLDPE. Advances in reactor design and catalyst technology have helped push the processing envelope of LLDPE. Reactors in series that produce bimodal MWD and metallocene LLDPE with sparse long chain branching are two examples.

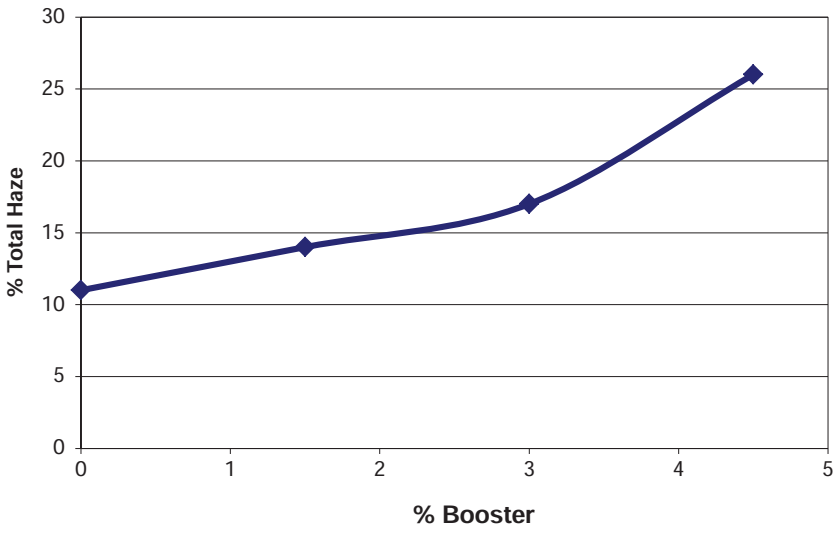


Figure 13.17 Effect of adding Booster on haze of a 25 μm LLDPE blown film. *Reproduced with permission from Morris BA. Modifier for increasing output and reducing gauge variation in LLDPE blown film. In: SPE polyolefins conference; 2008.*

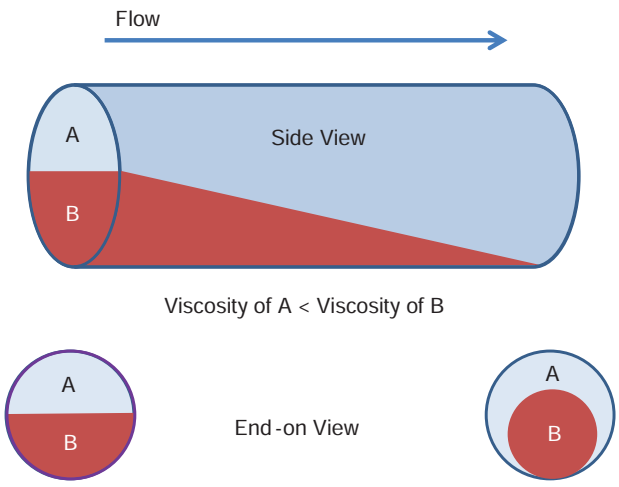


Figure 13.18 Illustration of encapsulation effect in steady-state flow. Layer A has a lower viscosity than layer B.

Improvements in blown film equipment have also helped boost the output of LLDPE blown film lines. These include better air ring and cooling designs that help keep the bubble stable.

Coextrusion of LLDPE with LDPE or other resins with superior melt strength is another avenue for reducing bubble instability and enhancing output without as much trade-off in film properties.

Processing parameters may also be adjusted to improve stability. Yoon [122] conducts a linear stability analysis and finds bubble stability is limited by both the BUR and thickness reduction ratio (ratio of final film thickness to die gap). The analysis also suggests there is an optimum frost line height. Their model agrees with observations of an LLDPE blown film line.

13.4.4 Layer Rearrangement in Coextrusion

Distortion or rearrangement of layers in coextrusion can occur if the viscous and elastic properties of the polymers are not well matched. This can lead to poor thickness control, and loss of barrier and other properties.

13.4.4.1 Shear Viscosity Effects

When two polymers of different shear viscosity flow down a channel, the lower viscosity resin will preferentially flow toward the region of highest shear rate. Han [54] attributes this behavior to the principle of minimum viscous energy dissipation. The result is that if the flow channel is sufficiently long and the viscosity difference is sufficiently large, the lower viscosity polymer will encapsulate the higher viscosity polymer. This is because the shear rate is highest near the channel wall. This encapsulation effect gives rise to layer maldistribution in coextrusion. This is illustrated in Fig. 13.18 where layer A tends to encapsulate layer B as they travel down the channel.

This is often more of a problem in flat die extrusion where the polymers travel together for long

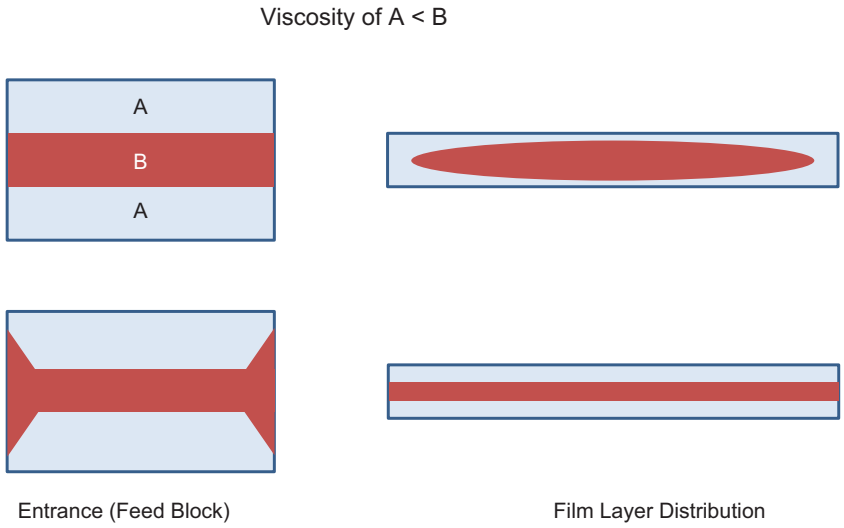


Figure 13.19 Layer redistribution in a three-layer coextrusion for the case where the skin layer A has lower viscosity than the core layer B. This results in A encapsulating B (upper diagram). If the feed channel is shaped with a "bow tie" contour, the layer distribution in the final film may be uniform (bottom diagram).
Adapted from Butler TI. Effects of flow instability in coextruded films. TAPPI J 1992;75(9):205–11.

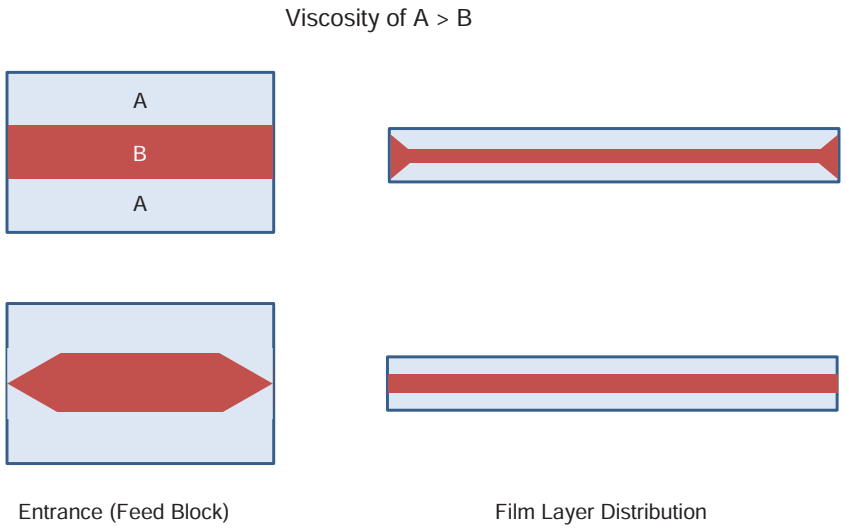


Figure 13.20 Layer redistribution in a three-layer coextrusion for the case where the skin layer A has a higher viscosity than the core layer B. This results in a dog bone or bow tie distribution in the final film. If the feed in contoured as in the bottom diagram, the final film distribution may be uniform.
Adapted from Butler TI. Effects of flow instability in coextruded films. TAPPI J 1992;75(9):205–11.

distances after being combined in a feedblock. In blown film, the polymers are usually combined closer to the die exit. Also, there are no edges in the annual flow in blown film, which helps reduce the distortion effects.

Some methods used to minimize this behavior include the following:

- Selecting polymers that match in viscosity.
- Minimizing the travel distance after the polymers are combined. Multi-manifold dies, for example, are less prone to this since the polymers are combined just prior to the die exit.
- Contouring the shape of the feed channel to compensate for the flow rearrangement. This is illustrated in Figs. 13.19 and 13.20 for a three-layer (A–B–A) structure. Some feedblock designs use inserts to contour the channel [55,56]. Other feedblocks have rotating pins that contour the channel. It may take some trial and error to come up with an acceptable contour that compensates for the maldistribution.

13.4.4.2 Elasticity Effects

Khan and Han [58,59] estimate the effect of differences in polymer elasticity on interface displacement and layer rearrangement. Their calculations show that the more elastic fluid will tend to encapsulate the less elastic one. They conclude, however, that viscosity plays the dominate role in determining the shape of the interface in steady flow [54].

In a series of elegant experiments and numerical simulations, Dooley et al. [60–66] show that polymer elasticity can lead to substantial layer rearrangement in coextrusion, particularly near the edges of a flat die. They eliminate the viscosity effects by conducting coextrusion experiments with the same polymer. The layers are pigmented to see the flow patterns. (The pigment is shown to not affect the flow.) They use several different feedblock configurations to visualize the flow down a channel. In the simplest, two layers of different color with a layer ratio of 20/80 are coextruded down a channel of different geometries. After establishing steady flow, they stop the extrusion, freeze the polymer in place, and open the channel to see the extrudate at different locations along the channel. In other experiments, they use special feedblocks to coextrude 165 layers or 49 strands to aid in the visualization of the flow.

Several different geometries are studied, including square, rectangular, teardrop, circular, and a rectangular manifold (to simulate what may happen in a die). Three polymers are used: polycarbonate (PC), polystyrene (PS), and LDPE. Rheology measurements show that the PS and LDPE are more elastic than PC.



Figure 13.21 Example of layer rearrangement due to secondary flows of elastic polymers. Cross section of two-layer coextruded polystyrene (colored white and black) structure as it progresses through a square channel. Progression is from upper left to lower right.
From Dooley J, Hyun KS, Hughes K. An experimental study on the effect of polymer viscoelasticity on layer rearrangement in coextruded structures. Polym Eng Sci 1998;38:1060–71.

Their results, some of which are illustrated in Fig. 13.21, show the following:

- PS and LDPE exhibits substantial layer distortion while flowing down noncircular channels. PC shows little or no distortion.
- The special feedblock configurations with 165 layers or 49 strands show secondary flow in the corners of the square and rectangular channels that cause the distortion. This is confirmed by numerical simulation. The secondary flows or vortices are due to the second normal stress difference (a measure of elasticity). Numerical simulations show that the amount of secondary flow correlates with the ratio of the second normal stress difference to the shear viscosity [67–69].
- The geometry of the channel influences the amount of distortion:
  - Circular channels do not show the distortion. The radial symmetry prevents the formation of secondary flows.
  - Square channels have the greatest amount of distortion.
  - Rectangular channels have less distortion and only in the corners.
  - Teardrop-shaped channels have six regions of secondary flows versus eight for rectangular and square.
  - A rectangular manifold channel shows distortion in the corners especially near the end of the channel. This geometry is similar to coat hanger style dies and suggests that more layer rearrangement may take place near the edges of the die than in the center. This is what is often seen in practice.
  - The entrance geometry (vertical or back) and manifold design of a coat hanger die affect the flow patterns [66].

The size of the secondary flows is several orders of magnitude smaller than the bulk flow in the channel, except near the walls or corners. In the coextrusion of two polymers of different viscosity and elasticity, the viscous encapsulation velocity

dominates near the entrance of the channel. The encapsulation velocity decreases as the polymers flow down the channel and the layers reach their equilibrium configuration. The elastic secondary velocity is steady throughout the channel, so that far down the channel the viscous and elastic flows are the same order of magnitude [70].

These results, as well as others [71,72], show that the viscosity and elasticity of the polymer must be taken into account during coextrusion. The selection of the polymers as well as the die design is important.

13.4.5 Interfacial Instabilities

In coextrusion, defects have been observed that are associated with the instability of flow between layers. These defects have been described in a number of ways, including chevrons, wood grain, orange peel, waves, ground glass appearance, and loss of see-through clarity. Their origins may differ and are often complex and poorly understood.

Interfacial instabilities have been categorized into four types:

- *Zigzag*. This is characterized by a high frequency, low amplitude wave, or zigzag. It may start out as an increase in surface roughness and haze and in its more severe form resemble wood grain patterns. Experiments have shown that this type of instability originates in the die land near the die exit [73]. Fig. 13.22 shows a photograph of a film with zigzag instability.
- *Wave*. This is characterized by a low frequency, large amplitude wave that often extends across the width of the film or sheet (Fig. 13.22). Several investigations show that this instability originates in the region where the polymers first merge together [74–77].
- *Scattering*. This instability is found in microlayer coextrusion involving greater than 100 layers with thicknesses less than 10 μm. Distinct layers are required. The mechanism is unknown but Ramanathan [74] speculates that a normal stress mismatch drives secondary flows near the die wall. Ramanathan [78] shows that adding a protective layer between the die wall and the microlayers can eliminate this instability.

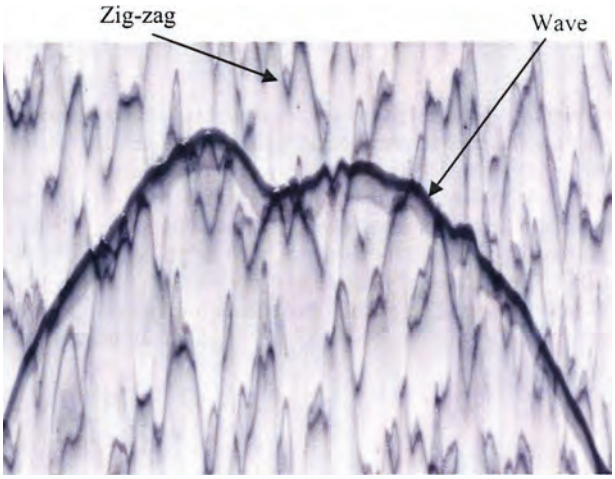


Figure 13.22 Photo of zigzag and wave-type instabilities in a coextruded cast film.
Reproduced with permission from Zatloukal M, Martyn M, Vlcek J, Saha P. Viscoelastic coextrusion flow modeling by advanced constitutive equations: the influence of the die design on interfacial instabilities. In: European TAPPI PLACE conference; 2005.

- *Interfacial adhesion*. This type of instability typically shows up as loss of see-through clarity or as a "ground glass" appearance as the observer looks through the film. It occurs in barrier packaging films where a reactive tie resin bonds to a barrier resin such as PA or ethylene vinyl alcohol (EVOH). A proposed mechanism is a local increase in MW at the interface between the reacting polymers, which creates viscosity mismatches and local stresses that may cause instabilities. For example, Levitt [79] amplifies the effect of interfacial interactions by measuring the extensional stress on specimens containing up to 100 layers of pairs of polymers. Combinations of pairs that form cross-links at the interface have stress values that are two orders of magnitude higher than nonreactive pairs. This type of instability can often be controlled by reducing the amount of chemical functionality in the tie resin. There is a limit to how effective this can be without adversely affecting adhesion. Special tie resin formulations have been developed to address this issue with mixed success [80].

13.4.5.1 Fundamental Studies

Interfacial instability has been studied for well over 40 years. Schrenk [73] and Han [82] find

evidence for a critical interfacial shear stress above which the onset of zigzag instability occurs. Their value for the critical stress is about 5×10^4 dyn/cm. Later investigators find that this value varies with polymer type, MWD, and other factors. There does not seem to be a universal value for the critical stress. Indeed, Wilson [83] says that the critical stress is not supported by theory and may even be misleading. Nevertheless, this concept is widely accepted, perhaps because it is easy to determine and known methods can be used to reduce the stress.

Perturbation methods are used to study flow instabilities in the engineering discipline of fluid mechanics. A periodic wave is introduced either experimentally or to model equations. If the wave grows as it travels through the medium, in this case as the polymer flows through the transfer pipes and die, the system is unstable. One of the earliest studies of this type was conducted by Yih [84] who studied Newtonian fluids. He finds that the viscosity ratio, thickness ratio, and initial wave frequency are important. Others have looked at viscoelastic polymers and find that the elasticity ratio and the flow channel geometry are also important [83,85–90].

A number of investigators focus on the region where the polymers merge. Changes in the channel geometry are more or less impactful on stability [74,76,91–93]. The acceleration of one flow stream into the other during the merge is hypothesized as being responsible for the wave instability, but simple velocity ratios have proven insufficient to predict the onset of instability [91–93]. Elongational viscosity and elasticity are thought to be involved [94]. Xiao [91] evaluates three different types of PE in blown film of (LDPE–tie–PE) and finds the more elastic polyethylene to be more prone to instability. Ramanathan [74] finds cast sheet/film structures with a large extensional viscosity ratio or a skin layer with a large extensional viscosity to be more prone to instability. Perdikoulias [92,93] finds LDPE coextruded with itself can generate instabilities; grades with broader MWD are more prone to instability. LDPE grades with broader MWD generally have more long chain branching, greater elasticity, and higher elongational viscosity. The stability of the broad MWD grades seems to be independent of the channel geometry and processing conditions, whereas narrower MWD grades exhibit instability that is associated with interfacial stress (which is related to channel geometry and processing conditions).

Zatloukal et al. [81,95–98] conduct numerical simulation of flow in the merge area to try to come up with predictors of instability. The results are compared against experimental data of Perdikoulias [92,93] and Martyn [75–77]. They propose criteria that goes by several names in successive papers, depending on which stress components they include. In an early version, it is known as the total normal stress difference (TNSD), which is essentially the TNSD (elasticity) averaged over the flow stream for each layer. It is positive when the major layer is stretched more than the minor layer and negative when the minor layer is stretched more. They correlate the sign and shape of this parameter with the onset of instability. If the sign goes negative or the shape is discontinuous, the flow is likely to be unstable. They conclude that skin layers that exhibit strain-hardening behavior in extension are more prone to instability.

The measurement of elongational viscosity and elasticity of polymer melts is challenging, as described in Chapter 5, especially under high extension rate conditions that simulate real polymer processing. Numerical methods using constitutive equations that can handle the elasticity characteristics of the polymer typically require material data that are not easily obtained, extensive knowledge of the flow channel geometry that is typically not available except to the equipment manufacturer and knowledge of numerical techniques. While these techniques have advanced the understanding of flow instabilities, they typically are too difficult to use as everyday tools for troubleshooting or selecting specific resins or structures.

13.4.5.2 Methods to Improve Stability

The theory discussed above suggests several methods for improving stability. One is to try to match the velocities of the polymers streams as they are combined in the feedblock or die. For example, some feedblocks have vanes that either automatically adjust the flow or can be manually adjusted. Other feedblocks have dividing plates to help distribute the velocity. Fixed geometry dies, such as blown film dies, generally have little leeway to adjust the velocity of the streams beyond changing the output of the extruder. Problems associated with mismatched velocities often occur as the converter

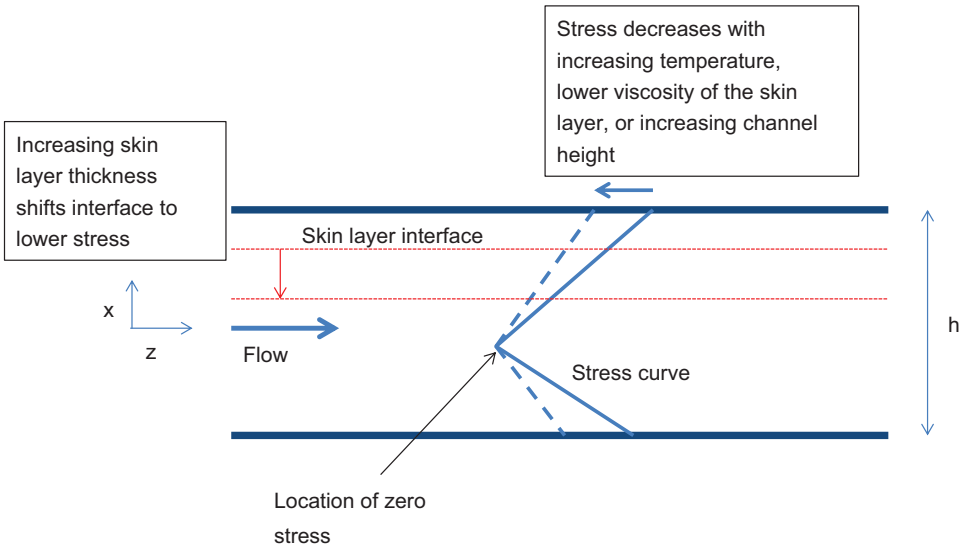


Figure 13.23 Ways to reduce interfacial stress in coextrusion. Depiction is of the stress profile in a rectangular flow channel of height *h*.

tries to make structures that are beyond the design optimum of the die. In other words, they try to put too much or too little through one of the layers. As the number of layers has increased in modern coextrusion systems, this has become less of an issue. Thick layers can be subdivided into several layers, each with their own extruder and flow channel, so that the process runs closer to its optimum. This allows the flow in each layer to better match with the other layers.

Another method to improve stability is to reduce the interfacial stress [57,73,82]. As shown in Fig. 13.23, stress varies linearly across the height of the channel. The stress is highest at the channel wall and goes to zero somewhere in the channel; for monolayer flow the stress is zero down the centerline of the channel. Fig. 13.23 outlines a number of ways to reduce the interfacial stress, which include the following:

- Increasing the temperature. Higher temperature reduces the viscosity of the fluid and reduces stress.
- Reducing the viscosity of the skin layers. This may be accomplished by raising the temperature or swapping out with a lower viscosity grade.
- Moving the skin layer away from surface (thicker skin layer). Since the stress is highest at the channel wall, moving the interface away from the wall reduces stress.
- Increasing the channel height. Stress is related to the pressure drop across the channel length. Opening the channel up reduces the pressure drop and the stress.
- Reducing the output. This is always an unfavorable action but may help to temporarily fix a problem until another solutions can be found.

Matching viscosities is an another approach that has been widely used with practical success. It is supported by the perturbation theories. While the fundamental studies suggest that matching elongational viscosity may help, data are hard to find. Elongational viscosity is generally not supplied by resin manufacturers and is difficult to measure. In some cases, it may be sufficient to consider the general family of polymers the resin belongs to. LDPE, for example, is known to strain harden during extension whereas LLDPE does not. At low extension rates, the elongational viscosity is equal to three times the shear viscosity; matching shear viscosity may at least provide directional trends toward matching elongational viscosity.

Shear viscosity is much easier to measure and data are generally readily available. A key question is what viscosity to use. A rather crude method is to match the melt flow rates of the polymers. This is not often very accurate since the viscosity changes with temperature and shear rate. A better method is to use the viscosity at the temperature and shear rate of the

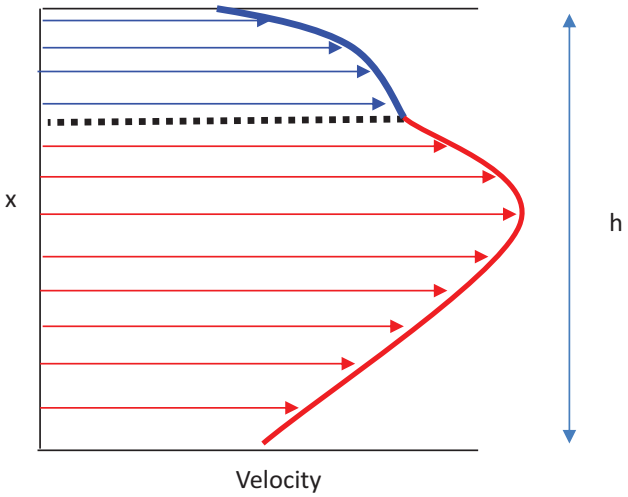


Figure 13.24 Velocity profile for a two-layer coextrusion.

interface. There are two challenges with this. One is that the location of the interface in the flow channel is unknown. Although the location of the interface in the final film is known, this location is not the same as that in the flow channel. This is due to the external constraints or boundary conditions on the flow. In the channel, the flow is bound by the walls; flow takes on a parabolic shape with zero velocity at the walls. At the channel exit, the boundary condition changes to a free surface. The individual layer flows change in response, shifting the location of the interfaces.

The second complication is that shear rate is discontinuous at the interface. This can be seen in Fig. 13.24, which shows the velocity profile of a two-layer flow. The velocity is continuous at the interface (the velocity of layer A = the velocity of layer B). This is a standard assumption in fluid mechanics called no-slip. The slope of the velocity curve is equal to the shear rate at a given point along the flow curve. At the interface the two slopes are not equal.

A better approach is to determine the shear stress at the interface. As mentioned earlier, the stress is continuous at the interface and varies linearly across the channel height. If the location of the interface can be determined, and the stress profile is known, the stress at the interface can be computed. It then becomes a simple matter of picking off the viscosity of each of the layers from their respective rheology curves (plotted as viscosity vs. shear stress, as illustrated in Fig. 6.21 or Fig. 13.25).

The location of the interfaces and the stress profile can be computed by solving the equations of motion for multilayer flow down a rectangular channel. Several references give the solution, including Han [54] and Han and Shetty [99] for isothermal power law fluids, Puissant [100] for nonisothermal power law fluids and Mavridis [94] and Pearson [101] for general nonisothermal viscoelastic fluids. The equations are nonlinear and require numerical methods to solve. The equations are more manageable if the flow is assumed to be Newtonian ($n = 1$ in the power law model) and isothermal. While not truly representing the flow of polymers, such an approach still provides reasonable estimates that have proven successful in minimizing stability problems [102]. A semi-numerical approach can be applied that involves starting at one channel wall and numerically

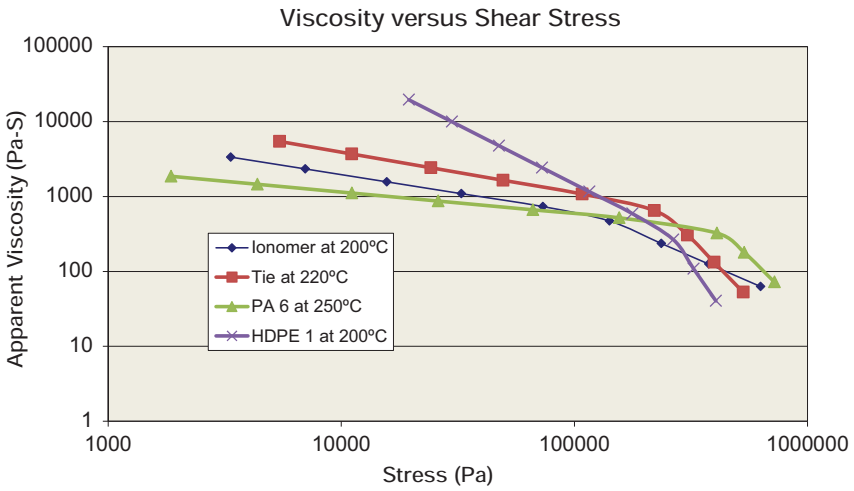


Figure 13.25 Viscosity versus shear stress curves for the four resins and temperatures in Table 13.4 (Scenario 1). Data are from capillary rheometry measurements, extrapolated to the given temperature using a double power law model with Arrhenius temperature dependence.
Courtesy of E. I. du Pont de Nemours and Company.

Table 13.4 Input Parameters for a Film Structure (Scenario 1)

Total throughput (kg/h)		260	
Width of channel (mm)		1100	
Height of channel (mm)		1.80	
Layer	**Resin**	**Thickness (μm)**	**Temperature (°C)**
1	Ionomer	20	200
2	Tie	7.5	220
3	PA6	12	250
4	Tie	7.5	220
5	HDPE 1	50	200
Total thickness		97	

marching across the height of the channel in small increments. At each step the flow rate for the first layer can be computed from the model equation and compared with the real flow rate obtained from the layer thickness in the film (times the line speed). When they match, the interface is found. This is repeated for each interface.

To illustrate the usefulness of such a tool, consider a five-layer coextruded film with the structure (Ionomer–tie–PA6–tie–HDPE). The throughput, dimensions of the channel, layer thicknesses, and temperatures are presented in Table 13.4. The viscosity versus shear stress curves for the four resins at their respective temperatures are shown in Fig. 13.25. Without some bounds on the shear stress in the channel it is difficult to determine how well matched the viscosities are. A simple method can be used to estimate the stress profile in the channel by first calculating the shear rate at the wall for Newtonian flow in a rectangular channel:

$$\dot{\gamma}_w = \frac{6Q}{wh^2} \tag{13.5}$$

where $\dot{\gamma}_w$ = shear rate at the wall; Q = total volumetric throughput (mass throughput divided by the average density of the melt); w = width of channel; h = height of channel.

The shear stress at each wall is determined from the rheology data for each of the skin layers, in this case the ionomer (wall 1) and HDPE (wall 2). This can be determined by replotting the rheology data in Fig. 13.25 as viscosity versus shear rate by recognizing

$$\tau = \eta\dot{\gamma} \tag{13.6}$$

where τ = shear stress; η = viscosity.

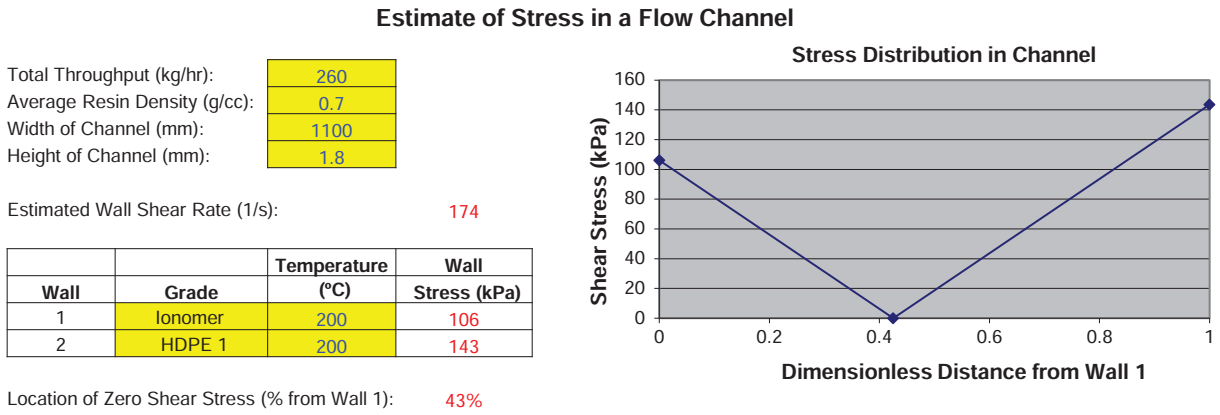


Figure 13.26 Estimate of stress profile in channel for flow of structure described in Table 13.4 (Scenario 1). *Courtesy of E. I. du Pont de Nemours and Company.*

Table 13.5 Results of a Multilayer Flow Model for the Input Conditions Found in Table 13.4 (Scenario 1)

Interface	Resin	Location of Zero Shear Stress			0.402		
		Distance From Wall	Shear Stress (kPa)	Shear Rate (1/s)	Viscosity (Pa s)	Viscosity Ratio	Comment
Wall 1	Ionomer	0.000	84.8	124	682		
1	Ionomer	0.304	20.7	15	1357	0.53	
	Tie			8	2554		
2	Tie	0.372	6.4	1	4792	3.67	Mismatch
	PA6			5	1305		
3	PA6	0.480	16.4	17	994	0.34	
	Tie			6	2894		
4	Tie	0.550	31.2	15	2054	0.22	Mismatch
	HDPE 1			3	9239		
Wall 2	HDPE 1	1.000	126.1	124	1014		

Courtesy of E. I. du Pont de Nemours and Company.

The result is shown in Fig. 13.26. The last piece of information that is needed is the location of the plane of zero shear stress, ξ. Since the stress profile is linear, ξ can be estimated by simple proportion:

$$\frac{\xi}{1-\xi} = \frac{\tau_{w1}}{\tau_{w2}} \tag{13.7}$$

where ξ = dimensionless distance from channel wall 1 (distance divided by the channel height); τ_{w1} = shear stress at wall 1; τ_{w2} = shear stress at wall 2.

The estimated stress profile is given in Fig. 13.26. The stress ranges from 0 to 140,000 Pa. The curves in Fig. 13.25 show that over this range the ionomer and tie resin viscosities are well matched, but the tie−PA and tie−HDPE combinations are not. To get more quantitative, the location of each interface needs to be estimated. This is done using a model described above. The results of

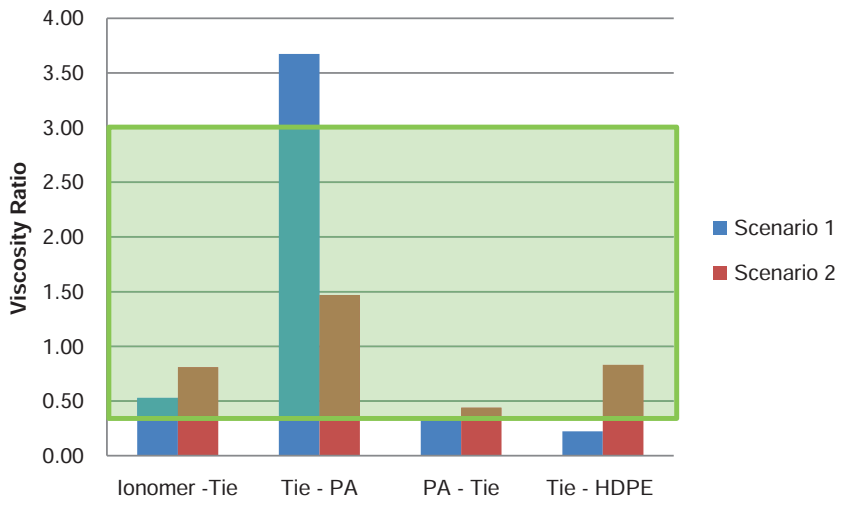


Figure 13.27 Viscosity ratios at each interface from Scenarios 1 and 2.

the model calculation are shown in Table 13.5. A general guideline based on practical experience is to keep the viscosity ratio between 3:1 and 1:3. The results show that the first tie—PA interface has a viscosity ratio of 3.7 and has the potential to be a source of flow instability. The second PA—tie interface is also very close to the bounds of the stability region and it too should be considered. Finally, the tie—HDPE interface also shows considerable viscosity mismatch. The viscosity ratios are plotted in Fig. 13.27.

There are several ways to address viscosity mismatch. These include:

- Adjusting the temperature of one or more layers. This changes the viscosity of the polymer. There are limitations to this approach. One is that resins may have thermal stability limits above which gel or other issues may occur (Section 13.1). Another is that the temperature must be well above the melting point or glass transition temperature of the polymer to achieve flow. Perhaps a greater limitation is the heat transfer that occurs between layers as they travel down the channel. This tends to equilibrate the temperature across the layers and maintaining large differences in temperature between layers may be impractical. Some models, such as the one developed by Mavridis and Shroff, incorporate heat transfer into the calculation. For those models that do not have heat transfer implicitly built into the equations, it can be useful to run the simulation at several temperatures to understand how sensitive the solution is to temperature effects.
- Swapping out one or more of the polymers with a grade with higher or lower MW (or melt viscosity).
- Increasing or decreasing the channel height (simulating or adjusting the die gap, for example). This changes the shear rate and stress profile in the channel, which may affect the viscosity ratios since different polymers have different shear thinning characteristics.
- Increasing or decreasing the throughput. This also changes the shear rate and stress in the channel.
- Changing the thickness of one or more of the layers. Increasing the thickness of a skin layer, for example, moves the interface further from the channel wall, which decreases the shear stress. Since the polymers may have different responses to changes in shear stress, moving the interface may change the viscosity ratio.

For this example, the first two approaches were used to bring the viscosities into better alignment. Changing the temperatures alone was not sufficient to eliminate the viscosity mismatches, particularly between the tie and HDPE. Replacing the HDPE with a lower MW grade (higher MI) along with adjusting the temperatures of the layers resulted in a good match at each interface. This scenario is shown in Table 13.6 and the results in Table 13.7. As shown in the bar graph in Fig. 13.27, the viscosity ratios in Scenario 2 all fall within the desired range. This is also seen in the viscosity versus shear stress

Table 13.6 Input Parameters for a Film Structure (Scenario 2)

Total throughput (kg/h)		260	
Width of channel (mm)		1100	
Height of channel (mm)		1.80	
Layer	**Resin**	**Thickness (μm)**	**Temperature (°C)**
1	Ionomer	20	200
2	Tie	7.5	240
3	PA6	12	245
4	Tie	7.5	225
5	HDPE 2	50	250
Total thickness		97	

Table 13.7 Results of a Multilayer Flow Model for the Input Conditions Found in Table 13.6 (Scenario 2)

Interface	Resin	Location of Zero Shear Stress			0.547		
		Distance From Wall	Shear Stress (kPa)	Shear Rate (1/s)	Viscosity (Pa-s)	Viscosity Ratio	Comment
Wall 1	Ionomer	0.000	84.8	124	682.1		
1	Ionomer	0.289	40.0	41	981.2	0.81	
	Tie			33	1213.4		
2	Tie	0.348	30.9	23	1358.1	1.47	
	PA6			33	923.8		
3	PA6	0.436	17.2	16	1097.2	0.44	
	Tie			7	2494.1		
4	Tie	0.489	9.0	3	3469.4	0.83	
	HDPE 2			2	4176.5		
Wall 2	HDPE 2	1.000	70.3	124	565.0		

Courtesy of E. I. du Pont de Nemours and Company.

curves for these resins at the new temperature profiles (Fig. 13.28).

Minimizing stress and matching viscosity are complementary approaches often used together to solve interfacial instability issues. Using one alone may not be sufficient, although both often result in similar tactics. The same model that is used to compute viscosity ratios also yields information about the interfacial stress. A few tactics do differ between the two approaches:

- The stress approach suggests decreasing the viscosity of the skin layer, even if it results in a mismatch in viscosity with the layer adjacent to it. In practice, this has proven effective in many situations.
- The stress approach suggests increasing the temperature across the board to reduce interfacial stress. This may be impractical in situations where melt strength (bubble stability) or thermal stability issues are a concern.

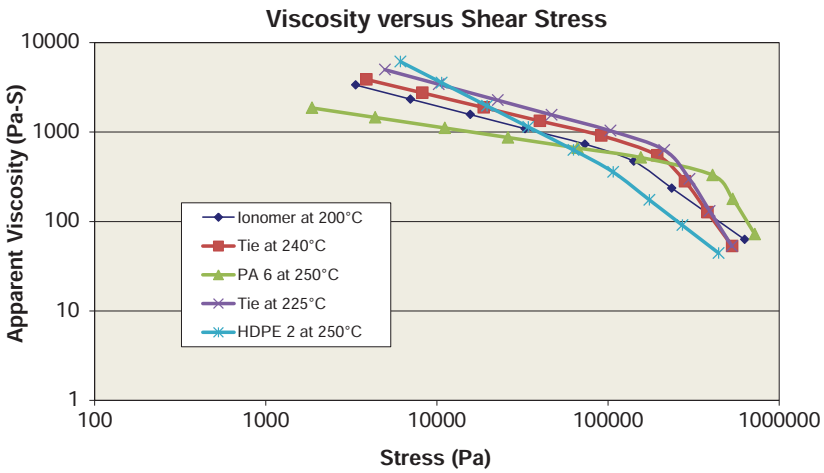


Figure 13.28 Viscosity versus shear stress curves for the five layers in Table 13.6 (Scenario 2). Data are from capillary rheometry measurements, extrapolated to the given temperature using a double power law model with Arrhenius temperature dependence. *Courtesy of E. I. du Pont de Nemours and Company.*

13.5 Curl

Curl is a term used to describe the tendency of a packaging film to roll up and not lay flat. Curl is undesirable because of the handling problems it creates on high-speed packaging lines. In extreme cases, curl may also detract from the appearance of the final package. Curl is particularly problematic in coextruded blown films when the layers are not symmetrically balanced. In particular, films containing barrier resins such as EVOH and PA are often difficult to make flat.

13.5.1 Causes

In coextrusion blown film, the primary cause of curl is the stress created when the layers shrink as the film is quenched or afterward during post-quench crystallization. Polymers shrink differently as they are quenched due to differences in freezing points, crystallinity, and coefficients of thermal expansion. The volume change of HDPE as it is slowly cooled from the melt is shown in Fig. 13.29. This curve was generated using a pressure–volume–temperature (PVT) apparatus [103–105]. For semicrystalline polymers, the volume undergoes a rapid reduction at the freezing point due to the formation of crystals. (The specific volume plotted here is the inverse of the density.) This decrease in volume is designated as ΔV_c (change in volume due to crystallization). The volume also changes due to thermal expansion and contraction, which is indicated by the positive slope leading up to the crystallization temperature.

Fig. 13.30 shows PVT data for three commonly used polymers in packaging films: HDPE, EVA (18 wt% VA), and EVOH (38 mol% ethylene). Their different freezing temperatures and ΔV_c clearly show up in this type of plot. Such data are useful for qualitatively understanding why some films curl more than others. For example, many snack films have the structure (HDPE–EVA), where the HDPE serves as a moisture barrier and the EVA gives low temperature sealability. These films typically have a very small amount of curl toward the EVA layer. While the HDPE undergoes a significant volume change as it crystallizes, the EVA is still molten when this occurs. It can flow to relieve stresses caused by the shrinking HDPE layer. When the EVA itself freezes, its volume change is much smaller, giving less of a tendency for curl. Furthermore, the EVA's modulus is considerably smaller than that of HDPE; the stiffness of the HDPE helps prevent curl.

For barrier applications, a layer of EVOH (and tie layers) can be added to a typical snack structure: (HDPE–tie–EVOH–tie–sealant). This structure has a strong tendency to curl towards the HDPE layer. The PVT data show why. The EVOH freezes first so that as the HDPE freezes, its shrinkage gives

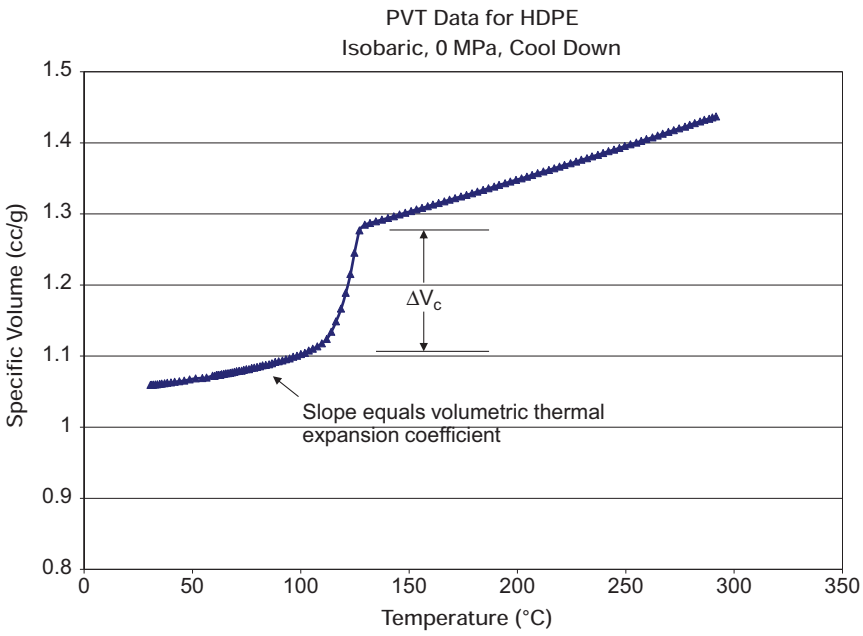


Figure 13.29 PVT data for HDPE. *Reprinted with permission from Morris BA. Reducing curl in multilayer blown film: experimental results, model development, and application to a cereal liner film. J Plast Film Sheeting 2003;19:31–54.*

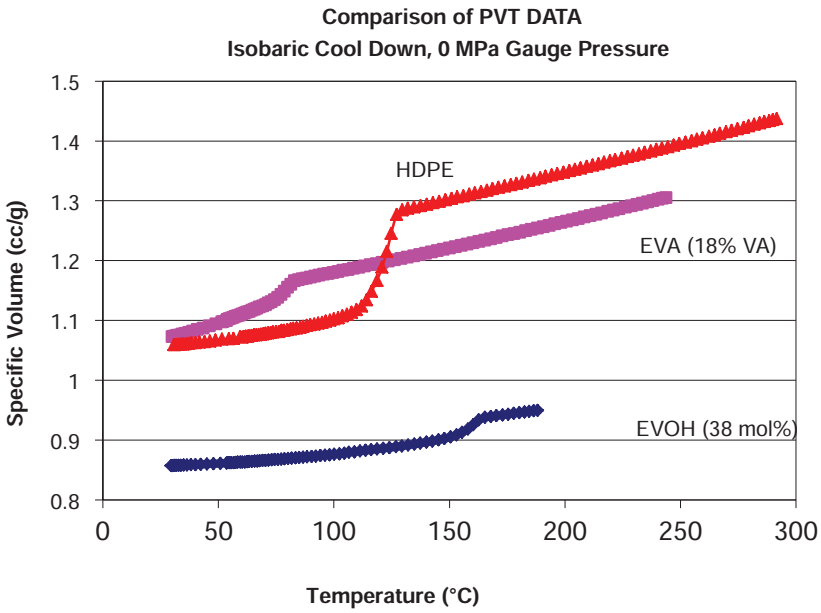


Figure 13.30 PVT data for EVOH, HDPE, and EVA.
Reproduced with permission from Morris BA. Reducing curl in multilayer blown film: experimental results, model development, and application to a cereal liner film. J Plast Film Sheeting 2003;19:31–54.

rise to stresses that cannot be relieved by melt flow of the EVOH layer. Also, the moduli of EVOH and HDPE differ only by a factor of about two. The combination of high-differential shrinkage and comparable moduli results in curl.

The PVT curves show what happens to the polymers as they are quenched when primary crystallization occurs. After quenching, some polymers will undergo further crystallization called secondary crystallization. The crystals that form are often less perfect than the primary crystals, filling in some of the space between spherulites, for example. They still can produce shrinkage that affects curl. PA, in particular, is known to undergo secondary crystallization when exposed to moisture. Moisturization is one technique used to control the curl of PA-containing films as described below [106–108].

The actual mechanism for curl is residual stress caused by differential shrinkage, and in some cases orientation from the film blowing process. A number of investigators in the fields of coatings and composites [109–111] have developed models for relating curl to residual stress between two thin films. The models rely on classical beam and plate theory of continuum mechanics. As depicted in Fig. 13.31, the residual stress is countered by a resisting force related to the stiffness and thickness of the layers in the structure. When the residual stress is strong enough to overcome the resisting force, the film bends or curls. A force and momentum balance is used to calculate these forces. In the appendix, the approach of Shen and Suresh [109] is used to develop a model that relates the curl of films to the modulus, thickness, location, and shrinkage of each layer.

Figs. 13.32 and 13.33 show the results of the model for two-layer films. A convenient way to characterize the curl of films is the curvature, which is the reciprocal of the radius of curvature (Fig. 13.34). The radius of curvature is the radius of a circle that circumscribes the curling film; its

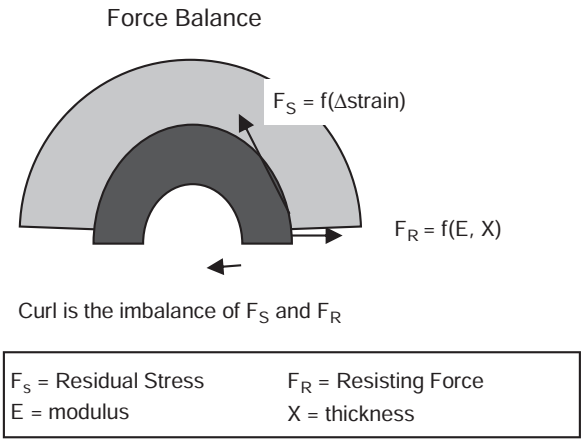


Figure 13.31 Forces acting on a two-layer film due to differential shrinkage.
From Morris BA. Reducing curl in multilayer blown film: experimental results, model development, and application to a cereal liner film. J Plast Film Sheeting 2003;19:31–54.

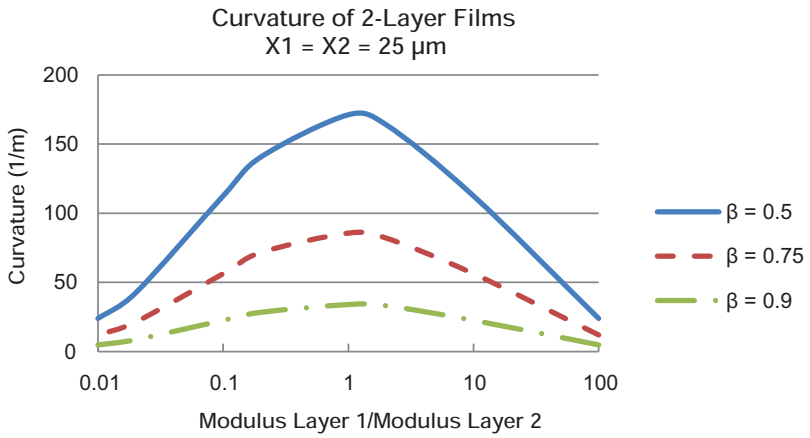


Figure 13.32 Model results for two-layer films showing effect of differential shrinkage (β) and modulus on curl. *Taken from Morris BA. Reducing curl in multilayer blown film: experimental results, model development, and application to a cereal liner film. J Plast Film Sheeting 2003;19:31–54.*

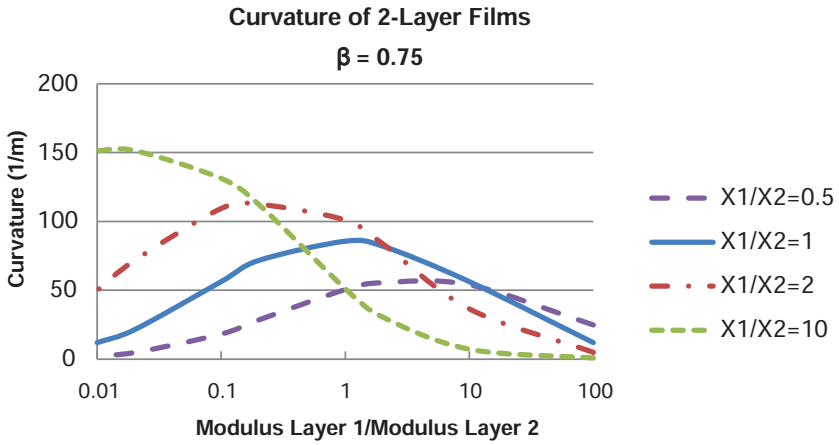


Figure 13.33 Model results for two-layer film showing the effect of thickness and modulus on curl. *Taken from Morris BA. Reducing curl in multilayer blown film: experimental results, model development, and application to a cereal liner film. J Plast Film Sheeting 2003;19:31–54.*

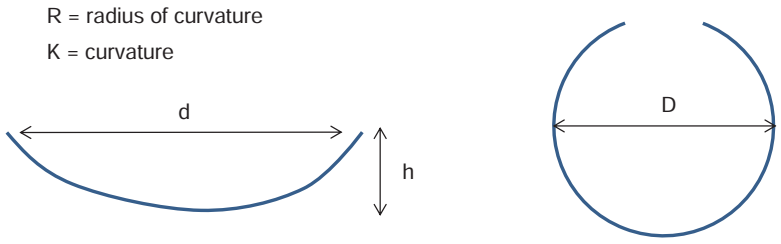


Figure 13.34 Measuring curl.

reciprocal is related to the severity of the curl. A flat film has a curvature of zero and films that curl tightly have large values of curvature. Fig. 13.32 plots the curvature versus the ratio of the stiffness (modulus) of the two layers. Here β represents the difference in shrinkage between the polymers (the ratio of the expansion coefficients). As β approaches 1, the differential shrinkage goes to 0. As β approaches 0, the differential shrinkage approaches ∞. Fig. 13.32 shows the model results for the case where the two layers are equal in thickness. The greatest curl occurs when the stiffness of the two layers is equal. As the stiffness of one layer dominates the other, the curl decreases. This agrees with practical experience: consider the painting of a metal part, such as an automotive door. As the paint dries, it shrinks relative to the door, but the door does not curl because it is so much stiffer than the paint. For the paint, the residual stress manifests itself in other ways, such as poor adhesion or pitting.

Fig. 13.32 also shows that as the differential shrinkage increases, the curl increases, as expected. In Fig. 13.33, the effect of varying the thickness of the film layers is demonstrated. The stiffness and thickness of the layers interact to varying degrees to resist the residual stress.

13.5.2 Strategies for Reducing Curl

With the residual stress mechanism as a foundation, several strategies are outlined for minimizing curl in film coextrusion.

13.5.2.1 Reduce the Crystallinity of the Polymers in the Film Structure, Particularly the Layer the Film is Curling Toward

Reducing the crystallinity of a polymer decreases ΔV_c and modulus, both of which can impact curl. Typically it is not the first layer to freeze that the film curls toward, even if that layer undergoes a large change in volume during crystallization. Its shrinkage occurs when the other layers are still molten and can flow in response. Later in the quenching process other layers begin to crystallize, imparting stresses against the already frozen first layer. It is these stresses that give rise to curl.

Table 13.8 Curl of Two-Layer Blown Film

Structure	Curls Toward	Severity
(HDPE−EVA)	EVA	Low
(HDPE−ionomer)	Ionomer	Low
(Ionomer−EVA)	EVA	Flat
(HDPE−EVOH)	HDPE	Very high
(HDPE−PA)	HDPE	Very high

Reproduced with permission from Morris BA. Reducing curl in multilayer blown film: experimental results, model development, and application to a cereal liner film. J Plast Film Sheeting 2003;19:31−54.

Morris [103,104] presents data for two-layer coextruded blown films of various layer ratios prepared on a laboratory blown film line. Table 13.8 shows the relative amount of curl for each combination of materials. Structures containing PA or EVOH curl tightly, whereas those containing only low crystalline polymers curl loosely. Interestingly, although the EVOH−HDPE film curls severely, when the two layers (which have poor adhesion to each other) are separated, the resulting films are flat. This validates the hypothesis that residual stress at the interface is involved.

In a second study, Morris conducts a statistically designed experiment looking at five factors on the curl of two layer films with the structure (EVOH−polyolefin). The variables are the following:

- polyolefin (PO) crystallinity (HDPE or EVA);
- BUR (1.6−2.9);
- ratio of thickness of PO to EVOH (0.5−2);
- frost line height (10−25 cm);
- Modification of EVOH by adding Surlyn AM7927 at 0−20%. AM7927 is an additive manufactured by DuPont that improves the thermoformability of EVOH and is expected to reduce the crystallinity and modulus of EVOH.

The parameters that are kept constant include the extrusion processing temperatures, final film thickness (113 μm), haul-off speed, and EVOH (38 mol% ethylene). Because the haul-off speed and film thickness are constant, as the BUR is increased the draw down ratio (DDR) decreases (from 8.6 to 4.8).

Curl measurements are made in both the MD and TD. For TD curl, 25-mm wide strips are cut in the

Table 13.9 Results of Statistically Designed Experiment Evaluating Curl of Two-Layer Blown Film

Factors That Reduce Curl	Effectiveness
↓ Crystallinity of PO (HDPE ⇒ EVA)	***
↓ BUR (↑ DDR)	**
↓ PO/EVOH thickness ratio	*
↑ Frost line height (MD curl)	***
↑ EVOH modifier (Surlyn AM7927)	Not significant

Asterisks represent statistical significance, which a higher number of asterisks meaning greater significance.
Reproduced with permission from Morris BA. Reducing curl in multilayer blown film: experimental results, model development, and application to a cereal liner film. J Plast Film Sheeting 2003;19:31–54.

MD (and vice versa for measuring MD curl). From these strips, 5-mm strips are cut and the curvature measured as illustrated in Fig. 13.34.

The analysis of the results is summarized in Table 13.9. In all cases, the curl is toward the polyolefin layer. The crystallinity of the polyolefin layer has the most statistically significant impact followed by the BUR and the thickness ratio. Frost line height is only significant for MD curl (not TD curl). EVOH modification has only a small impact on curl. Overall, it is found that the curl can be reduced (in order of greatest to least impact) by decreasing the crystallinity of the polyolefin layer (HDPE to EVA), increasing frost line height (MD only), reducing the BUR, and decreasing the polyolefin/EVOH thickness ratio.

In a third study, Morris looks at the effect of changing the crystallinity of the tie resin in the three-layer structure: (38-μm HDPE–13-μm tie–25-μm EVOH). The HDPE has a density of 0.960 g/cc and MI of 0.75 g/10 min. The EVOH is the 38-mol% ethylene grade used in the previous studies. The tie resins are all anhydride-modified ethylene copolymers. The base resins and corresponding freezing points are shown in Table 13.10 along with the curl results.

A tie resin with a low melting point may be fluid enough as the HDPE crystallizes to relieve the stress created by the differential shrinkage of the HDPE against the already solid EVOH. The data in Table 13.10, however, show that tie resin melt point has only a small effect on the curl (all the values are indicative of very tight curl). Furthermore, as the films aged (Fig. 13.35), the curl becomes more severe and all the films end up with about the same curl.

Aging is found to have a significant impact on curl. Samples of two-layer films containing PA or EVOH are aged in different moisture environments (desiccator at room temperature, 50% RH at room temperature, and 90% RH, 40°C). In general, the curl becomes more severe with time, but less so in the high humidity environments. The modulus of the layers is found to increase with time but not as much as the curl. This suggests that at high humidity, relaxation of stresses at the interface may be involved rather than a secondary crystallization or plasticization (from water) effect. For the case of PA, the presence of moisture can cause secondary crystallization [107–109], which causes further shrinkage with time. In either case, aging is just one of the many factors that makes understanding curl difficult.

Table 13.10 Effect of Changing Tie Resin on Curl of Coextruded Blown Film. Film Structure is (HDPE–tie–EVOH)

Tie Resin	Type	DSC T_c (°C)	K (m^{-1})	
			Mean	Standard Deviation
Tie1	EVA	58	123	9
Tie2	EVA	67	86	7
Tie3	LDPE	95	147	15
Tie4	LLDPE	112	152	55

Data from Morris BA. Reducing curl in multilayer blown film: experimental results, model development, and application to a cereal liner film. J Plast Film Sheeting 2003;19:31–54.

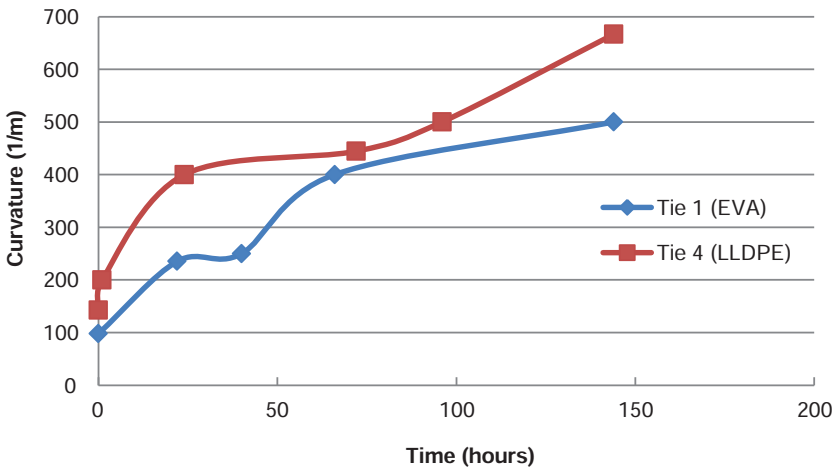


Figure 13.35 Effect of aging on curl of three layer films from Table 13.10. *Data from Morris BA. Reducing curl in multilayer blown film: experimental results, model development, and application to a cereal liner film. J Plast Film Sheeting 2003;19:31–54.*

13.5.2.2 Match the Shrinkage of the Layers So That They Cancel Out

This is a more theoretical than practical strategy since it is often difficult to achieve, but it provides a direction for modifying a structure to reduce curl. It explains why symmetric structures have little or no curl. For example, the structure (LLDPE–tie–EVOH–tie–LLDPE) where the layers on each side of the EVOH are the same should have no curl. As the film is quenched, the EVOH freezes first, followed by the LLDPE and tie resins on each side. Both sides shrink, but by the same amount so that the stress balances out. Increasing the thickness of one of the LLDPE layers, or increasing its density (which increases crystallinity and modulus) will cause the film to curl in that direction.

When creating unbalanced structures, trying to add some of the more crystalline polymer on the other side of the first layer to freeze may help. With the increased number of layers often available on modern coextrusion blown film lines, this is becoming more practical. In the past, with only three or five layers, this was a challenge. Consider a five-layer barrier structure: (HDPE–tie–EVOH–tie–EVA) with thicknesses (35/3/5/3/20 μm). This structure tends to curl toward the HDPE layer. Reducing the thickness of the HDPE layer would reduce the curl, but the thickness of this layer is needed to achieve moisture barrier specifications. With only five layers, many have tried increasing the crystallinity of the tie layer on the sealant side of the structure, perhaps switching from an EVA-based tie resin to an LLDPE or even HDPE-based tie resin. This has had limited success due to the thinness of this layer. With a nine-layer line, one has the flexibility to build in other layers on the sealant side to try to balance out the shrinkage and curl.

Another way to balance the shrinkage involves PA-coextruded films. Moisturizing the PA can cause secondary crystallization and shrinkage that may balance curl. This is discussed in more detail below.

13.5.2.3 Match the Freezing Points or Crystallization Rates of the Layers So That Shrinkage Occurs at the Same Time

In most coextruded film, the layers have different freezing points. The layer with the highest freezing point crystallizes first while the other layers are still molten and can flow in response. This layer provides a solid surface for the subsequent layers to shrink against, causing curl. So the order in which freezing takes place can affect the amount of curl. If the layers shrink at the same time, most of the shrinkage will cancel out.

For polyolefins, the freezing point varies with the class of polymer. The order from highest to lowest is polypropylene homopolymer (hoPP) > polypropylene random copolymer (coPP) > HDPE > LLDPE > LDPE. Specialty copolymers, such as metallocene plastomer, EVA, and ionomer, have lower freezing points than LDPE; their freezing points decrease with increasing comonomer content.

The freezing point of EVOH decreases with increasing ethylene content. For polyesters and PAs,

copolymers often have lower freezing points and crystallinity than the homopolymer. For example, PETG has a much lower melting and freezing point than PET.

Goetz [107,108] shows that the crystallization rate of PAs varies greatly with PA type and whether nucleating agents are added. Nucleating agents such as talc provide sites for crystals to form, generally increasing the temperature at which crystallization begins and the number of crystals that form (by several orders of magnitude). While the total amount of crystallinity ends up being about the same as unnucleated PA, the size of the crystals is substantially reduced. Nucleated PA blown film tends to have substantially less haze than unnucleated blown PA.

PA6 crystallizes faster than PA6/66 copolymers, and nucleated PA6 crystallizes faster yet. A PA grade that crystallizes slowly may overlap with the crystallization of PE in (PA—tie—PE) structures. For this reason, nucleated PA6 has higher curl than unnucleated PA6 in such structures. PA6/66 has even less curl, and blends of PA6/66 with amorphous PA (6I/6T, such as DuPont's Selar PA) crystallize in the same range as PE. Their crystallinity often cancels out the shrinkage of the PE and produce flat film. This is illustrated in Fig. 13.36.

13.5.2.4 Increase the Quench Rate

Increasing the quench rate during film fabrication suppresses the total amount of crystallinity, reducing overall shrinkage. It also lowers the temperature at which crystallinity occurs—through what is known as supercooling. This has the effect of clustering the freezing points of the layers, allowing some of the shrinkage to overlap and cancel out.

Cast films of the same composition typically have less curl than blown films due to the higher quench rate. Likewise, water-quench blown film curls less than air-quench blown film (Chapter 14). Crist [106] shows that a cast film of PA6 is almost amorphous, whereas a blown film of unnucleated PA6 has large spherulite crystals. Compared with blown films, cast films of PA6 are nearly transparent, have lower density, tensile strength and stiffness, and better formability.

13.5.2.5 Enhance Post-quench Crystallization

Most of the crystallization of semicrystalline polymers occurs as the polymer solidifies from the melt during the film-making process. Some polymers will continue to crystallize even at room temperature, although most do so at a very slow rate. Post-quench crystallization, known as secondary crystallization,

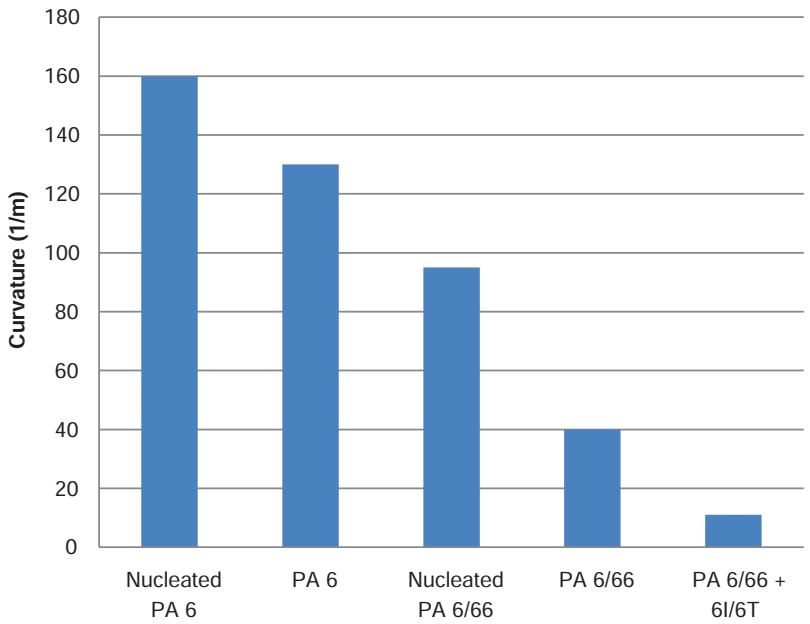


Figure 13.36 Curl of (PA—tie—LDPE) blown film (air quenched), total thickness 100 μm.
Data from Goetz W. Curl in multilayer PA/PE film. In: European TAPPI PLACE conference; 2001.

Table 13.11 Effect of Moisturization on Curl of (PA−tie−LDPE) Blown Films. Total Film Thickness is 100 μm. Results Are Reported as Curvature in Units of m^{-1}. Positive and Negative Values Indicate Curl Toward LDPE and PA Layers, Respectively

Water Bath	PA6/66	PA6/66 Nucleated	PA6 + PA6/66 (50:50)	PA6	PA6 Nucleated
None	40	80	100	180	200
25°C	−100	0			
40°C			0		
50°C				50	100
70°C				20	50

Data from Goetz W. Curl in multilayer PA/PE film. In: European TAPPI PLACE conference; 2001.

generally produces crystals that are less perfect and smaller than the primary crystals formed during quenching. This reordering of the molecules increases the density and shrinks the film. Some of the changes that occur include increased stiffness, dimensional change, and changes in curl. The aging effects shown in Fig. 13.35 may be related to post-quench crystallization among other things.

Post-quench crystallization is more likely to occur in films that experienced rapid quench rates, which suppresses the primary crystallization. A polymer has a certain preferred degree of crystallinity based on the ordering of the molecules into the lowest energy configuration. A rapid quench freezes the molecules in place before they have a chance to reach this preferred state. The driving force is still present to form crystals, yet the energy hurdle can be large particularly if the ambient temperature is below the glass transition temperature of the polymer. Molecular motion at room temperature may further be slowed by the presence of crystals that confine chain movement.

PA is a special case. PA6 and its copolymers absorb water, which plasticizes this highly polar polymer, disrupting the hydrogen bonds that bind the molecular chains together (the covalent bonds between atoms within the chain are not affected). Depending on the amount of moisture absorbed, the Tg decreases from about 55°C to 10°C. As the Tg drops below the ambient temperature, molecular motion increases, allowing secondary crystallization to occur. The secondary crystallization does not significantly increase the density but does cause 1−2% shrinkage over time. This time can be substantially accelerated by heating the polymer while it is exposed to moisture. Generally this is done by dipping the film into a heated water bath after quenching.

In a coextruded structure that is curling away from the PA, secondary crystallinity can help balance the shrinkage and reduce curl. If the film is already balanced, secondary crystallinity may induce curl toward the PA layer. Goetz [107,108] provides examples of three layer (PA−tie−PE) blown films exposed in-line to a post-quench water bath. The water is controlled to different temperatures and the residence time in the bath is 5 s. Excess water is removed from the surface of the films following the moisturization process and the films are conditioned at 23°C and 50% RH for 24 h prior to measuring curl.

The results are shown in Table 13.11. With no water bath exposure, the results are similar to Fig. 13.36; changing the PA grade to one with a higher natural level of primary crystallinity or rate of crystallinity increases the curl toward the PE layer. Exposure to room temperature, water is enough to switch the curl of the film containing PA6/66, the least crystalline PA, toward the PA. Those films with PA types with greater curl toward the PE layer require higher temperature water (more secondary crystallization) to reduce the curl. The curl of the film samples containing PA6 could not be completely eliminated even with exposure to boiling water. Control of the PA type, through selection of copolymers or blends, and moisturization conditions allows for the production of curl-free films.

13.5.2.6 Balance the Modulus, Thickness, Location, and Shrinkage of the Layers

This strategy is often the most practical approach. Materials selection is usually constrained by cost and functionality. For example, reducing the density of the HDPE layer may reduce curl, but at the cost of

reducing moisture barrier as well. Likewise, the option of significantly altering the blown-film process to achieve faster quench may be cost prohibitive for a given application. Also, changing quench conditions can have an impact on film properties (Chapter 14) and adhesion (Chapter 15). Thus, the converter is often left with trying to balance and rearrange layers to reduce curl using a trial and error approach that can both be costly and have no assurance of success. Clearly, a predictive model of the effect of thickness, layer arrangement, modulus, and shrinkage on curl would be of benefit to this process.

13.5.3 Modeling

One approach is to use statistically designed experiments to develop empirical models. A statistical model for the two-layer film developed by Morris was described earlier (Table 13.9). Kucejko and Pratt [112] use a design of experiments approach to reduce curl in a five-layer film with the structure (EVA−HDPE−LDPE−LDPE−HDPE). The nominal layer thicknesses are (10/20/50/20%) where the LDPE core (50%) represents the combination of the third and fourth layers. An eight-state screening design is run by varying the following:

- EVA melt temperature;
- outside HDPE layer melt temperature;
- total thickness;
- % HDPE (outside layer);
- % EVA (inside layer);
- Frost line height.

The HDPE and EVA layer thickness are varied at the expense of the LDPE core. The largest effect is % HDPE (lower gives less curl). Increasing output and decreasing thickness also helps reduce curl. Kucejko uses the model as a guide for making a film for a customer that has no curl.

Statistical-based models are very useful for a specific set of variables and provide predictions for inside the experimental design space. They are also helpful when many variables may be significant and the underlying mechanisms are not well understood. A more broadly useful tool is one based on first principles that can be applied to different structures.

Such a model has been developed by Morris [103−105] using classic beam theory and is derived in the appendix. Only the curl that develops during quenching of the film is considered (no secondary crystallization). The model inputs include the thickness, location in the multilayer structure, and tensile or secant modulus of each of the layers. These are either well known or can be easily obtained. More challenging is the thermal expansion coefficient, α, for each of the layers. Morris first assumed that α is the sum of the change in volume due to crystallization (from the PVT data) and the coefficient of linear thermal expansion in the solid state (obtained from thermal−mechanical analysis data):

$$\alpha_i = \alpha_T + \frac{\Delta V_c}{\Delta T} \tag{13.8}$$

where α_i = coefficient of thermal expansion for layer i; α_T = coefficient of linear thermal expansion (solid state); ΔV_c = volumetric change during crystallization; ΔT = temperature range for the analysis.

The final input parameter is the temperature range, ΔT, over which the polymer cools during quenching. The calculation is assumed to begin after the first layer freezes since any thermal contraction that occurs before that point is compensated by flow of the polymers. ΔV_c of the first layer to freeze is ignored and ΔT is taken as the difference between the crystallization temperature of the second layer to crystallize and room temperature.

This approach predicts film curvature that is substantially greater than what is actually measured, although it does correctly predict the direction of the curl. There are a number of reasons why this simple model does not yield quantitative results:

- Quench rate. The PVT data are generated at a cooling rate of 2°C/min, whereas commercial blown film lines quench the polymer at around 500−1500°C/min. A fast quench has the effect of reducing the temperature at which crystallization begins and the extent of crystallization due to undercooling of the melt. Spruiell et al. [113−115] developed a fast quench device for measuring crystallization kinetics with cooling rates up to 5000°C/min and published work on HDPE, LDPE, and PP. At fast quench rates, they find that crystallization becomes heat transfer limited. The exothermic heat of crystallization is balanced by the limited heat convection away from the film surface, giving rise to a temperature plateau several investigators have found in blown film [116,117]. Most of the

crystallization occurs in the plateau region and the crystals do not impinge until near the end of the plateau, suggesting much of the stress due to shrinkage during crystallization (ΔV_c) may relax. This would account for some of the overprediction of curl in the model. Spruiell finds that increasing the quench rate reduces the plateau temperature (which they equate to the freezing point), reduces the time for nucleation to occur, decreases the width of the plateau, increases the rate of crystallization, and reduces overall crystallinity.

- Stress-induced crystallization. As the blown film crystallizes, it also experiences stress and orientation. Stress is believed to accelerate the onset of crystallization by aligning the molecules and forming crystals along the chain. These crystals then nucleate the formation of chain-folded lamellae or "rows" of crystals. Most of the literature on flow-induced crystallization involves high-speed fiber spinning [118] where orientation is about an order of magnitude greater than for blown film. Lagasse and Maxwell [119] show, however, that even small amounts of strain/stress can substantially increase nucleation rates. Doufas and McHugh [120] develop a model of flow-induced crystallization of blown film. Faster quench rates act to delay crystallization, whereas stress acts to speed it up. More work is needed to understand the crystallization kinetics when both occur simultaneously as in the blown film process.
- Relaxation of strain (creep). Since the crystals do not impinge until most of the crystallization has taken place, some relaxation of strain imposed by shrinkage during crystallization is likely to happen. The amount of relaxation during crystallization and after is difficult to predict and may have a substantial influence on curl.
- Anisotropic shrinkage. It is assumed that the shrinkage is isotropic, yet the experiments described earlier show that factors such as BUR and DDR influence curl. This suggests that shrinkage and curl may be anisotropic.
- Secondary crystallization. As described above, some polymers continue to crystallize over time after they are quenched. Shrinkage due to secondary crystallization may balance out some of the curl. This is ignored in the model.
- Excessive deformation. The model is based on equations developed for small deflections of beams. Some structures, particularly ones involving EVOH or PA, curl very tightly. The model may no longer apply, particularly if the materials yield.

Morris works around these limitations by introducing a relaxation factor to Eq. (13.8):

$$\alpha_i = \alpha_T + \frac{\Delta V_c}{\Delta T} - \Re \tag{13.9}$$

where $\Re$ = relaxation factor.

The relaxation factor is determined experimentally from two-layer film curl data; the model is run backward to compute α from the curl results. By making measurements on different combinations of resins, a database of relaxation factors is built. Once $\Re$ is known for each resin, the model can be extended to any combination of resins and number of layers. To test the model, the curl of the (HDPE−tie−EVOH) structures described in Section 13.5.2.1 is computed. The measured curvature is around 140 m^{-1}, independent of tie layer, and ages up to 500 m^{-1}. Using an EVA to mimic the tie resin, the model predicts a curvature of 220 m^{-1}, which falls within the range of the experimental results. Furthermore, changing the parameters of the model to reflect different tie resins (such as LLDPE) does not appreciably change the results. This also agrees well with the experimental results.

To illustrate the utility of the model, Morris analyzes a barrier cereal liner film with the structure (HDPE−tie−EVOH−tie−sealant). The HDPE, typically 60% or more of the structure, provides a moisture barrier. The EVOH, around 7% of the structure, provides oxygen and aroma barrier. The sealant is typically an EVA or ionomer formulated for ease to open (peel seal). The tie layers comprise about 8% of the total structure. This combination of layers is often very difficult to make without significant curl. Qualitatively, this is because the EVOH freezes first and cannot flow in response to the substantial shrinkage of the HDPE layer as it freezes.

A sensitivity analysis is conducted using the model to predict which parameters most impact the curl for this structure. The results are given in Table 13.12 and Fig. 13.37. To simplify the analysis, the tie layers are ignored. The parameters are the thickness, modulus, and relative shrinkage (α) of each of the layers. The range for each parameter is

Table 13.12 Results of Parametric Study of Factors Affecting Curl of (HDPE–EVOH–Sealant) Film. Base Case Structure (40 μm HDPE–4 μm EVOH–19 μm Sealant)

Layer	Attribute	Attribute Range	K (m^{-1})
Sealant	Modulus, MPa	14–345	175–172
	α, m/m-°C	0.00002–0.0002	189–164
	Thickness (HDPE floats), μm	7.5–25	119–200
EVOH	Modulus, MPa	690–3450	88–5
	α, m/m-°C	0.00002–0.0001	208–8
	Thickness (HDPE floats), μm	2.5–7.5	133–263
HDPE	Modulus, MPa	6900–1730	227–147
	α, m/m-°C	0.00005–0.0004	−9.4–416

Base case K = *175 m^{-1}. Positive values indicate curl is toward the HDPE layer and negative layers toward the sealant. Adapted from Morris BA. Reducing curl in multilayer blown film: experimental results, model development, and application to a cereal liner film. J Plast Film Sheeting 2003;19:31–54.*

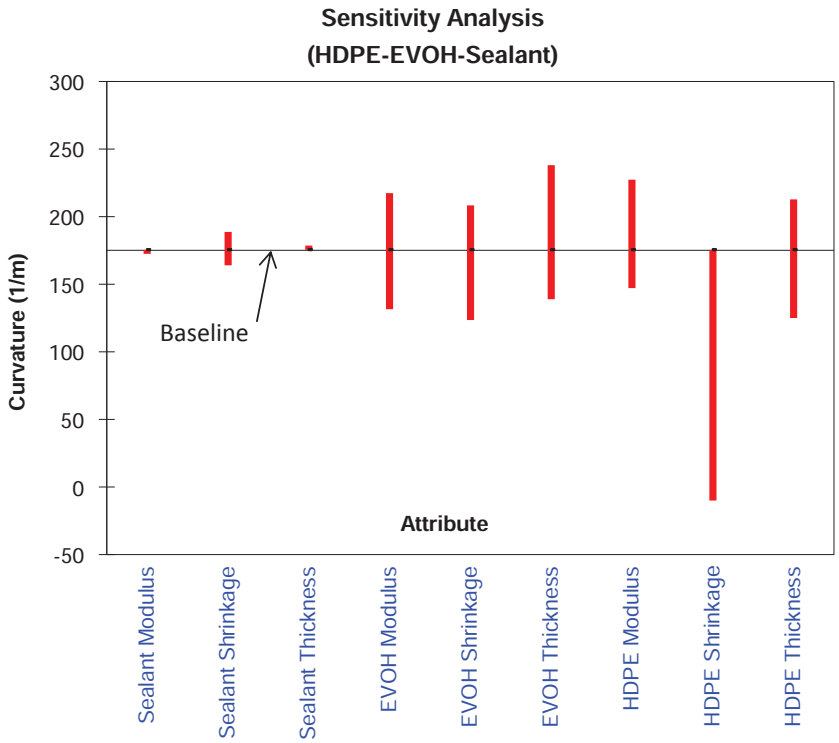


Figure 13.37 Sensitivity analysis of (HDPE–EVOH–sealant) film. *Adapted from Morris BA. Reducing curl in multilayer blown film: experimental results, model development, and application to a cereal liner film. J Plast Film Sheeting 2003;19:31–54.*

chosen to represent practical limits for that layer. The total thickness is kept constant. The analysis suggests that curl can be reduced in this structure by making the HDPE layer thicker, stiffer, and shrink less and making the EVOH layer thinner, less stiff, and shrink more. The HDPE layer has the greatest impact on the curl and the sealant layer has the least.

To validate the model predictions, eight films are made on a five-layer blown film line and their curl measured. The blown film line is equipped with five

extruders (63-mm diameter for the inside and outside layers, 50-mm diameter for the middle layers) feeding a 203-mm diameter coextrusion die equipped with a dual-lip air ring. The blowup ratio is 2.0, DDR 14, haul-off speed 19.8 m/min, frost line height 56 cm, and die gap 1.88 mm. Total film thickness is 69 μm. The structure is (HDPE−tie 1−EVOH−tie 2−sealant). Final barrel temperature set points and die temperature are 227°C.

Variables include the following:

- Sealant type (Table 13.13)—Three sealants are used, an EVA (18 wt% VA) and two ionomers commonly used in snack structures.
- EVOH type (Table 13.14)—A standard grade of EVOH (38 mol% ethylene) is evaluated along with two modifiers, an amorphous nylon and an ionomer, originally designed to enhance the thermoformability of EVOH. Adding amorphous nylon to PA6 is known to reduce curl.
- HDPE type (Table 13.15)—A standard grade and a talc-filled grade of HDPE are evaluated. The mineral filler reduces the shrinkage and increases the stiffness of the HDPE layer.
- HDPE thickness (63−84%)—Because of limitations on the HDPE extruder, this is accomplished by changing the tie 1 thickness from 4% to 25%. The standard and thick HDPE structures are illustrated in Fig. 13.38.
- EVOH thickness (7−4%).
- Sealant thickness (30−12%)—To keep the total thickness constant, the sealant thickness is reduced as the HDPE thickness is increased. Tie 2 (4%) is considered part of the sealant layer for the analysis.

Table 13.13 Sealants Used in Blown Film Trial

Code	Resin	Modulus (MPa)	Description
EVA	Elvax 3165	41	18%VA EVA
ION1	Surlyn 1650	275	Zn-ionomer
ION2	Surlyn 1855	150	Zn-ionomer
Tie2	Bynel 3930	83	EVA-based tie

From Morris BA. Reducing curl in multilayer blown film: experimental results, model development, and application to a cereal liner film. J Plast Film Sheeting 2003;19:31−54.

Table 13.14 EVOH Used in Blown Film Trial

Code	Resin	Modulus (MPa)	Description	Manufacturer
EVOH1	Eval LCH101A	2270	38-mol% ethylene	Kuraray
EVOH2	80% Eval LCH101A 20% Surlyn AM7927	1565	Blend	Kuraray DuPont
EVOH3	80% Eval LCH101A 20% Selar PA	2130	Blend	Kuraray DuPont

From Morris BA. Reducing curl in multilayer blown film: experimental results, model development, and application to a cereal liner film. J Plast Film Sheeting 2003;19:31−54.

Table 13.15 HDPE Used in Blown Film Trial

Code	Resin	Modulus (MPa)	Description	Manufacturer
HDPE	Sclair 19A	1140	0.96 g/cc	Nova chemical
Talc-HDPE	Zemid 641	1380	30% talc	DuPont Canada
Tie1	Bynel 4003	830	HDPE-based tie	DuPont

From Morris BA. Reducing curl in multilayer blown film: experimental results, model development, and application to a cereal liner film. J Plast Film Sheeting 2003;19:31−54.

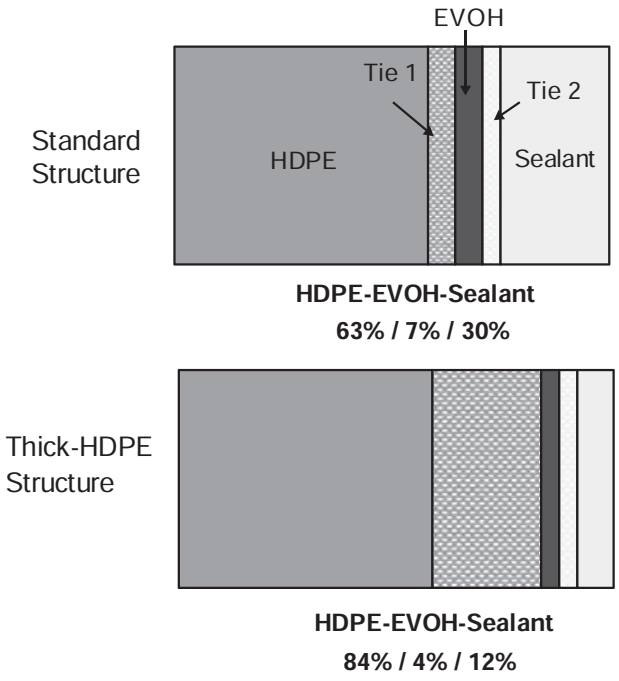


Figure 13.38 Structures in curl experiment.
From Morris BA. Reducing curl in multilayer blown film: experimental results, model development, and application to a cereal liner film. J Plast Film Sheeting 2003;19:31–54.

The design of the experiment is described in Table 13.16 along with the curvature results. The results are also plotted in Figs. 13.39–13.41. The results show the following:

- In the standard cereal liner structure, the curl is very tight toward the HDPE layer. The curl is in the MD. No value is recorded for the TD since the curl is too strong in the MD to get a meaningful measurement in the TD.
- Changing the sealant does not impact the curl very much, as predicted by the model. ION2 gave the least amount of curl of the sealants tested. Its performance may be enhanced by post-quench crystallization that is not accounted for by the model.
- Modifying the EVOH resin does not significantly reduce the curl in this structure. In other structures, however, this technique may be effective.
- Increasing the thickness of the HDPE layer significantly reduces curl, as predicted by the model.
- Using a mineral-filled HDPE significantly reduces curl. As shown by the model, this is due primarily to less shrinkage, although an increase in stiffness is also beneficial. The direction of curl changes from MD to TD.
- A combination of these factors yields essentially flat film.
- Overall, there is excellent agreement between the experimental results and the model predictions.

The films containing the talc–HDPE had poor tear resistance and barrier properties. A calcium carbonate-filled HDPE may be a better choice for practical application, since subsequent measurements on such a film showed excellent tear resistance and MVTR as good as a standard grade of HDPE.

Table 13.16 Design of Curl Experiment and Curvature Results

Name	Sealant	EVOH	HDPE	HDPE Thickness	Curvature (m^{-1})				
					Green		1-week		
					MD	TD	MD	TD	Model
Standard	EVA	EVOH 1	HDPE	Standard	250	0	250	0	188
Sealant 2	ION1	EVOH 1	HDPE	Standard	238	0	250	0	200
Sealant 3	ION2	EVOH 1	HDPE	Standard	182	0	192	0	192
EVOH 2	EVA	EVOH 2	HDPE	Standard	238	0	250	0	156
EVOH 3	EVA	EVOH 3	HDPE	Standard	333	0	250	0	182
Thick PE	EVA	EVOH 1	HDPE	Thick	147	0	98	0	91
Talc PE	EVA	EVOH 1	Talc–HDPE	Thick	0	105	0	48	59
Combined	ION2	EVOH 2	Talc–HDPE	Thick	0	50	0	25	45

Adapted from Morris BA. Reducing curl in multilayer blown film: experimental results, model development, and application to a cereal liner film. J Plast Film Sheeting 2003;19:31–54.

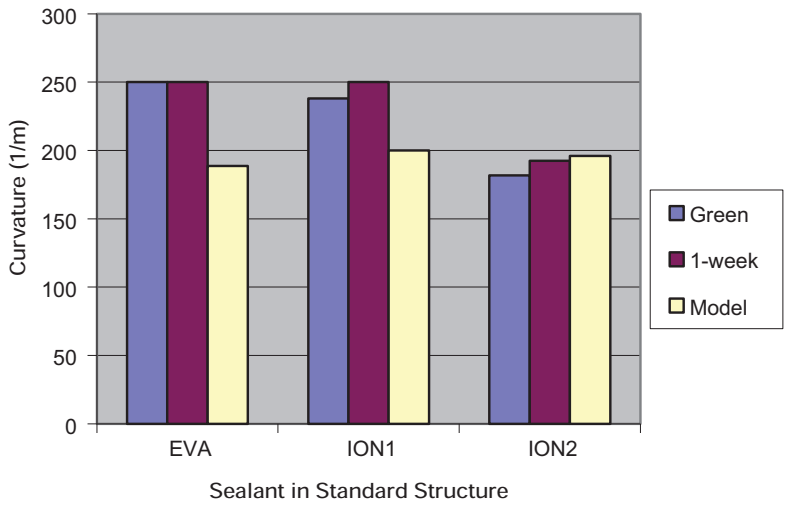


Figure 13.39 Curl results from blown film trial. Effect of sealant type.
Data from Morris BA. Reducing curl in multilayer blown film: experimental results, model development, and application to a cereal liner film. J Plast Film Sheeting 2003;19:31–54.

These evaluations show that the model makes fairly accurate predictions despite simplifying assumptions that include the following:

- Ignoring post-quench crystallization.
- Using a single relaxation "correction" factor to account for a number of physical attributes that are difficult to determine, including the effect of quench rate and stress on crystallization kinetics and the amount of stress relaxation.
- Assuming that shrinkage of adjacent layers occurring before a layer freezes-off does not contribute to the differential strain.
- Ignoring processing effects although processing conditions such as blowup ratio and draw down ratio are found in experiments to affect curl.
- Assuming that shrinkage is isotropic.
- Ignoring plastic yielding and other nonlinear effects due to large deformations in the continuum mechanics description of curl.

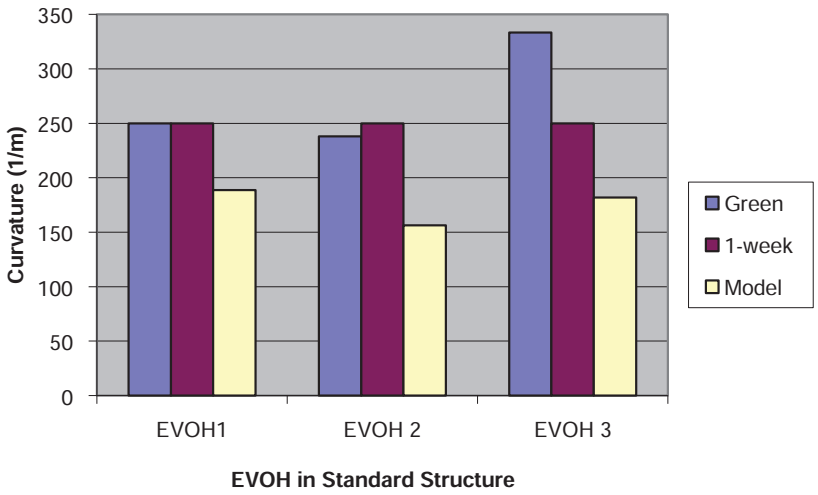


Figure 13.40 Curl results from blown film trial. Effect of EVOH type.
Data from Morris BA. Reducing curl in multilayer blown film: experimental results, model development, and application to a cereal liner film. J Plast Film Sheeting 2003;19:31–54.

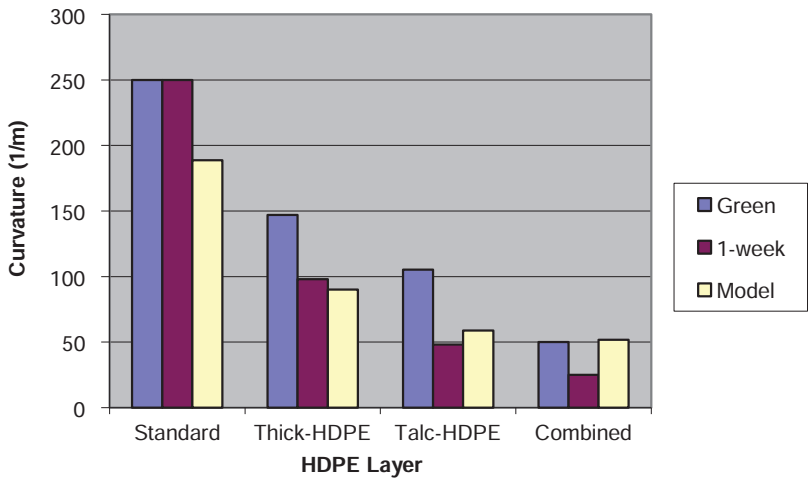


Figure 13.41 Curl results from blown film trial. Effect of HDPE type and thickness.
Data from Morris BA. Reducing curl in multilayer blown film: experimental results, model development, and application to a cereal liner film. J Plast Film Sheeting 2003;19:31–54.

Despite these limitations, the model does a remarkable job of predicting curl performance.

References

[1] Vlachopoulos J, Wagner JR, editors. The SPE guide on extrusion technology and troubleshooting. Brookfield (CT): The Society of Plastics Engineers; 2001.
[2] Rauwendaal C. Polymer extrusion. 4th ed. Munich: Carl Hanser Verlag; 2001.
[3] Campbell GA, Spalding MA. Troubleshooting & analysis of single-screw extrusion. New York: Hanser Gardner Publications; 2010. p. 484–90.
[4] Giles Jr HF, Mount III EM, Wagner Jr JR, editors. Extrusion: the definitive process guide and handbook. William Andrews; 2007. p. 453–63.
[5] Chung C. Extrusion of polymers: theory and practice. 2nd ed. Cincinnati (OH): Hanser Gardner Publications; 2000.
[6] Tadmor Z, Gogos C. Principles of polymer processing. 2nd ed. Hoboken (NJ): John Wiley & Sons; 2006.
[7] Tadmor Z, Klein I. Engineering principles of plasticating extrusion. New York: Van Nostrand Reinhold Co.; 1970.
[8] Bezigian T, editor. Extrusion coating manual. 4th ed. Atlanta: TAPPI Press; 1999.
[9] Butler TI. Gel troubleshooting. In: Butler TI, editor. 2005, Film extrusion manual. Atlanta: TAPPI Press; 2005. p. 275–86.
[10] Spalding MA, Garcia-Meitin E, Kodjie SL, Campbell GA. Troubleshooting and mitigating gels in polyolefin film products. In: SPE ANTEC conference; 2013.
[11] DuPont. The disco purge procedure for extrusion coaters. 2005. In: http://www.dupont.com//content/dam/dupont/products-and-services/packaging-materials-and-solutions/packaging-materials-and-solutions-landing/documents/disco_purge_procedure_.pdf.
[12] DuPont. Proper use of local exhaust ventilation during processing of plastics. 2011. http://www.dupont.com/content/dam/assets/products-and-services/plastics-polymers-resins/parts-shapes/documents/Ventilation_brochure_en_200108.pdf.
[13] Gander JD, Giacomin AJ. Review of die lip buildup in plastics extrusion. Polym Eng Sci 1997;37:1113–26.
[14] Musil J, Zatloukal M. Historical review of die drool phenomenon in plastics extrusion. Polym Rev 2014;54:16–34.
[15] Zatloukal M, Musil J. Die drool phenomenon in polymer extrusion. In: SPE ANTEC conference; 2014. p. 1048–54.
[16] Musil J, Zatloukal M. Experimental investigation of flow induced molecular weight fractionation during extrusion of HDPE polymer melts. Chem Eng Sci 2011;66:4814–23.
[17] Musil J, Zatloukal M. Experimental investigation of flow induced molecular weight

fractionation phenomenon for two linear HDPE polymer melts having same M_n and M_w but different M_z and M_{z+1} average molecular weights. Chem Eng Sci 2012; 81:146–56.
[18] Musil J, Zatloukal M. Investigation of die drool phenomenon for HDPE polymer melt. Chem Eng Sci 2010;65:6128–33.
[19] Hogan TA, Walla P, Dems BC. Investigation of the relationships between die build up and die swell. Polym Eng Sci 2009;49:333–43.
[20] Holtzen DA, Musiano JA. Die lip plate-out: a proposed mechanism. In: SPE regional technical conference (St. Louis); 1996.
[21] Zatloukal M, Chaloupkova K. Effect of die design and wall slip on die drool phenomenon for metallocene based LLDPE: theoretical and experimental investigation. In: SPE ANTEC conference; 2007.
[22] Chaloupkova K, Zatloukal M. Analysis of die drool phenomenon for metallocene based linear polyolefins. In: SPE ANTEC conference; 2006.
[23] Rakestraw JA, Waggoner MG. Polymer extrusion die and use thereof. U.S. Patent 5,458,836 A. 1995.
[24] Kurtz SJ, Szaniszio SR. Reduction of die drool in filled resins and product improvement. U.S. Patent 5,008,056. 1991.
[25] Koopmans R, Den Doelder J, Molenaar J. Polymer melt fracture. Boca Raton: CRC Press; 2011.
[26] Vergnes B. Extrusion defects and flow instabilities of molten polymers. Intern Polym Process 2015;XXX:3–28.
[27] Dealy JM, Wissbrun KF. Melt rheology and its role in plastics processing, theory and applications. Chapman & Hall; 1995. p. 336–40.
[28] Ramamurthy AV. Wall slip in viscous fluids and influence of materials of construction. J Rheol 1986;30:337.
[29] Silagy D, Demay Y, Agassant JF. Stationary and stability analysis of the film casting process. J Non-Newtonian Fluid Mech 1998;79: 563–83.
[30] Debbaut B, Marchal JM. Viscoelastic effects in film casting. In: Theoretical, experimental, and numerical contributions to the mechanics of fluids and solids. Z. Angew Math Phys 1995; 46(Special Issue):S679–98.
[31] Foederer BM, Morris BA. Use of IR technology to model temperature loss in the air gap. In: TAPPI PLACE conference; 2014.
[32] Dealy JM, Wissbrun KF. Melt rheology and its role in plastics processing, theory and applications. Chapman & Hall; 1995. p. 553–4.
[33] Dobroth T, Erwin E. Causes of edge beads in cast films. In: SPE ANTEC conference; 1985. p. 89–92.
[34] Dobroth T, Erwin E. Causes of edge beads in cast films. Polym Eng Sci 1986;26:462–7.
[35] Dobroth T, Erwin E. Elimination of edge beads in cast polymer films. In: SPE ANTEC conference; 1986. p. 893–900.
[36] Bezigian T. A survey of current bead reduction die technology. In: TAPPI polymers, laminations & coatings conference; 1997. p. 55–67.
[37] Bezigian T. A survey of current bead reduction die technology. In: Bezigian T, editor. 1999, Extrusion coating manual. 4th ed. Atlanta: TAPPI Press; 1999. p. 55–64.
[38] Dealy JM, Wissbrun KF. Melt rheology and its role in plastics processing, theory and applications. Chapman & Hall; 1995. p. 554.
[39] Christie A. Extrusion coaters: stop that edge weave. Plastics Technology; 2004. http://www.ptonline.com/articles/extrusion-coaters-stop-that-edge-weave.
[40] Bian B, Co A. Tension in multilayer film casting of polymer melts. In: SPE ANTEC conference; 1998. p. 113.
[41] Frey KR, Jerdee GD, Cleaver CD. The use of encapsulation dies for processing linear polyolefin resins in extrusion coating. In: SPE ANTEC conference; 2001.
[42] Butler TI. Blown film bubble instability induced by fabrication conditions. In: SPE ANTEC conferencevol. 58(1); 2000. p. 156–64.
[43] Tas P, Nguyen L, Marshall S, Kashanian M. Bubble stability and maximum output of SURPASS sLLDPE resin in blown film. In: TAPPI PLACE conference; 2004. p. 320–34.
[44] Han CD, Park JY. Studies on blown film extrusion. III. Bubble instability. J Appl Polym Sci 1975;19:3291.
[45] Han CD, Shetty R. Flow instability in tubular film blowing. I. Experimental study. IEC Fundam 1977;16:49.

[46] Kanae T, White JL. Kinematics, dynamics and stability of the tubular film extrusion of various polyethylenes. Polym Eng Sci 1984;24:1185.
[47] Kalyon DM, Yu D-W, Moy FH. Rheology and processing of linear low density polyethylene resins as affected by alpha-olefin comonomers. Polym Eng Sci 1988;28:1542.
[48] Obijeski TJ, Puritt KR. Improving the output and bubble stability of thick gauge blown film. In: SPE ANTEC conference; 1992. p. 150.
[49] Taylor J, Baik JJ. Benefits of coextruded LLDPE/LDPE film versus blended LLDPE/LDPE film. In: SPE ANTEC conference vol. 58(1); 2000. p. 209−15.
[50] Field GJ, Micic P, Bhattacharya S. Melt strength and film bubble instability of LLDPE/LDPE blends. Polym Int 1999;48:461−6.
[51] Savargaonkar N, Patel R, Karjala T, Salibi P, Liu L. Fundamentals of abuse performance of LLDPE/LDPE blends in blown film applications. In: SPE ANTEC conference; 2014. p. 880−4.
[52] Lue CT. Easy processing metallocene polyethylene. In: SPE ANTEC conference vol. 56(2); 1998. p. 1816−9.
[53] Morris BA. Modifier for increasing output and reducing gauge variation in LLDPE blown film. In: SPE polyolefins conference; 2008.
[54] Han CD. Multiphase flow in polymer processing. New York: Acedemic Press; 1981. p. 354−413.
[55] Dooley J, Stout B. An experimental study of the factors affecting the layer thickness uniformity of coextruded structures. In: SPE ANTEC conference; 1991. p. 62−5.
[56] Powers J, Dooley J. Coextrusion layer thickness distribution improvements via equipment design. In: SPE ANTEC conference; 1997. p. 328−33.
[57] Butler TI. Effects of flow instability in coextruded films. TAPPI J 1992;75(9):205−11.
[58] Khan AA, Han CD. On the interface deformation in the stratified two-phase flow of viscoelastic fluids. Trans Soc Rheol 1976;20:595−621.
[59] Khan AA, Han CD. A study on the interfacial instability in the stratified flow of two viscoelastic fluids through a rectangular duct. Trans Soc Rheol 1977;21:101−31.
[60] Dooley J, Dietsche. Numerical simulation of viscoelastic polymer flow − effects of secondary flows on multilayer coextrusion. Plast Eng April 1996;52(4):37−9.
[61] Dooley J, Ramanathan R. Coextrusion layer thickness variation − effects of geometry on layer rearrangement. In: SPE ANTEC conference; 1994. p. 89−93.
[62] Dooley J, Hitlon BT. Layer rearrangement in coextrusion. Plast Eng February 1994;50:25−7.
[63] Dooley J, Hughes K. Thickness variation in coextruded layers − effect of polymer viscoelasticity on layer uniformity. TAPPI J 1996;79(4):235−41.
[64] Dooley J, Hughes K. Coextrusion layer thickness variation − effect of polymer viscoelasticity on layer uniformity. In: SPE ANTEC conference; 1995. p. 69−74.
[65] Dooley J, Hyun KS, Hughes K. An experimental study on the effect of polymer viscoelasticity on layer rearrangement in coextruded structures. Polym Eng Sci 1998; 38:1060−71.
[66] Dooley J, Hughes K. Analyzing the flow through dies containing different channel geometries. In: SPE ANTEC conference; 1996. p. 236−40.
[67] Dietsche L, Dooley J. Numerical simulation of viscoelastic polymer flow − effect of secondary flows on multilayer coextrusion. In: SPE ANTEC conference; 1995. p. 188−93.
[68] Debbaut B, Avalosse T, Dooley J, Hughes K. On the development of secondary motions in straight channels induced by the second normal stress difference: experiments and simulations. J Non-Newtonian Fluid Mech 1997;69:255−71.
[69] Debbaut B, Dooley J. Secondary motions in straight and tapered channels: experiments and three-dimensional finite element simulation with a multimode differential viscoelastic model. J Rheol 1999;43:1525−45.
[70] Zryd JL, Dooley J. Relative effects of viscous and elastic forces on layer thickness uniformity in coextrusion. In: SPE ANTEC conference; 1998. p. 217.
[71] Shanker R, Ramanathan R, Schrenk WJ. Comparison of experimental velocity measurements in the manifold of an extrusion die with numerical simulation. In: SPE ANTEC conference; 1994. p. 75−9.

[72] Matsunage K, Kajiwara T, Funatsu K. Numerical simulation of multi-layer flow for polymer melts – a study of the effect of viscoelasticity on interfacial shape of polymers within dies. Polym Eng Sci 1998;38:1099–111.
[73] Schrenk WJ, Bradley NL, Alfrey Jr T, Maack H. Interfacial flow instability in multilayer coextrusion. Polym Eng Sci 1978;18:620–3.
[74] Ramanathan R, Shanker R, Rehg T, Jons S, Headley DL, Schrenk WJ. 'Wave' pattern instability in multi-layer coextrusion – an experimental investigation. In: SPE-ANTEC tech. papers, vol. 54; 1996. p. 224–8.
[75] Martyn MT, Gough T, Spares R, Coates PD. Visualization of melt interface in a co-extrusion geometry. In: SPE ANTEC conference; 2001.
[76] Martyn MT, Coates PD, Zatloukal M, Perdikoulias J. Visualisation and analysis of LDPE melt flows in a coextrusion geometry. In: TAPPI place conference, Boston, MA, vol. 1084; 2002. Also SPE ANTEC Conference, 2002.
[77] Martyn MT, Spares R, Coates PD, Zatloukal M. Imaging and analysis of wave type interfacial instability in the coextrusion of low-density polyethylene melts. J Non-Newtonian Fluid Mech 2009;156:150–64.
[78] Ramanathan R, Schrenk WJ, Wheatley JA. Coextrusion of multilayer articles using protective boundary layers and apparatus therefor. U.S. Patent 5,269,995 A. 1993.
[79] Levitt L, Macosko CW, Schweizer T, Meissner J. Extensional rheometry of polymer multilayers: a sensitive probe of interfaces. J Rheol 1997;41:671–85.
[80] Botros M, Lee C, Ward D, Schloemer T. New developments of Plexar® tie-layer adhesives in flexible and rigid applications. In: European TAPPI PLACE conference; 2005.
[81] Zatloukal M, Martyn M, Vlcek J, Saha P. Viscoelastic coextrusion flow modeling by advanced constitutive equations: the influence of the die design on interfacial instabilities. In: European TAPPI PLACE conference; 2005.
[82] Han CD, Shetty R. Studies on multilayer film coextrusion. II. Interfacial instability in flat film coextrusion. Polym Eng Sci 1978;18:180–6.
[83] Wilson GM. Interfacial instability in multilayer extrusion processes. In: SPE ANTEC conference; 1993.
[84] Yih CS. Instability due to viscosity stratification. J Fluid Mech 1967;27:337–52.
[85] Wilson GM, Khomami B. An experimental investigation of interfacial instabilities in multilayer flow of viscoelastic fluids, Part I. Incompatible polymer systems. J Non-Newtonian Fluid Mech 1992;45:355–84.
[86] Wilson GM, Khomami B. An experimental investigation of interfacial instabilities in multilayer flow of viscoelastic fluids, Part II. Elastic and nonlinear effects in incompatible polymer systems. J Rheol 1993;37:315–39.
[87] Wilson GM, Khomami B. An experimental investigation of interfacial instabilities in multilayer flow of viscoelastic fluids, Part III. Compatible polymer systems. J Rheol 1993;37:341–54.
[88] Hinch EJ, Harris OJ, Rallison JM. The instability mechanism for two elastic liquids being co-extruded. J Non-Newtonian Fluid Mech 1992;43:311–24.
[89] Valette R, Laure P, Demay Y, Agassant J-F. Experimental investigation of the development of interfacial instabilities in two layer coextrusion dies. Intern Polym Process 2004;XIX(2):118–28.
[90] Valette R, Laure P, Demay Y, Fortin A. Convective instabilities in the coextrusion process. Intern Polym Process 2001;XVI(2):192–7.
[91] Xiao K. Eliminating interfacial instability at PE/tie interface using a multi-layer stacked coextrusion die. In: SPE ANTEC conference; 2004. p. 362–6.
[92] Perdikoulias J, Tzoganakis C. Interfacial instability phenomena in blown film coextrusion of polyethylene resins. In: SPE ANTEC conference, vol. 53; 1995. p. 176–80.
[93] Perdikoulias J, Tzoganakis C. Interfacial instabilities during coextrusion of LDPEs. In: SPE ANTEC conference; 1997. p. 351–5.
[94] Mavridis H, Shroff RN. Multilayer extrusion: experiments and computer simulation. Polym Eng Sci 1994;34:559–69.
[95] Perdikoulias J, Zatloukal M, Tzoganakis C. Predicting the onset of interfacial instabilities in coextrusion flows. In: TAPPI polymers, laminations & coatings conference; 1999. p. 1003–10.
[96] Zatloukal M, Tzoganakis C, Vlcek J, Saha P. Numerical simulation of polymer coextrusion flows. Intern Polym Process 2001; XVI(2):198–207.
[97] Zatloukal M, Vlcek J, Saha P, Tzoganakis C. Viscoelastic stress calculation in multi-layer

coextrusion dies: die design and extensional viscosity effects on the onset of 'wave' interfacial instabilities. Polym Eng Sci 2002; 42:1520−33.
[98] Zatloukal M, Kopytko W, Lengalova A, Vlcek J. Theoretical and experimental analysis of interfacial instabilities in coextrusion flows. Polym Eng Sci 2005;98:153−62.
[99] Han CD, Shetty R. Studies on multilayer film coextrusion I. The rheology of flat film coextrusion. Polym Eng Sci 1976;16:697−705.
[100] Puissant S, Vergnes B, Demay Y, Agassant JF. A general non-isothermal model for one-dimensional multilayer coextrusion flows. Polym Eng Sci 1992;32:213−20.
[101] Pearson SD. Coextrusion flow analysis. TAPPI J 1994;77(6):193−7.
[102] Morris BA. Application of modeling to speed flexible package development. In: SPE ANTEC conference; 2012.
[103] Morris BA. Reducing curl in multilayer blown film: experimental results, model development, and application to a cereal liner film. J Plast Film Sheeting 2003;19:31−54.
[104] Morris BA. Reducing curl in multilayer blown film. Part I: experimental results, model development and strategies. In: TAPPI polymers, laminations and coatings conference; 2001.
[105] Morris BA. Reducing curl in multilayer blown film. Part II: application of predictive modeling to a barrier cereal liner film. In: TAPPI polymers, laminations and coatings conference; 2001.
[106] Crist MD, Do K, Noon E. Curl in nylon multilayer film. In: TAPPI polymers, laminations & coatings conference; 2000. p. 289−303.
[107] Goetz W. Curl in multilayer PA/PE film. In: European TAPPI PLACE conference; 2001.
[108] Goetz W. Curl in multilayer PA/PE film. In: TAPPI PLACE conference; 2002.
[109] Shen Y, Suresh S. Elastoplastic deformation of multilayered materials during thermal cycling. J Mater Res 1995;10:1200−15.
[110] Benabdi M, Roche A. Mechanical properties of thin and thick coatings applied to various substrates. Part I. An elastic analysis of residual stresses within coating materials. J Adhes Sci Technol 1997;11:281−99.
[111] Corcoran E. Determining stresses in organic coatings using plate-beam deflection. J Paint Technol 1969;41:635−40.
[112] Kucejko RM, Pratt JB. Curl in five layer coextruded film. Film extrusion TAPPI short course notes, 97. 1991.
[113] Ding Z, Spruiell J. Interpretation of the nonisothermal crystallization kinetics of polypropylene using a power law nucleation rate function. J Polym Sci B Polym Phys 1997;35:1077−93.
[114] Ding Z, Spruiell J. An experimental method for studying nonisothermal crystallization of polymers at very high cooling rates. J Polym Sci B Polym Phys 1996;34:2783−804.
[115] Supaphol P, Spruiell J. Nonisothermal bulk crystallization studies of high-density polyethylene using light depolarizing microscopy. J Polym Sci B Polym Phys 1998;36: 681−92.
[116] Butler TI, Patel R, Lai SY, Spuria J. Blown-film frost line-freeze line interactions. In: TAPPI polymers, laminations and coatings conference; 1993. p. 13.
[117] Morris BA. The effect of coextrusion on bubble kinematics, temperature distribution and property development in the blown-film process. In: SPE ANTEC conference; 1998.
[118] Ziabicki A, Kawai H, editors. High-speed fiber spinning. New York: Wiley; 1985.
[119] Lagassa R, Maxwell B. An experimental study of the kinetics of polymer crystallization during shear flow. Polym Eng Sci 1976;16:189.
[120] Doufas A, McHugh A. Modeling flow-induced crystallization in film blowing. In: SPE ANTEC conference; 2000.
[121] Canning K, Co A. Edge effects in film casting of molten polymers. J Plast Film Sheeting 2000;16:188−203.
[122] Yoon K-S, Park C-W. Stability of a blown film extrusion process. Intern Polym Process 1999;XIV:342−9.
[123] Pol H, Banik S, Azad LB, Thete S, Doshi P, Lele A. Nonisothermal analysis of extrusion film casting process using molecular constitutive equations. Rheol Acta 2014;53:85−101.
[124] Pol H, Thete SS, Doshi P, Lele AK. Necking in extrusion film casting: the role of molecular architecture. J Rheol 2013;57:559−83.
[125] Zatloukal M, Barborik T. Effect of extensional viscosity, elasticity and die exit stress state on neck-in phenomenon during extrusion film casting: theoretical study. In: SPE ANTEC conference; 2016.

[126] Chikhalikar K, Banik S, Azad LB, Jadhav K, Mahjan S, Ahmad Z, et al. Extrusion film casting of long chain branched polypropylene. Polym Eng Sci 2015;55:1977–87.

Appendix: Two-Layer Curl Model

A model for the curvature of a two-layer film subject to differential shrinkage during quenching is developed, following the approach of Shen and Suresh [109]. Although originally developed for thermal cycling in the solid state, the same equations describe the case for the quenching of coextrusion blown film if the volume changes due to crystallization and thermal contraction, and relaxation effects are properly accounted for. The stress in each layer is

$$\sigma_1 = E_1(\varepsilon - \alpha_1 \Delta T) \tag{13A.1}$$

$$\sigma_2 = E_2(\varepsilon - \alpha_2 \Delta T) \tag{13A.2}$$

where σ_i = stress in layer i; ε = strain; ΔT = change in temperature (from freezing point to room temperature during quenching); E_i = Young's modulus of layer i (for plane stress, divide E by the Poisson's ratio for the material); α_i = coefficient of thermal expansion for layer i.

When both materials remain in the solid state, as in the thermal cycling of composites below their melting points, α is simply the solid-state coefficient of linear thermal expansion. For the case of quenching of plastic film, the phase transition from melt to solid as well as relaxation effects are included. In general, α can be expressed as follows:

$$\alpha_i = \alpha_T + \frac{\Delta V_c}{\Delta T} - \Re \tag{13A.3}$$

where α_T = coefficient of linear thermal expansion (solid-state); ΔV_c = volumetric change during crystallization; $\Re$ = relaxation of strain.

For two-layer films, ΔV_c for the first material that freezes is ignored since the second layer can flow in response. Values for α_T and ΔV_c are obtained from TMA and PVT data, respectively. PVT data in combination with curl data on two-layer films are used to obtain $\Re$.

The strain is given by

$$\varepsilon = \varepsilon_o + Kx \tag{13A.4}$$

where ε_o = strain at the interface; x = distance from the interface, normal to the plane of the film; K = curvature (or curl) of the film.

A force and momentum balance give, respectively:

$$\int_{-X_1}^{0} \sigma_1 dx + \int_{0}^{X_2} \sigma_2 dx = 0 \tag{13A.5}$$

$$\int_{-X_1}^{0} \sigma_1 x\, dx + \int_{0}^{X_2} \sigma_2\, x\, dx = 0 \tag{13A.6}$$

where X_1 is the thickness of layer one and X_2 the thickness of layer 2.

Substituting Eqs. (13A.1), (13A.2), and (13A.4) into Eqs. (13A.5) and (13A.6) and solving yields the following expressions for ε_o and K (the reciprocal of the radius of curvature):

$$\varepsilon_o = \Delta T \frac{C_1}{C_2} \tag{13A.7}$$

$$K = \Delta T \frac{C_1 C_3 + C_2 C_4}{C_2 C_5} \tag{13A.8}$$

$$C_1 = \frac{1}{12}\alpha_1 E_1^2 X_1^4 + \frac{1}{12}\alpha_2 E_2^2 X_2^4 + E_1 E_2 X_1 X_2 \left(\frac{1}{3}\alpha_2 X_1^2 + \frac{1}{4}\alpha_2 X_1 X_2 + \frac{1}{4}\alpha_1 X_1 X_2 + \frac{1}{3}\alpha_1 X_2^2\right)$$

$$C_2 = \frac{1}{12}E_1^2 X_1^4 + \frac{1}{12}E_2^2 X_2^4 + E_1 E_2 X_1 X_2 \left(\frac{1}{3}X_1^2 + \frac{1}{2}X_1 X_2 + \frac{1}{3}X_2^2\right)$$

$$C_3 = \frac{1}{2}E_1 X_1^2 - \frac{1}{2}E_2 X_2^2$$

$$C_4 = -\frac{1}{2}E_1 \alpha_1 X_1^2 + \frac{1}{2}E_2 \alpha_2 X_2^2$$

$$C_5 = \frac{1}{3}E_1 X_1^3 + \frac{1}{3}E_2 X_2^3$$

14 Effect of Process on Properties

The properties of polymer films can never be separated from the process by which they are made. The stress and strain history imposed on the polymer as it is melted, extruded through the die, drawn to its final shape, and quenched affects orientation, crystallinity, and morphology of the film. These in turn impact the mechanical, optical, barrier, and other properties of the film. Process/structure/property relationships have been studied extensively; a comprehensive review is beyond the scope of this chapter. To illustrate the importance and complexity of the effect of processing on flexible packaging films, three examples involving blown film are presented:

- The effect of stress–strain history on film mechanical properties. In particular, the differences in strain history between monolayer and coextruded films and how this translates into property changes is highlighted.
- The effect of quench rate on properties. Key differences between air-quench versus water-quench blown film and their influence on the properties of barrier coextruded film are discussed.
- The effect of orientation on blend morphology.

14.1 Stress–Strain History in Blown Film

In the blown film process, the polymer exits the die in the form of a tube. Air is inserted inside the tube to inflate it outward into a bubble as it is drawn upward via a nipped set of rolls at the top of the film tower. A schematic of the process is shown in Fig. 14.1. Cooling air is blown across the bubble to quench the hot polymer. The shape of the bubble is determined by the inflation pressure, line speed, cooling rate, and the rheology of the polymer. The bubble shape influences the frozen-in stress, strain history, crystallinity, orientation, and other key attributes of the film and its properties.

The frost line is the point where the bubble no longer changes shape: both the diameter and velocity reach their final value at the frost line. It is often associated with crystallization, since for many films a hazy band can be seen across the bubble near the frost line. Recent studies with online X-ray scattering and Raman spectroscopy, however, show that less than 5% of the crystallinity occurs before the frost line [1–3]. Nevertheless, the region between the die exit and frost line has a profound effect on the stress history and property development of the film. It is only near the frost line where the bubble becomes stiff enough to sustain the stretching needed for the film to reach its final bubble diameter and velocity. High strain rates occur in this region that give rise to stress that is frozen in place as the film crystallizes. This stress orients the molecular chains, which in turn influences the extent of crystallization and its morphology.

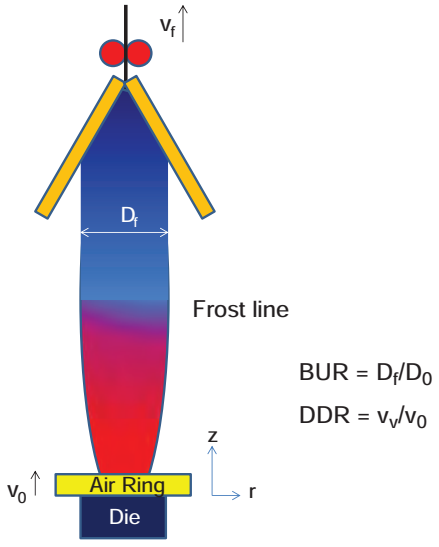


Figure 14.1 Schematic of blown film process.

The Science and Technology of Flexible Packaging. http://dx.doi.org/10.1016/B978-0-323-24273-8.00014-9
Copyright © 2017 Elsevier Inc. All rights reserved.

14.1.1 Monolayer Blown Film

The importance of the stress–strain history during processing of blown film has been well known since the early days of film fabrication. Huck and Clegg [4] published one of the earliest comprehensive studies of the effect of output, blowup ratio (BUR) and frost line height (FLH) on the mechanical and optical properties of LDPE film. Statistical analysis was used to identify key trends; an example of how the tear properties change with processing conditions is shown in Fig. 14.2. In addition to mechanical properties, an extensive investigation of how processing parameters affect optical properties is described (Chapter 12). The authors relate the mechanical properties to changes in the shape of the bubble and orientation measurements using birefringence. Numerous other investigators have studied the effect of processing variables on blown film crystallinity and property development, including online measurements of orientation and crystallinity [5–20]. For example, Shirodkar [9] found that dart impact and machine direction (MD) Elmendorf tear strength of linear low density polyethylene (LLDPE) films increases with increasing process time (Eq. (14.3)) and correlates this with orientation. The specific response of a polymer to processing conditions will depend on its molecular characteristics, such as molecular weight, molecular weight distribution, branching, and crystallinity, as well as how these characteristics affect the rheology of the polymer [6,21–29].

Scale-up guidelines have been proposed based on the analysis of stress, heat transfer, and crystallization during film blowing [9,30–33]. Dimensionless groups are used to estimate process parameters that will duplicate the properties of a film produced on one line to that on another line, such as a small pilot scale line. One such set of rules derived by Kanai [30] is summarized in Table 14.1. Here the BUR, take-up, or draw down ratio (DDR) and FLH/D_0 (frost line height/die diameter) are held constant. Studies [30,34,35] show that when using these rules the deformation history of the two processes is the same. Shirodkar [9] and Butler [31,32] propose holding process time constant as a scale-up rule. As shown in Table 14.1, this condition is a natural outcome of the Kanai rules.

Numerous studies have examined the effect of strain rate, stress, and temperature in the region between the die exit and nip roll on the microstructure of blown film: orientation, crystallinity, and crystalline morphology. These microstructural features are then related to macroproperties such as mechanical properties and permeability. Most of the studies have been on monolayer polyolefin film.

Perhaps the easiest quantity to measure is the temperature profile, using IR thermometry. A typical temperature profile measurement is shown in Fig. 14.3. The temperature steadily decreases until a plateau is reached. The onset temperature for the plateau is often called the crystallization line height (CLH). Other definitions are shown in Fig. 14.3. The end of the plateau is called the freezing line height in the early literature and was believed to be associated with the end of crystallization. Later, online measurements using small angle X-ray scattering [1,2] or Raman spectroscopy [14–16] showed that the polymer continues to crystallize well beyond the end of the plateau as shown in Fig. 14.3. The presence of the temperature plateau is best explained by Spruiell and coworkers [36–38], who duplicated the effect in very

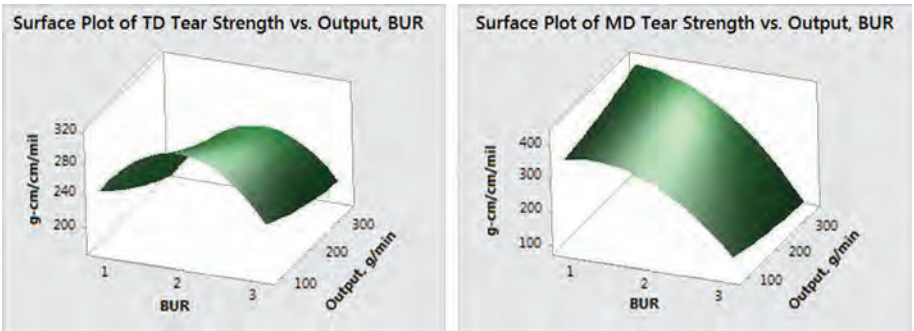


Figure 14.2 Effect of output and blowup ratio (BUR) on MD (left) and TD (right) Elmendorf tear strength. FLH was 14 inches (35.6 cm).
Adapted from Huck ND, Clegg PL. The effect of extrusion variables on the fundamental properties of tubular polythene film. In: SPE ANTEC Conference, 18-2. 1961. pp. 1–14.

Table 14.1 Scale-Up Rules for Blown Film Based on Kanai [30] Analysis. The symbol * indicates multiplication.

Parameter	Line 1	Line 2
Scaling Parameters (held constant)		
Melt temperature	Constant	Constant
BUR (D_f/D_0)	Constant	Constant
DDR (v_f/v_0)	Constant	Constant
FLH/D_0	Constant	Constant
Process Parameters		
Die diameter (D_0)	$D_{0,1}$	$D_{0,2}$
Film diameter (D_f)	BUR*$D_{0,1}$	BUR*$D_{0,2}$
Die gap (X_0)	$X_{0,1}$	$X_{0,2}$
Film thickness (X_f)	$X_{f,,1}$	$X_{f,1}*X_{0,2}/X_{0,1}$
Frost line height (FLH)	FLH_1	$FLH_1*D_{0,2}/D_{0,1}$
Haul-off speed (v_f)	$v_{f,1}$	$v_{f,1}*D_{0,2}/D_{0,1}$
Process time (t_f)	$FLH_1*\ln(DDR)/(v_{f,1}-v_{0,1})$	$t_{f,1}$ (constant)
Output (M)	$\pi D_0*BUR*X_f*v_f$	$M_1*(D_{0,2}/D_{0,1})^{2}*(X_{0,2}/X_{0,1})$

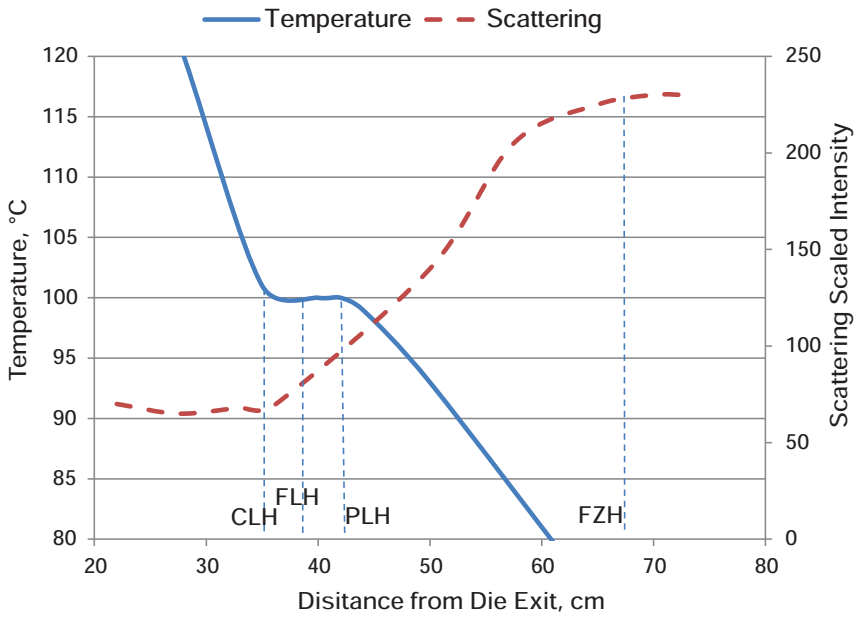


Figure 14.3 Crystallization and temperature profiles in blown film. *Data from Bullwinkel MD, Campbell GA, Rasussen DH, Brancewitz CJ. Structure development during film blowing. In: SPE ANTEC Conference. 2001 for an LLDPE resin*. Temperature was measured by IR and crystallinity by online small angle X-ray scattering. The data are smoothed. Scattering intensity is related to % crystallinity. *CLH*, Crystallization line height; *FLH*, frost line height; *FZH*, freezing line height; *PLH*, plateau line height (*Definitions are from Butler TI. Predicting blown film residual stress levels influence on properties. In: TAPPI PLACE Conference. 2006*).

rapid quench laboratory experiments (5000°C/min): the crystallization becomes heat transfer limited at rapid cooling rates. The exothermic heat of crystallization is balanced by the limited heat convection away from the film surface, giving rise to a temperature plateau.

The velocity of the polymer in the MD and transverse direction (TD) has been measured by a number of investigators [35,40–42]. A simple technique is to mark the bubble near the die exit and record the position of the mark using a video camera. By playing back the video one frame at a time, and knowing the number of frames per second, the position of the marker can be determined as a function of time. The velocity is calculated as the change in position with time. Similarly, the velocity in the TD can be determined by measuring the change in the diameter with time and position along the bubble. An example MD velocity profile for a monolayer high density polyethylene (HDPE) film is shown in Fig. 14.4.

The rate of strain or deformation can be computed from the velocity profiles:

$$\dot{\varepsilon}_1 = \frac{1}{v}\frac{dv}{dt} \tag{14.1}$$

$$\dot{\varepsilon}_2 = \frac{1}{v}\frac{dr}{dt} = \frac{v_z}{r}\frac{dr}{dz} \tag{14.2}$$

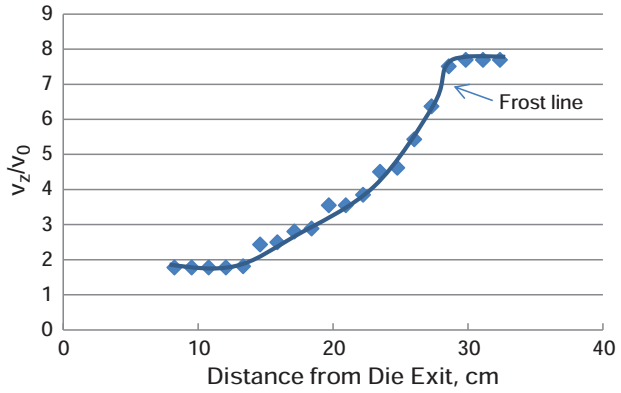


Figure 14.4 Machine direction velocity profile for a monolayer 50-μm HDPE blown film. Die diameter = 50 mm, frost line height = 27.5 mm, process time = 6.4 s.
From Morris BA. The effect of coextrusion on bubble kinematics, temperature distribution and property development in the blown film process. J Plastic Film Sheeting 1999;15(1):25–36 with permission.

where $\dot{\varepsilon}_1$ = rate of strain in the z-direction (machine), $\dot{\varepsilon}_2$ = rate of strain in the r-direction (cross or transverse), v = velocity, t = time, z = machine direction, r = radial direction.

The velocity data are fit to a polynomial and differentiated to find the rate of strain. An example for the rate of strain in the MD for a monolayer HDPE blown film is shown in Fig. 14.5. The maximum rate of strain occurs near the frost line.

The velocity and rate of strain data show that the change in bubble shape and velocity ceases near the frost line. The stress is related to the rate of strain, which reaches a maximum at the frost line and is locked-in. Many investigators have tried to correlate film properties with the deformation near the frost line with limited success [25,34,35,41,45–55]. Online birefringence measurements show some orientation occurs after the plateau region, after the rate of strain has fallen to zero [54]. The actual stress is a complex function of the total strain (DDR and BUR), rate of strain, temperature, crystallization, and orientation. Several investigators have tried to model the blown film process to determine the stress using mathematical or numerical simulation [3,21,22,39,47,48,53,56–64]. These models, for the most part, have resorted to simplifications to deal with the complications resulting from the rapid change in temperature, the melt viscoelasticity, thermal- and flow-induced crystallization, and the rheology of the semicrystalline phase. For example, as the melt begins to crystallize, the relationship

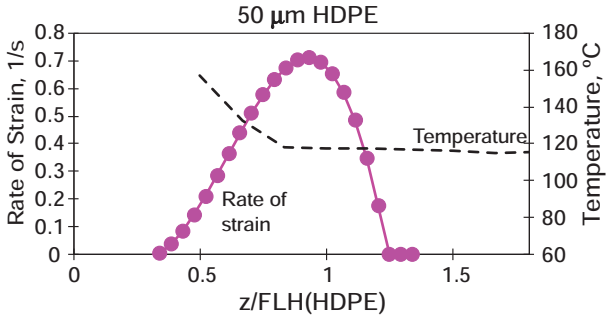


Figure 14.5 MD rate of strain from velocity measurements on a monolayer HDPE blown film line. Temperature profile is superimposed. X-axis is the vertical distance from the die exit (z) divided by the frost line height of the HDPE (FLH_{HDPE}).
From Morris BA. The effect of coextrusion on bubble kinematics, temperature distribution and property development in the blown film process. J Plastic Film Sheeting 1999;15(1):25–36 with permission.

between stress and deformation changes. The crystallization rate itself is complicated by the rapid cooling rate and strain imposed by the process. The rapid cooling rate, on the order of 1000−5000°C per minute, suppresses crystallization. Most measurements of polymer crystallinity are conducted using differential scanning calorimeter (DSC) where the cooling rate is typically 10−20°C per minute and can only go as high as about 100°C per minute. Special laboratory setups are needed to determine crystallization rates at cooling rates typical of blown film [36−38]. Ding and Spruiell [37] found that increasing the quench rate reduces the plateau temperature (which they equate to the freezing point), reduces the time for nucleation to occur, decreases the width of the plateau, increases the rate of crystallization, and reduces overall crystallinity.

Complicating things further is flow- or strain-induced crystallization. As the molecules line up in flow, the rate of crystallization may increase, sometimes by orders of magnitude [65,66]. This phenomenon is known to occur in high-speed fiber spinning [67] but also has been found to be important in blown film. Measurements of rate of crystallization under quiescent conditions (no-flow) can considerably underestimate the amount of crystallinity which develops.

Doufas and McHugh [3,68] have perhaps developed the best model to date to deal with all of these complications. Their model incorporates viscoelasticity of the melt and solid, nonisothermal dynamics as well as flow- and thermal-induced crystallization. The model does a good job of predicting how processing conditions affect crystallinity and orientation in the film and correctly predicts the position of the frost line, bubble shape, and velocity profiles. The model also computes the locked-in stress at the frost line, which Doufas [68] correlates well with measured mechanical properties.

The Doufas and McHugh and other models still have their limitations, which include the following:

- It is challenging to obtain the material parameters needed as inputs to the model. Many are difficult to measure. Indeed, in a recent article, Doufas uses data from the actual film line he is modeling to fit the parameters of the model. From this, he could correctly predict the effect of changing processing conditions. He also proposes that one can run lab-scale trials to obtain the model parameters for a given polymer, from which the model can predict the properties of films made on other lines. The models, however, are still a long way to being truly predictive from simple laboratory measurements on new polymers.
- The model does not predict the development of crystalline morphology (spherulites, lamella, and so on), which is known to be affected by polymer processing and to influence polymer properties [6,10,12,13,26,27,29,60,69−71]. Doufas [68] points out, however, that morphological features can be inferred by the stress levels that are predicted by the model.
- Models for general coextrusion have not been developed. Coextrusion adds an additional level of complexity with interfacial interactions and changes in the bubble kinematics, as described in the next section.

14.1.2 Coextrusion Blown Film

Almost all of the fundamental studies relating process to structure and properties have been conducted on monolayer film. Morris [43,44] was one of the first to study the deformation history of coextrusion blown film. His results show that the coextrusion process can significantly alter the deformation history compared with monolayer film, which in turn can change some properties. This work is discussed in detail below. It has been subsequently validated with more sophisticated online measurements by Giriprasath and Ogale [72,73] and illustrates some of the fundamental differences between coextrusion and monolayer extrusion.

Films are produced on a small-scale coextrusion blown film line equipped with a three-layer 50-mm diameter Brampton Slimline die and dual air ring. The die is fed by two 25-mm and one 38-mm diameter extruders. Two structures are made, a monolayer 50-μm HDPE film and a two-layer coextruded film with HDPE and ethylene vinyl alcohol (EVOH): (22.5 μm EVOH−45 μm HDPE) where the HDPE layer is on the outside of the bubble. The HDPE is Sclair 19A, a 0.75 MI, 0.960 g/cc density grade supplied by Nova Chemical. The EVOH is EVAL LCF101, a 1.5 MI, 32 mol% ethylene grade supplied by Kuraray.

The melt temperature (230°C), BUR (2:1), DDR (8:1 for monolayer, 6:1 for coex), and final thickness are kept constant in each series of films. The process

time (t_f), as defined by Eq. (14.3), is varied by changing FLH and haul-off speed (v_f):

$$t_f = \frac{\text{FLH}}{v_f - v_0} \ln\left(\frac{v_f}{v_0}\right) \tag{14.3}$$

where t_f = process time, FLH = frost line height, v_f = haul-off speed, v_0 = velocity of polymer at die exit.

The output of the extruders is changed with haul-off speed to keep the final film thickness constant.

There are two distinct visual "frost lines" observed when making the coextruded films, one for the HDPE layer and one for the EVOH layer. The results reported here are based on the FLH for the HDPE layer.

The temperature of the bubble as a function of vertical distance from the die exit (z direction) is measured using an IR thermometer (3.43 μm frequency). Velocity and bubble shape profiles are measured using a video camera and tracer technique described earlier [35,40–42]. Velocity profiles were fit to a fourth-order polynomial and differentiated to find the rate of strain profiles.

Fig. 14.6 shows the temperature profiles for a series of two-layer (EVOH–HDPE) coextruded films and one HDPE mono film. The curves have been normalized by dividing the vertical distance (z) by the FLH of the HDPE. The curves collapse onto a master curve, indicating the initial cooling rate is solely a function of the imposed quenching conditions. Note that state 7, a monolayer HDPE film, has the same initial cooling rate as the coextruded films. Since the HDPE layer is on the outside of the coextrusion and the IR frequency of 3.43 μm does not penetrate very deeply into the layer [74], the temperature measurement is not influenced by the temperature of the EVOH.

The width of the crystallization plateau differs from state to state. Ghaneh-Fard [54] finds the width of the plateau to be a function of FLH and flow rate. Butler [31] attributes this to inefficiencies in cooling as the frost line is moved further from the air ring. This relationship is refined in Fig. 14.7, where an excellent fit is found when the width of the plateau region in units of time [(CLH-PLH)/v_f] is plotted against process time.

Results of rate of strain calculations in the MD for a series of HDPE films are given in Fig. 14.8. The maximum rate of strain occurs near the CLH, as found by previous investigators: in monolayer extrusion, the maximum rate of change in bubble

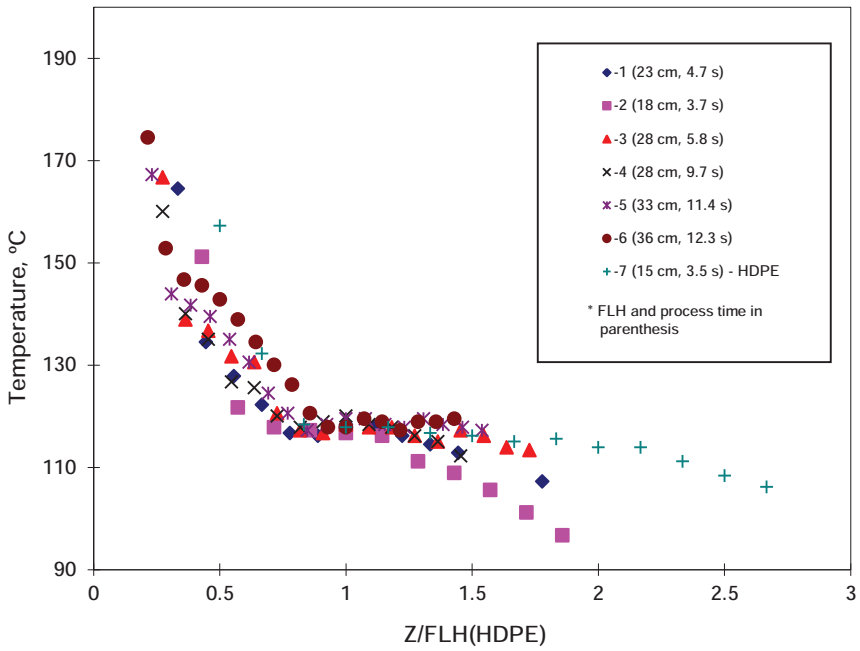


Figure 14.6 Normalized bubble temperature profile for (EVOH–HDPE) coextrusion or HDPE monolayer blown films.

Reproduced from Morris BA. The effect of coextrusion on bubble kinematics, temperature distribution and property development in the blown film process. J Plastic Film Sheeting 1999;15(1):25–36 with permission.

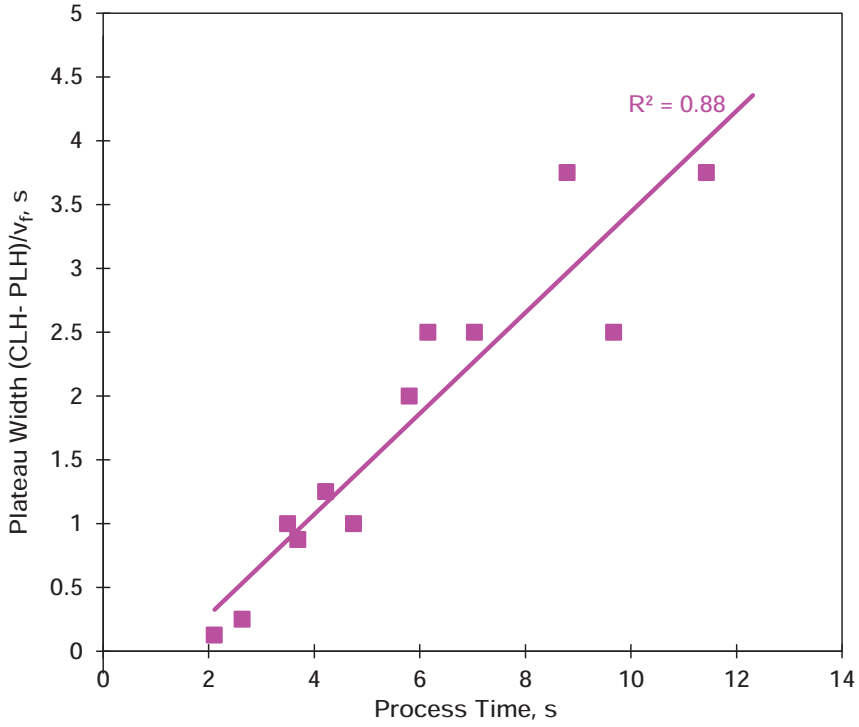


Figure 14.7 Width of temperature plateau (in units of time) plotted against process time (t_f).
Reproduced from Morris BA. The effect of coextrusion on bubble kinematics, temperature distribution and property development in the blown film process. J Plastic Film Sheeting 1999;15(1):25–36 with permission.

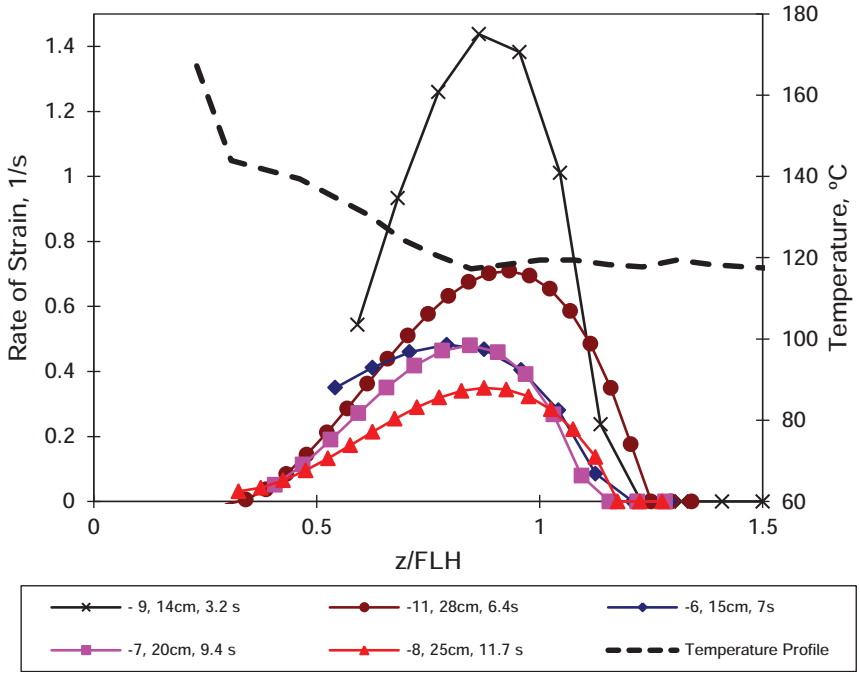


Figure 14.8 MD rate of strain for 50-μm HDPE monolayer films at different frost line heights and process times.
Reproduced from Morris BA. The effect of coextrusion on bubble kinematics, temperature distribution and property development in the blown film process. J Plastic Film Sheeting 1999;15(1):25–36 with permission.

shape and velocity occurs when the polymer has sufficient melt strength, which takes place near the crystallization plateau. The magnitude of the maximum rate of strain is a function of the process time as shown in Fig. 14.9 for the MD. With increasing process time, the maximum rate of strain (and hence stress) decreases. The TD rate of strain has the same features and is not shown here.

In coextrusion, the location of the maximum rate of strain is controlled by the material that freezes first. This is shown in Fig. 14.10 for the (EVOH–HDPE) coextrusion where the maximum

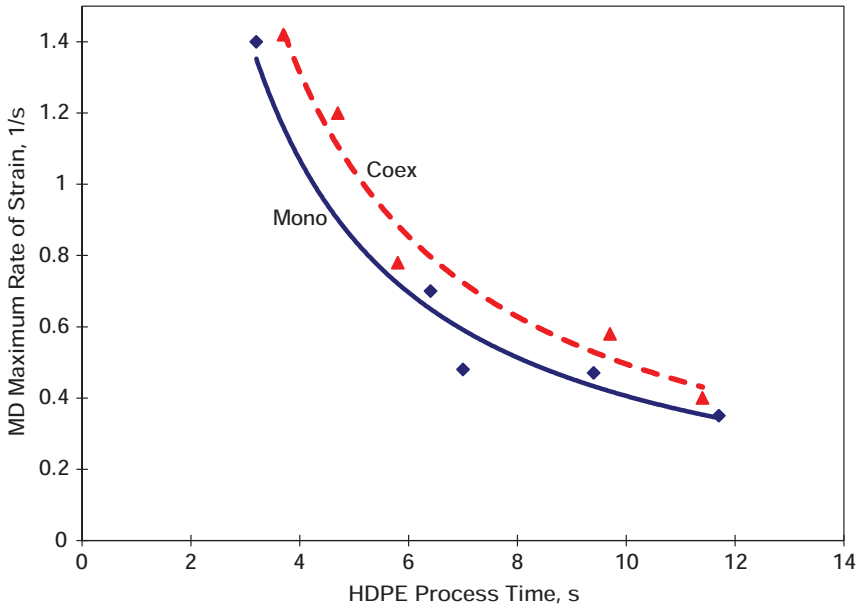


Figure 14.9 The effect of process time on MD maximum rate of strain.
Reproduced from Morris BA. The effect of coextrusion on bubble kinematics, temperature distribution and property development in the blown film process. J Plastic Film Sheeting 1999;15(1):25–36 with permission.

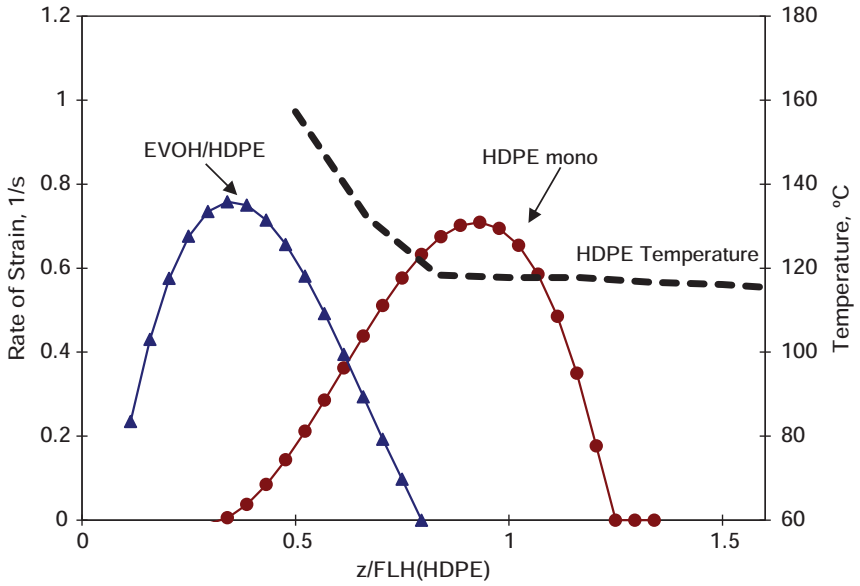


Figure 14.10 Effect of coextrusion on rate of strain.
Reproduced from Morris BA. The effect of coextrusion on bubble kinematics, temperature distribution and property development in the blown film process. J Plastic Film Sheeting 1999;15(1):25–36 with permission.

rate of strain of the HDPE is shifted from near the CLH of the HDPE (z/FLH$_{HDPE}$ of around 0.9) to the CLH of the EVOH (z/FLH$_{HDPE}$ of around 0.4). EVOH has a significantly higher crystallization temperature than HDPE (155 vs. 115°C by DSC). After the EVOH begins to freeze off, there is no significant change in bubble shape or velocity of any of the layers. This can have an effect on polymer properties in two ways. First, the maximum rate of strain of the HDPE layer at a given process time may be somewhat higher in this coextrusion, since the amount of stretching occurs over a shorter time span. This is shown in Fig. 14.9, but the effect is not substantial.

Secondly, and perhaps more importantly, the location of the maximum rate of strain of the HDPE is now shifted to a region where the temperature of the bubble is significantly higher. The HDPE is still fully molten and can flow and relax in response to the strain. The imposed stress is also lower due to the lower viscosity at the higher temperature: stress is equal to the elongational viscosity times the rate of strain.

Because of these effects, the film properties of a material within a coextruded structure may differ from a monoextruded film. This is illustrated in Tables 14.2 and 14.3 and Figs. 14.11–14.13 where several properties of approximately 50-μm

Table 14.2 Properties of 50-μm Monolayer HDPE Films

State No.	Haul-Off Speed (mm/s)	FLH (cm)	Process Time (s)	MD Yield Strength Mean (Std. Dev.) (MPa)	MD Elongation at Break Mean (Std. Dev.) (%)	TD Elmendorf. Tear Mean (Std. Dev.) (g/25 μm)
6	50.8	15	7.0	30.6 (0.6)	948 (100)	62.1 (5.8)
7	50.8	20	9.4			
8	50.8	25	11.7	30.9 (0.9)	1038 (106)	45.3 (4.4)
9	102	14	3.2	29.7 (0.6)	687 (300)	210 (22.3)
10	102	11	2.6	30.7 (0.8)	779 (135)	297 (54.9)
11	102	28	6.4	30.8 (1.3)	991 (181)	62.7 (5.1)

Reproduced from Morris BA. The effect of coextrusion on bubble kinematics, temperature distribution and property development in the blown film process. J Plastic Film Sheeting 1999;15(1):25–36 with permission.

Table 14.3 Properties of 45-μm HDPE Film Made by Coextrusion With EVOH. HDPE is Separated From the EVOH Prior to Testing

State No.	Haul-Off Speed (mm/s)	FLH (cm)	Process Time (s)	MD Yield Strength Mean (Std. Dev.) (MPa)	MD Elongation at Break Mean (Std. Dev.) (%)	TD Elmendorf Tear Mean (Std. Dev.) (g/25 μm)
1	102	23	4.7	28.8 (1.5)	914 (67)	51.4 (6.3)
2	102	18	3.7	29.6 (0.4)	847 (40)	63.2 (9.5)
3	102	28	5.8	29.5 (1.0)	927 (58)	52.1 (7.2)
4	61	28	9.7	29.7 (1.2)	897 (88)	41.1 (3.3)
5	61	33	11.4	28.9 (2.6)	884 (40)	36.7 (4.3)
6	61	36	12.3	29.8 (0.7)	1000 (53)	37.9 (8.3)

Reproduced from Morris BA. The effect of coextrusion on bubble kinematics, temperature distribution and property development in the blown film process. J Plastic Film Sheeting 1999;15(1):25–36 with permission.

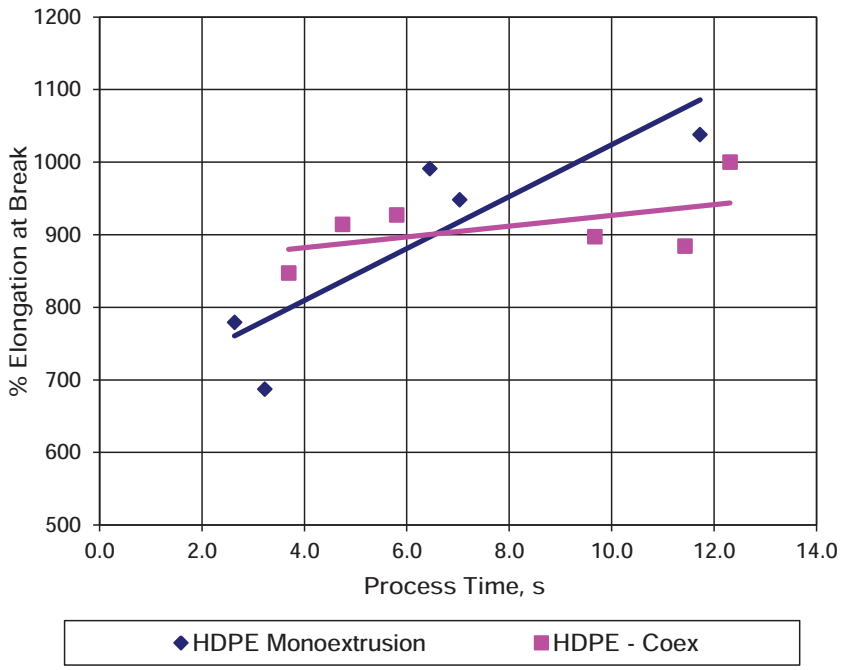


Figure 14.11 MD Elongation at break for HDPE films made by mono and coextrusion processes.
Reproduced from Morris BA. The effect of coextrusion on bubble kinematics, temperature distribution and property development in the blown film process. J Plastic Film Sheeting 1999;15(1):25–36 with permission.

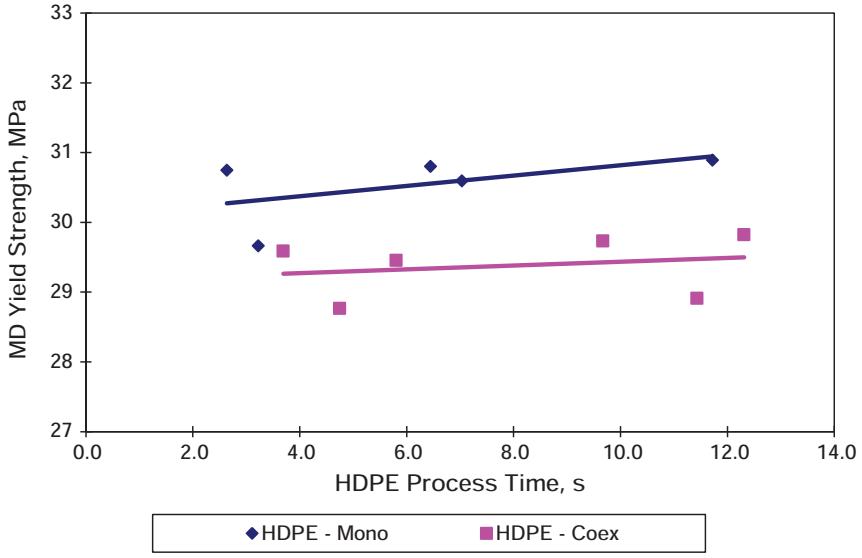


Figure 14.12 MD yield strength for HDPE films made by mono and coextrusion processes.
Reproduced from Morris BA. The effect of coextrusion on bubble kinematics, temperature distribution and property development in the blown film process. J Plastic Film Sheeting 1999;15(1):25–36 with permission.

mono- and coextruded HDPE film are compared. The coextrusion is with EVOH where the EVOH is removed from the HDPE before testing (EVOH and HDPE do not bond to one another). Fig. 14.11 shows that the elongation at break of monofilm is more sensitive to changes in process time than coextruded film. Fig. 14.12 displays lower yield strength in coextruded film. Fig. 12.13 shows a significant difference in TD tear properties as a function of process time.

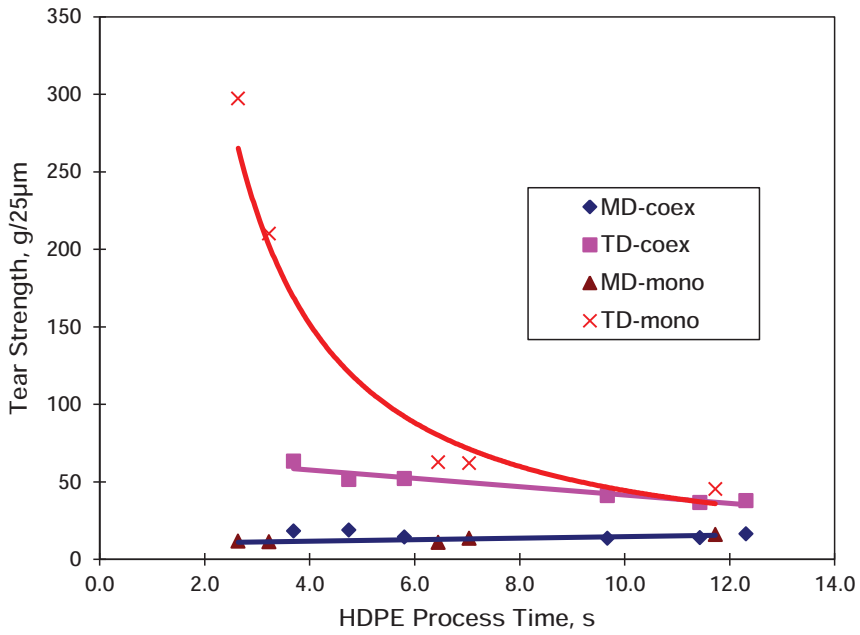


Figure 14.13 Elmendorf tear strength for HDPE films made by mono and coextrusion processes.
Reproduced from Morris BA. The effect of coextrusion on bubble kinematics, temperature distribution and property development in the blown film process. J Plastic Film Sheeting 1999;15(1):25–36 with permission.

The observed differences in physical properties may reflect fundamental differences in the amount of orientation that develops in these films. Shirodkar [9] shows that increasing the process time in monolayer extrusion significantly reduces orientation. This is because the stress on the polymer is highest near the frost line where small changes in rate of strain and relaxation time make a significant difference in stress. In the (EVOH–HDPE) coextrusion, the stress (and orientation) is not as sensitive to changes in process time, since the maximum rate of strain no longer is near the frost line; the stress on the HDPE is lower and so changes in process time do not influence physical properties as much. These effects could have an impact on other properties as well, such as barrier performance and interlayer adhesion.

Increasing process time (keeping BUR and DDR constant) decreases the amount of stress imparted during orientation by reducing the rate of strain (Fig. 14.9). The effect of processing parameters on the film properties of a polymer can be significantly changed when coextruding the polymer with a second polymer, even if the amount of the second polymer is comparatively small, provided the second polymer has a higher freezing point. In such a case, coextrusion changes the magnitude of the maximum rate of strain and shifts its location to regions of higher temperature. The results suggest that using monolayer film properties to predict coextrusion film properties may not be valid. Simple addition of individual layer film properties, such as physical and barrier properties, may not be sufficient when designing new film structures. The material properties and processing parameters interact in complex ways to influence the bubble kinematics and temperature distribution in coextrusion. Such considerations must be taken into account to fully predict film performance.

14.2 Air- Versus Water-Quench Blown Film

The quench rate has a substantial impact on the crystallinity of a polymer film, which influences physical, optical, and barrier properties as well as drawability and thermoformability. Conventional blown film uses air as the cooling medium. An air ring distributes air around the outside of the bubble. Air may also be distributed inside the bubble to further enhance the cooling rate. While the quench rate in conventional air-quench blown film lines is quite high, on the order of 1000°C/min or more, it is still slow compared with cast film cooling where the

Table 14.4 Characteristics of the Water-Quench (WQ) and Air-Quench (AQ) Blown Film Lines Used in the Experiments by Xiao [75,76]

	Air-Quench Line	Water-Quench Line
Extruders/layers	9	9
Extruder diameter	63.5 mm (2.5 inch)—2 50 mm (2 inch)—7	63.5 mm (2.5 inch)—9
Cooling	Inner bubble cooling (IBC) and air ring	Water ring on outside of bubble
Die diameter	450 mm	450 mm
Haul-off	Oscillating	Oscillating

melt is contacted with a cold roll. While quenching with air remains the predominant cooling technique for blown film lines, several equipment suppliers also offer water quench. In a water-quench line, the tube is extruded downward from the die. The tube is blown out and through an aperture with flowing water, called a water ring, which cools the bubble from the outside. Because water is a more effect heat transfer medium than air, the quench rate approaches that of the cast film process.

The advantages of water-quench over air-quench blown film include lower crystallinity, higher clarity, enhanced thermoformability, and reduced curl. Water-quench blown film lines provide a better balance of orientation than cast film lines and the opportunity for greater product diversity. Their versatility versus air-quench lines is more limited since the water ring is sized for a fixed BUR; to change the final film width or layflat, the water ring must be swapped out. Water-quench blown film lines also typically run at lower output than cast film lines.

Some of the crystallinity issues with air-quench blown film can be overcome with resin selection. For example, changing from polyamide 6 (PA6) to polyamide copolymers such as PA6/66 or adding an amorphous PA helps improve thermoformability and reduce curl. Water quench provides the opportunity to reduce the use of these more expensive resins.

Xiao, Armstrong, and Lee [75,76] compare the optical, barrier, and thermoforming properties of identical barrier films made on commercial scale water- and air-quenched blown film lines. Their work provides an excellent example of how the film fabrication process affects properties but also how secondary processes, in this case thermoforming, may also change performance. They made nine-layer barrier structures on two nearly identical Brampton Engineering blown film lines. The characteristics of these lines are summarized in Table 14.4.

Details of the structures and resins used in the study are provided in Tables 14.5 and 14.6. Three types of structures are made. Structure A is a symmetric structure with LLDPE on the outside and PA—EVOH—PA as the core. Structure B is nonsymmetric with PA on one of the outside layers and mPE on the other but with the same PA—EVOH—PA core. Sandwiching EVOH between layers of PA is often done to improve the formability of the film. Structure BT is a variation on structure B made with the layers reversed on the film line so that the PA layer is on the inside. The final structure, C, is symmetric with LLDPE as the outside layers but only EVOH as the barrier core. Structure C is included to evaluate the performance of a modified EVOH grade designed for improved thermoformability (EVOH3). The die diameter and output of the two lines are identical and all the films are 100-μm thick. No information is given about the individual layer thicknesses.

The films are tested for their optical properties (haze) and permeation to moisture (MVTR) and oxygen (OTR) prior to thermoforming. These results are designated as the "flat film" results. The films are thermoformed on two types of thermoforming equipment, a ZED batch former and a Multivac R5200 Solid Phase Pressure former. The barrier properties of the thermoformed packages are tested and an assessment of the thermoforming processing window is made from these trials.

The flat film haze results are graphed in Fig. 14.14. The haze of the air quenched films is significantly higher than for the water-quenched films. This was expected and is believed to be due to higher crystallinity in the air-quenched films. Indeed, optical

Table 14.5 Blown Film Structures Made and Tested in Quench Study by Xiao [76]. Layer 1 is on the Inside of the Bubble and Layer 9 on the Outside

Structure	1	2	3	4	5	6	7	8	9
A	LLDPE	LLDPE	Tie	PA6	EVOH1	PA6	Tie	LLDPE	LLDPE
A2	LLDPE	LLDPE	Tie	PA6	EVOH2	PA6	Tie	LLDPE	LLDPE
B	mPE	Tie	PA6	EVOH1	PA6	Tie	LLDPE	Tie	PA6
BT	PA6	Tie	LLDPE	Tie	PA6	EVOH1	PA6	Tie	mPE
C	LLDPE	LLDPE	LLDPE	Tie	EVOH1	Tie	LLDPE	LLDPE	LLDPE
C2	LLDPE	LLDPE	LLDPE	Tie	EVOH3	Tie	LLDPE	LLDPE	LLDPE

Adapted from Xiao K, Lee I-H, Armstrong R. Comparison of water-quench versus air-quench blown film processes – Part II: thermoformability. In: SPE ANTEC Conference. 2012. pp. 978–83.

Table 14.6 Description of Resins Used in Xiao [76] Blown Film Evaluation

Material	Characteristics
LLDPE	Octene, 0.918 g/cc density, 1 g/10 min MI
mPE	0.902 g/cc density, 1 g/10 min MI
Tie	Maleic anhydride-modified PE
PA	PA6
EVOH1	38 mol% ethylene
EVOH2	32 mol% ethylene
EVOH3	Modified 32 mol% ethylene

birefringence and wide angle X-ray (WAXS) measurements confirm that the air-quenched samples have significant crystallinity while the water-quenched films have very little.

One surprising result is the lower haze of the water-quenched nonsymmetrical structure when the PA layer is on the inside of the bubble (structure BT vs. B). The haze drops from 12% to 7% when the PA layer is moved from the outside to the inside. The authors hypothesize that when the PA is on the outside of the bubble, it acts as an insulating layer. The latent heat of crystallization of the PA layer slows the transfer of heat away from the interior layers, allowing them slightly more time to crystallize. When the PA is on the inside of the bubbles, the remaining layers are more directly exposed to the cooling water, increasing the rate of cooling. The overall level of crystallinity is still very low, as the WAXS data indicate. This explanation at least is consistent with the permeation results described below. The authors do not explore other possible mechanisms for the change in haze, such as possible differences in surface roughness, or plasticization of the outside PA layer by water, allowing more crystallization in that layer.

The permeation results for the flat films are provided in Figs. 14.15 and 14.16. Both the moisture vapor transmission rate (MVTR) and oxygen transmission rate (OTR) give similar trends. The water-quenched film has 30–50% higher moisture or oxygen permeability than its air-quenched counterpart. The permeability of a semicrystalline polymer is known to decrease with increasing crystallinity; the crystals act as impenetrable barriers to the gas molecules. So this result is not surprising. Once again, the position of the PA layer in the nonsymmetric film (B vs. BT) has an impact. The water-quenched structure B has lower permeability than BT. Like the haze results, this suggests that having PA on the outside results in higher crystallinity. Note that the permeability of the water-quenched B structure is still greater than the air-quenched B structure.

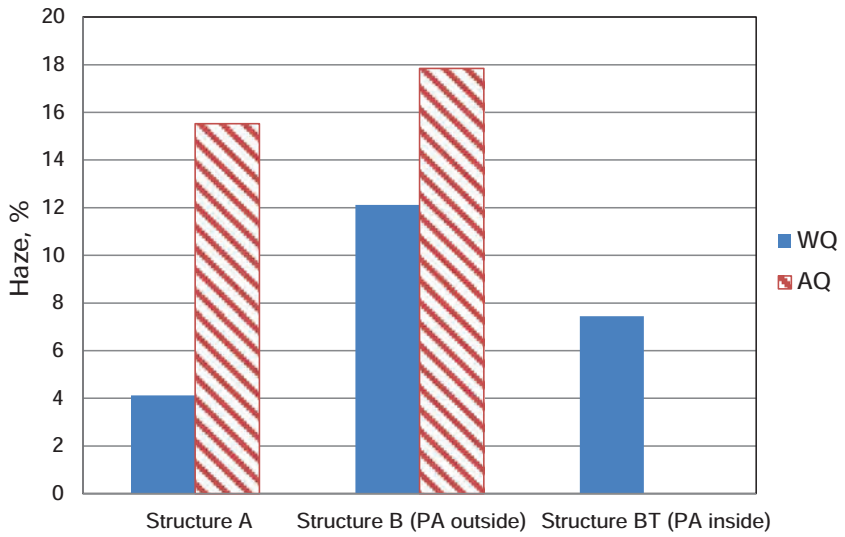


Figure 14.14 Results of haze measurements on flat films (prior to thermoforming) made via water quench (WQ) and air quench (AQ) blown film processes.
Adapted from Xiao K, Armstrong R, Lee I-H. Comparison of water-quench versus air-quench blown film processes – Part I: flat film properties. In: SPE ANTEC Conference. 2012. pp. 972–7.

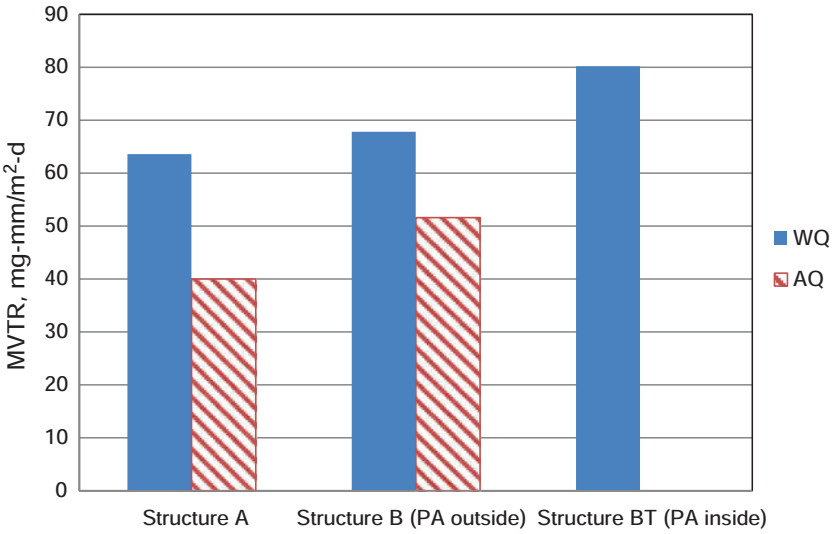


Figure 14.15 Moisture vapor transmission rate (MVTR) results comparing air-quenched (AQ) and water-quenched (WQ) blown films. Results are for flat films prior to thermoforming.
Adapted from Xiao K, Armstrong R, Lee I-H. Comparison of water-quench versus air-quench blown film processes – Part I: flat film properties. In: SPE ANTEC Conference. 2012. pp. 972–7.

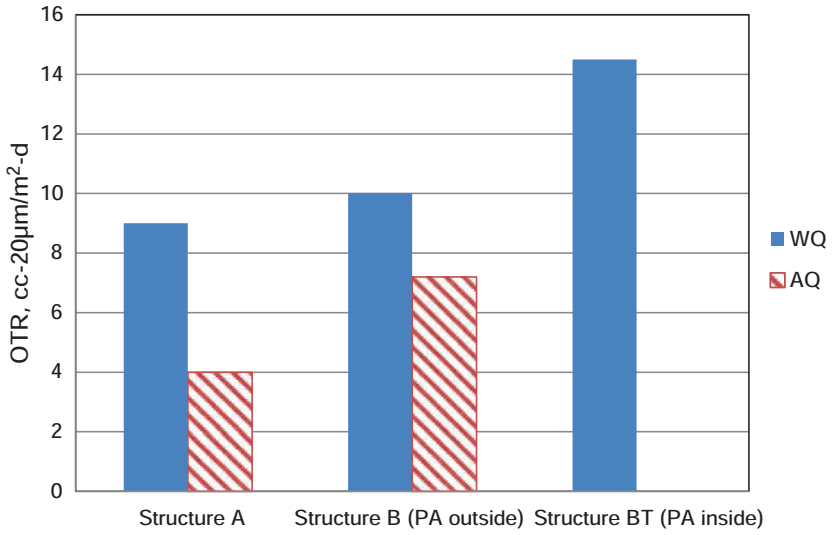


figure 14.16 Oxygen transmission rate (OTR) results comparing air-quenched (AQ) and water-quenched (WQ) blown films. Results are for flat films, prior to thermoforming. Test conditions are 85% RH at 30°C.
Adapted from Xiao K, Armstrong R, Lee I-H. Comparison of water-quench versus air-quench blown film processes – Part I: flat film properties. In: SPE ANTEC Conference. 2012. pp. 972–7.

The films are thermoformed on the ZED former at a draw depth of 4-cm with a corner radius of 0.6-cm. The OTR is measured by purging the inside of the formed cavity with nitrogen, sealing off the opening, controlling the outside atmosphere of the package to 100% RH and inside to 65% RH, and measuring the change in concentration of O_2 inside the package with time. The results for structure A and A2 are plotted in Fig. 14.17. After thermoforming, packages made from the water-quenched films have lower or equal OTR than their air-quenched counterparts. This is the opposite trend seen for the flat films. The water-quenched films, with their lower crystallinity, thermoform better: the appearance is superior and the

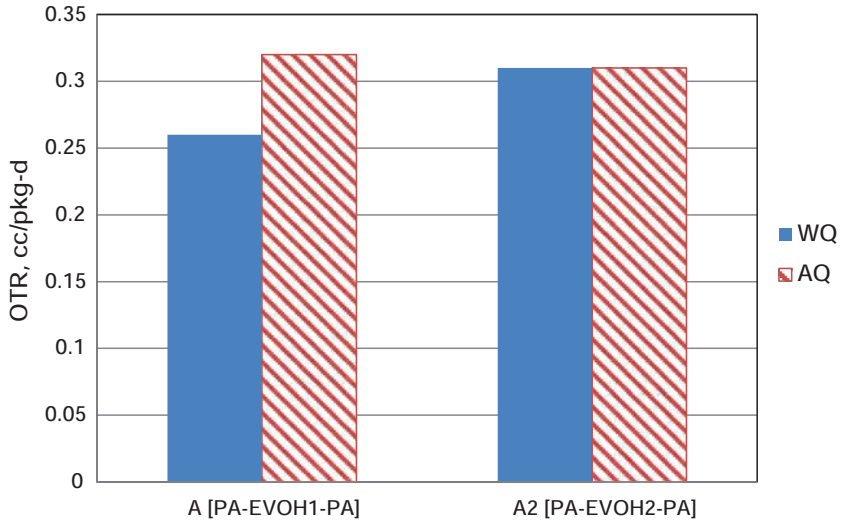


Figure 14.17 OTR results on thermoformed packages.
Adapted from Xiao K, Lee I-H, Armstrong R. Comparison of water-quench versus air-quench blown film processes – Part II: thermoformability. In: SPE ANTEC Conference. 2012. pp. 978–83.

gauge distribution is more uniform with less thinning in the corners. This is likely the reason for the improved barrier performance of the water-quenched films.

The thermoformability of the films is evaluated on the Multivac former. In this continuous roll fed process, the 325-mm wide film is heated between top and bottom plates prior to forming. For the trial, both plates are set at the same temperature. Either a two- or four-pocket mold is used. The majority of the trial is with the four-pocket, deep draw mold with dimensions 135-mm × 125-mm × 85-mm. The heating and forming times are held constant at 1 s and 2 s, respectively, and the temperature is varied to determine the forming window.

Three criteria are used to assess the formability:

- depth and quality of the pocket or cavity draw;
- number of cavities formed;
- degree of cavity breaks.

For cavities not fully formed, a gauge distribution across the pocket cross section is measured.

The C films, where the EVOH is not sandwiched between layers of PA6, did not form well. The results for the air-quenched versions are summarized in Table 14.7. Fifty percent or more of the cavities do not form or formed with breaks or blowouts. Gauge distribution of the cavities that did form show noticeably thinner EVOH in the corners. Even the modified grade of EVOH (EVOH3) does not perform well enough for the film structure, mold design, and process conditions considered in this trial. Comparing this with Film A, the authors conclude that encapsulating the EVOH with PA is critical for successfully thermoforming these structures.

Tables 14.8 and 14.9 show that the water-quenched versions of films A and B thermoform better than their air-quenched counter parts. They form more evenly at lower forming temperatures and form over a wider temperature window. Gauge distribution is more uniform for the WQ films, especially in the corners. One reason is that the forming temperature can be lower, which results in thicker corners.

This study illustrates how the film and packaging fabrication processes can have a significant impact on final package properties.

14.3 Development of Blend Morphology in Blown Film

Chapter 6 describes why most polymer–polymer blends are immiscible, forming separate phases with the minor component imbedded in the major component. Blend properties are influenced by the size, shape, and distribution of the phases, which collectively is known as the blend morphology. Polymer processing impacts the blend morphology through impartation of shear and elongation. Several

Table 14.7 Summary of Thermoformability Assessment of C Films

Temperature (°C)	Film C EVOH1 AQ	Film C2 EVOH3 AQ	Film A PA–EVOH1–PA AQ
90			XX
95			
100	XX	X	XX
105			
110	X	X	XX
115			
120	X	X	X
125			
130	X	X	Ø
135	X	X	
140	X		Ø
145			
150	X		

Key: XX, *100% could not form or pocket blow outs;* X, ≥*50% of pockets could not form, formed minimally or with pocket blow outs;* Ø, *100% formed, but with some variability in pocket appearance;* O, *good forming with consistent pockets.*
Adapted from Xiao K, Lee I-H, Armstrong R. Comparison of water-quench versus air-quench blown film processes – Part II: thermoformability. In: SPE ANTEC Conference. 2012. pp. 978–83.

Table 14.8 Summary of Thermoformability Assessment of A Films

Temperature (°C)	Film A PA–EVOH1–PA AQ	Film A PA–EVOH1–PA WQ
90	XX	XX
95		X
100	XX	O
105		
110	XX	O
115		
120	X	O
125		
130	Ø	Ø
135		
140	Ø	

Adapted from Xiao K, Lee I-H, Armstrong R. Comparison of water-quench versus air-quench blown film processes – Part II: thermoformability. In: SPE ANTEC Conference. 2012. pp. 978–83.

Table 14.9 Summary of Thermoformability Assessment of B Films

Temperature (°C)	Film B AQ	Film B WQ
90	XX	X
95	XX	X
100	X	X–Ø
105	X	X–Ø
110	Ø	O
115		
120	Ø	O
125	Ø–O	
130	Ø–O	O
135		
140		

Adapted from Xiao K, Lee I-H, Armstrong R. Comparison of water-quench versus air-quench blown film processes – Part II: thermoformability. In: SPE ANTEC Conference. 2012. pp. 978–83.

morphologies have been described for immiscible blends in blown film, including spheres and elongated particles, such as fibrils and ribbons. Forming elongated morphologies is a two-step process:

1. Sphere-like dispersed domains are formed during extrusion. Shear flows are the predominant type of flow in the extruder and die. These flows are inherently weaker than elongational flows that dominate once the polymer exits the die and are less likely to form elongated domains. The dispersed domain size is a function of
   a. the dispersed phase concentration;
   b. the ratio of the viscosity of the dispersed phase to the continuous phase (henceforth referred to simply as the viscosity ratio);
   c. interfacial tension;
   d. continuous phase viscosity;
   e. shear stress.
2. Stretching and orienting the spherical particles in the elongational flow fields at the extruder exit (blowing and drawing) causes formation of elongated structures. The morphology is influenced by
   a. initial domain size;
   b. polymer elasticity;
   c. minor component percentage;
   d. draw ratio and other film blowing parameters.

Fig. 14.18 shows an example of an elongated morphology in a blown film. Here polybutene-1 (PB) has been added to a polyolefin to create a peelable sealant. Pirtle [77] suggests that too much PB phase orientation in a peel seal blend can produce unwanted "stringy seals." Morphology control, therefore, is important for packaging applications.

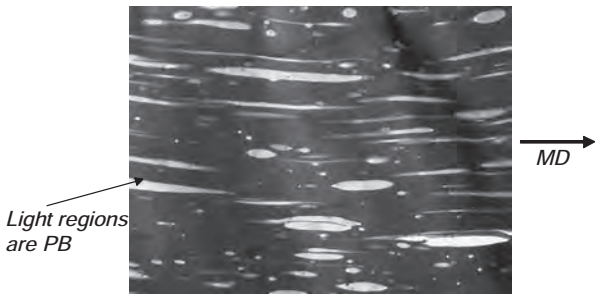


Figure 14.18 Elongated second phase (PB-1 in a polyolefin matrix) found in blown film.
Photograph courtesy of E. I. du Pont de Nemours and Company.

Eq. (6.8) is helpful for understanding how the material characteristics and processing parameters affect the morphology. It is repeated here:

$$Ca = \frac{\eta_c \dot{\gamma} D_d}{2\Gamma_{12}} \tag{14.4}$$

where Ca = capillary number, η_c = viscosity of the continuous phase, $\dot{\gamma}$ = shear rate, D_d = diameter of droplet (discontinuous phase), Γ_{12} = interfacial tension between the two polymers.

As is described in Chapter 6, there is a critical capillary number for droplet breakup that is a function of the viscosity ratio of the polymers. Fig. 6.16 shows that in shear flow, as the viscosity ratio increases, $Ca_{critical}$ decreases until the viscosity ratio reaches a value of around 1. Since the particle size (D_d) is proportional to Ca, the particle size reaches a minimum at a viscosity ratio of around 1. Eq. (14.4) also shows how the shear rate and interfacial tension affect the particle size at constant Ca (and constant viscosity ratio).

Some of the key material characteristics and processing factors influencing morphology development in blown film are now considered.

14.3.1 Material Characteristics

14.3.1.1 Viscosity Ratio

A viscosity ratio near one typically gives the smallest particle domains in the shear flow during extrusion. The smaller the particle size, the harder it is to deform and elongate. David's [78–80] studies of blends of PE with styrene block copolymers show that the dispersed phase viscosity needs to be less than the continuous phase viscosity to obtain elongated morphologies. For viscosity ratios greater than 1, the dispersed phase cannot be deformed enough to create the elongated morphologies.

14.3.1.2 Interfacial Tension

As described by Eq. (14.4), for a given capillary number, the lower the interfacial tension, the smaller the particle diameter. Chapter 6 describes ways to reduce interfacial tension, such as promoting specific interactions by matching solubility parameters or adding compatibilizers. This tends to reduce the

particle size and make elongated morphologies (such as laminar structures) more difficult to obtain [81–83].

14.3.1.3 Minor Phase Concentration in Blend

Increasing the dispersed phase volume fraction (ϕ_d) generally gives larger particle sizes, resulting in more fibril or laminar structures. The larger particle sizes may be due to coalescence, which becomes more significant as the concentration increases. Lopez-Barron [83] studies blends of PA6 and LDPE where LDPE is the continuous phase. The domain size of the PA6 increases with increasing concentration for uncompatibilized blends but is constant for a compatibilized system. The compatibilizer reduces interfacial tension and acts to reduce coalescence. David [78] finds co-continuous fibrils form as ϕ_d is increased. This is determined experimentally by extracting films with a solvent that selectively dissolves the minor component. As the volume fraction is increased, more minor phase polymer is extracted, suggesting co-continuous morphologies are forming. The onset of co-continuous fibril morphology occurs at a lower volume fraction than predicted by Eq. (6.9) which David [78,80] attributes to elongational effects.

14.3.1.4 Polymer Elasticity (Non-Newtonian Behavior)

Getlichermann and David [80] find that a viscosity ratio less than 1 is not sufficient to create elongated morphologies. If the dispersed phase is Newtonian in behavior, elongated morphologies are not observed after blowing and drawing. A polymer's non-Newtonian (elastic) behavior helps to stabilize the "threads" that forms during elongation, allowing more elongation without the threads breaking up into small particles.

They suggest that dispersed phase tension thickening is one attribute that should help stabilize the thread and help create elongated morphologies. Tension thickening or strain hardening refers to elongational viscosity measurements, which are difficult to perform. In general, linear polymers, such as LLDPE, have transient elongational viscosity that decreases with time (tension thinning), whereas the elongational viscosity of polymers with long chain branching (such as LDPE) tends to increase with time (tension thickening). Thus, polymers with long chain branching are more susceptible to the formation of elongated morphologies during film blowing.

14.3.2 Processing Factors

14.3.2.1 Extruder Speed

As extruder speed is increased, the shear rate increases, which should reduce the particle size. As discussed previously, smaller particles formed in the extruder and die are more difficult to elongate after they exit the die. Lee and Kim [82], however, found just the opposite for an LDPE–EVOH blend. They attribute this to the shorter extruder residence time at higher rpm. The EVOH, which is the discontinuous phase and melts at temperatures 50°C higher than the LDPE, has less time to melt fully and be dispersed. This gives rise to a larger particle size at the extruder exit and a greater tendency toward elongated laminar morphology.

14.3.2.2 Extruder Temperature

The extruder and die temperatures affect the morphology through their impact on the viscosity of both components. As the temperature is increased, η_c decreases. As described by Eq. (14.4), this results in less stress being applied to breaking up the droplets, giving larger particle sizes. Also, the polymers' viscosity temperature dependence may differ, altering the viscosity ratio.

14.3.2.3 Shear Stress in Extruder, Adaptor, and Die

During pressure-driven flow in an extruder, adapter pipe, and die, there is a shear stress distribution across the flow channel. The highest shear stresses occur at the wall. The polymer near the wall also experiences long residence time since the flow rate is lowest in this region. This may create a distribution of morphologies across the channel. Lee and Kim [82] find this to be true in LDPE–EVOH blends and it has also been documented for blends involving PB-1 and LDPE [84].

Lopez-Barron [83] observes a core-skin effect with uncompatibilized blends of PA6 and LDPE with the skin having small elongated domains and the core larger particles. They attribute this to a discontinuity at the die wall at the die exit. The polymer near the die wall in the die flow channel has zero or nearly

zero velocity (no slip boundary condition) and accelerates almost instantaneous to the free surface velocity at the die exit (see Fig. 13.2). This creates an intensive amount of stretching that may lead to the observations. Their compatibilized blends show no such effect.

14.3.2.4 Screw Design

For laminar morphologies, the literature teaches not to overmix the blend [85]. Careful screw design may be needed to accomplish this.

14.3.2.5 Draw Ratio

The minor component is typically spherical in shape as it exits the extruder [78–83,86]. It is the elongational flow fields imposed by the drawing and blowing process that give rise to the highly elongated structures. The degree of elongation depends on the process. David [78] finds the convergence/divergence in a capillary geometry only gives rise to elongated ellipsoids. A flat die produces fibrils in the MD and a blown film die gives fibrils and ribbons with two-dimensional orientation in the MD and TD as well as co-continuous fibrils.

The draw in the MD is characterized by the DDR or take-up ratio, which is defined as the haul-off speed divided by the polymer melt velocity as it exits the die (Section 2.2.1.3). The BUR characterizes the draw in the TD or hoop dimension. BUR is defined as the final bubble diameter divided by the die diameter. The DDR is inversely proportional to BUR times the final film thickness divided by the die gap (Eq. (2.7)):

$$\mathrm{DDR} = \frac{v_f}{v_0} \approx \frac{\text{Die Gap}}{\mathrm{BUR} \times \text{Film Thickness}} \qquad (14.5)$$

where DDR = draw down ratio or take-up ratio, v_f = haul-off speed, v_0 = velocity of polymer at die exit, BUR = blow up ratio = D_f/D_0.

DDR decreases with increasing BUR and film thickness and decreasing die gap. (In Eq. (14.5), the density change between solid and melt is ignored.)

David [78] finds that the fibril diameter is not a straightforward function of draw ratio. Without any drawing, the particles are spherical with a diameter of 0.5 μm. At a DDR of 5 and 20, the fibril diameters are 0.1 and 0.2 μm, respectively.

Robledo-Ortiz [86] shows that the stretching force increases with increasing DDR and decreasing FLH. The elongation of the minor phase domain (PA6 in their case) increases in the machine direction with increasing stretching force. The elongation in the hoop and radial (thickness) dimensions are balanced.

14.3.2.6 Frost Line Height and Process Time

Robledo-Ortiz shows that stretching force increases strongly with decreasing FLH. The elongation in the MD of PA6 in their PA6–LDPE blends increases accordingly. The frost line height is a component of the process time as shown in Eq. (14.3).

The effect of process time on the blend morphology has not been fully addressed in the literature. It encompasses critical aspects of the film blowing process, including the cooling and crystallization time. More important for this discussion is that the process time is inversely proportional to the elongation rate as shown in Fig. 14.10. Stress is related to the draw ratio and to the draw or elongation rate. Therefore, process time is inversely related to the stress imposed on the process; increasing process time should reduce elongation of the minor phase.

References

[1] Bullwinkel MD, Campbell GA, Rasussen DH, Brancewitz CJ. Structure development during film blowing. In: SPE ANTEC Conference; 2001.

[2] Bullwinkel MD, Campbell GA, Rasmussen DH, Krexa J, Brancewitz CJ. Crystallization studies of LLDPE during tubular blown film processing. Int Polym Process 2001;16:39–47.

[3] Doufas AK, McHugh AJ. Simulation of film blowing including flow-induced crystallization. J Rheol 2001;45:1085–104.

[4] Huck ND, Clegg PL. The effect of extrusion variables on the fundamental properties of tubular polythene film. In: SPE ANTEC Conference, 18-2; 1961. p. 1–14.

[5] Picot JJC. Molecular orientation in film extrusion of high-density polyethylene. Polym Eng Sci 1984;24:415–20.

[6] Haber A, Kamal MR. Morphology and orientation in polyethylene tubular blown films. In: SPE ANTEC Conference; 1987. p. 446.
[7] Butler TI, Patel R. Blown film bubble forming and quenching effects on film properties. J Plastic Film Sheeting 1993;9:181. Also 1993, SPE ANTEC Conference, pp. 51−57.
[8] Patel RM, Butler TI. Effect of fabrication conditions and molecular orientation on polyethylene blown film properties. In: TAPPI Polymers, Laminations and Coatings Conference; 1993. p. 303.
[9] Shirodkar PP, Firdaus V, Fruitwala H. Scale-up of LLDPE blown film extrusion. In: TAPPI Polymers, Laminations and Coatings Conference; December 1994. p. 405−13. Also, Plastics Engineering, p. 27.
[10] Simpson DM, Harrison IR. A study of the effects of processing parameters on the morphologies and tensile modulus of HDPE blown films: application of composite theories on a molecular level to characterize tensile modulus. J Plastic Film Sheeting 1994;10(Oct):302−25.
[11] Patel RM, Butler TI, Walton KL, Knight GW. Investigation of processing-structure-properties relationships in polyethylene blown films. Polym Eng Sci 1994;34:1506−14.
[12] van Gurp M, Kip BJ, van Heel JPC, de Boer S. On the development of orientation in LDPE blown films. J Plastic Film Sheeting 1994;10:156−76.
[13] Zhang XM, Elkoun S, Ajji A, Huneault MA. Oriented structure and anisotropy properties of polymer blown films: HDPE, LLDPE and LDPE. Polymer 2004;45:217−29.
[14] Cherukupalli S, Paradkar R, Ogale AA, McHugh AJ, Henrichsen L. Online measurements and heat transfer issues in blown film extrusion. In: SPE ANTEC Conference; 2002.
[15] Cherkupalli SS, Ogale AA. Online measurements of crystallinity using Raman spectroscopy during blown film extrusion. Polym Eng Sci 2004;44:1484−90.
[16] Cherkupalli SS, Gottlieb SE, Ogale AA. Real-time Raman spectroscopic measurement of crystallization kinetics and its effect on the morphology and properties of polyolefin blown films. J Appl Polym Sci 2005;98:1740−7.
[17] Fatahi S, Ajji A, Lafleur PG. Structure-property correlations for PE blown films. In: SPE ANTEC Conference; 2005. p. 1766−70.
[18] Legros N, Ghaneh-Fard A, Cole KC, Ajji A, Dumoulin MM. Tensile properties and orientation evolution with processing conditions in polyethylene blown films. In: SPE ANTEC Conference; 1998.
[19] Henrichsen LK, McHugh AJ. Analysis of film blowing with flow-enhanced crystallization. Intern Polym Process 2007;XXII:179−89.
[20] Ghaneh-Fard A. Effects of film blowing conditions on molecular orientation and mechanical properties of polyethylene films. J Plastic Film Sheeting 1999;15(3):194−218.
[21] Han CD, Kwack JY. Rheology-processing-property relationships in tubular blown film extrusion. I. High-pressure low-density polyethylene. J Appl Polym Sci 1983;28:3399−418.
[22] Kwack JY, Han CD. Rheology-processing-property relationships in tubular blown film extrusion. II. Low-pressure low-density polyethylene. J Appl Polym Sci 1983;28:3419−33.
[23] Sukhadia AM. Trade-offs in blown film processing-structure-property behavior of LLDPE type resins from chromium, metallocene and Ziegler-Natta catalysts. In: SPE ANTEC Conference; 1994. p. 202.
[24] Kennedy MA, Peacock AJ, Faila MD, Lucas JC, Mandelkern L. Tensile properties of crystalline polymers: random copolymers of ethylene. Macromolecules 1995;28:1407.
[25] Campbell GA, Babel AK. Physical properties and processing conditions correlations of the LDPE/LLDPE tubular blown films. Macromol Symp 1996;101:199.
[26] Yu T-H, Wilkes GL. Orientation determination and morphology study of high density polyethylene (HDPE) extruded tubular films: effect of processing variables and molecular weight distribution. Polymer 1996;37:4647−87.
[27] Yu T-H, Wilkes GL. Influence of molecular weight distribution on the melt extrusion of high density polyethylene (HDPE): effects of melt relaxation behavior on morphology and orientation in HDPE extruded tubular films. J Rheol 1996;40:1079−93.
[28] Krishmaswamy RK, Sukhadia AM. The relative influences of process and resin time scales on the MD tear strength of polyethylene blown films. In: SPE ANTEC Conference; 1999.
[29] Godshall D, Wilkes G, Krishnaswamy RK, Sukhadia AM. Processing-structure-property investigation of blown HDPE films containing

both machine and transverse direction oriented lamellar stacks. Polymer 2003;44:5397−406.
[30] Kanai T, Kimura M, Asano Y. Studies on scale-up of tubular film extrusion. In: SPE ANTEC Conference; 1986. p. 912.
[31] Butler TI, Lai SY, Patel R. Scale-up factors effecting crystallization in polyolefin blown film. In: TAPPI Polymers, Laminations and Coatings Conference; 1994. p. 289.
[32] Butler TI. Using dimensionless scale-up variables to predict LLDPE blown film properties. In: TAPPI Polymers, Laminations and Coatings Conference; 1995. p. 581−601.
[33] Kwack TH. Processing variables and the scaling parameters in blown film extrusion. In: SPE ANTEC Conference; 1999.
[34] Simpson DM, Harrison IR. The use of deformation rates in the scale-up of polyethylene blown film. In: SPE ANTEC Conference; 1991. p. 203−5.
[35] Simpson DM, Harrison IR. The use of deformation rates in the scale-up of polyethylene blown film. J Plastic Film Sheeting 1992;8:192−206.
[36] Ding Z, Spruiell J. Interpretation of the non-isothermal crystallization kinetics of polypropylene using a power law nucleation rate function. J Polym Sc.i B Polym Phys 1997;35:1077−93.
[37] Ding Z, Spruiell J. An experimental method for studying nonisothermal crystallization of polymers at very high cooling rates. J Polym Sci B Polym Phys 1996;34:2783−804.
[38] Supaphol P, Spruiell J. Nonisothermal bulk crystallization studies of high-density polyethylene using light depolarizing microscopy. J Polym Sci B Polym Phys 1998;36:681−92.
[39] Butler TI. Predicting blown film residual stress levels influence on properties. In: TAPPI PLACE Conference; 2006.
[40] Huang TA, Campbell GA. Deformation history of LLDPE/LDPE blends on blown film equipment. Adv Polym Technol 1985;5:181.
[41] Farber R, Dealy J. Strain history of the melt in film blowing. Polym Eng Sci 1974;14:435.
[42] Butler TI, Patel R, Lai SY, Spuria J. Blown film frost line-freeze line interactions. In: TAPPI Polymers, Laminations and Coatings Conference; 1993. p. 13.
[43] Morris BA. The effect of coextrusion on bubble kinematics, temperature distribution and property development in the blown film process. J Plastic Film Sheeting 1999;15(1):25−36.
[44] Morris BA. The effect of coextrusion on bubble kinematics, temperature distribution and property development in the blown film process. In: SPE ANTEC Conference; 1998. p. 118−22. Also TAPPI Polymers, Laminations and Coatings Conference, pp. 831−837.
[45] Han CD, Park JY. Studies on blown film extrusion. II. Analysis of the deformation and heat transfer process. J Appl Polym Sci 1975;19:3277.
[46] Han CD, Park JY. Studies on blown film extrusion. I. Experimental determination of elongational viscosity. J Appl Polym Sci 1975;19.
[47] Kanai T, White JL. Kinematics, dynamics and stability of the tubular film extrusion of various polyethylenes. Polym Eng Sci 1984;25:1185−201.
[48] Kanai T, White JL. Dynamics, heat transfer and structure development in tubular film extrusion of polymer melts: a mathematical model and predictions. J Polym Eng 1985;5:135−57.
[49] Yoon KS, Park CW. A study on two-layer blown film coextrusion. In: SPE ANTEC Conference; 1991. p. 2315.
[50] Babel AK, Campbell GA. Correlating the plastic strain with the properties of the low density polyethylene blown film. J Plastic Film Sheeting 1993;9(July):246.
[51] Babel AK, Campbell GA. Physical properties and processing conditions correlations of the LDPE/LLDPE tubular blown films. In: TAPPI Polymers, Laminations and Coatings Conference; 1994. p. 415−28.
[52] Babel AK, Campbell GA. A model linking process variables to the strength of blown films produced from LDPE and LLDPE. TAPPI J 1995;78(5):199−204.
[53] Campbell GA, Cao B, Babel AK. Kinematics, dynamics and physical properties of blown film. In: Kanai T, Campbell GA, editors. Film processing; 1999. p. 113−40.
[54] Ghaneh-Fard A, Carreau PJ, Lafleur PG. Study of kinematics and dynamics of film blowing of a linear low density polyethylene. In: SPE ANTEC Conference; 1996. p. 111−5.

[55] Carreau PJ, Ghaneh-Fard A, Lafleur PG. Rheological effects in film blowing. In: SPE ANTEC Conference; 1998.
[56] Pearson JRA, Petrie CJS. The flow of a tubular film. Part 1. Formal mathematical representation. J Fluid Mech 1970;40:1−19.
[57] Pearson JRA, Petrie CJS. The flow of a tubular film. Part 2. Interpretation of the model and discussion of solutions. J Fluid Mech 1970;42:609−25.
[58] Petrie CJS. A comparison of theoretical predictions with published experimental measurements on the blown film process. AIChE J 1975;21:275−82.
[59] Campbell GA, Cao B. Blowing film modeling − die to frostline. In: TAPPI Polymers, Laminations and Coatings Conference; 1986. p. 247−51.
[60] Kwack TH, Han CD, Vickers ME. Development of crystalline structure during tubular film blowing of low-density polyethylene. J Appl Polym Sci 1988;35:363.
[61] Ashok BK, Campbell GA. Two-phase simulation of tubular film blowing of crystalline polymers. Int Polym Process 1992;7:240−7.
[62] Pirkle Jr JC, Braatz RD. A thin-shell two-phase microstructural model for blown film extrusion. J Rheol 2010;54:471−505.
[63] Kolarik R, Zatloukal M. Modeling of nonisothermal film blowing process for non-Newtonian fluids by using variational principles. J Appl Polym Sci 2011;122:2807−20.
[64] Kuijk EW, Tas PP, Neuteboom P. A rheological model for prediction of polyethylene film properties. In: SPE ANTEC Conference; 1998. p. 30−4.
[65] Lagassa R, Maxwell B. An experimental study of the kinetics of polymer crystallization during shear flow. Polym Eng Sci 1976;16:189.
[66] Sentmanat M, Delgadillo-Velazquez O, Hatzikiriakos SG. Crystallization of an ethylene-based butene plastomer: the effect of uniaxial extension. Rheol Acta 2010;49:931−9.
[67] Ziabicki A, Kawai H, editors. High-speed fiber spinning. New York: Wiley; 1985.
[68] Doufas AK. A microstructural flow-induced crystallization model for film blowing: validation with experimental data. Rheol Acta 2014;53:269−93.
[69] Keller A, Machin MJ. Oriented crystallization in polymers. J Macromol Sci (Phys) 1967; B1:41−91.
[70] Gilbert M, Hemsley DA, Patel SR. Effect of processing conditions on the orientation and properties of polyethylene blown film. Br Polym J 1987;19:9−23.
[71] Gupta A, Simpson DM, Harrison IR. Crystalline morphology in oriented HDPE blown films. Plast Eng November 1993:33−6.
[72] Giriprasath G, Gotlieb S, Ogale AA. Process-structure-property relationships in bicomponent blow film extrusion using Roman spectroscopy. In: SPE ANTEC Conference; 2005. p. 158−62.
[73] Giriprasath G, Ogale AA. Processing-structure relationship in bilayer polyolefin blown films. In: SPE ANTEC Conference; 2006. p. 830−4.
[74] Cao B, Sweeney P, Campbell GA. Simultaneous surface and bulk temperature measurement of polyethylene during film blowing. J Plastic Film Sheeting April 1990;6:117.
[75] Xiao K, Armstrong R, Lee I-H. Comparison of water-quench versus air-quench blown film processes − Part I: flat film properties. In: SPE ANTEC Conference; 2012. p. 972−7.
[76] Xiao K, Lee I-H, Armstrong R. Comparison of water-quench versus air-quench blown film processes − Part II: thermoformability. In: SPE ANTEC Conference; 2012. p. 978−83.
[77] Pirtle S, Mergenhagen L, Wooster J, Cotton R. The effects of resin selection and extrusion variables on peelable seal performance. In: TAPPI PLACE conference; 2004.
[78] David C, Trojan M, Jacobs R, Piens M. Morphology of polyethylene blends: I. From spheres to fibrils and extended co-continuous phases in blends of polyethylene with styrene-isoprene-styrene triblock copolymers. Polymer 1991;32(3):510.
[79] David C, Getlichermann M, Trojan M, Jacobs R. Morphology of polyethylene blends. II: formation of a range of morphologies in blends of polyethylene with increasing content of styrene-isoprene-styrene triblock copolymers during extrusion-blowing. Poly Eng Sci 1992;32(1):6.
[80] Getlichermann M, David C. Morphology of polyethylene blends: III. Blend films of polyethylene with styrene-butadiene or styrene-isoprene copolymers obtained by extrusion-blowing. Polymer 1994;35(12):2542.
[81] Ronzalez-Nunez R, Favis B, Carreau R. Factors influencing the formation of elongated

morphologies in immiscible polymer blends during melt processing. Poly Eng Sci 1993;33(13):851.
[82] Lee S-Y, Kim S-C. Morphology and oxygen barrier properties of LLDPE/EVOH blends. Intern Polym Process 1996;XI:238.
[83] Lopez-Barron CR, Robledo-Ortiz JR, Rodrigue D, Gonzalez-Nunez R. Film processability, morphology, and properties of polyamide-6/low density polyethylene blends. J Plastic Film Sheeting 2007;23:149−69.
[84] Basell Product Literature. Polybutene-1 for use in seal-peel applications, customer presentation aid. 2001.
[85] Subramanian PM. Permeability barriers by controlled morphology of polymer blends. Poly Eng Sci 1985;25:483.
[86] Robledo-Ortiz JR, Ramiriz-Arreola D, Gonzalez-Nunez R, Rodrigue D. Effect of freeze-line position and stretching force on the morphology of LDPE-PA6 blown films. J Plastic Film Sheeting 2006;22:287−314.

15 Effect of Processing on Interlayer Adhesion

Adhesion is influenced by many factors, including the physical and chemical nature of the substrates and polymer being bonded, the process by which the structure is assembled and the environment the finished film undergoes in the end use. These elements are discussed in detail in Chapter 10. This chapter highlights two areas where the process strongly affects adhesion: (1) adhesion of polymer to substrate in extrusion coating and lamination and (2) interlayer adhesion in coextrusion cast film, blown film, and extrusion coating.

15.1 Adhesion to Substrates in Extrusion Coating

A number of elements influence the adhesion of polymers to solid substrates in extrusion coating and lamination, which include the following:

- the composition and quality of the substrate and polymer;
- extrusion and flow of the polymer through the die;
- oxidation and drawing in the air gap;
- wetting and quenching in the nip;
- adhesion testing methodology;
- environmental conditions during testing and in the end use.

The effect of composition and quality of the polymer and substrate are covered in Chapter 10. The substrate must be free of surface contamination and have an acceptable surface energy for wetting of the coating. Often flame, corona, or plasma treatment is used to clean and raise the surface energy of the substrate.

Fig. 15.1 outlines the processing factors that affect adhesion in extrusion coating and lamination. The critical regions of the process for adhesion are the following:

- The extruder and die where the polymer is melted and shaped into the melt curtain. Temperature and flow uniformity of the polymer as it exits the die are key for ensuring good gauge distribution and wetting later in the process.
- The air gap where the polymer is drawn to its final thickness and for some polymers, oxidation and other changes occur for adhesion.
- The nip where the polymer is contacted with the substrate and rapidly quenched.

15.1.1 Extruder and Die

The quality of the melt is important for good adhesion. Good quality means uniform thickness of the melt curtain, uniform temperature, constant output (no surging), and a lack of flow instabilities. Ensuring good melt quality starts with the extruder. A screw design that balances melting, mixing, and conveying without overheating the polymer is critical. An introduction to screw design is found in Section 2.1 where the reader is directed to several general references on extrusion and screw design for details. Barrel temperatures, screw speed, and back pressure also contribute to melt quality. The polymer at the extruder exit should be fully melted, uniform in temperature, and free of substantial pressure fluctuations.

The die must uniformly distribute the polymer melt so that the gauge and temperature is uniform at the die exit. Distributing the flow evenly across the width of wide dies can be a challenge. Various designs have been used, many using a manifold to help control the pressure drop across the die. Dies also typically have a preland region at the die exit that allows the polymer to relax prior to exiting the die. This can help relieve stress that may be detrimental to peel strength performance.

The Science and Technology of Flexible Packaging. http://dx.doi.org/10.1016/B978-0-323-24273-8.00015-0
Copyright © 2017 Elsevier Inc. All rights reserved.

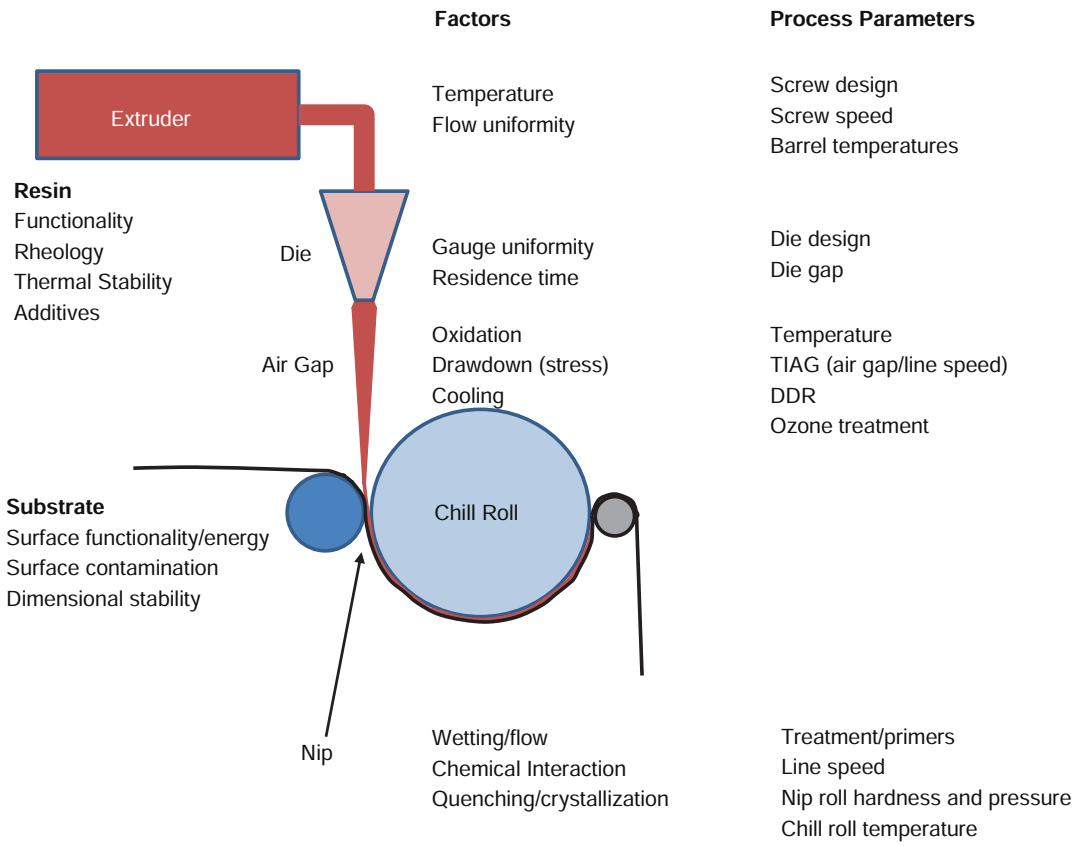


Figure 15.1 Factors of the extrusion coating process that influence adhesion. *DDR*, draw down ratio; *TIAG*, time in the air gap.

Streamlining the flow in the extruder, transfer pipes, and die helps prevent hang-ups and long residence time that can lead to excessive polymer degradation. Degradation can cause gel and other defects that detract from the quality of the coating. Degradation also changes the viscosity of the resin, which may affect its ability to wet the surface of the substrate.

Some amount of thermooxidative degradation may be desired to promote the formation of oxidative species for adhesion. Oxidation of low density polyethylene (LDPE) forms polar functional groups such as acids, aldehydes, and ketones that help with bonding to polar substrates. The oxidation process generally begins in the extruder and die, but most takes place in the air gap [1–3]. The oxidation of LDPE is explored in detail in Section 15.1.2.1.

15.1.2 Air Gap

The air gap is the region between the die exit and the chill roll where the polymer is drawn down to its final thickness. Drawing imparts orientation and stress on the polymer, which can influence the adhesion to the substrate. The polymer may also undergo oxidation in the air gap, which for nonpolar polymers, such as LDPE, is critical for adhesion to polar substrates, such as aluminum foil and paper. The amount of oxidation depends on the residence time and temperature.

The residence time in the air gap is historically known as the time in the air gap (TIAG) [4]. The simplest and most widely used expression for TIAG is given by Eq. (15.1):

$$\text{TIAG} = \frac{L}{v_f}. \tag{15.1}$$

where L = length of the air gap (distance between die exit and nip), v_f = final speed or line speed.

In English units, this can be written:

$$\text{TIAG (ms)} = \frac{L\ [\text{in.}]}{v_f\ [\text{ft/min}]} \times 5000. \tag{15.2}$$

In metric units:

$$\text{TIAG (ms)} = \frac{L\ [\text{mm}]}{v_f\ [\text{m/min}]} \times 60. \qquad (15.3)$$

While easy to calculate, TIAG fails to describe the actual physics of flow. As illustrated in Fig. 15.2, TIAG assumes that the velocity of the melt curtain instantaneously accelerates to the final velocity at the die exit. Other expressions have been proposed as described in Table 15.1. One method uses the average velocity (at the die exit and the line speed). Another assumes the velocity changes linearly from the die exit to the nip. Chapter 2 derives an expression for the residence time (which shall be called the process time in this chapter) assuming a Newtonian velocity profile [8].

$$t_f = \frac{L}{v_f}\left[\frac{\text{DDR} - 1}{\ln(\text{DDR})}\right] \qquad (15.4)$$

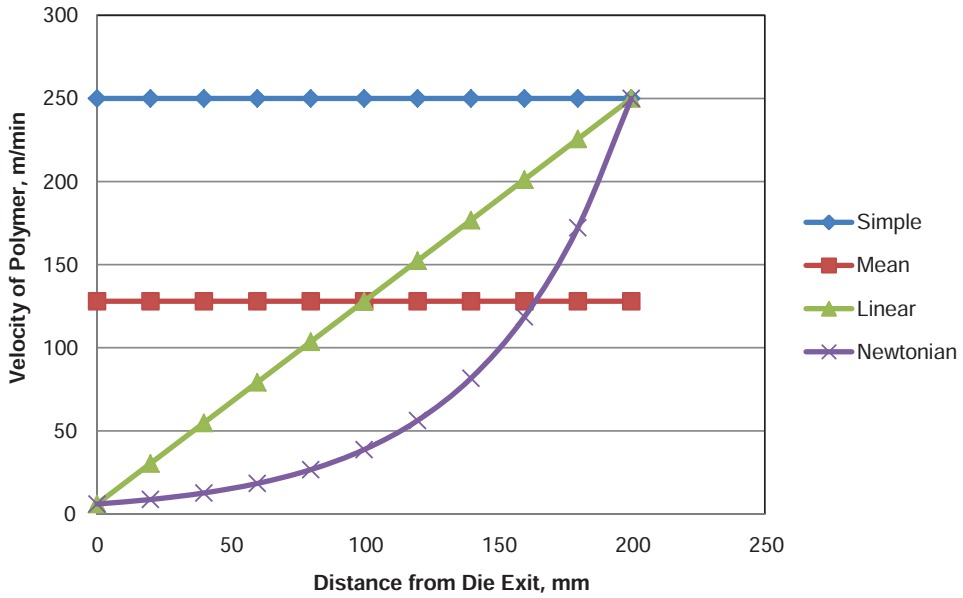


Figure 15.2 Velocity profiles in the air gap from various models for process time. Line speed = 250 m/min, die gap = 0.5 mm, air gap = 200 mm, coating thickness = 12 μm. Curves correspond to process time models shown in Table 15.1. The simple model assumes the velocity at the die exit is the same as the line speed. The mean model uses the average of the line speed and velocity at the die exit. The linear model assumes the velocity increases linearly as a function of the distance from the die exit and the Newtonian model assumes that the flow behaves like a Newtonian fluid ($v = \text{DDR}^{z/L}$). *DDR*, draw down ratio.

Table 15.1 Calculating Time in the Air Gap or Process Time

Model	Equation	References
Simple (TIAG)	$t_f^{\text{simple}} = \text{TIAG} = \frac{L}{v_f}$	Antonov and Soutar [4]
Mean	$t_f^{\text{mean}} = \frac{L}{0.5(v_0+v_f)} = \frac{L}{0.5v_f}\left(\frac{\text{DDR}}{\text{DDR}+1}\right)$	Morris [5]
Linear	$t_f^{\text{linear}} = \frac{L}{v_f}\left(\frac{\text{DDR}}{\text{DDR}-1}\right)\ln(\text{DDR})$	Morris [6,7]
Newtonian	$t_f^{\text{Newtonian}} = \frac{L}{v_f}\left(\frac{\text{DDR}-1}{\ln(\text{DDR})}\right)$	Morris [7,8]

L = *air gap*, v_f = *line speed*, v_0 = *velocity at die exit*, *DDR* = *draw down ratio* = v_f/v_0. TIAG, *time in the air gap.*

where t_f = process time (time between die exit and nip), DDR = draw down ratio (Eq. (2.18)).

Eq. (15.4) is a good compromise between ease of use and assuming a velocity profile that matches the actual physics of the flow in the air gap. As shown in Fig. 2.17, a Newtonian velocity profile agrees fairly well with the velocity profile for LDPE as measured by Canning [9]. More exact models require the use of non-Newtonian constitutive equations that are more difficult to compute using a hand calculator or simple spreadsheet program and often require material parameters that are challenging to measure. Example calculations for process time are provided in Table 15.2.

Many investigators have found that adhesion in extrusion coating increases with the TIAG. Antonov and Soutar [4] were among the first to summarize the data and show that the peel strength of the coating to the substrate increases with increasing TIAG for a wide variety of polymers and substrates. One set of data from this paper is reproduced in Fig. 15.3. A number of mechanisms may be responsible for this behavior, including time for oxidation of the melt curtain, stress effects, and cooling. These are explored in the following sections.

15.1.2.1 Oxidation

LDPE is the largest volume resin used in extrusion coating and lamination, yet it does not bond well by itself to polar substrates such as paper, aluminum foil, and chemically primed films. It is well recognized that LDPE undergoes oxidation during the extrusion coating process to create functional groups that favor adhesion. The mechanism for thermooxidation of LDPE is the formation of alkyl radicals (R*) through the splitting of covalent bonds, followed by reaction with oxygen to form

Table 15.2 Sample Process Time Calculations

Extrusion Coating Time in the Air Gap			
Input Parameters	**Unit**	**Value**	**Symbol**
Resin density (solid)	g/cc	0.92	ρ_f
Resin density (melt)	g/cc	0.73	ρ_o
Die width	mm	1000	w_o
Coating width	mm	900	w_f
Line speed	m/min	400	v_f
Die gap	μm	1000	X_o
Air gap	mm	400	L
Coating thickness	μm	12	X_f
Calculated Values			**Equation**
Velocity at die exit	m/min	5.4	$V_0 = V_f/\mathrm{DDR}$
DDR		73	$\mathrm{DDR} = \frac{X_f w_f \rho_f}{X_0 w_0 \rho_0}$
TIAG (simple model)	ms	60	$\mathrm{TIAG} = \frac{L}{v_f}$
t_f (mean velocity)	ms	118	$t_f^{\mathrm{mean}} = \frac{L}{0.5(v_0+v_f)}$
t_f (linear model)	ms	261	$t_f^{\mathrm{linear}} = \frac{L}{v_f}\left(\frac{\mathrm{DDR}}{\mathrm{DDR}-1}\right)\ln(\mathrm{DDR})$
t_f (newtonian model)	ms	1012	$t_f^{\mathrm{Newtonian}} = \frac{L}{v_f}\left(\frac{\mathrm{DDR}-1}{\ln(\mathrm{DDR})}\right)$

If melt density is unknown, a value of 0.7–0.75 g/cc is a good approximation for polyethylene and ethylene copolymers. DDR, *draw down ratio;* TIAG, *time in the air gap.*

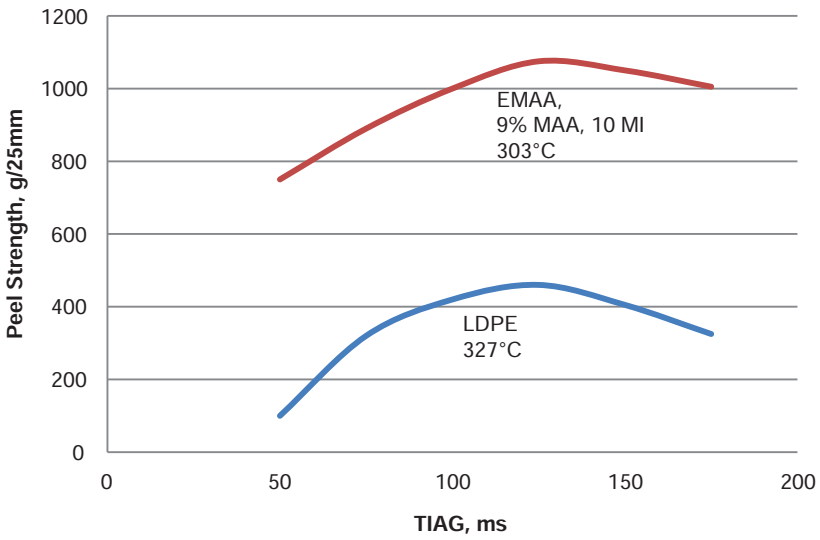


Figure 15.3 Peel strength to aluminum foil as a function of time in the air gap. *EMAA*, ethylene methacrylic acid; *LDPE*, low density polyethylene; *MAA*, methacrylic acid; *MI*, melt index; *TIAG*, time in the air gap.
From Antonov V, Soutar A. Foil adhesion with copolymers: time in the air gap. In: TAPPI 1991 polymers, laminations & coatings conference proceedings. Atlanta: TAPPI Press; 1991. p. 553. Reproduced with permission from E. I. du Pont de Nemours and Company.

hydroperoxides (ROOH). This occurs in a chain reaction [1,2,10–14].

$$RH \rightarrow R^{*} \rightarrow RO_2^{*} \rightarrow ROOH \rightarrow \text{Oxygenated products}$$

Here R represents the polymer chain. The products of oxidation include carboxylic acids, aldehydes, ketones, and alcohols.

The evidence that LDPE undergoes oxidation during the coating process and that the oxidation products are responsible for its adhesion to polar substrates is straightforward and incontrovertible:

- LDPE only adheres to polar substrates if the melt temperature is above about 285°C. This is shown by many investigators for bonding LDPE to paper or foil. One example is shown in Fig. 15.4. Typically, LDPE is extruded at 310°C and higher for extrusion coating applications.
- The onset of thermooxidative degradation of LDPE occurs at around 285°C and the rate of oxidation increases exponentially as the temperature is further increased. Several investigators [16–21] have linked the formation of oxidative species with processing temperature.
    - Laiho and Ylanen [16] correlate melt temperature with a carbonyl index (CI) that reflects the number of C═O groups that have formed. CI is obtained from Fourier transform infrared spectroscopy (FTIR) measurements by calculating the ratio of the peak height at 1720 cm^{-1} to a reference C-H peak at 2660 cm^{-1} [2]. As the melt temperature increases above 280°C, the CI increases substantially as shown in Fig. 15.5.
    - Ristey and Shroff [21] show similar results for two grades of LDPE. The grade with the lower density undergoes greater oxidation. This is explained by the chemistry: the lower density polymer has more short chain (methyl) branches and the branch points are more susceptible to oxidative reaction.
    - Andersson [2] shows similar results, which are reproduced in Fig. 15.6.
    - Briggs [17] uses ESCA (electron spectroscopy for chemical analysis, also known as X-ray photoelectron spectroscopy or XPS), a more sensitive surface analysis technique than FTIR. They find that the increase in adhesion of PE to aluminum with increasing processing temperature correlates with an increase in oxygen and nitrogen species at the surface of the PE.

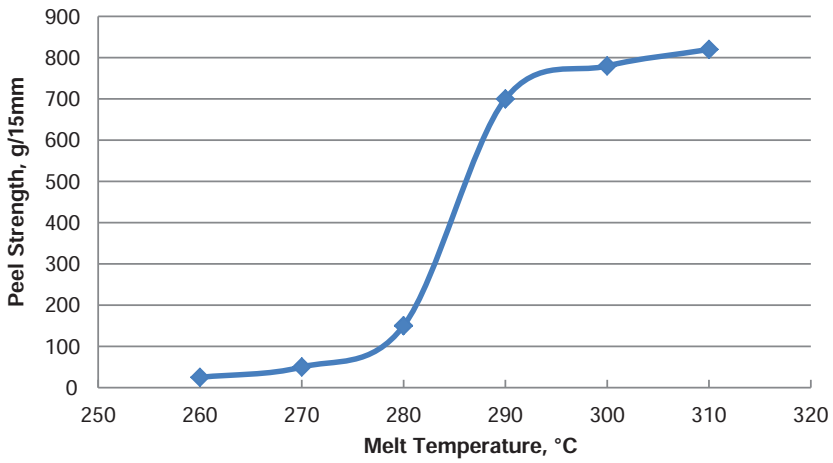


Figure 15.4 Adhesion of low density polyethylene (LDPE) to aluminum foil as a function of melt temperature. Line speed: 100 m/min, 20 μm coating.
Reproduced with permission from Sherman PB. Ozonation of polymer melt for improved adhesion. In: Bezigian, editor. Extrusion coating manual, 4th ed. Atlanta (GA): TAPPI Press; 1999. p. 75–88.

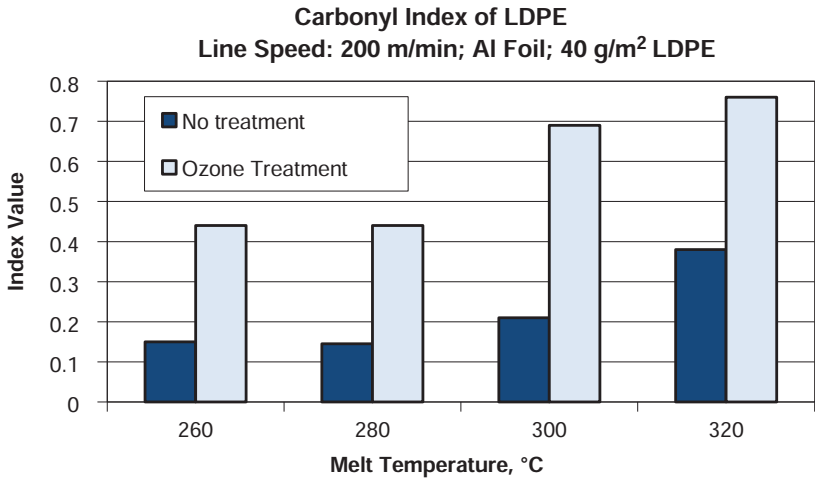


Figure 15.5 Oxidation, as measured by carbonyl index, as a function of melt temperature and ozone treatment. *LDPE*, low density polyethylene.
Reproduced with permission from Laiho E, Ylanen T. Flame, corona, ozone – do we need all pretreatments in extrusion coating. In: TAPPI polymers, laminations & coatings conference; 1997. p. 93.

- Some oxidative species are more effective for bonding to polar substrates than others. Hansen [18] looks specifically at the potential for these species to form acid–base interactions (the aluminum oxides on the surface of foil are basic) using a technique called flow microcalorimetry. They show that the acid functionality of LDPE fibers increases with increasing fabrication temperature (288–315°C).
- Decreasing the line speed or increasing the air gap increases the adhesion of LDPE to various substrates.
  - Croilius [22] relates this to the web exposure time or the time the polymer spends in the air gap.
  - Antonov and Soutar [4] later define the ratio of these two parameters as the TIAG as given by Eq. (15.1). Referring back to the

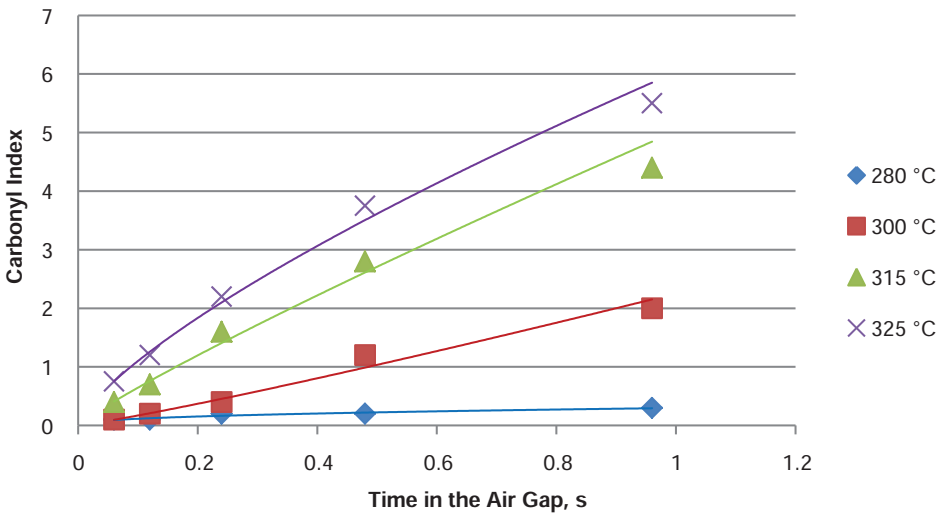


Figure 15.6 Oxidation as a function of time in the air gap (TIAG). Carbonyl index (CI) is a measure of oxidation obtained from Fourier transform infrared spectroscopy (FTIR) measurements.
Data from Andersson T, Stalbom B, Wesslen B. Degradation of polyethylene during extrusion. II. Degradation of low-density polyethylene, linear low-density polyethylene, and high density polyethylene in film extrusion. J Appl Polym Sci 2004;91:1525–1537.

typical plot shown in Fig. 15.3, the peel strength normally goes through a maximum at about 100 ms. The region below 100 ms is of most interest to coaters since it represents the region of higher productivity and output. In this region, increasing TIAG typically increases the adhesion to polar substrates. Sherman [15] suggests that this is due to an initiation effect; a certain time or temperature is required to initiate the oxidation reaction. At low TIAG, there is insufficient time for oxidation to begin.

- Andersson [2] relates TIAG directly to the CI by casting film into a water bath at different heights above the water while maintaining a constant line speed and output. The air gap ranges from 10 to 80 mm, corresponding to a range in TIAG of 0.12–1.92 s ($v_f = 5$ m/min). The plots of CI versus TIAG are shown in Fig. 15.6. The results show a monotonous increase in surface oxidation with increasing air gap (or equivalently TIAG).
- Ristey and Shroff [21] coat LDPE onto paper varying melt temperature, coat weight, and air gap while maintaining constant line speed (900 ft/min or 234 m/min). Increasing the air gap increases the CI and adhesion to paper. They find a certain minimum CI is needed to obtain good adhesion to paper.
- Hjertberg [20] measures peel strength of LDPE to aluminum as a function of CI and finds that the peel strength increases with increasing oxidation but plateaus at high values of CI. This is similar to a peel strength versus TIAG plot. Hjertberg attributes the plateau to a balancing of forces acting on the adhesion. The increased oxidation increases the polar functionality but at high levels causes chain scission. They measure the molecular weight distribution (MWD) of the oxidized LDPE and find a significant increase in the low MW fraction with increasing oxidation. Poor cohesive strength as a result of low MW may account for a loss in adhesion. This explanation is consistent with other investigations. Ristey and Shroff [21] measure the change in MWD and melt index (MI) of their coated LDPE. Plots of MI versus melt temperature are shown to have a U shape with a minimum around 330°C. At lower temperatures the polymer

degrades primarily by cross-linking, while at higher temperatures chain scission occurs. Andersson [2] reports similar results using an in-line rheometer during extrusion: chain extension or cross-linking dominates at lower temperature (<325°C), whereas chain scission dominates at higher temperatures. Linear low density polyethylene (LLDPE) and high density polyethylene (HDPE) show chain scission behavior over the whole temperature range.

  - Foster [23] recasts Ristey and Shroff's data in terms of TIAG and shows that CI increases with TIAG.

- The temperature at which adhesion of LDPE to polar substrates begins to take off also corresponds to an increase in generation of off-gases. Andersson [10–12] shows that the smoke at the die exit is comprised of oxidative by-products, including alcohols, acids, aldehydes, and ketones, the same functionality found in the LDPE films. The concentration of the by-products increases with increasing processing temperature and correlates with off-flavor of water samples subjected to the films, as determined by a human taste panel.
- Many investigators and processors have found treating the LDPE melt curtain with ozone promotes adhesion to polar substrates at lower extrusion temperatures or higher line speeds (shorter TIAG). This is attributed to enhanced surface oxidation [15,24,25], as shown in Fig. 15.5.
- Adding antioxidants to LDPE can inhibit adhesion [17,26]. One example is provided in Fig. 15.7 based on a study by Zambetti [26] using vitamin E as the antioxidant.

One of the drawbacks of LDPE is that its adhesion is dependent on the process: if sufficient oxidation does not occur, the adhesion will suffer. Excessive temperature causes off-flavor issues due to oxidative by-products and also loss of adhesion due to chain scission (the creation of low molecular weight species can weaken the bond strength). There is a relatively narrow temperature range for

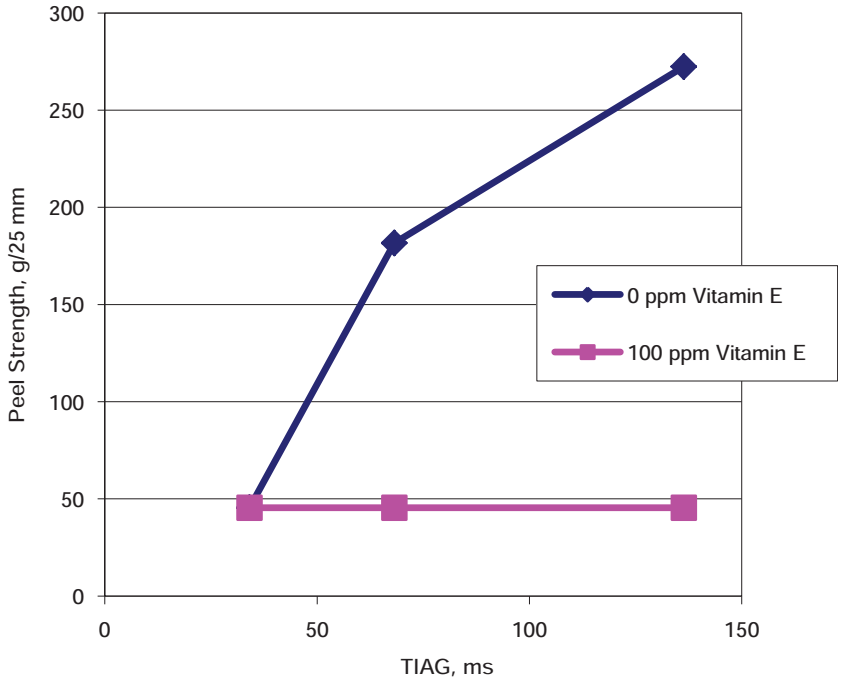


Figure 15.7 Effect of adding an antioxidant (vitamin E) to low density polyethylene (LDPE) on adhesion of LDPE extrusion coated onto aluminum foil. *TIAG*, time in the air gap.
Data are taken from Zambetti P, Baker S, Kelley D. Alpha tocopherol as an antioxidant for extrusion-coating polymers. TAPPI J 1995;78:167. Graph is reproduced from Morris BA, Suzuki N. The case against oxidation as a primary factor for bonding acid copolymers to foil. In: TAPPI polymers, laminations & coatings conference; 2000 with permission.

processing LDPE for optimum adhesion, typically between about 310 and 330°C.

Several approaches are used to mitigate these issues. One is to ozone treat the melt curtain. Hammond [24] shows that adhesion of LDPE to a chemically primed film can be achieved at substantially lower processing temperature or higher line speeds by using ozone treatment.

Another approach is to use functionalized polymers, such as acid copolymers and ionomers. These contain acid functionality incorporated into the backbone of the polyethylene chain during polymerization. There is no need of oxidation for these polymers to bond to polar substrates. Antonov and Soutar [4], however, show that these polymers exhibit an increase in peel strength to foil and paper with increasing TIAG, just like LDPE, but starting at much higher level of bond strength. This is illustrated in Fig. 15.3. Based on this evidence, many in the industry have assumed that oxidation is also involved in the adhesion of acid copolymers to polar substrates. Morris and Suzuki [25] examine this phenomenon and conclude that oxidation is not the underlying mechanism for these polymers. Their arguments and experimental results are summarized here:

- Oxidation does occur in acid copolymers during extrusion coating. In some unpublished work at DuPont in the 1980s, Golike [27] shows that oxidative species form during extrusion coating of acid copolymers at elevated temperatures (more than 280°C). The amount of oxidative species formed (as measured by headspace gas chromatography) increases with increasing melt temperature and correlates with changes in organoleptics. He concludes that the mechanism for oxidation of acid copolymers is similar to that of LDPE.
- The effect of melt temperature on the adhesion of acid copolymer resins (ACRs) is complex. Low-acid ACRs (typically 7% and lower) show an increase in peel strength to foil with increasing temperature similar to the trend found for LDPE. Higher acid polymers tend to be less sensitive to temperature above a certain minimum needed for wetting and spreading of the polymer onto the substrate. Antonov and Soutar [4] report that during an initial investigation of a 12% MAA (methacrylic acid), seven MI polymer, "adhesion was not related to melt temperature over the temperature range of 470−580°F (243−304°C)." This and other studies suggest that above about 280°C, the adhesion of high-acid ACRs does not substantially change with increasing temperature. Yet, organoleptic testing shows that more oxidative species form in acid copolymers when they are processed at these higher temperatures.
- One possible explanation comes from Hansen's flow microcalorimetry work [18]. They show that oxidation adds less than about 1 wt% acid functionality to LDPE. While this is significant for LDPE, this may be too little to make a difference for high-acid copolymers that already have 9−12 wt% acid functionality. Hester [28] finds that the effect of acid level on the adhesion of acid copolymers to foil is nonlinear (Fig. 15.8); when the ACR has less than 9% MAA adding additional acid functionality has a pronounced effect on adhesion. Above 9% acid, the effect is minimal.
- Morris [6] studies the effect of wetting and stress on the peel strength of acid copolymers to foil. This work is reviewed in Section 15.1.2.2. Wetting of the surface is quantified by measuring the contact angle (the angle between a liquid drop and the solid surface) of water on the coating surface. The greater the contact angle, the less tendency there is for the liquid to wet the surface. Thus, the contact angle is related to the surface energy and should change when oxidative species are formed at the surface. He finds, however, that measurements of the contact angle of water on the coating surface do not correlate with peel strength. The results suggest that at the TIAG and temperatures used in the study, oxidation is insignificant. Yet, large differences in peel strength are measured. Morris' analysis suggests that the increase in peel strength with increasing TIAG is associated with a reduction in stress. Specifically, TIAG is inversely related to the rate of elongation during coating. Increasing the rate of elongation (decreasing TIAG) increases the stress imparted on the polymer. Residual stress can negatively impact adhesion [29].
- Morris and Suzuki [25] conduct four experiments to better understand the mechanism for

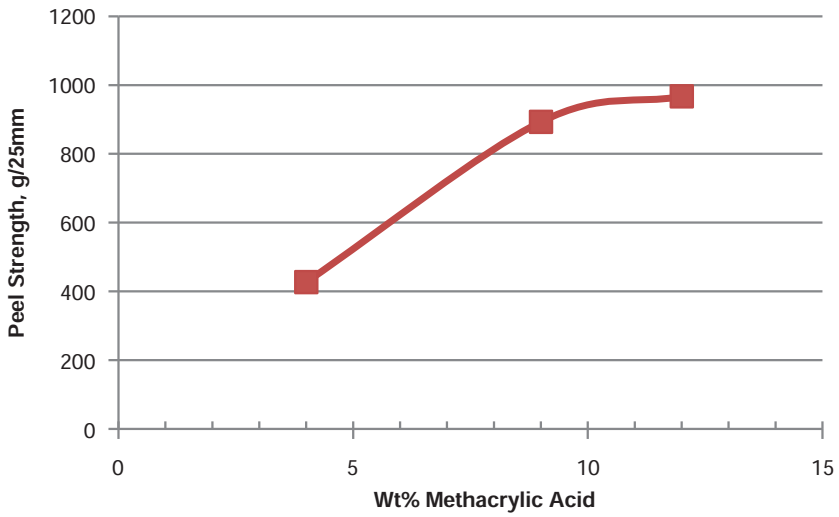


Figure 15.8 Effect of acid level on adhesion of acid copolymer (ethylene methacrylic acid, EMAA) to aluminum foil in extrusion coating. Structure is 25 μm EMAA/50 μm Al foil. Peel strength measured 1 week after coating. *Data from Hester D, Sadik S, Trouilhet Y. Using acid copolymers as coextrusion tie layers. In: TAPPI polymers, laminations & coatings conference; 1989. p. 459.*

the rise in peel strength with increasing TIAG for acid copolymers:

- In the first, two acid copolymers and an LDPE control are treated with ozone as they are coated onto foil. The structure is kraft paper (50 μm)/LDPE (20 μm)/Al foil (9 μm)/resin (20 μm). The resin is melted in a 65 mm diameter extruder and fed through an internal deckled die with a die gap of 0.8 mm and a width of 500 mm. The air gap is 120 mm and line speed 80 m/min for a TIAG of 90 ms. Four variables are tested: the resin type (two ACRs and one LDPE), the resin melt temperature, and the ozone concentration and flow rate. The resins are described in Table 15.3. Peel strength is measured using a T-peel test at a pull rate of 300 mm/min. Samples are measured at 1, 7, and 14 days after coating. The results of the 1-day peel tests are shown in Table 15.4 and Fig. 15.9 (7 and 14 days results show similar trends). The results indicate that ozone treatment has no positive effect on the adhesion of acid copolymers to foil. Indeed, at the lower processing

Table 15.3 Description of Resins Used in Morris and Suzuki Study of the Effect of Oxidation on Peel Strength of Acid Copolymers to Aluminum Foil

Code Name	Supplier	Grade Name	% Acid (MAA)	MI (g/10 min)
N0908	Mitusi-DuPont	Nucrel 0908C	9	8
N0407	Mitsui-DuPont	Nucrel AN4214C	4	7
N0910	DuPont	Nucrel 0910	9	10
N0910 + A/O	DuPont	Nucrel 0910 with 1000 ppm antioxidant	9	10
N1214	DuPont	Nucrel 1214	12	14

MAA, *methacrylic acid.*
From Morris BA, Suzuki N. The case against oxidation as a primary factor for bonding acid copolymers to foil. In: TAPPI polymers, laminations & coatings conference; 2000. Reproduced with permission from E. I. du Pont de Nemours and Company.

Table 15.4 Effect of Ozone Treatment on Peel Strength to Aluminum Foil

Resin	Ozone Conc. g/m^3	Ozone Flow m^3/h	Peel Strength, g/25 mm		
			At Extrusion Temperature		
			250°C	270°C	290°C
N0908	0	0	550	570	650
	15	0.5	520	600	630
	15	1.0	450	570	600
	15	2.0	330	550	600
	25	0.5	470	580	620
	25	1.0	320	580	600
Resin	**Ozone Conc. g/m^3**	**Ozone Flow m^3/h**	**Peel Strength, g/25 mm**		
			At Extrusion Temperature		
			270°C	**285°C**	**300°C**
N0407	0	0	500	520	530
	15	1.0	470	500	530
	25	1.0	430	480	500
Resin	**Ozone Conc. g/m^3**	**Ozone Flow m^3/h**	**Peel Strength, g/25 mm**		
			290°C Extrusion Temperature		
LDPE	0	0	30		
	15	1.0	250		
	15	2.0	230		
	25	1.0	250		
	25	2.0	230		
	35	1.0	250		
	35	2.0	250		

Measurements were made one day after extrusion coating. Structure is kraft paper/LDPE (low density polyethylene)/Al/resin. Resins are described in Table 15.3.
From Morris BA, Suzuki N. The case against oxidation as a primary factor for bonding acid copolymers to foil. In: TAPPI polymers, laminations & coatings conference; 2000. Reproduced with permission from E. I. du Pont de Nemours and Company.

temperatures, the peel strength is lower with ozone than without. This may be due to a cooling effect resulting from the flow of ozone onto the melt curtain. This contrasts with the LDPE case where the ozone treatment substantially increases the peel strength performance. The results suggest that increasing oxidation with ozone treatment does not enhance the adhesion of acid copolymers to foil. The results also show that even with ozone treatment, the adhesion of LDPE to foil is substantially less than the acid copolymer.

- In the second experiment, 1000 ppm of a hindered phenol antioxidant is added to an acid copolymer (N0910, described in Table 15.3). The N0910 is melt compounded with a concentrate made from the same base resin using a single-screw

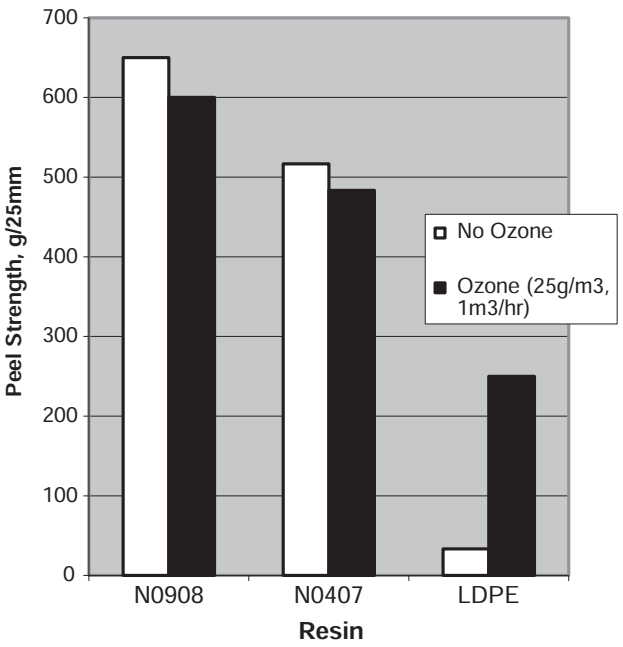


Figure 15.9 Effect of ozone treatment of melt curtain during extrusion coating on peel strength to aluminum foil for two acid copolymer resins and LDPE (low density polyethylene). Structure is kraft paper/LDPE/Al/resin. Resins are described in Table 15.3.
From Morris BA, Suzuki N. The case against oxidation as a primary factor for bonding acid copolymers to foil. In: TAPPI polymers, laminations & coatings conference; 2000. Reproduced with permission from E. I. du Pont de Nemours and Company.

compounding extruder at 190°C. For a control, the N0910 is put through the same extruder without the concentrate so that both resins have the same heat history. Both versions are extrusion coated onto 50 μm aluminum foil at a coating thickness of 25 μm. The melt temperature is set at 300°C and ranged from 290 to 308°C (measured by both an IR thermometer and thermocouple). The die gap is 0.63 mm. The air gap (127−254 mm) and line speed (61−244 m/min) are varied over a range so that the TIAG varies from 31 to 250 ms. Peel strength results are shown in Table 15.5 and Fig. 15.10. The results show that adding an antioxidant to the acid copolymer has no substantial effect on peel strength performance. These contrast with studies from the literature for LDPE (Fig. 15.7). ESCA is used to measure the amount of surface oxygen on the coatings. This technique measures the elemental composition near the surface of a material by bombarding the surface with high-energy electrons. The sampling depth is determined by the detection angle: 30° and 90° correspond to approximately 50 and 100 Å, respectively. The ESCA results are shown in Fig. 15.11. The unmodified N0910 shows an increase in surface oxidation whereas the addition of antioxidant effectively suppresses oxidation. Yet both give the same trend of increasing peel strength with increasing TIAG.

- The third experiment uses a high MI grade (N1214) to coat foil at 230°C, well below the onset of oxidation. The same structure and setup are used as for the antioxidant experiment. The N0910 run at 300°C is used for comparison. The peel strength results are shown in Fig. 15.12. Both the 1214 (230°C) and 0910 (300°C) show the characteristic increase in peel strength to foil with increasing TIAG. ESCA results are shown in Fig. 15.13. As expected, the N1214 shows no increase in surface oxygen concentration as a function of TIAG. The results show that greater oxidation is not required for the peel strength of acid copolymers to increase with increasing TIAG.
- The fourth experiment examines the effect of orientation on peel strength. Peel tests are conducted in the machine direction (MD) and transverse direction (TD) and compared with the mechanical properties of the coatings (% elongation at break). Returning to the same structure as in experiment 1, N0908 is coated onto the foil side of the structure paper/LDPE/Al. Coating thickness is 20 μm. The die gap is 0.8 mm. The melt temperature is 290°C. The air gap is 110 mm and line speed is varied from 80 to 200 m/min (resulting in TIAG ranging from 83 to 33 ms). To obtain samples of the coating for elongation measurements, 12 μm oriented polyester (OPET) slip sheets are inserted between the foil and coating during part of the run. The coating is then peeled away from the OPET for testing. The results of peel

Table 15.5 Results of Antioxidant and Low Temperature Experiments

Line Speed (m/min)	Air Gap (mm)	TIAG (ms)	Green Peel, g/25 mm		1 week Peel, g/25 mm		At% O by ESCA	
			Mean	Standard	Mean	Standard	30°	90°
50 μm Foil/N0910 (No Antioxidant) Coated at 300°C								
244	127	31	507	73	668	60	1.4	0.7
122	127	63	718	31	890	19	2.1	1.2
61	127	125	624	31	768	20	2.3	1.5
244	254	63	777	61	951	74	3.3	2.2
122	254	125	886	87	1130	107	2.6	1.8
61	254	250	776	33	893	78	2.2	1.3
50 μm Foil/N0910 + A/O Coated at 300°C								
244	127	31	444	65	502	58	1.9	1.2
122	127	63	449	82	470	91	2.3	1.3
61	127	125	724	50	910	33	2.3	1.3
244	254	63	748	34	801	33	2	1.2
122	254	125	812	74	950	69	2	1.1
61	254	250	931	86	1149	87	[a]	[a]
50 μm Foil/N1214 Coated at 230°C								
244	127	31	562	56	525	70	2.2	1.4
122	127	63	823	43	799	69	2.6	1.3
61	127	125	681	53	681	43	1.7	0.8
244	254	63	768	47	787	50	1.9	0.9
122	254	125	879	29	857	52	1.9	0.8
61	254	250	814	65	784	64	1.8	0.8

ESCA, *electron spectroscopy for chemical analysis;* TIAG, *time in the air gap.*

[a] *Value not reported due to sample contamination.*

From Morris BA, Suzuki N. The case against oxidation as a primary factor for bonding acid copolymers to foil. In: TAPPI polymers, laminations & coatings conference; 2000. Reproduced with permission from E. I. du Pont de Nemours and Company.

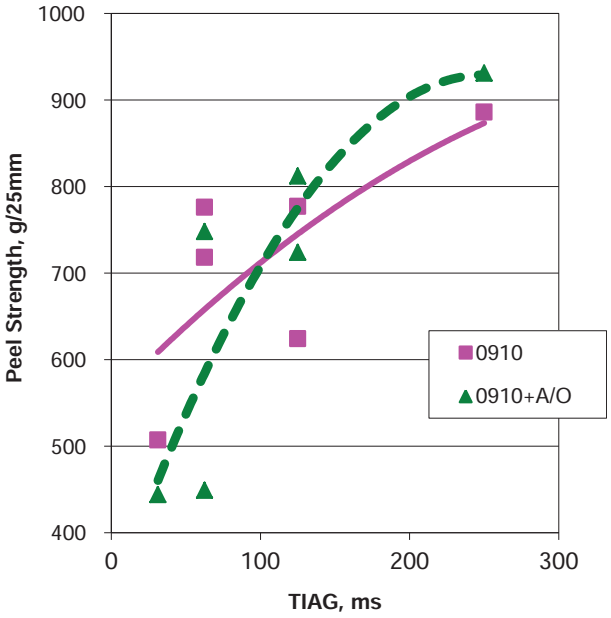


Figure 15.10 Effect of antioxidant on peel strength to foil of an acid copolymer resin. Results are for green peel strength. *TIAG*, time in the air gap.
From Morris BA, Suzuki N. The case against oxidation as a primary factor for bonding acid copolymers to foil. In: TAPPI polymers, laminations & coatings conference; 2000. Reproduced with permission from E. I. du Pont de Nemours and Company.

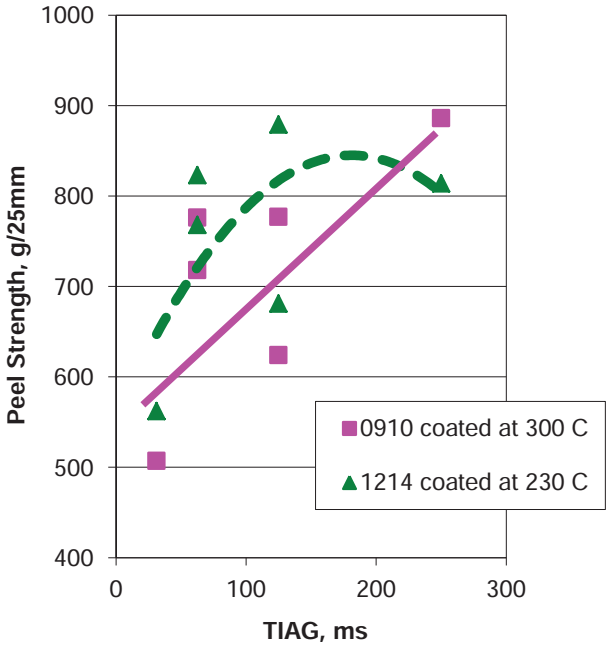


Figure 15.12 Effect of processing temperature on peel strength to aluminum foil. *TIAG*, time in the air gap.
From Morris BA, Suzuki N. The case against oxidation as a primary factor for bonding acid copolymers to foil. In: TAPPI polymers, laminations & coatings conference; 2000. Reproduced with permission from E. I. du Pont de Nemours and Company.

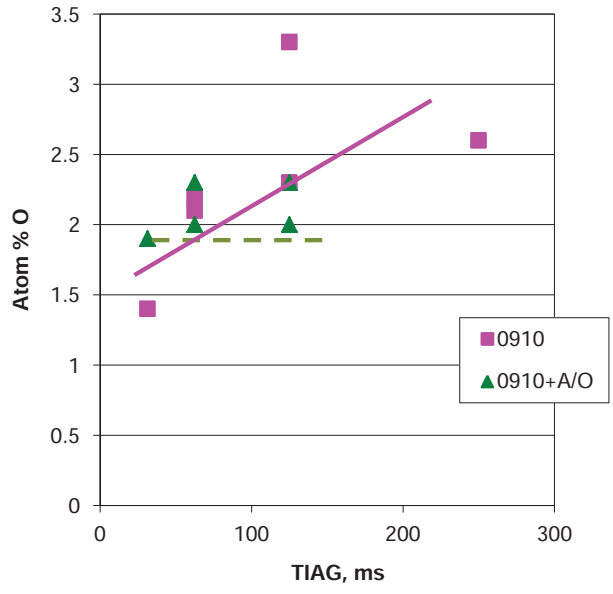


Figure 15.11 Effect of antioxidant on surface concentration of oxygen (ESCA results). *ESCA*, electron spectroscopy for chemical analysis; *TIAG*, time in the air gap.
From Morris BA, Suzuki N. The case against oxidation as a primary factor for bonding acid copolymers to foil. In: TAPPI polymers, laminations & coatings conference; 2000. Reproduced with permission from E. I. du Pont de Nemours and Company.

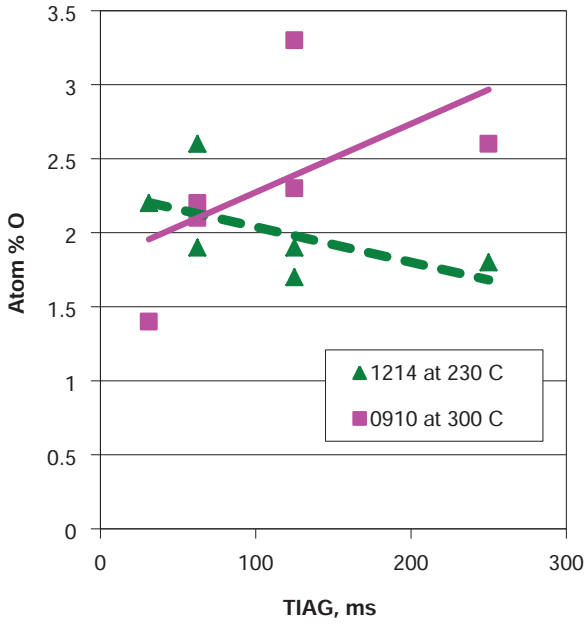


Figure 15.13 Effect of processing temperature on surface concentration of oxygen (ESCA results). *ESCA*, electron spectroscopy for chemical analysis; *TIAG*, time in the air gap.
From Morris BA, Suzuki N. The case against oxidation as a primary factor for bonding acid copolymers to foil. In: TAPPI polymers, laminations & coatings conference; 2000. Reproduced with permission from E. I. du Pont de Nemours and Company.

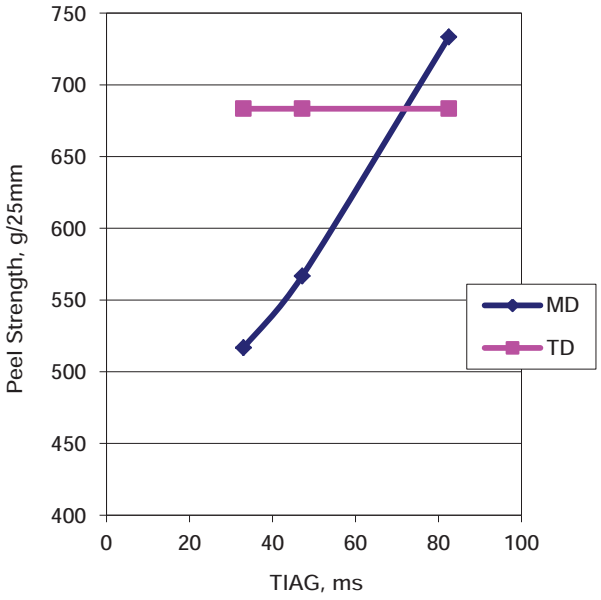


Figure 15.14 Effect of orientation on peel strength of N0908 acid copolymer to aluminum foil. Structure is kraft paper/LDPE/Al/resin. *LDPE*, low density polyethylene; *MD*, machine direction; *TD*, transverse direction; *TIAG*, time in the air gap.
From Morris BA, Suzuki N. The case against oxidation as a primary factor for bonding acid copolymers to foil. In: TAPPI polymers, laminations & coatings conference; 2000. Reproduced with permission from E. I. du Pont de Nemours and Company.

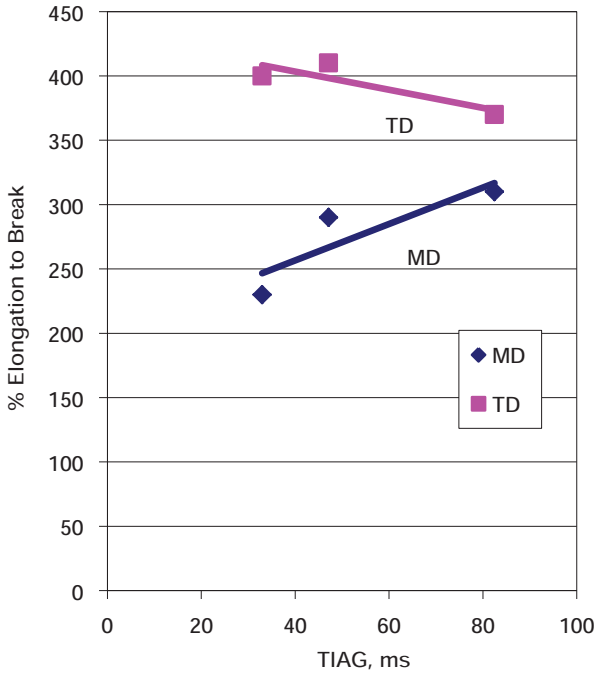


Figure 15.15 Effect of TIAG on % elongation at break of coatings from Fig. 15.14. *MD*, machine direction; *TD*, transverse direction; *TIAG*, time in the air gap.
From Morris BA, Suzuki N. The case against oxidation as a primary factor for bonding acid copolymers to foil. In: TAPPI polymers, laminations & coatings conference; 2000. Reproduced with permission from E. I. du Pont de Nemours and Company.

strength measurements in the MD and TD are shown in Fig. 15.14. In the MD, the peel strength increases with increasing TIAG, consistent with previous findings. In the TD, however, the peel strength is unchanged with increasing TIAG. If oxidation were the predominant mechanism, the peel strength should increase in both directions. The elongation at break of the coatings in the MD increases with TIAG, whereas it is relatively flat in the TD as shown in Fig. 15.15. This corresponds with the peel strength results. Two explanations are proposed. One involves stress. As TIAG increases, the stress decreases (Section 15.1.2.2). Lower stress results in less orientation of the polymer, resulting in higher elongation prior to breakage. Lower stress is also known to increase peel strength. The second explanation is related. The peel strength measurement captures the energy required to pull the specimen apart. This energy includes not only the inherent adhesion between the coating and substrate but also the energy needed to bend and elongate the peel arm. A fracture energy analysis shows that in these structures the energy to elongate the peel arm plays a substantial role [30]. Decreasing the % elongation of the peel arm reduces the peel strength (Section 10.2.3).

The practical implication of this study is that acid copolymers may provide more consistent peel strength performance to polar substrates than LDPE. They can be coated at lower temperatures, reducing organoleptic concerns, and at faster line speeds while still maintaining acceptable adhesion performance. As is discussed in Chapter 16, they also have better product resistance than LDPE, extending the shelf life of difficult products such as ketchup and salad dressings.

Acid copolymers and ionomers have their drawbacks, the most important being their higher price. Another approach to improving adhesion is to blend a functionalized ethylene copolymer with LDPE to enhance the adhesion to LDPE, making it more robust to processing variations. In Section 10.4.1.4, the development of Nucrel AE (adhesion enhancing), an acid-functionalized ethylene copolymer for blending with LDPE developed by DuPont is described [31]. The additive allows for higher line speeds and lower processing temperatures than LDPE alone and helps improve operational reliability [Fig. (10.20)].

The modifier approach is not for every situation. In particular, it does not provide the strong bond strength and resistance to aggressive products that the pure acid copolymer provides. But it is a good illustration of how understanding the manner in which adhesion performance is impacted by the process can lead to alternatives with better performance.

15.1.2.2 Stress and Orientation

As the polymer is drawn down to its final coating thickness in the air gap, it is subjected to stress. The stress arises from shear forces in the extruder and die, from extensional forces as the melt curtain is drawn down, and from shrinkage forces during crystallization. Morris [6] hypothesizes that these stresses may influence peel strength by impacting tensile properties and residual stress at the substrate−polymer interface. Stress is not one of the control parameters on an extrusion coating line that can be easily varied to directly test this hypothesis. Relationships between stress and common processing parameters such as air gap, die gap, melt temperature, and line speed are first required. Morris develops these relationships and conducts experiments changing processing parameters in a systematic way to alter the stress imposed on the polymer, using coating onto aluminum foil as a model system. Peel strength to foil varies by a factor of three, strongly suggesting that stress plays a role in peel strength performance. Stress developed during both extrusion and drawing are found to be important. This work is summarized in this section.

As described in Section 10.2.3, peel strength is the sum of the energy needed to create new surface area at the front of a crack traveling along the interface (this energy is known as the fracture energy) and the amount of energy dissipated by elongating and bending the peel arm. The fracture energy includes contributions from various adhesive forces such as thermodynamic and chemical interactions, as well as local deformation at the tip of the crack. The resistance to deformation is a function of the viscoelastic and tensile properties of the material. Changes in molecular orientation and crystalline morphology brought about by stress may affect these properties. For example, in polyethylene films the crystalline regions organize into lamellae or flat plates. High stress in the molten polymer has been shown to give a more ordered and twisted lamellae structure [32]. Such changes influence the bulk tensile properties of the polymer [33].

Another factor influencing peel strength is residual or frozen-in stress at the interface. This internal stress acts to reduce the fracture strength of the bond [29]. Internal stress may result when the oriented chains created during extrusion and drawing do not have time to relax back to their nature random coiled configuration due to the rapid quench. The ability of the stress to relax can be characterized by comparing the timescale of the process to the characteristic relaxation time of the polymer. The Deborah number is introduced in Chapter 5, a dimensionless number given by Eq. (15.5):

$$De = \frac{\lambda}{t_f} \tag{15.5}$$

where De = Deborah number, λ = relaxation time of the polymer, t_f = characteristic time of the process.

Methods for measuring the polymer relaxation time are given in Section 5.5.1. The characteristic process time is given by Eq. (15.4). When $De \ll 1$ ($t_f \gg \lambda$), stress is not likely to be frozen in since the polymer has time to relax. When $De \gg 1$, more of the internal stress will be frozen in place.

Stress may also arise from shrinkage of the polymer as it crystallizes. Increases in stress and orientation during the coating process may result in enhanced crystallinity and greater shrinkage (Section 13.5.3). For the purposes of this analysis, it is assumed that the stress due to shrinkage is either constant (independent of processing conditions) or is proportional to the net stress imparted during extrusion, drawing, and relaxation.

The net stress, therefore, is the sum of the stress imposed during extrusion (up to the die exit) and

drawing (in the air gap) minus any stress that has relaxed. An engineering analysis of the extrusion coating process is given in the Appendix where equations are developed relating processing variables to stress. The relationships between process variables and stress for the case of when the resin and coating thickness are held constant are summarized in Table 15.6. Here the symbol "∼" can be read as "goes as" or "scales as."

To examine the effect of stress on peel strength performance, 25 μm (1 mil) of an ethylene acrylic acid (EAA) copolymer (9 wt% AA with an MI of 10 g/10 min) is extrusion coated onto 50 μm (2 mil) aluminum foil under various processing conditions. A pilot scale line with a 107 cm wide T-slot die externally deckled to 71 cm and fed by a 114 cm diameter extruder is used for the coating. The air gap (13−34 cm), line speed (60−240 m/min), and die gap (0.38−1.01 mm) are varied, keeping coating thickness, deckled die width, and chill roll temperature constant. Goal melt temperature is 282°C (540°F); temperatures of the molten web measured with an IR thermometer range from 282 to 289°C at the die exit and from 276 to 282°C near the chill roll.

Peel strength of the acid copolymer to foil is measured by cutting 25 mm wide strips in the MD from the center of the web. These are separated between the acid copolymer and the foil and pulled in a tensile tester in a T-peel configuration at 305 mm/min. Measurements of contact angles using distilled water, tensile properties (ASTM 882), and wide angle X-ray scattering (WAXS) are conducted on selected samples.

The results of the trial are given in Table 15.7. Overall, peel strength varies by a factor of three, suggesting that stress is important to peel strength performance. Because of the interrelationships between stress imposed during extrusion (σ_{ext}) and the two parameters characterizing stress during drawing (rate of strain and total strain), it is difficult to isolate specific effects from the data. A statistical analysis software program is used to fit the data to a quadratic model. Plots of constant peel strength are given in Fig. 15.16. The statistical analysis shows the following trends:

- In general, peel strength decreases with increasing elongational rate of strain ($\dot{\varepsilon}$). The effect of rate of strain is stronger at higher total strains.
- At constant rate of strain and σ_{ext}, peel strength decreases with increasing total strain.
- The effect of σ_{ext} is more pronounced at low total strain. The elongational rate of strain can be increased by increasing line speed (increasing σ_{ext}) or reducing air gap (constant σ_{ext}). At low total strain, increasing the rate of strain while increasing σ_{ext} reduces peel strength further than by keeping σ_{ext} constant.

Polar contact angles (using water) are measured on the outside surface of the acid copolymer for selected

Table 15.6 Stress Equations for Extrusion Coating When Resin and Coating Thickness are Held Constant

Stress Factor	Equation	Equation Number
Stress imparted in the extruder and die (σ_{ext})	$\sigma_{ext} \sim \frac{m(T)\left(v_f^n\right)}{X_0^{2n}}$	15.6
Stress imparted during drawing (σ_d)	$\sigma_d \sim T,\ \dot{\varepsilon}, \varepsilon_{tot}$	15.7
	$\varepsilon_{tot} \sim \ln(\mathrm{DDR}) \sim \ln(X_0)$	15.8
	$\dot{\varepsilon} = \frac{v_f}{L}\left(\frac{\mathrm{DDR}-1}{\mathrm{DDR}}\right)$	15.9
Stress relaxation	$\mathrm{Relaxation} \sim \lambda(T),\ t_f$	15.10
	$t_f = \frac{L}{v_f}\left(\frac{\mathrm{DDR}}{\mathrm{DDR}-1}\right)\ln(\mathrm{DDR}) \sim \frac{L}{v_f}\ln(X_o)$	15.11

σ_{ext}, stress imposed by the extrusion; σ_d, stress imposed by drawing; ε_{tot}, strain at end of air gap; $\dot{\varepsilon}$, rate of strain (in air gap); λ, relaxation time of the polymer; T, temperature of molten polymer, v_f, line speed (velocity near the chill roll); X_o, die gap; m, n, power law viscosity model consistency index and exponent (Eq. (15A.3)); DDR, draw down ratio.

Table 15.7 Results From Extrusion Coating Trial Evaluating Factors Influencing Stress on Peel Strength

Experiment	Die Gap (mm)	Line Speed (m/min)	Air Gap (cm)	L/V_f (ms)	Process Time (ms)	σ_{ext} Relative [a]	σ_{draw}		Web Temperature (°C)		Peel Strength, g/25 mm			
											Green		1-week	
							ε_{tot} ln(DDR)	ε' (1/s)	At Die	At Chill Roll	Mean	Standard Deviation	Mean	Standard Deviation
1.1	0.64	61	13	125	400	0.66	3.0	7.3	286	279	**499**	345	**672**	309
1.2	0.64	122	25	125	400	1.00	3.0	7.3	286	278	**704**	32	**754**	182
1.4	0.64	244	25	63	200	1.52	3.0	14.5	293	287	**595**	163	**804**	168
2.1	0.64	122	13	63	200	1.00	3.0	14.5	286	284	**390**	118	**536**	154
2.2	0.64	122	18	88	280	1.00	3.0	10.5	286	283	**649**	114	**858**	109
2.3	0.64	122	25	125	400	1.00	3.0	7.3	286	279	**785**	36	**863**	59
2.4	0.64	122	34	169	540	1.00	3.0	5.4	287	276	**1035**	104	**1180**	104
4.1	0.38	122	13	63	172	1.85	2.5	13.6	288	287	**404**	68	**754**	50
4.2	0.38	122	18	88	241	1.85	2.5	9.7	288	283	**699**	36	**885**	59
4.3	0.38	122	25	125	344	1.85	2.5	6.8	287		**649**	14	**817**	45
4.4	0.38	122	34	169	465	1.85	2.5	5.0	288	278	**663**	45	**822**	23
4.5	0.38	61	13	125	344	1.22	2.5	6.8	290		**558**	127	**844**	95
4.6	0.38	171	34	121	332	2.26	2.5	7.0	283	280	**504**	218	**731**	209
4.7	0.38	244	25	63	172	2.80	2.5	13.6	282		**250**	27	**472**	132
5.1	1.02	122	13	63	227	0.57	3.5	15.1	286	283	**554**	209	**817**	54
5.2	1.02	122	25	125	453	0.57	3.5	7.5	287	282	**436**	145	**749**	68
5.3	1.02	122	32	156	566	0.57	3.5	6.0	287	280	**840**	182	**958**	114
5.4	1.02	122	36	175	634	0.57	3.5	5.4	289	280	**817**	127	**1017**	177
5.5	1.02	61	13	125	543	0.38	3.5	7.5	287	285	**722**	241	**908**	95
5.6	1.02	183	34	113	408	0.73	3.5	8.4	288	281	**658**	241	**849**	132
5.7	1.02	244	25	63	227	0.86	3.5	15.1	289	282	**322**	73	**622**	82

DDR, *draw down ratio.*

[a] *Extrusion stress computed using Eq. (15.6) with* n = *0.6 relative to experiment 1.2 (122 m/min line speed 0.64 mm die gap).*

From Morris BA. The influence of stress on peel strength of acid copolymers to foil. In: TAPPI polymers, laminations and coatings conference; 1998. Also Morris BA. J Reinf Plast Comp 2002;21:1243–55. Reproduced with permission from E. I. du Pont de Nemours and Company.

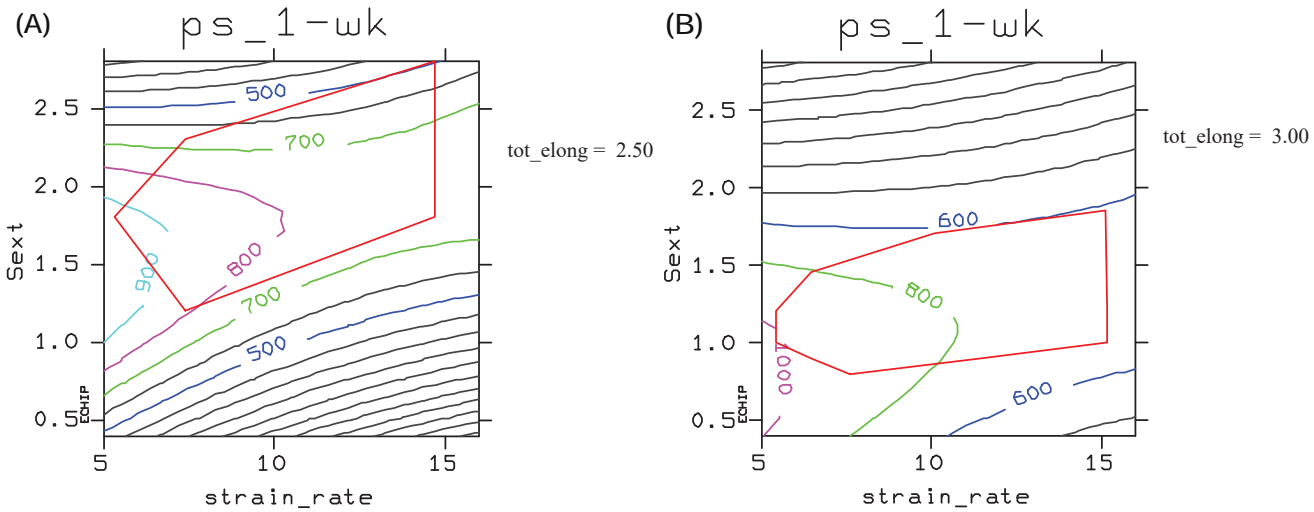


Figure 15.16 Contour plots of peel strength (PS). Vertical and horizontal axes are relative extrusion stress (Sext or σ_{ext}) and strain rate ($\dot{\varepsilon}$), respectively. Lines represent regions of constant peel strength (measured 1 week after coating). Plot (A) total strain of 2.5 and (B) total strain of 3.

From Morris BA. The influence of stress on peel strength of acid copolymers to foil. In: TAPPI polymers, laminations and coatings conference; 1998. Also Morris BA. J Reinf Plast Comp 2002;21:1243–55. Reproduced with permission from E. I. du Pont de Nemours and Company.

Table 15.8 Contact Angle Results

Sample	TIAG (ms)	T_o (°C)	PS—1-week (g/25 mm)	H_2O Contact Angle (degrees)
2.1	63	286	540	103.4
2.4	169	286	1180	112.4
5.1	63	286	820	108.5
5.4	175	289	1020	109.4
5.7	63	289	620	109.4

PS, *peel strength.*

From Morris BA. The influence of stress on peel strength of acid copolymers to foil. In: TAPPI polymers, laminations and coatings conference; 1998. Also Morris BA. J Reinf Plast Comp 2002;21:1243–55. Reproduced with permission from E. I. du Pont de Nemours and Company.

states to test whether oxidation may play a role in the peel strength results. As shown in Table 15.8, the polar contact angle does not correlate well with either TIAG (which represents the time for oxidation) or peel strength. The poor correlation is not what would be expected if oxidation were a key mechanism.

During experiment 5, Mylar OPET slip sheets were inserted between the foil and the coating so that samples of the coating could be isolated for testing. Table 15.9 shows the tensile properties of these samples. The DDR is 33.7 (die gap = 1 mm) and melt temperature around 282°C.

WAXS is used to assess relative molecular orientation differences between two of the samples, states 5.3 and 5.7. As shown in Table 15.9, these samples differ widely in $\dot{\varepsilon}$ and σ_{ext} as well as in tensile properties. Also, they give the largest difference in peel strength within the 5-series. The WAXS results, however, show no differences in orientation. The orientation in the plane of the film is random. There is slight orientation of the molecules in the thickness of the film (parallel to the MD) in both samples. The total amount of crystallinity of the samples also appears to be similar.

Table 15.9 Tensile Properties of 25-μm EAA Coating (Separated From Foil by Slip Sheets), DDR = 33.7, $T_0 = 281–287°C$

No.	ε' (1/s)	Relative (σ_{ext})	1 week PS (g/25 mm)	Yield Strength (MPa)	Tensile Strength at Break (MPa)	Elongation at Break (%)	Secant Modulus (MPa)
5.1	15.1	0.57	820	9.8	18.0	359	140
5.2	7.5	0.57	750	9.5	22.4	436	129
5.3	6.0	0.57	960	9.4	23.4	460	126
5.5	7.5	0.38	910	9.2	20.5	433	141
5.6	8.4	0.73	850	9.2	22.9	446	128
5.7	15.1	0.86	620	8.3	20.0	392	130

DDR, *draw down ratio;* EAA, *ethylene acrylic acid;* PS, *peel strength.*
From Morris BA. The influence of stress on peel strength of acid copolymers to foil. In: TAPPI polymers, laminations and coatings conference; 1998. Also Morris BA. J Reinf Plast Comp 2002;21:1243–55. Reproduced with permission from E. I. du Pont de Nemours and Company.

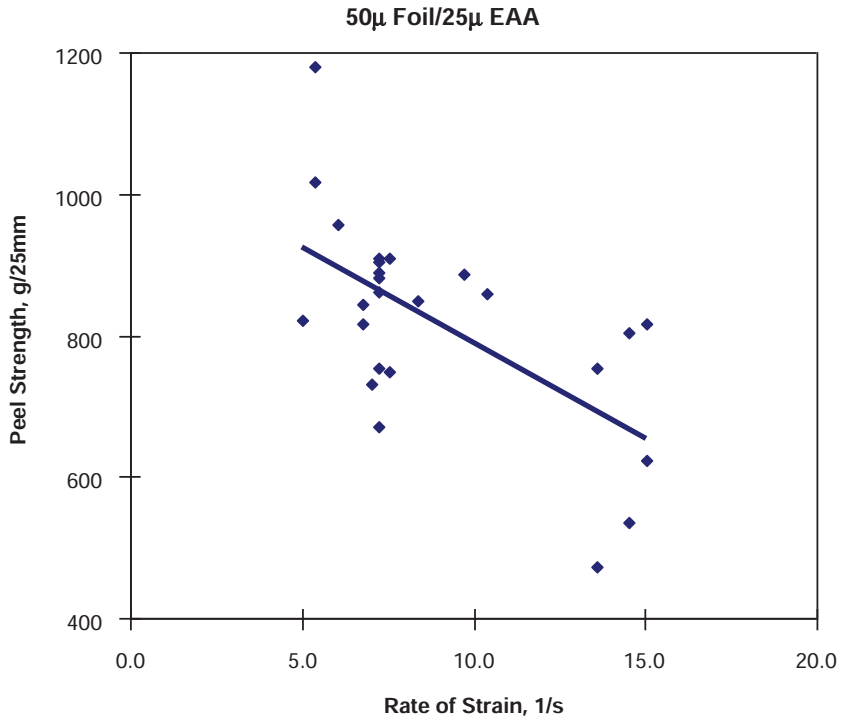


Figure 15.17 Effect of rate of elongation on peel strength to foil. *EAA*, ethylene acrylic acid.
From Morris BA. The influence of stress on peel strength of acid copolymers to foil. In: TAPPI polymers, laminations and coatings conference; 1998. Also Morris BA. J Reinf Plast Comp 2002;21:1243–55. Reproduced with permission from E. I. du Pont de Nemours and Company.

The peel strength results are consistent with the stress hypothesis. This can be seen when the results are cast in terms of the variables that influence stress ($\dot{\varepsilon}$, ε_{tot}, and σ_{ext}). Fig. 15.17 shows all of the peel strength data plotted versus rate of strain, $\dot{\varepsilon}$. As $\dot{\varepsilon}$ increases, the peel strength decreases. Since $\dot{\varepsilon}$ is directly related to the stress imposed during drawing, these results show that increasing stress results in lower peel strength. There is a considerable scatter in the data, however, suggesting other parameters are also involved. Much of this scatter is likely related to the effects of varying total strain and σ_{ext}.

Extensional flow that occurs in the drawing process is known as a strong flow compared to shear flow in the die [34]. The effect of extensional flow, characterized by total strain and rate of strain, should dominate σ_{ext} when the total strain is high. At low total extensional strain, the stress during drawing diminishes and σ_{ext} becomes important. The statistical model results support this. Thus, it is likely that stress imposed in the die and the air gap each play a role in peel strength performance.

A model by Kinloch [30] is used to analyze the effect of the differences found in the tensile property results shown in Table 15.9. The resultant changes in work required to bend and elongate the peel arm are not enough to explain the peel strength results. The WAXS data also show no differences in orientation of the coatings. This suggests that bulk changes in tensile properties may not explain these peel strength results. Local changes in viscoelastic properties or changes in residual stress, however, may play a key role.

Relating this back to the discussion at the beginning of this section on the increase of peel strength with increasing TIAG (Fig. 15.3), increasing TIAG reduces stress by decreasing the rate of strain $(\dot{\varepsilon})$, which is found to be significant in the experimental work of Morris. Other factors that influence stress are also important for peel strength performance.

15.1.2.3 Cooling

The melt curtain is cooled by convection and radiation heat transfer as it transverses the air gap. The amount of cooling increases with increasing TIAG. Cooling decreases the amount of oxidation, increases the viscosity, and slows chemical reaction at the melt–substrate interface. These all act to reduce adhesion, by decreasing wettability or chemical interaction. Too much cooling, therefore, may be detrimental to the formation of good bond strength.

The amount of cooling of the melt curtain is often insignificant, unless the coating thickness is very thin. This can be shown by modeling and experimental measurements. A heat balance on a differential element in the melt curtain, illustrated in Fig. 15.18, yields the following equation:

$$MC_p dT = -2hw(T - T_{air})dz \tag{15.12}$$

where M = mass flow rate, C_p = heat capacity, T = temperature of the web, h = heat transfer coefficient, w = width of the molten curtain, T_{air} = temperature of ambient air, z = distance from die exit.

Solving for T as a function of z by integrating the resulting differential equation yields

$$\frac{T - T_{air}}{T_0 - T_{air}} = \exp\left(-\frac{2hz}{\rho_f X_f C_p v_f}\right) \tag{15.13}$$

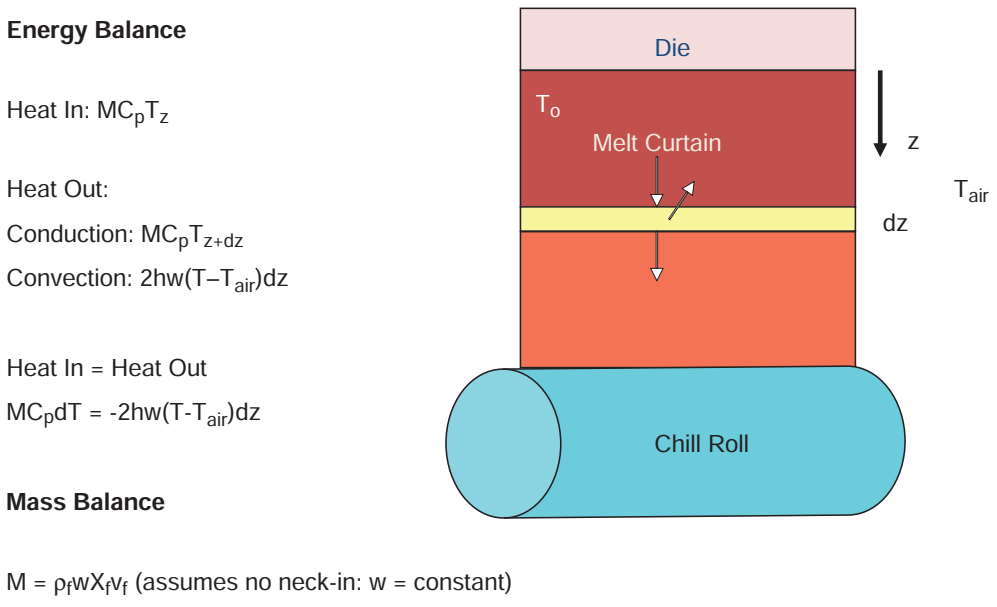


Figure 15.18 Heat balance on a differential element of the melt curtain in extrusion coating.

where v_f = line speed, X_f = coating thickness, ρ_f = density of coating (solid polymer), T_0 = temperature of polymer at the die exit.

Eq. (15.13) simplifies to the following equation when considering just the temperature at the nip, $T(z = L)$:

$$\frac{T - T_{air}}{T_0 - T_{air}} = \exp\left(-B\frac{\text{TIAG}}{X_f}\right) \quad \text{at } z = L, \quad (15.14)$$

where $B = \frac{2h}{\rho_f C_p}$.

Eq. (15.14) shows that the temperature at the nip decreases with increasing TIAG and decreasing coating thickness. This is illustrated in Fig. 15.19 assuming $B = 0.0073$ μm/ms, a typical value for LDPE.

The value of the heat transfer coefficient, h, is needed to use Eqs. (15.13) or (15.14). The heat transfer coefficient should have contributions from both convective and radiant heat transfer. Early investigators used correlations for h found in the general heat transfer literature that suggest the convective contribution ranges from about 5 to 30 W/m^2-K (1–5 Btu/h-ft^2-°F), and the radiant contribution is about 13 W/m^2-K (2.4 Btu/h-ft^2-°F) [35]. In the late 1960s, Van Ness [36] used the newly introduced IR thermometer to measure the molten web temperature in the air gap for the first time. As shown in Fig. 15.20, he found that the models considerably overestimated the temperature decrease in the air gap and hence the value of h.

Morris [8] finds that if h is set at 5.7 W/m^2-K (1 Btu/h-ft^2-°F), the model agrees well with measured values of the temperature near the chill roll at several line speeds and coat weights, as well as with Van Ness's original measurements. This is shown in Fig. 15.21. In a follow-up study using an IR camera, Foederer and Morris [37] measure the temperature profile in the air gap on two different extrusion coating pilot lines over a wide range of processing conditions (150–450 m/min, 6.35–25.4 μm coating thickness, 179–279 mm air gap, 8–33 draw ratio). The structure is paper/LDPE. A typical temperature scan is illustrated in Fig. 15.22. Their experimental results agree with the model using a value of $h = 9.9$ W/m^2-K (1.6 Btu/h-ft^2-°F) as shown in Fig. 15.23. This agrees well with the results of Morris [8].

The low value of h is puzzling. Devisme et al. [38] developed a model of the extrusion coating process that includes cooling in the air gap. They include both convective and radiant contributions, resulting in a value of $h = 31$ W/m^2-K. Their model agrees well with their experimental data for coating of

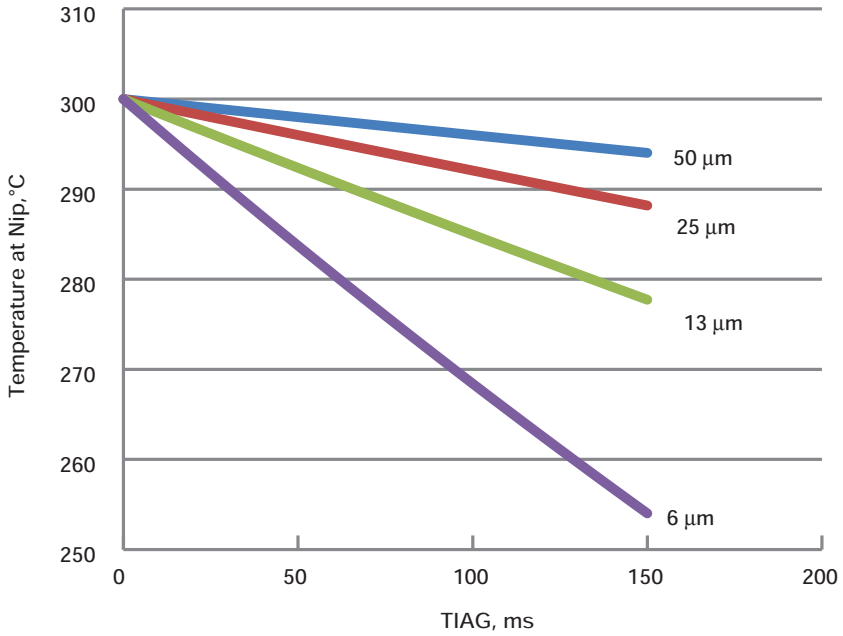


Figure 15.19 Temperature change in the air gap as a function of TIAG (time in the air gap) and coating thickness [from Eq. (15.14)]. Assumed the temperature at the die exit is 300°C and the surrounding air temperature is 25°C. *From Morris BA. Adhesion in extrusion coating: time in the air gap revisited. In: TAPPI PLACE conference; 2016. Reproduced with permission from E. I. du Pont de Nemours and Company.*

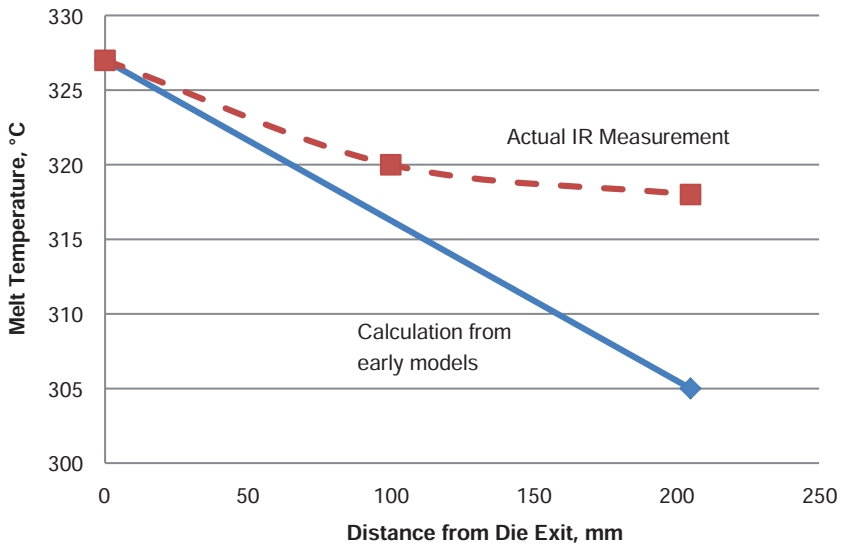


Figure 15.20 Comparison of temperature in the air gap from early models (*solid line*) with IR (infrared) thermometer readings (*dashed line*).
From Van Ness RT. Infrared thermometry – a useful tool for the coating industry. TAPPI 1968;51(12):39A–46A. Reproduced with permission from E. I. du Pont de Nemours and Company.

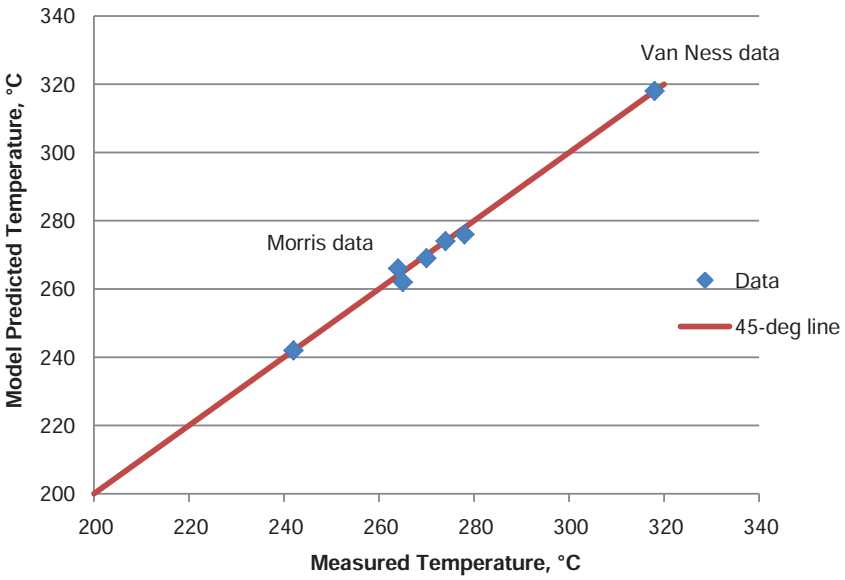


Figure 15.21 Comparison of experimental data from Morris [8] and Van Ness [36] with model results, assuming a convective heat transfer coefficient of 5.7 W/m^2-K (1 Btu/h-ft^2-°F).
Reproduced with permission from E. I. du Pont de Nemours and Company.

polypropylene (PP) onto aluminum foil: (PP–tie)/Al. Their coating thickness was 80 μm, considerably thicker than most commercial coating operations and what was used in the work of Van Ness, Morris, and Foederer. They also used a much slower line speed: 0.08–0.416 m/min. The DDR is only 4. Other parameters of the experiment are 60 mm air gap, 250 mm width, and 0.3 mm die gap. So under slow operating conditions, the heat transfer coefficient is in better alignment with conventional heat transfer theory. Perhaps at the higher speeds typical of commercial operations, other factors come into play not accounted for by the model. Nevertheless, the model predicts the correct trends in the data and can be used

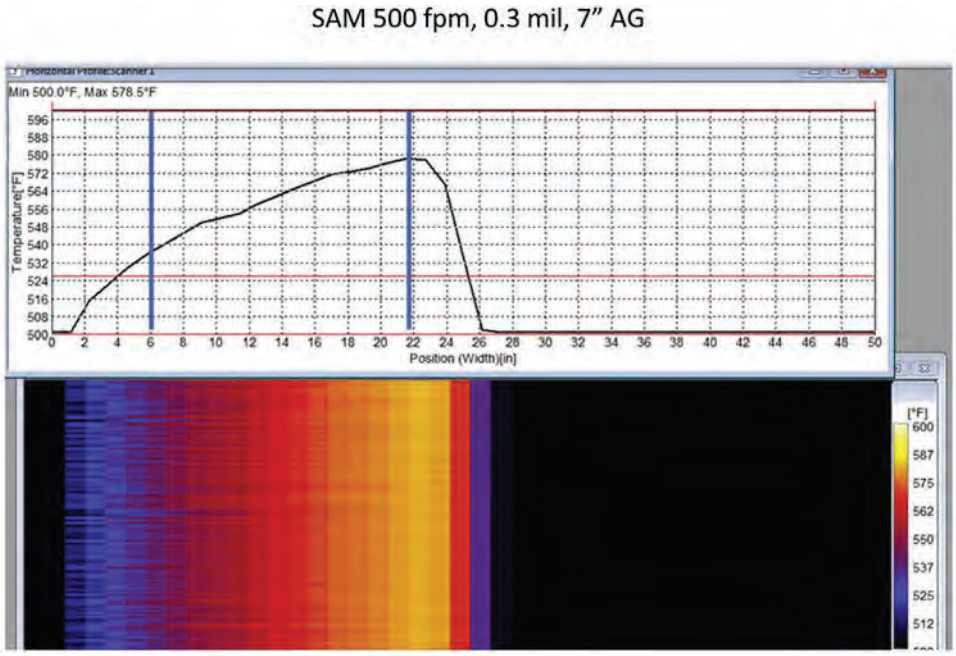


Figure 15.22 Example of a scan of the air gap with an IR thermometer. Conditions were 152.4 m/min line speed, 7.6 μm coating thickness, and 178 mm air gap.
From Foederer BM, Morris BA. Use of IR technology to model temperature loss in the air gap. In: TAPPI PLACE conference; 2014. Reproduced with permission from E. I. du Pont de Nemours and Company.

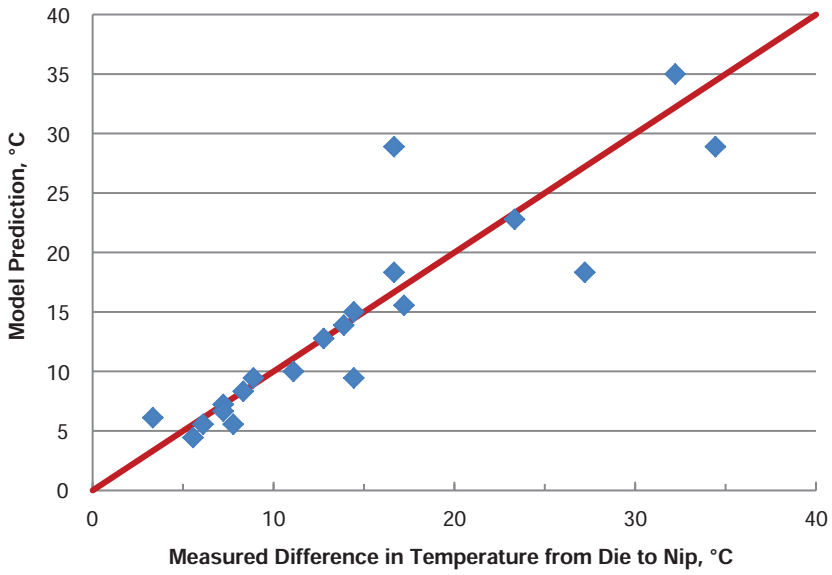


Figure 15.23 Comparison of model ($h = 9.9$ W/m^2-K) and experimental results from Foederer and Morris study. Data are for the difference in temperature at the die exit and at the nip [predicted (y-axis) and measured (x-axis)]. The line represents an exact fit.
From Foederer BM, Morris BA. Use of IR technology to model temperature loss in the air gap. In: TAPPI PLACE conference; 2014. Reproduced with permission from E. I. du Pont de Nemours and Company.

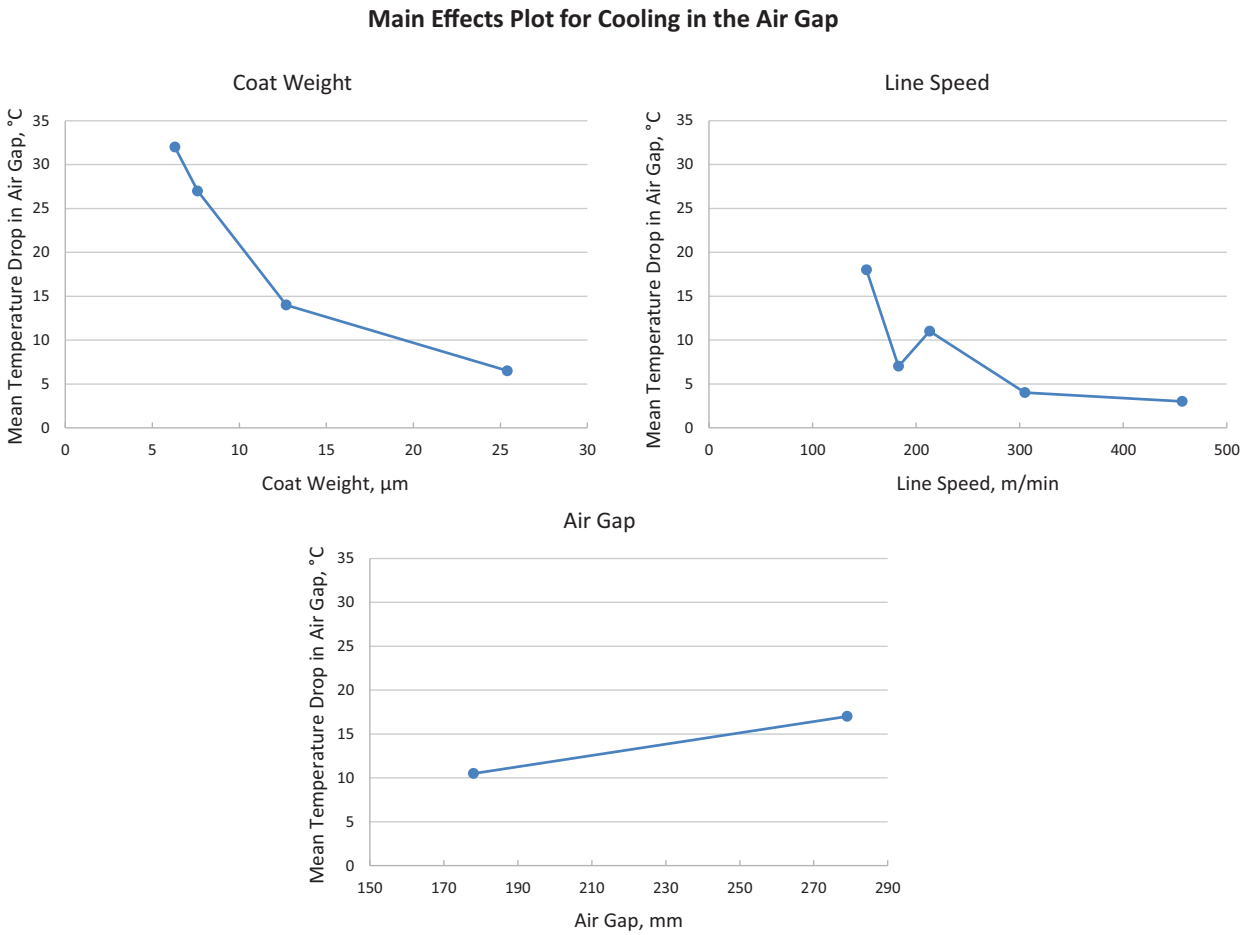


Figure 15.24 Main effects plot for cooling in the air gap (change in temperature between die exit and chill roll). *From Foederer BM, Morris BA. Use of IR technology to model temperature loss in the air gap. In: TAPPI PLACE conference; 2014. Reproduced with permission from E. I. du Pont de Nemours and Company.*

to make quantitative predictions provided the value for h is fit under conditions that are similar to the actual operation.

Foederer and Morris statistically analyze their data using an analysis of variance (ANOVA) method. The main effects plot, given in Fig. 15.24, shows that the cooling in the air gap decreases with increasing coating thickness and line speed and decreasing air gap. (In this graph, as well as in Fig. 15.23, the difference between the temperature at the die exit (T_0) and the temperature at the nip (T_L) is plotted. A greater value of this change in temperature indicates more cooling.) The air gap and line speed effects can be combined into TIAG ($= L/v_f$). This is done in Fig. 15.25, which shows that for a given coating thickness, as the TIAG is increased, the amount of cooling (ΔT) increases. This is in agreement with Eq. (15.14).

Figs. 15.24 and 15.25 show that of the variables tested, the coating thickness has the greatest impact on cooling in the air gap. This is an indication of the importance of the mass flow rate and is illustrated in Fig. 15.26 by plotting the temperature drop in the air gap versus the line speed for a 25 µm coating. Since the die gap and coat weight are kept constant, as the line speed is increased the mass flow rate increases (by increasing the extruder rpm). As the mass flow rate is increased, the amount of cooling decreases. This also agrees with the model.

These results show that at typical coat weights found in extrusion coating and lamination, the temperature does not change substantially in the air gap. This is particularly true for high output lines since the temperature drop in the air gap is related to the mass throughput. At very low coat weights, the

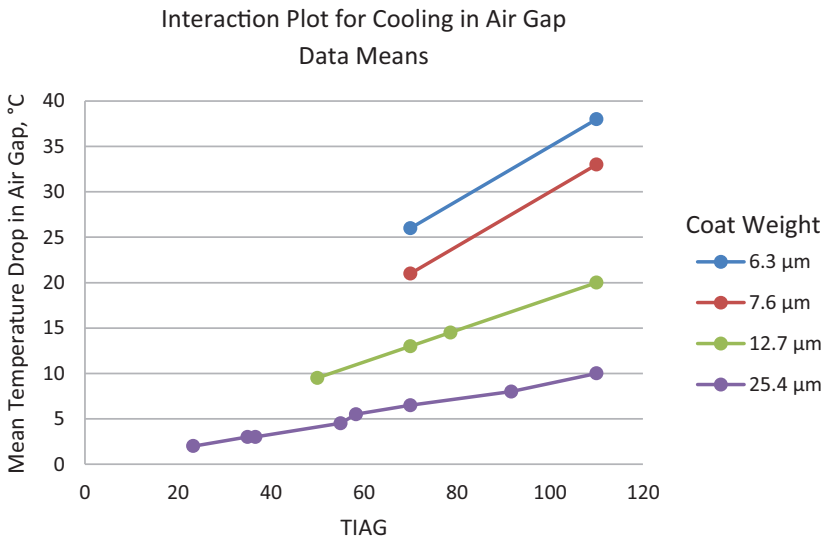


Figure 15.25 Interaction plot of mean temperature difference (between die exit and at nip) in the air gap versus time in the air gap (TIAG). *X*-axis scale is categorical rather than continuous.
From Foederer BM, Morris BA. Use of IR technology to model temperature loss in the air gap. In: TAPPI PLACE conference; 2014. Reproduced with permission from E. I. du Pont de Nemours and Company.

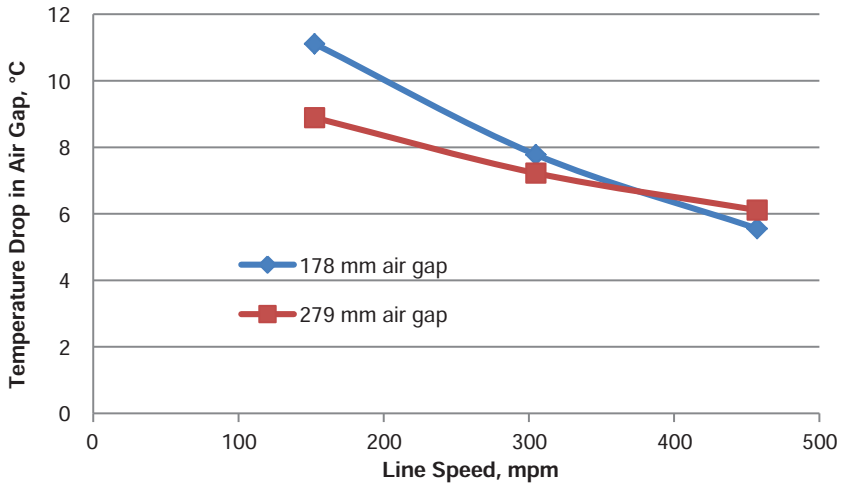


Figure 15.26 Effect of line speed on temperature change in the air gap. Data for 25 µm coating. Since coat weight is constant, line speed is directly proportional to extruder output.
From Foederer BM, Morris BA. Use of IR technology to model temperature loss in the air gap. In: TAPPI PLACE conference; 2014. Reproduced with permission from E. I. du Pont de Nemours and Company.

temperature drop begins to become significant and may be a factor in adhesion. The simple model developed here can be used to predict under what process conditions this may be a concern.

Both the model and the IR measurements give an average temperature across the thickness of the melt curtain at a given distance from the die exit (although IR measurement is more influenced by the temperature near the surface). This provides information regarding the flowability of the polymer as it contacts the substrate in the nip, but the surface temperature is also important if chemical reactions are taking place. An analysis shows that temperature is essentially uniform across the thickness of the curtain. The Biot (*Bi*) number is a dimensionless number that is the ratio of convection of heat from

Table 15.10 Air Gap Ranges to Obtain an Optimum Time in the Air Gap (TIAG) Between 50 and 100 ms

Line Speed		TIAG = 100 ms		TIAG = 50 ms	
m/min	ft/min	mm	in.	mm	in.
100	328	167	6.6	84	3.3
200	656	333	13.1	167	7.5
300	984	500	19.7	250	9.8
400	1312	667	26.2	333	13.1
500	1640	833	32.8	416	16.4

the melt curtain to the conduction of heat within the curtain:

$$Bi = hl/k \tag{15.15}$$

where Bi = Biot number, h = heat transfer coefficient (9.9 W/m^2-K), l = characteristic length scale (the thickness of the melt curtain), k = thermal conductivity (0.26 W/m-K).

When $Bi \ll 1$, the thermal conduction within the film is faster than the thermal convection at the surface and the temperature equilibrates across the thickness. For a web thickness of 0.75 mm (30 mils), $Bi = 0.03$. So even at the die exit, the temperature is constant across the thickness of the web.

An even temperature profile across the width of the melt curtain is important for ensuring uniform adhesion across the breadth of coated substrate. Air flow in the air gap can be complex, resulting in nonuniform convective cooling of the melt curtain. The air near the center of the curtain is entrained with the moving curtain and is forced down toward the chill roll. Once it gets there it has to turn, flowing upward, typically near the edges. Also there may be ventilation ducts near the die that affect the flow patterns. Both neck-in and the practice of thinning out the edges at the die exit to counter neck-in can result in the temperature at the edges of the curtain being different from the centerline temperature. The use of an IR thermometer or camera can be helpful for characterizing the temperature across the width of the melt curtain [37]. Countermeasures such as heating the edges of the die may help achieve more uniform temperature profiles.

Air flow patterns near the nip may push the curtain onto the chill roll prior to the substrate. Adjusting the position where the melt curtain is pinned to the substrate (known as the horizontal lay-on) so that the melt contacts the substrate first is favorable for adhesion. This allows the polymer more time to wet the substrate before being quenched.

15.1.2.4 General Guidelines

The conditions in the air gap have an impact on adhesion performance. In general, adhesion can be enhanced by the following factors:

- Increasing TIAG by increasing the air gap or reducing the line speed. This increases the amount of oxidation (for LDPE) and reduces stress. Antonov suggests running with a TIAG between 50 and 100 ms. Table 15.10 provides values of the air gap at different line speeds that fit within this range. Of the two factors that make up TIAG, the air gap is the better parameter to adjust from an operational point of view. Too long of an air gap, however, can lead to issues with neck-in or cooling in the gap.
- Increasing the melt temperature of the polymer at the die exit. This increases oxidation, reduces stress, improves wetting, and increases the energy available for chemical interaction. Too high temperature, however, can lead to thermodegradation, which may cause gel and black specs (cross-linking), embrittlement (chain scission), and taste and odor issues.
- Ozone treatment of nonpolar polymers such as LDPE.
- Adjusting the horizontal lay-on so that the polymer contacts the substrate prior to the chill roll.
- Reducing the die gap. This reduces the DDR and the stress generated in the air gap. Too narrow of a die gap, however, can lead to excessive stress in the die land.

- Stabilizing the air flow pattern or increasing the temperature of the die near the edges to ensure the melt curtain temperature is uniform across its width.
- Adding functionality to the polymer. For example, Fig. 15.3 shows the use of an acid copolymer improves peel strength compared with LDPE over a range of TIAG. This may allow the process to run at higher line speed or shorter air gap and still achieve adhesion goals. See Section 10.4.1 for details on tie resins in extrusion coating.

15.1.3 Nip

The nip is the region between the chill roll and rubber nip roll where the polymer contacts and wets the substrate and is rapidly solidified. The polymer needs to flow and wet the substrate, and any chemical interaction needed for bonding must take place in a very brief time frame before the polymer freezes off.

Wetting is covered in Chapter 10. In general, the substrate needs to have a higher surface energy than the molten polymer and be free of contamination. Often corona, ozone, plasma, or flame treatment is applied to the substrate prior to the nip to help clean and prepare the surface for wetting. Chemical primers can be applied to the substrate to promote adhesion. These must be properly dried or cured prior to the nip.

The flow in the nip region is very complex. The elongational flow in the air gap as the melt curtain is drawn down in thickness is followed by shear flow from the squeezing action of the nip roll. For porous substrates such as paper, it may be favorable for the polymer to flow into the pores to provide mechanical interlocking. Even for nonporous substrates, surface roughness may require the polymer to flow and wet small-scale crevices. This occurs as the polymer is rapidly changing temperature. The stress on the polymer has little time to relax before the polymer freezes. The stress can induce crystallinity and orientation, further complicating the rheology, and wetting in the nip region.

Devisme [38] develops a model of the temperature in the nip region, incorporating assumptions around barriers to heat transfer between the polymer and chill roll and strain-induced crystallization. Their approach uses several extrapolations and assumptions, especially around strain-induced crystallization kinetics, but provides good agreement with their experimental results. As described earlier, their experiments are run under slower conditions than those typically used in commercial extrusion coating operations. Nevertheless, the model provides insight into the effect high cooling rates and stretching has on crystallization in extrusion coating. It also suggests that the heat transfer coefficient between the polymer and chill roll may need to be adjusted for surface roughness.

Trouilhet and Morris [39] develop a model for calculating the temperature as a function of time in the nip. While it does not incorporate many of the complexities included by Devisme, it provides useful insight into a number of adhesion and processing issues. The model calculates the temperature profile in a multilayer film as a function of time. Because the dimensions along the surface of the film (MD and TD) are large compared to the thickness, a one-dimensional model is sufficient. For simplicity, the one-dimensional unsteady-state heat conduction equation with constant coefficients is used:

$$\frac{\partial T}{\partial t} = \alpha \frac{\partial^2 T}{\partial x^2} \tag{15.16}$$

where T = temperature; t = time, x = distance in the thickness dimension; α = thermal diffusivity = $\rho k/C_p$, ρ = density; k = thermal conductivity; C_p = heat capacity.

The thermal diffusivity is assumed to be constant, although the model allows for variation as a function of temperature. Such data are often hard to find and so the variation is ignored as a first approximation. Curvature is also neglected since the coated layers and substrate(s) are thin compared to the diameter of the rolls.

Initial and boundary conditions are needed to solve Eq. (15.16).

Initial condition

At $t = 0$, the melt curtain is assumed to be at T_0 and the substrate at ambient temperature.

Boundary conditions

1. At the external surfaces, $x = 0$ and X (X is the thickness of total multilayer structure)

   Three types of boundary conditions are allowed for in the model:

   - Type 1: Temperature is specified at the surface

$$\text{At} \quad x = 0 \text{ or } X, \quad T = T_1 \tag{15.17}$$

- Type 2: The surface is insulated from heat loss or gain. In mathematical terms, this means the change in temperature is zero

$$\text{At} \quad x = 0 \text{ or } X, \quad \frac{dT}{dx} = 0 \tag{15.18}$$

- Type 3: The surface of the film is being heated or cooled by heat convection with an outside medium such as air or water. Here it is convenient to introduce a heat transfer coefficient, h. The boundary conditions can be written as follows:

$$\text{At} \quad x = 0, -k\frac{dT}{dx} = h(T - T_{\text{inf}}) \tag{15.19}$$

$$\text{At} \quad x = X, \quad k\frac{dT}{dx} = h(T - T_{\text{inf}}) \tag{15.20}$$

here, T_{inf} is the temperature of the cooling or heating medium far away from the surface.

Note that the type 3 boundary condition is the most general of the three. When $h = 0$, the second boundary condition is obtained. Letting h approach infinity yields the first boundary condition. Typical values for h are given in many engineering texts. Radiant heat transfer may also be modeled by using an effective heat transfer coefficient.

For multiple layers, the heat flux at each interface is equal. For example, for layers 1 and 2:

$$k_1\frac{dT}{dx}\bigg|_1 = k_2\frac{dT}{dx}\bigg|_2 \tag{15.21}$$

A finite difference scheme is used to solve the previously mentioned equations. This method is chosen over analytical solutions (such as those found in Carslaw and Jaeger [40]) because of the geometry imposed by multiple layers. Also, the finite difference method lends itself well to more complex situations, such as geometries beyond films with parallel sides, incorporating the temperature dependence of the thermal parameters and considering the effect of phase changes. There are two general methods for solving finite difference problems, explicit and implicit. The particular scheme used here is an implicit algorithm. Implicit algorithms are generally more difficult to program than explicit algorithms, but they do not have the convergence problems of explicit schemes. For the most part, the methodology given by Carnahan et al. [41] is followed.

As polymers transition from the melt to the solid state, they release energy known as the enthalpy of crystallization. This can affect the change of temperature within the film. Such effects are generally small for polymers because most polymers are not very crystalline, especially when they are rapidly quenched. Thus, this model will capture most of the features of temperature change, even if the materials are undergoing phase transformations. In some cases, however, a more general model incorporating enthalpy effects is used. The methodology of Shamsundar and Rooz [42] is followed by using a nonlinear Gauss−Seidel iteration scheme to solve the enthalpy equations.

Several examples where the model provides useful insight are highlighted in the following sections.

15.1.3.1 Time in Nip and Solidification

One of the early adoptions of extrusion coating was for coating LDPE onto paper. A typical structure is 50-μm paper/25-μm LDPE. Fig. 15.27 shows the results of modeling the temperature development across the thickness of this structure as a function of time. The temperature of the melt curtain is assumed to be initially uniform. At time $t = 0$, the melt first comes in contact with the paper and the chill roll and heat exchange by conduction begins. For boundary conditions, the chill roll side of the LDPE is assumed to be 20°C (type 1 boundary condition). A type 3 boundary could be used here to account for the imperfect contact between the chill roll and polymer, but the type 1 boundary condition is found to be sufficient. For the paper surface against the rubber nip roll, a type 2 boundary condition (insulated) is used. This is illustrated in Fig. 15.28.

An LDPE with a density of 918 kg/m^3 crystallizes (solidifies) at 91°C (and melts at 106°C) under quiescent conditions. While the crystallization kinetics will differ due to the stress imposed by the process and rapid cooling rate, this crystallization temperature can be used for general discussion. Fig. 15.27 shows that the entire LDPE layer reaches 91°C and solidifies in about 3 ms. This time of solidification, t_s, is a useful parameter for characterizing the time available for wetting and adhesion but

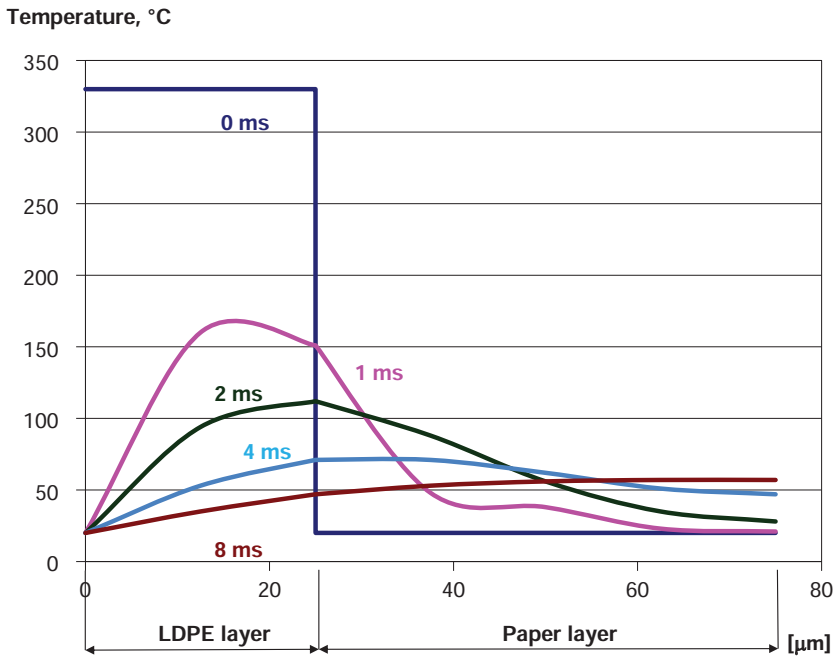


Figure 15.27 Model predictions of temperature profiles in the nip at different snapshots in time. Structure is 25-μm low density polyethylene (LDPE) initially at 330°C coated onto 50-μm paper initially at 20°C.
From Trouilhet Y, Morris BA. Prediction of temperature profiles across coating and substrate in the nip. In: TAPPI polymers, laminations and coatings conference; 1999. Reproduced with permission from E. I. du Pont de Nemours and Company.

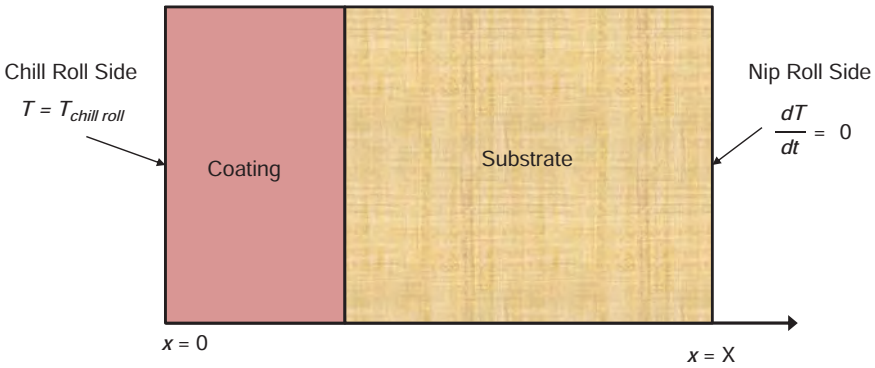


Figure 15.28 Boundary conditions in the nip region of extrusion coating.
From Trouilhet Y, Morris BA. Prediction of temperature profiles across coating and substrate in the nip. In: TAPPI polymers, laminations and coatings conference; 1999. Reproduced with permission from E. I. du Pont de Nemours and Company.

must be put into perspective by comparing it with the residence time in the nip, t_n.

The time in the nip is given by

$$t_n = \frac{d}{v_f} \tag{15.22}$$

where t_n = time in the nip, d = deformation of the rubber nip roll, v_f = line speed.

The deformation is a function of the force applied to the nip roll, the hardness of the rubber, the thickness of the rubber, and the diameter of the rubber roll and chill roll.

For example, if the deformation is 2 cm and the line speed is 240 m/min, then the time in the nip is 5 ms. Under these typical processing conditions, the LDPE layer solidifies completely in the nip since the time to solidify (3 ms) is smaller than the time in the nip (5 ms).

The melt solidifies under high pressure in the nip. The pressure in the nip rises to a maximum in the middle of the nip as shown on Fig. 15.29. The maximum pressure in the nip is given by:

$$P_m = 2\frac{f}{d} \tag{15.23}$$

where P_m = maximum pressure in the nip, f = force applied to the nip roll per width of substrate.

For typical values of $d = 2$ cm and $f = 30{,}000$ N/m, the maximum pressure in the nip reaches 3 MPa.

The line tension also exerts pressure on the coated layer around the chill roll, but this is typically negligible compared with the nip pressure. A force balance in the vertical direction gives:

$$pDW = 2T \tag{15.24}$$

where p (N/m^2) = pressure on the coating, D (m) = diameter of chill roll, W (m) = width of substrate, and T (N) = tension on substrate.

For a typical line with 2000 N of tension, 0.7 m chill roll diameter, and 1.5 m width of substrate, the pressure applied on the coating once it leaves the nip is only 0.004 MPa, which is about 1000 times less than the maximum pressure in the nip.

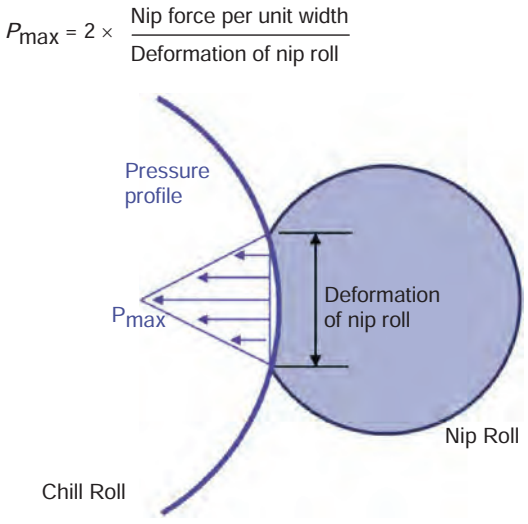


Figure 15.29 Pressure distribution in nip region. *From Trouilhet Y, Morris BA. Prediction of temperature profiles across coating and substrate in the nip. In: TAPPI polymers, laminations and coatings conference; 1999. Reproduced with permission from E. I. du Pont de Nemours and Company.*

Trouilhet and Morris propose the following condition for good adhesion:

$$t_n/2 < t_s < t_n. \tag{15.25}$$

When this condition is met, the melt solidifies under high pressure. When $t_s < t_n/2$, the melt does not experience the full pressure: wetting and flow are not optimal. For solidification times longer than the residence time in the nip, the pressure is released too early; bubble formation, chill roll sticking, and other problems may arise.

Various process parameters affect time in the nip and time of solidification. Fig. 15.30 shows how t_n varies with line speed and deformation of the rubber nip roll [as described by Eq. (15.22)]. Time in the nip varies from 1 to 30 ms for 600 m/min line speed and 1 cm deformation to 60 m/min line speed and 3 cm deformation, respectively.

The time to solidify (t_s) is calculated using the temperature in the nip model. Fig. 15.31 shows the calculated values as a function of LDPE thickness and polymer melt temperature (at first contact with the substrate). Typical melt temperatures range from a maximum of about 240°C for ethylene vinyl acetates (EVAs) to about 330°C for PEs that need to be oxidized. At 25-μm coating thickness, time to solidify varies from 1.5 to 3 ms. The time to solidify at a given initial melt temperature increases approximately with the square of the coating thickness, ranging from 0.75 ms at 12 μm to 12 ms at 50 μm.

Time to solidify is also shorter if the polymer solidifies at a higher temperature (higher freezing point) than LDPE. This is the case for PP, polyamide (PA), and polyethylene terephthalate (PET) and is one of the reasons these polymers are more difficult to extrusion coat than LDPE.

For short times of solidification, using a harder rubber surface on the nip roll may reduce time in the nip and improve adhesion to paper.

15.1.3.2 Other Examples

Trouilhet and Morris provide other examples of how a simple temperature model for the nip region can provide insight into extrusion coating problems. These examples were collected from actual problems in the industry.

- A two-layer coextrusion coating onto a primed OPET substrate was exhibiting poor adhesion.

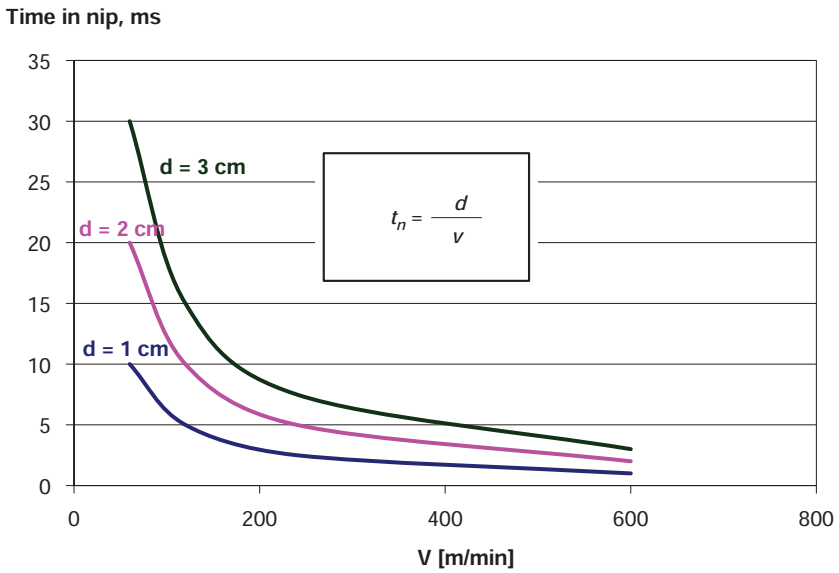


Figure 15.30 Time in the nip (t_n) as a function of line speed and nip roll deformation.
From Trouilhet Y, Morris BA. Prediction of temperature profiles across coating and substrate in the nip. In: TAPPI polymers, laminations and coatings conference; 1999. Reproduced with permission from E. I. du Pont de Nemours and Company.

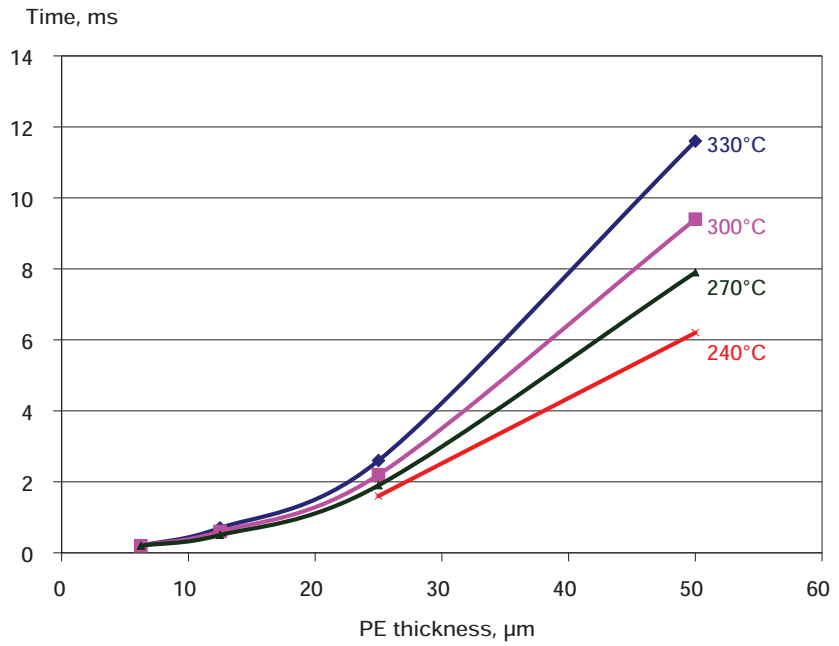


Figure 15.31 Time for solidification (t_s) of an low density polyethylene (LDPE) coating onto 50-μm paper at various melt temperatures. The solidification temperature is assumed to be 91°C.
From Trouilhet Y, Morris BA. Prediction of temperature profiles across coating and substrate in the nip. In: TAPPI polymers, laminations and coatings conference; 1999. Reproduced with permission from E. I. du Pont de Nemours and Company.

The two layers are both LDPE with the layer adjacent to the OPET extruded at 310°C to oxidize and bond to the primed surface of the OPET and the outside layer run at 280°C for improved organoleptics. For a line speed of 120 m/min and a nip deformation of 2 cm, time in the nip is calculated to be 10 ms. The temperature profiles predicted by the model for 1, 2, 5 (middle of nip where the nip pressure is at its maximum), and 10 ms

(end of nip) are given in Fig. 15.32. Part of the heat from the melt is transferred to the chill roll (set at 20°C) but part of the heat transfers to the OPET film shortly after contact.

The temperature of the two surfaces of the OPET film, one in contact with the LDPE and the other in contact with the rubber nip roll, is plotted as a function of time in Fig. 15.33. The temperature of the LDPE/OPET interface is at first higher than that at

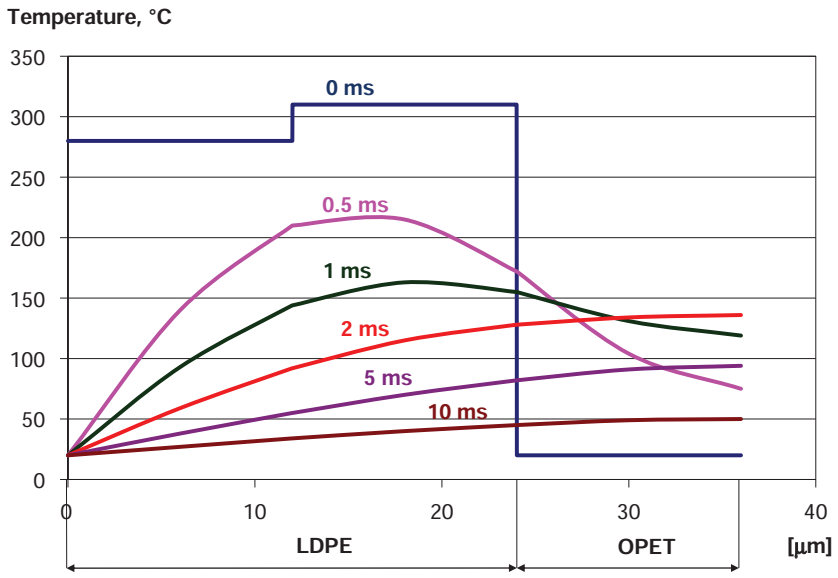


Figure 15.32 Model predictions of temperature profiles in the nip for coextrusion coating of low density polyethylene (LDPE) onto oriented polyester (OPET) substrate.
From Trouilhet Y, Morris BA. Prediction of temperature profiles across coating and substrate in the nip. In: TAPPI polymers, laminations and coatings conference; 1999. Reproduced with permission from E. I. du Pont de Nemours and Company.

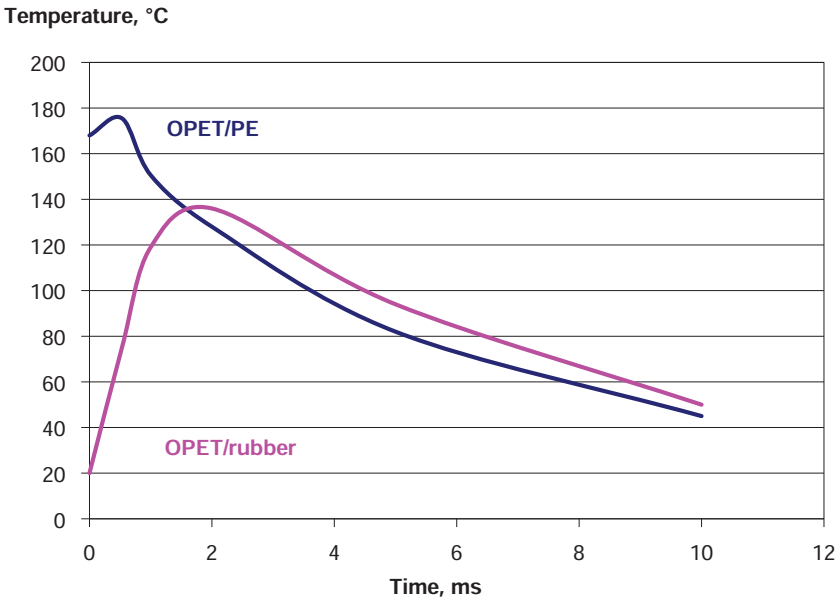


Figure 15.33 Model prediction of temperature of oriented polyester (OPET) film at the polyethylene (PE) and rubber interfaces.
From Trouilhet Y, Morris BA. Prediction of temperature profiles across coating and substrate in the nip. In: TAPPI polymers, laminations and coatings conference; 1999. Reproduced with permission from E. I. du Pont de Nemours and Company.

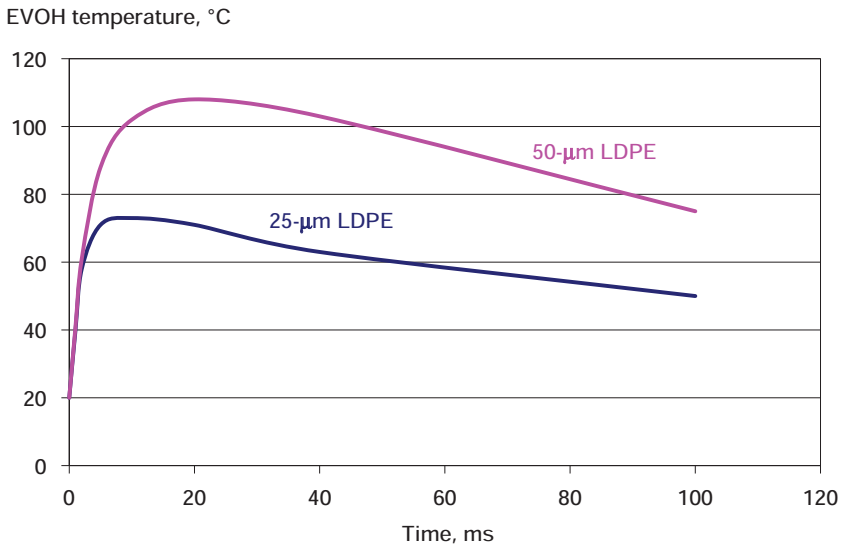


Figure 15.34 Model prediction of the temperature of the ethylene vinyl alcohol (EVOH) layer during lamination. Structure is 110 μm low density polyethylene (LDPE) film/LDPE/(20 μm-LDPE−5 μm-tie−10 μm-EVOH−5 μm-tie—20 μm-LDPE).

From Trouilhet Y, Morris BA. Prediction of temperature profiles across coating and substrate in the nip. In: TAPPI polymers, laminations and coatings conference; 1999. Reproduced with permission from E. I. du Pont de Nemours and Company.

the OPET/rubber interface; heat flows from the hot LDPE to the OPET film, which increases in temperature. The OPET film never melts, even at the PE/OPET interface as it is first contacted with the hot polymer. The OPET film reaches temperatures up to 136°C, however, which causes shrinkage of the film. It is hypothesized based on the model insight that the shrinkage was causing stresses at the interface and poor adhesion. The film was replaced with an OPET with higher dimensional stability at these temperatures and the adhesion improved.

- A barrier multilayer film with the structure (PE−tie−ethylene vinyl alcohol (EVOH)−tie−PE) [20/5/10/5/20 μm] is extrusion laminated with LDPE melt to an LDPE film (110 μm) in contact with the chill roll: the final structure is barrier film/LDPE/PE film. The film exhibits curl when the extrusion layer is thick (50 μm) but not when it was thin (25 μm). Curling in a multilayer structure occurs when at least one layer changes density while the others do not. A layer of a film can increase in density if it postcrystallizes (undergoes crystallization after quenching). Postcrystallization may occur if the polymer experiences temperatures above its glass transition temperature. The glass transition temperature of an EVOH with 32 mol% ethylene content is 69°C. The model prediction for the average temperature the EVOH experiences during the lamination process is plotted in Fig. 15.34 as a function of time for the two thicknesses of LDPE. The thinner extrusion layer keeps the EVOH temperature below T_g, whereas the thick extrusion layer transfers enough heat to the EVOH layer to bring it to temperatures well above T_g for prolonged times.
- Bubbles may form and get trapped in the laminating layer during extrusion lamination. An example is shown in Fig. 15.35. Among other things, bubbles affect the transparency and appearance of the laminate. Bubbles can arise from air or moisture entrapped in the resin that is allowed to expand as the pressure is released at the nip exit. This can occur if the polymer is still molten at the end of the nip ($t_s > t_n$). An example is a meat packaging film with the structure: PA6 film/LDPE/ionomer film. Two versions of different thickness are made by the converter:
  - thin film: 25/25/25 (total 75 μm)
  - thick film: 100/100/100 (total 300 μm)



Figure 15.35 Photomicrograph of bubble in extrusion lamination layer. *PA*, polyamide; *PE*; polyethylene.
From Trouilhet Y, Morris BA. Prediction of temperature profiles across coating and substrate in the nip. In: TAPPI polymers, laminations and coatings conference; 1999. Reproduced with permission from E. I. du Pont de Nemours and Company.

Bubbles form in the thick film during lamination but not in the thinner film. The thick film is produced at 60 m/min line speed and the thin film at 240 m/min. For a 2-cm nip deformation, t_n is 5 and 20 ms for the thin and thick films, respectively.

Temperature profiles in the film leaving the nip are given in Figs. 15.36 and 15.37 for the thinner and thicker films, respectively. Despite the longer residence time in the nip (20 ms instead of 5 ms), the PE temperature of the thicker film at the exit of the nip is higher. This is due to the thicker ionomer film between the melt and the chill roll acting to insulate the cooling effect of the roll, as well as the higher mass of hot LDPE. The model shows that the LDPE is still molten at the end of the nip for the thicker film but not for the thinner one, consistent with the bubble behavior.

15.1.4 Case Study: Effect of Coating Thickness on Peel Strength

As the coating thickness is reduced, the adhesive strength generally decreases. This was known from the early days of extrusion coating: Goslin and Sweeney's [43] and Guillotte and McLaughlin's [35] extensive work on the coating of paper with LDPE in the early 1960s is highlighted in Figs. 15.38 and 15.39. Here the adhesion is reported as % adhesion (adhesive force divided by the burst strength of the coating, as is illustrated in Fig. 15.40) so that the reduced physical strength of thinner coatings is

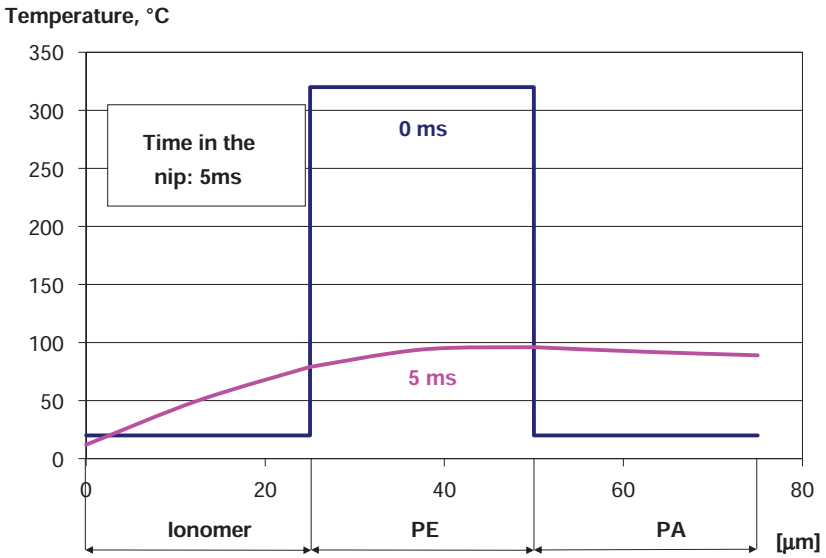


Figure 15.36 Model prediction of the temperature profile at the beginning and end of the nip region for the thin meat film structure: 25 μm-PA/25 μm-LDPE/25 μm-Ion. *LDPE*, low density polyethylene; *PA*, polyamide; *PE*, polyethylene.
From Trouilhet Y, Morris BA. Prediction of temperature profiles across coating and substrate in the nip. In: TAPPI polymers, laminations and coatings conference; 1999. Reproduced with permission from E. I. du Pont de Nemours and Company.

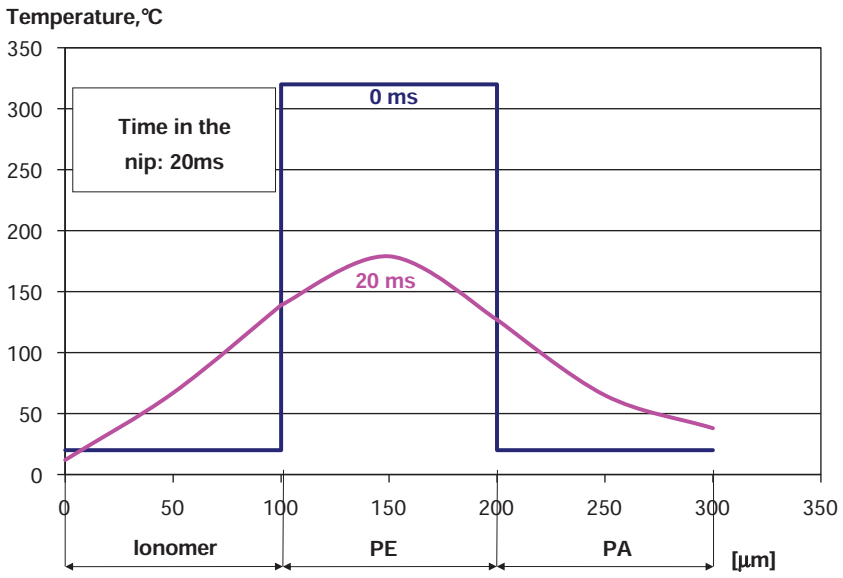


Figure 15.37 Model prediction of the temperature profile at the beginning and end of the nip region for the thin meat film structure: 100 μm-PA/100 μm-LDPE/100 μm-Ion. *LDPE*, low density polyethylene; *PA*, polyamide; *PE*, polyethylene.

From Trouilhet Y, Morris BA. Prediction of temperature profiles across coating and substrate in the nip. In: TAPPI polymers, laminations and coatings conference; 1999. Reproduced with permission from E. I. du Pont de Nemours and Company.

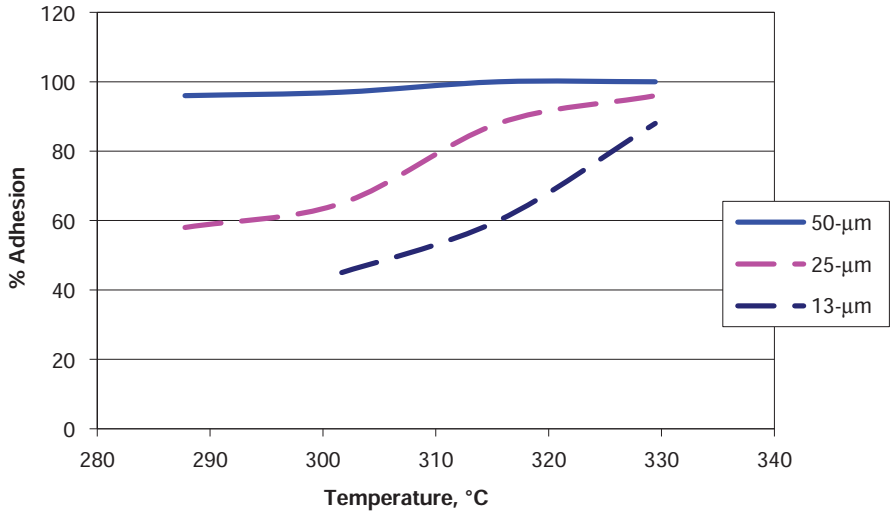


Figure 15.38 Adhesion of low density polyethylene (LDPE) to kraft paper. Conditions: 68 kg/hr, line speeds of 33.5, 65.5, and 134 m/min for 50, 25, and 13 μm coatings, respectively. This corresponds to time in the air gaps (TIAGs) of 125, 64, and 31 ms.

Reproduced with permission from Goslin JP, Sweeney HF. The interaction of processing variables, base materials, and resins in polyethylene extrusion coating. TAPPI 1960;43(5):434–47.

normalized out. For a given coating temperature, lower coating thickness gives lower % adhesion. Similar results were found for coating of nonporous substrates such as aluminum foil. Antonov and Soutar's [4] review in 1991 shows several examples of this, one of which is reproduced in Fig. 15.41.

The mechanism for the reduction in adhesion with decreasing coating thickness may involve a number of factors including the following:

- shorter time for oxidation in the air gap;
- faster cooling in the air gap;

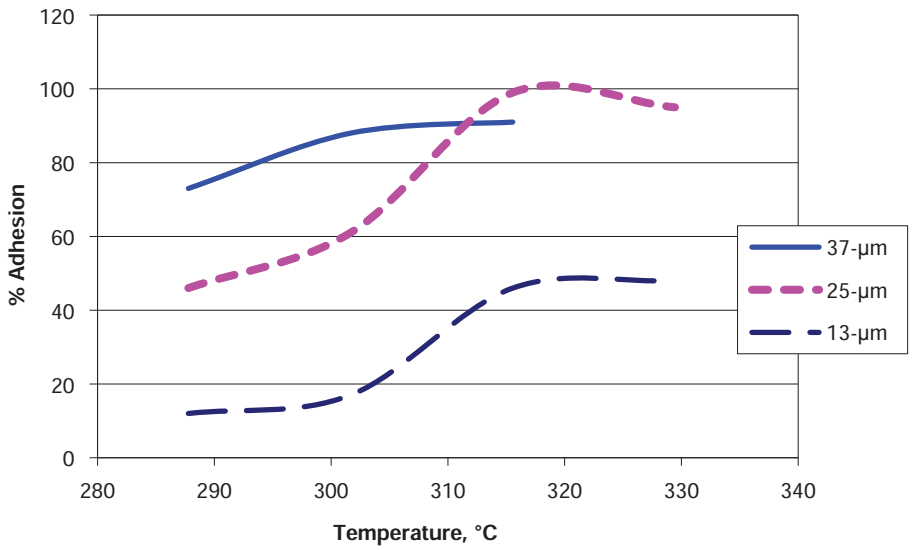


Figure 15.39 Adhesion of low density polyethylene (LDPE) to kraft paper. 114-mm air gap, 91.4 m/min line speed, 75 ms TIAG (time in the air gap).
Data from Guillotte JE, McLaughlin Jr TF. Calculating the adhesion of polyethylene coatings to Kraft paper. TAPPI 1962;45(3):200–208. Reproduced with permission from Morris BA. Understanding why adhesion in extrusion coating decreases with diminishing coating thickness. J Plastic Film Sheeting 2008;24:53–88.

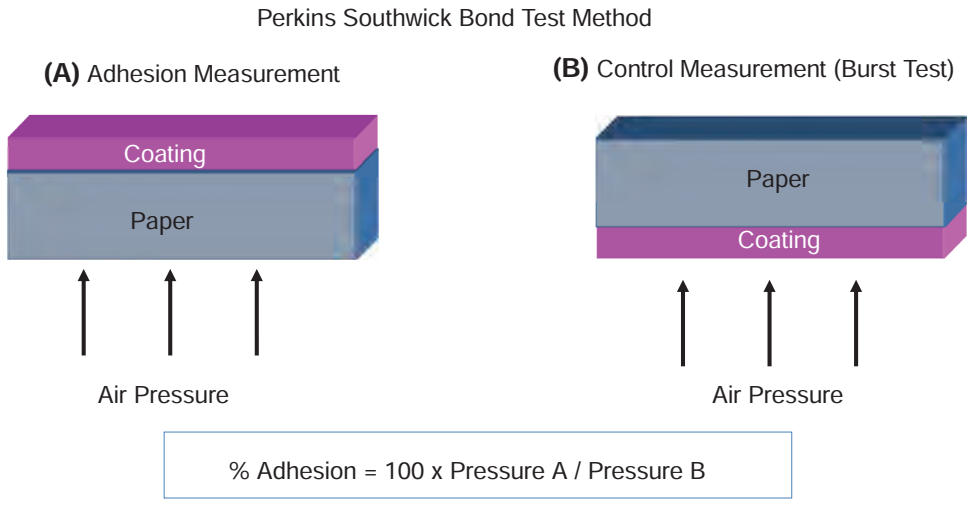


Figure 15.40 Illustration of the Perkins Southwick test method for measuring adhesion of LDPE (low density polyethylene) to paper. Two measurements are made. In (A), air pressure is used to measure the pressure to separate the coating from the paper (coating side away from the air source). In (B), the burst pressure of the coating is measured (coating side facing the air source). The ratio is reported as % adhesion.

- greater stress imposed during drawing in the air gap;
- more rapid cooling in the nip;
- changes in the peel test measurement.

Following the work of Morris [8,44–46], experiments and modeling are used to determine which of these factors are most important. The case study is divided into three parts:

- Section 15.1.4.1 explores the reduction in adhesion of LDPE to paper and other porous substrates. Several hypotheses are tested, including a reduction in oxidation time, faster cooling in the air gap, and more rapid

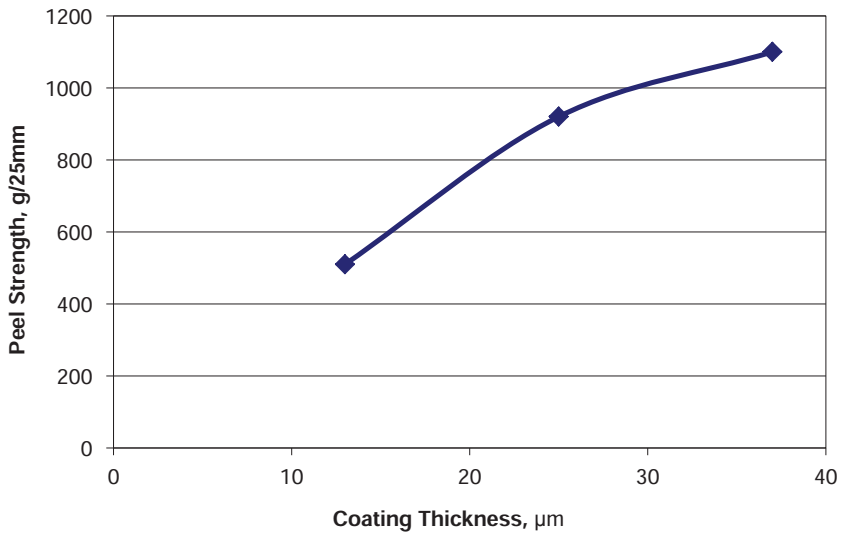


Figure 15.41 Peel strength of an acid copolymer to aluminum foil. Melt temperature = 303°C. TIAG (time in the air gap) = 80 ms.
Data from Antonov V, Soutar A. Foil adhesion with copolymers: time in the air gap. In: TAPPI 1991 polymers, laminations & coatings conference proceedings. Atlanta: TAPPI Press; 1991. p. 553. Reproduced with permission from Morris BA. Understanding why adhesion in extrusion coating decreases with diminishing coating thickness. J Plastic Film Sheeting 2008;24:53–88.

quenching in the nip. A model of the molten polymer penetration into the substrate shows that the greatest effect is cooling in the nip; thinner coatings have less time to flow into the substrate interstices once the chill roll contact is made. The model results agree well with experimental adhesion data from the literature.

- Section 15.1.4.2 examines the peel strength to aluminum foil and other nonporous substrates. Several hypotheses are proposed for why peel strength decreases in these structures, including a reduction in the air gap time, faster air gap cooling, more rapid nip quenching, and stress imposed during drawing. Modeling and experimental results show that cooling in the nip and stress have the greatest impact.
- Section 15.1.4.3 analyzes the peel test to understand why the peel strength of better adhering adhesives is more sensitive to changes in coating thickness. The analysis shows that changes in the critical dimension of the deformation region at the peel front may be responsible.

The case study illustrates how an understanding of process–property fundamentals leads to specific recommendations for improvement.

15.1.4.1 Porous Substrates

For porous substrates, such as paper, paperboard, and nonwovens, it is generally thought that adhesion is created by molten polymer penetration into the pores and around the fibers. This sets up conditions for good physical or mechanical bonds, although chemical bonds may also play a role. Early investigators proposed that web cooling in the air gap might be responsible for reduced adhesion with thinner coatings [35,43]. Thicker coatings retain more of their heat in the air gap so that they are more fluid when they contact the substrate. Cooling in the nip region may also affect penetration time and velocity.

Three potential factors are explored here:

- TIAG
- cooling in the air gap
- cooling in the nip.

For each factor, a hypothesis is proposed and tested with experimental data, modeling results, and logic.

15.1.4.1.1 Time in the Air Gap

Hypothesis: A significant portion of the decrease in adhesion performance is due to a reduction in TIAG.

Antonov and Soutar [4] show that adhesion decreases with decreasing TIAG for a variety of resins and substrates, including paperboard. For LDPE coatings, this is believed to be due to less time for oxidation as is described in Section 15.1.2.1.

TIAG, as defined by Eq. (15.1), is simply the air gap (L) divided by the line speed (v_f): $\text{TIAG} = L/v_f$. Often a processor may reduce the coating weight by increasing the line speed, keeping everything else constant. TIAG in this case will decrease with decreasing thickness. This is how Goslin and Sweeney conduct their experiment. As they reduce the thickness from 50 to 13 μm, the TIAG is reduced from 125 to 31 ms. This is in the range where Antonov and Soutar find that adhesion typically decreases with decreasing TIAG.

Increasing the line speed, however, is not the only way to reduce coating thickness. Other investigators, such as Guillotte and McLaughlin, have independently varied thickness, TIAG, and temperature. The curves plotted in Fig. 15.38 represent results at constant TIAG. These show that without changing TIAG, the adhesion still decreases with decreasing thickness. This is further reinforced by conducting an ANOVA of the Guillotte and McLaughlin data. The main effects are plotted in Fig. 15.42. On average, thickness has a much greater effect on % adhesion than either TIAG or coating temperature. Based on this analysis, the hypothesis is rejected:

- TIAG may have some effect on the reduction in adhesion with decreasing thickness but is not sufficient to explain it.
- The fact that adhesion increases with increasing TIAG (despite an increase in cooling, as shown in the next section) suggests chemical bonding due to oxidation may be contributing to the overall adhesion.

Eq. (15.4) is a more rigorous equation for the air gap time that better reflects the physics of the flow in the air gap. TIAG does not account for changes in the melt curtain draw down as thickness is altered. When the air gap and throughput are held constant, the decrease in process time given by Eq (15.4) with decreasing coating thickness is less than predicted by L/v_f. When the air gap or throughput is adjusted to keep TIAG constant (as in the Guillotte and McLaughlin data), the actual air gap time increases with

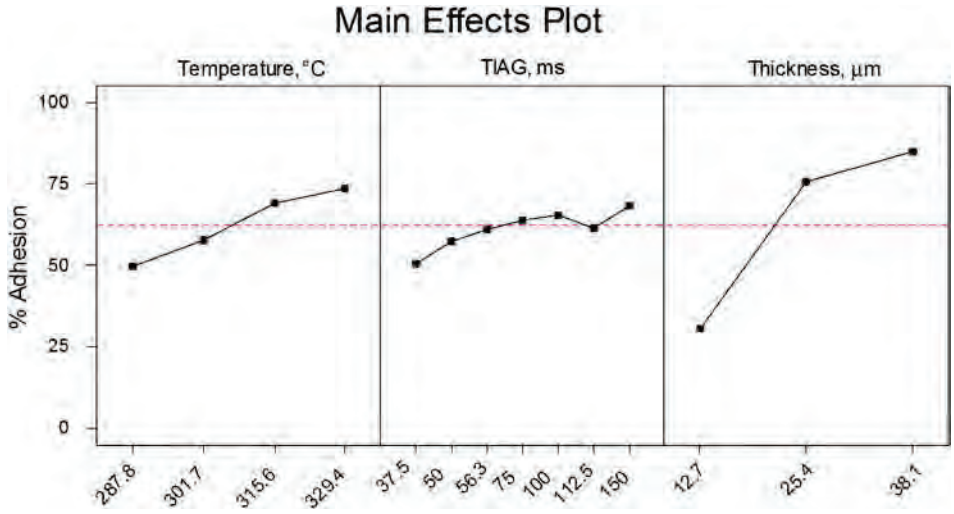


Figure 15.42 Main Effects Plot from ANOVA (analysis of variance) of Guillotte and McLaughlin [35]. *TIAG*, time in the air gap.

Data reproduced with permission from Morris BA. Understanding why adhesion in extrusion coating decreases with diminishing coating thickness. J Plastic Film Sheeting 2008;24:53–88.

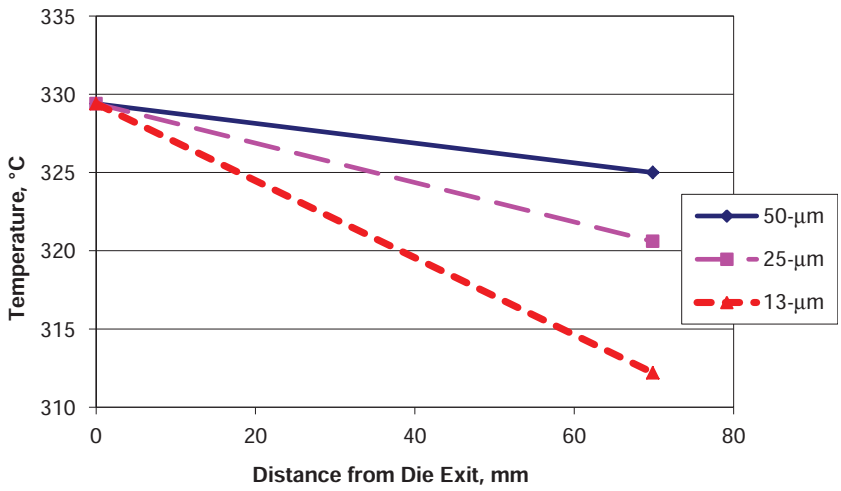


Figure 15.43 Calculation of temperature in the air gap using Eq. (15.13) based on processing parameters from Goslin and Sweeney [43].
Reproduced with permission from Morris BA. Understanding why adhesion in extrusion coating decreases with diminishing coating thickness. J Plastic Film Sheeting 2008;24:53–88.

decreasing coating weight. In either case, this does not alter the conclusions.

15.1.4.1.2 Cooling in the Air Gap

Hypothesis: Thinner coatings cool down more in the air gap, resulting in higher viscosity, less penetration of the coating into the porous substrate and therefore less adhesion.

The model developed in Section 15.1.2.3 is used to predict the temperature decrease in the air gap under the conditions used by Goslin and Sweeney (Fig. 15.38). As shown in Fig. 15.43, decreasing the thickness from 50 to 13 µm reduces the temperature in contact with the paper from 325 to 312°C.

The relative penetration velocity of the polymer melt into the paper at first contact is computed by assuming that the flow is fully developed and an average pore can be represented as a cylinder. For pressure-driven flow of a power law fluid down a cylindrical channel (Table 5.4) [47]:

$$v_{avg} = \frac{n}{3n+1}\left[\frac{R^{n+1}}{2m}\left(\frac{\Delta P}{l}\right)\right]^{1/n} \tag{15.26}$$

where v_{avg} = average velocity in the pore, n = power law exponent (Eq. (15.27)), m = power law constant (Eq. (15.27)), R = radius of cylinder representing the average pore, $\frac{\Delta P}{l}$ = pressure gradient, l = pore length.

Here a power law model is used to represent the viscosity:

$$\eta = m\dot{\gamma}^{n-1} \tag{15.27}$$

where η = shear viscosity, $\dot{\gamma}$ = shear viscosity.

An Arrhenius relationship is used to relate m to changes in temperature:

$$m = A\exp[-a(T - T_r)] \tag{15.28}$$

where A = constant, a = temperature exponent (related to the activation energy), T = temperature, T_r = Reference temperature.

Combining Eqs. (15.26)–(15.28), using typical values for LDPE ($a = 0.02$, $n = 0.4$) and assuming constant geometry (R) and pressure gradient in the nip $\left(\frac{\Delta P}{l}\right)$, the penetration velocity of the molten polymer at first contact with the substrate in the nip is:

$$V_p = \widehat{B}\exp\left[\left(\frac{a}{n}\right)T_s\right] = \widehat{B}\exp(0.05T_s) \tag{15.29}$$

where V_p = penetration velocity, $\widehat{B}$ = constant, T_s = temperature of the melt curtain at first contact with the substrate.

Fig. 15.44 shows the relative penetration velocity at first contact as a function of coating thickness and temperature (at the die exit). The results have been normalized to the penetration velocity of the 50 µm

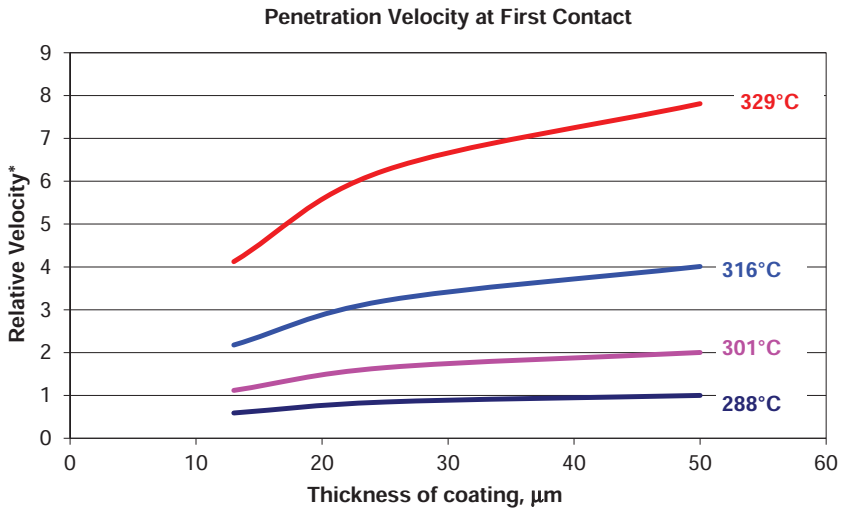


Figure 15.44 Initial penetration velocity from Eq. (15.29) based on cooling in the air gap. Conditions simulate data from Goslin and Sweeney [43].
Reproduced with permission from Morris BA. Understanding why adhesion in extrusion coating decreases with diminishing coating thickness. J Plastic Film Sheeting 2008;24:53–88.

coating at 288°C, which gives enough penetration for 100% adhesion (Fig. 15.38). If penetration is controlling adhesion, as the hypothesis implies, and if initial penetration velocity is the factor controlling penetration, then as soon as the relative penetration velocity exceeds 1, the adhesion should be 100%. The plot for 13 µm coating thickness shows that the penetration velocity should be sufficient for 100% adhesion at temperatures above 301°C.

Comparing this with Fig. 15.38, however, shows that even at 329°C (where the penetration velocity is four times that assumed necessary for 100% adhesion), the measured adhesion is still less than 100%. Thus, the hypothesis is rejected. While cooling in the air gap changes the penetration in the right direction, there is not a sufficient decrease in temperature and increase in viscosity to explain the adhesion results, at least by itself.[1]

[1]A sensitivity analysis on Eq. (15.29) shows that increasing n or decreasing $\widehat{B}$ reduces the change in velocity with temperature. While the slope of the curves may change, the conclusions are unaltered. The model results still show that there is enough penetration velocity of the 13 µm coating at around 300°C to achieve 100% adhesion, which is inconsistent with the adhesion measurements by Goslin and Sweeney.

15.1.4.1.3 Cooling in the Nip

Hypothesis: Faster cooling in the nip for thin coatings provides less time for penetration and for adhesion to develop.

Section 15.1.3 describes how cooling in the nip is rapid and the time available for penetration before the polymer solidifies is short. The solidification time (t_s) decreases with approximately the square of the coating thickness.

Total penetration is the product of the velocity and time: $P = V_p t$. In the air gap analysis, the time element is ignored. Time is an integral part of the current analysis. The time in the nip for the polymer to cool to its crystallization temperature and start to freeze is defined as t_s (Section 15.1.3). Well before the crystallization temperature, however, the viscosity becomes so high that flow essentially stops. In order to compute the relative penetration as a function of time, the temperature of the polymer as a function of time in the nip is first calculated using the unsteady-state heat conduction model developed in Section 15.1.1.3. This model shows that the temperature at the PE–paper interface decreases approximately exponentially with time in the nip.

The model uses a finite difference algorithm that calculates the temperature at each of many small time increments. The penetration velocity at a given time

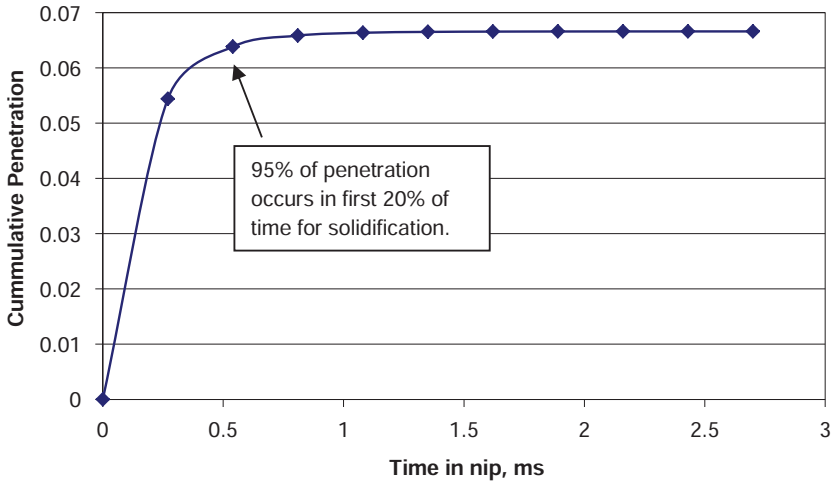


Figure 15.45 Penetration as a function of time in the nip for 25-μm coating onto paper. Initial temperature is 325°C. $t_s = 2.7$ ms.
Reproduced with permission from Morris BA. Understanding why adhesion in extrusion coating decreases with diminishing coating thickness. J Plastic Film Sheeting 2008;24:53–88.

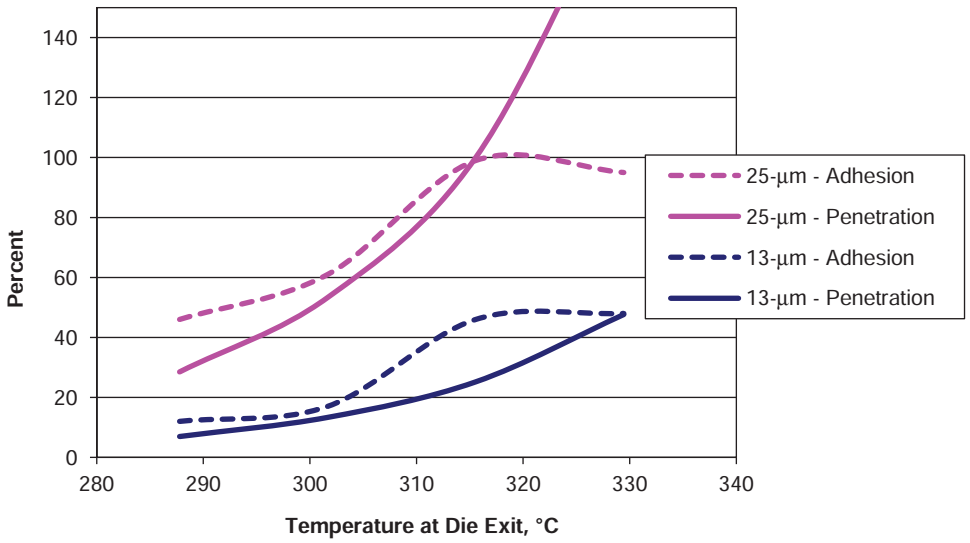


Figure 15.46 Comparison of penetration calculation with adhesion data of Guillotte and McLaughlin [35]. Cooling in the air gap is ignored. 100% penetration is set at 316°C and 25 μm, the onset of 100% adhesion in the Guillotte data.

increment is computed by replacing T_s in Eq. (15.29) with the temperature from the heat conduction model. The total penetration is found by integrating the velocity over time:

$$P = \int_0^{t_s} V_p(t)dt. \qquad (15.30)$$

A typical penetration curve is given in Fig. 15.45. Most of the penetration occurs in the first 20% of t_s.

The relative penetration of coatings under the conditions run by Goslin and Sweeney and Guillotte and McLaughlin is computed. For the first part of the analysis, cooling in the air gap is ignored and the temperature at first contact with the substrate (T_s) is assumed to be equal to the die exit temperature. Later the effects of cooling in the nip and in the air gap are combined.

Fig. 15.46 shows the results of the calculation for the Guillotte data. It is assumed that there is a minimum penetration threshold for 100% adhesion. Below the threshold, the adhesion increases linearly with penetration distance. Above the threshold, no further improvement in adhesion can be obtained

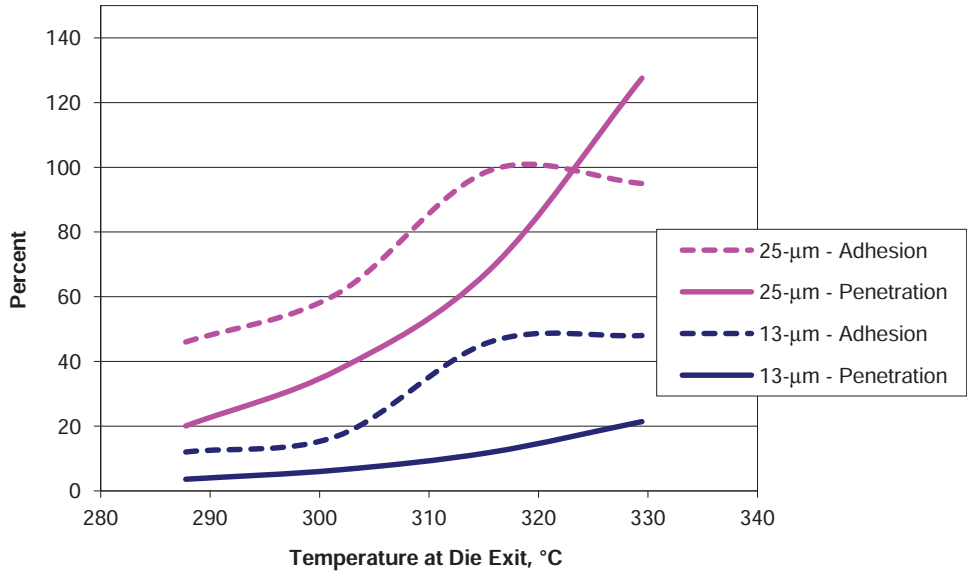


Figure 15.47 Comparison of penetration calculations with adhesion data of Guillotte and McLaughlin [35]. Cooling in the air gap is included. 100% penetration is set at 316°C and 25-μm, the onset of 100% adhesion in the Guillotte data.

Reproduced with permission from Morris BA. Understanding why adhesion in extrusion coating decreases with diminishing coating thickness. J Plastic Film Sheeting 2008;24:53–88.

(adhesion is greater than the coating burst strength, which corresponds to 100% adhesion). For the Guillotte data, this threshold appears to be the penetration achieved for the 25-μm coating at 316°C. This penetration is set to 1 and all the other penetration distances are computed relative to this. Relative penetration values greater than 1 should have 100% adhesion; values less than 1 should have relative adhesion that linearly corresponds to the relative penetration.

The results show the following:

- Increasing the coating temperature by 15°C doubles the penetration distance.
- Penetration increases with roughly the square of the coating thickness (in direct relation to t_s).
- Doubling the thickness is equivalent to increasing the coating temperature by about 30°C.

The penetration calculation tracks well with the adhesion data, but the adhesion is somewhat higher than predicted solely by penetration. One reason for this is that chemical bonding (from oxidation of the melt curtain) improves the adhesion and is not accounted for by the penetration model. Several simplifying assumptions used to develop the model may also be invalid and play a role. These include the following:

- Adhesion is a linear function of penetration.
- The flow is fully developed (even though the flow is transient and takes place in a few milliseconds before the polymer freezes).
- Entrance effects are negligible and can be ignored.
- The pressure gradient, $\frac{\Delta P}{l}$, is constant.

Finally, the effect of cooling in the air gap is combined with cooling in the nip. The output from the air gap cooling model is used as a starting point for the penetration calculation. The results are shown in Fig. 15.47. The trends are the same as for the cooling in the nip penetration model with the actual values of the penetration distance somewhat smaller since the starting temperatures are lower.[2] Similar results are obtained for the Goslin and Sweeney data.

[2]An order of magnitude calculation of the actual penetration at which 100% adhesion occurs gives values of around 5 μm [assumes $R = 5$ μm, $\Delta P = .4$ MPa, $\ell = 125$ μm in Eq. (15.26)].

15.1.4.1.4 Conclusions and Practical Implications

The results of the analysis are consistent with the hypothesis that cooling in the nip plays a substantial role in the change in adhesion with thickness. The conclusions for adhesion to porous substrates are the following:

- Faster quench times in the nip leads to less penetration of the molten polymer and less mechanical adhesion for thin coatings. This effect appears to be more important than cooling in the air gap.
- Penetration models predict the right trends in adhesion performance, although they tend to underpredict the amount of penetration/adhesion. Penetration approximately increases with the square of the coating thickness and doubles with every 10−15°C increase in temperature.
- Chemical bonding may also be important, as suggested by the TIAG analysis and the penetration model results.

The study suggests several strategies for improving the thin coating adhesion to porous substrates. These include the following:

- Increasing the coating temperature. This increases the polymer fluidity and the available penetration time before flow ceases. Most LDPE is already coated near its temperature limit, however. Higher temperatures may lead to excessive gel formation, chain scission (particularly for PP, but under severe conditions LDPE can unzip), smoking, and generation of oxidative species that contribute to off-flavors and odors.
- Increasing the coating resin MI. This allows more flow and penetration at a given temperature. High MI has its drawbacks, however. These include higher neck-in and poorer heat seal and hot tack strength.
- Adding chemical functionality to the coating or substrate. Materials such as acid copolymers and ethylene acrylate copolymers have chemical functionality that may help improve the adhesion strength to the substrate. Treatments such as corona, ozone, or plasma also increase functionality.
- Processing with a longer air gap. This promotes LDPE oxidation which adds to the polymer−substrate chemical adhesion. Drawbacks to this approach are increased air gap cooling, which has only a small impact on adhesion, and increased neck-in.
- Heating the substrate. Flame-treating paperboard has been used to help promote adhesion during coating.
- Increasing the nip pressure to increase the penetration driving force. This may also be accomplished by increasing the nip roll hardness.
- Decreasing the polymer freezing point. One reason that LDPE is a better coating resin than PP or PET is that it has a lower freezing point that allows more time in the nip before the polymer freezes and penetration ceases. Ethylene copolymers, such as EVA, ethylene methyl acrylate (EMA) and ethylene (meth)acrylic acid (EMAA or EAA), have lower freezing points than LDPE.
- Increasing the chill roll temperature. Usually there are practical limits to doing this due to chill roll sticking.

15.1.4.2 Nonporous Substrates

There are several possible mechanisms related to the coating process that may explain the observed decrease in adhesion with decreasing thickness to nonporous substrates such as aluminum foil. These include the following while coating onto 50 μm aluminum foil:

- less TIAG (reduces oxidation and increases stress);
- greater cooling in the air gap (increases viscosity and reduces wetting and chemical interaction);
- faster cooling in the nip (reduces time for wetting and chemical interaction);
- greater stress and orientation during drawing (increases residual stress).

As was done for porous substrates, a hypothesis is proposed for each of these potential mechanisms and tested using a combination of modeling and experimental results. One set of data that are used to test several of the hypotheses comes from a study

involving blending an additive into LDPE to enhance its adhesion to aluminum foil [31]. This work is described in Section 10.4.1.4. A statistically designed experiment (DOE) was conducted varying the following while coating onto 50 μm aluminium foil:

- the coating temperature at the die exit
- coating thickness
- TIAG
- percent of the adhesion-enhancing (AE) additive in the blend.

Peel strength to foil was the dependent variable. The results were fit to a statistical model, which is used in the analysis below and designated the AE DOE. An example of a plot of peel strength versus coating thickness from the model is shown in Fig. 15.48. The results were surprising in that the modified LDPE is more sensitive to changes in coating thickness than LDPE alone. This was the motivation for the study.

15.1.4.2.1 Time in the Air Gap

Hypothesis: A significant portion of the decrease in adhesion performance when decreasing coating thickness is due to a reduction in TIAG.

Section 15.1.2 describes how increasing TIAG increases peel strength of LDPE and acid copolymers to aluminum foil. For LDPE coatings, this is believed to be due to greater oxidation time; for acid copolymers, stress may be involved.

There are several studies that show peel strength decreases with decreasing thickness even at constant TIAG. An example is reproduced from Antonov and Soutar [4] in Fig. 15.49. Here the effect of thickness is much more pronounced than the effect of TIAG. The same is true for the AE DOE as shown in Fig. 14.48. In this experiment, the statistical analysis

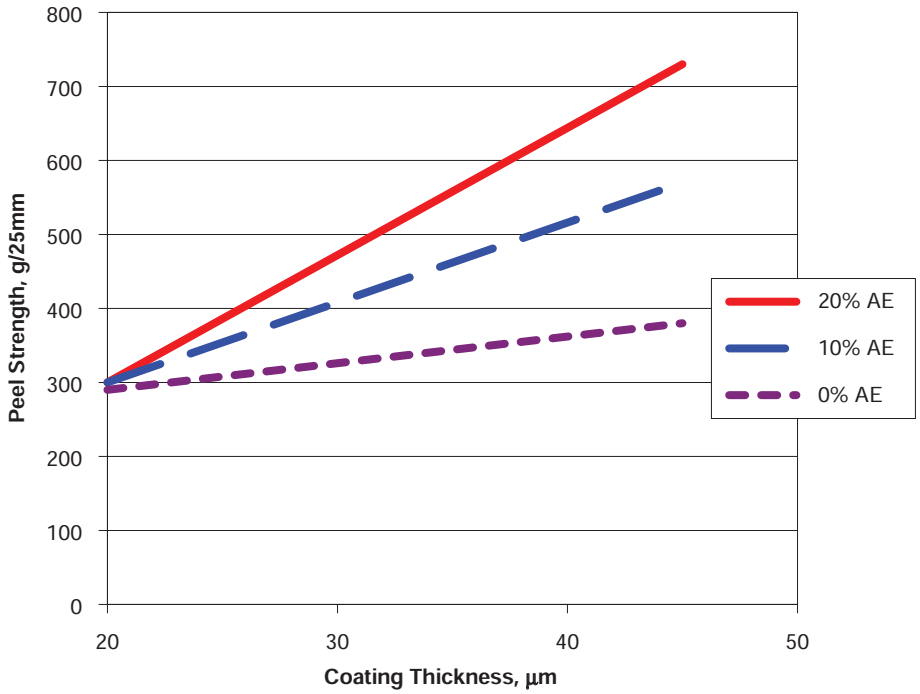


Figure 15.48 Results of DOE (design of experiment) varying coating thickness, coating temperature, time in the air gap (TIAG), and % AE (adhesion-enhancing) modifier in blend with low density polyethylene (LDPE). Here, temperature (310°C) and TIAG (80 ms) are kept constant and peel strength to aluminum foil as a function of thickness and %AE are plotted based on a statistical model of the experimental results. Structure is 50 μm Al/coating.

Data from Morris BA, Thai HT. Modifying LDPE for improved adhesion to aluminum foil In: TAPPI PLACE conference; 2004. Reproduced with permission from Morris BA. Understanding why adhesion in extrusion coating decreases with diminishing coating thickness. J Plastic Film Sheeting 2008;24:53–88.

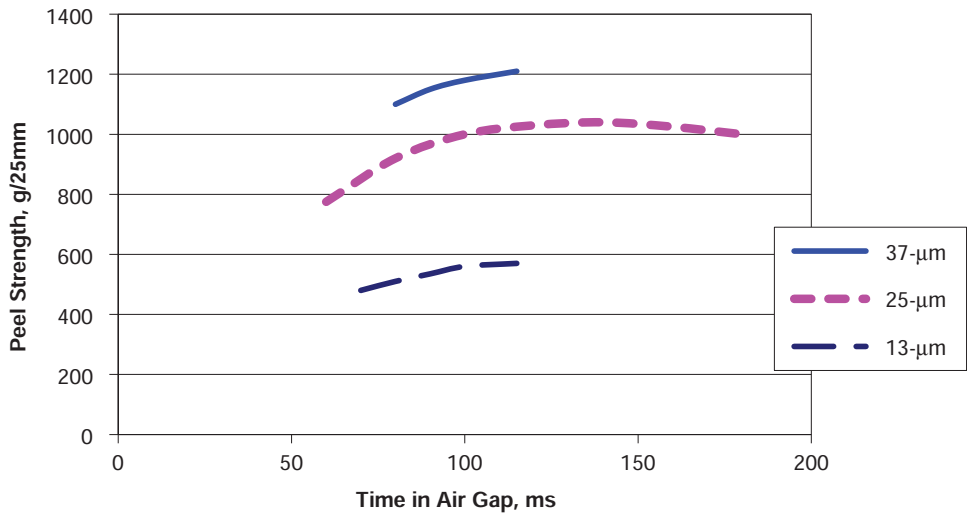


Figure 15.49 Adhesion of an acid copolymer to aluminum foil for three coating weights. Melt temperature = 303°C.

Data from Antonov V, Soutar A. Foil adhesion with copolymers: time in the air gap. In: TAPPI 1991 polymers, laminations & coatings conference proceedings. Atlanta: TAPPI Press; 1991. p. 553. Reproduced with permission from Morris BA. Understanding why adhesion in extrusion coating decreases with diminishing coating thickness. J Plastic Film Sheeting 2008;24:53–88.

shows that thickness has a greater impact than TIAG. This hypothesis, therefore, is rejected.

As discussed in Section 15.1.2, there are more accurate ways to compute the actual time in the air gap than TIAG; these methods, such as Eq. (15.4), take into account the draw down of the polymer. The results of such calculations, however, show that at constant TIAG and die gap, the actual time in the air gap increases with decreasing thickness, making the hypothesis even more difficult to support.

15.1.4.2.2 Cooling in the Air Gap

Hypothesis: Thinner coatings cool down more in the air gap, resulting in less wetting (due to higher viscosity) and chemical reaction when they come into contact with the substrate.

Sections 15.1.2.3 and 15.1.4.2 show that thinner coatings do cool down more in the air gap than thicker ones, but the actual amount of cooling in the air gap is relatively small. Nevertheless, this hypothesis can be tested directly by applying the web temperature model (Eq. (15.13)) to the AE DOE results. Fig. 15.50 shows the web temperature model results for two coatings at 45 and 20 µm, each with a 325°C die exit temperature. The thicker web cools to 321°C as it travels through the 152 mm air gap to the chill roll. The thinner web cools to 315°C.

Fig. 15.51 shows statistical DOE model predictions for the peel strength of the thick and thin coatings. These are 800 and 300 g/25 mm, respectively. To find out whether cooling in the air gap contributes to this decrease in adhesion, the web temperature model is used to determine what the die exit temperature needs to be for the thick coating to cool to the same temperature as the thin coating. This is represented by the dashed curve in Fig. 15.50. A die exit temperature of 320°C for the thick coating will duplicate the final temperature in the air gap of the thin coating. Plugging this value into the DOE model reveals no change in the peel strength, as illustrated by the final bar in Fig. 15.51. The hypothesis is rejected.

15.1.4.2.3 Cooling in the Nip

Hypothesis: Thin coatings cool faster in the nip, providing less time for wetting and chemical reaction and, hence, less adhesion to nonporous substrates.

Fig. 15.52 shows the results of the unsteady-state heat conduction model developed in Section 15.1.3 applied to an extrusion coating onto a foil laminate with the structure: (nip roll side) 13-µm OPET/19-µm LDPE/9-µm Al/coating (chill roll side). The coating is initially at 315°C and the foil laminate at 23°C. For boundary conditions, the outside coated

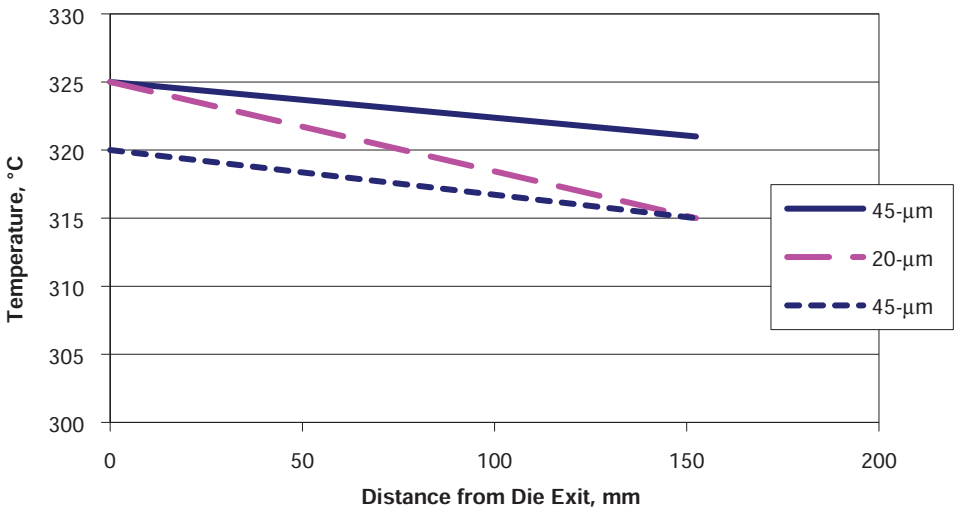


Figure 15.50 Web temperature model (Eq. (15.13)) applied to conditions of AE DOE (20% AE + 80% LDPE, 152 mm air gap, 91 m/min line speed, 100 ms TIAG). $h = 5.7$ W/m^2-K. *AE*, adhesion enhancing; *DOE*, design of experiment; *LDPE*, low density polyethylene; *TIAG*, time in the air gap.
Reproduced with permission from Morris BA. Understanding why adhesion in extrusion coating decreases with diminishing coating thickness. J Plastic Film Sheeting 2008;24:53–88.

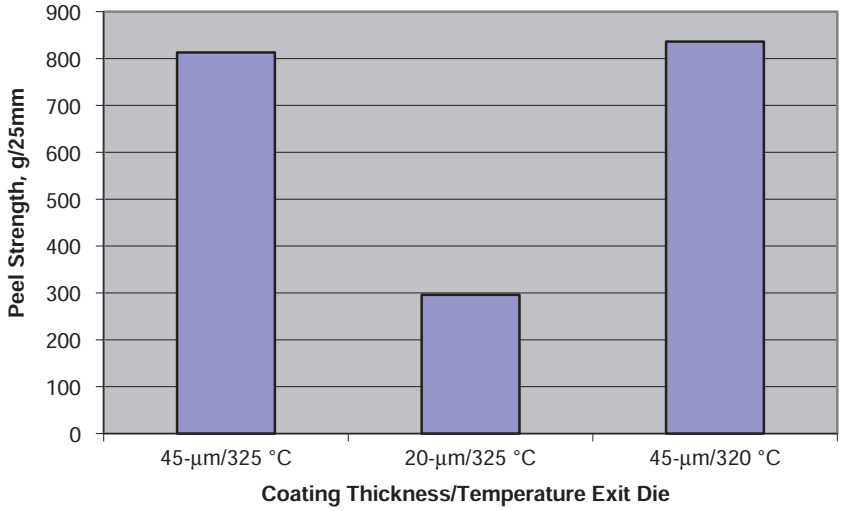


Figure 15.51 AE DOE model predictions for peel strength using coating thickness, die exit temperatures and processing parameters from Fig. 15.49. *AE*, adhesion enhancing; *DOE*, design of experiment.
Reproduced with permission from Morris BA. Understanding why adhesion in extrusion coating decreases with diminishing coating thickness. J Plastic Film Sheeting 2008;24:53–88.

surface is assumed to be in direct contact with the chill roll at 10°C and the outside foil laminate surface (OPET film) is in contact with a rubber nip roll (insulated). The results in Fig. 15.52 show the temperature at the foil surface versus time for 30- and 18-µm coating thicknesses. The foil surface temperature quickly rises from room temperature as the hot polymer contacts it. It reaches a maximum and slowly cools back down.

A key parameter proposed by Trouilhet and Morris [8] and described in Section 15.1.3 is the time until solidification, t_s. This represents the time until the polymer reaches its freezing temperature (91°C for LDPE). Once the polymer begins to crystallize, the

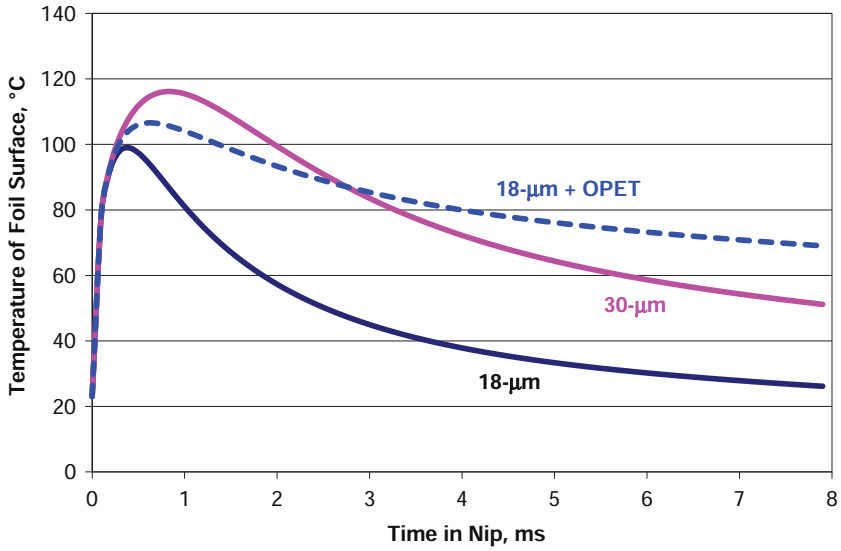


Figure 15.52 Heat transfer model calculations for the temperature of the foil surface during the coating of a foil laminate versus time in the nip. Dashed curve represents a way to slow the cooling of the 18-µm coating by inserting an OPET film between the coating and chill roll. Structure: 13-µm OPET/19-µm PE/9-µm Al/coating; coating temperature: 315°C; chill roll temperature: 10°C. *OPET*, oriented polyester; *PE*, polyethylene.
Reproduced with permission from Morris BA. Understanding why adhesion in extrusion coating decreases with diminishing coating thickness. J Plastic Film Sheeting 2008;24:53–88.

polymer chain movement is severely constrained, curtailing further flow, wetting, and rearrangement needed for chemical bonding. From Fig. 15.52, t_s for the 30- and 18-µm coatings is approximately 3 and 0.8 ms, respectively. This confirms that the thicker coatings have considerably more time for adhesion to develop before the onset of crystallization.

One way to try to determine the effect of the cooling rate in the nip on adhesion is to try to slow down the quench rate of the thin coating. Fig. 15.52 indicates how an experiment can be designed to do this. The bottom curve represents the temperature profile when an 18-µm coating is applied. The cooling of the thin coating can be slowed by inserting a film between the coating and chill roll. By selecting an appropriate film that has no adhesion to the coating, the film can be later removed for adhesion measurements. Fig. 15.52 shows the effect of using a 37 µm OPET film for this purpose in what essentially becomes an extrusion lamination. The structure is

Nip roll side [13-µm OPET/19-µm LDPE/9-µm Al/18-µm coating/37-µm OPET] chill roll side.

The presence of the OPET film insulates the interface between the coating and foil, extending t_s from 0.8 to about 3 ms. This is the same as the 30 µm coating without the insulating OPET layer.

The three structures in Fig. 15.52 were made on a pilot scale extrusion lamination line at DuPont. The coating resin is a blend of 20% AE modifier and 80% LDPE. Coating conditions and peel strength results are given in Fig. 15.53. As expected, the 18-µm coating has significantly less peel strength than the 30-µm coating. The peel strength of the 18-µm coating produced with the insulating layer of OPET (removed for the peel strength measurement) fell between the two. The results show that nip cooling is important for peel strength performance. The fact that the insulated 18-µm coating peel strength was not as good as the 30-µm coating, despite similar t_s values, suggests a couple of factors. One is that t_s may not be the proper scaling parameter for peel strength. A closer look at Fig. 15.52 shows that the insulated temperature curve does not match the 30-µm coating curve peak temperature. The higher 30-µm peak coating temperature may play a role. Second, the results suggest that other factors, besides nip cooling, may influence the effect thickness has on peel strength performance.

The hypothesis cannot be rejected. Cooling in the nip is important but is not likely the sole driving force behind the loss in peel strength at low thickness.

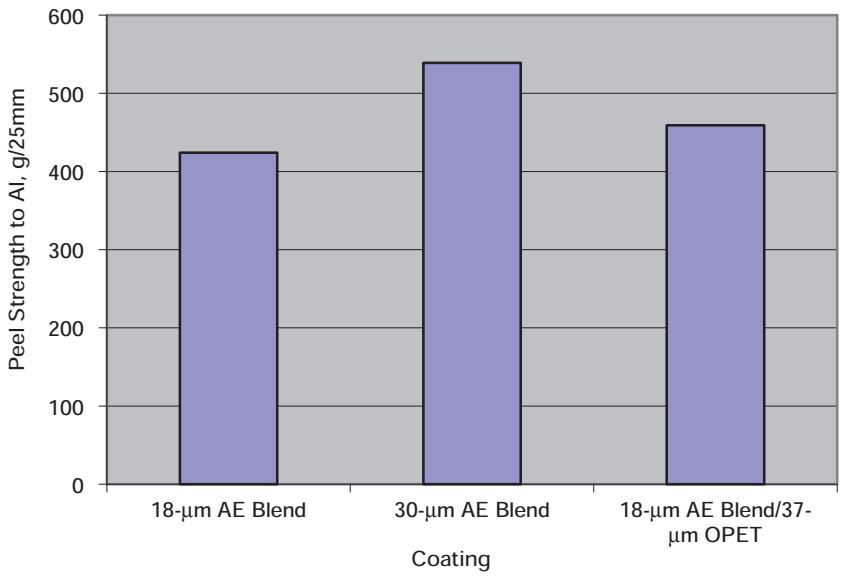


Figure 15.53 Peel strength results from coating trial duplicating structures from Fig. 15.52. Structure is OPET/PE/9-μm Al/coating. Coating conditions: 122 m/min line speed, 127 mm air gap, 75 mm TIAG, 332°C coating temperature, 10°C chill roll temperature, 60 psi nip pressure. *OPET*, oriented polyester; *PE*, polyethylene; *TIAG*, time in the air gap.

15.1.4.2.4 Stress

Hypothesis: Reducing the coating thickness puts more stress on the polymer, decreasing the peel strength.

Here the analysis from Section 15.1.2.2 and the Appendix is used to test the hypothesis. The stress imparted in the extruder and die is only weakly dependent upon thickness. Stress imparted during draw down in the air gap is related to three factors: the elongational strain rate, the total elongational strain, and the relaxation time. The strain rate is inversely proportional to TIAG, which has already been considered in Section 15.1.4.2.1. The total strain, ε_{tot}, is equal to the logarithm of the *DDR* as shown in Eqs. (15.8) and (15A.12). DDR is approximately equal to the die gap divided by the coating thickness (Eq. (15A.11)). Since the die gap is often kept constant while changing thickness, the *DDR*, and hence, stress increases with decreasing coating thickness.

One representation for the relaxation time is the process time (t_f) as defined by Eq. (15.4). If *TIAG* (L/v_f) is held constant, then $t_f \sim$ DDR/ln(DDR). Since DDR increases with decreasing coating thickness (at constant die gap), by this timescale, the time for relaxation increases when the thickness is decreased. The earlier analysis showed that TIAG does not affect adhesion as strongly as thickness does. This suggests that not much relaxation takes place in the air gap while the polymer is being drawn down. The time available for relaxation after the polymer hits the chill roll (t_s) and draw down has ceased may be a more relevant parameter.

Table 15.11 presents an analysis of the changes in stress, relaxation time, and peel strength under conditions that simulate the AE DOE. A 60% peel strength reduction occurs when changing the thickness from 45 to 20 μm, which is associated with a 33% increase in ε_{tot} and 88% decrease in t_s. Both associations support the hypothesis that stress plays a role in reducing peel strength with reductions in thickness.

15.1.4.2.5 Conclusions and Practical Implications

Based on this analysis, the hypotheses that cooling in the nip and stress play significant roles in the change in peel strength with thickness are not rejected. Neither mechanism can explain all the observations. In particular, understanding the increased sensitivity of higher performing adhesives, such as the AE-LDPE blends, to peel strength in coating thickness is still elusive and is taken up in Section 15.1.4.3.

Table 15.11 An Analysis of Stress, Relaxation Time, and Peel Strength Under the Conditions of the AE DOE

Parameter	45-μm Coating	20-μm Coating	% Change
Peel strength, g/25 mm	732	296	−60%
DDR	11.2	25.4	
ε_{tot} [ln(DDR)]	2.42	3.23	33%
TIAG, ms	80	80	
t_l, ms	338	603	78%
t_s, ms	5.9	0.7	−88%

AE, *adhesion enhancing;* DDR, *draw down ratio; DOE, design of experiment;* TIAG, *time in the air gap.*
Reproduced with permission from Morris BA. Understanding why adhesion in extrusion coating decreases with diminishing coating thickness. J Plastic Film Sheeting 2008;24:53–88.

The work suggests several strategies for improving the thin coating adhesion to nonporous substrates. These include the following:

- Reduce the cooling rate in the nip
  - Increase the coating temperature. Most coating resins, however, are already processed near their temperature limit. Higher temperatures may lead to other problems, as discussed in Section 15.1.4.4 and in Chapter 13.
  - Lower the polymer freezing temperature. Copolymers such as acid copolymers, EMA, ethylene butyl acrylate, and EVA have lower freezing points than LDPE, as does some grades of metallocene polyethylene.
  - Heat the substrate via flame treatment or other means to increase the time before the polymer freezes.
  - Increase the coating resin MI to allow more flow and wetting before the polymer freezes.
  - Increase the chill roll temperature. Usually there are practical limits to doing this due to chill roll sticking.
- Reduce stress
  - Decrease the die gap to reduce DDR and stress during drawing. Unfortunately, many modern edge bead reduction dies do not allow this.
  - Run with a longer air gap. This reduces stress and for nonpolar polymers such as LDPE promotes oxidation. The primary drawback is increased neck-in.
- Add chemical functionality to the coating or substrate. Resins such as acid copolymers and ethylene acrylate copolymers have chemical functionality that may help improve the adhesion strength to the substrate. Treatments such as corona, ozone, or plasma also increase functionality. Priming the substrate is another approach.

15.1.4.3 Analysis of Peel Test

The analysis so far has failed to discern the mechanism behind the results in Fig. 15.48 from the AE DOE [31], which show that the sensitivity of an adhesive's peel strength performance to changes in coating thickness increases as the bond strength increases. In this section, additional experimental results are shown that suggest these findings are general: for an acid copolymer which has strong bonds to foil, the peel strength is even more sensitive to changes in thickness than LDPE or the modified LDPE. An analysis of the peel strength measurement provides an explanation.

15.1.4.3.1 Experiment

Three resins of increasing acid functionality are extrusion coated onto a foil laminate to confirm the earlier work showing that the peel strength to foil of better performing adhesives is more sensitive to changes in coating thickness. The three resins are LDPE, a blend of 20% AE modifier [31] and 80% LDPE, and an EAA copolymer (9% AA,

10 MI). The AE modifier and EAA copolymer are supplied by DuPont. The coating conditions are the following:

- die: Cloeren edge bead reduction die
- substrate: 13-μm OPET/19-μm tie/9-μm Al
- coating thickness: 20−50 μm (coated onto the foil side of the substrate)
- coating temperature: 330°C for LDPE and AE−LDPE blend, 288°C for EAA
- die gap: 0.51 mm
- line speed: 122 m/min
- air gap: 127 mm
- chill roll temperature: 10°C
- nip pressure: 0.4 MPa.

The peel strength between the coating and foil is measured in the MD. The results are plotted versus coating thickness in Fig. 15.53 and show the following:

- The peel strength of the coating to aluminum foil is in the following order: LDPE < AE + LDPE < EAA.
- There is greater peel strength sensitivity to coating thickness when there is a stronger bond to the foil. This is indicated by the steeper slope for the EAA and AE + LDPE curves compared with the LDPE curve.

15.1.4.3.2 Peel Test Analysis

The peel test is a measure of the energy to pull the coating away from the substrate. The application of fracture mechanics to the peel test is described in Section 10.2.3. The peel force has contributions from elongating and bending the peel arms as well as the energy to create new interfacial area (known as the fracture energy). A mathematical expression is derived in Section 10.2.3 and reproduced here as Eq. (15.31) for convenience:

$$\frac{P}{b} = \frac{G_a + G_e + G_b}{1 + \varepsilon_a - \cos\theta} \tag{15.31}$$

where P = peel force, b = width of peel arm, G_a = fracture energy = energy to create new surfaces, G_e = energy dissipated during peel arm elongation, G_b = energy dissipated during bending of the peel arm, ε_a = inelastic extension of peel arm θ = peel angle.

The coating thickness impacts each element of the peel force:

- Elongation of peel arm (G_e): G_e is related to the peel arm thickness (X) times the area under the stress−strain curve:

$$G_e = X \int_0^{\varepsilon_a} \sigma d\varepsilon. \tag{15.32}$$

  Here σ is the stress. The peel arm tensile strain, ε_a, is a nonlinear function of the thickness, which affects G_e. At low thickness, the peel arm may yield. The integral term is large but X is small, so that G_e is small. As thickness increases, G_e increases. At some point, the peel arm stiffness prevents yielding: X is large but the integral term is small resulting in a decrease in G_e.
- Bending of peel arm (G_{db}): G_{db} arises from peel arm bending and can be significant if plastic yielding occurs. Gent and Hamed [48] studied the plastic yielding of OPET film during bending. They note that peel strength often has been observed to go through a maximum at intermediate thickness. Gent concludes that at low thickness, plastic yielding occurs, and the total energy that is dissipated is small. As thickness increases, more energy is dissipated and peel strength increases with G_{db}. Eventually, the peel arm gets too stiff and less yielding occurs, which leads to a reduction in G_{db} and peel strength. At high thickness, no yielding occurs and G_{db} is small.

  Gent also proposes that the adhesion strength at the interface can affect G_{db}. Low adhesion is less likely to lead to substrate yielding. High adhesion can lead to large energy dissipation within the substrate in the highly deformed region near the detachment: “plastic deformation of the stripping member can thus lead to an increase in peel strength in two ways:

  - directly, by an additional force representing the work required to propagate the bend in an elastic−plastic strip as peeling proceeds;
  - indirectly, by causing a larger deformation in the elastomeric substrate under the

higher peel forces and bringing about greater energy losses in this layer as a result." [48].

A similar argument can be made for G_e. Higher adhesion can also lead to a greater initial peel angle, θ_o, which can lead to a greater G_{db}. For example, Pascal [49] shows that the thickness affects the bending angle and peel strength in extrusion coating.

- Fracture energy (G_a): As described in Section 10.2.3, G_a can be decomposed into the product of two factors, the work of adhesion and the local energy dissipation at the peel front:

$$G_a = W_a(1 + \Phi(R, T)) \tag{15.33}$$

where W_a = work of adhesion or bonding, Φ = local viscoelastic energy dissipation, R = rate of pull, T = temperature.

W_a encompasses the thermodynamic and chemical adhesion that occurs at the interface. This term is typically quite small compared to the value of G_a but can be important because of its multiplying effect. In the experimental results, the AE−LDPE blend and the EAA copolymer have higher chemical functionality than LDPE. Their W_a is expected to be greater than that for LDPE.

The second term in Eq. (15.33), Φ, is the local energy that is dissipated as the detachment front, generally referred to as a crack, moves through. As described in Section 10.2.2.3, Φ arises from a zone of deformation created in front of the crack. At low thickness, the size of this zone is constrained by the layer thickness. As the thickness is increased, Φ and G_a increase with increasing thickness up to a critical value of the thickness, X_c. Once the thickness exceeds X_c, the size of the zone of deformation becomes small compared to the thickness; further increases in thickness have no effect on G_a. This is illustrated in Figs. 10.9 and 10.10.

The critical value of the thickness is derived in Section 10.2.2.3 and is related to the peel arm tensile properties and G_a:

$$X_c = \frac{1}{2\pi}\frac{G_a E}{\sigma_y^2} \tag{15.34}$$

where X_c = critical value of thickness where G_a transitions from a linear change to a plateau, E = tensile or Young's modulus, σ_y = yield strength.

The dependence of X_c on G_a makes sense in lieu of Gent's comments earlier. Higher G_a (through, for example, an increase in W_a) implies that the deformation zone is larger, which in turn should increase X_c.

15.1.4.3.3 Application of Peel Strength Model to Experimental Data

The analysis of the peel test mechanics shows that thickness significantly affects the measured peel force. Moreover, all three components, G_e, G_{db}, and G_a, are a function of the adhesive strength, which may explain the behavior in Figs. 15.48 and 15.54. To apply these concepts to the foil coating structures, a model developed by Kinloch, Lau, and Williams [30] is used (See Section 15.2.3). They derive analytical expressions for G_e, G_{db}, and G_a that are solved iteratively using a computer for conditions that simulate the AE DOE.

Model inputs include the imposed peel angle and the peel arm tensile properties [Young's modulus, plastic yield strain (e_y), and work-hardening parameter (α)]. Since Kinloch studied LDPE−foil laminates, their tensile data are used in the analysis. It is assumed adding AE to LDPE does not significantly change the tensile properties. A "T-peel" configuration is used in this study to measure peel strength, a geometry that is not explicitly included in the model. The imposed peel angle, θ, is set to 90° as an approximation.

Fig. 15.55 shows the results of the model for LDPE. The peel strength values (converted to the units of energy per area) as a function of thickness are taken from the AE DOE results (bottom curve in Fig. 15.48). The results show G_e is small, reflecting experimental observations that the peel arms did not elongate beyond the yield point. G_a is large but not very dependent on thickness. G_{db} has the greatest dependence on thickness.

Fig. 15.56 shows the results for the 20% AE, 80% LDPE blend (top curve from Fig. 15.48). Again G_e is small and will be ignored for the rest of this discussion. Here both G_a and G_{db} increase substantially with thickness. This may account for the blend's steeper peel strength curve in Fig. 15.48.

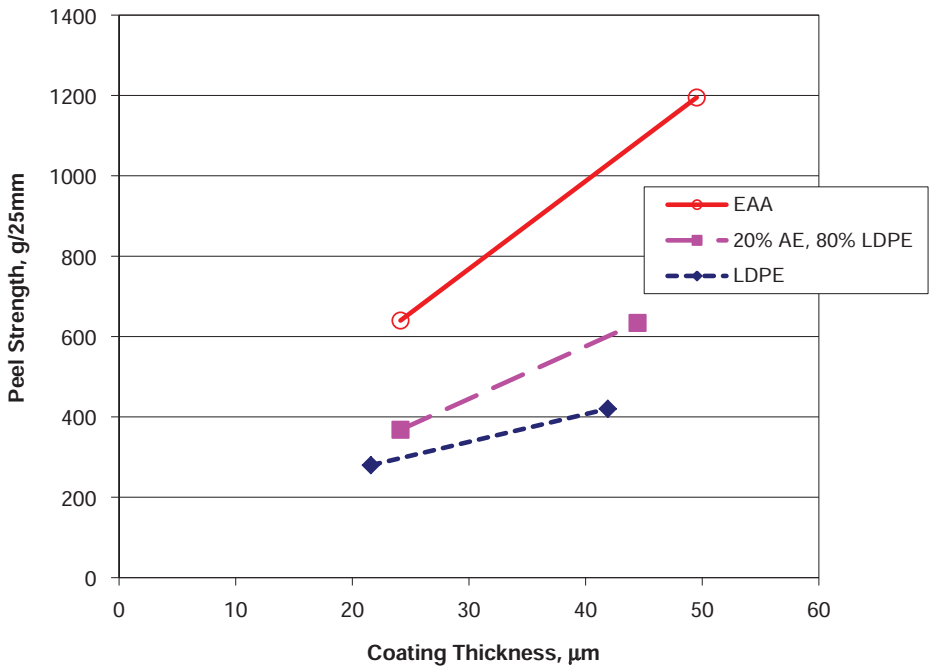


Figure 15.54 Results of coating trial. *AE*, adhesion enhancing additive; *EAA*, ethylene acrylic acid copolymer; *LDPE*, low density polyethylene.
Reproduced with permission from Morris BA. Understanding why adhesion in extrusion coating decreases with diminishing coating thickness. J Plastic Film Sheeting 2008;24:53–88.

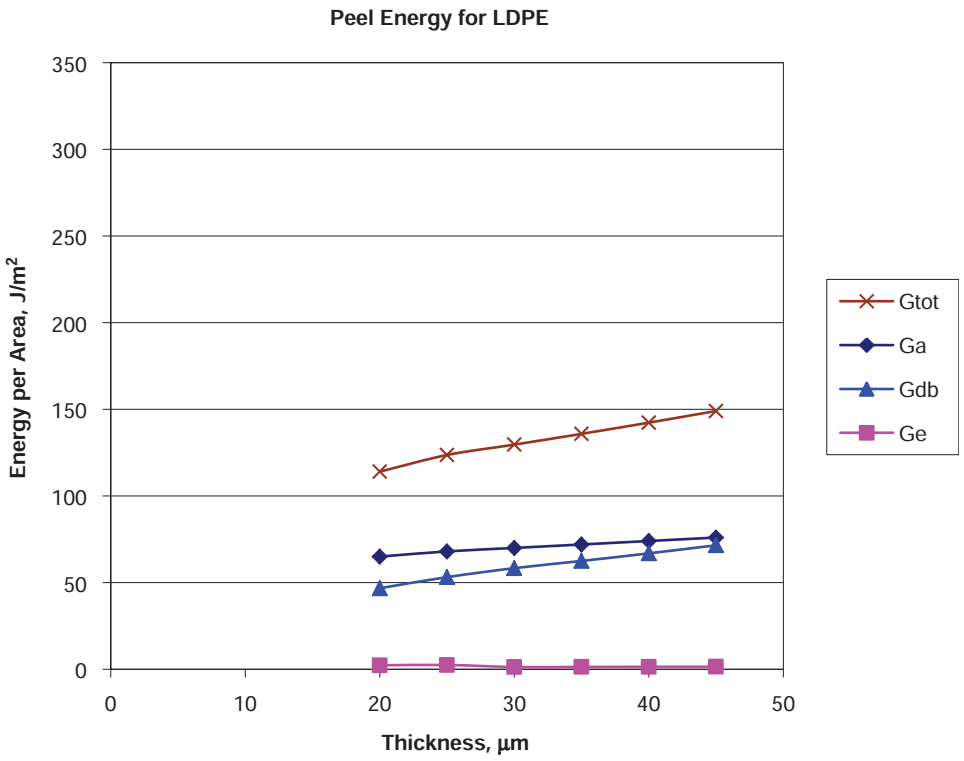


Figure 15.55 Results of energy analysis for low density polyethylene (LDPE) coatings. Peel strength and thickness data taken from AE DOE model (Fig. 15.48) with 80 ms time in the air gap (TIAG) and 310°C coating temperature. Peel energy model parameters: $E = 150$ MPa, $\alpha = 0.087$, $e_y = 6.2\%$, $\theta = 90°$.
Reproduced with permission from Morris BA. Understanding why adhesion in extrusion coating decreases with diminishing coating thickness. J Plastic Film Sheeting 2008;24:53–88.

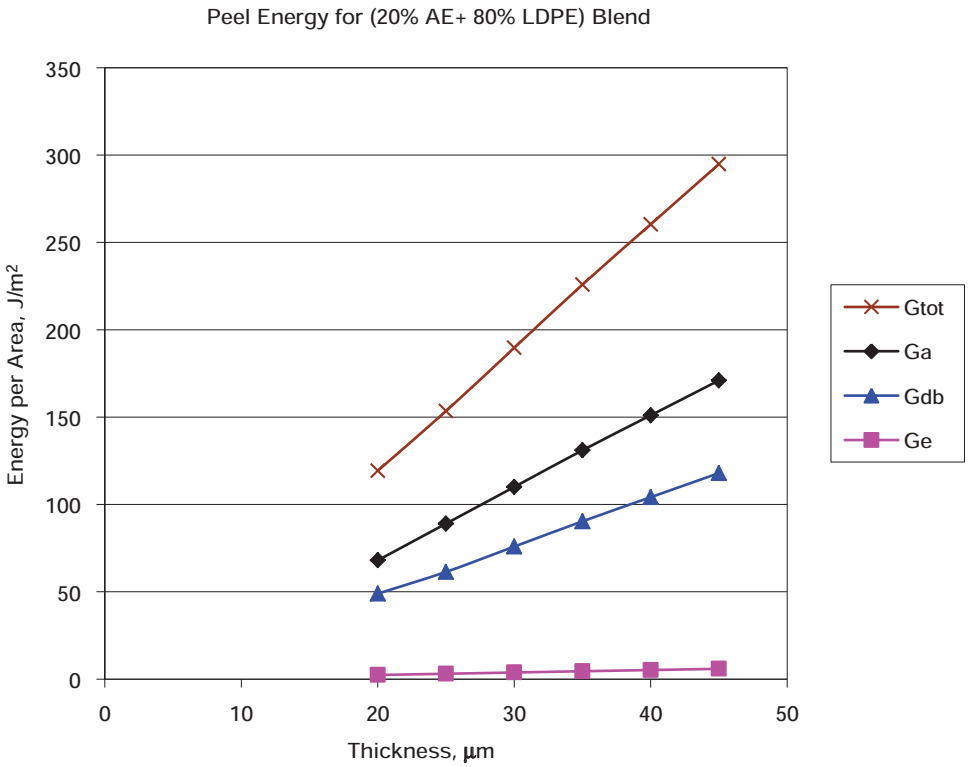


Figure 15.56 Results of energy analysis for 20% AE, 80% LDPE (low density polyethylene) coatings. Peel strength and thickness data taken from AE DOE model (Fig. 15.48) with 80 ms TIAG (time in the air gap) and 310°C coating temperature. Peel Energy model parameters: $E = 150$ MPa, $\alpha = 0.087$, $e_y = 6.2\%$, $\theta = 90°$. *Reproduced with permission from Morris BA. Understanding why adhesion in extrusion coating decreases with diminishing coating thickness. J Plastic Film Sheeting 2008;24:53–88.*

Comparing Figs. 15.55 and 15.56 shows that G_a for the blend is a stronger function of thickness than G_a for LDPE. Using Eq. (15.34), X_c is estimated to be around 10–20 µm for LDPE and 50–80 µm for the AE blend. Since the coating thickness is in the range of 20–50 µm, this suggests that the LDPE coatings are near the plateau region, whereas the AE blend coatings are still on the slope. This is illustrated in Fig. 15.57. Increasing the polymer-to-substrate bonding by adding chemical functionality increases X_c. Over the thickness range of interest, this change in critical thickness helps explain the peel strength sensitivity to thickness. X_c for the EAA coating is estimated to be 80–120 µm, which is consistent with its steeper slope in Fig. 15.54.

As noted earlier, G_{db} increases with increasing thickness for both LDPE and the AE–LDPE blend (Figs. 15.55 and 15.56). The AE blend slope, however, is considerably larger. Following the argument of Gent, it appears that adding AE to LDPE increases the energy dissipated during peel arm bending. This is achieved through a greater anchoring effect. Comparing the initial peel angles supports this. As shown in Fig. 15.58, model calculations indicate that the peel angle remains constant for the AE blend coating as the thickness is increased. For the LDPE coating, the initial peel angle decreases as thickness is increased. For a given thickness, the peel arm of the AE blend coating is pulled back at a higher angle than for LDPE, expending more energy during the peel strength measurement.

15.1.4.3.4 Conclusions and Practical Implications

The peel strength test mechanics help explain why thin coatings have low peel strength performance and higher bond strength leads to greater sensitivity of peel strength to changes in thickness. The energy dissipated during peel arm bending decreases with decreasing thickness. Moreover, both the fracture and bending energy are strongly influenced by adhesion. Higher adhesion increases the initial peel

angle, resulting in greater bending energy. In addition, the natural deformation zone size is enlarged, shifting the critical thickness (X_c) and onset of the plateau region to higher thickness. Within the coating range thickness explored in the experiments, this has the effect of putting the LDPE on the plateau region and the AE blend and acid copolymer on the sloping region. The greater bond strength provided by the chemical functionality in the AE blend and acid copolymer gives rise to a steeper climb in peel strength over a greater thickness range than for LDPE.

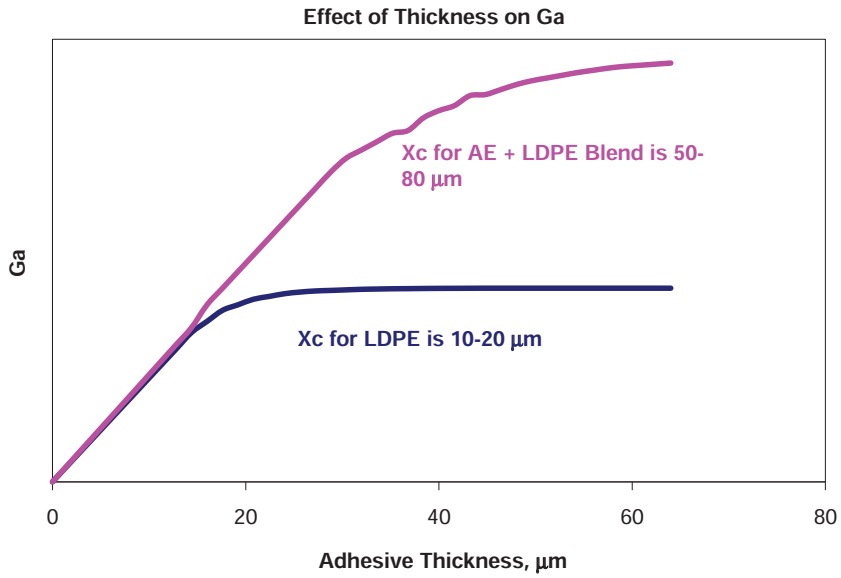


Figure 15.57 Scenario where G_a curves for low density polyethylene (LDPE) and AE (adhesion enhancing)–LDPE blends diverge because of differing values of X_c.
Reproduced with permission from Morris BA. Understanding why adhesion in extrusion coating decreases with diminishing coating thickness. J Plastic Film Sheeting 2008;24:53–88.

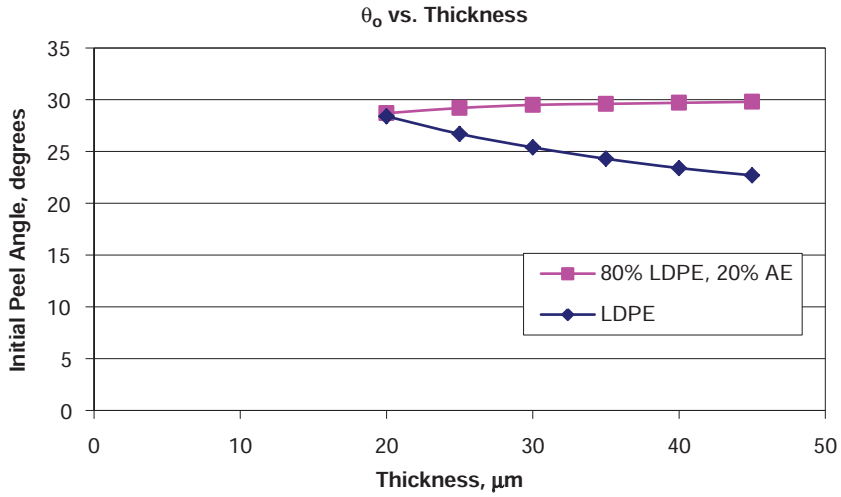


Figure 15.58 Comparison of initial peel angle (θ_0) for LDPE and AE–LDPE blend. Peel strength and thickness data taken from AE DOE model (Fig. 15.48) with 80 ms TIAG and 310°C coating temperature. Peel energy model parameters: $E = 150$ MPa, $\alpha = 0.087$, $e_y = 6.2\%$, $\theta = 90°$. *AE DOE*, adhesion-enhancing design of experiment; *LDPE*, low density polyethylene; *TIAG*, time in the air gap.
Reproduced with permission from Morris BA. Understanding why adhesion in extrusion coating decreases with diminishing coating thickness. J Plastic Film Sheeting 2008;24:53–88.

This work shows that increasing bond strength between the polymer coating and substrate does not always result in higher peel strength. The peel strength depends on many factors beyond the bond strength, which include the following:

- the local energy dissipation (Φ) at the peel front;
- the local peel angle; and
- whether the polymer yields or elongates.

These factors depend on stiffness, thickness, viscoelastic response, and the yield stress of the polymer. The physical properties, in turn, do not affect each peel strength component in the same way. For example, reducing stiffness may reduce the peel arm bending energy, but increase the fracture energy. The situation becomes even more complicated for extrusion laminations where the second substrate properties may become a factor.

Despite these complexities, the findings suggest several general strategies for increasing the peel strength at low coating thickness. For LDPE, increasing the bond strength by increasing oxidation (increasing temperature or using ozone treatment) or adding modifiers may help. But as is shown with the AE modifier work, this may be most effective for thick coatings. Without changing the physical properties, the bond strength may not be increased enough to significantly improve the peel strength of thin coatings. Acid copolymers have even stronger bond strength to aluminum foil than modified polyethylene. They are less crystalline than LDPE and, hence, have lower modulus and yield stress. Thus, their peel strength may be higher than LDPE at a given thickness, even though they may be more sensitive to changes in thickness. Further physical property changes can be obtained by incorporating soft comonomers such as acrylates or acetates into the ethylene backbone. EMA, EVA, or acid terpolymers (ethylene–acid–acrylate) are examples. Primers may be needed for some polymers to achieve good bond strength to the substrate.

In general, the polar ethylene copolymers, such as acid copolymers and EMA, have the right combination of stiffness, yield stress, and chemical functionality to improve peel strength over LDPE at low coating weights. One word of caution is that increasing the peel strength does not necessarily imply improved performance in a specific packaging application. Environmental and other end-use factors may need to be considered, as described in Chapter 16.

15.2 Interlayer Adhesion in Coextrusion

The mechanisms for adhesion in coextrusion are described in Chapter 10. Sufficient time and temperature for diffusion and chemical interaction at the interface are required for good adhesion. Complicating matters is the new interfacial area created as the melt is drawn to its final thickness just prior to quenching: as the interfacial area increases, the density of interfacial bonds decreases. Orientation and stress also impact peel strength performance. The time, temperature, and stress history of the polymer, therefore, affect interlayer peel strength in coextrusion coating, cast film, and blown film.

15.2.1 Initial Process Time Studies

The region between the die exit and the start of solidification (frost line for blown film and chill roll for cast film and extrusion coating) is a critical region for interlayer adhesion. The layers are drawn down to their final thickness with a commiserate increase in interfacial area. The polymer chains are subjected to orientation and stress and the polymer begins to cool. The process time is the characteristic time the polymer spends in this region. Following up on work by Shirodkar [50], Butler [51], and others showing process time in blown film correlates with a number of mechanical properties of film in monolayer extrusion. Morris [52] conducted an experiment showing process time also affects interlayer adhesion in coextrusion blown film. The equation for process time is provided in Chapters 2 and 13 and reproduced here:

$$t_f = \frac{h_f}{v_f - v_o} \ln\left(\frac{v_f}{v_o}\right) \tag{15.35}$$

where t_f = process time, h_f = frost line height, v_f = line speed, v_0 = velocity of polymer at die exit.

In terms of more commonly used parameters, the process time can be written as

$$t_f = \left[\frac{h_f}{v_f\left(1 - \frac{X_f \rho_f \mathrm{BUR}}{X_0 \rho_0}\right)}\right] \ln\left(\frac{X_0 \rho_0}{X_f \rho_f \mathrm{BUR}}\right). \tag{15.36}$$

where BUR = blown up ratio (ratio of final bubble diameter to die diameter), X_0 = die gap, X_f = final film thickness, ρ_0 = density of polymer at die exit (melt density), ρ_f = density of polymer in final film (solid density).

A three-layer blown film line is used to produce films with the structure (HDPE−tie−EVOH) with layer thicknesses (37.5/12.5/20 μm). Melt temperature, BUR, and film thickness are kept constant. The process time is varied by changing the frost line height (by varying the air quench speed) and the line speed. When the line speed is changed, the extruder output is adjusted to keep the final film thickness constant. Increasing the line speed increases take-up ratio (TUR), or DDR as it is sometimes called, and decreases BUR (Eq. (2.7)) since the film thickness and die gap are held constant.

The HDPE has a density of 960 kg/m^3, an MI of 0.75 g/10 min, melting point (T_m) of 137°C, and freezing point (T_c) of 115°C. The EVOH is a 32 mol % ethylene grade with an MFR (210°C/2160 g) of 3.0 g/10 min, T_m of 185°C, and T_c of 157°C. Three of the tie layers are listed in Table 15.12. These are anhydride-modified LLDPE resins that are often used to bond PE to EVOH in blown film (Section 10.4). The anhydride functionality reacts with the OH groups of the EVOH to form an ester. ADH1 and ADH2 are identical except for the amount of anhydride functionality. ADH2 has three times the amount as ADH1. ADH3 has an intermediate level of anhydride but is rubber modified, which gives it a lower modulus than the other two grades.

Peel strength between the tie resin and EVOH is measured using a T-peel configuration, pulled at 305 mm/min after 1 week of aging at 50% RH, 23°C. Plotted versus process time in Fig. 15.59, the results show a 10-fold increase in peel strength with increasing process time over the range explored. The results underscore the importance of processing on adhesion in coextrusion.

Morris finds similar behavior for a variety of combinations in coextrusion blown film, including the adhesion of EVA-based tie resins to EVOH [52], PP-based tie resins to EVOH [53], and PE-based tie resins to PA6 [53]. These are all combinations of immiscible polymers involving a chemical reaction at the interface. An increase in peel strength also occurs in nonreacting pairs where diffusion is the mechanism for adhesion. For example, bonding PE to ionomer is found to show this characteristic behavior.

Morris [7,54] later extends the study to coextrusion coating and cast film. Here the characteristic process time is the time between the die exit and chill roll, given by Eq (15.4). In one study, similar structures to that of the blown film study are made on a pilot scale coextrusion coating line. The structure is kraft paper//19-μm LDPE//(5-μm tie−6.3-μm EVOH−5-μm tie−25-μm LDPE). The kraft paper is coated with LDPE in one pass and coextrusion coated with the EVOH structure in a second pass. Corona treatment is applied to the LDPE-coated paper to ensure good adhesion between the tie layer and LDPE, since adhesion between the EVOH and tie layer is studied. The melt temperatures for the EVOH, tie, and LDPE layers are 232, 260, and 260°C, respectively. The air gap (13−25 cm) and line speed (61−183 m/min) are varied to change process time. Coating thickness, air gap (0.5 mm), and DDR (around 18) are kept constant. The tie resins, described in Table 15.13, are similar to those used in the blown film study, except for a somewhat higher MI for processing in extrusion coating. The LDPE is a standard extrusion coating grade and the EVOH, a 44 mol% ethylene grade.

The peel strength is measured between the outside tie resin and EVOH layers. The pull speed is 305 mm/min in a T-peel configuration. The results are shown in Fig. 15.60. Like the blown film results, the peel strength increases with increasing process time. Morris [54] also finds the peel strength of

Table 15.12 Tie Resins Used in Coextrusion Blown Film Trial

Grade	Type	MI g/10 min	Melt Point (°C)	Freeze Point (°C)	Modulus (MPa)	Anhydride (%)
ADH1	LLDPE	1.1	125	109	455	Standard
ADH2	LLDPE	1.1	129	115	434	3X standard
ADH3	LLDPE	3.1	130	112	207	2X standard

LLDPE, *linear low density polyethylene.*

Reproduced with permission from Morris BA. The effect of processing variables on peel strength in coextruded blown film. In: SPE ANTEC conference; 1996.

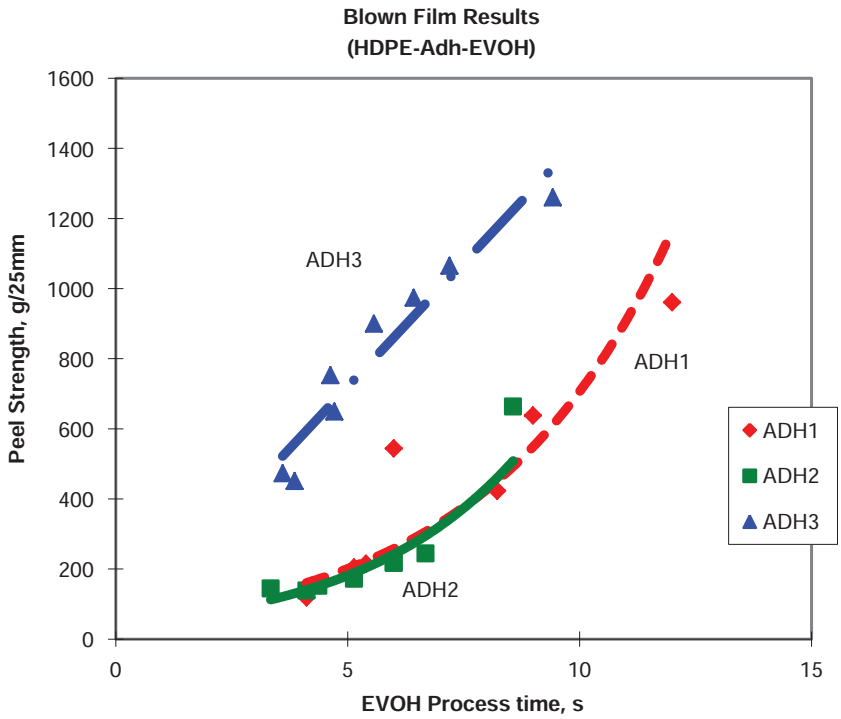


Figure 15.59 Peel strength to EVOH versus process time for blown film. The three-layer film has three frost lines, one for each layer. Here the process time is computed based on the EVOH frost line height, but the trends are the same for the process time computed on any of the frost line heights. *EVOH*, ethylene vinyl alcohol; *HDPE*, high density polyethylene.
Reproduced with permission from Morris BA. The effect of processing variables on peel strength in coextruded blown film. In: SPE ANTEC conference; 1996.

Table 15.13 Tie Resins Used in Coextrusion Coating Experiment

Grade	Type	Description
Tie A	LLDPE	Standard anhydride level
Tie B	LLDPE	3X standard anhydride level
Tie C	LDPE	2X standard anhydride, rubber modified

LLDPE, *linear low density polyethylene; LDPE, low density polyethylene.*
Data from Morris BA. Effect of time, temperature and draw down on interlayer peel strength during coextrusion coating, film casting and film blowing. In: TAPPI PLACE Conference; 2008.

LDPE–EAA copolymer increases with increasing process time in coextrusion coating.

While the peel strength increases with increasing process time for both processes and all six tie resins, there are differences that merit closer examination. In the blown film study, the peel strength curves for ADH1 and ADH2 fall on top of one another, even though ADH2 has three times as much chemical functionality. This suggests that the reaction kinetics between the EVOH and anhydride groups on the tie resins is faster than the process time. If the chemical reaction were the limiting factor, the peel strength curve would be expected to be shifted upward for ADH2, especially at short process times.

A stress mechanism is consistent with the results. As described in Chapter 14, increasing the process time in blown film decreases the stress during blowing. The process time is inversely related to the rate of strain. This can influence peel strength in a several ways. First, the reduced orientation resulting from the lower stress at long process time may change the physical properties of the film. As described in Sections 10.2.3 and 15.1.4.3, the bending and elongation of the peel arm during the peel test affect the peel energy. Chapter 14 describes how the coextrusion process affects such properties as elongation at break and yield strength. More directly, stress imparted during the orientation of the

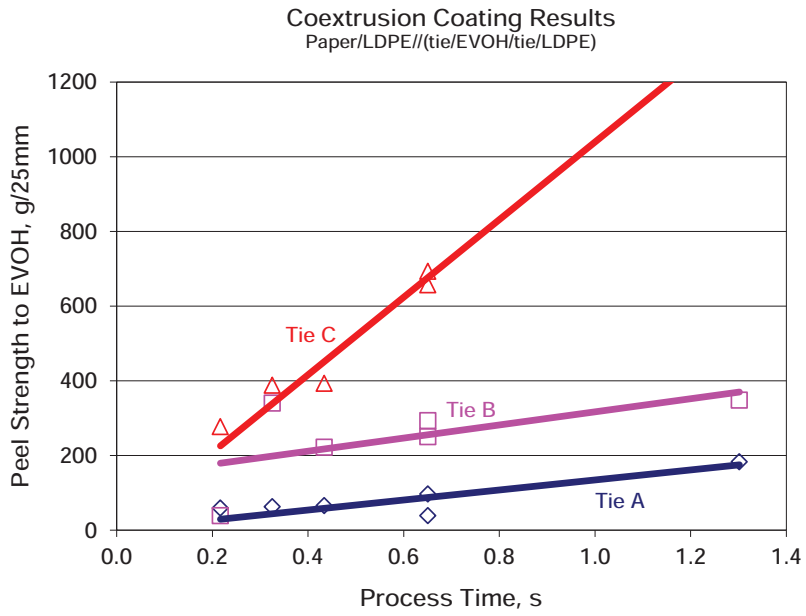


Figure 15.60 Peel strength to EVOH versus process time for coextrusion coating. *LDPE*, low density polyethylene; *EVOH*, ethylene vinyl alcohol.
From Morris BA. Effect of time, temperature and draw down on interlayer peel strength during coextrusion coating, film casting and film blowing. In: TAPPI PLACE Conference; 2008. Reproduced with permission from E. I. du Pont de Nemours and Company.

film can be frozen in during quenching if the polymer has not had time to relax. Wu [29] describes how residual stress generally reduces peel strength. Finally, subtle changes in the viscoelastic properties can affect the fracture energy—the energy required to create new interfacial area as the peel is made.

The work of Zhang [55] provides an example of the effect of residual stress on peel strength. The interlayer adhesion between various layers of a 20-layer coextruded sheet of repeating layers of polystyrene (PS) and polymethyl methacrylate (PMMA) is measured. These are two immiscible polymers with poor adhesion. The shear stress during extrusion is higher near the channel wall. Peel strength measurements on the quenched sheets show that the interfacial adhesion near the outside of the sheet, where the residual stress is highest, is about one-third lower than near the center.

The behavior of ADH3 in Fig. 15.59 further supports the stress hypothesis. The peel strength curve for this tie resin is parallel to the curves for ADH1 and ADH2 (same slope) but is shifted upward to higher levels of peel strength. This can be explained by examining the equation for fracture energy. As described by Eq. (15.33), the fracture energy is often written as the product of two factors, W_a and Φ. Here W_a represents the bonding at the interface (from either chemical interaction or diffusion), and Φ represents the local energy dissipated during deformation of the polymer as the peel front propagates through. Since Φ is a function of the viscoelastic properties of the polymer, a rubber-modified tie resin is likely to have a greater value of Φ than a nonrubber-modified one.

The anhydride level in ADH3 is intermediate to that of ADH1 and ADH2. Since ADH1 and ADH2 fall on the same curve, W_a is constant. The effect of rubber modification is to increase G_a through an increase in Φ. The curve for ADH3 is simply shifted upward with the same slope.

The coextrusion coating results have different behavior. Comparing tie A and B, increasing the anhydride level results in a shift upward to higher values of peel strength but does not change the slope of the curves. The rubber-modified tie C has a greater slope than the curves for tie A and B. Both of these observations suggest the formation of adhesive bonds may be limited by the timescales involved in extrusion coating (and, since the process is similar, for cast film). The first result, increasing anhydride level from tie A to tie B, directly supports this: if the extent of reaction is rate limited, increasing the reactant

concentration should result in more bonds forming. The greater extent of reaction shifts the curve for tie B upward. The timescale is much shorter in the coating process than for blown film. The reaction may not be complete in the time allowed by the process. Increasing the time should allow for more reaction (or diffusion in the case of nonreacting interfaces) to take place.

The second observation can be shown to support the reaction hypothesis by referring to Eq. (15.33). Unlike the blown film case, W_a increases with increasing process time due to more time for reaction. The product of an increasing W_a with a higher value of Φ due to rubber modification should result in a higher slope. This is exactly what is seen for tie C in Fig. 15.60.

15.2.2 Time, Temperature, and Area Creation

The differences highlighted by Figs. 15.59 and 15.60 are the result of different timescales and temperature profiles for the blown and coating/cast film processes, and how these relate to new interfacial area creation. Here, cast film and coextrusion coating are lumped together since they have similar timescales.

There are two timescales to consider—the time between the die exit and when the polymer first reaches its crystallization or solidification temperature (process time) and the time it takes crystallization to be completed once it has begun (crystallization time). The former has already been shown to be important. The latter may be important because up to the point where the polymer fully crystallizes there may be some mobility of the molecules that can affect adhesion. The process time for blown film is about an order of magnitude greater than for cast film and coextrusion coating: 5−10 s versus 0.2−1.5 s. This can be seen directly by comparing Figs. 15.59 and 15.60.

The crystallization time for blown film is related to the temperature plateau near the frost line as shown in Fig. 14.3. As described in Chapter 14, the cooling of the melt overshoots, resulting in a plateau in the temperature as the heat transfer from the surface cannot keep up with the exothermic heat generated by the crystallizing polymer. The width of this plateau was found to increase with increasing process time as shown in Fig. 14.7. While investigators have found that the polymer continues to crystallize beyond the plateau region, the mobility of the polymer chains is likely hindered enough to use the plateau time as the crystallization time. The study by Morris [56] described in Chapter 14 shows that the crystallization time is on the order of 2−5 s. This will vary depending on the inherent crystallinity of the polymer and whether inner bubble cooling is used.

The crystallization time is difficult to measure for cast film and extrusion coating. Instead, the melt curtain temperature and nip heat conduction models developed in Sections 15.1.2 and 15.1.3 are used. Once the melt curtain contacts the chill roll, heat is rapidly removed. The results of the model simulating the conditions of the coextrusion coating trial described in Section 15.2.1 are given in Fig. 15.61. The temperature drops only a few degrees in the air gap and very rapidly cools once contact with the chill roll is made. A close-up of the model calculations after contact with the chill roll is shown in Fig. 15.62. There is only a brief temperature plateau as the latent heat of crystallization is removed. The crystallization time is on the order of 5 ms, three orders of magnitude less than for blown film.

The increase in the interfacial area during drawing can dilute the density of bonds that have formed per unit area. The relationship between when the new area generation occurs, temperature (needed to form new bonds) and time available for new bond generation is important. The increase in the interfacial area is related to the elongation of the polymer during processing. As the polymer is stretched, its thickness decreases. To conserve mass, the area increases proportionally:

$$\frac{A(z)}{A_0} = \frac{X_0}{X(z)} \frac{W_0}{W(z)} \frac{\rho_0}{\rho_f} \tag{15.37}$$

where $A(z)$ = interfacial area as a function of distance from the die exit; A_0 = initial interfacial at die exit; $X(z)$ = thickness of the melt curtain as a function of distance from the die exit; W_0 = initial width at die exit for flat dies and initial circumference for tubular dies; $W(z)$ = width of the melt as a function of distance from the die exit.

For the rest of the analysis, the density ratio is ignored. For polyolefins, the density ratio is typically 0.7−0.8.

For extrusion coating and cast film, a simple mass balance shows that the area ratio is equal to the DDR;

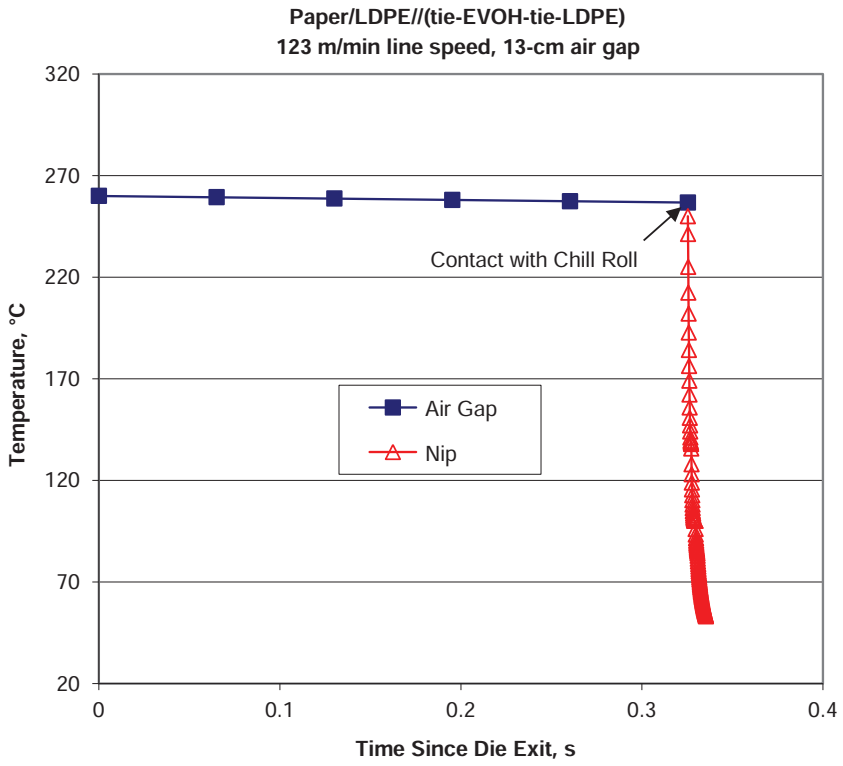


Figure 15.61 Calculation of temperature profile in the air gap and nip for the coextrusion coating experiment described in Fig. 15.60. *EVOH*, ethylene vinyl alcohol; *LDPE*, low density polyethylene.
From Morris BA. Effect of time, temperature and draw down on interlayer peel strength during coextrusion coating, film casting and film blowing. In: TAPPI PLACE Conference; 2008. Reproduced with permission from E. I. du Pont de Nemours and Company.

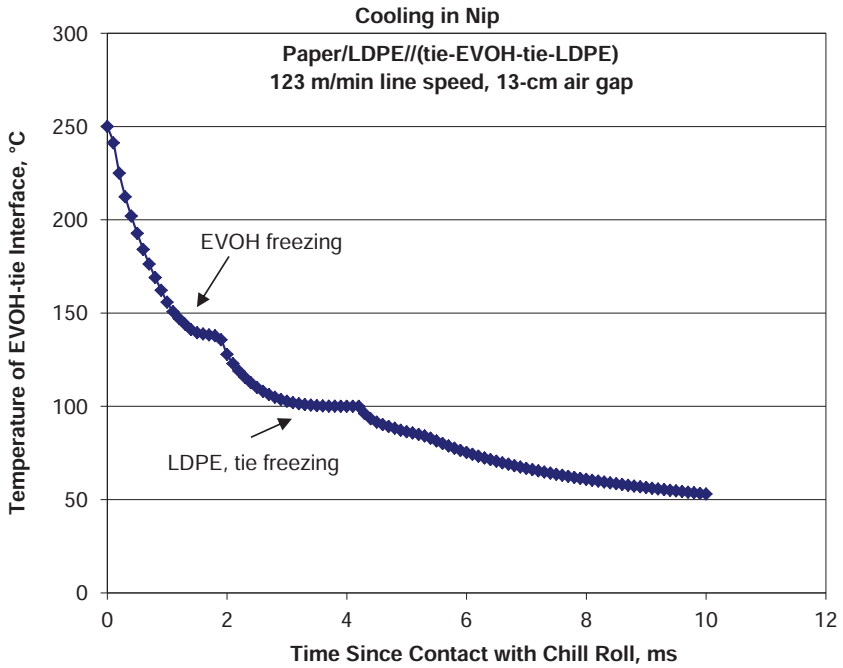


Figure 15.62 Close-up of temperature profile in the nip from Fig. 15.61 computed from heat conduction model. *EVOH*, ethylene vinyl alcohol; *LDPE*, low density polyethylene.
From Morris BA. Effect of time, temperature and draw down on interlayer peel strength during coextrusion coating, film casting and film blowing. In: TAPPI PLACE Conference; 2008. Reproduced with permission from E. I. du Pont de Nemours and Company.

for blown film, it is equal to the product of the BUR and TUR or DDR:

$$A_f/A_o = \text{DDR(extrusion coating and cast film)} \quad (15.38)$$

$$A_f/A_o = (\text{DDR})(\text{BUR})(\text{blown film}) \quad (15.39)$$

Increasing the DDR directly increases the amount of the new interfacial area created after the die exit. Fig. 15.63 shows the calculated change in the interfacial area in the air gap for the extrusion coating trial. Superimposed on the graph is the temperature profile from Fig. 15.61. The interfacial area is created while the polymer is still very hot, which is important for bond formation and interlayer diffusion. The creation of new interfacial area, however, exponentially increases with distance from the die exit (z) so that a large increase in area occurs just before the polymer contacts the chill roll ($z/L = 1$). From Fig. 15.61, once contact with the chill roll is made, quenching occurs quickly, crystallization time is short, and there is little time for new bond formation.

Chapter 14 describes a study by Morris [56] that uses an IR thermometer and video techniques to measure the temperature, velocity, and bubble diameter profiles along the bubble in the blown film process. Data for a coextrusion of (HDPE−EVOH) from this study is shown in Fig. 15.64, along with the calculation for the area ratio, which is the product of the bubble diameter and velocity profiles. The area ratio exponentially increases with distance from the die exit, similar to what was found for cast film/extrusion coating. The increase in interfacial area ceases at around $z/L = 1$, where L is the frost line height for the EVOH layer (which freezes first). The temperatures are much lower at this point than what was found in the extrusion coating example. The time available for bonding, however, is much longer. The HDPE layer does not start to freeze until about $z/L = 1.5$ or about 3 s after the interfacial area stops increasing. If a tie layer were present, it would not start freezing until even later since it would typically have an even lower freezing point. This is because in coextrusion blown film, the bubble shape and velocity profiles are determined by the layer that freezes first (Section 14.1.2). This can have an impact on the

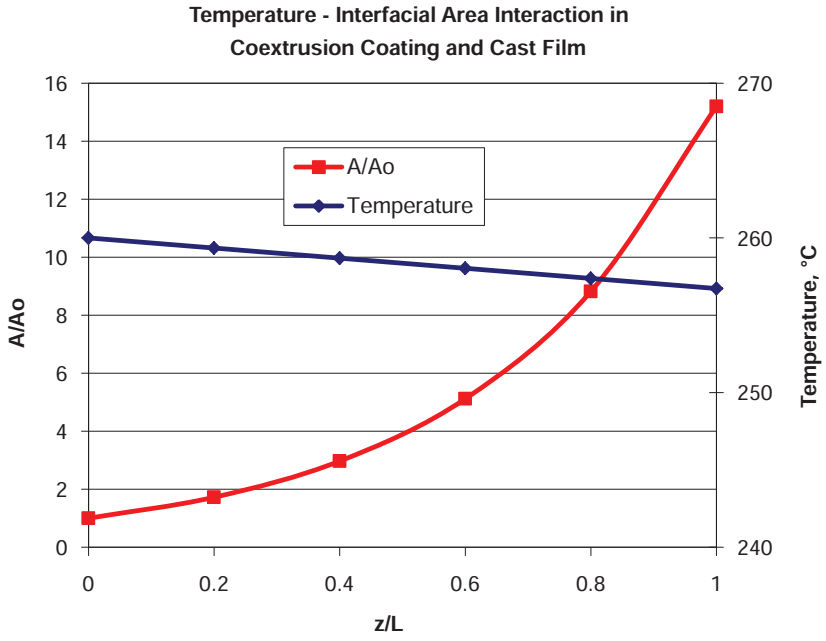


Figure 15.63 New interfacial area creation and temperature in the air gap in coextrusion cast film or coextrusion coating. The quantity z/L is the dimensionless distance from the die exit (L = air gap distance).
From Morris BA. Effect of time, temperature and draw down on interlayer peel strength during coextrusion coating, film casting and film blowing. In: TAPPI PLACE Conference; 2008. Reproduced with permission from E. I. du Pont de Nemours and Company.

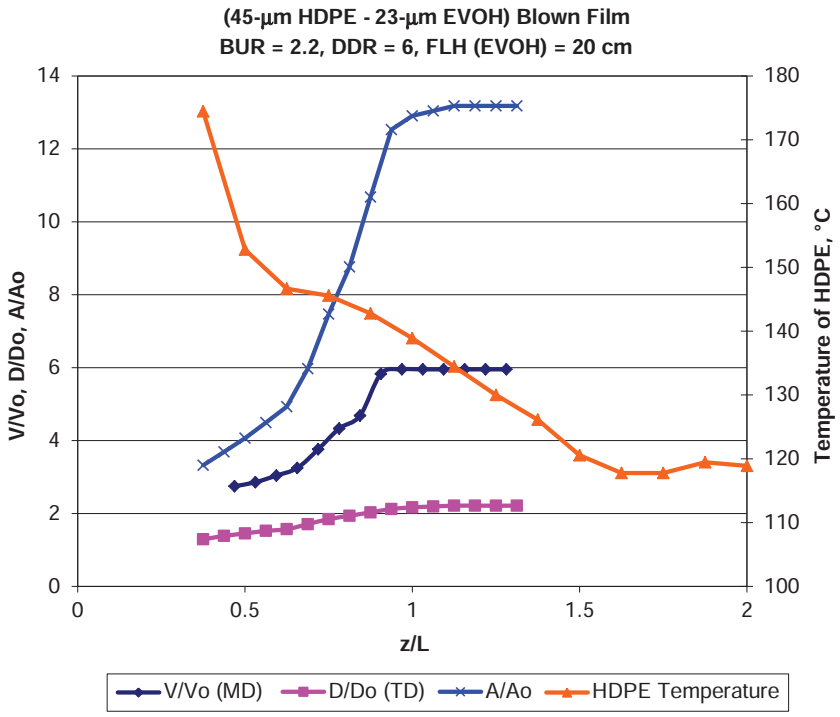


Figure 15.64 Temperature, bubble diameter, velocity, and new interfacial area creation in blown film as a function of distance from the die exit. Based on data from Morris [56]. z = distance from die exit and L = EVOH frost line height. *BUR*, blown up ratio; *DDR*, draw down ratio; *EVOH*, ethylene vinyl alcohol; *HDPE*, high density polyethylene; *MD*, machine direction; *TD*, transverse direction.
From Morris BA. Effect of time, temperature and draw down on interlayer peel strength during coextrusion coating, film casting and film blowing. In: TAPPI PLACE Conference; 2008. Reproduced with permission from E. I. du Pont de Nemours and Company.

physical properties of the film. It may also have an effect on adhesion, shifting the point where the interfacial area ceases to grow to a region of higher temperature and, hence, greater molecular mobility and reactivity. This may allow more time for adhesion to take place before solidification sets in. Since many commercially important coextruded blown films involve a barrier polymer with a high freezing point (eg, PA or EVOH) and a polyolefin-based tie resin with a much lower freezing point, this effect may be fairly widespread.

To summarize, cast film/extrusion coating is characterized by high temperatures and an exponential increase in interfacial area in the air gap followed by a very rapid freezing of the polymer layers. There may be little time for bond formation in the newly created interfacial regions. Blown film also shows a rapid increase in the interfacial area near the frost line of the layer that freezes first. The time available for bonding before crystallization is complete is several orders of magnitude longer than for cast film/extrusion coating. These differences in time, temperature, and area creation during drawing may help explain the differences in the behavior of the peel strength versus process time curves. The development of adhesion in these processes is complex, and other factors besides the reaction kinetics and diffusion also likely play a role, including the development and relaxation of stress and orientation during drawing and quenching and the effect these may have on crystallinity.

The work has several practical implications for converters of coextrusion cast film or extrusion coating. One is that tie resin formulations for cast film or extrusion coating may require higher levels of functionality than those used in blown film. The work shows that premium tie resins with rubber and other modifiers may be particularly beneficial for these processes.

Song [57] provides a formula for determining the effective contact time between layers during

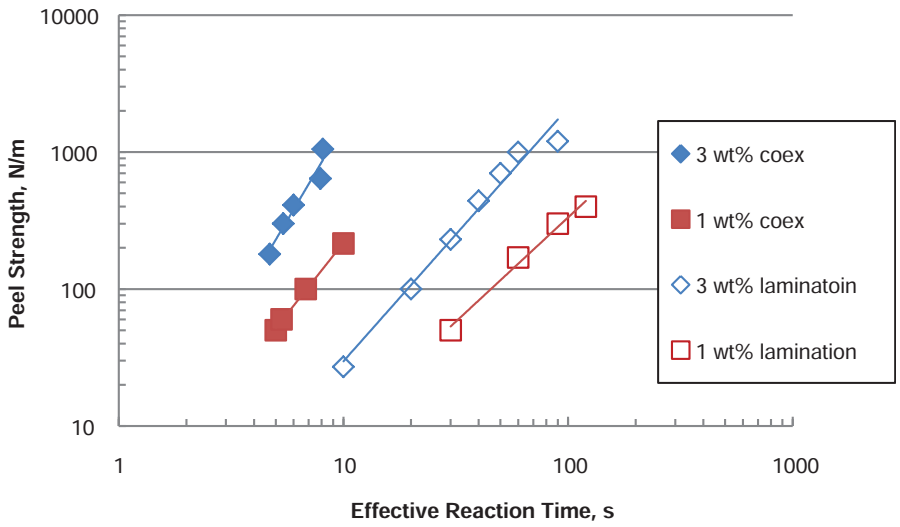


Figure 15.65 Peel strength versus effective contact time for bonding of polyurethane to an amine-modified polyethylene via coextrusion and thermal lamination. Weight percent refers to the amount of amine functionality on the polyethylene.

Reproduced with permission from Song J, Ewoldt RH, Hu W, Silvis HC, Macosko CW. Flow accelerates adhesion between functional polyethylene and polyurethane. AIChE J 2011;57:3496–506.

coextrusion taking into account the bulk motion (advection) and interfacial area creation:

$$t_{\text{eff}} = \frac{1}{Q} e^{\int_0^z f(z)dz} \left\{ \int_0^z e^{-\int_0^z f(z)dz} X(z)W(z)dz \right\} \tag{15.40}$$

where t_{eff} = effective reaction time or contact time, z = machine direction, $X(z)$ = thickness, $W(z)$ = width, $f(z)$ = areal dilation.

The areal dilation is given by

$$f(z) = \frac{1}{X(z)} \frac{dX(z)}{dz} \tag{15.41}$$

Eq. (15.40) is derived from a conservation expression with the simplifying assumption of plug flow.

Song illustrates the approach by considering the reaction time in a sheet line, calculating the contributions from the feedblock to the die entrance, the spreading in the die body, flow in the die land, and finally the draw down from the die exit to the chill roll. Laboratory results for a coextrusion of polyurethane with an amine-modified polyethylene are presented. The urethane reacts with the amine groups to form a block copolymer at the interface. The peel strength is found to correlate with the total reaction time, as is shown in Fig. 15.65. As is described in Chapter 10, Song also measures the number of reacted groups at the interface and finds the density of bonds per area increases with the effective reaction time.

A significant portion of the effective contact time in Song's experiment occurs in the draw down region after the die exit. They find the peel strength decreases with increasing DDR, as shown in Fig. 15.66. In these experiments, the volumetric flow rate, Q, is held constant and DDR is increased by increasing the line speed, v_f. Although Song's effective contact time is not exactly the same as TIAG or t_f (Eq. (15.4)), the relationship between TIAG and DDR can be used to understand the trend in Fig. 15.66. Since DDR = v_f/v_0 and $Q = X_0 W v_0$, Eq. (15.1) can be rewritten in terms of DDR:

$$\text{TIAG} = \left[\frac{LX_0W}{Q}\right] \frac{1}{\text{DDR}} \tag{15.42}$$

where TIAG = time in air gap, L = air gap, X_0 = die gap, Q = volumetric flow rate, DDR = draw down ratio.

Under the conditions of Song's experiment, the term in brackets is constant. The peel strength is inversely related to DDR, which in turn is inversely related to TIAG. This suggests that peel strength increases with TIAG. Replotting the data in terms of

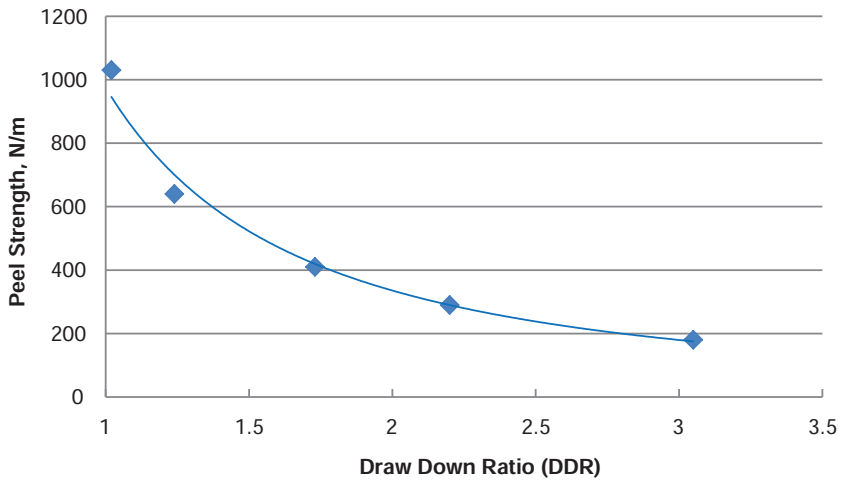


Figure 15.66 Effect of draw down ratio (DDR) on peel strength performance for a coextrusion of polyurethane and amine-modified PE (polyethylene).
Data from Song J, Ewoldt RH, Hu W, Silvis HC, Macosko CW. Flow accelerates adhesion between functional polyethylene and polyurethane. AIChE J 2011;57:3496–506.

TIAG and t_f in Fig. 15.67 confirms this. This is the same relationship found by Morris [7].

15.2.3 Process Time Master Curve

The peel strength versus process time curves for blown film and coextrusion coating in Figs. 15.59 and 15.60 have different timescales and slopes. Other results reported by Morris [52,53] indicate that different tie resins have different slopes. This is illustrated in another set of experiments by Morris [7,58,59]. Two sets of films are made, one by blowing and the other by casting.

The blown film study is conducted using the same equipment and procedures as in the original work [52]. A three-layer blown film line equipped with a 76 mm (3 in.) Brampton Slimline (stackable-type) die with a 50 mm (2 in.) opening and an Uni-Flow dual lip air ring is used. Three 25 mm (1 in.) diameter extruders feed the die. No inner-bubble cooling is used. Melt temperature, die gap (1 mm), final film thickness, and BUR (2:1) are kept constant. Process time is varied by changing frost line height (through adjusting quench air velocity and temperature) and haul-off speed.

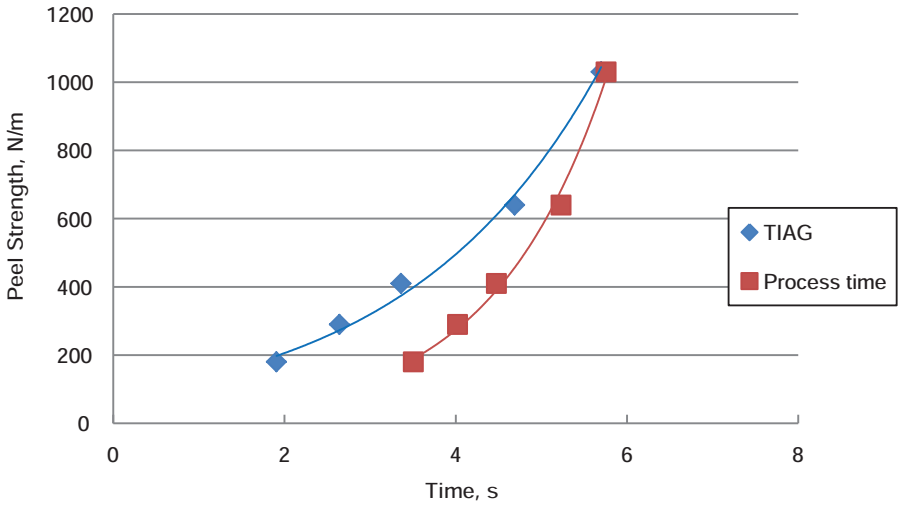


Figure 15.67 Data from Fig. 15.64 replotted in terms of process time. *TIAG*, time in the air gap.
Data from Song J, Ewoldt RH, Hu W, Silvis HC, Macosko CW. Flow accelerates adhesion between functional polyethylene and polyurethane. AIChE J 2011;57:3496–506.

The test structure is (HDPE−tie−EVOH). The layer thicknesses are 37.5/12.5/20 μm (1.5/0.5/0.8 mils), respectively. Final barrel temperatures are 230°C for all three extruders, as is the die temperature. The HDPE has a density of 960 kg/m^3, an MI of 0.75 g/10 min (190°C/2160 g), melting point (T_m) of 137°C, and freezing point (T_c) of 115°C. The EVOH is a 32 mol% ethylene grade with an MFR (210°C/2160 g) of 3.0 g/10 min, T_m of 185°C, and T_c of 157°C. A description of the tie resins is given in Table 15.14. All are anhydride-modified polyethylene or ethylene copolymers.

The cast film samples are made on a coextrusion coating line. The 50 μm (2 mil) structure is (LDPE−tie−EVOH−tie−LDPE) with nominal layer distribution of (13−4−6−4−23 μm). The film is coextrusion coated onto 48-gauge (12 μm) OPET with the thinner LDPE side on the OPET surface. (The OPET is stripped away from the film before testing.) The tie and LDPE extruders are set at 260°C (500°F) and the EVOH extruder at 232°C (450°F). The Cloeren edge bead reduction die is set at 252°C (485°F). The air gap is varied from 13−25 cm (5−10 in.) and line speed from 122 to 244 m/min (400−800 feet per minute). The die gap is 0.69 mm (27 mils). The LDPE has a density of 0.918 g/cc and MI of 7 g/10 min. The EVOH contains 44 mol% ethylene and has a MI of 5.5 g/10 min. The tie resins are described in Table 15.14.

For the blown films, peel strength is measured in the MD between the EVOH and tie layer. One-inch strips are pulled in a T-peel configuration at a crosshead speed 305 mm/min. Results reported are an average of five determinations.

The cast films are too thin to conduct standard peel tests. The LDPE is too stretchy and breaks before the pull tabs can be established. Instead, the cast films are separated from the OPET and heat-sealed lengthwise (in the MD) at the thin LDPE−LDPE interface at 132°C (270°F), 0.5 s dwell, and 0.27 MPa (40 psi). Values of peel strength represent an average of at least three 1/2-in. wide strips cut from the sealed area and tested at a pull rate of 150 mm/min (6-in. per minute), corrected to reflect 25-mm (1-in.) wide strips. Testing is carefully observed to note when the LDPE seal layers break through to the tie−EVOH interface and seal strength recorded from that point forward. Iodine staining is used to confirm the failure mode. The long seal length is necessary in order to allow time for the seal to break through to the weakest interface.

The results from the two trials are plotted in Fig. 15.68. The curves have distinct characteristics:

- As in previous studies, the peel strength to EVOH increases with increasing process time.
- The process time for blown film is longer than for cast film.
- In the blown film results, tie resins based on linear polymer (LLDPE) give a steeper slope than those based on LDPE or EVA, which contain long chain branching (LCB).

Table 15.14 Tie Resins Used in Coextrusion Blown and Cast Film Study

Resin	Base Resin	Process	Melt Index[a] (g/10 min)	Young's Modulus (MPa/kpsi)
Tie 1	EVA (9% VA)	BF	1	132/19
Tie 2	EVA (25% VA)	BF	2	34/5
Tie 5	LLDPE	BF	1	455/66
Tie 6	mLLDPE	BF	1	414/60
Tie 7	LLDPE (rubber modified)	BF, CF	3	338/49
Tie 8	LLDPE	CF	4	428/62

BF, *blow film process;* CF, *cast film process;* EVA, *ethylene vinyl acetate;* LLDPE, *linear low density polyethylene;* mLLDPE, *metallocene LLDPE.*

[a] *2160 g/190° C.*

Reproduced with permission from Morris BA. Effect of process and material parameters on interlayer peel strength in coextrusion coating, film casting and film blowing. J Plastic Film Sheeting 2010;26:343−76.

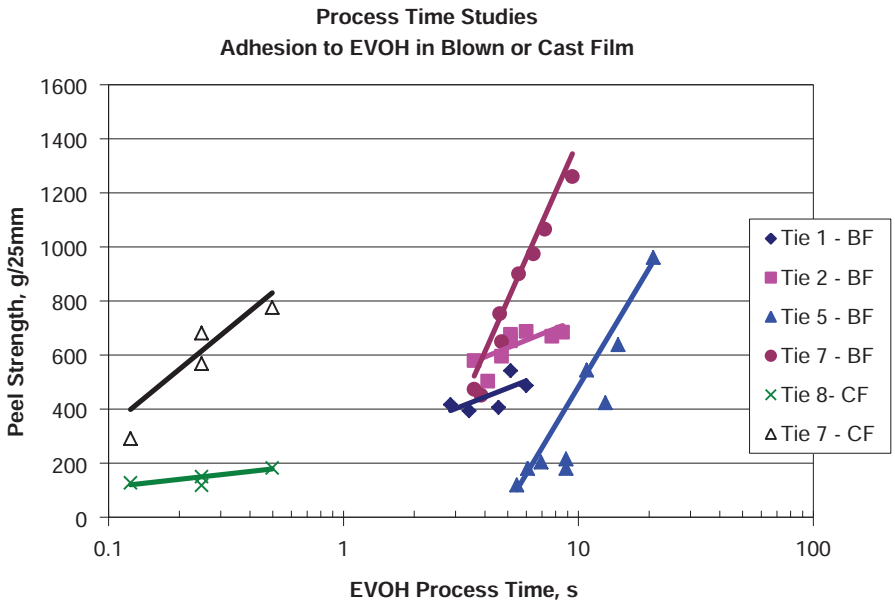


Figure 15.68 Peel strength to ethylene vinyl alcohol (EVOH) results from blown and cast film coextrusion trial. *Reproduced with permission from Morris BA. Effect of process and material parameters on interlayer peel strength in coextrusion coating, film casting and film blowing. J Plastic Film Sheeting 2010;26:343–76.*

- Lower modulus tie resins of the same chemistry have curves that are shifted upward to higher values of peel strength (compare tie 5 with 7 and tie 1 with 2).
- Tie resins of similar composition exhibit a steeper slope in blown film than in cast film (compare tie 5 with 8 and tie 7 with 7).

At first glance, each tie resin and process has its own peel strength versus process time curve, making general use of this information difficult. The trends in the data, however, suggest a way to transform the data into a useful master curve using concepts from a stress analysis.

The process time in blown and cast film is inversely proportional to the rate of strain (Sections 14.1.2 and 15.1.2.2). Increasing the process time decreases stress by decreasing the rate of strain. The blown film results suggest that the tie resins based on linear polyethylene are more sensitive to changes in stress than the branched polymers since the slopes of the linear polyethylene tie resins are steeper. The influence of LCB and broader MWD on the response of the peel strength to process time is likely related to differences in elongational viscosity and relaxation behavior. Elongational viscosity is known to increase with increasing LCB due to entanglement effects. Likewise, the ability of a polymer to relax is hindered by LCB. An estimate of average relaxation time can be obtained from the inverse of the frequency where the storage modulus (G') and the loss modulus (G'') are equal in dynamic mechanical measurements (DMAs). Results of DMA measurements at 190°C for three of the tie resins are given in Table 15.15. The EVA-based tie resin has about an order of magnitude larger relaxation time than the two LLDPE-based ones. The flatness of the peel strength versus process time curve for the EVA-based tie resin may be due to the inability of the EVA to respond to greater times for relaxation during the process.

The Deborah number (*De*) is introduced in Eq. (15.5) as the relaxation time of the polymer divided by the process time. The *De* number relates to the ability of the polymer to react to stresses during the timescale of the process. Large *De* signifies the polymer behaves like an elastic solid, whereas small *De* indicates the polymer acts like a viscous fluid. Relaxation time is a function of temperature, as given by an Arrhenius relationship:

$$t_{\text{relaxation}}(T) = a_T(T)t_{\text{relaxation}}(T_{\text{ref}}) \qquad (15.43)$$

where $a_T(T) = e^{E_a/RT} - e^{E_a/RT_{\text{ref}}}$; T = characteristic temperature of the process [K]; T_{ref} = reference

Table 15.15 Relaxation Time Data for Three Tie Resins From Fig. 15.67

Tie	Base Resin	Frequency at $G' = G''$ s^{-1}	Estimated t_{relax} (190°C) s
Tie 1	EVA	7.5	0.130
Tie 5	LLDPE	100	0.009
Tie 6	mLLDPE	140	0.007

EVA, *ethylene vinyl acetate;* LLDPE, *linear low density polyethylene.*
Reproduced with permission from Morris BA. Effect of process and material parameters on interlayer peel strength in coextrusion coating, film casting and film blowing. J Plastic Film Sheeting 2010;26:343–76.

temperature [K], 190°C = 463 K; R = gas constant; E_a = activation energy.

The characteristic temperature for the blown film process is taken to be 125°C. This is based on the analysis in Chapter 14 showing that the maximum rate of elongation occurs near the frost line of the layer that freezes first in the coextrusion. For this structure, the EVOH freezes first and has a freezing temperature of around 125°C where the tie resin is still molten. The characteristic temperature for the cast film structures is taken to be 260°C. This is based on the model calculations presented in Fig. 15.61. Using Eq. (15.43) with an activation energy of 30 kJ/mol, relaxation times for each of the tie resins at the characteristic temperature for the cast and blown film processes are computed and recorded in Table 15.16.

Morris [7,59] finds that all the curves from Fig. 15.68 collapse onto a single master curve when the x- and y-axes are transformed, as shown in Fig. 15.69. For the x-axis, the process time is divided by the relaxation time of the tie resin (at the characteristic temperature of the process). This should be recognized as the inverse of the Deborah number. The increase in peel strength with increasing $1/De$ indicates that the adhesion increases as the polymer becomes more viscous and less elastic in nature.

The vertical shift factors for the y-axis were chosen to obtain a good fit. Fig. 15.70 shows that these vertical shift factors correlate well with the Young's modulus of the tie resin. This suggests that the y-axis is related to the peel strength times the modulus. Other material properties such as yield strength may also correlate with the vertical shift factors but no attempt was made to establish such a relationship.

The origin of the vertical shift factors is likely from the local viscoelastic energy dissipation of the polymer. A more explicit equation is derived by equating the energy balance from Eq. (15.33) with a

Table 15.16 Characteristic Relaxation Time Data for Tie Resins

Tie	Base Resin	Process	t_{relax} (s)	Vertical Shift Factor
Tie 1	EVA	BF	0.464	1.25
Tie 2	EVA	BF	0.464	0.67
Tie 5	LLDPE	BF	0.032	25
Tie 6	LLDPE	BF	0.025	20
Tie 7	LLDPE	BF	0.018	5
Tie 7	LLDPE	CF	0.0018	5
Tie 8	LLDPE	CF	0.0032	25

Data are shifted to 125° C for blown film and 260° C for cast film using Eq. (15.43).
EVA, *ethylene vinyl acetate;* LLDPE, *linear low density polyethylene.*
Reproduced with permission from Morris BA. Effect of process and material parameters on interlayer peel strength in coextrusion coating, film casting and film blowing. J Plastic Film Sheeting 2010;26:343–76.

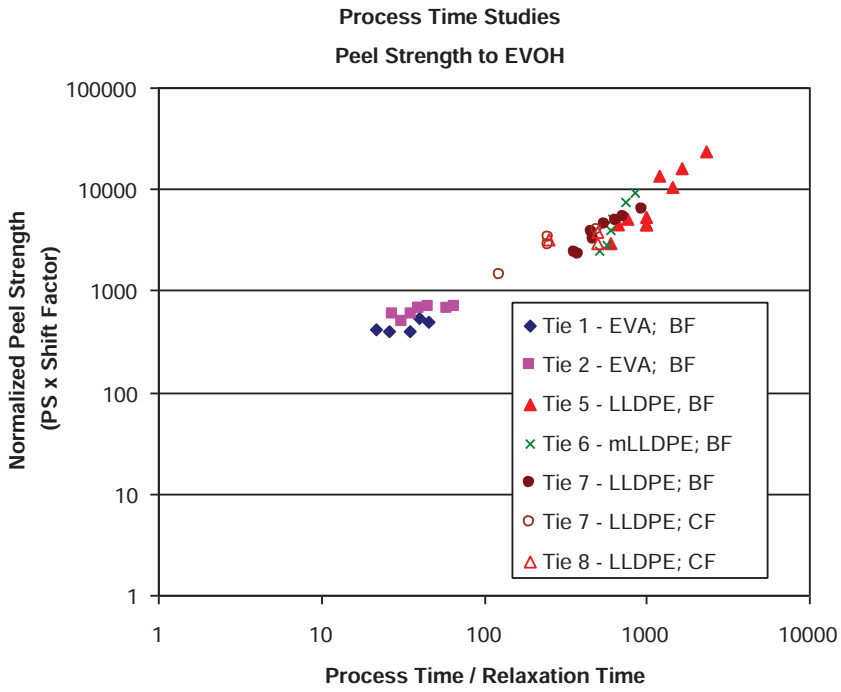


Figure 15.69 Transformed data into master peel strength versus process time curve. *EVA*, ethylene vinyl acetate; *LLDPE*, linear low density polyethylene.
Reproduced with permission from Morris BA. Effect of process and material parameters on interlayer peel strength in coextrusion coating, film casting and film blowing. J Plastic Film Sheeting 2010;26:343–76.

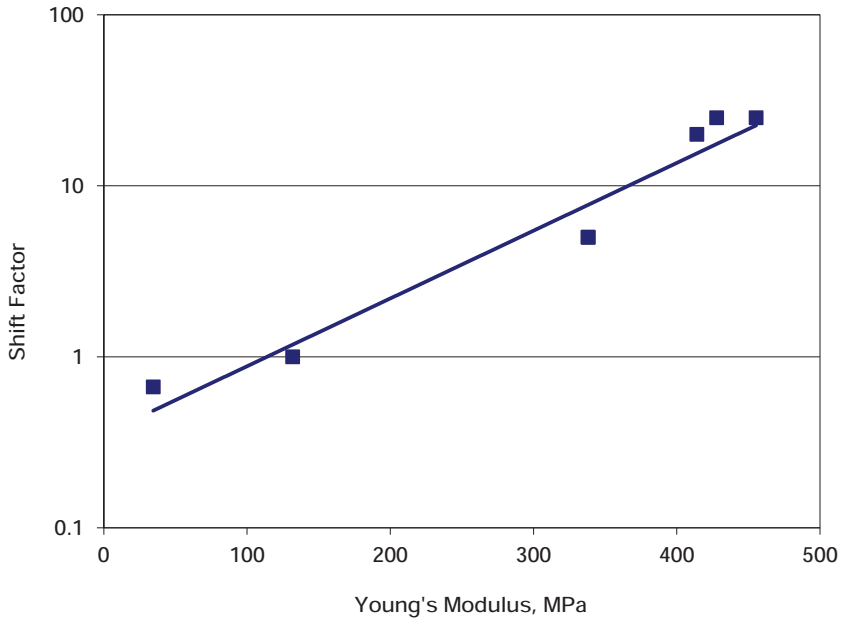


Figure 15.70 Vertical shift factors for Fig. 15.69 plotted versus Young's modulus. Modulus was measured from tensile bars.
Reproduced with permission from Morris BA. Effect of process and material parameters on interlayer peel strength in coextrusion coating, film casting and film blowing. J Plastic Film Sheeting 2010;26:343–76.

force balance (stress analysis) on the peel test. The result, derived in Section 10.2.3, is

$$K_I^2 = G_a E \tag{15.44}$$

where K_I = stress intensity factor, G_a = fracture energy, E = Young's modulus.

K_I is equal to the maximum stress at the crack tip (or peel front) divided by the imposed stress. Fracture occurs when the maximum local stress equals the local cohesive or adhesive strength. Typically, failure at the interface occurs at imposed loads that are considerably less than the idealized strength of the interface. The stress intensity factor characterizes the amplification of the stresses at the crack tip that leads to failure. Thus the stress intensity factor takes into account the adhesive strength at the interface and the material parameters of the tie resin.

There are a number of limitations to the analysis. The relaxation times are estimates based on linear viscoelastic measurements when elongation flow dominates in these processes. The thickness of the tie and other layers likely play a role. The tie resins themselves are often complex multicomponent alloys that defy the simple characterizations given here. The chemical reaction rate effects found to be important in cast film (Section 15.2.1) are ignored, although Eqs. (15.43) and (15.44) may implicitly take these into account.

Nevertheless, Fig. 15.69 represents a powerful tool toward better understanding the effect of process and material parameters on adhesion in coextrusion. For the first time, a correlation for peel strength performance in similar films made on two very different processes has been obtained. The approach takes into account the differences in the stress–strain history (through t_f and $t_{relaxation}$), temperature (through $t_{relaxation}$), and time (through t_f) of the process as well as differences in molecular architecture (LCB, MWD, crystallinity, and modulus) of the tie resin (through E and $t_{relaxation}$). The work suggests that stress may be as important as the kinetics of chemical reaction and diffusion at the interface for determining the process time response of the cast film process. The work shows that increasing output (inversely related to process time) reduces peel strength, but that this effect can be mitigated to some extent by the appropriate choice of the tie resin (modulus and relaxation time). The work also points to how tie resins might be optimized for a given process and set of processing parameters.

15.2.4 Flow Accelerated Reaction Rate

Song [57] finds that flow accelerates the chemical interaction at the interface in coextrusion. The formation of block copolymers through reaction at the interface between polyurethane and amine-modified polyethylene is studied in both coextrusion and thermal lamination. The coextrusion results are discussed in Section 15.2.2, where the peel strength is shown to correlate with effective reaction time. The thermal lamination experiments are conducted using a laboratory press at different hold-up times, followed by quenching in ice water. The lamination is conducted so that the layers are not squeezed down in thickness during the process. The results for the polyurethane–amine-modified PE are shown in Fig. 15.65 for both the coextrusion and thermal lamination. The time to achieve a given peel strength value is two orders of magnitudes shorter for the coextrusion. Song directly relates peel strength to the formation of block copolymers at the interface using XPS, as described in Section 10.3.4.

In a follow-up experiment, Song [60] coextrudes PA6 with maleic anhydride-grafted HDPE (HDPE-g-MAH) using a coextrusion sheet line with two die configurations. In one die, the flow is compressive—as the polymer is spread to its final width it is also compressed in the thickness dimension. This is typical of a standard cast film die. The second die is designed to be noncompressive. Thermal laminations of the same materials are also produced using a laboratory press.

The PA6/HDPE-g-MAH layer combination is typical of many flexible packaging structures. The anhydride reacts with the amine end groups on the PA6 to form an imide. Like the polyurethane–amine modified PE combination, XPS shows that formation of an in situ block copolymer through the formation of the imide group correlates with the development of peel strength at the interface. The peel strength is found to develop 100 times faster in the compressive die than the noncompressive die, suggesting the formation of the block copolymer is accelerated by the compressive flow. The reaction rate in the compressive die is about 80 times that found in the thermal lamination experiment. The reaction rate of the noncompressive die is about the same as lamination. Scanning electron microscopy (SEM) shows similar behavior in the morphology for the compressive coextrusion and longtime lamination (high peel

strength). Adhesion measurements, XPS, and SEM all show evidence of acceleration of adhesion in coextrusion with the compressive die. Furthermore, experiments on the lab press where the thickness of the laminate is reduced during lamination (compression) have accelerated reaction rates comparable to the coextrusion with the compressive die.

Song discusses possible causes for the accelerated reaction rate during coextrusion:

- Shear stress. The interface between the two layers is deliberately placed near the centerline of the flow channel where the shear stress is zero and there is no mixing. This eliminates shear stress as a factor. The DDR is also small, suggesting that elongational stress is also negligible.
- Pressure. This is not expected to be a significant effect for liquid−liquid reactions over the pressure range experienced in their experiments.
- Crystallinity at interface. Song measures crystallinity and finds no significant difference in samples made with the different dies. Also, the stress−strain curves for coextrusion and lamination samples are nearly identical.
- Diffusive flux. Compressive flow reduces the diffusion length scale. A dimensionless group analysis (Damkohler number, the ratio of reaction rate to diffusion rate) shows, however, that this change is not substantial enough to change the regime from reaction limited to diffusion limited. They conclude that this is not the cause.
- Flow-induced orientation. This is known to induce crystallization kinetics. Also "flow stress and strain is known to break and promote reactions of groups in the polymer backbone."

Song expands upon the last point by computing the Weissenberg number (*Wi*), which is equal to the shear rate times the relaxation time of the polymer. The orientation of the chains is expected to increase with increasing *Wi* and total strain [ln(DDR)]. The DDR ranged from 1.07 to 3.08 in their experiment. The *Wi* number, however, is substantially higher in the compressive die (83) than the noncompressive die (2.7).

Song speculates that the enhanced reaction rate during orientation is the result of functional polymers being driven to the interface and stretched, increasing the collision probability of the functional groups. Song cites examples from the literature that indicates the compressive/elongational flow in coextrusion or polymer compounding accelerates the reaction rate at the interface. Macosko [62] shows the reaction rate between components of a heterogeneous blend during mixing is 1000-fold greater than under quiescent conditions and still around 300-times greater after accounting for the increase in interfacial area. Botros [63] reports similar behavior when mixing an anhydride-functionalized tie resin and EVOH. The diffusion rate near an interface is an order of magnitude slower than in the bulk [61]. Flow seems to force the reactive species to penetrate into the interface and increase the concentration of reactive species at the interface.

References

[1] Andersson T, Wesslen B. Degradation of LDPE, LLDPE and HDPE in film extrusion. In: TAPPI PLACE conference; 2004.
[2] Andersson T, Stalbom B, Wesslen B. Degradation of polyethylene during extrusion. II. Degradation of low-density polyethylene, linear low-density polyethylene, and high density polyethylene in film extrusion. J Appl Polym Sci 2004;91:1525−37.
[3] Gregory BH. Extrusion coating, a process manual. Victoria, Canada: Trafford; 2005. p. 73−92.
[4] Antonov V, Soutar A. Foil adhesion with copolymers: time in the air gap. In: TAPPI 1991 polymers, laminations & coatings conference proceedings. Atlanta: TAPPI Press; 1991. p. 553.
[5] Morris BA. Adhesion in extrusion coating: time in the air gap revisited. In: TAPPI PLACE conference; 2016.
[6] Morris BA. The influence of stress on peel strength of acid copolymers to foil. In: TAPPI polymers, laminations and coatings conference; 1998. Also Morris BA. J Reinf Plast Comp 2002;21:1243−55.
[7] Morris BA. Effect of process and material parameters on interlayer peel strength in coextrusion coating, film casting and film blowing. J Plastic Film Sheeting 2010;26: 343−76.

[8] Morris BA. Understanding why adhesion in extrusion coating decreases with diminishing coating thickness. J Plastic Film Sheeting 2008;24:53–88.
[9] Canning K, Bian B, Co A. Film casting of a low density polyethylene melt. In: SPE ANTEC conference; 1999. p. 386–90.
[10] Andersson T, Wesslen B, Sandstrom J. Degradation of low density polyethylene during extrusion. I. Volatile compounds in smoke from extruded films. J Appl Polym Sci 2002;86:1580–6.
[11] Andersson T, Nielsen T, Wesslen B. Degradation of low density polyethylene during extrusion. III. Volatile compounds in extruded films creating off-flavor. J Appl Polym Sci 2005;95:847–58.
[12] Andersson T, Holmgren MHJ, Nielsen T, Wesslen B. Degradation of low density polyethylene during extrusion. IV. Off-flavor compounds in extruded films of stabilized LDPE. J Appl Polym Sci 2005;95:583–95.
[13] Andersson T, Wesslen B. Degradation of low density polyethylene during extrusion. V. Effects of oxygen content in air gap. J Appl Polym Sci 2005;96:1767–75.
[14] Gugumus F. Physico-chemical aspects of polyethylene processing in an open mixer 6. Discussion of hydroperoxide formation and decomposition. Polym Degrad Stab 2000;68:337–52.
[15] Sherman PB. Ozonation of polymer melt for improved adhesion. In: Bezigian, editor. Extrusion coating manual. 4th ed. Atlanta (GA): TAPPI Press; 1999. p. 75–88.
[16] Laiho E, Ylanen T. Flame, corona, ozone – do we need all pretreatments in extrusion coating. In: TAPPI polymers, laminations & coatings conference; 1997. p. 93.
[17] Briggs D, Brewis D, Lonieczko M. X-ray photoelectron spectroscopy studies of polyethylene-aluminum laminates. Eur Polym J 1978;14:1.
[18] Hansen M, Finlayson M, Vaughn M. Characterizing aluminum adhesion for low-density polyethylene. In: TAPPI polymers, laminations & coatings conference; 1991. p. 349.
[19] Brewis D, Briggs D. Adhesion to polyethylene and polypropylene. Polymer 1981;22:7.
[20] Hjertberg T, Sultan B, Sorvik E. The effect of corona discharge treatment of ethylene copolymers on their adhesion to aluminum. J Appl Polym Sci 1989;37:1183.
[21] Ristey WJ, Shroff RN. The degradation and surface oxidation of polyethylene during the extrusion coating process. In: TAPPI paper synthetics proceedings; 1978.
[22] Croilius V, Ebeling W, Parsons R. The effect of processing variables on the adhesion strength of polyethylene-coated aluminum foil. TAPPI J 1962;45:352.
[23] Foster BW. Effect of extrusion coating parameters on activation of a primed film. In: TAPPI place conference; 2002.
[24] Hammond DR. Improving oxidation of the extrusion melt at higher line speeds and lower melt temperature. Eur TAPPI PLACE Conference; 2013.
[25] Morris BA, Suzuki N. The case against oxidation as a primary factor for bonding acid copolymers to foil. In: TAPPI polymers, laminations & coatings conference; 2000.
[26] Zambetti P, Baker S, Kelley D. Alpha tocopherol as an antioxidant for extrusion-coating polymers. TAPPI J 1995;78:167.
[27] Golike R. DuPont internal report. 1987.
[28] Hester D, Sadik S, Trouilhet Y. Using acid copolymers as coextrusion tie layers. In: TAPPI polymers, laminations & coatings conference; 1989. p. 459.
[29] Wu S. Polymer interface and adhesion. New York: Marcel Dekker, Inc.; 1982. p. 465.
[30] Kinloch A, Lau CC, Williams JG. The peeling of flexible laminates. J Fract 1994;66:45–70.
[31] Morris BA, Thai HT. Modifying LDPE for improved adhesion to aluminum foil. In: TAPPI PLACE conference; 2004.
[32] Keller A, Machin MJ. Oriented crystallization in polymers. J Macromol Sci (Phys) 1967;B1(1): 41–91.
[33] Kwack TH, Han CD, Vickers ME. Development of crystalline structure during tubular film blowing of low-density polyethylene. J Appl Poly Sci 1988;35:363–89.
[34] Dealy JM, Wissbrun KF. Melt rheology and its role in plastics processing, theory and applications. New York: Van Nostrand Reinhold; 1990.

[35] Guillotte JE, McLaughlin Jr TF. Calculating the adhesion of polyethylene coatings to Kraft paper. TAPPI 1962;45(3):200−8.
[36] Van Ness RT. Infrared thermometry − a useful tool for the coating industry. TAPPI 1968;51(12):39A−46A.
[37] Foederer BM, Morris BA. Use of IR technology to model temperature loss in the air gap. In: TAPPI PLACE conference; 2014.
[38] Devisme S, Haudin J-M, Agassant J-F, Rauline D, Chopinez F. Numerical simulation of extrusion coating. Intern Polym Process 2007;XXII:90−104.
[39] Trouilhet Y, Morris BA. Prediction of temperature profiles across coating and substrate in the nip. In: TAPPI polymers, laminations and coatings conference; 1999.
[40] Carslaw HS, Jaeger JC. Conduction of heat in solids. Oxford University Press; 1959.
[41] Carnahan B, Luther HA, Wilkes JO. Applied numerical methods. New York: Wiley; 1969.
[42] Shamsundar N, Rooz E. Numerical methods for moving boundary problems. In: Minkowycz WJ, et al., editors. Handbook of numerical heat transfer. New York: John Wiley & Sons; 1988.
[43] Goslin JP, Sweeney HF. The interaction of processing variables, base materials, and resins in polyethylene extrusion coating. TAPPI 1960;43(5):434−47.
[44] Morris BA. Understanding why adhesion in extrusion coating decreases with diminishing coating thickness, part I: penetration of porous substrates. In: SPE ANTEC conference and TAPPI place conference; 2005.
[45] Morris BA. Understanding why adhesion in extrusion coating decreases with diminishing coating thickness, Part II: non-porous substrates. In: SPE ANTEC conference and TAPPI PLACE conference; 2006.
[46] Morris BA. Understanding why adhesion in extrusion coating decreases with diminishing coating thickness, part III: analysis of peel test. In: SPE ANTEC conference and TAPPI PLACE conference; 2007.
[47] Vlachopoulos J. Melt flow through channels. In: Introduction to polymer processing. 2nd ed. McMaster University; 1994.
[48] Gent AN, Hamed GR. Peel mechanics for an elastic-plastic adherend. J Appl Polym Sci 1977; 21:2817−31.
[49] Pascal J. Ultraversatile adhesives to broaden the possibilities of extrusion lamination. In: TAPPI PLACE conference; 2006.
[50] Shirodkar PP, Firdaus V, Fruitwala H. Scale-up of LLDPE blown film extrusion. Plast Eng 1994:27.
[51] Butler TI. Using dimensionless scale-up variables to predict LLDPE blown film properties. In: TAPPI polymers, laminations and coatings conference; 1995. p. 581.
[52] Morris BA. The effect of processing variables on peel strength in coextruded blown film. In: SPE ANTEC conference; 1996.
[53] Morris BA. Peel strength issues in the blown film coextrusion process. In: TAPPI polymers, laminations and coatings conference; 1996.
[54] Morris BA. Effect of time, temperature and draw down on interlayer peel strength during coextrusion coating, film casting and film blowing. In: TAPPI PLACE conference; 2008.
[55] Zhang J, Lodge TP, Macosko CW. Interfacial slip reduces polymer-polymer adhesion during coextrusion. J Rheol 2006;50:41−57.
[56] Morris BA. The effect of coextrusion on bubble kinematics, temperature distribution and property development in the blown film process. J Plastic Film Sheeting 1999;15(1):25−36.
[57] Song J, Ewoldt RH, Hu W, Silvis HC, Macosko CW. Flow accelerates adhesion between functional polyethylene and polyurethane. AIChE J 2011;57:3496−506.
[58] Morris BA. Correlation of interlayer peel strength to post die processing times in coextrusion blown and cast film. In: SPE coextrusion Topcon, Cincinnati, OH, October 21−22, 2008; 2008.
[59] Morris BA. The effect of post die process time on adhesion in coextrusion blown and cast film. In: TAPPI PLACE conference; 2010.
[60] Song J, Baker AM, Macosko CW, Ewoldt RH. Reactive coupling between immiscible polymer chains: acceleration by compressive flow. AIChE J 2013;59:3391−402.
[61] Zheng X, Rafailovich MH, Sokolov J, et al. Long-range effects on polymer diffusion induced by a bounding interface. Phys Rev Lett 1997;79(2):241−4.

[62] Macosko CW, Jeon HK, Hoye TR. Reactions at polymer-polymer interfaces for blend compatibilization. Prog Polym Sci 2005;30:939–47.
[63] Botros MG. Investigation of adhesion and failure mechanisms in tie-layer adhesive/EVOH systems. J Plastic Film Sheeting 1996;12: 195–211.

Appendix: Relating Stress to Process Control Variables

Nomenclature

DDR	Draw down ratio $= v_f/v_o \sim X_o/X_f$
G	Modulus
X_o	Die gap
X_f	Final coating thickness
L	Air gap
m	Power law viscosity preexponent
n	Power law viscosity exponent
Q	Volumetric flow rate
T	Temperature of molten web
T_o	Temperature of web at the die exit
TIAG	Time in the air gap (Eq. (15.1))
t	Time
t_f	Characteristic process time
V	Velocity of an element of polymer
v_f	Line speed
v_o	Initial speed of polymer as it exits the die
w	Width of die
z	Position (distance from die exit)
ε_{tot}	Total strain or elongation of the molten web
$\dot{\varepsilon}$	Rate of strain or elongation
$\dot{\varepsilon}_{avg}$	Average rate of strain (in elongation)
$\dot{\gamma}$	Shear rate
$\dot{\gamma}_{app}$	Apparent shear rate
η	Shear viscosity
η_e	Elongational or extensional viscosity
σ_{ext}	Stress during extrusion
σ_d	Stress during drawing of the molten web

Analysis

The stress on the molten polymer is the sum of the stress imposed during extrusion (σ_{ext}) and drawing (σ_d), minus the amount of stress that has relaxed. To represent stress during extrusion, consider pressure-driven flow through two flat plates (as in the land region of the die, where the shear rate is typically the highest during extrusion). The stress is the product of the shear viscosity and shear rate:

$$\sigma_{ext} = \eta\dot{\gamma}. \tag{15A.1}$$

For a non-Newtonian fluid, a power law model can be used to relate viscosity to shear rate:

$$\eta = m\dot{\gamma}^{n-1}. \tag{15A.2}$$

In Table 5.4, an expression for the shear rate at the wall is derived which has the form:

$$\dot{\gamma}_w = \frac{4n+2}{n}\frac{Q}{wX_0^2}. \tag{15A.3}$$

Recognizing that $Q = wX_f v_f$ and combining Eqs. (15A.1)–(15A.3), the following relationship for stress imparted in the die land is obtained:

$$\sigma_{ext} = \left(\frac{4n+2}{n}\right)^n \frac{mv_f^n X_f^n}{X_0^{2n}}. \tag{15A.4}$$

Note that m is a function of temperature and polymer molecular weight.

The stress imparted during drawing, σ_d, is more difficult to characterize. For a liquid, the stress is proportional to the rate of strain, but for a solid, the stress is related to the strain:

$$\sigma_d = \eta_e\dot{\varepsilon} \quad \text{for a viscous liquid, and} \tag{15A.5}$$

$$\sigma_d = G\varepsilon_{tot} \quad \text{for an elastic solid.} \tag{15A.6}$$

Since polymer melts are viscoelastic with characteristics of both liquids and solids, it is likely that the stress is related to both $\dot{\varepsilon}$ and ε_{tot}. Both modulus and viscosity are functions of temperature. When dealing with a single material, Eqs. (15A.5) and (15A.6) can be combined into the following expression:

$$\sigma_d = f(T,\ \varepsilon_{tot}, \dot{\varepsilon}). \tag{15A.7}$$

Relationships for $\dot{\varepsilon}$ and ε_{tot} in terms of extrusion coating variables are needed.

The velocity of an element of polymer within the molten web is equal to its change in position with time:

$$V = \frac{dz}{dt}. \tag{15A.8}$$

The instantaneous rate of strain is equal to the change in velocity with respect to distance:

$$\dot{\varepsilon} = \frac{dV}{dz} = \frac{1}{V}\frac{dV}{dt}. \tag{15A.9}$$

The total strain is found by integrating the instantaneous rate of strain over time:

$$\varepsilon_{\text{tot}} = \int_0^{t_f} \dot{\varepsilon} dt = \int_0^{t_f} \frac{1}{V}\frac{d\dot{V}}{dt} dt = \ln\left(\frac{v_f}{v_0}\right). \tag{15A.10}$$

The ratio of the final velocity to initial velocity is known as the DDR and is related to the ratio of the die gap to final coating thickness:

$$\text{DDR} = \frac{v_f}{v_o} \cong \frac{X_o}{X_f}. \tag{15A.11}$$

Here the relationship between DDR and the film gauge is determined by mass balance between the die exit and the chill roll, neglecting density differences. Combining Eqs. (15A.10) and (15A.11), the following expression for the total strain is obtained:

$$\varepsilon_{\text{tot}} = \ln(\text{DDR}). \tag{15A.12}$$

Eq. (15A.9) gives the instantaneous rate of strain. For the purpose of this analysis, the average rate of strain will suffice. The average rate of strain is equal to the total change in velocity divided by the change in distance. For the region between the die exit and the chill roll, this becomes

$$\dot{\varepsilon}_{\text{avg}} = \frac{\Delta V}{\Delta z} = \frac{v_f - v_0}{L}. \tag{15A.13}$$

Eq. (15A.11) can be used to put (15A.13) into terms of DDR:

$$\dot{\varepsilon}_{\text{avg}} = \frac{v_f}{L}\left(\frac{\text{DDR} - 1}{\text{DDR}}\right). \tag{15A.14}$$

The amount of stress relaxation is a function of the characteristic relaxation time of the polymer (a material parameter influenced by MW, MWD, branching, and so on), processing temperature, and time. A characteristic time for the process can be defined as the total strain divided by the average rate of strain:

$$t_f = \frac{\varepsilon_{\text{tot}}}{\dot{\varepsilon}_{\text{avg}}}. \tag{15A.15}$$

Substituting (15A.12) and (15A.14) into (15A.15) gives the following relationship for process time:

$$t_f = \frac{L}{v_f}\left(\frac{\text{DDR}}{\text{DDR} - 1}\right)\ln(\text{DDR}). \tag{15A.16}$$

Note that this is the form of the linear velocity model in Table 15.1.

16 End-Use Factors Influencing the Design of Flexible Packaging

The interaction of the package with its physical environment and the product it contains can influence package performance. These end-use factors, as well as cost, must be considered when designing films for flexible packaging. The cost involves not just the materials and film-converting costs but also the total cost of using the package, including packing productivity, package failures during packaging and the end use, and product shelf life. For perishable food products, usually the cost of the product is greater than the package and the benefit of extending shelf life may overwhelm an increase in package cost. Increasingly, the cost to the environment must also be considered, such as greenhouse gas (GHG) emissions, renewable energy content, water usage, and end-of-life scenarios. This chapter describes some of these factors beginning with how the external influences of temperature, humidity, and pressure affect film properties and suitability of materials for use. In-package sterilization processes are also considered. This is followed by a section covering food product−package interactions that may affect shelf life: migration of components of the food into the package or from the package to the food may negatively affect film performance or food taste and odor. The properties of polymer films may change over time as molecules relax and reorganize. Accounting for these aging effects must be considered during package design. Finally, the total cost of packaging is discussed.

16.1 Environmental Effects on Package Performance

16.1.1 Temperature

Films may be exposed to conditions in the end use not accounted for by room temperature tests. These may involve high or low temperatures. Examples of high temperature exposure include the following:

- Retort sterilization, where the filled package is subjected to temperatures of 121°C or higher for 30−60 min in a steam autoclave. This process was originally developed for food packaged in metal cans.
- In-package pasteurization where the temperature may exceed 90°C. Many prepared meat products are pasteurized in the package following filling as an extra insurance against dangerous microbes such as *Listeria* and *Escherichia coli*.
- Hot fill of the product during packaging.
- Cook-in where the product is literally cooked in the package. Processed deli meats are prepared in this way. Various meat cuts are blended together with binders, fillers, extender ingredients, and water and molded into the package. The meat−water slurry is cooked for several hours at 80−100°C, depending on the product. This is a rather demanding application not just because of the elevated temperatures; the package must withstand stress induced by the cooking process and prevent migration of oily components of the food through the package. Furthermore, marinade and other liquids may be injected into the meat during cooking. The vacuum-packaging process may pull out some of the liquids that are injected or naturally form during cooking, giving an unsightly liquid "purge" in the package. Good adhesion of the film material to the meat protein, and the ability to tightly surround the meat during cooking helps reduce purge. Functionalized polyethylenes, such as acid copolymers, ionomers, and maleic anhydride-modified linear low density

The Science and Technology of Flexible Packaging. http://dx.doi.org/10.1016/B978-0-323-24273-8.00016-2
Copyright © 2017 Elsevier Inc. All rights reserved.

polyethylene (LLDPE), are often used as the sealant layer.

- Packaging that is designed to be microwaved by the consumer. These packages often contain susceptors that help generate and concentrate the heat during microwaving. Temperatures can get very hot. Some packages are designed with lidding or other components that give way when high temperatures are reached. These are used for self-venting packages to allow steam and other gases to escape during cooking so that dangerous levels are not reached inside the package.
- Dual ovenable packaging. Here the product is designed to be cooked in a microwave or conventional convection oven. Crystalline polyethylene terephthalate (CPET) trays are often used for this type of package for their temperature resistance.

Examples of low temperature environments, a package may experience include cold temperature storage and transport of frozen foods in the distribution chain, as well as storage by the consumer in a home freezer. Consumer freezers are typically kept at −18°C or lower. Industrial blast freezers may subject the package to evaporative temperatures of −30 to −40°C, although the core temperature will typically be −7 to −18°C.

Polymers undergo fundamental thermal transitions that affect their physical properties. For amorphous polymers such as polystyrene (PS), amorphous polyethylene terephthalate (PET), and amorphous polylactic acid (PLA), the glass transition temperature (T_g) is an important benchmark. The T_g is the transition between the glassy and rubbery phases of the polymer. Below T_g the polymer chains are constrained and do not flow. As the temperatures increases through the glass transition temperature, the stiffness and other key physical properties of the polymer significantly decreases. Standard grades of PLA, for example, have a T_g of around 55°C. Since temperature may exceed 55°C during standard shipping, packages made from amorphous PLA must be shipped in refrigerated trucks. This limits their use for many applications. Crystalline versions of PLA films/trays can be made with higher temperature resistance, but the crystallinity reduces the transparency of the package. The T_g for various amorphous polymers can be found in Table 16.1.

Table 16.1 Typical Glass Transition Temperatures and Melting Points of Resins Used in Flexible Packaging

Polymer	T_g (°C)	T_m (°C)
Amorphous Polymers		
APET	67	
PS	100	
PLA	55–60	
PA 6I/6T	132	
PVC	80	
Semicrystalline Polymers		
EVA		75–100
Ionomer		80–100
Acid copolymer		85–105
LDPE	−85 to −130 (depends on data source)	110
HDPE	−70 to −125 (depends on data source)	130–135
LLDPE–Ziegler–Natta	−78	120–125
LLDPE–metallocene		55–120
PP homopolymer	−18	160–165
PP random copolymer		135–155
PA6	57 (dry), <0 wet	220
PA6/66		195
EVOH, 44 mol% ethylene	53 (dry)	165
EVOH, 32 mol% ethylene	57 (dry)	183
PET (crystalline) or OPET	70–80	254–267

For semicrystalline polymers such as PE, polypropylene (PP), polyamide (PA), and crystalline PET, the melt point (T_m) is the critical temperature. The melting of semicrystalline polymers typically occurs over a range of temperatures; the onset of the decrease in physical properties with increasing

temperature may occur at a temperature below the peak melting point. This is illustrated in Fig. 16.1 where the storage modulus of a homopolymer PP from dynamic mechanical analysis is plotted versus temperature. The T_m of PP homopolymer is around 161°C, but the modulus drops well below this.

The melting points of commonly used polymers in flexible packaging are given in Table 16.1. In multilayer film structures, the sealing layer is often selected to have a lower T_m than the heat resistant or structural layer. Depending on the nature of the temperature exposure (whether the film is under stress), the package may maintain its integrity even if T_m for one of the layers is exceeded, as long as the melt strength or hot tack of that layer is sufficient.

In addition to thermal transitions that may affect the mechanical properties of the polymer and render it unfavorable for a high temperature application, there may be regulatory hurdles. Specific regulatory requirements may be needed for applications subjected to elevated temperature such as microwave or convection oven cooking or retort. Migratory species in polymer films may diffuse into the food product faster at elevated temperatures, depending on the polymers. The regulations have specific testing protocols for high temperature use (see Chapter 4 for more information on regulatory requirements).

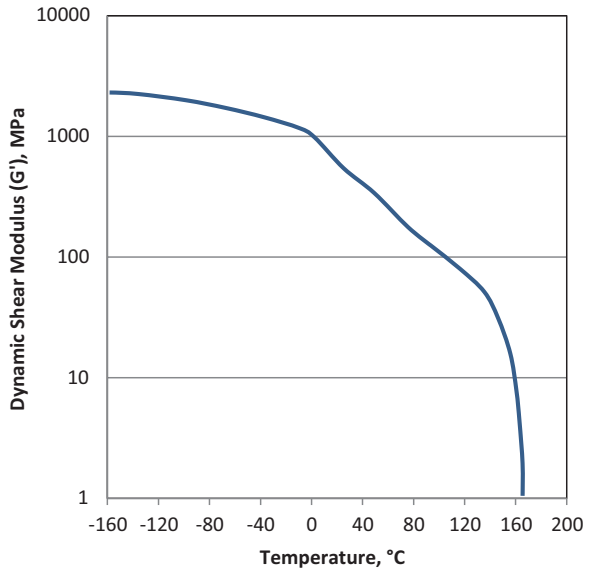


Figure 16.1 Storage modulus (G') as a function of temperature for semicrystalline PP homopolymer. *Data are from Osswald T. "Mechanical behavior of polymers," understanding polymer processing: processes and governing equations. Hanser; 2011 sample chapter, viewed November 24, 2015 at, http://www.hanserpublications.com/SampleChapters/9781569904725_9781569904725_Understanding%20Polymer%20Processing_Osswald.pdf.*

Elevated temperatures in the end use increase oxygen and moisture permeation and the migration of small molecules to or from the package (scalping and impartation, described in Section 16.2). These need to be planned for when designing the packaging structure or the shelf life may be compromised.

For low temperature environments, embrittlement of the polymer may become an issue. When the temperature drops below the T_g of the polymer, toughness often substantially decreases. Polymers with low T_g may be favored or be used as a modifier. For example, PP has a T_g of around −18°C, whereas the T_g of polyethylene (PE) is around −80°C or lower. PE is tougher than PP at freezer temperatures. The PP may be modified with a rubbery phase to improve its cold temperature toughness either through copolymerization (impact copolymers) or by blending in a toughener such as ethylene propylene diene rubber, ethylene-propylene rubber, or metallocene polyethylene plastomer. Similarly, PET ($T_g = 80$°C) is often modified with ethylene methyl acrylate copolymer ($T_g \sim -40$°C) to prevent CPET trays from shattering if they are dropped by the consumer as they remove them from the freezer.

16.1.2 Humidity

Moisture acts as a plasticizer for some polymers, affecting their gas permeation and mechanical properties. The effect of relative humidity on the oxygen permeation of ethylene vinyl alcohol (EVOH), PA, and other polymers is described in detail in Section 8.4.1.2.4.3. Moisture pickup in the end use increases the permeation of gas molecules through these films, as is illustrated in Fig. 8.1 for EVOH. Barrier performance can be compensated by the following:

- Selecting barrier polymers that are less sensitive to relative humidity.
- Increasing barrier layer thickness.
- Moving the barrier layer toward the surface exposed to the lower humidity environment, since the effective relative humidity varies within the thickness of the package films. Design equations to estimate the relative humidity the barrier layer sees in its end use are provided in Section 8.4.1.2.4.3.

The combination of high relative humidity and temperature can be particularly problematic for barrier performance of water-sensitive barrier polymers such as EVOH. During retort sterilization, the packaged product is exposed to 121°C in a saturated steam environment for 30–60 min. A number of factors conspire against maintaining barrier performance under these conditions:

- Permeation increases with increasing temperature.
- Permeation increases with increasing relative humidity. Polyolefin layers that may otherwise provide some moisture protection of the oxygen barrier layer over short times (until equilibrium is established) are no help; their moisture barrier becomes almost nonexistent under these conditions.
- The heat and water change the crystalline structure of EVOH so that following retort, the oxygen barrier performance does not return to its original value [2–5]. This is known as retort shock and is described in detail in Section 8.4.1.2.4.4. Not only does extra oxygen enter during the retort process itself, but because the EVOH does not fully recover, the additional oxygen that is allowed into the package following retort must be considered when designing the package to meet shelf life requirements.

Alternative barrier materials and packaging structures may offer improved performance over EVOH for retort of flexible packaging. Some examples of oxygen permeation of several structures before and after retort are shown in Fig. 16.2.

Schubert [7] describes aluminum foil-based laminates used for retort stand-up pouches with the structure PET/adh/Al/adh/OPA/adh/PP. The adhesive is typically a two-component polyurethane–polyester. The adhesion often improves during retort—moisture passes through the polymer layers and helps with the bonding of silanol groups in the adhesive to oxides on the aluminum foil. Bubbles can form, however, where the adhesive does not cover the aluminum foil (due to "dry spots" caused by the adhesive being applied to the printing ink). The moisture and oxygen in the bubble causes oxide growth on the foil surface. The spots can expand and evolve hydrogen.

Since moisture can act as a plasticizer for some polymers, such as PA6, the stiffness, or modulus of films containing these polymers may decrease over time if the package is subjected to a high relative humidity environment. The loss in stiffness is usually

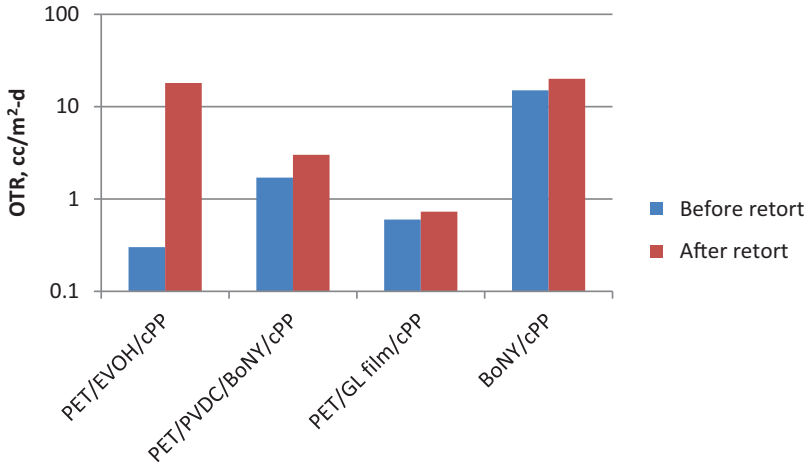


Figure 16.2 Oxygen transmission rate (OTR) of multilayer films before and after retort (125°C, 20 min). OTR is measured at 25°C, 70% RH. cPP = cast polypropylene, GL film is silica-deposited laminated film from Toppan Printing Co., Ltd., and BONY is oriented PA film.

Reproduced with permission from Mokwena KK, Tang J. Ethylene vinyl alcohol: a review of barrier properties for packaging shelf stable foods. Crit Rev Food Sci Nutr 2012;52:640–50. Data from Hernandez RJ, Giacin JR. Factors affecting permeation, sorption and migration processes in package-product systems. In: Taub IA, Singh RP, editors. Food storage stability. Boca Raton, FL: CRC Press; 1998. p. 269–330.

associated with a gain in toughness. Indeed, for some applications, films containing PA6 are purposely subjected to a high moisture environment to provide toughness. Section 13.5 describes how moisturization can also be used to induce secondary crystallization in PA6, which induces changes in dimension and curl.

16.1.3 Pressure

Pressure variations due to changes in altitude during shipping can put stress on package seals, as is described in Chapter 7. A "ballooning" effect occurs when a packaged sealed at sea level is transported to high elevations as the surrounding air pressure is diminished, allowing the air molecules inside the package to expand. End-use seal strength specifications should be set sufficiently high to prevent delamination during such changes in altitude.

In general, the differences in pressure that a typical package is subjected to in its use has little effect on the mechanical and barrier properties of flexible packaging films. A new technology, however, for in-package pasteurization of food products is gaining favor called high pressure processing (HPP) where the packaged product is subjected to extreme pressures of 600 MPa (87 kpsi). Microbes are deactivated by disrupting the cell wall and the cell's ability to repair the damage. Time at pressure for this to occur depends on the acidity and water activity of the food product, as well as the type of microbe to be deactivated. Gram positive microbes (eg, *Listeria*) are more difficult to deactivate than gram negative ones. Spores are particularly resistant to high pressure [8–12].

The use of HPP is growing for extending the shelf life of refrigerated foods such as processed meats, salsa, and various fruits and vegetables. The best packages for HPP turn out to be rigid or flexible packages with little or no headspace. The package deflects up to 15% during the high pressure treatment. As long as the package has a conformable lid or sidewall and is sealed well, it generally holds up well. HPP, therefore, seems ideally suited for flexible packaging. Shelf life extensions of two times or more have been reported, depending on the product. As the shelf life is extended by prevention of microbial growth, spoilage by oxidation becomes more of an issue. The substitution of oxygen barrier film structures for nonbarrier ones may be needed.

16.1.4 Irradiation

Electron beam and gamma ray radiation (from radioactive isotopes cobalt-60 and cesium-137) are used for medical device sterilization, food irradiation and sterilization, and sanitation of packaging materials. At the typical dosage required to reduce microbial contamination, no heat is generated, which is beneficial for retaining the nutritional and sensory value of food. Most commercial operations prefer to sterilize the device or food product after packaging to avoid recontaminating the product during packaging. The package, therefore, needs to withstand the effects of radiation.

Radiation can cause cross-linking or chain scission of polymers, which affects mechanical properties such as tensile strength, elongation, and impact resistance. Chemical changes may also occur, such as the creation of peroxides through reaction with oxygen. The peroxides may undergo further reaction over time, sometimes in the presence of moisture. The effects of radiation may not be immediately apparent and require extensive testing when considering new materials. Chemical interactions with the polymer, or various additives that may be in the polymer such as antioxidants, may create low molecular weight (MW) species that alter the odor, taste, or safety of the product. For these reasons, government agencies regulate the use of materials that are used in irradiated packaging. In the United States, irradiation of food packaging is regulated by the U.S. FDA under Title 21 of the Code of Federal Regulations (CFR), Part 179.25 (General provisions for food irradiation). Packaging materials must comply with 21 CFR 179.45 (packaging materials for use during the irradiation of prepackaged foods). Unfortunately, many modern packaging materials and structures are not listed in CFR 179.45. New packaging structures/materials not already listed, or the subject of a Food Contact Notice, requires a premarket safety assessment. This includes chemistry, toxicology, and environmental components.

For selecting packaging materials exposed to radiation sterilization of medical devices, some basic rules can be considered [13]:

- Materials designed for medical devices are generally durable to radiation.
- Higher MW and narrower molecular weight distribution grades generally have greater radiation resistance.

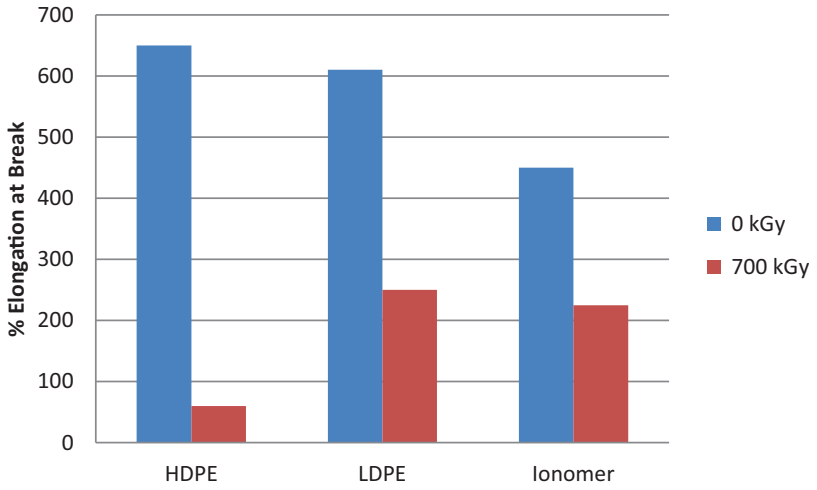


Figure 16.3 Effect of radiation on elongation at break of ethylene polymers. Polymers are subjected to 700 kGy of radiation.

Data from Lyons BJ, Weir FE. The effect of radiation on the mechanical properties of polymers. In: Dole E, editor. The radiation chemistry of macromolecules, vol. 2. Academic Press; 1973 and graph is reproduced with permission from Hoh G, Cumberbatch GM. Stability of Surlyn® films to radiation, In: TAPPI polymers, laminations and coatings conference; 1990. p. 251–92.

- Aromatic polymers are more resistant than aliphatic ones.
- Amorphous polymers are more resistant than semicrystalline polymers.
- Higher levels of antioxidant improve radiation resistance. (Caution: for food packaging, some antioxidants may create by-products that are not on the regulatory lists.)
- Lower density polymers are more resistant than higher density ones.
- For semicrystalline polymers, lower levels of crystallinity improve radiation resistance. An example is presented in Fig. 16.3 showing the elongation at break for high density polyethylene (HDPE), low density polyethylene (LDPE), and an ionomer before and after exposure. The order of higher to lower level of crystallinity is HDPE > LDPE > ionomer, which is the same order as the effect of radiation on elongation.
- Small pendent side groups can improve radiation resistance. For example, the alpha olefin side chains in LLDPE lower its density and crystallinity and improve radiation resistance over HDPE.
- Materials with low oxygen permeation are more radiation resistant.
- A mnemonic is to avoid materials that are APT to fail [acetal, polypropylene (unstabilized), or Teflon (PTFE)].
- Materials must be compliant with appropriate regulations.

The effect of radiation depends on its dosage and the exposure environment (oxygen, moisture, temperature). There are two main units of radiation dosage: Gy and Rad. One Gy is equal to 1 J of energy absorbed per 1 kg of matter. One Rad is equal to 100 erg absorbed per gram of matter. Therefore, 10 kGy = 1 MRad. Most medical devices are sterilized with 25 kGy or less. End users of medical device packaging typically specify that the material must withstand 25 or 50 kGy, the latter in case of two passes through the sterilization process. For food irradiation, the maximum dosage is typically 10 kGy, except for some spices which are exposed to 30 kGy. A list is shown in Table 16.2. At these relatively low doses, most flexible packaging structures retain their mechanical properties and heat seal performance [16]. Hoh [15], for example, shows that ionomers show no negative impact on mechanical properties from radiation exposure up to 50 kGy.

Komolprasert [16] reviews the literature on the effect of radiation on the creation of regulated

Table 16.2 Foods and Dosage Levels Permitted to Be Irradiated by the FDA (21 CFR 179.26)

Food Product	Purpose	Maximum Dosage (kGy)
Pork carcasses	Control of *Trichinella spiralis*	1 (0.3 minimum)
Fresh foods	Growth and maturation inhibition	1
Food	Disinfestation of arthropod pests	1
Enzyme preparations	Microbial disinfection	10
Dry or dehydrated spices/ seasonings	Microbial disinfection	30
Fresh or frozen uncooked poultry	Control food-borne pathogens	3
Frozen, packaged meats for NASA space program	Sterilization	44 minimum
Refrigerated uncooked meat products	Control food-borne pathogens and extend shelf life	4.5
Frozen uncooked meat products	Control food-borne pathogens and extend shelf life	7
Fresh shell eggs	Control *Salmonella*	3
Seeds for sprouting	Control of microbial pathogens	8
Fresh or frozen molluscan shellfish	Control of *Vibrio* bacteria and other food-borne microorganisms	5.5
Fresh iceberg lettuce and spinach	Control food-borne pathogens and extend shelf life	4

Date from U.S. Code of Federal Regulations 21 CFR 179.26, viewed November 30, 2015 at, http://www.accessdata.fda.gov/scripts/cdrh/cfdocs/cfcfr/cfrsearch.cfm?fr=179.26.

by-products in different packaging materials. Most by-products are below the regulated threshold for daily consumption, but some associated with the breakdown of additives in the polymers are not listed in the regulations. One class of additives, hindered phenol antioxidants, has been found to degrade into species that affect organoleptics and may have regulatory hurdles. These must be considered when selecting materials and designing packaging structures.

16.2 Packaging–Product Interactions

The product may interact with the package to affect the performance of the package or the quality of the product. Three areas of food packaging are explored here:

- loss of package integrity from product component migration into the package and causing interlayer delamination or stress cracking;
- organoleptic issues resulting from scalping of flavor components from the food into the package or migration of components from the package into the food;
- shelf life extensions from active packaging.

16.2.1 Loss of Package Integrity

In nonbarrier flexible packaging, the primary concern with product–packaging interactions is product loss over time, which can result in loss of

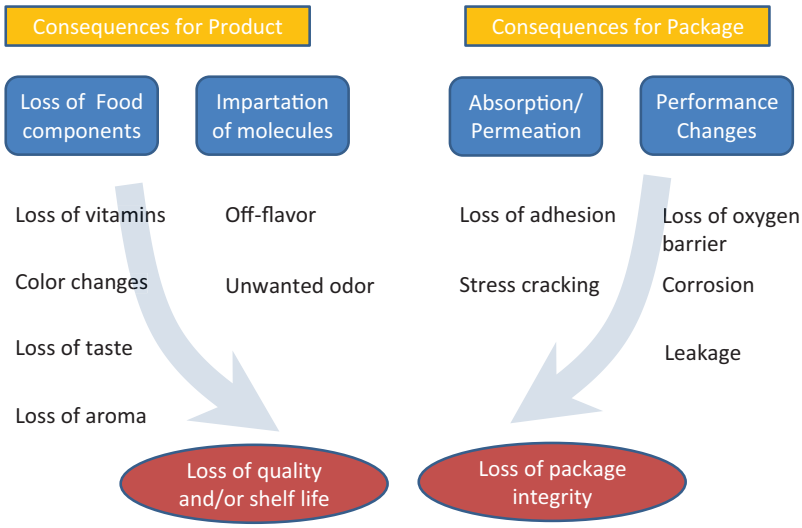


Figure 16.4 Negative consequences of product–package interactions.
Adapted from Pieper G. Interaction phenomenon in multilayer flexible packaging. In: Ackermann P, Jagerstad M, Ohlsson T, editors. Foods and packaging materials – chemical interactions, vol. 162. Special Publication–Royal Society of Chemistry; 1995. p. 95–100.

vitamins and nutrients, color changes, and altered taste and aroma. These are taken up in more detail in Section 16.2.2. In barrier packaging, the primary concern is the absorption of food components by the contact layer. However, there can also be deleterious interactions between food components and the package, affecting packaging integrity and ultimately product quality. Categories of negative interactions are illustrated in Fig. 16.4. Food components such as fatty acids may migrate to the barrier interface and outcompete for reaction sites, causing loss of adhesion and delamination. This may lead to loss of barrier and impact product quality. Environmental stress cracking (ESC) may also lead to a loss of barrier, corrosion of foil layers, and leakage.

As described in Chapter 8, the migration of organic molecules in plastic films is complex and not well studied. Migration depends on the molecule first being sorbed by the film, which often involves swelling and other mechanisms in concert with other ingredients in the product. This is followed by diffusion of the molecule to the interface. The effect of these molecules on interlayer adhesion is even less studied. Several examples from the literature are described here to illustrate the consequences and challenges.

16.2.1.1 Peel Strength and Delamination

Schroeder [19] studies the effect of flavorant sorption on adhesion in two adhesive lamination packaging structures:

1. 15-μm polyvinylidene chloride (PVDC) ctg/46-μm OPET/ink/adh/51-μm EVA (ethylene vinyl acetate copolymer) (6% VA). The adhesive is a one component polyurethane based on 4,4′-diphenyl methane diisocyanate.
2. The same as A except the sealant layer is LLDPE.

Two food products are tested: a natural strength lemon juice and a branded hot sauce. A 3 wt% citric acid solution is used to simulate lemon juice without organic components like d-limonene and 3% acetic acid to simulate the hot sauce without the organic components. The laminates are immersed in the food or simulants in a test cell such that only the food contact side is exposed. The samples are stored at 45°C for 30 days and the peel strength is periodically measured.

Their results show the following:

- Both laminates delaminate when exposed to the food products but not to the simulants. This suggests low MW flavor components, such as

d-limonene in the lemon juice, are responsible for the loss of adhesion.

- The locus of failure is between the ink and adhesive layers for structure B (LLDPE) and loss of cohesion within the adhesive layer for structure A (EVA). This is determined by ESCA (electron spectroscopy for chemical analysis, also known as X-ray photoelectron spectroscopy) and SEM (scanning electron microscopy).
- Peel strength reduction is a poor predictor of delamination; significant peel strength reduction occurs in some samples that do not delaminate.
- The greatest peel strength reduction occurs when the laminates are exposed to the food. Some reduction occurs just from heating or with the simulant.
- d-limonene is the likely cause of delamination for lemon juice but the hot sauce is too complicated to implicate a specific molecule.

Olafsson [20–24] investigates the effect of organic acids on adhesion of LDPE to aluminum foil. Laminates with the structure LDPE/paperboard/LDPE/Al/LDPE are prepared by extrusion coating/lamination by Tetra Pak, a major manufacturer of barrier laminates for liquid packaging. Various acids are stored at room temperature in pouches made from the laminates. Periodically the laminates are tested for peel strength, examined for evidence of delamination, and analyzed with FTIR and ESCA. They find the following:

- The LDPE delaminates from the foil within 3 days when exposed to 3 wt% acetic acid. Over the course of the next 3 days, the peel strength recovers to about half its original value. FTIR reveals the formation of aluminum acetate at the interface that leads to the partial recovery of the peel strength (by forming hydrogen bonds with the polymer).
- Laminates exposed to propionic acid show complete delamination after 8 days and do not recover. Propionic acid has a longer chain length (extra methyl group) than acetic acid. FTIR shows more propionic acid migrates than acetic acid, which the authors attribute to its greater solubility in LDPE (due to its longer chain length).
- Citric acid, lactic acid, and water have no effect on the peel strength. Compared with acetic acid, citric acid has an extra hydroxyl group and lactic acid has an extra carboxyl group, both of which should impede their migration in LDPE due to an increase in polarity. Higher polarity decreases solubility in the nonpolar LDPE.
- A series of fatty acids of different chain length (C10 to C18) and saturation (0–3 carbon double bonds) are tested. The amount of fatty acid sorbed by the inner LDPE increases with increasing chain length for saturated fatty acids. The sorption decreases with increasing degree of unsaturation for unsaturated fatty acids. Most of the sorption occurs within the first 2 days of exposure.
- Pouches containing monounsaturated fatty acids are found to quickly delaminate between the LDPE and foil. Pouches containing C18:2 (18 carbon atoms, 2 double bonds) and C18:3 showed a substantial drop in peel strength but recover to 50–75% of the control over time. A second study with saturated fatty acids shows no delamination but a drop-off in peel strength by about 40%.
- Separate permeation measurements show that the permeation increases with increasing chain length for saturated fatty acids. The permeation decreases with increasing unsaturation.

In discussing the results, Olafsson concludes the following:

- The chemical structure of the acid affects sorption, migration, and the ability of the acid to affect adhesion. The very polar organic acids are not expected to diffuse very quickly through nonpolar LDPE; Olafsson suggests they may diffuse as dimers. Acetic and propionic acids are linear and so diffuse faster than citric or lactic acids.
- The partial recovery of some of the bond strengths is due to the formation of metal salts at the interface.
- Fat absorption from fatty foods swells PE, causing an increase in migration [25–27].

- Free fatty acid concentration in foods is generally initially low but can increase with time due to hydrolysis. The concentration in oils and fats vary widely: 0.02−0.05 in refined oils such as rapeseed oil, 0.5−1% in virgin olive oil, 0.002% in fresh milk (4% fat), and 0.16% in butter.
- Adhesive forces between LDPE and Al are believed to be mainly due to acid−base interactions, including hydrogen bonds and van der Waals forces between the aluminum oxides on the foil and oxidized functional groups on the LDPE.
- Delamination is believed to be due to the fatty acid penetrating through the LDPE and accumulating at the foil interface, creating a weak boundary layer of acid−base interactions between the low MW fatty acid and oxide surface of the foil.
- The sorption (and migration) effects of the different fatty acids can be explained by differences in molecular structure:
  - Longer chain length gives rise to more van der Waals interactions and greater solubility in LDPE.
  - Greater unsaturation makes the molecule more rigid, which results in slower diffusion.
- The different adhesion results from the two fatty acid studies can be explained as being due to differences in the solutions (the first contains water, and the second just ethanol as the solvent). Water in the first study may be responsible for the delamination—it strongly forms hydrogen bonds that may interfere with the adhesion, whereas the bonds with ethanol are not as strong.

To improve product resistance, ethylene acrylic or methacrylic acid copolymers (EAA or EMAA) or ionomers are often used as tie resins between LDPE and foil. Product resistance generally increases with increasing acid level and thickness of the acid copolymer layer [28−30]. Bernacki [28] extrusion coats 25-μm of sealant onto the foil side of the laminate 50 lb Kraft paper/12-μm LDPE/0.00035 g Al. The coating is either monolayer or a coextrusion of LDPE and EAA. Pouches are made from the laminates and filled with product. Peel strength between the coating and foil is measured after storage for 3 weeks at 49°C and after 6 weeks at 49°C and 23°C. The products tested included ketchup, orange juice, Hidden Valley Party Dip, blue cheese dressing, mustard, vegetable oil, wintergreen tobacco, shampoo, Ben Gay lotion, lemon juice, and iodine. The results show the following:

- Monolayer EAA (9 wt%) exhibits the best product resistance.
- The peel strength in pouches containing Ben Gay lotion and Hidden Valley Party Dip decreases when stored at 49°C but increases in the pouches containing the others products, suggesting the other products are not very aggressive.
- EAA and ionomers offer improved product resistance over LDPE.
- The polymers with higher acid levels provide better product resistance.
- In the coextrusion structures, a 9% AA grade offers protection when used as a tie layer comprising 50% and 20% of the sealant coating, whereas a 3% AA grade does not offer protection at 20%.
- None of the pouches hold up to iodine. Ben Gay is also very aggressive. These are consistent with Antonov and Soutar [29] who list a number of products that should not be packaged in unprimed foil/acid copolymer laminates:
  - Anything with pH below 2.5−3. Certain condiments containing vinegar ketchup in the United States is suitable but differs around the world. Some chilli sauces are not suitable;
  - Methyl salicylate. Low concentrations for flavoring may be fine but products for sore muscles (Ben Gay) are not;
  - Curry and some pepper products;
  - Povidone−iodine;
  - Turpentine;
  - Chloroform;
  - High concentrations of flavoring oils, such as peppermint.

Accelerated shelf life testing at elevated temperatures can be misleading and should be confirmed with long-term storage tests. Elevated temperature

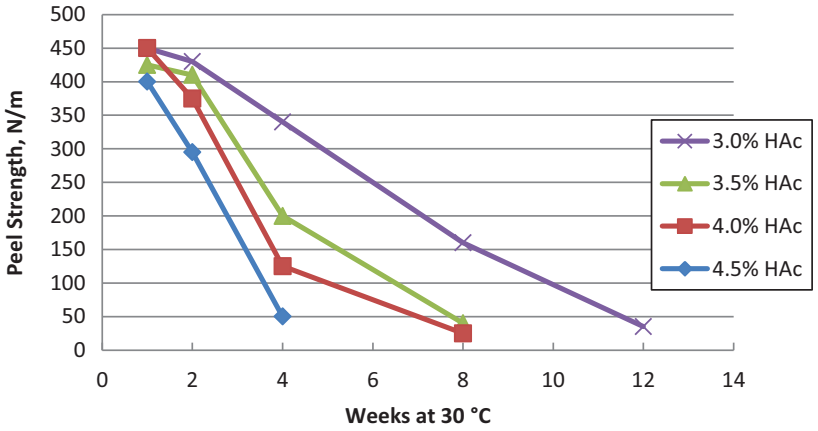


Figure 16.5 Effect of acetic acid concentration on peel strength between an ACR or ionomer tie resin and aluminum foil in a barrier laminate structure.
Reproduced with permission from Pieper G. Interaction phenomenon in multilayer flexible packaging. In: Ackermann P, Jagerstad M, Ohlsson T, editors. Foods and packaging materials – chemical interactions, vol. 162. Special Publication–Royal Society of Chemistry; 1995. p. 95–100.

may anneal the sample and increase the bond strength if the product is benign. Elevated temperatures may also cause product interactions to take place that would not at room temperature.

Pieper [18] shows shelf life data with acetic acid stored in commercial LDPE/paperboard/LDPE/Al/(ACR-LDPE) laminate structures. Here ACR stands for acid copolymer resin, which includes EAA, EMAA, and ionomers. Fig. 16.5 shows the effect of acetic acid concentration on shelf life, as measured by peel strength between the ACR and foil. Increasing the acid concentration in the product reduces the shelf life. One strategy to extend shelf life is to increase the acid content of the tie layer, as described by Bernacki. This must be balanced by the loss in adhesion between the ACR and LDPE. Most commercial applications use acid copolymers with acid levels in the range of 6–9 wt%. Hester [30] shows that while increasing the acid level in the ACR reduces the initial adhesion to LDPE, higher acid helps reduce the loss in adhesion when exposed to acetic acid.

Another strategy for increasing shelf life is to increase the thickness of the ACR layer. Fig. 16.6

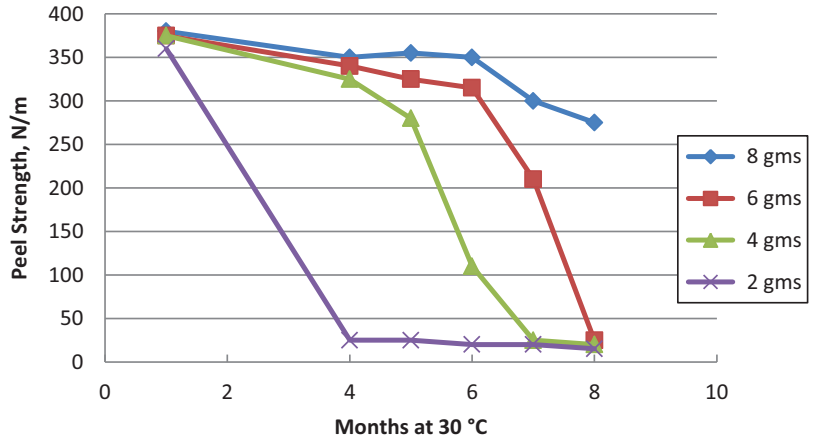


Figure 16.6 Effect of tie layer thickness on peel strength durability in the presence of orange juice stored at 30°C. Peel strength is measured between the ACR tie layer and aluminum foil barrier layer.
Reproduced with permission from Pieper G. Interaction phenomenon in multilayer flexible packaging. In: Ackermann P, Jagerstad M, Ohlsson T, editors. Foods and packaging materials – chemical interactions, vol. 162. Special Publication–Royal Society of Chemistry; 1995. p. 95–100.

shows the effect of increasing the ACR thickness from 2 to 8 gsm (approximately 2−8 μm) from the work of Pieper. Here the peel strength between the ACR and foil is reported for orange juice stored for up to 8 months at 30°C.

Pieper also considers inserting other polymers between the tie and foil to protect the adhesion. Permeability of acetic acid in orange juice is measured for PA, PET, EVOH, and (LDPE−EAA). The PET has the lowest permeability followed closely by the LDPE−EAA and then the PA. Surprisingly, the EVOH performs poorly, showing that the acetic acid permeability does not track with oxygen permeation.

Retort sterilization is especially challenging even for foil-based packaging. Fat and fatty acids can quickly migrate through polyolefins at elevated temperatures due to their affinity. Long chain fatty acids do not react with aluminum at room temperature, but they do above 100°C. Aluminum soaps or carboxylates form which may cause delamination. Formation of soaps is also partly responsible for adhesion of acid copolymers to foil. When the low MW fatty acids are present, they may out compete the acid copolymer for the oxides at the foil surface, resulting in a weak boundary layer and delamination [7].

Schubert [7] conducts an experiment simulating retort of an aluminum foil laminate in the presence of a food simulant. Triglycerides are found to migrate into the coating. These are present with phospholipids (natural emulsifiers) and smaller fatty acids. The migration is detected by attenuated total reflectance infrared spectroscopy at penetration depths of up to 3 μm. SEM images show layer destruction, fat-filled voids, and defects in the coating after retort. When the simulants contain fatty acids, delamination occurs and defects similar to what is found in commercial packages are found. At the delaminating interface, additional aluminum soaps are found. Schubert concludes that delamination failure is the result of progressive replacement of the polymer−oxide bonds with fatty acid−aluminum soap bonds.

16.2.1.2 Environmental Stress Cracking

Polymers in contact with fats and oils may undergo ESC, where the polymer becomes brittle and cracks, especially in regions of high stress. Cracking can lead to package failure. Pieper [18] finds that fats, oils, and formulated tomato products (with salts and acids) are effective stress-cracking agents. When packaging these products, special caution is advised.

Polyethylene forms plate-like crystalline structures called lamella in films and coatings. The lamella are held together by tie molecules. Pieper explains ESC using the model of Lustiger and Markham [31], which attributes cracking of polymers under long periods of low stress levels to untangling of tie molecules between crystalline lamella.

LDPE can be an effective contact layer if a grade is selected with good environmental stress crack resistance. In general, this means a high concentration of tie molecules. High MW grades are preferred for this reason.

Mannheim [32] conducts transportation vibration simulation studies on orange juice aseptically packaged in three structures (adhesive layers not shown):

- PE/met-PET/PE;
- PE/EVOH/PE;
- PET-met/met-PET/PE.

The third structure has the lowest initial oxygen permeation value (OPV), but the orange juice packaged and stored at 25°C deteriorates the fastest in this package. Flex cracking during the vibration test increases oxygen permeability from 1.6 to 16.8 cc/d/bag. The combined effects of oxygen permeability and product interactions reduce shelf life of citrus products compared with glass. Transportation simulation is important for understanding how well the package will survive abuse—pinholes, flex cracking, puncture, or seal failure may occur, any one of which can deteriorate shelf life.

16.2.2 Organoleptics

Taste and odor changes to the food product can arise from migration of low MW species from the package (or the external environment through the package) into the product (impartation) or by migration of flavor or aroma components from the product into the package (scalping). Material selection, film structure design, and film fabrication processing can impact both of these.

16.2.2.1 Impartation

Low MW species may diffuse through the flexible film and desorb into the product. In some cases,

active components such as antioxidants or antimicrobials are intended to migrate to the surface and interact with the product. This is discussed in Section 16.2.3. Here, unwanted migration that may negatively impact sensory perception or cause regulatory concerns is briefly described.

The unwanted migratory species may arise from the substrate or resin, from the environment, or be created during processing [103]. Examples include the following:

- Residual monomer, catalyst, low MW oligomers, or processing aids (such as slip agents, plasticizers, and lubricants) in the polymer resin. Sometimes the resin itself is clean but a masterbatch containing pigment or processing aid contains additives not accounted for;
- Mineral oils from recycled paperboard used in a secondary package, for example, in bag-in-box packaging;
- Uncured components of adhesives;
- Solvent and other components of inks;
- Oils on the surface of aluminum foil;
- Various additives from paper or paperboard;
- Oxidative by-products from extrusion of the polymer;
- Reactive by-products from irradiation (see Section 16.1.4).

There also may be migratory species that are regulated from a food or product safety perspective. Some components have been banned for use in certain applications, such as BPA containing polymers for baby bottles. Often various simulants are used to conduct migratory studies to satisfy regulatory agencies such as the U.S. FDA and the European Union Commission (EU 10/2011). These are described in Chapter 4.

Communication along the supply chain is important for ensuring the package does not create issues from impartation at the end user. It is important to note that materials with food regulatory compliance may still cause organoleptic issues. Often the offending components are by-products or residuals from the manufacturing process that are not controlled by the resin manufacturer. Other components may come from unforeseen sources, such as additive manufacturers, adhesives, and printing components. In multilayer films and laminates, components from the outside layer may transfer to the inside product-contact layer while the film is wound in the roll. This in turn may provide a source of impartation to the product during packaging. Finally, the film-converting process itself can generate unwanted migratory species.

The amount of impartation depends on a number of factors, which include the following:

- The concentration of migratory species in the package structure (or the environment if the origin of the species is outside the package).
- The concentration of the migratory species in the product. Ultimately, it is the concentration difference that drives diffusion from the package to the product.
- The solubility of the migrating species in the package material. If the species is strongly bonded to the package material, it is less likely to migrate out. This depends on the chemistry of the migratory species and the material.
- The size and shape of the species. Larger molecules generally diffuse more slowly than smaller ones. Linear molecules may diffuse faster than ones with branches or bulky side groups. Longer chain aliphatic molecules may have greater solubility in polyethylene.
- Barrier layers that may be between the layer containing the species and product (functional barrier in the language of regulators).
- The chemistry of the product. Acidic or fatty foods may have a different affinity for the migratory species than water. This affects the solubility and desorption of the species from the package to the food itself. Most migrants have a hydrophobic character and so more readily desorb into fatty foods. Some components of the product may plasticize or swell the polymer, allowing more migration to take place.
- Temperature. Higher temperature generally favors faster diffusion rates. Hot fill, retort, in-package sterilization, or even storage in a nonrefrigerated warehouse in the summer may contribute to greater migration. Refrigeration will slow migration.
- Relative humidity. Some polymers are plasticized by water, allowing migrating species to diffusion faster through them.

The oxidative degradation of polyethylene during cast film and extrusion coating and its effect on organoleptics has been well studied in a series of papers by Andersson [33–38]. The thermo-oxidative degradation of polyethylene results in the formation of alkyl radicals (R*) through cleavage of covalent bonds, followed by reaction with oxygen to form hydroperoxides (ROOH) in a chain reaction: RH → R* → RO_2* → ROOH → oxygenated products. The oxidation may start in the extruder but mostly occurs in the air gap between the die exit and chill roll (Section 15.1.2.1). Some of the key findings include the following:

- Oxidation creates degradation by-products consisting of alcohols, aldehydes, ketones, and carboxylic acids in the C_4–C_{12} range that can be found in the resulting films/coatings. (These same functional groups are also bound to the longer polymer chains and are responsible for the increase in adhesion of LDPE to polar substrates, as described in Section 15.1.2.1.)
- Smoke collected at the die exit contains volatile aldehydes, ketones, and carboxylic acids. More by-products are found with thicker coatings/films.
- The amount and type of degradation by-products depend on the exposure time in the air gap and temperature. At short times the by-products are mainly branched alkanes; at longer times acids, alcohols, ketones, and aldehydes form.
- The extrusion degradation by-products correlate with off-flavor in water packaged in the films, as determined by a sensory panel. The presence of aldehydes and ketones has the clearest effect on off-flavor with C_7–C_9 ketones and C_5–C_8 aldehydes having the greatest impact.
- The amount of oxidation, as measured by the carbonyl index (an IR method described in Section 15.1.2.1 measuring the amount of carbonyl groups that form), correlates with the degree of off-flavor determined by the sensory panel. The carbonyl index increases with increasing temperature, oxygen concentration in air gap, and time in the air gap.
- Adding scavengers can help reduce the off-taste. At low processing temperatures, reactive additives, such as maleic anhydride-grafted polyolefins, can help control the release of off-flavor components. Zeolites are also effective even at higher extrusion temperatures.
- Antioxidants added to the polyethylene are effective for preventing off-flavor, but they must be selected with processing temperature in mind. Thermal instability of the antioxidant can jeopardize the intended effect. A mixture of antioxidants is found to be most effective.

16.2.2.2 Scalping

Scalping involves migration of aroma or flavor components from the product into the package. The resulting loss of components affects the sensory quality of the product. Selecting materials and designing packaging structures that minimize scalping may help extend the shelf life of the product.

The interplay between the package and product can be very complex and is the subject of several review papers [39–45]. Migration involves sorption and partition of the molecule between the product and package, and diffusion. Partition relates to the equilibrium concentration of the species between the package and the product and is related to solubility. Diffusion is the time-dependent movement of the species between the two mediums. Partitioning is influenced by temperature, pH, the chemical structure of the migrant, molecular size and structure, fat content, and degrees of crystallinity [41,42].

The barrier to migration of organic molecules, oil and grease resistance, and chemical resistance are briefly described in Chapter 8. A few examples from the literature are provided here to illustrate the complexity. One food product that has garnered a considerable attention in the literature is orange juice. Pieper [18,46] stores orange juice is glass jars containing plastic packaging laminates for 24 weeks at 4°C and tests for absorption of 19 aroma compounds. The package structures are the following:

1. LDPE/board/LDPE/AP/EVOH/AP/LDPE (4/9 gsm for last two layers);
2. LDPE/board/LDPE/Al/AP/PET/AP/LDPE (0.5/26 gsm);
3. LDPE/board/LDPE/Al/AP/LDPE (8/34 gsm).

Here AP stands for adhesive polymer. Package number three (with the most amount of LDPE) absorbs more d-limonene and aroma compounds than

the other two packages. The order of absorption is glass < Pkg 1 < Pkg 2 < Pkg 3. Some compounds show little absorption while others up to 50%. A sensory panel finds no significant difference among any of the samples at any time during the study.

For nonpolar LDPE, the absorption of the nonpolar aroma molecule d-limonene is particularly an issue, since it is a major contributor to citrus juice flavor/aroma. The extent of absorption depends on the thickness of the contact layer and the surface to area ratio of the package.

Pieper comments that polyolefins have only minor differences in solubility but the diffusion rate is in the following order: LDPE > HDPE > PP. Polar polymers like PET show very little affinity for both polar and nonpolar aroma components.

Kwapong [47] stores strips of LDPE and two grades of ionomer in glass jars containing aqueous aroma compounds, including limonene, citral, ethyl butyrate, and linalool. Essential oils are also tested. A sensory panel finds significant differences between the control and test samples for all essential oils investigated. A significant difference is not found for benzaldehyde and citral. Limonene has the greatest affinity for the LDPE and ionomers. Orange oil sorbs considerably less than limonene, which the authors attribute to the chemistry. Limonene is nonpolar and has a greater permeability through nonpolar polymers like LDPE. They conclude that the compound characteristics are more important than the polymer for the materials they studied.

Mannheim [32,48] reviews previous work showing LDPE absorbs d-limonene. One study says this may be an advantage since d-limonene is a precursor to off-flavor compounds. Other studies have shown that increasing the thickness of the PE layer in contact with the juice increases the loss of d-limonene, LDPE absorbs more than an ionomer sealant and IR measurements indicate the limonene is absorbed rather than adsorbed. SEM studies show that LDPE swells as it absorbs d-limonene, which may be a factor in migration.

In Mannheim's study, orange juice is stored at 25°C for 12 weeks in PE/board/Al/PE cartons and compared with glass. Greater retention of ascorbic acid and less browning of orange juice occurs in glass. Greater amounts of d-limonene are found in the carton. A taste panel can tell the difference between orange juice packaged in glass and cartons after 2.5 months of storage.

Mannheim also immerses the PE layer into model solutions. Corona- and noncorona-treated LDPE films are used. The PE film accelerates ascorbic acid degradation with the treated film having the greatest effect. They also find differences between LDPE processed at high temperature followed by corona treatment (simulating carton production) and the LDPE liner used in bag-in-box package (made at lower temperature with no treatment). The liner shows no adverse effect on browning or ascorbic acid degradation but a loss in d-limonene. The taste panel cannot discern differences with a control.

Sheung [49] studies the absorption of d-limonene, α-pinene, ethyl butyrate, and octanal into laminated polymeric packaging materials containing LDPE, PET, PVDC, and EVOH. The packaging materials are stored in orange juice for 28 days at 25°C. The absorption of ethyl butyrate and octanal is the same for all four structures. Addition of a layer of EVOH or PET reduces the absorption of d-limonene and α-pinene by 50% and 20%, respectively.

Van Willige [50] stores packaging strips in orange juice and model simulants for 29 days at 20°C in the dark. In a model simulate with seven flavorants, absorption is much greater in LDPE than PET or polycarbonate (PC). In LDPE, absorption of valencene >> decanal, hexyl acetate, octanal, and nananone. In PC and PET, valencene is the lowest absorbed and decanal is the highest. The polarity of the flavorant molecule and polymer has a considerable impact on absorption.

In orange juice, limonene is absorbed readily by the LDPE, while myrcene, valencene, pinene, and decanal absorb much less. In PC and PET, only small quantities of limonene, myrcene, and decanal are absorbed. Loss of flavor compounds from the simulant or orange juice does not affect taste perception by a sensory panel from any of the three packaging materials.

Haugaard [51] stores fresh orange juice at 4°C for 14 days in HDPE, PS, and PLA. They find significantly greater loss of ascorbic acid in HDPE and PS than for PLA. Less color change is found for PS and PLA than for HDPE. There is no detectable loss of d-limonene in PS and PLA while a large loss is found for HDPE.

Lebosse [52] studies food interactions with a PP film using an acidic model solution with 10 aroma compounds. They comment that sorption protects the most reactive terpenes from degradation and thus

minimizes the formation of compounds which could behave as off-flavors (eg, α-terpineol).

Other studies have highlighted some of the chemistry and polymer science involved in scalping of flavor and aroma molecules:

- Gavara [53] finds that sorption of aroma compounds is selective. For example d-limonene has 2.5 times higher absorption in LLDPE than does ethyl caproate. The selectivity may account for perception differences in sensory panel evaluations. In general, they find a PET copolymer (co-PET) provides lower scalping of aroma compounds than an ionomer, which is better than LLDPE.
- Hernandez-Munoz [54] studies the effect of sorbed oil on aroma loss in ULDPE, ionomer, and co-PET packaging materials. The oil apparently swells the polymer, increasing the solubility but not the diffusivity (the holes generated by swelling are filled by the long oil molecules). The permeability of nonpolar compounds is considerably increased but not polar compounds. This has consequences for packaging of fatty foods—fat sorption may affect the rate of sorption of nonpolar aroma compounds. The study underscores the importance of testing with the food contaminates present. Chang [55] explores some of the computational aspects of this behavior.
- In a second study, Hernandez-Munoz [56] examines the influence of four fatty food simulants (95% ethanol, sunflower oil, n-heptane, and isooctane) on the sorption of six food aroma compounds in the same three packaging materials. They find that the aroma scalping is highly dependent on the food simulant. Polar aroma components are more sorbed into polymers in the presence of a nonpolar fatty food simulant and vice versa. In general, co-PET had the lowest partition coefficient for nonpolar components while ULDPE showed the lowest partition for polar aromas.
- Halek [57] considers the polarity and crystallinity aspects of polymers on their performance in food packaging. The permeant can change the mechanical properties of the polymer, increasing chain mobility and diffusion. He uses as an example the effect of relative humidity on the OPV of PVOH to show how cross-effects can affect permeation. The polar water molecule interacts with the polar bonds in the PVOH, swelling the structure and retarding interaction with polar permeants.
- Imai [58] measures the partition of aroma compounds in LDPE, EVOH, and a polyester copolymer (co-PET). Three probe compounds are tested: d-limonene, neral and geranial. The co-PET has significantly less sorption than the other two films. EVOH is better than LDPE, but the co-PET shows almost no sorption of d-limonene. Sorption occurs within a day in EVOH and LDPE but only slowly over 24 days in co-PET.
- Colomines [59] studies the influence of crystallinity on the interaction of PLA with the aroma compound ethyl acetate. An increase in crystallinity results in a decrease in ethyl acetate sorption. The aroma compound plasticizes the PLA: increasing the concentration decreases the T_g from around 60°C to well below room temperature.
- Lopez-Carballo [60] shows that sorption of α-pinene and ethyl butyrate in EVOH increases with increasing relative humidity. Even in the worst case (100% RH), however, EVOH outperforms LDPE as a barrier to organic vapors by at least 500,000-fold.
- Safa [61] studies the sorption of esters in PP packaging materials and finds the size and shape of the diffusion molecules matters.
- Van Willige [62] examines the effect of storage time and temperature on sorption of a 10-component model solution of flavor compounds. The absorption rate and amount increase with increasing temperature (4−40°C in the study). Depending on storage temperature, polyolefin (LLDPE and OPP) absorption is 3−2400 times that of polyesters (PET, PC, and polyethylene naphthalate).

To summarize, product−package interactions can be complex, resulting in loss of flavor or aroma components in the packaged product and shortening shelf life. Many factors are involved, which include the following:

- External factors, such as time, temperature, and relative humidity during storage;

- Composition of layers in the package structure, especially the polarity of the food contact layer and its surface area and thickness. Higher crystallinity in semicrystalline polymers tends to reduce sorption. In amorphous polymers, rubbery polymers (temperature above the T_g) have a greater affinity for sorption than stiff, glassy polymers;
- Chemistry (polarity), size, structure, and concentration of the migrating molecule;
- Chemistry of the food medium (pH and so on)
- Temperature of the food medium;
- Presence of other compounds that may swell the polymer, such as oils.

16.2.3 Active Packaging

Active packaging is a term used to describe packaging that purposely interacts with the product to extend shelf life or enhance the product quality. The interaction provides active rather than passive protection. Passive and active packaging are often used together, such as the combination of an oxygen barrier layer (passive) with an oxygen scavenger (active). Whereas scalping and impartation involve unwanted migration of molecules, active packaging usually involves the migration, sequestering, and emission of molecules to produce a desired outcome.

Some examples of active packaging include the following:

- Oxygen scavenging—see Section 8.5.1. Sachets for oxygen scavenging are one of the largest applications of active packaging.
- Odor scavenging to reduce undesirable aromas from food that has not yet spoiled.
- CO_2 scavenging or emission. One application is for scavenging CO_2 from fresh roasted or ground coffee in hermetically sealed packages to prevent pressure build and bursting [63]. CO_2 emitters have been used to extend modified atmosphere packaging (MAP).
- Moisture scavenging, typically in the form of desiccant sachets.
- MAP. This is the largest use of active packaging, although it does not involve an active interaction between the package and product.
- Ethylene scavenging/emitting for plant growth regulation.
- Antimicrobial activity.
- Antioxidation. An example is adding vitamin E to the package film with the intent of it migrating into the food product.

A number of articles provide good reviews of the technology [63–71]. Most successes have been at the academic level or with the use of sachets. Commercial applications have small and narrow markets in flexible packaging [72].

There are a number of challenges, both technical and financial. Chapter 8 describes the technology and challenges for oxygen scavenging. Two additional examples are highlighted here: odor scavenging and antimicrobials. The first has been more successful than the second.

16.2.3.1 Odor Scavenging

Ebner [68] provides a good grounding on the issues with odor scavenging that is summarized here. Many food products develop "confinement" odors—unpleasant odors that the consumer experiences when the package is first opened. These may arise from a number of sources, which include the following:

- sulfurous compounds from amino acid or carbohydrate breakdown;
- amines;
- aldehydes and ketones from lipid oxidation or carbohydrate degradation;
- fatty acids.

The basic causes are oxidation, enzymatic reactions, and bacteria growth, all of which can occur during product storage. Despite the odors, the product may be perfectly safe.

Many food types may benefit from reducing confinement odor, including poultry, bone-in meats, seafood, smoked and processed meats, baked goods, coffee, nuts, baking mixes, and snack foods. To design an optimal system the odor profile needs to be known. Each situation may need a different solution.

An odor scavenger system must meet a number of CTQs (critical to quality attributes or basic requirements), which include the following [68]:

- removes odors quickly;
- does not remove desirable odors;

- does not mask spoilage;
- is extrudable or coatable;
- is readily incorporated into a package structure, label, sachet, and so on;
- is colorless;
- has food law approval;
- is invisible to the consumer.

The chemistry of removing odor molecules suggests three possible approaches:

- Adsorbing or binding the odor molecule onto the surface of a scavenging agent. Examples include activated charcoal and silica gel.
- Absorbing the odor molecule into the pores of a solid. Examples include zeolites, molecular sieves, and cyclodextrins.
- Reacting with the odor molecule on the surface of the film to tie it up (chemisorption). An example is the reaction of hydrogen sulfide with iron or copper to form a metal sulfide.

The scavenging agent or solution may be extruded into the packaging film, coated onto the surface of the film, or contained in an absorbent pad or sachet. Ebner provides a list of typical odor scavengers and gives an example of their efficacy for reducing hydrogen sulfide.

Besides adding agents to the film, Hausmann [73] shows that the selection of the sealant resin may help control odor for certain foods and package forms. An ionomer sealant is compared with a standard polyethylene sealant for the vacuum skin packaging of beef loin. The package structure is (PA—EVOH—PA—tie—sealant) (80 μm). Samples are tested after 28, 42, and 56 days of storage at 4°C. The packages with ionomer sealant show reduced bacteria growth, lower drip (or purge) loss, and lower odor while keeping an acceptable meat color. A second study with skin packaging of pork roast, beef flank, and beef loin shows that the ionomer sealant provides lower drip loss, higher bonding of water to the meat (which correlates with more tender meat), and slightly better color after 2 weeks.

16.2.3.2 Antimicrobial

The drivers for antimicrobial packaging include improving food safety (controlling deleterious microbes such as *Listeria*); maintaining product color, taste, and odor; preventing spoilage; and extending shelf life. Retort sterilization, in-package pasteurization, irradiation; and HPP are technologies used to destroy microbes in food products. All of these technologies have shortcomings: thermal treatments may cause undesirable changes to the food taste, irradiation has labeling and cost issues and HPP is just emerging as a sterilization technology. Antimicrobial packaging may provide additional options for the food company. Refrigeration and control of temperature excursions during handling, transportation and storage is also important.

An ideal antimicrobial active package solution would meet the following CTQs [68]:

- GRAS (generally accepted as safe) and/or FDA, USDA, EPA, FTC, and other regulatory agency compliant;
- effective against a broad range of microorganisms;
- nontoxic, nonallergenic, and harmless to human health;
- stable at a wide range of temperatures, lighting and environmental conditions;
- fast acting, even in the presence of organic or biological substances;
- functional at refrigerated conditions;
- imparts no color, odor, or taste;
- effective over the life of the packaged product;
- ideally extrudable into the packaging;
- inexpensive.

There are three general strategies for using antimicrobials to control microbial growth inside the package. One is to add the antimicrobial agent to the food product itself, as an ingredient; this food additive approach is subject to different regulations from those for packaging. Another is to add the agent to the headspace. Sachets and MAP work in this way. MAP provides an initial environment for controlling microbial growth, but since the headspace atmosphere changes with time, the microbial growth rate may accelerate with passing time. Also, since MAP typically is a low oxygen environment, control of anaerobic microbe growth is critical (see Section 3.2.4 for more information about MAP).

The third strategy is to add the agent to the package material. Since antimicrobial additives typically need to contact the food to be effective, the additive either needs to be food grade (regulatory approval as a food ingredient) or be tightly bound to the package surface so that it is not extracted into the food. Most microbial growth occurs on the surface of solid and semisolid food products. There must be a mechanism for the antimicrobial agent to transfer from the package to the surface of the food. One method is to use volatile agents, where the agent can transfer from the film into the headspace and from there to the food product. If the agent is a nonvolatile migrating agent or is immobile, the food must be in direct contact with the surface of the packaging film. The package form can help provide direct contact; vacuum packaging, for example, provides contact with solid products. Some types of food products, such as ground meat, are not amenable to direct contact strategies.

There are several methods for applying antimicrobial agents as food additives or to the package itself. One is to dip coat the agent onto the product prior to packaging. This may not be effective for long as the agent diffuses from the surface to the core of the product. Another is to spray the agent as a solution onto the package. The final method is to incorporate the agent into the packaging structure. This includes the use of sachets, coatings, surface attachment, and extrusion into the film.

Han [66] provides a good review of antimicrobial systems tested in the last 20 years. Almost all the studies are academic. Many antimicrobial systems show promise in lab cultures but fail in actual food systems. Antimicrobial packaging has many challenges:

- Extrusion of organic antimicrobials into the film poses several difficulties. The extrusion temperature for most packaging polymers is too high for most organic molecules. Volatile molecules vaporize and are lost. Nonvolatile molecules such as enzymes are prone to thermal degradation. Low MW additives do not mix well with high MW polymers due to their difference in viscosity. Polar additives are incompatible with nonpolar polymers.
- Some additives may change the physical properties of the film or the heat sealability.
- Encapsulation by the polymer may prevent the agent from getting to the surface of the film to be effective.
- The agent itself or its degradation by-products from extrusion may cause organoleptic issues.
- Migrating agents must have a rate of migration that matches the rate of loss of the agent at the surface of the product. If the migration rate is too fast, and the agent is too soluble in the product, the agent may initially be effective at reducing the microbial population, but this will subside as the agent diffuses into the core of the product. Similarly, if the migration is too slow, not enough of the agent will get to the product surface to effectively control the microbial population. It is very difficult to control the migration rate without using a controlled release system that adds considerable cost.
- Inorganic agents such as silver, silver salts, and zinc salts are very effective antimicrobial agents in the lab. In practice, once a layer of dead cells cover the sliver molecule, it is shielded from affecting other microbes. Also, sulfur-containing amino acids present in some proteins can react with silver and render the surface inactive.
- Chelating agents such as chitosan may react with components of the food such as lipids and so be unavailable to react with the microbes.
- The efficacy of antimicrobial agents is influenced by many factors. Antimicrobials that can survive the extrusion or coating process may not be suitable for the food environment (pH, water activity, salt concentration, intrinsic enzymes, antioxidants, and other microbes) or withstand the storage environment (light or dark, warm or cold). Refrigerated environments are particularly problematic. Finally, the agent may not deactivate the type of microbe that needs to be controlled.
- Regulatory approval is required. Depending on the food and region, various regulatory agencies are involved.
- Label laws. For natural foods, compliance with the standard of identity might be compromised. Migratory agents may need to be listed as an ingredient in the food. One anecdote involves a volatile antimicrobial that was found to very

effective for a particular cheese product. No trace of the agent could be found on the product itself, but the company's legal team argued that since the agent was shown to be effective, it must be there. Adding the ingredient to the food product would have required the product to be relabeled as a different category of food due to labeling conventions. This was unacceptable to the company and commercialization of the system was abandoned.

16.3 Aging

The properties of polymers may change over time due to a number of factors:

- Environmental exposure. Temperature, pressure, humidity, and irradiation are discussed in Section 16.1. UV radiation is an another factor for some applications but is generally not an issue in flexible packaging since the shelf life of most goods is short and the product is usually stored indoors.
- Chemical attack. Oil, grease, and chemical resistance are discussed in Chapter 8. Food interactions are described in Section 16.2.
- Physical aging—the subject of this section.

Physical aging is generally the result of the movement of molecular chains over long time scales to more energy favorable configurations [74–77]. As the film is fabricated, it is cooled too quickly for the polymer chains to be in their equilibrium state. This results in excess-free volume. Chains can move even below T_g, albeit very slowly. Over time they fill the free volume: chains get closer together and interact more. As a result the polymer may get stiffer and stronger (due to more chemical interactions among the polymer chains) but lose ductility. For semicrystalline polymers, chain movement may result in the thickening of crystalline lamellae or the formation of smaller, secondary crystals. This behavior occurs as long as the ambient temperature is above the beta transition temperature of the polymer, which for most polymers is below room temperature (for example, for PET it is −5°C). The change in the polymer is more rapid at elevated temperatures (up to T_g or T_m).

Sepe [74] provides an example of how this affects packaging. PET bottles introduced in the 1970s became brittle when stored in warehouses at 50°C. Impact resistance decreased while strength and modulus increased. Several explanations were considered:

- loss of MW due to hydrolytic instability (over long time – similar to what happens at short times in an extruder);
- UV degradation;
- chemical exposure;
- increase in crystallinity.

Each of these was eliminated as possible mechanisms: the conditions were not severe enough to cause hydrolytic or thermal degradation, the bottles were not exposed to sunlight, no chemicals were present, and the temperature was not high enough for crystals to form. The loss in ductility, however, fits well with the physical aging hypothesis.

Aging can be delayed by storing the film/part at cold temperature. Higher MW decreases aging, as does cooling the polymer more slowly during film fabrication.

Some polymers are more susceptible to aging than others. Ionomer films, for example, exhibit an increase in modulus over the first week after fabrication. This behavior correlates with the onset and growth of a secondary melting peak in a differential scanning calorimeter (DSC) curve. Upon reheating, the peak disappears only to reform with storage time. The exact origin of this peak is debated in the literature [78–84], but it is likely a combination of the formation of secondary polyethylene crystals and reorganization within the ionic clusters. The same behavior is seen for acid copolymers and other ethylene copolymers (ECPs), although to a lesser extent. Conditions that suppress primary crystallization, such as increasing neutralization of the acid groups, gives rise to the greater formation of the secondary crystals [78].

PA6 undergoes secondary crystallization, especially in high humidity environments, that affects stiffness and dimensional stability. This is described in Section 13.5 as it pertains to film curl.

Beyond physical property changes, and often subtle changes in dimension, adhesion is most

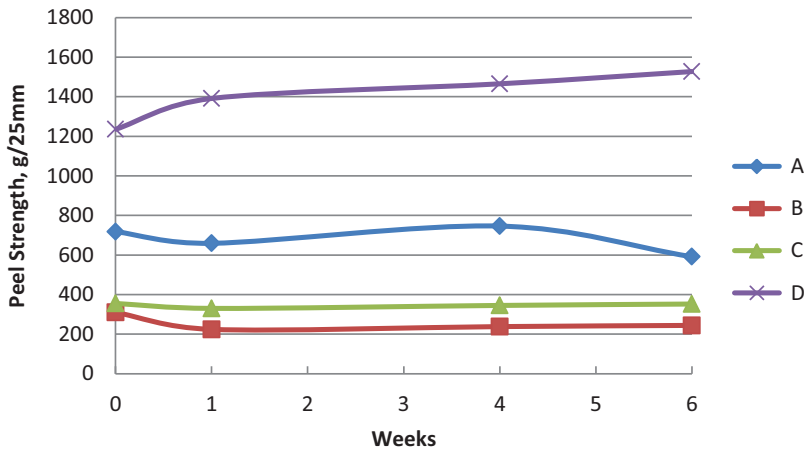


Figure 16.7 Example of peel strength as a function of storage time for an extrusion lamination. Structure is 12 μm OPET/19 μm ACR/9-μm Al/19 μm ECP/51 μm LLDPE film. Peel strength is between the ethylene copolymer (ECP) and Al foil layers. Storage was at 23°C, 50% RH. Samples A–D are different ethylene-based copolymers or homopolymers.

affected by aging. Peel strength may age up or down with time. An example showing the change in peel strength with time of several ethylene-based polymers to foil is shown in Fig. 16.7. A number of factors may cause peel strength to age up, which include the following:

- The movement of polymer chains or functional groups near the interface to create additional bond sites, particularly polar interactions between the two substrates.
- Bulk movement of polymer chains near the interface to fill in free volume. Lee and Wool [85–87] describe this phenomenon (Section 10.3.3). During bonding, the formation of reacted sites at the interface sterically hinders the positioning of the bulk chains near the interface. They postulate that this creates a region of lesser density near the interface, contributing to lower peel strength. Over time, as the chains move to fill in the voids and increase entanglement, the strength near the interface increases.
- Stiffening of the peel arms due to secondary crystallinity or physical aging. This may increase the energy needed to bend the peel arm during the peel test. The actual angle of separation and the amount of elongation may also change. These may act to either increase or decrease the peel strength.
- Changes in viscoelastic dissipation at the peel front due to physical aging. This may affect the peel strength measurement. The local energy dissipation at the peel front is likely linked to changes in crystallinity and free volume.
- Relaxation of residual stress as the molecules rearrange.

Age down of peel strength may also occur. Some of the factors that may be involved include the following:

- Migration of competing species to the interface, such as residual acids and processing oils, or in the case of product interactions, acids from the product itself, as described in Section 16.2.
- An increase in stress due to shrinkage from secondary crystallization. This is thought to be behind the cracking and age down of bonds between LDPE and metallized films.
- Changes in the chemistry of the one or both substrates. Moisture, for example, may change the oxide structure of aluminum foil (Section 16.1.2).
- Changes in the stress versus strain behavior of the polymer due to physical aging, resulting in a change in failure mode during the peel test.

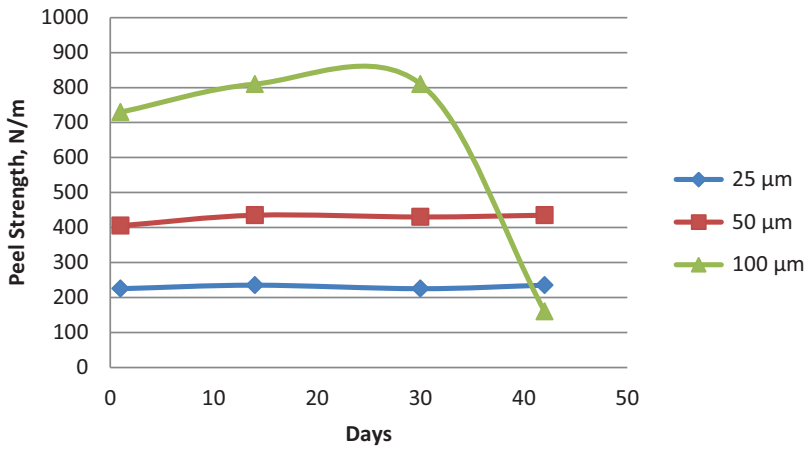


Figure 16.8 Peel strength of EMAA to aluminum foil as a function of storage time and coating thickness.
Reproduced with permission from Hoh G, Sadik SA, Gates JA. Aluminum foil adhesion of ethylene/methacrylic acid copolymer extrusion coatings. In: TAPPI polymers, laminations and coatings conference. 1989. p. 361–6.

An example of the last point is described by Hoh [88]. They found that the peel strength of thin extrusion coatings of EMAA (12 wt% MAA) on aluminum foil increased slightly with age. Aging was conducted at room temperature in a standard lab environment (no product present) for 42 days. The peel strength of a thick coating of 100 µm aged up for 28 days and then decreased to less than a quarter of its original value. This is illustrated in Fig. 16.8.

They found that the yield stress and secant modulus of the thick coating increased over the 4-week time period, as shown in Fig. 16.9. They attribute this to rearrangement of hydrogen bonded groups within the polymer, but secondary crystallization may also be involved. They use an analysis by Kaelble [89] to explain the results. Kaelble derives equations for the peel force when pulling a flexible membrane from a rigid substrate. The peel strength is related to the thickness of the film raised to the $^{3}/_{4}$ power and the modulus to the $^{1}/_{4}$ power:

$$\text{Peel Strength} \propto X^{3/4} E^{1/4} \tag{16.1}$$

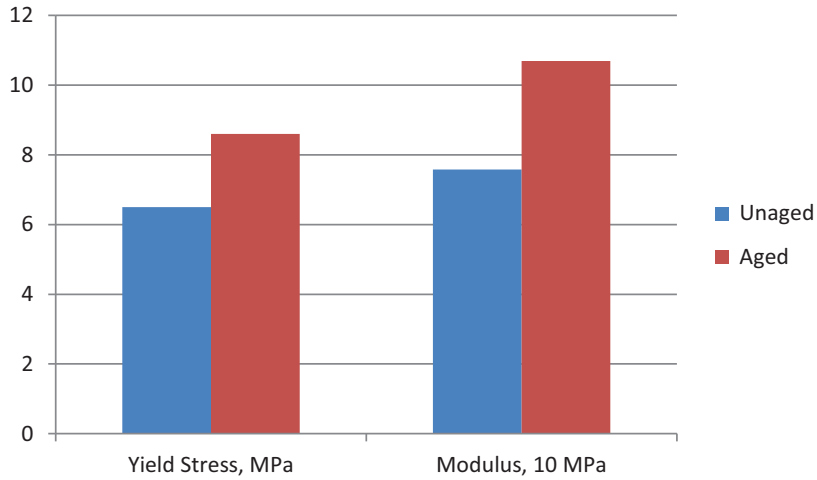


Figure 16.9 Aging of yield stress and secant modulus of EMAA film.
Data from Hoh G, Sadik SA, Gates JA. Aluminum foil adhesion of ethylene/methacrylic acid copolymer extrusion coatings. In: TAPPI polymers, laminations and coatings conference. 1989. p. 361–6. Modulus is in units of 10 MPa; multiply by 10 to get MPa.

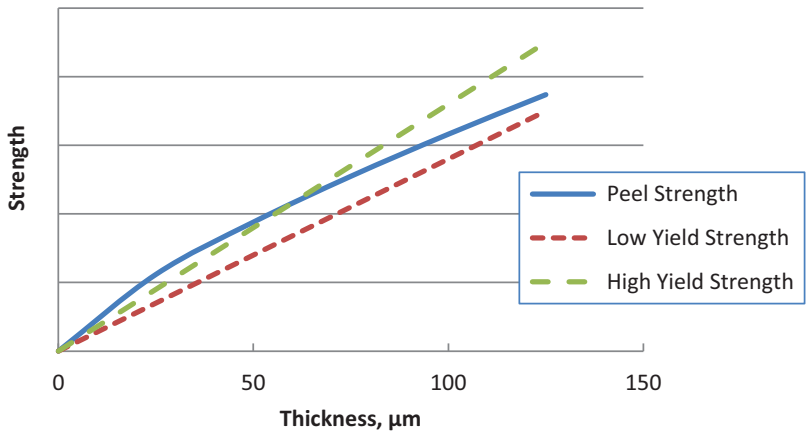


Figure 16.10 Effect of yield strength changes on apparent adhesion.
Reproduced with permission from Hoh G, Sadik SA, Gates JA. Aluminum foil adhesion of ethylene/methacrylic acid copolymer extrusion coatings. In: TAPPI polymers, laminations and coatings conference. 1989. p. 361–6.

where X = film thickness and E = tensile modulus of the film.

As the thickness of the coating is increased, its yield strength (yield stress times the cross-sectional area) increases. At some critical thickness, it will equal the peel strength. Below the critical thickness, the peel arm yields and elongates, distributing the energy of the peel test. Above the critical thickness, the peel arm does not yield and the peel energy is concentrated at the peel front, lowering the overall peel strength.

One way to illustrate is in Fig. 16.10. Here the peel strength versus thickness curve is shown as the solid curved line ($X^{3/4}$). The yield strength is a linear function of thickness as represented by the straight line. Initially, the yield strength curve is below the peel strength curve; yielding takes place during the peel test. As the yield stress increases with age, the yield strength curve crosses the peel strength curve. For this system, this occurs around 38–75 µm. Once the thickness crosses the threshold, yielding no longer takes place and the peel strength decreases.

Another way to visualize the effect of the change in yield strength is to plot the stress vs strain curve, as shown in Fig. 16.11. The horizontal line represents the interfacial stress threshold above which failure occurs. If the yield stress is below this threshold, the sample will yield and elongate until the threshold is reached (bottom curve). The peel strength is related to the area under the curve. With aging, the yield stress increases. If the increase takes it above the failure threshold, the peel arm does not elongate prior to failure and the area under the curve is considerably smaller.

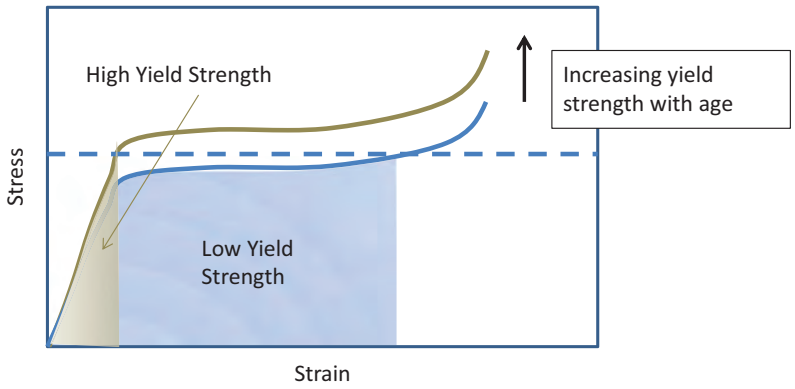


Figure 16.11 Energy analysis of the effect of changing yield strength on peel strength. Peel strength is related to the area under the stress versus strain curve.

16.4 General Considerations

The examples in Sections 16.1–16.3 underscore the need to test the packaging structure under conditions that simulate the end use. Changes in properties due to the environment, sterilization processes, product interactions, and physical aging may compromise the integrity of the package. The package may affect the quality of the product, especially the sensory perception of the product due to loss or gain of migratory species. Often these changes are complex and cannot be easily predicted in advance. Also simple testing may not be sufficient. For example, simulating scalping with a single food simulate may not capture the effects of coagents that may swell the polymer. Accelerated testing, especially at elevated temperature may also create confounding results—degradation mechanisms or polymer transitions that would not take place at the actual use temperature may provide spurious results.

16.5 Cost

Cost is a critical consideration for the end user. The driving force behind growth in flexible package, and specifically multilayer flexible packaging, is cost savings over other forms of packaging. The total cost of procuring and using the film should be considered, both from a financial and increasingly from a sustainability perspective.

16.5.1 Financial Costs

The cost of a packaging solution must be weighed against the total value the package provides and the next best competitive alternative. When comparing alternatives, differences in the price of the film, packaging line efficiencies, and throughput and failure rates (at the packer, during distribution and at the retailer) should be considered. These factors are outlined in Table 16.3.

Table 16.3 Financial Cost Factors in Flexible Packaging

Material Costs	Converting Costs	Packing/Brand Owner Costs
Material selection	Line speed	**Labor and overhead**
Structure design (thicknesses)	Length of runs (transitions)	Labor rate
Price	First quality yield	Number of workers
Quality	Number of processing steps (coex vs lamination)	Machine hour rate
Density	Ability to reuse scrap	Roll stock cost
	Labor rates	Transition losses
	Energy costs	Output (line speed)
	Profit margin	**Package failures**
		Off-machine rewraps
		Off-machine losses (including product)
		In-store losses
		Other
		Environmental taxes, fees
		Waste due to package form (eg, thermoforming round shapes in rectangular sheet)

16.5.1.1 Material Costs

The majority of the cost to make a roll of film comes from the raw materials. Judicious selection of raw materials and effective use of structure design allows the material costs to be optimized. Optimized is a better word than minimize. Often using a higher cost material lowers the total cost through better package performance (fewer failures), increased packing efficiencies, or lower roll stock costs (through material substitution, thickness reduction, or greater productivity in the converting process). Premium materials have their place but not for every application.

The density of the material affects its cost since most materials are sold on a weight basis but the final film is used on an area basis. Polyolefins enjoy a large share of the flexible packaging market not only because of their excellent properties, but because they have a lower density than most other polymers. On OPP film weighs 35% less than an OPET film of the same thickness.

Quality is an often overlooked factor in material costs. A material that is more consistent with fewer defects will run more efficiently in the film-converting process, increasing first quality yield.

16.5.1.2 Converting Costs

A number of factors impact the cost of converting the raw materials and substrates into flexible packaging films and laminates, as described in Table 16.3. There are often several different processes that can be used to implement a packaging solution: lamination, extrusion coating, coextrusion cast film, coextrusion blown film, and so on. The lowest cost process may depend on the size of the run and may change during the product's life cycle. Short runs may favor lamination or blown film, whereas large dedicated cast or coating lines may be used as the product scales up to larger quantities.

A number of technologies, many described elsewhere in this book, have helped improve productivity and reduce cost. Some examples include the following:

- the development of coextrusion, eliminating lamination steps for some packaging structures;
- the development of more robust metallized films that replace foil;
- the increase in the number of layers available for coextrusion, allowing the asset to be more flexible for making different structures and increasing the control over individual layer thickness;
- improved air rings in blown film for helping maintain bubble stability (allowing higher output and better control over film thickness);
- edge bead reduction dies that reduce edge trim in cast film and extrusion coating;
- encapsulation dies that allow edge trim of multilayer films to be recycled;
- higher melt strength resins that help improve bubble stability in blown film and reduce neck-in in cast film/extrusion coating.

16.5.1.3 Packing Labor and Overhead Costs

Higher packaging line speeds generally translate into lower cost since the machine time and labor is spread out over more packages. The line speed will depend on what the rate limiting step is. If the machine is hand fed, investment in automation or more laborers may help. Often the bottleneck is the sealing process—getting heat to the interface to melt and bond the sealant. Switching to a sealant with a lower seal initiation temperature may help. Alternative methods of sealing, such as ultrasonics, may be considered.

16.5.1.4 Indirect Packing Costs Due to Package Failure

The cost of package failures due to poor sealing, puncture, or general abuse through handling and distribution can be significant. The failure rate typically ranges from less than one percent to several percent. The cost will depend on the cost of the product and volume: leakers may be more costly per item in terms of returns for a fresh meat product than for a bag of potato chips, but because the sheer volume and scale, small reductions in failure rates are a big driver for snack food companies.

The failures can be categorized into three types. Off-machine rewraps are those that the operator notices during packing. The product is returned to be repackaged and so the loss is only the film itself.

Off-machine losses are those that are detected while the product is still at the packer but both the film and product must be disposed. In-store losses are returns and credits from failures detected at the retailer. These involve loss of both product and film. A fourth category that is difficult to quantify are those packages that prematurely fail after the consumer has purchased the product. Many of these go unreported but can potentially damage brand image and result in loss of repeat sales.

16.5.1.5 Other Costs

Some countries or regions, such as Europe, have enacted laws imposing taxes or fees on packaging structures to help encourage reducing and recycling of packaging. In some cases, the roll stock cost of the film can be somewhat higher if it results in a lower environmental fee.

Other costs include the waste associated with package form. An example is thermoforming of round shapes from a rectangular sheet. About 50% of the sheet is not used due to simple geometric considerations. If this portion of the sheet cannot be reused in the existing structure, it often must be downgraded, sold at a loss, or disposed of.

16.5.1.6 Modeling Financial Costs

Models are available that estimate the financial costs of packaging. A simple model is available online from DuPont called the Sealant Value Estimator tool [90]. It was originally developed in the 1980s as a tool to help packers understand the value premium sealants provide in terms of lower total cost. It includes the roll stock cost, direct packaging costs (except the transition losses), and indirect packaging costs due to failures. The tool is used here to illustrate the benefit of designing structures for improved throughput and reduced failure rate.

To demonstrate the utility of cost modeling, a hypothetical cereal liner bag-in-box structure is considered. A flexible packaging structure with a Surlyn ionomer sealant is compared with another sealant (designated "Other"). This may be an EVA sealant, for example. In this analysis, it is assumed the performance of the Other structure is known and fixed. The analysis shows how much saving might occur if the package performance was to be improved and how sensitive this is to the cost of the roll stock and other cost parameters.

The inputs to the model are provided in Table 16.4. A 10% improvement in line speed and 50% lower failure rate is assumed for the Surlyn sealant. The roll stock cost is 6% higher for the film containing Surlyn.

The analysis results are given in Table 16.5 and shown graphically in Fig. 16.12. In this example, switching to the ionomer sealant increases the package material costs but reduces the overall costs by $140,000 per year through savings in labor and overhead and a reduction in waste (including loss of product).

The model includes a sensitivity analysis where each input parameter is varied while the others are held constant. This provides an assessment of how much of a change is needed for that input parameter to match the cost performance of the Other film. An example is shown in Fig. 16.13 for the effect of line speed. The Other film is assumed to be constant (at 58 pkg/min) since it is the known control. The cost of using the Surlyn film at various line speeds is plotted; at low line speed the cost is high due to the greater machine hour time and labor to produce the same number of packages. The cost decreases with increasing line speed. Where the two curves intersect is the breakeven point. Keeping all the other inputs constant, the analysis shows that the Surlyn film would still be cost-effective at $>$ 49 pkg/min, 16% less than the 58 pkg/min of the Other film. The cost saving due to the improved failure rate allows for this, if needed. More than likely, however, Surlyn will allow higher line speed than the incumbent because of its low seal initiation temperature.

A similar breakeven analysis is shown in Fig. 16.14 for roll stock costs. The result shows that the price of the Surlyn film could be 10% higher than the value used in the original analysis (and 17% higher than the Other film) and still be more cost-effective than the Other film.

These types of analyses can be very helpful for determining very quickly whether a premium material is worth considering for a given application.

16.5.2 Environmental Costs

Flexible packaging is well suited for its first life purpose of protecting the product, reducing spoilage of foodstuffs, reducing cost, and providing consumer convenience. It uses less material, requires less

Table 16.4 Example Input Table for the Sealant Value Estimator (SaVE) Tool for a Hypothetical Cereal Liner. The Model Compares Two Film Structures, One With a Surlyn Ionomer Sealant and Another (Other)

Sealant Value Estimator (SaVE)		
Case Name: Cereal Liner		
Packing Line Input		
Number of employees	1	
Cost per man-hour (labor rate), US$ per hour	20	
Fixed overhead and equipment costs per hour, US$	20	
Packages produced per week (in thousands)	596	
Weeks per year packing product	50	
Product cost per 1000 packages, US$	500	
Film Specific Input	**Surlyn**	**Other**
Packaging line speed, packs per minute	64	58
Roll stock price per 1000 in^2, US$	0.09	0.0854
Surface area of roll stock used per package, per 1000 in^2	0.65	0.65
Percent off-machine rewraps	1.5	3
Percent off-machine losses	0.5	1
Percent in-store losses	0.5	1

Based on input screen from the DuPont ND. Sealant value estimator: are you paying too much for sealed packaging? DuPont, viewed November 28, 2015 at http://www2.dupont.com/Packaging_Resins/en_US/Modeling_Tools/SaVE/index.html.

Table 16.5 Example Output Table for the Sealant Value Estimator (SaVE) Tool for a Hypothetical Cereal Liner

Analysis		
Summary of Costs: US$ per 1000 packages	**Surlyn**	**Other**
Package materials cost	58.5	55.51
Labor and Overhead cost	10.42	11.49
Waste cost due to off-machine package failures	3.88	7.68
Waste cost due to in-store package failures	2.84	5.67
Total packaging costs with store rejects	75.64	80.35
Total Savings, US$		
Savings per 1000 packages using Surlyn	4.71	
Savings per week using Surlyn	2810	
Savings per year using Surlyn	140503	
Savings per machine hour	18	

Based on output screen from the DuPont ND. Sealant value estimator: are you paying too much for sealed packaging? DuPont, viewed November 28, 2015 at http://www2.dupont.com/Packaging_Resins/en_US/Modeling_Tools/SaVE/index.html. Reproduced with permission from E.I. du Pont de Nemours and Company.

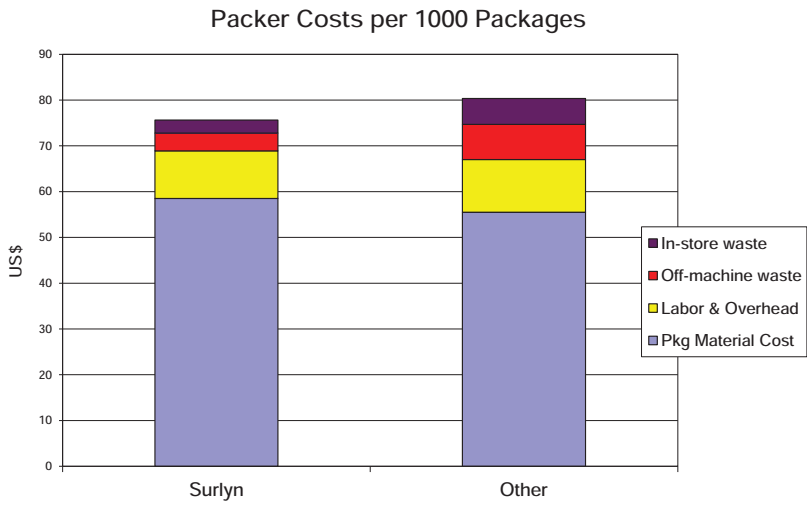


Figure 16.12 Graphical output from DuPont's SaVE tool for a hypothetical cereal liner film application comparing Surlyn ionomer sealant with another sealant.
Data from Morris BA. Optimizing flexible packaging … with unique tools from DuPont, In: Presentation at PackExpo; 2011. Reproduced with permission from E.I. du Pont de Nemours and Company.

energy to produce and transport, and has a lower environmental footprint than other packaging formats. Indeed, flexible packaging has a net benefit to society when the prevention of product waste is considered; the environmental cost of the wasted product overwhelms the environmental footprint of the package. Yet flexible packaging has its issues, particularly when it comes to end-of-life scenarios. Very little postconsumer flexible packaging is currently recycled and multimaterial films and laminates make them more challenging to reuse. This

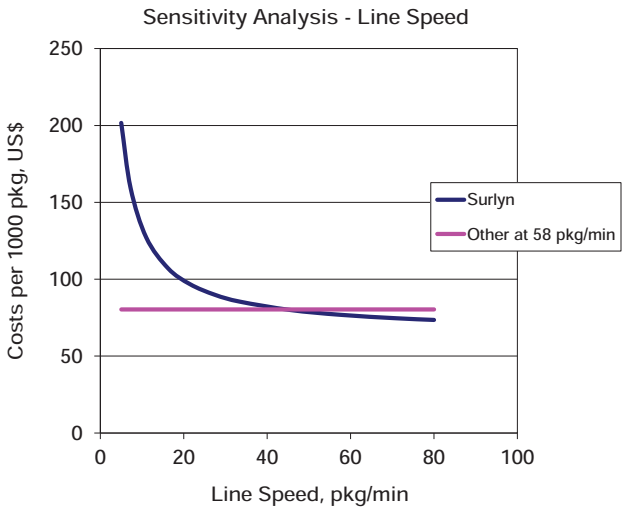


Figure 16.13 Breakeven analysis for line speed.
Based on output from DuPont ND. Sealant value estimator: are you paying too much for sealed packaging? DuPont, viewed November 28, 2015 at, http://www2.dupont.com/Packaging_Resins/en_US/Modeling_Tools/SaVE/index.html. Reproduced with permission from E.I. du Pont de Nemours and Company.

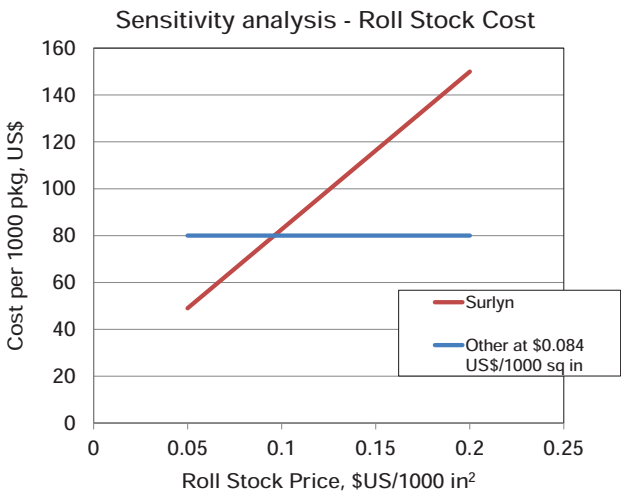


Figure 16.14 Breakeven analysis for roll stock price.
Based on output from DuPont ND. Sealant value estimator: are you paying too much for sealed packaging? DuPont, viewed November 28, 2015 at, http://www2.dupont.com/Packaging_Resins/en_US/Modeling_Tools/SaVE/index.html. Reproduced with permission from E.I. du Pont de Nemours and Company.

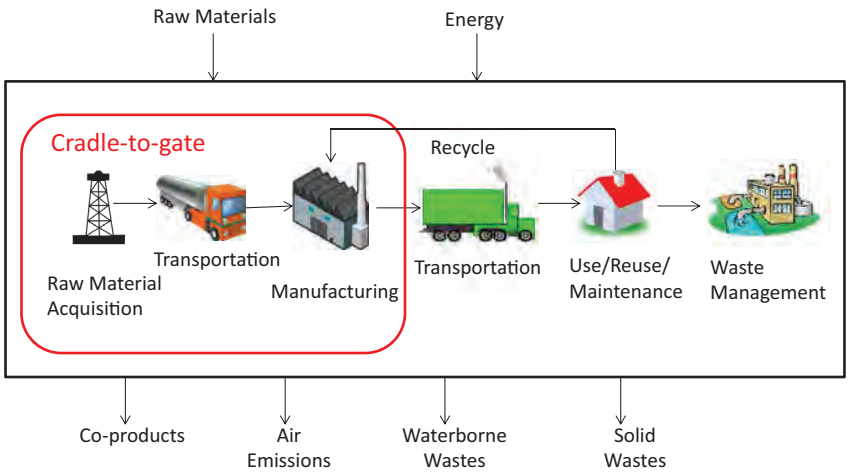


Figure 16.15 Schematic of a product life cycle.
Courtesy of E.I. du Pont de Nemours and Company.

section examines how the environmental costs of packaging are quantified (using life cycle analysis (LCA) methodology) and end-of-life issues.

16.5.2.1 Life Cycle Analysis[1]

The packaging industry is becoming more sophisticated in understanding the nuances of what represents a truly sustainable product. Initially, the industry focused on such factors as bio-based content and package weight reduction. While these factors are readily measured and communicated, they are not measures of actual environmental impact. As such, there is the possibility of a seemingly sustainable solution to have a negative environmental impact relative to the so-called nonsustainable incumbent. LCA has emerged as the premier technology to access sustainability; standards have been adopted and results are increasingly becoming available to the public.

An LCA is a detailed assessment of the environmental impact of a product or offering throughout its life cycle. Depending on the scope of the LCA, different environmental impacts can be considered. Typically, LCA focuses on nonrenewable energy consumed and greenhouse gas (GHG) emitted (also called global warming potential). Other environmental impacts may also be considered, such as acidification, eutrophication, ozone depletion, smog generation, and water use. The nonrenewable energy consumed is net of any energy generated and recycled in the process and is reported as megajoules/unit, typically megajoules per kg of product (MJ/kg). The GHG emissions include emissions from utility generation (eg, electricity, steam), as well as process emissions of any GHG, and are reported as kilograms of carbon dioxide equivalent/unit, again typically per kilogram of product (kg eq. CO_2/kg).

The scope of the LCA is important. Referring to Fig. 16.15, a cradle-to-grave LCA covers raw materials, manufacturing, use, and end-of-life phases. While it is certainly desirable to understand the environmental footprint all the way through the life cycle, the number of value chain participants makes it extremely difficult to obtain reliable data. For this reason, most available LCA data is for the so-called cradle-to-gate, which includes the environmental footprint of the production of raw materials and all required manufacturing steps. Although the scope of a cradle-to-gate LCA is narrower than that of cradle-to-grave, it is still very much a challenge to get reliable and complete data sets so sensible assumptions and approximations are often unavoidable. Also, comparing LCA results from different sources can be challenging since each study may make different assumptions on, for example, heat and electricity generation, which may result in slight differences of the final results. For these reasons, in general, the accuracy of any given LCA should be considered to be no better than ±10% when comparing studies not performed within the exact same scope.

[1]Based on Casarino, Morris and Veith [94].

A cradle-to-gate LCA for a polymer supplier includes monomers, additives, process chemicals, and so on. The resin manufacturer obtains data on the energy and GHG for each raw material—this is often called the embodied or feedstock energy or embodied GHG. Embodied energy and GHG data can be obtained from a variety of sources—public databases, LCA software packages, from the supplier, or depending on the degree of backward integration, from the resin manufacturer's own operations. The LCA also includes manufacturing, which for the polymer supplier may include polymerization, pelletization, compounding, and so on.

Key inputs to enable a packaging converter to conduct his or her own cradle-to-gate LCA is the embodied energy and GHG in the resins used to make packaging structures. There are a growing number of publically available databases providing data for a number of monomers, ingredients, and resins. Examples include PlasticsEurope, ACC, Ecoinvent, and other LCA software databases. These are generally based on industry averages and/or input from key industry players, and the results are aggregated to conceal any individual organization's proprietary information. As such, these data are generally available only for large volume commodity materials. Data for nonrenewable energy consumption and GHG for several polymers used in packaging are given in Table 16.6.

LCA data are helpful for polymer manufacturers to help them prioritize process improvements or product development that may have significant footprint reduction potential. LCAs can help film converters optimize packaging structures by allowing comparison between functional alternatives. For films, this will typically mean footprint per unit area that gives the same degree of product protection, shelf appeal, handling, abuse resistance, and other properties. While LCAs are typically computed in terms of energy requirements or emissions per unit weight, converting such information into meaningful functional alternatives is not always straightforward. For example, when comparing different package forms, the functional unit should be posed in terms of the unit of product packaged (such as per kg of food product), or even better would be per unit of food waste avoided. Another challenge is that packaging structures can be put together in a number of ways using a variety of converting processes. If the film-converting processes are assumed to have similar footprints, then the overall impact of multilayer film structures can be compared by summing the material quantities and footprint/kg of each material that makes up the structure.

Casarino [94] provides an example comparing three resins used to make a clamshell package: amorphous polyester (APET), high impact polystyrene (HIPS), and PLA. Some of the characteristics

Table 16.6 LCA Data for Packaging Resins and Films

Polymer	Nonrenewable Energy Consumption (MJ/kg)	Greenhouse Gas Emissions (kg eq. CO_2/kg)	Sources
PET resin	69	2.3	PlasticsEurope (2013) [92]
PA6 resin	129	6.7	PlasticsEurope (2014) [92]
HDPE resin	79	1.8	PlasticsEurope (2014) [92]
LDPE resin	82	1.9	PlasticsEurope (2014) [92]
LDPE film	88	2.4	PlasticsEurope, 2005 [92]
LLDPE resin	79	1.8	PlasticsEurope (2014) [92]
PP resin	77	1.6	PlasticsEurope (2014) [92]
OPP film	98	3.2	PlasticsEurope (2005) [92]
APET	80	3.3	PlasticsEurope (2005) [92]
HIPS	87	3.4	PlasticsEurope (2005) [92]
PLA	54	1.8	Vink [93]

Table 16.7 Properties of Clamshell Resins

Resin	Cost ($/m^3)	Tensile Modulus (GPa)	OPV (cc-25 μm/m^2-d)	MVTR (g-25 μm/m^2-d)
APET	2500	2	45–90	15
HIPS	2300	1.8	4700–9300	155
PLA	2500	3.4	620	325

Reproduced with permission from Casarino CM, Morris BA, Veith SR. Resin life cycle estimation to help guide sustainability choices, In: SPE ANTEC conference; 2009.

of these resins are given in Table 16.7. The traditional approach is to compare these materials based on cost and physical properties. The price and densities of these resins differ; however, on a unit volume basis, all three materials cost about the same. Because of its lower oxygen and moisture permeability, APET is favored for applications requiring moderate barrier. HIPS is favored for applications requiring breathability.

Environmental factors can also be considered. Table 16.6 lists the nonrenewable energy consumption and GHG emissions for these materials. This information needs to be put on an equal basis for comparison. The high stiffness of PLA may allow it to be downgauged in this structure while maintaining the overall feel and function of the package. The bending stiffness of a film/sheet scales as the modulus times the thickness cubed (Chapter 9). For comparison, the APET sheet is selected as the control with a thickness of 0.38 mm (15 mil). The thickness of HIPS and PLA sheet is computed to be 0.39 and 0.32 mm, respectively, to have the same bending stiffness as the APET sheet. A correction for the density of the resins is also made. The combination of the density and thickness allows the conversion of the footprint data from per kilogram basis to the functional basis of per unit area. Table 16.8 gives the results of the calculations, which show the following:

- Using HIPS allows some reduction in energy and GHG emissions over APET because of its lower density.
- PLA gives the greatest reduction in energy and GHG emissions as a result of having an inherently lower footprint and the opportunity for reducing the package thickness (downgauging). Downgauging may also allow for cost reduction.

In the above example, it is assumed the brittleness and use temperature limitations of PLA can be ignored. The analysis highlights the potential of PLA if these problems can be mitigated through the use of additives or other solutions [95,96].

LCA information can be incorporated into packaging design models. An example of this is provided in Chapter 17.

16.5.2.2 End-of-Life Scenarios

Flexible packaging generates less waste than other package formats due to its small physical footprint.

Table 16.8 Results of LCA Calculation for Clamshell Packaging

Resin	Density (g/cc)	Thickness (mm)	Weight/ Area (kg/m^3)	NREC (MJ/m^2)	Reduction (%)	GHG (kg eq. CO_2/kg)	Reduction (%)
APET	1.35	0.38	0.51	41	0	1.7	0
HIPS	1.05	0.39	0.41	36	−12	1.4	−17
PLA	1.24	0.32	0.40	21	−48	0.7	−58

NREC = Nonrenewable energy consumption.
Reproduced with permission from Casarino CM, Morris BA, Veith SR. Resin life cycle estimation to help guide sustainability choices, In: SPE ANTEC conference; 2009.

Flexible Packaging Europe [104], for example, calculates that the use of 26.5 million tons of packaging material (or 77% by weight) could be prevented if all of packaging in Europe were switched to flexible packaging. Nevertheless, flexible packaging has several negative end-of-life issues around disposal, littering, ocean pollution, reuse, and recycling. These issues are due to the following [97]:

- lack of collection and recycling infrastructure that can handle the collection, sorting and recycling of films. This is particularly true for multilayer films and laminates for barrier packaging;
- slow environmental degradation of many of the materials used; and
- food waste contamination—often 10–20% of package weight.

Flexible packaging also has a visibility problem. Even though it makes up only a small portion of the municipal waste stream, it often is seen as the problem. Public perception is a challenge to the industry. Sustainability is often equated with recycling, ignoring the positive benefits flexible packaging brings to society.

Several approaches are being taken by the industry to enhance recycling and recovery of flexible packaging. These include the following [97]:

Monolayer and coated barrier systems. Europe is considering mandates toward a "circular" economy for flexible packaging [98]. This means reusing, repairing, refurbishing, and recycling existing materials and products in a more focused way. This is driving new monomaterial approaches to packaging. An example is an all-polyethylene stand-up pouch developed by Dow Chemical [99]. Various barrier-coating technologies are also being researched in the industry, such as SiOx, AlOx, nanoclays, carbon nanocoats, that would be recyclable in the polymer stream. As Cooper [97] points out, there is still a problem of collection and sorting to separate and recycle these packages mechanically into the base polymer stream. This may be no easier than using multilayer barrier materials, which can be recovered to produce energy or fuels. Also, there still remains the problem of film contamination, particularly with food waste, that is hard to clean from postconsumer film for recycling.

Improved collection, marking, and sorting systems. These are needed to increase the recycle rate substantially. A number of entities are working on developing technology, including UK REFLEX, U.S. Recycling Partnership and the Sustainable Packaging Coalition. Among UK REFLEX's goals is to develop polymer blends from flexible packaging for new uses, improved identification, marking and sorting systems, and water-based ink removal systems. As a first step, Resource Recycling Systems is evaluating the effectiveness of existing sorting equipment at municipal recycle centers for use with flexible packaging. The goal is to allow flexible packaging to be included in mixed waste curb-side collection programs.

Delamination technology to separate layers in multilayer packaging. Saperatec is working on a low-energy mechanical method to separate layers after the waste has been shredded. A proprietary surfactant microemulsion breaks up the layers. It was originally developed for rigid packaging and is being extended to flexible.

Anaerobic and pyrolytic waste-to-energy, waste-to-fuel, and waste-to-chemicals processes. A number of companies are working in this field. For example, Enerchem [105] has pilot facilities in Canada for making syngas from garbage using a thermochemical process. Municipal solid waste is sorted to remove recyclable items and fed into a gasification reactor, which produces a syngas rich in hydrogen and carbon monoxide. The gas goes through a series of cleaning and catalytic synthesis steps to produce chemical grade syngas and renewable biofuels and chemicals, including methanol.

Pyrolysis is a promising anaerobic technology that differs from incineration, which is an aerobic process. It generates low levels of emissions and GHGs, yields useful chemical or fuel products, and produces no dioxins. Pyrolysis processes have advantages in that the packaging can be mixed with other refuse and no market needs to be found for the recycled product. Sorting and contamination are no longer issues.

Some NGOs, consumers, and lawmakers do not consider these methods "true" recycling, however. It is unclear if the infrastructure for pyrolysis and other waste-to-chemical technology will be built to handle postconsumer waste on a large scale.

Other existing technologies have so far failed to make a substantial impact on end-of-life issues with flexible packaging. These include the following:

- Compostable packaging. Polymers such as PLA, PBAT (eg, BASF's Ecoflex), and other aliphatic polyesters, and thermoplastic starches are compostable in industrial facilities. They generally do not degrade fast enough to be home composted (they require higher temperatures) or to degrade naturally in the environment or in landfills. Since large-scale industrial composting facilities do not exist in most regions, these compostable polymers are typically used in closed system settings, such as amusement parks and sports stadiums.
- Biodegradation additives. These are additives that are added to petroleum-based polymers such as polyethylene that promote breakdown of the polymer over time. They typically act through oxidation catalysts or enzymatic activity to fragment the polymer into microscopic pieces that are more amendable for biological activity. They are controversial for a number of reasons, including their contribution to littering (products labeled as biodegradable are more likely to be littered by the consumer), contribution of fossil carbon dioxide to the atmosphere if they do break down aerobically (causing a net increase in atmospheric carbon dioxide) and methane, an even more powerful GHG, if they break down anaerobically (such as in a landfill). The rate of degradation slows when in deep water oceans and so the additives may not mitigate marine pollution. The jury is still out on these additives with industry groups pitted against one another making conflicting claims [100–102].

The end-of-life issues with flexible packaging reflect those of other multicomponent systems and will be the subject of continued research and regulation going forward. These may drive the development of new package forms and structures in the future.

References

[1] Osswald T. "Mechanical behavior of polymers," understanding polymer processing: processes and governing equations. Hanser; 2011. sample chapter, viewed November 24, 2015 at, http://www.hanserpublications.com/SampleChapters/9781569904725_9781569904725_Understanding%20Polymer%20Processing_Osswald.pdf.

[2] Tsai BC, Jenkins BJ. Effect of retorting on the barrier properties of EVOH. J Plastic Film Sheeting 1988;4:63–71.

[3] Lopez-Rubio A, Lagaron JM, Gimenez E, Cava D. Morphological altercations induced by temperature and humidity in ethylene-vinyl alcohol copolymers. Macromolecules 2003;36:9467–76.

[4] Lopez-Rubio A, Hernandez-Munoz P, Gimenez E, Yamamoto T, Gavara R, Lagaron JM. Gas barrier changes and morphological alterations induced by retorting in ethylene vinyl alcohol-based food packaging structures. J Appl Polym Sci 2005;96:2192–202.

[5] Mokwena KK, Tang J. Ethylene vinyl alcohol: a review of barrier properties for packaging shelf stable foods. Crit Rev Food Sci Nutr 2012;52:640–50.

[6] Hernandez RJ, Giacin JR. Factors affecting permeation, sorption and migration processes in package-product systems. In: Taub IA, Singh RP, editors. Food storage stability. Boca Raton, FL: CRC Press; 1998. p. 269–330.

[7] Schubert G. Adhesion of aluminum foil coatings – stick with it. In: TAPPI European PLACE conference; 2004.

[8] Fersti C, Fersti P. High pressure processing: insights on technology and regulatory requirements. NFL White Paper Series, vol. 10. The National Food Lab; 2013. Viewed on November 22, 2015 at, http://www.thenfl.com/wp-content/uploads/High-Pressure-Processing-Insights_20131.pdf.

[9] Avure HPP Food Processing, ND. viewed on November 22, 2015 at http://www.avure-hpp-foods.com/.

[10] Hiperbaric USA, ND. High pressure processing for food & beverage products, viewed on November 22, 2015 at http://www.hiperbaric.com/en.

[11] U.S. Food and Drug Administration. Kinetics of microbial inactivation for alternative food processing technologies – high pressure

processing. 2014. Viewed on November 22, 2015 at, http://www.fda.gov/Food/FoodScienceResearch/SafePracticesforFoodProcesses/ucm101456.htm.
[12] Multivac, ND. HPP: high pressure preservation, viewed on November 22, 2015 at, http://www.multivac.com.au/our-products/hpp-high-pressure-preservation.html.
[13] Hemmerich KJ. Polymer materials selection for radiation-sterilized products. MDDI; 2000. viewed November 24, 2015 at, http://www.mddionline.com/article/polymer-materials-selection-radiation-sterilized-products.
[14] Lyons BJ, Weir FE. The effect of radiation on the mechanical properties of polymers. In: Dole E, editor. The radiation chemistry of macromolecules, vol. 2. Academic Press; 1973.
[15] Hoh G, Cumberbatch GM. Stability of Surlyn® films to radiation. In: TAPPI polymers, laminations and coatings conference; 1990. p. 251–92.
[16] Komolprasert V. Packaging for foods treated with ionizing radiation. In: Han JH, editor. Packaging for non thermal processing of food. Blackwell Publishing; 2007. viewed November 25, 2015. From http://www.fda.gov/Food/IngredientsPackagingLabeling/IrradiatedFoodPackaging/ucm081399.htm.
[17] U.S. Code of Federal Regulations 21 CFR 179.26, viewed November 30, 2015 at, http://www.accessdata.fda.gov/scripts/cdrh/cfdocs/cfcfr/cfrsearch.cfm?fr=179.26.
[18] Pieper G. Interaction phenomenon in multilayer flexible packaging. In: Ackermann P, Jagerstad M, Ohlsson T, editors. Foods and packaging materials – chemical interactions, 162. Special Publication–Royal Society of Chemistry; 1995. p. 95–100.
[19] Schroeder MA, Harte BR, Giacin JR, Hernandez RJ. Effect of flavor sorption on adhesive and cohesive bond strengths in laminations. J Plastic Film Sheeting 1990;6:232–46.
[20] Olafsson G, Jaegerstad M, Oeste R, Wesslen B. Delamination of polyethylene and aluminum foil layers of laminated packaging material by acetic acid. J Food Sci 1993;58:215–9.
[21] Olafsson G, Jagerstad M, Oste R, Wesslen B, Hjertberg T. Effects of different organic acids on the adhesion between polyethylene film and aluminum foil. Food Chem 1993;47:227–33.
[22] Olafsson G, Hildingsson I. Sorption of fatty acids into low density polyethylene and its effect on adhesion with aluminum foil in laminated packaging material. J Agr Food Chem 1995;43:306–12.
[23] Olafsson G, Hildingsson I, Bergenstahl B. Transport of oleic and acetic acids from emulsions into low-density polyethylene; effects on adhesion with aluminum foil in laminated packaging. J Food Sci 1995;60:420–5.
[24] Olafsson G, Hildingsson I. Interactions between carboxylic acids and laminated food packaging material. In: Ackermann P, Jagerstad M, Ohlsson T, editors. Foods and packaging materials – chemical interactions, 162. Special Publication – Royal Society of Chemistry; 1995. p. 101–7.
[25] Koch J, Robinson L, Figge K. Determination of fat release by foods. I. Methods. Fette Seifen Anstrichm 1976;78:371.
[26] Koch J, Figge K. Determination of fat release by foods. II. Application of method to additional foods. Fette Seifen Anstrichm 1978;80:158.
[27] Bieber WD, Figge K, Koch J. Interaction between plastic packaging materials and foodstuffs with different fat content and different fat release properties. Food Addit Contam 1985;2:113–24.
[28] Bernacki R. Adhesive polymers for extrusion coating and lamination. In: TAPPI polymers, laminations & coatings conference proceedings. Atlanta: TAPPI Press; 1985. p. 311–8.
[29] Antonov V, Soutar A. Foil adhesion with copolymers: time in the air gap. In: TAPPI 1991 polymers, laminations & coatings conference proceedings. Atlanta: TAPPI Press; 1991. p. 553.
[30] Hester D, Sadik S, Trouilhet Y. Using acid copolymers as coextrusion tie layers. In: TAPPI polymers, laminations & coatings conference; 1989. p. 459.
[31] Lustiger A, Markham RL. Importance of tie molecules in preventing polyethylene fracture under long-term loading conditions. Polymer 1983;24:1647–54.
[32] Mannheim CH, Miltz J, Passy N. Interaction between aseptically filled citrus products and laminated structures. In: Hotchkiss JH, editor. Food and packaging interactions, American

chemical society symposium series; 1988. p. 68−82.
[33] Andersson T, Wesslen B. Degradation of LDPE, LLDPE and HDPE in film extrusion. In: TAPPI PLACE conference; 2004.
[34] Andersson T, Wesslen B, Sandstrom J. Degradation of low density polyethylene during extrusion. I. Volatile compounds in smoke from extruded films. J Appl Polym Sci 2002;86:1580−6.
[35] Andersson T, Stalbom B, Wesslen B. Degradation of polyethylene during extrusion. II. Degradation of low-density polyethylene, linear low-density polyethylene, and high density polyethylene in film extrusion. J Appl Polym Sci 2004;91:1525−37.
[36] Andersson T, Nielsen T, Wesslen B. Degradation of low density polyethylene during extrusion. III. Volatile compounds in extruded films creating off-flavor. J Appl Polym Sci 2005;95:847−58.
[37] Andersson T, Holmgren MHJ, Nielsen T, Wesslen B. Degradation of low density polyethylene during extrusion. IV. Off-flavor compounds in extruded films of stabilized LDPE. J Appl Polym Sci 2005;95:583−95.
[38] Andersson T, Wesslen B. Degradation of low density polyethylene during extrusion. VI. Effects of oxygen content in air gap. J Appl Polym Sci 2005;96:1767−75.
[39] Cooksey K. Interaction of food and packaging contents. In: Wilson CL, editor. Intelligent and active packaging for fruits and vegetables. CRC Press; 2007. p. 187−99.
[40] Duncan SE, Webster JB. Sensory impacts of food-packaging interactions. Adv Food Nutr Res 2009;56:17−64.
[41] Sajilata MG, Savitha K, Singhal RS, Kanetkar VR. Scalping of flavors in packaged foods. Compr Rev Food Sci Food Saf 2007;6:17−35.
[42] Tehrany EA, Desobry S. Partition coefficients in food/packaging systems: a review. Food Addit Contam 2004;21:1186−202.
[43] Linssen JPH, Van Willige RWG, Dekker M. Packaging-flavor interactions. In: Ahvenainen R, editor. Novel food packaging techniques. CRC Press; 2003. p. 144−71.
[44] Fayoux SC, Seuvre A-M, Voilley AJ. Aroma transfers in and through plastic packagings: orange juice and d-limonene. A review. Part II: overall sorption mechanisms and parameters - a literature survey. Packag Technol Sci 1997;10:145−60.
[45] Fayoux SC, Seuvre A-M, Voilley AJ. Aroma transfers in and through plastic packaging: orange juice and d-limonene. A review. Part I: orange juice aroma sorption. Packag Technol Sci 1997;10:69−82.
[46] Pieper G, Borgudd L, Acermann P, Fellers P. Absorption of aroma volatiles of orange juice into laminated carton packages did not affect sensory quality. J Food Sci 1992;57:1408−11.
[47] Kwapong OY, Hotchkiss JH. Comparative sorption of compounds by polyethylene and ionomer food-contact plastics. J Food Sci 1987;52:761−85.
[48] Mannheim CH, Miltz J, Letzter A. Interaction between polyethylene laminated cartons and aseptically packed citrus juices. J Food Sci 1987;52:737−40.
[49] Sheung KSM, Min S, Sastry SK. Dynamic head space analyses of orange juice flavor compounds and their absorption into packaging materials. J Food Sci 2004;69:C549−56.
[50] Van Willige RWG, Linssen JPH, Legger-Huysman A, Voragen AGJ. Influence of flavour absorption by food-packaging materials (low-density polyethylene, polycarbonate and polyethylene terephthalate) on taste perception of a model solution and orange juice. Food Addit Contam 2003;20:84−91.
[51] Haugaard VK, Weber CJ, Danielsen B, Bertelsen G. Quality changes in orange juice packed in materials based on polylactate. Eur Food Res Technol 2002;214:423−8.
[52] Lebosse R, Ducruet V, Feigenbaum A. Interactions between reactive aroma compounds from model citrus juice with polypropylene packaging film. J Agric Food Chem 1997;45:2836−42.
[53] Gavara R, Catala R, Hernandez-Munoz P. Study of aroma scalping through thermosealable polymers used in food packaging by inverse gas chromatography. Food Addit Contam 1997;14:609−16.
[54] Hernandez-Munoz P, Catala R, Gavara R. Effect of sorbed oil on food aroma loss through packaging materials. J Agric Food Chem 1999;47:4370−4.

[55] Chang S-S, Guttman CM, Sanchez IC, Smith LE. Theoretical and computational aspects of migration of packaging components to food. In: Hotchkiss JH, editor. Food and packaging interactions, American chemical society symposium series; 1988. p. 106–17.
[56] Hernandez-Munoz P, Catala R, Gavara R. Food aroma partition between packaging materials and fatty food simulants. Food Addit Contam 2001;18:673–82.
[57] Halek GW. Relationship between polymer structure and performance in food packaging applications. In: Hotchkiss JH, editor. Food and packaging interactions, American chemical society symposium series; 1988. p. 195–202.
[58] Imai T, Harte RR, Giaicin JR. Partition distribution of aroma volatiles from orange juice into selected polymeric sealant films. J Food Sci 1990;55:158–61.
[59] Colomines G, Ducruet V, Courgneau C, Guinault A, Domenek S. Barrier properties of poly(lactic acid) and its morphological changes induced by aroma compound sorption. Polym Int 2010;59:818–26.
[60] Lopez-Carballo G, Cava D, Lagaron JM, Catala R, Gavara R. Characterization of the interaction between two food aroma components, α-pinene and ethyl butyrate, and ethylene-vinyl alcohol copolymer (EVOH) packaging films as a function of environmental humidity. J Agri Food Chem 2005;53:7212–6.
[61] Safa L, Abbes B. Experimental and numerical study of sorption/diffusion of esters into polypropylene packaging films. Packag Technol Sci 2002;15:55–64.
[62] Van Willige R, Schoolmeester D, Van Ooij A, Linssen J, Voragen A. Influence of storage time and temperature on absorption of flavor compounds from solutions by plastic packaging materials. J Food Sci 2002;67:2023–31.
[63] Day BPF. Active packaging. In: Coles R, McDowell D, Kirwan MJ, editors. Food packaging technology. Boco Ratan, FL: CRC Press; 2003. p. 282–302.
[64] Robertson GL. Active and intelligent packaging. In: Food packaging: principles and practice. 2nd ed. Boca Raton, FL: CRC Press; 2006 [chapter 14].
[65] Brody AL, Strupinsky ER, Kline LR. Active packaging for food applications. Lancaster, PA: Technomic Publishing Co; 2001.
[66] Han JH. Antimicrobial packaging systems. In: Ebnesajjad S, editor. Plastic films in food packaging: materials, technology and applications. Amsterdam: Elsevier; 2013. p. 151–80.
[67] Rooney ML. Introduction to active food packaging technologies. In: Ebnesajjad S, editor. Plastic films in food packaging: materials, technology and applications. Amsterdam: Elsevier; 2013. p. 127–38.
[68] Ebner C. Successes and challenges encountered in the development of active packaging for food. In: SPE FlexPackCon Conference; 2015.
[69] Ozdemir M, Floros JD. Active food packaging technologies. Crit Rev Food Sci Nutr 2004;44:185–93.
[70] Rooney ML. History of active packaging. In: Wilson CL, editor. Intelligent and active packaging for fruits and vegetables. CRC Press; 2007. p. 11–30.
[71] Pereira de Abreu DA, Cruz JM, Paseiro Losada P. Active and intelligent packaging for the food industry. Food Rev Int 2012;28:146–87.
[72] Cooksey K. What's next in active and intelligent food packaging?. Packaging World; 2014. viewed November 24, 2015. From http://www.packworld.com/trends-and-issues/smartactive-packaging/whats-next-active-and-intelligent-food-packaging.
[73] Hausmann K, Ziche L, Schenck H. More sustainable meat packages through novel sealant solutions. In: European TAPPI PLACE conference; 2015.
[74] Sepe M. Materials: the mystery of physical aging: part 1. Plastics Technology; 2014. November Issue, viewed December 02, 2015 at, http://www.ptonline.com/columns/the-mystery-of-physical-aging-part-1.
[75] Sepe M. Materials: the mystery of physical aging: part 2. Plastics Technology; 2014. December Issue, viewed December 02, 2015 at, http://www.ptonline.com/columns/the-mystery-of-physical-aging-part-2.
[76] Sepe M. Materials: the mystery of physical aging: part 3. Plastics Technology; 2015. January Issue, viewed December 02, 2015 at,

http://www.ptonline.com/columns/materials-the-mystery-of-physical-aging-part-3.
[77] Struik LCE. Physical aging of plastics and other glassy materials. Polm Engr Sci 1977;17:165–73.
[78] Morris BA, Chen JC. The stiffness of ionomers: how it is achieved and its importance to flexible packaging applications. In: SPE ANTEC conference; 2003.
[79] Yoshimizu H, Tsujita Y. Applications of NMR spectroscopy to the structure and ionic aggregates of ionomers. Ann Rep NMR Spectrosc 2001;44:1–21.
[80] Kutsumizu S, Tadano K, Matsuda Y, Goto M, Tachino H, Hara H, et al. Investigation of microphase separation and thermal properties of noncrystalline ethylene ionomers. 2. IR, DSC, and dielectric characterization. Macromolecules 2000;33:9044–53.
[81] Hirasawa E, Yamamoto Y, Tadano K, Yano S. Formation of ionic crystallites and its effect on the modulus of ethylene ionomers. Macromolecules 1989;22:2776.
[82] Tadano K, Hirasawa E, Yamamoto H, Yano S. Order-disorder transition of ionic clusters in ionomers. Macromolecules 1989;22:226–33.
[83] Goddard R, Grady B, Cooper S. The room temperature annealing peak in inomers: ionic crystallites or water absorption? Macromolecules 1994;27:1710–9.
[84] Marx CL, Cooper SL. The crystallinity of ionomers. J Macromol Sci Phys 1974;9:19–33.
[85] Lee I, Wool RP. Optimum polymer solid interface design for adhesion strength. J Adhes 2001;75:299–324.
[86] Lee I, Wool RP. Polymer adhesion vs substrate receptor group density. Macromolecules 2000;33:2680–7.
[87] Gong L, Friend AD, Wool RP. Polymer-solid interfaces: influence of sticker groups on structure and strength. Macromolecules 1998;31:3706–14.
[88] Hoh G, Sadik SA, Gates JA. Aluminum foil adhesion of ethylene/methacrylic acid copolymer extrusion coatings. In: TAPPI polymers, laminations and coatings conference; 1989. p. 361–6.
[89] Kaelble DH. Theory and analysis of peel adhesion: bond stresses and distribution. Trans Soc Rheol 1960;IV:45–73.
[90] DuPont, ND. Sealant value estimator: are you paying too much for sealed packaging?: DuPont, viewed November 28, 2015 at, http://www2.dupont.com/Packaging_Resins/en_US/Modeling_Tools/SaVE/index.html.
[91] Morris BA. Optimizing flexible packaging … with unique tools from DuPont. In: Presentation at PackExpo; 2011.
[92] PlasticsEurope Association of Plastics Manufacturers, viewed December 02, 2015 at http://www.lca.plasticseurope.org/main2.htm.
[93] Vink ETH, Rabago KR, Glassner DA, Gruber PR. Applications of life cycle assessment to NatureWorks® polylatide (PLA) production. Polym Degrad Stab 2003;80:403–19.
[94] Casarino CM, Morris BA, Veith SR. Resin life cycle estimation to help guide sustainability choices. In: SPE ANTEC conference; 2009.
[95] Morris BA, Kirschbaum D. Modification of PLA for improved processing and properties. In: Bioplastics processing conference, Charlotte, NC; 2007.
[96] Uradnisheck J. Improved dimensional stability of thermoformed polylactic acid articles. In: SPE ANTEC conference; 2009.
[97] Cooper TA. The challenge of flexible packaging recycling and recovery: multilayer films, barrier structures, and pouches. In: SPE FlexPackCon conference; 2015.
[98] European Commission. Moving towards a circular economy. 2015. viewed November 29, 2015 at, http://ec.europa.eu/environment/circular-economy/index_en.htm.
[99] Spinner J. Dow collaboration leads to 'revolutionary' recyclable pouch. FoodProduction Daily.com, William Reed Business Media; 2013. viewed November 19, 2015 at, http://www.foodproductiondaily.com/Packaging/Dow-collaboration-leads-to-revolutionary-recyclable-pouch.
[100] Clark T. Plastics: establishing the path to zero waste, a pragmatic approach to sustainable management of plastic materials. Enso Plastics; 2015. viewed December 02, 2015 at, http://www.ensoplastics.com/download/Plastics_EstablishingthePathtoZeroWaste.pdf.
[101] Sustainable Packaging Coalition. The SPC position against biodegradability additives for petroleum-based plastics. 2015. viewed December 02, 2015 at, http://www.

sustainablepackaging.org/content/?type=5&id=position-against-biodegradability-additives-for-petroleum-based-plastics.

[102] Kershaw PJ. Biodegradable plastics & marine litter: misconceptions, concerns and impacts on marine environments. United Nations Environment Program; 2015. viewed December 02, 2015 at, http://unep.org/gpa/documents/publications/BiodegradablePlastics.pdf.

[103] Brown H, Williams J. Packaged product quality and shelf life. In: Coles R, McDowell D, Kirwan MJ, editors. Food packaging technolgoy. Boca Raton, FL: CRC Press; 2003. p. 65–94.

[104] Flexible Packaging Europe, ND. Sustainability, viewed January 25, 2016 at http://www.flexpack-europe.org/sustainability-new.html.

[105] Enerchem. Technology. 2015. viewed on January 25, 2016 at, http://enerkem.com/about-us/technology/.

17 Analytical and Modeling Tools for Structure Design and Process Optimization

Chapter 1 introduces the general needs along the value chain for flexible packaging. For a specific application, these needs should be translated to CTQs (critical to quality attributes) that provide the criteria for designing the film structure. The CTQs typically involve sealing, barrier, strength, stiffness, abuse resistance, interlayer adhesion, and optical properties described in Part IV while being subjected to end-use conditions (Part VI). The challenge to the package engineer is to meet the package CTQs with the optimum combination of materials at minimum cost. As is discussed in Part V, the converting process cannot be ignored; the process not only affects the economics of the film but also film properties. In addition, the combination of some materials may pose special processing difficulties. For example, flow instabilities, curl, adhesion, and other factors may make producing a given design a challenge.

A number of mathematical, statistical, and numerical models have been introduced in previous chapters that aid in the fundamental understanding of process—structure—property relationships. This chapter summarizes the general approach to modeling for structure design, provides examples of models useful for product development and process optimization, and presents a case study of how they may be used in practice.

Often it is helpful to look at how similar products are packaged; or if the goal is to improve upon the existing structure, understand what it is made of and how it is manufactured. The first section of this chapter briefly describes three analytical techniques that are helpful for structure identification.

17.1 Identification of Packaging Structures

There are a number of reasons for analyzing the structure of an existing commercial packaging film, including the following:

- Surveying the market to understand what types of materials are used.
- Investigating what structures are used for similar products.
- Understanding how a competitor is approaching a similar application.

There are three invaluable analytical tools that are helpful for identifying the structure of multilayer flexible packaging films: optical microscopy, Fourier transform infrared spectroscopy (FTIR), and differential scanning calorimetry (DSC).

17.1.1 Microscopy

Microscopy is used to determine the number of layers in a flexible package film and their thicknesses. Generally optical microscopy is sufficient, although scanning electron microscopy and transmission electron microscopy are sometimes used if very thin layers are involved, such as microlayer technology introduced in Sections 8.5.2, 9.4.6 and 12.2.4. In practice, the resolution limit of an optical microscope is about 0.2 μm [1]. A standard optical microscope with magnification of 4—100X works well. The ability to take a picture and calibrate the dimensions of the image is very helpful. Modern equipment can do this electronically.

The film sample is viewed in the cross section as shown in Fig. 17.1. Sample preparation is critical to obtaining a good image without "ghost" layers. These are artifacts that appear as layers that are not really present. One method is to microtome the specimen. A procedure is described by Garcia-Meitin [2]. Cryogenic microtoming of thin sections allows the microscope to be used in the transmission light mode. Differential interference contrast or cross-polarized light can be used to obtain details about interfaces, caulkability, and seal failures in coextruded films [2].

Another specimen preparation method is to use a metal frame. The film is sandwiched between the

The Science and Technology of Flexible Packaging. http://dx.doi.org/10.1016/B978-0-323-24273-8.00017-4
Copyright © 2017 Elsevier Inc. All rights reserved.

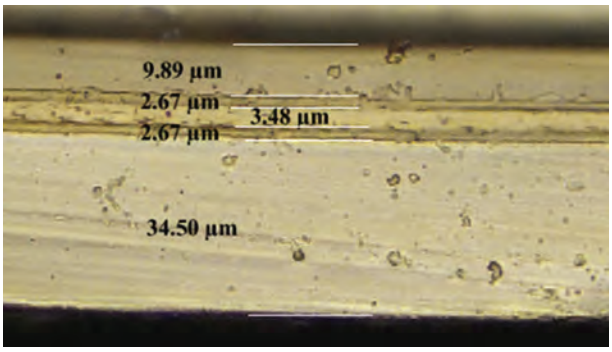


Figure 17.1 Cross-sectional view of a packaging film using optical microscope.
Courtesy of E. I. DuPont de Nemours and Company.

ends of the frame and clamped in place. A razor blade is used to cut a fresh surface of the film flush with the ends of the frame. With practice and replacing the razor blade frequently, a good surface can be obtained for viewing under the microscope using reflected or transmitted light.

Staining can be used to help improve the contrast between layers and make a preliminary identification of the material type. One commonly used stain is tincture of iodine, which stains ethylene vinyl alcohol (EVOH) dark brown and polyamide 6 (PA6) light brown.

In addition to determining the structure of unknown film samples, microscopy is very useful for quality control of layer thicknesses during coextrusion film production. Microscopy can also be used to establish whether layers contain blends with mineral fillers or with other polymers.

17.1.2 Fourier Transform Infrared Spectroscopy

When infrared radiation (IR) is directed through a film, some of the radiation is absorbed by the material and the rest passes through. In IR spectroscopy, this transmitted radiation is detected and converted into a spectrum that reveals a unique fingerprint of the material. Fourier transforms are a mathematical construct used to convert the signal into a useful spectrum, hence the name Fourier transform infrared spectroscopy. FTIR is a powerful technique for identifying the types of polymers in a packaging film. Each polymer type has its own characteristic IR absorption spectrum. Analytical chemists can use FTIR to identify functional groups on a polymer by knowing the spectra of different molecular groups, such as acids or aldehydes. Some of these are tabulated in Table 17.1. Greater detail can be found in reference handbooks [3]. Databases of spectra of standard materials exist that the technician can use as a starting point to determine what materials are present. These libraries, however, may not provide details of specific grades or blends. This takes experience. Many resin suppliers and film converters have built up this experience over time and are good places to consult for help in identifying structures.

There are several different FTIR sampling methods, two of which are often used for film identification [5].

- Transmission. This is the simplest method and requires no special accessory. The film is put directly into the IR beam, which passes through the specimen. For multilayer films, however, this creates a spectrum of all the materials present. Some spectra may overlap, making interpretation of the spectrum difficult.
- Attenuated total reflectance (ATR). In this method an internally reflected IR beam generates an evanescent wave that is contacted with the sample. The wave is attenuated in the regions of the spectrum where the sample absorbs IR radiation. The attenuated wave is recorded by a detector and is converted into an IR spectrum. The evanescent wave decays exponentially with distance from the surface, and so this technique is ideal for measuring the composition of surfaces of films, or for thicker films where strongly absorbing materials create intense peaks in transmission mode. The spacial resolution of ATR is about 150 µm and penetrates a depth of about 2 µm.

Both ATR and transmission FTIR can be helpful for identifying layers in packaging films. ATR can be used on the outside surfaces and provides the most definitive identification (free of interference from other layers). Sometimes the film can be stretched to expose other layers in the structure which also can be identified with ATR. Modern FTIR equipment can be used in conjunction with microscopy to look at samples in cross section. Traversing across the section with multiple scans can help when trying to identify thin layers. Cross sections often get distorted

Table 17.1 IR Frequencies of Chemical Compounds and Examples of Polymers That Contain Them

Bond	Compound Type	Polymer	Frequency Range ($cm^{-1'}$)
C–H	Alkanes	PE, PP, ethylene copolymers	2850–2960 1350–1470
C–H	Alkenes	Unsaturated fatty acid slip agents	3020–3080 675–1000
C–H	Aromatic rings	PET, PS	3000–3100 675–870
C–H	Alkynes		3300
C=C	Alkenes	Unsaturated fatty acid slip agents	1640–1680
C≡C	Alkynes		2100–2260
C–C	Aromatic rings	PET, PS	1500, 1600
C–O	Alcohols, ethers, carboxylic acids, esters	EAA, EMAA, EVA, EVOH, PET	1080–1300
C=O	Aldehydes, ketones, carboxylic acids, esters	EAA, EMAA, EVA, EVOH, PET, PA	1690–1760
O–H	Alcohols, phenols	EVOH	3610–3640 3200–3600
N–H	Amines	PA6	3300–3500
C–N	Amines	PA6	1180–1360
C≡N	Nitriles		1515–1560
$-NO_2$	Nitro compounds		1345–1385

PE, Polyethylene*; PP,* polypropylene*; PS,* polystyrene*; PET,* polyethylene terephthalate*; EAA,* ethylene acrylic acid*; EMAA,* ethylene methacrylic acid*; EVA,* ethylene vinyl acetate*; EVOH,* ethylene vinyl alcohol*; PA,* polyamide.
Data from Morrison RT, Boyd RN. Organic chemistry. 3rd ed. New York: Allyn and Bacon, Inc.; 1976.

when they are mounted and thin layers may be below the resolution of the instrument. A single scan will likely be of a combination of layers rather than an isolated spectrum of a single layer. By taking multiple scans across the sample, the changes in the peaks can often provide a clue as to the identity of each layer.

FTIR techniques are very useful for identifying the type of polymers present. They may not be able to differentiate between types or grades of polymer within a polymer family. For example, different types polyethylene [high density polyethylene (HDPE), linear low density polyethylene (LLDPE), low density polyethylene (LDPE)] have similar IR spectra. The same is true of some types of polyamide and grades of EVOH. Polymer blends may also be a challenge, especially if the spectra overlap. Sometimes FTIR can identify qualitatively if a type of polymer or functional group is present, but without careful calibration curves generated from known standards, it may not be possible to determine how much is present in a blend or coextrusion. If the film can be delaminated, ATR can be run on the exposed surface to determine the composition of that layer.

17.1.3 Differential Scanning Calorimetry

DSC is a method that measures changes in the heat capacity of a material. A sample of known mass is heated or cooled and the change in heat capacity is recorded as changes in heat flow. This allows the detection of thermal transitions: glass transition temperature, melting point, and freezing point [6]. These transitions can be very useful for identifying materials in an unknown packaging film. In particular, it may help identify the particular type of polymer within a polymer family: the melting point of LDPE is distinct from HDPE, for example. Different polyamides have distinct melting points, as do grades of EVOH. Table 16.1 provides thermal transitions for some commonly used polymers in flexible packaging.

For multilayer films, sometimes the melt transition peak for one layer will overlap with another, hiding

one or more of the layers (delaminating the layers prior to testing may help). Also, it can be difficult to differentiate between some polymers that have similar melting points, such as specific grades of ethylene vinyl acetate (EVA) and metallocene VLDPE. For these reasons, DSC is often used together with FTIR and microscopy to determine the identity of each of the layers. One method alone may not tell the whole story.

17.1.4 Other Techniques

In general, optical microscopy, FTIR, and DSC will provide a good basis for the identification of a packaging film structure. They are easy to run, the results are straightforward to interpret, and the equipment relatively inexpensive to acquire. There are a number of other analytical techniques that may be helpful for answering specific questions regarding the composition of a packaging structure. Several of these are given in Table 17.2. Most of these techniques require expensive equipment to run and expertise to interpret the results. Also, many of these techniques work best on a single material—separating the layers may be needed before running them.

17.2 Modeling

Designing new flexible packaging structures can be a time-consuming and expensive task. The packaging engineer must take into consideration many factors, including the package strength, ability to withstand abuse during filling and shipping, barrier, sealability, optical properties, and cost (including not only the cost of the materials but also converting, packaging, waste, and cost to the environment). In addition to these performance and cost factors, the engineer also needs to determine if the proposed package structure can be made on converting equipment at a productive rate.

Often developing a new package structure requires several iterations of producing and testing prototypes. Unless developmental scale equipment is available in the lab, this involves breaking into production to make prototypes, which can incur significant cost and delays as commercial orders typically take priority over development trials.

Table 17.2 Analytical Techniques That May Be Useful for Identifying the Composition of a Flexible Packaging Film

Method	Uses for Flexible Packaging Identification
Optical and electron microscopy	Number and thickness of layers
FTIR (Fourier transform infrared spectroscopy)	Chemical identity of layers
DSC (differential scanning calorimetry)	Thermal transitions—complements FTIR for identifying layers
DMA (dynamic mechanical analysis)	Thermal transitions
ESCA/XPS and TOF-SIMS (electron spectroscopy for chemical analysis or X-ray photoelectron spectroscopy and time of flight secondary ion mass spectroscopy)	Presence and composition of additives on surface
LC (liquid chromatography)	Molecular weight distribution and branching
TREF (temperature rise elution fractionation)	Comonomer distribution in PE
NMR (nuclear magnetic resonance)	Chemical structure
Mass spectroscopy/GC (gas chromatography)	Identity of volatiles
SAXS/WAXS (small angle or wide angle X-ray scattering)	Crystalline structure
Ash	Amount of inorganic filler
ICP/XRF (Inductively conductive plasma spectroscopy/X-ray fluorescence spectroscopy)	Identification of metals

Testing at outside labs can also involve lengthy delays.

Computer modeling and simulation can help minimize iterations and allow the engineer to optimize function and cost on the computer before any film is made. It can also help determine if problems such as poor extrusion, flow instabilities, or curl may occur during film fabrication. If so, potential solutions involving material selection, structure, and process can be scoped out prior to running on the production line. Process models can also be used to troubleshoot problems with production of existing structures.

17.2.1 Types of Modeling

There are three general types of models that are used in flexible packaging: attribute, empirical/statistical, and fundamental/theoretical.

17.2.1.1 Attribute Models

Attribute-based modeling is a way to quantify choices among options that have several qualities. An example is a sealant selector tool developed by DuPont [7]. This tool embodies the information in Section 7.11. The user selects the attributes that are most important for their application and ranks their importance on a scale of 1−10. For example, the sealant layer in the package may be called upon to provide low temperature sealability, be transparent, and provide grease and oil resistance. Some sealant resins may work well for one or more of the attributes but not as well as other options for the others. The model embodies the knowledge of an expert panel that has rated different sealant polymers based on these attributes. The model calculates a numerical score for each resin type based on the importance of the attribute to the user and the performance of that resin based on the expert panel. The output provides a quantitative comparison of the resins as a starting point for the user to consider in the package design. An example illustrating the use of this tool is provided in Section 17.2.3.

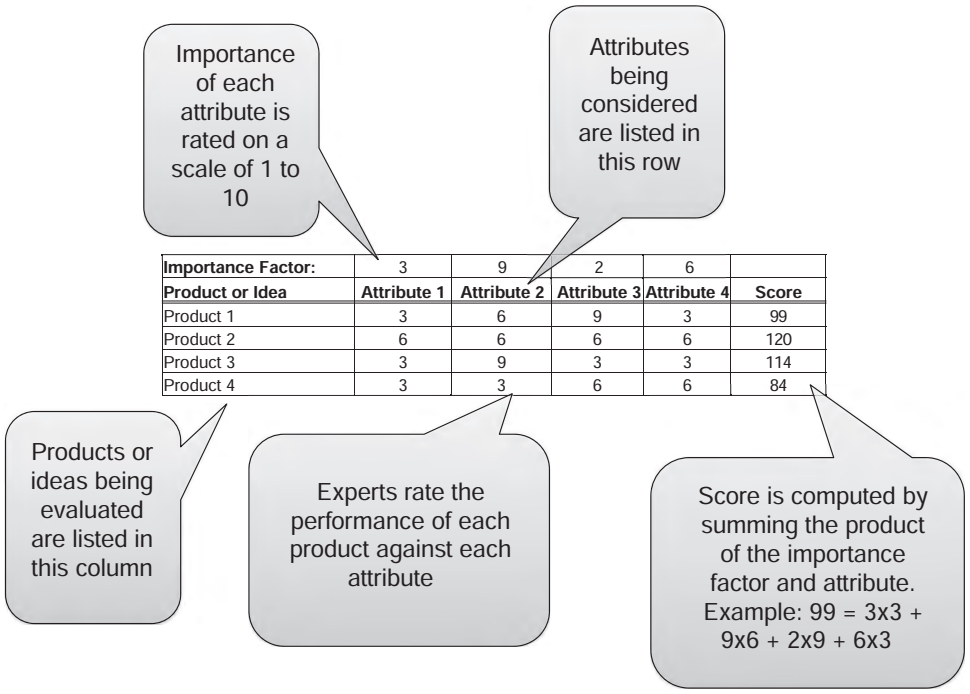
Attribute models are a type of expert system. As well as providing selection tools such as the one illustrated above, they are useful for capturing the expert knowledge of an organization, evaluating project ideas, and many other things. A simple version of an attribute model is a cause and effect matrix. This is typically a spreadsheet, as illustrated in Fig. 17.2. Here the products or ideas being evaluated are listed in the first column. Along the top, the attributes that are important are listed. For each attribute, the user rates their importance on a scale of 1−10. These are placed above the attribute in the spreadsheet. An expert panel (which may be the user) rates the performance of each product against each attribute on a scale of 1−10. A numerical score is computed by summing up the product of the importance factor and attribute rating. The resulting scores show the relative performance of each product versus the weighted importance of the attributes.

17.2.1.2 Empirical and Statistical Models

Statistical- or empirical-based models do not rely on the underlying science behind the property being considered. Instead, they use statistically based tools to develop predictive equations. Often industrial systems are complex with a number of possible variables and phenomena that may influence the outcome of a particular test result. In these situations, theoretical understanding may not exist or what does exist does not explain all of the variability in the system. Furthermore, complex systems can be very difficult to model theoretically or numerically. The use of statistics allows predictive capability where it may not otherwise be possible and often with an economy of experiments.

One of the most powerful techniques in empirical modeling is statistical design of experiments (DOEs). In scientific experiments, often all the possible variables are held constant except for one, which is varied systematically to determine the response of the system. If the system has many variables, varying each one at a time will require a substantial amount of experiments. DOE uses statistical-based algorithms to economize on the design by simultaneously combining multiple factors. Rather than varying one variable at a time, all the variables are varied and only a few of the possible combinations are used. The results are analyzed to determine which variables and their interactions are statistically important and a statistical-based model is obtained. A number of good references are available that provide details into the method [8−14].

The first step in designing a DOE is to determine the independent and response variables. The independent variables are those factors that may influence the outcome of the experiment. It is important at the



Importance Factor:	3	9	2	6	
Product or Idea	**Attribute 1**	**Attribute 2**	**Attribute 3**	**Attribute 4**	**Score**
Product 1	3	6	9	3	99
Product 2	6	6	6	6	120
Product 3	3	9	3	3	114
Product 4	3	3	6	6	84

Figure 17.2 Cause and effect matrix for attribute modeling.

beginning of a project to consider a wide range of possible factors that may affect the final properties. One tool that may be useful is to construct a fishbone diagram, which can help identify possible factors to consider or causes of a problem. An example given in Fig. 17.3 for a heat seal issue resulted from a team consideration of possible causes in the general categories that make up the fish bones: personnel, materials, measurements, environment, methods, and machines. From this input the most important factors can be used to conduct the experiments and construct the model.

The response variables are the outcomes, such as tear strength or impact resistance. Multiple response variables may be measured and analyzed. One of the benefits of the analysis is that it can be used to optimize for more than one response, such as maximum tear resistance with minimum haze.

Often there are a number of possible independent variables that may impact the responses. A two-step process is used to decrease the number of experiments. A screening design uses just a few experiments, typically on the order of 10–20 states, to test up to 10 variables for importance. The model that arises from such an experiment is enough to discern the direction of the response (such as increasing film thickness increases impact resistance) but does not provide information on interactions between variables. A second experiment is typically conducted using the three or four most important variables coming out of the screening experiment. Called a response surface design, the second experiment will usually involve more states to determine curvature and interaction effects.

Commercial software is available to design and analyze DOEs, such as JMP [15] and Minitab [16]. A number of designs are possible and the complexity of the design depends on whether the variables are continuous (eg, thickness or temperature) or categorical (nonnumerical, such as grade names or polymer types), and whether any variables are constrained in certain regions of the design space (some combinations of variables may not be possible, such as high haul-off speed and high film thickness). If some variables are more difficult to change (eg, extruder temperature), blocking can be used to minimize the number of changes.

One of the most useful types of DOE is the factorial design. A simple two-level factorial design considers the high and low value of each independent variable. In a full factorial design, each combination of factors is run. The number of runs or states is simply 2^n where n is the number of variables. For example, if there are three variables, the number of states is 8. Such an experiment can be conceptualized by the corners of a cube, as shown in Fig. 17.4. Here

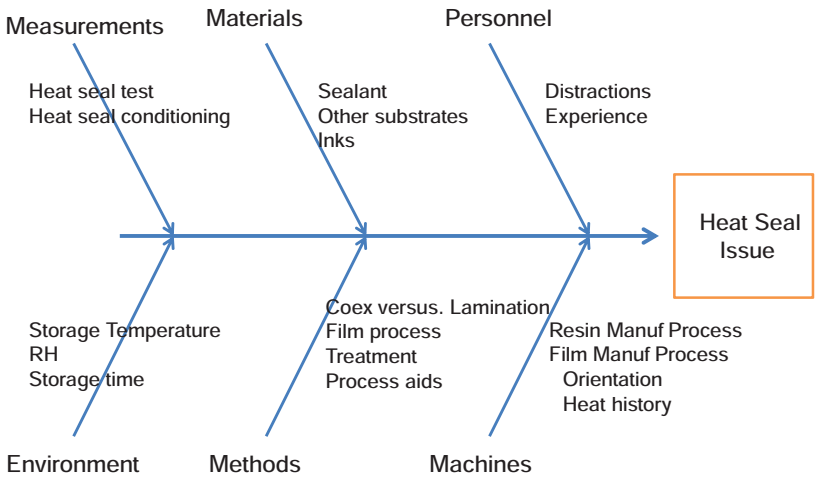


Figure 17.3 Example of a fishbone diagram for a heat seal problem.

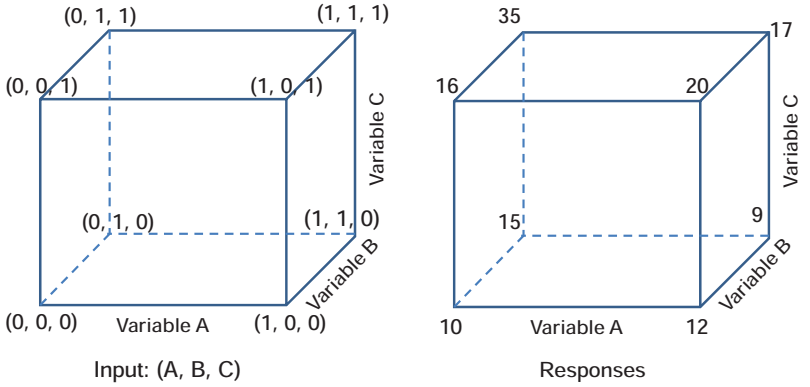


Figure 17.4 Graphical representation of a three-variable factorial design.

the range of each variable is arbitrarily set from 0 to 1 (low to high). The responses can be plotted on the corners of the cube to visually see the effects of the variables. In the example in Fig. 17.4, the results show that variable C has the strongest effect: increasing C increases the response. Variables A and B have weaker effects by themselves but have some strong interactions. For example, at low A, increasing B increases the response, but at high A, the opposite is true.

For more general designs contour plots are often used to graphically depict the results. Examples of contour plots can be seen in Figs. 10.18 and 10.19.

To complete the DOE, replicates are needed for two or more states so that the statistical analysis can calculate the replicate error. Once the replicate error is known, the software computes the level of confidence that one or more of the variables has a statistical impact on the response. In statistical terms, the analysis computes a p-value for each term of the model. If the p-value is less than 0.1, the independent variable is important.

An important consideration when designing a DOE experiment is to choose the range of each variable to be as large as practically possible. This is because statistical models generally work well inside the original design space but not very well when extrapolating outside the design space. This is one of the fundamental limitations of this approach.

Many DOE experiments are reported in the literature. For example, Borse [17] uses a full factorial DOE approach to optimize the properties of a three-layer blown film. The structure is (sLLDPE–PE blend–sLLDPE) where sLLDPE is a single site-

catalyzed LLDPE and the PE core layer is a blend of either butene or hexene LLDPE (Ziegler–Natta) with LDPE. The independent variables are the thickness ratio of the skin to core layers, the type of LLDPE in the core (butene or hexene), the % of LDPE in the core layer and the film gauge. The responses include a number of mechanical and optical properties. One set of results is reproduced in Fig. 17.5, which shows the predicted response of varying layer ratio and % LDPE in the core for a 25 μm film with the core layer containing b-LLDPE. The results show that low gloss and high puncture energy can be obtained at 20% LDPE in the core with a layer ratio of 20/60/20.

Several examples of DOE experiments and models are given in this book. One can be found in Section 10.4.1.4 where a response surface design was used to explore the effects of line speed, extrusion temperature, coating thickness, and percent of a modifier added to LDPE on the peel strength of LDPE to aluminum foil in extrusion coating. The model predicts the processing conditions needed to obtain a given peel strength at the optimum additive level. Another example can be found in Section 13.5 on curl.

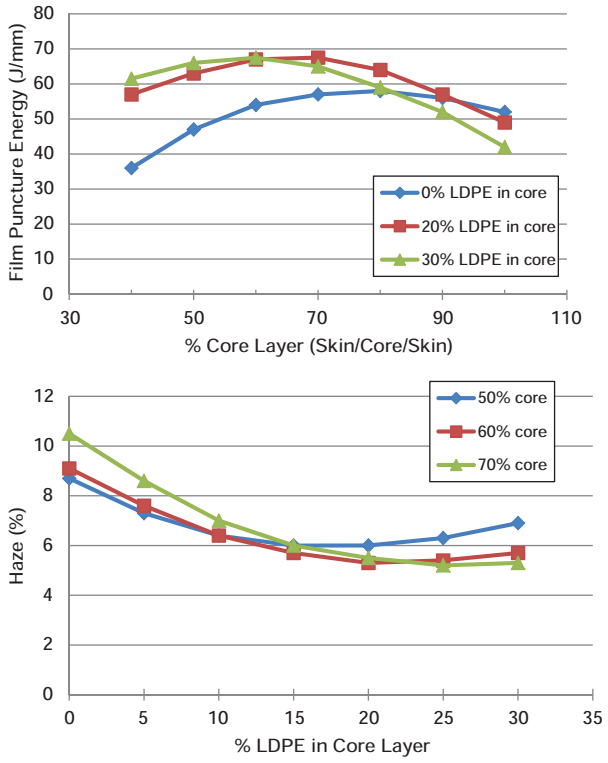


Figure 17.5 Effect of layer ratio and % LDPE in the core for a 25-μm coextruded blown film with structure (sLLDPE–bLLDPE + LDPE core–sLLDPE). Top graph is statistical model predictions for film puncture energy and bottom graph is for haze.
Reproduced from Borse N, Aubee N. Predicting physical and optical properties of co-extruded blown films using design of experiment based model. In: SPE ANTEC Conference. 2015. pp. 1584–8 with permission from the Society of Plastics Engineers.

Regression analysis and other techniques used to fit experimental data with a mathematical formula is another type of statistical model. For example, Blom [18] (Section 9.4.3.4) uses graphical and regression techniques to gain insight into the abrasion resistance of plastic films. The work led to the definition of an abrasion coefficient (Eq. (9.12)) as a material parameter.

Todd [19] uses a nonlinear regression model to develop a new grade of HDPE with a good balance of mechanical properties for a barrier film application. The barrier of HDPE film generally increases with higher crystallinity (density) and melt index (MI). Higher MI decreases film mechanical properties. What was unknown is the effect of molecular weight distribution (MWD). Blown films from 14 different HDPE resins with different density, MI, and MWD are made and tested for Elmendorf tear strength, dart drop impact resistance, and MVTR. A statistical model is fit to the results and used to design a new resin, which when tested, validates the model.

A combination of theoretical and statistical analysis can be used to produce models that better fit the data. Wang [20] looks at the effect of LLDPE resin parameters (MW, MWD, and comonomer distribution, as measured by MI, stress exponent, and TREF (temperature rise elution fractionation)), melt relaxation time from rheology measurements and blown film parameters (die gap, film thickness, blow up ratio, melt temperature, and output) on dart impact. Rather than simply use the parameters as is, some are combined or transformed into fundamental factors, such as the strain rate and a corrected Deborah number (Eq. (15.5)). They find that the fit is better than if simply using the raw parameters. The resulting model is highly nonlinear with significant interactions. For example, the dart impact depends on the Deborah number raised to the power of 3.75 and the strain rate to the power of 3. The model is fairly robust and is able to predict dart impact of resins made on pilot and commercial resin manufacturing lines, as well as resins from a competitor.

Section 15.1.2.2 describes how common extrusion coating process parameters are related to fundamental factors that describe the stress imparted on the melt curtain during coating, such as the stress imparted in the extruder and die, total elongation in the air gap, the rate of elongation in the air gap, and the process time. Because of the interactions among the parameters, a DOE approach is used and the results are fit to a quadratic statistical model. The results of the analysis (Figs. 15.16 and 15.17) are used to draw conclusions about the effect of stress on peel strength performance [21].

As shown in Section 15.1.4, the use of DOE models can be used to test hypotheses about the fundamental factors that influence the properties of films and coatings. In this case study, the model developed in Section 10.4.1.4 is used to test potential mechanisms governing the effect of coating thickness on peel strength.

The primary limitation of DOE and other statistical modeling approaches is that they generally cannot be extended beyond the original experimental design space. They are excellent for troubleshooting problems and optimizing processes or film structures, but for totally new structures and processes they may be limiting.

17.2.1.3 Theoretical/Fundamental Models

Theoretical or fundamental models are derived from scientific or engineering first principles. Examples include the bending stiffness (Section 9.2.2), curl (Section 13.5.3), heat seal (Section 7.6), permeability (Section 8.4.1.1), and heat transfer (Section 15.1.3) models discussed in this book. These are derived from equations that describe the underlying physics or chemistry behind the phenomenon.

Numerical or computer simulations also fit into this category. Examples include simulations for extrusion, blown film, and cast film. Engineering analysis of films and packages is another example, using finite elements, finite difference, and finite volume techniques to optimize package design.

Theoretical models are very powerful since they can be used to extend beyond the original design space, provided they accurately capture the fundamental mechanism behind the response. But they have their limitations. One is that industrial processes are generally complex and noisy. Several phenomena or mechanisms may be influencing the outcome that a simple model cannot accurately project.

Fully representing a physical phenomenon requires complex partial differential equations in three spacial dimensions and a time component. For example, Agassant [22] describes 10 equations that must be solved for polymer flow simulation arising from mass, momentum, and energy balances. Coupled with this are complex constitutive equations that describe relationships between stress and flow. Solving these systems of equations analytically usually requires many simplifications to make the math tractable. For example, the flow may be assumed to be Newtonian when it actually is highly viscoelastic. The system may be assumed to be isothermal even though temperatures are changing. These simplifications must be carefully evaluated for the system being analyzed. In many cases, simple analytical models can provide tremendous insight into complex processes but may result in significant error when making quantitative predictions.

The alternative is to solve the equations numerically. Tremendous strides have been made in the last 50 years in the field of numerical simulation, but there still are many limitations. Agassant [22] discusses a number of these limitations as they pertain to flow simulation, but the comments apply to modeling mechanical processes as well:

- Finite element, volume, or difference techniques are typically used. These involve dividing the space into a mesh of volumes. The accuracy of the simulation can depend on how representative the volumes are, which can be computationally difficult for complex flow situations.
- Nonlinear behavior is difficult to model. For flow simulation, for example, constitutive equations relating the stress tensor to the rate of strain tensor may have many parameters that are challenging to measure with standard lab techniques.
- The most sophisticated constitutive equation may not be the best for a given simulation. It will depend on the type of flow, the available computing power of the facility, and the ability to measure the parameters.
- Direct analysis can take a lot of computational time and may not be practical for parametric studies. The equations can sometimes be

simplified through use of dimensional analysis and other techniques. Often is not obvious, however, whether the direct or approximate approach is best for a given situation.

- Modeling has become progressively more sophisticated over the years. It is now possible to use commercial software, such as Moldflow or Polyflow in the area of polymer flow simulations, to simulate many industrial processes. A trend is toward a "black box" approach where the user simply plugs in the conditions into the model. This may be fine for some situations, but often complex flows require some judgment as to what approximations to make. It is best to develop a good physical understanding of the process, make appropriate simplifications and realistic rheology assessments before using the black box approach. Extensional flow remains an area where accurate simulation is uncertain. No universal constitutive equation exists for single phase polymer melts, much less blends, and other multiphase materials. Melt transitions (solid to melt and vice versa) are still a challenge to model accurately. Crystallization is particularly a challenge, and the effect of flow exacerbates this. The future challenge is to model orientation and crystalline morphology development to predict mechanical properties.

When it comes to numerical simulation of the mechanical performance of films and packages, obtaining the model material parameters at the appropriate rate of strain is challenging. The properties of plastics are rate dependent and less understood from a modeling perspective than metals. The lower stiffness and deformation resistance of polymer films, as well as inhomogeneous strain fields, makes testing of polymeric materials difficult [23]. Special test rigs may need to be developed [24]. Another approach, employed by Carbajal [25], is to model the test method itself. To model high-speed impact puncture resistance of multilayer films, they needed high-speed mechanical properties of the individual layers. Using lower speed tensile properties as a starting point, they tweaked the parameters by comparing numerical simulations of the test rig with experimental results. Their work is explored more fully in the next section.

17.2.2 Examples of Models and Their Use in Flexible Packaging

Models for flexible packaging can be grouped into two categories: package design and processing/converting. The package design tools help the user select materials and design the flexible film structure to meet the packaging needs and minimize cost. The process tools help the user determine if the structure can be made and troubleshoot in advance potential problems. A summary of the modeling tools described here is provided in Table 17.3.

17.2.2.1 Package Design

As described throughout this book, most flexible packages have multilayer constructions to achieve the desired functional requirements in a cost-

Table 17.3 Examples of Models for Package Development

Package Design	Processing/Converting
Oxygen and moisture permeability	Extrusion simulation
Sealant selection	Blown/cast film/extrusion coating simulation
Migration/impartation	Flow instability in coextrusion
Sealant performance	Heat transfer in air gap and nip
Tie resin selection	Curl
Physical properties: bending stiffness, other	COF/slip migration
Physical properties: engineering analysis	Adhesion
Cost analysis	
Life cycle assessment	

effective manner. Each layer has its role. Often multiple materials are available for each functional role, and some materials may play more than one role. Various tools are available or can be developed, which help optimize the structure and select the best materials for a given application.

An important consideration in many packaging applications is limiting the amount of oxygen that permeates into the package. Barrier polymers, such as EVOH, poly vinylidene chloride (PVDC) or PA6, or barrier films, such as aluminum foil or metalized oriented polypropylene (VM-OPP) or oriented polyester (VM-OPET), are incorporated into the structure. In modified atmosphere packaging, the headspace is injected with a mixture of gases designed to extend the shelf life of the product. It is important that this mixture should not permeate out of the package. In other applications, moisture barrier is important. The permeability of gases through a multilayer package is a function of the inherent permeability and thickness of each of the materials.

Chapter 8 develops the equation for predicting the permeability of a multilayer film structure given the permeability and thickness of the layers (Eq. (8.21)). This equation can be incorporated into a permeability calculator to help select the best resin and thickness for a given barrier need. Such tools can be found online or can be easily programmed into a spreadsheet. More sophisticated models use finite element and other techniques to compute the oxygen ingress of complex packages (eg, bottles) or to predict the composition of modified atmosphere packages over time. The simple approach works well for many applications.

The sealant is the innermost layer of the structure that provides a hermetic seal to protect the product. Ethylene copolymers are often used as sealants because of their low melting points. These include LDPE, EVA, LLDPE, metallocene polyethylene plastomers (mPE), acid copolymers (ACR), and ionomers. The selection of the best sealant for a given application depends on what the sealant needs to contribute to the overall performance of the package. Several such attributes are described in Section 7.11. An attribute-based model for selecting the sealant that best meets the criteria is described in Section 17.2.1.1.

Migration of unwanted compounds (monomers, oligomers, additives, solvents, and so on) from the package to the product may affect the sensory perception of a food product (Section 16.2.2.1) as well as has food regulatory compliance issues. The European Union Commission Regulation No. 10/2011 on the use of plastic materials that come in contact with food has specific migration limits for compounds [26]. The regulation calls for the testing of the migration of these compounds in food simulates according to food type and shelf life requirements. Such testing often requires sophisticated techniques and can be very expensive. The regulation allows for the use of migration modeling to predict migration under extreme conditions so that the regulations are not exceeded.

A number of migration models are available commercially, including those by Combase [27], AKTS [28], FABES [29], and ICIPC [30]. These models numerically solve the time-dependent diffusion equation (Eq. (12.11)) by finite difference or element techniques to estimate the maximum amount of the compound that migrants into the food [31–33]. Similar to the model described in Chapter 12 for slip agent migration, these models use as inputs the partition coefficient of the compound between the contact layer and food medium and the diffusion coefficient of the compound in the polymer. The former is estimated based on the polarity of the compound and medium derived from measurements in octanol and water. The diffusion coefficient is estimated based on generally recognized molecular diffusion models for noninteracting compounds where only the molecular weight of the compound, storage temperature, and several parameters specific to the polymer are required [28,33]. This allows for a wide range of migratory species and polymers to be modeled.

Cost is an important consideration, both financial cost as well as cost to the environment, and is covered in detail in Chapter 16. Downgauging the thickness is one approach to reducing cost, but unless material or process changes are made, the overall stiffness and strength of the package may suffer. Bending stiffness is a complex function of the thickness, modulus, and position of each of the layers. A model is described in Section 9.4.2 that has proven very useful for designing structures with less material without sacrificing bending stiffness. This is accomplished through material substitution and position, sometimes in ways that may not be thought of without the use of the model [34]. The model can be combined with information on the material cost, as well as environmental cost from a life cycle analysis

(described in Section 17.2.3.4), to provide overall guidance on cost versus performance [35].

Other physical properties of multilayer film have also been modeled usually with statistical-based approaches. Examples include abrasion resistance [18], tear resistance [17,36], energy to break [17], and tensile strength [17]. Carjabal et al. [25] used finite element analysis to model high-speed impact resistance of multilayer films. Their approach is worth highlighting since their combination of experimental and modeling work allowed them to overcome the challenges with material parameter measurement.

As described in Chapter 9, Carjabal et al. [37] study impact puncture during filling of crackers on a vertical form-fill-seal line. The drop of the sharp cracker creates pinholes at high impact velocities. Two characteristics of their study are important for the model development. First, they took the time to understand the fundamentals of what happens as the cracker impacts the film. Using high speed video they record individual drops. They find that the impact is a high speed event (around 4 m/s), the cracker does not significantly deform during the event, and the size of the pinhole is much smaller than typical laboratory impact tests. Based on this information they design, test, and validate a new laboratory test that is described in Section 9.4.3.2. The fundamental study also provides insight into how to model the impact. Because the video shows that duration of the event is only a few thousandths of a second in duration, it is necessary to select software that can deal with short time frames. The lack of deformation of the cracker allows them to represent the cracker in the model as a rigid object, simplifying the calculations.

Second, the test method they develop can also be used to fine-tune the material parameters needed for the model. The test, a high-speed reverse impact test, provides information on the work vs displacement during the puncture of the film with a needle probe. Since the model is expected to provide insight into the contribution of individual layer properties, thickness, and position within the film structure, each material must be considered explicitly. This requires material parameters at high strain rates. Films of the individual layers are made and the tensile properties at low strain rates are measured. For each individual material, the work versus displacement is measured using the reverse impact tester. Using the low strain rate tensile properties as a starting point, the parameters are tweaked until there is a good agreement between the model prediction and experimental result.

The approach proves to be very successful. Shown in Fig. 17.6 is a comparison of the model predictions with the test results of the ultimate work to puncture for seven different barrier snack films. The films have the general structure (HDPE—tie—PA—tie—sealant) and vary by composition (% PA, thickness, and so

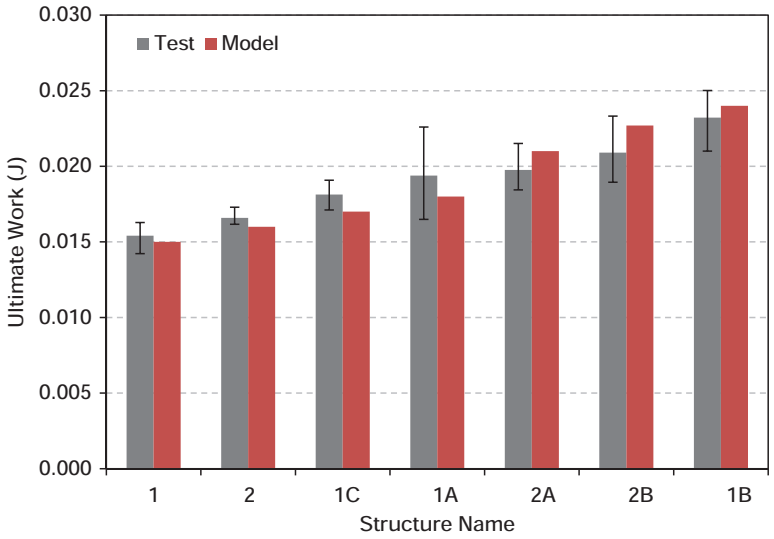


Figure 17.6 Comparison of model prediction with test results on seven five-layer barrier blown films.
Reproduced from Carbajal LA, Jiao R, Hahm DM, Morris BA, Kendzirski RR. Predicting the impact puncture response of multilayer flexible food packages using explicit finite element models. In: SPE ANTEC Conference. 2016 with permission from the Society of Plastics Engineers.

on). The model and test results are in excellent agreement and are able to discriminate among the samples. The model also provides insight into the dynamics of the impact event, such as the fluttering of the film (Fig. 17.7) that qualitatively agrees with high-speed video images. Further, the model parameters are the same as those used in a second model of a bullet drop test, which is utilized in the initial study to validate the reverse impact puncture test. Bullets are chosen since they have better flying stability than crackers (or screws, which are often used in empirical drop tests). The bullets have similar weight and tip dimensions as the crackers. The model predictions agree well with the measured puncture velocities of the multilayer films. Now that the model is correctly predicting impact performance of the test films, it can be used to explore design concepts such as replacing or repositioning materials within the structure.

Once a candidate structure has been determined, it is helpful to know how well it will seal. This will determine what packaging line speeds may be obtainable, which affects total cost to the packer. Morris [38] and Moffitt [39] have developed heat seal models which can help with this assessment. These are described in Section 7.6.1. They take into account the heat transfer through the film, melting of the sealant, molecular diffusion, and strength buildup. As is shown in Section 7.6.1, Morris's model agrees well with experiments on a packaging line.

Cost is an overriding consideration of package design. Total cost to the packer should be considered, including the roll stock costs (which incorporate material and converting costs) and packing costs. The packing costs will depend on the packing labor and equipment costs (including overhead), packaging efficiencies, and waste. Using a premium sealant, for example, may increase the roll stock cost but reduce the overall cost by increasing line speed and reducing leakers and waste. Section 16.5.1.6 describes a simple packing cost model developed by DuPont that is available online [40].

An engineering analysis using numerical simulation such as finite elements (FEA) can be helpful in some situations. FEA is widely used in rigid packaging but is only beginning to see use in flexible packaging. Yuan [24] explains that the flexibility of flexible pouches creates simulation challenges such as structural instabilities, wrinkles, and complex contact situations. Accurate characterization of the film for the specific loading situation is critical to success. But once done, it can be very useful for package design.

Morris [35] provides an example where FEA is used for the design of the seal geometry of a dual compartment pouch. The concept for the design is shown in Fig. 17.8. When the consumer squeezes the pouch, the internal seal bursts and the contents mix. The design of this structure requires a special ionomer sealant as well as a seal geometry that focuses the stress in a way that facilitates opening between compartments and not at the pouch edge. An FEA model is used to predict the forces on the seal area of different seal configurations. One such example is shown in Fig. 17.9.

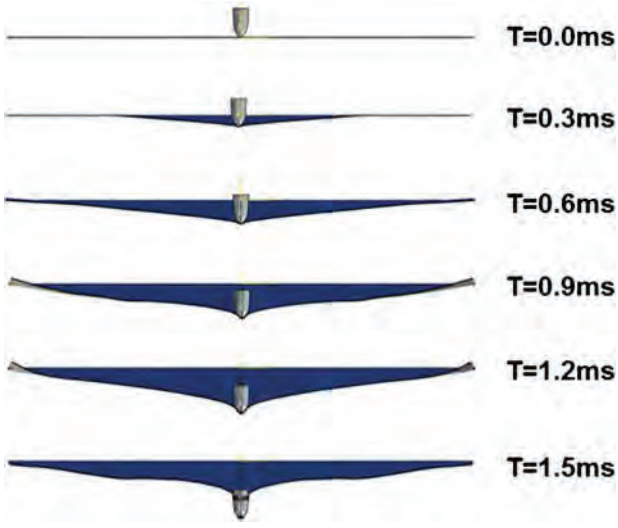


Figure 17.7 Typical predicted deformed shapes. *Reproduced from Carbajal LA, Jiao R, Hahm DM, Morris BA, Kendzirski RR. Predicting the impact puncture response of multilayer flexible food packages using explicit finite element models. In: SPE ANTEC Conference. 2016 with permission from the Society of Plastics Engineers.*

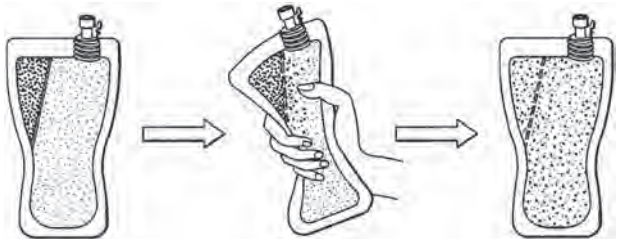


Figure 17.8 Dual compartment pouch concept. *Reproduced from Bourque RA, et al. Multiple compartment pouch and beverage container with frangible seal. US Patent 7306095 B1. 2007.*

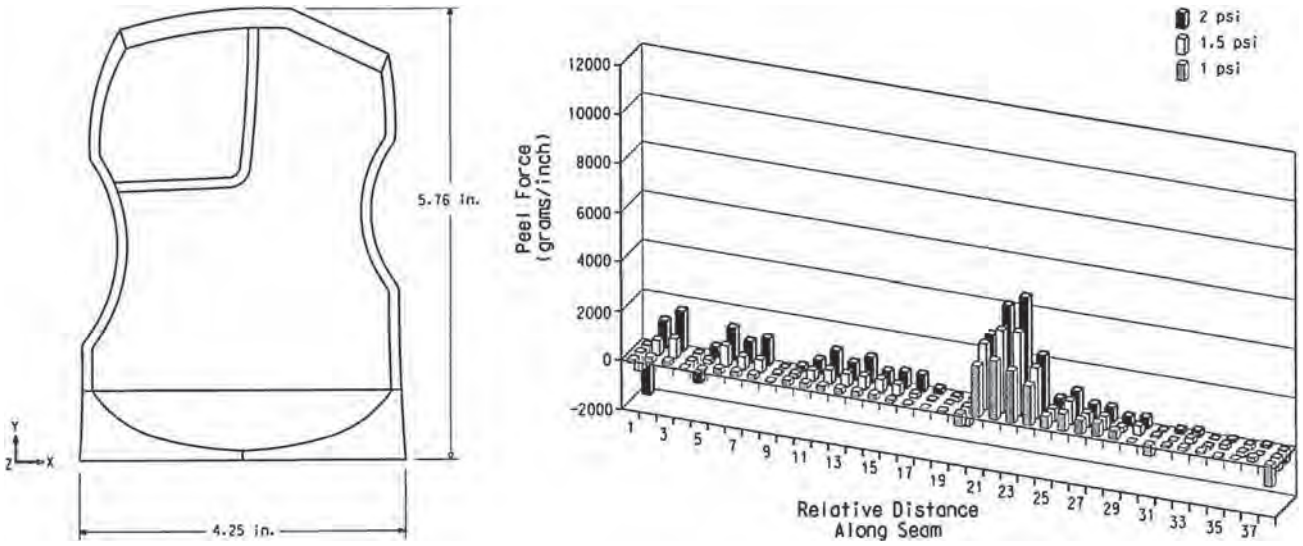


Figure 17.9 Prediction of peel force (right) using finite element analysis of a dual compartment pouch (left) at different pressures as a function of position along the interior seam.
Reproduced from Bourque RA, et al. Multiple compartment pouch and beverage container with frangible seal. US Patent 7306095 B1. 2007.

Yuan [24] provides six case studies where FEA is applied to pouches:

- Case 1: Venting seal bar design for microwavable and retortable pouches. The seal must be strong enough to withstand the temperature and pressure during retort sterilization (121°C, 15–25 psig) without debonding, but weak enough to open up after 90 s of microwaving for venting at 99°C and 4–5 psig. One challenge for the simulation is obtaining a good debonding model, which required measuring peel strength at different angles. This underscores the importance of good experiments to go along with the model development. The model successfully predicts the pressure of the venting and pressure and where partial separation occurs in the package.
- Case 2: Stand-up pouch filling. An FEA model is developed to simulate a filling operation: folding, followed by opening for filling, stand-up base opening, filling with liquid or solid, and heat sealing. The model is used to determine the optimum location of side suction cups, the magnitude of air pressure, and grip locations.
- Case 3: Pouch heat sealing. The top of the pouch is initially an oval during sealing; closing and sealing without forming wrinkles is a challenge. An FEA simulation successfully captures the formation of a wrinkle caused by improper transfer grips and is used to design a solution.
- Case 4: Retort sterilization. The integrity of the seal can be compromised by the creep behavior of the polymer and hot spots that occur during the cooling portion of the retort cycle. Simulation is used along with a seal failure model to predict where the hot spots will be, accounting for the creep behavior.
- Case 5: Pouch drop impact. In this dynamic situation, the critical performance attribute is ductility under high strain rate loading and under biaxial stress. The peak strain rate in a 3-ft (0.91 m) drop can be 30 s^{-1}, 100 times higher than in a tensile test. The stress state dependence of the material is needed since the strain rate and stress differ at each location during the impact event. The authors devise custom fixtures to test the materials at high strain rates and stresses. Comparison between the drop impact test results and the simulation is excellent.
- Case 6: Pouch tear-opening. Consumers want a consistent, easy tear-opening experience. Developing a good propagation of tear model is important. The material properties may change due to thermal exposure during retort

or hot fill. These changes need to be accounted for in the propagation model. If done properly, the tear performance can be correctly predicted.

17.2.2.2 Processing/Converting

The first step in converting polymer to film is extrusion. There are several commercially available single screw extrusion simulation tools including those from Compuplast, Polydynamics, and the University of Paderborn. These programs simulate the solids conveying, melting, and pumping or metering sections of the extruder based on fundamental models from the literature [42,43]. They compute melting, temperature, and pressure profiles along the extruder as well as output rates. They are particularly useful for extrusion engineers for designing screws and troubleshooting extrusion issues [44]. They have limited value for packaging design although may be useful if new materials are being considered.

Combining dissimilar materials in coextrusion can result in flow instabilities where the materials are combined or near the die exit. These instabilities manifest themselves as "wood grain," "orange peel," or waves or zigzag patterns. Sophisticated numerical simulation has been employed to understand the origins of these instabilities, as described in Section 13.4.5. These models often require detailed knowledge of the flow channels and material parameters that may be difficult to measure. A simpler modeling approach is outlined in Section 13.4.5.2. Commercial software is also available to help with these calculations. These tools are helpful for flagging potential problems with matching viscosities and developing strategies for dealing with them, such as changing grades, thicknesses, output, or flow channel dimensions.

Numerical simulations have been used to better understand flow in dies. A number of studies have been published [45–53] with a representative set of examples provided in the cited references (a complete review is beyond the scope of this book). The function of the die is to distribute the flow so that it is uniform across the width or circumference at the exit. Various methods are used to accomplish this, such as the use of multiple manifolds in flat dies and spirals in annual dies. Rheology, especially viscous encapsulation and elastic effects (Section 13.4.4.2), may affect the uniformity of the output and film thickness, especially in coextrusion. These models are mostly in the domain of the equipment manufacturers who design the dies, but it is important for the converter and package designer to know that equipment manufacturers have tools that can help them optimize dies for a given application.

The region past the die exit, where the polymer is drawn down to its final thickness and quenched, has a substantial impact on film properties. There are several models that have been developed in the literature for blown film [54–60]. Compuplast [86] and Polydynamics [87] also have commercial simulation software available. The goal of these models is to try to predict the temperature, bubble shape, and velocity and stress profiles in the film. The stress near the frost line is particularly important for predicting film properties. These models, however, are still mostly of academic interest. The challenges with modeling blown film are described in Section 14.1.1. Limitations of these numerical simulations include the following:

- Simplifications that are typically used to make the computations tractable. These may limit the applicability of the model.
- Difficulties in measuring the material parameters needed for simulation. For example, Doufas [59] has created one of the more advanced models that accounts for many of the physical phenomena that occur during film blowing, including flow-induced crystallization. To obtain the material parameters, however, he resorts to running the material first on the line he is modeling to fit the model to the experimental results.
- Lack of good models for coextrusion.
- Challenges in modeling the cooling part of the process (air flow, heat transfer, and so on) and scaling this up to commercial lines to include both air ring design and inner bubble cooling [61,62].

These models are good for understanding the fundamentals of the process and continue to progress. For now, however, they have not reached the point where the package engineer can use them to predict the properties of untested structures.

Similar statements can be made for cast film. Most of the simulations that can be found in the literature use sophisticated numerical methods and are still in the academic domain [63–79]. A sampling of studies reported in the literature is

summarized in Table 17.4. Simplifying assumptions regarding the number of dimensions, type of flow (Newtonian or viscoelastic), and temperature change is made to various degrees to make the computation tractable. One-dimensional models fix the width and so provide no information on neck-in or edge bead (Section 13.4.2). These models can provide information on draw resonance and thickness uniformity. Two dimensional models use a membrane approximation where the thickness is assumed to be small and the melt curtain behaves as a thin sheet in the state of planar stress. This simplifies the computations. These models can provide information about neck-in and edge bead. Very few investigations model the full three-dimensional case, which would be required to capture the effect of modern edge bead reduction dies.

Heat transfer models like the one developed in Section 15.1.3 have been used to simulate cooling in the nip of extrusion coating [80,81] and sheet lines [82]. They have also been helpful for evaluating new concepts for blown film cooling [83] and annealing of thin sheet and films [84]. The output of the model is particularly helpful for troubleshooting adhesion issues. Commercial software is available for conductive heat transfer modeling, and some specialized programs such as one developed by IKV [82] for sheet cooling are available. These can be versatile tools for troubleshooting not only adhesion issues, but heat sealing and anywhere heat is involved.

During the quenching of a multilayer film, the layers may shrink by different amounts, resulting in film curl. This is described in detail in Section 13.5. A model is developed in Section 13.5.3 based on beam theory that has proven very helpful for troubleshooting curl issues [85].

Models for thermoforming of sheet and film are described in Section 11.1.4. These can be useful for screening new film structures, although obtaining material parameters can be a challenge.

Section 12.1.4.2 describes models for predicting the level of slip accumulating at the surface as a function of time, polymer thickness, and initial slip concentration. Presumably, one then could correlate slip surface concentration with COF, using empirical relationships. These models have been used primarily to better understand the mechanisms of slip

Table 17.4 Summary of Simulation Studies of the Cast Film Process

Study	Model Dimensions	Constitutive Equation	Comment
Yeow [63]	1	Newtonian	Stability analysis
Anturker [64]	1	Viscoelastic	Draw resonance
Iyenjar [65,66]	1	Viscoelastic (Giesekes)	Isothermal
Pis-Lopez & co [67,68]	1	Viscoelastic (Giesekes)	Multiple layers
Pol [69]	1	Viscoelastic (extended Pom Pom)	Isothermal, neck-in
Pol [70]	1	Viscoelastic (extended Pom Pom)	Nonisothermal, neck-in
Chikhalikar [71]	1	Viscoelastic (extended Pom Pom)	Isothermal, neck-in
Lamberti [72]	1	Viscous (cross)	Nonisothermal, flow induced crystallization
Zatloukal [73]	1	Viscoelastic (Leonov)	Isothermal, neck-in
Debbaut [74]	2	Viscoelastic	Isothermal
Silagy [75]	2	Viscoelastic (Maxwell)	Isothermal
Rajagopalan [76]	2	Viscoelastic (Giesekes)	Isothermal
Sollogoub [77]	2	Viscoelastic	Nonisothermal
Cox [78]	2	Viscoelastic (Giesekes)	Nonisothermal
Sakaki [79]	3	Newtonian	Isothermal

migration and have limitations for predicting actual COF in packaging films. One of these limitations is the lack of knowledge of how slip agents are partitioned at interfaces between layers in a multilayer film. This knowledge would be required to extend the approach to coextruded films.

Chapter 15 covers a number of fundamental studies on the effect of processing on adhesion, such as a peel strength master curve that relates the material properties of the tie resin, the timescales of the process and polymer relaxation to peel strength (Section 15.2.3). The master curve approach can be used to predict adhesion performance.

Finally, there are scale-up relationships for duplicating the properties obtained on a lab line on a larger commercial line. Such relationships are discussed in Section 14.1.1 for blown film.

17.2.3 Case Study

To illustrate the use of models to speed the development of flexible packaging, a hypothetical package development is considered. The analysis is based on a case study presented by Morris [35] that describes the use of modeling tools developed at DuPont.

Table 17.5 Requirements of Barrier Bag-in-Box Liner Used in Case Study

Package Requirements:
Easy open function
Moisture barrier: <0.3 g/day/package
Oxygen barrier: OTR <3 cc O_2/day/package
Puncture resistance
Cost-effective and easy to run on vertical form fill seal line

The example package is a barrier bag-in-box snack package. The inner liner is made and filled on a vertical form-fill-seal line and then placed into a secondary paperboard box. The first step in the design process is to determine the requirements for the package. The brand owner or end user generally provides these. The converter or designer must translate the stated needs into engineering requirements that can be used in the design process. The requirements considered for this case study for the barrier bag are given in Table 17.5.

Because of the barrier requirements, the general structure (HDPE—tie—barrier—tie—sealant) is considered. This is a fairly standard structure used in these types of applications, as is shown in Appendix B. The HDPE provides moisture barrier. Either polyamide or EVOH is typically used as the oxygen barrier layer. The sealant is an EVA or ionomer formulated for easy opening. The models and tools will help determine which materials to use, their thicknesses, how cost-effective it may be, as well as whether any difficulties in making the structure might be encountered. Table 17.6 describes some of the resins that will be considered in the analysis.

17.2.3.1 Barrier Selection

A simple permeability calculator based on Eq. (8.21) can be used to determine what barrier resin to use. An example spreadsheet is shown in Fig. 17.10. The requirements call for a fairly moderate oxygen barrier to prevent spoilage. Oxygen barrier is also often used as a predictor for aroma barrier, even though aroma involves larger molecules and may not correlate with oxygen permeability (Section 8.2.4). Highly flavored

Table 17.6 Description of Resins Used in the Case Study

Resin	Description	MI (g/10 min)	Tensile Modulus (MPa)
EVA	18% VA	2.5	70
Ionomer 1	Zinc neutralized	5.3	240
Ionomer 2	Zinc neutralized	0.7	480
Tie	LLDPE-based	1.1	210
PA6	Nylon 6		700
HDPE	0.95 g/cc	0.26	770

Permeabilty Calculator
(Fill in Cells in Blue)

Square inches of film: 130 0.084 square meters
Film Thickness (mils): 4.1 104.1 microns

		% of	Thickness		OPV	MVTR
Layer	Resin	Thickness	mil	microns	cc-mil/100in2-d-atm	g-mil/100in2-d-atm
1	Ionomer 1	25	1.03	26.0	350	1.75
2	tie	7.5	0.31	7.8	550	1.2
3	PA6	12	0.49	12.5	6	13
4	tie	7.5	0.31	7.8	550	1.2
5	HDPE	48	1.97	50.0	220	0.5
6						
7						
8						
9						
Total		100			10.5	0.2

Summary Results:

OTR (cc/100in2-d-atm)	10.5	MTR (g/100in2-d-atm)	0.2
OTR (cc/m2-d-atm)	163.2	MTR (g/m2-d-atm)	3.1
OTR cc/day (100% O2)	13.69	MTR (g/day)	0.26
OTR cc/day (air)	2.87		

Calculation:

OTR = 1/(thickness1/OPV1 + thickness2/OPV2 + thickness3/OPV3)
OTR (cc/day) = OTR(cc/100in2-d-atm)*Square inches of film/100

Figure 17.10 Permeability calculator showing results for a barrier snack package example. *MTR*, Moisture transmission rate; *MVTR*, moisture vapor transmission rate; *OPV*, oxygen permeation value; *OTR*, oxygen transmission rate.
Reproduced from Morris BA. Application of modeling to speed flexible packaging development. In: SPE ANTEC Conference. 2012. Also Morris BA. J. Plastic Film & Sheeting 2013;29:pp. 249–70 with permission for the Society of Plastics Engineers.

snacks and cereals may require an aroma barrier to prevent too much of the aroma from permeating through the package and into the grocery aisles. The model results given in Fig. 17.10 show that a 12 μm layer of PA6 will be sufficient. EVOH could be used but may be overengineered. Less than 1 μm would be needed to achieve the barrier requirement, but limitations on coextrusion equipment generally constrain the thickness to about 3 μm or higher. Furthermore, films containing PA generally have better impact puncture resistance than EVOH. The results show that 50 μm of HDPE will provide enough moisture barrier performance.

17.2.3.2 Sealant Selection

The attributes the sealant needs to bring to the structure are tabulated in Table 17.7. Each attribute has been assigned an importance rating on a scale of 1–10. These are entered into the DuPont sealant selector tool (Section 17.2.1.1). The results are shown in Fig. 17.11. The functional score for each sealant type has been normalized to a scale of 0–10. The length of each bar is the sum of the importance factors multiplied by the matrix score for each attribute. The individual contribution from each attribute is highlighted by color and can be used to quickly see why one sealant is scoring better than another. In this example, ionomers and EVA have the highest scores. The ionomer has strong contributions from its ability to be formulated as an easy-open sealant while maintaining a hermetic seal, perforation resistance, grease and oil resistance, and low seal temperatures.

17.2.3.3 Stiffness and Life Cycle Assessment Model

DuPont has developed a model that computes bending stiffness and provides a cradle-to-gate life cycle assessment of the materials used in the package

Table 17.7 Input to the Sealant Selector Tool for the Snack Film in the Case Study. Scale is From 1 to 10 With 10 Being Most Important

Attribute	Importance Rating (1–10 scale)
Blown film processing	3
Low-seal initiation temperature	10
Broad hot tack temperature range	5
Seal around contamination	3
Caulk gussets; seal through wrinkles	3
Grease and oil resistance	6
Perforation resistance	10
Easy to open seal technology	10

Reproduced from Morris BA. Application of modeling to speed flexible packaging development. In: SPE ANTEC Conference. 2012. Also Morris BA. J. Plastic Film & Sheeting 2013;29:pp. 249–70 with permission from the Society of Plastics Engineers.

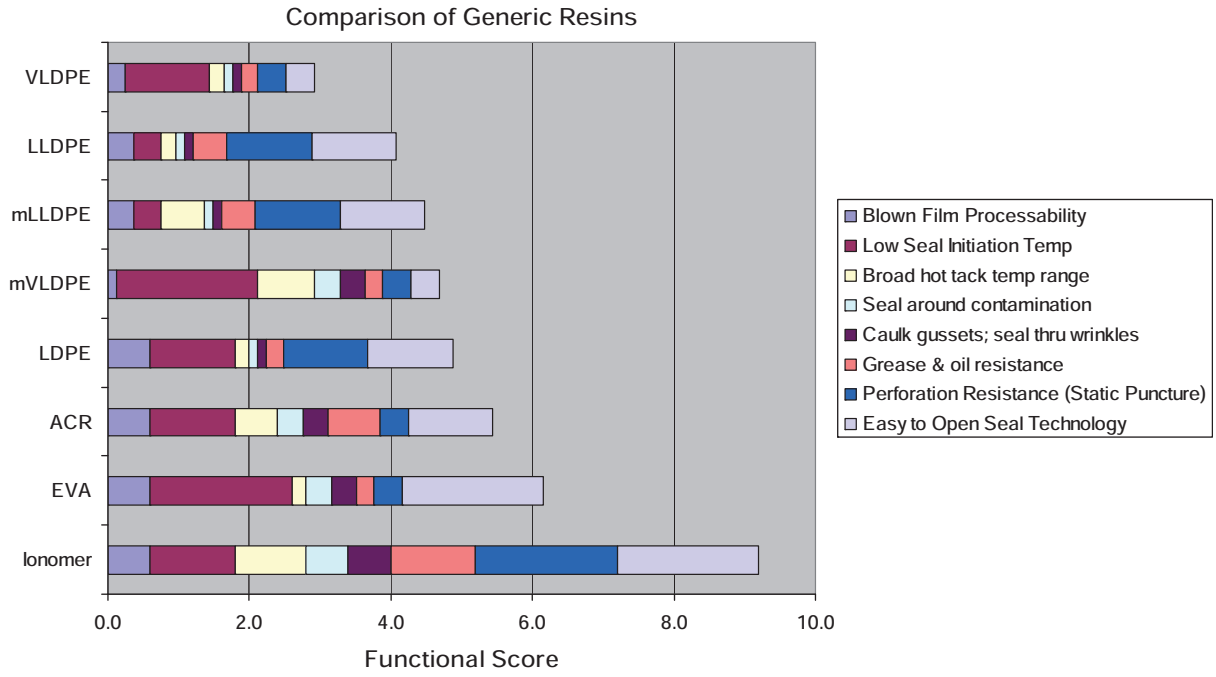


Figure 17.11 DuPont sealant selector tool [40] results for the snack film example. *ACR*, Acid copolymer resin; *EVA*, ethylene vinyl acetate copolymer; *LDPE*, low density polyethylene; *LLDPE*, linear low density polyethylene; *mLLDPE*, metallocene linear low density polyethylene; *mVLDPE*, metallocene very low density polyethylene plastomer; *VLDPE*, very low density polyethylene.

Reproduced from Morris BA. Application of modeling to speed flexible packaging development. In: SPE ANTEC Conference. 2012. Also Morris BA. J. Plastic Film & Sheeting 2013;29:pp. 249–70 with permission from the Society of Plastic Engineers.

structure. Table 17.8 shows the typical output from this model. Material cost can also be computed by the model, but it is not shown here. Summary inputs are given in the first six columns, and the computed results are given in the final column. By running several cases, the user can see how changes in materials and thickness can affect package performance (stiffness) and cost (material cost, nonrenewable energy consumption, and greenhouse gas emissions).

This is shown in Figs. 17.12–17.14 where the model results graphed for the barrier bag-in-box liner film. As is described in Section 9.4.2, the stiffness of

Table 17.8 Example Output From Stiffness/LCA Model

Example							
Barrier Bag in Box Base Case							
Layer Description	**Thickness (microns)**	**Modulus (M Pa)**	**Density (g/cm^3)**	**Nonrenewable Energy Consumption (MJ/kg)**	**Greenhouse Gas Emissions (eq CO_2/kg)**	**Model Results**	
HDPE	50.8	770	0.95	76	1.9	Weight:	0.102 kg/m^2
Tie	7.5	210	0.91	76.9	2.1	Thickness:	104.2 μm
PA6	13	700	1.2	120	9.1	Stiffness factor:	2.56
Tie	7.5	210	0.91	76.9	2.1	Neutral axis from top:	36.7 μm
EVA	25.4	70	0.95	76.9	2.1	Total material cost:	0.220 $\$/m^2$
						Nonrenewable energy consumption:	8.46 MJ/m^2
						Greenhouse gas emissions:	0.313 eq CO_2/m^2

This tool is suitable for quickly exploring technology options. For supporting business decisions, more comprehensive studies are necessary. The peer review conducted on this tool does not imply an endorsement of any comparative assertions based on the results.
Reproduced from Morris BA. Application of modeling to speed flexible packaging development. In: SPE ANTEC Conference. 2012. Also Morris BA. J. Plastic Film & Sheeting 2013;29:pp. 249–70 with permission from the Society of Plastics Engineers.

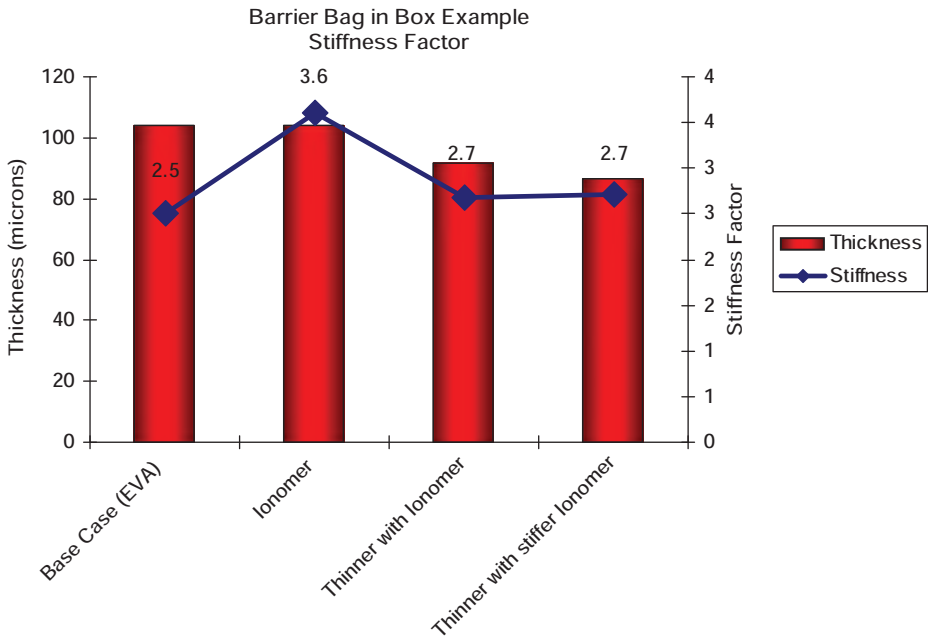


Figure 17.12 Cross-plot of model output of thickness and bending stiffness (stiffness factor) for snack film structures.
Reproduced from Morris BA. Application of modeling to speed flexible packaging development. In: SPE ANTEC Conference. 2012. Also Morris BA. J. Plastic Film & Sheeting 2013;29:pp. 249–70 with permission from the Society of Plastics Engineers.

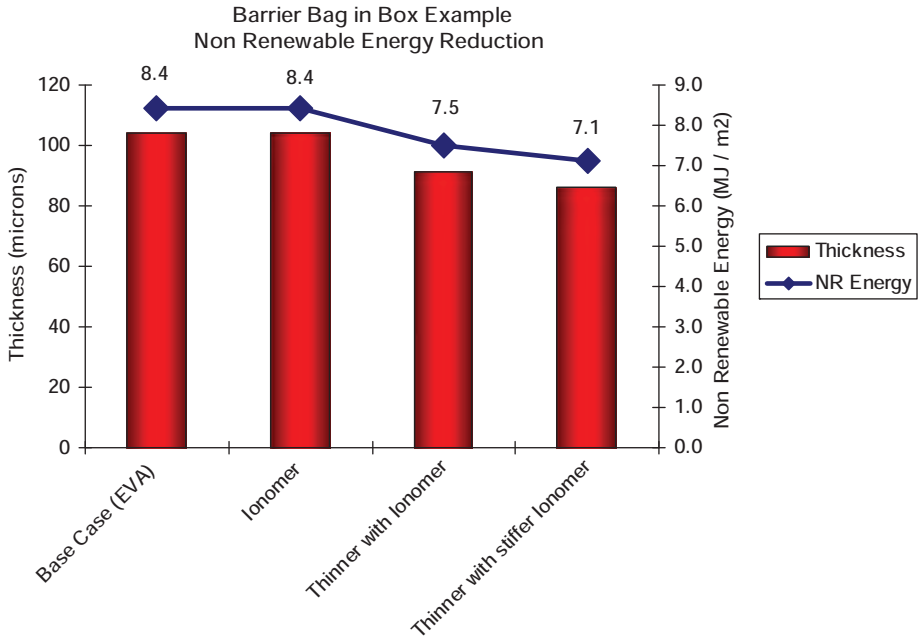


Figure 17.13 Cross-plot of model output of thickness and nonrenewable energy for snack film structures.
Reproduced from Morris BA. Application of modeling to speed flexible packaging development. In: SPE ANTEC Conference. 2012. Also Morris BA. J. Plastic Film & Sheeting 2013;29:pp. 249–70 with permission from the Society of Plastics Engineers.

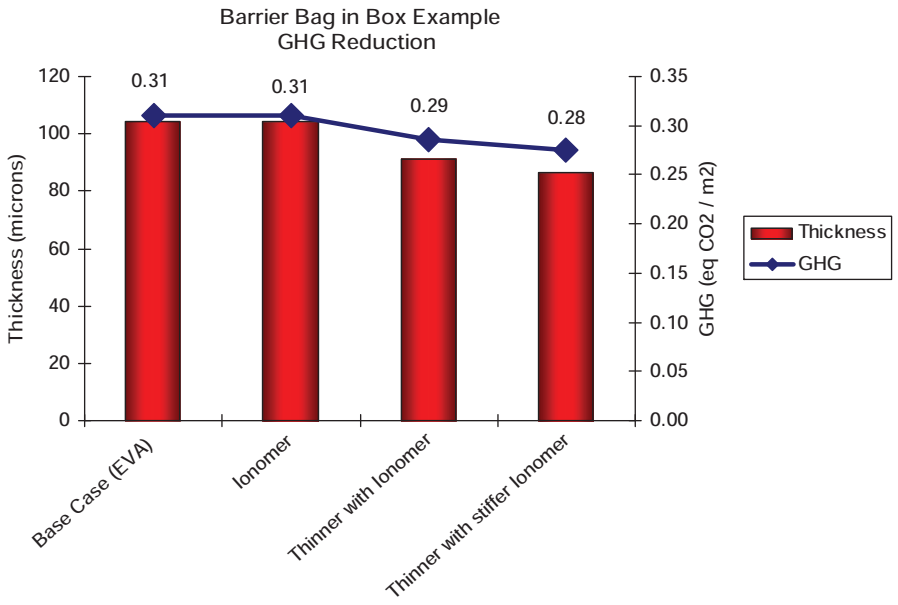


Figure 17.14 Cross-plot of model output of thickness and greenhouse gas emissions for snack film structures. *Reproduced from Morris BA. Application of modeling to speed flexible packaging development. In: SPE ANTEC Conference. 2012. Also Morris BA. J. Plastic Film & Sheeting 2013;29:pp. 249–70 with permission from the Society of Plastics Engineers.*

the sealant layer often has a disproportionate influence on the overall bending stiffness of a film. Table 17.6 shows that the ionomers have a substantially higher modulus than EVA. Substituting an ionomer sealant for an EVA sealant increases the film stiffness (Fig. 17.12). This may allow the sealant layer to be downgauged (third bar in Fig. 17.12) while maintaining overall package stiffness. A package using an ionomer with a higher modulus can be further downgauged, which results in additional reductions in the environmental footprint (Figs. 17.13 and 17.14). Of course there are practical limits to how thin the sealant layer can be and maintain good seal functionality. For example, if the sealant is too thin is may not caulk well into wrinkles and other imperfections. The model provides directional guidance; the results should always be tested under conditions of actual use.

17.2.3.4 Packing Costs

Fig. 17.15 shows the output from the DuPont SaVE tool [40], a packaging cost model described in Section 16.5.1.6. The structure with an ionomer sealant to is compared with one with an EVA sealant. The packaging material costs are higher for the ionomer structure (bottom/blue bar), but the overall packaging cost is lower (total bar height) due to lower cost of labor, overhead, and waste. Here it is assumed the line speed is 10% faster (64 packages/min) and leaker rates 50% lower for the ionomer film.

As is discussed in Section 16.5.1.6, the SaVE tool also provides a sensitivity analysis on each of the key input variables such as line speed, leaker rate, and roll stock cost. This example is the same at the one used in Section 16.5.1.6—the analysis shows that the line speed could be as low as 49 packs/min and the ionomer film would still save cost due to its lower leaker rate.

17.2.3.5 Heat Seal

Fig. 17.16 shows experimental and model results of plateau seal temperature vs dwell time for ionomer films from work described in Section 7.6.1 [38]. The snack package structure is roughly 100 μm thick. The model predicts for a sealing temperature of 130°C that the dwell time will be around 0.5 s. At this dwell time, a typical vertical form-fill-seal machine will have a packing speed of 60 packs/min (assuming the heat seal is 50% of the cycle). This is consistent with the assumptions used in the total cost model. The high sealing temperature may be close to causing distortion of the HDPE layer, which has a peak

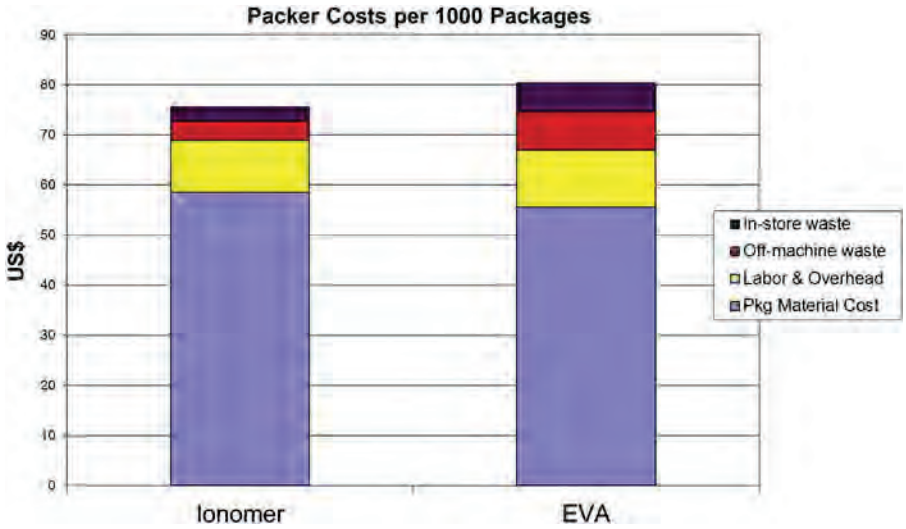


Figure 17.15 Example output from the DuPont Sealant Value Estimator tool.
Reproduced from Morris BA. Application of modeling to speed flexible packaging development. In: SPE ANTEC Conference. 2012. Also Morris BA. J. Plastic Film & Sheeting 2013;29:pp. 249–70 with permission from the Society of Plastics Engineers.

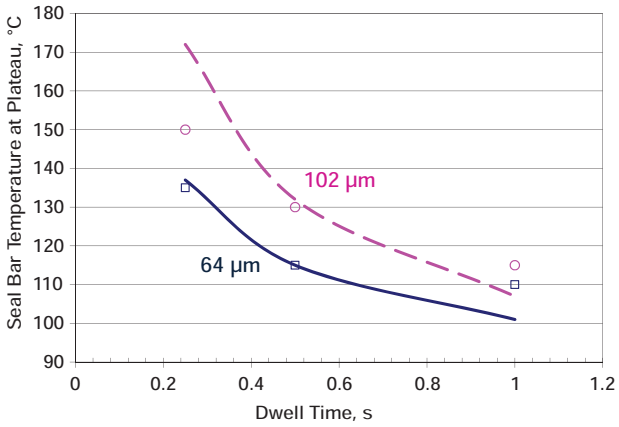


Figure 17.16 Heat seal model (*curves*) and experimental results (*data points*) for ionomer films. Plateau seal temperature is the minimum temperature at which the maximum heat seal strength is obtained. Films have structure OPET/ionomer (5), where *OPET*, oriented polyester film.
Reproduced from Morris BA. Application of modeling to speed flexible packaging development. In: SPE ANTEC Conference. 2012. Also Morris BA. J. Plastic Film & Sheeting 2013;29:pp. 249–70 with permission.

melting point of around 135°C. The model suggests switching to a grade of ionomer with a lower seal initiation temperature may be advantageous.

17.2.3.6 Flow Instabilities in Coextrusion

The flow matching model from Section 15.4.5.2 is used to estimate whether the designed structure may have flow instability issues. The input parameters for the model are given in Table 17.9. The output is shown graphically in Fig. 17.17. The shaded region in the middle is the ideal region for no flow instabilities (where the ratios to fall within the 3:1 to 1:3 viscosity ratio criteria). The analysis suggests that the PA viscosity is too low compared to the tie resin; the ratio of the PA viscosity to the first and second tie layers is almost 1:4 and 1:2.6. A better match can be obtained by reducing the PA extrusion temperature or switching to a higher molecular weight grade of PA (both approaches increase the viscosity of the PA layer). Lowering the viscosity of the tie layer may also be effective but this may cause problems at the HDPE–tie interface. These parameters can be adjusted in the model to determine the best approach without resorting to trial and error on the film line.

Note that the analysis is not symmetrical in that the viscosity ratio of the tie 1–PA and PA–tie 2 is not the inverse of one another even though the tie is the same composition, thickness and temperature on both sides of the PA. This is due to differences in shear stress (and shear rates) on each side of the PA layer.

Table 17.9 Input for the Flow Matching Model for Predicting Onset of Coextrusion Instabilities

Viscosity Matching in Coextrusion

Input Parameters

Total throughput (kg/hr): 260

Width of channel (mm): 1100

Height of channel (mm): 1.80

Layer	Resin	Thickness microns	Temperature Degrees C
1	Ionomer	20	200
2	Tie 1	7.5	220
3	PA6	12	250
4	Tie 1	7.5	220
5	HDPE	50	200
	Total thickness	97	

Reproduced from Morris BA. Application of modeling to speed flexible packaging development. In: SPE ANTEC Conference. 2012. Also Morris BA. J. Plastic Film & Sheeting 2013;29:pp. 249–70 with permission from the Society of Plastics Engineers.

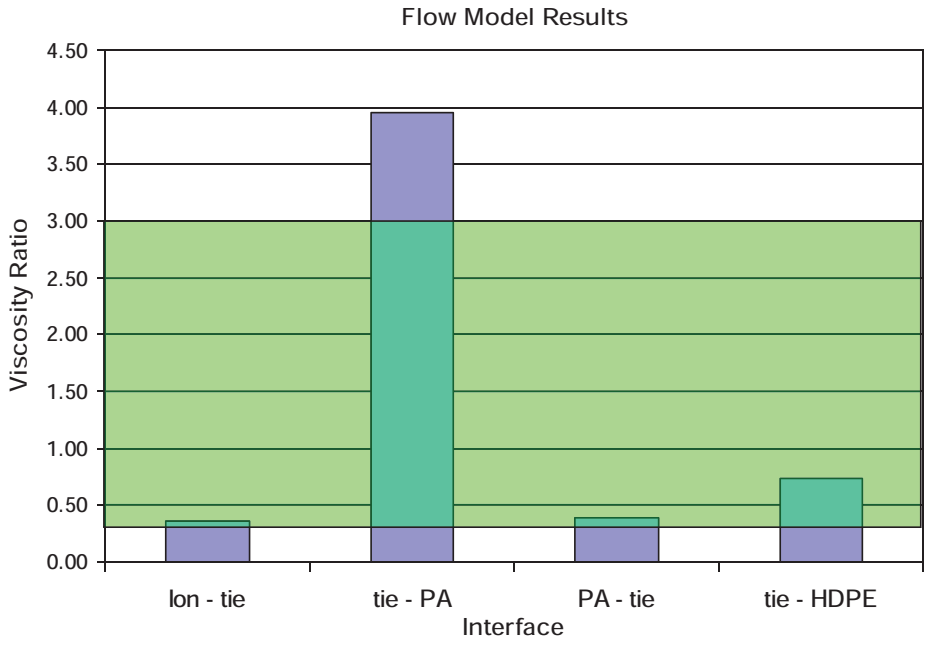


Figure 17.17 Graphical representation of flow model output. (*HDPE*, High density polyethylene; *Ion*, ionomer, *PA*, polyamide 6). The viscosity ratio is the ratio of the viscosity of the first resin on the list to the viscosity of the second at the shear stress and temperature at the interface. The shaded region is the desired region for good flow.

17.2.3.7 Curl

Curl can be significant in blown films of this structure. The PA layer freezes first followed by the HDPE layer. As it freezes, the HDPE shrinks due to the more ordered structure (higher density) of the crystal domains. The combination of the shrinkage, stiffness, and thickness of the HDPE layer causes the film to curl toward the HDPE layer. The sealant side of the structure, being thinner and less crystalline, is generally not enough to compensate.

The curl model [85] described in Section 13.5.3 is used to estimate the curvature of the films. The model results suggest films with either an EVA or an ionomer sealant will have a significant curl toward the HDPE. Changing the thickness of the sealant has little impact. Techniques that have been found to reduce curl include increasing the quench rate and adding amorphous PA to PA6. PA6 is also known to undergo post-quench crystallization, especially if the film is moisture conditioned, which can balance out some of the curl toward the HDPE layer. Post-quench crystallization is not captured by the model.

References

[1] Nikon ND. Microscopy U: Resolution, viewed December 06, 2015 at: https://www.microscopyu.com/articles/formulas/formulasresolution.html.

[2] Garcia-Meitin EI, Lai CY, O'Connell P, Bensason S. Development of sealants for flexible packaging using light microscopy. In: SPE ANTEC Conference; 2015.

[3] Weast RC, editor. Handbook of chemistry and physics. 56th ed. Cleveland (OH): CRC Press, Inc.; 1975. F245–54.

[4] Morrison RT, Boyd RN. Organic chemistry. 3rd ed. New York: Allyn and Bacon, Inc.; 1976.

[5] Thermo Scientific, ND. FTIR basics, viewed December 05, 2015 at: http://www.thermoscientific.com/en/about-us/general-landing-page/ftir-basics.html.

[6] Perkin Elmer. Differential scanning calorimetry (DSC), frequently asked questions. 2013. viewed December 06, 2015 at: http://www.perkinelmer.com/CMSResources/Images/44-74542GDE_DSCBeginnersGuide.pdf.

[7] DuPont ND. Sealant selector, viewed on August 02, 2014, from: http://www2.dupont.com/Packaging_Resins/en_US/Modeling_Tools/Sealant_Selector_Guide/index.html.

[8] Box GE, Hunter WG, Hunter JS, Hunter WG. Statistics for experimenters: design, innovation, and discovery. 2nd ed. Wiley; 2005.

[9] Montgomery DC. Design and analysis of experiments. 8th ed. John Wiley and Sons, Inc.; 2012.

[10] Box GEP, Draper NR. Empirical model building and response surfaces. John Wiley and Sons; 1987.

[11] Cornell J. Experiments with mixtures: models, and the analysis of mixture data. 3rd ed. John Wiley and Sons; 2002.

[12] Myers RH, Montgomery DC, Anderson-Cook CM. Response surface methodology: process and product optimization using designed experiments. 3rd ed. John Wiley and Sons; 2016.

[13] Mason RL, Gunst RF, Hess JL. Statistical design & analysis of experiments with applications to engineering and science. 2nd ed. John Wiley and Sons; 2003.

[14] Hinkelmann K, Kempthorne O. Design and analysis of experiments, volume I: introduction to experimental design. 2nd ed. John Wiley and Sons; 2008.

[15] SAS ND. JMP®, discover the unexpected, viewed December 06, 2015 at: http://www.jmp.com/en_us/software/jmp.html.

[16] Minitab, ND. Put your data to work, viewed December 06, 2015 at: https://www.minitab.com/en-us/.

[17] Borse N, Aubee N. Predicting physical and optical properties of co-extruded blown films using design of experiment based model. In: SPE ANTEC Conference; 2015. p. 1584–8.

[18] Blom H. Flexible packaging durability studies. In: SPE FlexPackCon Conference; 2014.

[19] Todd WG, Podborny WR. Predictive models helps develop new high-performance HDPE for barrier film application. In: SPE ANTEC Conference; 2001.

[20] Wang X. A predictive model for dart impact strengths of solution octene LLDPE film resins. In: SPE ANTEC Conference; 2003. p. 1386–90.

[21] Morris BA. The influence of stress on peel strength of acid copolymers to foil. In: TAPPI Polymers, Laminations and Coatings Conference; 1998. Also Morris, B. A., 2002, J. Reinforced Plastics and Composites, 21, pp. 1243–55.

[22] Agassant JF, Mackley MR. A personal perspective on the use of modeling simulation for polymer melt processing. Intern Polym Process 2015;XXX:121–40.
[23] Bergstrom J, Quinn D, Schmitt E, Brown S, Chow S. High strain rate testing and modeling of polymers for impact simulations. In: SPE ANTEC Conference; 2014. p. 2305–7.
[24] Yuan JZ, Haynes CA. Predictive analysis of flexible pouch performance. In: SPE ANTEC Conference; 2014. p. 1436–40.
[25] Carbajal LA, Jiao R, Hahm DM, Morris BA, Kendzirski RR. Predicting the impact puncture response of multilayer flexible food packages using explicit finite element models. In: SPE ANTEC Conference; 2016.
[26] European Union Commission Regulation No 10/2011. On plastic materials and articles that come into contact with food, viewed December 05, 2015 at: https://www.fsai.ie/uploadedFiles/Reg10_2011.pdf.
[27] Combase: combined database for predictive microbiology, viewed December 05, 2015 at: http://www.combase.cc/.
[28] AKTS ND. AKTS-SML software, viewed December 05, 2015 at: http://www.akts.com/sml-diffusion-migration-multilayer-packaging/download-diffusion-prediction-software.html.
[29] FABES ND. Analysis and evaluation of diffusion processes: Migratest ESP, viewed December 05, 2015 at: http://www.fabes-online.de/software.php?lang=en&mode=migratest.
[30] ICIPC ND. Migrasoft version: 2015-07-23, viewed December 05, 2015 at: http://tools.icipc.org/migrasoft/.
[31] Roduit B, Borgeat CH, Cavin S, Fragniere C, Dudler V. Application of finite element analysis (FEA) for the simulation of release of additives from multilayer polymeric packaging structures. Food Addit Contam 2005;22:945–55.
[32] Pocas MF, Oliveira JC, Oliveira FAR, Hogg T. A critical survey of predictive mathematical models for migration from packaging. Crit Rev Food Sci Nutr 2008;48:913–28.
[33] Lopez ID, Estefan JC, Betancur A. Packaging and food interactions modeling: validation for compliance with specific migration regulations. In: SPE ANTEC Conference; 2015. p. 1545–9.
[34] Morris BA, Vansant JD. The influence of sealant modulus on the bending stiffness of multilayer films. In: TAPPI Polymers, Laminations and Coatings Conference; 1997.
[35] Morris BA. Application of modeling to speed flexible packaging development. In: SPE ANTEC Conference; 2012. Also Morris, B. A., 2013, J. Plastic Film & Sheeting, 29, pp. 249–70.
[36] Wu R-Y, McCarthy LD, Stachurski ZH. Tearing resistance of multi-layer plastic films. Intern J Fract 1994;68:141–50.
[37] Carbajal LA, Jiao R, Hahm DM, Morris BA, Kendzirski RR. Impact puncture resistance of multilayer flexible food packages. In: SPE ANTEC Conference; 2015.
[38] Morris BA. Predicting the heat seal of ionomer films. J Plastic Film Sheeting 2002;18:157–67.
[39] Moffitt RD. A mathematical model for the heat sealing of linear, semi-crystalline polymers. In: SPE ANTEC Conference; 2006. p. 1027–32.
[40] DuPont ND. Sealant value estimator: are you paying too much for sealed packaging?. DuPont, viewed November 28, 2015 at: http://www2.dupont.com/Packaging_Resins/en_US/Modeling_Tools/SaVE/index.html.
[41] Bourque RA, et al. Multiple compartment pouch and beverage container with frangible seal. 2007. US Patent 7306095 B1.
[42] Tadmor Z, Gogos CG. 1982, Principles of polymer processing. New York: John Wiley & Sons; 1979.
[43] Agur EE, Vlachopoulos J. Numerical simulation of a single-screw plasticating extruder. Polym Eng Sci 1982;22:1084–94.
[44] Vleck J, Perdikoulias J. Application of a single screw extrusion simulation towards design. In: SPE ANTEC Conference; 2002.
[45] Vaddiraju SR, Kostic M, Reifneider L, Pla-Dalmau A, Rykalin V, Bross A. Extrusion simulation and experimental validation to optimize precision die design. In: SPE ANTEC Conference; 2004. p. 76–80.
[46] Gupta M. Three dimensional simulation of coextrusion in a complex profile die. In: SPE ANTEC Conference; 2010. p. 2030–6.
[47] Perdikoulias J, Svabik J. 3D FEM simulation of feed-block profiling for flat die coextrusion. In: SPE ANTEC Conference; 2002.

[48] Lee PC, Macosko CW. Die design for layer thickness uniformity in multilayer coextrusion. In: SPE ANTEC Conference; 2009. p. 1542−6.
[49] Sun Y, Gupta M, Dooley J, Koppi KA, Spalding MA. Experimental and numerical investigation of the elongational viscosity effects in a coat-hanger die. In: SPE ANTEC Conference; 2005. p. 81−5.
[50] Catherine O. Effect of typical melt temperature non-uniformity on flow distribution in flat dies. In: SPE ANTEC Conference; 2012.
[51] Iuliano S, Svenningsen A. The effect of flow channel aspect ratio on layer uniformity in flat extrusion dies. In: SPE ANTEC Conference; 2016.
[52] Kihara S, Gouda T, Matsunaga K, Funatsu K. Numerical simulation of three-dimenional viscoelastic flow within dies. Polym Eng Sci 1999;39:142−63.
[53] Debbaut B, Dooley J. Secondary motions in straight and tapered channels: experiments and three-dimensional finite element simulation with a multimode differential viscoelastic model. J Rheol 1999;43:1525−45.
[54] Pearson JRA, Petrie CJS. The flow of a tubular film. Part 1. Formal mathematical representation. J Fluid Mech 1970;40:1−19.
[55] Pearson JRA, Petrie CJS. The flow of a tubular film. Part 2. Interpretation of the model and discussion of solutions. J Fluid Mech 1970;42:609−25.
[56] Ashok BK, Campbell GA. Two-phase simulation of tubular film blowing of crystalline polymers. Int Polym Process 1992;7:240−7.
[57] Doufas AK, McHugh AJ. Simulation of film blowing including flow-induced crystallization. J Rheol 2001;45:1085−104.
[58] Pirkle Jr JC, Braatz RD. A thin-shell two-phase microstructural model for blown film extrusion. J Rheol 2010;54:471−505. Ashok, B. K. and Campbell, G. A., Int Polym Process, 7, 240−7 (1992).
[59] Doufas AK. A microstructural flow-induced crystallization model for film blowing: validation with experimental data. Rheol Acta 2014;53:269−93.
[60] Kolarik R, Zatloukal M. Modeling of nonisothermal film blowing process for non-Newtonian fluids by using variational principles. J Appl Polym Sci 2011;122:2807−20.
[61] Sidiropoulos V, Vlachopoulos J. Numerical simulation of blown film cooling. In: SPE ANTEC Conference; 2000.
[62] Jonas M, Wortberg J, Uniewski T, Blume S. A prediction model for the numerical optimization of a novel blown film cooling system. In: SPE ANTEC Conference; 2014. p. 1194−9.
[63] Yeow YL. On the stability of extending films: a model for the film casting process. J Fluid Mech 1974;66:613−22.
[64] Anturkar NR, Co A. Draw resonance in film casting of viscoelastic fluids: a linear stability analysis. J Non-Newt Fluid Mech 1988;28:287.
[65] Iyengar VR, Co A. Film casting of a modified Giesekus fluid: a steady-state analysis. J Newt Fluid Mech 1993;48:1−20.
[66] Iyengar VR, Co A. Film casting of a modified Giesekus fluid: a steady-state analysis. Chem Eng Sci 1996;51:1417−30.
[67] Pis-Lopez ME, Co A. Multilayer film casting of modified Giesekus fluids Part 1. Steady-state analysis. J Newt Fluid Mech 1996;66:71−93.
[68] Pis-Lopez ME, Co A. Multilayer film casting of modified Giesekus fluids Part 2. Linear stability analysis. J Newt Fluid Mech 1996;66:95−114.
[69] Pol H, Thete SS, Doshi P, Lele AK. Necking in extrusion film casting: the role of molecular architecture. J Rheol 2013;57:559−83.
[70] Pol H, Banik S, Azad LB, Thete S, Doshi P, Lele A. Nonisothermal analysis of extrusion film casting process using molecular constitutive equations. Rheol Acta 2014;53:85−101.
[71] Chikhalikar K, Banik S, Azad LB, Jadhav K, Mahjan S, Ahmad Z, et al. Extrusion film casting of long chain branched polypropylene. Polym Eng Sci 2015;55:1977−87.
[72] Lamberti G. Flow-induced crystallization during isotactic polypropylene film casting. Polym Eng Sci 2011;51:851−61.
[73] Zatloukal M, Barborik T. Effect of extensional viscosity, elasticity and die exit stress state on neck-in phenomenon during extrusion film casting: theoretical study. In: SPE ANTEC Conference; 2016.
[74] Debbaut B, Marchal JM. Viscoelastic effects in film casting. Special Issue, Theoretical, experimental, and numerical contributions to the

mechanics of fluids and solids Z Angew Math Phys 1995;46:S679–98.
[75] Silagy D, Demay Y, Agassant JF. Stationary and stability analysis of the film casting process. J Newt Fluid Mech 1998;79:563–83.
[76] Rajagopalan D. Impact of viscoelasticity on gage variation in film casting. J Rheol 1999;43:73–83.
[77] Sollogoub C, Demay Y, Agassant JF. Non-isothermal viscoelastic numerical model of the cast film process. J Newt Fluid Mech 2006;138:76–86.
[78] Cox C, von Oehsen JB. A finite element model of non-isothermal viscoelastic flow in the cast film process. In: SPE ANTEC Conference; 2007. p. 1596–600.
[79] Sakaki K, Katsumoto R, Kajiwara T, Funatsu K. Three-dimensional flow simulation of a film-casting process. Polym Eng Sci 1996;36:1821–31.
[80] Trouilhet Y, Morris. Prediction of temperature profiles across coating and substrate in the nip. In: TAPPI Polymers, Laminations and Coatings Conference; 1999.
[81] Devisme S, Haudin J-M, Agassant J-F, Rauline D, Chopinez F. Numerical simulation of extrusion coating: contribution to the understanding of adhesion mechanisms between grafted polypropylene and aluminum. Intern Polym Process 2007;XXII:90–104.
[82] AiXtrusion. Film and sheet extrusion – simulation of cooling, viewed 10 December 10, 2015 at: https://translate.google.com/translate?hl=en&sl=de&u=http://aixtrusion.de/leistungen/produkte/prozesssimulation/sheetcoolaix-abkuehlvorgaenge/&prev=search.
[83] Hopmann C, Hennings M. Increased throughputs in blow film extrusion by using a contact cooling sleeve. In: SPE ANTEC Conference; 2016.
[84] Huang W, Spalding MA, Read MD, Hogan TA. Heat transfer simulation for a continuous annealing process of plastic sheets. In: SPE ANTEC Conference; 2015.
[85] Morris BA. Reducing curl in multilayer blown film: experimental results, model development, and application to a cereal liner film. J Plastic Film Sheeting 2003;19:31–54.
[86] Compulast. Compuplast virtual laboratory™ – blown film extrusion. 2014, viewed February 02, 2016 at: http://www.compuplast.com/product/extrusion-packages/blown-film-extrusion.
[87] Polydynamics ND. B-film 2. viewed February 02, 2016 at: http://www.polydynamics.com/fra_programs.htm.

Appendix A: Writing Guide for Packaging Films and Other Multilayer Structures

S.B. Marks
E.I. du Pont de Nemours & Company, Wilmington, DE, United States

A wide variety of multilayer structures are used in the flexible and rigid packaging industry, which are put together by an assortment of techniques including: extrusion lamination, adhesive lamination, extrusion coating, as well as coextrusion blown film, cast film, sheet and blow molding.

Currently, there does not exist a standard method for communicating structures in a written format between companies (and for the most part, even within companies). The guidelines described below are derived from formats used within DuPont. While no one method is best, we have found this guide to be useful in that it presents a systematic way to not only communicate the components of the structure but also the technology used to put it together. By following the guidelines, one can better understand whether, for example, a structure is manufactured using either coextrusion or tandem extrusion coating. Such concise writing can improve communication. Thus we offer these guidelines to the industry in the hope that they will increase communication effectiveness and understanding between all persons in our business.

The format guidelines allow for use in handwritten communication or for typing using a keyboard, which is especially important for the electronic communication methods in use today.

One commonly misunderstood character is the dash or minus sign. There are actually three different dashes available in most word processors. They are:

- The minus sign−(a short length dash)
- An En dash−(a medium length dash) {With the "Num Lock" on, hold down the Alt key and type 0150 on the keypad.}, or {With the "Num Lock" on, hold down the Ctrl key and type "-" on the keypad.}
- An Em dash—(a long length dash) {With the "Num Lock" on, hold down the Alt key and type 0151 on the keypad.}, or {With the "Num Lock" on, hold down the Ctrl &Alt keys and type "-" on the keypad.}

In Microsoft Word, they are also shown on the Special Character tab of the symbol window.

Table A.1 Key Definitions

Primer	A bonding agent that is applied in a liquid form to a solid surface. It is intended to promote the adhesion of another liquid or molten material that will subsequently be applied on top of the primer. Typically, it is dried, prior to having the subsequent material applied to it. *(This is usually associated with extrusion coating.)* In some parts of the world these are referred to as anchor coatings (*AC*). Adhesion generally increases after curing time.
Adhesive	A bonding agent that is applied in a liquid or paste form to one or more solid surfaces. It is intended to promote adhesion of the solid surfaces to one another. The adhesive is typically dried, and then the solid surfaces are brought together with heat and/or pressure to active the adhesive. *(This usually is associated with water based, solvent based, or solventless dry lamination.)* Adhesion generally increases after curing time. An adhesive can be abbreviated as "ADH," or "adh."

Multilayer Flexible Packaging, ISBN: 9780815520214
Copyright 2009 Elsevier Inc. All rights of reproduction, in any form, reserved.

In this guide the dash is called out for one symbol and is meant to have a space before and after the dash to make the code more legible. One can also use the En dash to replace the dash with the before and after spaces.

Note: The information contained herein is only a guide. The structures listed herein are a mixture of actual and potential applications, but users should not rely upon it absolutely for specific applications since performance properties will vary with processing and specific end-use conditions. It is given and accepted at user's risk and confirmation of its validity and suitability in particular cases should be obtained independently. We make no guarantees of results and assume no obligation or liability in connection with its advice. This publication is not to be taken as a license to operate under, or recommendation to infringe, any patents (Tables A.1–A.14).

Table A.2 Key Abbreviations

VM	A vacuum metallization process for applying a thin metal layer to a solid surface, such as OPET and OPP films. This can also be applied to paper, printed surfaces, and other materials. (*VM* can also be written, *"met.")* The metal is usually aluminum, but can also be other metals such as copper, gold, tin, etc. (If it is not aluminum, please specify in your communication.)
vm	Vacuum metallized
met.	Metallized
SiO_x	A silicon oxide coating that is typically applied to a film such as OPET. This usually transparent coating is applied in a vacuum deposition process.
O.L.	An overlacquer that is applied over ink to add scratch protection and gloss.
W.O.	White opaque. This is a white pigmented material with higher opacity.

(Continued)

Table A.2 Key Abbreviations (*Continued)*

Tie	Generically indicates a coextrudable adhesive resin. This is used in structure notations when the resin brand or grade is unknown. If the tie material base resin is known then please indicate: for example, LLDPE tie, EVA tie, PP tie, etc. If the brand is known, please indicate, such as DuPont Bynel, or Mitsui Admer. If the grade number is known, please indicate.
MB	A "masterbatch" or concentrate. This could be for pigments such as TiO_2 (white MB) or for slip and antiblock concentrates. For example: white MB, slip MB, etc.

Table A.3 Key Symbols

/	The boundary between a solid interface and a liquid or molten material being applied to it. For example: *OPET/ink/primer/33 μm EMAA* is an oriented polyester film, printed with one or more inks, and dried. A primer is applied to the printed surface, dried, then extrusion coated with 33 μm of an EMAA resin.
()	A set of parentheses. These indicate that the materials within are being coextruded. Look for a short dash " – " sign with spaces or an En dash "–" between materials.
" – "	Indicates the boundary between two molten materials being coextruded together. They should be enclosed in a set of parentheses, "()". Use a space on each side of the dash or En dash. For example: *(1 mil LDPE–2 mil EAA)* is a two-layer coextruded film of low-density polyethylene and EAA.

(Continued)

Table A.3 Key Symbols (*Continued)*

[ ]	A set of straight-sided brackets. These indicate that the materials within are being blended. If known, percentages by *weight ratio* for the materials being blended should be indicated. Look for a plus sign between the materials.
"+"	Indicates two materials being blended together. They should be enclosed in a set of straight-sided brackets, "[ ]." Use a space on each side the plus. For example: *([75% Nylon 6 + 25% Amorphous PA] − tie − LLDPE)* is a blend of Nylon 6 and Amorphous Nylon, in the *weight ratios* indicated, is the outer layer of a three-layer coextrusion. The middle layer is an unknown coextrudable adhesive resin, and the inner layer is an LLDPE.
//	Indicates the boundary between two solid surfaces, one is a film, and the other is a film that is often coated with an adhesive. (Typical for adhesive lamination.) For example: *OPET/adhesive//25 μm ionomer film* an oriented polyester film that has an adhesive applied to it and dried. An ionomer film is then combined, typically with a heated nip roll to activate the adhesive.
"//TL or BL//"	Indicates the boundary between two warm solid layers that are joined together by only heat and pressure. Examples would be: "//TL//" Thermally laminated films. Two films (or one film and one foil), combined typically between rubber rolls, following preheating of one or both films. "//BL//" Blown films that are intentionally blocked in the collapsing nip. A "*B*locked

(Continued)

Table A.3 Key Symbols (*Continued)*

	*L*amination." In addition, surround the structure with braces or curly brackets, "{}," to indicate a combined web. See examples in the following pages.
< or >	Indicates direction to which a surface treatment has been applied, such as; flame, corona, ozone, plasma. For example: *Paper < flame/LDPE/foil/ LDPE.*

Table A.4 Materials (Generic Representations) for Webs/Films/Substrates

OPET or BOPET	Biaxially oriented polyester film. (Occasionally called BOPET.) Using "OPET" will prevent confusion with extruded PET.
VM-OPET	Vacuum-metallized OPET film Metallization on the left
OPET-VM	Vacuum-metallized OPET film Metallization on the right
OPET-SiO*x*	OPET film with silicon oxide on the right side of the film
SiO*x*-OPET	OPET film with silicon oxide on the left side of the film
OPET-PVdC	Oriented polyester film with a PVdC coating on the right
PVdC-OPET	Oriented polyester film with a PVdC coating on the left
PVdC-OPET-PVdC	Oriented polyester film, two side coated with PVdC
OPP or BOPP	Biaxially oriented polypropylene film
VM-OPP	Oriented polypropylene film, with metallization on the left side
OPP-VM	Oriented polypropylene film, with metallization on the right side

(Continued)

Table A.4 Materials (Generic Representations) for Webs/Films/Substrates (*Continued)*

OPP-A	Oriented polypropylene film, with an acrylic coating on the right side
A-OPP	Oriented polypropylene film, with an acrylic coating on the left side
CPP	Cast polypropylene film
VM-CPP	Cast polypropylene film with metallization on the left side
CPP-VM	Cast polypropylene film with metallization on the right side
C-Nylon	Cast nylon film, also written as *Cast PA,* for cast polyamide film
O-Nylon	Uniaxially oriented nylon film
BONy	Biaxially oriented nylon film
BOPA	Biaxially oriented polyamide (nylon) film
K-Nylon	Biaxially oriented nylon film, with PVdC on one side
BONy-PVdC	"K-Nylon," but written to specify PVdC on the right side
Alu	Aluminum (Aluminium), can also be written as "*AL*"
Foil	Usually thin aluminum. Can be other metals, if not aluminum, specify. Examples: tin foil, gold foil. (In Europe the word "foil" is used to indicate any thin film, and can cause communication issues globally.)
Cello	Plain, uncoated cellophane
K-Cello	Two-side PVdC-coated cellophane
NC-Cello	Two-side nitrocellulose-coated cellophane
Paper	Lightweight paper-based webs. Please specify when possible: Kraft, Bleached Kraft, SBS, clay coated, etc.
Board	Heavy weight paper-based webs. Please specify when possible.
Nonwoven	Nonwoven webs. If the brand is unknown, use nonwoven HDPE, nonwoven PP, and nonwoven PET. Use brand name if known; such as DuPont Tyvek, PGI Reemay, PGI Typar.
Woven Fabric	Fabric weaves. For example: "tight weave;" woven PP, woven HDPE, woven PP.
Scrim	Woven mesh type fabrics with an "open weave;" for example: Scrim PP, Scrim PET, Scrim HDPE.

(Continued)

Table A.4 Materials (Generic Representations) for Webs/Films/Substrates (*Continued)*

Table A.5 Thickness or Gauge Representations

#	"pounds per ream" (a ream being 3000 square feet)
Mils	English measurement of 0.001 or 1/1000 of an inch.
Inches	English unit for thick layers, such as in bottles and sheet applications
μm	Metric measurement (micron), 0.001 of a millimeter (it is common in this industry to also just write the "μ" symbol when referring to microns or micrometers, instead of the full "μm.")
mm	Millimeters, metric unit used for thick layers, such as in bottle and sheet applications
gsm	grams per square meter
pt.	"point," which is a unit of thickness for paperboard. (1 pt. approximately = 1 mil)
ga	"gauge" of a film in some systems. e.g. 100 ga = 1 mil = 25.4 μm: 48 ga = 12 μm = 0.5 mils

Table A.6 Adhesives and Primers

PUR	Polyurethane; *PUR adhesive or PUR primer;* can be solvent or water based
PEI	Polyethylene-imine; *PEI primer,* usually a water-based primer
EAA	Ethylene acrylic acid; *EAA primer* (water based)
EAC	Ethylene acrylate; *EAC primer* (water based)
Other primers	(there are several others such as organic titanates, etc.)

Table A.7 Surface Treatments

Corona	Electron discharge excitement of atmospheric air over the film surface.
Plasma	Electron discharge excitement of a gas other than standard air over the film surface. Examples would include: nitrogen, argon, helium, neon, etc. (as well as gas mixtures.)
Flame	Surface treatment with burning gases. The gas mixture could be either an oxidizing flame, reducing flame, or stoichiometric flame.
Ozone	Molten web oxidation by exposing the polymer to a dry ozone flow created off-line and pumped to the molten web area, through a tube with small outlet holes along its length. Occasionally seen on extrusion coating lines.

Table A.8 Extrudable Resins (Generic Names for When Brand/Grade is Unknown)

HMW-HDPE	High Molecular Weight HDPE
HDPE	High-Density polyethylene
MDPE	Medium-density polyethylene
LDPE	Low-density polyethylene
LLDPE	Linear low-density polyethylene

(*Continued*)

Table A.8 Extrudable Resins (Generic Names for When Brand/Grade is Unknown) (*Continued*)

HMW-HDPE	High Molecular Weight HDPE
VLDPE	Very low-density (linear) polyethylene (also- VLLDPE)
ULDPE	Ultra low-density polyethylene (also- ULLDPE)
mPE	Metallocene polyethylene, generic
mLMDPE	Metallocene linear medium-density polyethylene
mLLDPE	Metallocene linear low-density polyethylene
mVLDPE	Metallocene very low (linear) density polyethylene (sometimes referred to as a "plastomer"), such as ExxonMobil Exact, Dow Engage, Dow Affinity, LG Chem Lucene
PP	Polypropylene (generic indication when minimal information is known)
CoPP	Copolymer polypropylene
HoPP	Homopolymer polypropylene
ACR	Acid copolymer resin, generic name for EAA and EMAA resins
EAA	Ethylene acrylic acid copolymer, such as DuPont Nucrel, Dow Primacor, and ExxonMobil Escor
EMAA	Ethylene methacrylic acid copolymer, such as DuPont Nucrel
Ionomer	Ionomer copolymer resins, such as DuPont Surlyn
Acrylate	Acrylate copolymers, such as Arkema Lotryl, DuPont Elvaloy AC, ExxonMobil Optema, Westlake EMAC
EBA	Ethylene butyl acrylate
EEA	Ethylene ethyl acrylate
EMA	Ethylene methyl acrylate
EMMA	Ethylene methyl methacrylate
EiBA	Ethylene /*so*-butyl acrylate

(*Continued*)

Table A.8 Extrudable Resins (Generic Names for When Brand/Grade is Unknown) (*Continued*)

HMW-HDPE	High Molecular Weight HDPE
EnBA	Ethylene normal-butyl acrylate
EVA	Ethylene vinyl acetate; such as DuPont Elvax, Celanese Ateva, LyondellBasell Ultrathene, ExxonMobil Escorene Ultra
PS	Polystyrene
EPS	Expanded (or foamed) polystyrene
HIPS	High impact polystyrene
GPPS	General purpose polystyrene
PVC	Polyvinyl chloride
PVdC	Polyvinylidene chloride. Most commonly seen as a coating on a film, but there are also extrudable grades, such as Dow Saran, and Solvay Ixan
PA	Polyamide, commonly called *Nylon*
Nylon	Polyamide, when unspecified, quite often is *Nylon 6*
Nylon 6	Polymer from caprolactam (also written "PA 6")
Nylon 6.6	Polymer from adipic acid & hexamethylenediamine (also written "PA 6,6" or "PA 6:6" or "PA 66")
Nylon 6/6.6	Copolymer of 6 and 6.6 types of polyamide (also written *"PA 6/6.6"* or *PA 6:66)*
Nylon (other)	other nylon polymers: Nylon 11, Nylon 12, Nylon 6/12, etc...
Amorphous PA	Amorphous nylon; DuPont Selar PA, or EMS Grivory
MXD6	Crystalline nylon; Mitsubishi Nylon-MXD6
EVOH	Ethylene vinyl alcohol; Kuraray Eval, Nippon-Gohsei Soarnol, Arkema/CCPC Evasin
PAN	Polyacrylontrile, sometimes written as "an"
SAN	Styrene acrylonitrile copolymer

(*Continued*)

Table A.8 Extrudable Resins (Generic Names for When Brand/Grade is Unknown) (*Continued*)

HMW-HDPE	High Molecular Weight HDPE
AN-MA	Acrylonitrile methyl acrylate copolymer (such as Ineos Barex, which was being decommissioned end of 2014)
ABS	Acrylonitrile butadiene styrene copolymer
LCP	Liquid crystal polymer
COC	Cyclic olefin copolymer, such as TAP Topas, or Mitsui Apel
PUR	Polyurethane, extrudable type when seen in a coextrusion, for example
SBC	Styrene butadiene copolymer (such as Chevron Philips K-Resin)
PET	Extruded polyester. Could be monolayer or in a coextrusion
PET ext.ctg.	Extrusion coating of polyester
APET	Amorphous polyester
CPET	Crystalline polyester
PETG	Polyester copolymer with glycol
PEN	Polyethylene napthalate
PLA	Polylactic acid
PGA	Polyglycolic acid
PHA	Polyhydroxyalkanote

Table A.9 Terpolymers

EVACO	Terpolymer of ethylene, vinyl acetate, and carbon monoxide, such as DuPont Elvaloy
EnBACO	Terpolymer of ethylene, normal-butyl acrylate, and carbon monoxide, such as DuPont Elvaloy
EiBAMAA	Terpolymer of ethylene, isobutyl acrylate, and methacrylic acid
Other terpolymers	(There are various other terpolymers in the industry based using a variety of monomers...)

Table A.10 Grafted Resins

EVA-gMAh	Ethylene vinyl acetate with a graft of maleic anhydride
LLDPE-gMAh	LLDPE with a graft of maleic anhydride
Other grafted polymers	(There are various other grafted resins in the industry based on HDPE, PP, LDPE, EPR, EPDM, PS, etc.)

Table A.11 Others

Peel Seal or Easy Peel	Generic name for a peelable sealant resin of unknown brand/grade. If brand is known, please indicate, such as DuPont Appeel, Mitsui-DuPont CMPS, Yasuhara Hirodyne, or Toyo Topco
H.S. lacquer	Generic name for a "heat seal lacquer," usually applied by gravure
Hot Melt	Generic name for a hot melt adhesive applied as a sealant

Table A.12 Trademarks

Arkema	Evatane, Lotader, Lotryl, Orevac, Orgalloy, Pebax, Rilsan, and Evasin (in conjunction with Chang Chun Petrochem (Taiwan)
Avintiv	Reemay, Typar
Celanese	Ateva
Chevron Phillips Chemical:	K-Resin, Marlex, MarFlex
Bemis Company, Inc.:	EZ Peel
Dow Chemical:	Affinity, Amplify, Attane, Dowlex, Elite, Engage, Flexomer, Infuse, Nordel, Primacor, Saran, Tuflin, Versify
DuPont-Teijin Films	Mylar, Melinex
E.I. du Pont de Nemours & Co.	Appeel, Booster, Bynel, Conpol, Elvaloy, Elvaloy AC, Elvax, Entira, Fusabond, Hytrel, Nucrel, Selar, Surlyn, Tyvek, Zytel
EMS Group:	Grivory, Grilon
LyondellBasell Chemical	Ultrathene, Petrothene, Plexar, Pro-Fax, Moplen, Adflex, Adstif, Adsyl, Toppyl
Evonik	Vestamid
ExxonMobil Chemical:	Enable, Escor, Escorene, Exact, Exceed, Exxelor, Optema, Vistalon, Vistamaxx
Ineos:	Barex
Kuraray Chemical:	Eval
Mitsui Chemical:	Apel, Admer
Mitsubishi Chemical:	Modic
Mitsui-DuPont Chemical:	CMPS
Nippon Gohsei	Soarnol
Phillips 66	Copylene
Solvay Chemical:	Ixan (resin), Diofan (dispersion)
Topas Advanced Polymers:	Topas
Toyo Chemical:	Topco
Westlake Chemical:	Hifor, Elevate, EMAC, EBAC, Mxsten, Tymax
Yasuhara Chemical:	Hirodyne, Hirotac

(Continued)

Table A.12 Trademarks (*Continued)*

Table A.13 Structure Examples (Structures Should Be Written From "Outside to Inside," With Regards to the Order of Layers, Starting From the Left)

OPET/ink/adhesive//CPP
An adhesive lamination of cast polypropylene film to reverse printed polyester film. An unknown adhesive is applied to the printed polyester film surface.
OPET/primer/CoPP
An extrusion coating of copolymer polypropylene on to an unprinted polyester film. There is an unknown primer applied to the OPET.
48 ga OPET/ink/PEI primer/28# LDPE
A reverse printed 48-gauge OPET film that is primed with a PEI primer, and then extrusion coated with 28 pounds per ream of low density polyethylene.
15 μm BONy/ink/PUR adh//88 μm LDPE
An adhesive lamination of an LDPE film to a reverse printed biaxially oriented nylon film. The PUR adhesive is applied to the reverse printed nylon film.
0.5 mils OPET-PVdC/ink/primer/0.8 mils LDPE/1.5 mils Peel Seal
A 0.5-mils OPET film with PVdC coating is reverse printed on the PVdC side. The printed side is then primed and extrusion coated with 0.8-mils LDPE. A 1.5-mils Easy Peel or Peel Seal extrusion coating resin is applied onto the LDPE. This is done in either tandem or a two-pass extrusion coating.
12 μm OPET/primer/15 μm LDPE/6 μm alu/(11 μm EMAA–25 μm Easy Peel)
A 12-μm OPET film is primed and extrusion laminated with 15 μm of LDPE to 6 μm aluminum foil. The bare aluminum side is then coextrusion coated with a two-layer coating that is 11 μm of EMAA and 25 μm of Easy Peel resin.
OPET/primer/(LDPE–[LDPE + white MB]–LDPE)/foil/EMAA
An OPET film which is primed, and then has foil extrusion laminated to it using a three-layer coextrusion, with the center layer containing a white masterbatch. The foil is then extrusion coated on the other side with EMAA.
20 μm OPP/ink/adhesive//7 μm alu/33 gsm EAA
A 20-μm OPP film that is reverse printed, then adhesively laminated to 7 μm aluminum foil. The adhesive is applied to the printed surface, not the aluminum. The laminate is then extrusion coated with 33 gsm of EAA.
20 μm OPP-PVdC/low temp PUR primer/35 μm EVA
PVdC coated OPP extrusion coated with an 18% EVA. A special low activation temperature PUR primer is used to allow for direct extrusion coating of an EVA at 235°C onto a primed film.
BONy/ink/solventless adh//(LLDPE–LDPE–Ionomer)
A solventless adhesive lamination of a reverse printed biaxially oriented nylon film to a three-layer coextruded film. The adhesive is applied to the printed surface of the nylon film.
(Nylon 6:66–Tie A–Nylon 6–Tie B–Ionomer)
A five-layer coextruded film. You will need to specify if this is made by a cast film or blown film process. In a straight coextrusion, this is helpful to know for physical property issues.
OPP < corona/solvent adhesive//([LLDPE + LDPE]–tie–Nylon 6–tie–LLDPE–LDPE–Ionomer)
An OPP film that is corona treated in-line, then has a solventless adhesive applied to its surface. This film is then combined with a seven-layer coex film, likely with a typical heated pressure nip.

(Continued)

Table A.13 Structure Examples (Structures Should Be Written From "Outside to Inside," With Regards to the Order of Layers, Starting From the Left) (*Continued)*

O.L./ink/40# Paper < flame/0.7 mils LDPE/0.35 mils alu/1.8 mils Ionomer
A surface printed and overlacquered paper is flame treated, and extrusion laminated using LDPE to aluminum. The other side of the aluminum is then extrusion coated with the Ionomer. You will need to specify if this is done in a two-pass operation on a single station extrusion coating line, or one pass on a tandem extrusion coating line.
O.L./ink/Paper/EMAA/alu/[Ionomer + Slip MB]
A surface printed and overlacquered paper that is extrusion laminated to aluminum with EMAA. The other side of the aluminum is then extrusion coated with a blend of Ionomer and masterbatch.
(CoPP − tie A − Nylon 6 − EVOH − Nylon 6 − tie B − Ionomer)
A seven-layer coextruded film. The tie layer resins are not known, but it is known that there are two different grades being used in the one structure. You will need to specify whether it is made by a cast film or blown film process.
(Nylon 6 − tie − Nylon 6 − tie − LLDPE − mPE − Ionomer)
A seven-layer coextruded film. The tie layers are believed to be the same, so are not labeled differently. A mPE is used to adhere the Ionomer to the LDPE. An upgrade would be to specify the mPE grade or density and the Ionomer grade. You will need to specify whether it is made by a cast film or blown film process.
(15 μm Nylon 6 − 5 μm LLDPE tie − 45 μm LLDPE)
A three-layer coextruded film. As each layer thickness is known, they are specified in the structure. While the tie resin grade is not known, it is known to be based on LLDPE. You will need to specify whether it is a cast film or blown film.
(20 μm [Nylon 6 + Amorphous PA] − 4 μm tie − 40 μm LLDPE)
A three-layer coex film. The outer layer blend ratio is unknown. The layer thickness for each layer is specified. You will have to specify if this is made by a blown or cast film process.
([80% Nylon 6 + 20% Amorphous PA] − tie − EVOH − tie − LLDPE)
A five-layer coextruded film. The outer layer is an 80% Nylon 6 plus 20% amorphous nylon blend. You will need to specify if the film is made by a blown or cast process.
OPET/ink/adh//SiOx-OPET/primer/(LDPE − Ionomer)
A reverse printed OPET is adhesively laminated to a silicon oxide coated OPET. The adhesive is applied to the printed surface of the outer OPET. Then the plain side of the silicon oxide coated OPET is primed and coextrusion coated with a two-layer LDPE and Ionomer coating.
OPET/ink/primer/met/adhesive//(Nylon - tie–LLDPE)
A reverse printed OPET is primed on the ink surface, then metallized. This film is then adhesively laminated to a three-layer coex film. The adhesive is applied to the metallized surface.
OPET/ink/adhesive//OPET-VM/(LDPE - Ionomer)
A reverse printed OPET is adhesively laminated to a metallized OPET. The adhesive is applied to the ink surface. The metallized layer is facing to the inside of the package structure, not the outside. The metallized surface is coex-extrusion coated with a two-layer LDPE and Ionomer coating.
OPP/ink/primer/LDPE/primer/VM-CPP
A reverse printed OPP that is extrusion laminated using LDPE to a metallized cast polypropylene film. Primers are applied to the printed OPP, and the metallized CPP.

(Continued)

Table A.13 Structure Examples (Structures Should Be Written From "Outside to Inside," With Regards to the Order of Layers, Starting From the Left) (*Continued)*

OPP/ink/primer/LDPE/VM-OPET//adhesive/CPP
A reverse printed OPP that is extrusion laminated using LDPE to a metallized OPET. This is then adhesively laminated to a cast polypropylene film. The adhesive is applied to the CPP film.
OPET/ink/primer/LDPE/VM-OPET/adhesive//CPP
A reverse printed OPET that is extrusion laminated using LDPE to a metallized OPET. This is then adhesively laminated to a cast polypropylene film. The adhesive is applied to the OPET film.
12 μm OPET/met/adh//15 μm BONy/adhesive//corona > (20 μm LLDPE − 10 μm LDPE − 45 μm EVA)
An OPET that has been metallized, then adhesively laminated to BONy film. The other side of the nylon film is then adhesively laminated to a coex film which has been in-line corona treated (likely re-treated to burn off slip agents in the film).
OPET/ink/primer/LDPE/met-OPET < corona/primer/LDPE/LLDPE film
A reverse printed OPET film that is coated with an unknown primer, and then extrusion laminated to metallized PET film using LDPE. The plain side of the PET film is then corona treated and primed then extrusion laminated to LLDPE film using LDPE.
20 μm OPP/ink/primer/15 μm LDPE/13 μm met-OPET < corona/primer/12 μm LDPE/12 μm EVA
A reverse printed OPP that is extrusion laminated to a metallized PET film. The plain side of the PET film is extrusion coated with LDPE, and the LDPE is extrusion coated with EVA.
(LLDPE − W.O. LLDPE − LDPE) film/EAA/alu/EAA/(LDPE − LLDPE) film
An extrusion lamination with EAA of a three-layer film to one side of the aluminum. The outer film is white, but the pigment is only in the middle layer. The other side of the aluminum has a two-layer film extrusion laminated to it with an EAA.
50 μm Blue EAA//TL//alu//TL//50 μm EAA
A thermal lamination of blue pigmented EAA film to aluminum on one side. Another film of clear EAA is thermally laminated to the other side of the alu. (A cable shielding type structure.)
Green EAA/200 μm alu/EAA
An extrusion coating of green pigmented EAA is applied to one side of the 200 μm aluminum. A clear EAA is extrusion coated to the other side of the aluminum. (A cable shielding type structure.)
(LDPE − EAA)//TL//150 μm alu//TL//(EAA − LDPE)
150 μm aluminum that has coex films thermally laminated to each side. (A cable shielding type structure.)
{ (mLLDPE − LDPE − tie − Nylon − EVOH − Nylon − EVA tie)//BL//(EVA tie − Nylon − EVOH − Nylon − tie − LDPE − mLLDPE) }
A 13-layer structure that is made by intentionally blocking a coex blown film in the main collapsing nip. The film from the die is actually seven layers. In the main nip, the bubble is blocked on purpose. The nip rolls may be heated to help this. The tower height is usually very short so that the film is still quite warm entering the nips. The tie resin at the blocking interface is known to be an EVA based tie resin, but the exact grade is not known.
Cello/ink/primer/LDPE/alu/EMAA
Cellophane that is reverse printed, primed, and extrusion laminated to aluminum with LDPE. The other side of the aluminum is then extrusion coated with EMAA.
K-Cello/ink/primer/LDPE/alu/Ionomer

(Continued)

Table A.13 Structure Examples (Structures Should Be Written From "Outside to Inside," With Regards to the Order of Layers, Starting From the Left) (*Continued)*

A PVdC coated cellophane (two side coated), that is reverse printed, primed, and extrusion laminated to aluminum with LDPE. The other side of the aluminum is then extrusion coated with an ionomer.
O.L./Ink/50 gsm Paper/LDPE/7 μm Alu/35 μm EAA (made on a tandem extrusion line)
Paper that is surface printed and overlacquered. It is extrusion laminated with LDPE to aluminum. The other side of the aluminum is extrusion coated with EAA. This is specified as being processed by tandem extrusion lamination instead of two-pass coating.
LDPE/ink/18 pt. Board/LDPE/alu/(EAA- LDPE)
A surface printed 18 Point Paperboard that is surface extrusion coated with LDPE, and then extrusion laminated with LDPE to aluminum. The other side of the aluminum is then coextrusion coated with a combination of LDPE and EAA.
(850 μm HDPE − 55 μm HDPE tie − 55 μm Nylon 6)
A three-layer coextrusion, which by looking at the thickness, likely is a coex blow molded bottle. This layer thickness is often used for barrier bottles, such as for agricultural chemicals, where nylon is often used as the inner layer. Please indicate the application when drafting out structures such as this to prevent confusion, as this could also be a sheeting application.
(725 μmHDPE − 12 μm regrind − 55 μm HDPE tie − 55 μm Nylon 6)
Similar to above structure for an agchem bottle, except with a layer of regrind material between the outer HDPE and the tie layer.
(225 μm PP − PP tie − 35 μm EVOH − PP tie − 175 μm PP)
A coextrusion that by the thickness is likely a sheet material. The structure may seem to indicate that it might be used to thermoform into a cup or tray. A description of the actual application for the structure should be included in any communication.
OPET/primer/LDPE/sealant//TL//leather
An oriented polyester film that is primed and extrusion coated with LDPE and then the sealant resin. This structure is then thermally laminated to leather. (The application may be for an emblem or other fabric decoration that requires surface protection.)
Ink/30 μm alu < flame/(EMAA − Easy Peel)
A surface printed aluminum foil that is in-line flame treated, and then coextrusion coated with a two-layer coextrusion. The EMAA would be for high foil adhesion. The "easy peel" is a sealant to various cup stock materials.

Table A.14 Sample Structures for Practice Descriptions

K-Nylon,corona/adhesive//(mLLDPE − 12% EVA − peel seal resin)
BONy-PVdC/adhesive//(mLLDPE − mLLDPE − EMAA)
BONy-PVdC/primer/(LDPE − LDPE − EMAA)
OPET/ink/adh/alu/adhesive//(LLDPE − LLDPE − EMAA)
PET-VM/adhesive//BONy/adhesive//corona. (LLDPE − LDPE − EVA)
OPP/ink/adh//met-OPET/primer/(LDPE − Ionomer)
OPET-PVdC/ink/adhesive/(LDPE − EMAA − Ionomer)
OPP/ink,corona/(tie resin-[LDPE + adhesion modifier].corona/met-OPET,corona/primer/LDPE

Appendix B: Examples of Flexible Packaging Film Structures

This appendix is adapted from sections of Butler, T. I. and Morris, B. A., 2016, "PE-based multilayer film structures," in Wagner, J. (ed.), *Multilayer flexible packaging*, 2nd ed., Elsevier, Oxford, pp. 281−310.

Packages may be formed in-line by several techniques or may be supplied to the packer as preformed pouches or bags. Packaging may also be created by wrapping or shrinking a basic film around a bundle of goods. In-line package-forming examples include vertical form-fill-seal (VFFS), horizontal form-fill-seal (HFFS), and thermoform-fill-seal (Chapter 3). In VFFS operations, film from a roll is guided through rollers and then shaped by a forming collar into a tube. The film moves in a vertical direction (down) over a filling tube. A vertical seal is made, forming the film into a continuous tube. As the film continues through the machine, a horizontal seal is made, perpendicular to the film machine direction, forming the bottom end-seal of the bag being formed and the top seal of the previously filled bag. The product is dropped into the partially formed bag, advanced to the seal bars and the next bottom and top end-seal is made. The process may operate in a stepwise or continuous manner. One example of a product normally packaged on VFFS equipment is fresh-cut produce. In HFFS operations, the film moves in a horizontal direction during the packaging step. One application that typically uses HFFS equipment is chunk cheese. In thermoform-fill-seal operations, a bottom web is formed, product is added and the top web, which is normally flat, is sealed to the bottom web. Thermoform-fill-seal packaging is frequently used for bacon and processed meats. Stand-up pouches and other types of packaging may be formed in-line with the filling equipment, or may be fully or partially prefabricated prior to the filling step.

Markets for flexible packaging films have continued to grow in many applications. Polyethylene and the various copolymers account for more than 75% of the flexible packaging film. Some major market segments where coextruded film is used include the following:

- medical packaging
- food packaging
- heavy duty shipping bags
- stretch wrap
- trash bags
- condiment sachets (ketchup, salad dressing, and so on)
- aseptic juice packaging
- towelettes
- condoms
- laminates for toothpaste tubes—PE (polyethylene) film/(LDPE (low density polyethylene)−EAA (ethylene acrylic acid)/Al/(EAA/LDPE)/PE film
- stand-up pouches—OPET (oriented polyester)/print/adh/m-OPP (oriented polypropylene)/adh/(LLDPE (linear low density polyethylene)−HDPE (high density polyethylene)−LLDPE) and variations.

The sections that follow provide some of the package requirements and past structures used to meet these requirements. They are drawn primarily from North America. By no means are the structures provided exhaustive in what has or could be used for the application. Nor are they meant to predict what structures may be best for the future. They are merely provided as a reference and thought starter. As described throughout this book, there are often many ways to construct a flexible package structure to meet the needs of the application. Overall economics is typically the driving force for selecting one polymer or structure over another. This, however, depends on the

capabilities and assets of the provider, as well as the desires of the packager. Factors such as sustainability may drive different material and structural choices in the future.

B.1 Medical Packaging

A wide variety of structures are used in the medical packaging area (Table B.1). The structure requirements include the following:

- sterilization capability
- microbial barrier
- linear tear properties
- puncture resistance.

Sterilization methods used for medical device packaging include ethylene oxide gas and radiation. The package is typically a forming web and a nonwoven fabric (like Tyvek), which lets the ethylene oxide in and out of the package. Medical device packaging usually does not require oxygen barrier properties so ethylene vinyl alcohol (EVOH) is normally not required. Blown film, cast film, and extrusion coating processes are used to produce structures for medical packaging applications. Coextrusion processes are growing in this market. Films ranging from 3 to 11 layers are now available. These markets often require many years to meet the required qualifications.

The forming webs were historically three-layer ethylene vinyl acetate (EVA) and ionomer films, which are still in use today. Heavy gauge films were sometimes produced by combining a three-layer film to form six layers. Newer film structures have seen more layers being used and incorporating polyamide (PA) for forming and puncture resistance.

Table B.1 Medical Device Packaging Structures

3-Layer Structure	**Layers (%)**	**Gauge (μm)**
(EVA–ION–EVA)	(20/60/20)	50–400
(ION–EAA–EVA)	(30/30/40)	50–400
Paper/LDPE/Al	Lamination	
5-Layer Structure		
(LLDPE–tie–PA–tie–LLDPE)	(40/5/10/5/40)	50–400
(mLLDPE–tie–PA–tie–mLLDPE)	(40/5/10/5/40)	50–400
(LLDPE–tie–PA–tie–PA)	(70/5/10/5/10)	50–400
LDPE/paper/LDPE/foil/LDPE	Lamination	
OPET/adh/(LDPE–EVA–ION)	Lamination	
7-Layer Structure		
(LLDPE–tie–PA–EVOH–PA–tie–LLDPE)	(30/5/10/10/10/5/30)	50–400
9-Layer Structure		
(PE–tie–PA–tie–PE–tie–PA–tie–PE)	(20/5/10/5/20/5/10/5/20)	50–400
(LLDPE–LDPE–tie–PA–EVOH–PA–tie–LDPE–LLDPE)	(10/15/10/10/10//10/10/15/10)	50–400

EVA, *ethylene vinyl acetate;* EVOH, *ethylene vinyl alcohol;* LLDPE, *linear low density polyethylene;* LDPE, *low density polyethylene;* PA, *polyamide;* OPET, *oriented polyester.*

Consumer and industrial heath-care products using flexible packaging include the following:

- medical disposables
- surgical instruments
- syringes and hypodermic needles
- sutures
- pharmaceutical
- condoms and towelettes.

Lidding stock is normally produced by extrusion coating and/or lamination processes and combines paper, polymers, and foil to form multilayer structures. Sachets for condom and towelette packaging typically use the structure OPET/print/LDPE/Al/ION and variations, with ionomers used as the sealant for its chemical and flex crack resistance.

B.2 Food Packaging

B.2.1 Primal Meat Packaging (Shrink)

Packaging primal and subprimal meat requires a package that:

- provides high shrinkage to fully collapse around irregular shapes;
- has excellent optical properties;
- shrinks at low temperature to prevent product damage;
- imparts good softness and elasticity;
- provides excellent oxygen, moisture, odor, and grease barrier protection;
- prevents freezer burn;
- facilitates using individual cuts by food preparers;
- helps reduce purge loss;
- extends shelf life;
- offers easy disposal;
- has good machinability; and
- has an oxygen transmission rate (OTR) less than 15 cc/m^2-day-atm (nonfrozen only).

Shrinkable polyvinylidene chloride (PVDC) barrier films with the sealant layer designed to provide toughness and puncture resistance are often used. These films must be oriented to provide acceptable shrink properties using a double bubble process. PA and EVOH have replaced PVDC in some applications. Table B.2 shows some typical film structures used in shrink film for primal and subprimal meat packaging.

B.2.2 Processed Meat Packaging

Processed and cook-in meats such as luncheon meat, ham, bologna and salami are packaged in barrier films that are designed to keep oxygen from entering the package. This extends shelf-life and gives the retailer longer product display times. It also allows the consumer to keep the product in their refrigerator, unopened, for some time after purchase. These packages are often printed with eye-catching

Table B.2 Primal and Subprimal Meat Packaging

5-Layer Structure	Layers (%)	Gauge (μm)
(ULDPE–EVA–PVDC–EVA–ULDPE)	(40/5/10/5/40)	50–120
(mLLDPE–EVA–PVDC–EVA–mLLDPE)	(40/5/10/5/40)	50–120
(PA–EVOH–tie–LLDPE–mLLDPE)	(30/40/10/10/10)	50–120
(PA–EVOH–tie–LLDPE–ION)	(30/40/10/10/10)	200–300
OPA/PVDC/(LLDPE–EVA–ION)	(20/30/35/5/10)	50–100

Note:/PVDC/is an adhesive lamination with PVDC. See appendix for convention used.
EVA, *ethylene vinyl acetate;* EVOH, *ethylene vinyl alcohol;* LLDPE, *linear low density polyethylene;* OPA, *oriented polyamide;* PA, *polyamide;* PVDC, *polyvinylidene chloride;* ULDPE, *ultralow density polyethylene.*

graphics to increase sales. These films may contain the following:

- a barrier polymer;
- printing surface, such as PET or PA, that also provides thermal resistance during sealing and helps provide abuse resistance during distribution;
- LLDPE or VLDPE (very low density polyethylene) toughness layers;
- a sealant layer that is typically an EVA, LLDPE, polyolefin plastomer (POP or mPE), or ionomer.

The processed meat package comprises a forming film and a backing film. The forming film is thermoformed to the meat product shape. In addition, low oxygen permeability, abuse resistance, and seal integrity are critical to maintaining the proper atmosphere inside the package. Optical properties, such as high gloss and high clarity, are important on the backing film where reverse-printed PET is used to create consumer appeal. Barrier requirements for processed meats range from 3 to 15 cc/m^2-day-atm for OTR and 3−8 g/m^2-day for water vapor transmission rates (WVTR). Table B.3 shows some typical film structures used in processed meat packaging.

B.2.3 Poultry/Fish Packaging

Moisture barrier properties are critical for poultry and fish packaging. The package form is normally vacuum packaging with a good sealant polymer such as EVA, ionomer, or LLDPE (Table B.4).

B.2.4 Cereal Box Liners

Cereal box liners also require good moisture barrier properties to provide good taste and freshness protection. HDPE polymers are typically used to provide moisture barrier. Sealant polymers such as EVA, ionomer, mPE, or blends are used for low temperature seals, form-fill-seal packaging, and easy opening seals. Certain products have additional requirements, such as puncture resistance to keep the product from poking through the packaging film and flavor and aroma barrier for highly flavored cereals. Heat seal initiation temperatures of 90°C and below are commonly required. Moisture vapor transmission rates less than or equal to 15 g/m^2-day-atm are often required. Packages requiring aroma or taste barrier properties will contain either PA or EVOH polymers (Table B.5).

B.2.5 Snack Food Packaging

Potato chips are often packaged in structures that contain metallized films (Table B.6). Polymer film metallization provides oxygen barrier, moisture barrier, and light barrier. The light barrier is to protect the potato chips from ultraviolet radiation that initializes an oxidation mechanism. Seal strength must be optimized to provide a secure package that can be easily opened by the consumer. Seal integrity and consumer appeal are also critical.

B.2.6 Salty Snack Packaging

Salty snacks are frequently high in fat content and may require a package that provides an oxygen barrier in order to prevent the fat in the food from going rancid. They may also require grease resistance to keep the package from leaving an oily spot. Salty snacks may be packaged in barrier films containing foil, a metallized polymer film, or a barrier polymer such as EVOH or PVDC and are gas flushed with nitrogen to maintain a low oxygen concentration inside the package (Table B.7).

B.2.7 Bakery

Moisture barrier is normally the critical property in bakery applications. Polymers used for moisture barrier include LDPE, LLDPE, HDPE, or PP. Typically EVA polymers are used for sealability and optics. Applications such as cake mix pouches require aroma, taste, and moisture barrier properties. PA is used for taste and aroma barrier. In bread bags, the toughness of LLDPE allows down gauging, while LDPE provides good optics and printability (Table B.8).

B.2.8 Cheese Packaging

Most cheese sold in the United States is prepackaged in flexible packaging. The cheese packaging includes the following:

- individually wrapped slices of processed cheese
- chunk cheese
- shredded cheese.

Table B.3 Processed Meat Packaging Film Structures

Product Structure	Layers (%)	Gauge (μm)
Ground Beef		
(PA–tie–LLDPE)	(20/5/75)	150–200
(PA–EVOH–tie–LLDPE)	(10/10/5/75)	150–200
(LLDPE–tie–PA–EVOH–PA–tie–LLDPE)	(25/10/10/10/10/10/25)	40–150
Barrier Overwrap		
(PA–EVOH–tie–LLDPE–mLLDPE)	(10/10/10/40/30)	150–200
(PA–EVOH–tie–LDPE–LDPE–mLLDPE)	(15/10/15/10/15/20)	150–200
Chub Films		
PA//PVDC/LLDPE	(20/5/75)	150–200
Food Service Portion: Steaks/Chops/Roasts		
Forming Web		
(PA–EVOH–tie–LLDPE)	(15/5/5/75)	150–200
(PA–EVOH–tie–ION)	(15/5/5/75)	150–200
(PA–tie–LLDPE)	(20/5/75)	150–200
(PA–ION)	(20/80)	150–200
PA//PVDC/(EVA–ION)	(25/5/10/60)	150–200
(LLDPE–tie–PA–EVOH–PA–tie–LLDPE)	(25/10/10/10/10/10/25)	150–200
Nonforming Web		
(PA–EVOH–tie–LLDPE)	(10/10/10/70)	50–80
(PA–EVOH–tie–ION)	(10/10/10/70)	50–80
OPET//PVDC//LLDPE	(10/5/85)	50–80
OPET//PVDC//ION	(10/5/85)	50–80
(PA–tie–ION)	(10/10/80)	50–80
(LLDPE–tie–PA–EVOH–PA–tie–LLDPE)	(25/10/10/10/10/10/25)	50–80
Skin Packaging Forming Web		
(EVA–tie–EVOH–tie–ION)	(35/10/10//10/35)	150–250
Skin Packaging Nonforming Web		
(EVA–tie–EVOH–tie–ION)	(35/10/10//10/35)	50–80
Luncheon Meat		
Forming Web		
(PA–EVOH–tie–LLDPE)	(15/5/5/75)	150–200
(PA–EVOH–tie–ION)	(15/5/5/75)	150–200
(PA–EVOH–tie–mLLDPE)	(15/5/5/75)	150–200
(LLDPE–tie–PA–EVOH–PA–tie–LLDPE)	(25/10/10/10/10/10/25)	150–200

(*Continued*)

Table B.3 Processed Meat Packaging Film Structures (*Continued*)

Product Structure	Layers (%)	Gauge (μm)
Nonforming Web		
OPET//PVDC//(EVA–LLDPE)	(25/5/10/60)	50–100
OPET//adh//(EVOH–tie–mLLDPE)	(25/2/5/10/60)	50–100
OPET//adh//(EVOH–tie–ION)	(25/2/5/10/60)	50–100
(PA–EVOH–tie–LLDPE)	(25/10/5/25)	50–100
OPA//PVDC//LLDPE	(65/5/25)	50–100
(PA–EVOH–PA–tie–LLDPE)	(10/10/10/10/60)	50–100
(LLDPE–tie–PA–EVOH–PA–tie–LLDPE)	(25/10/10/10/10/10/25)	50–100
Frankfurters		
Forming Web		
PA–EVOH–tie–LLDPE)	(15/5/5/75)	150–200
(PA–EVOH–tie–mLLDPE)	(15/5/5/75)	150–200
(PA–EVOH–tie–EVA)	(15/5/5/75)	150–200
(PA–EVOH–tie–ION)	(15/5/5/75)	150–200
(LLDPE–tie–PA–EVOH–PA–tie–LLDPE)	(25/10/10/10/10/10/25)	150–200
(PA–tie–PA–EVOH–PA–tie–ION)	(15/20/10/5/10/25/15)	150–200
(PA–tie–PA–EVOH–PA–tie–LLDPE)	(15/15/10/5/10/25/20)	150–200
(PP–tie–PA–EVOH–PA–tie–ION)	(15/20/10/5/10/25/15)	150–200
Nonforming Web		
OPA//PVDC/(EVA–LLDE)	(10/5/25/60)	50–100
OPET//adh/(EVOH–tie–mLLDPE)	(15/10/15/60)	50–100
OPET//PVDC//ION or EVA	(10/5/85)	50–100
(LLDPE–tie–PA–EVOH–PA–tie–LLDPE)	(25/10/10/10/10/10/25)	50–100
OPET//adh//(LLDPE–ION)	(25/2/48/25)	50–100
OPET//adh//(LLDPE–tie–EVOH–tie–ION)	(15/2/38/10/10/10/15)	50–100
Sausage		
Forming Web		
(LLDPE–LDPE–tie–EVOH–PA–tie–EVA)	(30/5/10/10/10/5/30)	150–200
(PA–EVOH–tie–mLLDPE)	(75/5/5/15)	150–200
(PA–EVOH–tie–ION)	(15/5/5/75)	150–200
(LLDPE–tie–PA–EVOH–PA–tie–LLDPE)	(25/10/10/10/10/10/25)	150–200
(PA–tie–PA–EVOH–PA–tie–ION)	(15/25/10/5/10/20/15)	150–200
(PA–tie–PA–EVOH–PA–tie–LLDPE)	(15/25/10/5/10/15/20)	150–200
(PP–tie–PA–EVOH–PA–tie–ION)	(15/25/10/5/10/25/15)	150–200

Table B.3 Processed Meat Packaging Film Structures (*Continued*)

Product Structure	Layers (%)	Gauge (μm)
(OPET//adh//(EVOH–tie–LLDPE)	(15/2/14/10/14/60	50–100
(PA–EVOH–tie–mLLDPE)	(15/10/15/60)	50–100
(LLDPE–tie–PA–EVOH–PA–tie–LLDPE)	(25/10/10/10/10/10/25)	50–100
Shrink Bags		
(EVA–PVDC–EVA)	(48/5/47)	50–80
(EVA–tie–EVOH–tie–EVA)	(38/10/5/10/37)	50–80
(LLDPE–tie–PA–EVOH–PA–tie–LLDPE)	(25/10/10/10/10/10/25)	50–80
Ham		
Forming Web		
(PA–EVOH–tie–LLDPE)	(15/10/15/60)	150–200
(PA–EVOH–tie–ION)	(15/10/15/60)	150–200
(LLDPE–tie–PA–EVOH–PA–tie–LLDPE)	(25/10/10/10/10/10/25)	50–100
Nonforming Web		
PA//PVDC//LLDPE	(25/5/70)	50–80
PA//PVDC/ION	(35/5/70)	50–80
OPET//PVDC//LLDPE	(25/5/70)	50–80
OPET//PVDC//ION	(25/5/70)	50–80
(LLDPE–tie–PA–EVOH–PA–tie–LLDPE)	(25/10/10/10/10/10/25)	50–100
Shrink Bags		
(EVA–PVDC–EVA)	(48/5/47)	50–80
(EVA–tie–EVOH–tie–EVA)	(38/10/5/10/37)	50–80
(mLLDPE–tie–EVOH–tie–mLLDPE)	(30/10/10/10/30)	50–80
Bacon		
(PA–EVOH–tie–ION)	(30/10/10/50)	50–100
PA/primer/(PE–ION)	(15/50/35)	50–100
(PA–tie–PA–EVOH–PA–tie–ION)	(15/20/10/5/10/20/20)	50–100
Deli Meats		
Shrink Bags		
(EVA–PVDC–EVA)	(48/5/47)	50–80
(EVA–tie–EVOH–tie–EVA)	(38/10/5/10/37)	50–80
(mLLDPE–tie–EVOH–tie–mLLDPE)	(30/10/10/10/30)	50–80
Forming Web		
(PA–EVOH–tie–LLDPE)	(10/5/5/80)	200–250
(PA–EVOH–tie–ION)	(10/5/5/80)	200–250
(LLDPE–tie–PA–EVOH–PA–tie–LLDPE)	(25/10/10/10/10/10/25)	50–100

(*Continued*)

Table B.3 Processed Meat Packaging Film Structures (*Continued*)

Product Structure	Layers (%)	Gauge (μm)
Nonforming Web		
LLDPE/adh/(PA–EVOH–tie–EVA)	(40//10/10/20/30)	50–80
(PA–EVOH–tie–ION)	(15/10/15/60)	50–80
(LLDPE–tie–PA–EVOH–PA–tie–LLDPE)	(25/10/10/10/10/10/25)	50–100
Casings		
OPA//LLDPE	(30//70)	50–80
LLDPE//OPA//PVDC	(70//20//10)	50–80

EVA, *ethylene vinyl acetate;* EVOH, *ethylene vinyl alcohol;* LDPE, *low density polyethylene;* LLDPE, *linear low density polyethylene;* OPA, *oriented polyamide;* OPET, *oriented polyester;* PA, *polyamide;* PP, *polypropylene;* PVDC, *polyvinylidene chloride.*

Table B.4 Poultry/Fish Packaging

7-Layer Structure	Layers (%)	Gauge (μm)
(LLDPE–tie–PA–EVOH–PA–tie–LLDPE)	(25/10/10/10/10/10/25)	40–150
(LLDPE–tie–PA–EVOH–PA–tie–ION)	(25/10/10/10/10/10/25)	40–150

EVOH, *ethylene vinyl alcohol;* LLDPE, *linear low density polyethylene;* PA, *polyamide.*

Table B.5 Cereal Packaging

Market Structure	Layers (%)	Gauge (μm)
Bag-in-Box		
(HDPE–HDPE–EVA + PB)	(45/45/10)	40–60
(HDPE–HDPE–ION)	(45/45/10)	40–60
Bag-in-Box (Peelable Seal)		
(HDPE–HDPE–EVA + ION)	(45/45/10)	40–60
Bag-in-Box (Barrier Bag)		
(HDPE–tie–EVOH–tie–EVA + PB)	(60/10/10/10)	40–60
(HDPE–tie–PA–tie–EVA + PB)	(60/10/10/10)	40–60

EVA, *ethylene vinyl acetate;* EVOH, *ethylene vinyl alcohol;* HDPE, *high density polyethylene.*

Both chunk cheese and shredded cheese require substantial oxygen barrier to prevent mold growth and spoilage. EVOH, PVDC, or PVOH (polyvinyl alcohol) may provide the oxygen barrier. While EVOH is generally coextruded into the film structure, PVDC or PVOH may be coated onto a film via a coating process. Cheese packaging also requires excellent seal integrity and abuse resistance to prevent the controlled atmosphere inside the package from being lost. Cheese packages are often laminations made with reverse printed outer webs containing PET or PA for superior graphical presentation. The sealant layer may be extrusion coated onto the outer layer or adhesively laminated. Sealant layers

Table B.6 Snack Food Packaging Films

Structure	Layers (%)	Gauge(μm)
Potato Chips (OTR 2.0, MVTR 0.02)		
OPP//met-OPP	(50/50)	20–60
OPP//LDPE// met-OPP	(25/50/25)	20–60
OPP-met// (HDPE-EVA)	(15/70/15)	40–80
Tortilla and Corn Chips (OTR <2.0, MVTR <0.35)		
OPP//LDPE//OPP	(25/50/25)	20–60
OPP//PVDC//OPP	(50/5/45)	20–60
Pretzels (OTR <2.0, MVTR <0.5)		
OPP//LDPE// OPET	(25/50/25)	30–80
OPP//LDPE//OPP	(25/50/25)	30–80
OPP//PVDC/OPP	(45/5/50)	30–60
Meat Snacks		
OPET//PVDC// LDPE	(50/5/45)	30–60
(PA–tie–EVOH–tie–LLDPE)	(10/10/10/10/60)	40–80

EVA, *ethylene vinyl acetate;* EVOH, *ethylene vinyl alcohol;* HDPE, *high density polyethylene;* LDPE, *low density polyethylene;* LLDPE, *linear low density polyethylene;* MVTR, *moisture vapor transmission rate;* OPET, *oriented polyester;* OPP, *oriented polypropylene;* OTR, *oxygen transmission rate;* PVDC, *polyvinylidene chloride.*

Table B.7 Snack Nuts Packaging

Structure	Layers (%)	Gauge (μm)
OPP//LDPE//OPP	(20/60/20)	40–60
OPP//LDPE//foil// LDPE	(10/20/5/65)	40–60

LDPE, *low density polyethylene;* OPP, *oriented polypropylene.*

may consist of EVA, ionomer, or mPE. Low heat seal initiation temperature (90°C or below) and good seal through contamination performance are required. Processed cheese typically requires films with OTR of 9–15 cc/m^2-day-atm and WVTR of 15 g/m^2-day (Table B.9).

Table B.8 Bakery Packaging

Structure	Layers (%)	Gauge (μm)
cPP/PP/cPP	(10/80/10)	30–60
PP/EVA	(80/20)	30–60
(HDPE–EAA–PA–EAA)	(70/10/10/10)	30–70
(LLDPE–PP–LLDPE)	(10/80/10)	30–60
(PA–EVOH–PA–tie–LLDPE)	(20/10/20/10/30)	100–160

EAA, *ethylene acrylic acid;* EVOH, *ethylene vinyl alcohol;* HDPE, *high density polypropylene;* LLDPE, *linear low density polyethylene;* PA, *polyamide;* PP, *polypropylene.*

An acrylic, PVOH-coated OPP film is also used in cheese packaging in both extrusion and adhesive laminations. Acrylic is coated on one side and PVOH on the other side.

B.2.9 Milk Pouches

LLDPE or LDPE/LLDPE blends provide the sealant in both milk powder and liquid pouches (Table B.10). If oxygen barrier is required for long shelf-life, then PA or EVOH layers are included.

B.2.10 Frozen Food

Frozen foods are packaged in a variety of packaging types. Examples of frozen foods packaged in flexible packaging include the following:

- Frozen fruits
- Vegetables
- French fries
- Individually packed quick frozen chicken breasts.

Many frozen foods are packaged in surface-printed polyethylene films. In recent years in the United States, reverse-printed laminations, which may be shaped into stand-up pouches, have grown in use in the frozen food supermarket aisle. These packages have attractive graphics and may incorporate

Table B.9 Cheese Packaging

Structure	Layers (%)	Gauge (μm)
Natural Chunk Cheese Pouches		
OPET/adh/(EVOH–tie–LLDPE)	(15/5/10/10/55)	40–60
LLDPE//PVDC//OPP//OPP//PVDC//LLDPE	(15/10/75)	50–60
OPET//PVDC//LLDPE	(15/10/75)	45–50
EVA//PVDC	(95/5)	50–60
OPA//PVDC//LLDPE	(15/10/75)	45–50
Vacuum Bags for Aging		
OPA//PVDC//EVA	(110/5/85)	40–100
(PA–tie–LLDPE)	(10/10/80)	40–100
(PA–tie–EVA)	(10/10/80)	40–100
Shredded Cheese		
PVDC//PA//LDPE	(5/20/75)	80–100
PVDC//PET//LDPE	(5/20/75)	80–100
(PA–EVOH–tie–LDPE)	(10/10/10/PA)	80–100
Processed Cheese Slices		
OPP//EVA	(50/50)	20
PP/EVA	(20/80)	35–40

EVA, *ethylene vinyl acetate;* EVOH, *ethylene vinyl alcohol;* LDPE, *low density polyethylene;* LLDPE, *linear low density polyethylene;* OPET, *oriented polyester;* OPP, *oriented polypropylene;* PA, *polyamide;* PVDC, *polyvinylidene chloride.*

Table B.10 Milk Packaging

Structure	Layers (%)	Gauge (μm)
(LLDPE–tie–PA–tie–LLDPE)	(35/10/10/10/35)	40–70
HDPE/(LDPE + LLDPE)	(40/60)	40–80

HDPE, *high density polyethylene;* LDPE, *low density polyethylene;* LLDPE, *linear low density polyethylene;* PA, *polyamide.*

convenience features such as self-venting for microwave cooking.

Key requirements for frozen food packaging are the following:

- low temperature toughness
- modulus
- high hot tack strength
- high seal strength.

Some packages are clear and require good clarity, while others are pigmented and require good gloss. LLDPE, ULDPE, EVA, and mPE resins are all commonly used in creating frozen food packaging. Stiffness must be adequate for high speed packaging and packaging films must have tear and puncture strength high enough to prevent package damage during transportation and storage (Table B.11).

B.2.11 Fresh-Cut Produce

Key performance requirements for fresh-cut produce packaging include proper oxygen and carbon dioxide permeability, seal integrity, machinability, and consumer appeal. Consumer appeal includes both feel and appearance. Feel is generally determined by film thickness and modulus while appearance is governed by print quality and film optical properties, such as clarity, haze, and gloss. In order to extend the shelf life of the produce being packaged, films must provide the proper oxygen permeability that is matched to the packed produce respiration rate. Cut produce respires after

Table B.11 Frozen Food Packaging

Structure	Layers (%)	Gauge (μm)
(EVA–LLDPE–EVA)	(15/70/15)	40–80
PET//tie//(LDPE–ION)	(15/5/40/40)	40–80
(mLLDPE–LLDPE–mLLDPE)	(15/70/15)	40–80
(HDPE–MDPE–EVA)	(15/70/15)	40–80

EVA, *ethylene vinyl acetate;* HDPE, *high density polyethylene;* LDPE, *low density polyethylene;* LLDPE, *linear low density polyethylene;* MDPE, *medium density polyethylene.*

harvesting, consuming oxygen, and giving off carbon dioxide. By controlling the permeation of gases through the package, the environment inside the package is controlled, respiration is slowed, and shelf life is extended. The bags must have complete seal integrity in order to prevent the unplanned transfer of gases between the bags and the environment. Bags may contain PP, LLDPE, ULDPE, EVA, or mPE. OTR requirements vary widely depending on the produce being packaged, but common items range from about 1500 cc/m^2-day-atm for Caesar salad mixes to 2300–3000 cc/m^2-day-atm for iceberg salad mixes and 3000–5500 cc/100in^2-day-atm for specialty salad mixes such as baby greens and exotic lettuces. Perforation may be used to obtain high transmission rates for some applications.

B.2.12 Retortable Pouches

A growing flexible packaging use is in the replacement of metal cans with retortable pouches. These pouches are typically laminations containing biaxially oriented PA for toughness, aluminum foil for oxygen barrier and a polypropylene sealant film. These pouches may contain items like tuna, pet food and soup. The food items are held at elevated temperature after packaging, so the packages must remain intact at elevated temperatures. In addition to temperature resistance, toughness, seal strength and barrier properties are critically important.

B.2.13 Edible Oil Packaging

The packaging of cooking oil uses PA to provide oxygen barrier properties. EAA is typically used as the sealant layer. The seal type determines the PA layer location (Table B.12).

Table B.12 Edible Oil Packaging

Structure	Layers (%)	Gauge (μm)
(PA–tie–EAA)	(10/15/75)	50–150
(EAA–tie–PA–tie–EAA)	(35/10/10/10/35)	50–150
(EAA–PA–EAA)	(40/20/40)	50–150

EAA, *ethylene vinyl acetate;* PA, *polyamide.*

Table B.13 Bag-in-Box Packaging Structures

Structure	Layers (%)	Gauge (μm)
(LLDPE–tie–PA–tie–LLDPE)	(35/10/10/10/35)	40–80
(EVA–tie–PA–tie–EVA)	(35/10/10/10/35)	40–80
(LLDPE–tie–EVOH–tie–LLDPE)	(35/10/10/10/35)	40–80

EVA, *ethylene vinyl acetate;* EVOH, *ethylene vinyl alcohol;* LLDPE, *linear low density polyethylene;* PA, *polyamide.*

B.2.14 Bag-in-Box

Coextruded films containing oxygen barrier polymers are replacing some metallized film laminates where flex crack resistance is required. LLDPE or EVA polymers are used as sealants (Table B.13).

B.3 Industrial/Consumer Films

B.3.1 Stretch Wrap

Stretch film, or stretch/cling film, is used to unitize goods for transportation. A thin film is stretched, either by machine or by hand and wrapped around packages to hold the goods together. The film clings to itself and to the pallet, securing the load. In its most common form, stretch/cling film is applied to a stacked pallet using a power prestretch pallet wrapper in an automated operation. In this operation, the film is stretched, between 100% and 300%, by rollers turning at different speeds and is then applied to a loaded pallet, which sits atop a moving turntable. Machine wrap film is typically supplied on rolls that are 20 or 30 inches (51 or 76 cm) wide. Hand wrap film is supplied on smaller rolls. Stretch/cling films may be manufactured by either a cast or blown film process. Most stretch/cling films are coextruded structures containing three to seven layers. LLDPE is the primary component in most stretch films. For specialized applications, coextrusions containing minor PP, EVA, POP, *m*-LLDPE, or ULDPE layers may be employed (Table B.14). For most stretch film structures, a resin with good inherent cling is used on either one or both surface layers. A tackifier,

Table B.14 Stretch Cling Pallet Wrap

Structure	Layers (%)	Gauge (μm)
Stretch Cling Film		
(EVA–ULDPE–LLDPE)	(10/80/10)	15–30
(ULDPE–LLDPE–ULDPE)	(10/80/10)	15–30
(ULDPE–LLDPE–mLLDPE–LLDPE–ULDPE)	(10/25/30/25/10)	15–30
One-Side Cling Film		
(mLLDPE–LLDPE–MDPE)	(10/80/10)	15–30
(EMA–LLDPE–PP)	(10/80/10)	15–30
(POP–LLDPE–PP)	(10/80/10)	15–30
(ULDPE–LLDPE–LLDPE–eLLDPE–PP)	(10/20/30/30/10)	10–30

EMA, *ethylene methacrylic acid;* EVA, *ethylene vinyl acetate;* LLDPE, *linear low density polyethylene;* MDPE, *medium density polyethylene;* PP, *polypropylene;* POP, *polyolefin plastomer;* ULDPE, *ultralow density polyethylene.*

such as polyisobutylene, can also be added to the structure to provide the desired cling force. Stretch film is used to unitize entire or partial pallets stacked with products such as resin bags, fertilizer bags, consumer goods, and food products during distribution. Most stretch film is removed by the retailer prior to displaying the packaged items for sale. Stretch films must have good:

- cling
- stretchability
- load retention and
- puncture resistance.

B.3.2 Heavy Duty Bags (Shipping Bags)

Heavy duty shipping sacks are used to transport items such as the following:

- resin
- salt
- pet food
- fertilizer
- chemicals
- topsoil
- bark mulch
- compressed bales of fiberglass insulation.

When filled they weigh 40 pounds (18 kg) or more. Heavy duty shipping sacks may be supplied as preformed bags or as roll stock, which is formed into bags in a continuous VFFS operation. Special machinery is required to form heavy duty shipping sacks on VFFS machinery in a high-speed continuous operation. These bags need moderate COF because they must easily pass through the packaging equipment, but stacked bags must not slide off each other. Bags filled with hot products, such as salt, must also withstand the filling temperatures without excessive stretching or dimpling. Film toughness and creep resistance are also important in many heavy duty shipping sack applications. LLDPE has allowed significant gauge reduction. LDPE is used to reduce creep and improve processability. HDPE and PP are used for stiffness and higher end-use temperature resistance. EVA polymers are used for low temperature sealability in form-fill-seal applications (Table B.15).

B.3.3 Trash Bags

LLDPE introduction accelerated using coextrusion in trash (or refuse) bags (Table B.16). Downgauging and using recycled material allows for improved economics and sustainability. High molecular weight HDPE polymers are also finding increased usage due to further downgauging opportunities. This is the largest coextruded film market segment.

Table B.15 Heavy Duty Bags

Structure	Layers (%)	Gauge (μm)
(LLDPE–EPE–LLDPE+LDPE)	(20/60/20)	100–200
(EPE–PP–EPE)	(20/60/20)	100–200

EPE, *enhanced polyethylene;* LDPE, *low density polyethylene;* LLDPE, *linear low density polyethylene;* PP, *polypropylene.*

Table B.16 Trash Bag Coextrusion Structures

Structure	Layers (%)	Gauge (μm)
(LLDPE–LLDPE)	(50/50)	15–70
(LLDPE–Recycle–LLDPE)	(33/34/33)	15–70
(LLDPE–HMW-HDPE–LLDPE)	(10/80/10)	15–25

HMW-HDPE, *high molecular weight-high density polyethylene;* LLDPE, *linear low density polyethylene.*

Table B.17 Grocery Bags

Structure	Layers (%)	Gauge (μm)
(LLDPE–HMW-HDPE–LLDPE)	(10/80/10)	12–20

HMW-HDPE, *high molecular weight-high density polyethylene;* LLDPE, *linear low density polyethylene.*

B.3.4 Grocery Sacks (Merchandise Bags)

High molecular weight-HDPE coextruded with LLDPE provides improved sealability with good downgauging potential (Table B.17). This film is typically made on high stalk HDPE blown film coextrusion lines.

B.3.5 High-Clarity Shrink Film (Oriented)

Oriented, high-clarity shrink film is used to protect and display high value consumer goods. It is distinguished from regular shrink film by its superior clarity and appearance, as well as increased shrinkage properties and higher stiffness. Goods are packaged by wrapping the film loosely around the goods, sealing the film to make a completely enclosed bag, and then shrinking the film in a shrink tunnel or oven. Small holes may be poked in the film before wrapping to allow air to escape while the film is shrinking. As in industrial shrink film, heat causes the polymer molecules to relax, causing the film to return to its original unoriented size and shrink tightly around the packaged goods. Since the polymer molecules in oriented shrink film are much more highly oriented, greater shrinkage may be obtained. Boxed retail goods and stationery products are often wrapped with high-clarity shrink film. Ice cream cartons and other food products are also wrapped in high-clarity shrink film. Optical properties, seal properties, shrinkage, and holding force are key requirements for oriented shrink film. These structures are normally biaxially oriented films of LLDPE and PP (Table B.18).

Table B.18 High-Clarity Shrink Film

Structure	Layers (%)	Gauge (μm)
(PP–LLDPE–PP)	(25/50/25)	15–25

LLDPE, *linear low density polyethylene;* PP, *polypropylene.*

Index

'*Note:* Page numbers followed by "f" indicate figures and "t" indicate tables.'

A

AA. *See* Acrylic acid (AA)
Abrasion resistance, 252
ABS. *See* Acrylonitrile-butadiene-styrene (ABS)
Abuse resistance, 310–311, 327, 334–335
  engineering principles for multilayer films, 318–345
  flex fatigue, 317
  mechanical properties, 311–313
  puncture and impact resistance, 315–316
  scratch and abrasion resistance, 316–317
  shipping tests for package durability, 317–318
  stiffness, 313–314
  tear strength, 314
  typical values, 318
Acid copolymer resins (ACRs), 196, 547. *See also* Ethylene acrylic acid; Ethylene methacrylic acid
Acid copolymers, 129, 182, 275, 470, 554
ACRs. *See* Acid copolymer resins (ACRs)
Acrylic acid (AA), 275
Acrylic acid-grafted polyethylene (PE-g-AA), 364–365
Acrylonitrile-butadiene-styrene (ABS), 150
Active packaging, 633–636
  antimicrobial, 634–636
  odor scavenging, 633–634
  oxygen scavenging, 293
Additive technology for control of film friction
  migrating additives, 439–440
  migratory slip additive performance factors, 441–453
  nonmigrating additives, 440–441
  strategies to reduce COF, 438f
  theory of friction and how additives work, 437–439
Additives, 94, 140–141. *See also* Modifiers
  fillers, 104
  in flexible packaging, 104
  inorganic antiblocking agent, 104
  modifiers, 98–104
  stabilizers, 94–98
  and treatments, effect on heat seal performance, 197–198
Adherend chemistry, 380–384
Adhesion, 70, 428–429, 501–502, 539. *See also* Interlayer adhesion
  to aluminum foil, 251
  of multilayer films, 351, 360
    adhesion of coatings, 354
    boundary layer, 370–371
    chemical interaction, 367–370
    diffusion, 366–367
    fracture mechanics analysis of peel test, 354
    mechanical interlocking, 365–366
    oxidation of LDPE, 351–352
    peel test, 352–354
    polymers in coextrusion, 352t
    tie resin technology, 351, 371–396
    wetting and work of adhesion, 361–365
  to PE, 251
  to substrates in extrusion coating, 539
    air gap, 540–566
    die, 539–540
    effect of coating thickness on peel strength, 573–594
    extruder, 539–540
    nip, 566–573
Adhesive application, 42
Adhesive lamination, 42, 43f
  extrusion coating and lamination *vs*., 44
  key components, 42–43
  key factors affecting properties, 43–44
Adhesives, 16, 89
Advanced coatings, 299–300
  ALD, 300
  DLC, 300
Aesthetics, 70
AFM. *See* Atomic force microscopy (AFM)
Aging, 636–639, 638f
  effects, 246
Air gap, 540
  antioxidant and low temperature experiments, 551t
  contact angle results, 557t
  cooling, 559–565, 578–579, 584
  effects plot for cooling in, 563f
  extrusion coating trial evaluating factors, 556t
  guidelines, 565–566
  with IR thermometer, 562f
  Newtonian velocity profile, 541–542
  orientation, 554–559
  oxidation, 542–554
  ozone treatment
    of melt curtain, 550f
    on peel strength, 549t
  sample process time calculations, 542t
  stress, 554–559
  tensile properties of 25-mm EAA coating, 558t
  TIAG, 540, 565t
Air ring, 30
Air-quench blown film. *See also* Coextrusion blown film; Monolayer blown film
  process, 447
  water-quench blown film, *vs*., 525–530, 526t–527t, 528f, 531t
ALD. *See* Atomic layer deposition (ALD)
Alkoxy radicals ($RO^{\cdot}$), 95
Alkyl radicals ($R\cdot$), 95
Aluminum foil, 4, 104–105, 272, 364
Amide structure, 446–447
Amorpha in Turkey, 4f
Amorphous polyester (APET), 74, 90, 646–647
Amorphous polymers, 410
Anaerobic and pyrolytic waste-to-energy process, 648
Analysis of variance method (ANOVA method), 563
Analytical techniques, 247
Anisotropic shrinkage, 503
Annealing, 104
  temperature, 418–419

ANOVA method. *See* Analysis of variance method (ANOVA method)
Antagonistic effects, 456, 456f
Antiblock, 99
  additives, 57–58, 440–441
Antifog, 103
  additives, 435
Antimicrobial, 634–636
Antioxidant system, 95
Antistat additives, 101–102, 435
APET. *See* Amorphous polyester (APET)
Area creation, 598–603, 601f
Area ratio, 600–601
Arrhenius equation, 214, 578
Aseptic packaging, 54
Assembling package, 15–18
ASTM D1003, 453
ASTM D1306 method, 315
ASTM D1746, 453
ASTM D2457, 453
ASTM D2838, 414, 427
ASTM D3354, 437
ASTM D5342 method, 313
ASTM D747 method, 313
ASTM D882, 311
ASTM E96, 268
ASTM F1249 method, 268–269
ASTM F1921, 187
ASTM F392 method, 317
Atomic force microscopy (AFM), 247, 446, 451
Atomic layer deposition (ALD), 299–300
Attenuated total reflectance (ATR), 658
Attribute models, 661, 662f
Auto adhesion, 198
  early theories, 199–200

B

Backside transfer, 245
Bag-in-box packaging, 707, 707t
Bakery packaging, 700, 705t
"Ballooning" effect, 621
Bar sealing, 61
Barrier, 69–70
  bag-in-box liner requirements, 673t
  screws, 27
  selection, 673–674
Barrier packaging, 259
  antimicrobial packaging, 261
  barrier needs by food type, 262t
  degree of protection, 265t
  deleterious pathogens, 260
  emerging technologies, 293–300
  extrinsic factors, 259, 259t
  intrinsic factors, 259, 259t
  measurement, 261
    conversion factors, 266t
    gas permeation, 266–268
    moisture vapor transmission rate, 268–269
    organic molecules permeation, 269
    oxygen permeation value (OPV), 261
  modified atmosphere packaging (MAP), 260
  permeation values, 269–278
  scalping, 261
  science of permeation, 278–293
Base films, 420
Basket weaving, 3–4
Bend under own weight, 313
Bending stiffness, 309, 323–327
  comparison of adhesive and extrusion laminated films, 325t
  force and deflection, 324f
  model results, 326t
  redesign of thermoforming web, 327f
Beta gauges, 31
Biaxial orientation, 415, 419, 423
Biaxial-orientated polyester (BOPET), 44, 412–413
Biaxial-orientated polypropylene (BOPP), 44, 412–413
Biobased polymers, 91
  biosourced monomer-based polymers, 92
  PBS, 93–94
  PHAs, 92–93
  PLA, 92
  starch polymers, 94
Biodegradation additives, 649
Biosourced monomer-based polymers, 92
Biot number (*Bi* number), 564–565
Birefringence, 413
"Black box" approach, 666
Bleached paper, 107
Blend morphology, 167f, 530–532
  development in blown film, 530–532
    effect of minor phase concentration, 533
    elongated second phase, 532f
    material characteristics, 532–533
    processing factors, 533–534
Blending, 149–150, 155. *See also* Melt blending
  melt blending, 152–155
  morphology development in immiscible blends, 160–169
  pellet premixing, 151–152
  processes, 150–155
  properties *vs*. percent of polymer, 156f
  TEMs, 156f
  thermodynamics, 157–160
Blister packaging, 55
Block copolymers, 78
Blocking, 57–58, 437
  force measurement, 437f
Blooming additives, 101
Blow-up ratio (BUR), 33, 337–338, 417, 479–480, 516, 594–595
Blown film, 421, 441–442
  air ring, 30
  air-quench blown film *vs*. water-quench blown film, 525–530, 526t
  bubble instability, 479–483, 479f–480f
  cast film processes *vs*., 39, 39t
  coextrusion blown film, 32, 519–525
  collapsing frame, 30
  cylindrical spiral mandrel die design, 29f
  development of blend morphology in, 530–534
  dual lip air ring, 30f
  examples, 515
  extruder, 29
  gauge control, 30–31
  haul-off roll, 30
  inner bubble cooling, 30
  key factors affecting properties, 32–35
  line, 504–505
  polymers, 28
  process, 7, 29, 29f, 515f
  scale-up, 35, 35t, 516, 517t
  stress–strain history in, 515–525
  tubular die, 29–30
  winders, 31f
  windup, 31–35
Bond strength, 367. *See also* Seal strength; Peel strength
Bonding at interface, 200. *See also* Adhesion
BOPET. *See* Biaxial-orientated polyester (BOPET)
BOPP. *See* Biaxial-orientated polypropylene (BOPP)
Bottom web, 54
Boundary layer adhesion mechanism, 370–371
Branched PE, 77
Branching, 77–78, 140, 140f
  Long chain (LCB), 77
  Short chain (SCB), 77
Breakeven analysis, 644f
Brookfield viscometer, 132
Bullet drop test model, 668–669
BUR. *See* Blow-up ratio (BUR)

C

Cache strain, 311
Calcium carbonate ($CaCO_3$), 98
Cantilever tests, 313
Capillary melt shear viscometry, 133

basic equations, 133−134
corrections to capillary rheology data, 134−135, 134f
Capillary number, 161
Capillary rheology data, corrections to, 134−135, 134f
Carbon double bonds, 439
Carbonyl index (CI), 543
Carreau−Yasuda model, 222, 223t
Cast film, 36, 36f
blown film processes *vs*., 39, 39t
cast film/extrusion coating, 601
chill roll, 36−37
coextrusion, 37
die, 36
extruder, 36
key factors affecting properties, 37−39
pinning technology, 36−37
windup, 37
CED. *See* Cohesive energy density (CED)
Cellophane, 4, 106
Cereal box liners, 700, 704t
CFR. *See* Code of Federal Regulations (CFR)
Chamfering, 469
Channel leakers, 245−246
Chaotic flow, 471
CHDM. *See* Cyclohexane dimethanol (CHDM)
Cheese packaging, 700−705, 706t
Chelating agents, 635
Chemical interaction, 367−370
Chemical resistance, 278
Chemistry, 204−205
Chill roll
cast film, 36−37
extrusion coating and lamination, 41
release, 99−101
Chlorotrifluoroethylene (CTFE), 69
Christensen models, 410
Chrome plating, 363
Chromium-based catalysts, 76, 79
CI. *See* Carbonyl index (CI)
Clamshell packaging, 54−55
Clamshell resins properties, 647t
Clarifying agents, 102−103, 457
Clay-coated paper, 108
CLH. *See* Crystallization line height (CLH)
Cling additives, 440
Cling films, 426−428
Clostridium botulinum (*C. botulinum*), 59, 260
co-PET. *See* PET copolymer (co-PET)
"Coat hanger" dies, 36
Coating
adhesion, 354
adhesive resin, 375−378
and lamination
adhesive lamination, 42−44
extrusion coating and lamination, 40−42
Coating thickness, 554, 559−563
on peel strength, 573−574
adhesion of LDPE, 574f−575f
nonporous substrates, 582−588
peel test analysis, 588−594
Perkins Southwick test method, 575f
porous substrates, 576−582
Coca-Cola, 11−12
COCs. *See* Cyclic olefin copolymers (COCs)
Code of Federal Regulations (CFR), 111, 621
Coefficient of friction (COF), 57, 99, 197, 435−437, 436f. *See also* Dynamic COF; Static COF
correlation of kinetic, 444f
effect of sled weight, 437f
Coextrudable adhesives, 378−396
coextrudable tie resin technology, 378−380
factors affecting peel strength, 380−392
Coextrudable tie resin, 392−396
Coextruded films, 322, 707
Coextrusion, 14, 450−451, 455−456, 455f, 465
cast film, 37
extrusion coating and lamination, 41
layer multiplier technology, 369
layer rearrangement in, 483−486
layer redistribution in three-layer coextrusion, 483f−484f
Coextrusion blown film, 32, 519−525. *See also* Air-quench blown film; Monolayer blown film; Water-quench blown film
effect of coextrusion, 522f
effect of process time, 522f
Elmendorf tear strength, 525f
machine direction (MD)
elongation, 524f
rate, 521f
yield strength, 524f
normalized bubble temperature profile, 520f
properties, 523t
width of temperature plateau, 521f
COF. *See* Coefficient of friction (COF)
Coffee package, 423−424
Cohesive energy density (CED), 157−158, 281
Collapsing frame, 30
Compatibility, 156
Compatibilizers, 104
Complex viscosity, 136, 406, 407f
Compostable packaging, 649
Compression ratio, 26−27
Compuplast, 671
Computer modeling and simulation, 661
Condensation, 76
polymers, 470
Conductive sealing (CS). *See* Hot bar sealing
Cone and plate viscometer, 135, 135f
Constitutive equations, 141−144, 141f
Consumer Packaging Goods (CPG), 12
Consumption patterns, 9−11
Contact angle, 361
Contamination, 244−245
Converting costs, 641
Converting processes, 25, 25t
coating and lamination, 40−44
extrusion, 25−29
film converting, 29−40
orientation, 44−46
printing, 46−47
single screw extruder, 25f, 26t
Cooling, 559−565
in air gap, 578−579
nonporous substrates, 584
porous substrates, 578−579
kinetics, 33−34
in nip
nonporous substrates, 584−586
porous substrates, 579−581
Coordination catalyst polymerization, 76
Copolymers, 78
CoPP. *See* Random copolymer polypropylene
Corotating twin-screw extruder, 154−155
Cost, 640, 667−669
environmental costs, 642−649
financial costs, 640−642, 640t
Covalent bonds, 76
Cox-Merz rule, 136
CPET. *See* Crystalline polyethylene terephthalate (CPET)
CPG. *See* Consumer Packaging Goods (CPG)
Crack or peel front, 590. *See also* Fracture; Peel test
Cradle-to-gate LCA, 645
Creep, 130, 141−144, 141f
Creep test, 402−403
Creep/recovery, 142−144, 142f−143f
Critical attribute, 456
Critical surface tension, 361
Critical to quality (CTQ), 13, 633−634

Critical thickness (for adhesion), 359–360, 359f, 590
Cryogenic microtoming, 657
Crystalline
  morphology, 75, 337, 415
  regions, 273
Crystalline polyethylene terephthalate (CPET), 90, 618
Crystallinity, 402, 609
Crystallization, 205–206
  continuum of molecular forces, 205f
  half time, 406–407, 408f
  model calculation, 206f
  secondary, 500–501, 503
  stress and strain induced, 208–209, 503
  time, 598–603, 601f
  types of molecular forces, 205t
Crystallization line height (CLH), 516–518
Crystals, 74, 281–282
CTFE. *See* Chlorotrifluoroethylene (CTFE)
CTQ. *See* Critical to quality (CTQ)
Cup method, 268
Curing, 42, 44
Curl, 494, 496f, 506f, 681
  aging of three layer films, 499f
  causes, 494–497
  changing tie resin of coextruded blown film, 498t
  design of experiment and curvature results, 506t
  differential shrinkage, 495–497, 495f–496f
  measuring curl, 496f
  modeling, 502–508
  strategies for reduction, 497
    balance modulus, thickness, location, and shrinkage of layer, 501–502
    matching freezing points or crystallization rates, 499–500
    matching shrinkage of layers, 499
    post-quench crystallization, 500–501
    quench rate increase, 500
    reducing polymer crystallinity, 497–498, 498t
  of two-layer blown film, 497t
Cyclic olefin copolymers (COCs), 69, 85–86, 85f, 273, 425–426. *See also* Biobased polymers
Cyclohexane dimethanol (CHDM), 90
Cylindrical spiral mandrel die design, 29f

D

Dairy products, 260
DDR. *See* Draw down ratio (DDR)
Deadweight
  hot tack test, 185f
  tests, 185
Deborah number (*De*), 35, 122–123, 468–469, 474f, 554, 605–606, 664
Deformation, 311
Delamination, 624–628
  peel–seal technology, 351
  technology for recycling multilayer films, 648
Design of experiments (DOEs), 661–664
  experiments, 663–664
  factorial design, 662–663, 663f
  primary limitation, 665
Diamondlike coatings (DLC), 300
Dichroism, 413
Die, 539–540
  cast film, 36
  drool, 467–470, 468t
  exit region, 469, 469f
  extrusion coating and lamination, 40
  swell, 468
Die drip; *See* Die—drool
Die lip buildup; *See* Die—drool
Differential scanning calorimetry (DSC), 194, 403, 405f, 518–519, 657, 659–660
Diffusion, 207, 279, 366–367, 380–381, 630
  coefficient, 269, 443
  diffusion-in experiment, 443
  diffusion-out experiment, 443–444
  at interface, 200–201
    heat seal process effects, 202
    polymer properties, 203–205
Diffusive flux, 609
Dimensional stability, 90
Dimensional thermoformability index (DTI), 403–404
Dioctyl phthalate, 101
Dipole forces, 77
Directional tear technology, 340–342
Dispersion, 159–160
  of rigid particles, 169–171
  stabilization, 162
DLC. *See* Diamondlike coatings (DLC)
DMA. *See* Dynamic mechanical analysis (DMA)
DMTA. *See* Dynamic mechanical thermal analysis (DMTA)
DOEs. *See* Design of experiments (DOEs)
Dog bone profile, 472
Domain size, 457–458
Double bubble processes, 45–46, 45f, 412, 415
Dow chemical hot tack tester, 185f
Down gauging, 309
Draw down ratio (DDR), 32–33, 321–322, 417, 497, 516, 534, 595, 602, 603f
Draw ratio, 473, 474f, 479, 534
Draw resonance, 42, 478–479
Drying, 42, 95
DSC. *See* Differential scanning calorimetry (DSC)
DTI. *See* Dimensional thermoformability index (DTI)
Dual bore capillary rheometer, 135f
Dual compartment pouch concept, 669f
Dual ovenable packaging, 618
DuPont, 661, 674–675
  bending stiffness test method, 313, 314f
  company, 4
  disco purge method, 466, 467f
  sealant selector tool, 675f
  Selar PA, 297
  spring hot tack test, 185–186, 186f
Dwell time, 63, 183, 191
Dynamic COF, 436
Dynamic mechanical analysis (DMA), 403, 605
Dynamic mechanical thermal analysis (DMTA), 403
Dynamic rheology measurements, 135–136
Dyne test, 361

E

E-beam irradiation, 404. *See also* Irradiation, Pasteurization; Sterilization
E/GMA. *See* Ethylene-coglycidyl methacrylate (E/GMA)
EAA. *See* Ethylene acrylic acid (EAA)
Easy-open seal technology, 230
  examples, 231–232, 233f
  lidding films, 235–238
  mechanisms, 231f
  PB-1 blends, 232–235, 234f, 236f
EBA. *See* Ethylene butyl acrylate (EBA)
Ecoflex, 94
ECPs. *See* Ethylene copolymers (ECPs)
Edge bead, 40, 129, 472–478, 474f
  forces on melt curtain leading to, 477f
Edge Tear Instabilities, 478–479
Edge weave, 42, 129, 478–479
Edible oil packaging, 707, 707t
Elastic modulus. *See* Tensile modulus

Elasticity, 125
effects, 484–486, 485f
Electrical theory of adhesion, 199–200
Electron beam irradiation. *See* E-beam irradiation
Electron spectroscopy for chemical analysis (ESCA), 247, 368–369, 446–447, 543, 625
Elmendorf tear resistance test, 314
Elongation, 311
Elongational viscosity, 121f
measurements, 533
EMA. *See* Ethylene methyl acrylate (EMA)
EMAA. *See* Ethylene methacrylic acid (EMAA)
Emerging barrier technologies
advance coatings, 299–300
layer multiplication, 294–297
nanocomposites, 297–299
oxygen scavenging, 293–294
Empirical and statistical models, 661–665
fishbone diagram for heat seal problem, 663f
Encapsulation, 635
End use, 130, 391–392
factors influencing flexible packaging design, 617
aging, 636–639
cost, 640–649
environmental effects on package performance, 617–623
general considerations, 640
packaging–product interactions, 623–636
End-of-life scenarios, 647–649
Engineering strain, 312
Engineering stress, 312
Environmental costs, 642–649. *See also* Financial costs
breakeven analysis, 644f
end-of-life scenarios, 647–649
LCA, 645–647
product life cycle, 645f
SaVE Tool, 643t, 644f
Environmental effects on package performance. *See also* Packaging–product interactions
foods and dosage levels, 623t
humidity, 619–621
irradiation, 621–623
pressure, 621
storage modulus, 619f
temperature, 617–619
Environmental stress cracking (ESC), 623–624, 628
EPDM. *See* Ethylene propylene diamine monomer (EPDM)
EPR. *See* Ethylene–propylene rubber (EPR)
Erucamide, 100t, 439, 442, 444t
correlation with COF, LLDPE film, 444f
surface concentration on LLDPE film, 442–443, 444f, 444t
ESC. *See* Environmental stress cracking (ESC)
ESCA. *See* Electron spectroscopy for chemical analysis (ESCA)
Essential work of fracture (EWF), 343–344
Ethylene, 79
ethylene-based ionomers, 76–77
ethylene-bis-stearamide, 439
scavenger, 260
Ethylene acrylic acid (EAA), 70, 203, 364–365, 555, 697
N,N-Ethylene bisamide, 439
Ethylene butyl acrylate (EBA), 374
Ethylene copolymers (ECPs), 82–83, 248, 636. *See also* Biobased polymers
in flexible packaging, 82t
Ethylene methacrylic acid (EMAA), 203
Ethylene methyl acrylate (EMA), 70, 203, 364–365, 582
EMA-based tie resin, 465
Ethylene propylene diamine monomer (EPDM), 103, 150
Ethylene vinyl acetate (EVA), 6–7, 70, 150, 182, 274, 364–365, 435, 569, 659–660, 698
EVA-based tie resin, 465
Ethylene vinyl alcohol (EVOH), 7, 58, 69, 87–88, 87f, 150, 269–272, 406, 407t, 408f, 503, 505, 505t, 507f, 572, 595, 619–620, 658, 698
Ethylene-coglycidyl methacrylate (E/GMA), 369
Ethylene–propylene rubber (EPR), 158, 383–384
EUP. *See* European Pharmacopeia (EUP)
European Pharmacopeia (EUP), 113
EVA. *See* Ethylene vinyl acetate (EVA)
EVA copolymer–styrene vinyl phenol (EVA–StVPh), 159
EVOH. *See* Ethylene vinyl alcohol (EVOH)
EWF. *See* Essential work of fracture (EWF)
Exfoliation, 170, 297
Extensional flow, 122f
Extensional measurements, 136–137
extrudate drawing test, 138f
Extensional viscosity, 121f, 403
Extrinsic factors affecting food quality, 259, 259t
Extrudate distortion, 125–128, 470–472, 471f
Extruder, 539–540
blown film, 29
cast film, 36
extrusion coating and lamination, 40
speed, 533
temperature, 533
Extrusion, 25–29, 124–125
in blown film, 129–130
elasticity, 125
equations for simple shear flows, 126t–127t
film fabrication processes, 129–130
flow in transfer pipes, 125
flow instabilities, 128–129, 470–493
flow of polymers, 125
haze, 454
melt fracture. *See also* Extrudate distortion, 125–128
melt swell, 128f
processes, 7
recirculation secondary flows, 128f
shear thinning behavior, 124–125
velocity profile, 128f
viscosity, 125
Extrusion coating, 7, 540f
adhesion to substrates in, 539
air gap, 540–566
effect of coating thickness on peel strength, 573–594
die, 539–540
extruder, 539–540
nip, 566–573
and lamination, 40, 40f, 371–378
adhesive lamination *vs*., 44
coating adhesive resin, 375–378
coextrusion, 41
examples, 374–375
key components, 40–41
key parameters affecting properties, 41–42
polymer, 373–374
substrate, 371–373

F

Factorial design, 662–663, 663f
Failure analysis for heat sealing, 242. *See also* Heat sealing
analytical techniques, 247
causes, 242–247, 243t–244t

Failure analysis for heat sealing (*Continued*)
troubleshooting checklist, 247–248
types of seal failures, 242
Falling dart impact test, 315–316
Fast quench process, 447
Fatty acid amides, 99, 439–440, 439t, 447
FCNs. *See* Food Contact Notifications (FCNs)
FDA. *See* U.S. Food and Drug Administration (FDA)
FEA. *See* Finite element analysis (FEA)
Feedblock technology, 32, 37
Fick's first law, 265–266, 279, 442–443
Fick's second law, 279
Fickian diffusion equations, 269
Fillers, 104, 140–141
Filling, 58–59
Film, 291–292, 291f
blocking, 435
converting, 245
blown film, 29–31
cast film, 36–39
film-to-film COF properties, 436
film-to-metal COF properties, 436
lamination and printing, 12
structure, 386–388, 405–406
temperature, 406–409, 406t
thermal properties and thermoforming temperatures, 407t
thickness, 193–194, 276–277
and additive level, 447–448, 448f
measurement, 31, 401
heat seal curves, 194f
Film fabrication, 124–125, 234–235, 442, 447
additives and treatments, 197–198
in blown film, 129–130
elasticity, 125
equations for simple shear flows, 126t–127t
film fabrication processes, 129–130
film thickness, 193–194
flow in transfer pipes, 125
flow instabilities, 128–129
flow of polymers, 125
LLDPE extrudate distortion, 129f
melt fracture, 125–128
melt swell, 128f
and package design, 195–197
recirculation secondary flows, 128f
sealant resin, 194–195
shear thinning behavior, 124–125
substrate adhesion, 195
thickness measurement, 31
velocity profile, 128f
viscosity, 125
Financial costs, 640–642, 640t. *See also* Environmental costs
converting costs, 641
indirect packing costs, 641–642
material costs, 641
modeling, 642
other costs, 642
packing labor and overhead costs, 641
Finite element analysis (FEA), 669
Finite element model, 411
Finite velocity, 467
Flame treatment, 364
Flaring of die exit to reduce die drool, 469
Flex fatigue, 317
Flexible packaging, 3, 9, 642–645, 648. *See also* Modeling flexible packaging structures
film structures
food packaging, 699–707
industrial/consumer films, 707–709
medical packaging, 698–699, 698t
flexible packaging films, markets for, 697
rheology, importance in, 123–131. *See also* Rheology
end use, 130
extrusion and film fabrication, 124–130
polymer characterization, 130–131
typical shear rate ranges, 124f
value chain, 11f
Flexible Packaging Association, 9
Flexographic printing, 47, 47f
FLH. *See* Frost line height (FLH)
Flood feeding in extrusion, 25. *See also* Extrusion
Flow
accelerated reaction rate in coextrusion, 608–609
flow-induced orientation, 609
instabilities in coextrusion, 679
maldistribution and instability issues, 470
bubble instability in blown film, 479–483
draw down, 472–479
interfacial instabilities, 486–493
layer rearrangement in coextrusion, 483–486
sharkskin and extrudate distortion, 470–472
microcalorimetry, 544
Fluoroelastomers, 125–128
Fluoropolymer, 469–470
Food Contact Notifications (FCNs), 111
Food packaging, 10, 110–111, 266–268. *See also* Industrial/consumer films; Medical packaging
bag-in-box packaging, 707, 707t
bakery packaging, 700, 705t
cereal box liners, 700, 704t
cheese packaging, 700–705, 706t
edible oil packaging, 707, 707t
fresh-cut produce, 706–707
frozen food packaging, 705–706, 706t
milk pouches, 705, 706t
poultry/fish packaging, 700, 704t
primal meat packaging, 699, 699t
processed meat packaging, 699–700
film structures, 701t–704t
regulatory compliance
in European Union, 112–113
in United States, 111–112
retortable pouches, 707
salty snack packaging, 700
snack food packaging, 700, 705t
subprimal meat packaging, 699t
Foreign contamination, 465
Forming process, 401–402
Fourier transform infrared spectroscopy (FTIR spectroscopy), 109, 247, 287, 368–369, 450, 465, 543, 657–659
IR frequencies of chemical compounds, 659t
trichroism, 337–338
Fracture
energy, 130, 211, 554, 590
model, 363
mechanics, 210–212
analysis of peel test, 354
Free radical polymerization, 75
Free volume, 443
Freezing line height, 516–518
Fresh-cut produce, 706–707
Frictional properties, 435
additive technology, 437–441
blocking, 437
coefficient of friction, 436–437
importance, 435–436
Frost line, 515
Frost line height (FLH), 33–34, 516, 534
Frozen food packaging, 705–706, 706t
FTIR spectroscopy. *See* Fourier transform infrared spectroscopy (FTIR spectroscopy)

G

Gamma backscatter techniques for measuring film thickness, 31
Gamma capacitance techniques for measuring film thickness, 31
Gamma gauges for measuring film thickness, 31
Gamma ray transmission for measuring film thickness, 31
Gas, 86
  fading, 98
  flush packaging, 59–60
  permeation, 266–268
    standard methods for measuring, 267t
  phase-fluidized bed reactor, 79
Gas barrier, 69, 269
  EVOH, 269–272
  OPV and MVTR values for high barrier polymers, 270t
  OTR and MVTR values for barrier substrates, 271t
  PA, 272
  PVDC, 272
  resins and substrates, 272
Gas chromatography (GC), 266
Gas sealing. *See* Hot air sealing
Gauge control, 30–31
GC. *See* Gas chromatography (GC)
Gelbo flex test, 317
Generally accepted as safe (GRAS), 111, 634
GHG emissions. *See* Greenhouse gas emissions (GHG emissions)
"Glass" oxide coatings, 290
Gloss, 453, 458
Good and Girifalco equation, 160
Grafted PE, 84
Graham's law, 293
GRAS. *See* Generally accepted as safe (GRAS)
Gravure printing, 46–47, 46f
Grease resistance and barrier, 69, 274
  acid copolymers, 275
  film thickness, 276–277
  ionomers, 275–276
  and oil resistance, 251, 251f
  oil type, 277
  paper, 108
  PE, 274–275
  PP, 276
"Greaseproof paper", 107
Greenhouse gas emissions (GHG emissions), 617
Grocery sacks, 709, 709t
Gross melt fracture, 128, 471
Gussets, 245–246

H

Halogens, 425–426
HALS. *See* Hindered amine light stabilizers (HALS)
Haul-off roll, 30
Haze, 481–482, 482f
Haze and transparency, 454
  coextrusion, 455–456
  factors, 456–458
  monolayer polyethylene film, 454–455
HDPE. *See* High density polyethylene (HDPE)
Health-care packaging, 113
Heat seal, 212–216, 215f
  coatings, 235–237
  model, 214f, 678–679, 679f
  operation
    dwell time, 191
    pressure, 192
    product contamination, 192–193
    seal bar design, 192
    temperature, 191–192
  process effects, 202
  results of horizontal form fill seal trial, 216f
  temperature curves, 63f, 188–190, 189f
  temperature window, 189f–190f
Heat seal initiation temperature (HSIT), 63, 188
Heat sealing, 60–61, 130, 181, 198
  bonding at interface, 200
  crystallization, 205–206
  die design, 62
  diffusion at interface, 200–205
  early theories of auto adhesion, 199–200
  easy-open seal technology, 230–238
  factors influencing performance, 62–65, 191–198
  failure analysis, 242–248
  in flexible packaging, 181
  fracture mechanics, 210–212
  hot tack, 182f, 207–210, 216–219
    curves, 190–191
  interfacial bond strength, 205–206
  laboratory tests
    comparing with packaging line studies, 188
    heat seal tests, 183–184
    hot tack measurement, 184–188
  mechanisms of self-adhesion, 198f
  reclosable seal technologies, 238–239
  science of, 198–212
  seal crimper, 62
  seal strength of packages, 182–183
  sealant, 182
    layer, 181
  selecting sealant resins, 248–253
  squeeze flow, 219–230
  troubleshooting, 242–248
  types, 61–62
  ultra sonic (US), 239–242
Heat transfer models, 672
Heavy duty bags, 708, 708t
Hencky strain. *See* Logarithmic strain
Henry's law, 265
Herman's orientation function, 339
Heterogeneous nucleation, 102
HFFS. *See* Horizontal form fill seal (HFFS)
High barrier
  polymers, 277
  substrates, 272
High density polyethylene (HDPE), 6, 62, 69, 81–82, 150, 187–188, 195, 273, 467, 494, 545–546, 595, 659, 673, 697
  blown film trial, 505t
  HDPE–tie–barrier–tie–sealant structure, 673
  HDPE–tie–EVOH test structure, 604
High impact polystyrene (HIPS), 91, 646–647
High pressure processing (HPP), 621. *See also* Pasteurization; Sterilization
High speed puncture, 315–316
High stress region, 469
High-clarity shrink film, 709, 709t
Highly crystalline polyolefins, 69
Hindered amine light stabilizers (HALS), 95–98
HIPS. *See* High impact polystyrene (HIPS)
HMW–HDPE films, 421
Homogeneous nucleation, 102
homopolymer polypropylene (hPP or hoPP), 321–322
"Hook", 371
Hookean solids, 122–123
Horizontal form fill seal (HFFS), 51–53, 53f, 697
Horizontal thermoform fill seal, 53–54, 53f
Hot adhesion, 207
Hot air sealing, 61
Hot bar sealing, 195, 239, 242
Hot knife sealing, 61
Hot tack, 51, 65, 65f, 130, 181–182, 182f, 207–210, 216–219, 217f, 219f

Hot tack (*Continued*)
comparison of hot tack performance, 208f
curves, 190–191, 190f
effect of delay time, 220f
DSC, 209f
master hot tack curve, 218f
model prediction, 221f
resin design strategies, 208f
strain or stress induced crystallization, effect on, 208–209
temperature window breadth, 251
transient elongation viscosity, 210f
Hot tack initiation temperature (HTIT), 187, 190–191
Hot wire sealing, 61
HPP. *See* High pressure processing (HPP)
hPP. *See* homopolymer (hPP)
HSIT. *See* Heat seal initiation temperature (HSIT)
HTIT. *See* Hot tack initiation temperature (HTIT)
Humidity. *See* Relative humidity
Hydrocarbon resins, 103
Hydrodynamics, 470
Hydrogen bonding, 77, 415
Hydrogen chloride (HCl), 94–95
Hydroperoxide (ROOH), 95, 260, 630
Hydroxyl (OH), 368
Hydroxyl radicals (˙OH), 95
Hyperelastic constitutive models, 410
Hyperelastic model, 410

I

6I. *See* Isophthalic acid (6I)
I-beam, 323–324
ICH. *See* International Conference on Harmonization (ICH)
Immiscible blends, 156
Impact resistance, 315
high speed puncture, 315–316
slow puncture, 315
Impartation, 628–630
Improved collection, marking, and sorting systems, 648
Impulse sealing, 61
In-package
pasteurization, 617
sterilization processes, 617
Indirect packing costs, 641–642
Induction
force, 77
sealing, 61
Industrial/consumer films. *See also* Food packaging; Medical packaging
grocery sacks, 709, 709t
heavy duty bags, 708, 708t
high-clarity shrink film, 709, 709t
stretch cling pallet wrap, 708t
stretch wrap, 707–708
trash bags, 708
coextrusion structures, 692t–695t
Infrared (IR), 155–156. *See also* ATR; FTIR
detectors, 268–269
radiation, 658
spectroscopy, 31
Initial process time studies, 594–598
Inner bubble cooling, 30
Inorganic agents, 635
Institute of Mechanical Engineers study, 8
Interaction parameter, 157
Intercalation of clay, 297
Interfacial/interface, 361
adhesion, 486
bond strength, 205–206
continuum of molecular forces, 205f
model calculation, 206f
types of molecular forces, 205t
defect model, 363
instabilities, 486
fundamental studies, 486–487
input parameters for film structure, 490t, 492t
methods to improving stability, 487–493
velocity profile of two-layer flow, 489f
tension
adhesion to substrates, 361, 363. *See also* Surface tension; Thermodynamics; Wetting
polymer blends, 149, 160–161, 532–533
relationship to solubility parameters, 160, 363
Interlayer adhesion. *See also* Adhesion
in coextrusion, 594
crystallization time, temperature, and area creation, 598–603, 601f
flow accelerated reaction rate, 608–609
initial process time studies, 594–598
interfacial area creation and temperature, 600f
process time master curve, 603–608
after forming, 410
relating stress to process control variables, 612–613
Intermolecular forces. *See* Van der Waals forces
International Conference on Harmonization (ICH), 113
Intramolecular forces, 77
Intrinsic factors for food safety, 259, 259t
Ionic bonding, 415
Ionic bonds, 76–77
Ionomers, 76–77, 82–83, 129, 206, 251, 275–276, 415, 415f–417f, 450, 554
chemical structure, 83f
morphology, 83f
sealant bonds, 206
IR. *See* Infrared (IR)
Irradiation, 420, 621–623. *See also* Sterilization
ISO 2493 method, 313
ISO 7765–2 method, 316
Isomerism, 77–78
polypropylene, 78f
Isophthalic acid (6I), 86
Isotactic polymer, 78
Isotactic polypropylene, 84f

J

Japanese Pharmacopeia (JP), 113
JMP, 662

K

K-BKZ models, 410–411
Kinetic coefficient of friction (COF). *See* Coefficient of friction; Dynamic COF
Kraft paper, 107

L

L/D. *See* Length to diameter ratio (*L/D*)
Labeling laws, 8, 59, 635–636
Laboratory heat seal tests, 183–184
Laboratory hot tack measurement, 184–188
deadweight hot tack test, 185f
Dow chemical hot tack tester, 185f
DuPont spring test, 186f
Packforsk hot tack tester, 186f
Laboratory puncture tests, 330

Lako Tool, 62
Lamella (polymer crystals), 337, 628. *See also* Crystalline morphology
Laminates, 328–332
Laminations, 420
  extrusion coating and, 371–378
Layer multiplication, 294–297, 345
LCA. *See* Life cycle analysis (LCA)
LCB. *See* Long chain branching (LCB)
LDPE. *See* Low density polyethylene (LDPE)
Leakers, 641
Length to diameter ratio (*L/D*), 131, 468, 471
Lidding films, 235, 423
  heat seal coatings, 235–237
  peelable seal resins, 237–238
Lidding stock, 699
Life cycle analysis (LCA), 645–647
  calculation for clamshell packaging, 647t
  data for packaging resins and films, 646t
  model, 674–678, 676t, 677f
Light barrier, 69, 278
  packaging, 260
Limiting tear resistance, 342
Limonene (also d-limonene), 277, 624, 630–633
Linear low density polyethylene (LLDPE), 6, 70, 79–81, 124–125, 129, 150, 182, 195, 274, 327–328, 421, 422f, 439, 441, 444f, 444t, 470–471, 473f, 478–479, 545–546, 617–618, 659, 697, 707–708
  bubble stability, 480
    melt strength additive, 480f, 481, 482f
  elmendorf tear resistance, 481f
  LLDPE–LDPE monolayer films, 414–415, 480f
  melt strength measurements, 480f
Linear polymer, 77
Linear stability analysis, 483
Linear thermal shrinkage, 413
Linear viscoelasticity, 131
Listeria monocytogenes (*L. monocytogenes*), 260
LLDPE. *See* Linear low density polyethylene (LLDPE)
Lockup seal, 230
Logarithmic strain, 312
Long chain branching (LCB), 77, 402, 604
Longer-chain polyamides, 272
Loss modulus, 136
Low density polyethylene (LDPE), 5, 56, 70, 79, 124–125, 150, 182, 373, 439–440, 471, 474f, 478, 540, 542–543, 628, 659, 697
  LDPE/paperboard/LDPE/Al/LDPE structure, 625
  LDPE–LLDPE blends, 158–159
  LDPE–tie–EVOH film, 410, 410f
  LDPE–tie–EVOH–tie–HDPE films, 421, 604
Low residual stress, 401
Low-melting
  polymers, 435
  sealant layers, 435
Lubricants, 101

M

m-LLDPE. *See* Metallocene LLDPE (m-LLDPE); Metallocene polyethylene plastomer
MAA. *See* Methacrylic acid (MAA)
Machine direction (MD), 323, 334, 412, 516, 550–553
Machine direction orientation (MDO), 390
  films, 44, 45f, 46
  processes, 401, 417, 418f
Machine wrap film, 707–708
Maddock screw element, 155f
Magnetic flux, 401
Maleic anhydride grafted polyethylene, 84, 84f, 451
MAP. *See* Modified atmosphere packaging (MAP)
Material costs, 641
Material selection, 69
Maxwell model, 142–143
Maxwell–Stephan equation, 292
MD. *See* Machine direction (MD)
MDO. *See* Machine direction orientation (MDO)
Mechanical interlocking, 365–366
Medical packaging, 698–699, 698t. *See also* Food packaging; Industrial/consumer films
Melt
  flow index. *See* Melt index (MI); Melt flow rate (MFR)
  forming processes, 406
  fracture, 102, 125–128. *See also* Extrudate distortion
  strength, 122, 252, 403
  stretching, 419
  swell, 125
    ratio, 125
Melt blending, 152
  barrier energy transfer screw, 155f
  circulatory flow patterns, 153f
  corotating twin-screw extruder, 154–155
  distributive and dispersive mixing, 152f
  Maddock screw element, 155f
  melting mechanism, 152–153
  mixing, 152
    elements, 153–154
    pin mixing section, 154f
    Saxton mixing section, 154f
  stress and velocity distribution, 153f
  twin-screw extruder modular elements, 155f
Melt flow rate (MFR), 131–132, 132t. *See also* Melt index
  ranging, 415
  viscosity *vs*. shear rate curves, 132f
Melt index (MI), 108–109, 131–132, 132t, 171, 212, 545–546, 664. *See also* Melt flow rate
  viscosity *vs*. shear rate curves, 132f
Melt strength additive (MSA), 481, 481t
Metalized OPP. *See* Metalized oriented polypropylene (Metalized OPP)
Metalized oriented polypropylene (Metalized OPP), 274
Metallized film, 105–106, 372
  balloon film, 423
Metallocene catalysts, 81
Metallocene LLDPE (m-LLDPE), 158–159, 455
Metallocene polyethylene plastomer (mPE), 150, 210
Methacrylic acid (MAA), 275, 547
Methyl ethylene, 84. *See also* Polypropylene
MFR. *See* Melt flow rate (MFR)
MI. *See* Melt index (MI)
Microbes, 621
Microlayer. *See also* Layer multiplier technology
  films specialty, 458
  technology, 294–295, 344–345
Microscopy, 247, 657–658, 658f
Migrating additives, 435, 439–440. *See also* Antistat additives; Chill roll release; Slip additives
  effect of increasing film thickness, 446f
  equilibrium surface concentration increases, 446f
  model calculation, 445f
  slip additives of, 442–446

Migrating agents, 635. *See also* Migrating additives
Migratory slip additive performance factors, 441
  additives, effect of, 449–450
  amide structure, 446–447
  coextrusion, 450–451
  fatty acid amide slip problems, 451
  film fabrication, 447
  film thickness and additive level, 447–448
  migration of slip additives, 442–446
  multilayer structures, 450–451
  polymer surface, 441–442
  storage temperature, 449
  tips and classic references, 452–453
Milk pouches, 705, 706t
Minitab, 662
Mixing, 152
  elements, 153–154
  pin mixing section, 154f
  Saxton mixing section, 154f
MMT. *See* Montmorillonite (MMT)
Modeling, 410–411, 502–508
  base case structure, 504t
  financial costs, 642
  sensitivity analysis, 504f
Modeling flexible packaging structures, 660–681. *See also* Flexible packaging; Packaging structure identification
  attribute models, 661
  case study, 673–681
    barrier bag-in-box liner requirements, 673t
    barrier selection, 673–674
    curl, 681
    flow instabilities in coextrusion, 679
    heat seal model, 678–679, 679f
    input for flow matching model, 680t
    packing costs, 678
    sealant selection, 674, 675t
    stiffness and LCA model, 674–678, 676t, 677f
  empirical and statistical models, 661–665
  examples, 666–673, 666t
  package design, 666–671
  processing/converting, 671–673
  theoretical/fundamental models, 665–666
Modified atmosphere packaging (MAP), 59–60, 260, 633–634
  in food packaging, 60t
  gases in, 60t
Modifiers. *See also* Additives
  antiblock, 99
  antifog, 103
  antistats, 101–102
  chill roll release, 99–101
  clarifying agents, 102–103
  compatibilizers, 104
  lubricants, 101
  nucleating agents, 102–103
  opacifiers, 98
  pigments, 98
  plasticizers, 101
  process aids, 102
  slip agents, 99
  tackifiers, 103
  toughenners, 103
Modulus, 122
Moisture vapor barrier, 272, 273f
  PCTFE, 272–273
  Polyolefins, 273
  PVDC, 273
Moisture vapor transmission rate (MVTR), 252, 268–269, 270t, 421, 528, 529f
Moisture-related issues, 470
Moisturization technique for polyamide, 495, 501t
Molecular architecture, effect on heat sealing, 203–204
Molecular chain length variations, 371
Molecular factors affecting melt rheology, 139
  additives, 140–141
  branching, 140
  chemical interactions, 140
  fillers, 140–141
  MW, 139
  MWD, 140
Molecular forces, 76
  effect of bonding on polymer properties, 77
  primary bonds, 76–77
  secondary bonds, 77
Molecular weight (MW), 72, 139, 158–159, 204, 272, 402, 443, 465
  species, 621
Molecular weight distribution (MWD), 72–74, 129, 131, 140, 140f, 158–159, 195, 281, 412, 443, 471, 479, 487, 545–546, 664
Monolayer and coated barrier systems, 648
Monolayer blown film, 516–519, 516f. *See also* Air-quench blown film; Coextrusion blown film; Water-quench blown film
  crystallization and temperature profiles, 517f
  machine direction velocity profile, 518f
  MD rate, 518f
  scale-up rules, 517t
Monolayer extrusion, 470
Montmorillonite (MMT), 297
Mooney–Rivlin models, 410
Mooning, 246–247
  of seals, 191
Morphology, 149, 156–157
Morphology development of polymer blends
  blend morphology, 167f
  in blown film, 169
  calculating viscosity ratio, 167f
  compatibilizers in reducing coalescence, 166f
  HDPE–PS blend viscosity ratio, 167f
  in immiscible blends, 160–169, 160f
  morphology development, 168f
  single droplet breakup mechanisms, 166f
  single screw extrusion solid bed melting model, 168f
  viscoelastic droplet deformation, 163t–165t
mPE. *See* Metallocene polyethylene plastomer (mPE)
MSA. *See* Melt strength additive (MSA)
Multi-manifold dies, 37
Multilayer barrier shrink film and bags, 420–421
Multilayer films, 12, 342
  engineering principles for, 318
    bending stiffness, 323–327
    EWF, 343–344
    mechanical properties, 318–323
    microlayer technology, 344–345
    puncture, scratch, and abrasion resistance, 327–335
    tear resistance, 335–342
Multilayer nonshrink barrier films, 421–424
Multilayer structures, 450–451
MVTR. *See* Moisture vapor transmission rate (MVTR)
MW. *See* Molecular weight (MW)
MWD. *See* Molecular weight distribution (MWD)
MXD6, 86

N

"Nano" scratch tests, 317
Nanocomposites, 169–171, 171f, 297–299, 298f–299f
Nanoparticles, 171
Near-infrared spectroscopy (Near-IR spectroscopy), 31
Neck-in, 40, 129, 472–478, 473f–474f, 475t, 476f
Net stress, 554–555
Net ultimate hot tack (NUHT), 217
Neutral axis, 323–324
Newtonian fluid, 122
Newtonian model, 124
Newtonian plateau, 123–124
Nip, 566
  boundary conditions, 566–567
  cooling in, 579–581, 584–586
  examples, 569–573
  extrusion coating and lamination, 41
  solidification, 567–569
  thermal diffusivity, 566
  time in, 567–569
Nitrocellulose-based waterproof coatings, 106
Nitrogen flushed packaging, 260
No-slip condition, 469–471, 489
Nominal stress, 312
Non-Fickian diffusion, 279
Non-Newtonian behavior, 533
Nonmigrating additives, 435
Nonpolar polymers, 198
Nonporous substrates, extrusion coating on, 582. *See also* Porous substrates
  cooling
    in air gap, 584
    in nip, 584–586
  practical implications, 587–588
  stress, 587
  TIAG, 583–584
Normal force, 436–438
NO_x. *See* Oxides of nitrogen (NO_x)
Nucleating agents, 75, 102–103, 457
Numerical simulation, 671
NUHT. *See* Net ultimate hot tack (NUHT)
Nylon, 86, 156–157. *See also* Polyamide

O

OBCs. *See* Olefin block copolymers (OBCs)
Odor scavenging, 633–634
Ogden models, 410
OGTR. *See* Oxygen gas transmission rate (OGTR)
OH. *See* Hydroxyl (OH)
Oil
  barrier, 69. *See also* Grease barrier
  resistance, 274
    acid copolymers, 275
    film thickness, 276–277
    ionomers, 275–276
    PE, 274–275
    PP, 276
  type, 277
Oleamide, 100t, 439, 442
Olefin block copolymers (OBCs), 382
Oleophobic chemicals, 107–108
Oleyl palmitamide, 100t, 439
OPA. *See* Oriented polyamide (OPA)
Opacifiers, 98
OPET. *See* Oriented polyethylene terephthalate (OPET)
OPP. *See* Oriented polypropylene (OPP)
Optical microscopy, 292
Optical properties, 453
  definitions and measurement, 453
  gloss, 458
  haze and transparency, 454–458
  Microlayer films specialty, 458
OPV. *See* Oxygen permeation value (OPV)
Organic molecule permeation, 269
Organoleptics, 294, 628–633
  impartation, 628–630
  scalping, 630–633
Orientation, 44, 411–429, 554–559. *See also* Biaxial orientation
  affecting factors
    oriented multilayer films, 420–429
    polymer characteristics, 415–416
    processing factors, 416–420
  double bubble process, 45–46, 45f
  machine orientation process, 45f
  MDO process, 46
  release stress, 414
  tenter frame process, 44f, 45
Oriented multilayer films
  adhesion, 428–429
  base films, 420
  laminations, 420
  multilayer barrier shrink film and bags, 420–421
  multilayer nonshrink barrier films, 421–424
  shrink films and labels, 424–426
  stretch and cling films, 426–428
Oriented polyamide (OPA), 420
Oriented polyester, 69, 105, 272, 420, 550–553, 569–572, 667, 697. *See also* Biaxial-oriented polyester
Oriented polyethylene terephthalate (OPET), 309
Oriented polypropylene (OPP), 69, 104, 188–189, 697. *See also* Biaxial-oriented polyester
Oscillatory flow, 471
OTR. *See* Oxygen transmission rate (OTR)
Oxidation
  adhesion of LDPE in extrusion coating/lamination, 542–554
  food quality, 260
Oxides of nitrogen (NO_x), 98
Oxygen
  barrier, 252
  headspace (MAP), 59
  scavenging, 293–294
Oxygen gas transmission rate (OGTR), 265
Oxygen permeation value (OPV), 261, 270t, 421, 628
Oxygen transmission rate (OTR), 265, 424, 528, 529f–530f, 620f, 699

P

PA. *See* Polyamide (PA)
PA66, 86, 86f
PA6I/6T, 86. *See also* DuPont—Selar PA
Package(s), 697
  design, 195–197, 666–671
    dual compartment pouch concept, 669f
    hot tack, 197f
  development models, 666t
  failures, 617, 628, 641–642
  integrity loss, 623–628
    environmental stress cracking, 628
    peel strength and delamination, 624–628
  shipping tests for durability, 317–318
Packaging, 3, 259, 618. *See also* Environmental effects on package performance; Flexible packaging; Modeling flexible packaging structures
  Amorpha, 4f
  assembling package, 15–18
  benefits, 7–9
  blowpipe, 4
  Cellophane advertisement, 5f–6f
  consumption patterns, 9–11
  drivers and trends, 18t
  five layer flexible packaging structures, 17t
  flexible packaging value chain, 11f
  hunter-gatherer societies, 3

Packaging (*Continued*)
line studies, lab results to, 188
LLDPE, 6
machinery, 7
milestones in history, 3f
needs along value chain, 13−15
packaging−product interactions, 623
active packaging, 633−636
negative consequences, 624f
organoleptics, 628−633
package integrity loss, 623−628
PE, 5
plastics materials, 7
structure identification, 657−660
analytical techniques, 660t
DSC, 659−660
FTIR, 658−659
microscopy, 657−658, 658f
technology, 260−261
three layer flexible packaging structures, 17t
trends in context of value chain, 18−19
two-layer flexible packaging structures, 16t
value chain, 11−13
Packaging equipment, 51
aseptic packaging, 54
horizontal thermoform fill seal, 53−54, 53f
pouch machines, 51−53
retail packaging, 54−56
tray sealer, 54
unit operations, 56−65
uses, 52t
Packforsk
hot tack tester, 186f
test, 187
Packing
costs, 678
labor and overhead costs, 641
Paper, 106
paper-based packaging, 4
paper-making process, 364
types in packaging, 107−108
Paperboard, 56, 106
for packaging, 108
Pasteurization, 617, 621
PB-1. *See* Polybutene-1 (PB-1)
PBAT. *See* Poly(Butylene Adipate co-Terephthalate)
PBS. *See* Polybutylene succinate (PBS)
PC. *See* Polycarbonate (PC)
PC-PMMA. *See* Polycarbonate/polymethyl methacrylate (PC-PMMA)
PC-SAN. *See* Polycarbonate/styrene acrylonitrile (PC-SAN)
PCL. *See* Poly caprolactone (PCL)
PCTFE. *See* Polychlorotrifluoroethylene (PCTFE)
PDI. *See* Poly-dispersity index (PDI)
PE. *See* Polyethylene (PE)
PE film/LDPE−EAA/Al/(EAA/LDPE)/PE film, 697
PE-g-AA. *See* Acrylic acid-grafted polyethylene (PE-g-AA)
Peak hot tack strength, 248
Pebax, 101−102. *See also* Antistat additives
PECVD. *See* Plasma-enhanced chemical vapor deposition (PECVD)
Peel
angle, 237, 354−360
arms, 182
force, 130
rate, 357−359
seals, 230. *See also* Easy open seal technology; Peelable seal resins
speed, 237
Peel strength (PS), 130, 554, 557f, 595, 624−628, 637f
affecting factors, 380
end use, 391−392
film structure, 386−388
processing, 388−391
tie resin functionality, 384−386
tie resin matrix and adherend chemistry, 380−384
coating thickness effect on, 573−574
adhesion of LDPE, 574f−575f
nonporous substrates, 582−588
peel test analysis, 588−594
Perkins Southwick test method, 575f
porous substrates, 576−582
effective contact time, *vs*., 602f
of EMAA to aluminum foil, 638f
to EVOH, 605f
to EVOH *vs*. process time
for blown film, 596f
for coextrusion coating, 597f
Peel test(s), 182−183, 183f, 184t, 352−354, 550−553
analysis, 588−590
application of peel strength model, 590−592
experiment, 588−589
fracture mechanics analysis, 354
peel angle, 354−360
peel rate, temperature, and viscoelasticity, 357−359
practical implications, 592−594
thickness, 359−360
viscoelastic energy dissipation, 355
Peelable seal resins, 237−238. *See also* Easy open seal technology
PEI. *See* Polyethylene imide (PEI)
Pellet mixers, 151
Pellet premixing, 151−152, 151f
PEN. *See* Polyethylene naphthalate (PEN)
Pendant drop method, 361−362
Pendulum impact test, 316
PEO. *See* Polyethylene oxide (PEO)
Permanent additives, 101−102
Permeability, 69
co-efficient, 279
Permeant, 261
Permeation, 261, 278
chemical resistance, 278
through defects, 290−293
factors affecting permeability, 281
environmental effects, 284−290
permeant factors, 282−284
polymer factors, 281−282
thickness, 282
gas barrier, 269−272
grease and oil resistance, 274−277
light barrier, 278
moisture vapor barrier, 272−274
through multilayer films, 280
organic molecules, 277
through perforations, 290, 292−293
through pinholes, 290−292
through polymer films, 278−293
Peroxy radicals ($ROO^{\cdot}$), 95
Perturbation methods, 487
PET. *See* Polyethylene terephthalate (PET)
PET copolymer (co-PET), 632
PETG. *See* Polyethylene terephthalate glycol (PETG)
Pharmaceutical packaging, 259
PHAs. *See* Polyhydroxyalkanoates (PHAs)
Phase inversion onset, 169
Phenolic antioxidants, 95
Phosphite antioxidant, 95
Physical aging, 636
PIB. *See* Polyisobutylene (PIB)
Pigments, 98, 150
Pinning technology, cast film, 36−37

PLA. *See* Polylactic acid (PLA)
Plasma-enhanced chemical vapor deposition (PECVD), 299–300
Plasticizers, 101
Plate-out. *See* Die drool
Plateau hot tack strength, 217
Plateau initiation temperature, 63, 188
Plug-assisted thermoforming, 409
Pneumatic sealing, 61
PO. *See* Polyolefin (PO)
Polar ethylene copolymers, 205
Polar polymers, 69–70, 470
Polar sealants, 200
Poly caprolactone (PCL), 295–296
Poly-dispersity index (PDI), 74
Poly(Butylene Adipate co-Terephthalate) (PBAT), 94
Polyamide (PA), 44, 86, 95, 156–157, 272, 404, 501, 569, 618–619, 698
Polyamide 6 (PA6), 6–7, 69, 86, 86f, 150, 326–327, 636, 658
  crystallizes, 500
  PA6/HDPE-g-MAH layer combination, 608–609
Polybutene-1 (PB-1), 85, 150, 231–232
  blends, 232–235, 234f, 236f
Polybutylene succinate (PBS), 93–94
Polybutylene terephthalate (PBT), 90
Polycarbonate (PC), 150, 391, 484, 631
Polycarbonate/polymethyl methacrylate (PC-PMMA), 344
Polycarbonate/styrene acrylonitrile (PC-SAN), 344
Polychlorotrifluoroethylene (PCTFE), 89, 89f, 272
Polydynamics, 671
Polyester, 89–91
Polyethylene (PE), 5, 15, 75, 77–79, 248, 274–275, 318–321, 404, 435, 466, 619, 697
  blown film, 454
  chain structure differences, 81f
  chemical structure, 78f
  ethylene copolymers, 82–83, 82t
  films, 327–328, 336–340
    DuPont static puncture test of multilayer film, 329f
    fracture mechanics parameters, 336t
    HDPE, 338f
    LDPE, 340f
    plate-like lamellae structure, 337f
  grafted PE, 84
  HDPE, 81–82
  LDPE, 79
  LLDPE, 79–81
  oxidative degradation, 630
Polyethylene imide (PEI), 368
Polyethylene naphthalate (PEN), 90, 272
Polyethylene nucleation, 102
Polyethylene oxide (PEO), 295–296
Polyethylene terephthalate (PET), 15, 54, 69, 132, 150, 184, 188–189, 272, 366, 465, 569, 618
Polyethylene terephthalate glycol (PETG), 90, 425–426, 465
Polyhydroxyalkanoates (PHAs), 92–93
Polyisobutylene (PIB), 427
Polylactic acid (PLA), 92, 93f, 157, 277, 618
  biaxially oriented film, 93t
  thermal properties, 93t
Polylactide (PLA). *See* Polylactic acid (PLA)
Polymer blending
  blending, 149–150
    physics, 155–169
    processes, 150–155
  dispersion of rigid particles, 169–171
  morphology, 149
  morphology development in blown film, 169
  nanocomposites, 169–171, 171f
  for packaging applications, 149
  rheology, 171–172
Polymer processing aids (PPAs), 469–470
Polymer(s), 121, 201, 373–374, 618, 649. *See also* Biobased polymers; Lidding films
  blends, 457–458
  chains, 411, 412f
  characterization, 130–131
  chemistry, 72
    branching and isomerism, 77–78
    crystallinity, 74–75
    molecular forces, 76–77
    MW, 72
    MWD, 72–74
    polymerization process, 75–76
  crystallizes, 439–440
  elasticity, 533
  films, 515
  pellets, 25
  polymer-free volume, 447
  properties
    chemistry, 204–205
    molecular architecture, 203–204
    thermal properties, 203
  substrates, 364
  surface, 441–442
Polymerization process, 75
  condensation, 76
  coordination, 76
  free radical, 75
Polyolefin (PO), 85–86, 273, 497
  antioxidants for stabilizing, 96t–97t
  autooxidative degradation, 95f
  labels, 426
  polyolefin-based shrink labels, 426
  polyolefin-based tie resin, 380
  slip agents for, 100t
Polyolefin plastomer (POP), 700. *See also* Metallocene polyethylene plastomer
Polyoxymethylene (POM), 157
Polypropylene (PP), 69, 84–85, 150, 182, 273, 276, 466, 471, 560–563, 618–619
Polystyrene (PS), 91, 91f, 344–345, 471, 484, 618
Polytrimethyl terephthalate (PTT), 90
Polyvinyl alcohol (PVOH), 69, 87, 87f, 269–270
Polyvinyl chloride (PVC), 55, 91, 91f, 282, 412
Polyvinylidene chloride (PVDC), 6–7, 69, 88–89, 88f, 272, 421, 624, 699
POM. *See* Polyoxymethylene (POM)
Porous substrates, extrusion coating onto, 576. *See also* Nonporous substrates
  cooling in air gap, 578–579
  cooling in nip, 579–581
  practical implications, 582
  TIAG, 577–578
Post-quench crystallization, 500–501, 500f
Potassium ionomers, 101–102
Pouch(es), 51
  drop impact, 670
  heat sealing, 670
  machines, 51
    HFFS machine, 51–53
    VFFS machine, 51
  tear-opening, 670–671
Poultry/fish packaging, 700, 704t
Power law model, 578
PP. *See* Polypropylene (PP)
PP-tie-EVOH-tie-PP sheet, 407–409, 408f–409f, 416
PPAs. *See* Polymer processing aids (PPAs)
Pressure, 65, 139, 192, 284, 409, 437, 609, 621
Pressure-sensitive adhesives (PSAs), 238

Pressure−volume−temperature apparatus (PVT apparatus), 494, 494f
PRF. *See* Puncture resistance factor (PRF)
Primal meat packaging, 699, 699t
Primary bonds, 76−77
Printability, 70
Printing, 46−47
Process aids, 102
Process time, 542, 577−578
  calculating TIAG, 541t
  initial process time studies, 594−598
  master curve, 603−608
  sample calculations, 542t
Processed meat packaging, 699−700, 701t−704t
Processing effect on quality
  curl, 494−508
  die drool, 467−470
  flow maldistribution and instability issues, 470−493
  moisture-related issues, 470
  thermal stability, 465−467
Processing parameters, 409
Processing/converting, 671−673, 672t
Product contamination, 192−193, 193f
Propene, 84. *See also* Polypropylene
PS. *See* Peel strength (PS); Polystyrene (PS)
PSAs. *See* Pressure-sensitive adhesives (PSAs)
PTT. *See* Polytrimethyl terephthalate (PTT)
Puncture resistance, 253, 315, 327
  high speed puncture, 315−316
  laminates, 328−332
  polyethylene films, 327−328
  slow puncture, 315
Puncture resistance factor (PRF), 329
Pure surface winders, 31
Purge compounds, 466−467
PVC. *See* Polyvinyl chloride (PVC)
PVDC. *See* Polyvinylidene chloride (PVDC)
PVOH. *See* Polyvinyl alcohol (PVOH)
PVT apparatus. *See* Pressure−volume−temperature apparatus (PVT apparatus)
Pyrolysis, 648

Q

Quality, 641
  processing effect
    curl, 494−508
    die drool, 467−470
    flow maldistribution and instability issues, 470−493
    moisture-related issues, 470
    thermal stability, 465−467
Quality control tests (QC tests), 109
Quench rate, 500, 502−503, 525−526

R

Random copolymer polypropylene (rPP or coPP), 321−322
Rate of elongation. *See* Rate of strain
Rate of strain, 33, 121, 138
Rate of stretching. *See* Rate of strain
Reclosable seal technologies, 238−239. *See also* Easy-open seal technology
Refractive indices (RI), 440, 458
Registration, 57−58
Regression analysis, 664
Regulatory considerations, 110
  food packaging regulatory compliance
    in European Union, 112−113
    in United States, 111−112
  health-care packaging, 113
Relative humidity (RH), 69, 265, 284−287
  effect on oxygen permeability, 69, 265, 271f, 284−287
  EVOH, 88f
  End-use effects, 619−621
Relaxation, 141−144, 141f. *See also* Stress relaxation
  factor, 503
Reptation theory, 201
Resins, 272
  adhesion, 70
  aesthetics, 70
  barrier, 69−70
  in flexible packaging, 72, 72t−73t
    additives, 94−104
    biobased polymers, 91−94
    EVOH, 87−88
    PCTFE, 89
    polyamides, 86
    polyester, 89−91
    polyethylene, 78−84
    polymer chemistry, 72−78
    polyolefins, 85−86
    polypropylene, 84−85
    polystyrene, 91, 91f
    polyvinyl chloride, 91, 91f
    PVDC, 88−89
    PVOH, 87
    tie resins and adhesives, 89
  function, 69
  material specifications, 108−110
  sealing, 70, 248−253, 249t−250t
  structural integrity, 69
  typical properties, 70−71, 71t
Respiration, 260
Retail packaging, 54
  blister packaging, 55
  clamshell packaging, 54−55
  comparison of types, 56, 57t
  skin packaging, 55−56, 56f
"Retort shock", 287
Retort sterilization, 287−290, 617, 628, 670
Retortable pouches, 707
Retrogradation, 94
Reverse printing, 16
Reverse-side transfer, 370−371
RH. *See* Relative humidity (RH)
Rheology, 109, 123−124, 671
  constitutive equations, 141−144, 141f
  creep, 141−144, 141f
  elongational viscosity behavior, 123f
  extensional flow, 122f
  factors influencing polymer rheology, 138−141
  in flexible packaging, 123−131
  measurements, 131−137
  modes of strain, 121
  normal force, 124f
  polymer blends, 171−172
  relaxation, 141−144, 141f
  shear flow, 121f
  stress, 122
  units for stress and viscosity, 122t
  viscosity
    of materials, 123t
    shear rate curve, *vs*., 123f
Rheotens test, 137, 403
RI. *See* Refractive indices (RI)
Riboflavin, 260
Rigid packaging, 4
Rigid particle dispersion, 169−171
$RO^{\cdot}$. *See* Alkoxy radicals ($RO^{\cdot}$)
$ROO^{\cdot}$. *See* Peroxy radicals ($ROO^{\cdot}$)
ROOH. *See* Hydroperoxide (ROOH)
Room temperature (RT), 446
Rosin resins, 103
Rotary abrasion test, 317
rPP. *See* random copolymer polypropylene (rPP or coPP)
RT. *See* Room temperature (RT)
Rubber modifier, 103
Rutile titanium dioxide, 278

S

Salty snack packaging, 700
SaVE tool. *See* Sealant Value Estimator tool (SaVE tool)
Saxton mixing section, 154f

Scalping, 261, 630–633
Scanning electron microscopy (SEM), 337–338, 368–369, 608–609
Scattering, 486
  light, 453
Scavenging
  odor, 633–634
  oxygen, 293–294
  rate, 294
Scratch resistance, 316–317, 327, 332–334
Screw design, 534
Scrubbing additives, 466–467
Seal. *See also* Heat seal; Heat sealing; Peel strength
  bar design, 62, 192
  initiation temperature, 248
  strength, 248
    packages, 182–183, 183f, 184t
  types of failures, 242
Sealant, 70, 667
  composition, 237
  layer, 181
  polymers, 700
  resin, 194–195
    abrasion resistance, 252
    adhesion to aluminum foil, 251
    adhesion to PE, 251
    breadth of hot tack temperature window, 251
    clarity and transparency, 252
    DSC curve for PE, 195f
    DSC peak melting temperature, 196t
    grease and oil resistance, 251, 251f
    melt strength, 252
    moisture vapor transmission rate, 252
    oxygen barrier, 252
    peak hot tack strength, 248
    puncture resistance, 253
    seal initiation temperature, 248
    seal strength, 248
    seal through contamination, 251
    selection, 248, 249t–250t
    stiffness, 252f, 253
    tear strength, 252
  selection, 242, 674, 675t
  type, 505, 505t, 507f
Sealant Value Estimator tool (SaVE tool), 643t, 644f, 678, 679f
Sealing, 70. *See also* Heat sealing
  seal through contamination, 251
  time, 183
  variables, 242–244
Secant modulus, 312
Second Newtonian plateau, 124
Secondary bonds, 77
Secondary forces, 77
Self-adhesion, 198, 198f
Self-healing effect, 402
SEM. *See* Scanning electron microscopy (SEM)
Semicrystalline polymers, 74, 410, 426f
Sensitivity analysis, 579
Sequential orientation, 419
Sharkskin, 125–128
  extrudate distortion, 470–472
  LLDPE, 129f
Shear flow, 121f
Shear force, 121
Shear stress, 121, 489, 489f, 493f, 609
  in adaptor, 533–534
  in die, 533–534
  in extruder, 533–534
  multilayer flow model, 491t, 493t
  stress profile in channel, 490f
Shear thinning behavior, 122
Shear viscosity, 483–484, 483f, 488–489, 489f
Shipping Bags, 708
Shrink, 411–429
  affecting factors
    oriented multilayer films, 420–429
    polymer characteristics, 415–416
    processing factors, 416–420
  film, 412, 424–426, 425t
  force, 413–415
  labels, 424–426, 425t
  tension, 414, 426f
Silicone oil, 453
Simultaneous orientation, 419
Single droplet breakup mechanisms, 166f
Single screw extruder, 25f, 26t, 152
  melting in, 27f
  metering section, 27f
Skin packaging, 55–56, 56f
Slip additives or agents, 99, 100t, 438, 440–441. *See also* migrating additives; nonmigrating additives
  equilibrium surface concentration, 446f
  effect of increasing film thickness, 446f
  migration, 442–446, 444f
  model calculation, 445f
Slip concentrations, 452
Slip velocity, 467
Slip-stick flow, 467, 471
Slow puncture, 315
Slurry loop process, 80
Snack food packaging, 700, 705t
Snack nuts packaging, 705t
Snap-back forming, 409
Soft annealing, aluminum foil, 364
Softwood pulp, 106
Solid phase pressure forming (SPPF), 406
Solid state stretching, 419. *See also* Orientation
Solidification, 567–569
Solubility parameter, 157–158, 159t, 160
Solution casting, 87
Solution viscosity, 132–133
Solventless adhesives, 42
Spencer impact test, 316
Spherulites, 74, 102
SPPF. *See* Solid phase pressure forming (SPPF)
Squeeze flow, 219–220, 221f
  experimental results, 222–224, 222t, 223f–224f
  insights and limitations, 226–230, 229f–230f
  model development, 220–222, 222t
  model results, 224–226, 225f–228f
Stabilizers, 94–98
Staining, 658
Stand-up pouch filling, 670
Standard temperature and pressure (STP), 261
Standard screw design, 26–27
Static COF, 436
Statistical-based models, 502
Stearyl erucamide, 439
Stephan's equation, 221
Sterilization methods, 287, 617, 621–623, 698. *See also* Pasteurization
Stiff materials, 69
Stiffness, 252f, 253, 309, 313
  bend under own weight, 313
  cantilever tests, 313
  engineering principles for multilayer films, 318–345
  factor, 313
  flex fatigue, 317
  geometry of test frame, 313
  and LCA model, 674–678, 676t, 677f
  measurement, 311–318
  shipping tests for package durability, 317–318
  tensile modulus, 310
  three-point flex, 313–314
  typical values, 318
Storage modulus, 136, 619f
Storage temperature, 449
STP. *See* Standard temperature and pressure (STP)
Strain, 121, 138, 311
  hardening, 122, 402
  rate, 402

Strain (*Continued*)
ratio, 311–312
strain-hardening parameter, 313
Strength, 309. *See also* Peel strength
engineering principles for multilayer films, 318–345
flex fatigue, 317
measurement, 311–318
shipping flexible package, 310f
shipping tests for package durability, 317–318
tear strength, 314
typical values, 318
Stress, 121, 554–559, 587
factor, 309
relaxation, 141–142, 141f–142f, 555t, 613
stress-induced crystallization, 503
Stress–strain, 32–33
behavior, 130
history in blown film, 515
coextrusion blown film, 519–525
monolayer blown film, 516–519, 516f
Stretch
cling pallet wrap, 708t
films, 426–428
rate, 417–418
ratio, 417
wrap, 707–708
Stretching, 412
temperature, 416–417, 417f
Structural integrity, 69
Styrene (St), 159
Subprimal meat packaging, 699t
Substrate(s), 272, 371–373
adhesion, 70, 195
air gap, 540–566
effect of coating thickness on peel strength, 573–594
die, 539–540
extruder, 539–540
in extrusion coating, 539
nip, 566–573
aesthetics, 70
barrier, 69–70
chemistry, 237
in flexible packaging, 104
aluminum foil, 104–105
cellophane, 106
metallized film, 105–106
oriented polyester, 105
oriented polypropylene, 104
paper and paperboard, 106–108
in flexible packaging, 72t
function, 69
material specifications, 108–110
regulatory considerations, 110
food packaging regulatory compliance in European Union, 112–113
food packaging regulatory compliance in United States, 111–112
health-care packaging, 113
sealing, 70
structural integrity, 69
typical properties, 70–71, 71t
unwind and preparation, 40–41
Suppliers, 108
Surface energy. *See* Surface tension
Surface resistivity, 102
Surface tension, 361. *See also* Thermodynamics; Wetting
factors affecting
density, 362
surface crystallinity, 362, 362t
temperature, 362
guidelines for adhesion, 363–364
measurement, 361
contact angle. *See* contact angle
Dyne test, 361
pendant drop, 361–362
Zisman plot, 361
relationship to interfacial tension, 363
typical values
polymer melts, 362t
polymer solids, 361t
Syndiotactic polymer, 78
Synergistic effects, 455, 456f

T

6T. *See* Terephthalic acid (6T)
T-peel test, 183f
Tackifiers, 103
Tacticity, 84
Take-up ratio (TUR). *See* Draw down ratio (DDR)
Takeoff ratio, 417
TD. *See* Transverse direction (TD)
Tear resistance, 335–336
directional tear technology, 340–342
multilayer films, 342
polyethylene films, 336–340
Tear resistance, 310
Tear strength, 252, 314. *See also* Peel strength
Teflon, 184
TEM. *See* Transmission electron microscopy (TEM)
Temperature, 69, 138–139, 138f, 183, 191–192, 284, 357–359, 598–603, 601f, 617–619
viscosity changes, 139t
Temperature rise elution fractionation (TREF), 664
Tensile modulus, 310–312, 404
Tensile strength, 312
Tensile tester, 311, 314
Tenter frame process, 44f, 45, 415
Terephthalic acid (6T), 86
Terminal relaxation time, 213
Terpene resins, 103
Theoretical/fundamental models, 665–666
Thermal diffusivity, 566
Thermal expansion coefficient, 502
Thermal lamination, 12
Thermal properties, 203
Thermal stability, 465–467
Thermal–mechanical analysis (TMA), 247
Thermodynamics, 157–160, 159f
adhesion, 361–365. *See also* Wetting
cohesive energy density, 157f
critical solubility parameter for miscibility of polymer blends, 158t
driving force for additive migration, 441–442
interfacial tension, 361
surface tension, 361
effect of surface crystallinity, 362t
effect of temperature, 362
guideline for adhesion, 363–364
polymer melts, 362t
solid polymer films, 361t
Thermoforming, 58, 130, 401
factors affecting, 405–410
material properties and testing, 402–405
measurement, 31, 401
testing, 401–402
Thermoplastic silicones, 441
Thermoplasticolefin (TPO), 427
Three-point flex test for bending stiffness, 313–314
Threshold of regulation (TOR), 111
Threshold temperature, 470
TIAG. *See* Time in air gap (TIAG)
Tie layer technology, 351
coextrusion, 378–396
choosing, 392–396
factors affecting performance, 380–392
resin technology, 378–380
extrusion coating and lamination, 371–378

choosing, 375–378
effect of substrate chemistry, 371–373
examples from literature, 374–375
polymer chemistry, 373–374
Tie resin(s), 89, 351. *See* Tie resin technology
coextrudable adhesives or tie resins, 378–396
extrusion coating and lamination, 371–378
functionality, 384–386
matrix, 380–384
technology, 371
Time in air gap (TIAG), 37–38, 540, 541t, 602
nonporous substrates, 583–584
porous substrates, 577–578
Time of flight secondary ion mass spectroscopy (TOF-SIMS), 247
Tin foil, 4
Titanium dioxide (TiO_2), 13, 16, 69, 98, 150, 278, 468
TMA. *See* Thermal–mechanical analysis (TMA)
TNSD. *See* Total normal stress difference (TNSD)
TOF-SIMS. *See* Time of flight secondary ion mass spectroscopy (TOF-SIMS)
Top web, 54
TOR. *See* Threshold of regulation (TOR)
Total normal stress difference (TNSD), 487
Tougheners, 103
TPO. *See* Thermoplasticolefin (TPO)
TR. *See* Transmission rate (TR)
Transmission, 658
Transmission electron microscopy (TEM), 156f, 240
Transmission rate (TR), 265
Transverse direction (TD), 323, 334, 412, 518, 550–553
Trash bags, 709t, 708
Tray sealer, 54
TREF. *See* Temperature rise elution fractionation (TREF)
Troubleshooting sealing, 242
analytical techniques, 247
causes, 242–247, 243t–244t
checklist, 247–248
types of seal failures, 242
Trouser tear method, 314
True strain. *See* Logarithmic strain
True stress, 312
Tubular die, 29–30
TUR. *See* Take-up ratio (TUR)
Twin-screw extruder modular elements, 155f
Two drum winders, 31

U

U.S. Food and Drug Administration (FDA), 111
U.S. Pharmacopeial Convention (USP), 113
UK REFLEX, 648
Ultimate seal strength, 188. *See also* Peel strength
Ultrasonic sealing (US), 61, 239–242, 241f
Uncoated film, 106
Unit operations
filling, 58–59
gas flush packaging, 59–60
heat sealing, 60–61
modified atmosphere packaging, 59–60
packaging equipment, 56
registration, 57–58
thermoforming, 58. *See also* Thermoforming
United Nations Food and Agriculture Organization, 8
Unwind and surface preparation, 42
US. *See* Ultrasonic sealing (US)
USP. *See* U.S. Pharmacopeial Convention (USP)
UV stabilization, 95–98

V

VA. *See* Vinyl acetate (VA)
Vacuum forming, 409
Vacuum packaging, 260
Value chain
flexible packaging, 11f
needs along, 13
consumer needs, 13
converter needs, 14–15
end-user needs, 13–14, 15t
packaging trends in, 18–19
Van der Waals forces, 77, 199, 367
Vegetable oils, 277
Venting seal bar design, 670
Vertical form fill seal machine (VFFS machine), 51, 52f, 697, 708
Vertical shift factors, 606, 607f
Very low density polyethylene (VLDPE), 81, 275–276, 700
VFFS machine. *See* Vertical form fill seal machine (VFFS machine)
Vinyl acetate (VA), 159
Vinyl free radical polymerization, 75
Vinyl phenol (VPh), 159
Vinylidene dichloride. *See* Polyvinylidene chloride (PVDC)
Viscoelastic/viscoelasticity, 357–359
constitutive models, 410
fluids, 122–123
polymers, 468
Viscosity, 109, 121, 125, 225
mismatches, 486, 492–493
ratio, 161, 167f, 491–492, 491f, 532
Visking Company, 7
Vitamin B2, 260
VLDPE. *See* Very low density polyethylene (VLDPE)
Voigt model, 143
Volumetric systems, 59
VPh. *See* Vinyl phenol (VPh)

W

Waste-to-chemicals process, 648
Waste-to-fuel process, 648
Water
quench system, 29
resistance paper, 108
ring, 525–526
Water vapor transmission rates (WVTR), 700
Water-quench blown film, 447. *See also* Coextrusion blown film; Monolayer blown film
air-quench blown film *vs*., 525–530, 526t–527t, 528f, 531t
Water-soluble films, 87
Waterproof packaging, 7
Wave instability, 486
WAXS. *See* Wide angle X-ray scattering (WAXS)
Weissenberg effect, 123
Weissenberg number (*Wi* number), 609
Wetting, 42, 200, 363
adhesion, 361
practical guidelines, 363–365
surface tension (energy) of inks, 363–364
surface tension of polymer melts, 362t
surface tension of solid polymer films, 361t
WHO. *See* World Health Organization (WHO)
Wi number. *See* Weissenberg number (*Wi* number)

Wide angle X-ray scattering (WAXS), 321–322, 526–528, 555, 557
Williams–Landel–Ferry model (WLF model), 411
Winders, 31f
Windup, 31–35
WLF model. *See* Williams–Landel–Ferry model (WLF model)
Wood pulp, 4
World Health Organization (WHO), 113

X

X-ray diffraction, 413
X-ray photoelectron spectroscopy (XPS). *See* Electron spectroscopy for chemical analysis (ESCA)

Y

Yield strength, 312
Yield stress, 312, 402
Young's equation, 361
Young's modulus. *See* Tensile modulus

Z

Zero shear viscosity, 123–124
Ziegler–Natta catalysts, 76, 79–81
Ziegler–Natta LLDPE (ZN-LLDPE films), 79, 81, 441–442, 454, 456
Zig-zap instability, 128–129, 486, 486f
Zipper(s), 238
  technology, 238
Zisman plot, 361. *See also* Surface tension
ZN-LLDPE films. *See* Ziegler–Natta LLDPE (ZN-LLDPE films)